NASA Conference Publication 3221
Part 1

Eleventh Workshop for Computational Fluid Dynamic Applications in Rocket Propulsion

Compiled by
R.W. Williams
George C. Marshall Space Flight Center
Marshall Space Flight Center, Alabama

Proceedings of a workshop held at
NASA George C. Marshall Space Flight Center
Huntsville, Alabama
April 20–22, 1993

NASA
National Aeronautics and
Space Administration
Office of Management
Scientific and Technical
Information Program
1993

TABLE OF CONTENTS

Page

PART I

TABLE OF CONTENTS (Continued)

TABLE OF CONTENTS (Continued)

TABLE OF CONTENTS (Continued)

TABLE OF CONTENTS (Continued)

TABLE OF CONTENTS (Continued)

Overview of MSFC

CFD Activities

Presented to:
11th Workshop for CFD
Applications in Rocket
Propulsion
April 20, 1993

Paul McConnaughey
Chief, CFD Branch
Fluid Dynamics Div.
NASA MSFC

Overview of MSFC CFD Activities

Overview

- **Current Activities**
  - Program-supporting applications
  - Other analyses in progress
  - Codes in use
- **CFD Consortium for Applications in Propulsion Technology**
  - Turbine Team
  - Pump Team
  - Combustion Team
- **Future Directions**
  - Programs
  - Major technology initiatives
  - CFD technology

Overview of MSFC CFD Activities

Program Supporting Applications

- **Space Shuttle Main Engine (SSME)**
  - Advanced Main Combustion Chamber
  - Hydrostatic bearing inlet cavity (TTB issue)
  - Preburner exit temperatures, first stage nozzle hot spot
- **Alternate Turbopump Development Program (LOX pump)**
  - Inducer/impeller analysis
  - Balance piston flow analysis and dynamic coefficients
  - Pump inlet volute configurations
  - Bearing cavity flows
  - Turn-around duct/heat exchanger vane redesign
- **Alternate Turbopump Development Program (Fuel pump)**
  - Unsteady turbine blade loads

Program Supporting Applications

- **Advanced Solid Rocket Motor (ASRM)**
  - Multiport ignitor analysis
  - Aft end flow and actuator hinge moments
  - Bore/slot flow and propellant deformation
  - Simulation of MSFC wind tunnel cold flow tests

- **Redesigned Solid Rocket Motor (RSRM)**
  - Pressure drop down motor
  - Unsteady pressure fluctuations
  - STS-54 pressure transient investigation
  - Ignitor joint defect analysis

- **Hybrid Rocket Motors**
  - 11" motor simulation
  - combustion stablitiy assessment

Overview of MSFC CFD Activities

Program Supporting Applications

- **Space Station Freedom (SSF) Environmental Controls and Life Support Systems**
  - Node/module flow analysis
  - Contaminant tracking
  - MSFC wind tunnel benchmark test (LDV data)
- **Space Transportation System (Shuttle)**
  - Assessment of current launch commit criteria
  - Booster aerothermal environment on launch pad
- **Rarified Gas Flows**
  - Gravity Probe B nozzle
  - AGARD benchmarks

VELOCITY MAGNITUDE COLOR CONTOURS

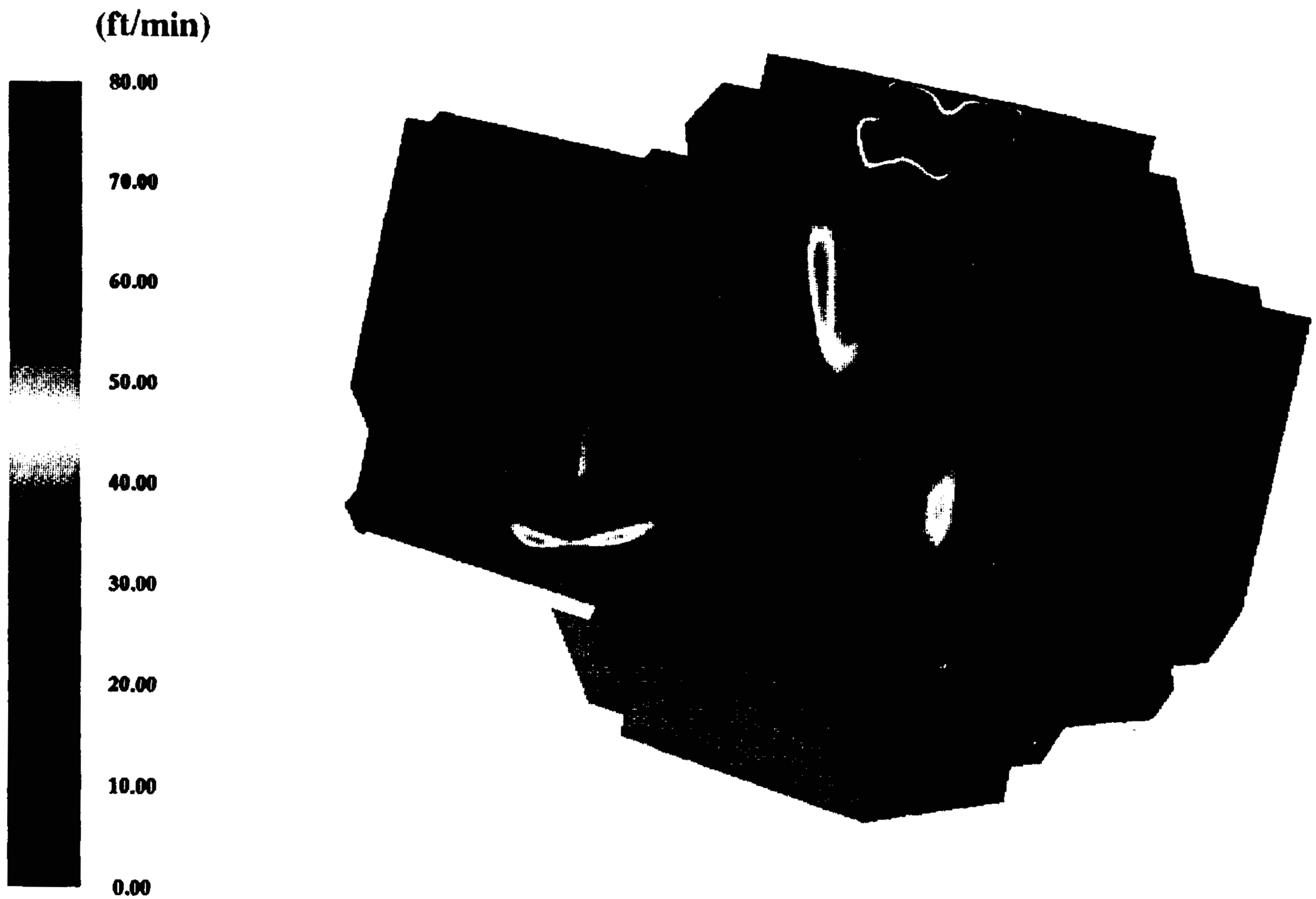

Overview of MSFC CFD Activities

Other Analyses in Progress

- **Liquid Propulsion Technologies**
  - Hydrostatic bearing flows
  - CFD-based rotor dynamic coefficient predictions
- **Vehicle Base Flow and Heating**
  - Supersonic backward facing step benchmark
  - Four engine cluster plume/base flow benchmark
  - F-1 nozzle and S-1C plume predictions
- **Vehicle External Flow Environments**
  - NLS-II
  - MSFC wind tunnel tests
    - Axisymetric vehicles
    - Multi-body configurations
- **Consortium Supporting Activities**

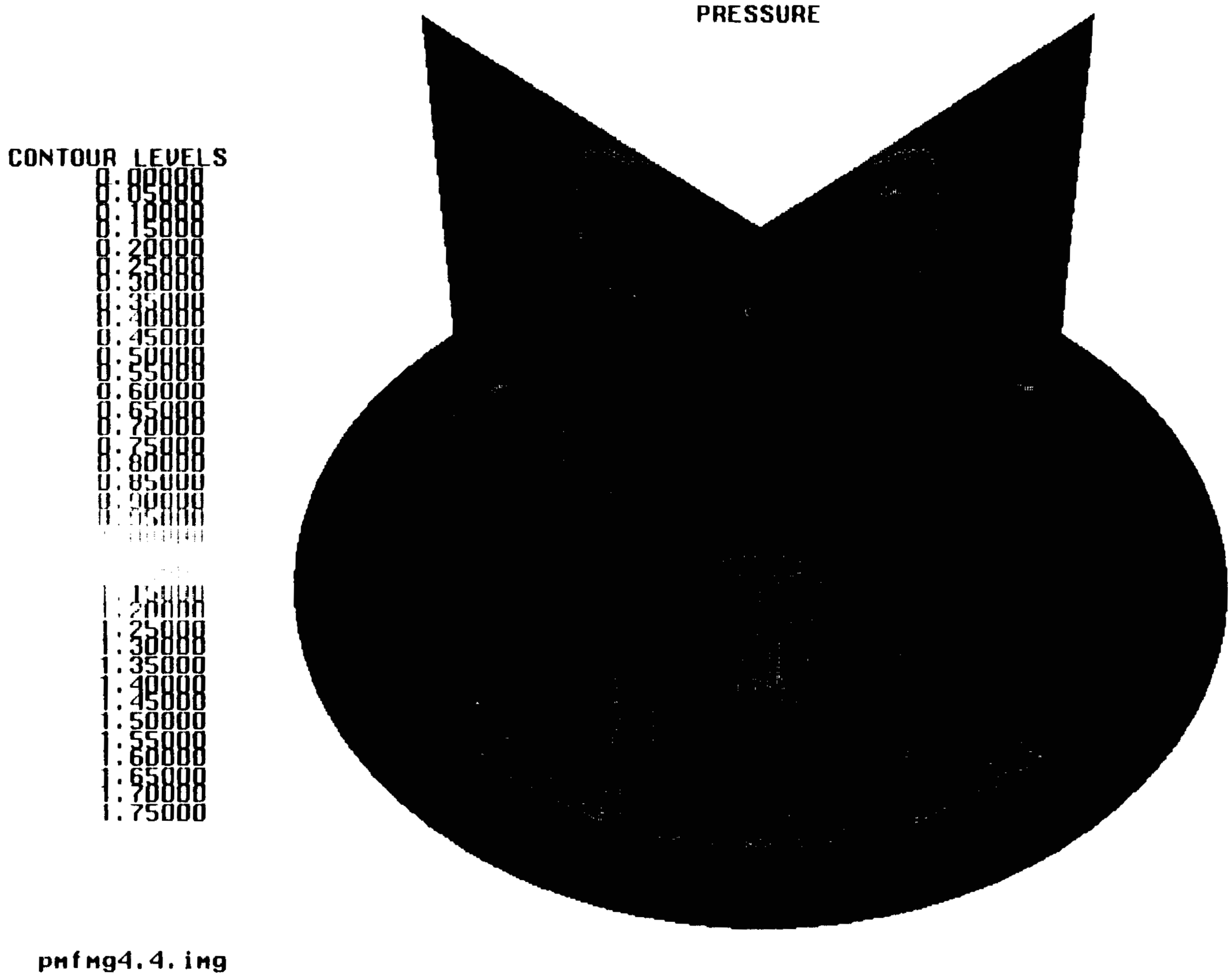
PRESSURE
CONTOUR LEVELS
0.00000
0.05000
0.10000
0.15000
0.20000
0.25000
0.30000
0.35000
0.40000
0.45000
0.50000
0.55000
0.60000
0.65000
0.70000
0.75000
0.80000
0.85000
0.90000
1.20000
1.25000
1.30000
1.35000
1.40000
1.45000
1.50000
1.55000
1.60000
1.65000
1.70000
1.75000
pmfmg4.4.img

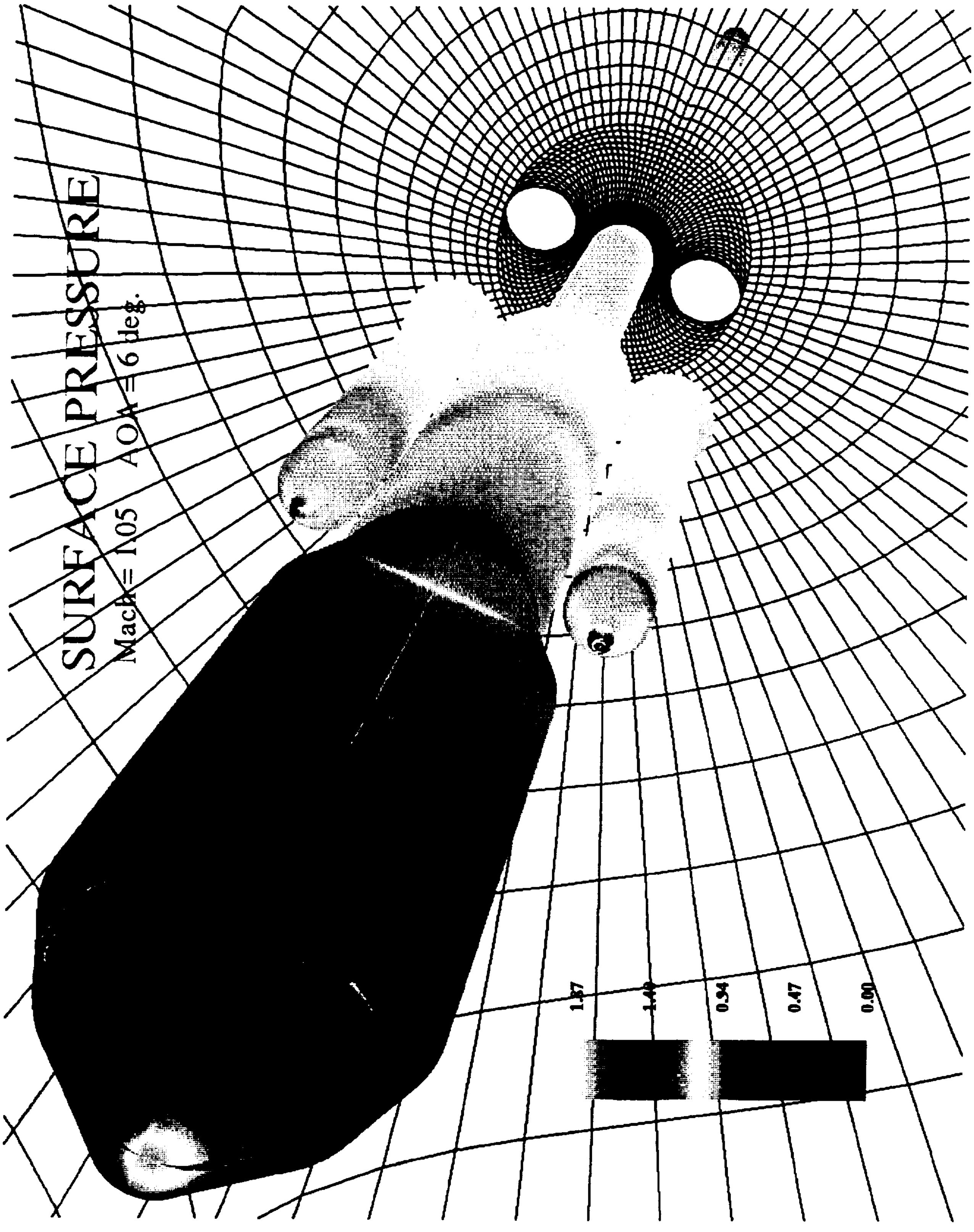
SURFACE PRESSURE
Mach = 1.05 AOA = 6 deg.
1.87
1.40
0.94
0.47
0.00

Codes in Use

- **Philosophy**
  - Public domain codes
  - Utilize 'best' code for a particular application

- **Grid Generation**
  - GENIE++
  - GEN2D / GEN3D
  - NGP and RAGGS currently being assessed

- **Flow Solvers**
  - CELMINT
  - FDNS3D
  - HAH3D
  - INS3D
  - ROTOR
  - REFLEQS
  - UBIFLOW

- **Post Processing**
  - PLOT3D
  - FAST

CFD Consortium for Applications in Propulsion Technology (CAPT)

- **Objective**
  - Maturation of CFD for design applications and the development of advanced hardware concepts
- **Approach**
  - Form three component-based teams
    - Turbine
    - Pump
    - Combustion Driven Flows
  - MSFC, NASA Research Centers, Industry, DoD, Universities
  - CFD code developers, appliers, designers, experimentalists, program
  - Technology based funding (ETO), SBIR, programs, codes D and C
  - Product oriented, focused on and program design point and schedule
  - Meet quarterly, 24 to 40 attendees
- **Products**
  - Benchmark datasets
  - Validated codes for subcomponent applications
  - CFD-derived Advanced Hardware Concepts

CFD Consortium for Applications in Propulsion Technology (CFD CAPT)

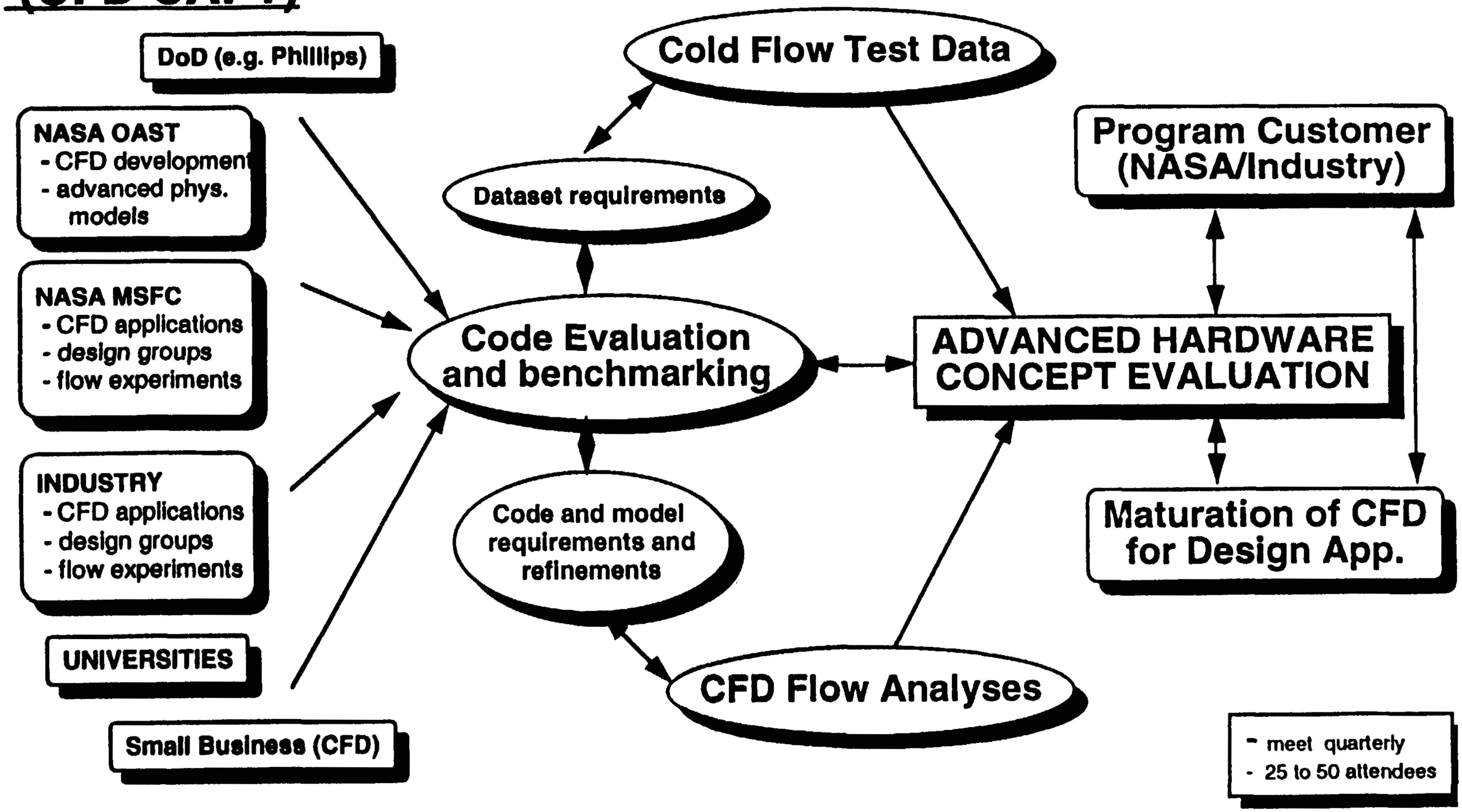

CAPT TURBINE TECHNOLOGY TEAM

Past Results

- **Advanced hardware concept turbine, Generic Gas Generator Turbine, developed**
  - Highly cambered rotor airfoils (160 degrees) predicted to be aerodynamically sound by six CFD analyses
  - Reduced parts over conventional designs by 55 percent
  - Increased predicted efficiency over conventional designs by 10 percent
  - Optimal spacing determined with unsteady CFD analyses
    - Reduced predicted blade loading/stress by 24 percent

- **Incorporated high-turning blade concept in the STME Gas Generator Oxidizer Turbine**
  - Predicted aerodynamically sound by five CFD analyses
  - Enabled single-stage design resulting in estimated savings of $71 million dollars in STME LCC
  - Reduced parts count over conventional designs by 50 percent
  - Increased predicted efficiency over conventional designs by 2 percent

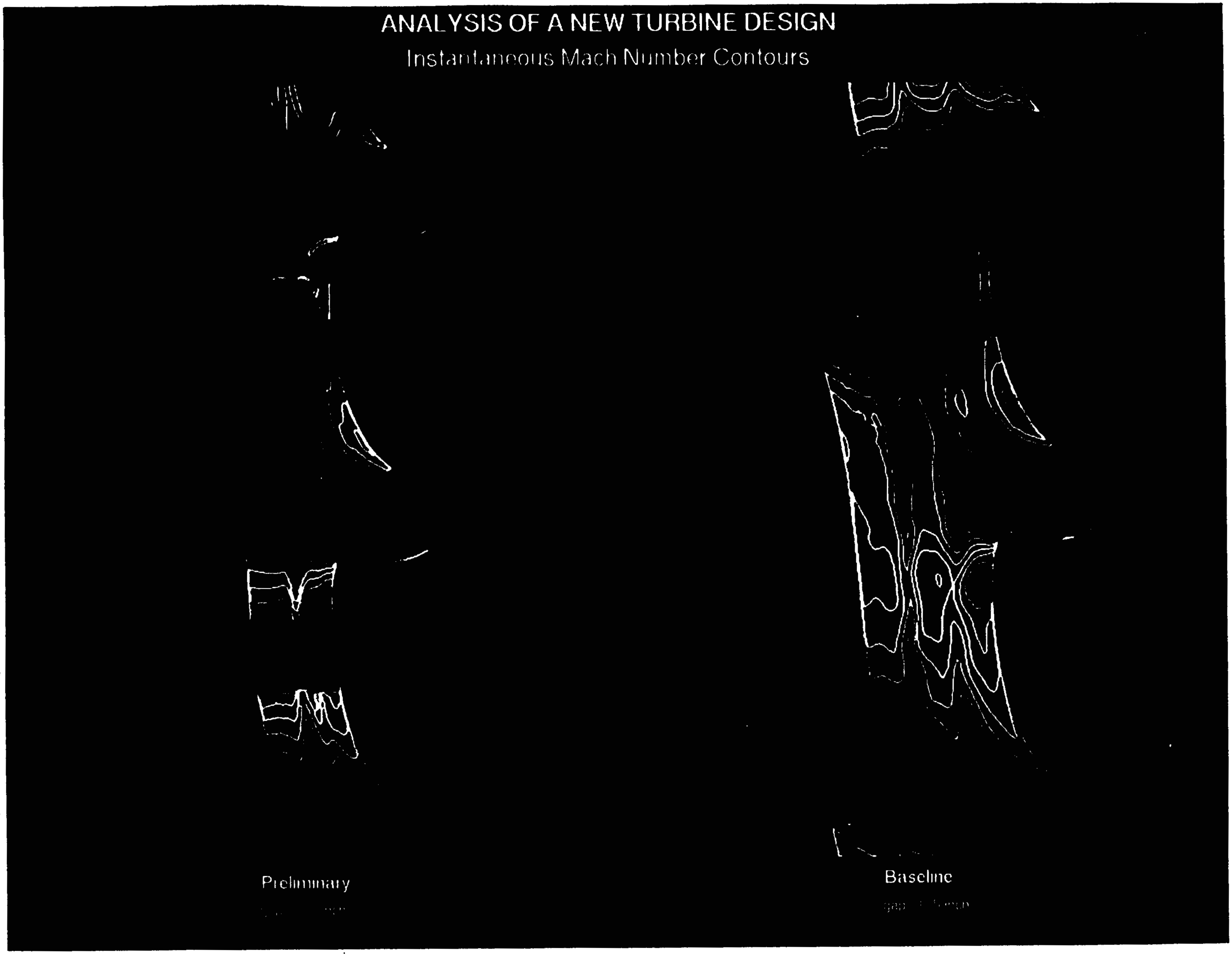
ANALYSIS OF A NEW TURBINE DESIGN
Instantaneous Mach Number Contours
Preliminary
Baseline

CAPT TURBINE TECHNOLOGY TEAM

Current Activities

- **Volute Development**
  - Designed baseline inlet and exit volutes for Gas Generator Oxidizer Turbine
  - Analysis with three CFD codes in progress
  - Grid and boundary condition study in progress

- **Verification/Validation Testing**
  - Designed and built turbine test article (turbine stage and volutes) for the Gas Generator Oxidizer Turbine (test in summer, 1993 at MSFC)
  - Verify environment of baseline turbine/volute system
  - Provide unique set of turbine and volute data for CFD validation

- **Advanced Concepts for Turbine Loss Control**
  - Team currently exploring mechanisms to reduce losses in the Gas Generator Oxidizer Turbine
    - Minishrouds
    - Blade and endwall fences
    - Labyrinth effects

CAPT TURBINE TECHNOLOGY TEAM

Future Work

- **Subsonic Turbine Development**
  - Validate/calibrate codes with benchmark data obtained for baseline Gas Generator Oxidizer Turbine
  - Incorporate promising loss control mechanisms into advanced Gas Generator Oxidizer Turbine
  - Achieve optimum design based on CFD predictions

- **Volute Development**
  - Modify/enhance CFD codes based on benchmark data
  - Develop design improvements based on parametric studies conducted with enhanced codes

- **Verification/Validation Testing**
  - Design, build, and test advanced Gas Generator Oxidizer Turbine system model
    - Design verification
    - Code validation

CAPT PUMP TEAM

Past Results

- **Validated six CFD codes for axial pump flows**
  - Rocketdyne .3 flow coefficient inducer

- **Obtained benchmark data for Rocket engine impeller**
  - SSME HPFTP impeller

- **Benchmarked six CFD codes for impeller flows**

- **Designed high head coefficient, low distortion impeller**
  - Efficiency: ~ SSME, Ψ + 11%, distortion: -12%, blade count: -50%
  - Designed optimized using CFD

- **Verified advanced impeller design experimentally**

11 INCH SSME HPFTP IMPELLER

LASER VELOCIMETER TEST DATA

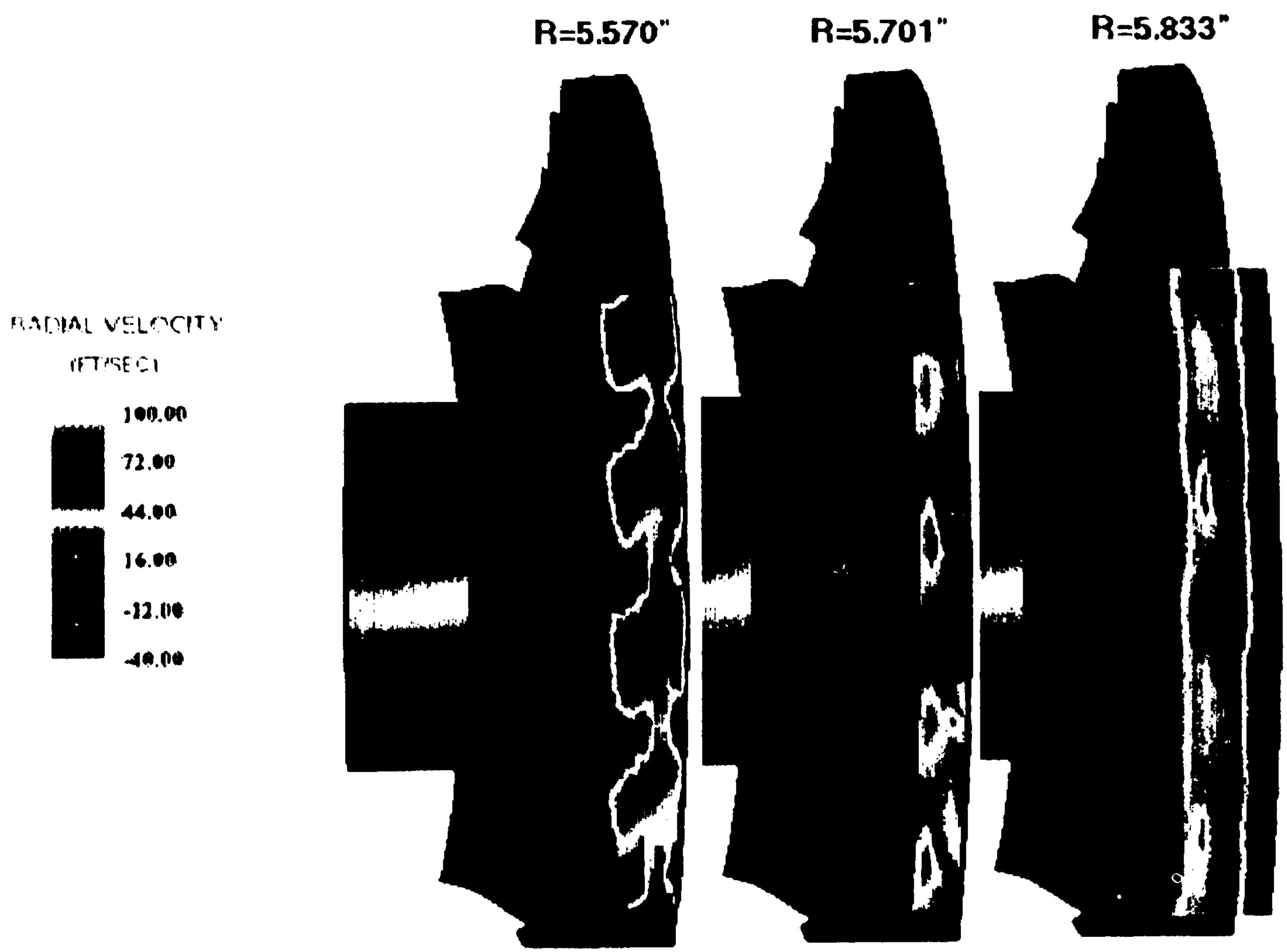

VT28 - Hydrodynamic Design of Advanced Pump Components

TURBOMACHINERY
TECHNOLOGY

Particle Trace of the Flow Field

Original Design

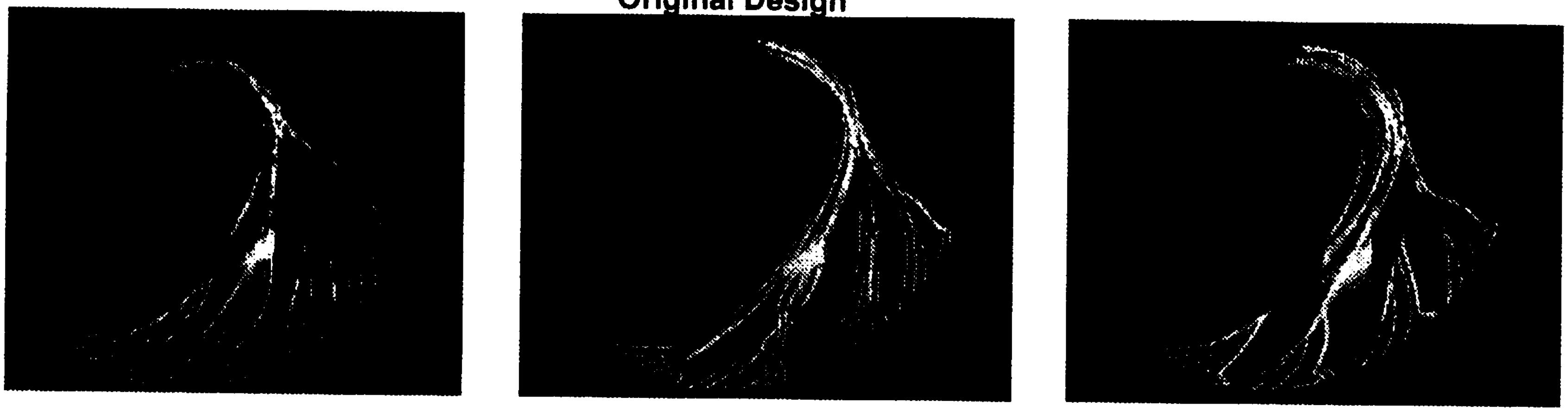

Advanced Concept: Blade Lean

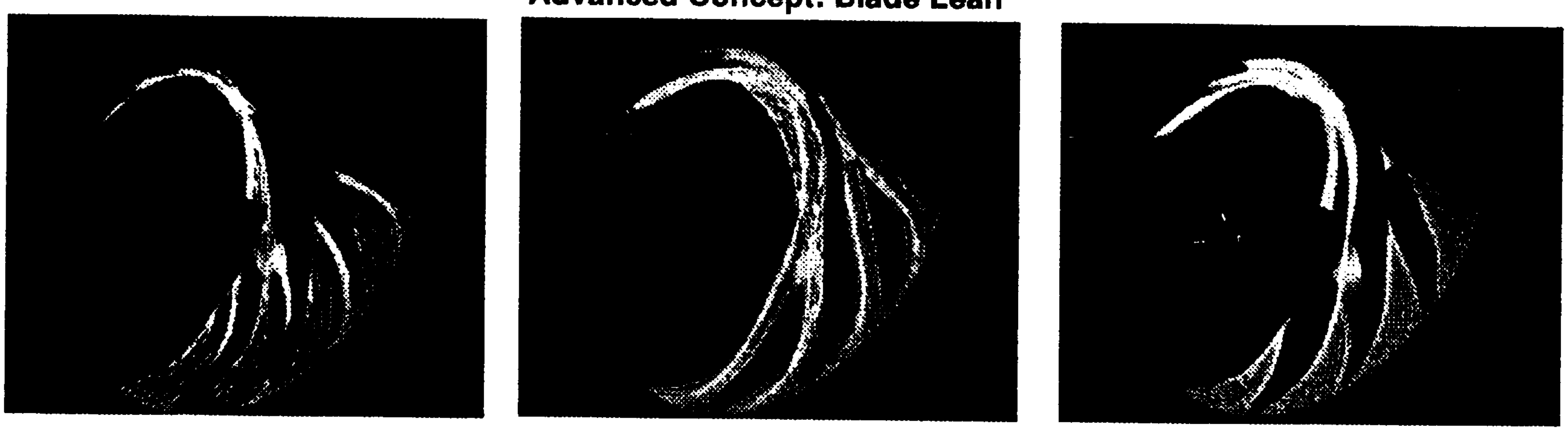

Hub Surface | Mid Span | Tip Surface

CAPT PUMP TEAM

Current Activities

- **Evaluating Advanced impeller concepts using CFD**
  - Tandem blades
  - Impeller axial length
  - Partial blade location and length
  - Blade loading distribution (3D blade)
  - Impact of shroud/hub cavity flows

- **Goal is to further reduce distortion and increase performance**

- **Preparing experimental rig for inducer benchmark data collection**
  - Non-cavitated, three velocity components
  - Minimum of five axial planes
  - Typical rocket engine inducer

- **Performed a first order impeller-diffuser interaction prediction**
  - Used existing Caltech data

CAPT PUMP TEAM

Future Work

- **Manufacture and test the advanced concept impeller**
  - Obtain performance and L2F data
- **Design an advanced diffuser**
  - Use CFD in the design process
- **Manufacture and test advanced diffuser**
  - Obtain interaction data, L2F velocities
- **Obtain 3D data for inducer flowfield**
- **Perform non-cavitated inducer benchmark**
  - Assess practicality of persuing cavitation modeling

CAPT COMBUSTION-DRIVEN FLOW TECHNOLOGY TEAM

Past Results

- **Code Validation Activities**
  - Film cooling/jet injection (five codes, heat transfer data)
  - Over 35 validation cases to assess NLS base heating issue
  - Miscellaneous cases pertinent to specific problems

- **Advanced Hardware Concepts**
  - STME subscale film cooled nozzle
    - 3D Navier-Stokes analysis resulted in manifold changes
    - 2D Navier-Stokes analysis improved injection geometry
    - Design tool available for STME nozzle coolant injection issues
  - NLS base flow/heating analysis (1.5 stage vehicle)
    - Assessed baseline environments at 10 and 50k ft altitudes
    - Analysis used to check scaling of S1-C flight data
    - Complex six-engine vehicle base flow analysis with finite rate chemistry
    - Parametrically assessed turbine exhaust location using Navier-Stokes analysis

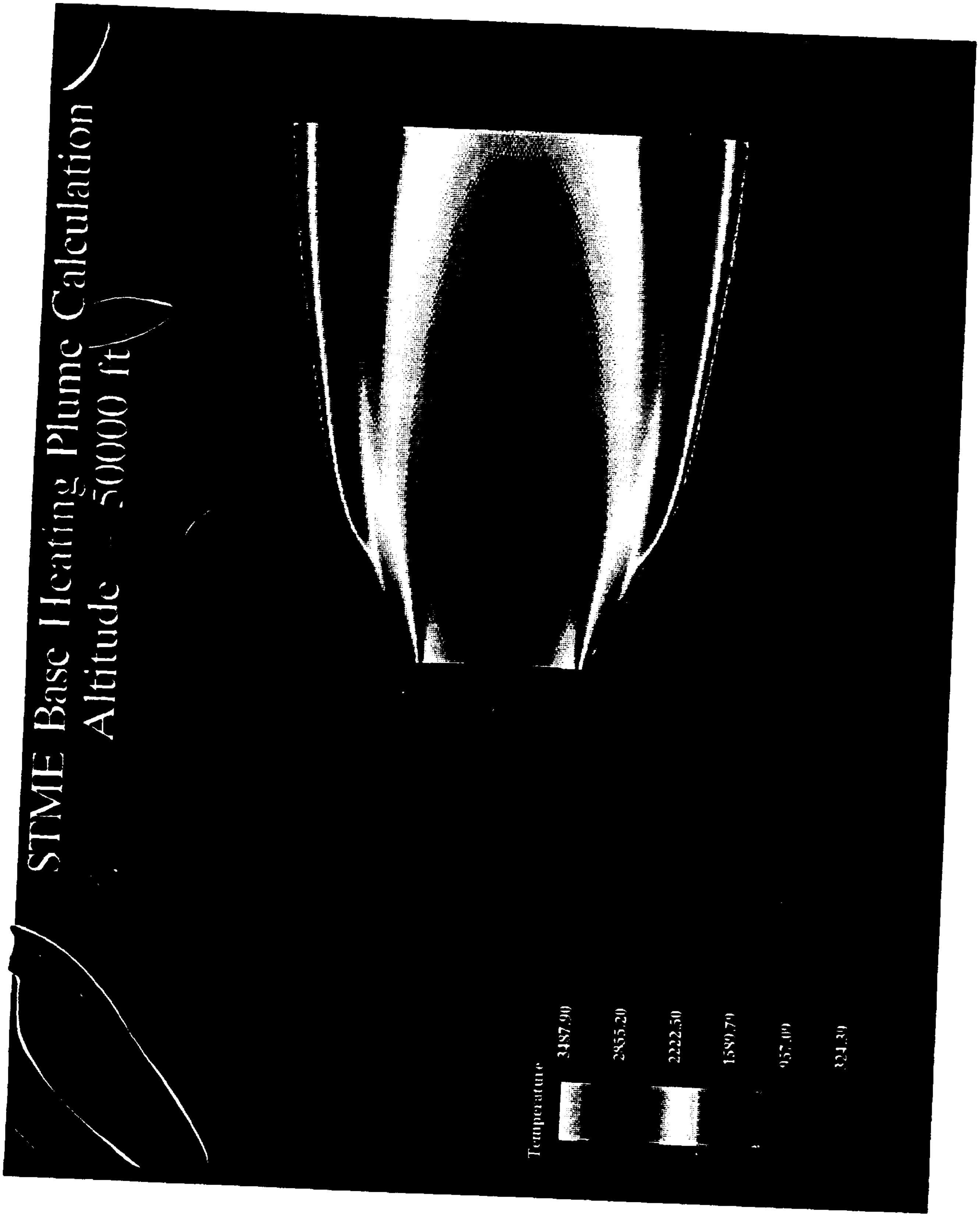
STME Base Heating Plume Calculation
Altitude 50000 ft
Temperature
3487.90
2855.20
2222.50

COMBUSTION-DRIVEN FLOW TECHNOLOGY TEAM

- **Advanced Hardware Concepts (Continued)**
  - AMCC
    - Assessed large throat chamber flowfield
    - Predicted hot side wall temperature distribution (iter. w/thermal)
  - 11" hybrid motor
    - Steady-state, finite rate solution on coarse grid
    - Fine grid case is complete
    - Computational capability demonstrated

COMBUSTION-DRIVEN FLOW TECHNOLOGY TEAM

Current Activities

- **Injector/chamber analysis**
  - Upgrade of Navier-Stokes codes for injector analysis
    - -- 3D Navier-Stokes analysis
      - 2-phase flow with efficient spray transport models
      - Upgraded physical models for atomization, vaporization
  - Verification of submodels using code flow/hot flow, gas/gas, gas/liquid single element/ multi-element injector data sets

Future Work

- **Application of Navier-Stokes codes for inject/chamber compatibility**
  - Capability will allow the evaluation in the design phase of injector parameters which determine compatibility with the chamber
- **Continuation of work on hybrid motor**
- **Expansion/deflecting nozzles**

Future Directions - Programs

- **STS Enhancements**
  - ATD High Pressure Fuel Turbopump (HPFTP)
  - Large throat AMCC/platelet combustion chamber
  - ASRM
- **Space Station Freedom Redesign**
  - Ventilation analysis
- **Spacelifter**
  - Main engine (?)
- **SIMPLEX turbopump**
  - 40K LOX turbopump for hybrid test motor
  - Low performance, low part count, non-flight configuration
- **Other directions as a result of Access to Space studies**

George C. Marshall Space Flight Center
Science and Engineering Directorate

Propulsion Laboratory
Component Development Division
Turbomachinery and Combustion Devices Branch

SIMPLEX TURBOPUMP (STP) PRELIMINARY DESIGN STATUS

NASA
National Aeronautics and Space Administration

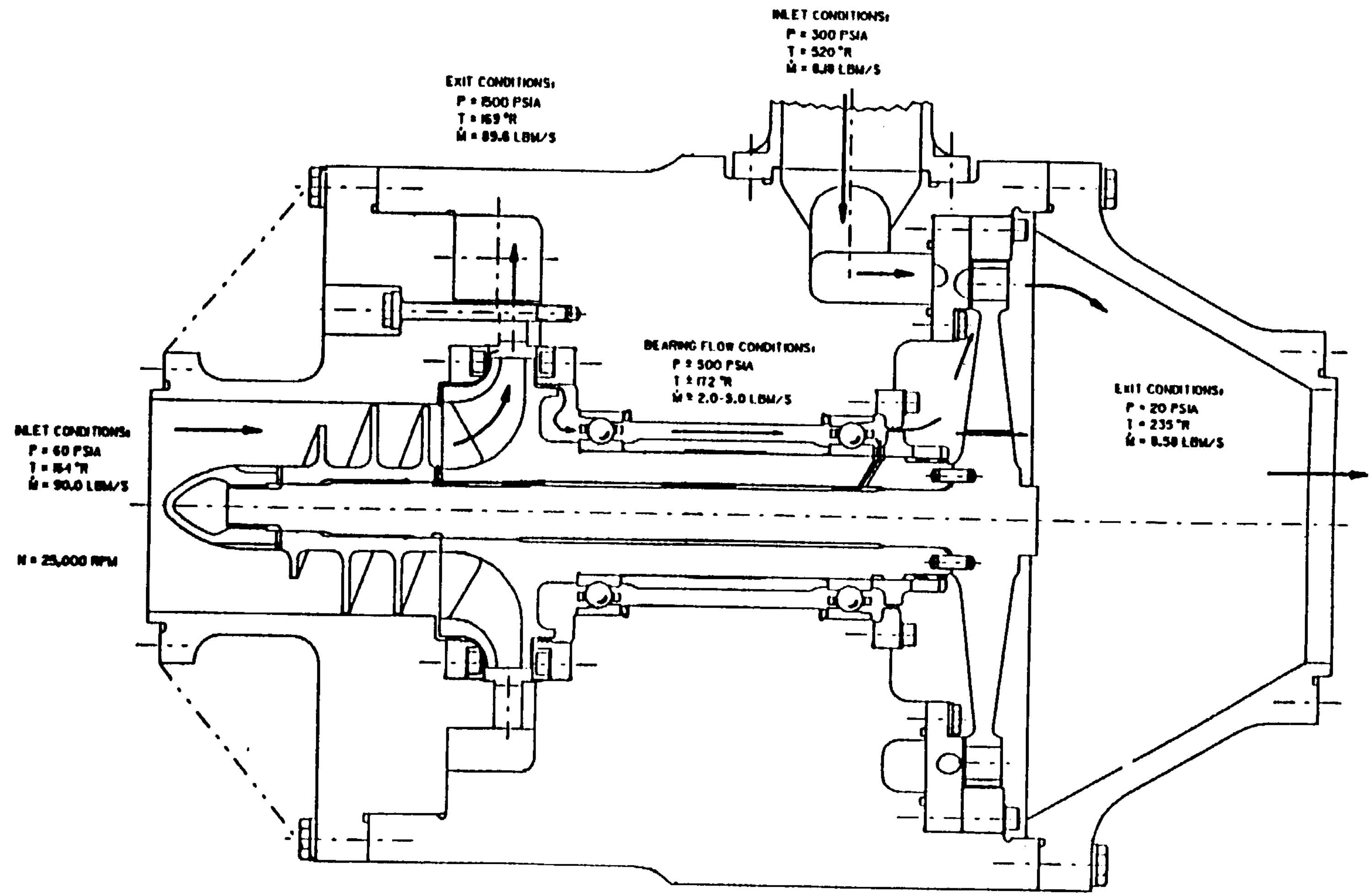

PRIMARY FLOW PATH REQUIREMENTS
AND ESTIMATE OF SECONDARY FLOWS
31 MARCH 1993

MWM 4/6/93

Overview of MSFC CFD Activities

Future Directions - Major Technology Initiatives

- **Hybrid Rocket Motor Development**
  - NRA released 4-9-93, code D funding (majority)
  - 100K, 250-350K, and 750K-1.0M thrust level motors
  - Code for performance and environment prediction
  - Jerry Cook, EP54

- **Advanced Technology Low Cost Turbopump**
  - Earth-to-Orbit (ETO) funding
  - Large turbopump design, fabricate, and test
  - Will utilize and integrate developed ETO technologies
  - Innovative design, manufacturing, and management methods to lower cost
  - Expect NRA to be released 4Q-93
  - Henry Stinson, EP62

Future Directions - Major Technology Initiatives

- **Advanced Technology Low Cost Engine**
  - Funding from development (code D) in progress
  - 50K, 200-750K, and 1.5-2.0M engines
  - Commonality in designs
  - Jan Monk, EE83

- **Technology Reinvestment Project**
  - CBD announcement 3-12-93, proposals due 7-23-93
  - Advanced Research Projects Agency (ARPA)
  - Emphasis on dual-use technology and manufacturing, conversion of defense capabilities to commercial applications
  - Small business, industry, and federal agency teams
  - ARPA looking for 'in-kind' contributions
  - Cannot count NASA cooperation as part of 'industry matching funds'
  - Dollars contributed by NASA subtract from ARPA funding
  - Use of NASA facilities and manpower does not affect ARPA funding (may be viewed as favorable)

WHAT IS ATLCE?

ADVANCED TECHNOLOGY LOW COST ENGINES (ATLCE)

- CONCEPT SUPPORTS FAMILY OF PROPULSION SYSTEMS
  - 50K Upper Stage
  - 200-750K Booster/Core
  - 1500-2000K Booster Engine
  - High Thrust/Weight SSTO Applications
  - Multiple Propellant Combinations
  - Lox Turbomachinery Satisfies Hybrid Requirement
  - SUPPORTS BLAIR REPORT
    - Upper Stage Engine
    - Hydrocarbon Engine

- LOW PRESSURE STAGED COMBUSTION CYCLE
  - 900-1000 psia Chamber Pressure
  - Gas / Gas Main Injector
  - High Performance

- ADVANCED COMPOSITES THRUST CHAMBER
  - Reduced Costs
  - Low Weight

- SIMPLEX SINGLE STAGE TURBOMACHINERY
  - Hydrostatic Bearings
  - Minimum Number of Parts

- OXIDIZER RICH OXIDIZER PREBURNER
  - Low Turbine Temperatures

- LOW COSTS
  - 50K Upper Stage Engine < $1M
  - Simple Design Supports Minimum Development Program

REFERENCE CYCLE

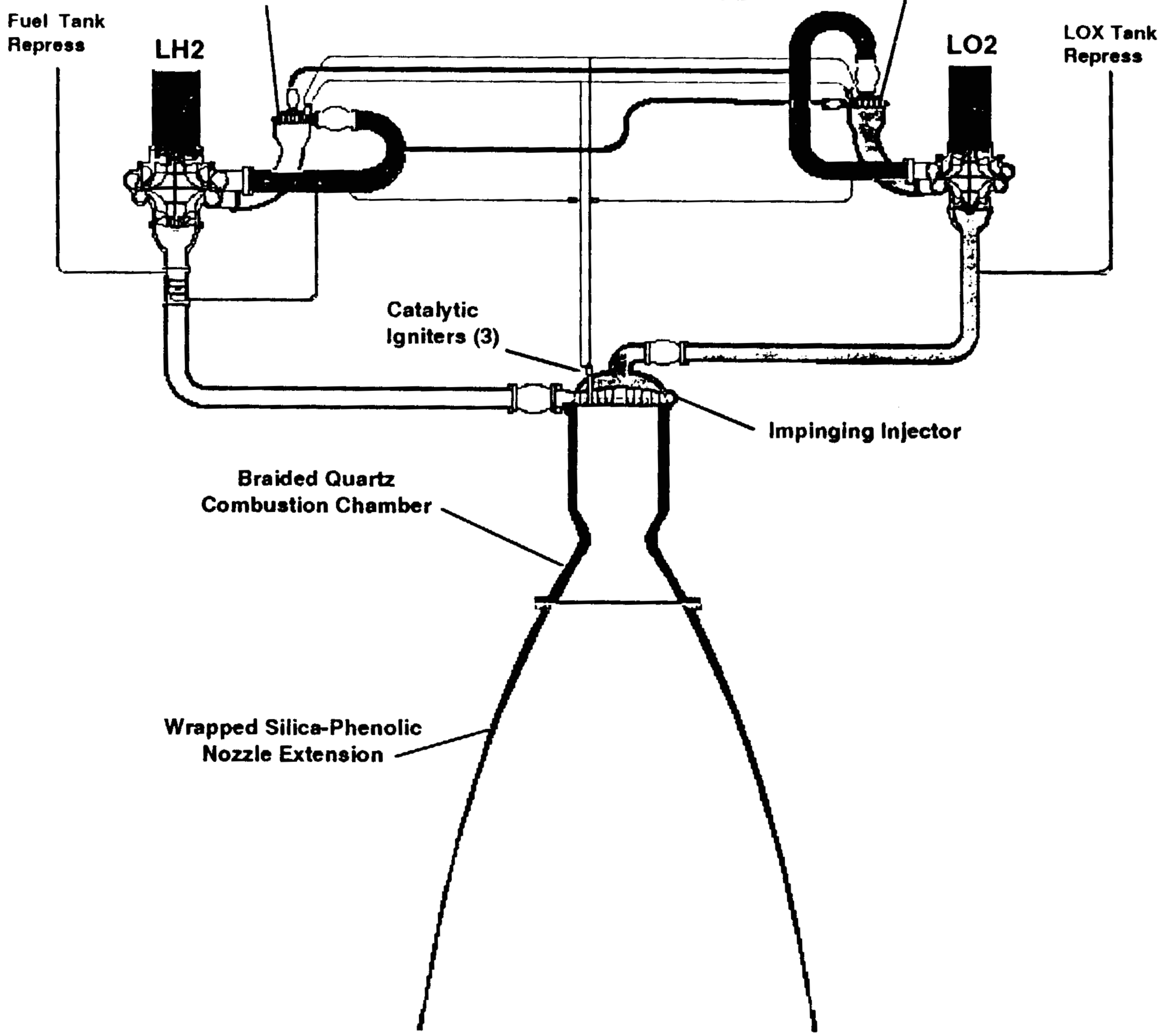

JCM 3-31-93

ATLCE

KEY PERFORMANCE PARAMETERS

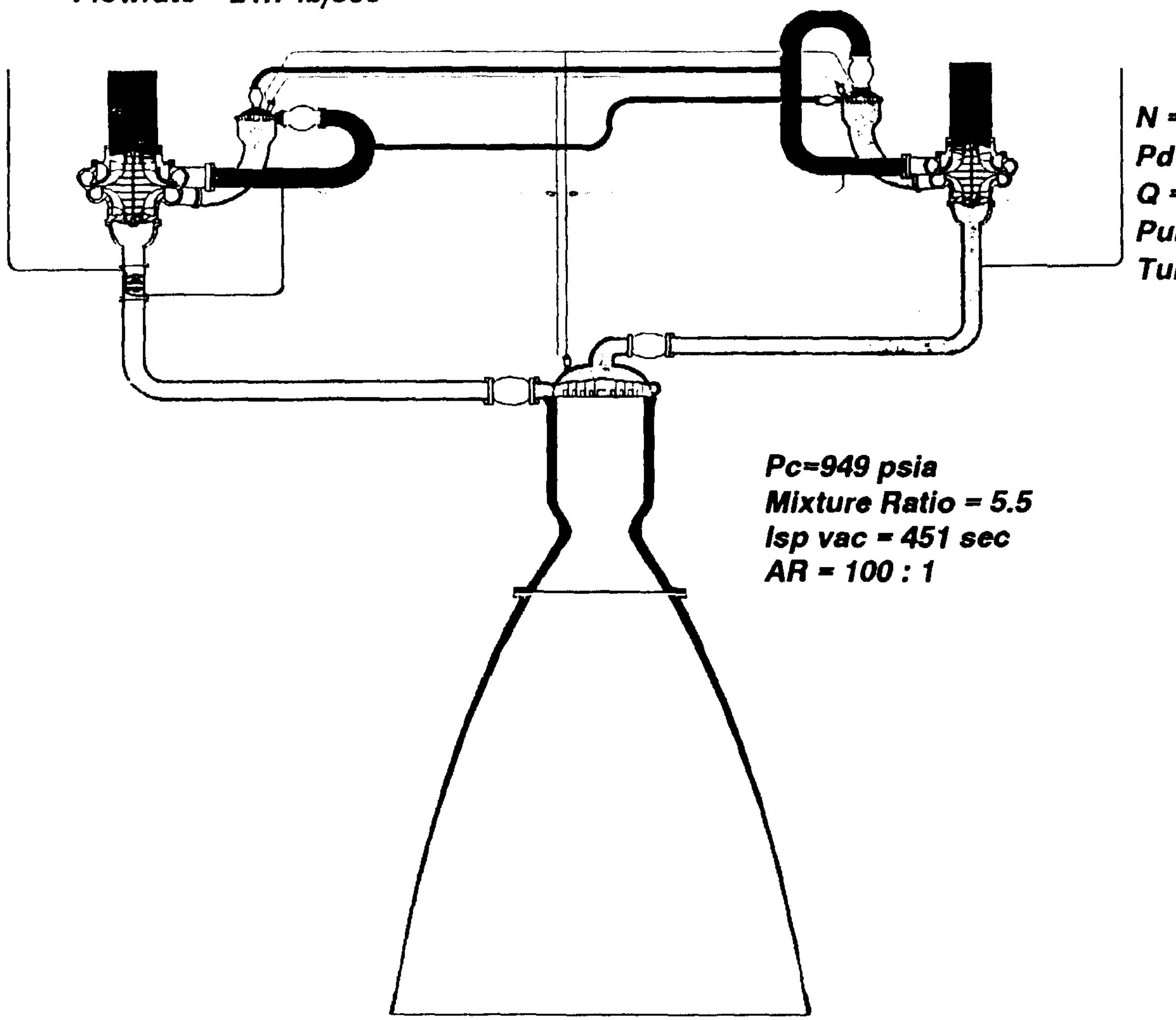

JCM 4-5-93

Future Directions - CFD Technology

- **GOAL - CFD as an accepted and necessary design tool**
  - Stress and life assessments need accurate steady and dynamic loads
  - Must improve current performance predictions
  - Codes must be accurate, robust, and reasonably efficient on avaliable computer hardware
  - Analysts must look for engineering solutions, not perfect solutions
  - CFD analysis must be delivered in a timely and cost-effective manner
  - Move codes out of CFD specialty groups
- **Reasonable progress in**
  - Code generalization
  - Grid generation/adaption
  - Physical models and implementation
  - Benchmarking
  - Program-supporting applications
  - Integration of CFD into design organizations

Future Directions - CFD Technology

- **Code Standards and/or Standard Codes**
  - NASTRAN, ANSYS, SINDA, TRASYS
  - No analogs in CFD community
    - Limited investment for a single code or family of codes
    - Redundant efforts across country
    - Kept CFD as a technology, limited design impact

- **Integrated codes for non-specialist applications**
  - Custom models to run on a range of platforms
  - Workstations, Class VI computers, coarse and massively parallel environments
  - A NASTRAN-type family of CFD codes should be within reach

- **Continue basic work in**
  - unstructured solvers
  - adaption techniques and error estimates
  - algorithm/hardware architecture optimization

Summary and Conclusions

- Significant progress in integration of CFD into programs and design organizations
- Limited opportunity for major program impact in near future
- Expanded opportunities to integrate CFD into advanced space hardware programs, applications for dual-use technologies, and for code commercialization.

N95- 23616

51-37
43735
P- 19

3-D CFD ANALYSIS OF HYDROSTATIC BEARINGS

Shyi-Jang Lin and Robert I. Hibbs
Rocketdyne Division, Rockwell International

ABSTRACT

The hydrostatic bearing promises life and speed characteristics currently unachievable with rolling element bearings alone. In order to achieve the speed and life requirements of the next generation of rocket engines, turbopump manufacturers are proposing hydrostatic bearing to be used in place of, or in series with, rolling element bearings.

The design of a hydrostatic bearing is dependent on accurate prediction of the pressure in the bearing. The stiffness and damping of the hydrostatic bearing is very sensitive to the bearing recess pressure ratio. In the conventional approach, usually ad hoc assumptions were made in determining the bearing pressure of this approach is inherently incorrect.

In the present paper, a more elaborate approach to obtain the bearing pressure is used. The bearing pressure and complete flow features of the bearing are directly computed by solving the complete 3-D Navier-Stokes equation .

The code used in the present calculation is a modified version of REACT3D code.

Several calculations has been performed for the hydrostatic bearing designed and tested at Texas A&M. Good agreement has been obtained between computed and test results. Detailed flow features in the bearing will be also described and discussed.

3-D CFD Analysis of Hydrostatic Bearings

by

Robert Hibbs, Jr., and Shyi-Jang Lin

Benefits of Hydrostatic Bearings in High Power Density Turbomachinery Led Rocketdyne to Pursue Aggressive IR&D Initiative to Improve Analysis Capability

Rockwell International
Rocketdyne Division

UNCLASSIFIED

HYDROSTATIC BEARING
(CUTAWAY)

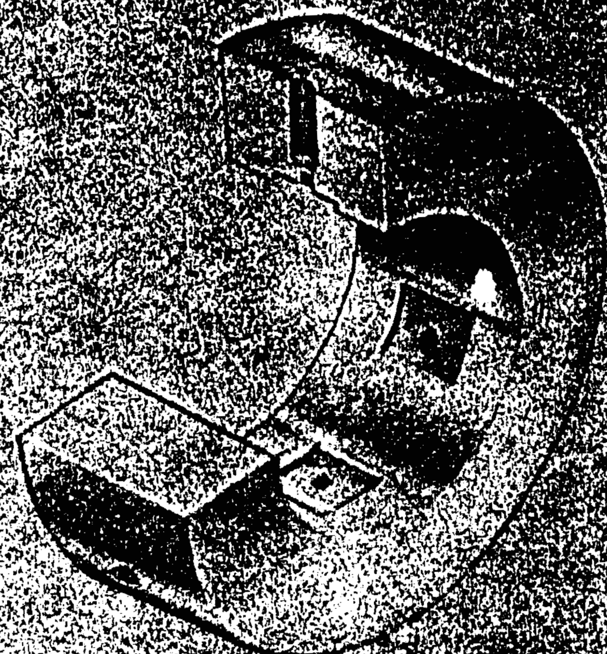

SC89C-31-76
564

NASP ROCKETDYNE

Rockwell International

UNCLASSIFIED

ORIGINAL PAGE IS
OF POOR QUALITY

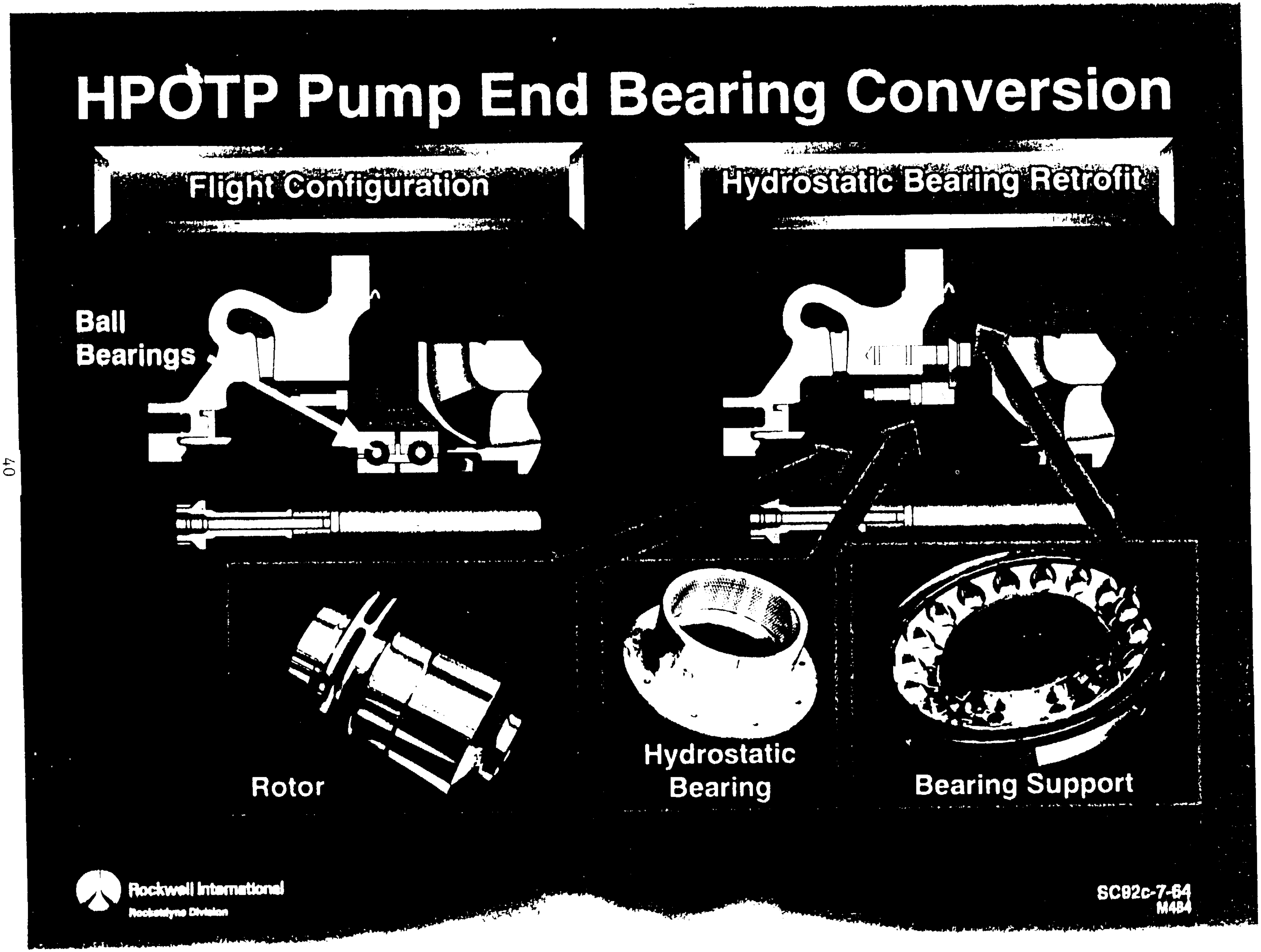
HPOTP Pump End Bearing Conversion
Flight Configuration
Hydrostatic Bearing Retrofit
Ball Bearings
Rotor
Hydrostatic Bearing
Bearing Support
Rockwell International
Rocketdyne Division
SC92c-7-64
M484

FUEL PUMP FOR NLS

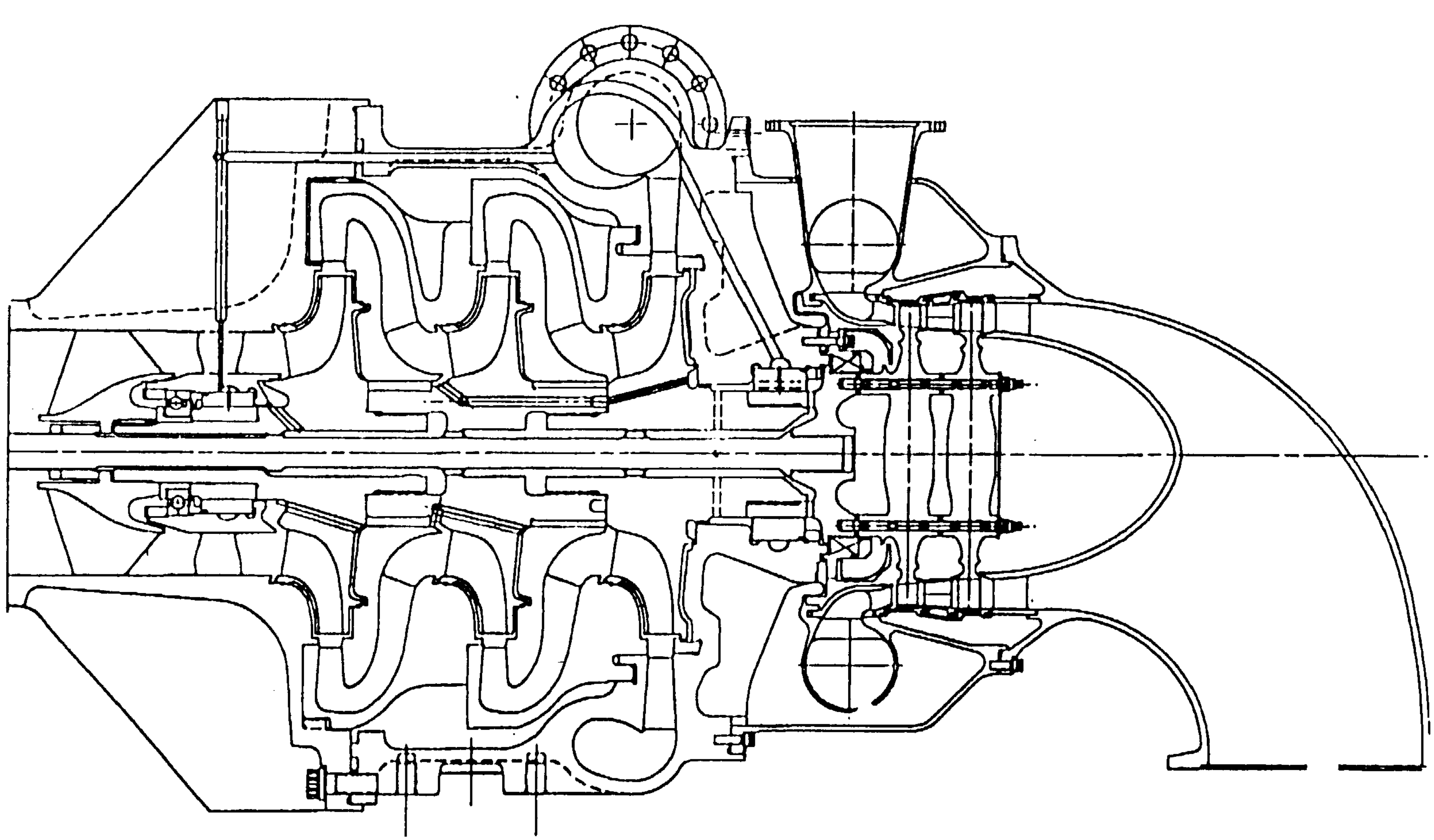

Benefits:

- Low-Wear/ No Known Life LImit
- Reasonable Hardware Cost

Rockwell International
Rocketdyne Division

Significantly Improved Life & Power Level Margin With Hydrostatic Bearing

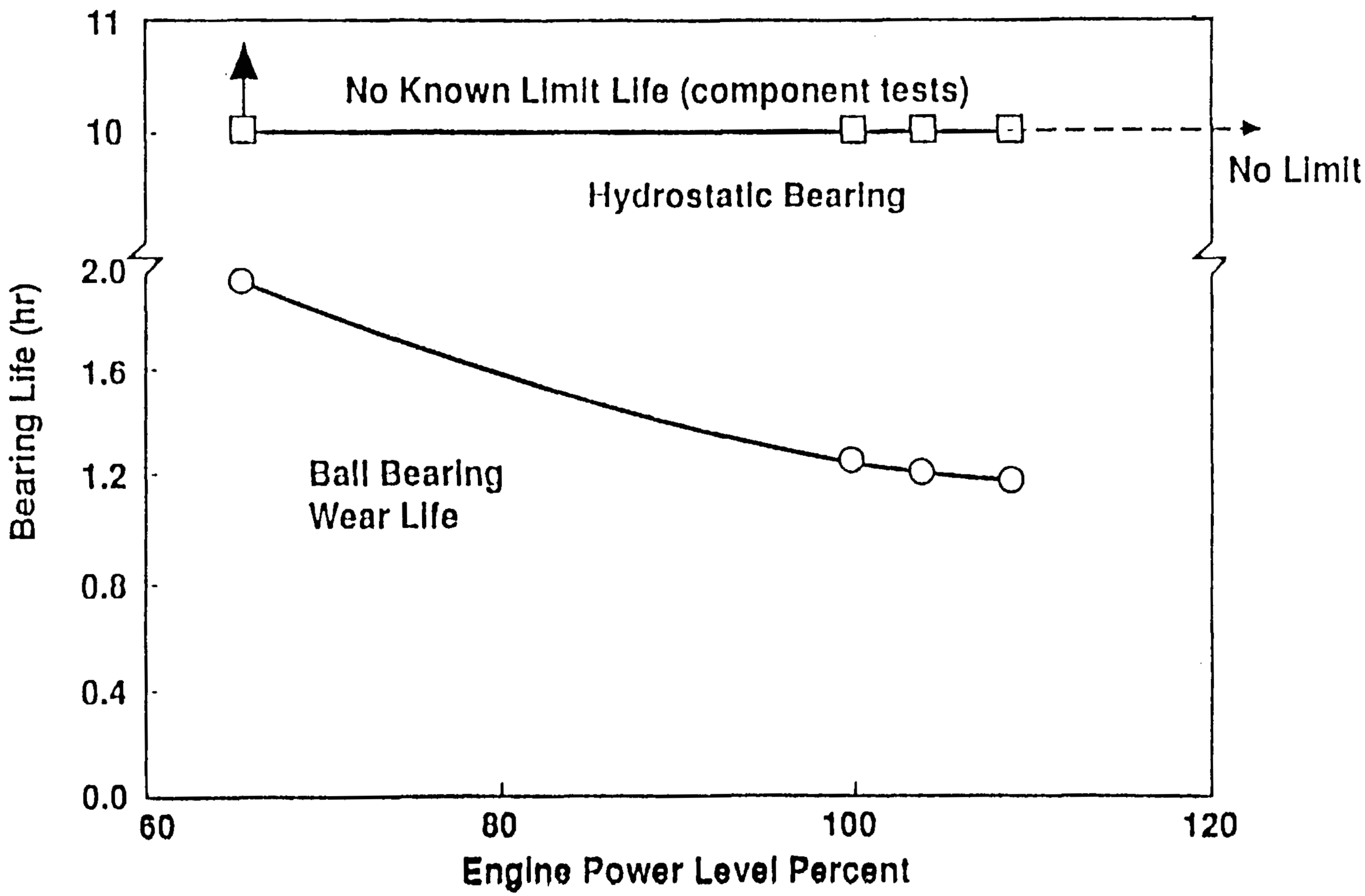

Rockwell International
Rocketdyne Division

92c-4-631
M669

Analysis Requirement:

- Improve Accuracy of Rotordynamic Model Input
    - Direct Stiffness
    - Cross-Coupled Stiffness
    - Direct Damping
    - Added Mass

Rockwell International
Rocketdyne Division

Analysis Method:

- Bulk-Flow Analysis Operational and Anchored
  - Film-averaged Navier Stokes Eqn Across Lands
  - Recess Pressure Constant / Including orifice
  - Loss Coefficient Used to Determine Pressure at Entrance to Bearing Land
- Currently Improving with Steady-State 3-D CFD
  - Anchor Loss Coefficients for Bulk Flow Model
- Full Bearing Perturbation Solution of 3D Steady-State Solution
- Steady Solution with Eccentric Shaft
- Unsteady Solution with Whirling Shaft

Rockwell International
Rocketdyne Division

COMPARISON OF THEORY AND EXPERIMENT
TEXAS A&M HYDROSTATIC BEARING TESTING

	Difference MIN	Difference AVG	Difference MAX
Direct Stiffness (K_{xx})	-5%	+7%	+20%
Cross-Coupled Stiffness (K_{xy})	-26%	+2%	+16%
Direct Damping (C_{xx})	-22%	-5%	+13%
$WFR = K_{xy} / \omega C_{xx}$ Whirl Frequency Ratio	-15%	+1%	+8%

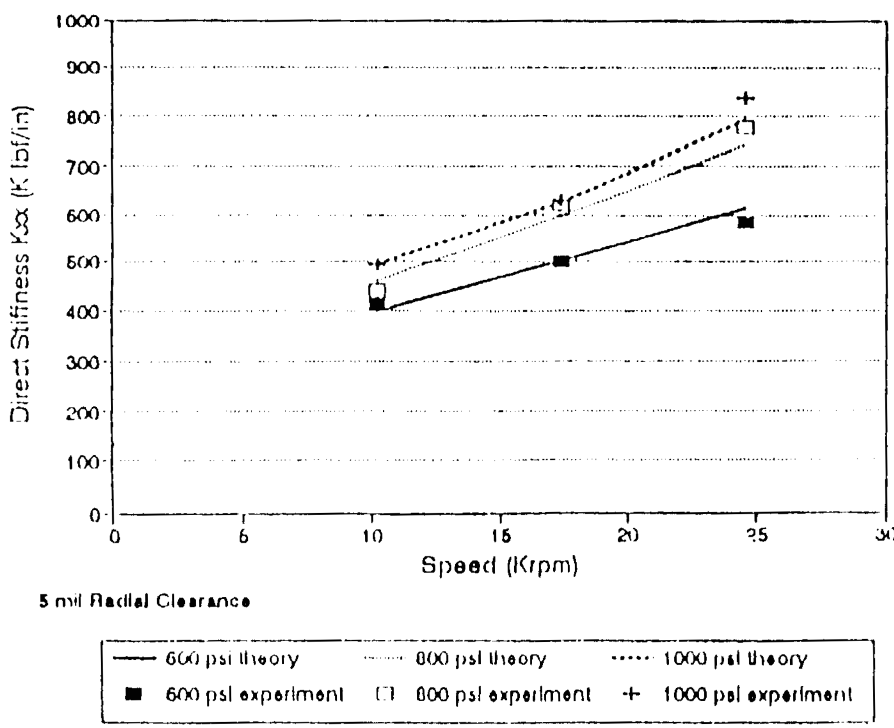

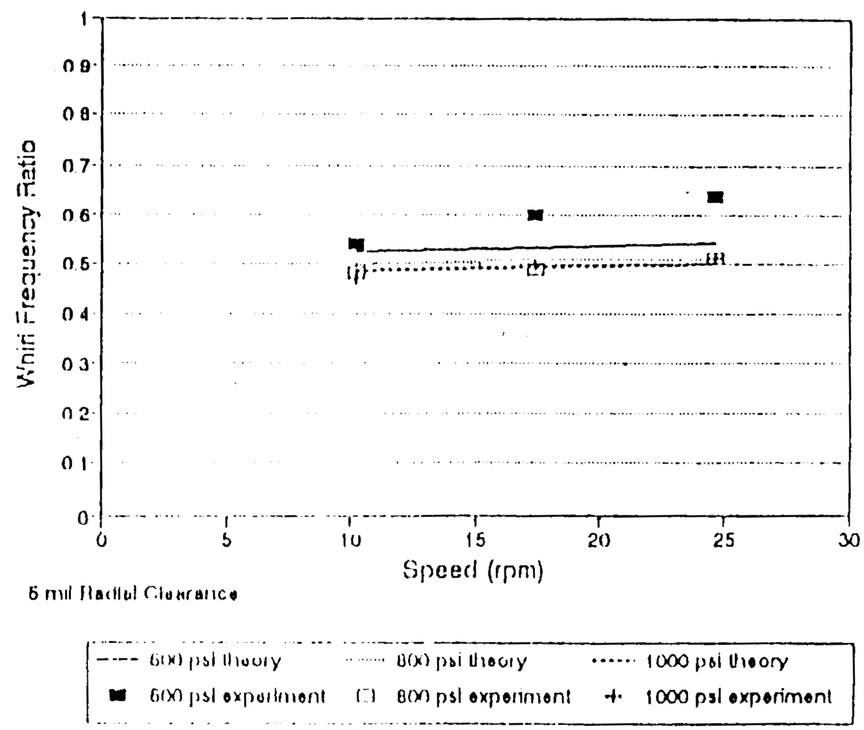

Rockwell International
Rocketdyne Division

Grid Generation Challenges:

- Circular Orifice to Square Recess
- Circular Orifice Matching Recess Curvature
- Aspect Ratio in Bearing Land
- Solved Through Multi-Zone Approach
    - 5 Zones

Entrance	22X8X8
Orifice	10X8X8
Recess	6X20X20
Land-1	6X32X17
Land-2	6X32X17

- Total in Model - 10976

Rockwell International
Rocketdyne Division

3D Multi-Zone Grid of H/S Bearing

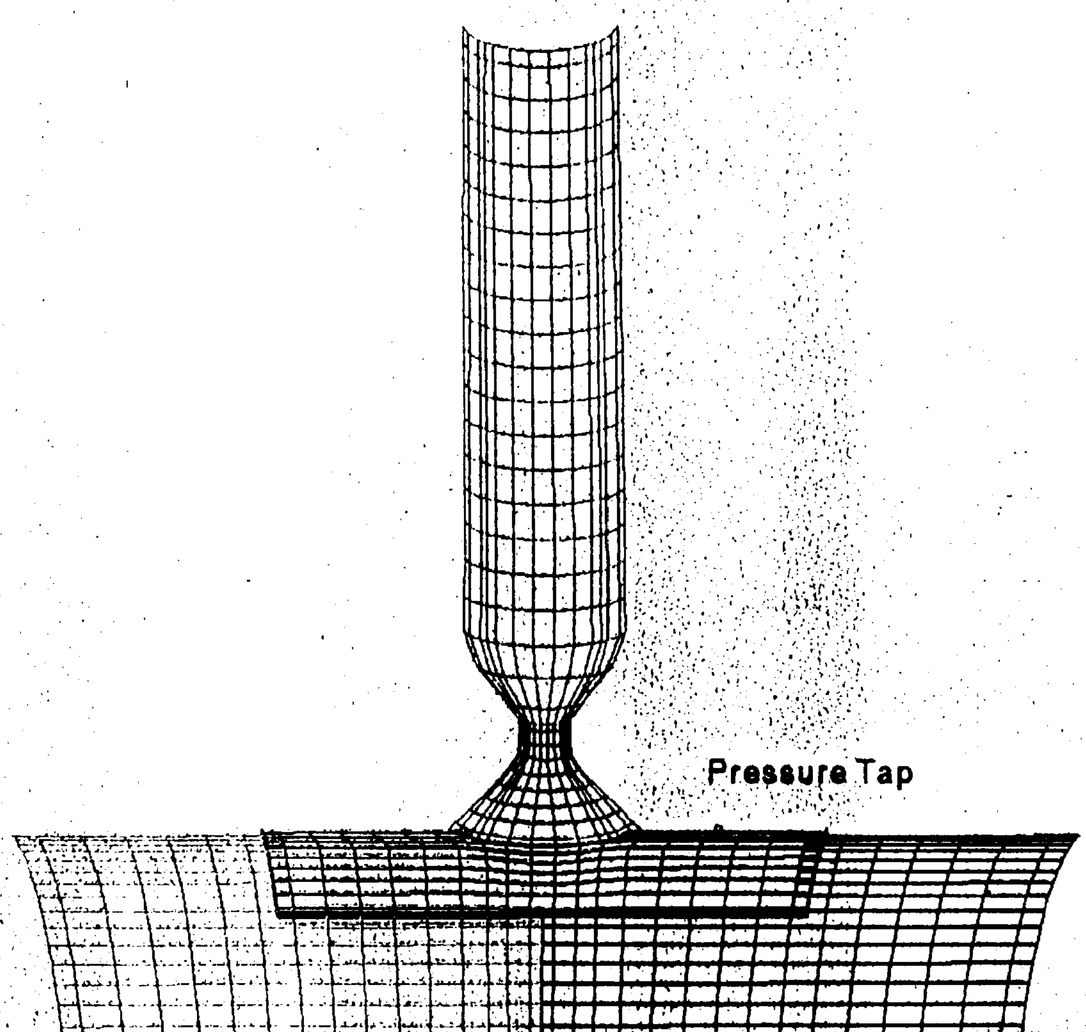

Rockwell International
Rocketdyne Division

Methodology

- 3 D Steady-State Accurate Finite Volume Formulation in Generalized Coordinates
- Full Navier-Stokes (FNS) 1st and 2nd Order Upwind/Central Spatial Discretization
- Simple Based Velocity-Pressure Coupling
- k- ε Turbulence Modelling with Wall Function
- Multiple Zone Approach

Rockwell International
Rocketdyne Division

Boundary Conditions

- No-slip at stationary wall
- Specify velocities at the inlet
- Extrapolate the flow velocity variables from the interior point at the outlet
- No slip relative to the rotating shaft
- Periodic conditions between recesses
- Consistent formulation of interface Zonal conditions

Results:

- Within 5% of Recess Pressure Loss
- Qualitative Agreement of Flowfield
- Matches Assumptions of Bulk Flow Model

Rockwell International
Rocketdyne Division

Code Development and Verification

TAMU Data Compared to CFD Solution

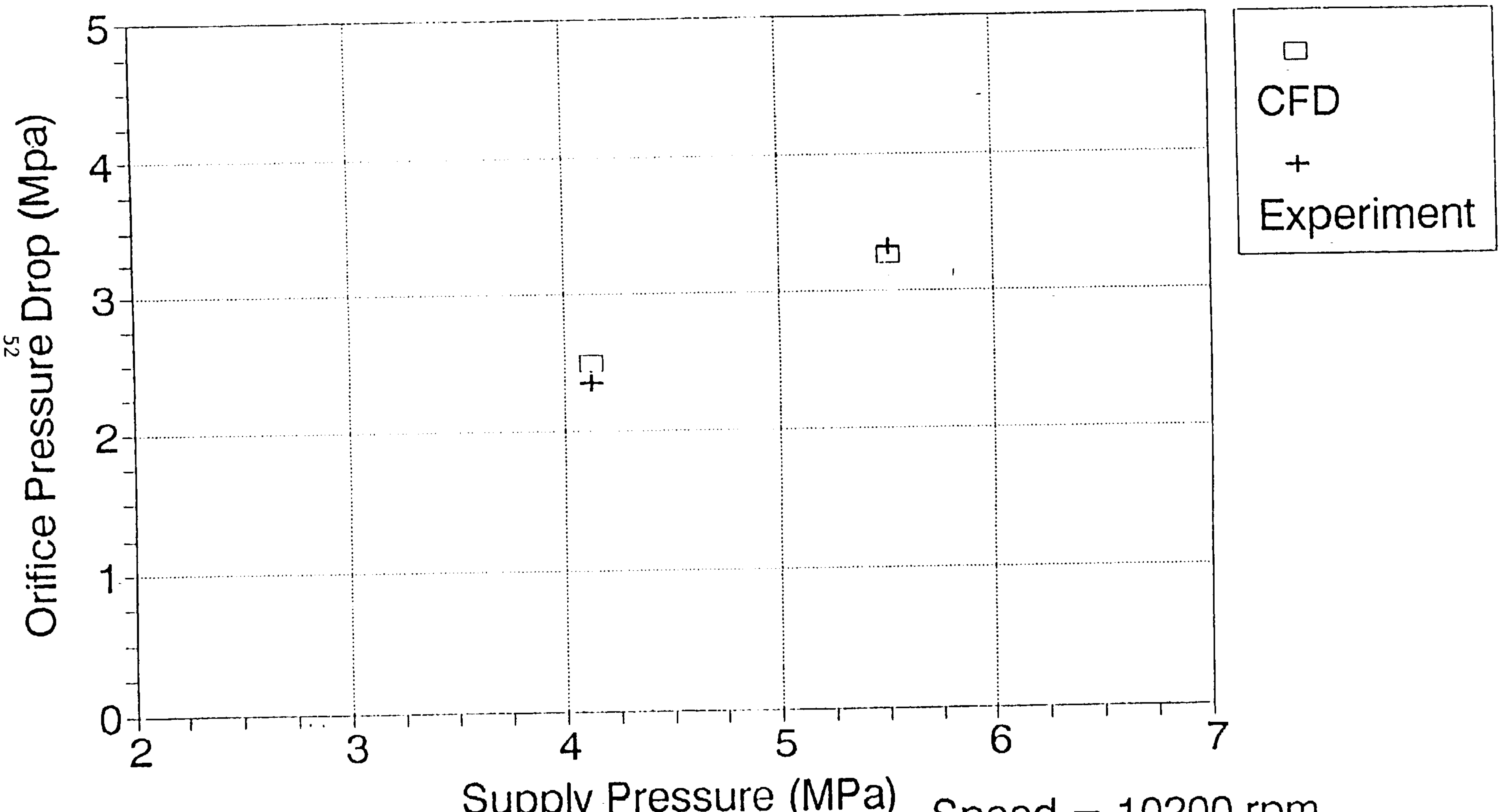

Speed = 10200 rpm

Clearance = 0.126 mm

Rockwell International
Rocketdyne Division

3-D CFD Pressure Solution

Axial Line Plot in Bearing Clearance

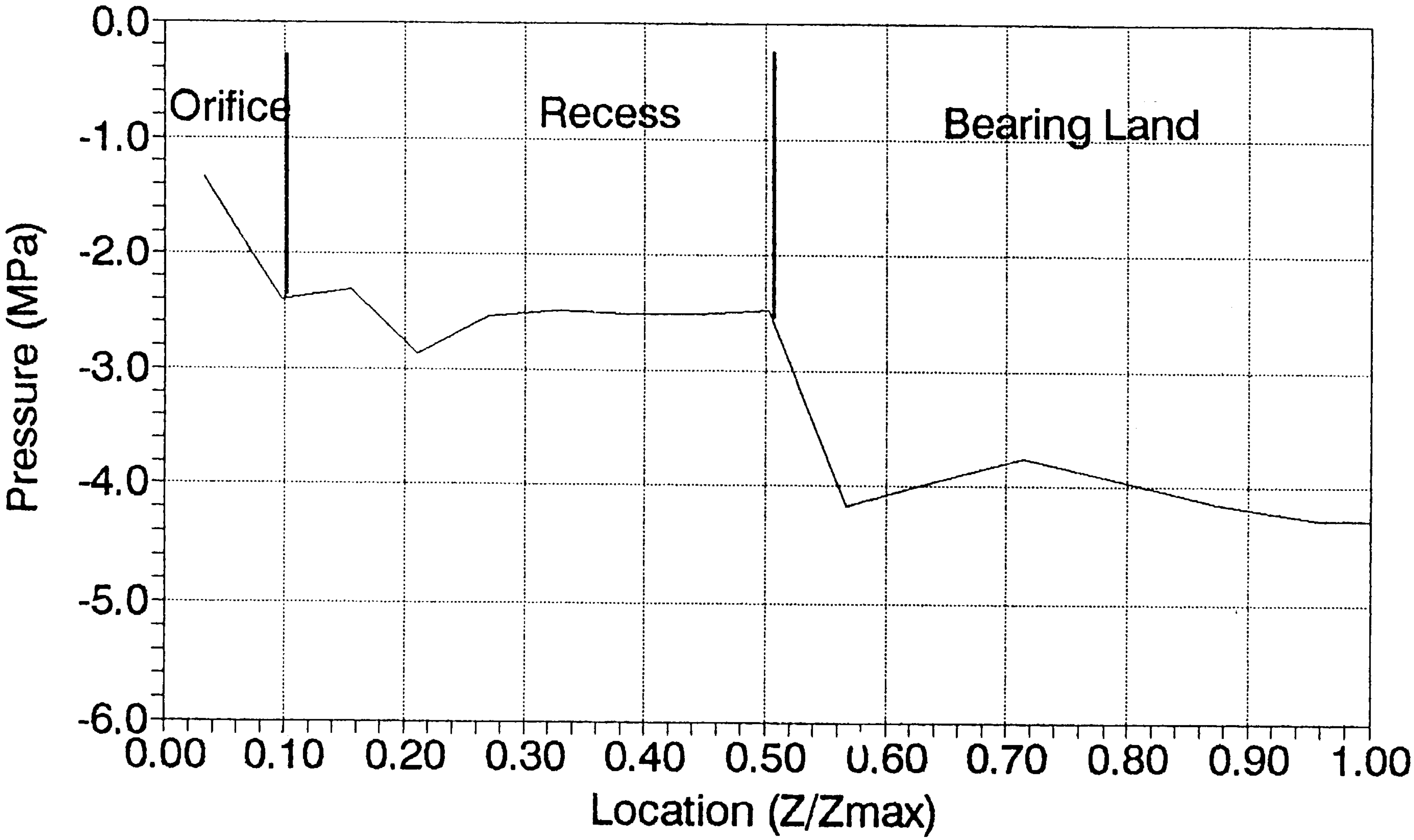

Rockwell International
Rocketdyne Division

Pressure Contour at Clearance Radial Plane

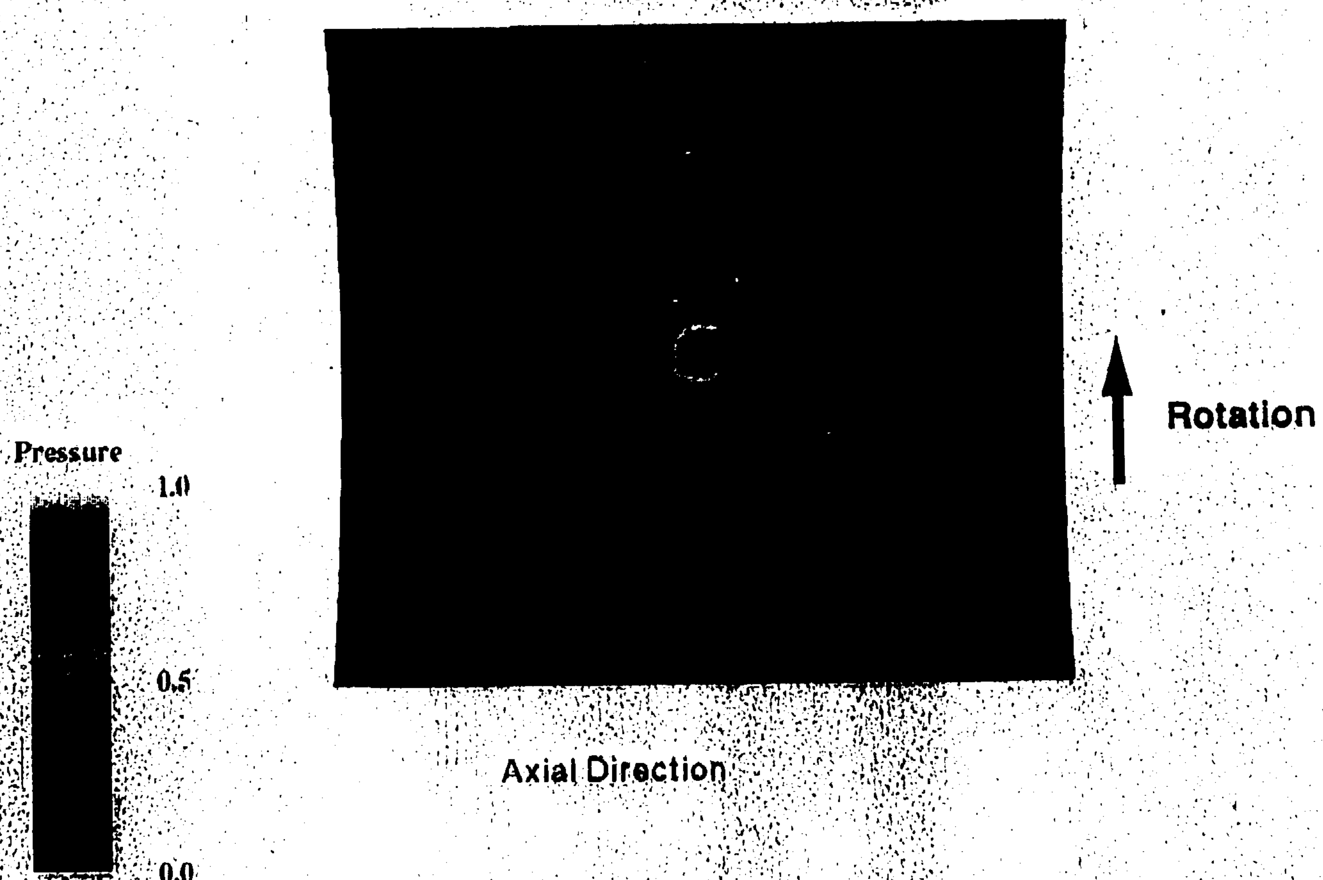

Conclusions:

- REACT3D Successfully Predicted Hydrostatic Bearing Solution on Actual Concentric Geometry
- 3-D CFD Solution Supports Main Assumptions of Bulk- Flow Model
    - Flow Variables Constant Across Bearing Clearance
    - Recess Pressure Constant
- Improvements to Bulk -Flow Solution will be Determined by Evaluation of Differences
    - Pressure Recovery at Entrance to Recess and Land

Rockwell International
Rocketdyne Division

N95- 23617

S2-34
44720

Finite-difference Solutions of the Alternate Turbopump Development High-pressure Oxidizer Turbopump Pump-end Ball-bearing Cavity Flows

p-18

by

Theodore G. Benjamin, Roberto Garcia, Paul K. McConnaughey,
Ten-See Wang and Bruce T. Vu
Computational Fluid Dynamics Branch
George C. Marshall Space Flight Center
National Aeronautics and Space Administration
Huntsville, Alabama
and
Youssef Dakhoul
Sverdrup Technologies
Huntsville, Alabama

These analyses were undertaken to aid in the understandng of flow phenomena in the Alternate Turbopump Development (ATD) High-pressure Oxidizer Turbopump (HPOTP) Pump-end ball bearing (PEBB) cavities and their roles in turbopump vibration initiation and bearing distress. This effort was being performed to provide timely support to the program in a decision as to whether or not the program should be continued.

In the first case, it was determined that a change in bearing throughflow had no significant effect on axial preload. This was a follow-on to a previous study which had resulted in a redesign of the bearing exit cavity which virtually eliminated bearing axial loading.

In the second case, a three-dimensional analysis of the inner-race-guided cage configuration was performed so as to determine the pressure distribution on the outer race when the shaft is 0.0002" off-center. The results indicate that there is virtually no circumferential pressure difference caused by the offset to contribute to bearing tilt.

In the third case, axisymmetric analyses were performed on an outer-race guided cage configuration to determine the magnitude of tangential flow entering the bearing. The removed-shoulder case was analyzed as was the static diverter case. A third analysis where the preload spring was shielded by a sheet of metal for the baseline case was also performed. It was determined that the swirl entering the bearing was acceptable and the project decided to use the outer-race-guided cage configuration.

In the fourth case, more bearing configurations were analyzed. These analyses included thermal modeling so as to determine the added benefit of injecting colder fluid directly onto the bearing inner-race contact area. The results of these analyses contributed to a programmatic decision to include coolant injection in the design.

FINITE-DIFFERENCE SOLUTIONS OF THE ALTERNATE TURBOPUMP HIGH-PRESSURE OXIDIZER TURBOPUMP PUMP-END BALL-BEARING CAVITY FLOWS

T. Benjamin
R. Garcia
P. McConnaughey
B. Vu
T. Wang
NASA / MSFC

Y. Dakhoul
Sverdrup Technologies/ Huntsville, Alabama

Computational Fluid Dynamics Branch
Fluid Dynamics Division
Structures and Dynamics Laboratory
Science and Engineering Directorate
Marshall Space Flight Center

Eleventh Workshop for CFD
Applications in Rocket Propulsion
Huntsville, Alabama
April 20-22, 1993

OVERVIEW

- Introduction
- Objective
- Approach
- Results
- Future work

INTRODUCTION

- Distress (increased temperature rise across bearings, high wear rate) observed in pump-end ball bearings in testing at Pratt & Whitney
  - Possible cause is loss of preload on the bearing
  - Second possible cause is loss of solid-film lubricant transfer to bearing contact areas because bearing outer-race tilt causes excessive ball temperature, which inhibits lubricant transfer
    - ◊ One potential agent for bearing tilt is asymmetric pressure loading on bearing
  - Third possible cause is inadequate cooling
- Some design changes implemented to mitigate distress
  - Move bearing cage to outer race to increase throughflow of fluid to inner-race contact areas
  - Remove material from inlet-side inner-race shoulder to increase flow to inner-race contact areas
  - Inject cooler flow near inner-race contact areas to reduce ball temperatures
  - Silicon nitride balls

Computational Fluid Dynamics Branch
Fluid Dynamics Division
Structures and Dynamics Laboratory
Science and Engineering Directorate
Marshall Space Flight Center

ATD SSME High Pressure Oxidizer Turbopump

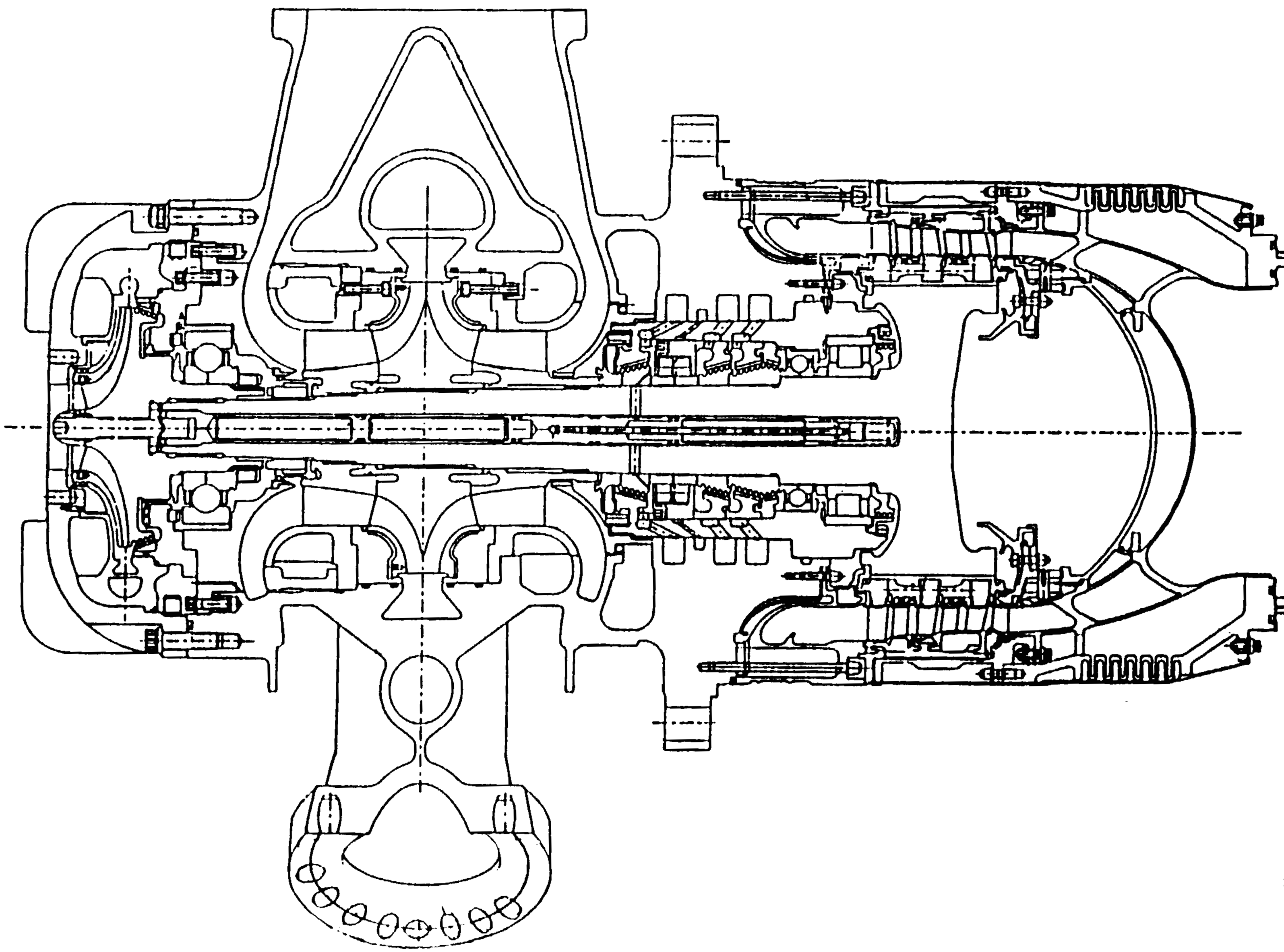

20 April 1993

Computational Fluid Dynamics Branch
Fluid Dynamics Division
Structures and Dynamics Laboratory
Science and Engineering Directorate
Marshall Space Flight Center

Finite-difference Solutions of the Alternate Turbopump Development High-pressure Oxidizer Turbopump Pump-end Ball-bearing Cavity Flows

Baseline Configuration

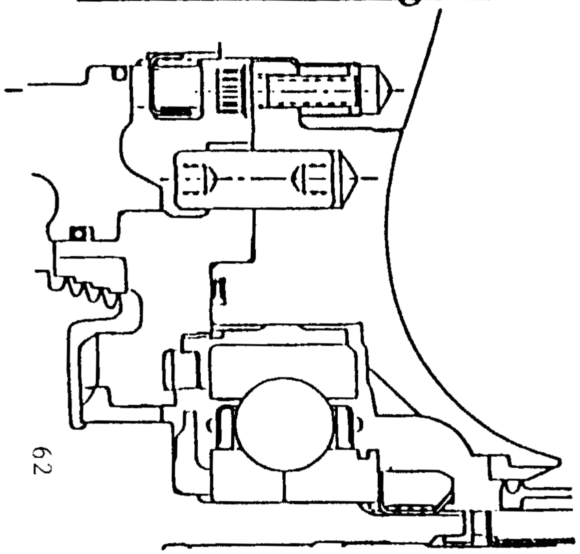

Removed Race Shoulder

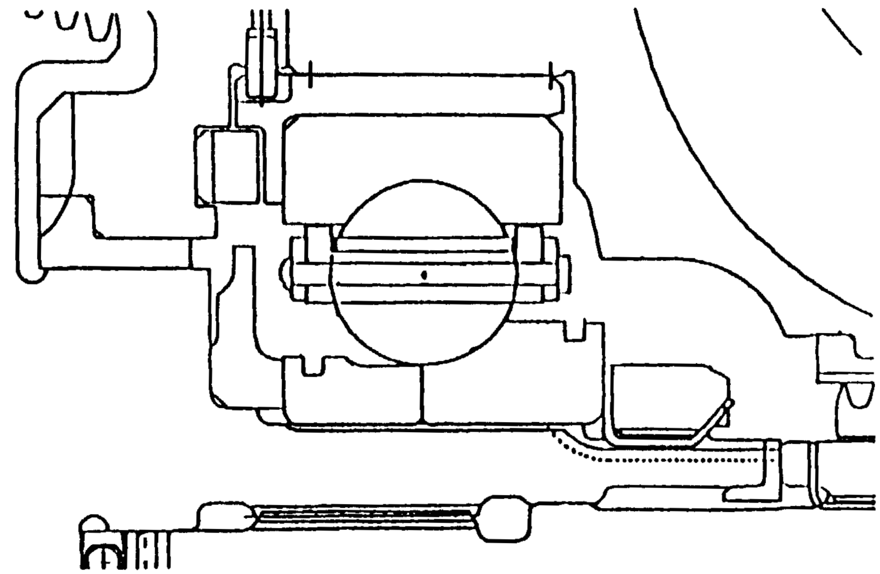

Inner Race Injection

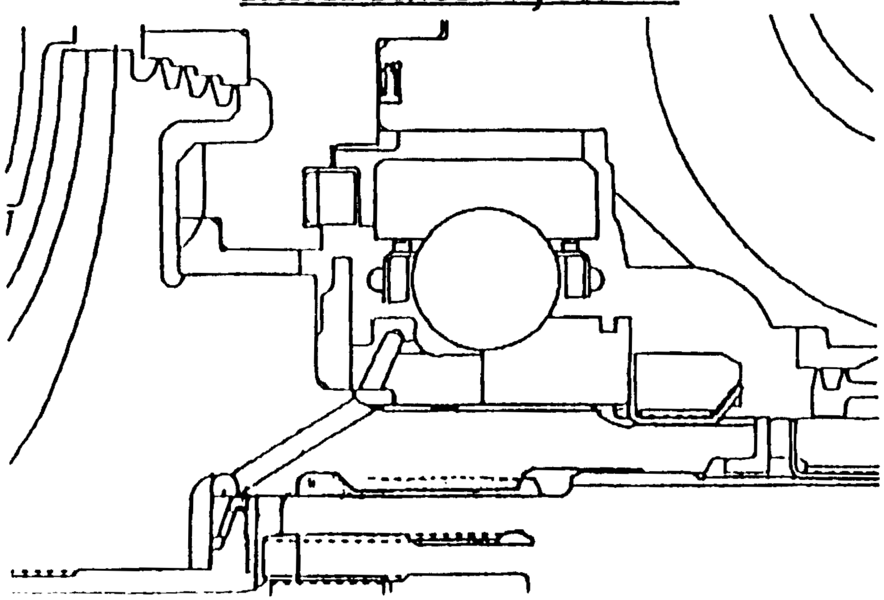

Static Diverter

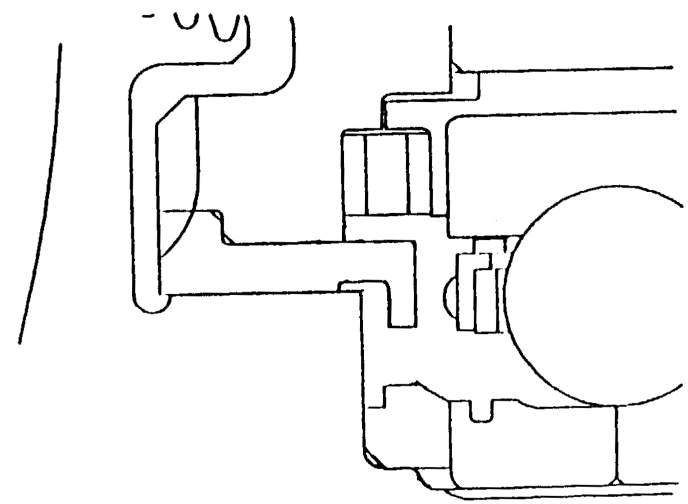

Computational Fluid Dynamics Branch
Fluid Dynamics Division
Structures and Dynamics Laboratory
Science and Engineering Directorate
Marshall Space Flight Center

OBJECTIVE OF CFD ANALYSIS

- Determine effect of flow rate upon axial preload
- Quantify pressure field asymmetry due to rotor offset as cause of bearing tilt
- Determine effect of design changes upon bearing inlet swirl (viscous heating)
- Quantify effectiveness of design changes to enhance cooling

Computational Fluid Dynamics Branch
Fluid Dynamics Division
Structures and Dynamics Laboratory
Science and Engineering Directorate
Marshall Space Flight Center

APPROACH

- All analyses
  - K-ε turbulence model with wall functions
  - Neglected ball
  - Incompressible
  - Fixed inlet velocity field
- Effect on axial preload
  - Previous analysis indicated at 9 pps flow rate through bearing, pressure forces on inlet and outlet faces of bearing balanced such that preload was unaffected
  - Analyzed axisymmetrically and isothermally with finite-difference Navier-Stokes code (FDNS) and finite-volume Navier-Stokes co-located code (REFLEQS)
  - Analyzed for 15 pps flow rate to augment previous 9 pps analysis
- Pressure field asymmetry
  - Analysis of inlet cavity with 0.0002" shaft static offset and flow rate of 15 pps
  - Three-dimensional isothermal analysis using FDNS

<u>APPROACH</u> (continued)

- Asses bearing design effects on bearing inlet swirl
  - Analyses of inlet cavity with outer-race-guided cage with flow rate of 15 pps
  - Utilized three configurations
  - Axisymmetric isothermal analysis using FDNS
- Cooling enhancement
  - Analyses of inlet cavity for outer-race-guided cage configuration
    - ◊ Lowered shoulder analyzed for three different ball/inner-race heat-generation levels with 15 pps through bearing
    - ◊ Injection cases analyzed for three different ball/inner-race heat-generation levels with 7.5 pps entering through seal (230 °R) and 7.5 pps injected through inner race (190 °R)
  - Axisymmetric thermal analyses using REFLEQS
  - Effectiveness determined by maximum temperature in bearing area

RESULTS

- Change in flow rate does not affect axial preload
- No circumferential pressure field asymmetry due to shaft offset to contribute to bearing tilt
- Moving bearing cage to outer race increases inlet swirl
  - Baseline: bearing inlet swirl = 15 ft/sec
  - Removed race: bearing inlet swirl = 31 ft/sec
  - Shielded preload spring: bearing inlet swirl = 105 ft/sec
  - Static diverter: bearing inlet swirl = 55 ft/sec
- For silicon nitride balls, cooling enhancement keeps ball temperatures in desirable range
  - For inner race guided cage with no EHD, maximum temperature 325 °R
  - For outer race guided cage:

Elastohydrodynamic film (Q)	Lowered shoulder	Coolant injection
None (0.56 Btu/sec)	255 °R	213 °R
Partial (0.23 Btu/sec)	240 °R	204 °R
Full (0.028 Btu/sec)	231 °R	198 °R

Computational Fluid Dynamics Branch
Fluid Dynamics Division
Structures and Dynamics Laboratory
Science and Engineering Directorate
Marshall Space Flight Center

Finite-difference Solutions of the Alternate Turbopump Development High-pressure Oxidizer Turbopump Pump-end Ball-bearing Cavity Flows

Bearing-face Pressures

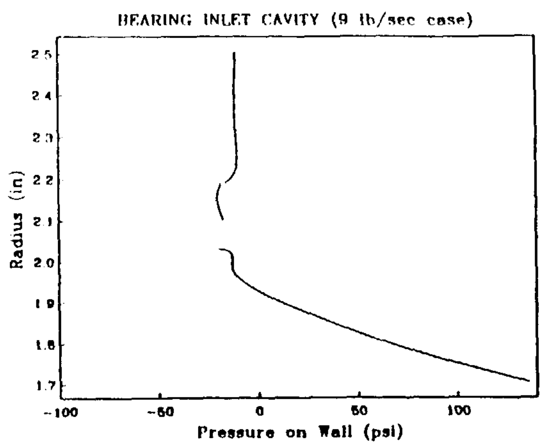

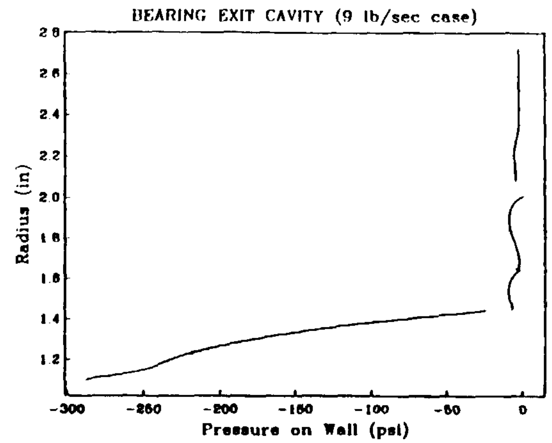

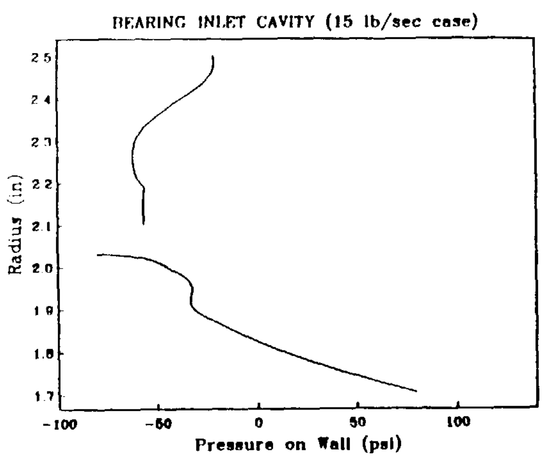

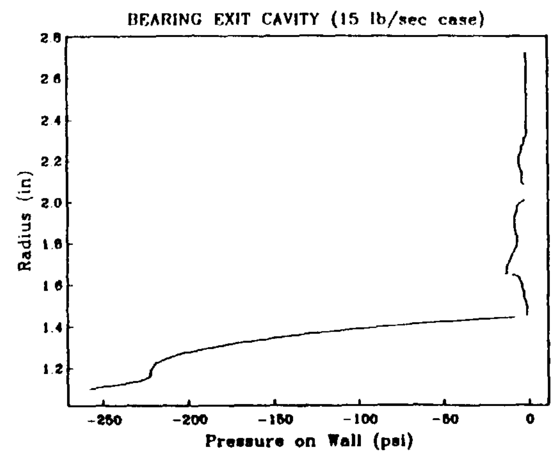

20 April 1993

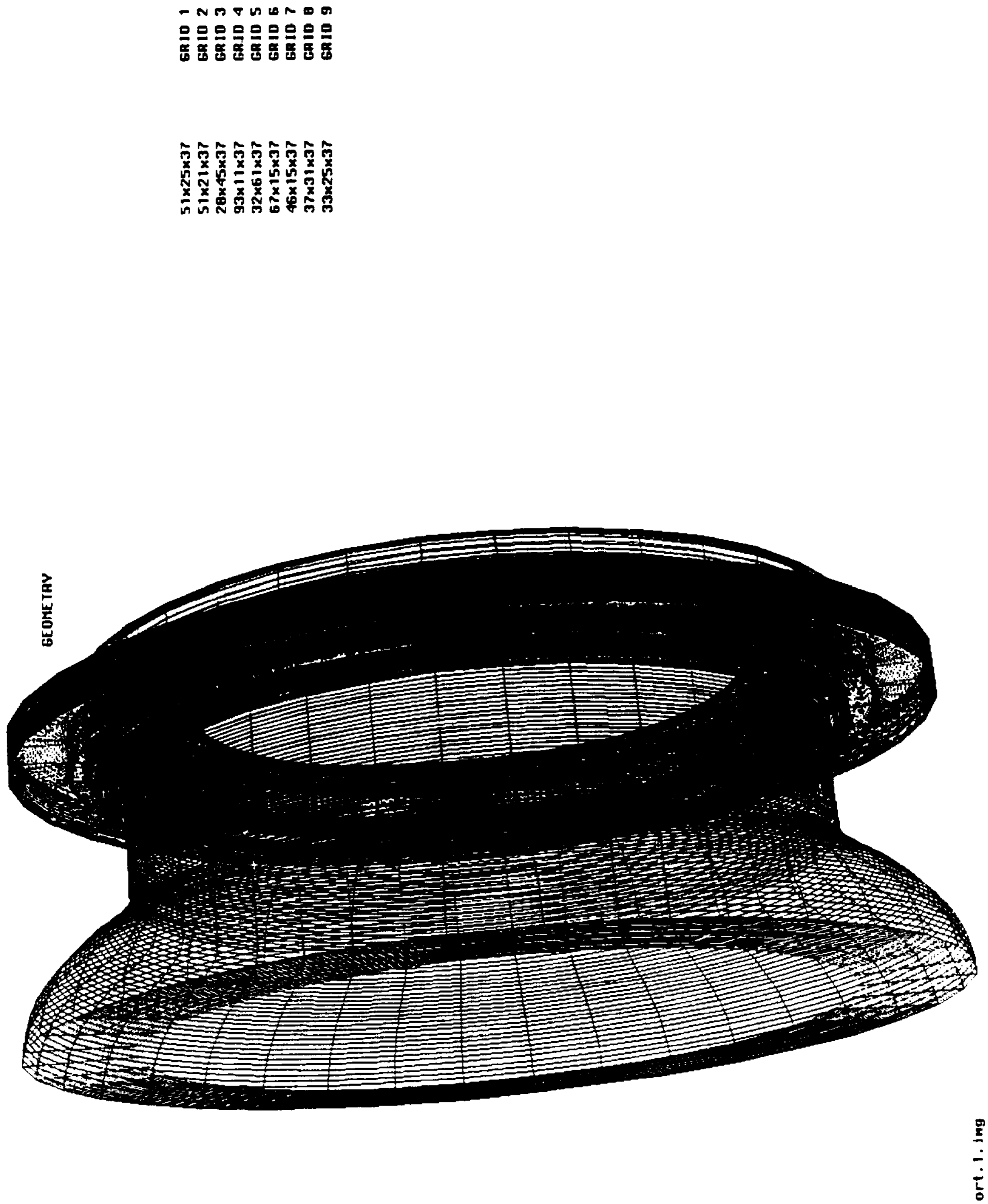
GEOMETRY
GRID 1 51x25x37
GRID 2 51x21x37
GRID 3 28x45x37
GRID 4 93x11x37
GRID 5 32x61x37
GRID 6 67x15x37
GRID 7 46x15x37
GRID 8 37x31x37
GRID 9 33x25x37
fort.1.img

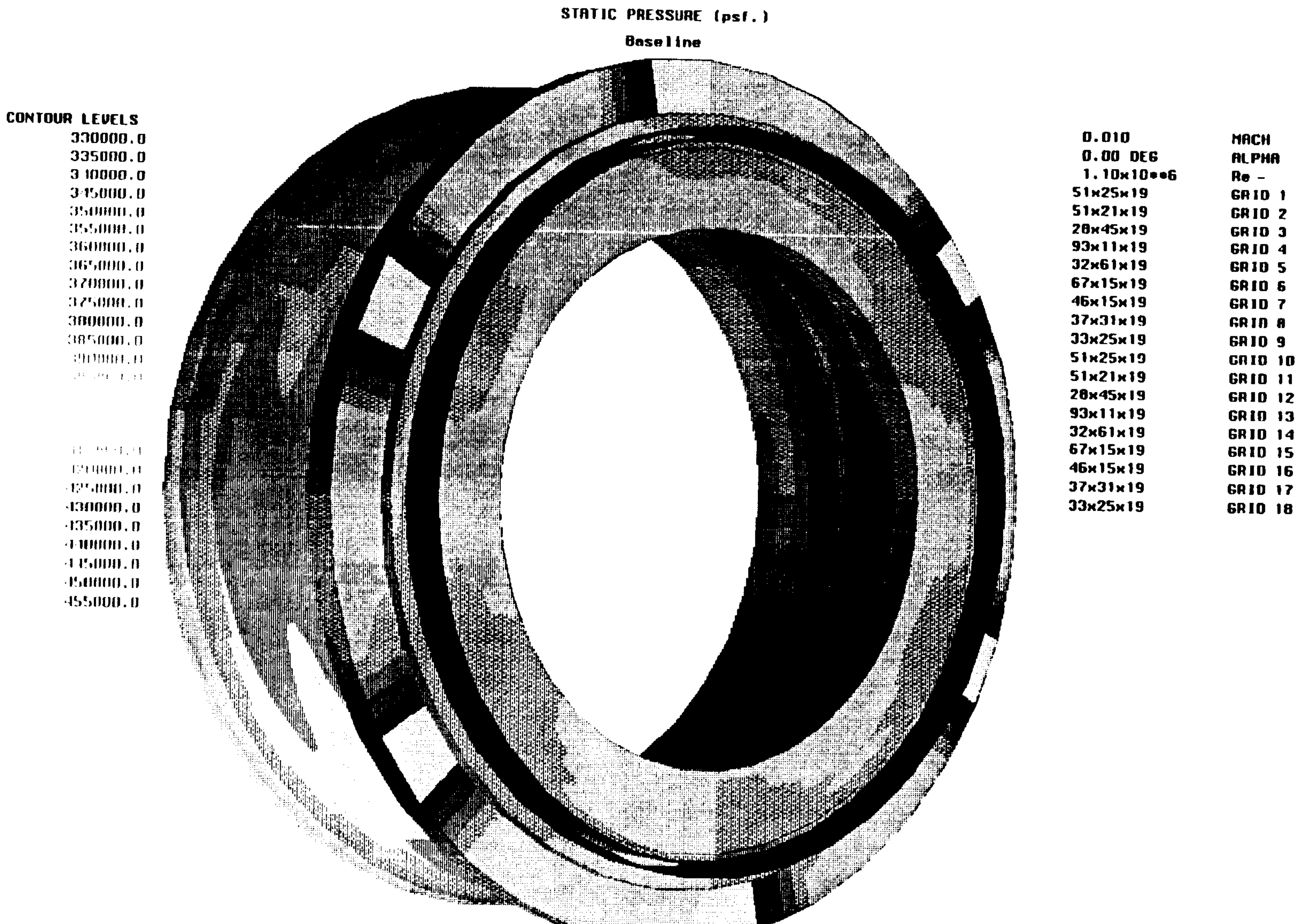
STATIC PRESSURE (psf.)
Baseline
CONTOUR LEVELS
330000.0
335000.0
340000.0
345000.0
350000.0
355000.0
360000.0
365000.0
370000.0
375000.0
380000.0
385000.0
390000.0
420000.0
425000.0
430000.0
435000.0
440000.0
445000.0
450000.0
455000.0
0.010 MACH
0.00 DEG ALPHA
1.10x10**6 Re -
51x25x19 GRID 1
51x21x19 GRID 2
28x45x19 GRID 3
93x11x19 GRID 4
32x61x19 GRID 5
67x15x19 GRID 6
46x15x19 GRID 7
37x31x19 GRID 8
33x25x19 GRID 9
51x25x19 GRID 10
51x21x19 GRID 11
28x45x19 GRID 12
93x11x19 GRID 13
32x61x19 GRID 14
67x15x19 GRID 15
46x15x19 GRID 16
37x31x19 GRID 17
33x25x19 GRID 18

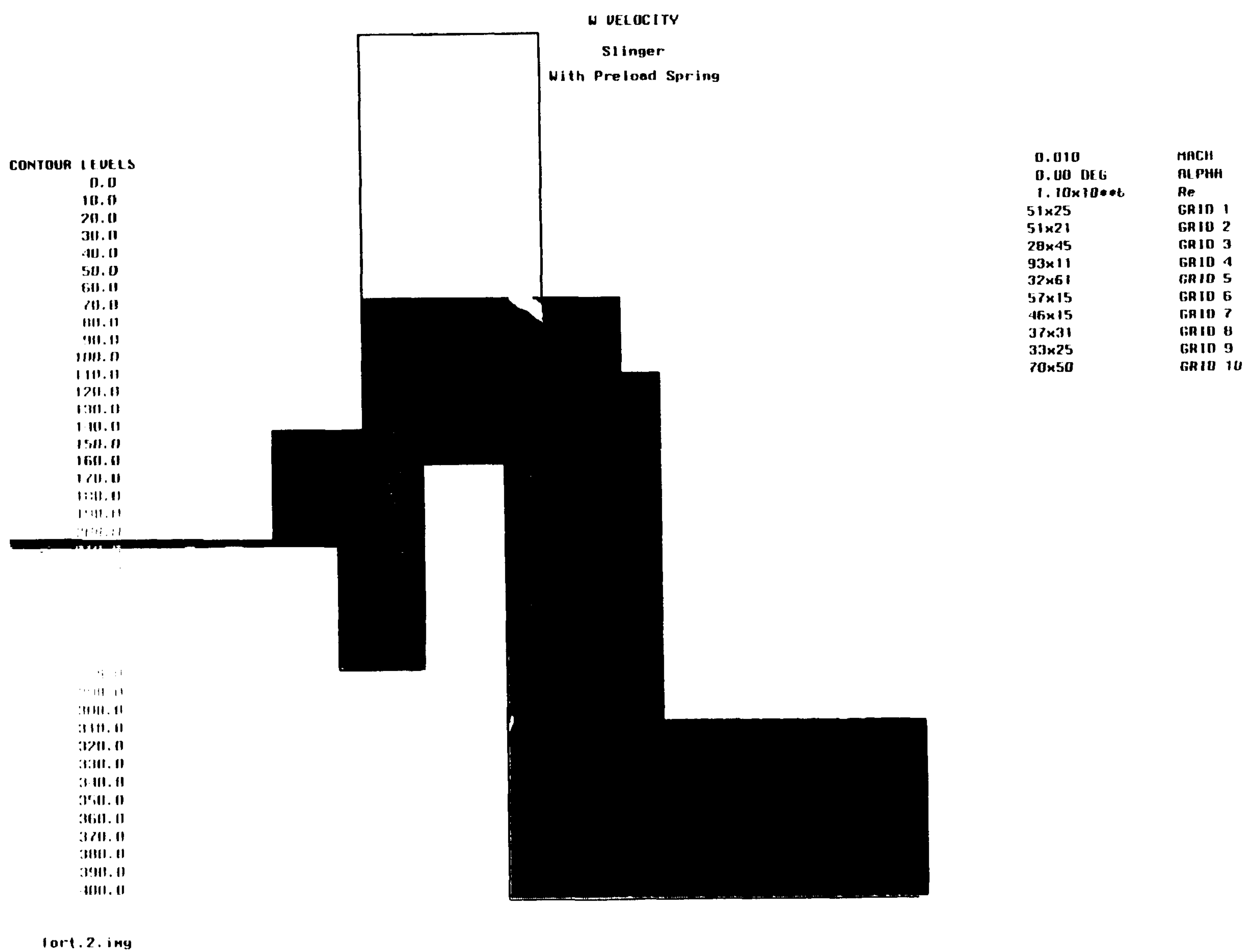
W VELOCITY
Slinger
With Preload Spring
CONTOUR LEVELS
0.0
10.0
20.0
30.0
40.0
50.0
60.0
70.0
80.0
90.0
100.0
110.0
120.0
130.0
140.0
150.0
160.0
170.0
180.0
190.0
300.0
310.0
320.0
330.0
340.0
350.0
360.0
370.0
380.0
390.0
400.0
fort.2.img
0.010 MACH
0.00 DEG ALPHA
1.10x10**6 Re
51x25 GRID 1
51x21 GRID 2
28x45 GRID 3
93x11 GRID 4
32x61 GRID 5
57x15 GRID 6
46x15 GRID 7
37x31 GRID 8
33x25 GRID 9
70x50 GRID 10

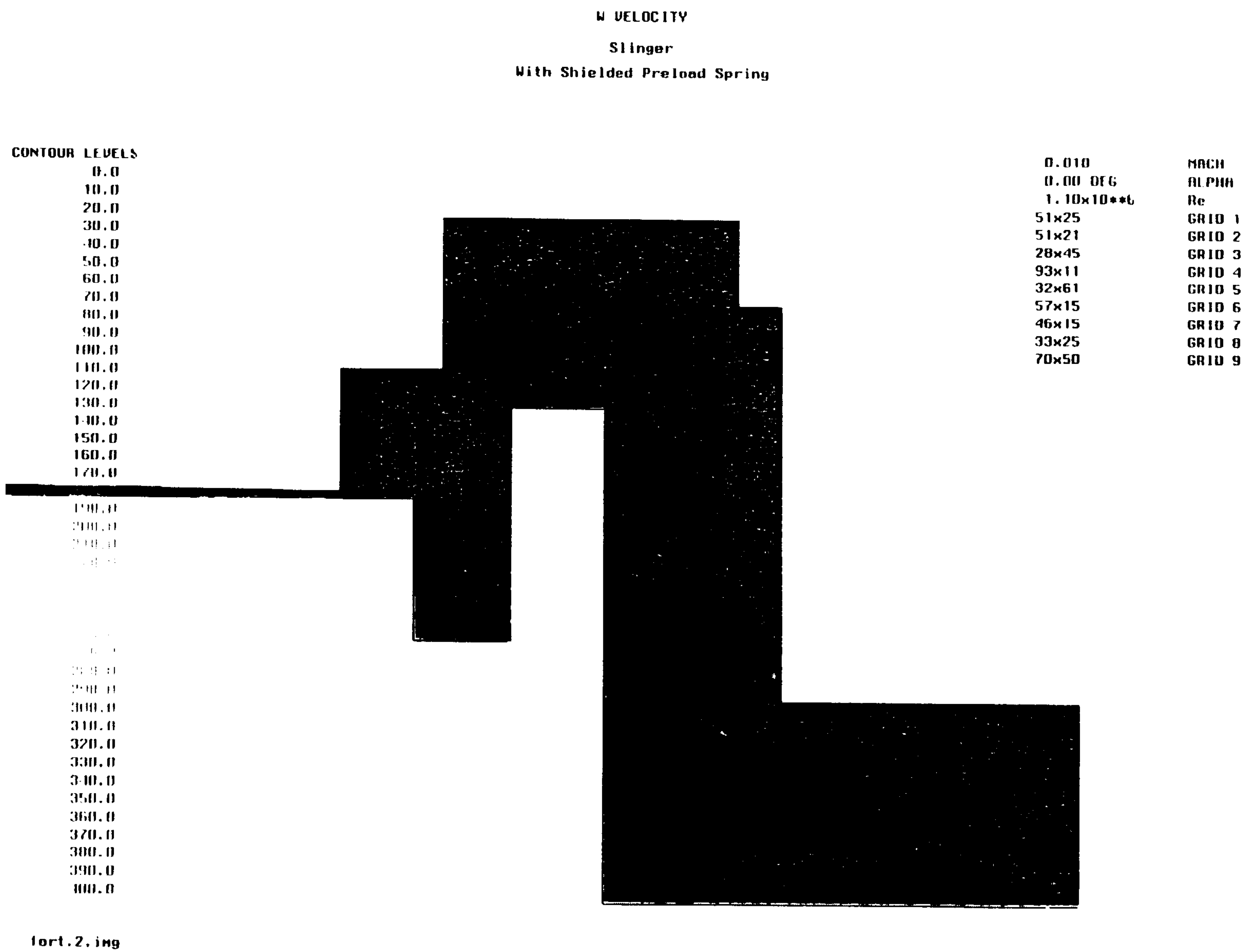
W VELOCITY
Slinger
With Shielded Preload Spring
CONTOUR LEVELS
0.0
10.0
20.0
30.0
40.0
50.0
60.0
70.0
80.0
90.0
100.0
110.0
120.0
130.0
140.0
150.0
160.0
170.0
190.0
200.0
290.0
300.0
310.0
320.0
330.0
340.0
350.0
360.0
370.0
380.0
390.0
400.0
fort.2.img
0.010 MACH
0.00 DEG ALPHA
1.10x10**6 Re
51x25 GRID 1
51x21 GRID 2
28x45 GRID 3
93x11 GRID 4
32x61 GRID 5
57x15 GRID 6
46x15 GRID 7
33x25 GRID 8
70x50 GRID 9

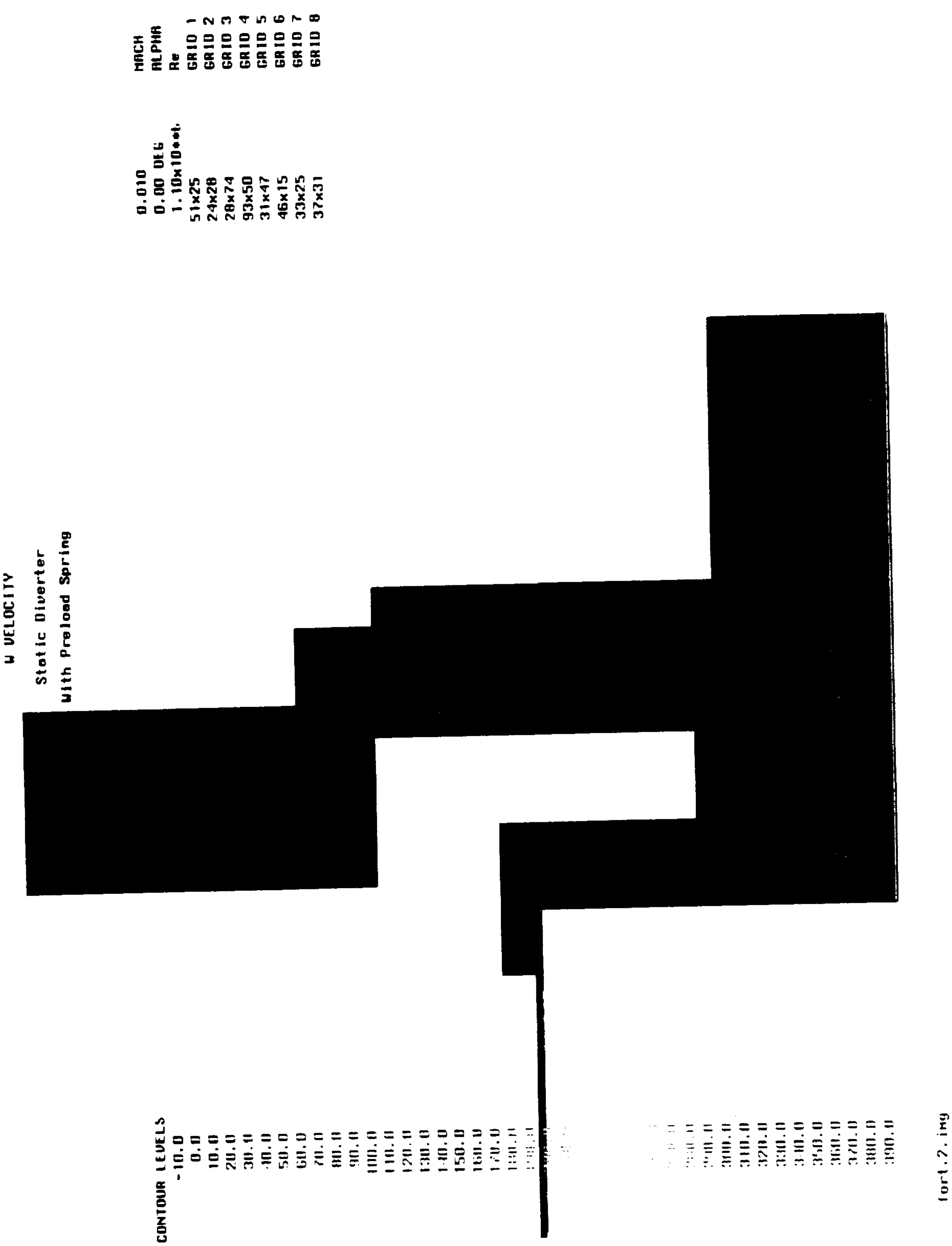
W VELOCITY
Static Diverter
With Preload Spring
MACH 0.010
ALPHA 0.00 DEG
Re 1.10x10**6
GRID 1 51x25
GRID 2 24x28
GRID 3 28x74
GRID 4 93x50
GRID 5 31x47
GRID 6 46x15
GRID 7 33x25
GRID 8 37x31
CONTOUR LEVELS
-10.0
0.0
10.0
20.0
30.0
40.0
50.0
60.0
70.0
80.0
90.0
100.0
110.0
120.0
130.0
140.0
150.0
160.0
170.0
300.0
310.0
320.0
330.0
340.0
350.0
360.0
370.0
380.0
390.0
fort.2.img

CFD ANALYSIS OF ATD BEARING FLOWS
FLOW STREAMLINES COLORED BY FLUID TEMPERATURE

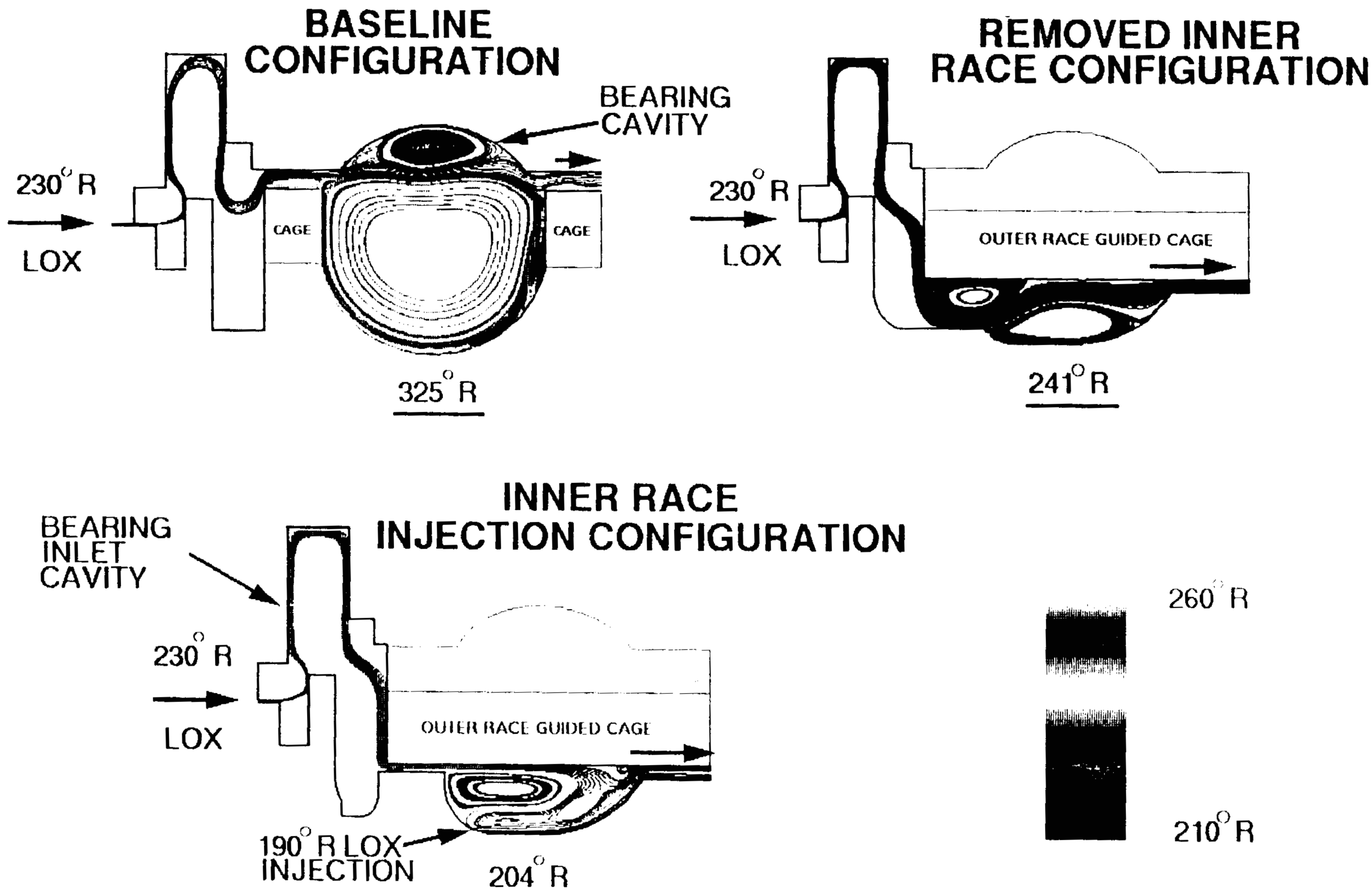

Computational Fluid Dynamics Branch
Fluid Dynamics Division
Structures and Dynamics Laboratory
Science and Engineering Directorate
Marshall Space Flight Center

Future Work

- Optimizing inner-race injection design
  - Sweep angle
  - Injection flow rate
  - Axial flow angle
  - Other possibilities
    - ◊ Shoulder height
    - ◊ Hole location, size, number

N95-23618

S3-34
p. 23

NAVIER-STOKES FLOW FIELD ANALYSIS OF COMPRESSIBLE FLOW IN A PRESSURE RELIEF VALVE

Bruce Vu & Ten-See Wang
Computational Fluid Dynamics Branch
NASA - Marshall Space Flight Center

Ming-Hsin Shih & Bharat Soni
Engineering Research Center for Computational Field Simulation
Mississippi State University

Abstract

The present study was motivated to analyze the complex flow field involving gaseous oxygen (GOX) flow in a relief valve (RV). The 9391 RV, pictured in Figure 1, was combined with the pilot valve to regulate the actuation pressure of the main valve system. During a high-pressure flow test at Marshall Space Flight Center (MSFC) the valve system developed a resonance chatter, which destroyed most of the valve body. Figures 2-4 show the valve body before and after accident. It was understood that the subject RV has never been operated at 5500 psia. In order to fully understand the flow behavior in the RV, a computational fluid dynamics (CFD) analysis is carried out to investigate the side load across the piston sleeve and the erosion patterns resulting from flow distribution around piston/nozzle interface.

Grid Topology

The safety RV consists of a main cylinder and a piston, with a smaller diameter inlet. An intersection technique was developed to model the piston-cylinder configureation (Figure 5). To simplify the geometry, the diameter of the cylinder is kept constant.

An O-type grid in the axial plane was initially considered for this geometry. However, it would become very difficult to generate grid lines around the piston on the upper part of the main cylinder, if not impossible. H-type grid was then chosen to model this internal flow geometry. The main cylinder was cut into half at the plane of symmetry to reduce the size of domain. It was again cut into halves at the bottom face of the piston to divide the computational domain into upper part and lower part. To model the field geometry, the descritization was carried out into five-block zonal grid; the inlet itself formed a block, the lower part of the main cylinder formed another block, and the upper part of the main cylinder was cut into 3 more blocks. The 5-block grid is shown in Figures 6-7. Compared to the original O-type grid, this H-type grid topology greatly reduced the grid distortion, especially near the piston .

Grid Generation

GENIE++ (Ref. 1-3), a general purpose three-dimensional grid generation package, was used to generate the grid for this geometry. GENIE++ is the Mississippi State University updated version of INGRID (Ref. 4-5) developed by Arnold Engineering Development Center (AEDC).

In order to perform the surface intersections of the piston, as well as the inlet, with the main cylinder, an intersection algorithm with Newton-Ralphson method was used to obtain the intersection curves. Weighted transfinite interpolation (Weighted TFI) (Ref. 2) algorithm is used to generate the algebraic grid. Weighted TFI can be formulated as uniform TFI with grid distribution mesh, where the grid distribution mesh is obtained by performing uniform TFI on normalized arc length distribution on associated boundaries (or surfaces in volume grid).

Since the selected grid topology reduced the distortion of grid lines, the resulting algebraic grid was very satisfactory, and no elliptic smoothing was performed for the present computation. However, for future grid-dependent study, elliptic solver will be applied to refine the local grids while maintaining a packed, viscous grid on the surface.

Governing Equations and Computational Scheme

The present numerical simulation uses a non-staggered grid, pressure based transport equation solver with an extended version of two-equation k-ε turbulence model. While the computer code has all-speed capability for both compressible and incompressible flows, the present study only uses the compressible feature. The basic equations employed to describe the momentum and heat transfer in the computational domain are the three-dimensional Reynolds-averaged transport equations. To solve the system of coupled nonlinear partial differential equations, it uses finite difference approximations to establish a system of linearized algebraic equations. An adaptive upwinding scheme is utilized to model the convective terms of the momentum, energy and continuity equations, which is based on the second and fourth order central differencing with artificial dissipation. Discretization of viscous fluxes and source terms uses a second-order central difference approximation. For velocity-pressure coupling, the present solution procedure employs pressure-based, predictor followed by multi-corrector approach. Details of the present numerical methodology are given by Wang and Chen (Ref. 6).

Due to symmetry, the computational domain occupies only the front half of the RV. Along all solid walls, no-slip condition is applied for velocities, and temperature is assumed constant. For near-wall turbulence treatment, it uses a wall function with modified flux source and a velocity profile capable of providing a smooth transition between logarithmic law-of-wall and linear variation in viscous sublayer. Such a treatment significantly reduces the flux dependence on the near-wall spacing. The inlet conditions are fully developed profiles for velocities and turbulence parameters, and the outlet conditions satisfy the conservation of mass.

Result and Discussion

The preliminary computations have been performed to simulate the flow field of GOX in the 9391 RV at 5500 psia and 1000° R. Results indicated no viscous heating due to low temperature gradients near the piston surface (Figure 8). The surface pressure contours in Figure 9 also indicated an insignificant side load across the piston sleeve. The force obtained from integrating all pressure points around the piston surface, from the bottom up to the piston sleeve is found to be only 70 lbf, under this adverse condition. The velocity vectors, magnitude, and Mach contours are shown in Figures 10-12, respectively. Finally, the vortex formations in Figure 13-14 predicts reasonable erosion patterns in the gap between the cylinder elbow and the bottom of the piston. Evidently these patterns are in agreement with the damaged hardware which indicates clear signs of burns and scratches near the piston/throat region.

References

1. Soni, B.K., Thompson, J.F., Stokes, M., and Shih, M.H.,"GENIE++, EAGLEView, and TIGER: General and Special Purpose Graphically Interactive Grid Systems", AIAA-92-0071, AIAA 30th Aerospace Sciences Meeting and Exhibit, Reno, Nevada, 1992.

2. Soni, B.K., "Grid Generation for Internal Flow Configurations", Computers Math. Application, Vol. 24, No. 516, pp.191-201, 1992.

3. Soni, B.K., "Two and Three Dimensional Grid Generation for Internal Flow Application of Computational Fluid Dynamics", AIAA-85-1526, AIAA 7th Computational Fluid Dynamics Conference, Cincinnati, Ohio, 1985.

4. Soni, B.K., and Dorrell, E.W., "INGRID Interactive Geometry-Grid Generation for Two Dimensional Applications", AEDC-TR-86-49.

5. Dorrell, E.W., and McClure, M.D., "3D INGRID: Interactive Three-Dimensional Grid Generation", AEDC-TR-87-40.

6. Wang, T.S. and Chen, Y.S., "A Unified Navier-Stokes Flowfield and Performance Analysis of Liquid Rocket Engines," AIAA-90-2494, AIAA/SAE/ASME/ASEE 26th Joint Propulsion Conference, Orlando, FL, July 1990.

Navier-Stokes Flow Field Analysis of Compressible Flow in a Pressure Relief Valve

By

B.T. Vu & T.S. Wang
Marshall Space Flight Center

M.H. Shih & B.K. Soni
Mississippi State University
Engineering Research Center

For

Workshop for CFD Applications in Rocket Propulsion
April 20-22, 1993
Huntsville, Alabama

BACKGROUND

TS116 Mishap Investigation:

- Mishap occured at X-15 while 40K test system was supposed to be in static state.
- The pressure relief valves have never been operated at 5500 psi.
- There are no data except valve activation times, personnel observations, and remaining parts of the subject relief valve.

OBJECTIVE

To investigate the following action items:

- Friction due to hot GOX flow across nozzle/piston interface
- Side load on piston sleeve
- Velocities at valve inlet nozzle
- Erosion patterns caused by vortex formations

APPROACH

- 1-D analytical solutions assuming convergent-divergent nozzle flow for initial flow field
- 3-D, multi-block, H-type grid generated by Genie++ using new intersection technique
- Numerical solutions by a pressure-based flow solver (FDNS-3D) assuming flow to be viscous, turbulent and compressible

RESULTS & DISCUSSION

- FDNS performs well on the coarse grids.
- F=70 lbf, based on 3-D analysis for the single-phase flow through a wide gap (0.16"). This side load results from integrating all pressure points (computed by FDNS) around the piston surface, from the bottom up to the piston sleeve.
- No viscous heating due to low temperature gradients.
- Low pressure drops across the piston indicate insignificant side loads.
- 3-D calculation indicates recirculation around piston/throat region.
- Vortex formation patterns agree with physical evidence from the damaged hardware.

SUMMARY

- Multi-block, 3-D, H-type grid was generated. Total of 91,612 grid points.
- Side loads calculated.
- Flow conditions provided to failure investigation team.
- Due to the complexity of grid and flow definition, 3-D problem becomes very expensive, e.g. the cost for a converged single-phase solution is recorded as:

  1000 iterations = 9.5 cpu hours = 79.2 calendar hours

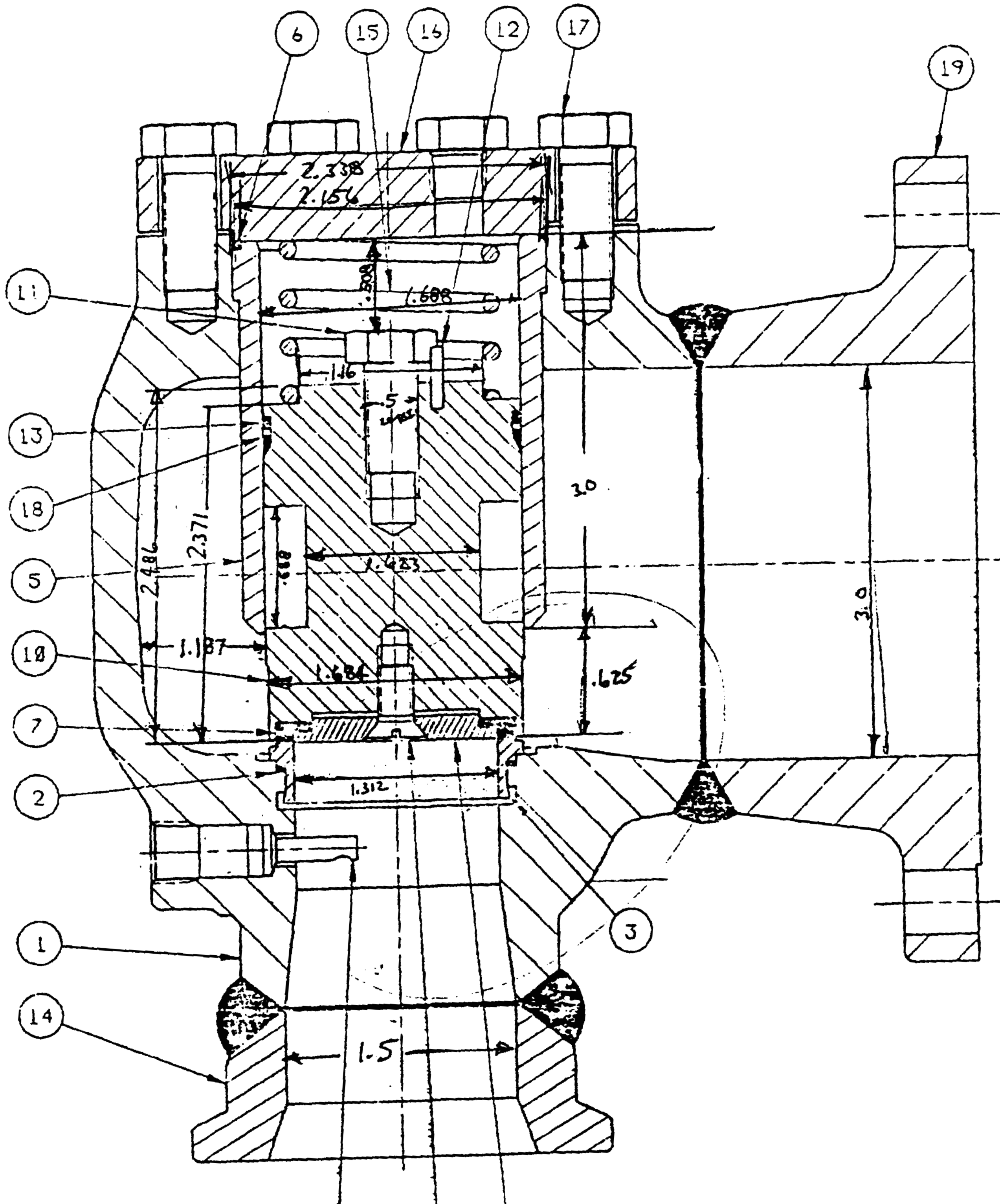

Figure 1. Valve schematic

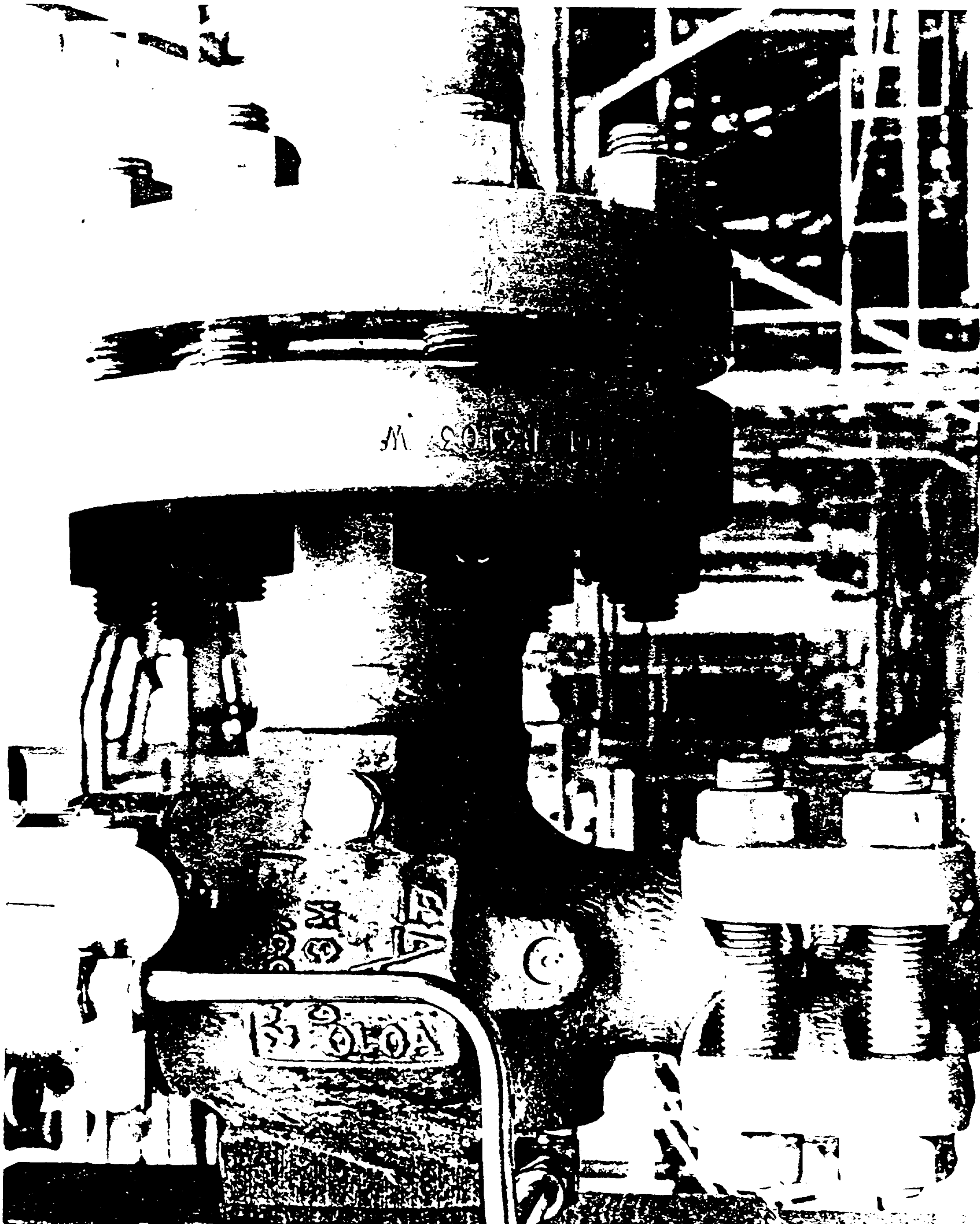

Figure 2. Valve photo (before accident)

Figure 3. Side-view photo (after accident)

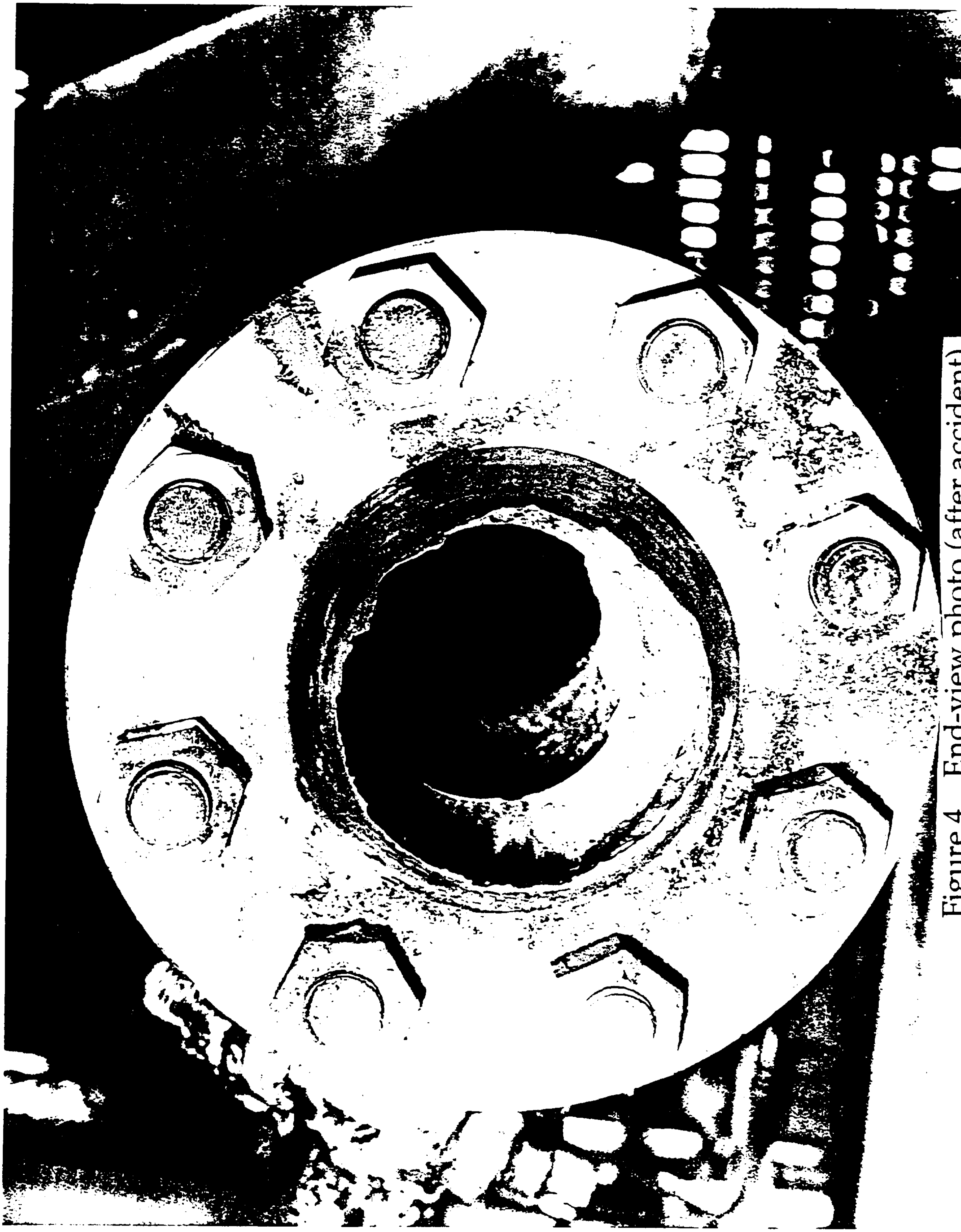

Figure 4. End-view photo (after accident)

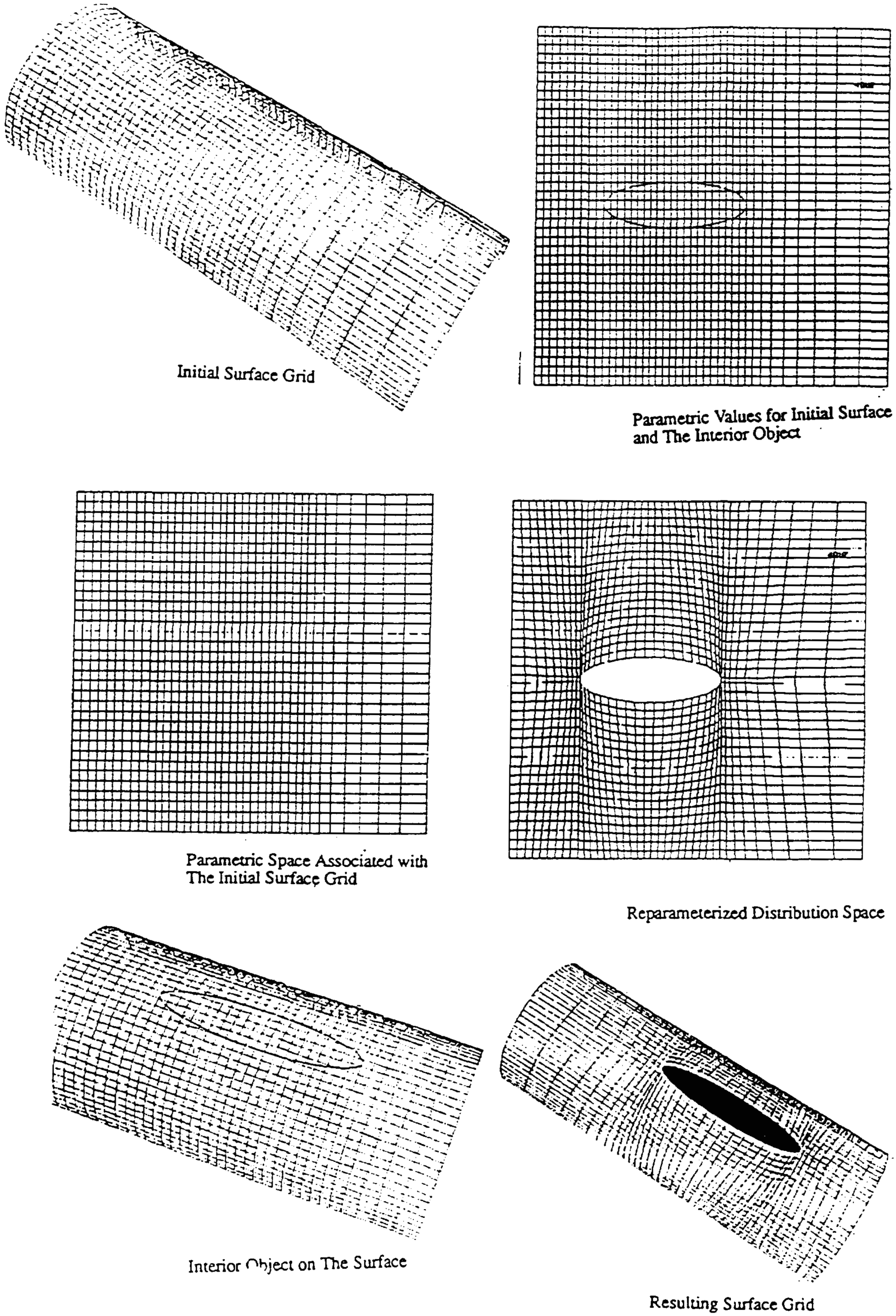

Figure 5. Intersection technique

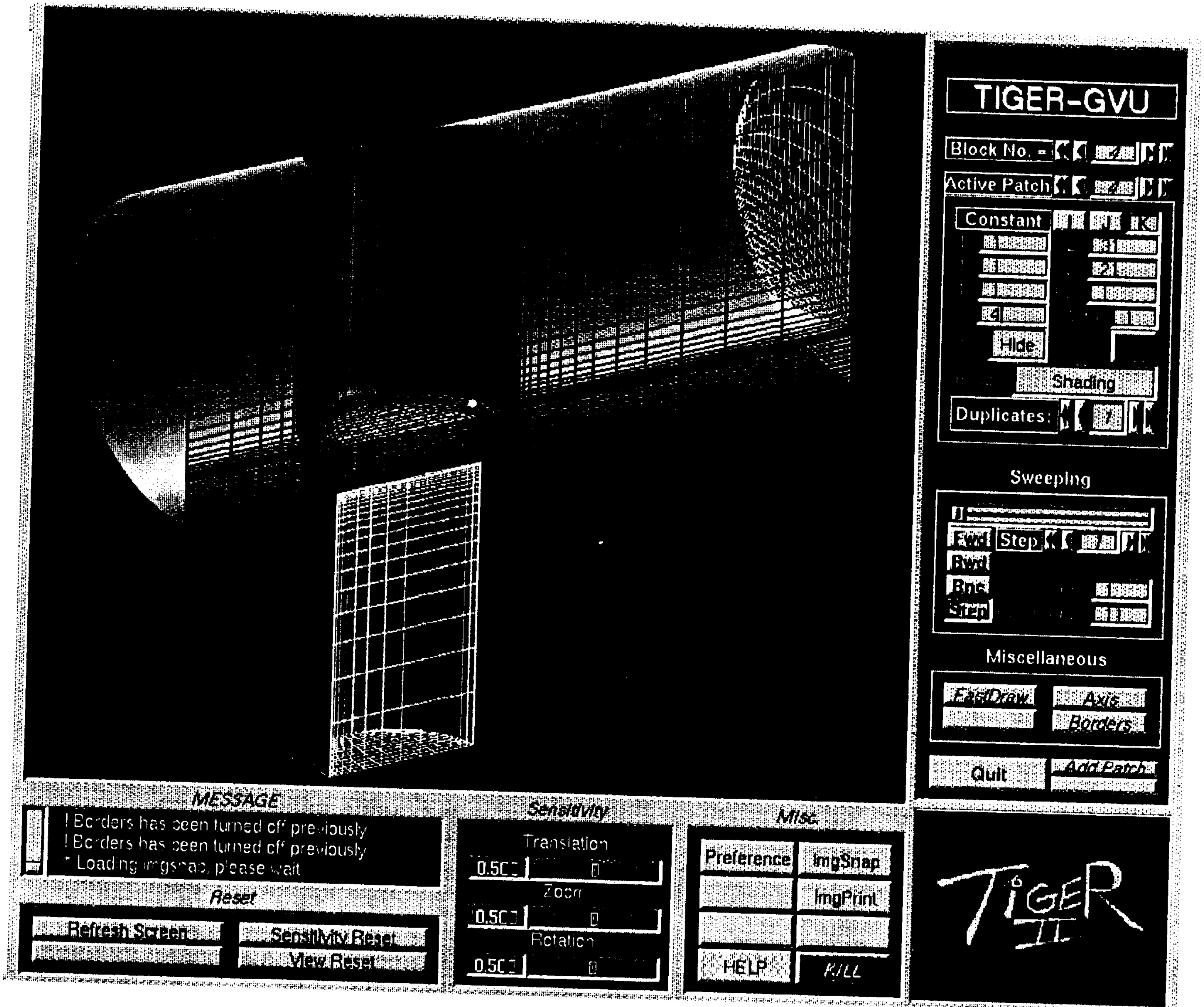

Figure 6. Three-dimensional grid (side-view)

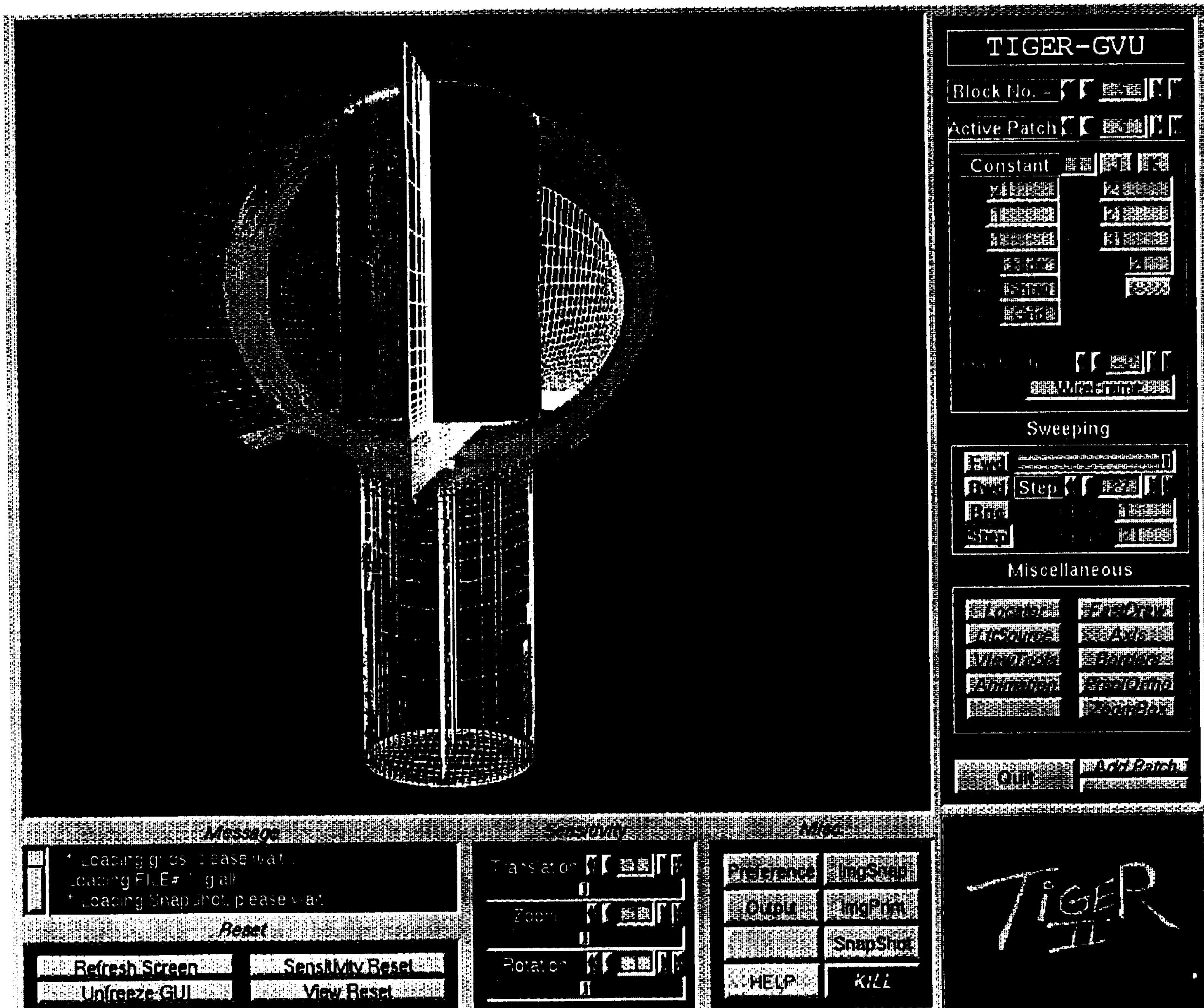

Figure 7. Three-dimensional grid (end-view)

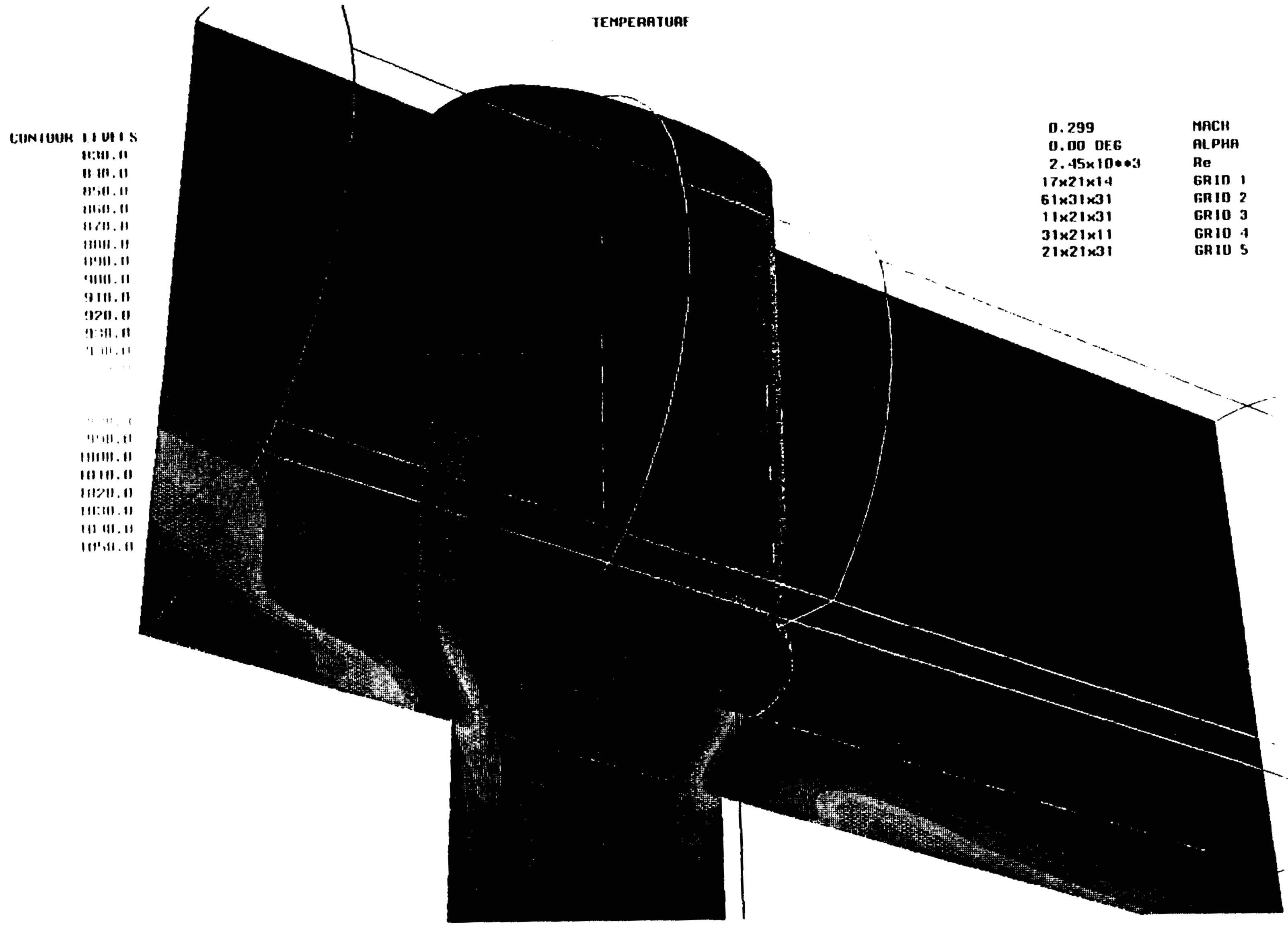

Figure 8. Temperature contours

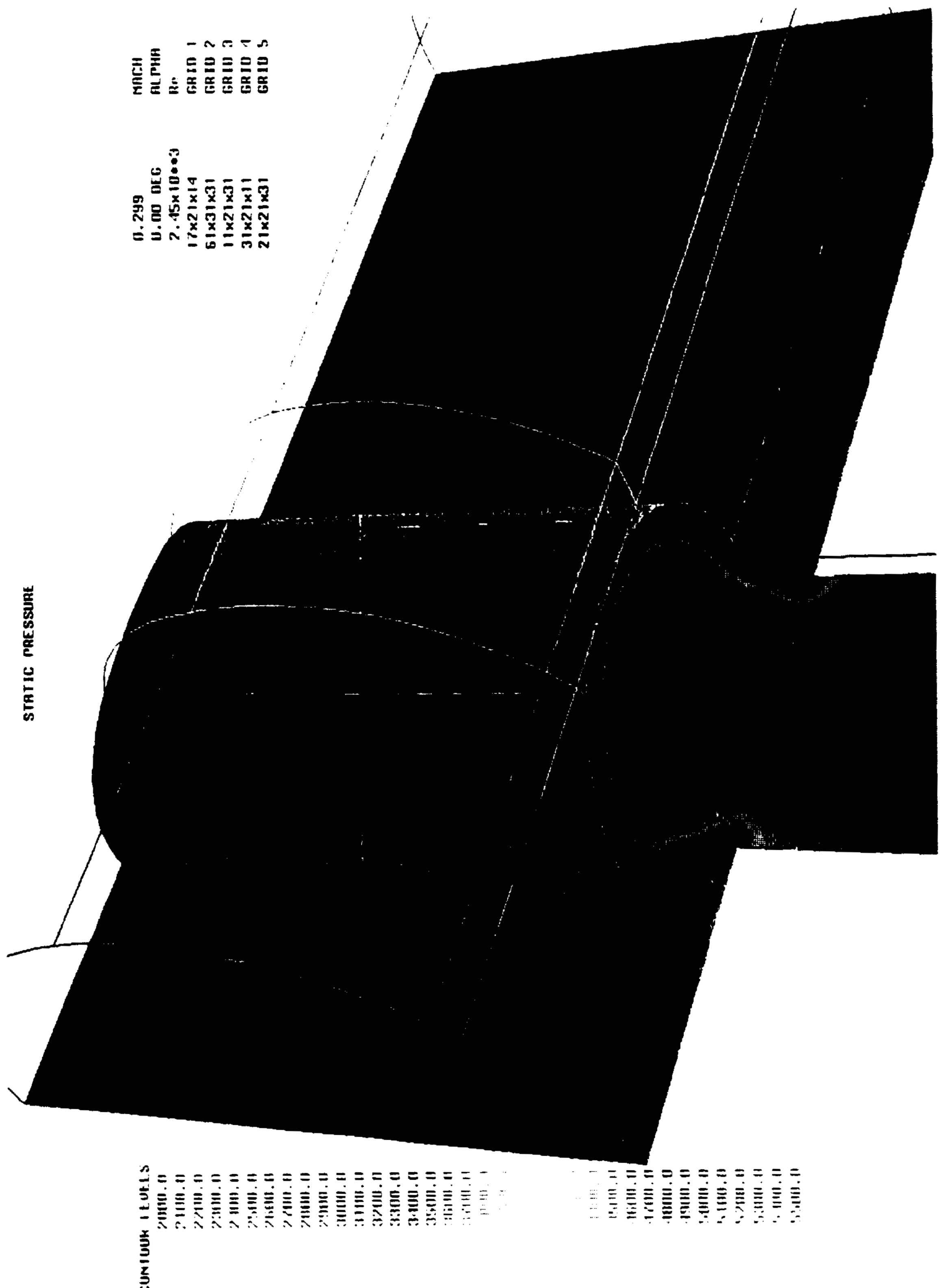

Figure 9. Pressure contours

ORIGINAL PAGE IS
OF POOR QUALITY

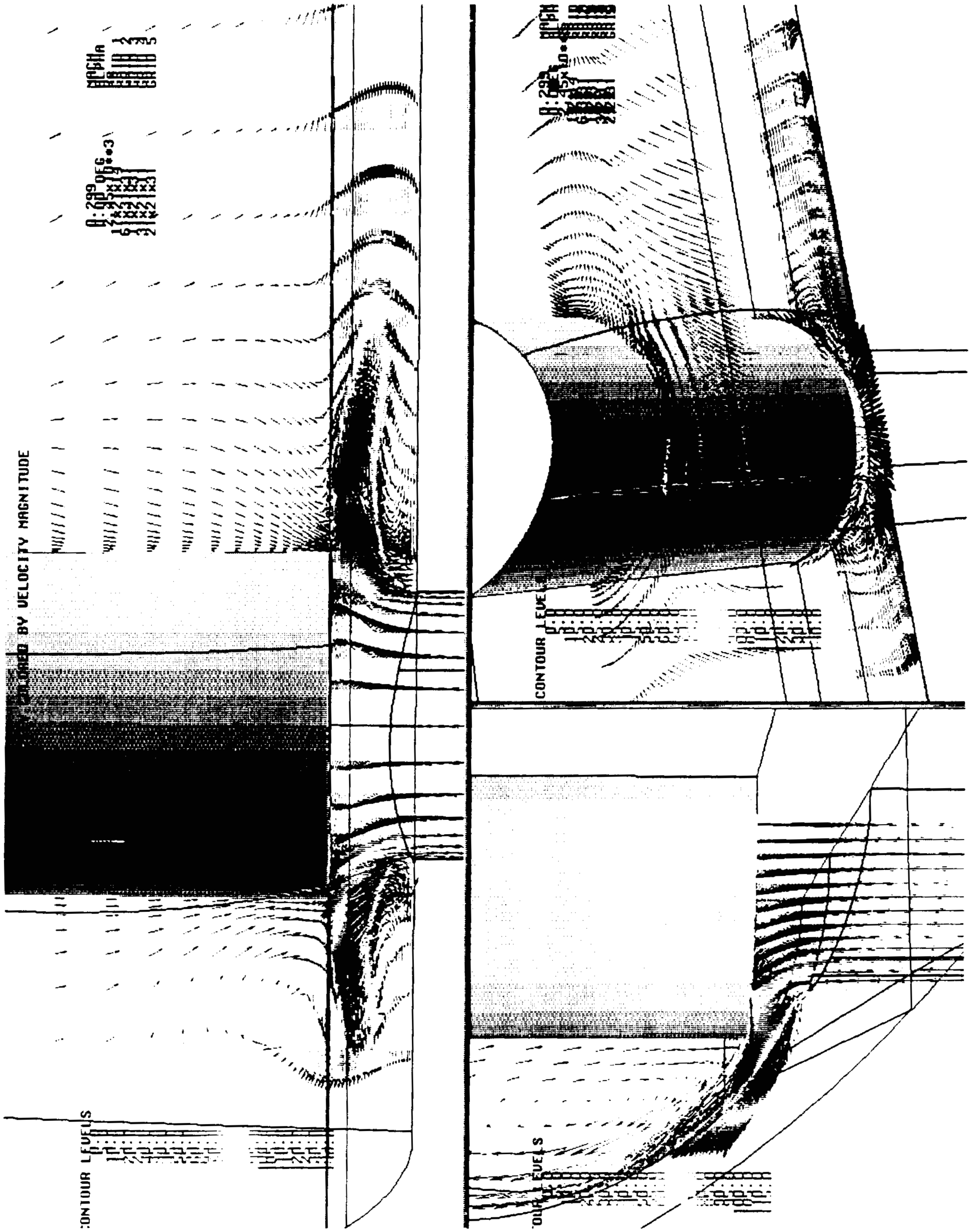

Figure 10. Velocity vectors

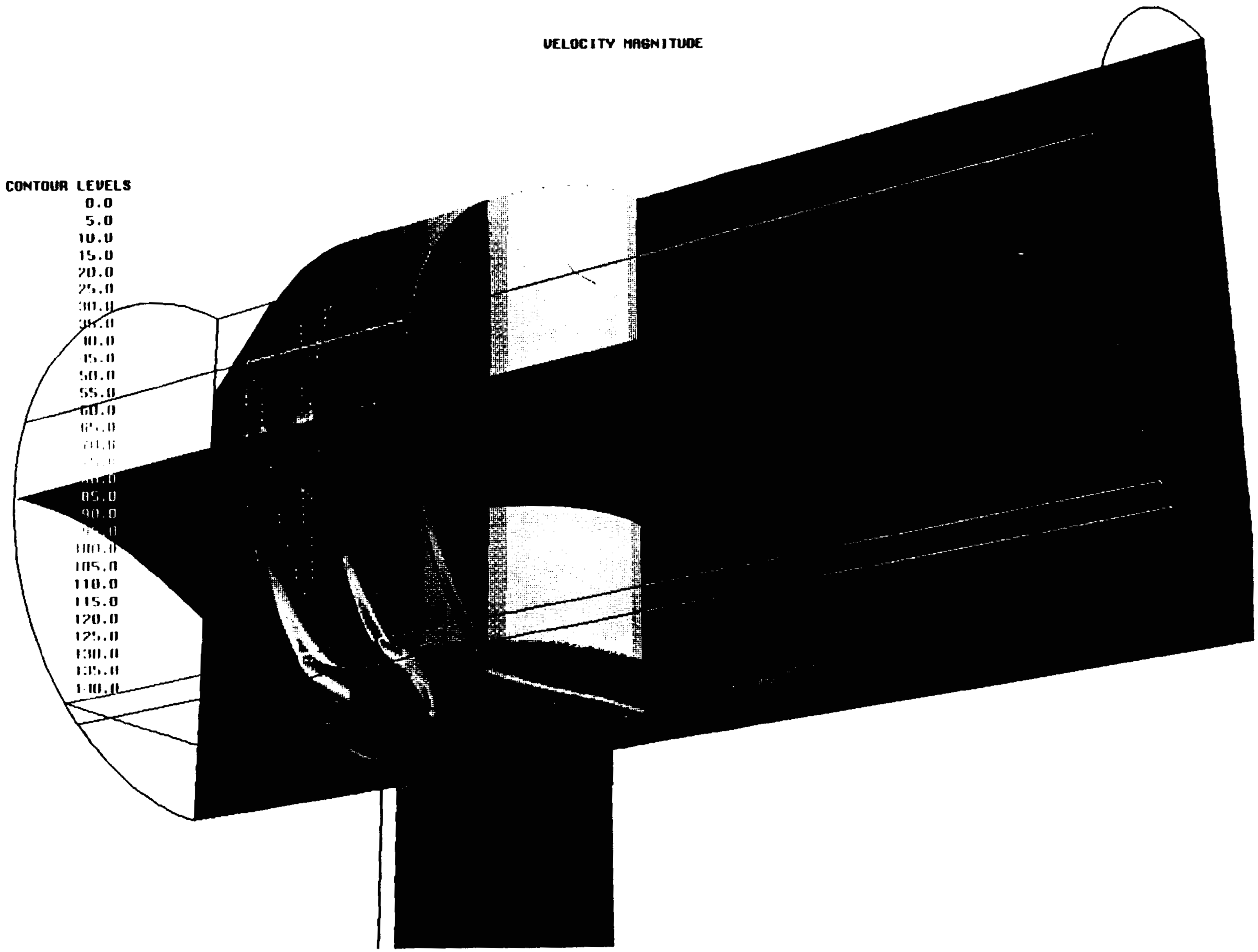

Figure 11. Velocity contours

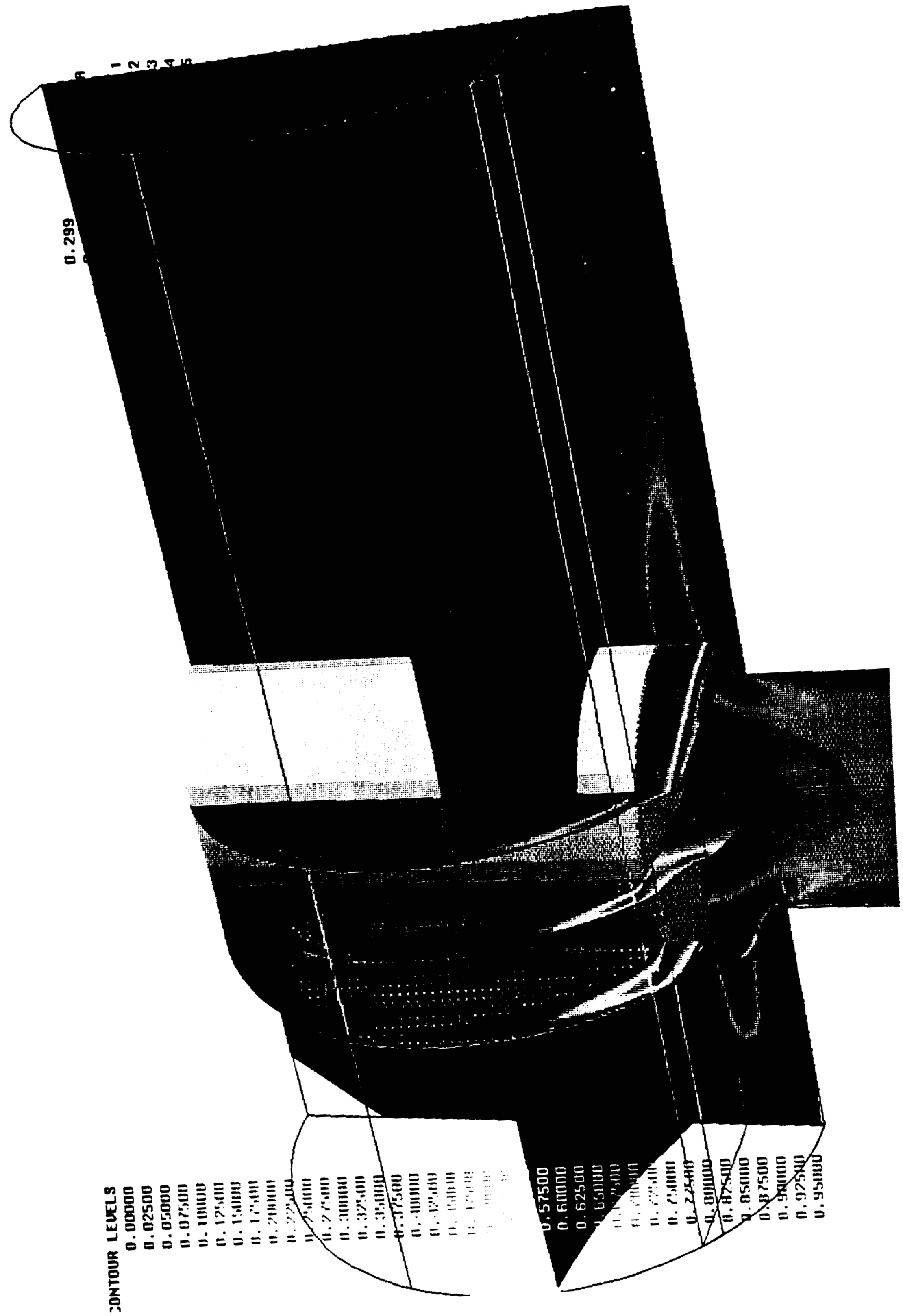

Figure 12. Mach contours

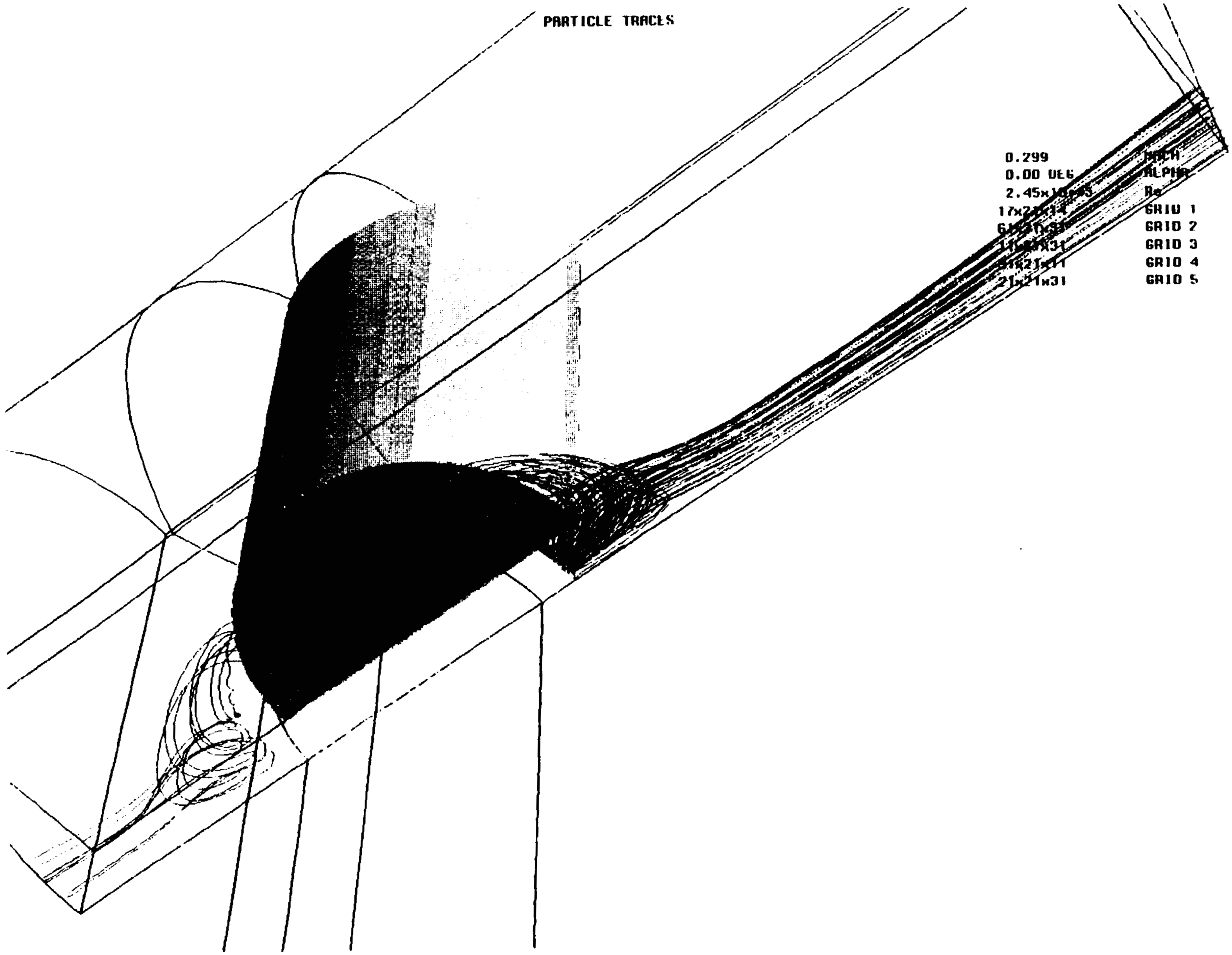

Figure 13. Particle tracing

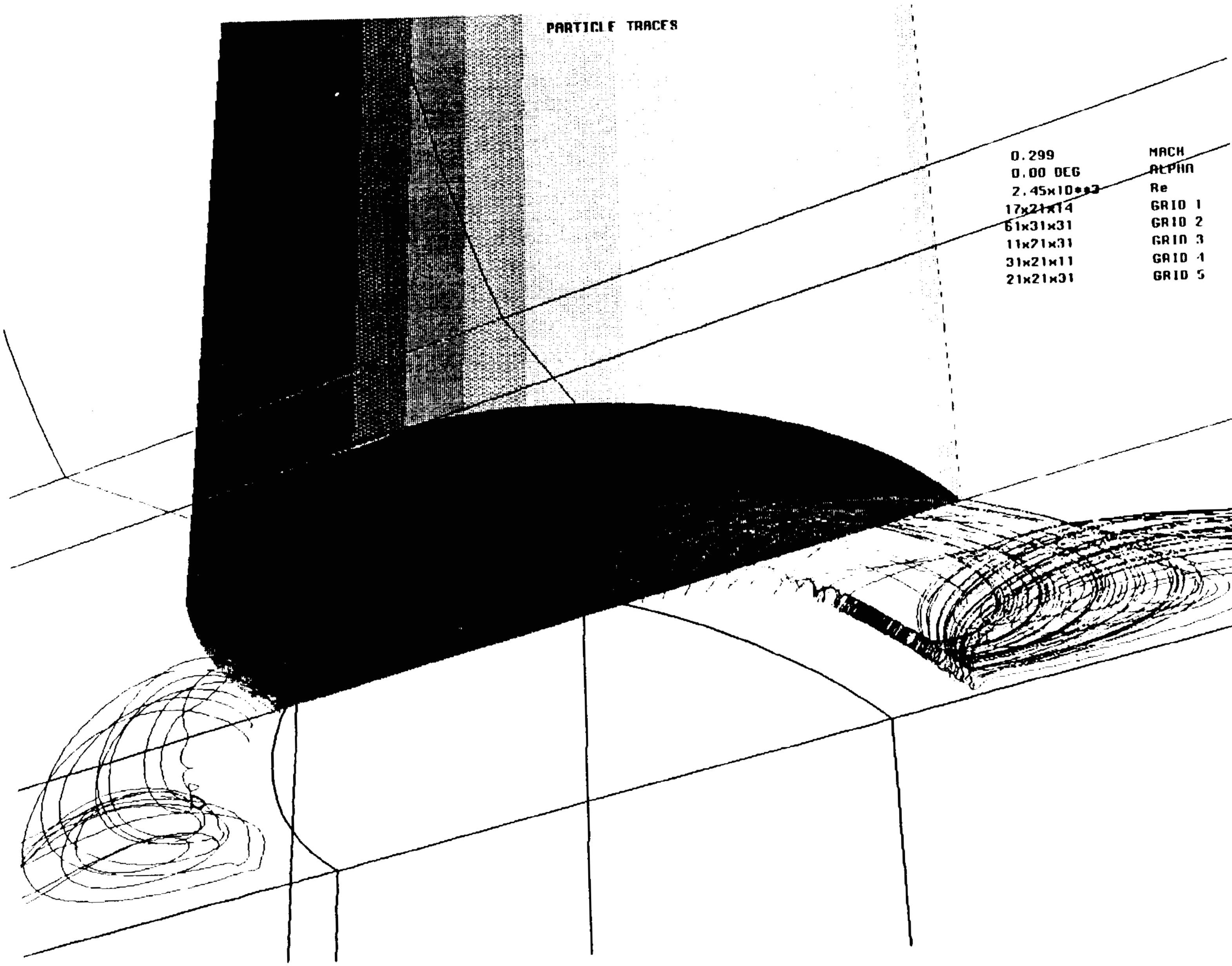

Figure 14. Particle tracing (close-up)

N95-23619

24-34
p. 24

COMPUTATIONAL FLUID DYNAMICS (CFD) ANALYSES IN SUPPORT OF SPACE SHUTTLE MAIN ENGINE (SSME) HEAT EXCHANGER (HX) VANE CRACKING INVESTIGATION

R. Garcia, T. Benjamin, and J. Cornelison
NASA/Marshall Space Flight Center, Alabama

A. J. Fredmonski
Pratt & Whitney, West Palm Beach, Florida

Integration issues involved with installing the alternate turbopump (ATP) High Pressure Oxygen Turbopump (HPOTP) into the SSME have raised questions regarding the flow in the HPOTP turnaround duct (TAD). Steady-state Navier-Stokes CFD analyses have been performed by NASA and Pratt & Whitney (P&W) to address these questions. The analyses have consisted of two-dimensional axisymmetric calculations done at Marshall Space Flight Center and three-dimensional calculations performed at P&W. These analyses have identified flowfield differences between the baseline ATP and the Rocketdyne configurations. The results show that the baseline ATP configuration represents a more severe environment to the inner HX guide vane. This vane has limited life when tested in conjunction with the ATP but infinite life when tested with the current SSME HPOTP. The CFD results have helped interpret test results and have been used to assess proposed redesigns. This paper includes details of the axisymmetric model, its results, and its contribution towards resolving the problem.

AXISYMMETRIC CFD ANALYSIS IN SUPPORT OF THE SSME HEAT EXCHANGER (HX) VANE CRACKING INVESTIGATION

R. Garcia
T. Benjamin
J. Cornelison
NASA/MSFC

A. J. Fredmonski
Pratt & Whitney/West Palm Beach, FL

11th Workshop for CFD
Application in Rocket Propulsion
Huntsville, AL
April 20-22, 1993

OVERVIEW OF MSFC CFD SUPPORT OF HX VANE CRACKING INVESTIGATION

OVERVIEW

- **Introduction/objective**
- **Approach:**
  - Testing
  - CFD analysis
- **Results**
  - Axisymmetric analysis
- **Conclusion/future work**

OVERVIEW OF MSFC CFD SUPPORT OF HX VANE CRACKING INVESTIGATION

INTRODUCTION

- **The inner Heat Exchanger (HX) guide vane cracks when tested with the Pratt & Whitney oxygen turbopump**
  - Flow environment about the vane varies with turbopump used (Pratt & Whitney vs. Rocketdyne)
  - HX vanes have not cracked when tested with Rocektdyne's oxygen turbopump
  - Inspection of cracked vanes indicates failure due to high cycle fatigue

OBJECTIVE

- **Identify potential sources of vane unsteady loading**
  - Differences between Rocketdyne and Pratt & Whitney configuration
- **Identify configurational changes to the turbopump to reduce unsteady loading**

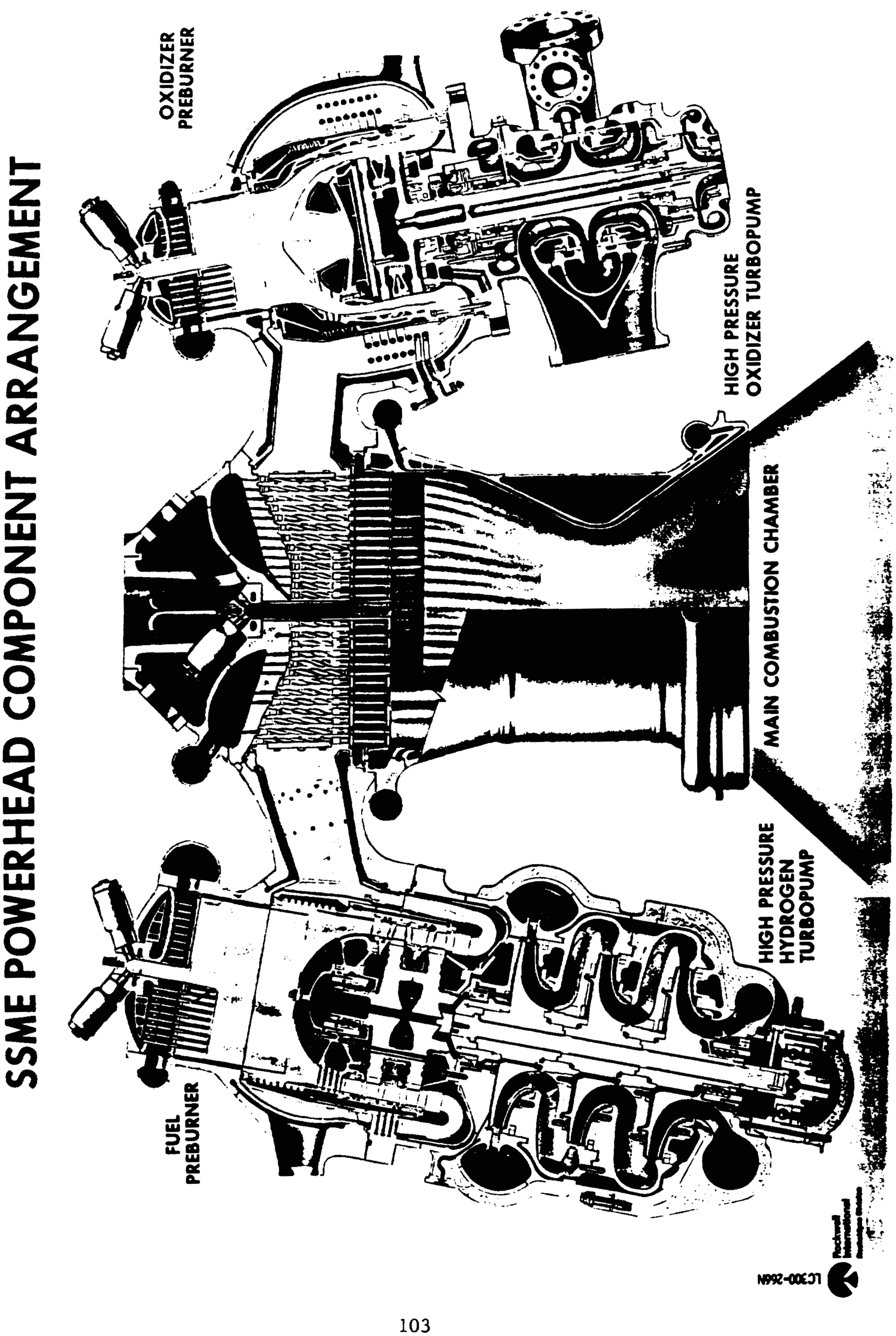
SSME POWERHEAD COMPONENT ARRANGEMENT
OXIDIZER PREBURNER
HIGH PRESSURE OXIDIZER TURBOPUMP
MAIN COMBUSTION CHAMBER
HIGH PRESSURE HYDROGEN TURBOPUMP
FUEL PREBURNER
LC300-266N

LOX TANK PRESS HEAT EXCHANGER ASSY

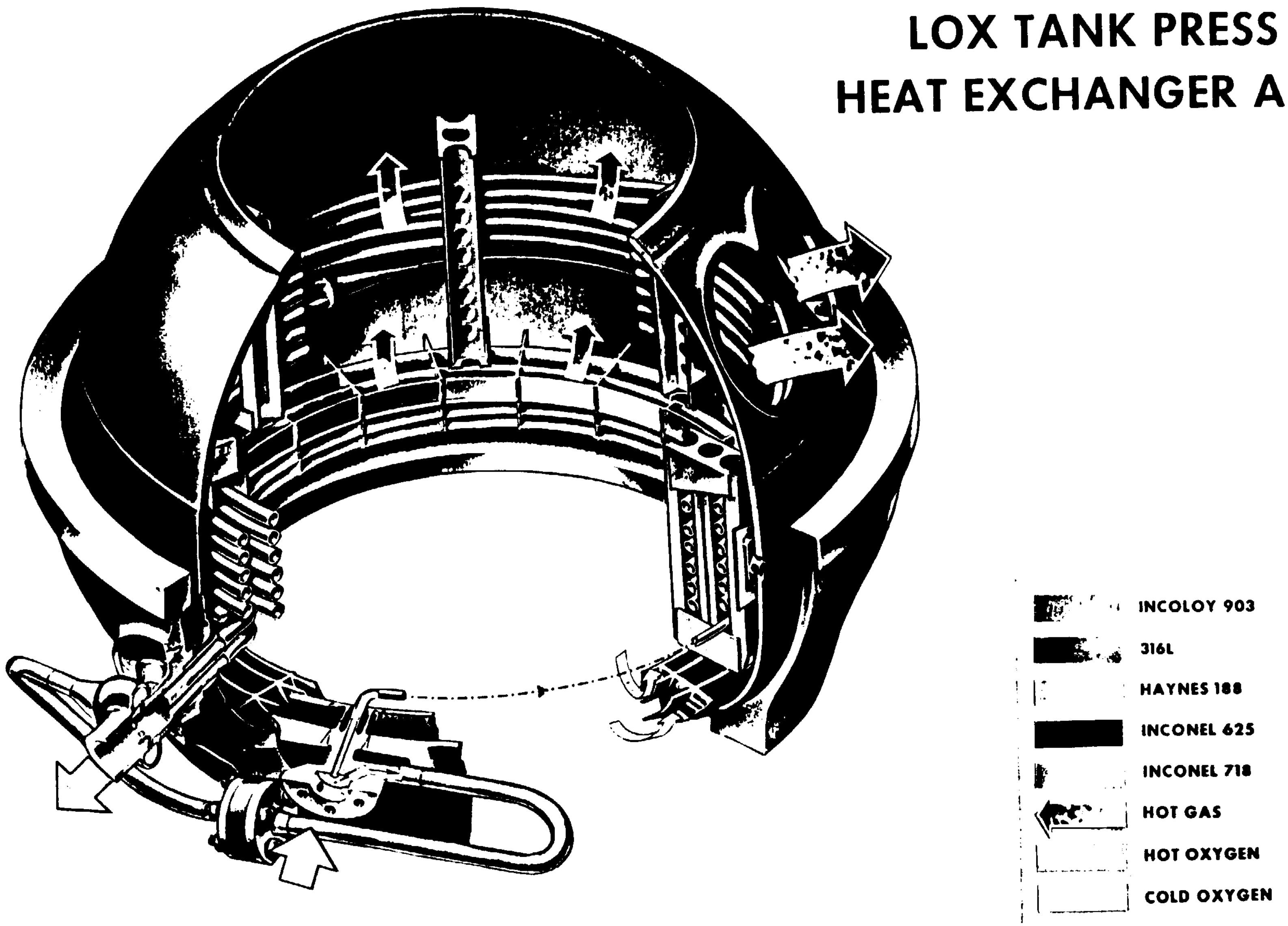

LC301-394D

Rocketdyne Division
Rockwell International

APPROACH: TESTING

- **2D Water-flow rig (Rocketdyne and Pratt & Whitney)**
  - Used for flow visualization and qualitative CFD results validation
- **2D air-flow rig (Rocketdyne)**
  - Provides turbulent pressure fluctuations and preliminary evaluation of potential fixes
- **3D air-flow rig (MSFC)**
  - Full simulation of duct geometry
  - Provides unsteady pressure levels and vane strain levels
- **Hot fire testing (Pratt & Whitney and SSC)**
  - Actual environment, duration testing
  - Provides HX vane strain levels

APPROACH: CFD ANALYSIS

- **Modified Euler, multi-stage turbine analysis (Pratt & Whitney)**
  - Provided duct inlet velocity field for both baseline geometries
- **Single stage Navier-Stokes turbine analysis (Rocketdyne, REACT3D)**
  - Verified modified Euler predictions
- **Axisymmetric steady CFD analysis (MSFC, REFLEQS)**
  - Provided two day turnaround capability
  - Used to identify differences between baseline configurations
  - Used to evaluate all proposed fixes, and test rig configurations
- **3D symmetric discharge CFD analysis (Pratt & Whitney)**
  - Included effect of axial strut on flowfield
- **Axisymmetric, unsteady CFD analysis (Rockwell, USA)**
  - Used to identify unsteady flow features not captured by the steady analysis

APPROACH: AXISYMMETRIC, STEADY ANALYSIS

- **Assembled a three member team: grids, codes, and post-processing**
- **Geometries to be analyzed generated at Pratt & Whitney or at MSFC**
- **Grids generated using GENIE**
  - Typical grid size: 175 X 51
- **Model included splitter vanes, HX vanes, and the first five HX coils**
  - Axial struts and asymmetric discharge not included
- **CFD code REFLEQS with the K-ε turbulence model**
  - Pressure based, finite volume method
  - Fully implicit formulation
  - SIMPLEC solution algorithm
  - On YMP: 118 μsec/point/iteration, 136 words/point

OVERVIEW OF MSFC CFD SUPPORT OF HX VANE CRACKING INVESTIGATION

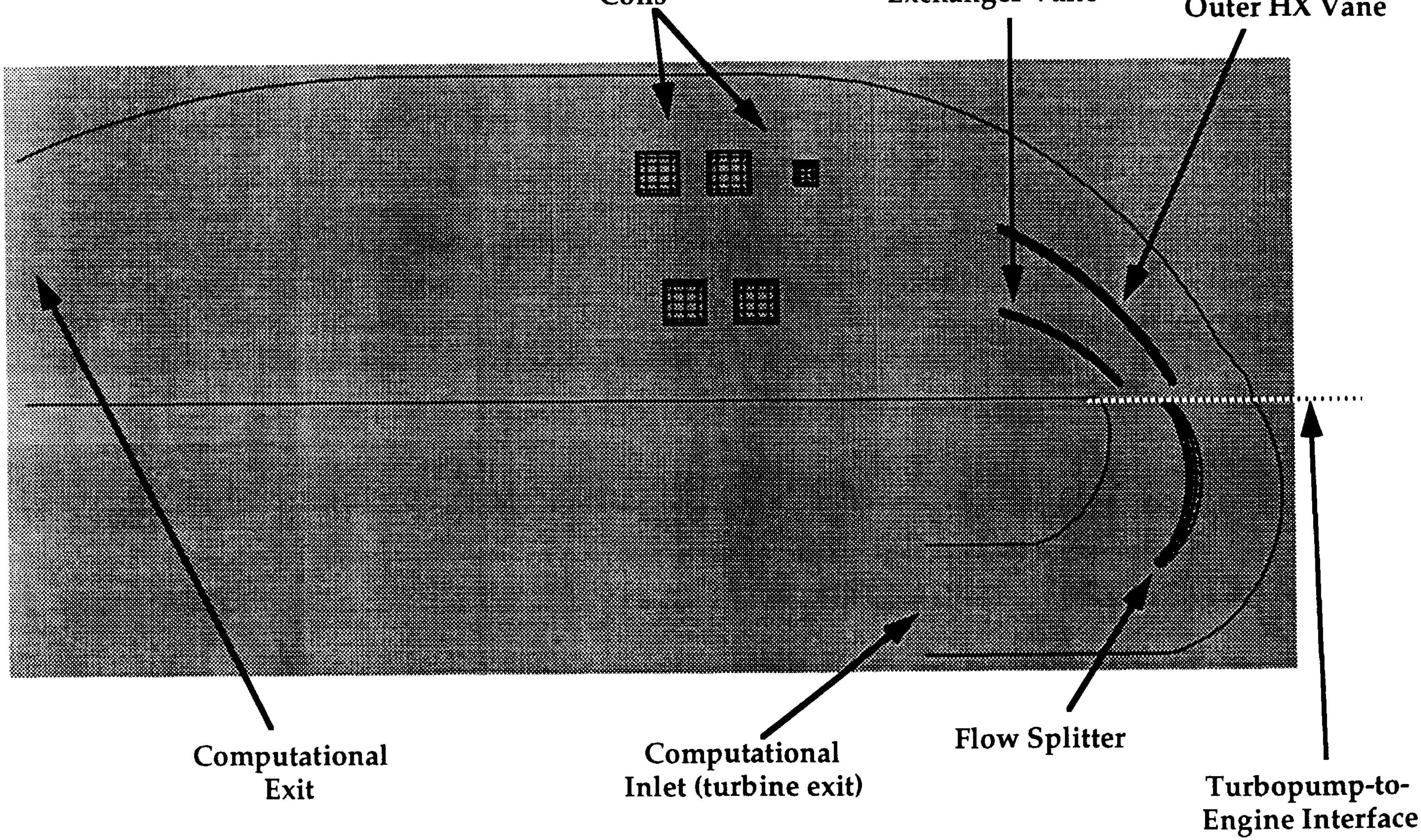

APPROACH: AXISYMMETRIC, STEADY ANALYSIS

- **Full-upwind formulation used to obtain solutions**
- **Fixed inlet velocity field, fixed exit pressure**
- **Solution process initiated with inlet condition, "empty" flowfield, heavy under-relaxation**
- **Engineering solution typically obtained with 1,500 iterations**
  - Always continued to run to at least 3,000 iterations
- **Sensitivity of solution to various parameters assessed**
  - Grid spacing, differencing scheme, inlet turbulence levels
- **Solutions qualitatively compared to 2D test rigs**
- **Code solutions used to obtain relative comparisons between configurations**
  - Absolute quantities treated with caution
- **Goal was to try to match the Rocketdyne velocity and turbulence fields**

RESULTS

- **Primary difference between Rocketdyne and Pratt & Whitney baseline flowfields due to turbine exit flow**
  - Rocketdyne has radially inward flow, Pratt & Whitney radially outward
- **Turbine exit flow difference leads to higher velocities in the inner HX vane region for the Pratt & Whitney configuration**
  - Higher dynamic pressure, more severe turbulence buffeting
- **Approximately 45 cases modeled to date**
  - Approximately half were of different configurations
- **Solutions have been evaluated for:**
  - Flow split across the splitter
  - Velocity and turbulence intensity profile at the turbopump-to-engine interface
  - Velocity and turbulence intensity profile at the HX coils

OVERVIEW OF MSFC CFD SUPPORT OF HX VANE CRACKING INVESTIGATION

Turbine Exit Profiles:

ATD: Radially outward flow vector

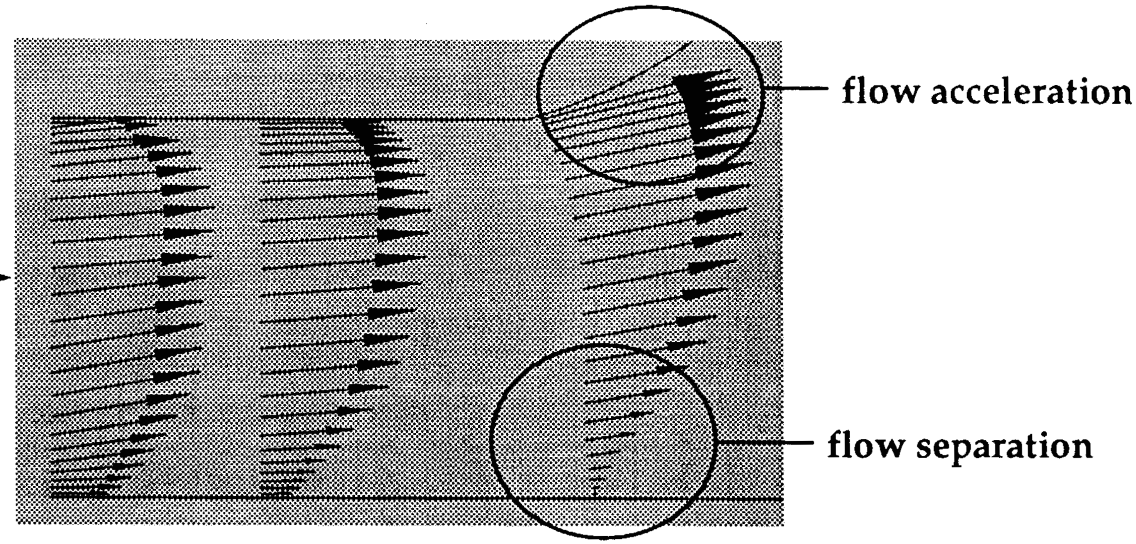

Rkdn: Radially inward flow vector

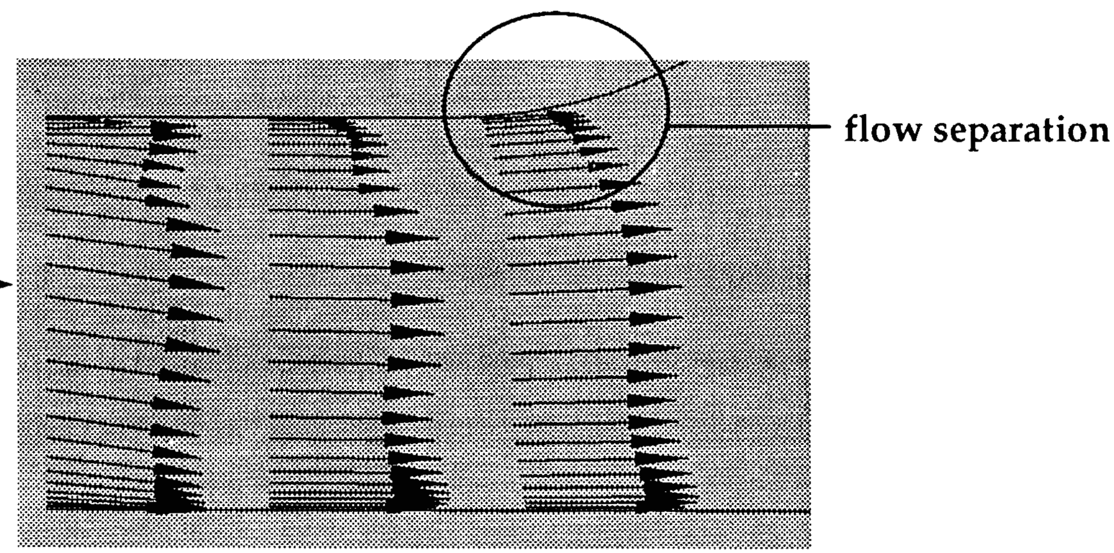

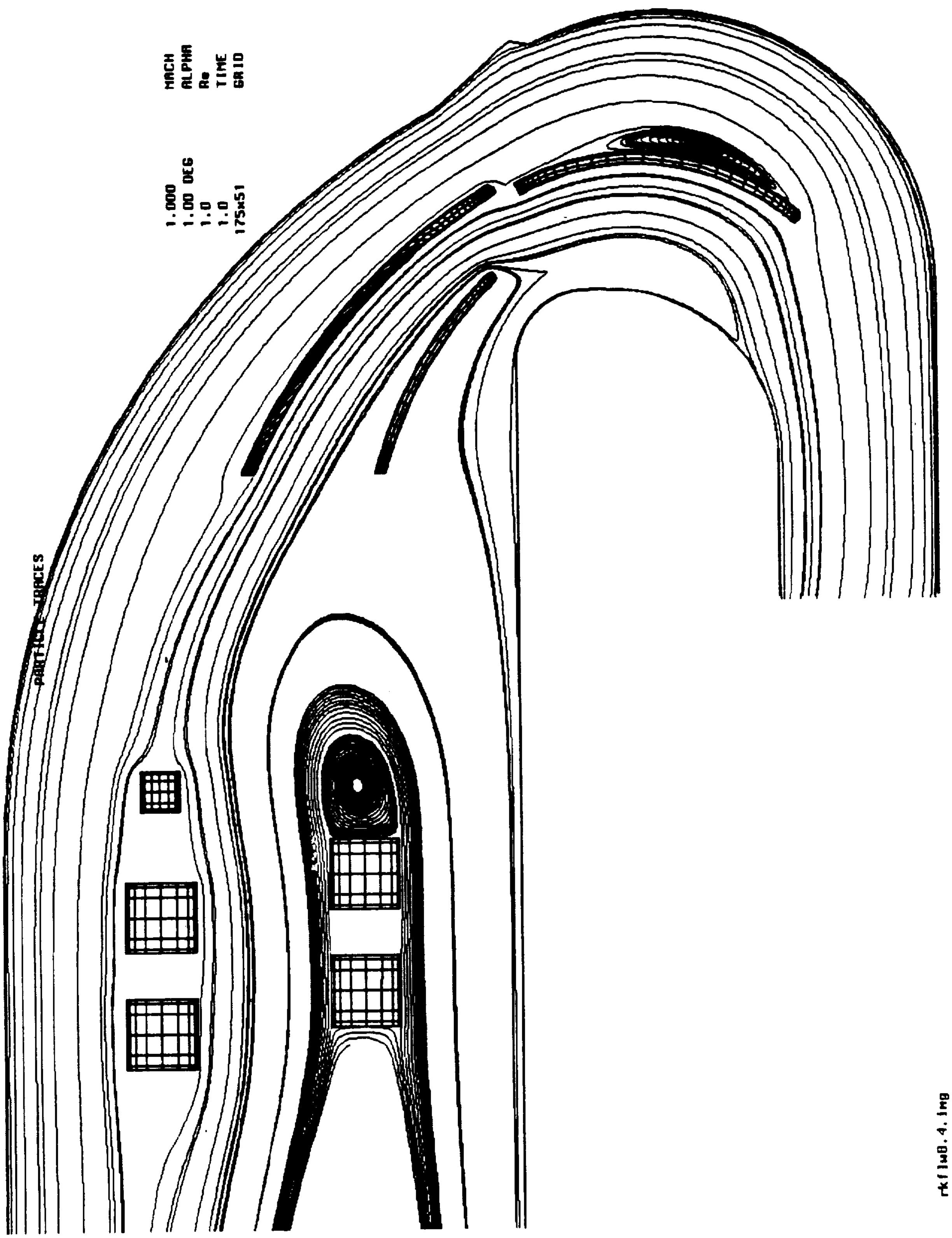
PARTICLE TRACES
1.000 MACH
1.00 DEG ALPHA
1.0 Re
1.0 TIME
175x51 GRID
rkflw0.4.img

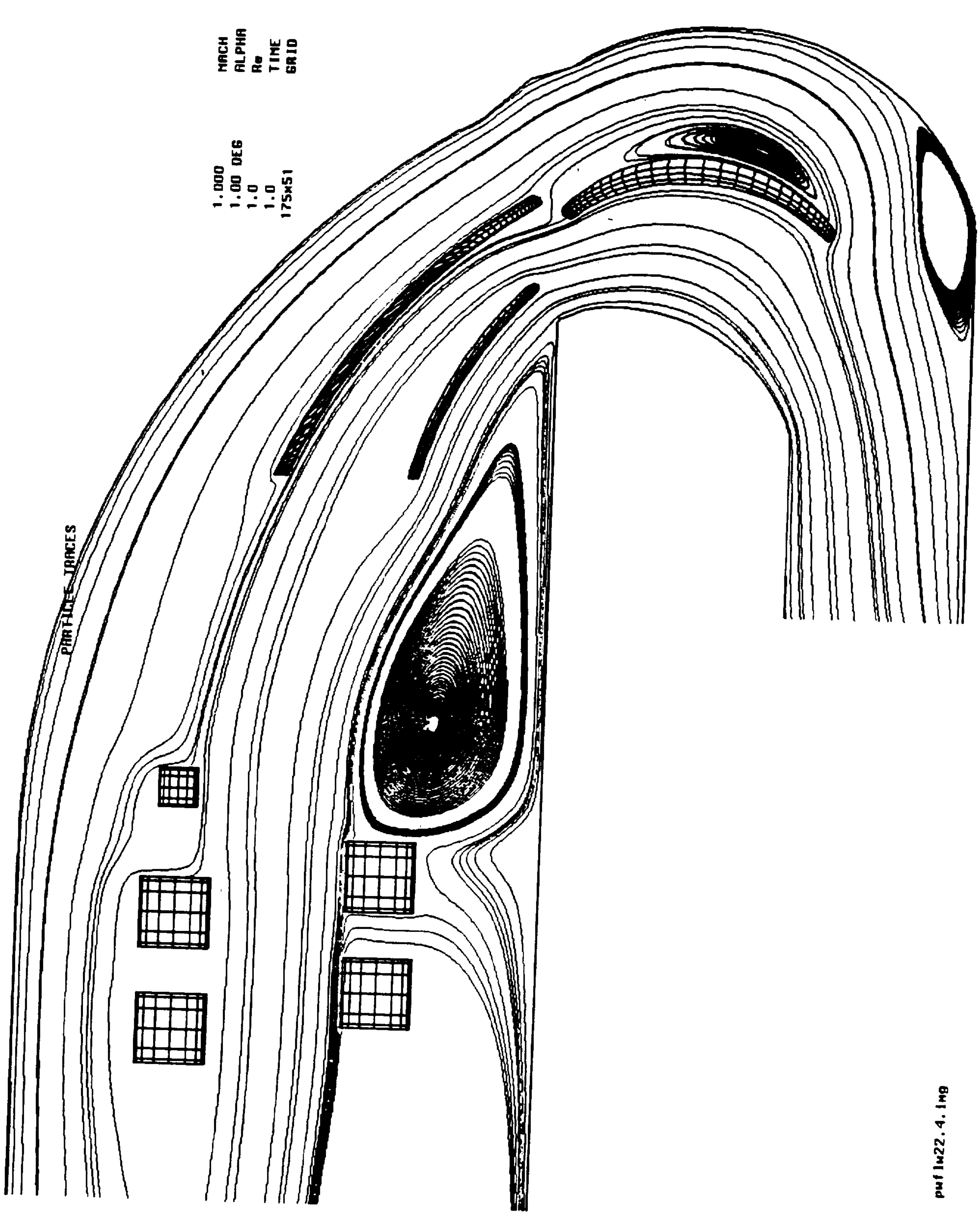

PARTICLE TRACES
MACH 1.000
ALPHA 1.00 DEG
Re 1.0
TIME 1.0
GRID 175x51
pwflw22.4.img

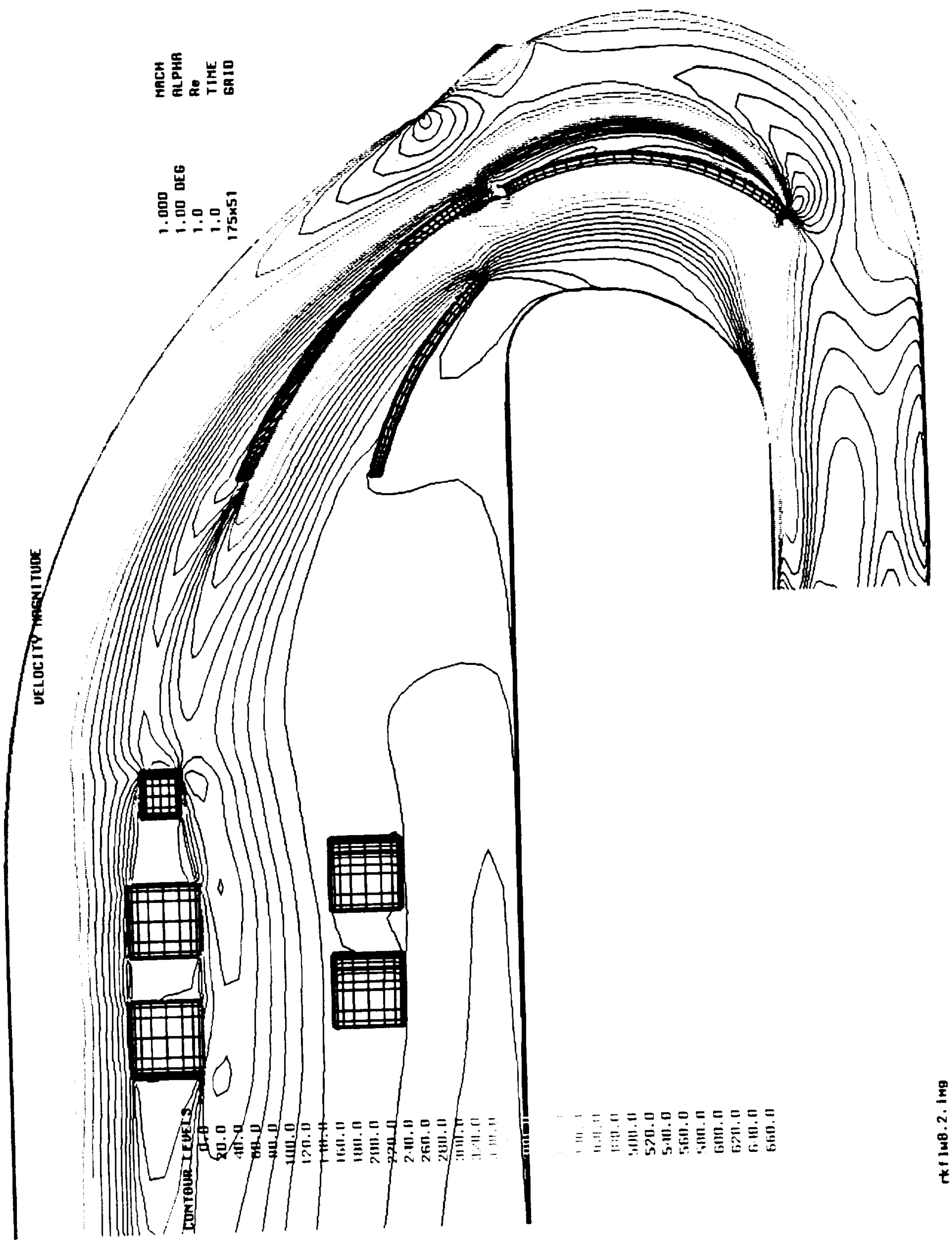
VELOCITY MAGNITUDE
MACH 1.000
ALPHA 1.00 DEG
Re 1.0
TIME 1.0
GRID 175x51
CONTOUR LEVELS
520.0
540.0
560.0
620.0
660.0
rkflw8.2.img

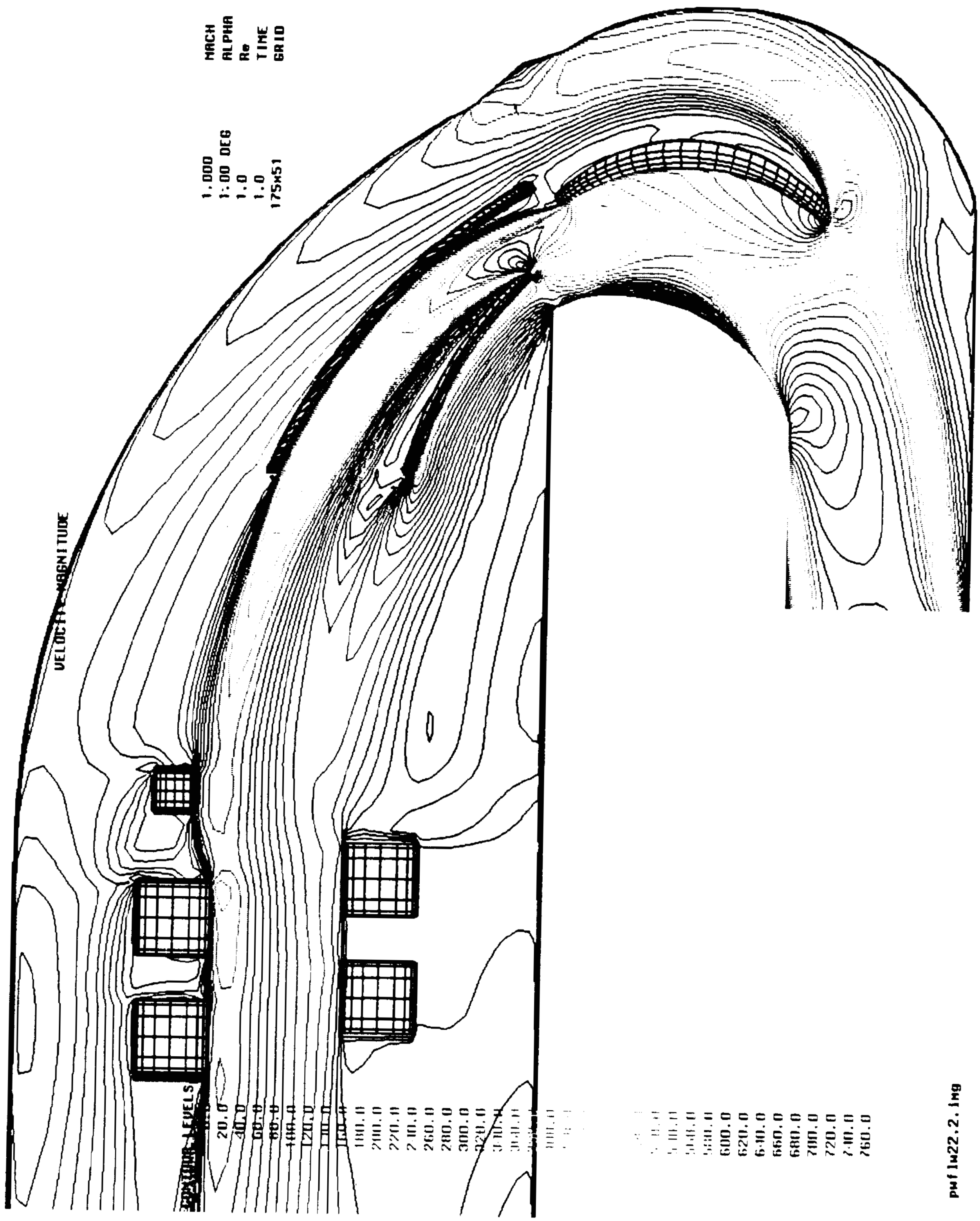
VELOCITY MAGNITUDE
MACH 1.000
ALPHA 1.00 DEG
Re 1.0
TIME 1.0
GRID 175x51
CONTOUR LEVELS
20.0
40.0
600.0
620.0
660.0
680.0
700.0
720.0
760.0
pwflw22.2.img

Examples of Geometries Modeled

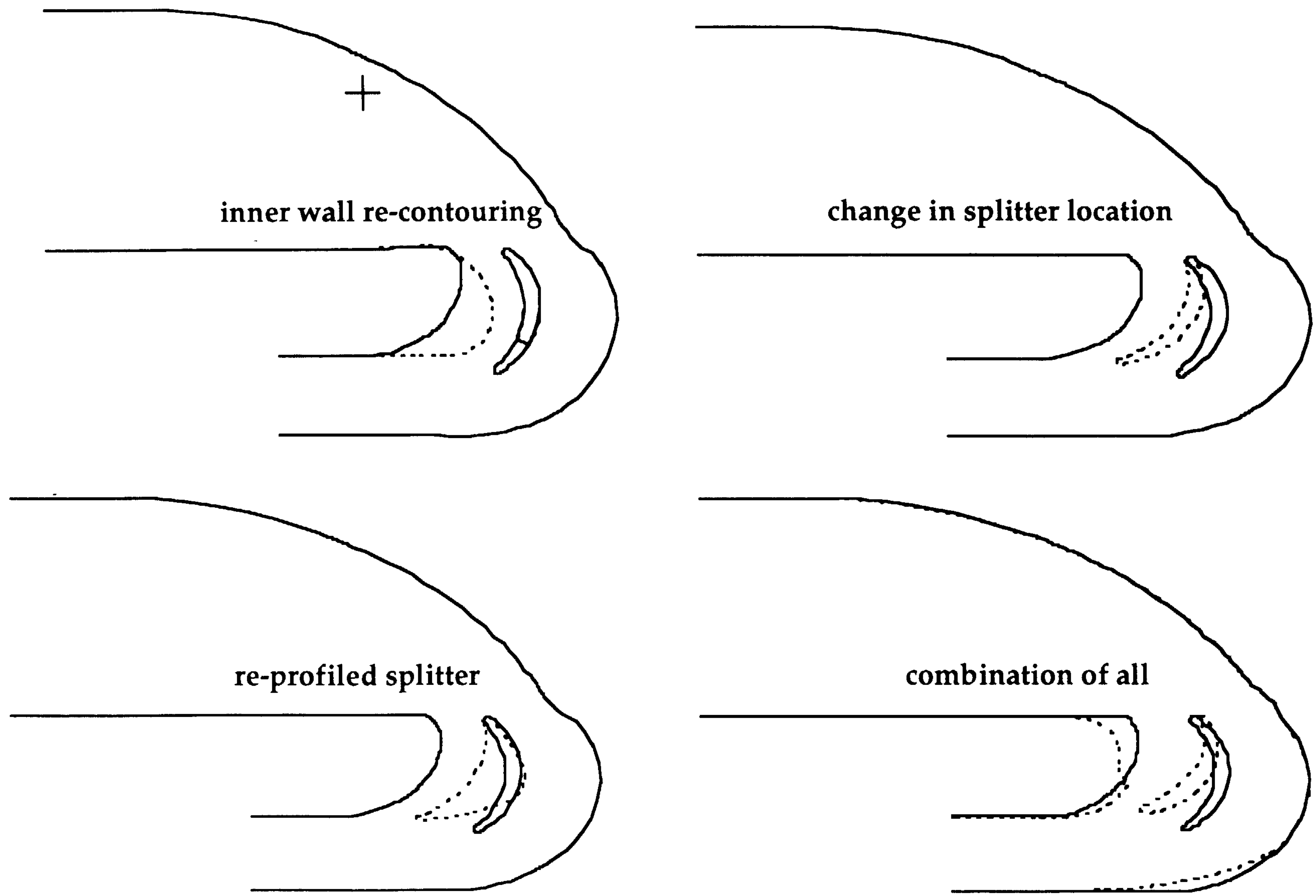

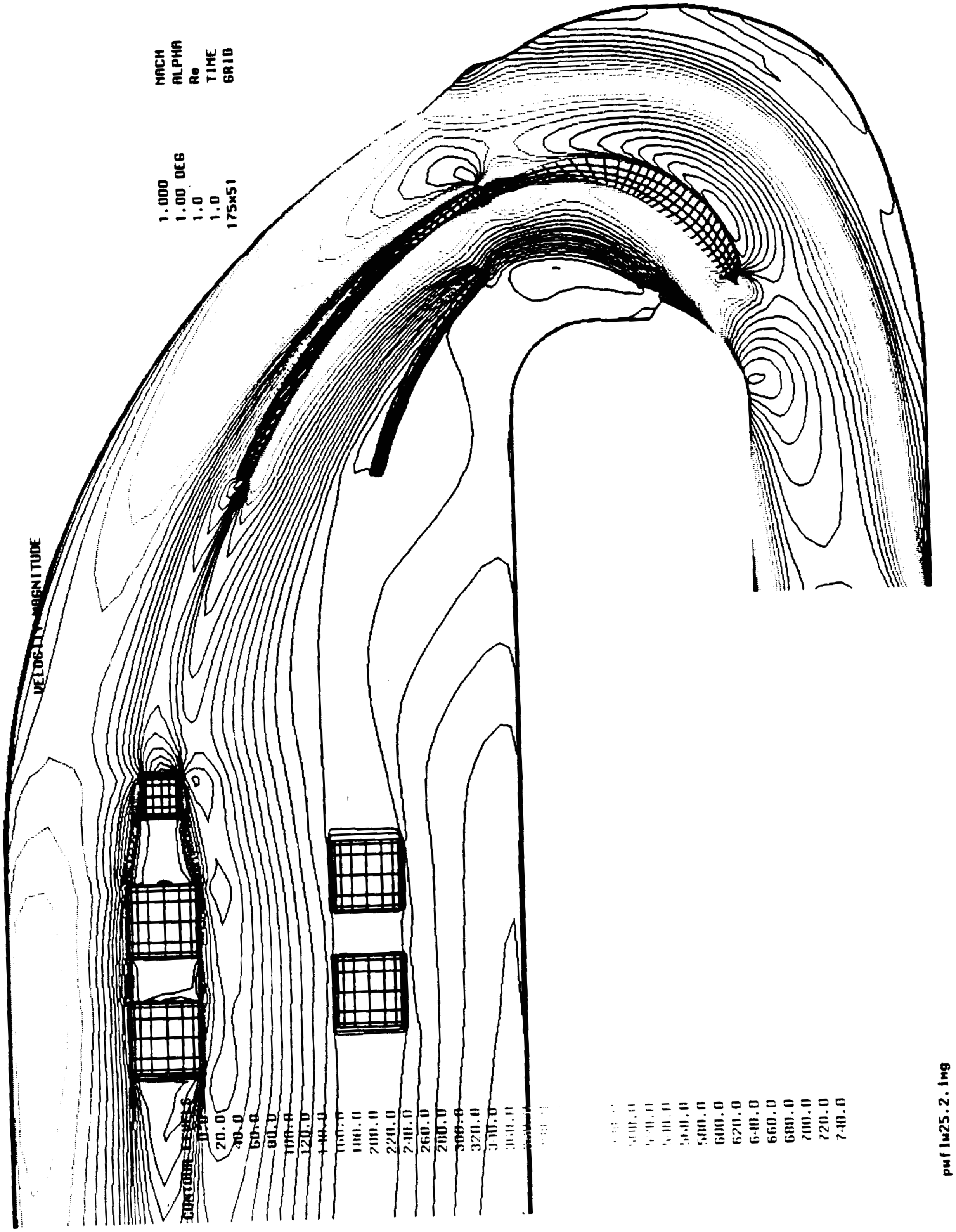

ORIGINAL PAGE IS
OF POOR QUALITY

RESULTS

- **Configuration identified that closely matches the Rocketdyne baseline velocity profile at the engine interface**

- **Predicted turbulence intensity similar to Rocketdyne configuration**
  - Peak turbulence intensity near the vane surfaces reduced ~ by a factor of 2

- **Environment in the HX coils region similar to or better than Rocketdyne baseline**

CONCLUSION/FUTURE WORK

- **Quick turnnaround CFD capability demonstrated**

- **Potential source and fix to the problem identified**

- **Increased sensitivity among analysts to turbulence field**
  - K prediction, shear layer strengths

- **Presently generating full 3D grid**
  - To identify circumferential variation that may intensify turbulence levels
  - To assure that the proposed fix is not impaired functionally by 3D effects

OVERVIEW OF MSFC CFD SUPPORT OF HX VANE CRACKING INVESTIGATION

Velocity Profile at the Engine Interface
Radial Velocity

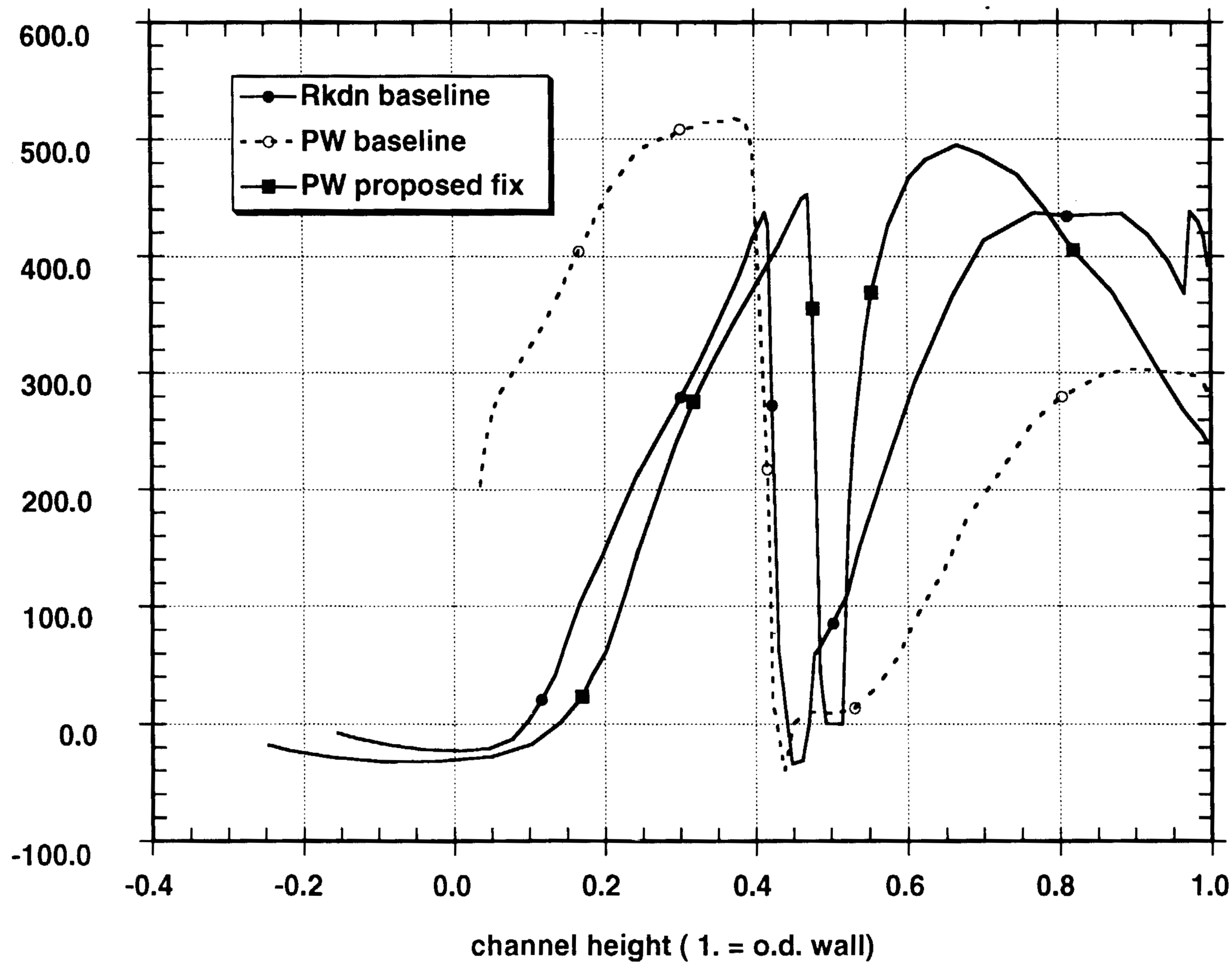

Relative Peak Turbulence Intensity

(Rkdn levels used as reference at each loca

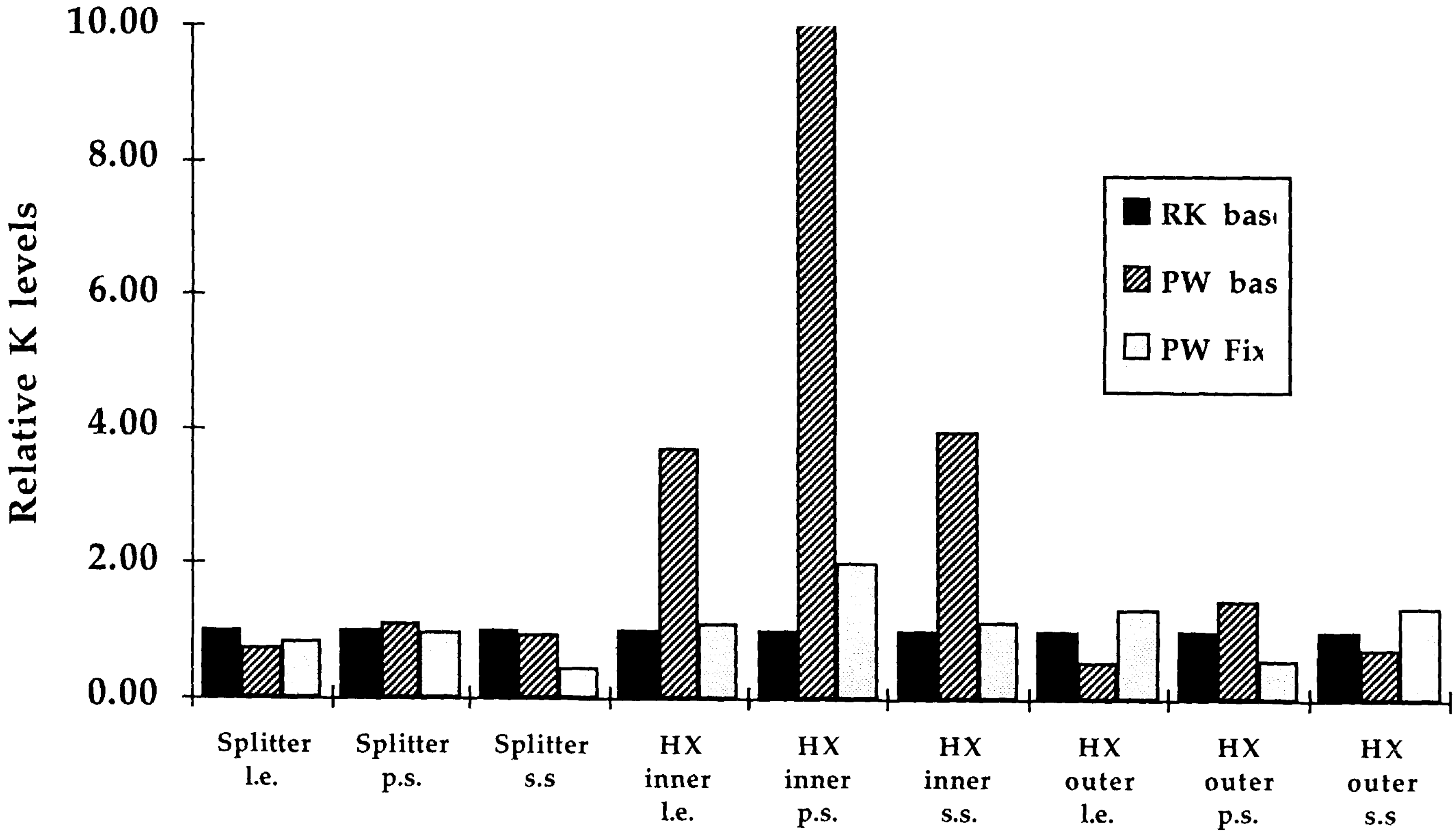

OVERVIEW OF MSFC CFD SUPPORT OF HX VANE CRACKING INVESTIGATION

Velocity Profile at the HX Coils
Axial Velocity

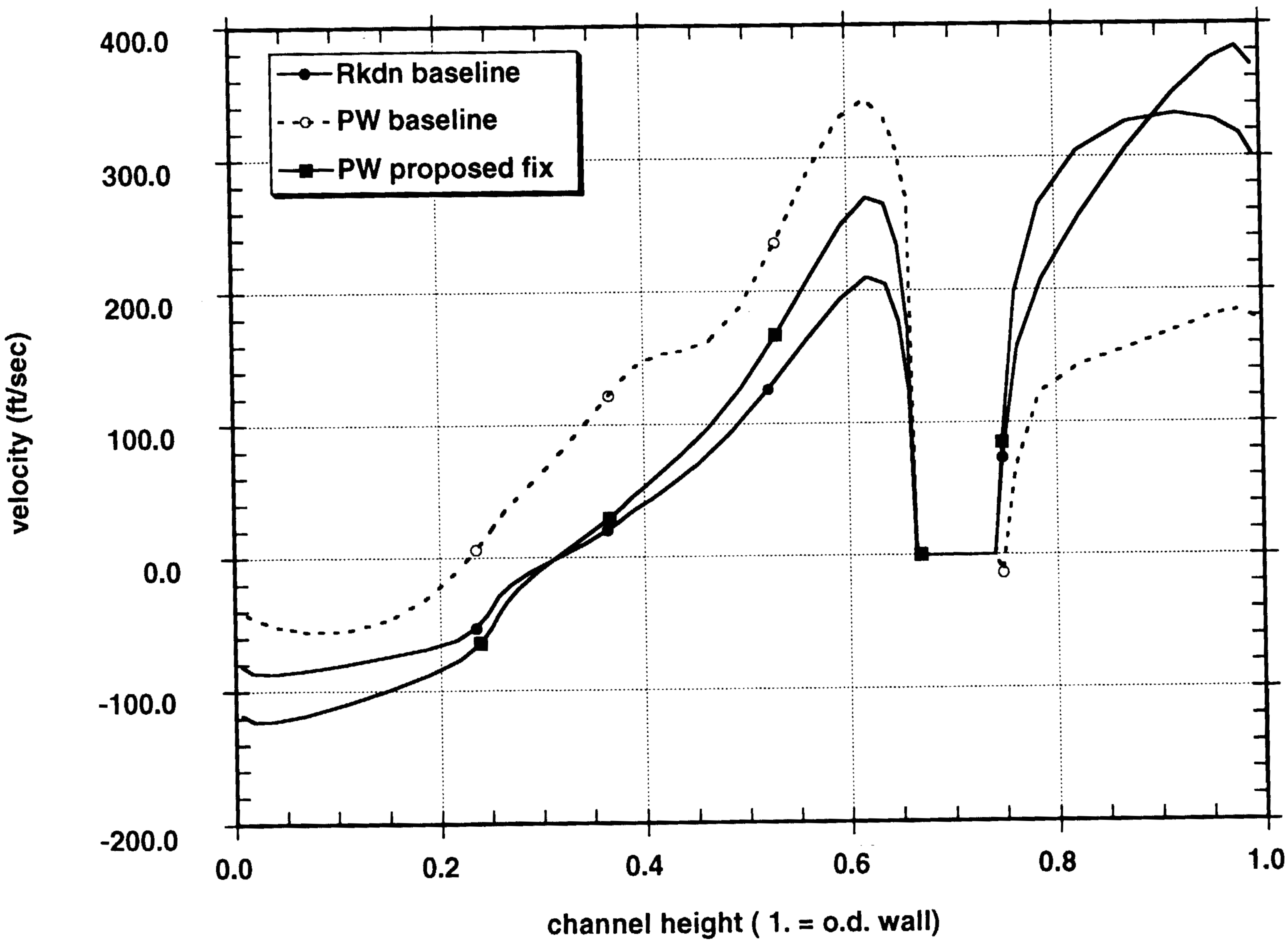

N95- 23620

3D FLOW ANALYSIS OF THE ALTERNATE SSME HPOT TAD

C.A.Kubinski
Government Engines & Space Propulsion Division
West Palm Beach, Florida

ABSTRACT

This paper describes the results of numerical flow analyses performed in support of design development of the Space Shuttle Main Engine Alternate High Pressure Oxidizer Turbine Turn–around duct (TAD). The flow domain has been modeled using a 3D, Navier–Stokes, general purpose flow solver. The goal of this effort is to achieve an alternate TAD exit flow distribution which closely matches that of the baseline configuration. 3D Navier Stokes CFD analyses were employed to evaluate numerous candidate geometry modifications to the TAD flowpath in order to achieve this goal. The design iterations are summarized, as well as a description of the computational model, numerical results and the conclusions based on these calculations.

Workshop for Computational Fluid Dynamics Applications in Rocket Propulsion, NASA MSFC

3D Flow Analysis of the Alternate SSME HPOT TAD

Cheryl A. Kubinski
Pratt & Whitney (GESP)
April 20, 1993

SSME ATD HPOT TAD REDESIGN

Outline

I. Problem Overview

II. Background – Differences Between Rocketdyne Baseline and ATD HPOT TAD

- Geometrical
- Aerodynamic

III. Approach

- Minimize Differences using CFD tools to predict flowfield differences

IV. Status

- Modified ATD TAD Configuration Defined Which Emulates Rocketdyne Baseline

SSME ATD HPOT TAD REDESIGN

Problem Overview

Engine Turning Vane Cracking Investigation

- Engine turning cracking occurs at inside vane leading edge, pressure and suction side.

Heat Exchanger

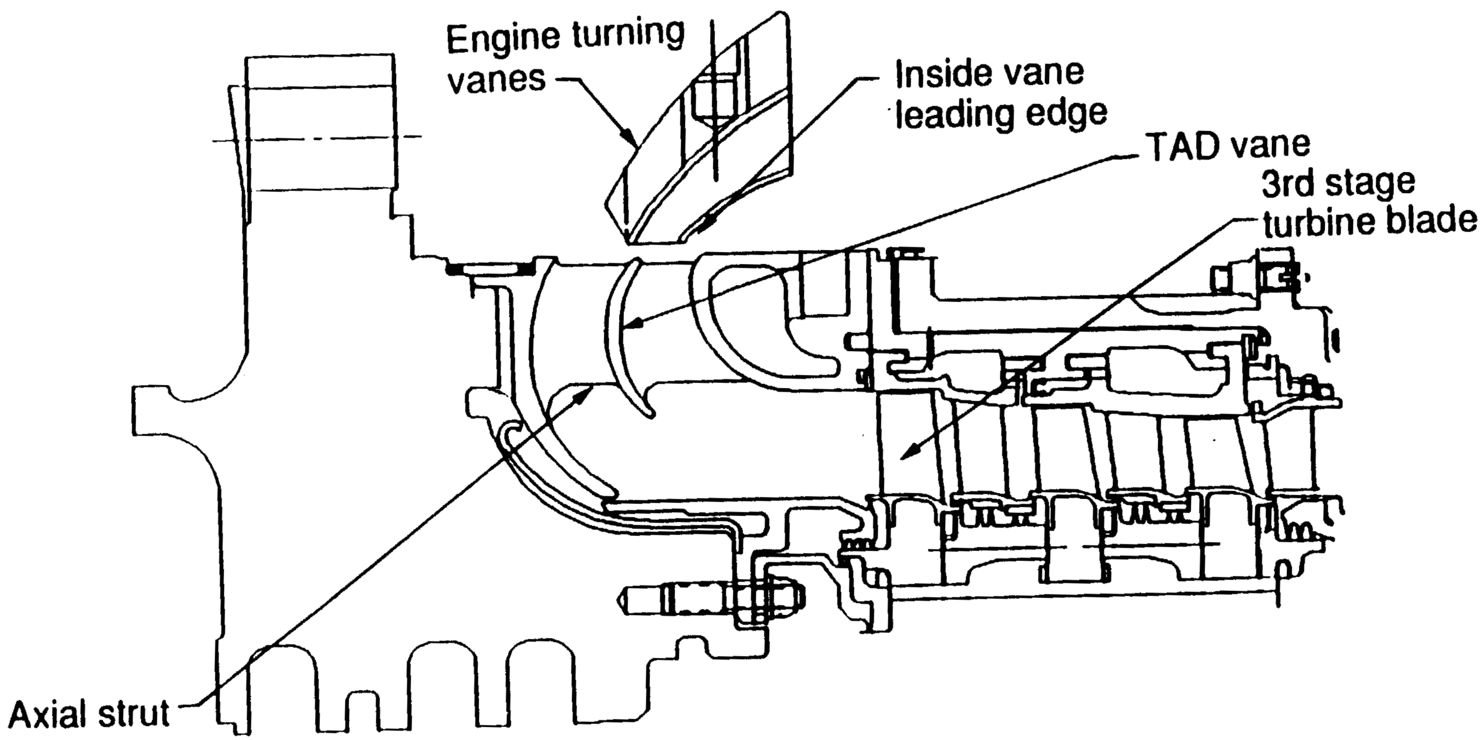

SSME ATD HPOT TAD REDESIGN

Problem Overview

- Engine turning vane cracking occurs with P&W HPOTP
- Fractography analysis indicates cracking is due to HCF.
- Fault tree failure analysis indicates flow environment induced loads result in HCF incidents.
- Flow environment induced loads may result from:
  - Interface velocity distribution
  - Unsteadiness/turbulence
  - Turbine thermal profiles

SSME ATD HPOT TAD REDESIGN

Geometrical Differences

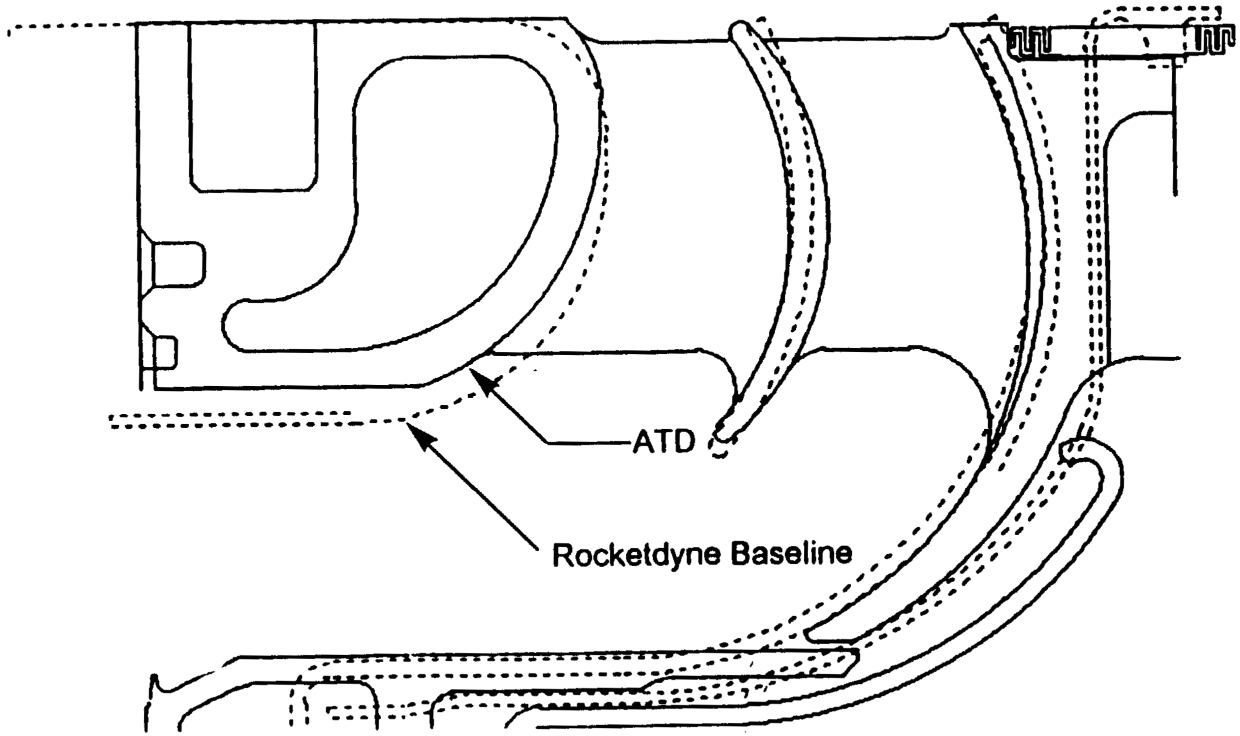

SSME ATD HPOT TAD REDESIGN

TAD Inlet Gas Profile Differences

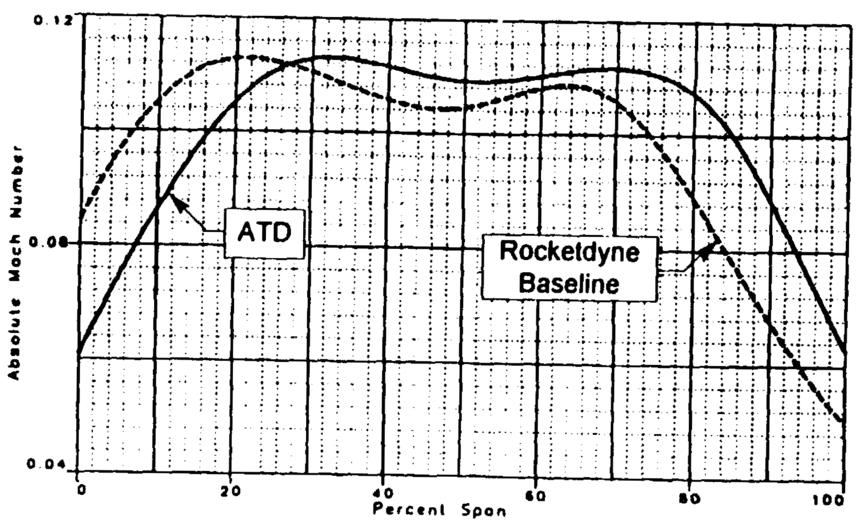

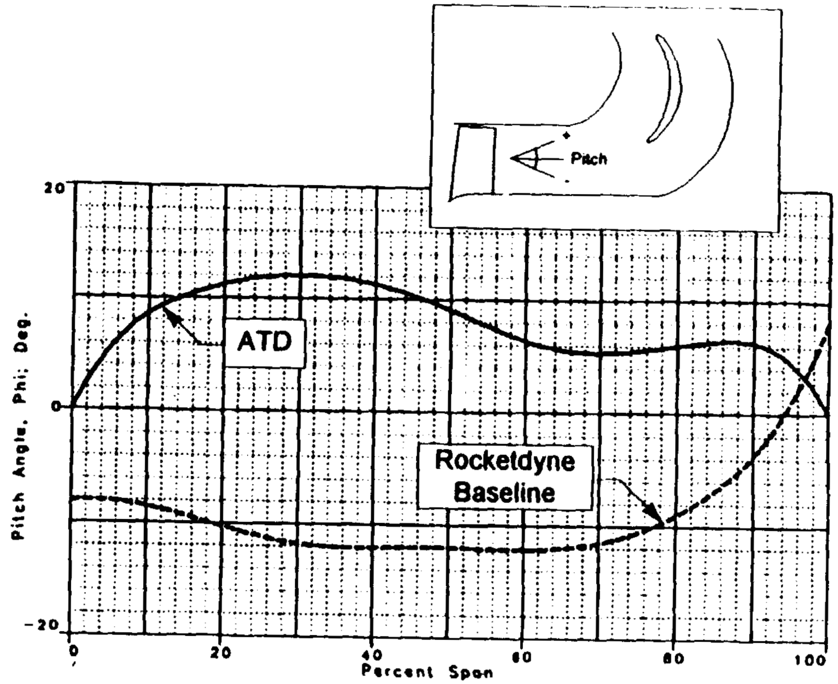

SSME ATD HPOT TAD REDESIGN

CFD Support for TAD Modification – Design Process

Geometry Definition

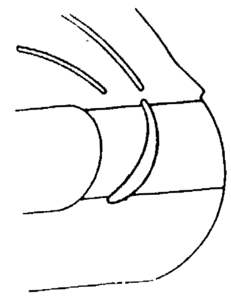

CFD Analysis

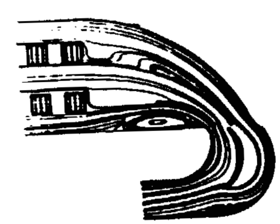

TAD Modified to Match Baseline Interface Conditions

SSME ATD HPOT TAD REDESIGN

Description of STAR–CD

- General Purpose, 3D Navier Stokes Flow Solver
- Body–Fitted, Unstructured Mesh allows for modelling of Complex Geometries
- Rapid Turn–Around
- TAD Calibration Cases
  - Arizona State University Test Case (D.Metzger)
  - NASA–Ames Test Case (D.Monson)

SSME ATD HPOT TAD REDESIGN

Code Verification

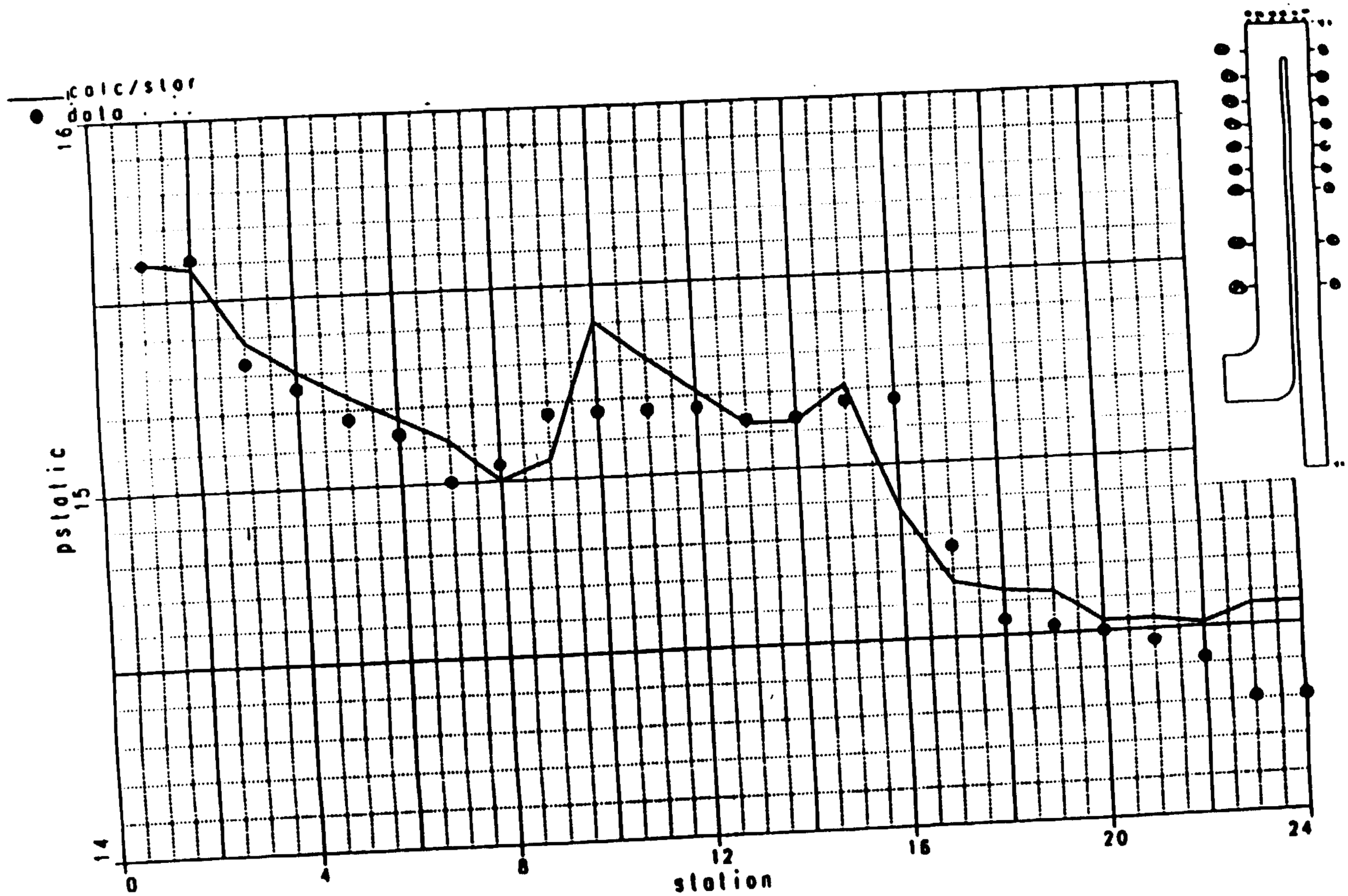

Measured / CFD Predicted Static Pressure With Trip Strips

SSME ATD HPOT TAD REDESIGN

Code Verification

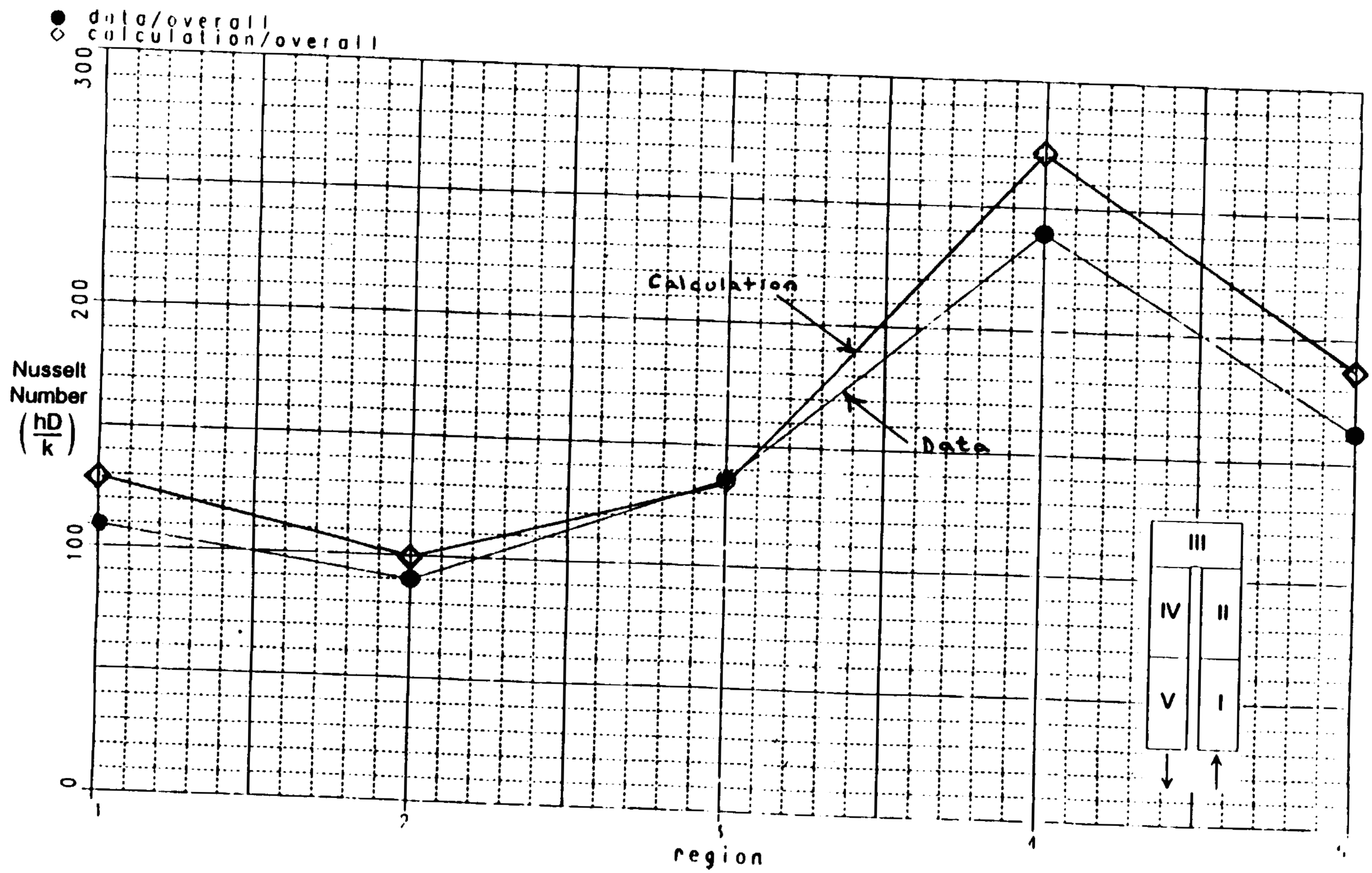

Measured vs Predicted Nusselt Number For Model Without Trip Strips

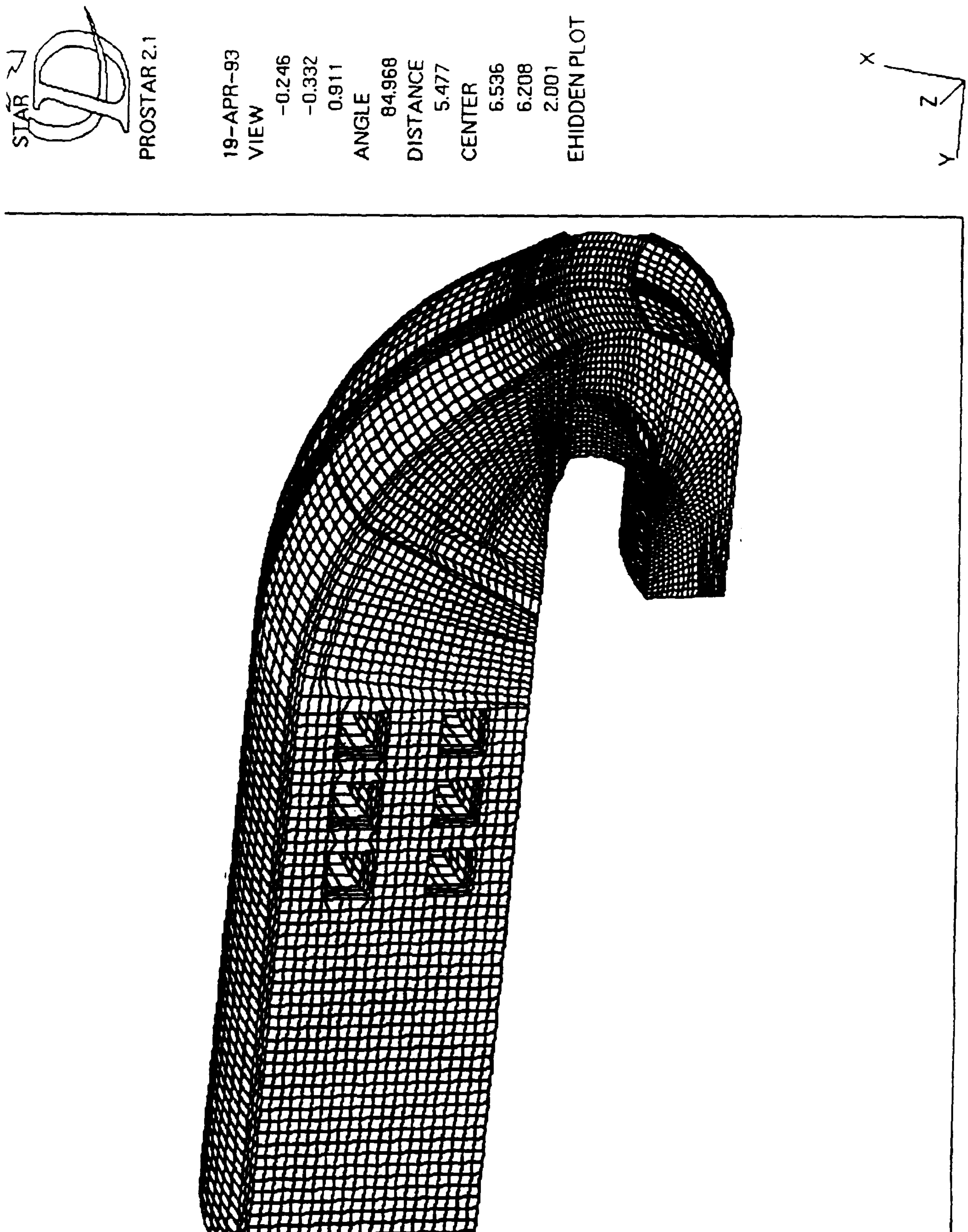
STAR
PROSTAR 2.1
19-APR-93
VIEW
-0.246
-0.332
0.911
ANGLE
84.968
DISTANCE
5.477
CENTER
6.536
6.208
2.001
EHIDDEN PLOT
X
Z
Y

SSME ATD HPOT TAD REDESIGN

Predicted TAD Flow Pattern Differences

Rocketdyne Baseline

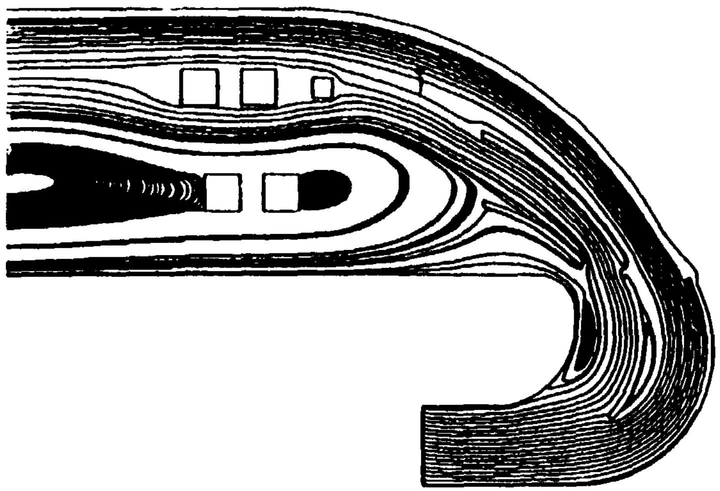

ATD

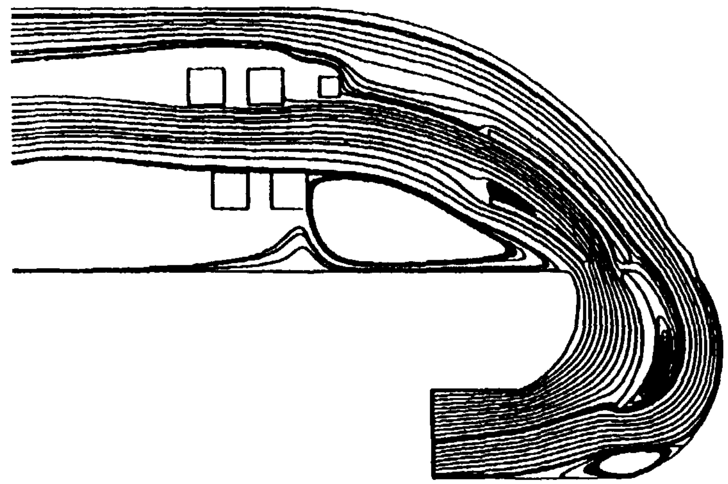

REFLEQX Axisymmetric Analysis (MSFC)

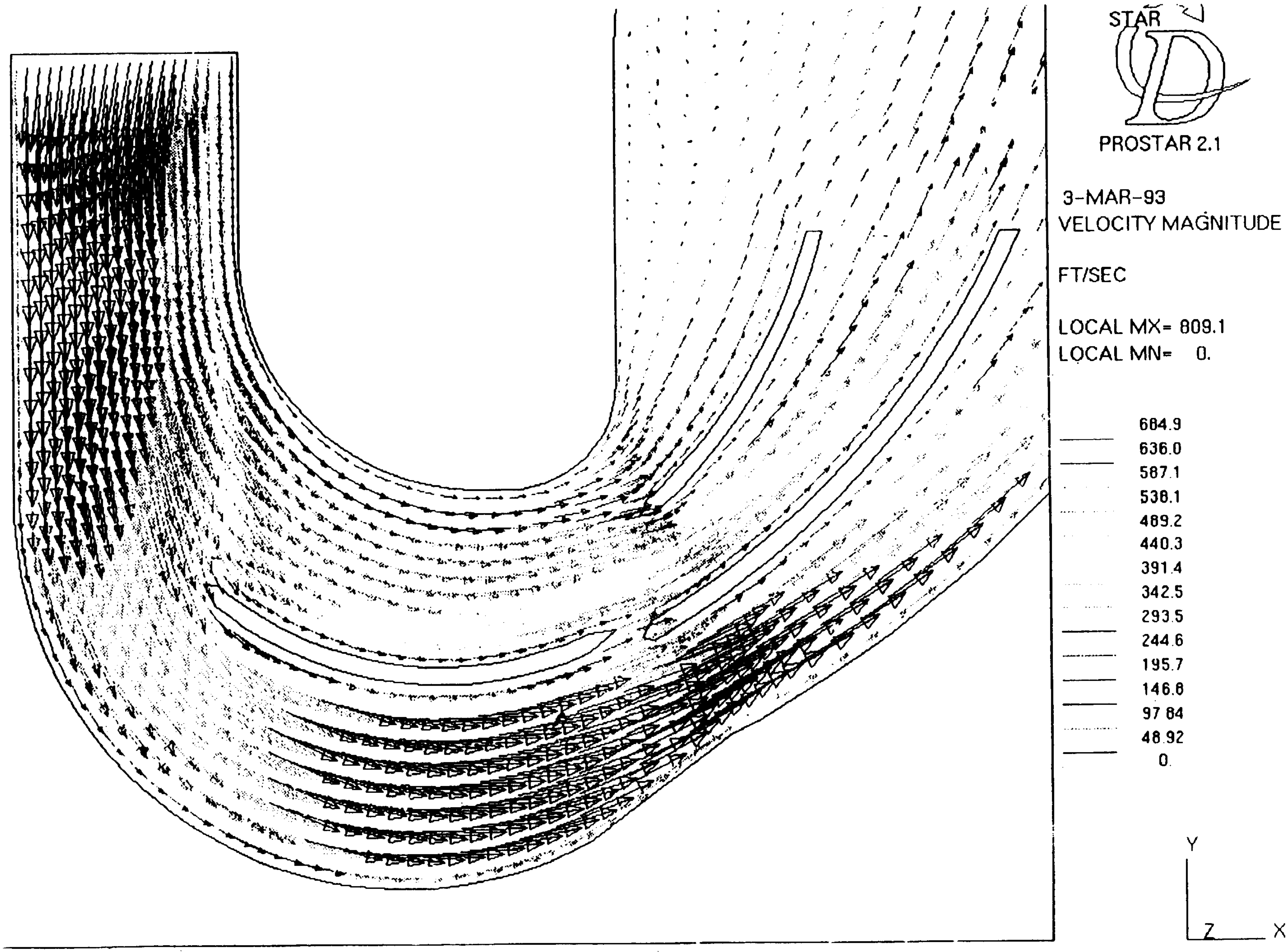

rocketdyne model..

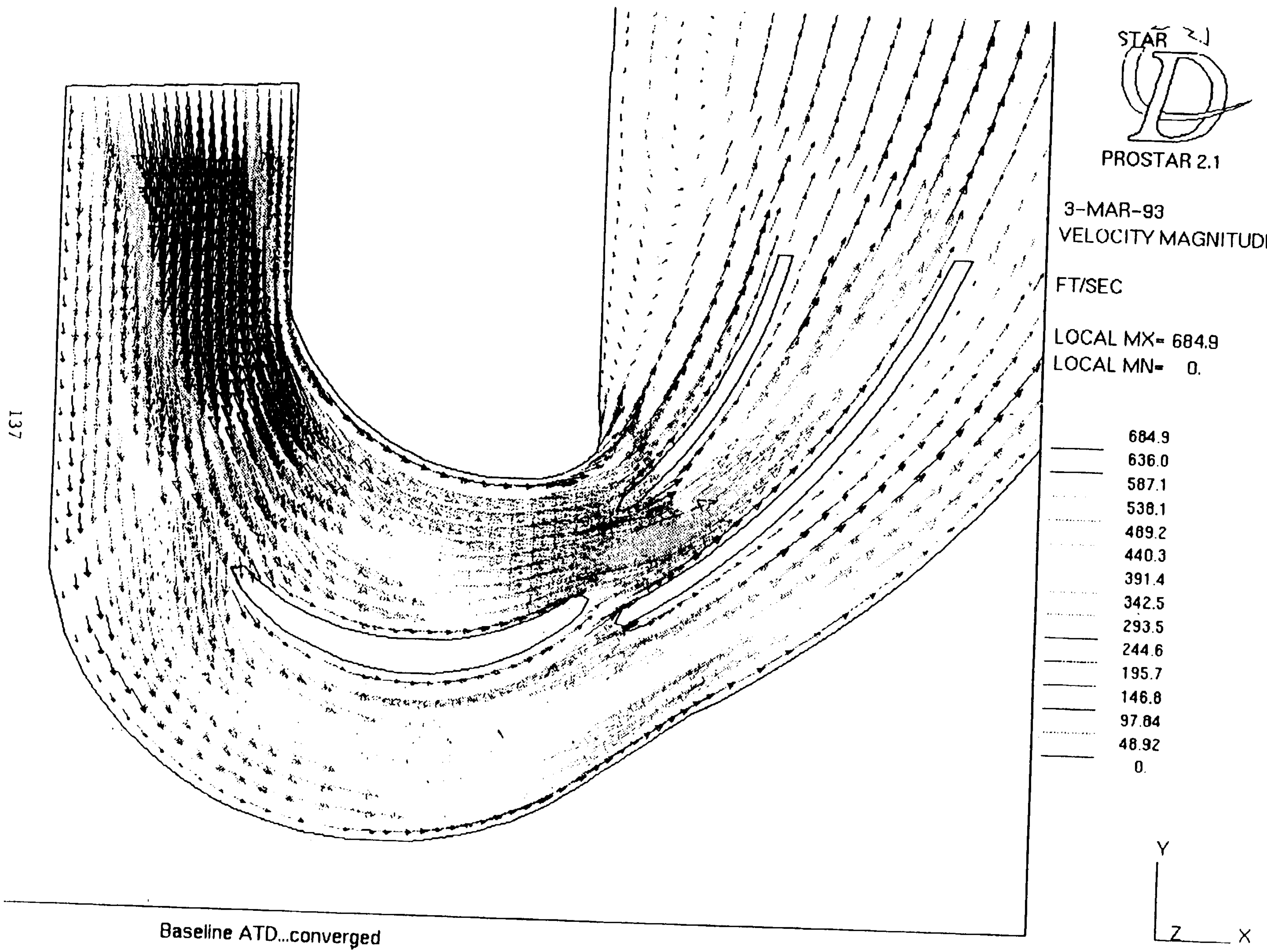

Baseline ATD...converged

SSME ATD HPOT TAD REDESIGN

Differences in Velocity Distributions at Interface Plane

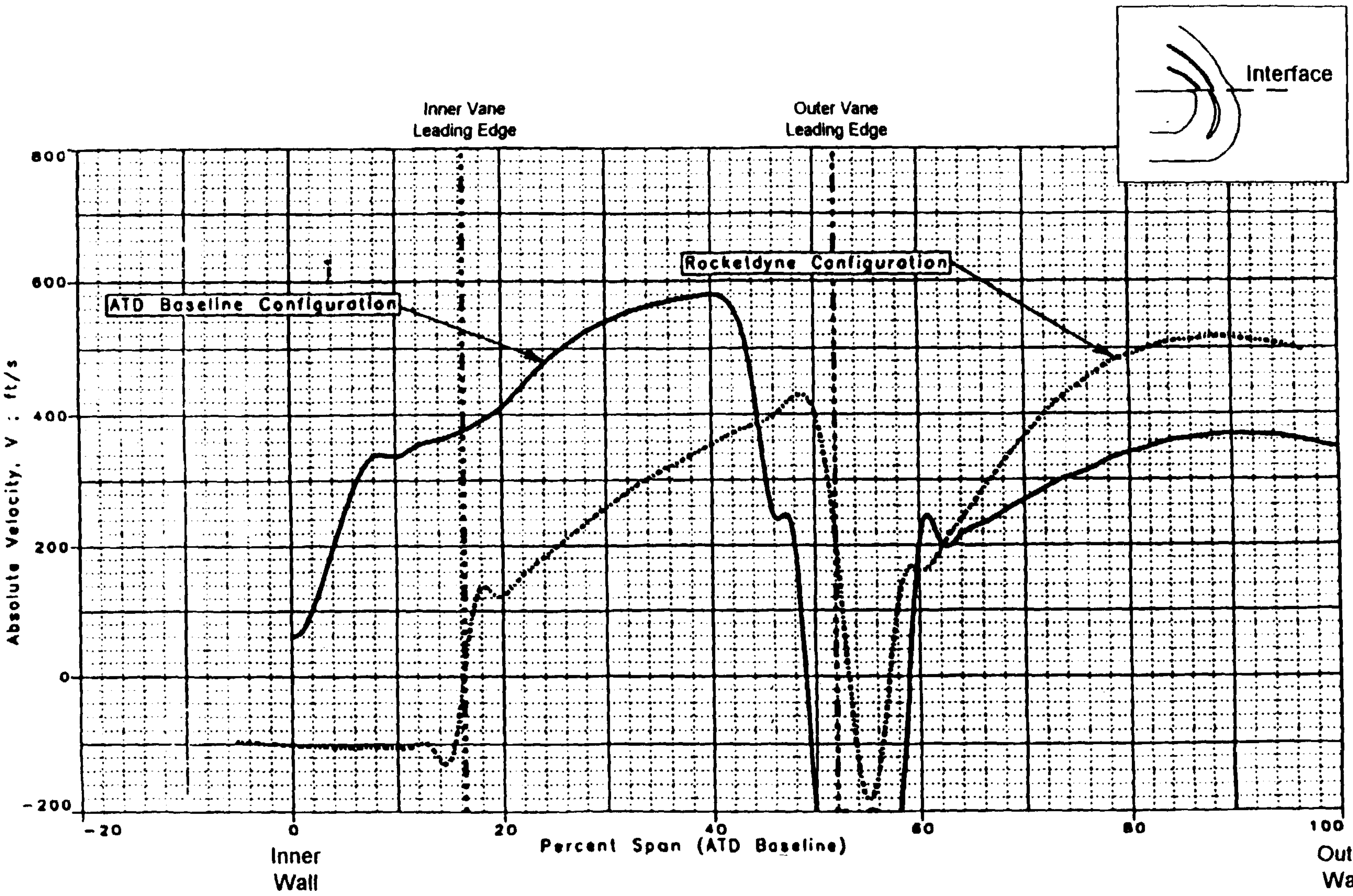

REFLEQX Axisymetric Analysis (MSFC)

SSME ATD HPOT TAD REDESIGN

Differences in Velocity Distributions at Interface Plane

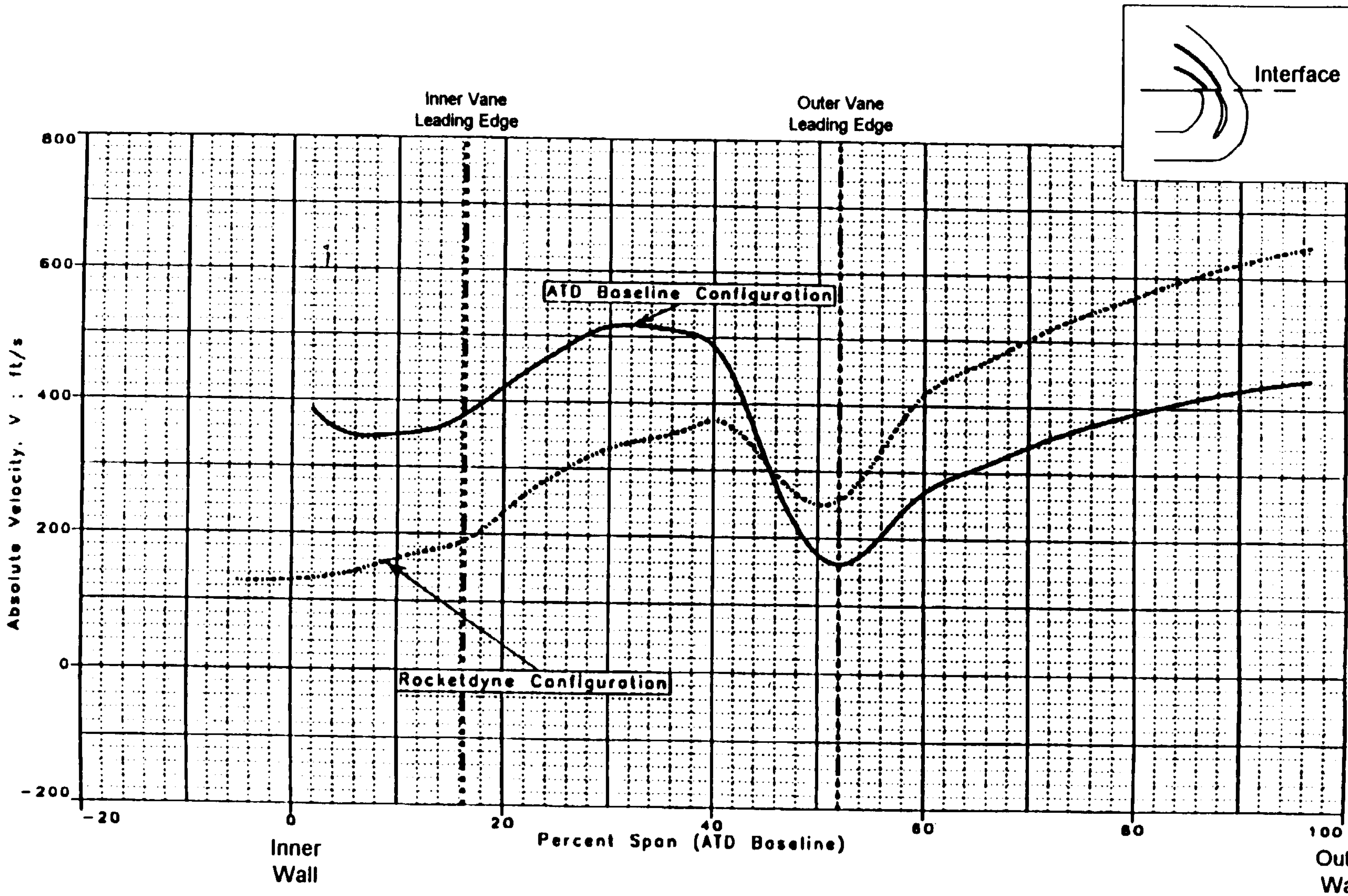

3D Analysis

SSME ATD HPOT TAD REDESIGN

Splitter and Inner Turn Contours Modified to Reduce Velocity Near Inner Vane

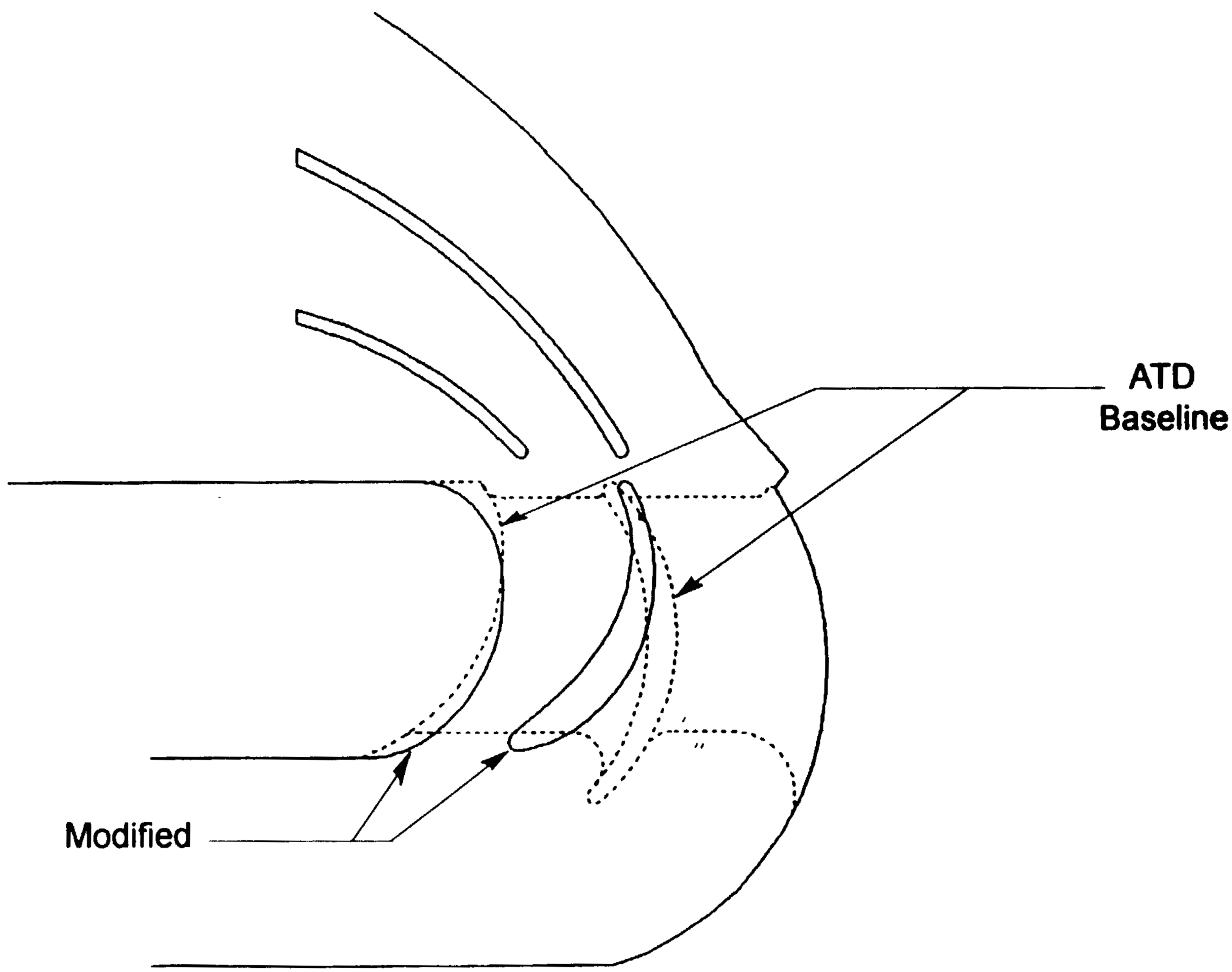

SSME ATD HPOT TAD REDESIGN

CFD Models Differ in Prediction of Flow Separation For Modified TAD

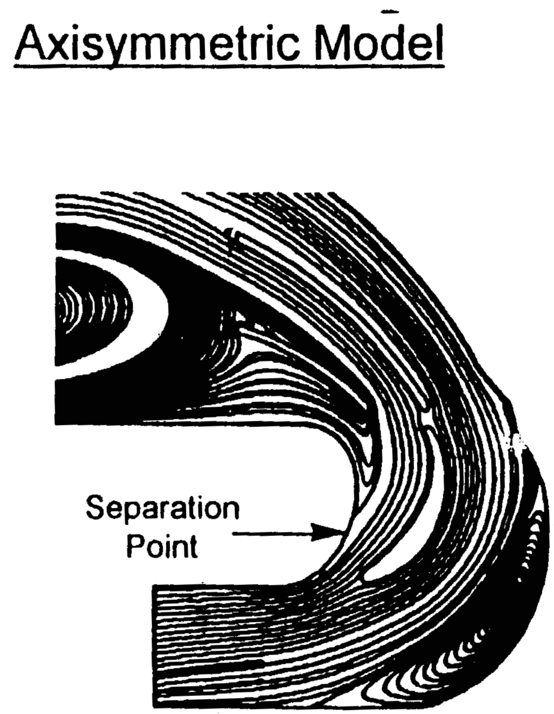

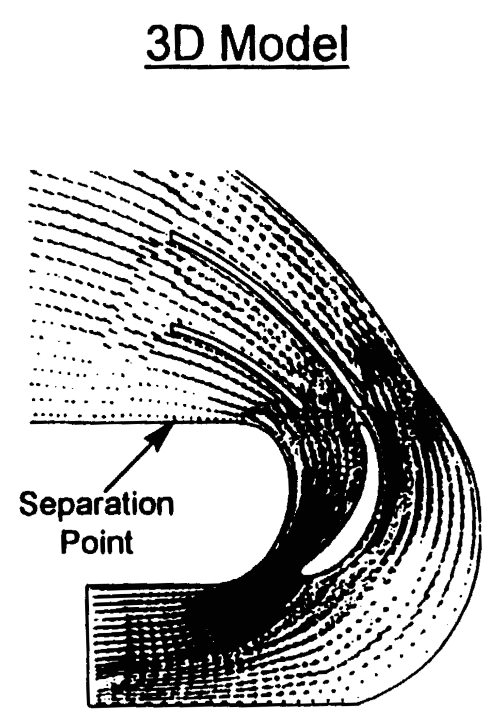

SSME ATD HPOT TAD REDESIGN

ATD TAD Redesign Configuration

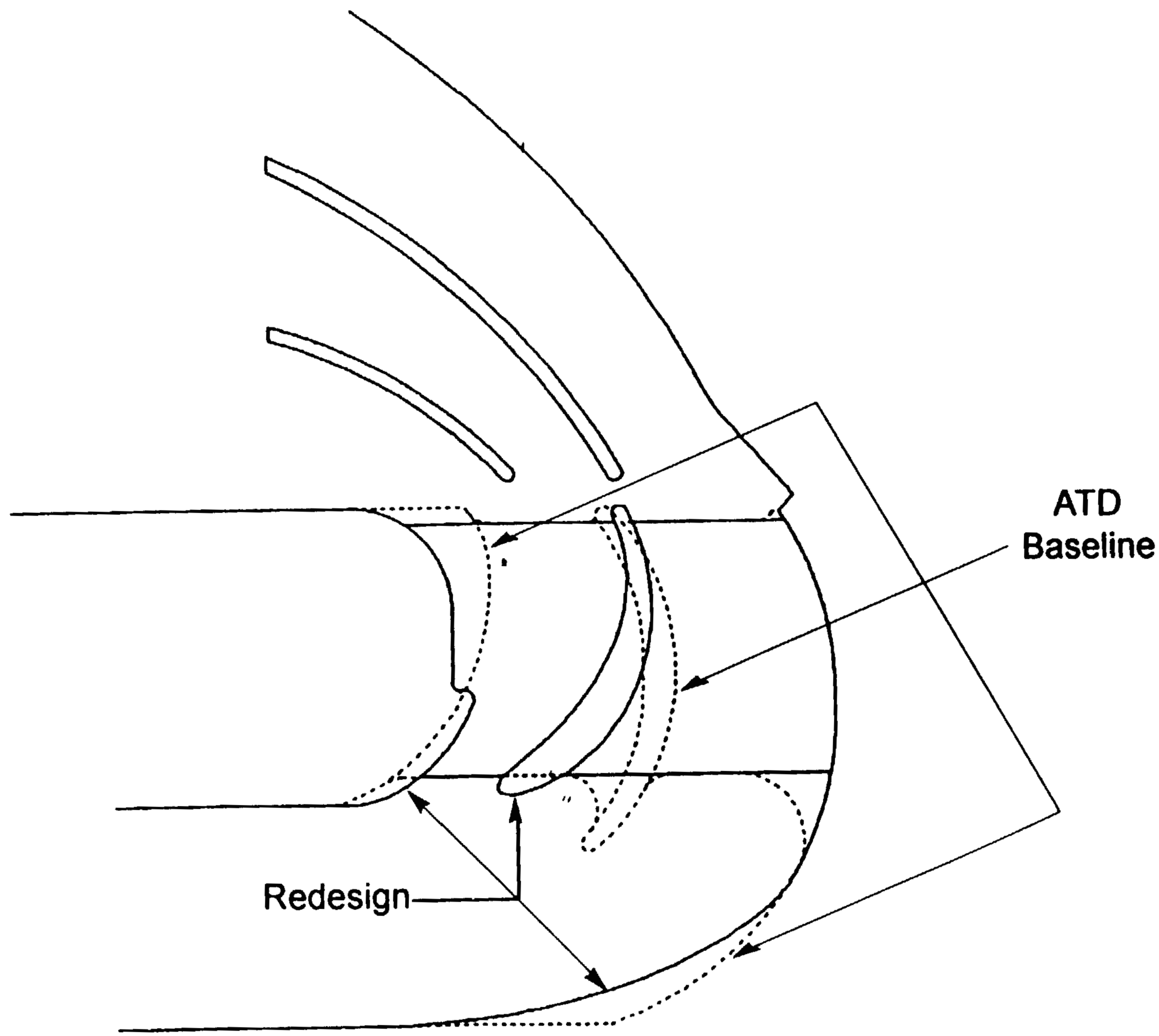

SSME ATD HPOT TAD REDESIGN

ATD Redesign – 2D Axisymmetric Analysis

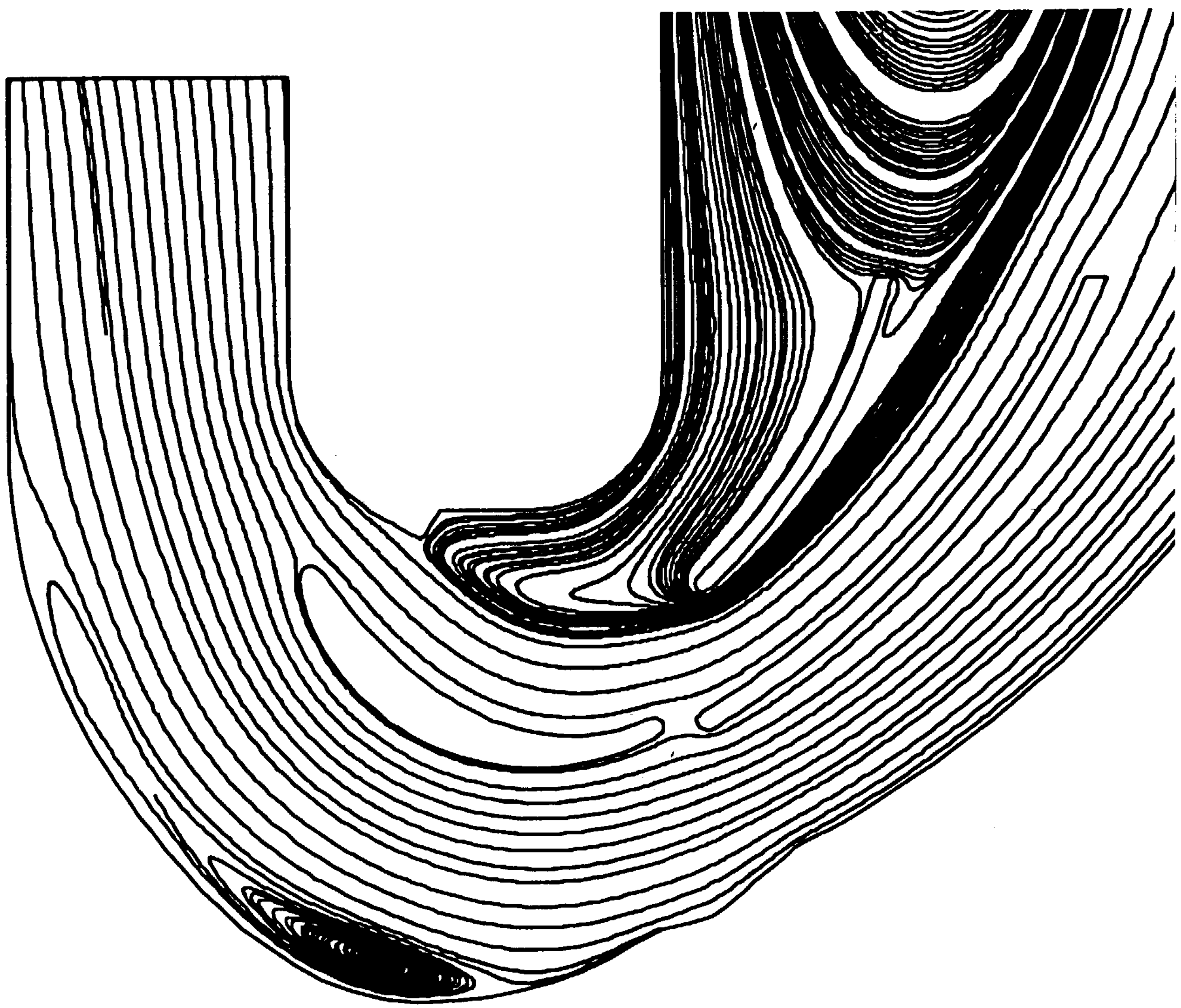

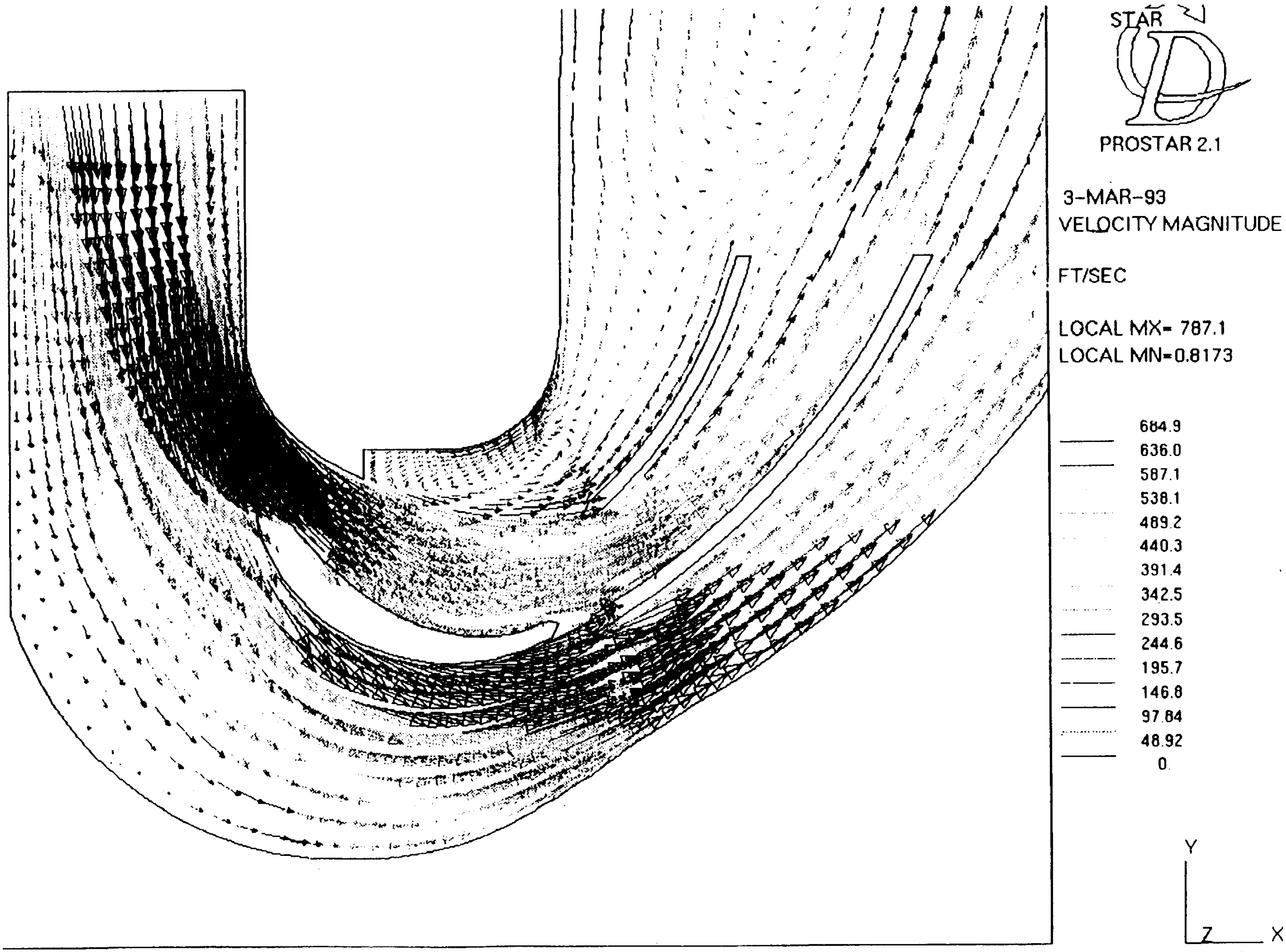

ATD Redesign

SSME ATD HPOT TAD REDESIGN

Axisymmetric Analysis Indicates Velocity Near Inner Vane Still At Goal Level

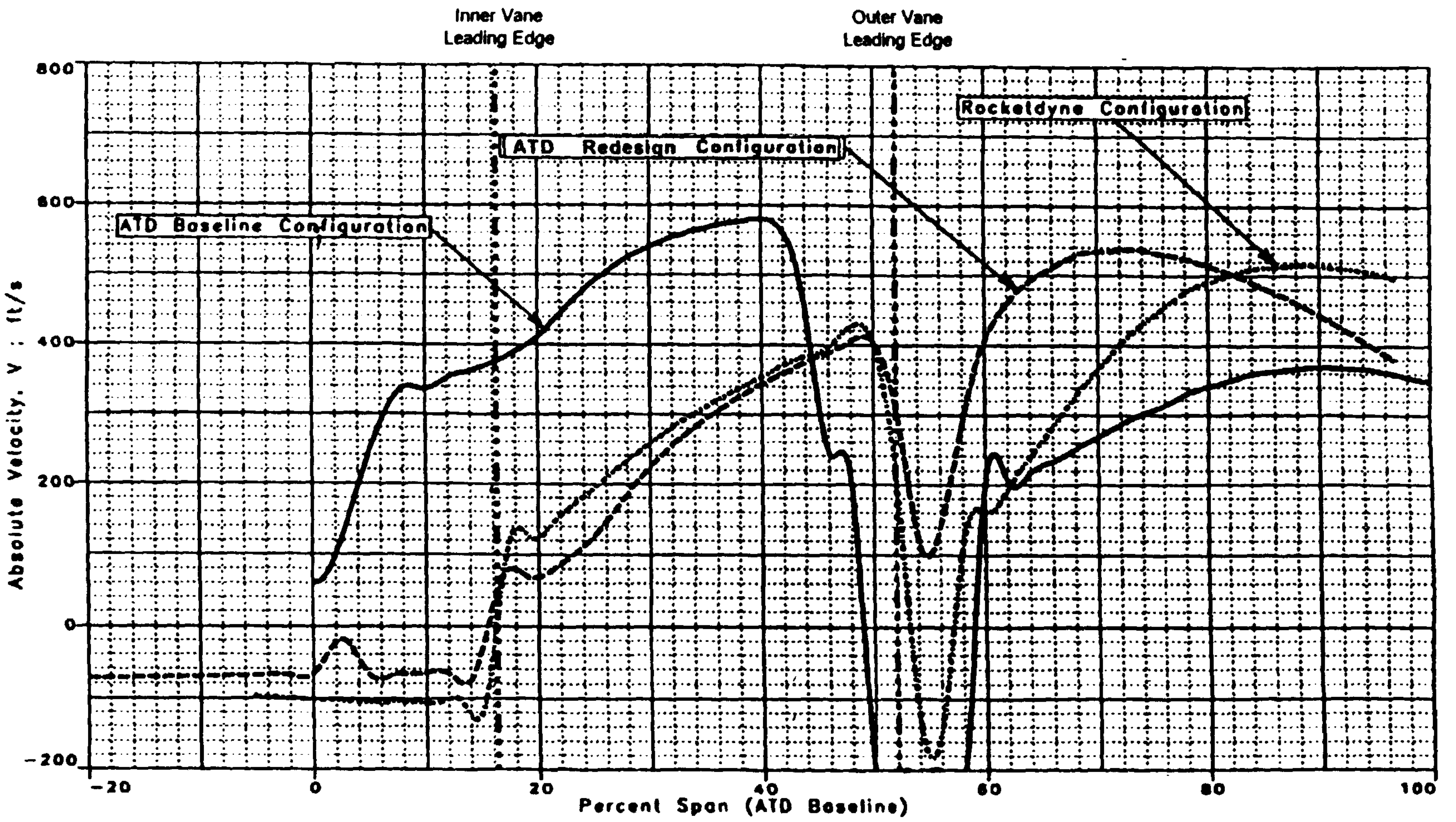

SSME ATD HPOT TAD REDESIGN

3D Analysis of ATD Redesign TAD Indicates Velocity Near Inner Vane At Goal Level

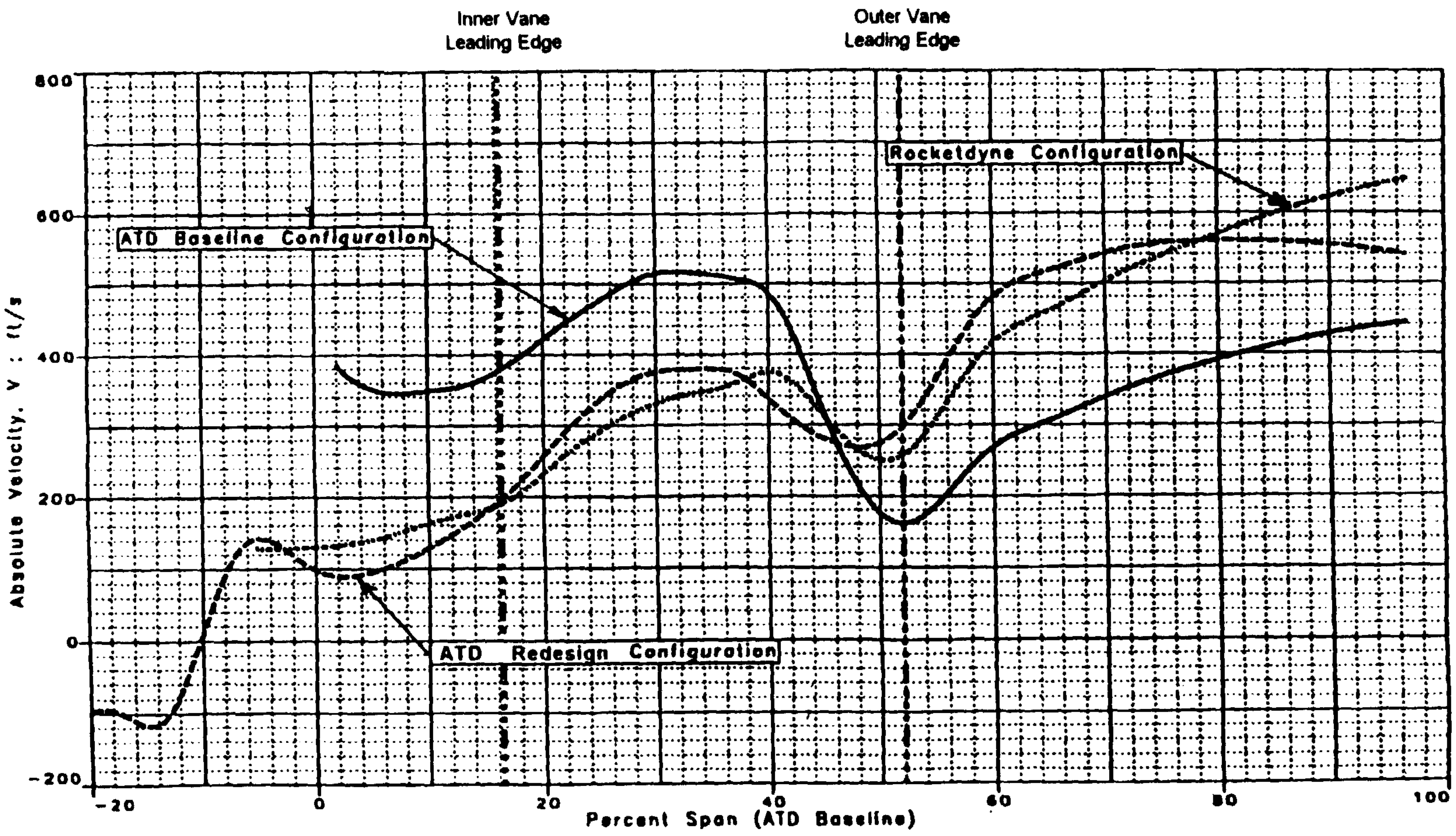

SSME ATD HPOT TAD REDESIGN

Summary

- Major Differences Between the Rocketdyne and ATD TAD's Have Been Identified and Addressed
  - Interface Velocity Distribution
  - TAD Mass Flow Split
  - Fluctuating Pressures Along GOX Hex Vanes
  - Engine–Side Cavities
- Modified ATD TAD Recommended for Incorporation Into the ATD HPOT – Supported By:
  - Axisymmetric CFD Results
  - 3D CFD Results

N95- 23621

-6-34

p_21

UNSTEADY FLOW SIMULATIONS IN SUPPORT OF THE SSME HEX TURNING VANE CRACKING INVESTIGATION WITH THE ATD HPOTP

by

N. S. Dougherty, D. W. Burnette, and J. B. Holt
Rockwell International
Space Systems Division
Huntsville, AL 35806

and

T. Nesman
MSFC/ED33
Marshall Space Flight Center, AL 35812

ABSTRACT

Unsteady flow computations are being performed with the P&W (ATD) and the Rocketdyne baseline configurations of the SSME LO_2 turbine turnaround duct (TAD) and heat exchanger (HEX). The work is in support of the HEX inner turning vane cracking investigation. Fatigue cracking has occurred during hot firings with the P&W configuration on the HEX inner vane, and it appears the fix will involve changes to the TAD splitter vane position and to the TAD inner wall curvature to reduce the dynamic loading on the inner vane. Unsteady flow computations on the P&W baseline and fix and on the Rocketdyne baseline reference follow steady-flow screening computations done by MSFC/ED32 on several trial configurations arriving at the fix.

The P&W TAD inlet velocity profile has a strong radial velocity component that directs the flow toward the inner wall and raises the local velocity a factor of two and the dynamic pressure a factor of four. The fix is intended to redistribute the flow more evenly across the HEX inner and outer vanes like the Rocketdyne baseline reference. Vane buffeting at frequencies around 4,000 Hz is the leading suspected cause of the problem. Our simulations (work in progress) are being done with the USA 2D axisymmetric code approximating the flow as axisymmetric u+v 2D (axial, u, and radial, v, components only). The HEX coils are included in the model to make sure the fix does not adversely affect the HEX environment.

Turbulent kinetic energy, k, levels where $k = 1/2\ v'\ rms^2$ are locally as high as 10,000 ft^2/sec^2 for the P&W baseline at the engine interface (between the TAD and HEX) at the HEX inner vane location. However, k is less than 8,000 on the HEX outer vane and only about 4,500 on the HEX inner vane for the Rocketdyne baseline. Unsteady turbulence intensity, v'rms/v, and pressure, p', are being computed in the present computations to compare with steady-flow Reynolds-averaged computations where p'rms = const (ρk) for overall rms random turbulence from 0.1 to 12,000 Hz frequency. Random overall static, p'rms fluctuations as large as 1.7 psi are estimated from k on the HEX inner vane for the P&W baseline configuration but only about 0.7 psi for the Rocketdyne configuration.

UNSTEADY FLOW SIMULATIONS IN SUPPORT OF THE SSME HEX TURNING VANE CRACKING INVESTIGATION WITH THE ATD HPOTP

APRIL 20, 1993

N.S. Dougherty, J.B. Holt, and D.W. Burnette
Rockwell International
Huntsville, AL
and
T. Nesman
MSFC/ED33

RENG002557.01

ENGINE HEX TURNING VANE CRACKING INVESTIGATION UNSTEADY CFD ANALYSIS

OBJECTIVE

- PROVIDE UNSTEADY FLOW SIMULATIONS OF THE ATD HPOTP TURNAROUND DUCT/HEAT EXCHANGER FLOW TO SUPPORT IDENTIFICATION OF A "FIX" THAT:

  1) ELIMINATES HEX INNER VANE CRACKING, AND

  2) DOES NOT ADVERSELY AFFECT THE HEX COIL ENVIRONMENT

ENGINE HEX TURNING VANE CRACKING INVESTIGATION
UNSTEADY CFD ANALYSIS

APPROACH

- DENSITY-BASED TIME-ACCURATE CFD CODE
  - 2ND-ORDER ACCURATE
  - PREVIOUSLY BENCHMARKED ON SIMPLE FLOW
    - RECTANGULAR CAVITY (ROSSITER)
    - EDGETONE (BROWN)
    - CURVED VANE (4 KHZ LO_2 SPLITTER VANE)
  - AXISYMMETRIC u AND v
- GEOMETRY, BOUNDARY CONDITIONS, AND REFERENCE QUANTITIES SAME AS IN STEADY-FLOW CFD ANALYSIS
- RESULTS COMPARED FOR GEOMETRY CHANGE
  - BASELINE CONFIGURATION
  - "FIX" CONFIGURATION

RENG002568.01

MODELING APPROACH

BENEFITS

- CAN SHOW POTENTIALS FOR UNSTEADY BEHAVIOR
  – FLOW INSTABILITIES, UNSTEADY SEPARATION, BUFFETING
- MATCHES 2D STEADY-FLOW CFD (MEAN VALUES)
- PROVIDES HEX VANE UNSTEADY LOADING - - p', (t, ℓ)
- CAN PROVIDE p' AT AIRFLOW MEASUREMENT LOCATIONS
- AIDS UNDERSTANDING OF HOT FIRE AND AIRFLOW TEST DATA

AREAS FOR IMPROVEMENT

- 2D (INSTEAD OF 3D) TRUNCATED GEOMETRY CAN ALLOW ACOUSTICS TO DOMINATE
- TURBULENCE TREATMENT IS ALWAYS A QUESTION

ENGINE HEX TURNING VANE CRACKING INVESTIGATION
UNSTEADY CFD ANALYSIS

BASELINE CONFIGURATION GRID

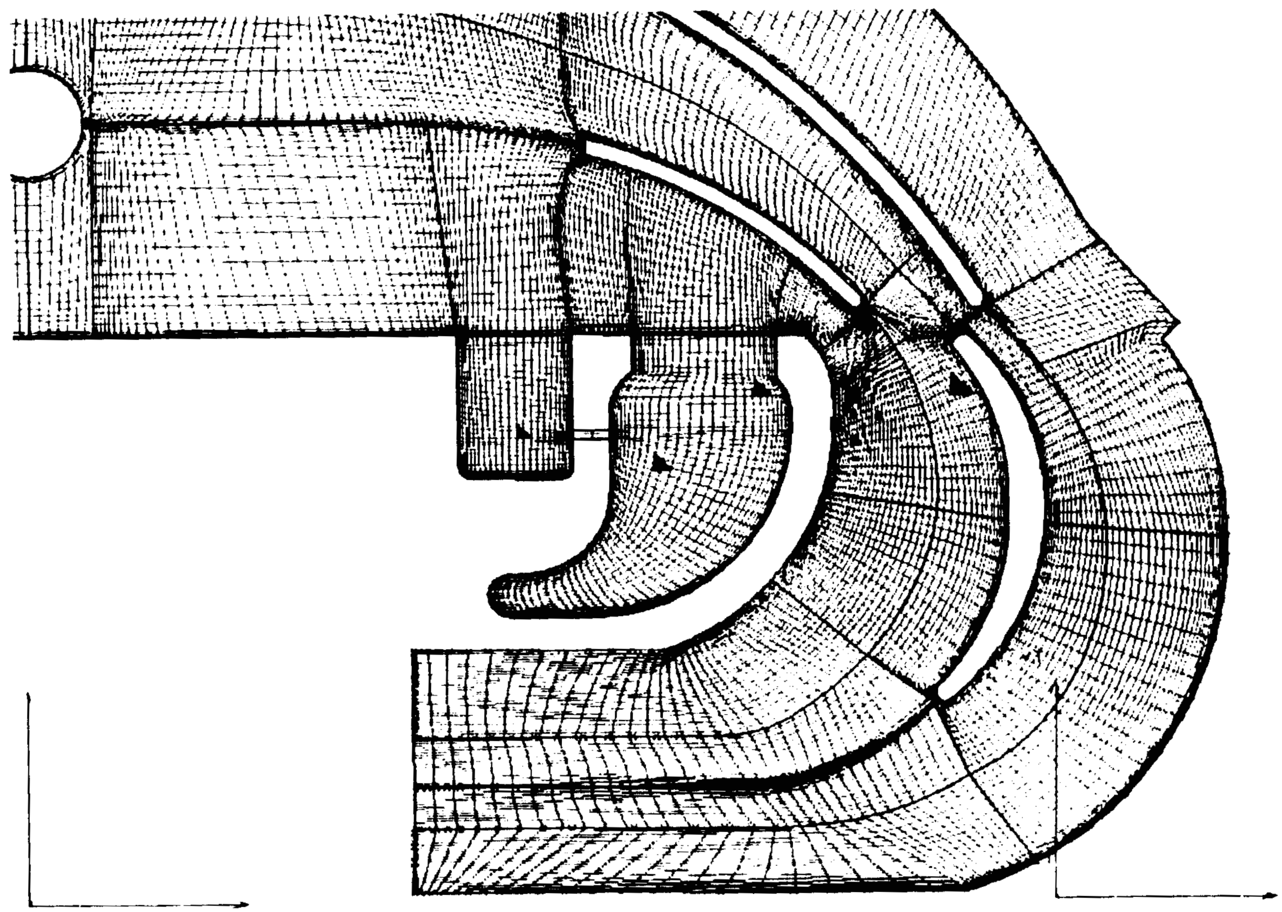

RENG002566.01

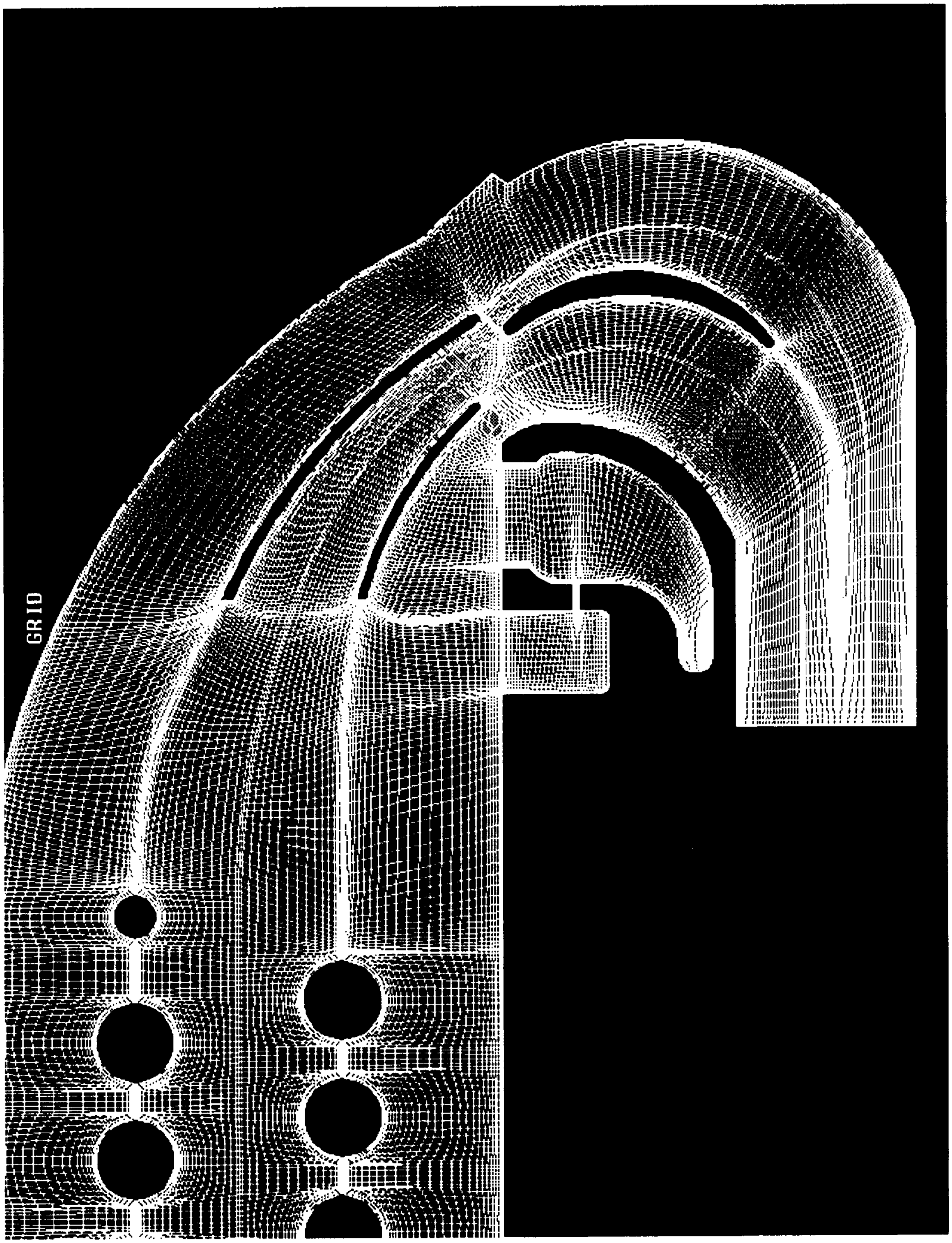
GRID

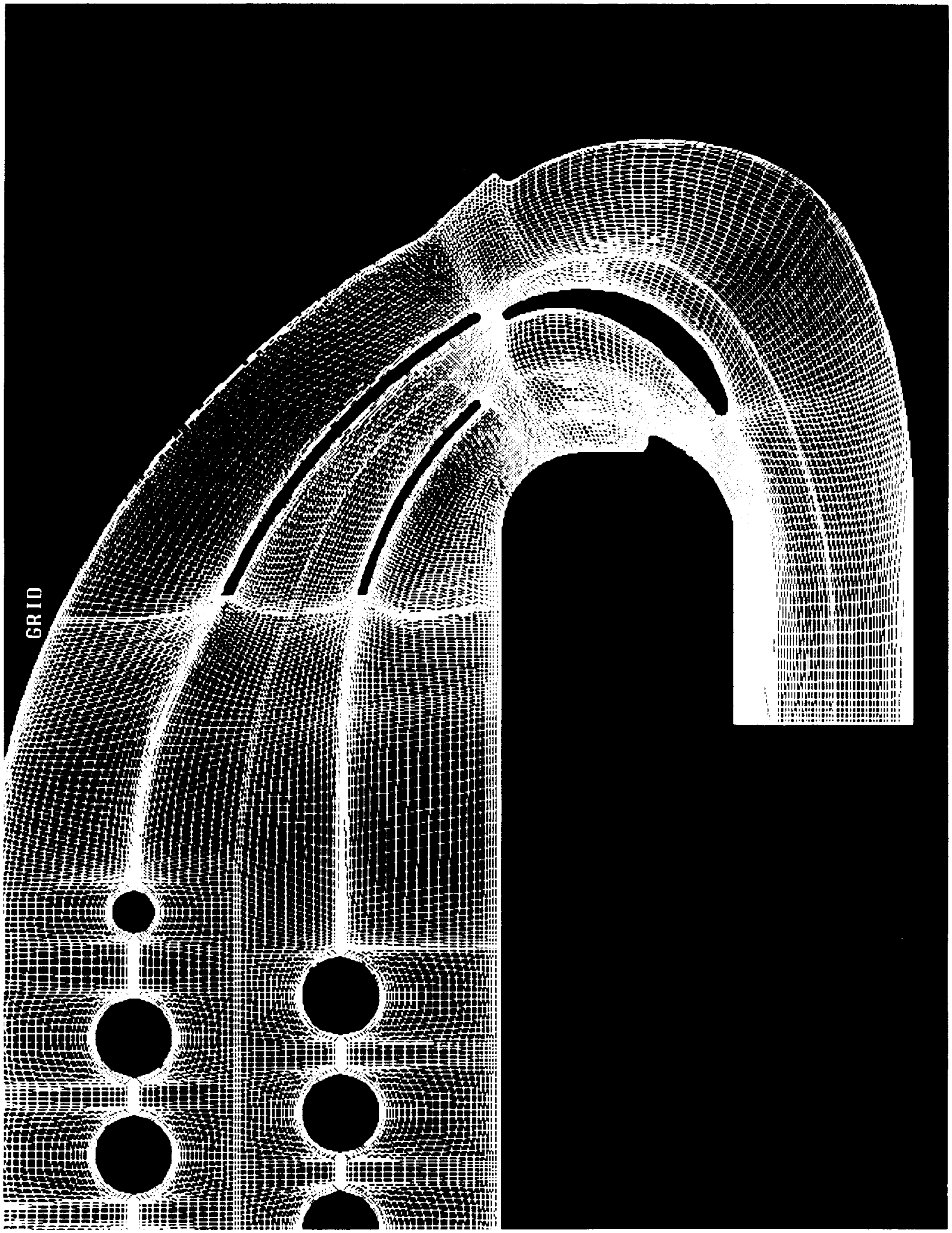
GRID

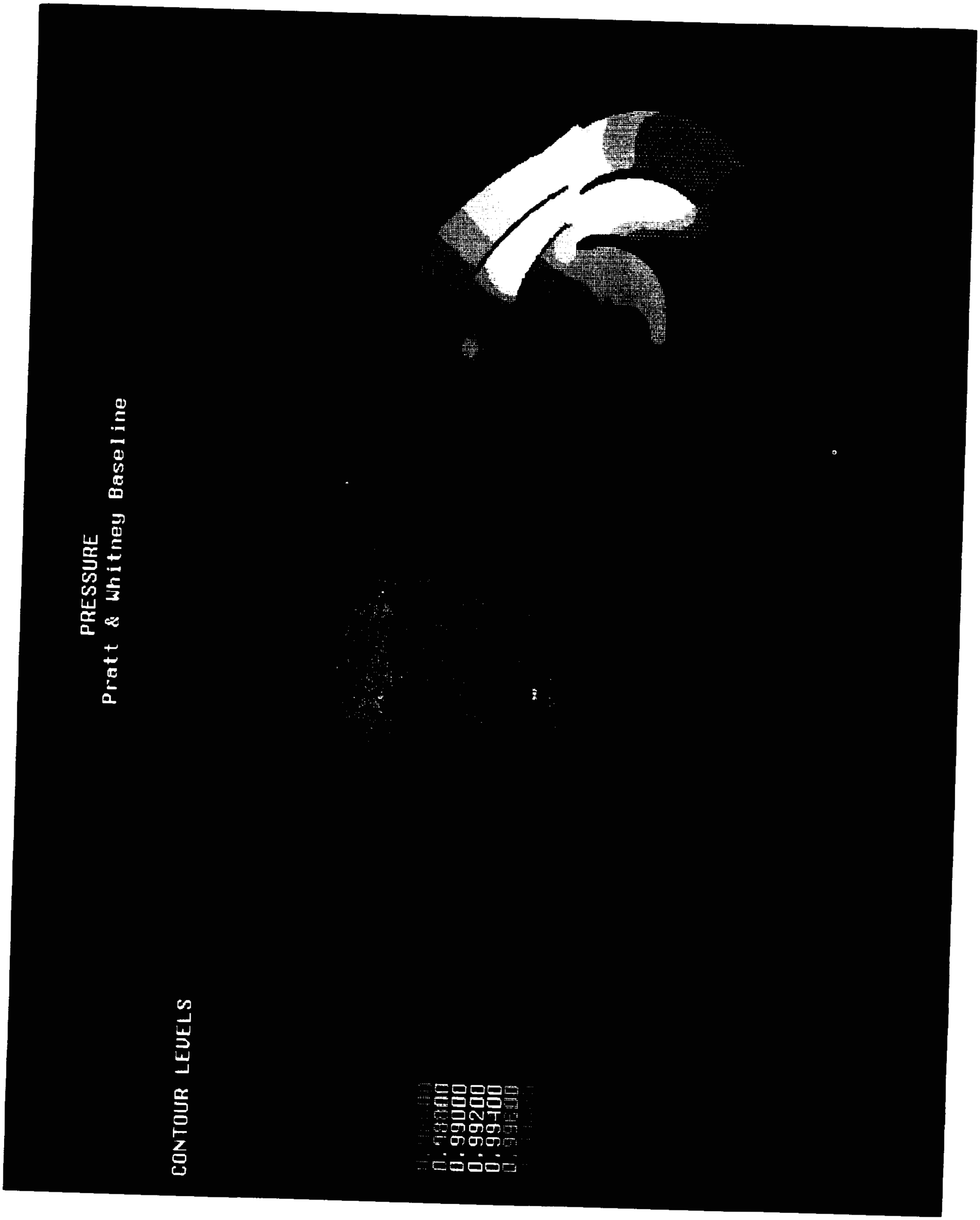
PRESSURE
Pratt & Whitney Baseline
CONTOUR LEVELS
0.99000
0.99200
0.99400

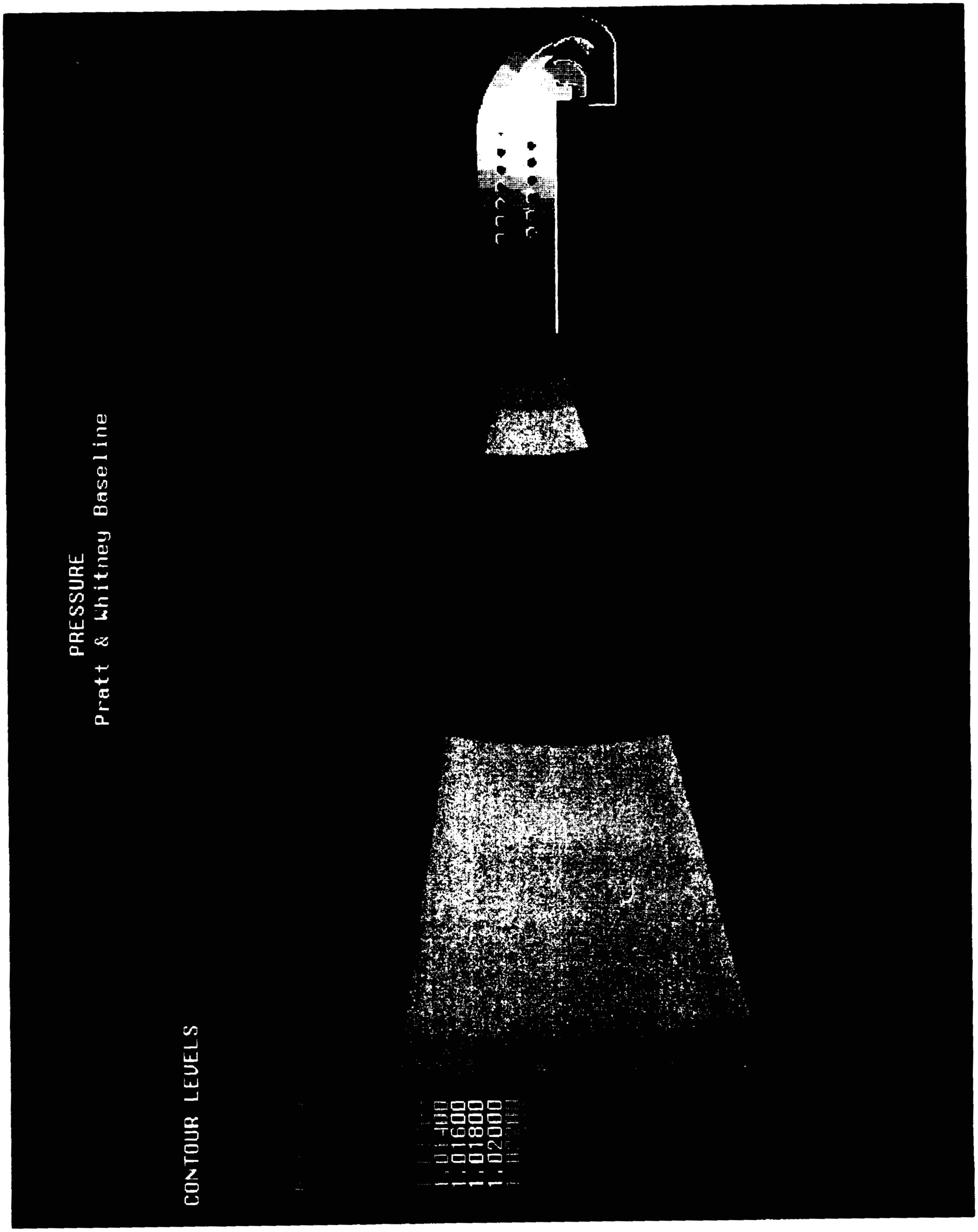
PRESSURE
Pratt & Whitney Baseline
CONTOUR LEVELS
1.01600
1.01800
1.02000

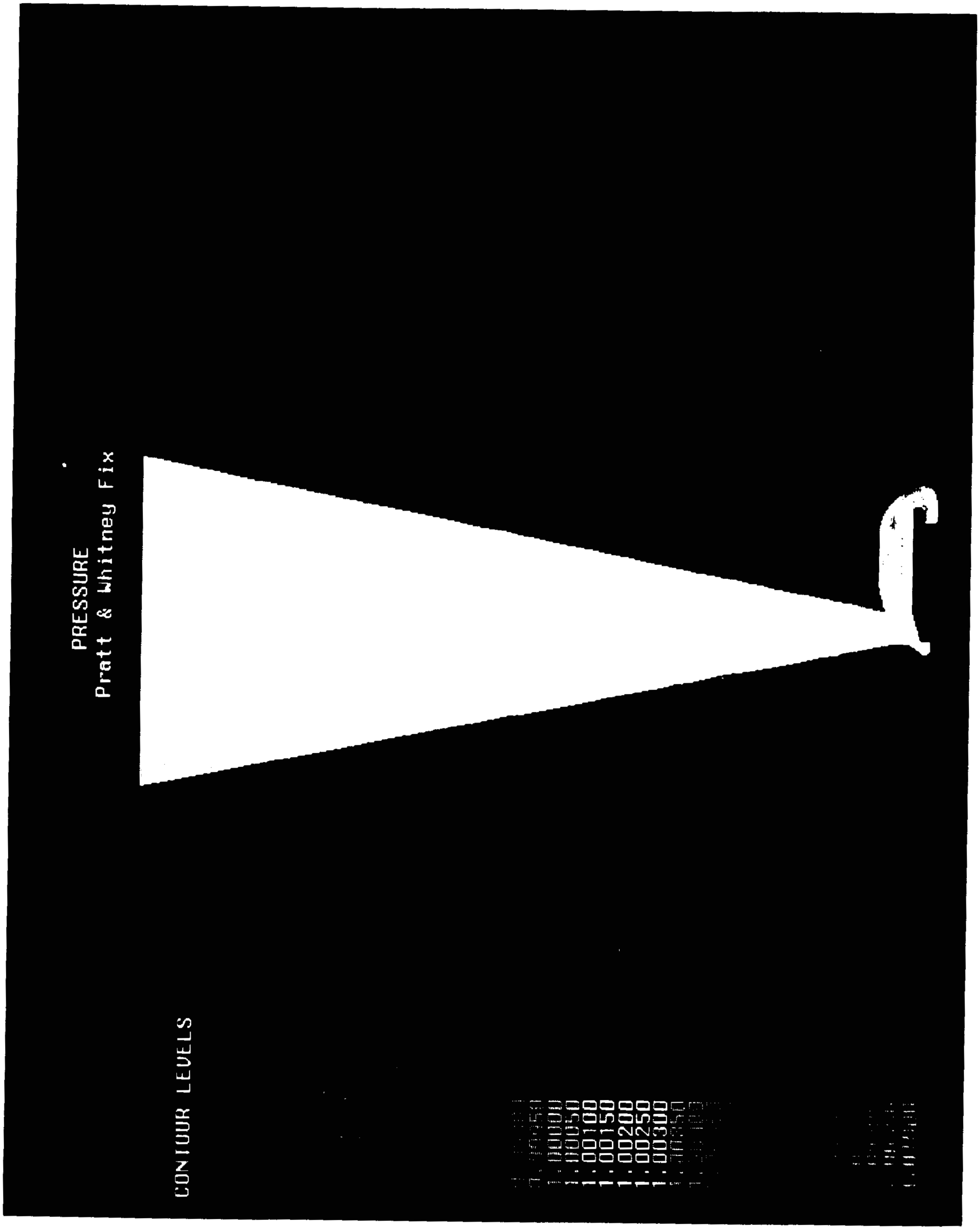
PRESSURE
Pratt & Whitney Fix
CONTOUR LEVELS
1.00000
1.00050
1.00100
1.00150
1.00200
1.00250
1.00300

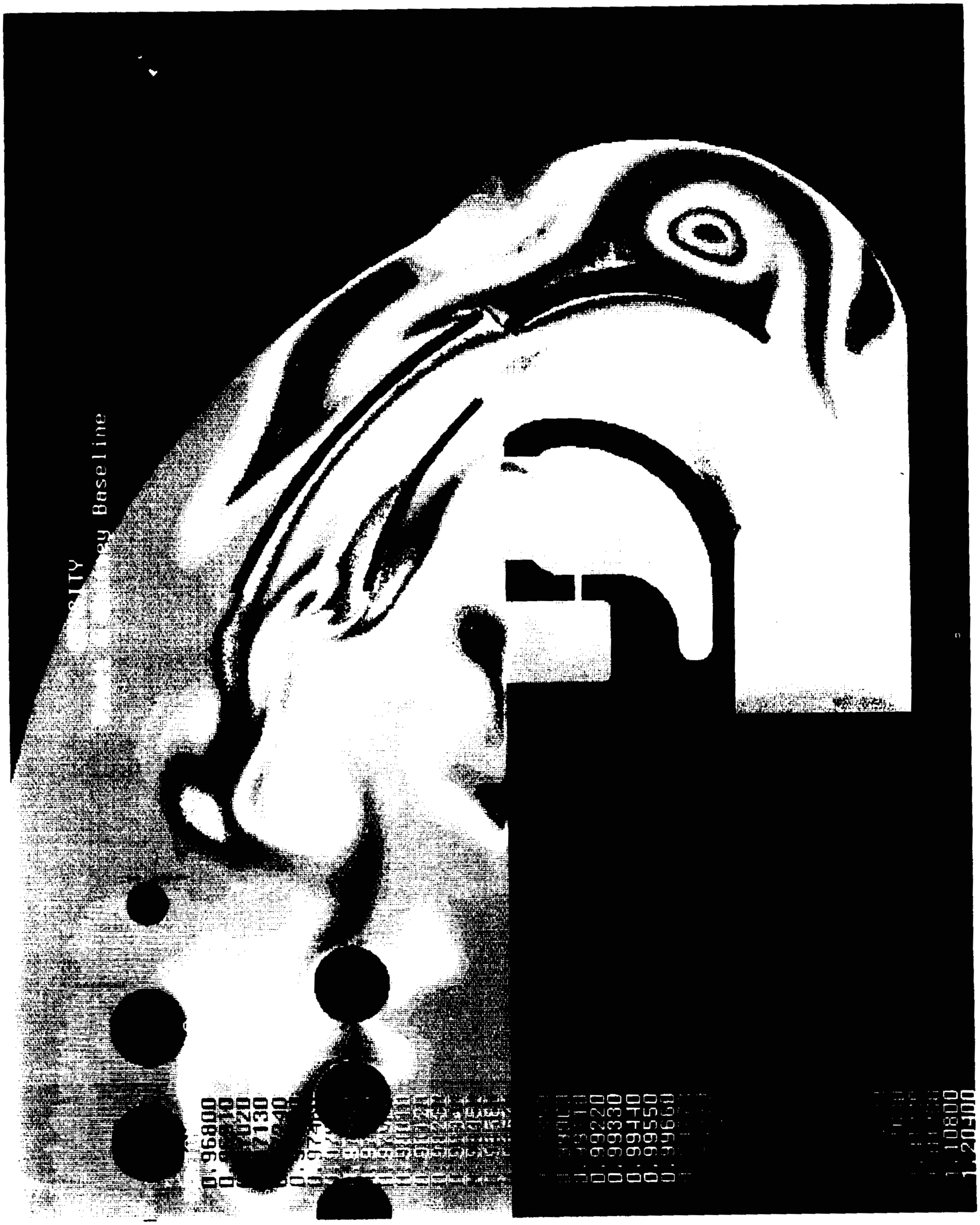

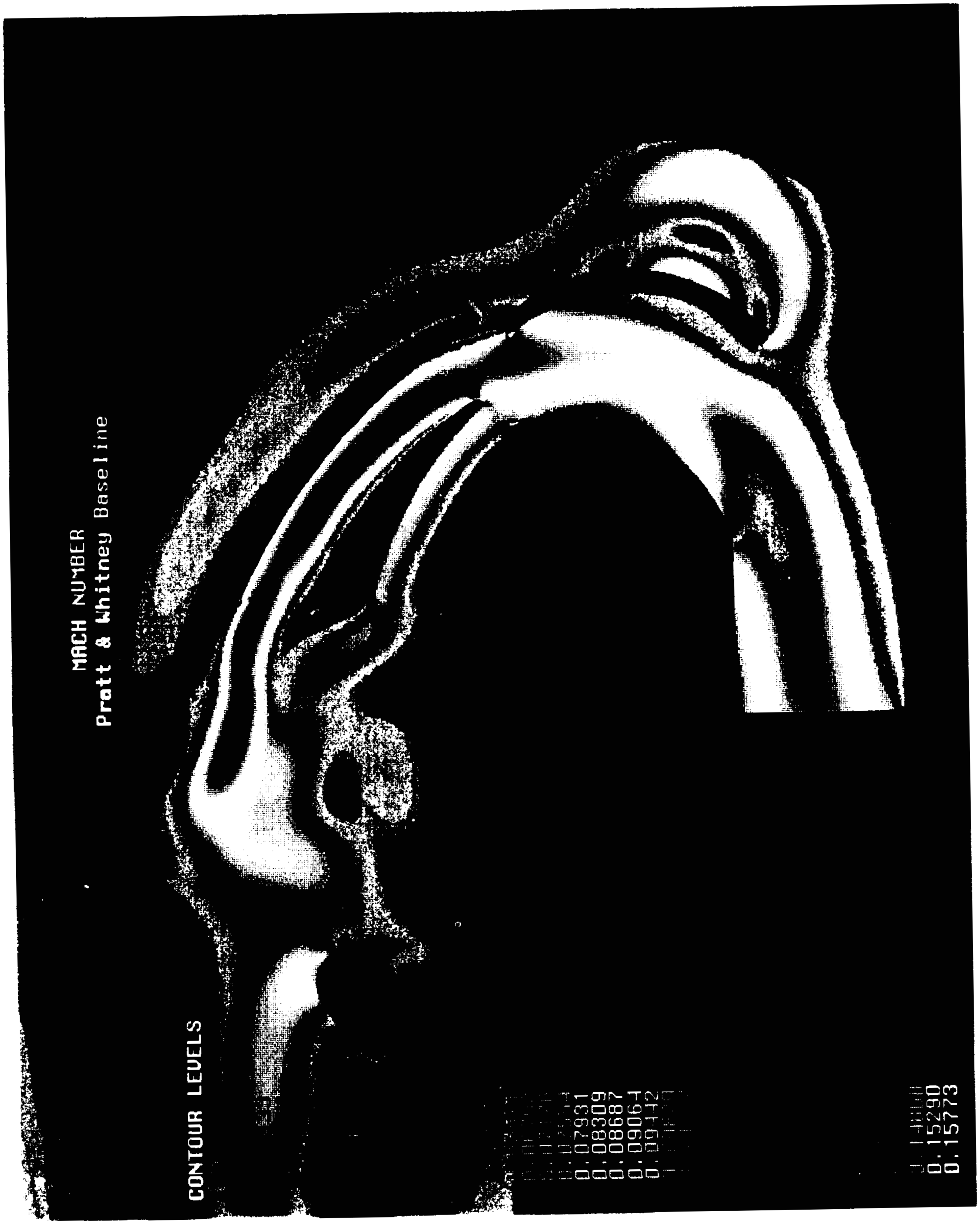

ORIGINAL PAGE IS
OF POOR QUALITY

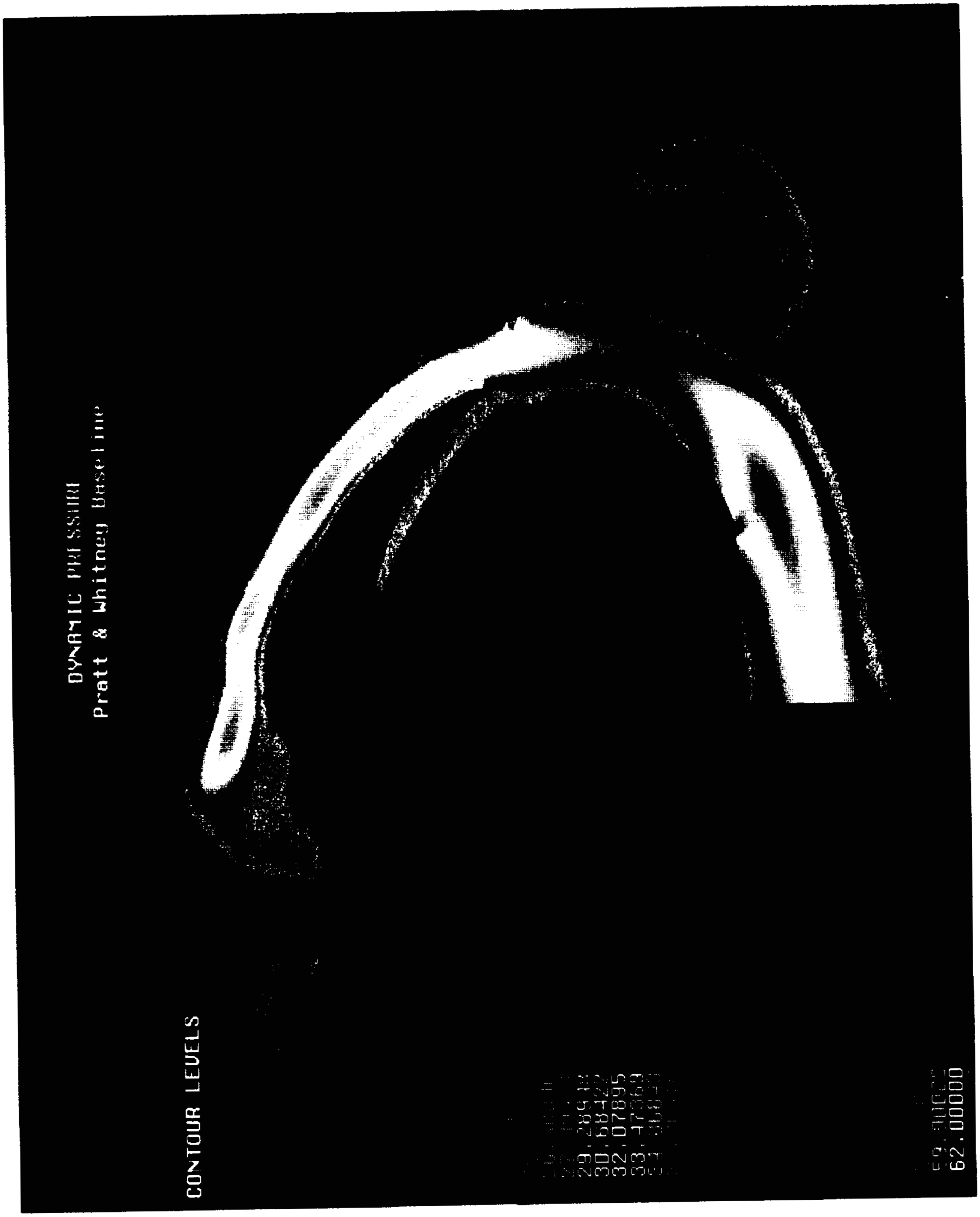
DYNAMIC PRESSURE
Pratt & Whitney Baseline
CONTOUR LEVELS
32.07895
62.00000

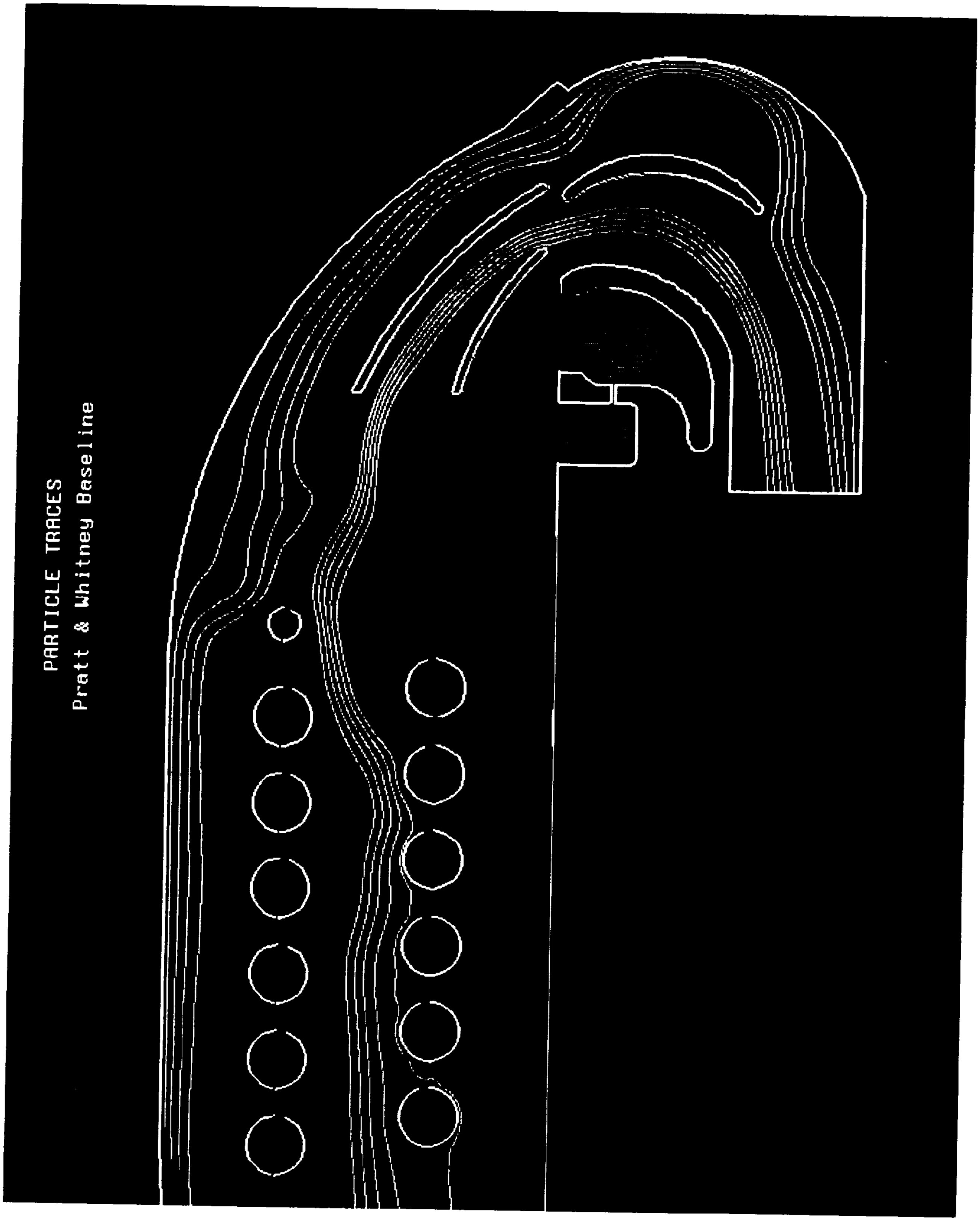
PARTICLE TRACES
Pratt & Whitney Baseline


0.96800
0.96910
0.97020
0.97130
0.99220
0.99330
0.99440
0.99550

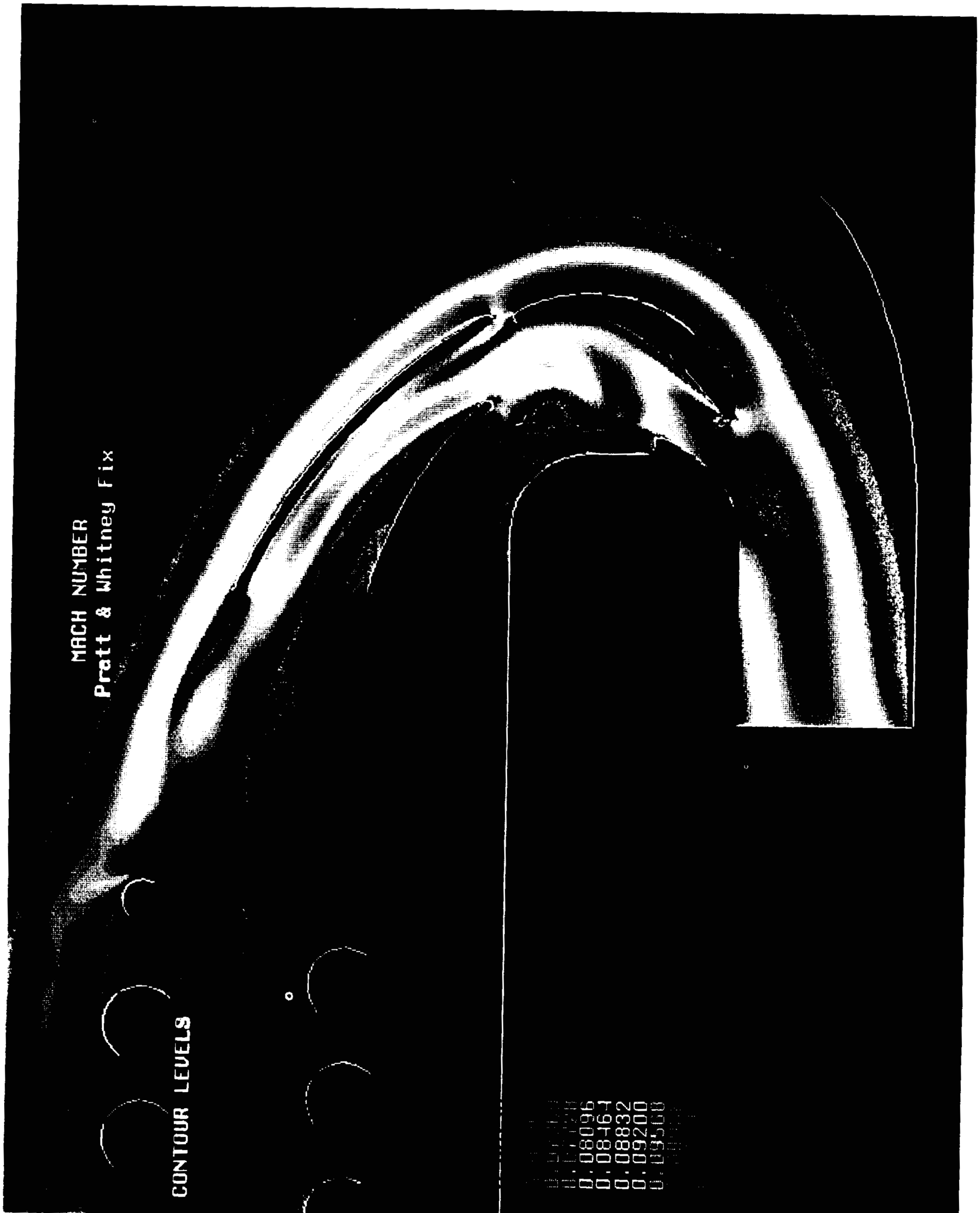
MACH NUMBER
Pratt & Whitney Fix
CONTOUR LEVELS
0.08096
0.08464
0.08832
0.09200

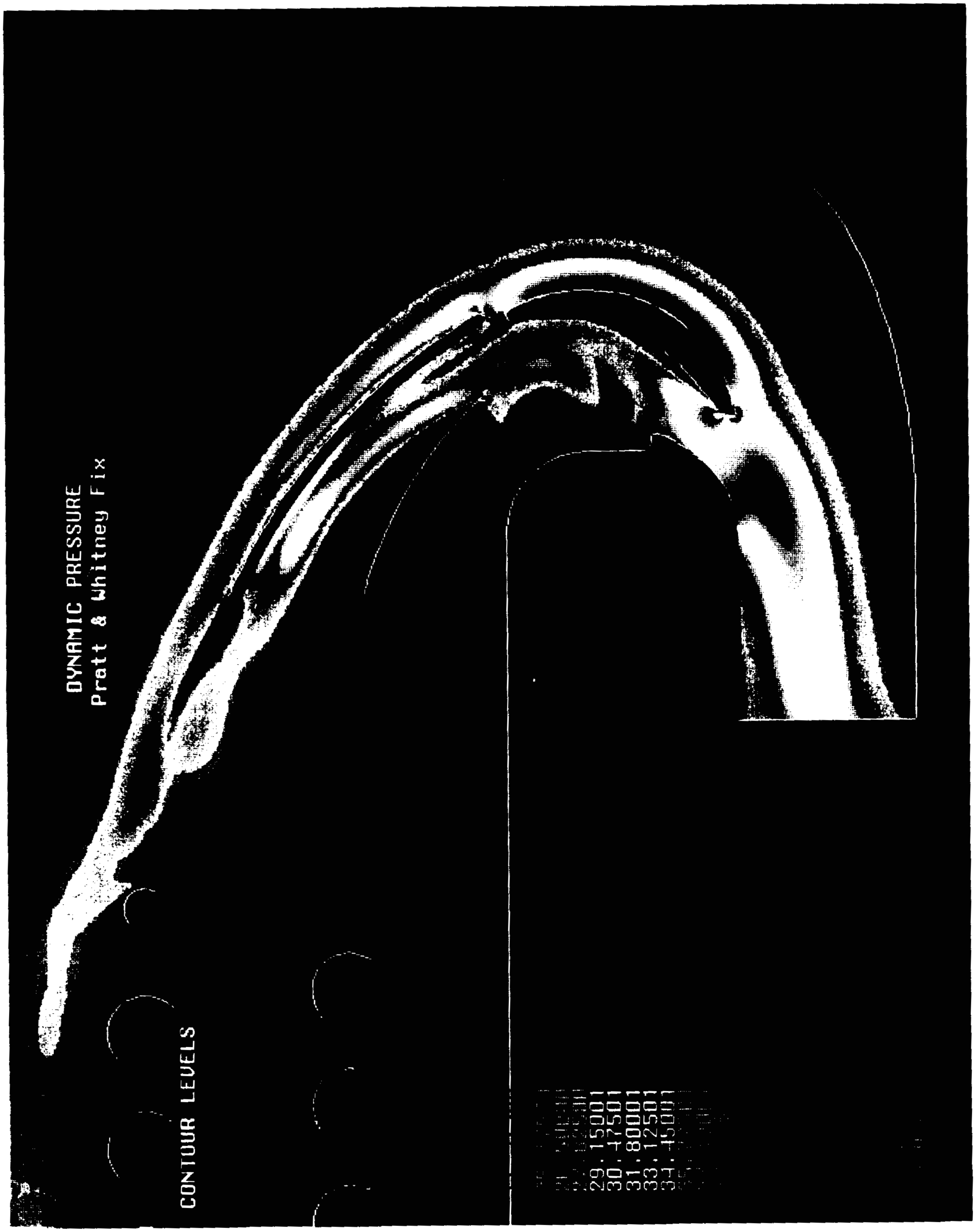
DYNAMIC PRESSURE
Pratt & Whitney Fix
CONTOUR LEVELS
29.15001
30.47501
31.80001
33.12501

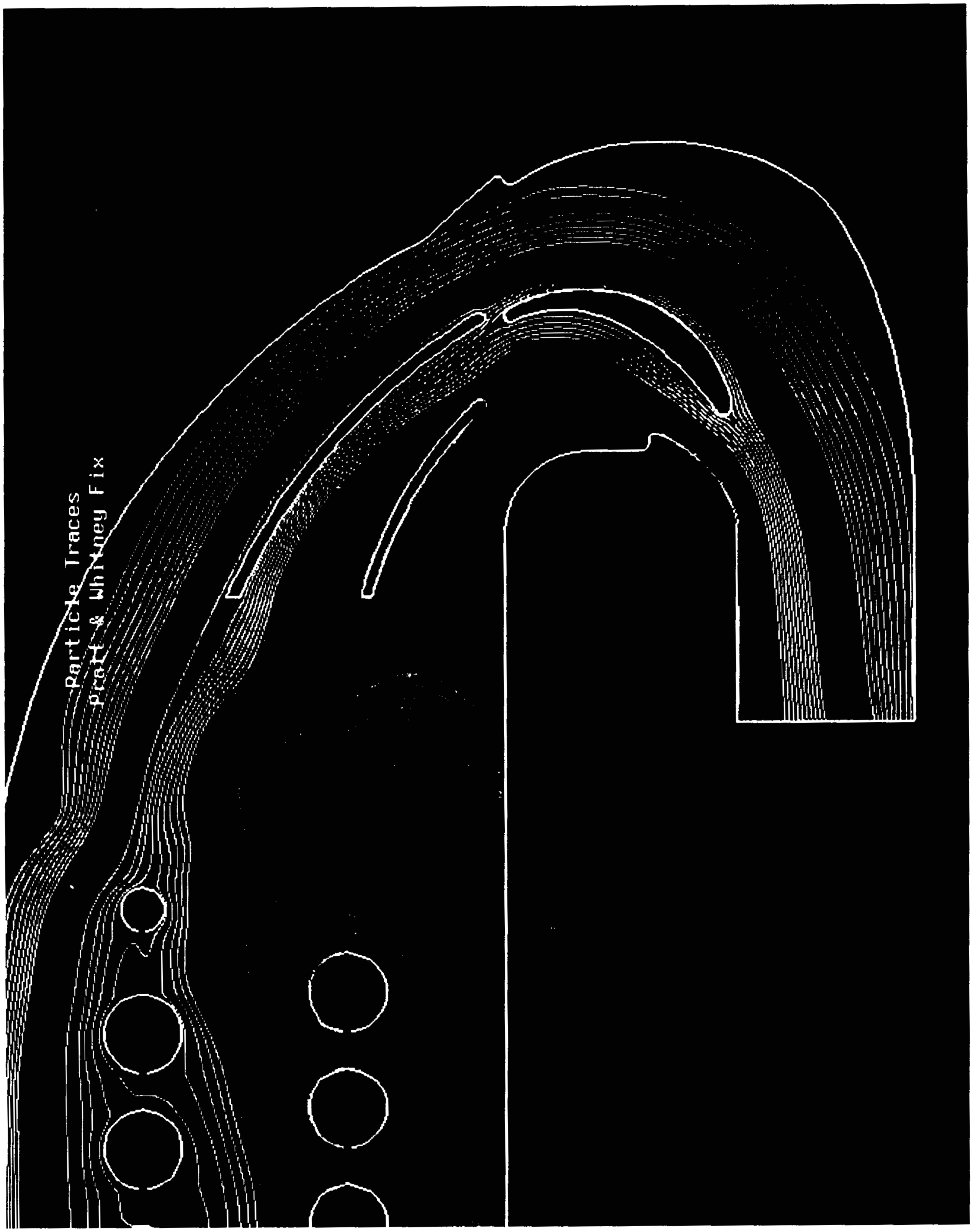
Particle Traces
Pratt & Whitney Fix

ENGINE HEX TURNING VANE CRACKING INVESTIGATION
UNSTEADY CFD ANALYSIS

THE ACOUSTICALLY-TUNED P&W BASELINE WITH CAVITIES CASE GAVE ABSOLUTE AND DIFFERENTIAL LOADINGS ON THE HEX INNER VANE - - AS LARGE AS 4 PSID

P_{REF} = 3625 PSI

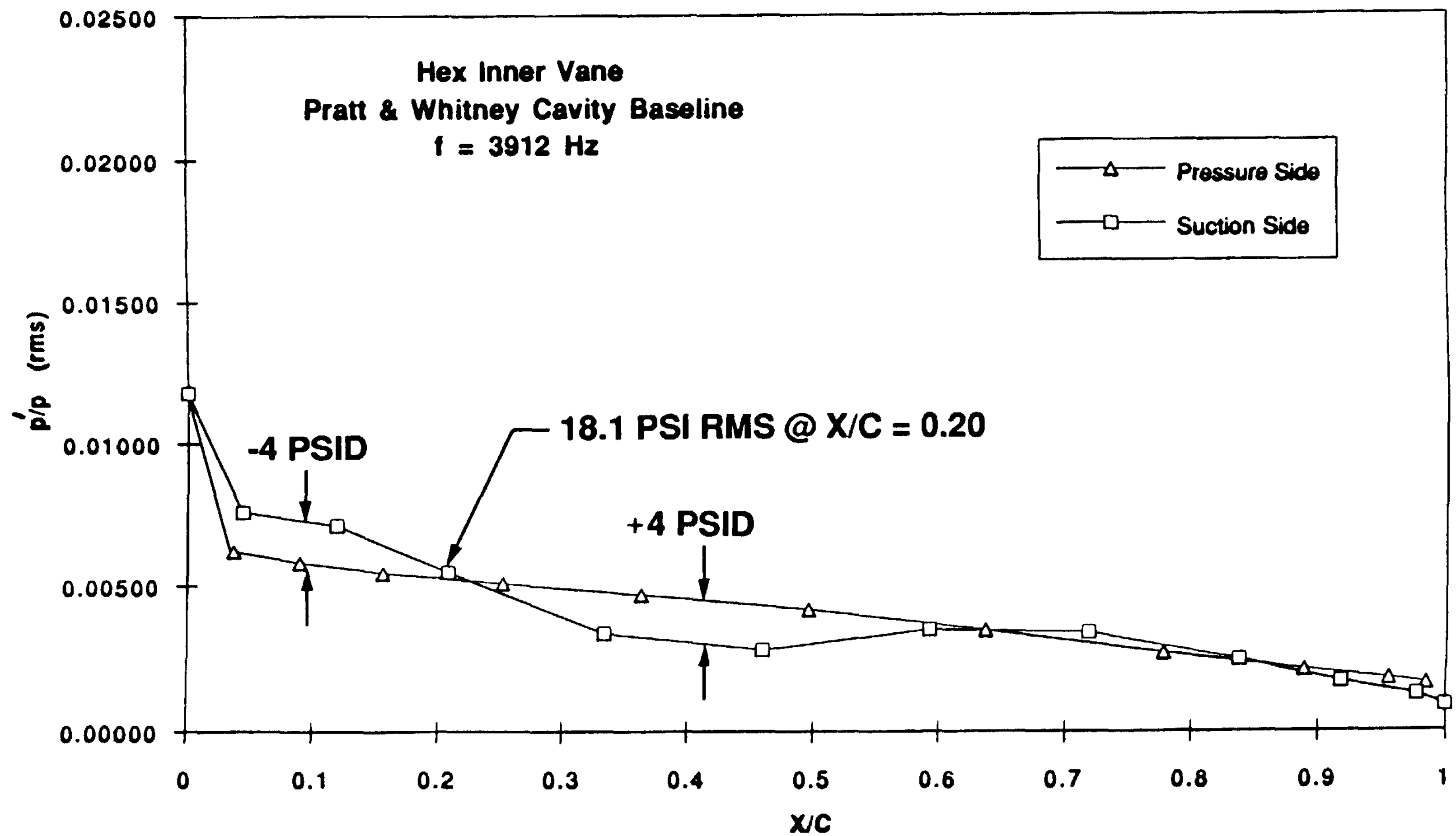

RENG002492.03

ENGINE HEX TURNING VANE CRACKING INVESTIGATION
UNSTEADY CFD ANALYSIS

PRELIMINARY CONCLUSIONS

1) UNSTEADY PRESSURE DIFFERENTIAL LOADINGS WERE PRODUCED LARGE ENOUGH TO CRACK THE HEX INNER VANE IN THE BASELINE CONFIGURATION. (WITH EXCESSIVE ACOUSTIC TUNING, THEY WERE LARGE ENOUGH TO CRACK THE HEX OUTER VANE ALSO)

2) UNSTEADY PRESSURE DIFFERENTIAL LOADINGS WERE SOMEWHAT REDUCED ON THE HEX INNER VANE FOR THE "FIX" CONFIGURATION BUT THE HEX COIL ENVIRONMENT IS INCREASED

NOTE: ANALYSIS OF COMPUTATIONAL RESULTS STILL IN PROGRESS
DUE: APRIL 26, 1993

ASC

Advanced
Scientific
Computing
Corp.

COMPARISON BETWEEN PREDICTED AND EXPERIMENTALLY MEASURED FLOW FIELDS AT THE EXIT OF THE SSME HPFTP IMPELLER

George Bache'

Advanced Scientific Computing Corp.
4721 Broome Place
El Dorado Hills, CA 95762

N95- 23622

ABSTRACT

Validation of CFD codes is a critical first step in the process of developing CFD design capability. The MSFC Pump Technology Team has recognized the importance of validation and has thus funded several experimental programs designed to obtain CFD quality validation data. The first data set to become available is for the SSME High Pressure Fuel Turbopump Impeller. LDV Data was taken at the impeller inlet (to obtain a reliable inlet boundary condition) and three radial positions at the impeller discharge.

Our CFD code, TASCflow, is used within the Propulsion and Commercial Pump Industry as a tool for pump design. The objective of this work, therefore, is to further validate TASCflow for application in pump design. TASCflow was used to predict flow at the impeller discharge for flowrates of 80, 100 and 115 percent of design flow. Comparison to data has been made with encouraging results.

Approach

- Develop Computational Model
  - TRUEGRID
  - ICEM CFD

- Set Inlet Boundary Condition Based on Measured Inlet Conditions
  - LDV Measurements Obtained From Rocketdyne and NASA/MSFC at Q/Qd=0.8, 1.0, and 1.15

- Compute Flow for SSME HPFTP Impeller at Q/Qd=0.8, 1.0, and 1.15.
  - Computations Performed With ***TASCflow***

- Compare Predicted Exit Velocity Profiles to Measured
  - LDV Measurements Obtained From Rocketdyne and NASA/MSFC at Q/Qd=0.8, 1.0, and 1.15
  - Non-Dimensional Velocities (Vel/Utip)

ASC

Computational Grid

89x29x60 (154860 Nodes)

Advanced
Scientific
Computing
Corp.

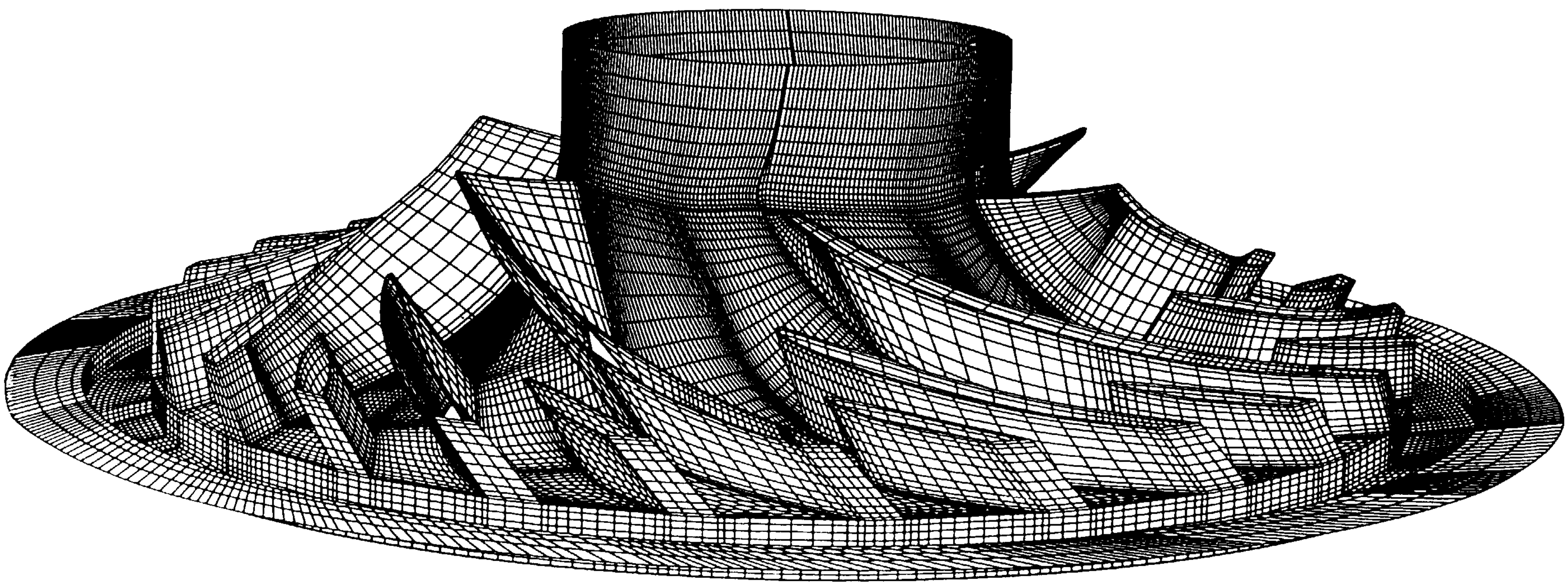

ASC

Computational Grid

89x29x60 (154860 Nodes)

Advanced
Scientific
Computing
Corp.

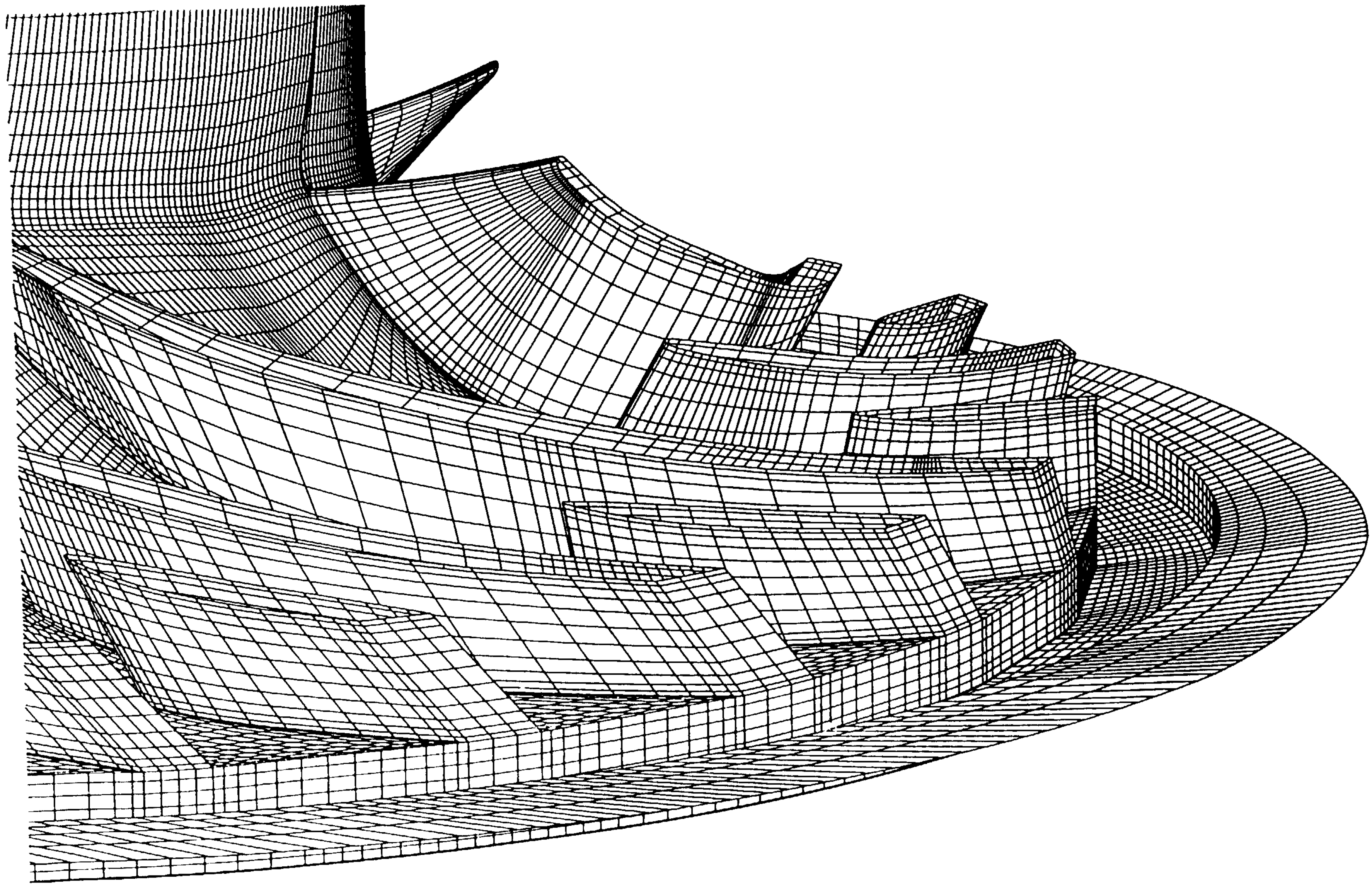

ASC

Advanced
Scientific
Computing
Corp.

SSME HPFTP IMPELLER COMPUTATIONAL DOMAIN AND BOUNDARY CONDITIONS

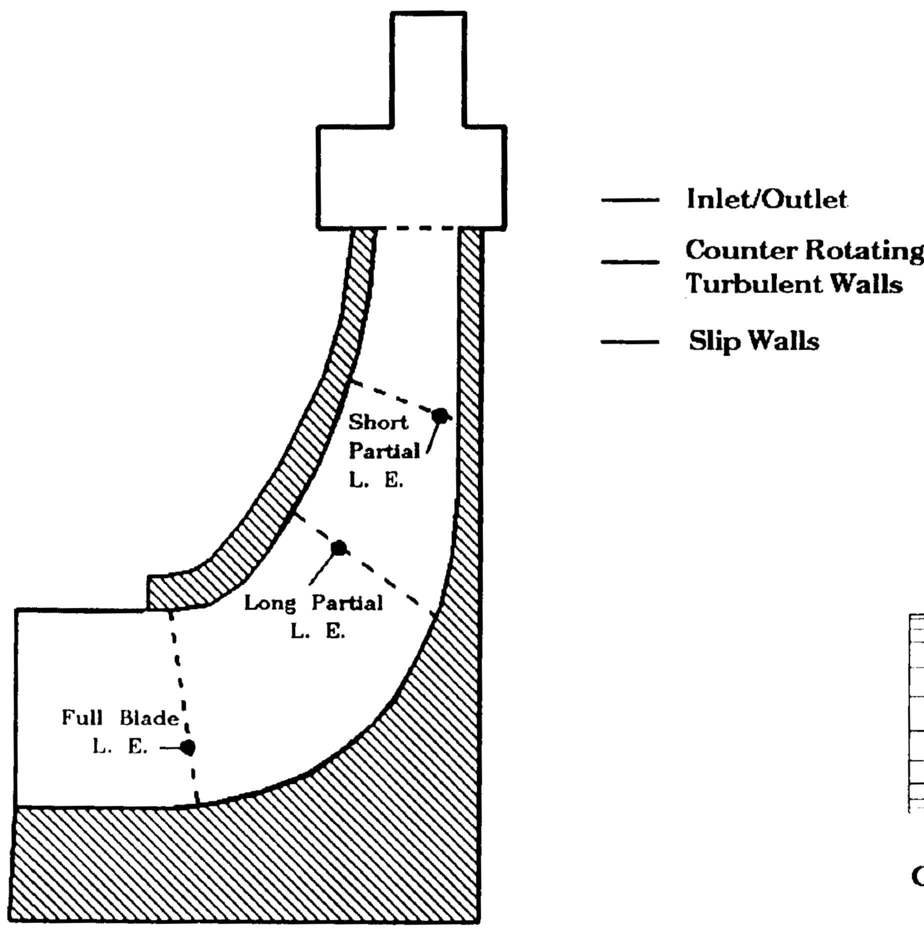

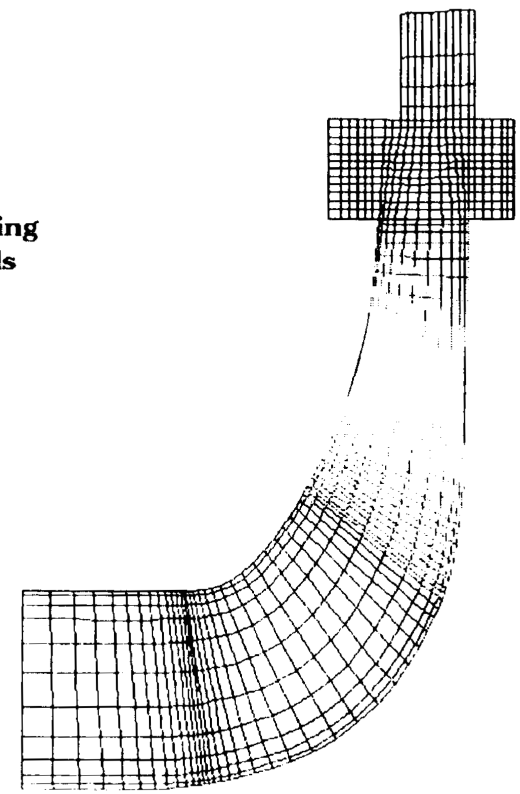

GRID COLORED BY PRESSURE

ASC

TASCflow

Advanced
Scientific
Computing
Corp.

Collocated, Finite Volume, Primitive Variable

Incompressible - Subsonic - Transonic - Supersonic

Viscous - Laminar or Turbulent (k-e)

Steady or Unsteady

Stationary or Rotating Frame of Reference

Porous Media

Heat Transfer Including Conjugate Heat Transfer

Natural Convection

Species Transport

Chemical Reaction

ASC

Advanced
Scientific
Computing
Corp.

SSME HPFTP IMPELLER
LASER VELOCIMETER DATA SURVEY LOCATIONS

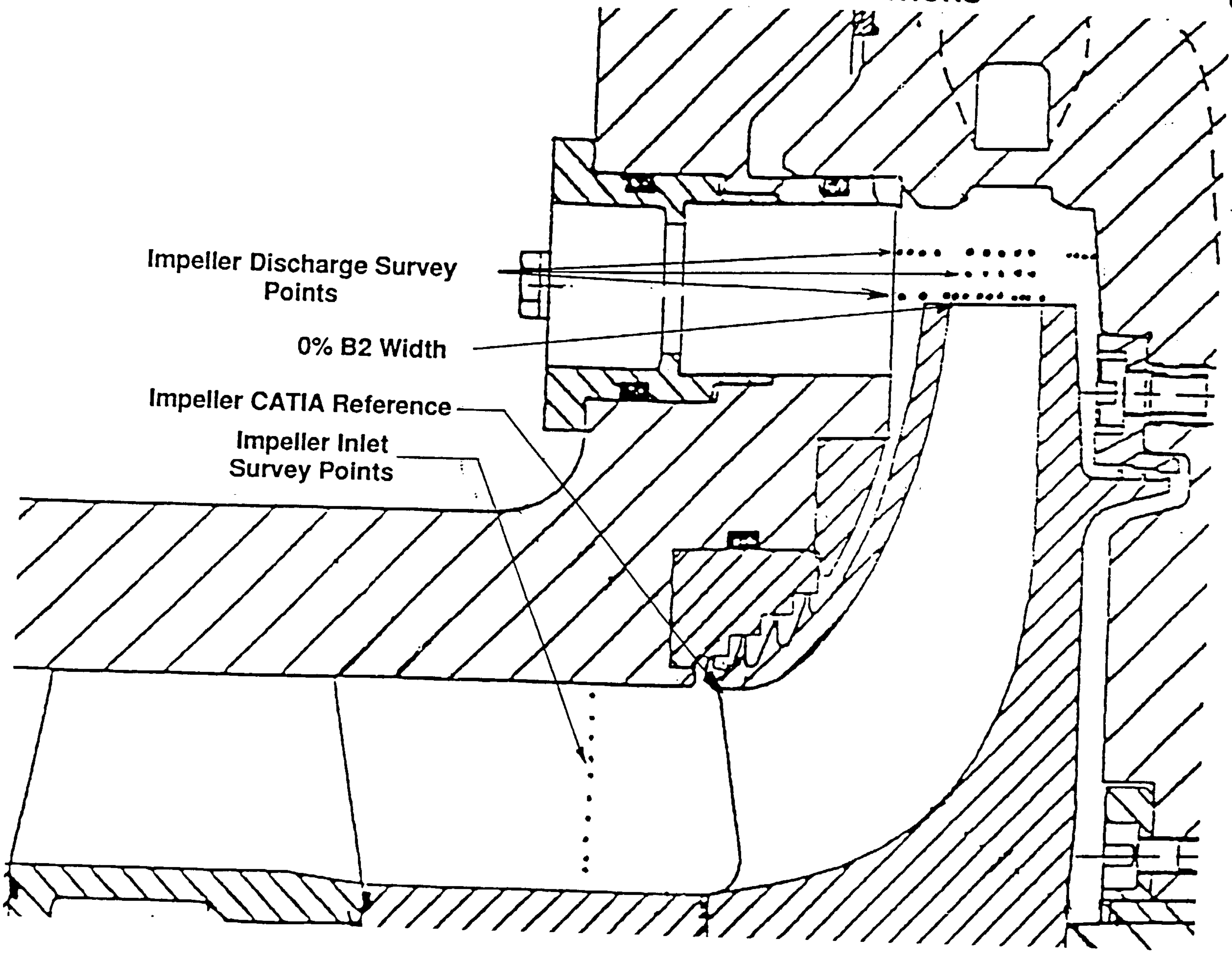

GRID STRUCTURE AT R/RTIP=1.Ø13

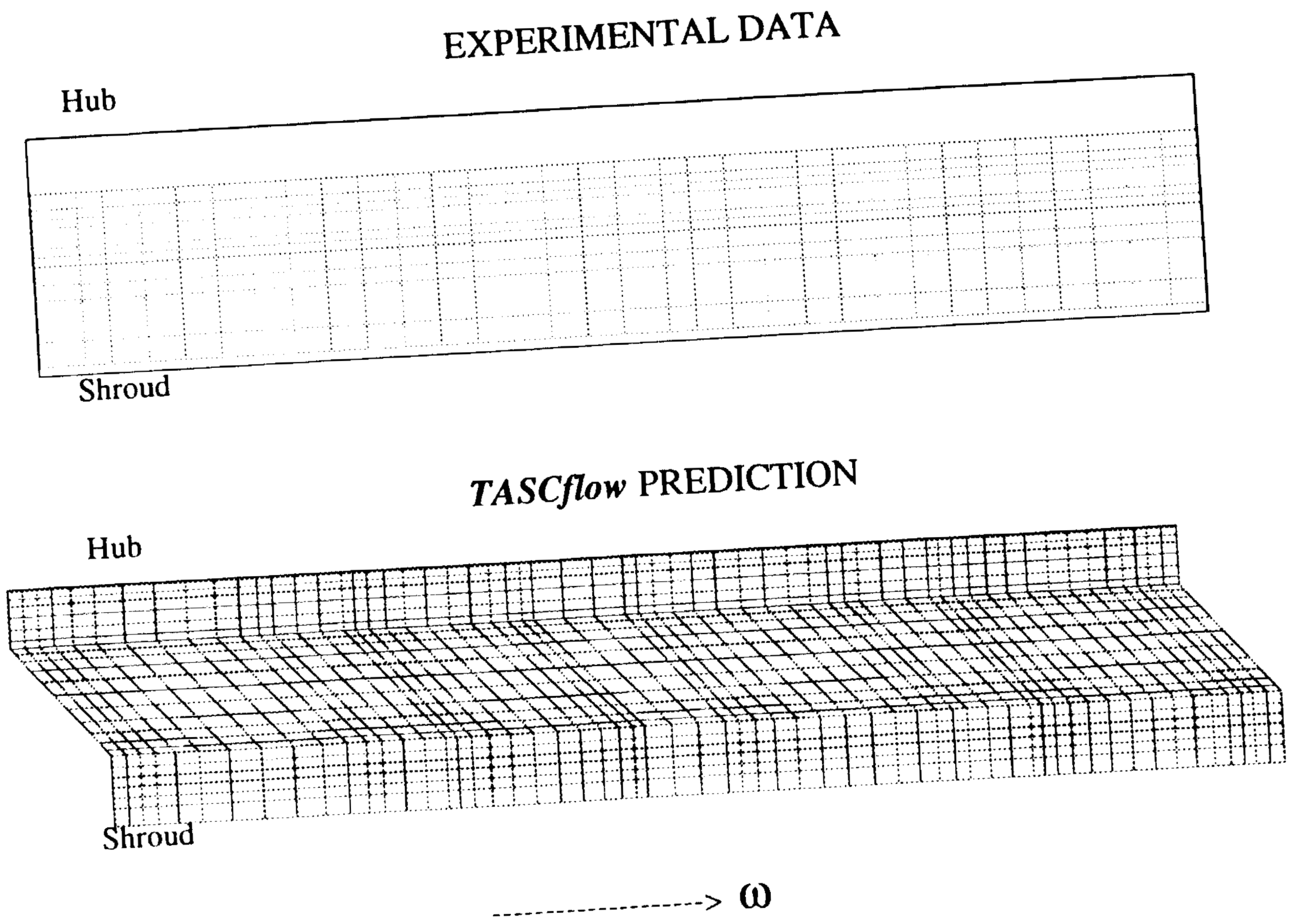

ABS. VELOCITY FOR Q/QD=1.Ø. R/RTIP=1.Ø13

EXPERIMENTAL DATA

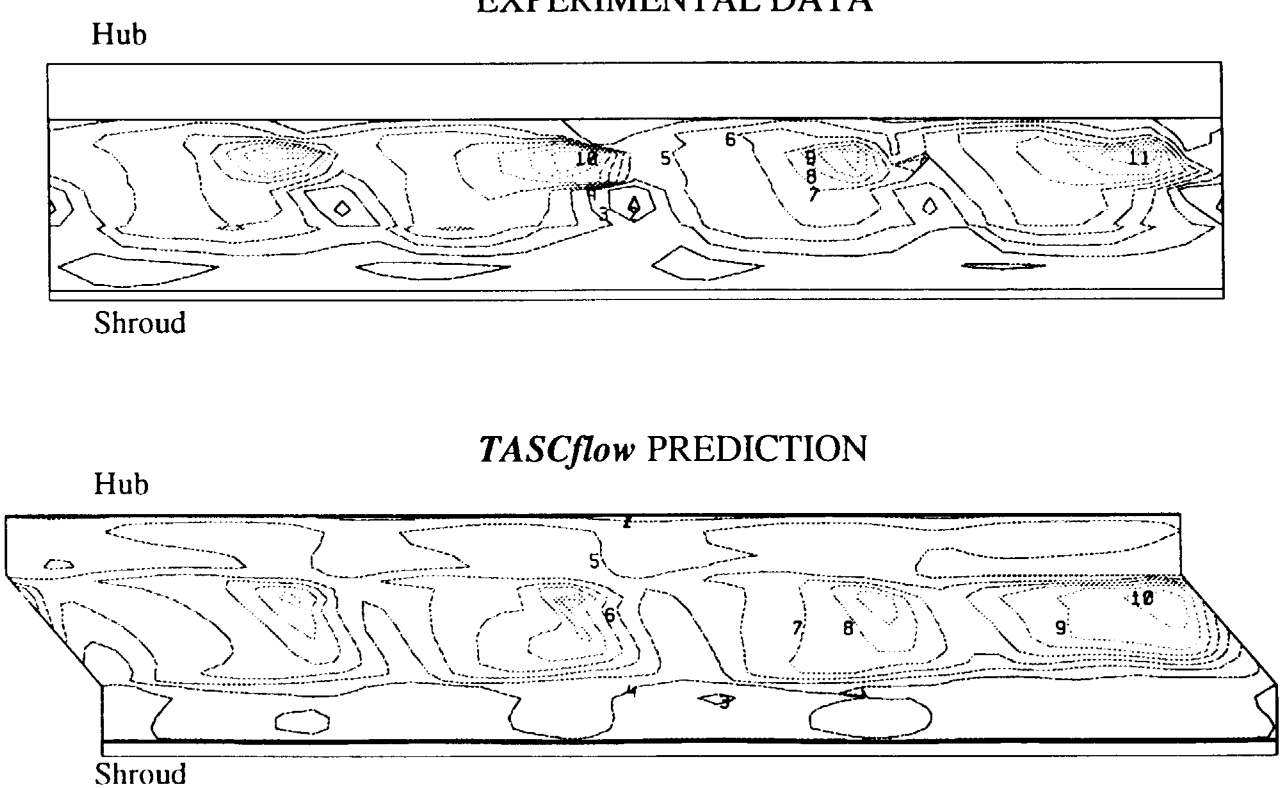

--------------------> ω

	C
12	9.5ØØE-Ø1
11	9.ØØØE-Ø1
1Ø	8.5ØØE-Ø1
9	8.ØØØE-Ø1
8	7.5ØØE-Ø1
7	7.ØØØE-Ø1
6	6.5ØØE-Ø1
5	6.ØØØE-Ø1
4	5.5ØØE-Ø1
3	5.ØØØE-Ø1
2	4.5ØØE-Ø1
1	4.ØØØE-Ø1

ASC ABSOLUTE VELOCITY. 50 PERCENT B2

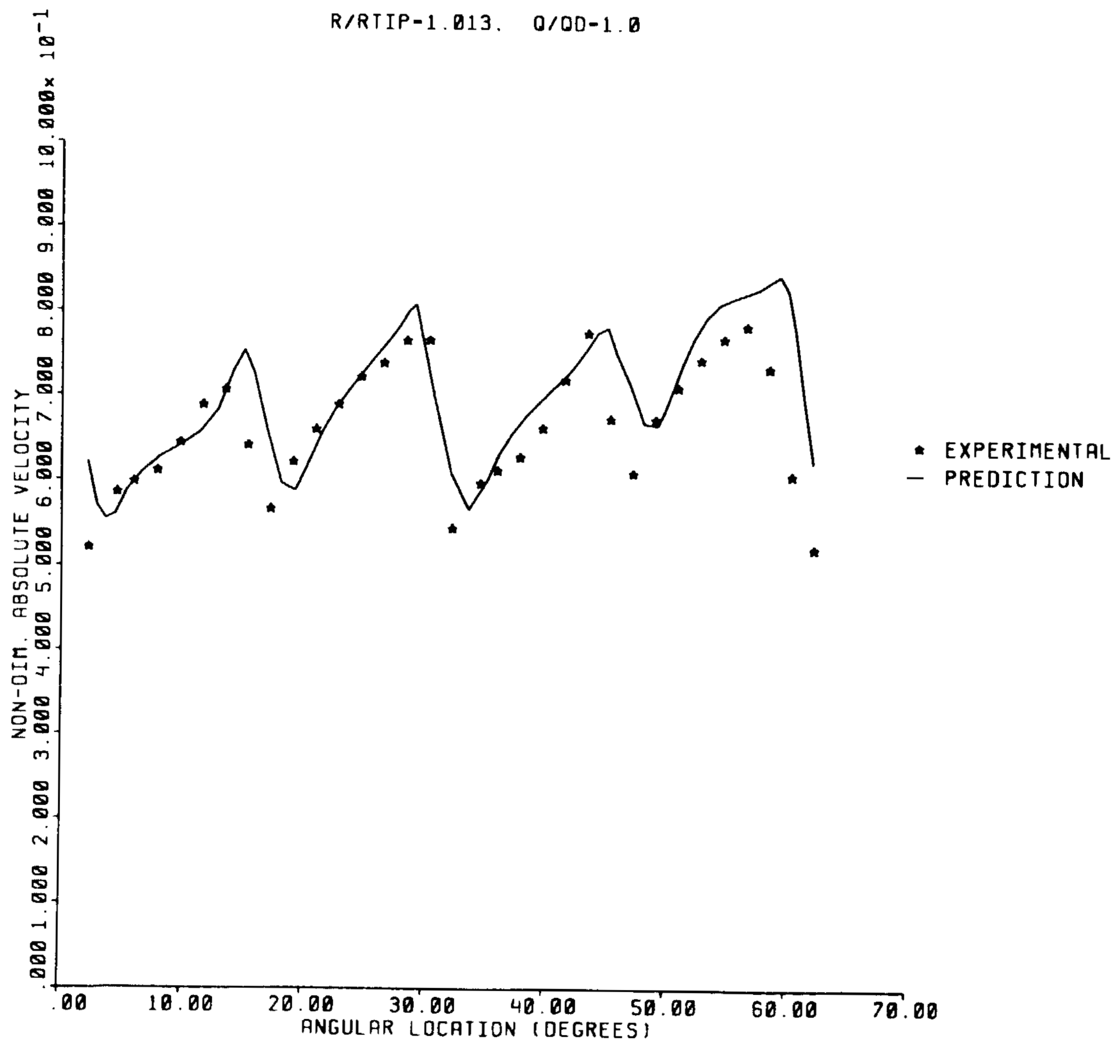

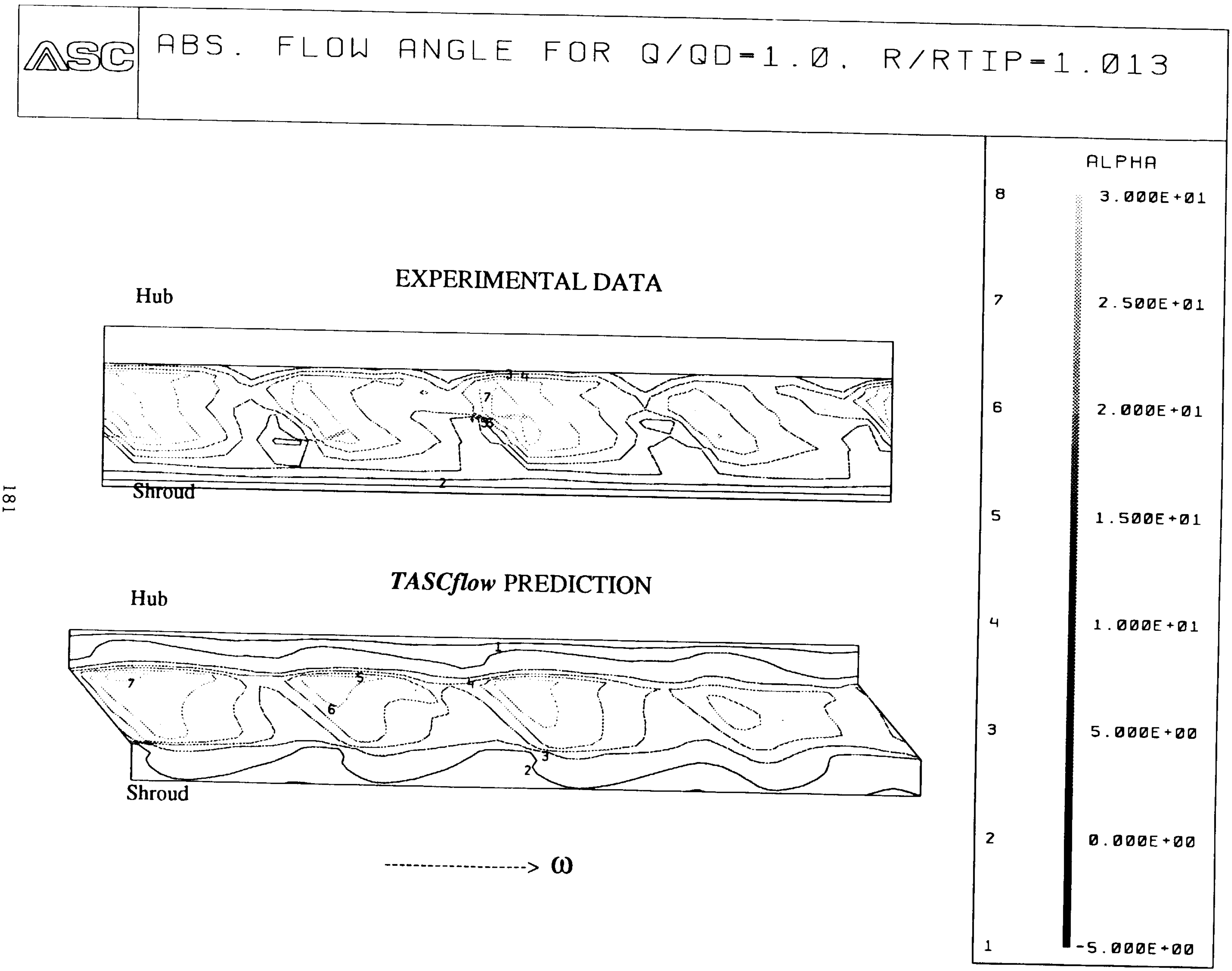
ASC
ABS. FLOW ANGLE FOR Q/QD=1.Ø. R/RTIP=1.Ø13
ALPHA
8 3.ØØØE+Ø1
7 2.5ØØE+Ø1
6 2.ØØØE+Ø1
5 1.5ØØE+Ø1
4 1.ØØØE+Ø1
3 5.ØØØE+ØØ
2 Ø.ØØØE+ØØ
1 -5.ØØØE+ØØ
EXPERIMENTAL DATA
Hub
Shroud
TASCflow PREDICTION
Hub
Shroud
-------------------> ω

ABSOLUTE FLOW ANGLE, 5Ø PERCENT B2

R/RTIP-1.Ø13, Q/QD-1.Ø

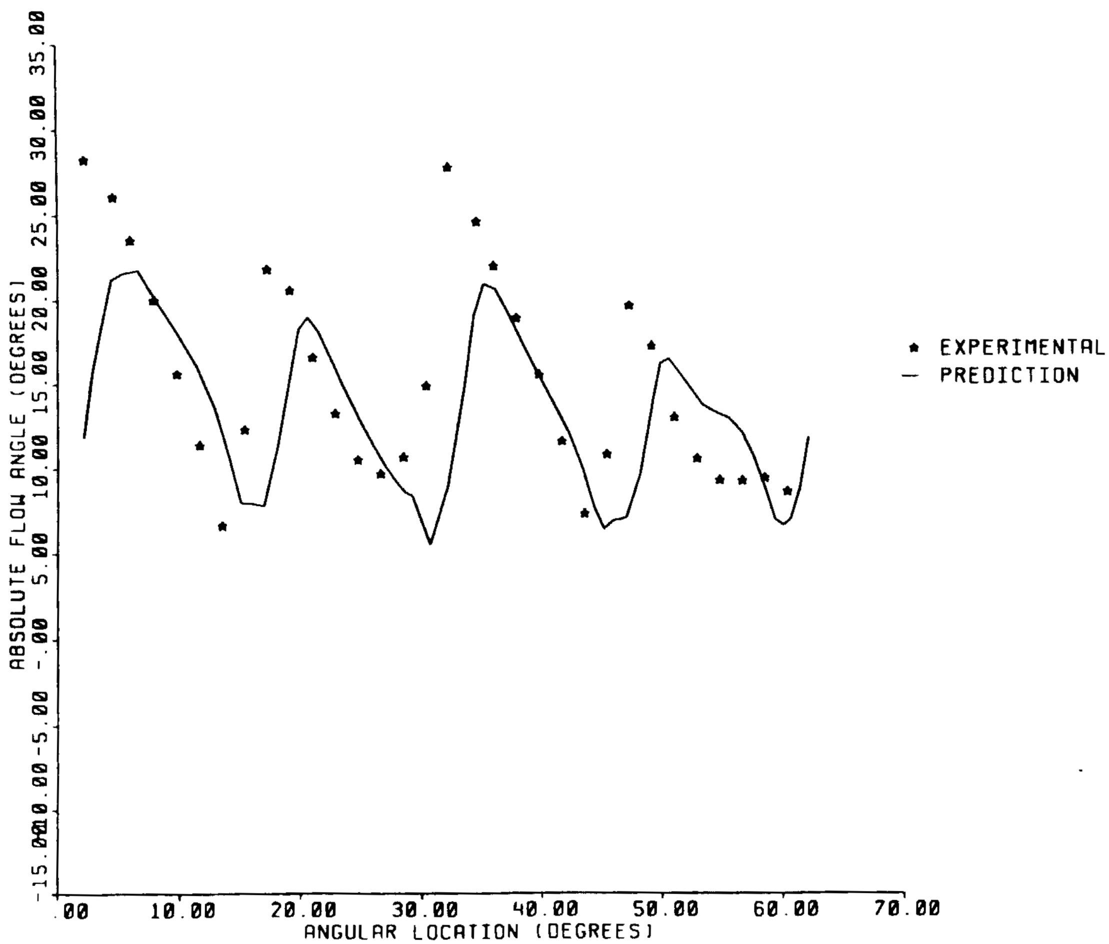

GRID STRUCTURE AT R/RTIP=1.036

EXPERIMENTAL DATA

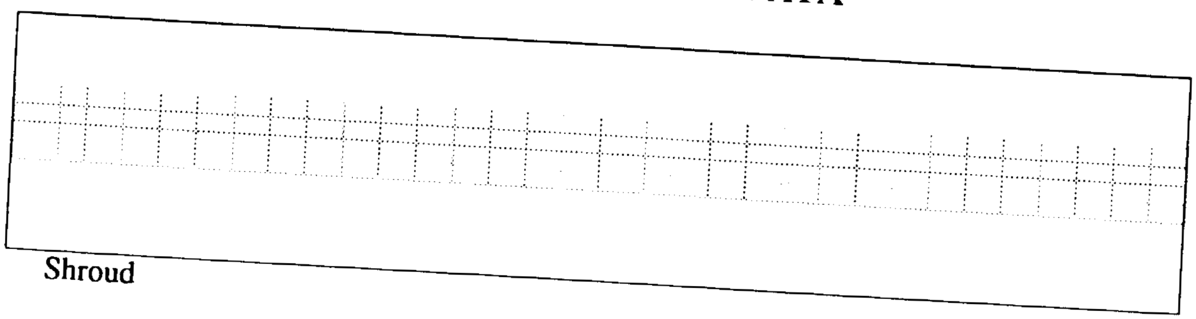

TASCflow PREDICTION

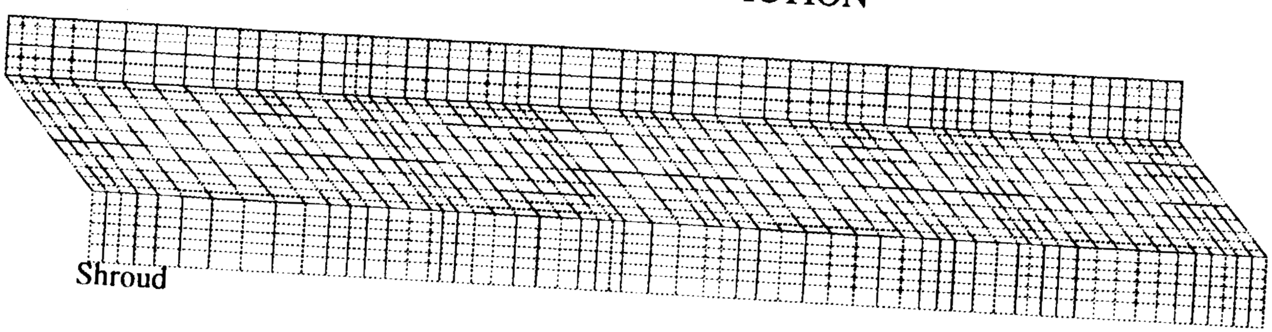

-------------------> ω

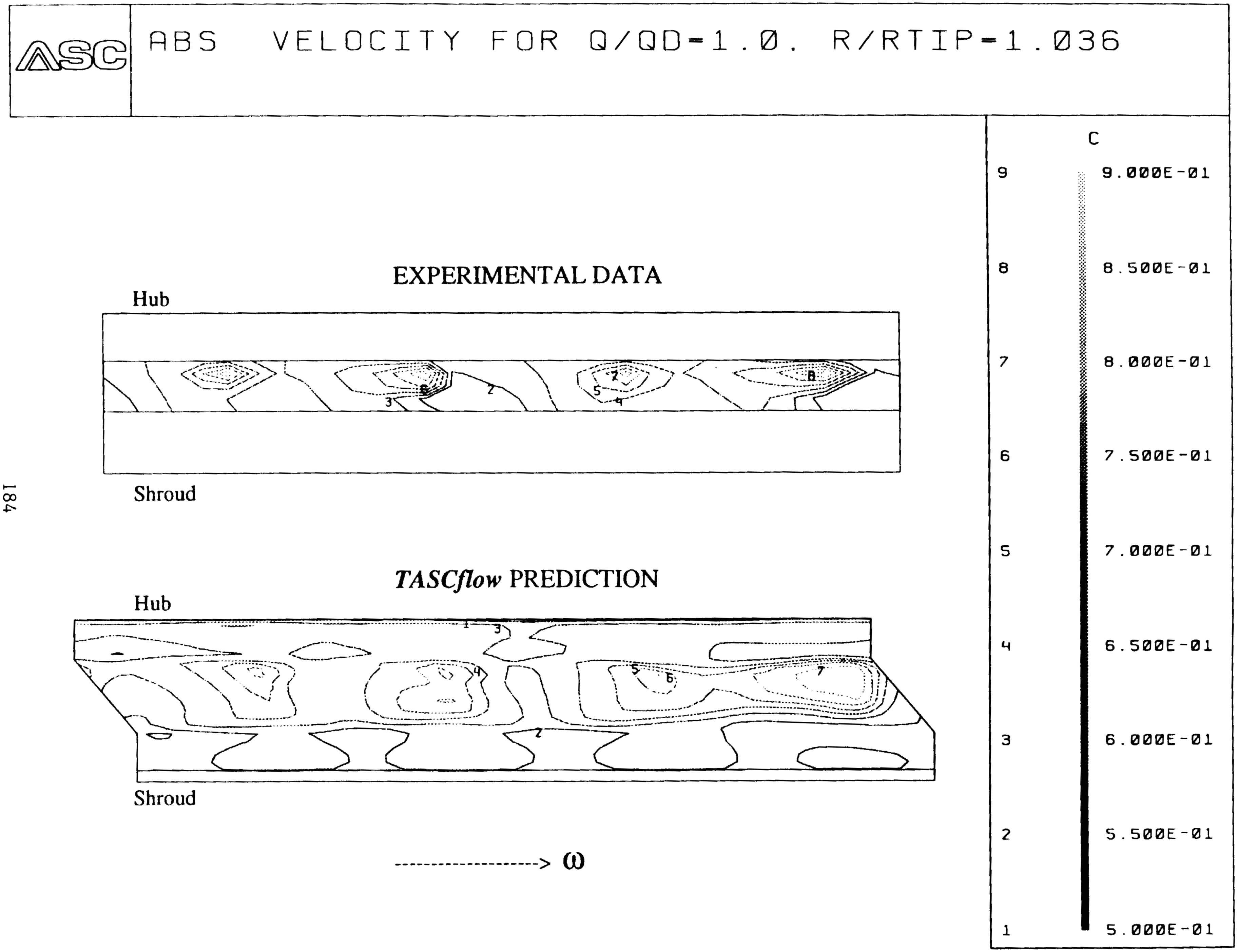
ASC
ABS VELOCITY FOR Q/QD=1.0. R/RTIP=1.036
EXPERIMENTAL DATA
Hub
Shroud
TASCflow PREDICTION
Hub
Shroud
ω
C
9 9.000E-01
8 8.500E-01
7 8.000E-01
6 7.500E-01
5 7.000E-01
4 6.500E-01
3 6.000E-01
2 5.500E-01
1 5.000E-01

C-3.

ABSOLUTE VELOCITY. 50 PERCENT B2

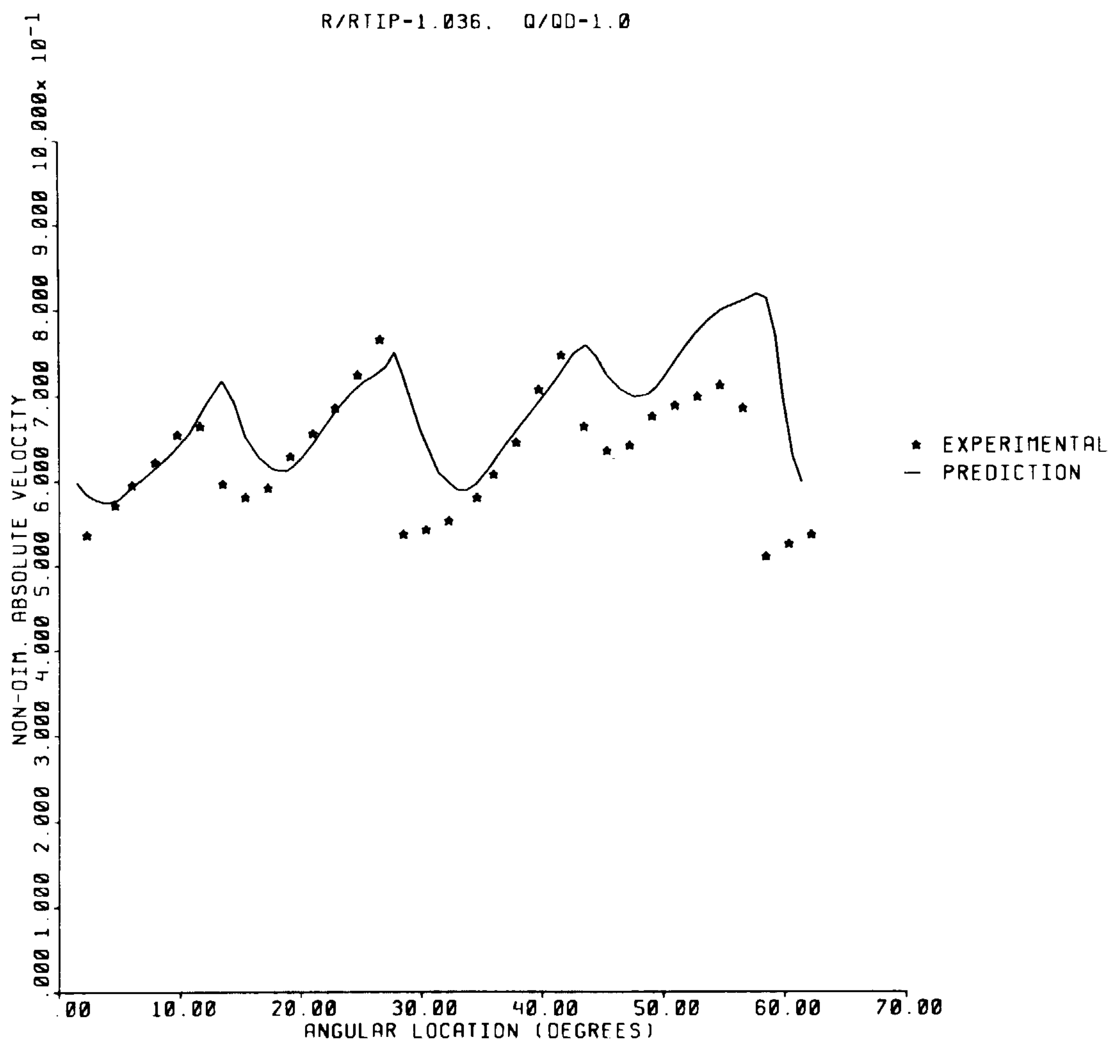

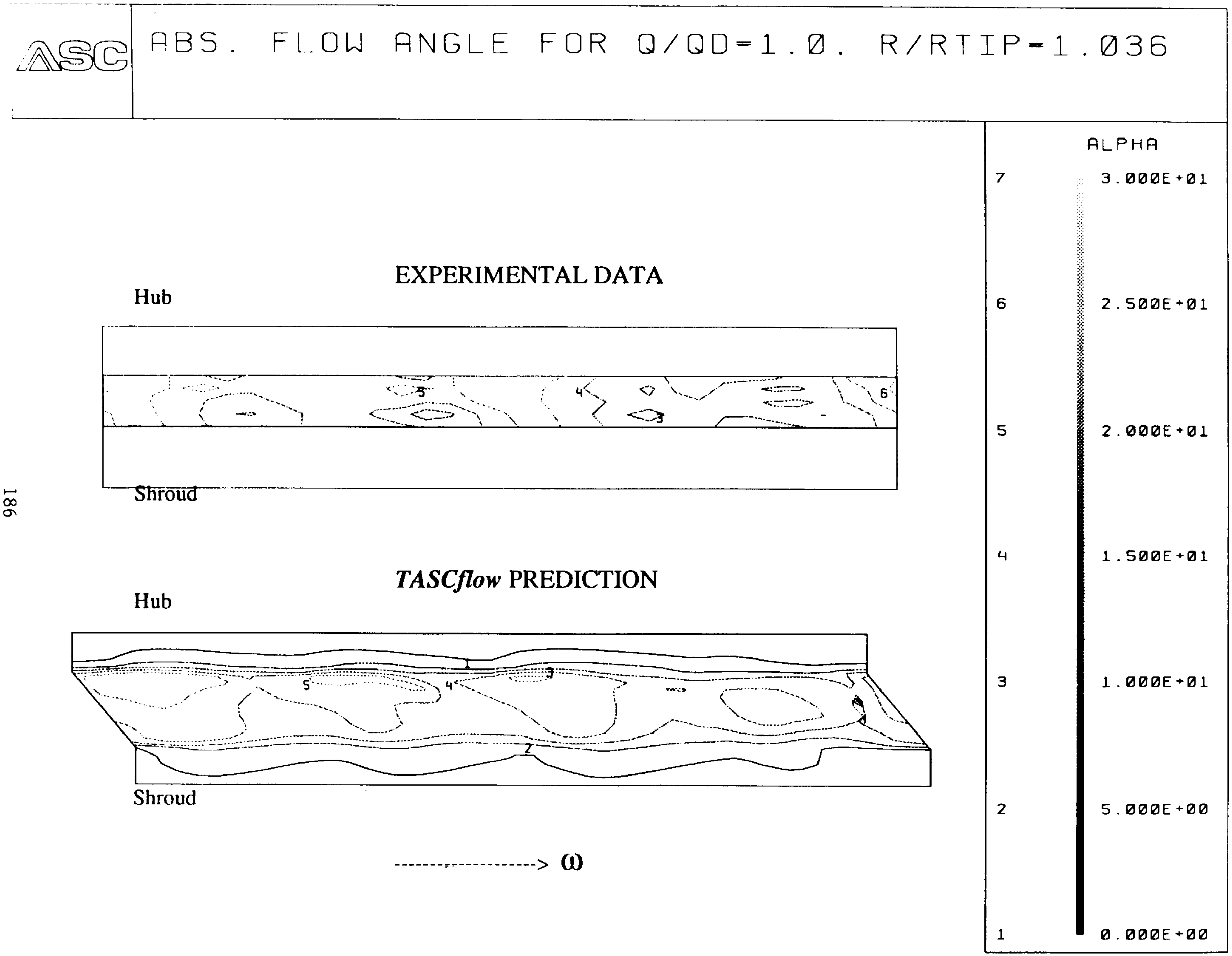
ABS. FLOW ANGLE FOR Q/QD=1.Ø. R/RTIP=1.Ø36
EXPERIMENTAL DATA
Hub
Shroud
TASCflow PREDICTION
Hub
Shroud
ω
ALPHA
7 3.ØØØE+Ø1
6 2.5ØØE+Ø1
5 2.ØØØE+Ø1
4 1.5ØØE+Ø1
3 1.ØØØE+Ø1
2 5.ØØØE+ØØ
1 Ø.ØØØE+ØØ

ASC ABSOLUTE FLOW ANGLE. 50 PERCENT B2

R/RTIP-1.036. Q/QD-1.0

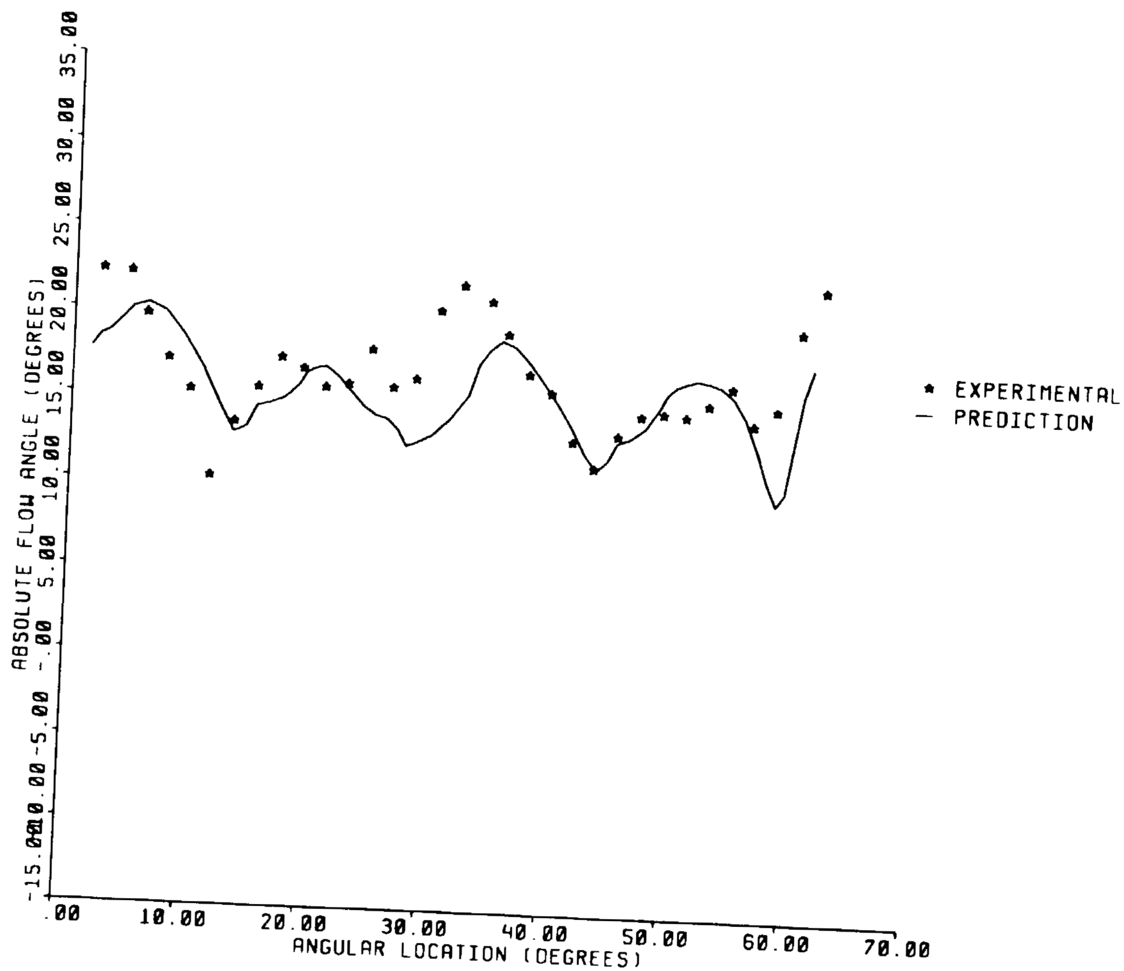

ASC GRID STRUCTURE AT R/RTIP=1.060

EXPERIMENTAL DATA

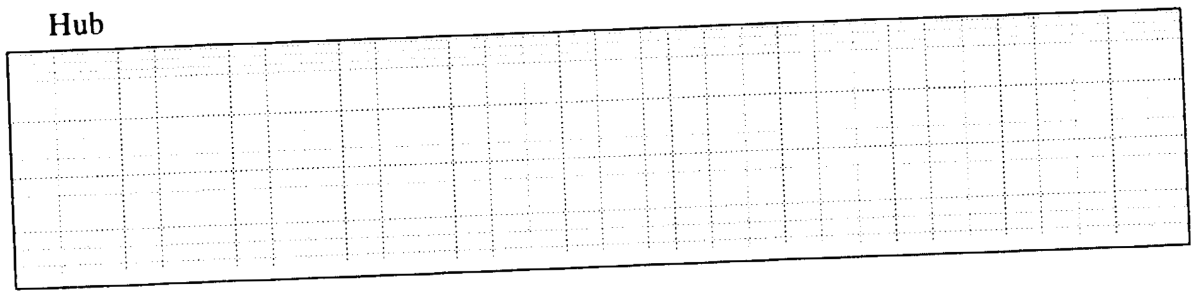

TASCflow PREDICTION

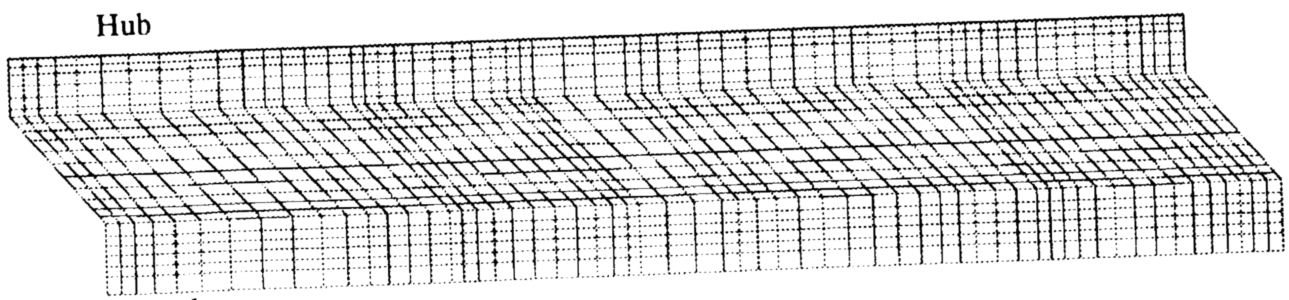

-------------------> ω

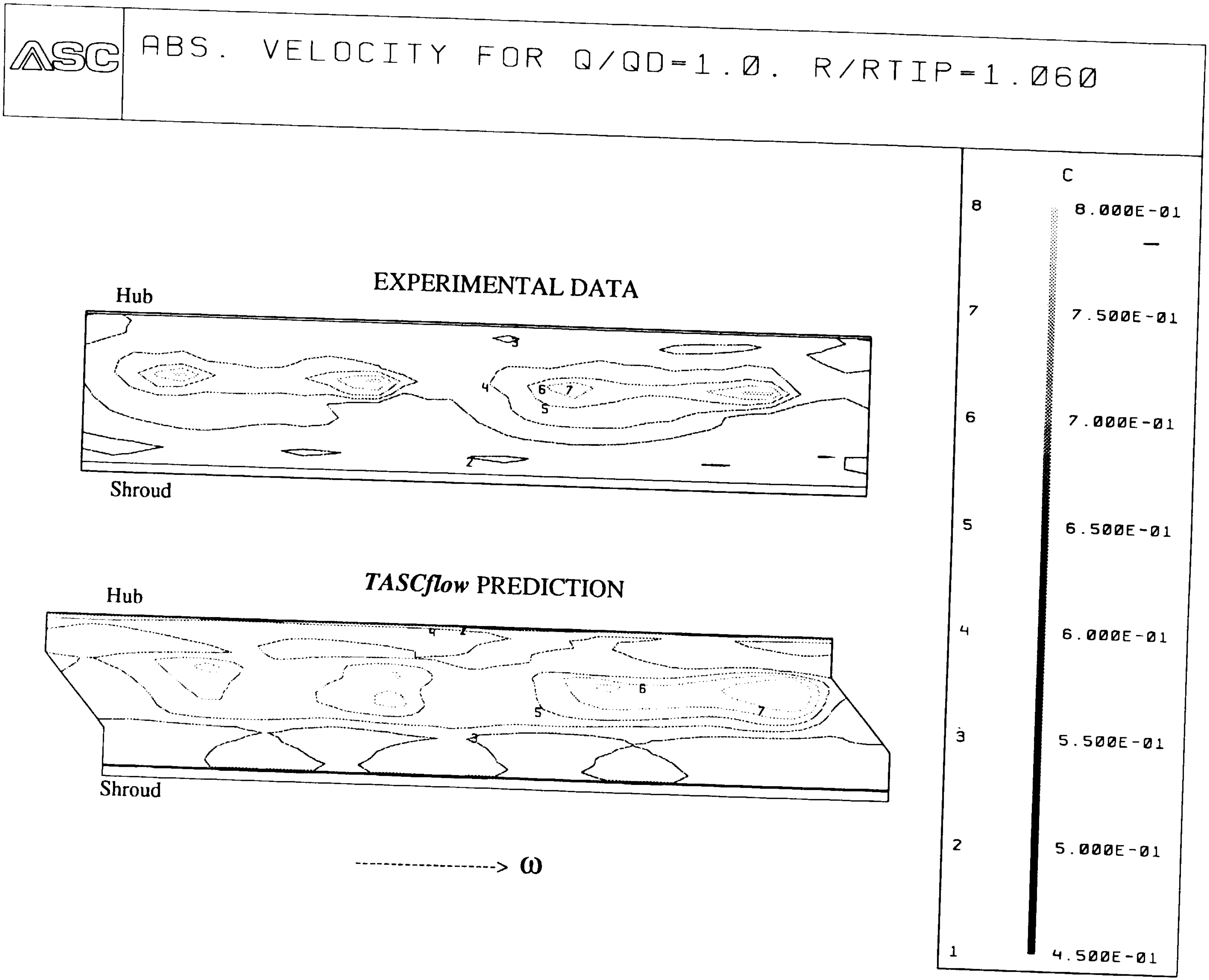
ABS. VELOCITY FOR Q/QD=1.0. R/RTIP=1.060
EXPERIMENTAL DATA
Hub
Shroud
TASCflow PREDICTION
Hub
Shroud
ω
C
8 8.000E-01
7 7.500E-01
6 7.000E-01
5 6.500E-01
4 6.000E-01
3 5.500E-01
2 5.000E-01
1 4.500E-01

ABSOLUTE VELOCITY. 50 PERCENT B2

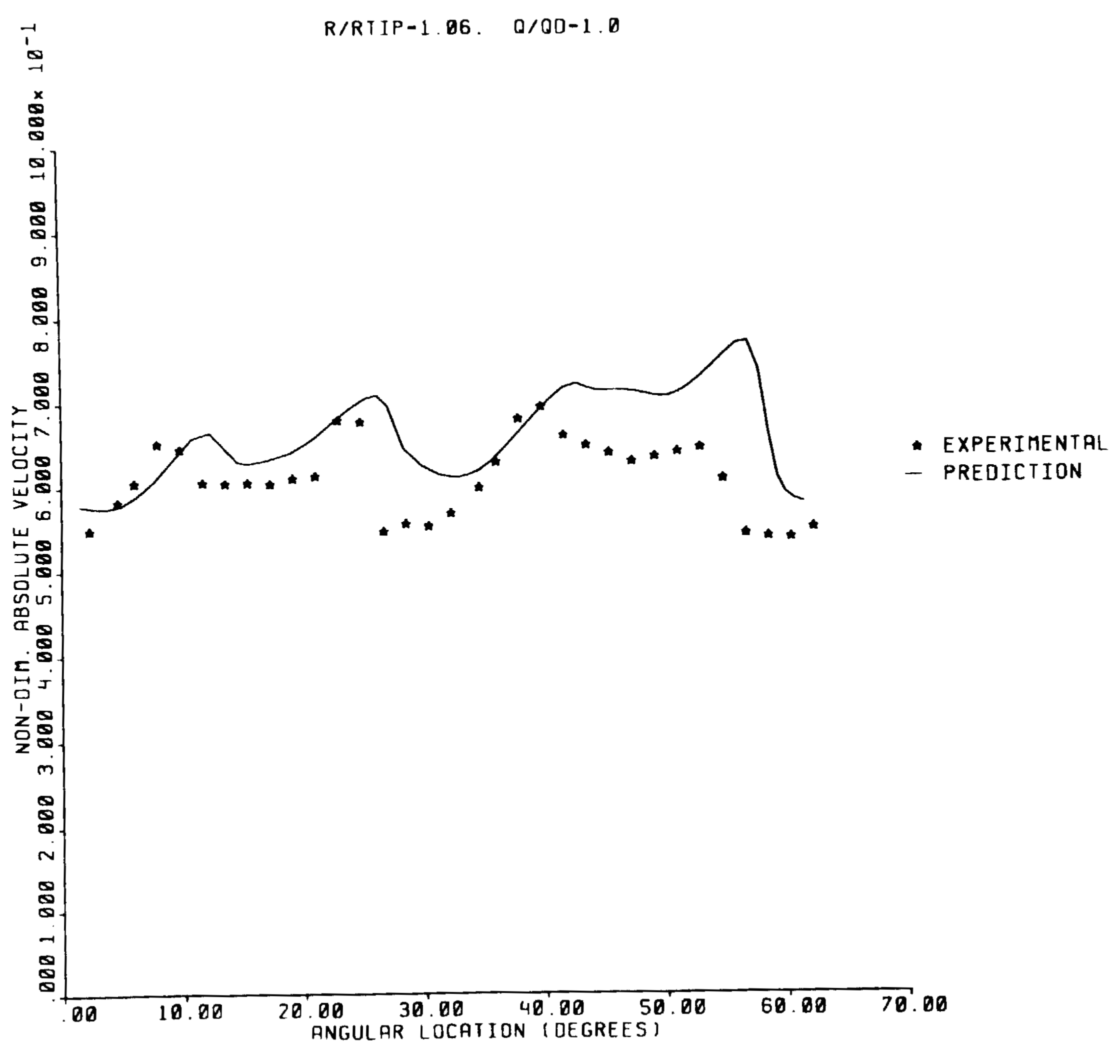

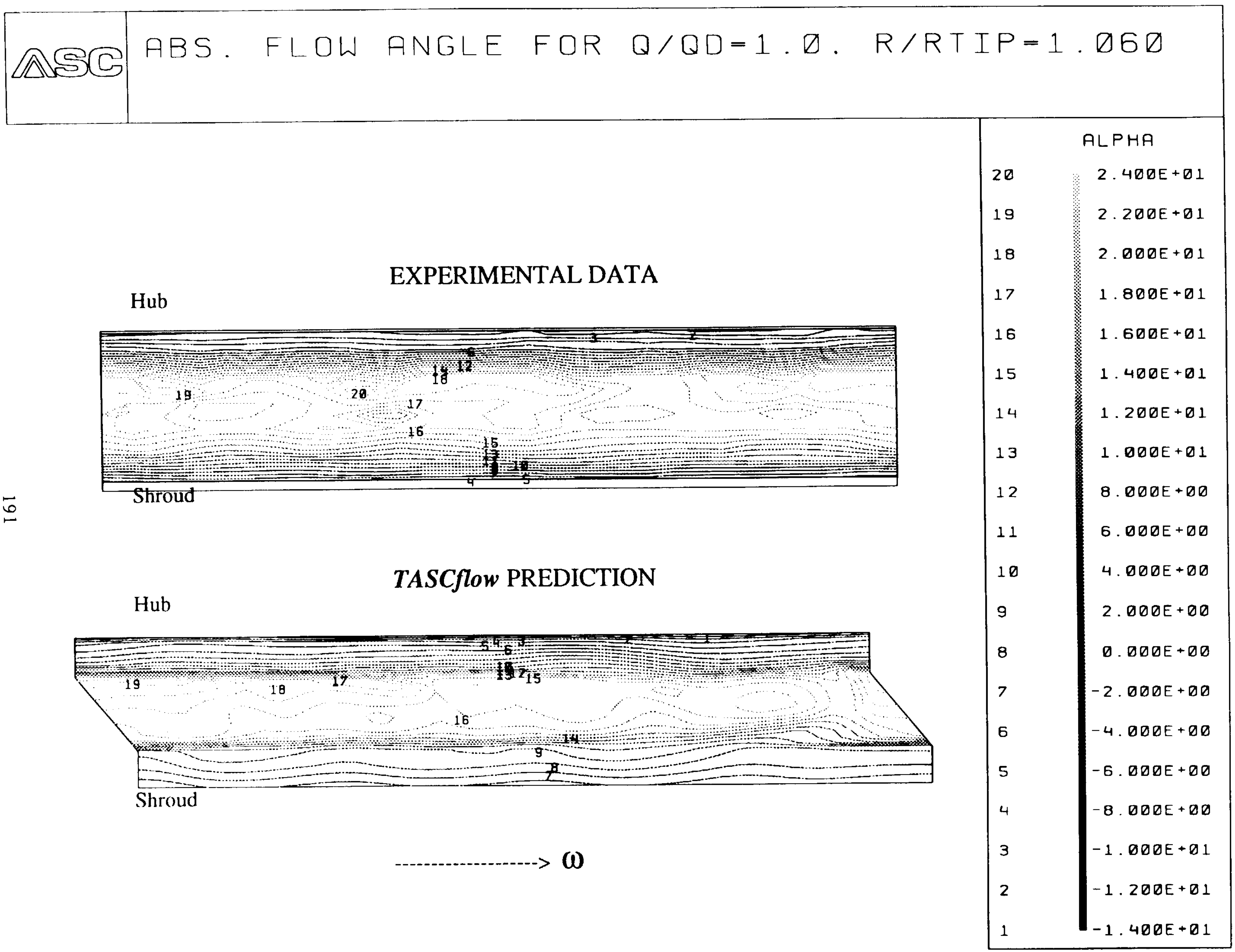

ASC
ABS. FLOW ANGLE FOR Q/QD=1.0. R/RTIP=1.060
EXPERIMENTAL DATA
Hub
Shroud
TASCflow PREDICTION
Hub
Shroud
---------> ω
ALPHA
20 2.400E+01
19 2.200E+01
18 2.000E+01
17 1.800E+01
16 1.600E+01
15 1.400E+01
14 1.200E+01
13 1.000E+01
12 8.000E+00
11 6.000E+00
10 4.000E+00
9 2.000E+00
8 0.000E+00
7 -2.000E+00
6 -4.000E+00
5 -6.000E+00
4 -8.000E+00
3 -1.000E+01
2 -1.200E+01
1 -1.400E+01

ABSOLUTE FLOW ANGLE, 50 PERCENT B2

R/RTIP-1.06, Q/QD-1.0

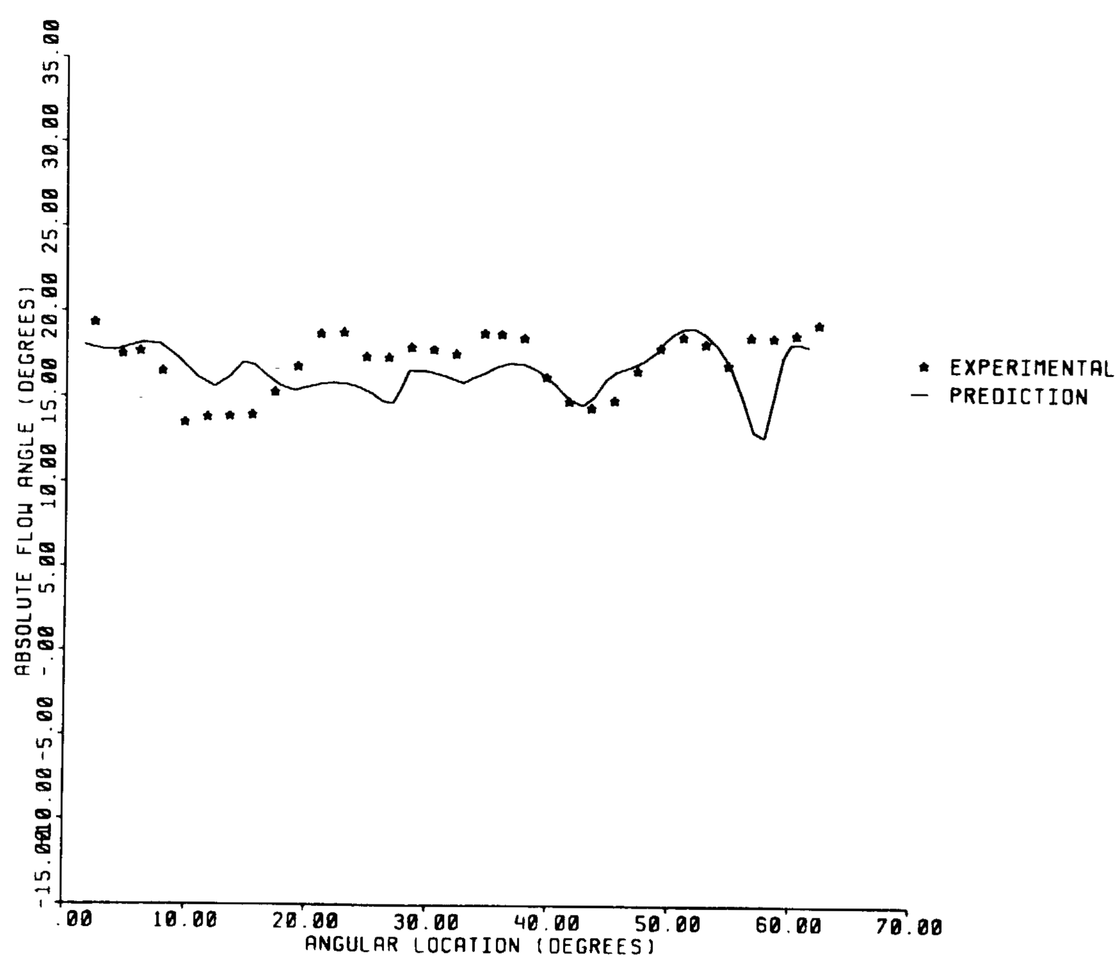

ASC

Absolute Velocity (C/Utip) at Impeller Discharge

Advanced Scientific Computing Corp.

Abs. Velocity: C/Utip at R/Rtip=1.013, 50% B2

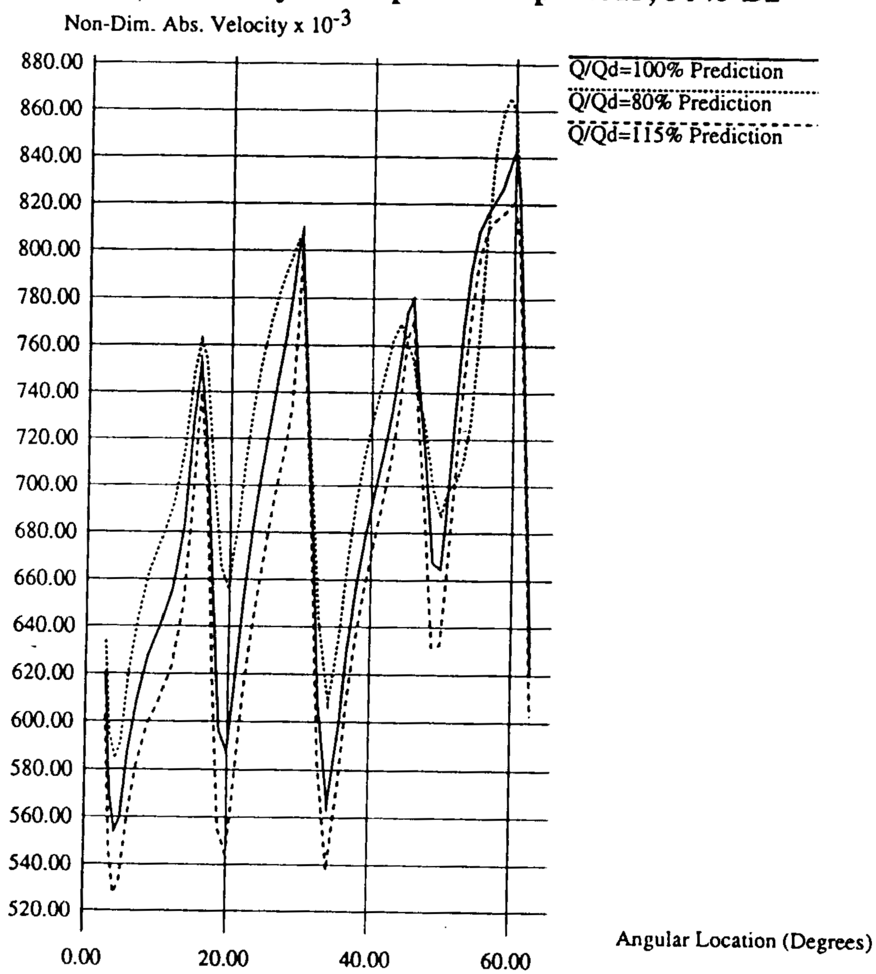

Abs. Velocity: C/Utip at R/Rtip=1.060, 50% B2

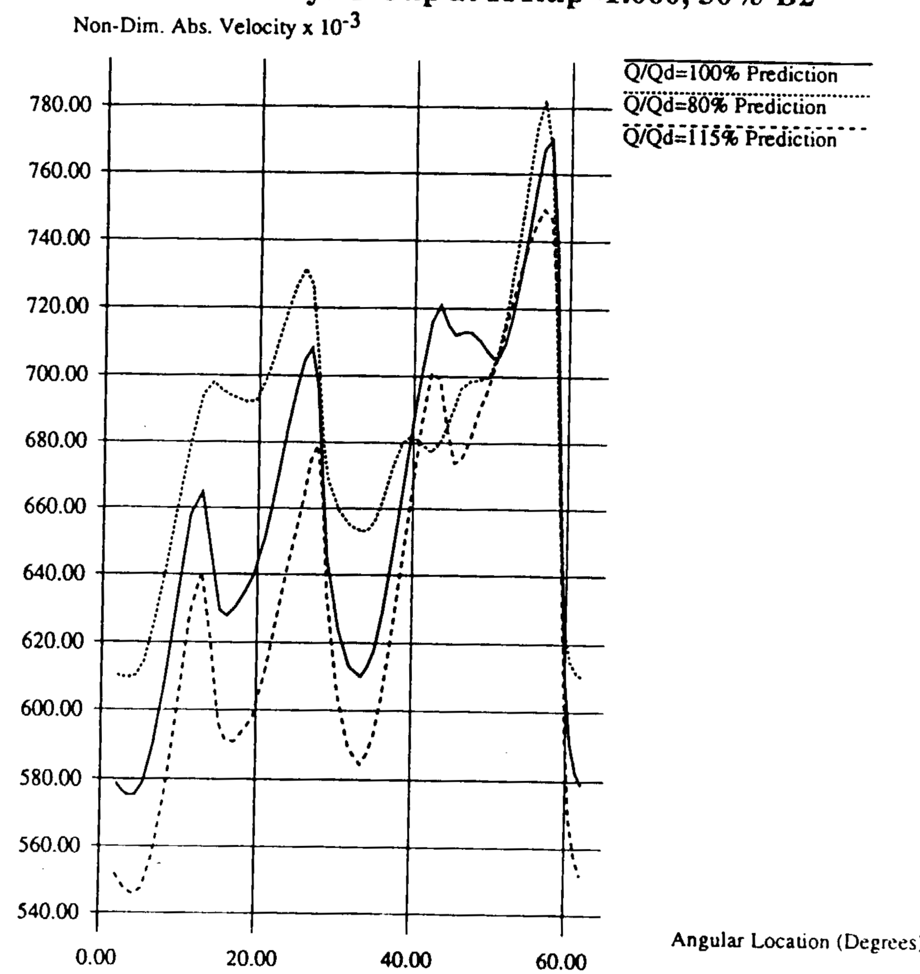

Absolute Flow Angle at Impeller Discharge

Abs. Flow Angle: Alpha at R/Rtip=1.013, 50% B2

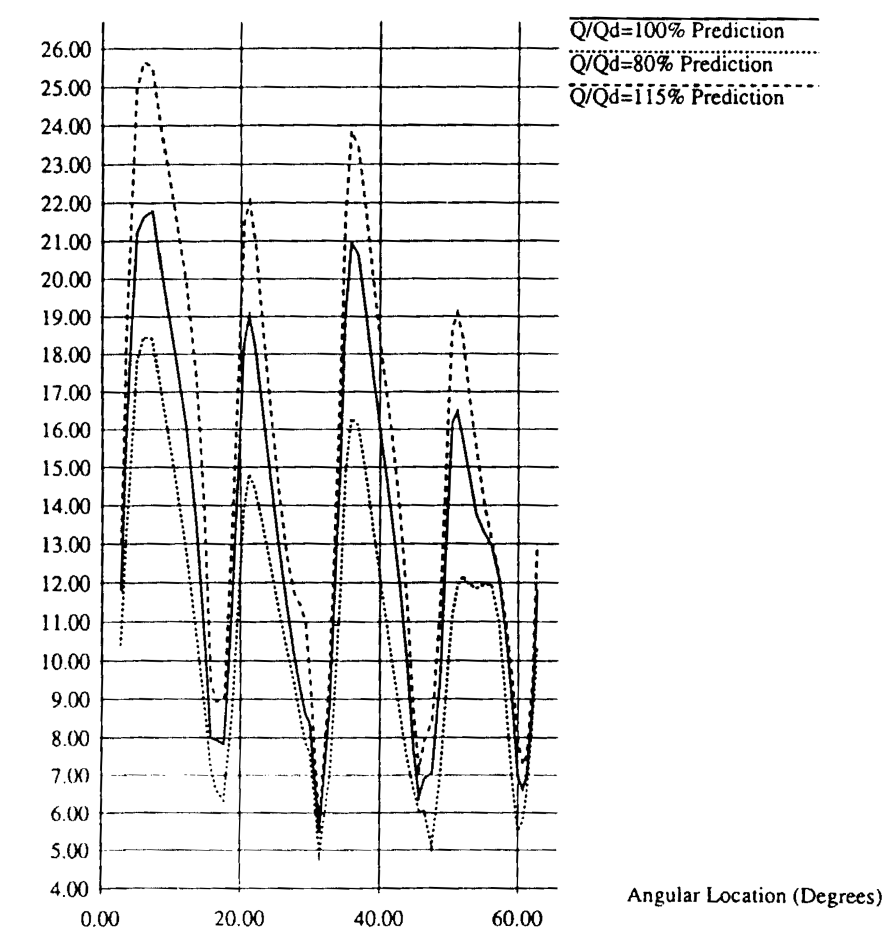

Abs. Flow Angle: Alpha at R/Rtip=1.060, 50% B2

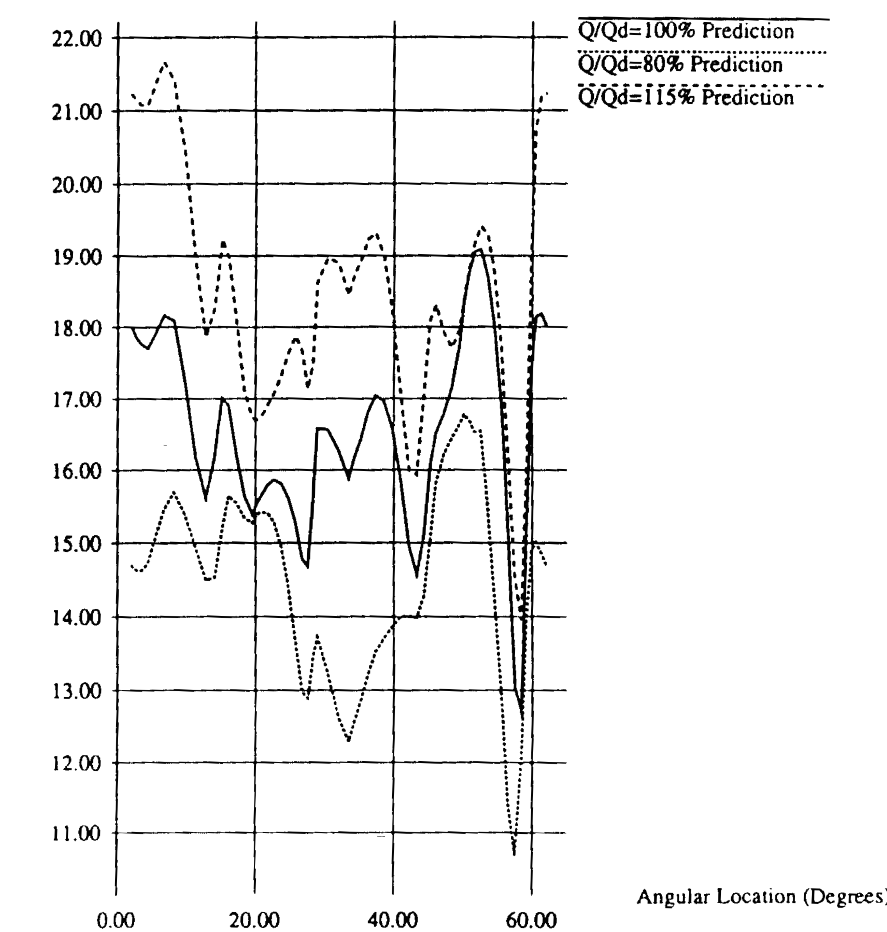

N95- 23623

33-34
p. 93

Three-Dimensional Flow Analysis Inside Consortium Impeller at Design and Off-Design Conditions

C.Hah, J. Loellbach, F-L. Tsung, and D. A. Greenwald

NASA Lewis Research Center

R. Garcia

NASA Marshall Space Flight Center

Three-dimensional flow fields inside the Consortium impeller were analyzed with a Navier-Stokes code. The numerical results at the design and off-design conditions are compared with the experimental data.

THREE-DIMENSIONAL FLOW ANALYSIS INSIDE CONSORTIUM IMPELLER AT DESIGN AND OFF-DESIGN CONDITIONS

C. HAH, J. LOELLBACH, F. TSUNG, AND D. A. GREENWALD

NASA LEWIS RESEARCH CENTER

R. GARCIA

NASA MARSHALL SPACE FLIGHT CENTER

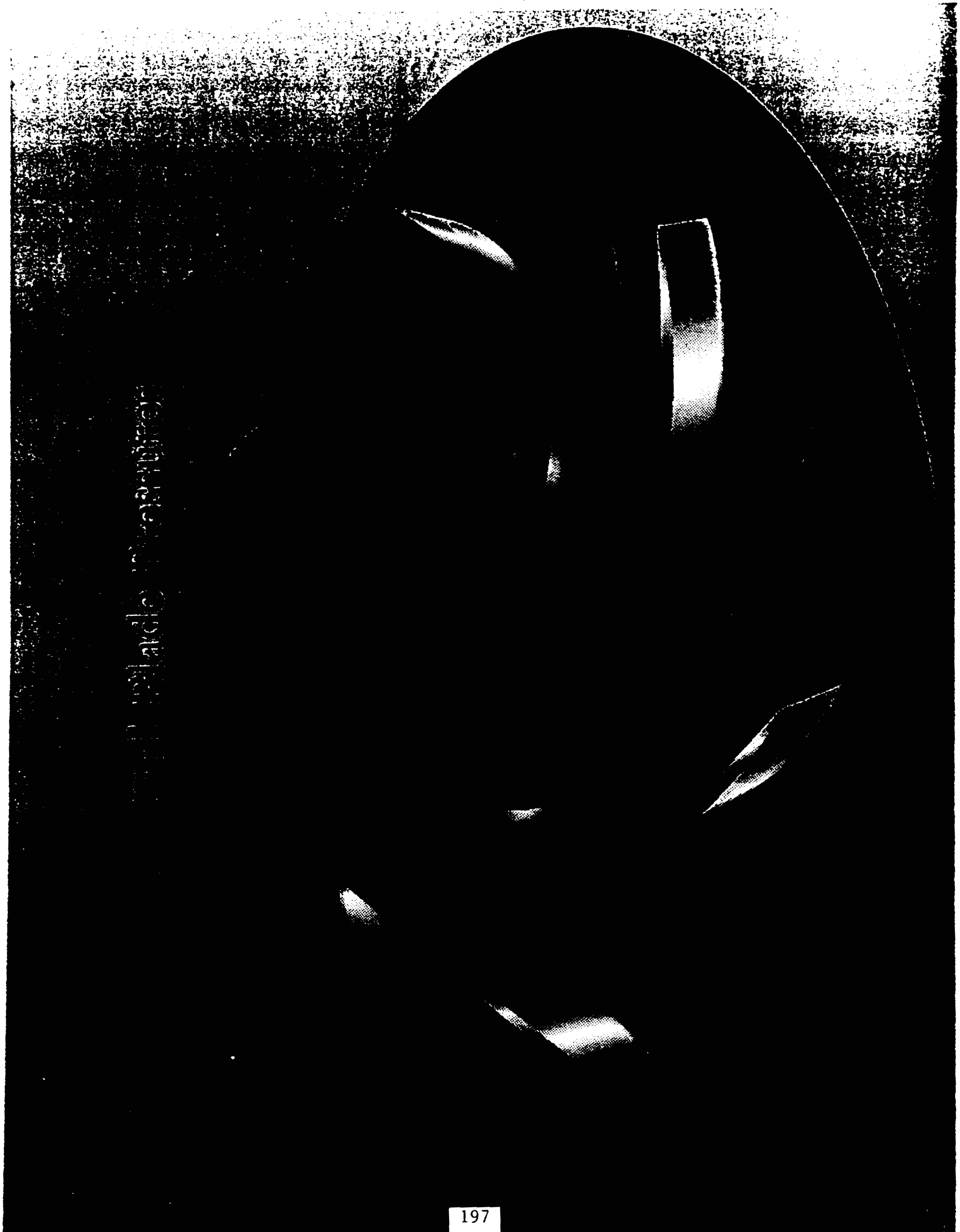

Objective

- Design and Off-Design Performance
- Numerical Optimization of Splitter

Computational grid

- o I-GRIDS
- o 40x24x123, 30x24x123, and 12x12x80

Computational Grid

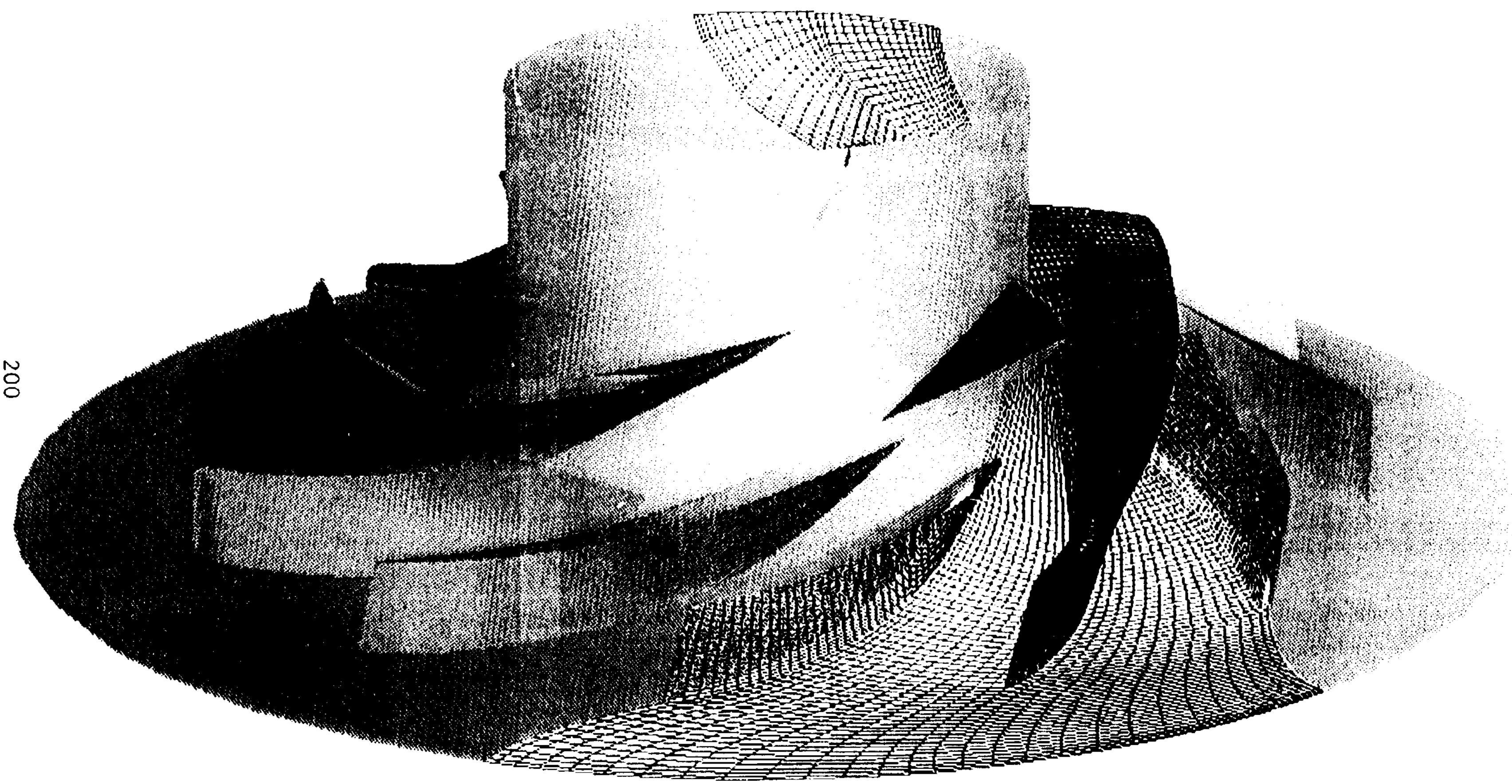

Impeller Partial Blade Configurations

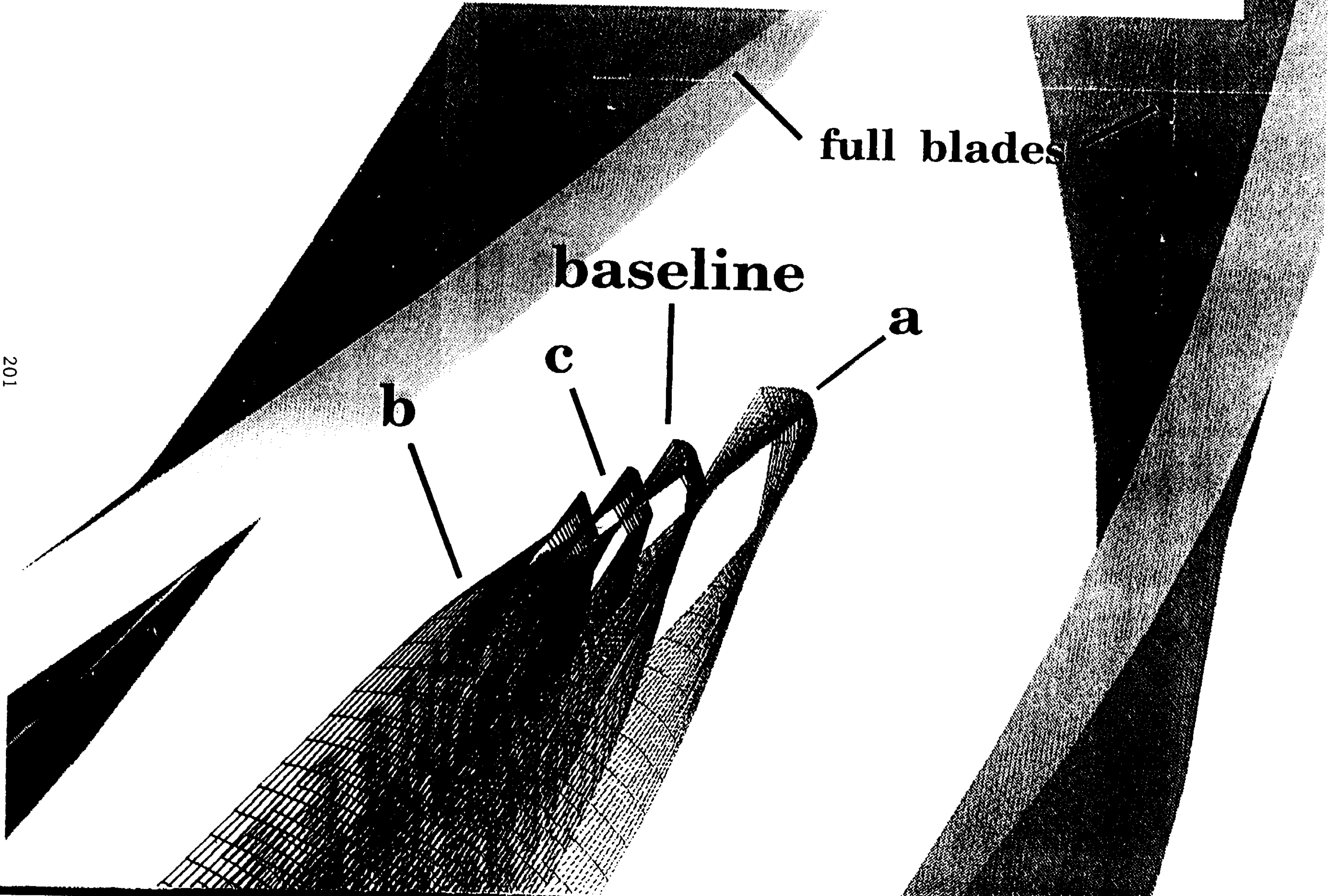

Flow Cases Studied

- o Baseline
  - o Design Flow
  - o 120 % Design Flow
  - o 88 % Design Flow
- o Optimization of Splitter
  - o Baseline
  - o Cases A, B, C

- **Baseline**
  - **Design Flow**
  - **120 % Design Flow**
  - **88 % Design Flow**

Blade Surface Pressure Contour

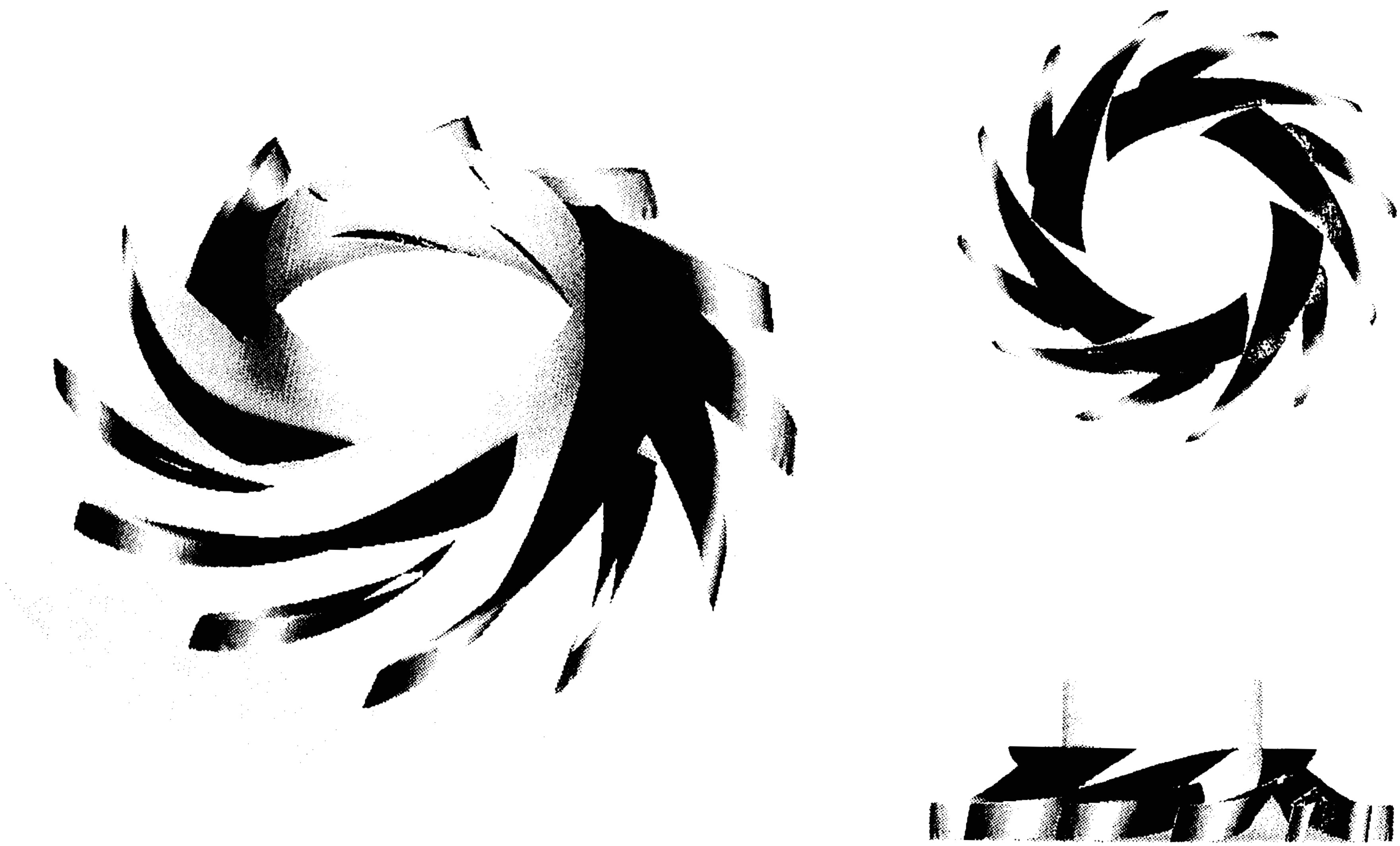

Hub Surface Pressure Contour

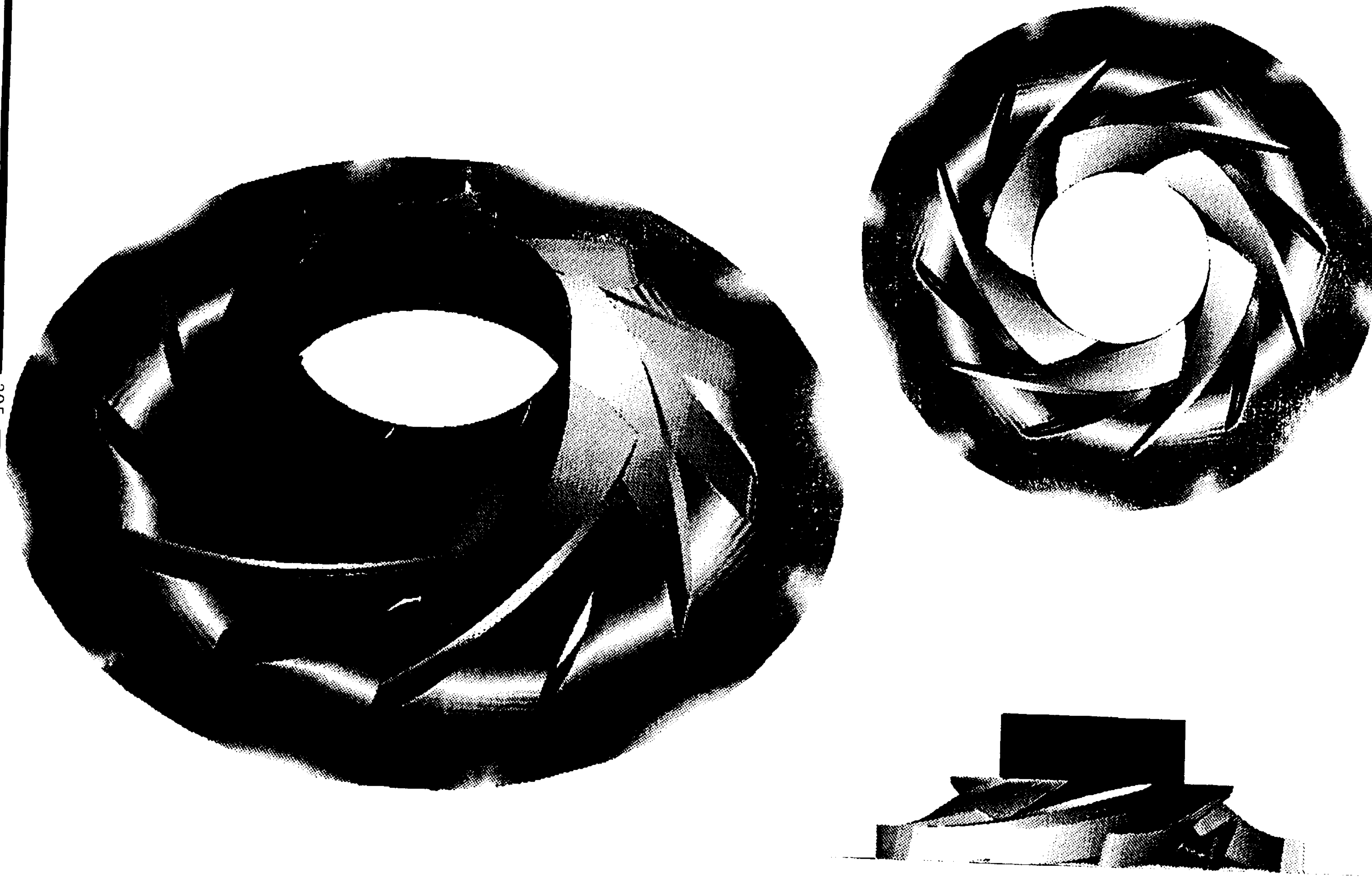

Relative Velocity Vector

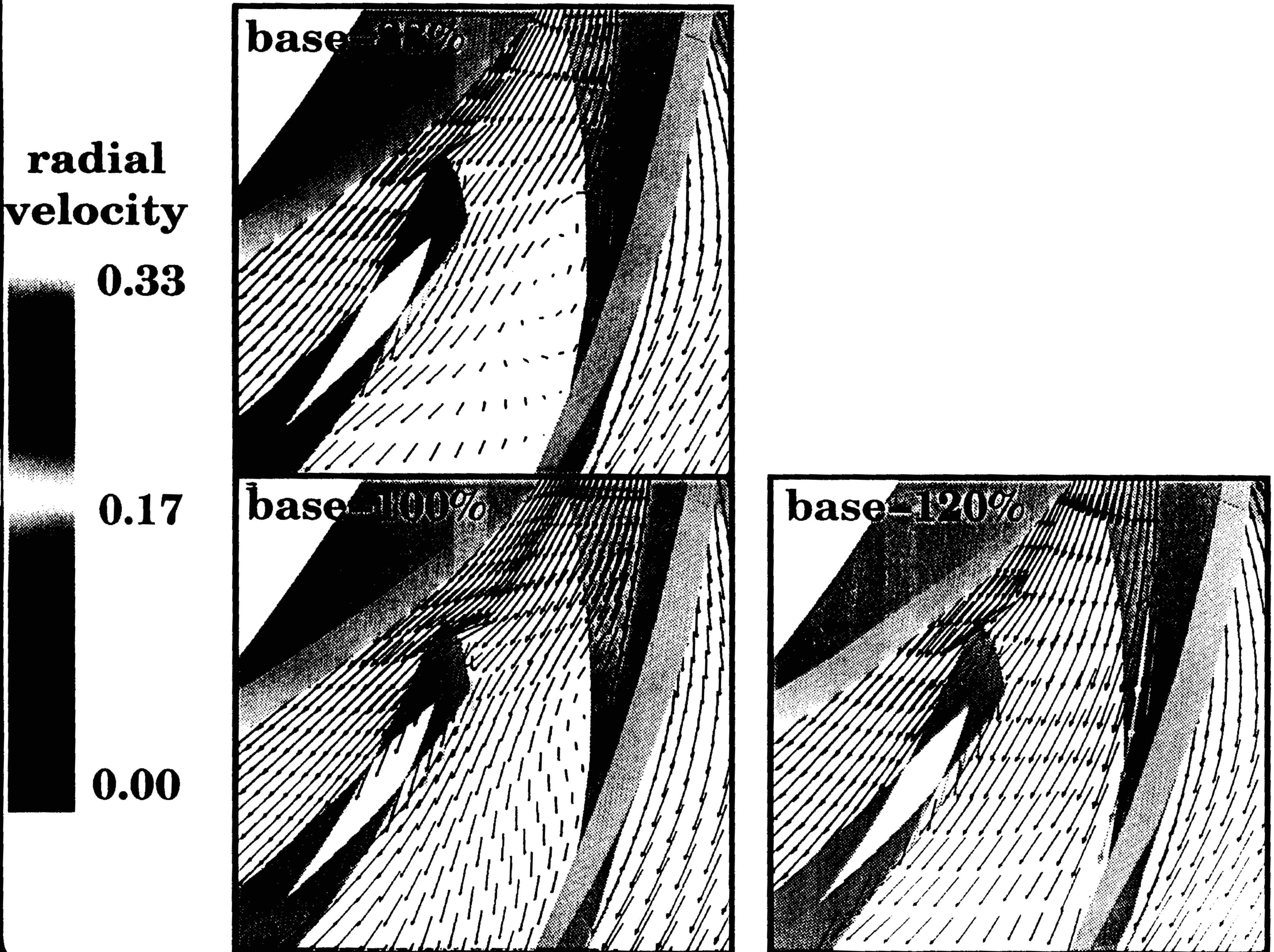

Nondimensional Radial Velocity

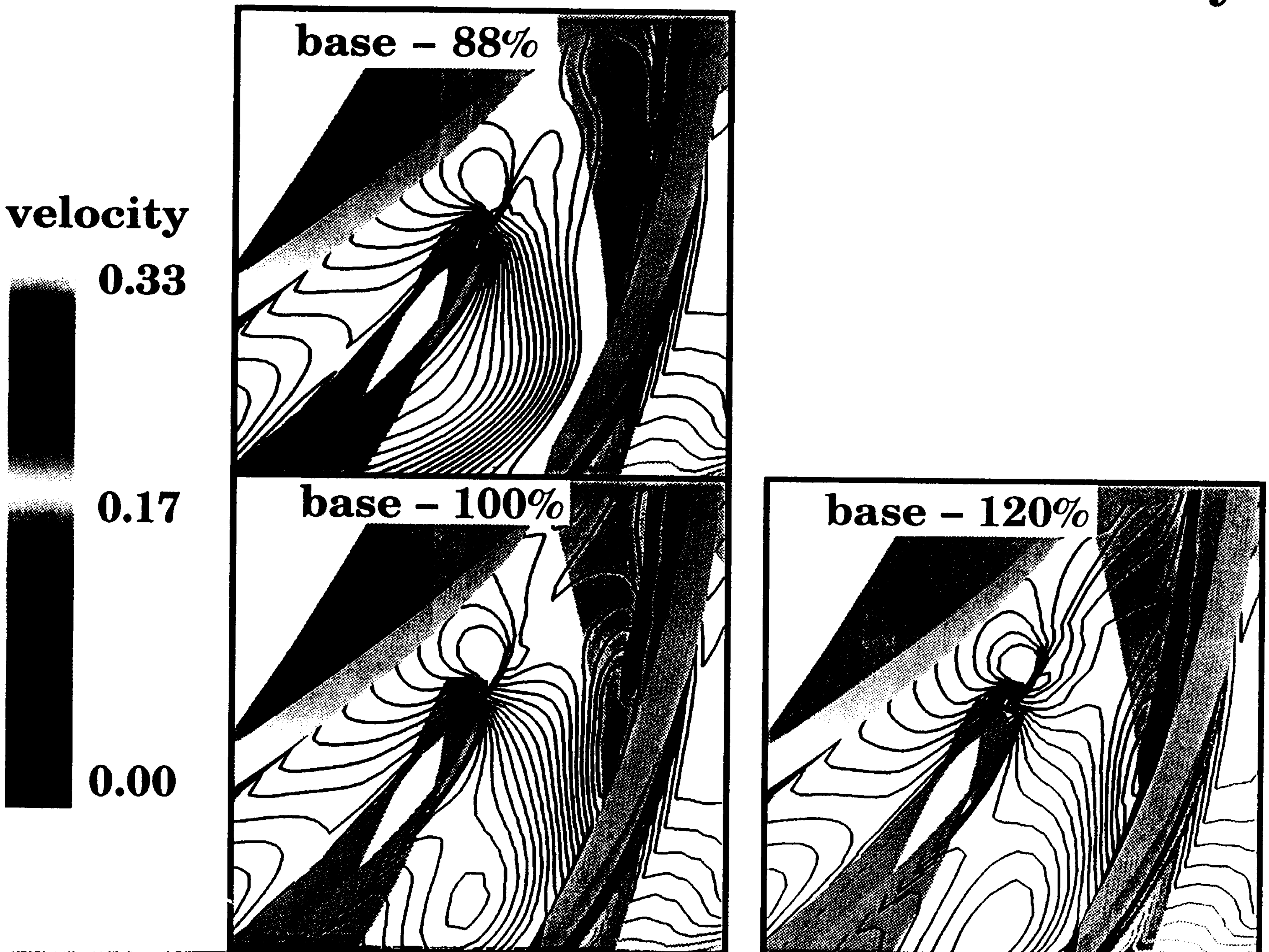

Particle Trace

baseline–coarse

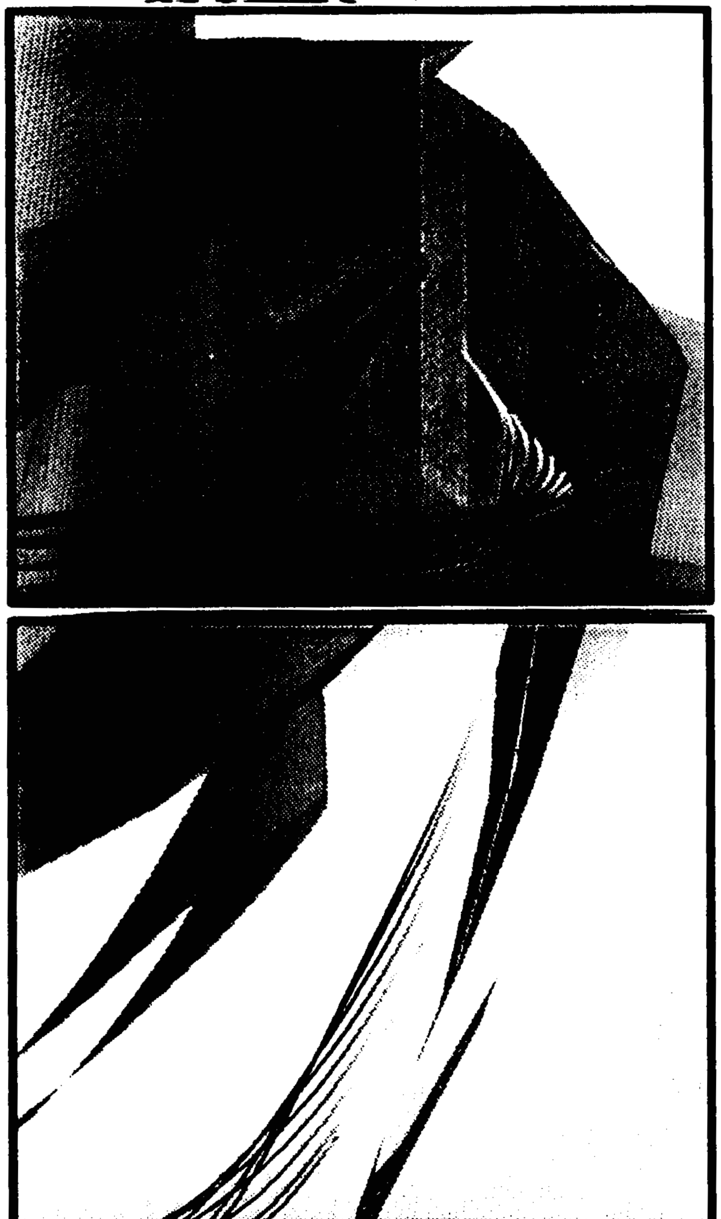

baseline–dense

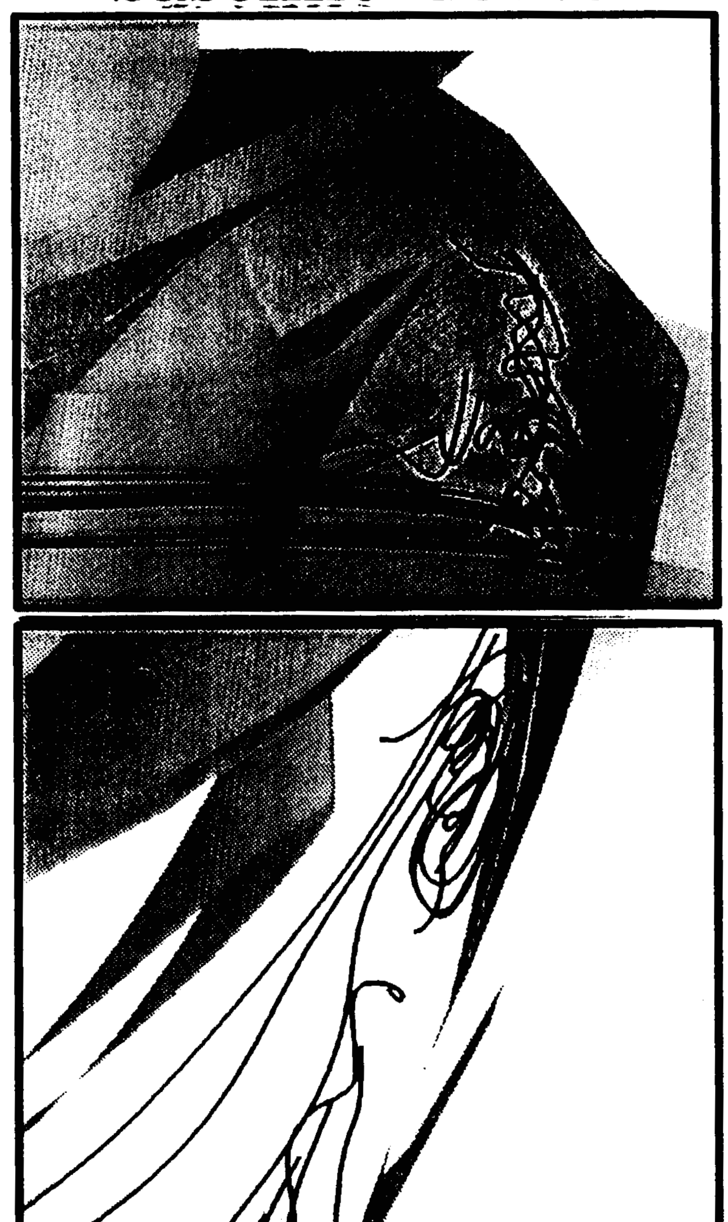

Particle Trace

base – 88%

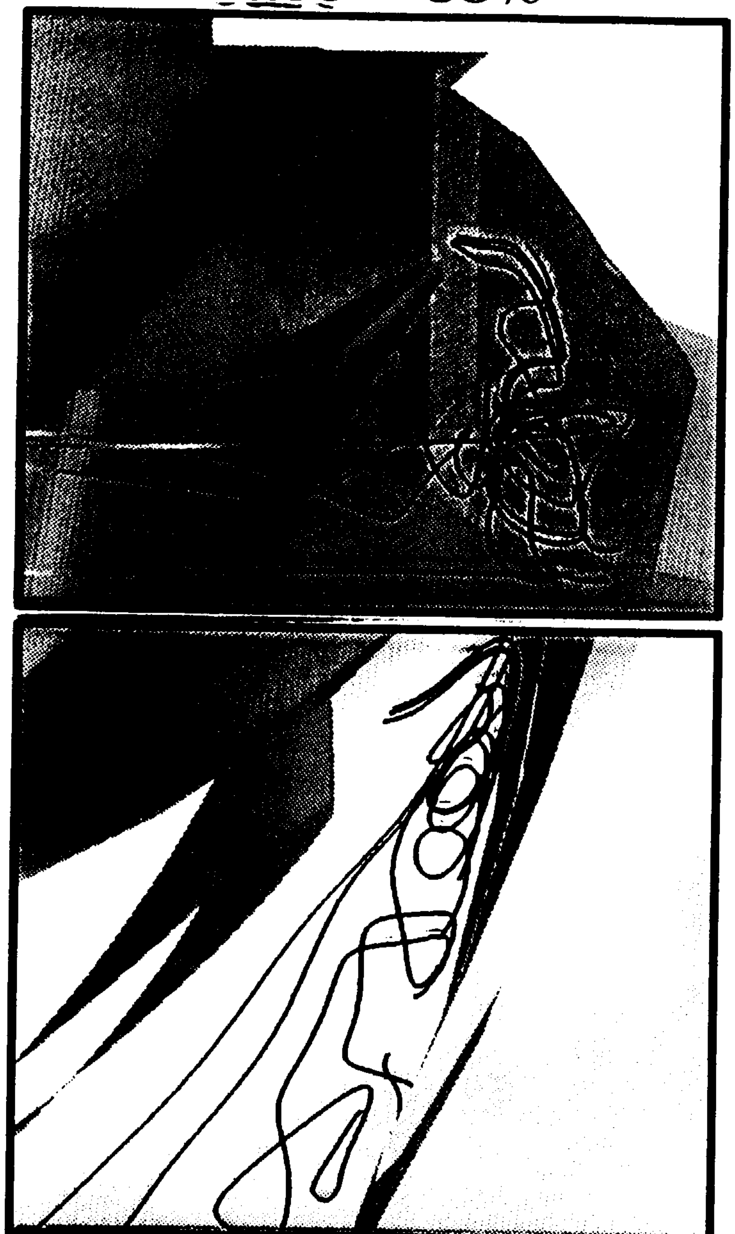

base – 120%

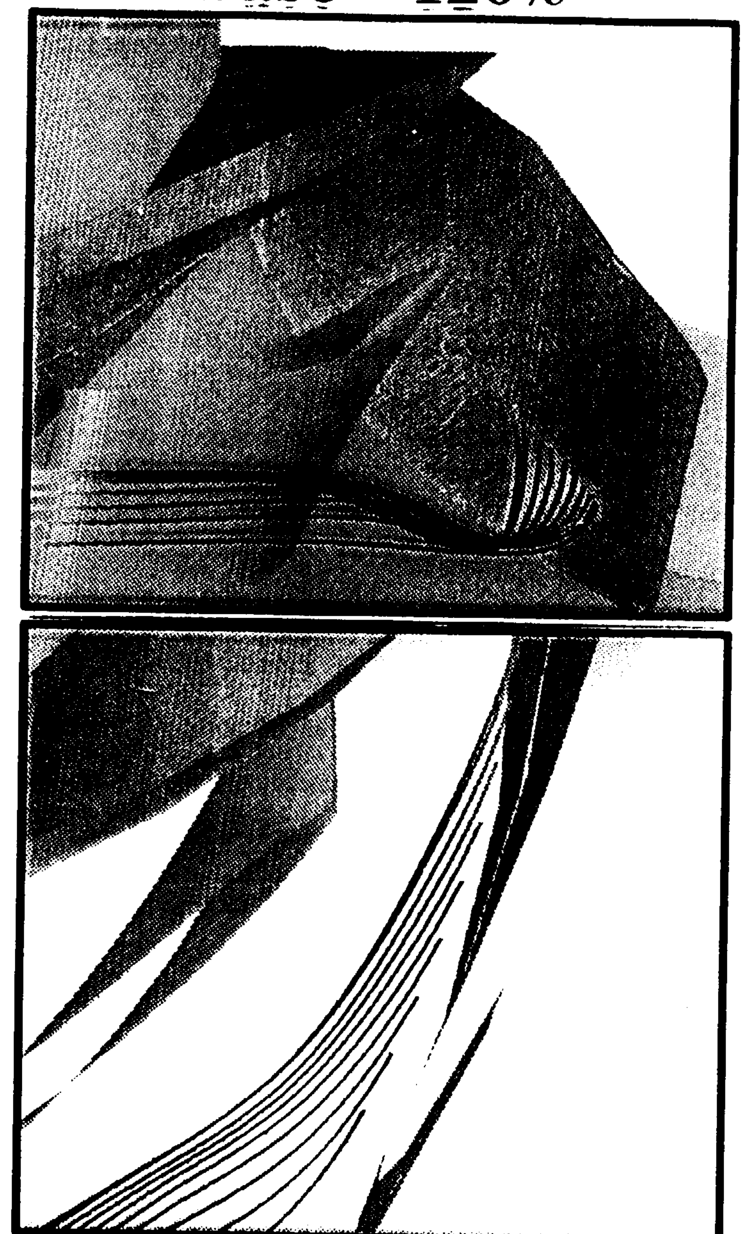

Flow Split

88 % Flow : .46/.54

100 % Flow : .49/.51

120 % Flow : .52/.48

Observation

o Small Flow Separation at Design Flow rate

o Large Flow Separation at 88 % Flow rate

o No Flow Separation at 120 % Flow rate

- **Optimization of Splitter**
  - **Baseline**
  - **Cases A, B, C**

Relative Velocity Vector

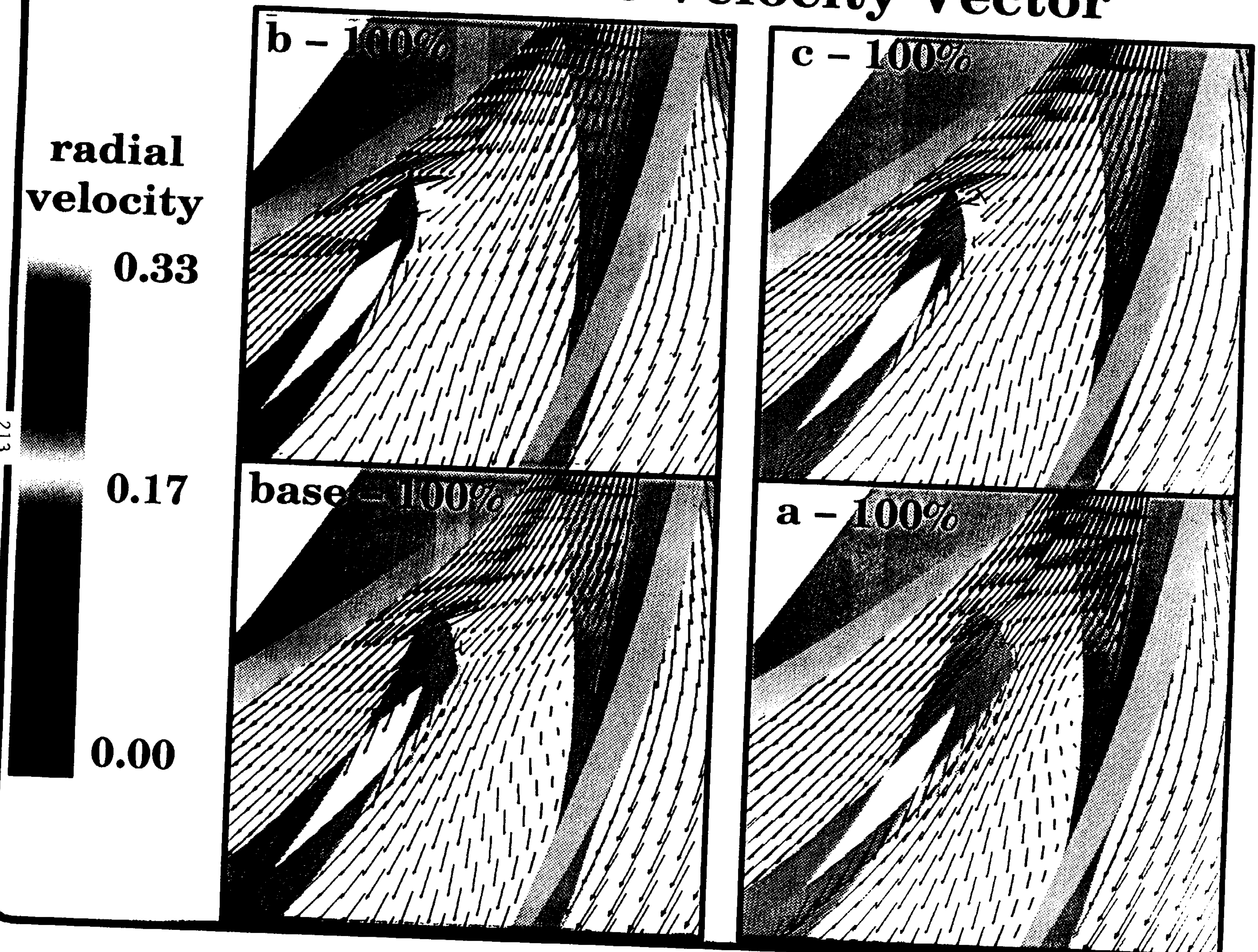

Nondimensional Radial Velocity

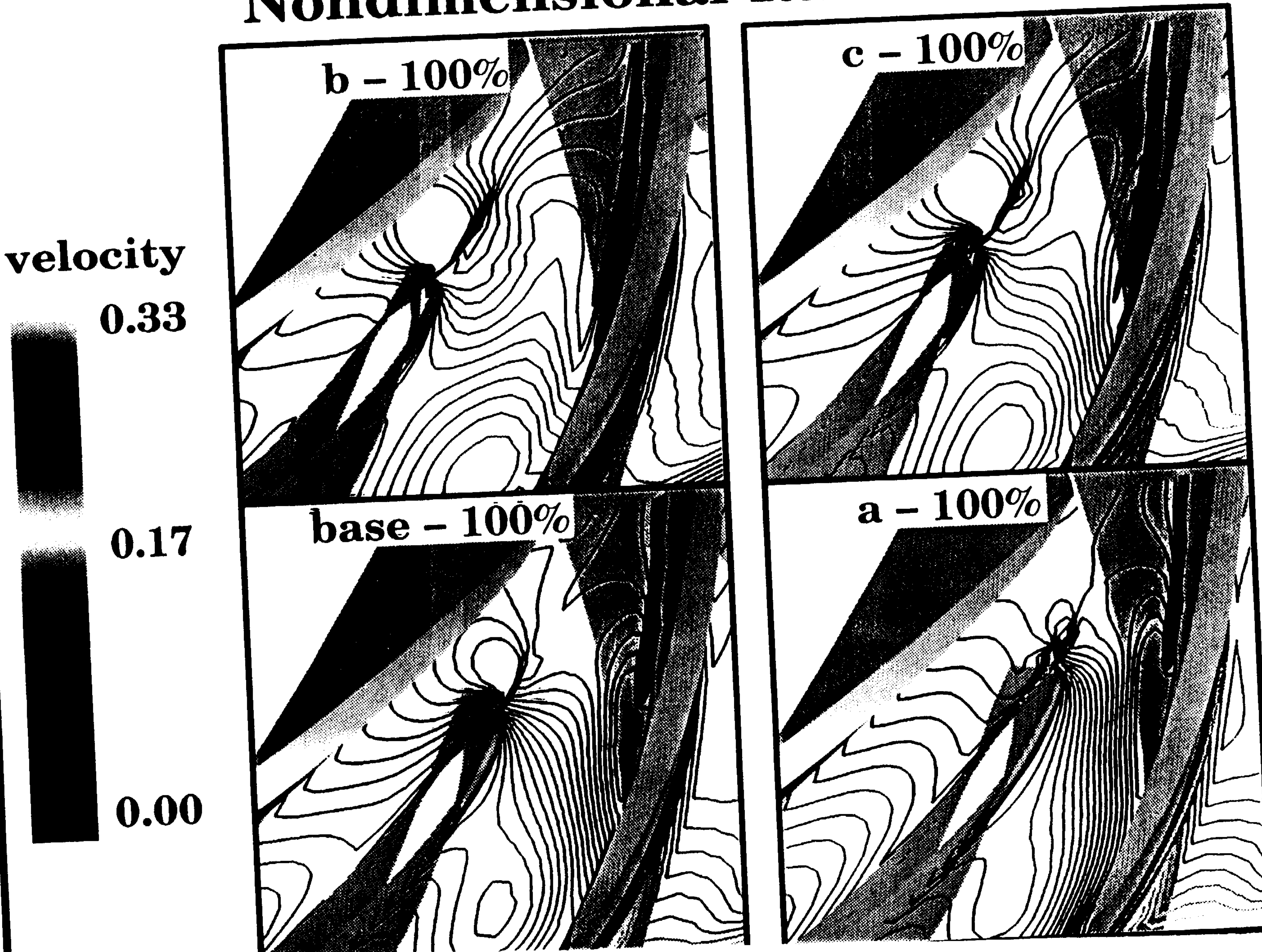

Particle Trace

base – 100%

a – 100%

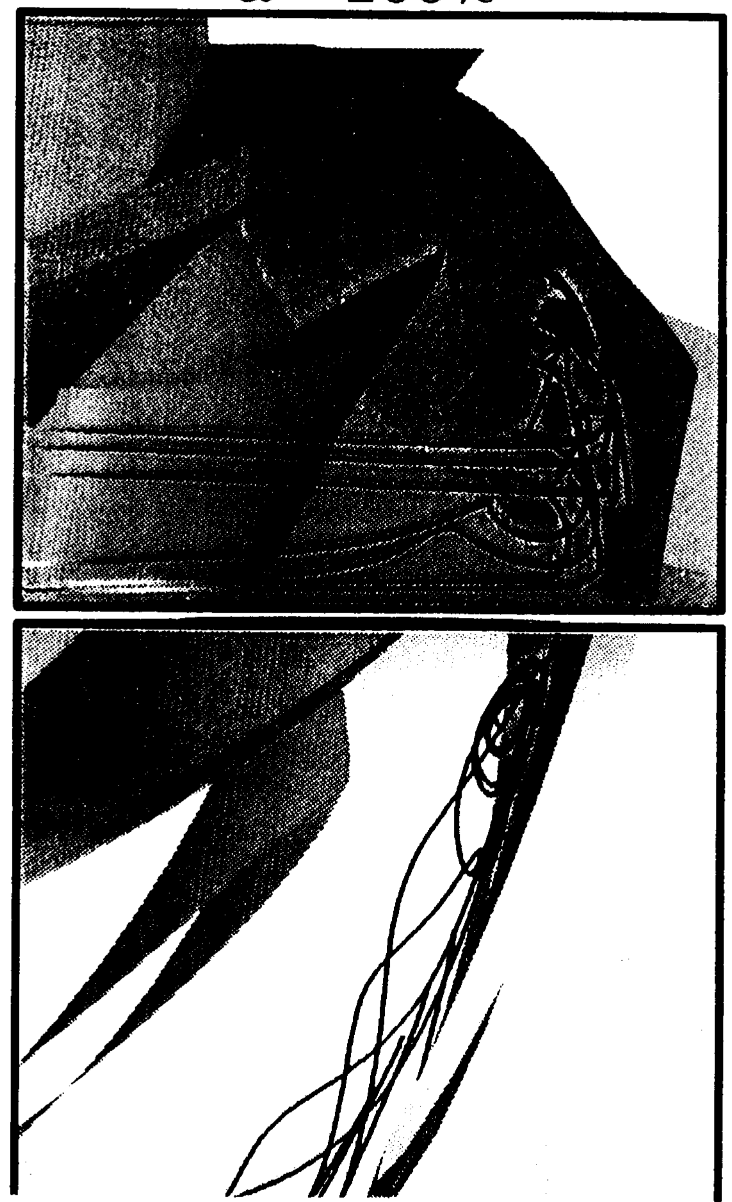

Particle Trace

b – 100%

c – 100%

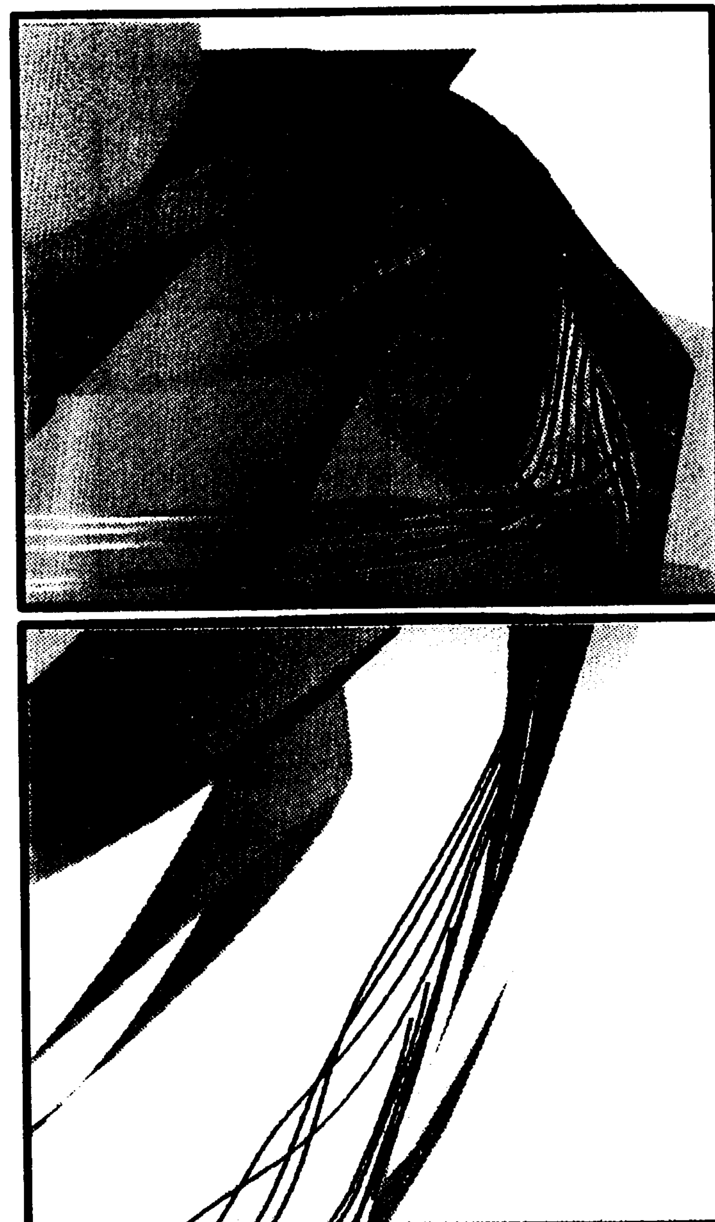

Observation

- o Small Flow Separation for Baseline Design
- o Large Flow Separation for Design A
- o No Flow Separation For Design B
- o Design C is a Good Compromise

N95- 23624

OPTIMIZATION OF A CENTRIFUGAL IMPELLER DESIGN THROUGH CFD ANALYSIS

W. C. Chen, A. H. Eastland, D. C. Chan
Rockwell International, Rocketdyne Division
R. Garcia
NASA, Marshall Space Flight Center

This paper discusses the procedure, approach and Rocketdyne CFD results for the optimization of the NASA consortium impeller design. Two different approaches have been investigated. The first one is to use a tandem blade arrangement, the main impeller blade is split into two separate rows with the second blade row offset circumferentially with respect to the first row. The second approach is to control the high losses related to secondary flows within the impeller passage. Many key parameters have been identified and each consortium team member involved will optimize a specific parameter using 3-D CFD analysis. Rocketdyne has provided a series of CFD grids for the consortium team members. SECA will complete the tandem blade study, SRA will study the effect of the splitter blade solidity change, NASA LeRC will evaluate the effect of circumferential position of the splitter blade, VPI will work on the hub to shroud blade loading distribution, NASA Ames will examine the impeller discharge leakage flow impacts and Rocketdyne will continue to work on the meridional contour and the blade leading to trailing edge work distribution. This paper will also present Rocketdyne results from the tandem blade study and from the blade loading distribution study. It is the ultimate goal of this consortium team to integrate the available CFD analysis to design an advanced technology impeller that is suitable for use in the NASA Space Transportation Main Engine (STME) fuel turbopump.

PRECEDING PAGE BLANK NOT FILMED

PAGE 218 INTENTIONALLY BLANK

OPTIMIZATION OF A CENTRIFUGAL IMPELLER DESIGN THROUGH CFD ANALYSIS

BY

WEI-CHUNG CHEN, ANTHONY H. EASTLAND, DANIEL C. CHAN

ROCKETDYNE DIVISION, ROCKWELL INTERNATIONAL CORPORATION

AND

ROBERT GARCIA

NASA MARSHALL SPACE FLIGHT CENTER

PRESENTED AT NASA MARSHALL SPACE FLIGHT CENTER

11TH WORKSHOP FOR CFD APPLICATIONS IN ROCKET PROPULSION

APRIL 20-22. 1993

Rockwell International

Rocketdyne Division

OPTIMIZATION OF A CENTRIFUGAL IMPELLER DESIGN THROUGH CFD ANALYSIS

- OBJECTIVES
  - DEVELOP ADVANCED CONCEPT HIGH HEAD COEFFICIENT IMPELLER DESIGN WITH MINIMIZED EXIT FLOW DISTORTION
  - DESIGN HIGH HEAD COEFFICIENT IMPELLER AND REDUCE 3 STAGES STME FUEL PUMP TO 2 STAGES
- APPROACH
  - INCORPORATE CFD AS DESIGN TOOL AND OPTIMIZE IMPELLER DESIGN THROUGH CFD ANALYSIS
  - WATER TEST TO CONFIRM IMPELLER PERFORMANCE

Rockwell International
Rocketdyne Division

CONSORTIUM 2STAGE FUEL PUMP

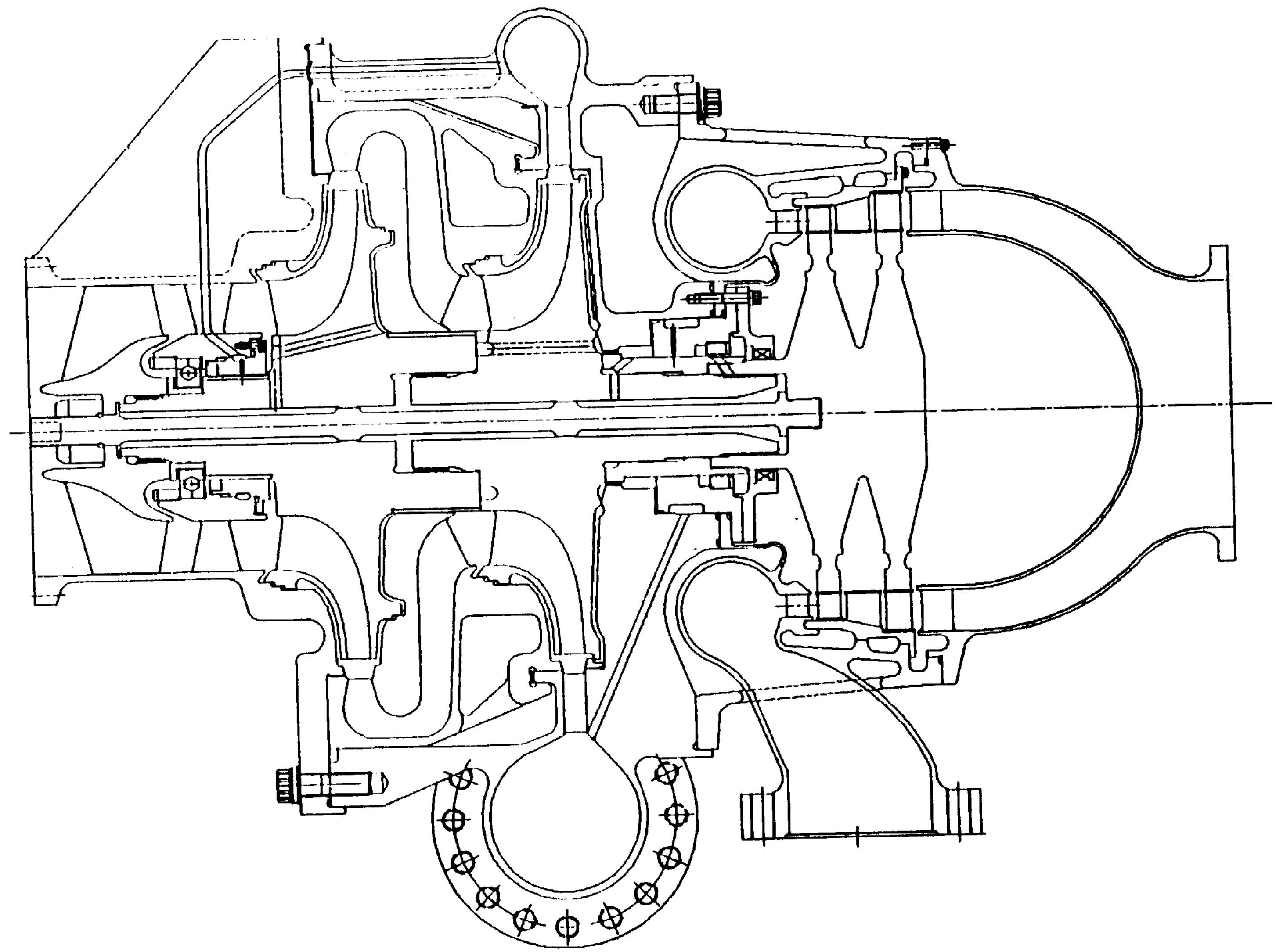

Rockwell International
Rocketdyne Division

OPTIMIZATION OF A CENTRIFUGAL IMPELLER DESIGN THROUGH CFD ANALYSIS

- EXISTING BASELINE DESIGN
  - SUCESSFULLY COMPLETED WATER TEST
    - TEST RESULTS PRESENTED IN SEPARATE PAPER
  - ACHIEVED REQUIRED HEAD
  - GOOD AGREEMENT BETWEEN CFD RESULTS AND LASER MEASUREMENT
    - PRESENTED IN JAN. 1993 NASA PUMP CONSORTIUM MEETING
  - MINOR REVERSE FLOW AND FLOW SEPARATION NEAR SUCTION SIDE SHROUD REGION
- BASELINE DESIGN OPTIMIZED THROUGH CFD ANALYSIS BY ALL CONSORTIUM MEMBERS
- ROCKETDYNE CONTRIBUTION
  - TANDEM BLADE APPROACH
  - CONTROL IMPELLER BLADE LOADING FROM L.E. TO T.E.

Rockwell International
Rocketdyne Division

COMPUTATIONAL GRID

MERIDIONAL VIEW: (BASELINE DESIGN)

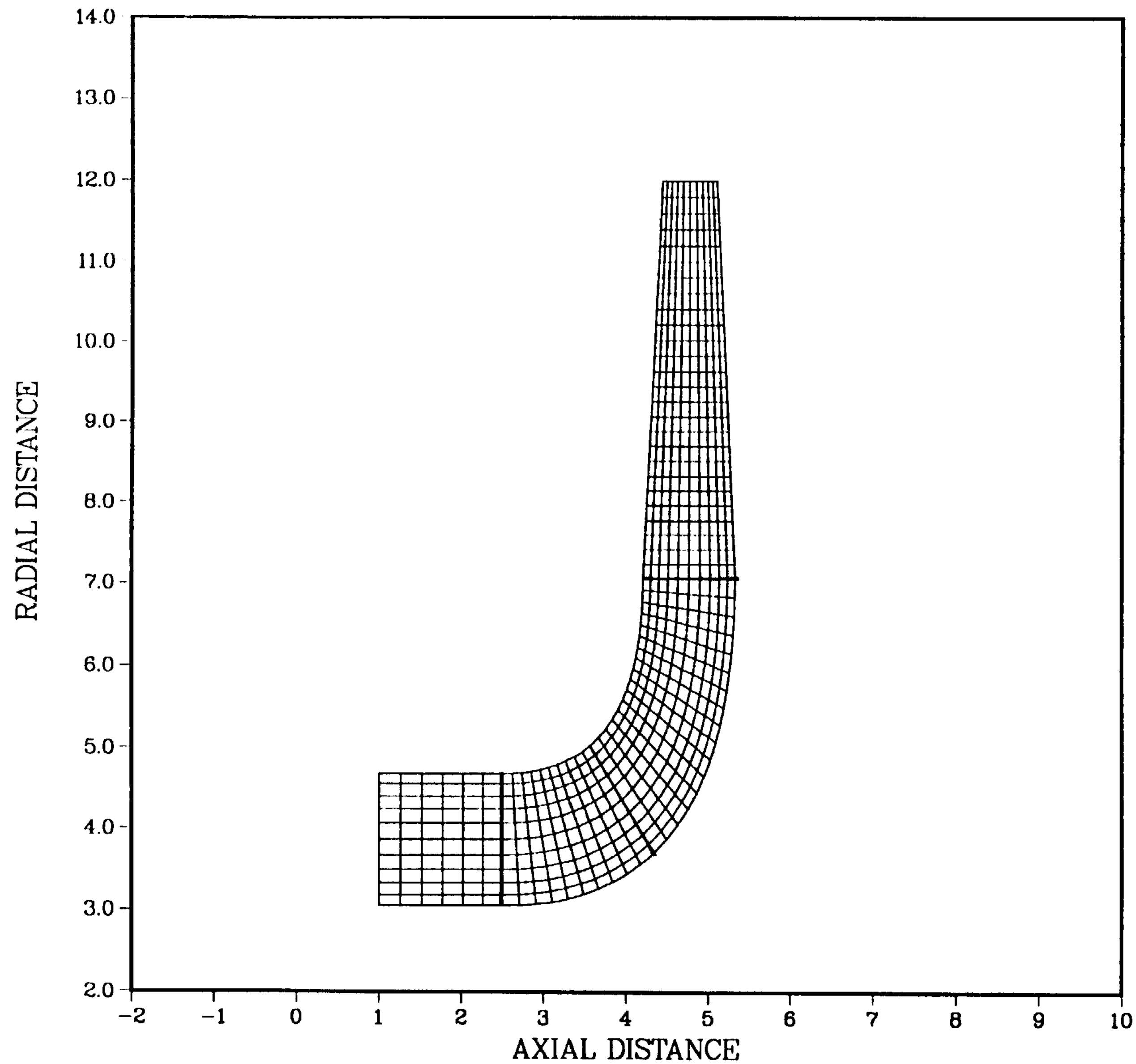

Rockwell International

Rocketdyne Division

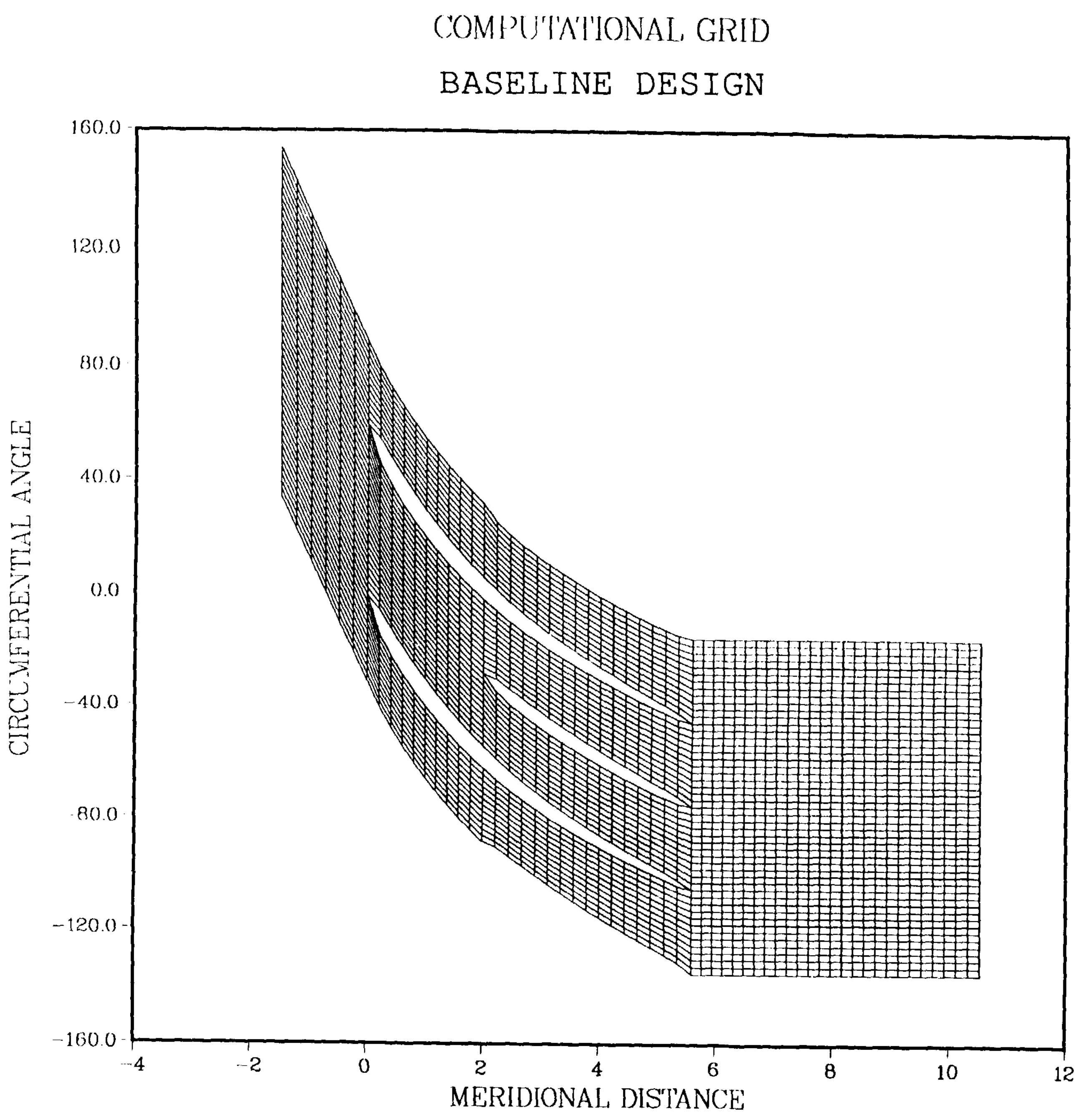

Rockwell International
Rocketdyne Division

COMPARISON OF CFD SOLUTION TO TEST DATA
AVERAGED ABSOLUTE RADIAL VELOCITY
PLANE 1, $Q_D=100\%$, RADIUS=4.700 INCH

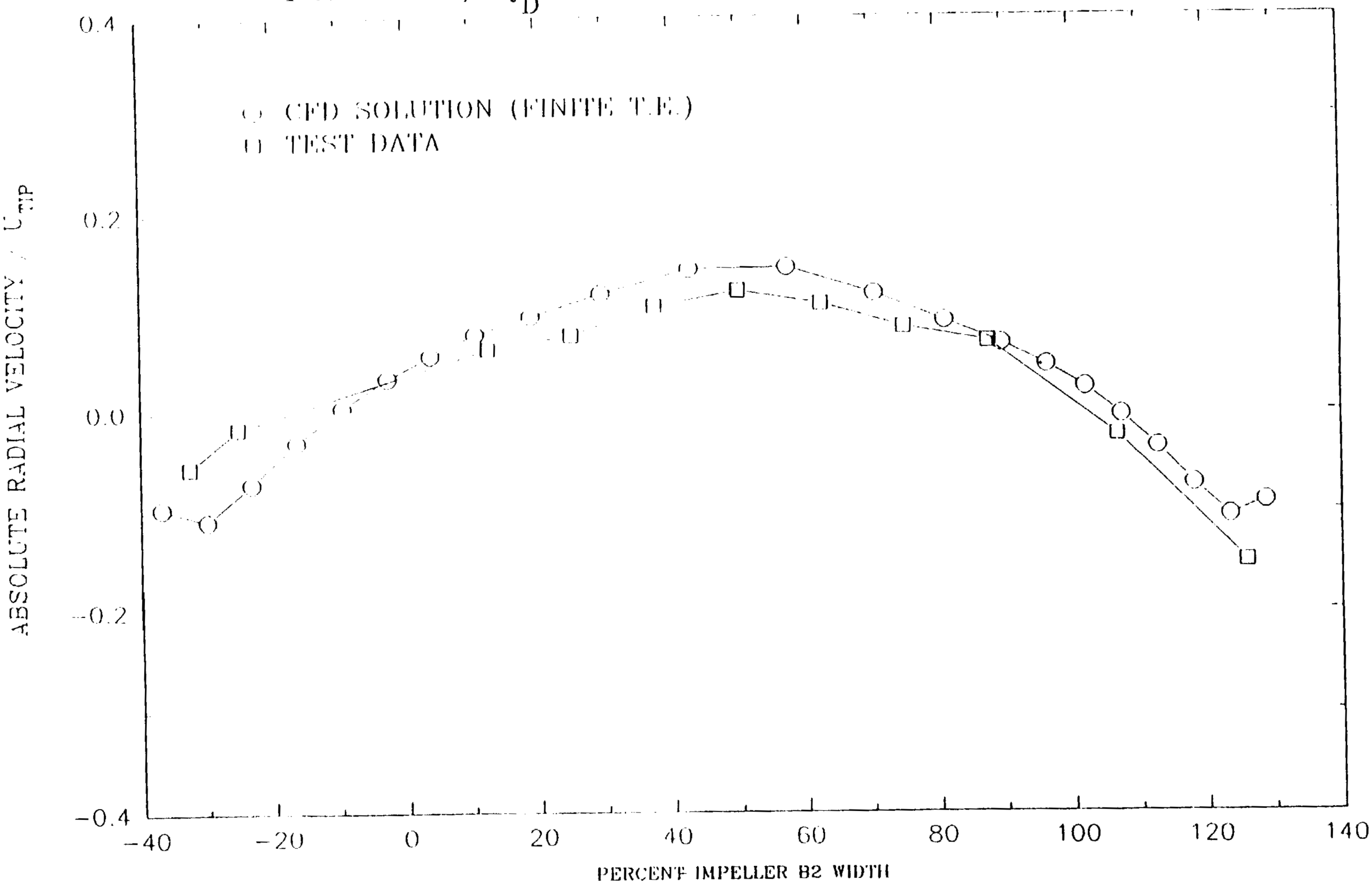

01/28/93

Rockwell International
Rocketdyne Division

ORIGINAL PAGE IS
OF POOR QUALITY

COMPARISON OF CFD SOLUTION TO TEST DATA
AVERAGED ABSOLUTE FLOW ANGLE
PLANE 1, $Q_D = 100\%$, RADIUS=4.700 INCH

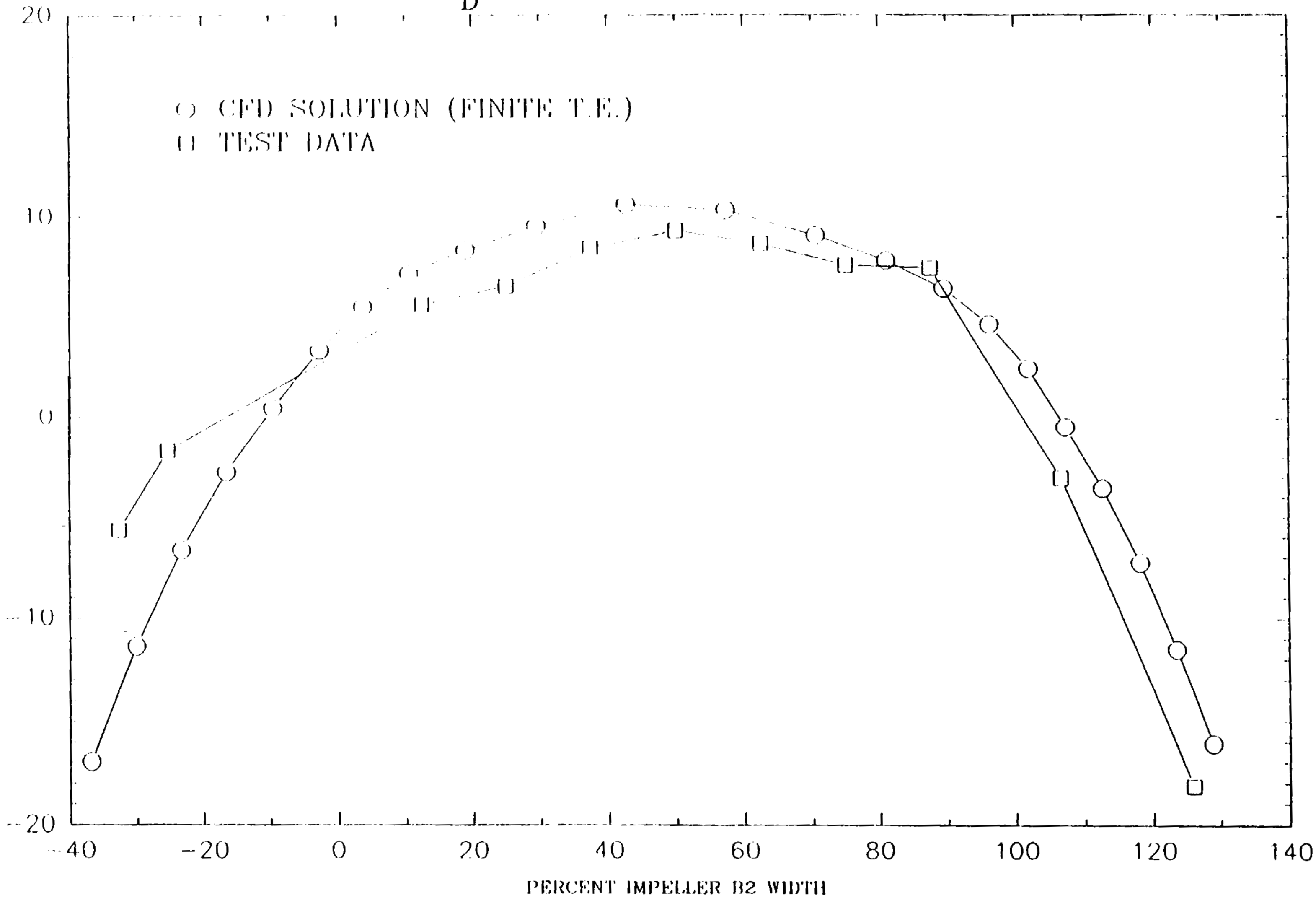

01/26/93

Rockwell International
Rocketdyne Division

OPTIMIZATION OF A CENTRIFUGAL IMPELLER DESIGN THROUGH CFD ANALYSIS

- TANDEM BLADE APPROACH
  - CUT 1 (TANDEM LOCATE AT BLADE L.E.)
  - CUT 2 (TANDEM LOCATE AT MIDSECTION OF BLADE)
  - CUT 3 (TANDEM LOCATE NEAR T.E. OF BLADE)
- TANDEM BLADE CFD RESULTS
  - MINIMUM PERFORMANCE IMPROVEMENT WITH LARGE ADDITIONAL BLADE FABRICATION COMPLEXITY
  - CUT 1 MORE EFFECTIVE THAN CUT 2 AND CUT 3 TO CONTROL FLOW
  - SMALL CLOCKING ANGLE MORE BENIFICIAL THAN LARGE CLOCKING ANGLE
  - DETAILED CFD RESULTS PRESENTED IN OCTOBER, 1992 NASA CONSORTIUM MEETING
  - INDEPENDENT ANALYSIS IN WORK TO CONFIRM RESULTS

Rockwell International
Rocketdyne Division

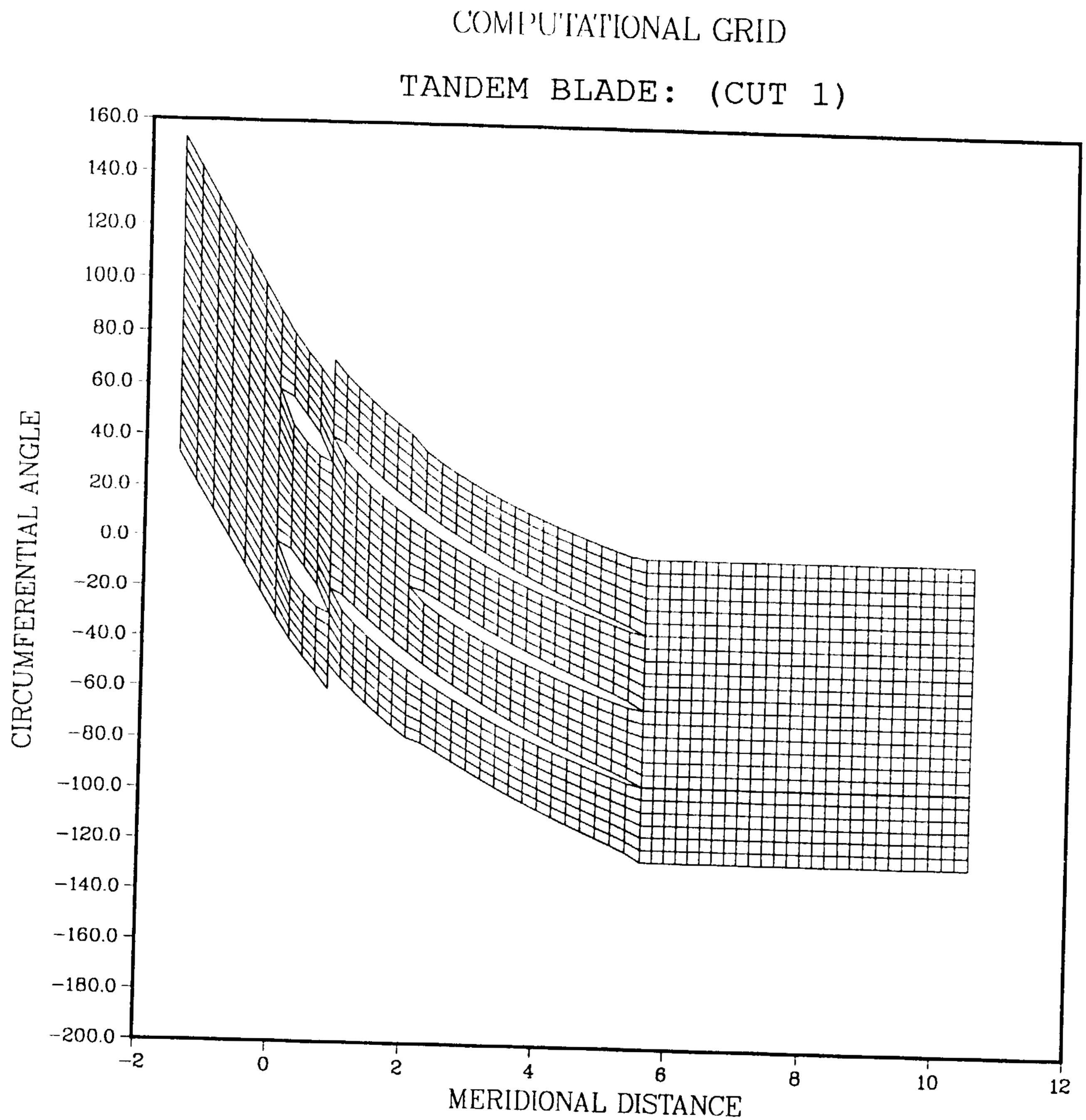

Rockwell International
Rocketdyne Division

COMPUTATIONAL GRID

TANDEM BLADE: (CUT 2)

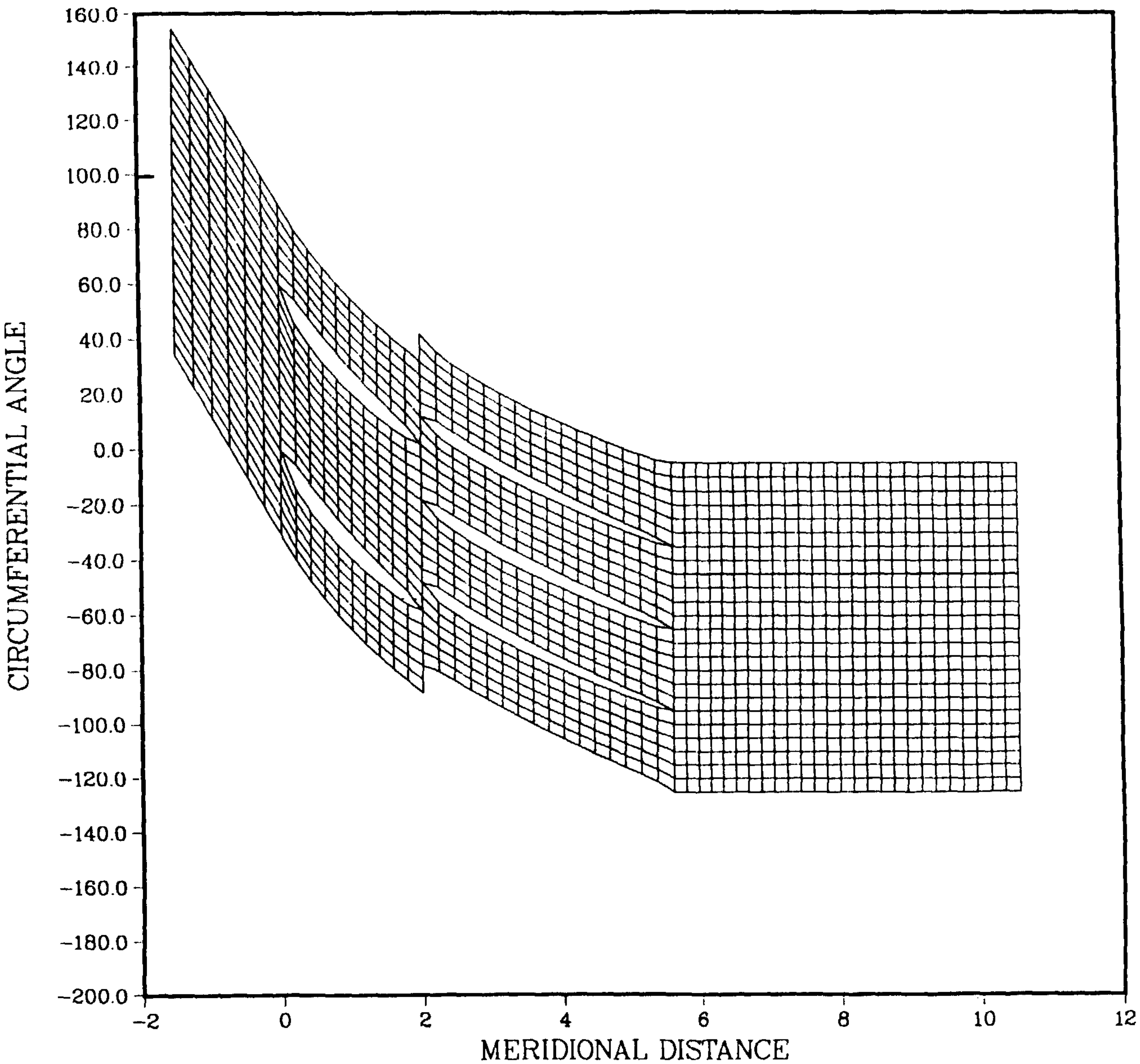

Rockwell International
Rocketdyne Division

COMPUTATIONAL GRID

TANDEM BLADE: (CUT 3)

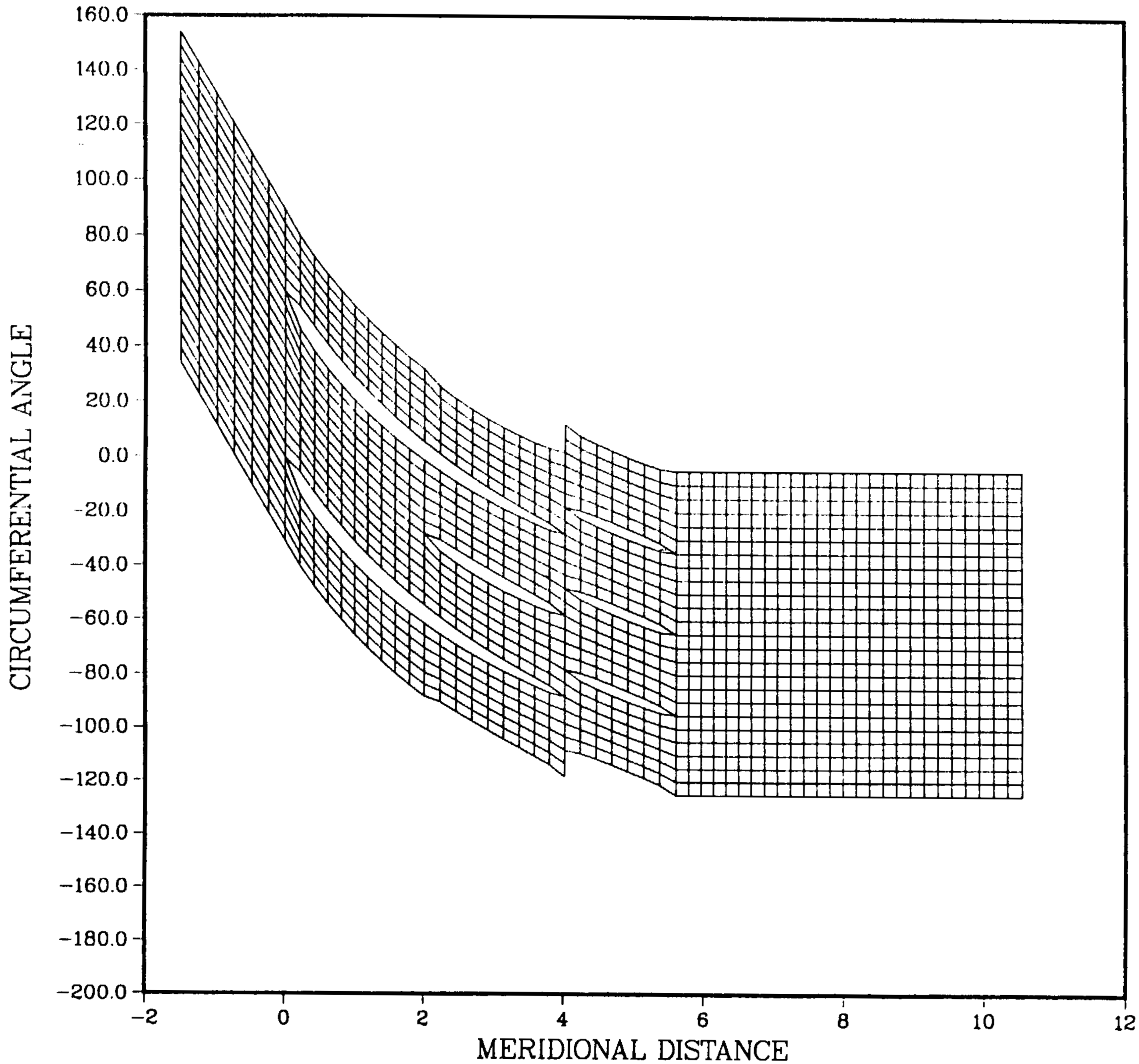

Rockwell International
Rocketdyne Division

OPTIMIZATION OF A CENTRIFUGAL IMPELLER DESIGN THROUGH CFD ANALYSIS

- CONTROL OF IMPELLER BLADE LOADING FROM L.E. TO T.E.
  - REDISTRIBUTE BLADE LOADING BUT PRESERVE BASELINE BLADE CONTOUR
    - BASB, UNLOAD AT L.E. AND T.E. BUT INCREASE LOADING AT MID-SECTION
    - BASC, INCREASE BLADE LOADING AT L.E. AND T.E. BUT UNLOAD AT MID-SECTION
    - BASG, L.E. LOADED
    - BASH, T.E. LOADED
  - CHANGE IMPELLER MERIDIONAL CONTOUR WITH B2 WIDTH REDUCED BY 20%
    - 3 AXIAL LENGTHS (3.87, 3.40, 2.82) ALL WITH DISCHARGE BLADE ANGLE 41.5 (GOOX, GOOY, GOOZ)
    - 3 AXIAL LENGTHS (3.87, 3.40, 2.82) ALL WITH DISCHARGE HUB BLADE ANGLE 50 DEGREE AND TIP BLADE ANGLE 35 DEGREE (GOOF, GOOH, GOOK)

Rockwell International
Rocketdyne Division

NASA CONSORTIUM IMPELLER

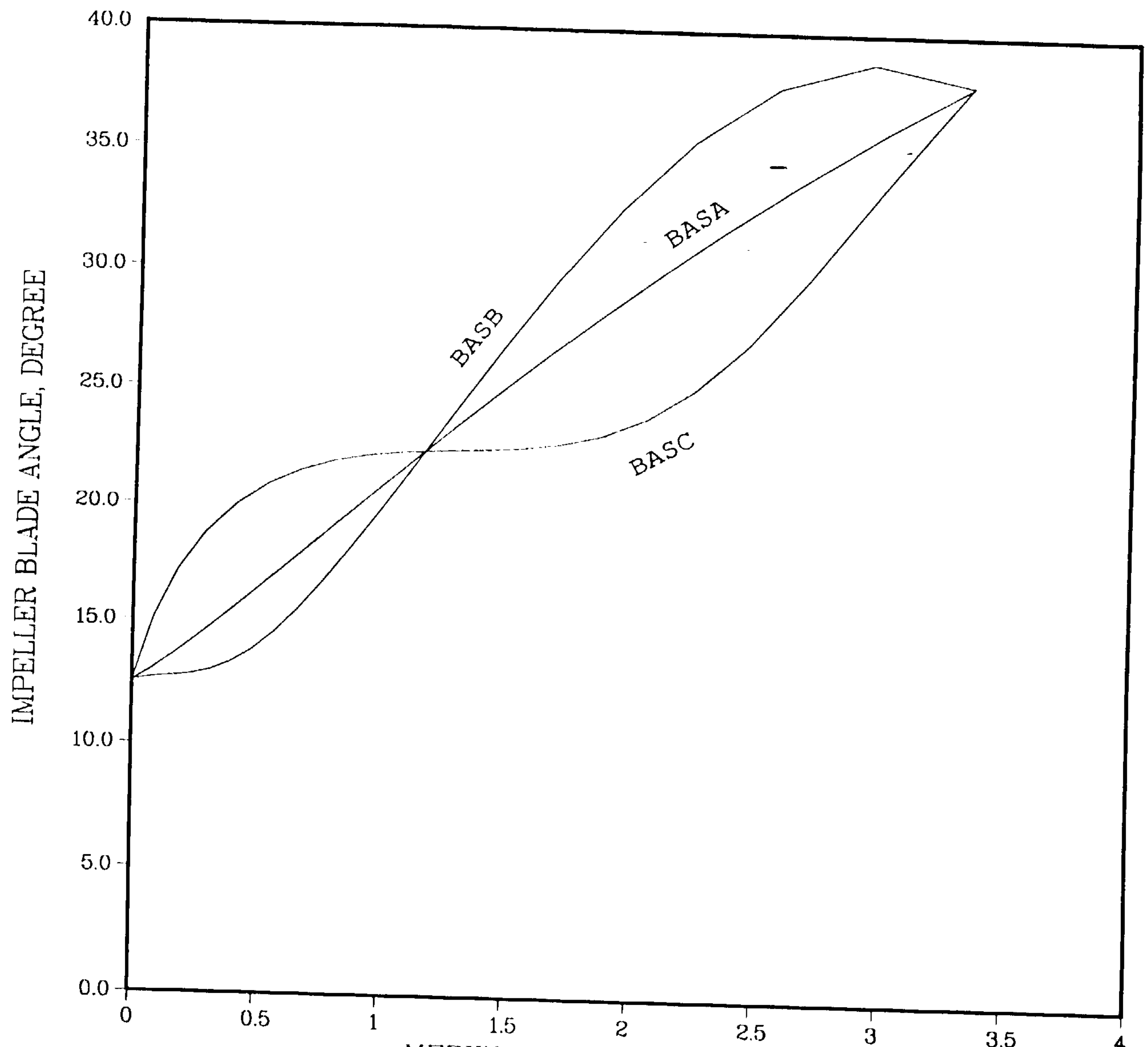

Rockwell International
Rocketdyne Division

NASA CONSORTIUM IMPELLER

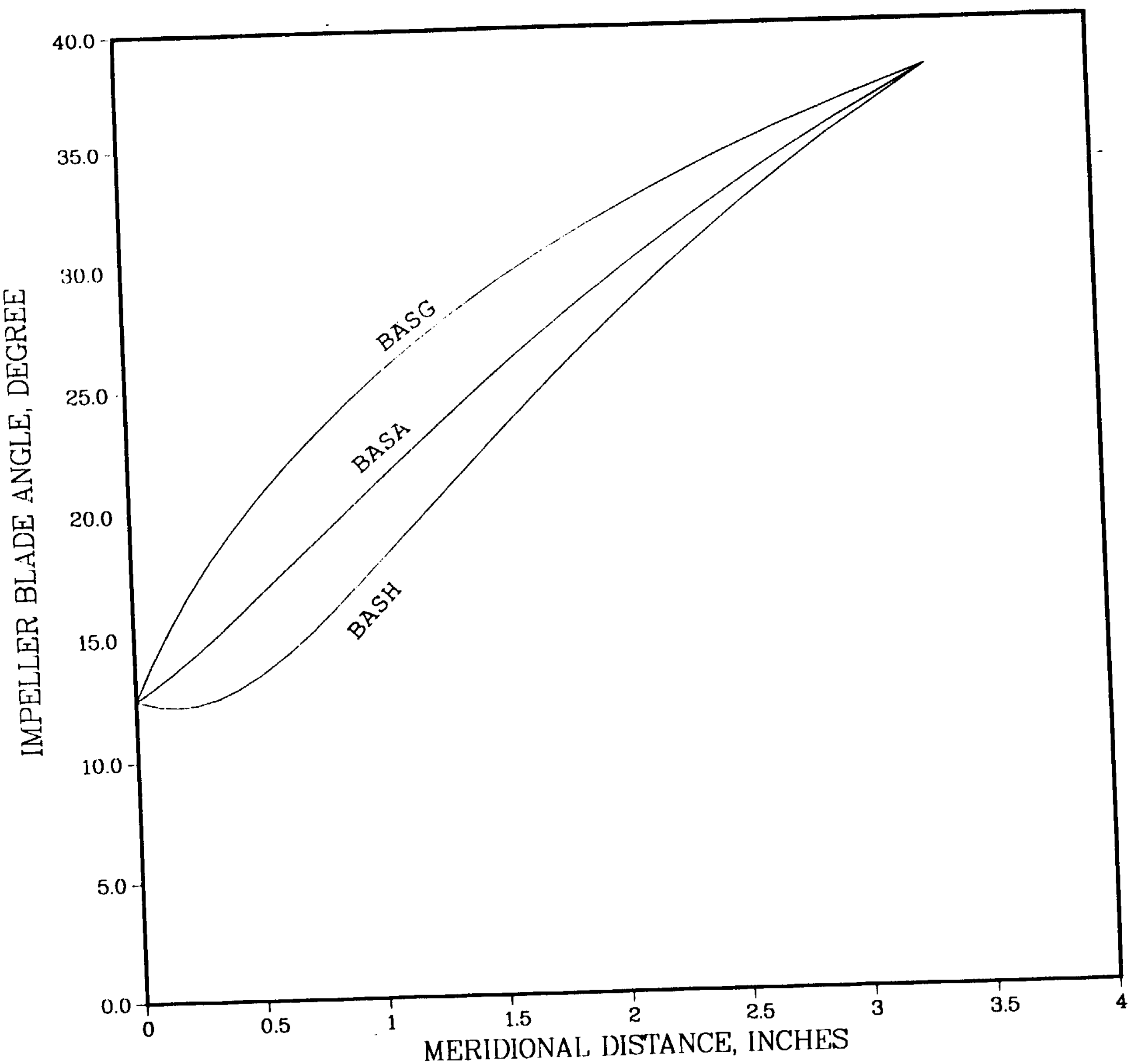

Rockwell International
Rocketdyne Division

NASA CONSORTIUM IMPELLER

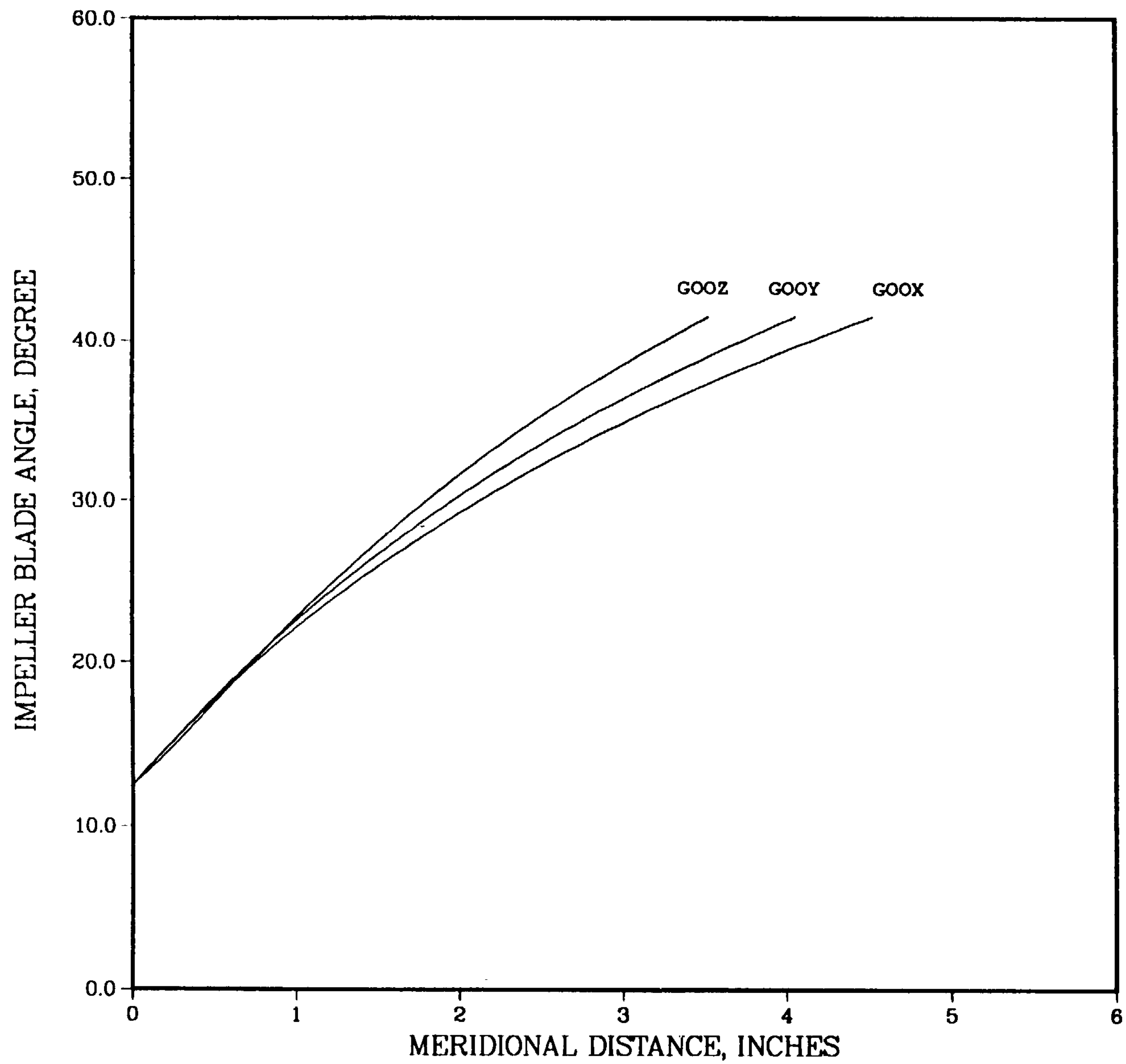

Rockwell International
Rocketdyne Division

NASA CONSORTIUM IMPELLER

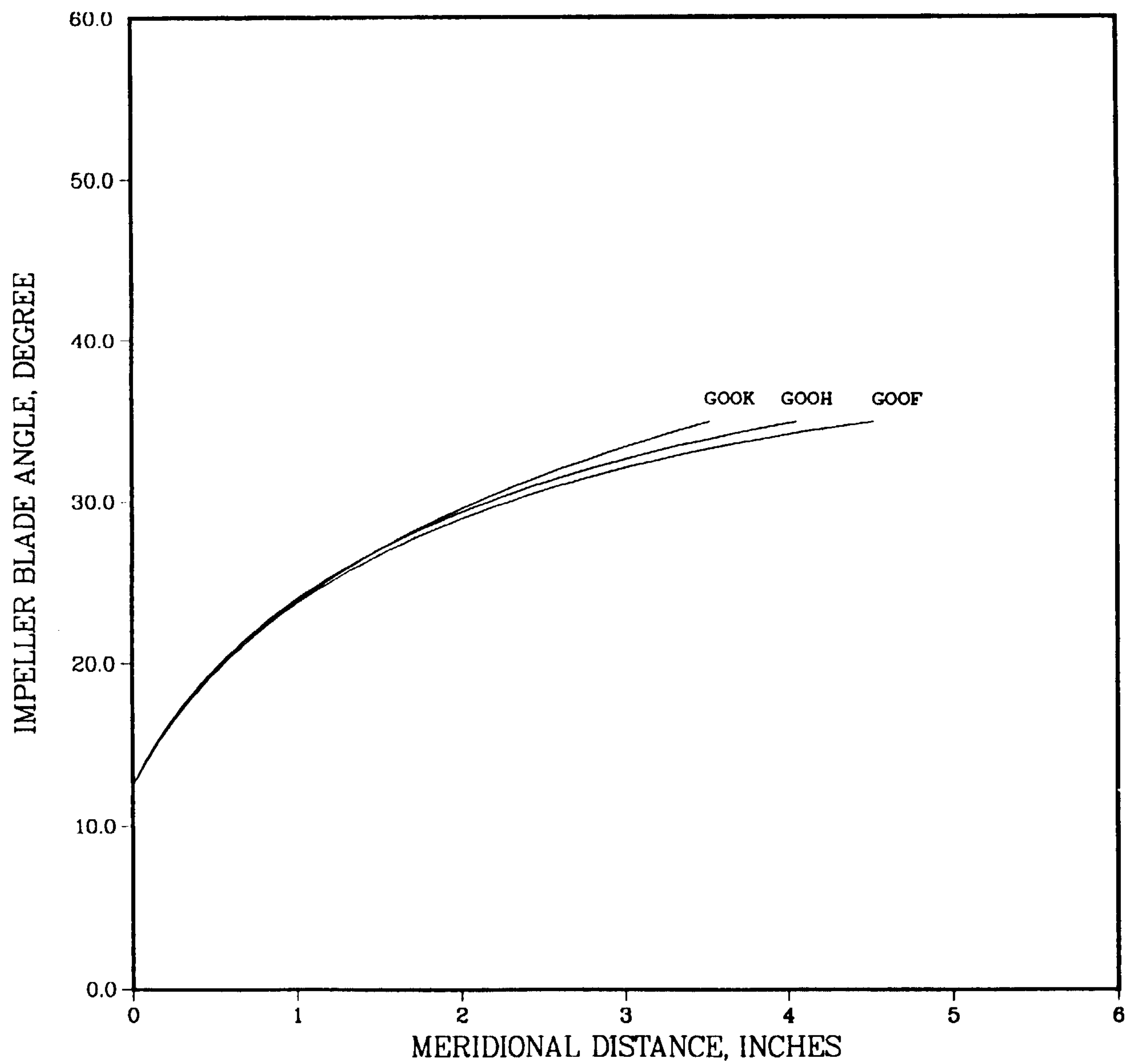

Rockwell International
Rocketdyne Division

OPTIMIZATION OF A CENTRIFUGAL IMPELLER DESIGN THROUGH CFD ANALYSIS

- RESULTS OF CFD ANALYSIS

  - NO SIGNIFICANT IMPACT ON IMPELLER OVERALL PERFORMANCE BY REDISTRIBUTING L.E. TO T.E. BLADE LOADING
  - REDUCED B2 INCREASES OUTLET RADIAL VELOCITY AND ELIMINATES REVERSE FLOW AND BLADE SUCTION SIDE SEPARATION
  - INCREASED AXIAL LENGTH IMPROVE IMPELLER EFFICIENCY UP TO 1% AND REDUCES BLADE TO BLADE DYNAMIC LOADING UP TO 18%
  - VARYING OUTLET BLADE ANGLE SLIGHTLY IMPROVES HUB TO TIP FLOW DISTORTION WITH NO IMPROVEMENT OF BLADE TO BLADE NONUNIFORMITY

Rockwell International
Rocketdyne Division

NASA CONSORTIUM IMPELLER PERFORMANCE

CASE / PERFORMANCE	BASA	BASB	BASC	BASG	BASH	GOOF	GOOH	GOOK	GOOX	GOOY	GOOZ
EFFICIENCY (%)	95.1	95.1	95.0	95.1	95.1	96.0	95.5	95.4	95.95	95.7	95.2
EULER HEAD (FT)	1329.8	1320.7	1337	1342.8	1329.2	1332.5	1332.9	1321.5	1336.3	1334.9	1326.4
INLET PT (PSI)	29.2	29.2	29.2	29.2	29.1	29.7	29.7	29.5	29.7	30.0	29.9
OUTLET PT (PSI)	576.1	572.4	578.7	581.5	575.5	582.9	580.2	571.7	584.1	582.3	576.3
HUB TO TIP FLOW DISTORTION (DEGREE)	3.00	3.08	3.15	1.80	3.00	2.72	2.46	2.39	3.53	2.94	2.53
BLADE TO BLADE DYNAMIC LOAD	0.78E4	0.77E4	0.79E4	0.81E4	0.74E4	0.71E4	0.75E4	0.79E4	0.64E4	0.68E4	0.77E4
FLOW SPLIT ZONE II, ZONE III	54.7 45.3	55.2 44.8	53.5 46.5	58.8 41.2	51.0 49.0	53.3 46.7	55.0 45.0	55.6 44.4	53.6 46.4	55.3 44.7	57.2 42.8
IMPELLER HEAD COEFF.	0.653	0.649	0.656	0.66	0.653	0.661	0.657	0.651	0.662	0.660	0.653
OUTLET FLOW SEPARATION	YES	YES	YES	YES	YES	NO	NO	NO	NO	NO	NO
OUTLET FLOW RECIRCULATION	YES	YES	YES	YES	YES	NO	NO	NO	NO	NO	NO

Rockwell International
Rocketdyne Division

NASA CONSORTIUM IMPELLER

BASA

VELOCITY VECTORS IN MIDPLANE

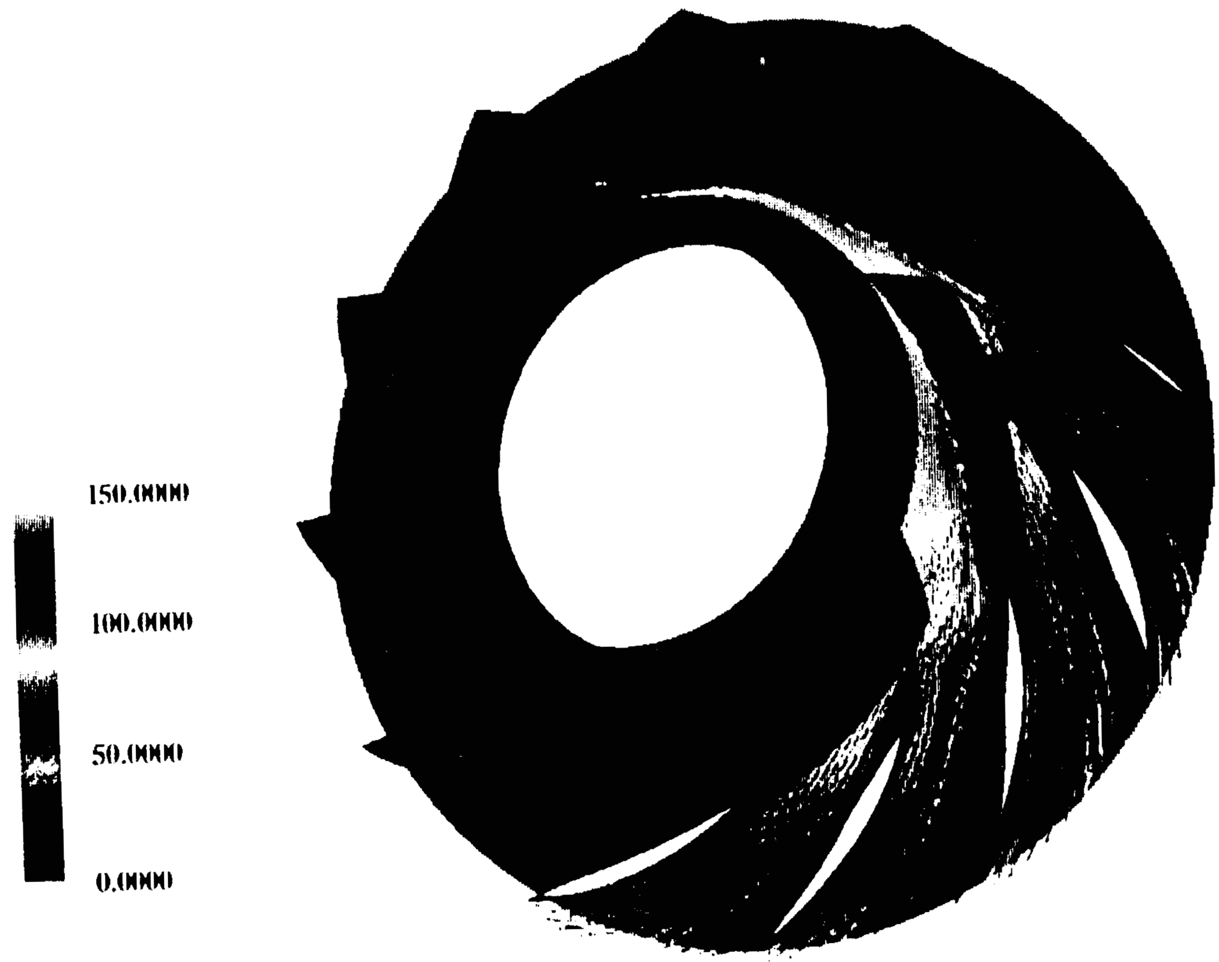

NASA CONSORTIUM IMPELLER

BASH

VELOCITY VECTORS IN MIDPLANE

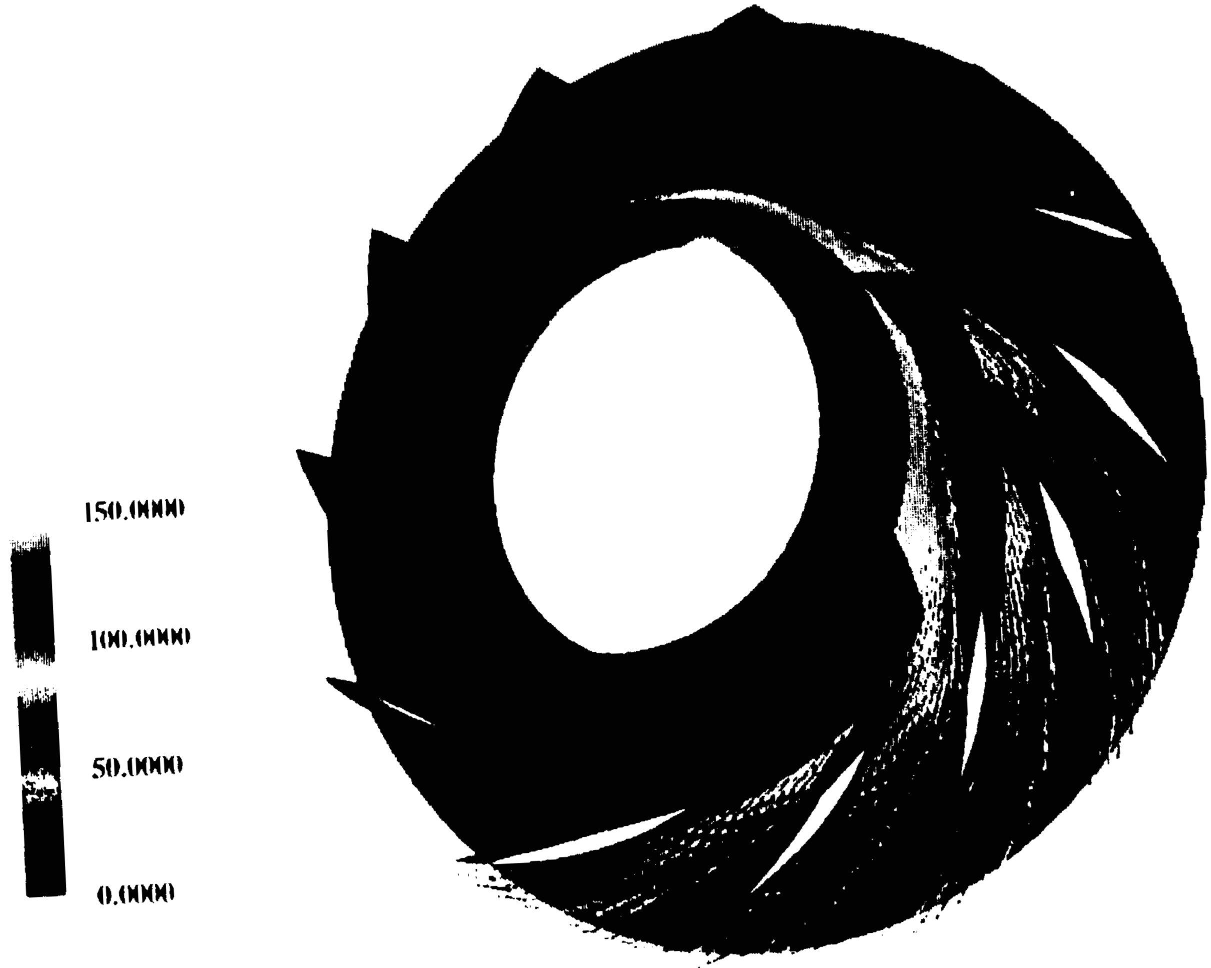

IMPELLER DISCHARGE RADIAL VELOCITY:

(BASELINE DESIGN)

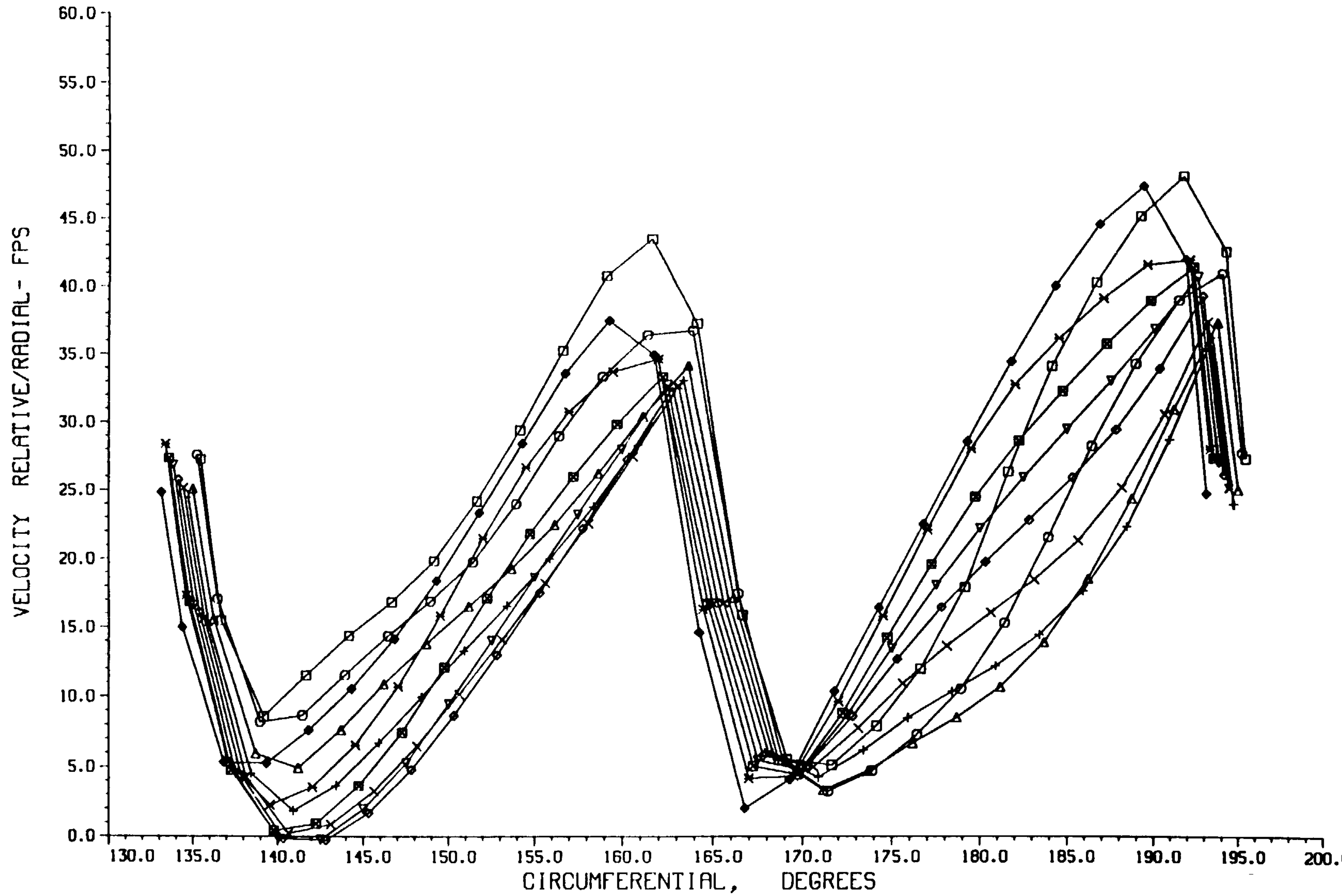

Rockwell International
Rocketdyne Division

IMPELLER DISCHARGE RADIAL VELOCITY: (GOOX DESIGN)

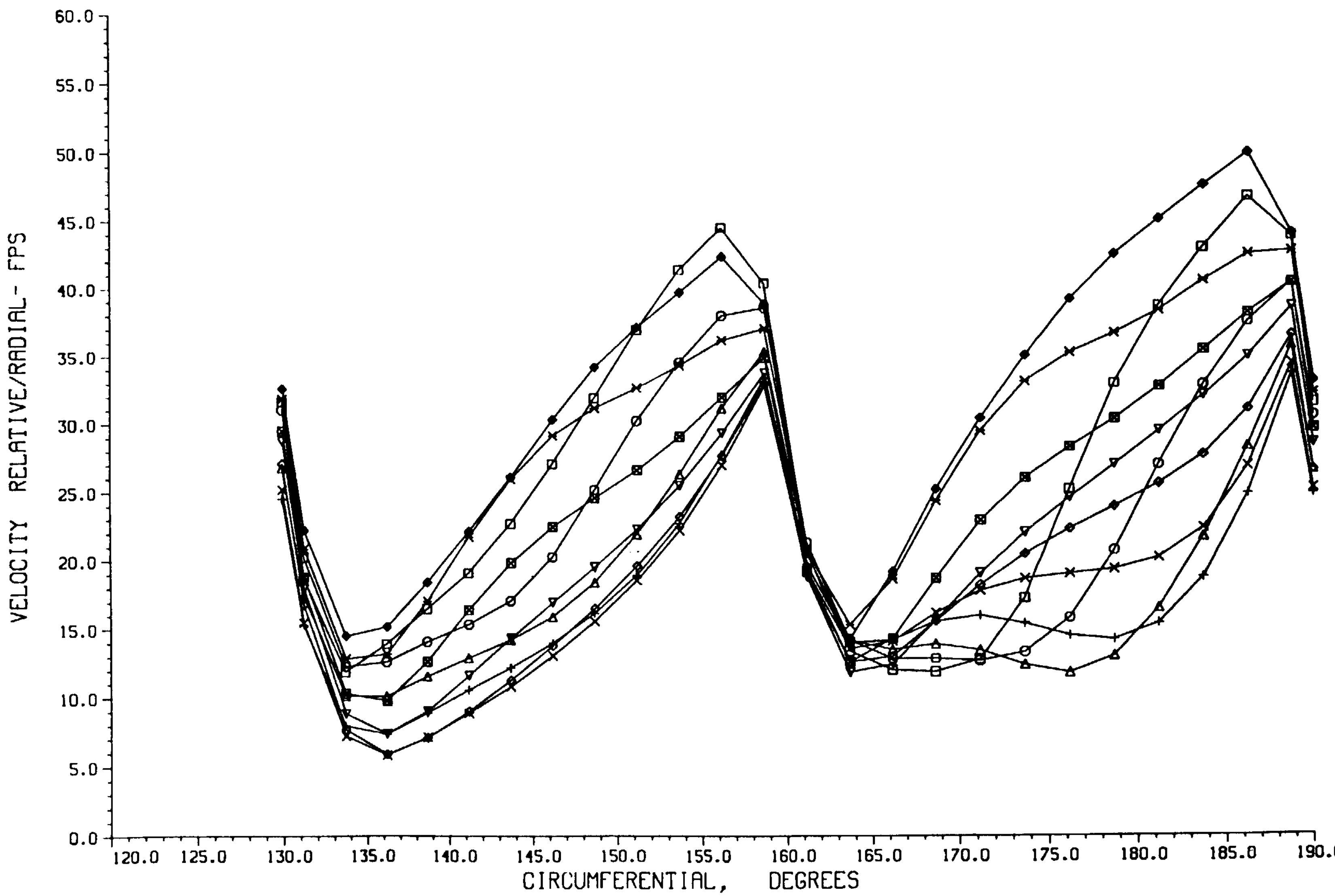

Rockwell International
Rocketdyne Division

NASA CONSORTIUM IMPELLER PERFORMANCE

CASE / PERFORMANCE	BASA	BASB	BASC	BASG	BASH	GOOF	GOOH	GOOK	GOOX	GOOY	GOOZ
EFFICIENCY (%)	$\boxed{95.1}$	95.1	95.0	95.1	95.1	96.0	95.5	95.4	$\boxed{95.95}$	95.7	95.2
EULER HEAD (FT)	1329.8	1320.7	1337	1342.8	1329.2	1332.5	1332.9	1321.5	1336.3	1334.9	1326.4
INLET PT (PSI)	29.2	29.2	29.2	29.2	29.1	29.7	29.7	29.5	29.7	30.0	29.9
OUTLET PT (PSI)	576.1	572.4	578.7	581.5	575.5	582.9	580.2	571.7	584.1	582.3	576.3
HUB TO TIP FLOW DISTORTION (DEGREE)	3.00	3.08	3.15	1.80	3.00	2.72	2.46	2.39	3.53	2.94	2.53
BLADE TO BLADE DYNAMIC LOAD	$\boxed{0.78E4}$	0.77E4	0.79E4	0.81E4	0.74E4	0.71E4	0.75E4	0.79E4	$\boxed{0.64E4}$	0.68E4	0.77E4
FLOW SPLIT ZONE II, ZONE III	54.7 45.3	55.2 44.8	53.5 46.5	58.8 41.2	51.0 49.0	53.3 46.7	55.0 45.0	55.6 44.4	53.6 46.4	55.3 44.7	57.2 42.8
IMPELLER HEAD COEFF.	0.653	0.649	0.656	0.66	0.653	0.661	0.657	0.651	0.662	0.660	0.653
OUTLET FLOW SEPARATION	YES	YES	YES	YES	YES	NO	NO	NO	NO	NO	NO
OUTLET FLOW RECIRCULATION	YES	YES	YES	YES	YES	NO	NO	NO	NO	NO	NO

Rockwell International
Rocketdyne Division

NASA CONSORTIUM IMPELLER

BASA

ROTARY STAGNATION PRESSURE   REDUCED STATIC PRESSURE

NASA CONSORTIUM IMPELLER

GOOF

ROTARY STAGNATION PRESSURE   REDUCED STATIC PRESSURE

NASA CONSORTIUM IMPELLER PERFORMANCE

CASE / PERFORMANCE	BASA	BASB	BASC	BASG	BASH	GOOF	GOOH	GOOK	GOOX	GOOY	GOOZ
EFFICIENCY (%)	95.1	95.1	95.0	95.1	95.1	96.0	95.5	95.4	95.95	95.7	95.2
EULER HEAD (FT)	1329.8	1320.7	1337	1342.8	1329.2	1332.5	1332.9	1321.5	1336.3	1334.9	1326.4
INLET PT (PSI)	29.2	29.2	29.2	29.2	29.1	29.7	29.7	29.5	29.7	30.0	29.9
OUTLET PT (PSI)	576.1	572.4	578.7	581.5	575.5	582.9	580.2	571.7	584.1	582.3	576.3
HUB TO TIP FLOW DISTORTION (DEGREE)	3.00	3.08	3.15	1.80	3.00	2.72	2.46	2.39	3.53	2.94	2.53
BLADE TO BLADE DYNAMIC LOAD	0.78E4	0.77E4	0.79E4	0.81E4	0.74E4	0.71E4	0.75E4	0.79E4	0.64E4	0.68E4	0.77E4
FLOW SPLIT ZONE II, ZONE III	54.7 45.3	55.2 44.8	53.5 46.5	58.8 41.2	51.0 49.0	53.3 46.7	55.0 45.0	55.6 44.4	53.6 46.4	55.3 44.7	57.2 42.8
IMPELLER HEAD COEFF.	0.653	0.649	0.656	0.66	0.653	0.661	0.657	0.651	0.662	0.660	0.653
OUTLET FLOW SEPARATION	YES	YES	YES	YES	YES	NO	NO	NO	NO	NO	NO
OUTLET FLOW RECIRCULATION	YES	YES	YES	YES	YES	NO	NO	NO	NO	NO	NO

Rockwell International
Rocketdyne Division

OPTIMIZATION OF A CENTRIFUGAL IMPELLER DESIGN THROUGH CFD ANALYSIS

- CONCLUSION
  - CFD RESULTS SHOW MINIMAL PERFORMANCE IMPROVEMENT OF TANDEM BLADE CONFIGURATION FOR THIS HIGH HEAD COEFFICIENT AND HIGH EYE TO TIP RATIO
  - IMPELLER DISCHARGE REVERSE FLOW CAN BE CONTROLLED BY THE B2 WIDTH
  - THE IMPELLER EFFICIENCY AND EXIT FLOW DISTORTION CAN BE IMPROVED BY CONTROL OF THE IMPELLER AXIAL LENGTH
  - BASELINE DESIGN CAN BE FURTHER OPRIMIZED TO MEET STRUCTURAL AND HYDRODYNAMIC REQUIREMENT
    - PARTIAL BLADE SOLIDITY, PARTIAL BLADE POSITION, T.E. BLADE LEAN PENDING OTHER CONSORTIUM TEAM MEMBER RESULTS

Rockwell International
Rocketdyne Division

OPTIMIZATION OF A CENTRIFUGAL IMPELLER DESIGN THROUGH CFD ANALYSIS

TABLE I : DESCRIPTION OF CHANGES FOR EACH CASE

BASA: EXISTING BASELINE DESIGN WITH WATER TEST RESULTS

BASB: SAME BLADE ENVELOPE AS BASA WITH LARGER LOAD AT BLADE L.E. AND T.E. BUT SMALLER LOAD AT MID-SECTION

BASC: SAME BLADE ENVELOPE AS BASA WITH LARGER LOAD AT MID-SECTION, BUT SMALLER LOAD AT L.E. AND T.E.

BASG: SAME MERIDIONAL CONTOUR AS BASA WITH HEAVY LOAD AT L.E. AND GRADUAL UNLOADING TOWARD T.E.

BASH: SAME MERIDIONAL CONTOUR AS BASA WITH VERY SMALL LOAD AT L.E. AND GRADUAL INCREASE IN LOADING TOWARD T.E.

GOOF: INCREASE AXIAL LENGTH BY 37%, REDUCE B2 BY 20% AND CHANGE OUTLET BLADE ANGLE FROM HUB=50 TO TIP=35

GOOH: INCREASE AXIAL LENGTH BY 20%, REDUCE B2 BY 20% AND CHANGE OUTLET BLADE ANGLE FROM HUB=50 TO TIP=35

GOOK: NO CHANGE OF AXIAL LENGTH, REDUCE B2 BY 20% AND CHANGE OUTLET BLADE ANGLE FROM HUB=50 TO TIP=35

GOOX: INCREASE AXIAL LENGTH BY 37%, REDUCE B2 BY 20% AND USE CONSTANT OUTLET BLADE ANGLE 41.5

GOOY: INCREASE AXIAL LENGTH BY 20%, REDUCE B2 BY 20% AND USE CONSTANT OUTLET BLADE ANGLE 41.5

GOOZ: NO CHANGE OF AXIAL LENGTH, REDUCE B2 BY 20% AND USE CONSTANT OUTLET BLADE ANGLE 41.5

NASA CONSORTIUM IMPELLER GEOMETRY

CASE / GEOMETRY	BASA	BASB	BASC	BASG	BASH	GOOF	GOOH	GOOK	GOOX	GOOY	GOOZ
AXIAL LENGTH (INCH)	2.82	2.82	2.82	2.82	2.82	3.87	3.40	2.82	3.87	3.40	2.82
B2 WIDTH (INCH)	1.12	1.12	1.12	1.12	1.12	0.90	0.80	0.90	0.90	0.90	0.90
HUB WRAP (DEGREE)	0~105	0~105	0~105	0~91	0~114	0~100	0~90	0~80	0~100	0~90	0~80
TIP WRAP (DEGREE)	20~103	20~103	20~103	20~91	20~114	0~100	0~90	0~80	0~100	0~90	0~80
OUTLET LEAN (DEGREE)	16	20	14	0	0	0	0	0	0	0	0
HUB OUTLET BLADE ANGLE	38	38	38	38	38	50	50	50	41.5	41.5	41.5
TIP OUTLET BLADE ANGLE	38	38	38	38	38	35	35	35	41.5	41.5	41.5
HUB INLET BLADE ANGLE	20	20	20	20	20	20	20	20	20	20	20
TIP INLET BLADE ANGLE	12.5	12.5	12.5	12.5	12.5	12.5	12.5	12.5	12.5	12.5	12.5

Rockwell International
Rocketdyne Division

N95- 23625

USE OF BLADE LEAN IN TURBOMACHINERY REDESIGN

John Moore, Joan G. Moore, and Alex Lupi

Mechanical Engineering Department
Virginia Polytechnic Institute and State University
Blacksburg, Virginia 24061-0238

Blade lean is used to improve the uniformity of exit flow distributions from turbomachinery blading. In turbines, it has been used to control secondary flows by tailoring blade turning to reduce flow overturning and underturning and to create more uniform loss distributions from hub to shroud.

In the present study, the Pump Consortium centrifugal impeller has been redesigned using blade lean. The flow at the exit of the baseline impeller had large blade-to-blade variations, creating a highly unsteady flow for the downstream diffuser. Blade lean is used to redesign the flow to move the high loss fluid from the suction side to the hub, significantly reducing blade-to-blade variations at the exit.

Axial Flow Turbine Stators

Consortium Pump Impeller Problem

Secondary Flow Analysis for a Rotor

Stable Location of High Loss Fluid

Impeller Redesign

Improved Performance

Use of Blade Lean
in
Axial Flow Turbine Stators

∇P in Cross-Sections

Controlling Exit Loss Distributions

Linear Cascade

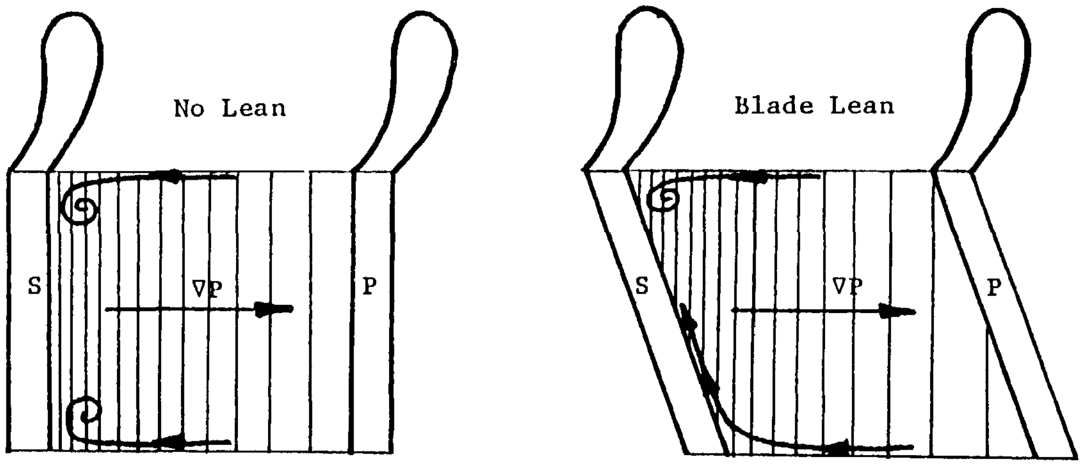

Static pressure contours established by primary flow.

Boundary layer flow towards top endwall/ suction side corner region.

Boundary layer accumulation towards midspan.

Annular Cascade

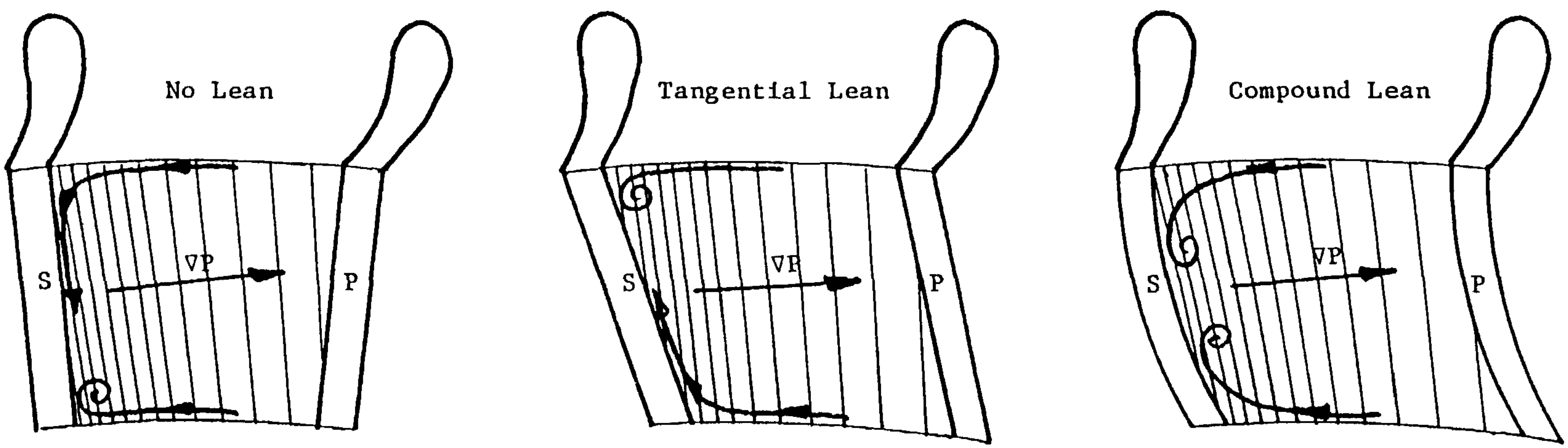

Expect more losses in hub/suction side corner region.

Opposing radially inward flow in suction side boundary layer.

Spreading loss spanwise.

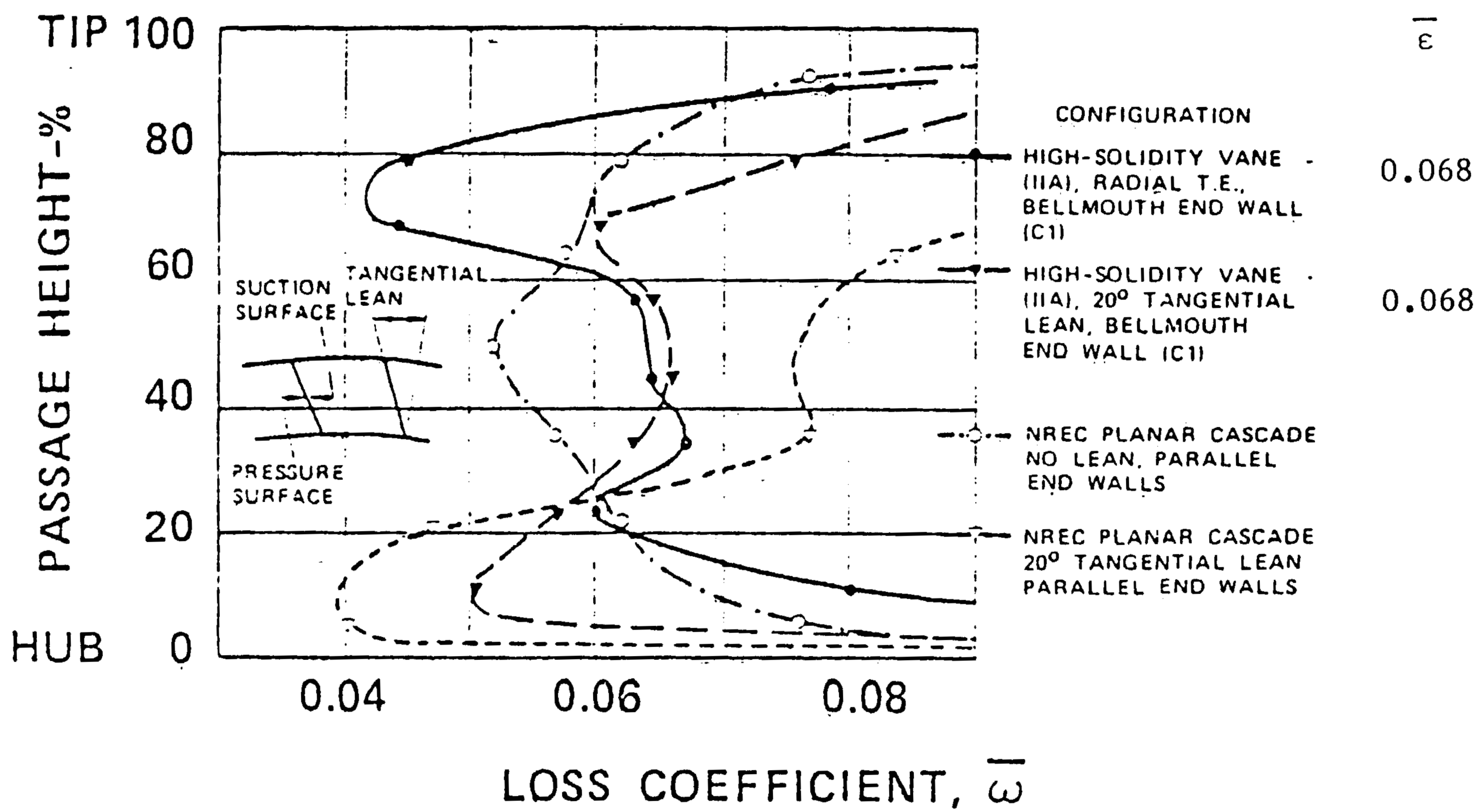

Effect of tangential lean on stator vane losses

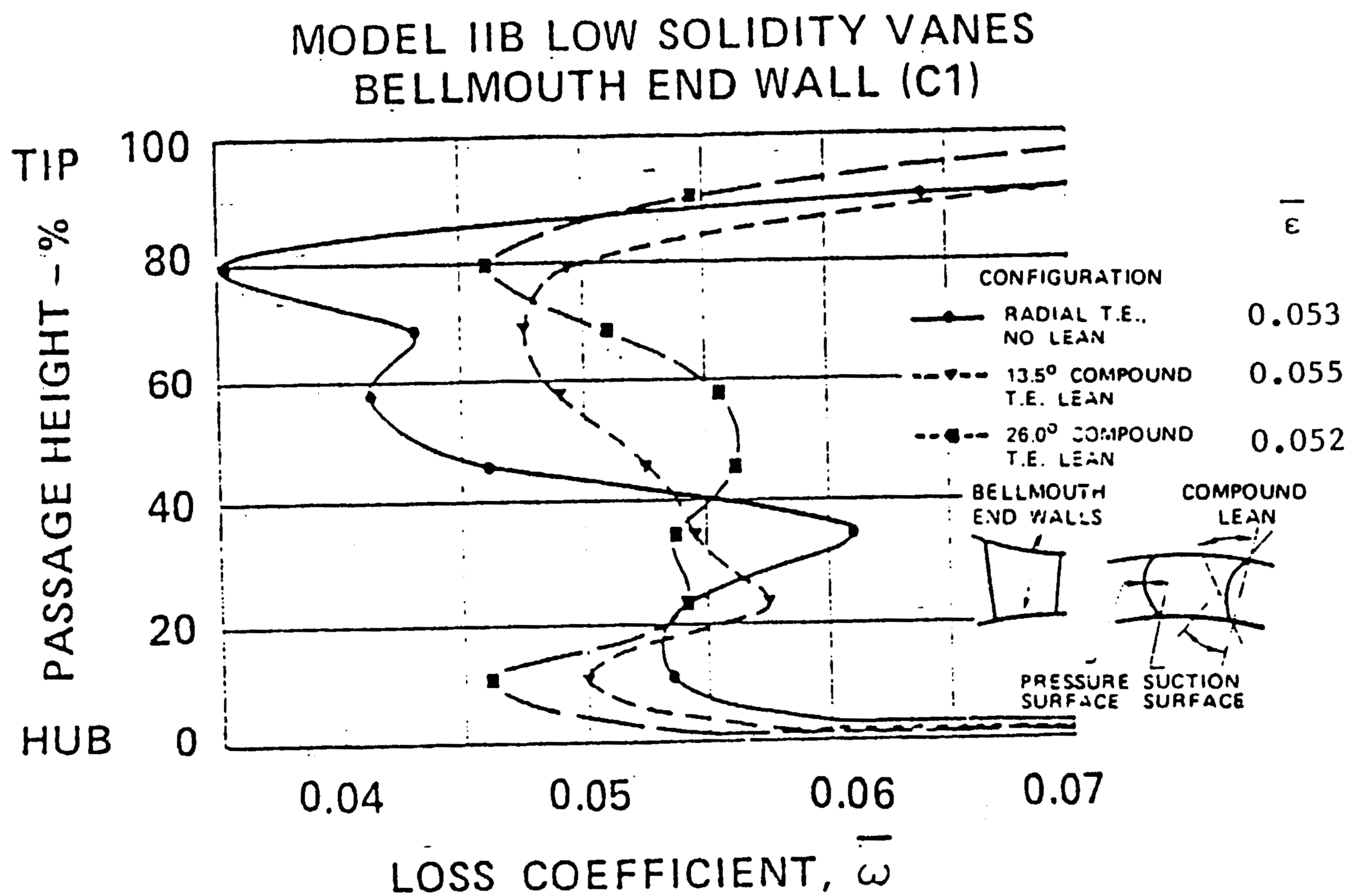

Effect of compound lean on stator vane losses

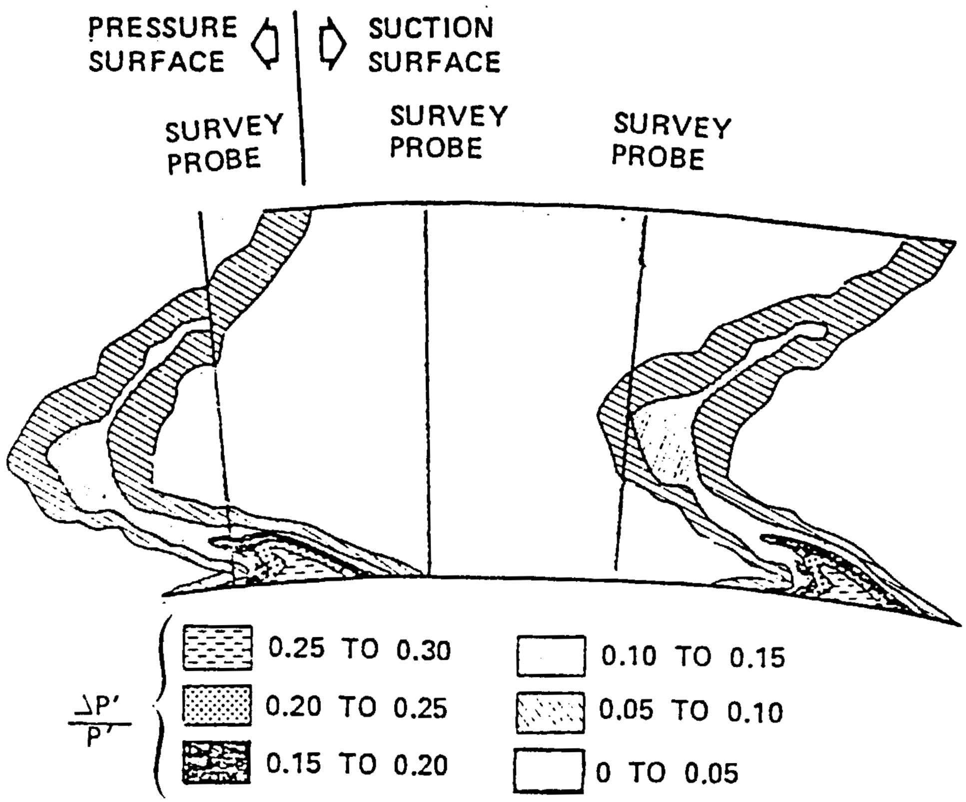

Total pressure loss contours: Phase II stator

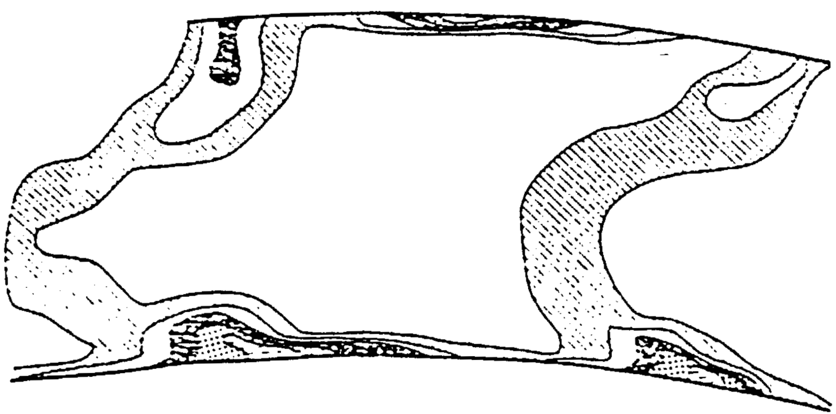

Total pressure loss contours: Phase I/ Model D stator

CONSORTIUM IMPELLER BASELINE DESIGN

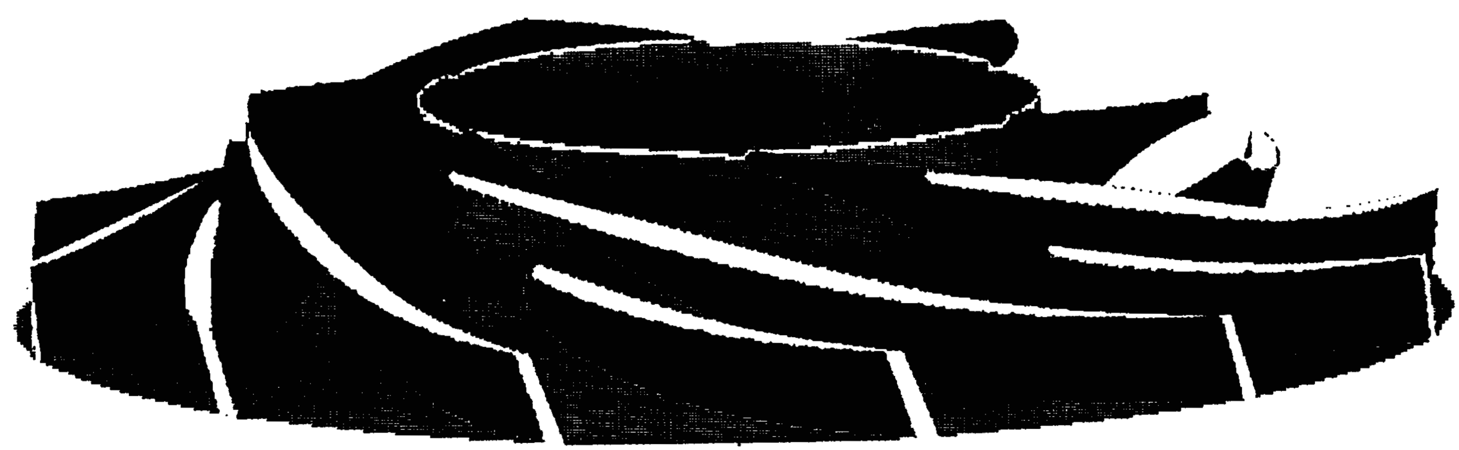

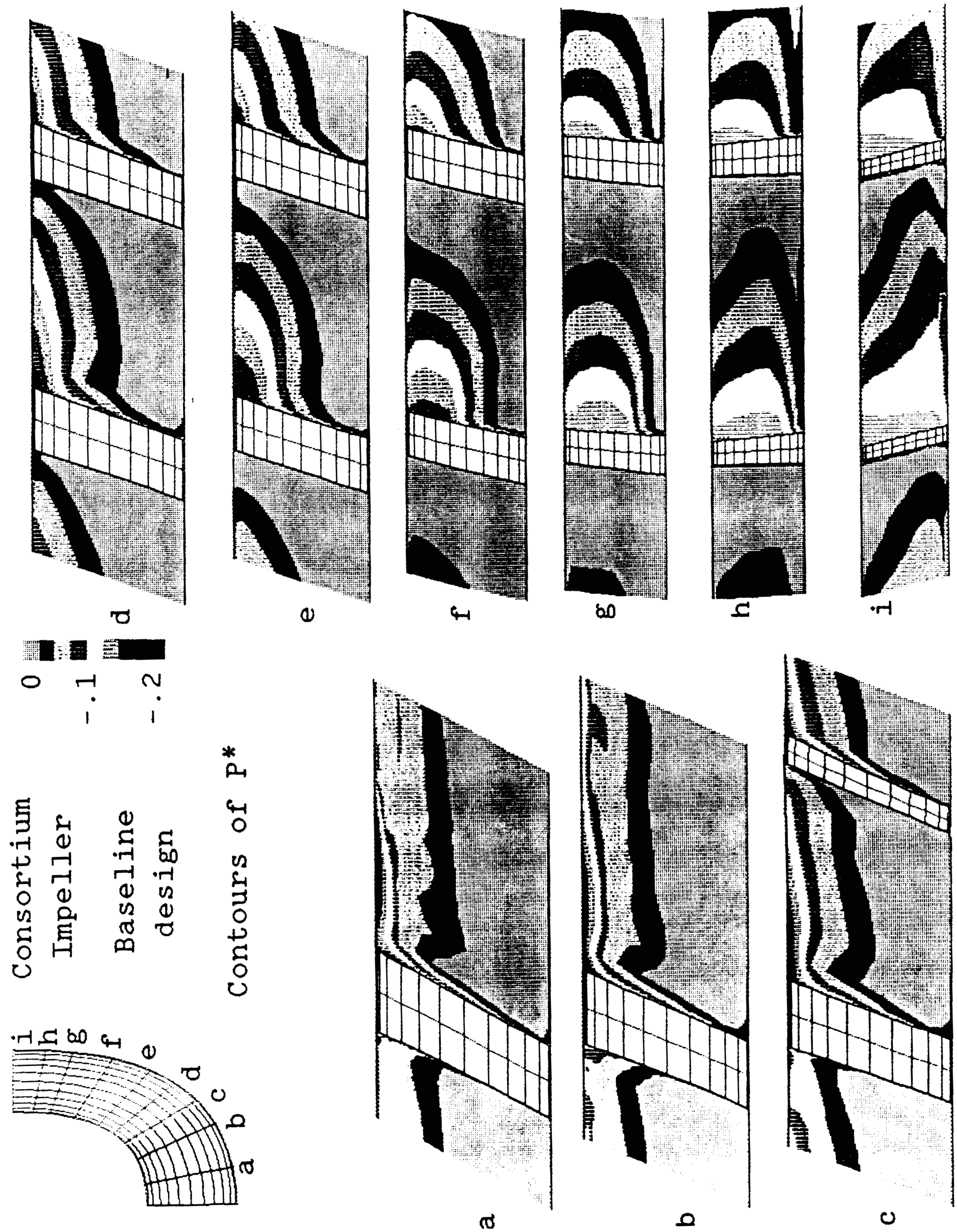
Consortium
Impeller
Baseline
design
Contours of P*
0
-.1
-.2
a
b
c
d
e
f
g
h
i

Consortium Impeller, Baseline Design
Exit Plane Distortion

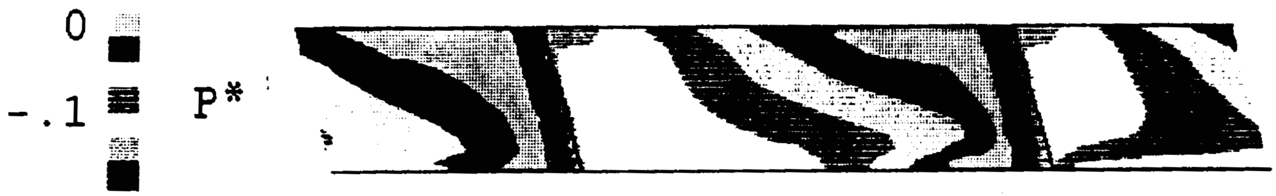

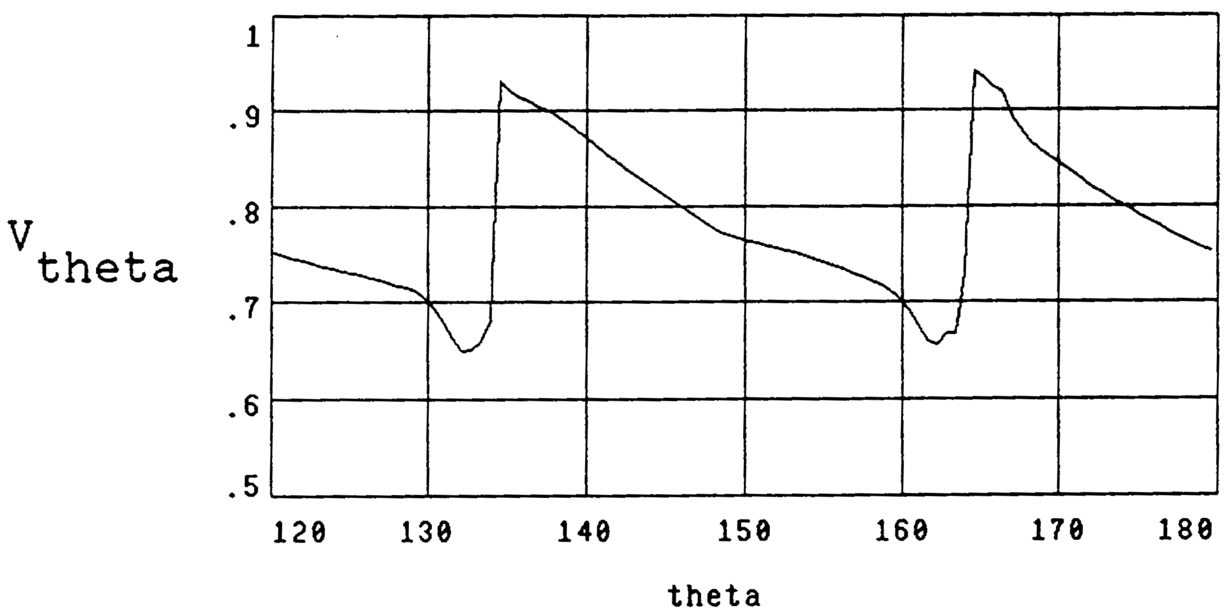

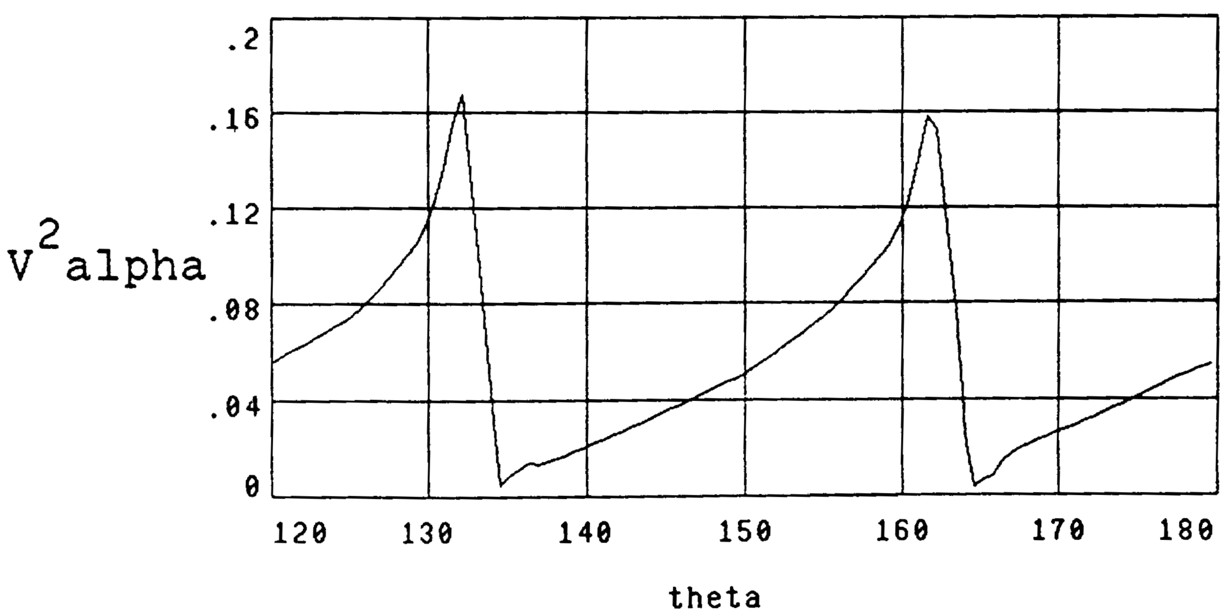

Equations for Incompressible Flow in a Rotating System

Reduced static pressure

$$p_r = p - \frac{1}{2}\rho\omega^2 r^2.$$

Rotary stagnation pressure

$$p^* = p + \frac{1}{2}\rho W^2 - \frac{1}{2}\rho\omega^2 r^2$$

Absolute vorticity

$$\underline{\Omega} = \nabla \times \underline{V} = \nabla \times \underline{W} + 2\underline{\omega}$$

Momentum, inviscid flow

$$(\underline{W} \cdot \nabla)\underline{W} + 2\underline{\omega} \times \underline{W} = -\frac{1}{\rho}\nabla p_r$$

Determining the Stable Orientation Vector for Secondary Vorticity Suppression in Rotating Systems

Secondary Circulation, Hawthorne

$$\frac{\partial}{\partial s}\left[\frac{\Omega_s}{W}\right] = \frac{2}{\rho W^2}\left[\frac{1}{R_n}\frac{\partial p^*}{\partial b} + \frac{\omega}{W}\frac{\partial p^*}{\partial z}\right]$$

From momentum

$$\underline{W} \times \underline{\Omega} = \frac{1}{\rho}\nabla p^*$$

or

$$\underline{W} \cdot \nabla p^* = 0, \qquad \nabla p^* \perp \underline{W}$$

Generation of secondary circulation = 0 when

$$\underline{W} \cdot \left\{[-\frac{1}{\rho}\nabla p_r - \underline{\omega} \times \underline{W}] \times \nabla p^*\right\} = 0$$

I.e. the component of the vector

$$-\frac{1}{\rho}\nabla p_r - \underline{\omega} \times \underline{W}$$

perpendicular to the relative velocity points to the stable location of high loss fluid.

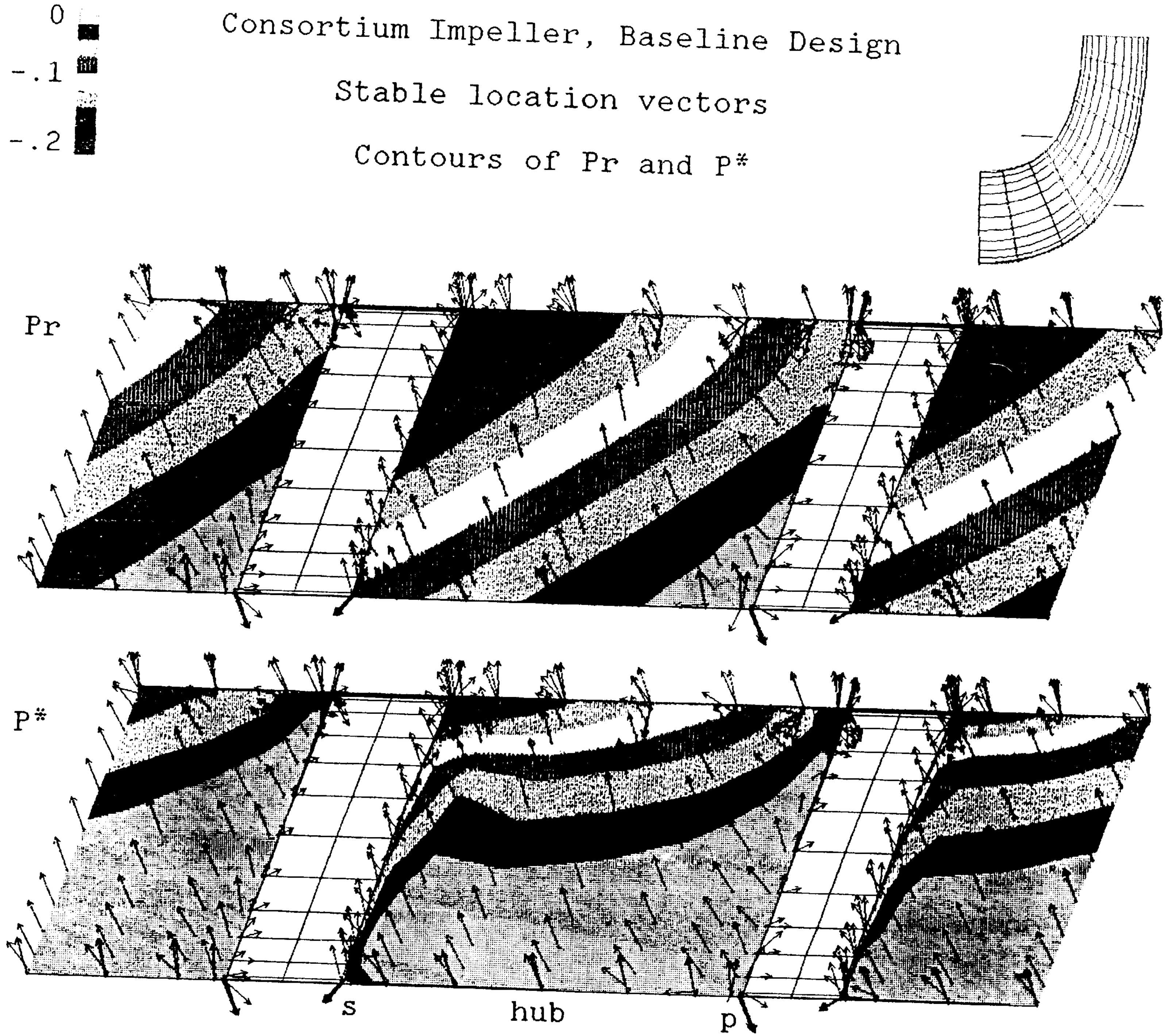
Consortium Impeller, Baseline Design
Stable location vectors
Contours of Pr and P*
0
-.1
-.2
Pr
P*
s
hub
p

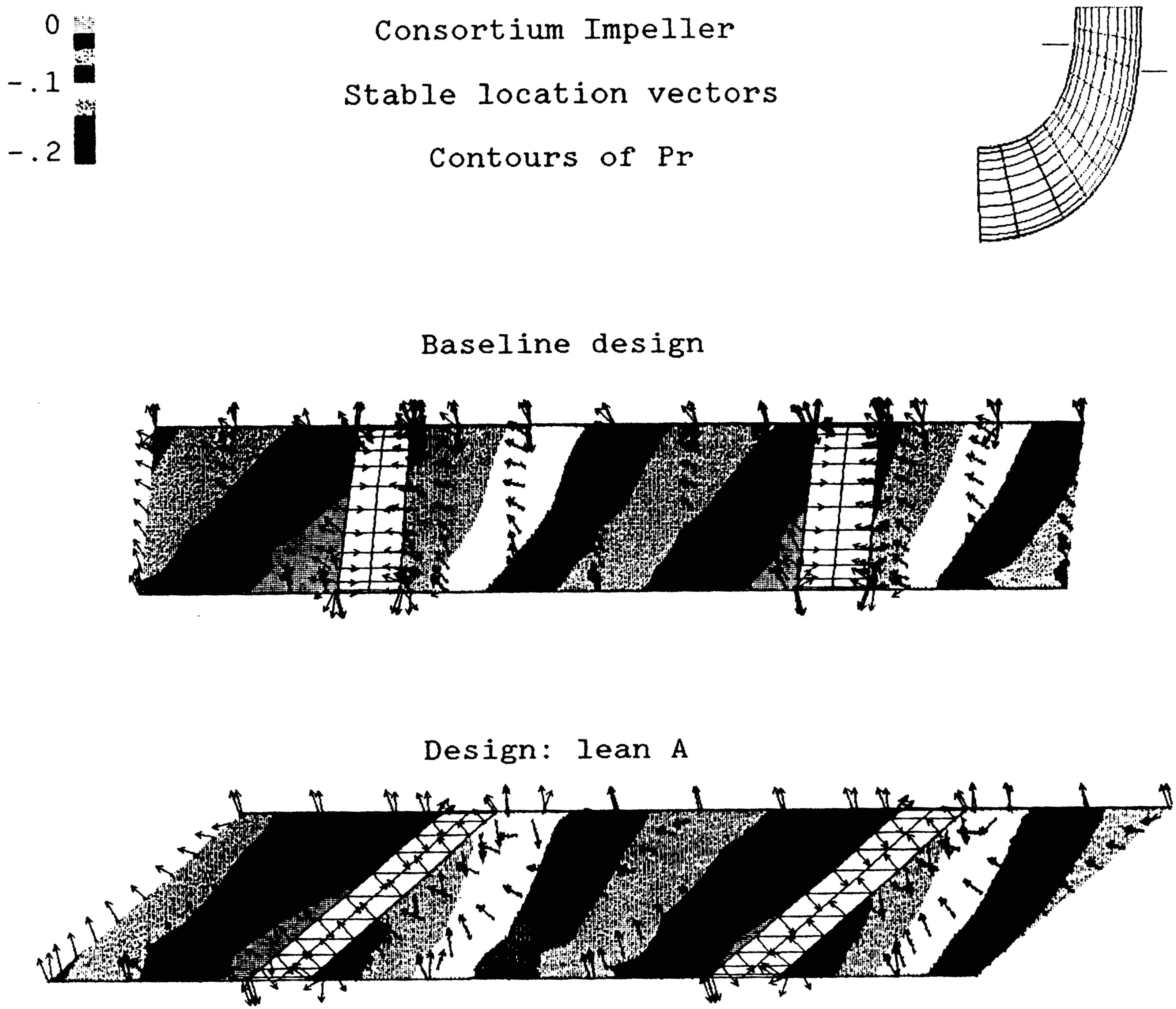
0
-.1
-.2
Consortium Impeller
Stable location vectors
Contours of Pr
Baseline design
Design: lean A

CONSORTIUM IMPELLER REDESIGN: LEAN A

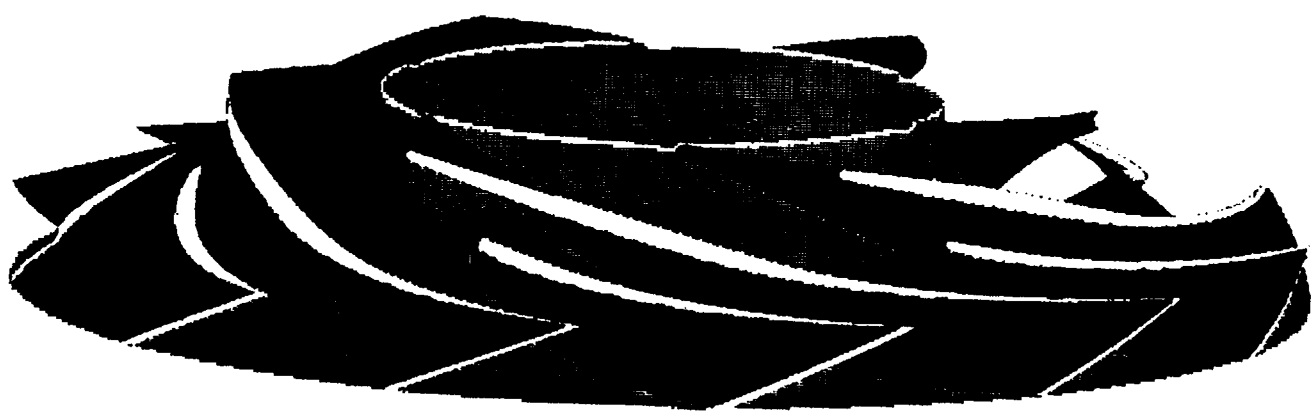

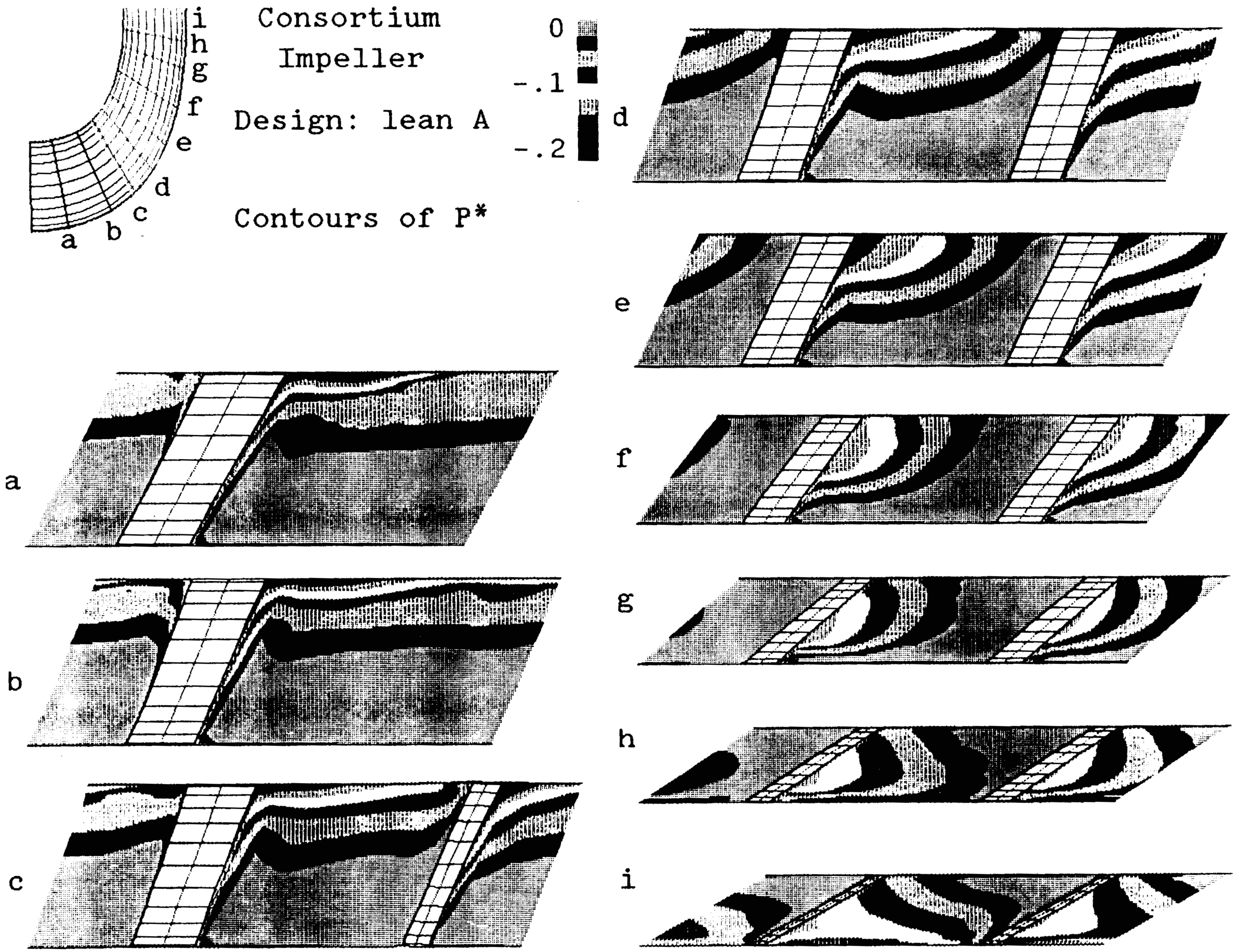
Consortium
Impeller
Design: lean A
Contours of P*
0
-.1
-.2
a
b
c
d
e
f
g
h
i

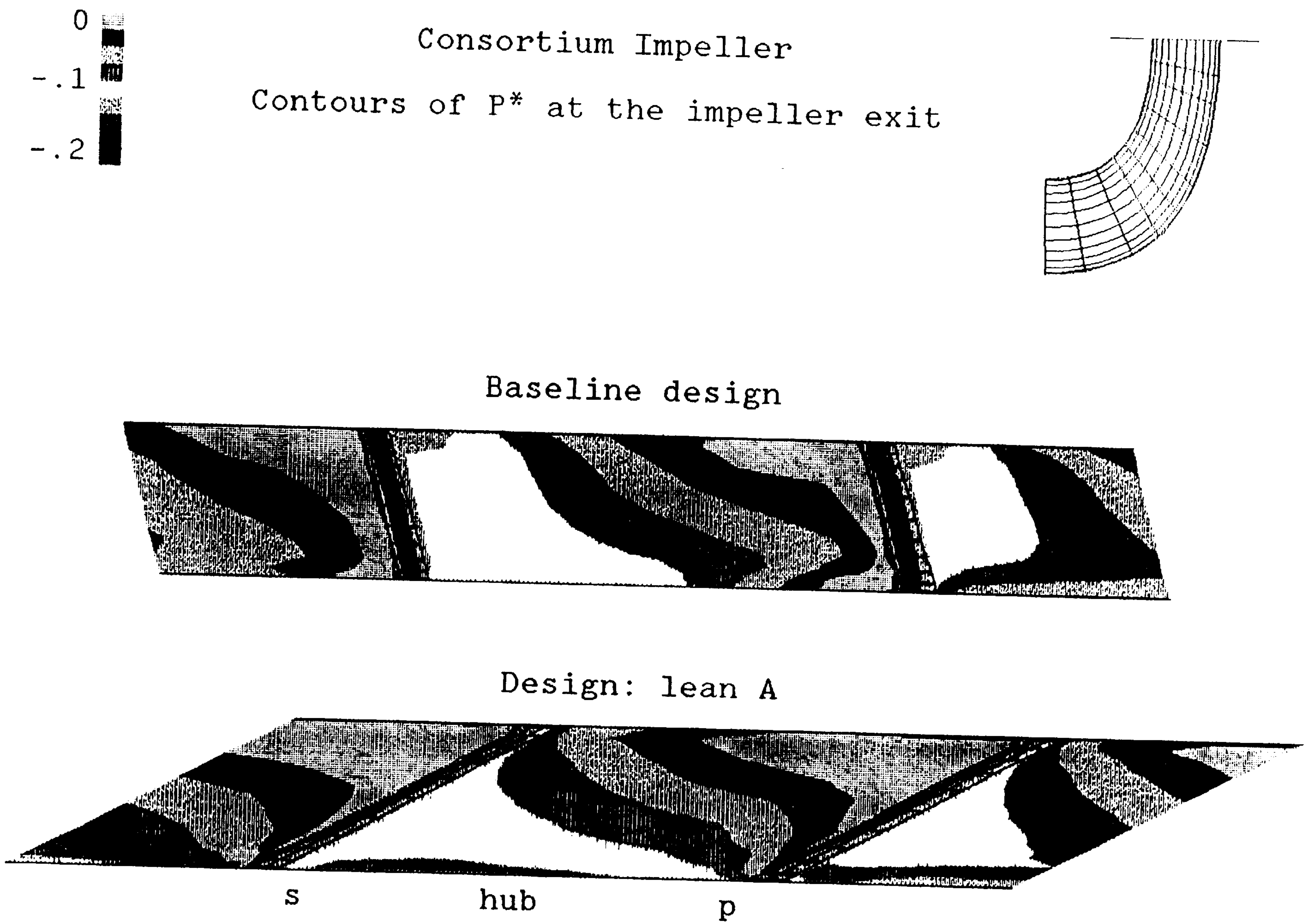
Consortium Impeller
Contours of P* at the impeller exit
0
-.1
-.2
Baseline design
Design: lean A
s
hub
p

Consortium Impeller, Design: Lean A
Exit Plane Distortion

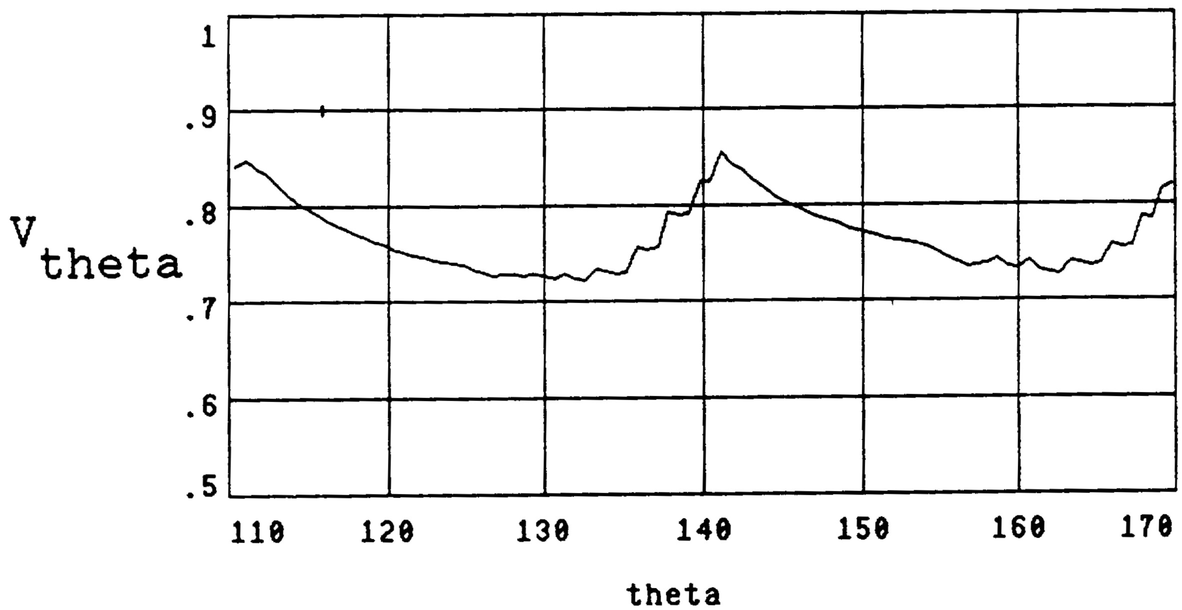

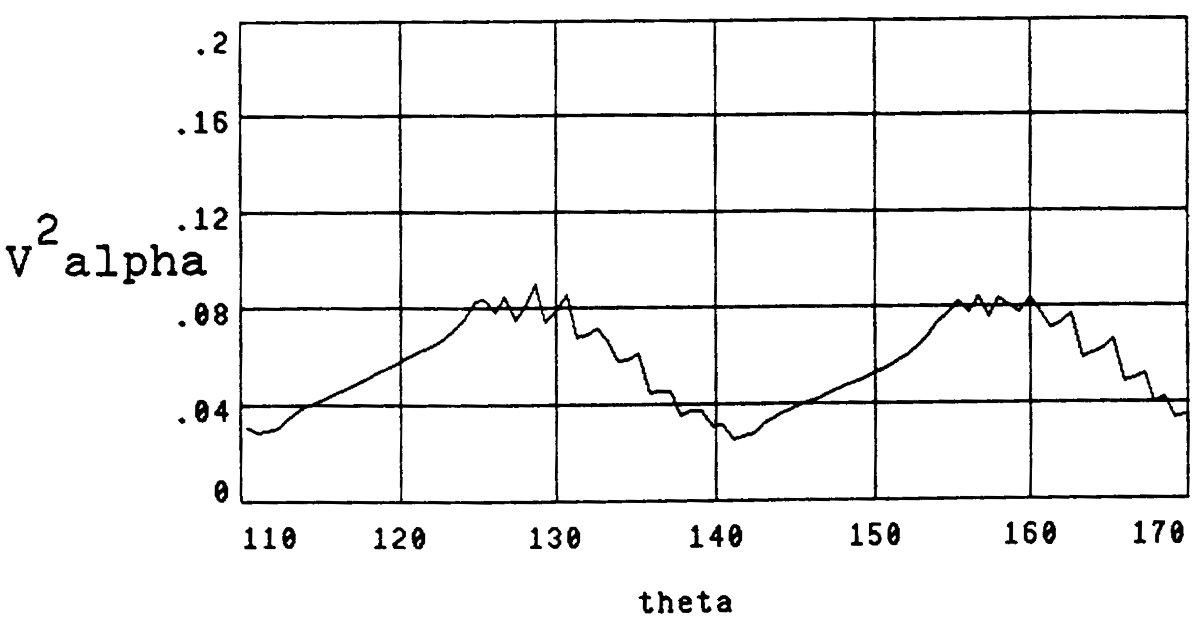

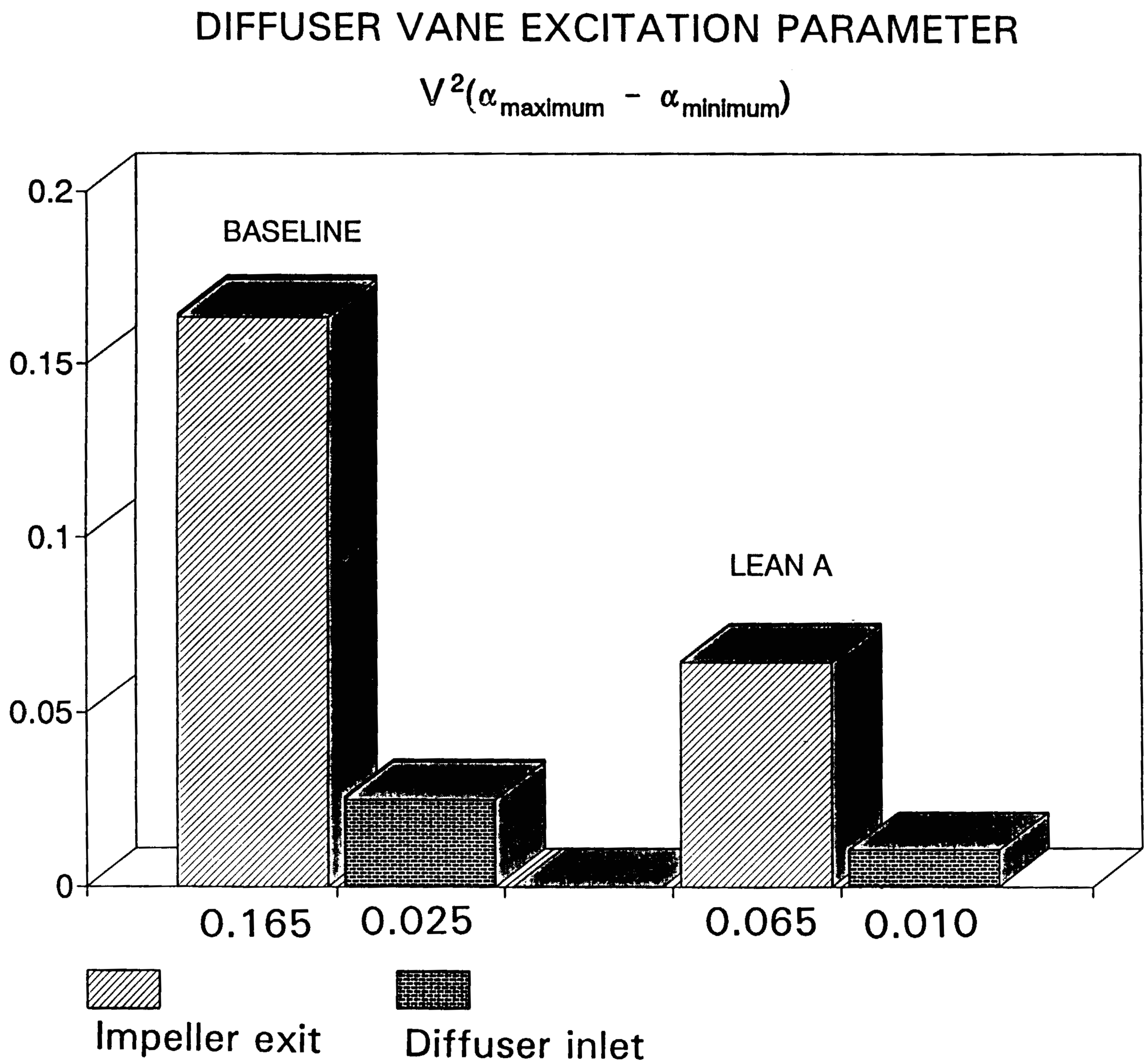
DIFFUSER VANE EXCITATION PARAMETER
$V^2(\alpha_{maximum} - \alpha_{minimum})$
0.2
0.15
0.1
0.05
0
BASELINE
LEAN A
0.165
0.025
0.065
0.010
Impeller exit
Diffuser inlet

Circumferential Averages

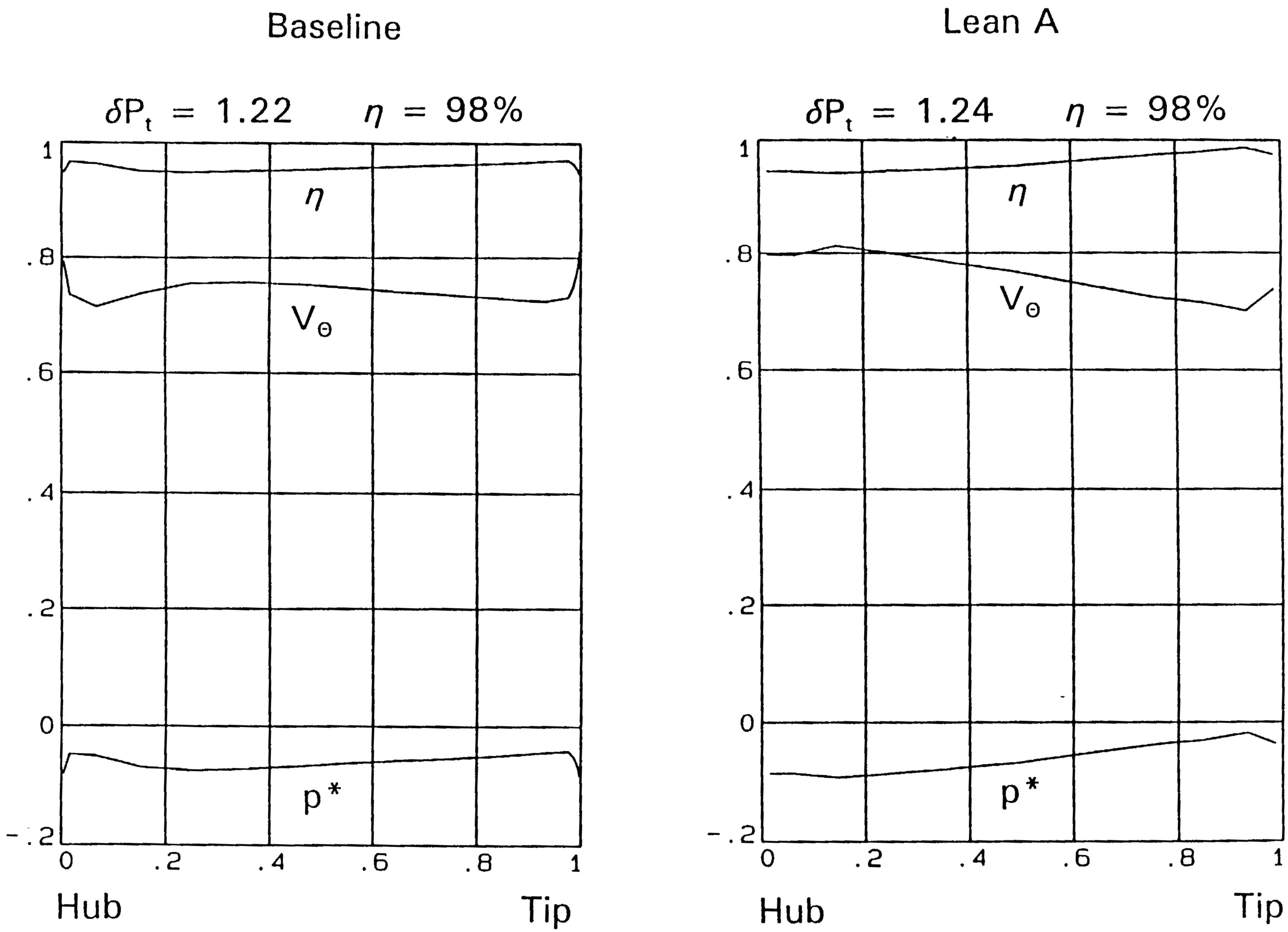

CONCLUSIONS

Consortium Pump Impeller

Redesigned using Blade Lean

Improved tangential uniformity of exit flow distribution

Reduced diffuser vane excitation forces

N95- 23626

34

11345

P. 33

CFD PARAMETRIC STUDY OF CONSORTIUM IMPELLER

Gary C. Cheng*, Y.S. Chen†, R. Garcia‡, and R.W. Williams§

Abstract

Current design of high performance turbopumps for rocket engines requires effective and robust analytical tools to provide design impact in a productive manner. The main goal of this study is to develop a robust and effective computational fluid dynamics (CFD) pump model for general turbopump design and analysis applications. A Finite Difference Navier-Stokes flow solver, FDNS, which includes the extended k-ε turbulence model and appropriate moving interface boundary conditions, was developed to analyze turbulent flows in turbomachinery devices. A second-order central difference scheme plus adaptive dissipation terms was employed in the FDNS code, along with a predictor plus multi-corrector pressure-based solution procedure. The multi-zone, multi-block capability allows the FDNS code to efficiently solve flow fields with complicated geometry. The FDNS code has been benchmarked by analyzing the pump consortium inducer, and it provided satisfactory results. In the present study, a CFD parametric study of the pump consortium impeller was conducted using the FDNS code. The pump consortium impeller, with partial blades, is a new design concept of the advanced rocket engines. The parametric study was to analyze the baseline design of the consortium impeller and its modification which utilizes TANDEM blades. In the present study, the TANDEM blade configuration of the consortium impeller considers cut full blades for about one quarter chord length from the leading edge and clocks the leading edge portion with an angle of 7.5 or 22.5 degrees. The purpose of the present study is to investigate the effect and trend of the TANDEM blade modification and provide the result as a design guideline. A 3-D flow analysis, with a 103 x 23 x 30 mesh grid system and with the inlet flow conditions measured by Rocketdyne, was performed for the baseline consortium impeller. The numerical result shows that the mass flow rate splits through various blade passages are relatively uniform. Due to the complexity of blade geometries, the TANDEM blade configurations were analyzed with the multi-zone grid structure. Both the 7.5°- and the 22.5°-clocking TANDEM blade cases utilized a 80K mesh system. The numerical result of two TANDEM blade modifications indicates the efficiency and the head are worse than those of the baseline case due to larger flow distortion. The gap between the TANDEM blade and the full blade allows the flow passes through and heavily loads the pressure side of the partial blade such that flow reversal occurs near the suction side of the splitter. The flow split at the exit of impeller blades is very non-uniform for TANDEM blade cases, and this will greatly induce the side load on the diffuser. Therefore, the TANDEM blade modification in the present CFD analysis does not improve the performance of the consortium impeller.

* SECA, Inc., 3313 Bob Wallace Ave., Suite 202, Huntsville, AL

† Engineering Sciences, Inc., 4920 Corporate Dr., Suite K, Huntsville, AL

‡ ED 32, NASA/Marshall Space Flight Center, Huntsville, AL

§ ED 32, NASA/Marshall Space Flight Center, Huntsville, AL

CFD PARAMETRIC STUDY OF CONSORTIUM IMPELLER

-- 100% DESIGN FLOW CASE --

Gary C. Cheng, SECA, Inc.

Y.S. Chen, ESI

R. Garcia and R.W. Williams
NASA Marshall Space Flight Center

NASA Contract No. NAS8-38868

ELEVENTH WORKSHOP FOR CFD APPLICATIONS IN ROCKET PROPULSION
NASA/MSFC, APRIL 20-22, 1993

OBJECTIVE

- DEVELOP A ROBUST AND EFFECTIVE CFD PUMP MODEL FOR THE DESIGN AND ANALYSIS OF TURBOPUMP COMPONENTS
- BENCHMARK THE PUMP MODEL AND COMPUTE THE CONSORTIUM IMPELLER WITH THE BASELINE GEOMETRY AT 100% DESIGN FLOW RATE
- STUDY THE EFFECT OF TANDEM BLADE MODIFICATIONS ON THE CONSORTIUM IMPELLER PERFORMANCE

TEST CONFIGURATION SETUP

- **BASELINE IMPELLER**
  - ONE ZONE, 103 x 23 x 30 GRIDS
  - I: STREAMWISE DIRECTION
  - J: HUB-TO-TIP DIRECTION
  - K: BLADE-TO-BLADE DIRECTION (SUCTION TO PRESSURE)

- **TANDEM BLADE WITH 7.5° CLOCKING**
  - FOUR ZONES: Zone #1, 15 x 33 x 23; Zone #2, 51 x 7 x 23; Zone #3, 51 x 17 x 23; Zone #4, 51 x 11 x 23; Zone #5, 31 x 33 x 23
  - I: STREAMWISE DIRECTION

- J: BLADE-TO-BLADE DIRECTION (PRESSURE TO SUCTION)
- K: HUB-TO-TIP DIRECTION

- **TANDEM BLADE WITH 22.5° CLOCKING**
  - FOUR ZONES: Zone #1, 15 x 33 x 23; Zone #2, 51 x 13 x 23; Zone #3, 51 x 17 x 23; Zone #4, 51 x 5 x 23; Zone #5, 31 x 33 x 23
  - I: STREAMWISE DIRECTION
  - J: BLADE-TO-BLADE DIRECTION (PRESSURE TO SUCTION)
  - K: HUB-TO-TIP DIRECTION

NUMERICAL METHOD

- NAVIER-STOKES FLOW SOLVER: **FDNS** CODE
- PRESSURE BASED FINITE DIFFERENCE APPROACH
- PREDICTOR PLUS MULTI-CORRECTOR TIME MARCHING SCHEME
- MULTI-ZONE, BODY-FITTED COORDINATE SYSTEM
- SECOND-ORDER CENTRAL PLUS DISSIPATION SCHEME FOR CONVECTION TERMS
- MULTI-BLOCK, IMPLICIT POINT-BY-POINT SOLVER
- STANDARD AND EXTENDED K-ε TURBULENCE MODELS

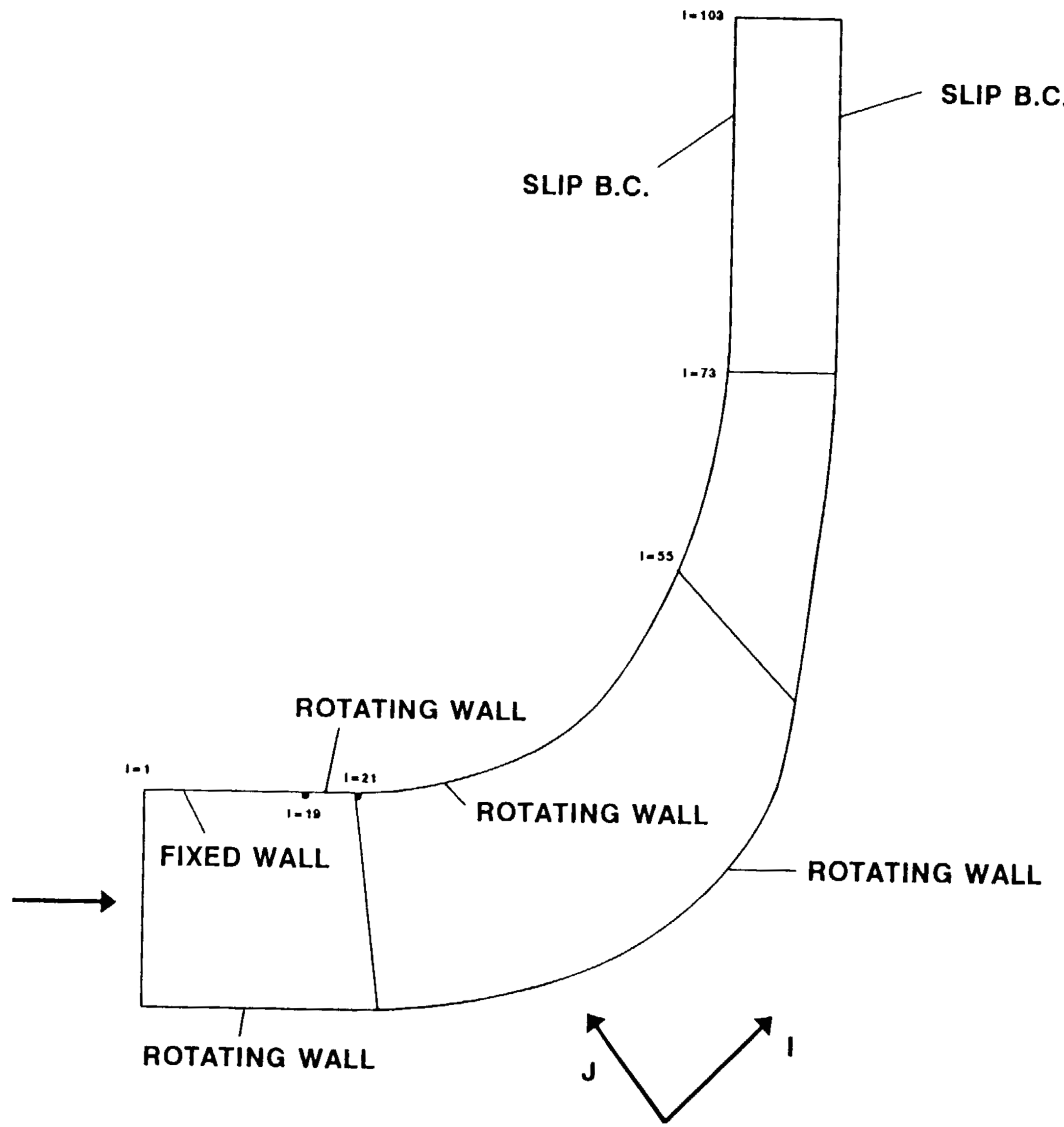

The Mesh System Layout for the Consortium Impeller (Hub-to-Tip)

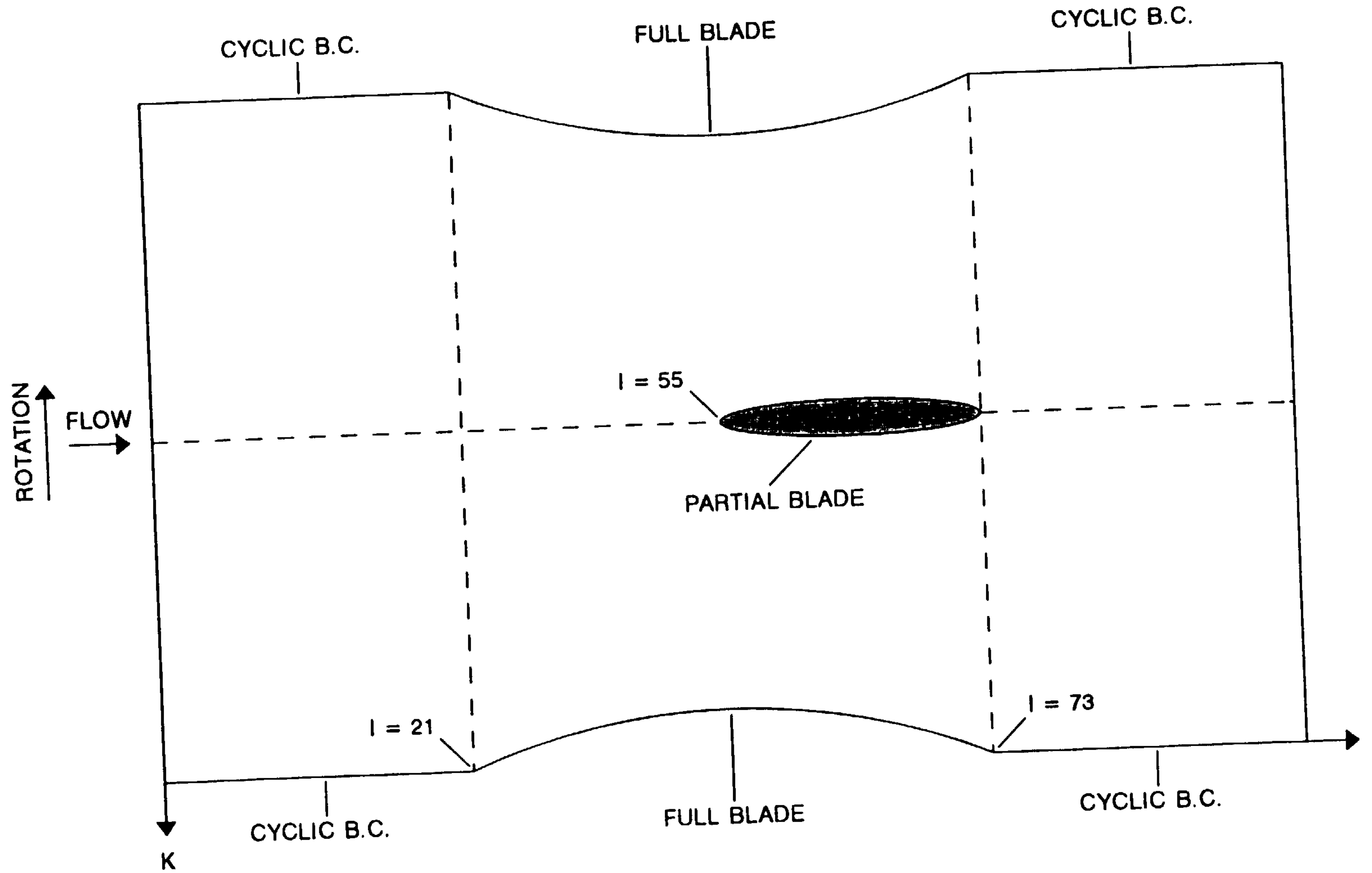

The Mesh System Layout for the Baseline Consortium Impeller

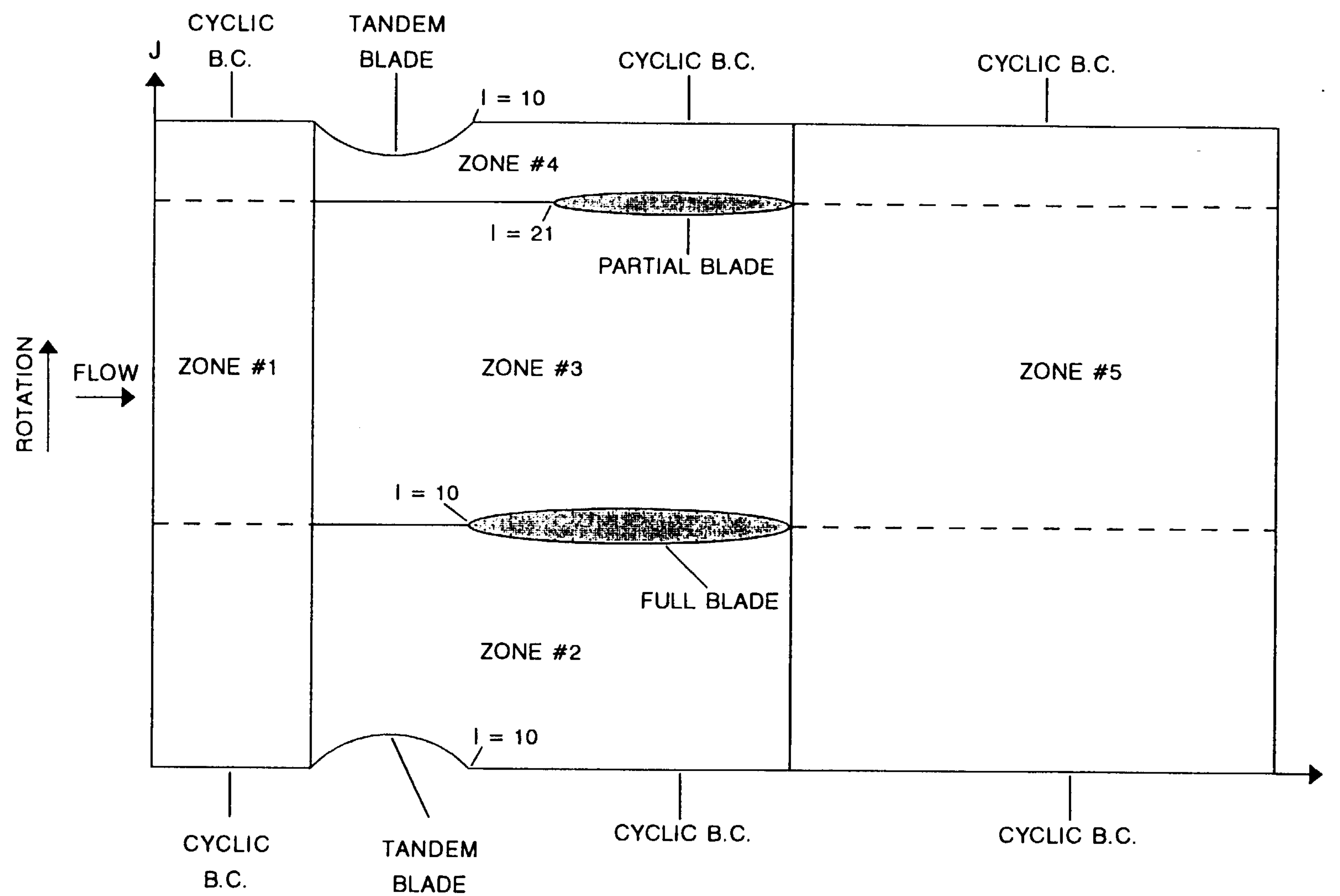

The Mesh System Layout for 22.5° Clocking TANDEM Blade Impeller

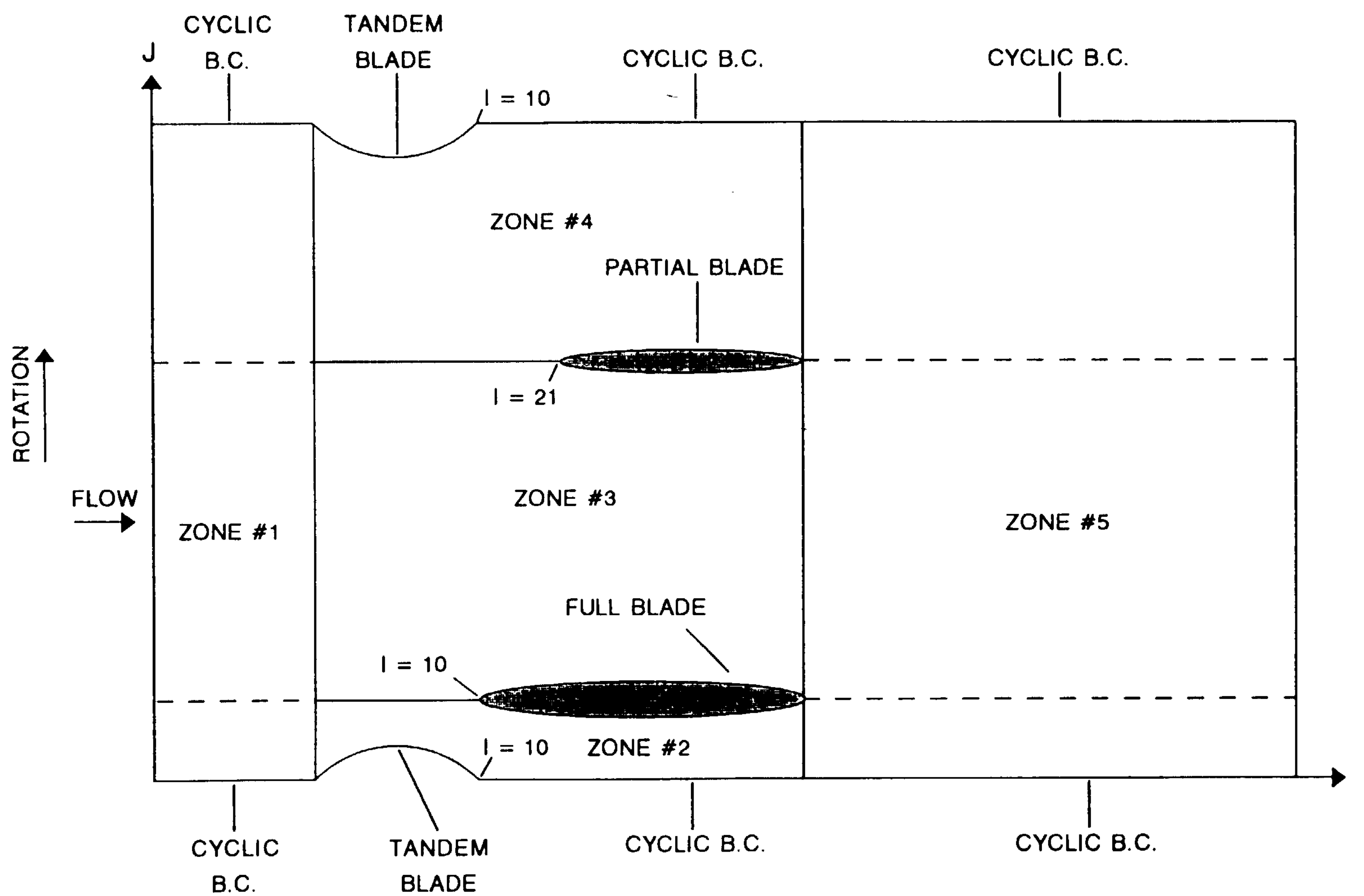

The Mesh System Layout for 7.5° Clocking TANDEM Blade Impeller

- **TEST CONDITIONS**

Full Blades/Partial Blades	6/6
Working Medium	Water (70 °F)
Shaft Speed	6322 rpm
Exit Tip Diameter	9.045 inches
Inlet Hub Diameter	3.9 inches
Inlet Tip Diameter	6.0 inches
Reference Velocity	23.41 ft/sec
Reference Reynolds Number	1.59×10^7 ft^{-1}
Mass Flow Rate	160.8 lb/sec

- MEASURED AXIAL AND TANGENTIAL VELOCITY PROFILES DOWNSTREAM OF THE INDUCER EXIT ARE USED AS INLET CONDITIONS TO THE IMPELLER

SECA, Inc.

BASELINE

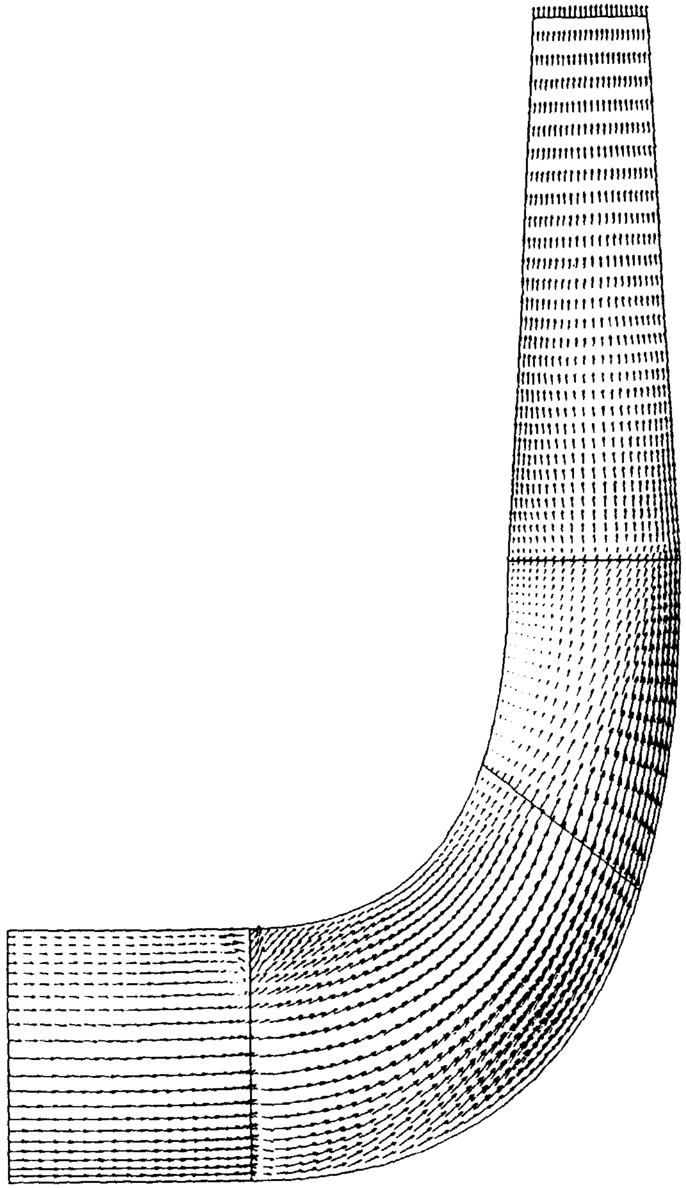

Suction Side of Full Blade

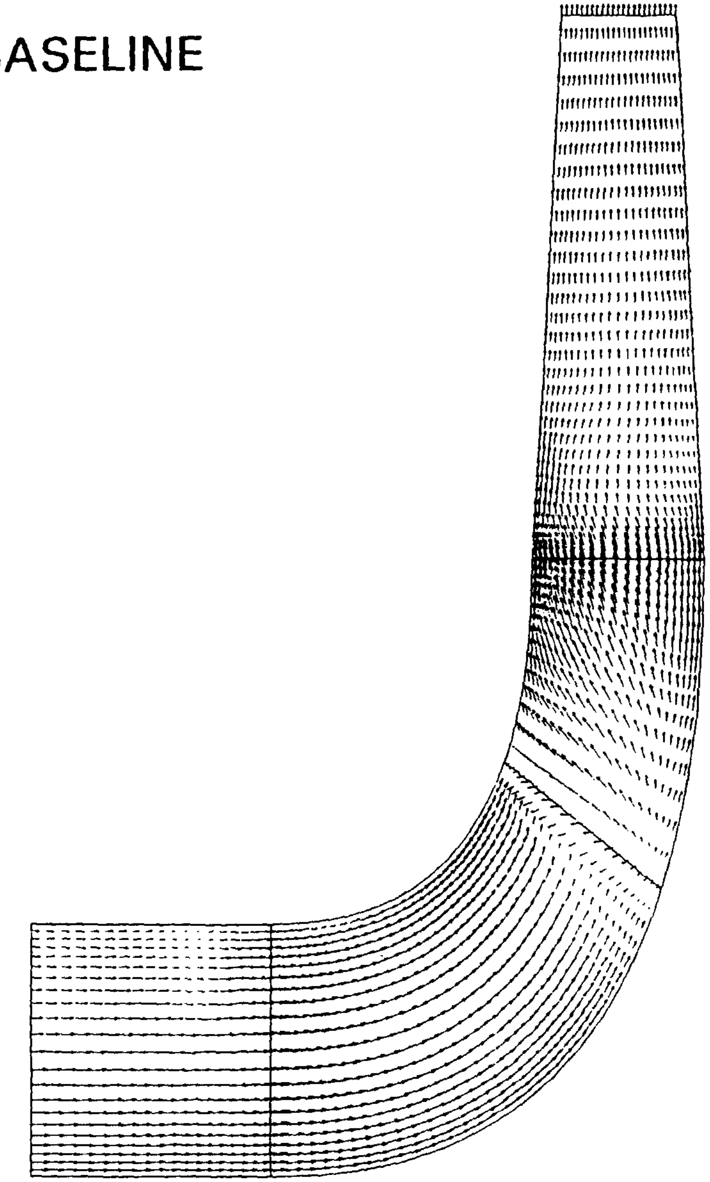

Pressure Side of Partial Blade

BASELINE

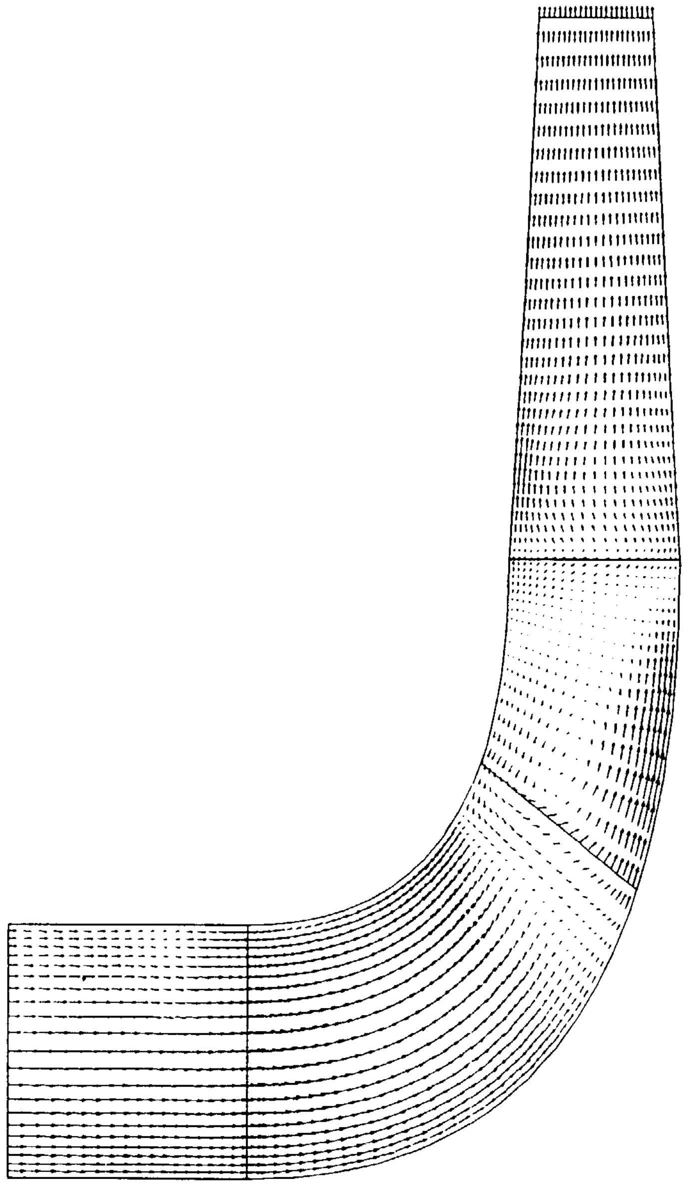

Suction Side of Partial Blade

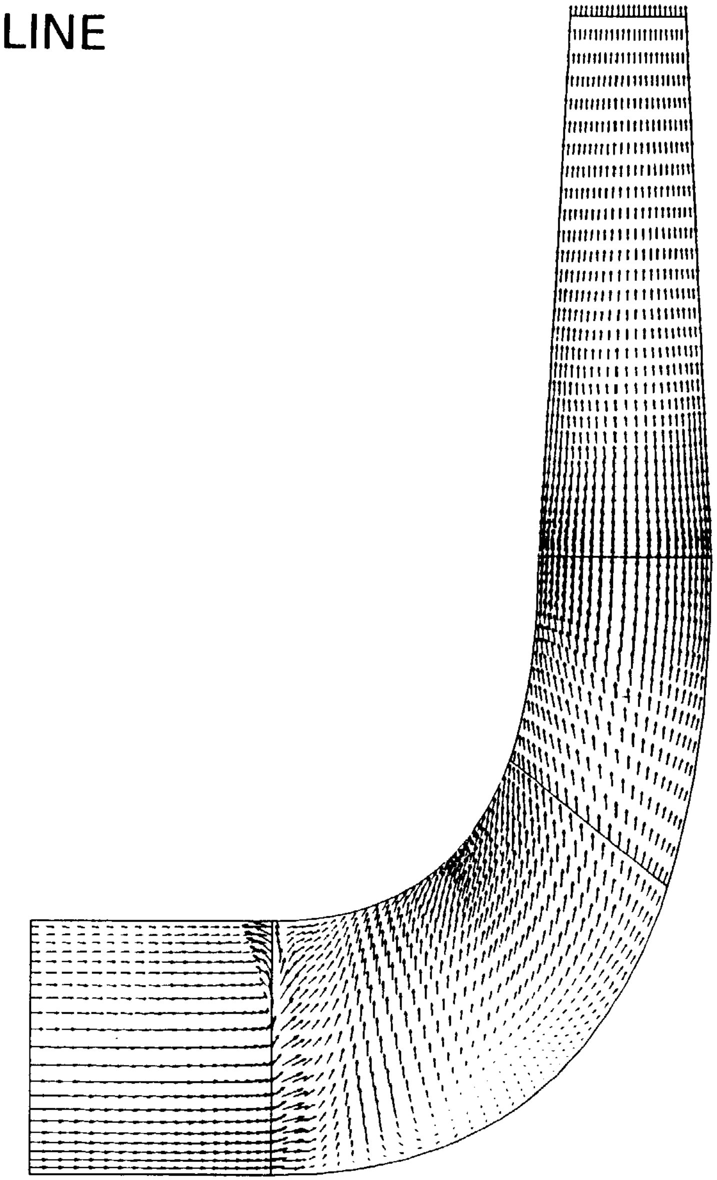

Pressure Side of Full Blade

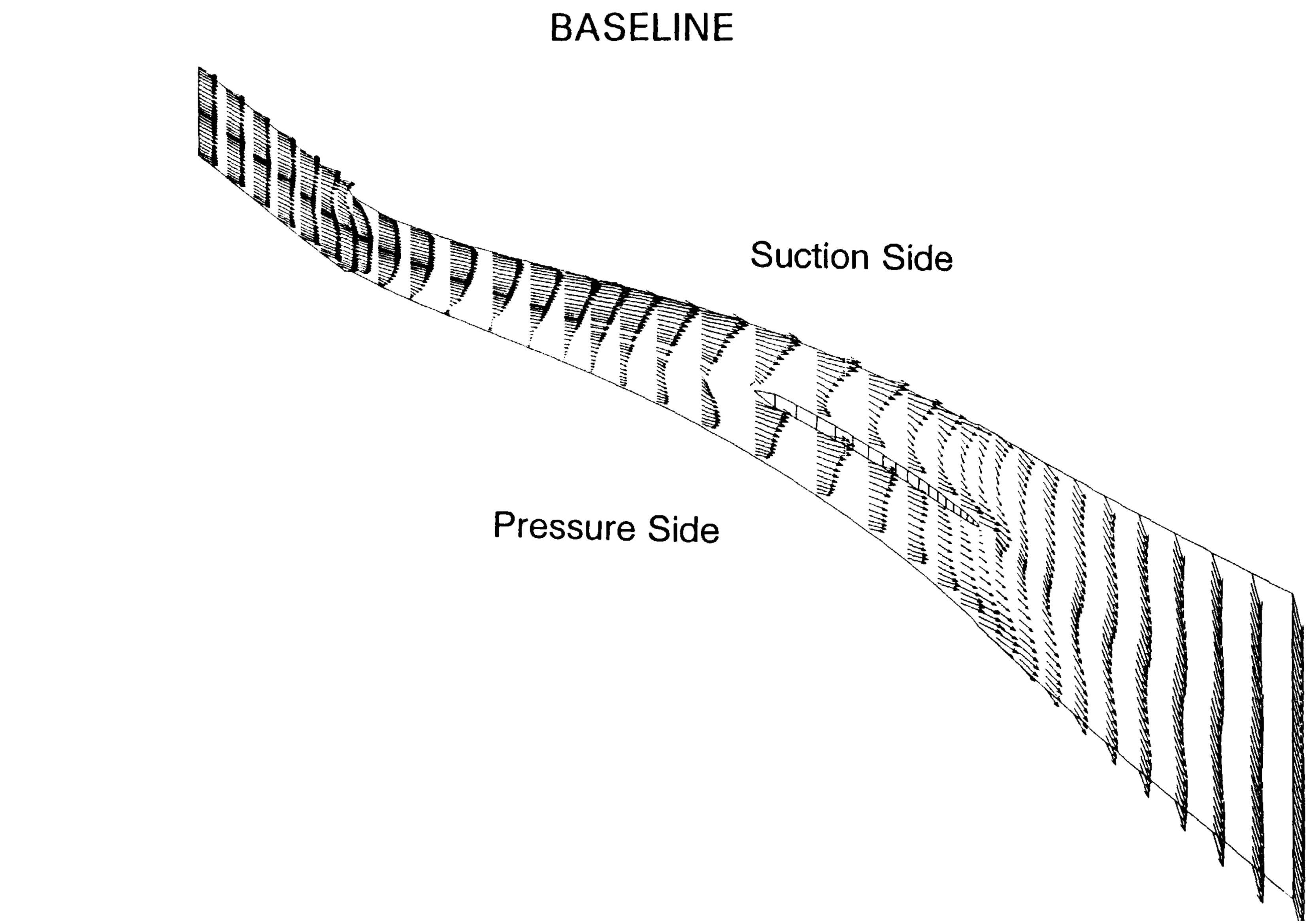

Velocity Vectors Near the Hub

BASELINE

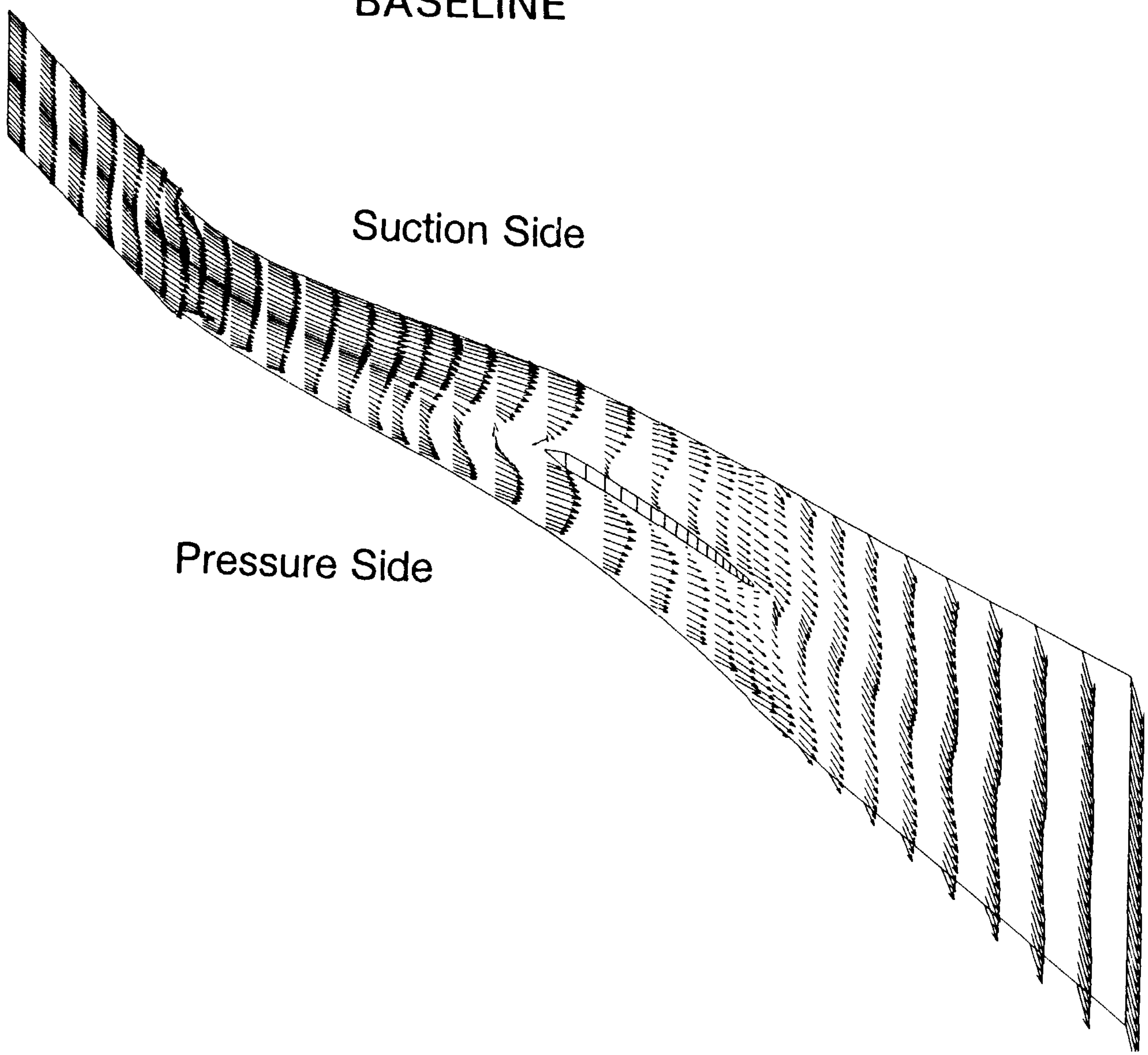

Velocity Vectors at the Mid Span

BASELINE

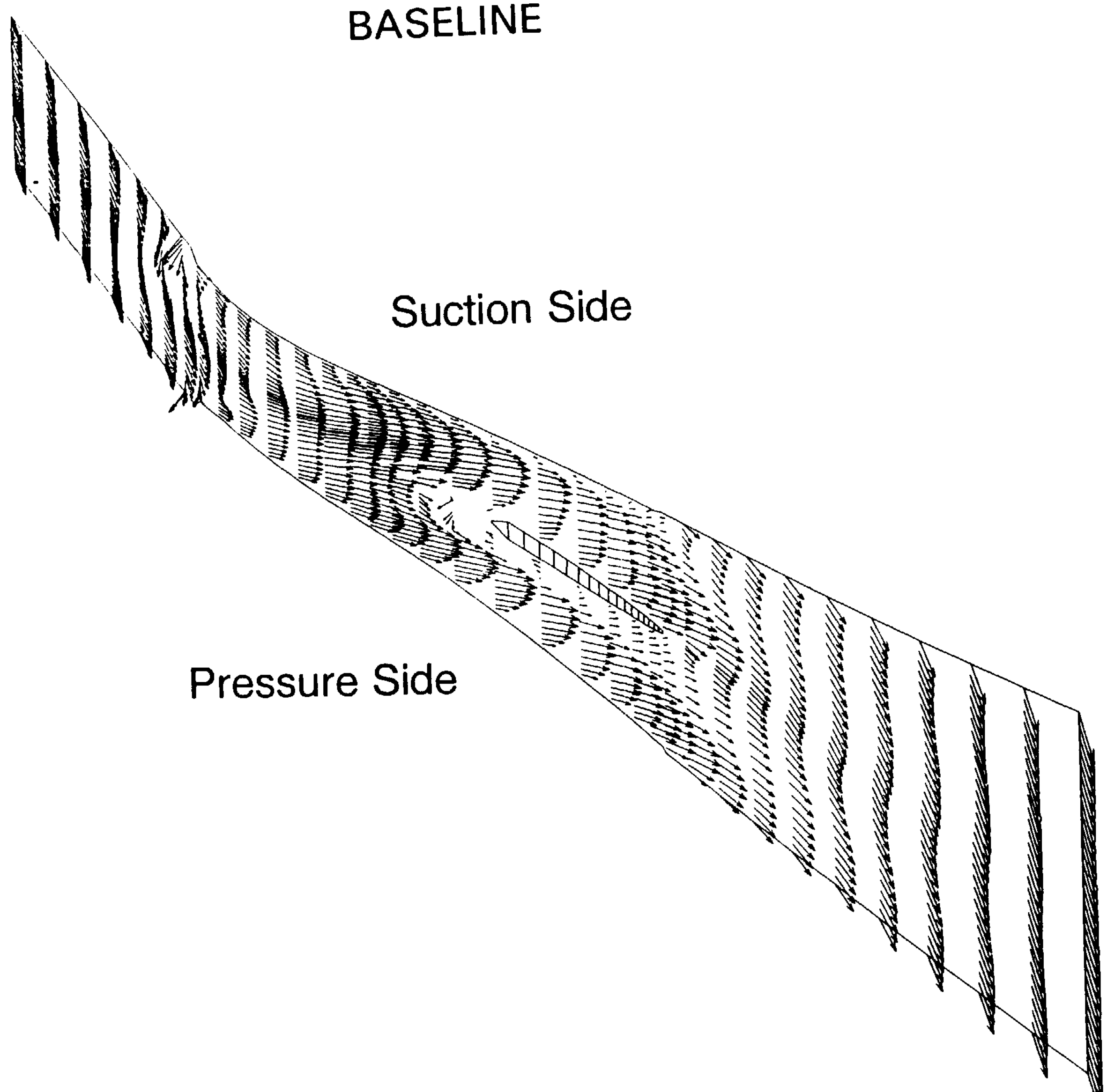

Velocity Vectors Near the Shroud

7.5° TANDEM
Blade

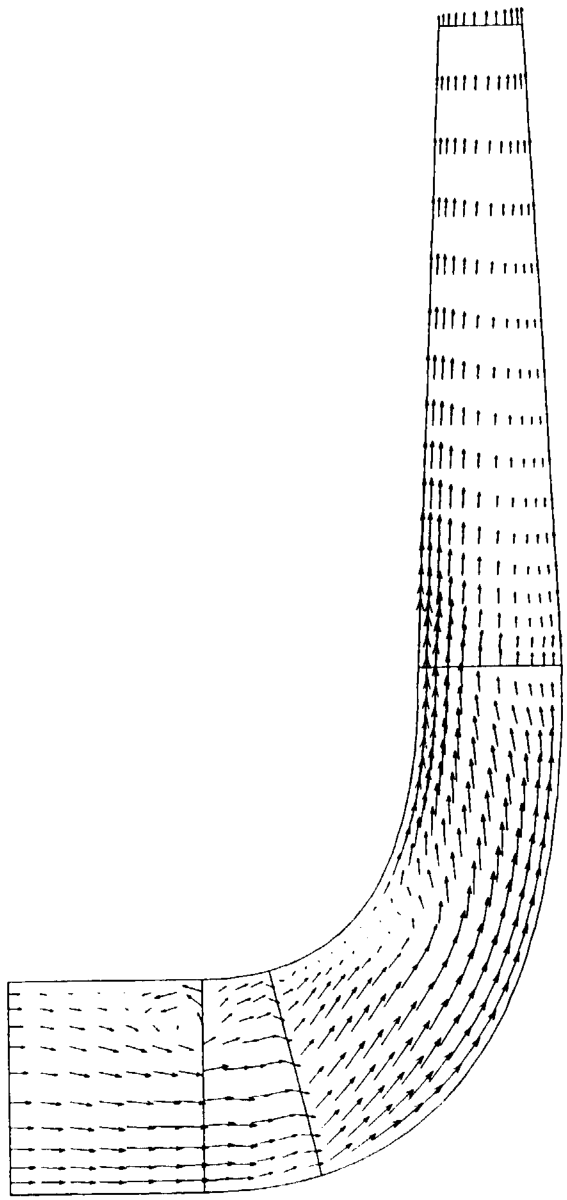

Pressure Side of Tandem Blade

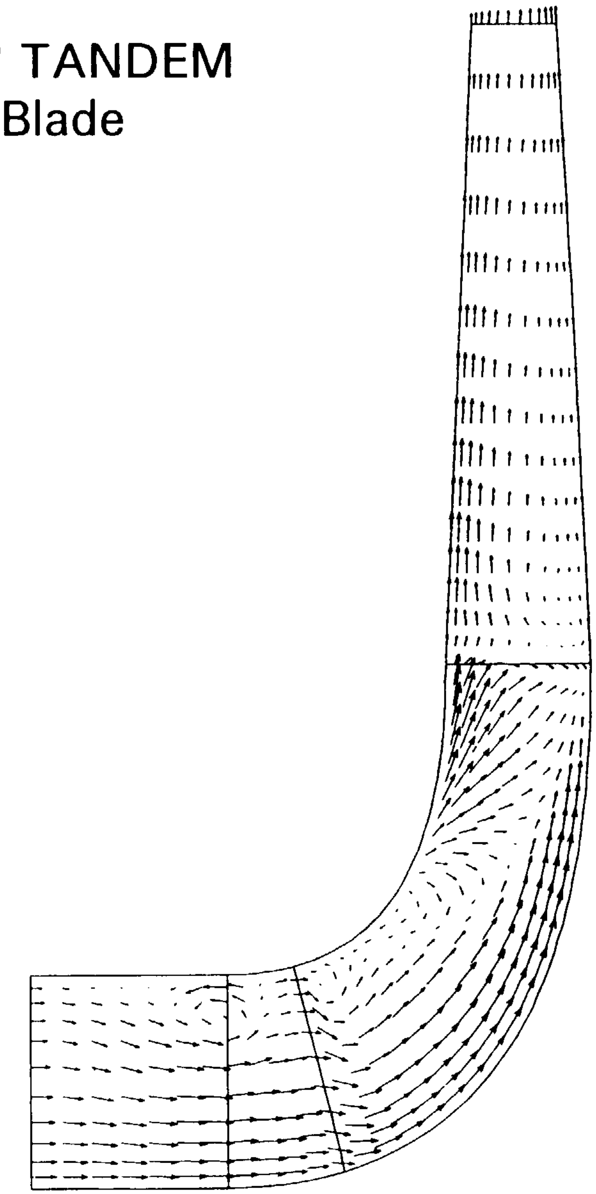

Suction Side of Full Blade

7.5° TANDEM
Blade

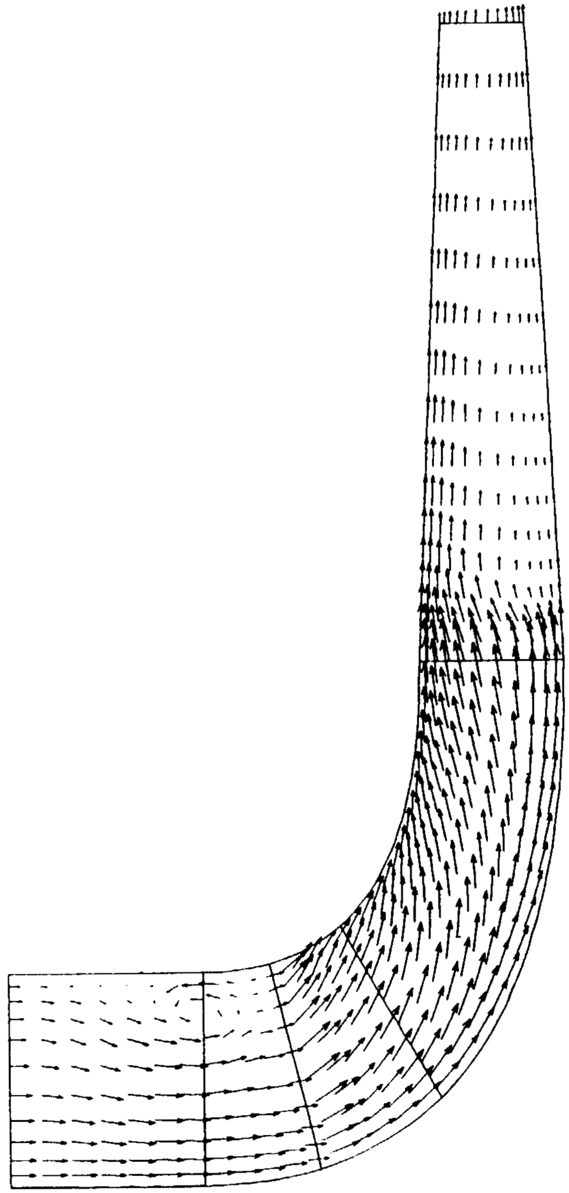
Pressure Side of Full Blade

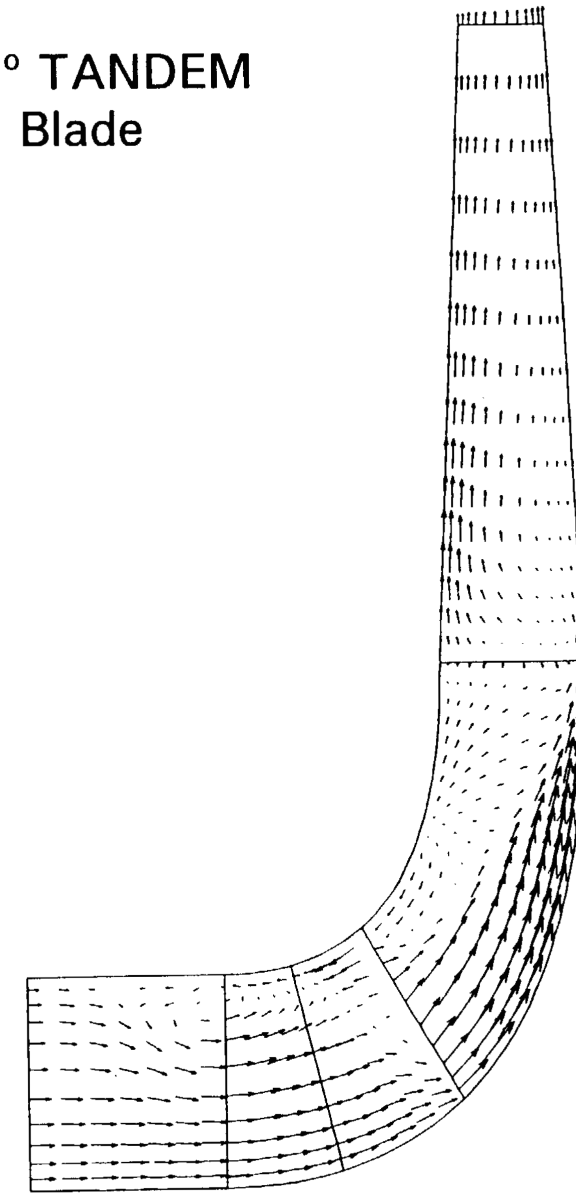
Suction Side of Partial Blade

7.5° TANDEM
Blade

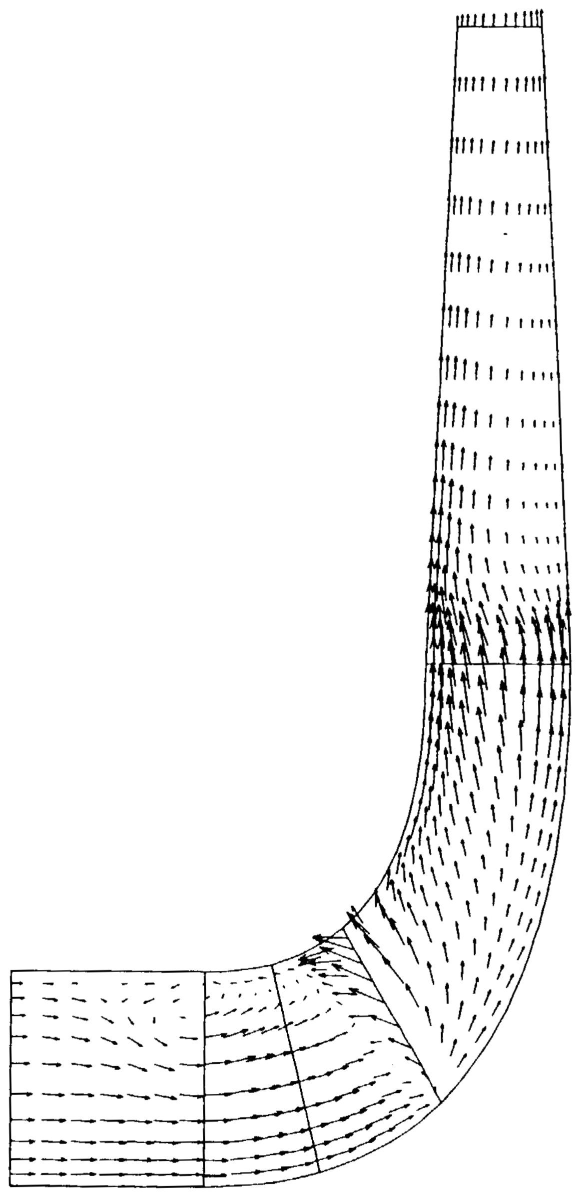

Pressure Side of Partial Blade

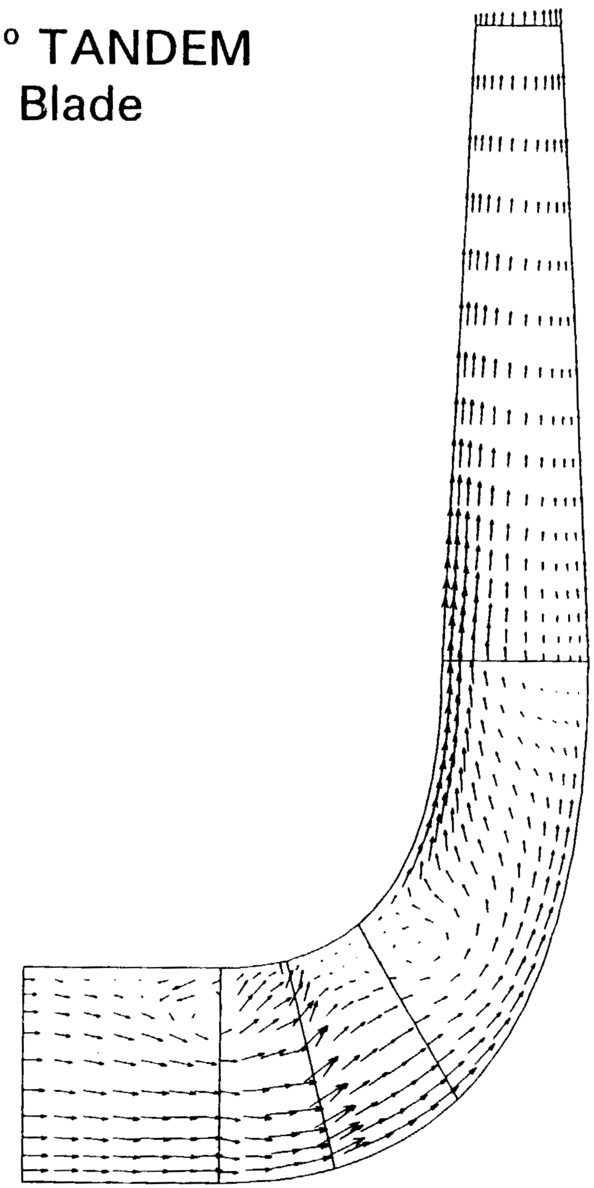

Suction Side of TANDEM Blade

7.5° TANDEM Blade

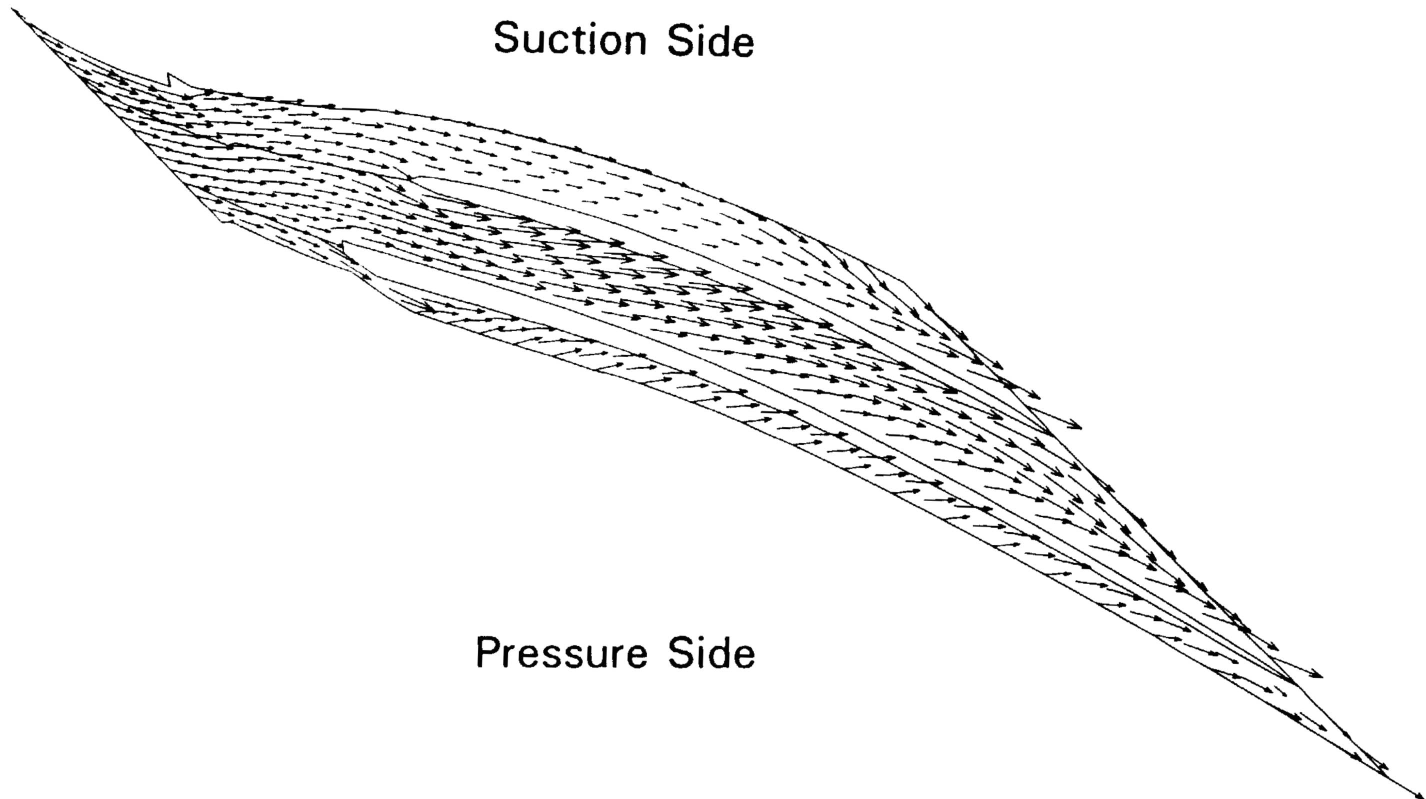

Velocity Vectors Near the Hub

7.5° TANDEM Blade

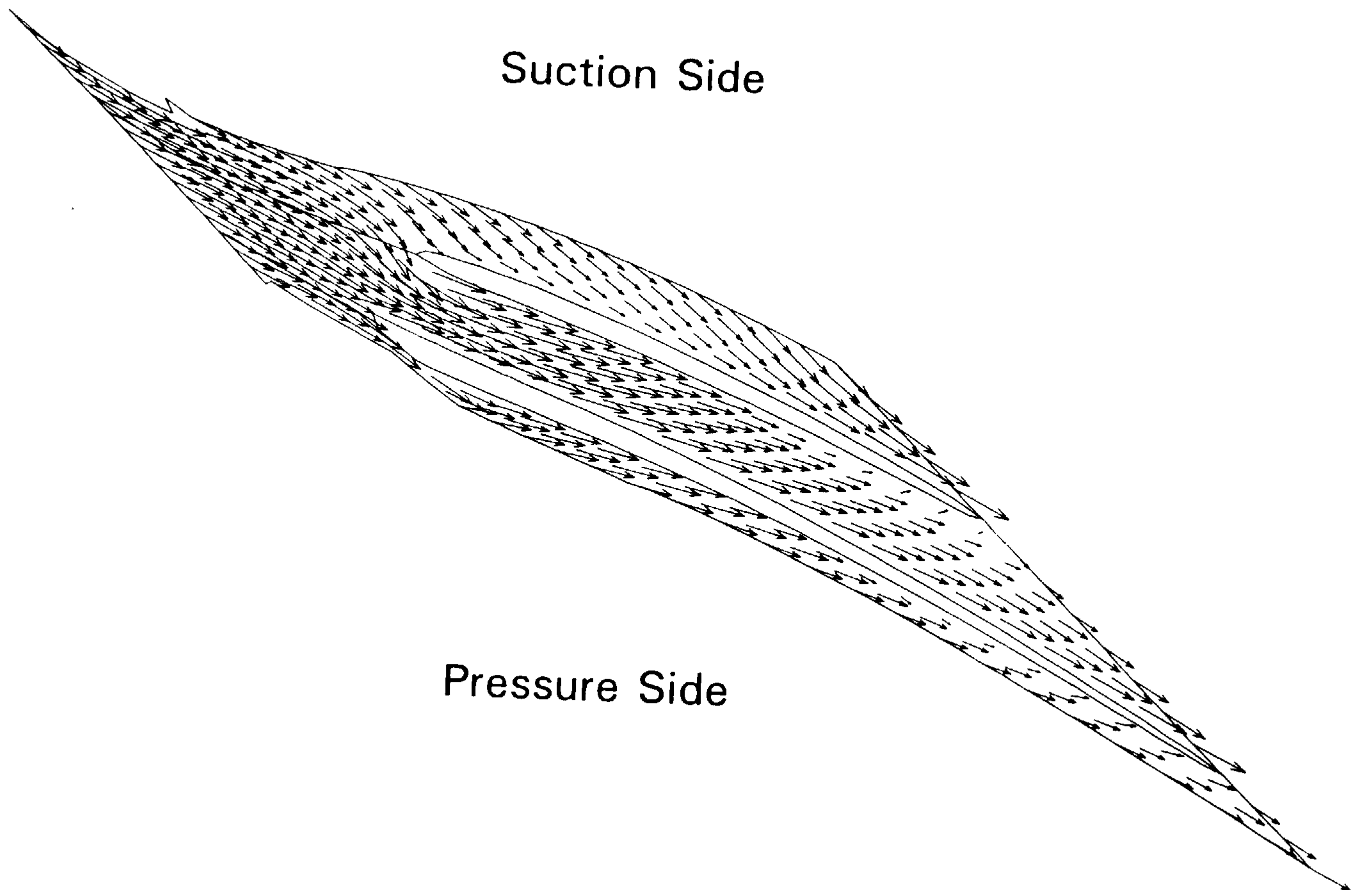

Velocity Vectors at the Mid Span

7.5° TANDEM Blade

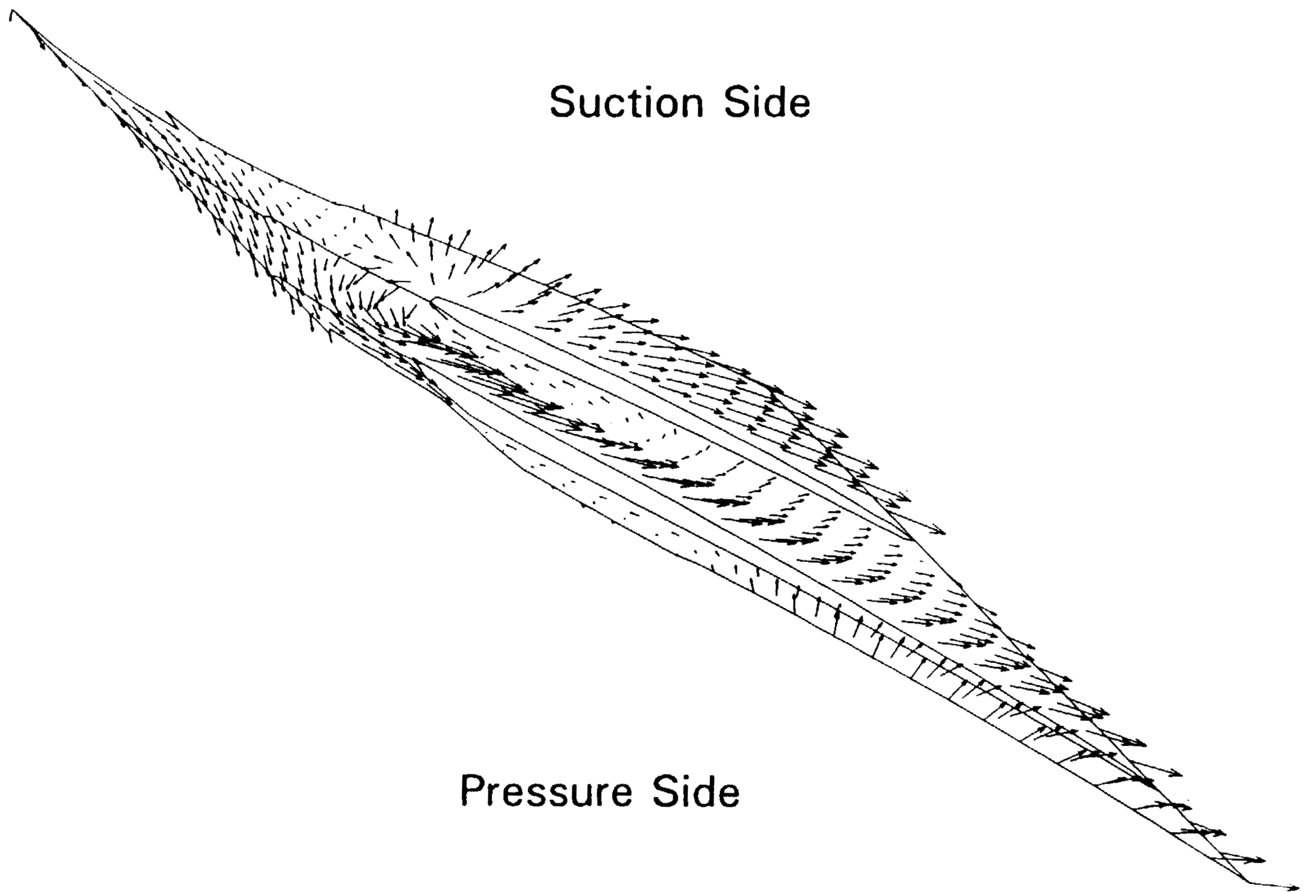

Velocity Vectors Near the Shroud

22.5° TANDEM Blade

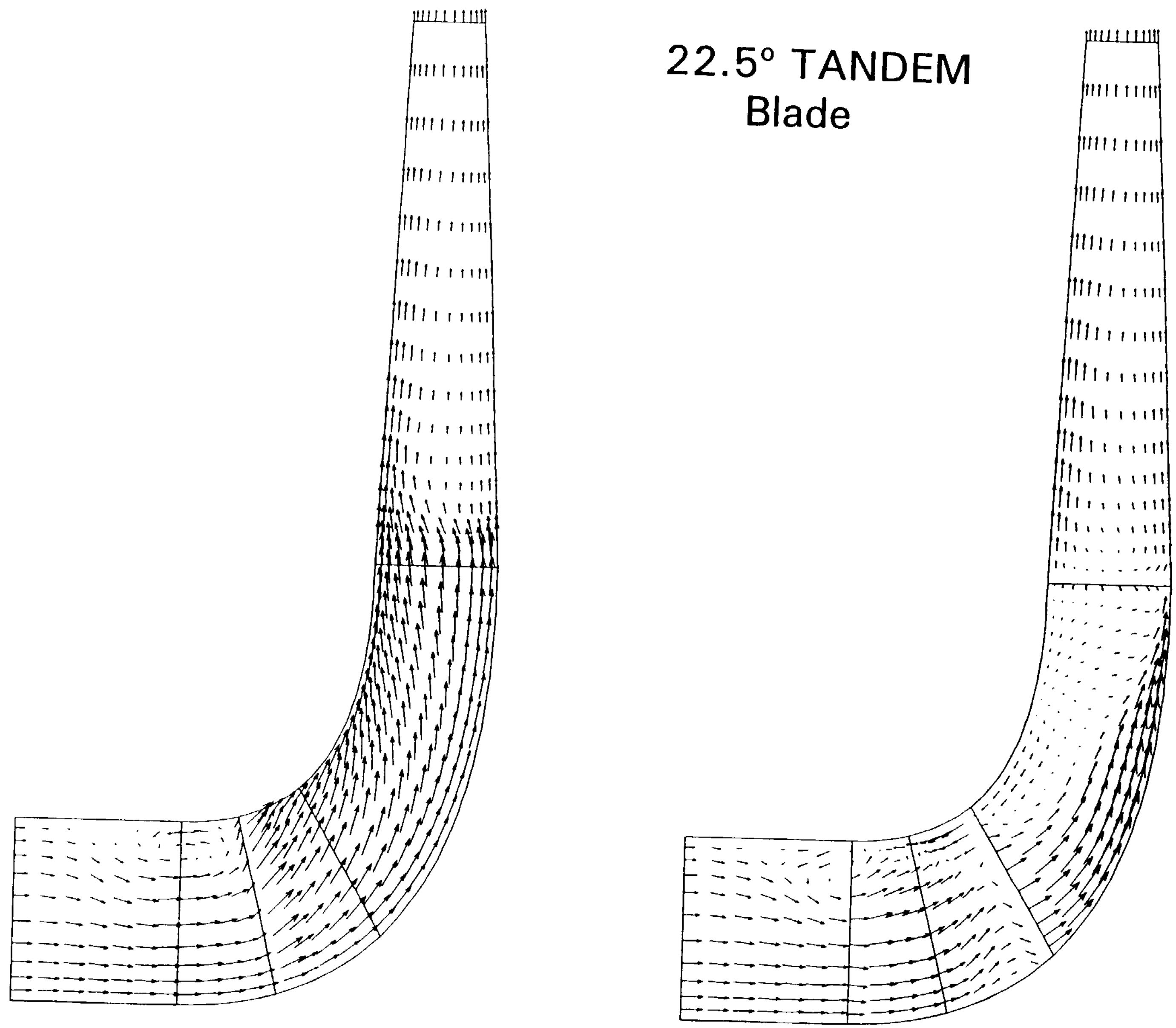

Pressure Side of Full Blade

Suction Side of Partial Blade

22.5° TANDEM
Blade

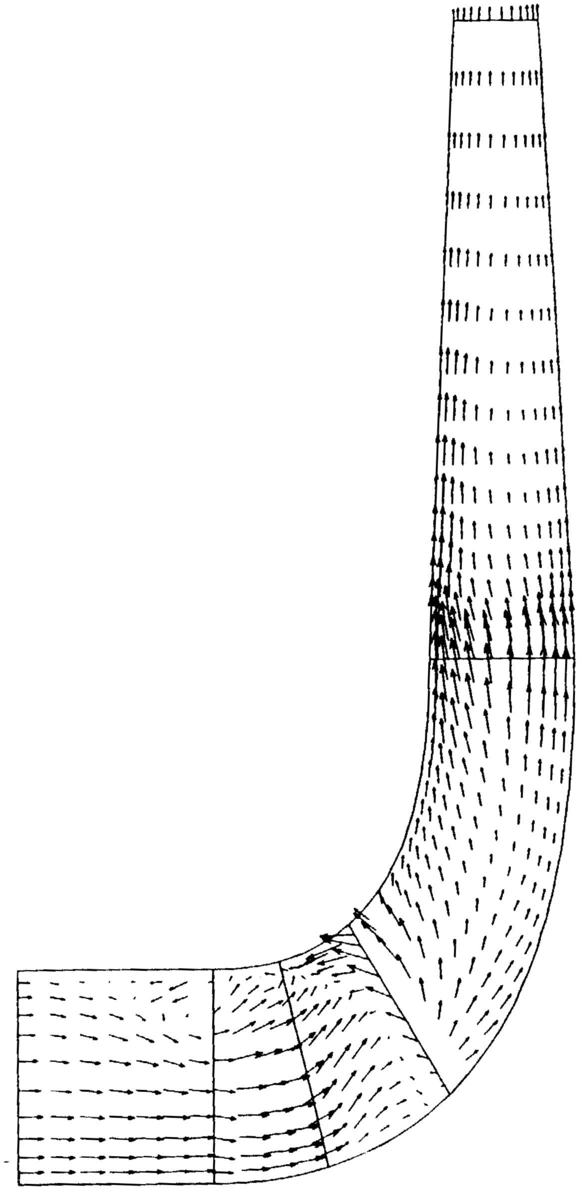

Pressure Side of Partial Blade

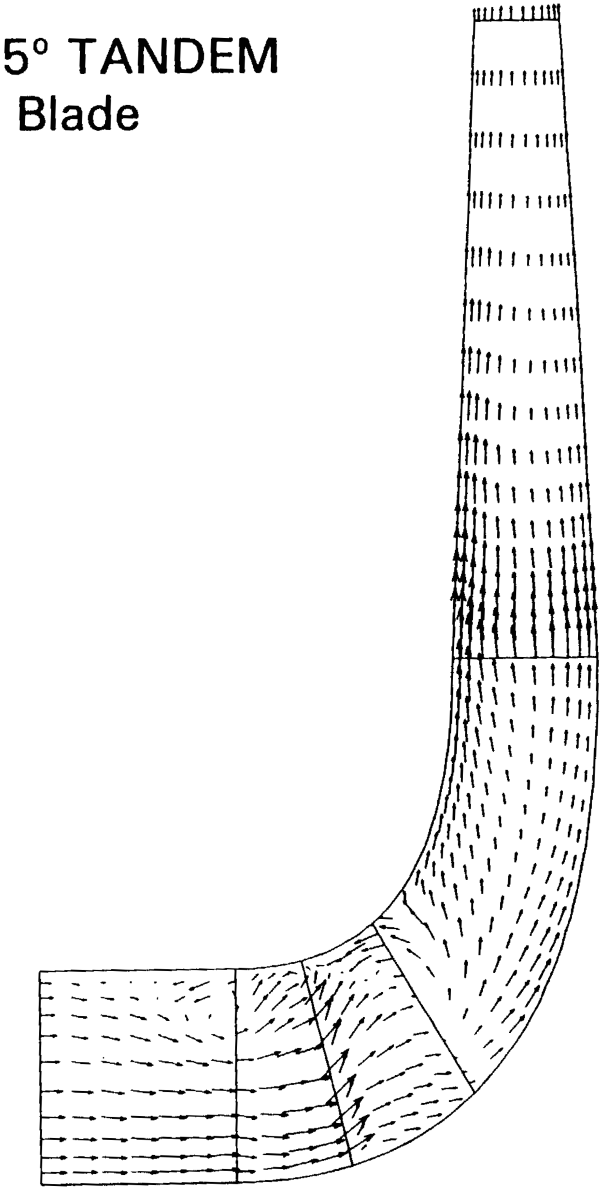

Suction Side of TANDEM Blade

22.5° TANDEM Blade

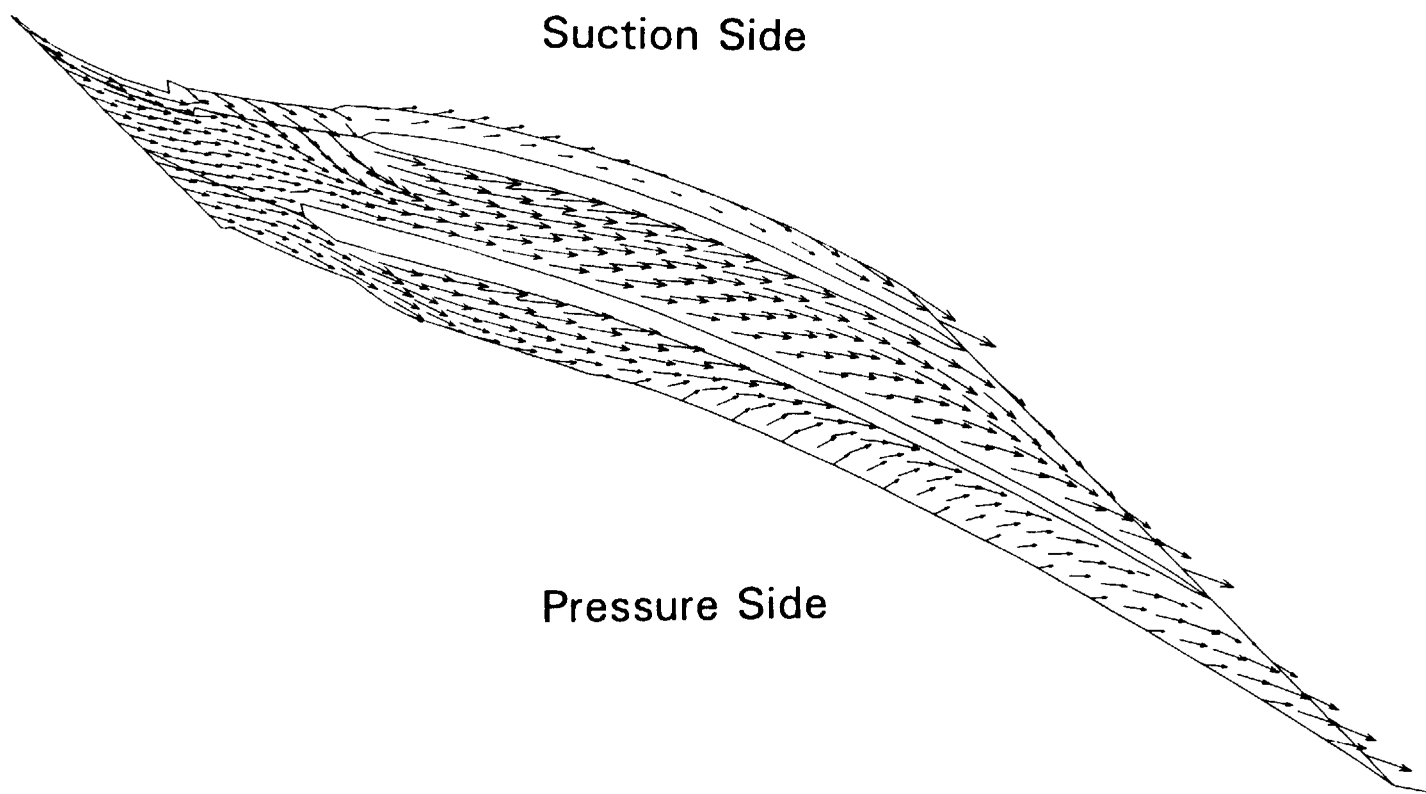

Velocity Vectors Near the Hub

22.5° TANDEM Blade

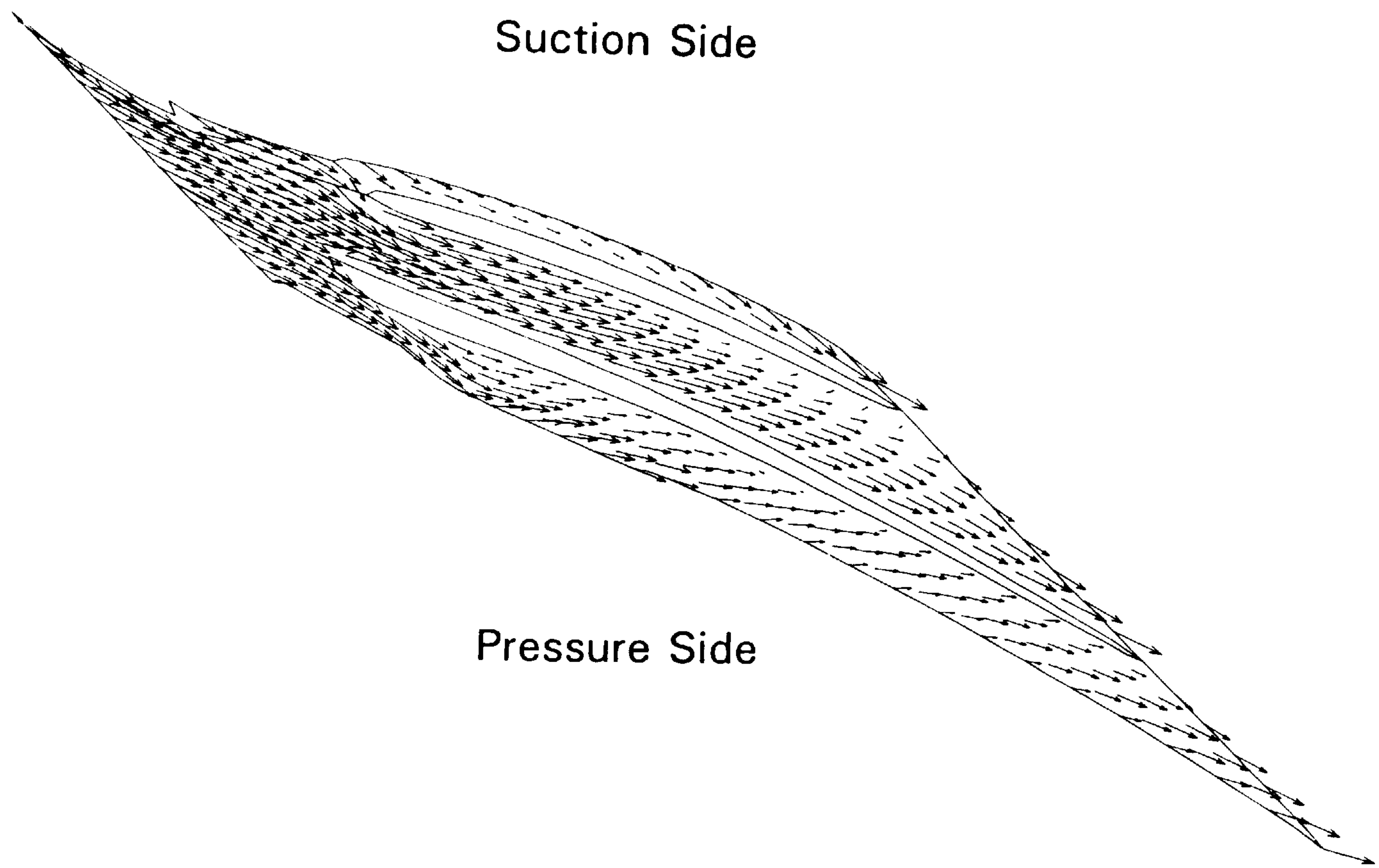

Velocity Vectors at the Mid Span

22.5° TANDEM Blade

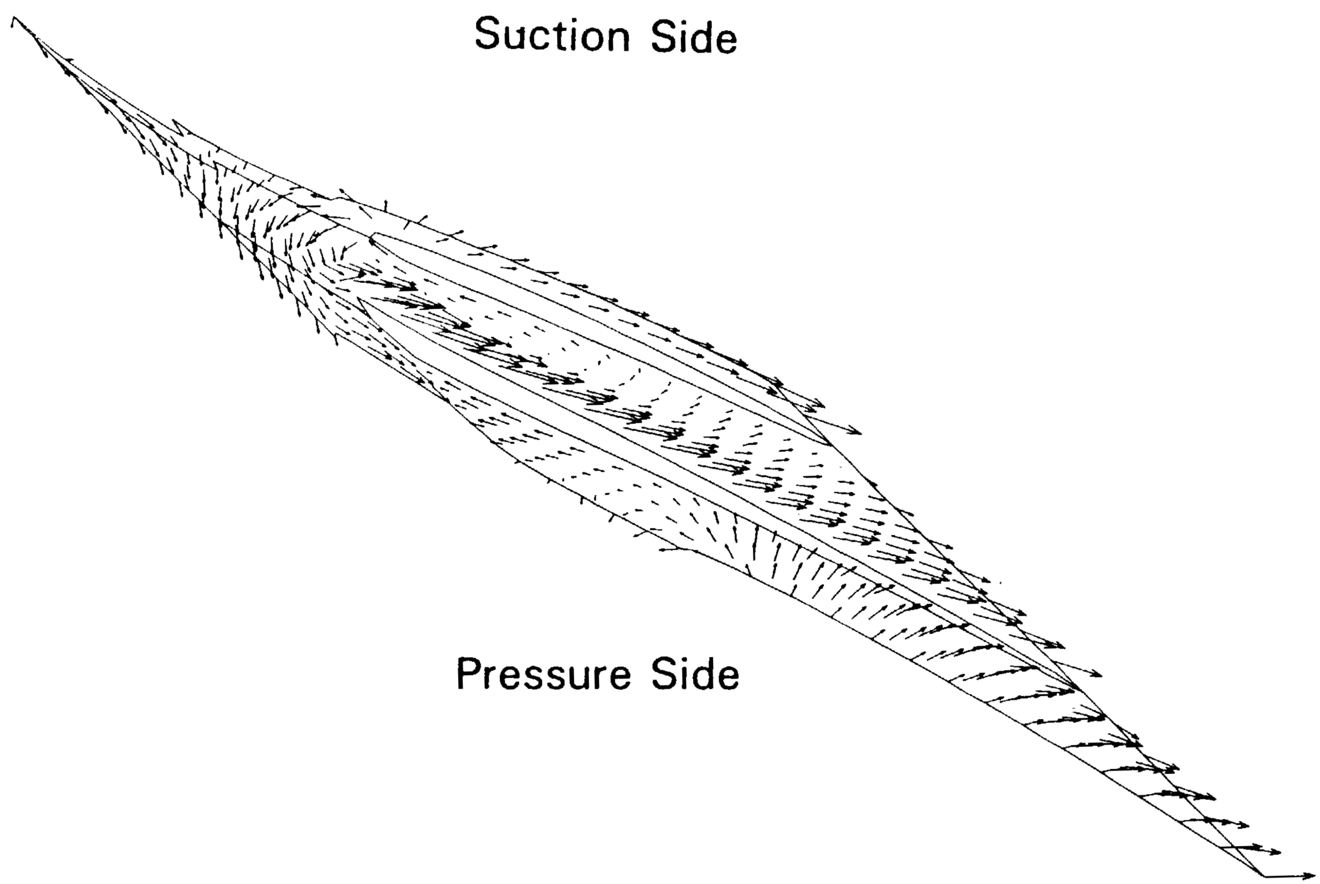

Velocity Vectors Near the Shroud

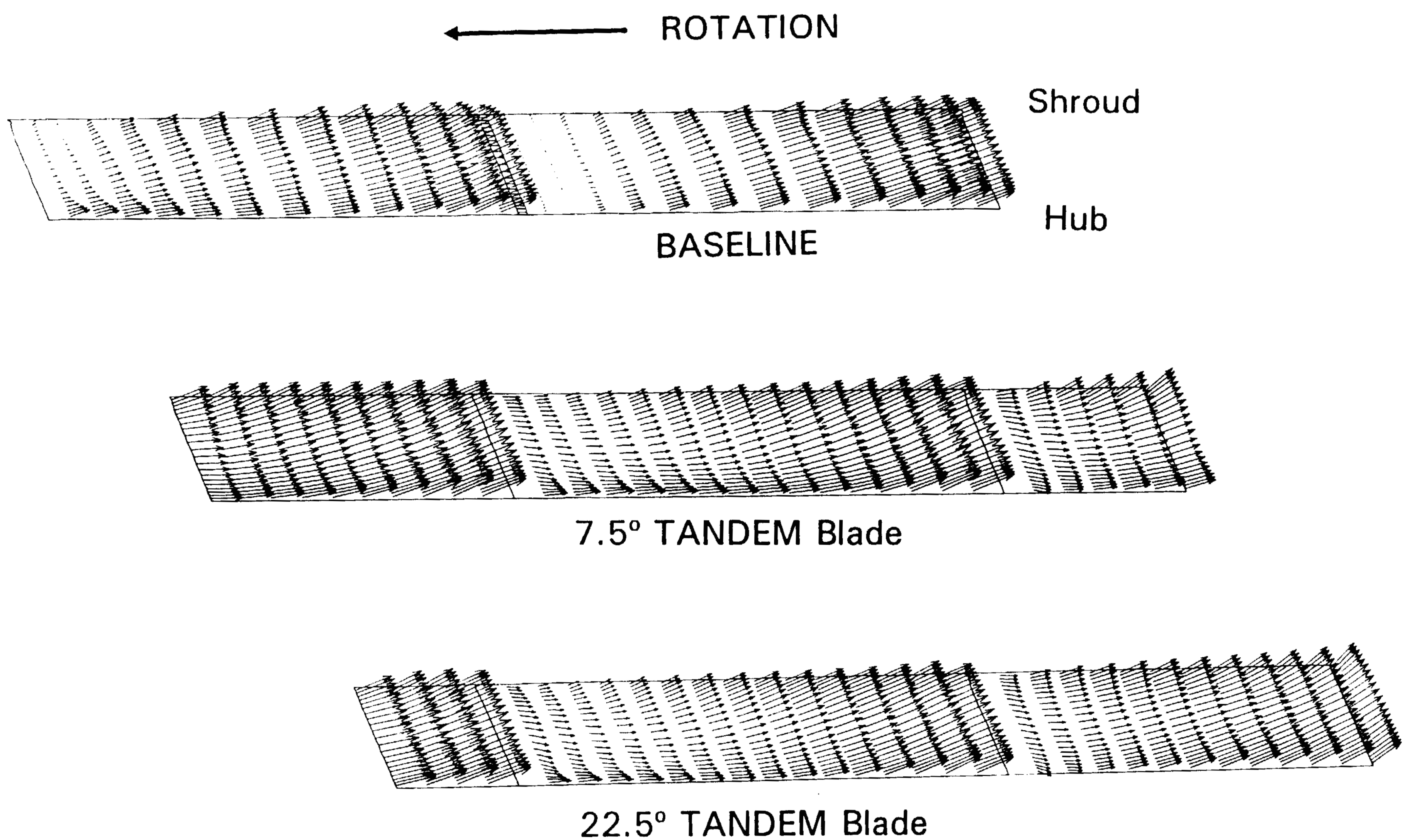

Velocity Vectors at the Exit of Impeller Blade

Advanced Impeller Parametrics: Tandem Blades

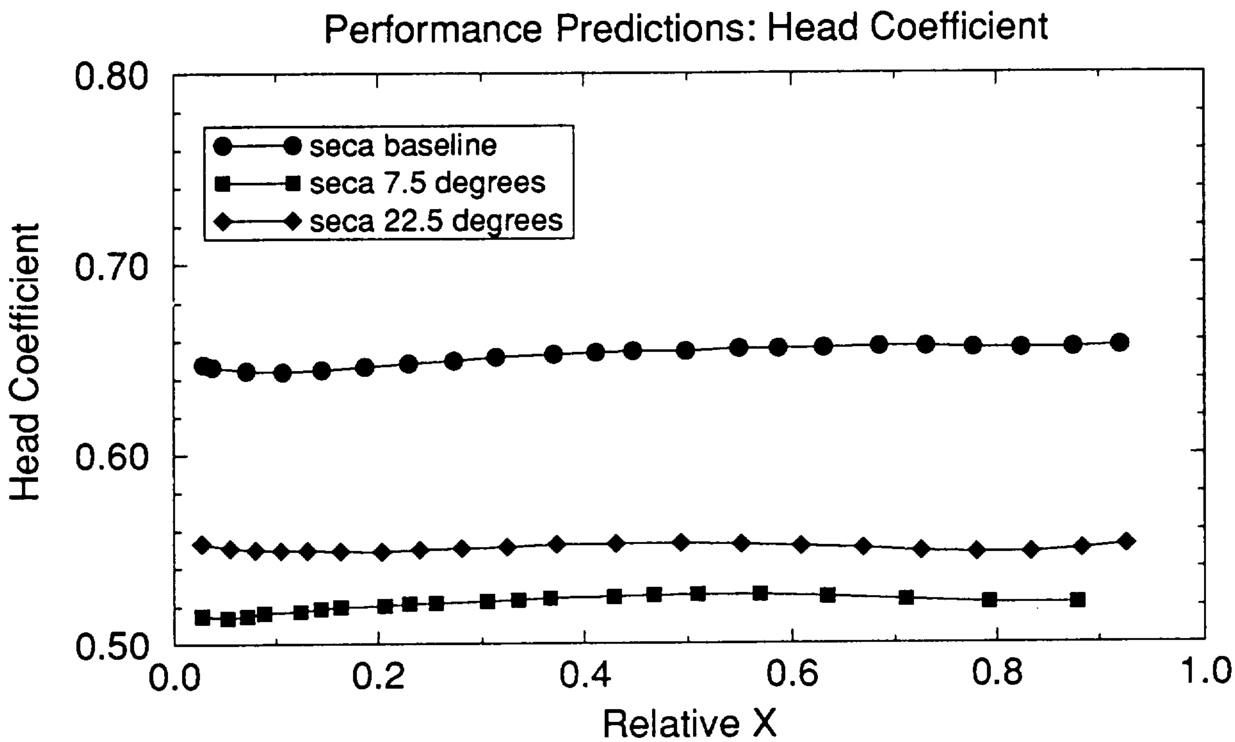

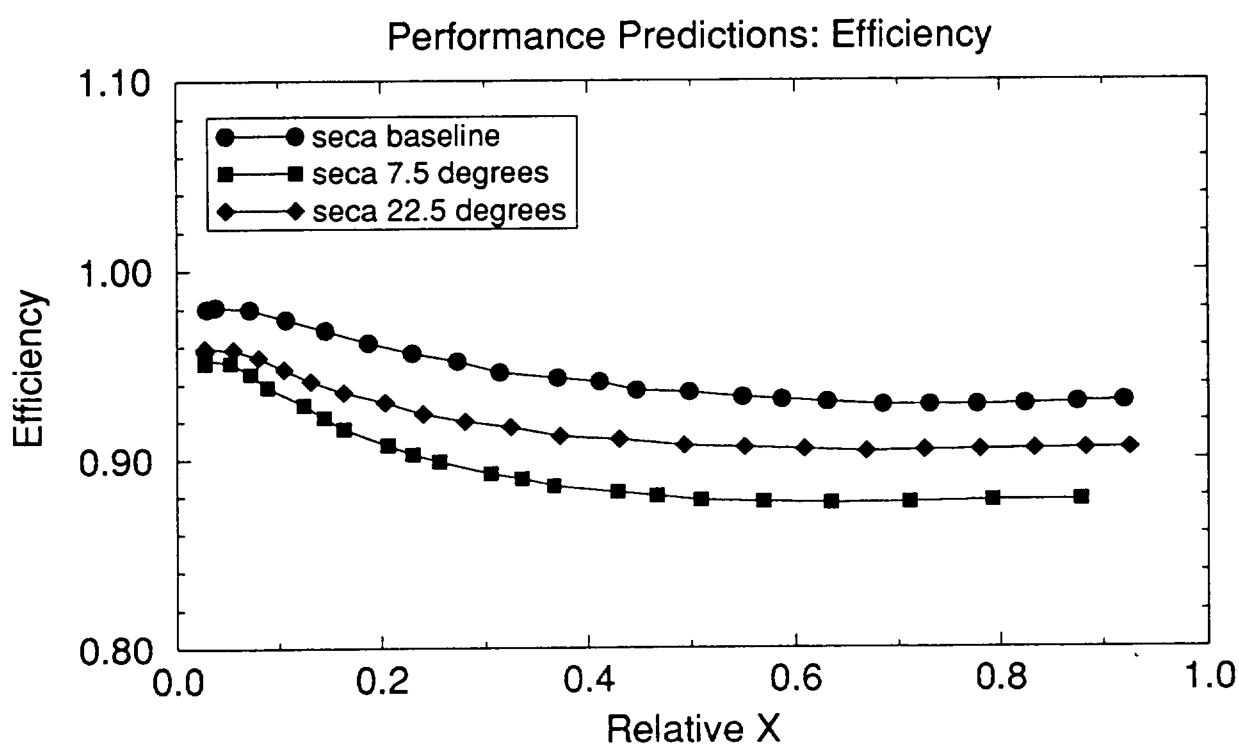

Advanced Impeller Parametrics: Tandem Blades

Performance Predictions: Static Head Coeff.

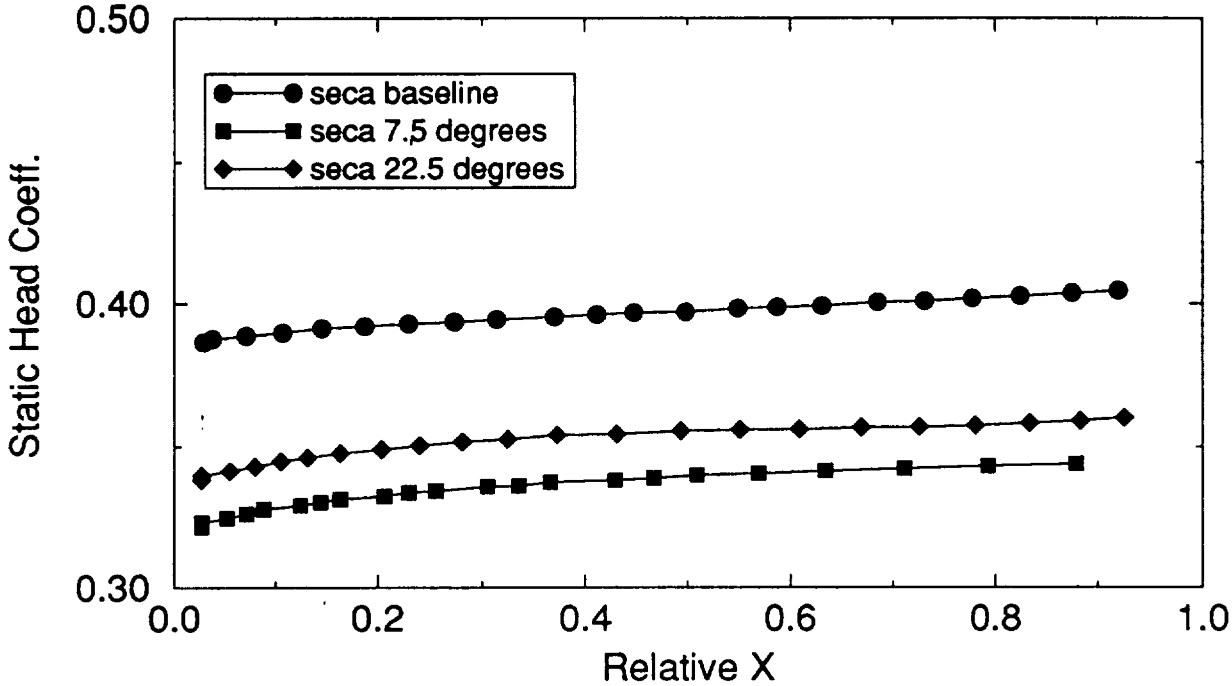

Performance Predictions: Euler Head Coeff.

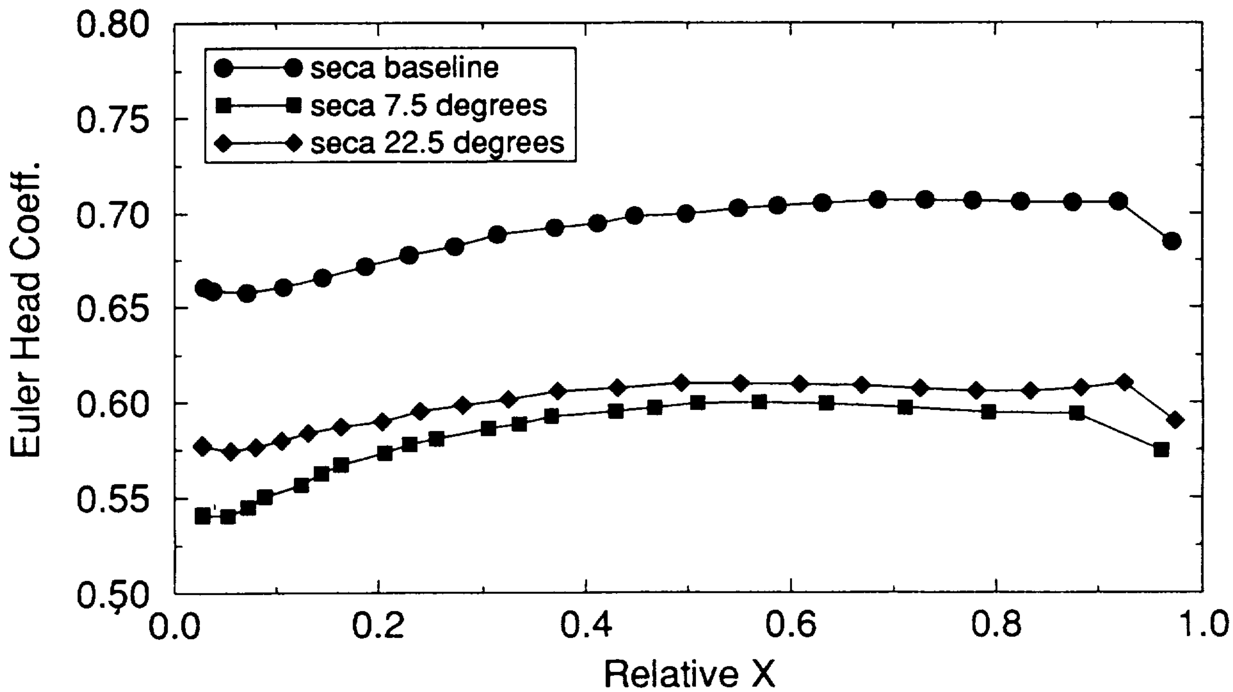

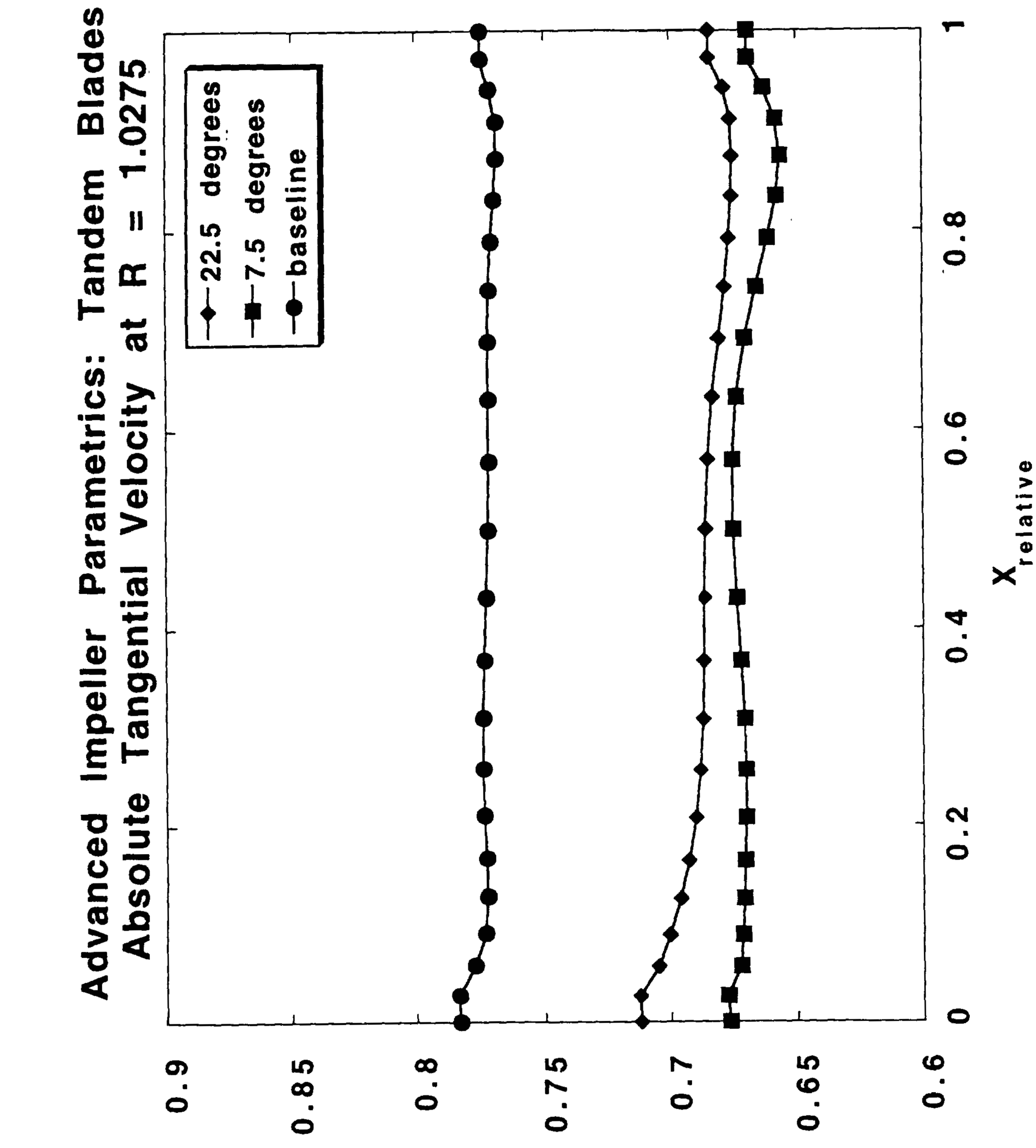
Advanced Impeller Parametrics: Tandem Blades
Absolute Tangential Velocity at R = 1.0275
22.5 degrees
7.5 degrees
baseline
C_u
$X_{relative}$
0.9
0.85
0.8
0.75
0.7
0.65
0.6
0
0.2
0.4
0.6
0.8
1

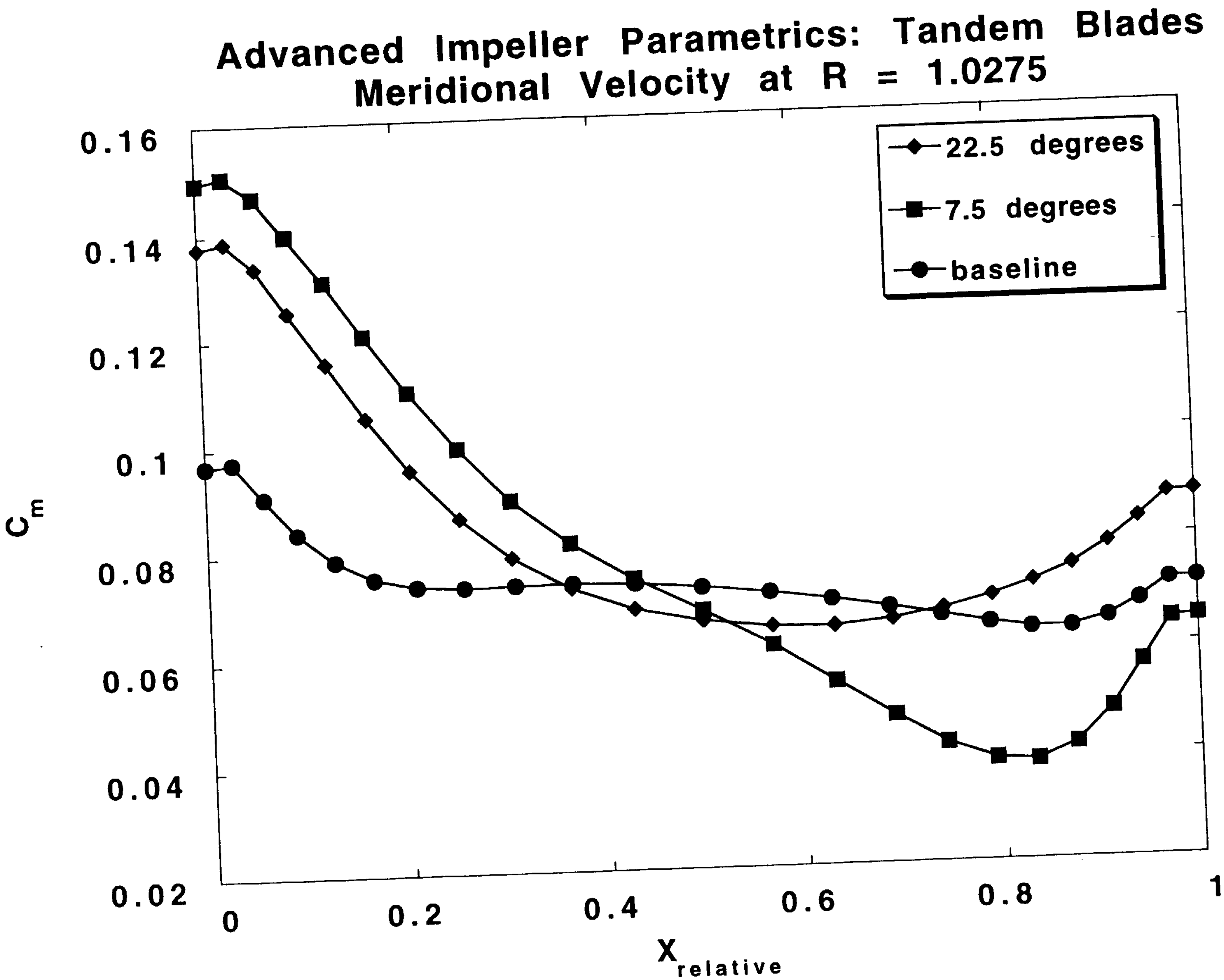

Advanced Impeller Parametrics: Tandem Blades
Meridional Velocity at R = 1.0275
22.5 degrees
7.5 degrees
baseline
0.16
0.14
0.12
0.1
0.08
0.06
0.04
0.02
0
0.2
0.4
0.6
0.8
1
C_m
$X_{relative}$

SUMMARY

- THE MASS FLOW RATE SPLIT

BLADE ROW	S.F.B.-P.P.B. / S.P.B.-P.F.B.
BASELINE IMPELLER	48/52
7.5° TANDEM BLADE	56/44
22.5° TANDEM BLADE	60/40

- THE TANDEM BLADE MODIFICATION DID NOT IMPROVE THE IMPELLER PERFORMANCE

N95- 23627

p. 31

Abstract of a proposed presentation at workshop for
CFD Applications in Rocket Propulsion to be held at
NASA Marshall Space Flight Center, AL, April 20-22, 1993

INCOMPRESSIBLE NAVIER-STOKES CALCULATIONS IN PUMP FLOWS

Cetin Kiris, Leon Chang
MCAT Institute, Moffett Field, CA

and

Dochan Kwak
NASA-Ames Research Center, Moffett Field, CA

Flow through pump components, such as the SSME-HPFTP Impeller and an advanced rocket pump impeller, is efficiently simulated by solving the incompressible Navier-Stokes equations. The solution method is based on the pseudocompressibility approach and uses an implicit-upwind differencing scheme together with the Gauss-Seidel line relaxation method. The equations are solved in steadily rotating reference frames and the centrifugal force and the Coriolis force are added to the equation of motion. Current computations use one-equation Baldwin-Barth turbulence model which is derived from a simplified form of the standard $k - \epsilon$ model equations. The resulting computer code is applied to the flow analysis inside an 11-inch SSME High Pressure Fuel Turbopump impeller, and an advanced rocket pump impeller. Numerical results of SSME-HPFTP impeller flow are compared with experimental measuremnts. In the advanced pump impeller, the effects of exit and shroud cavities are investigated. Flow analyses at design conditions will be presented.

INCOMPRESSIBLE NAVIER-STOKES COMPUTATIONS IN PUMP FLOWS

Cetin Kiris, Leon Chang
MCAT Institute

Dochan Kwak
Computational Algorithms and Applications Branch
NASA-Ames Research Center

Workshop for CFD Applications in Rocket Propulsion
NASA-MSFC, April 20-22, 1993

Outline

- Introduction
- Method of Solution
- Previous Work
- SSME-HPFTP Impeller Results
- Advanced Pump Impeller Analysis
- Summary

Introduction

- Motivation
  - ≫ Increase efficiency and reliability of the pump components in advance liquid rocket engine.
- Objective
  - ≫ To enhance, and validate a computational procedure for pump flow analysis.
- Approach
  - ≫ CFD validation cases parallel to experimental studies (MSFC Pump Consortium Team)
  - ≫ Component analysis in steadily rotating frames
  - ≫ 3-D viscous incompressible flow solver (INS3D-UP)
  - ≫ One-equation Baldwin-Barth turbulence model
  - ≫ Coarse/medium size grid for engineering purposes (150K - 600K).

Solution Method (INS3D-UP)

- Based on method of pseudocompressibility
- Both steady-state and time-accurate formulation
- Multi-Zone and Overlapped grid scheme capability
- Central differencing for viscous fluxes
- Upwind differencing for convective fluxes
  - 3rd and 5th order flux-difference splitting is used for the right hand side terms
- Implicit Gauss-Seidel line relaxation scheme
- Inflow and Outflow boundaries based on Method of Characteristics
  - Inflow Boundary : Three velocity components specified
  - Outflow Boundary : Static pressure specified
- Quasi-implicit boundary conditions at zonal interfaces

Steady-State Formulation

- Introduce pseudocompressibility term to the continuity equation

$$\frac{\partial p}{\partial \tau} = -\beta \left(\frac{\partial \hat{U}}{\partial \xi} + \frac{\partial \hat{V}}{\partial \eta} + \frac{\partial \hat{W}}{\partial \zeta} \right)$$

$$\frac{\partial \hat{q}}{\partial \tau} = -\frac{\partial}{\partial \xi}(\hat{e} - \hat{e}_v) - \frac{\partial}{\partial \eta}(\hat{f} - \hat{f}_v) - \frac{\partial}{\partial \zeta}(\hat{g} - \hat{g}_v) + S$$

≫ β is an pseudocompressibility constant
≫ τ is a pseudo-time step
≫ S is a source term for centrifugal and coriolis forces

- Euler Implicit time discretization

- Solve system of equations iteratively in pseudo-time until solution converges to a steady state

Previous Work

- Flow analysis for a high-flow-coefficient inducer was completed. The results from one-equation Baldwin-Barth turbulence model compare fairly well with the experimental data.
- Advanced impeller design was analyzed for baseline and optimized geometries. Inflow conditions were not avialable experimentally.
- Advanced impeller design was analyzed for design and off-design conditions (100, 120, 80, and 60 percent of design flows).
- The effect of downstream boundary conditions was investigated.

Recent Work

- 11 inch SSME-HPFTP impeller was analyzed. Exit cavities were included.
- Advanced impeller design was analyzed with the recent inflow conditions.
- The effect of exit cavities were investigated.
- The shroud cavity calculation is currently underway.

SSME-HPFTP Impeller Computations

- Grid 1 : 108 x 25 x 33
- Grid 2 : 108 x 25 x 33
- Grid 3 : 108 x 25 x 33
- Grid 4 : 108 x 25 x 33 / TOTAL : 633 K
- Grid 5 : 37 x 132 x 33
- Grid 6 : 21 x 132 x 21
- Grid 7 : 21 x 132 x 21

SSME HPFTP Impeller Grid

TOTAL 633,000 GRID POINTS

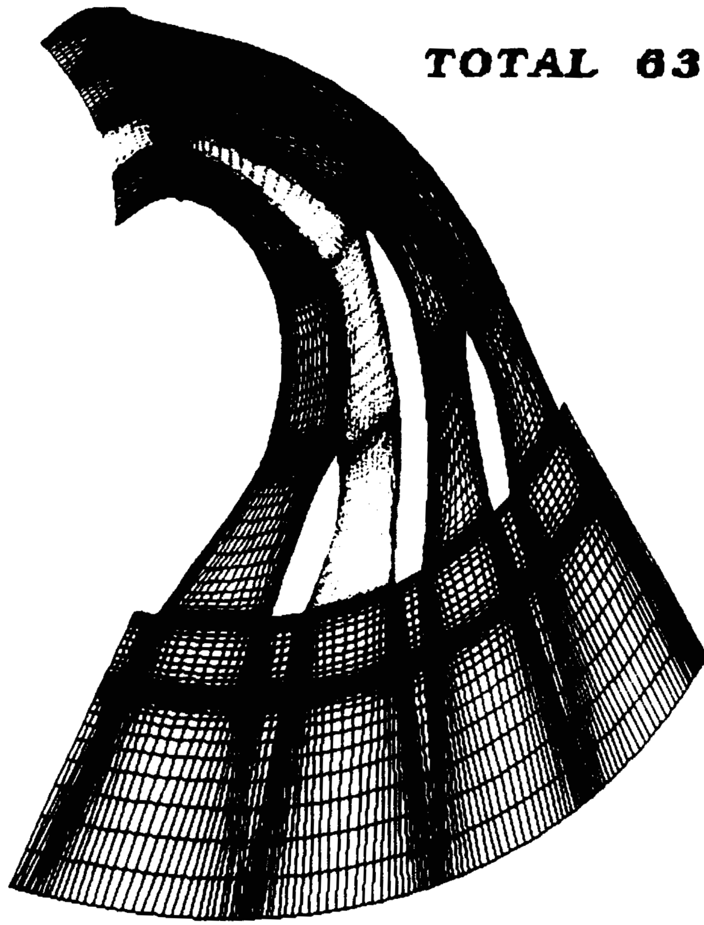

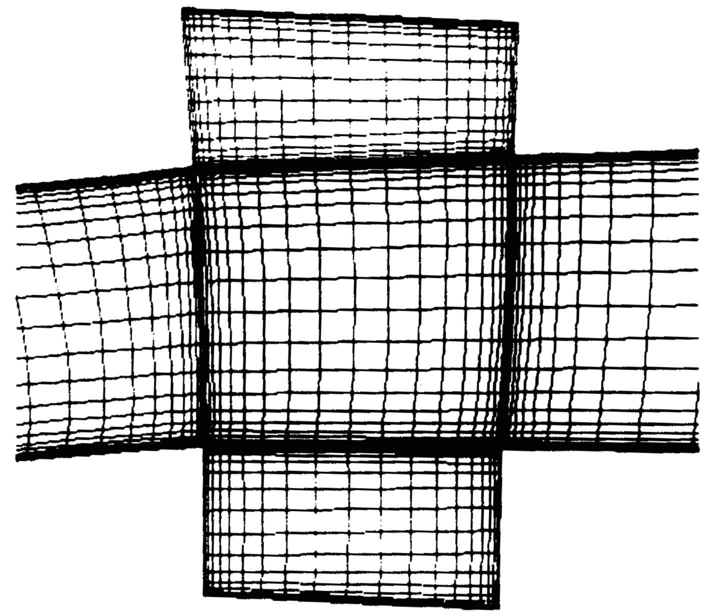

Grid 1 ■
Grid 2 ■
Grid 3 ■

Grid 4 ■
Grid 5 ■

Grid 1 ■
Grid 5 ■
Grid 6 ■
Grid 7 ■

SSME-HPFTP Impeller Computations

Flow Split

- Full Blade S.S. - Short Partial P.S. : % 19.7 (comp) % 20.84 (exp)
- Short Partial S.S. - Long Partial P.S. : % 25.3 (comp) % 26.48 (exp)
- Long Partial S.S. - Short Partial P.S. : % 25.7 (comp) % 24.54 (exp)
- Short Partial S.S. - Full Blade P.S. : % 29.3 (comp) % 28.14 (exp)

SSME-HPFTP Impeller

downstream of impeller exit plane

(51 % of blade height)

Impeller exit radius : 5.5 in.

V* : Impeller exit wheel speed (303.5 ft/sec)

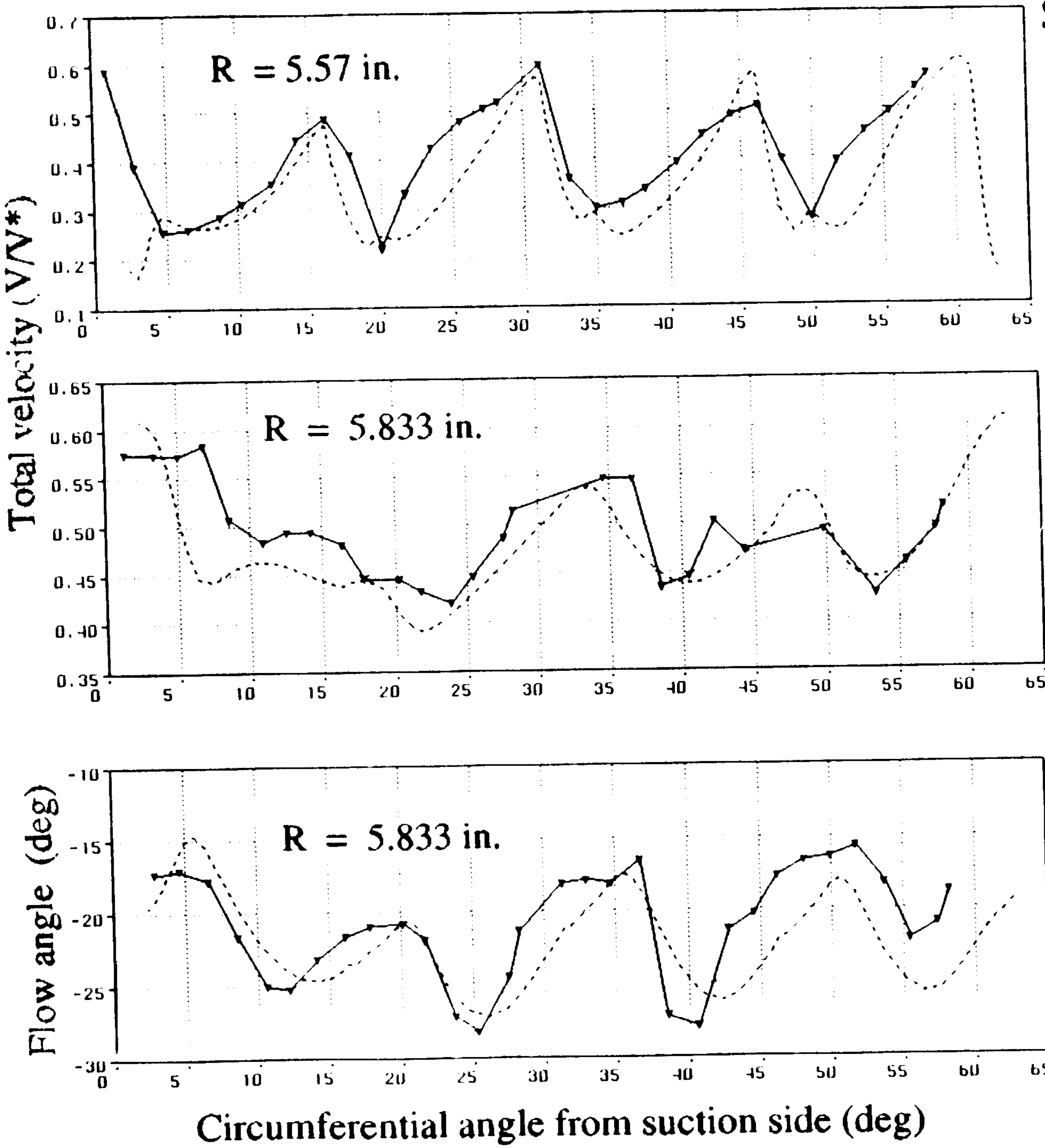

11 INCH SSME HPFTP IMPELLER

particle traces colored by relative total velocity magnitude

total velocity

0.00000
0.05000
0.10000
0.15000
0.20000
0.25000
0.30000
0.35000
0.40000
0.45000
0.50000
0.55000
0.60000
0.65000
0.70000
0.75000
0.80000
[illegible]
0.90000
0.95000
1.00000
1.05000
1.10000
1.15000
1.20000
1.25000
1.30000
1.35000
1.40000
1.45000

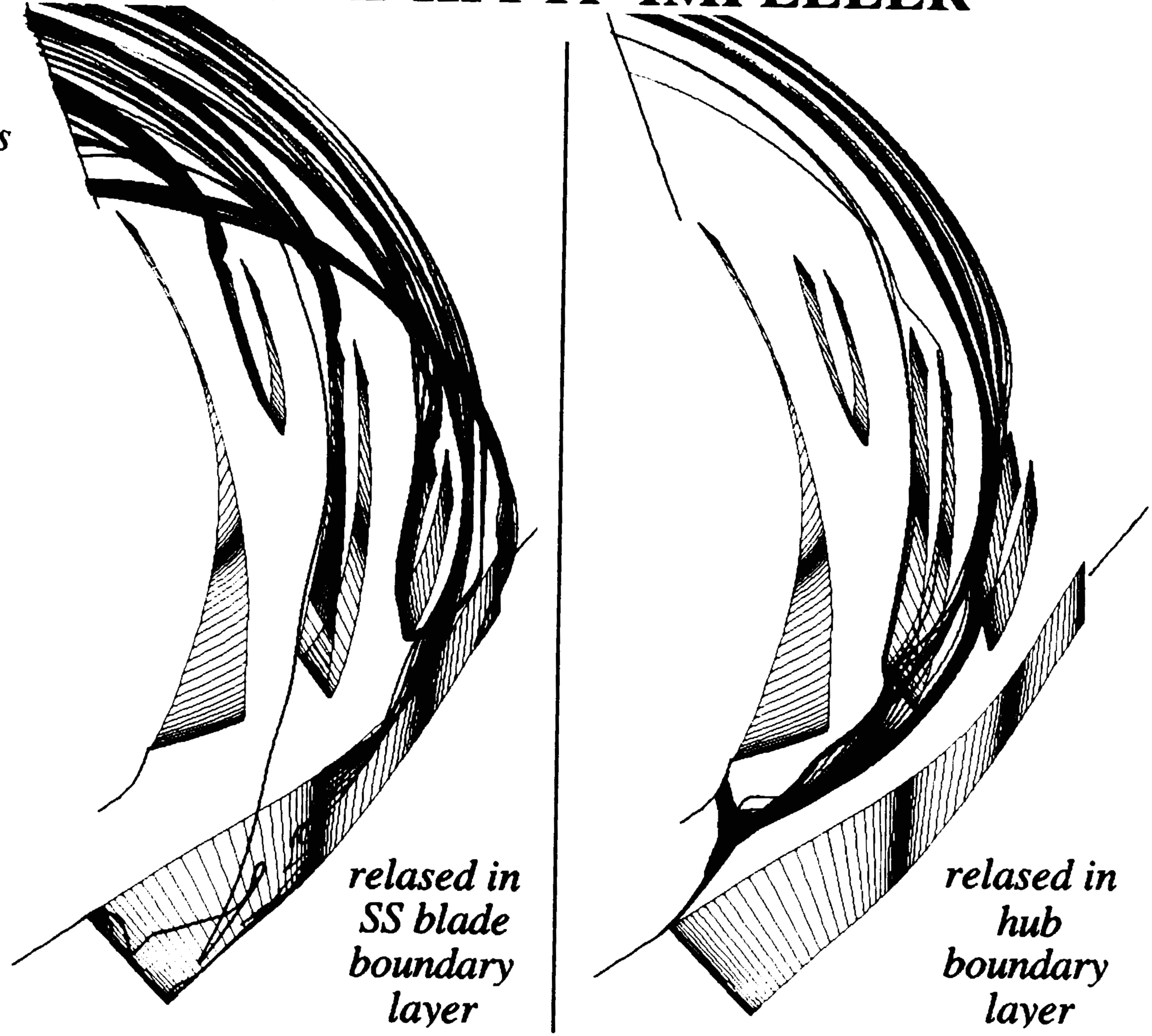

11 INCH SSME HPFTP IMPELLER

particle traces
colored by
relative
total
velocity
magnitude

total
velocity

0.00000
0.05000
0.10000
0.15000
0.20000
0.25000
0.30000
0.35000
0.40000
0.45000
0.50000
0.55000
0.60000
0.65000
0.70000
0.75000
[illegible]
[illegible]
[illegible]
1.00000
1.05000
1.10000
1.15000
1.20000
1.25000
1.30000
1.35000
1.40000
1.45000

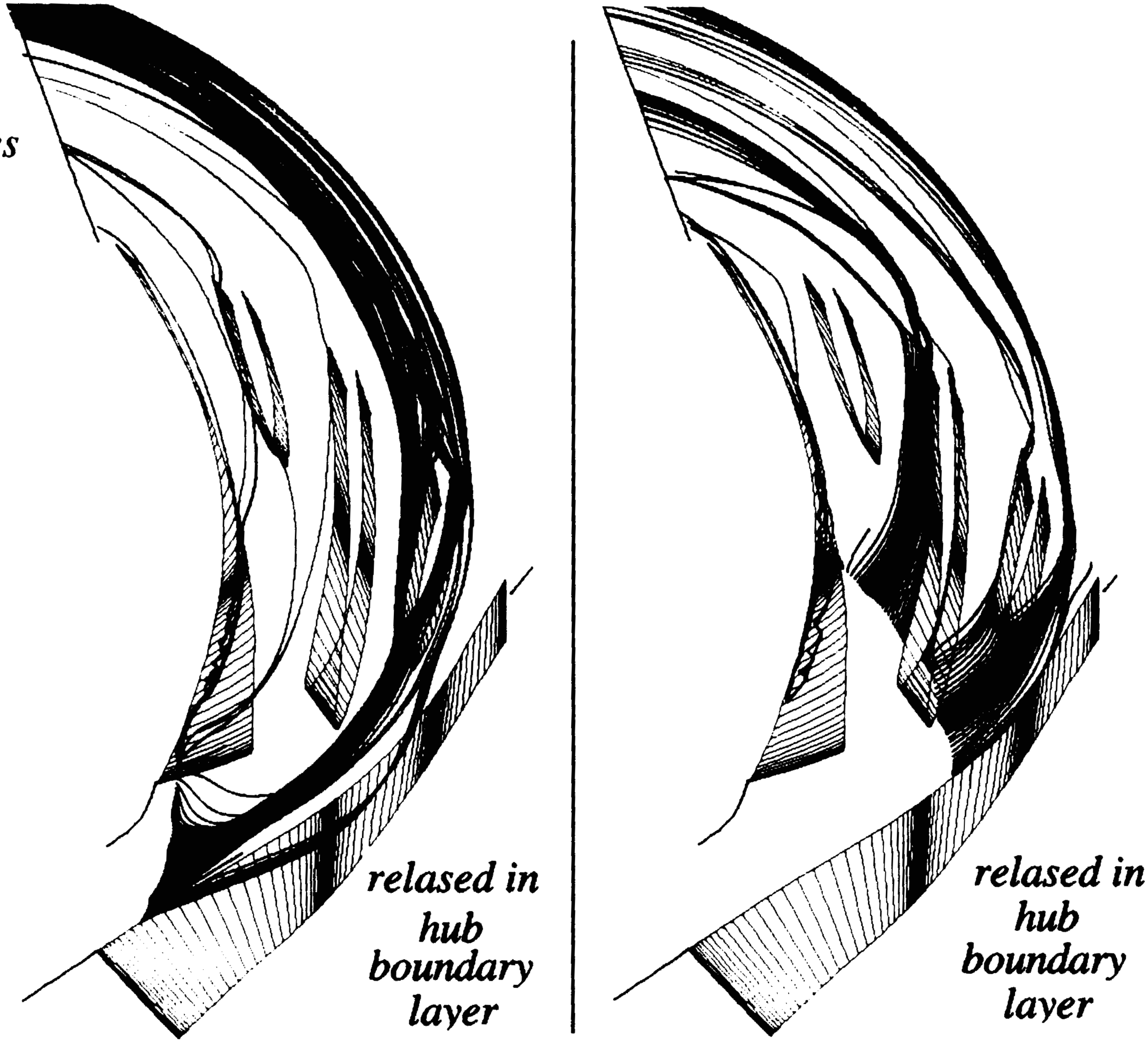

11 INCH SSME HPFTP IMPELLER

particle traces colored by relative total velocity magnitude

total velocity

0.00000
0.05000
0.10000
0.15000
0.20000
0.25000
0.30000
0.35000
0.40000
0.45000
0.50000
0.55000
0.60000
0.65000
0.70000
0.75000
0.80000
[illegible]
0.90000
0.95000
1.00000
1.05000
1.10000
1.15000
1.20000
1.25000
1.30000
1.35000
1.40000
1.45000

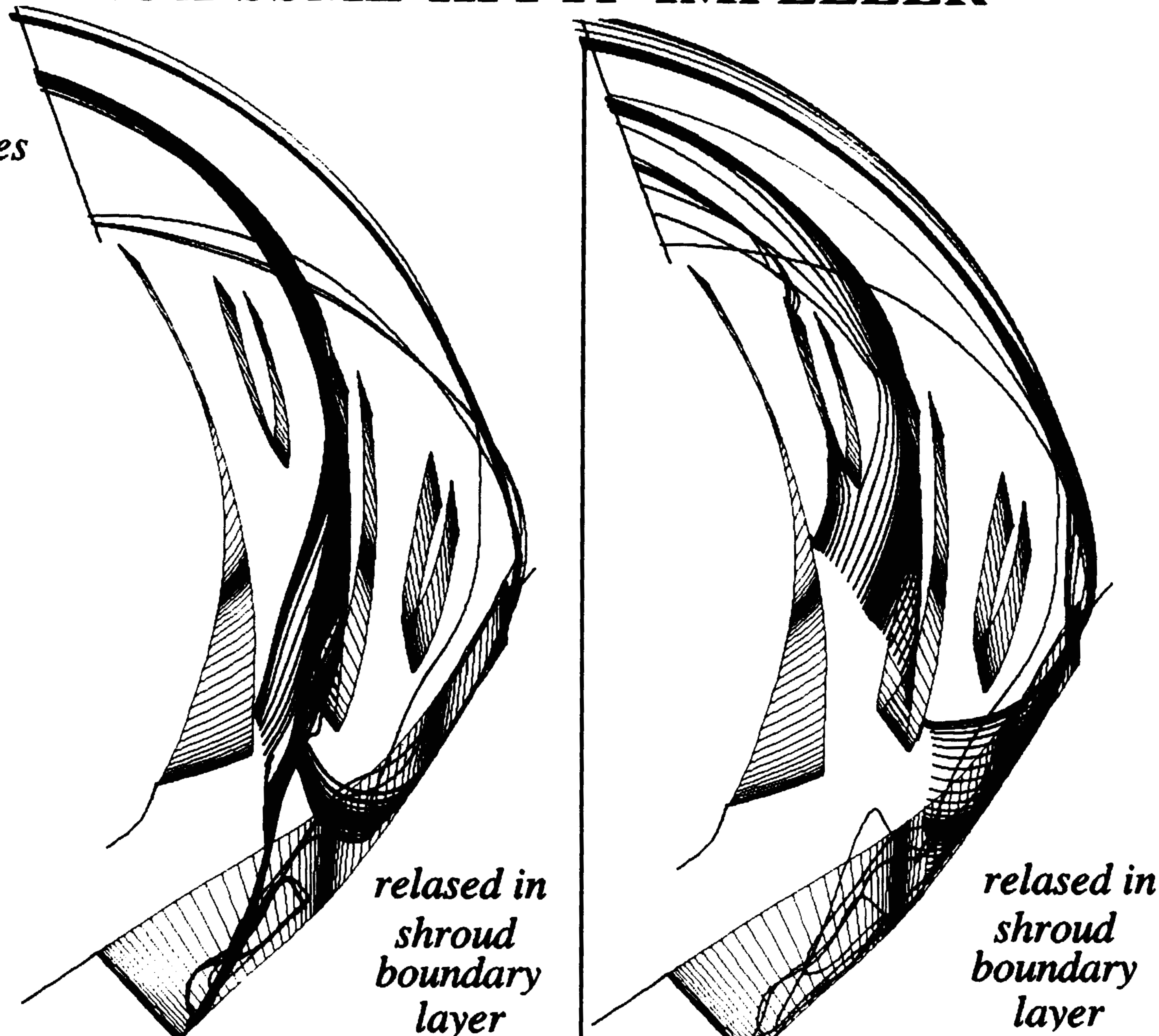

Advanced Rocket Pump Impeller

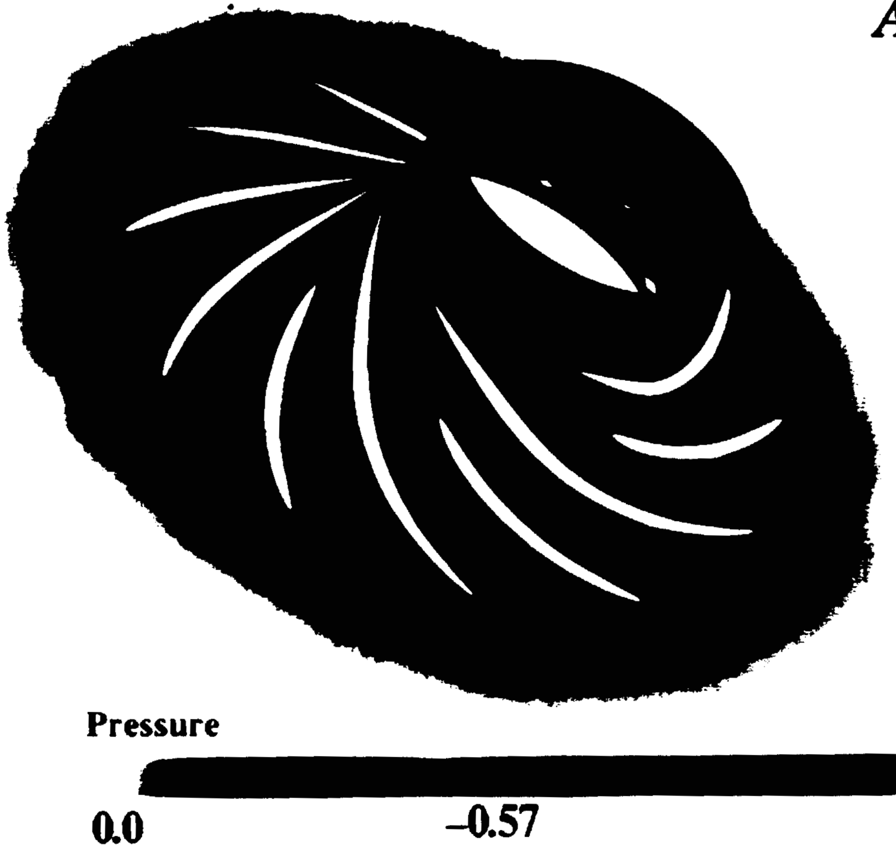

Shrouded impeller

6 full blades

6 partial blades

Impeller shaft speed : 6322 rpm

Impeller exit wheel speed :

249.5 ft/sec

Impeller exit diameter : 9.045 in.

Reynold Number : 1.81e+5

Reference length : 1 inch

Reference velocity : 284 in/sec

Fluid medium : water at 70 F

Baseline Impeller

Case 1 – No cavities (slip downstream b.c.)

Case 2 – Exit cavities

Case 3 – Exit cavities + shroud cavity

Advanced Impeller Computations

- Grid 1 : 111 x 25 x 33
- Grid 2 : 111 x 25 x 33
- Grid 3 : 61 x 72 x 33 / slip b.c. total : 328 K
- Grid 4 : 45 x 72 x 33
- Grid 5 : 45 x 72 x 33 / + exit cavities total : 542 K
- Grid 6 : 52 x 72 x 15 / + shroud cavity total : 598 K

Flow Split

- Full Blade S.S. - Short Blade P.S. : % 48.7 (comp) % 49.0 (exp)
- Short Blade S.S. - Full Blade P.S. : % 51.3 (comp) % 51.0 (exp)

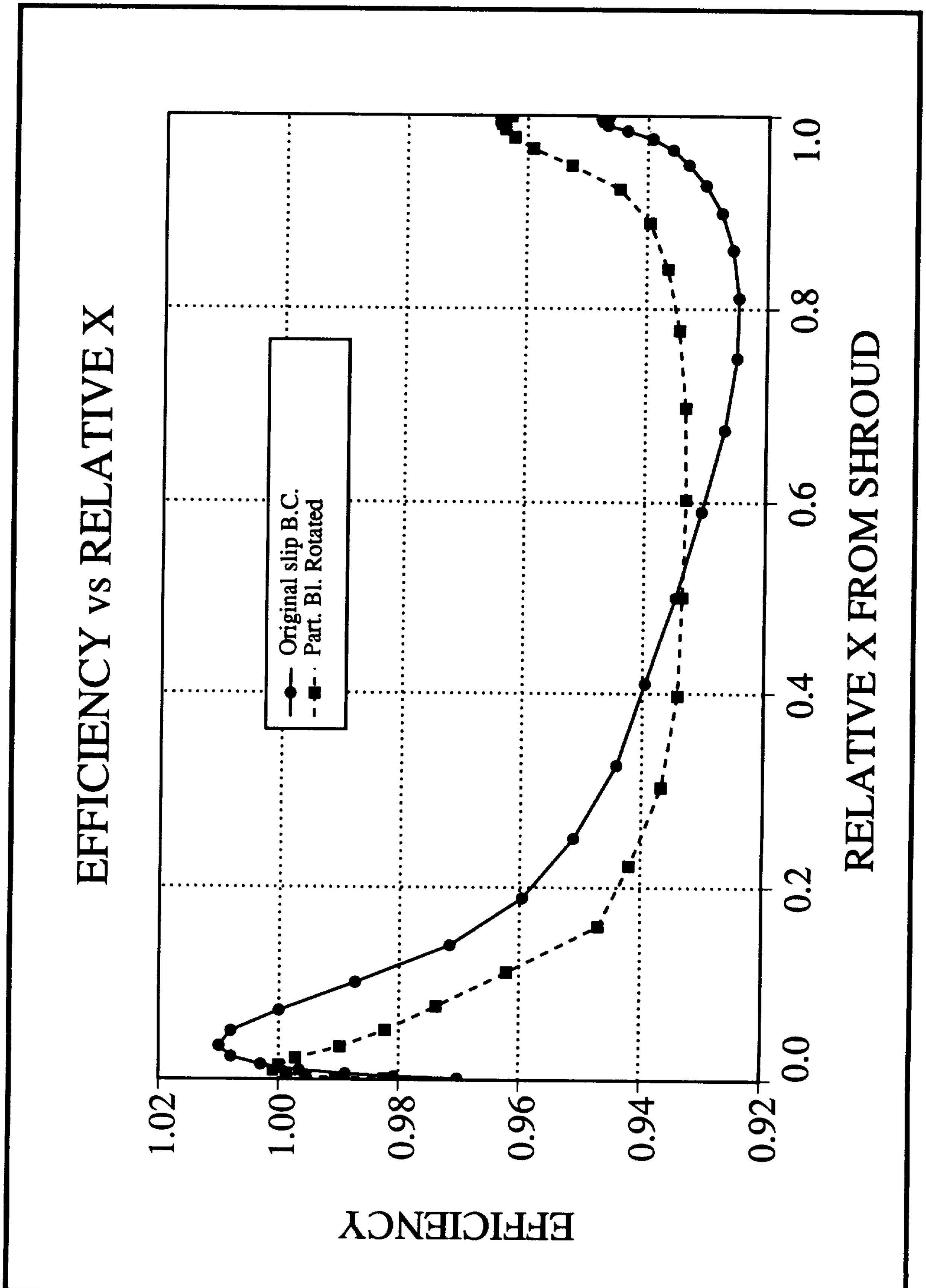
EFFICIENCY vs RELATIVE X
EFFICIENCY
RELATIVE X FROM SHROUD
Original slip B.C.
Part. Bl. Rotated
1.02
1.00
0.98
0.96
0.94
0.92
0.0
0.2
0.4
0.6
0.8
1.0

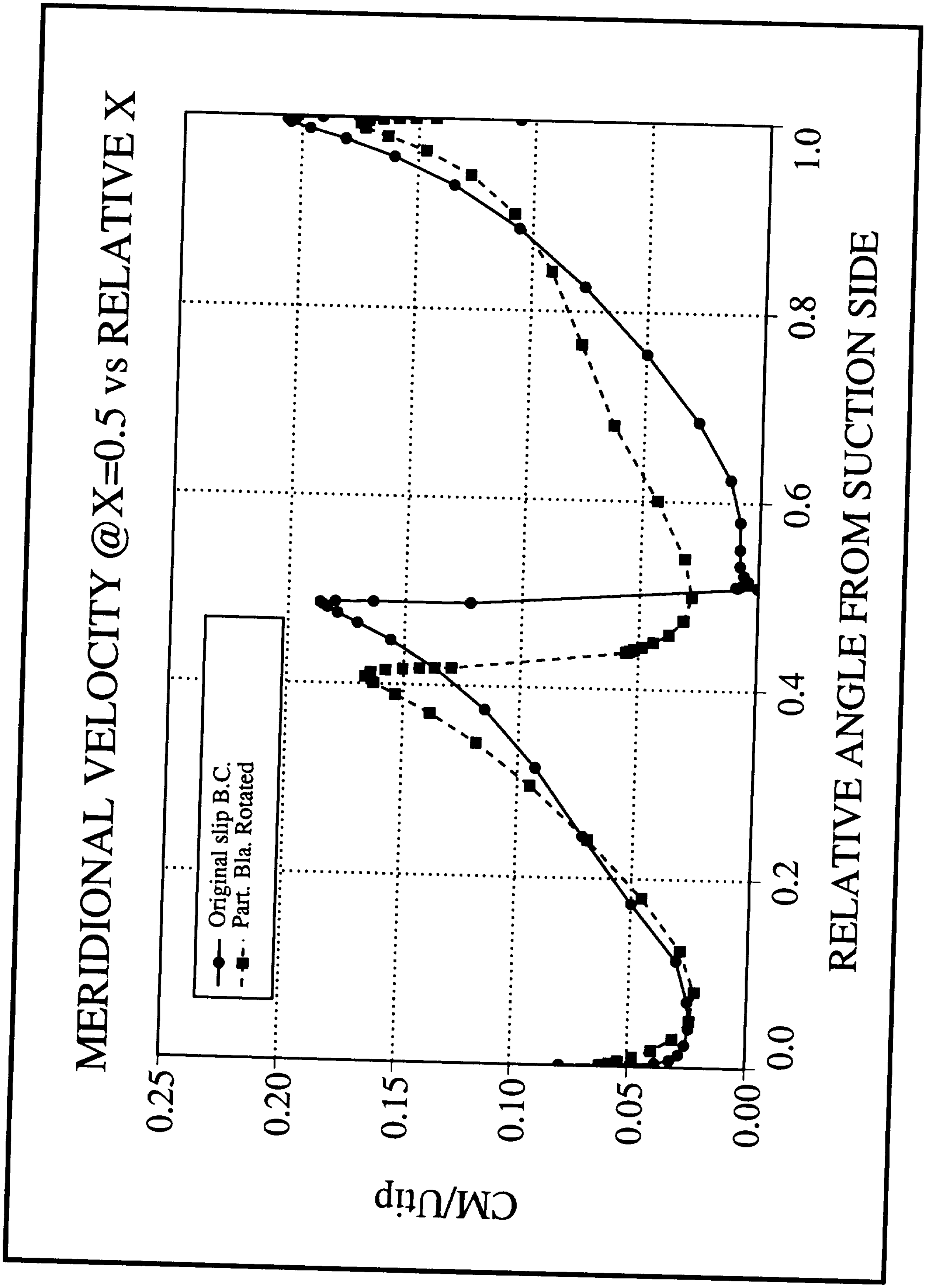
MERIDIONAL VELOCITY @X=0.5 vs RELATIVE X
CM/Utip
RELATIVE ANGLE FROM SUCTION SIDE
Original slip B.C.
Part. Bla. Rotated
0.25
0.20
0.15
0.10
0.05
0.00
0.0
0.2
0.4
0.6
0.8
1.0

Advanced Impeller Concept

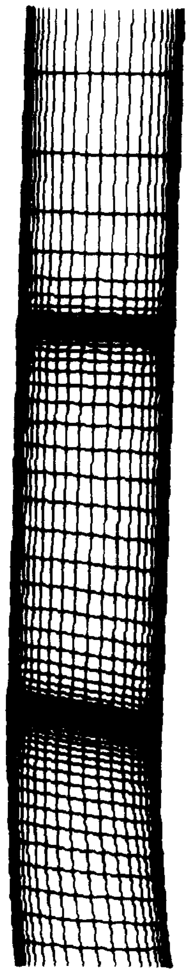

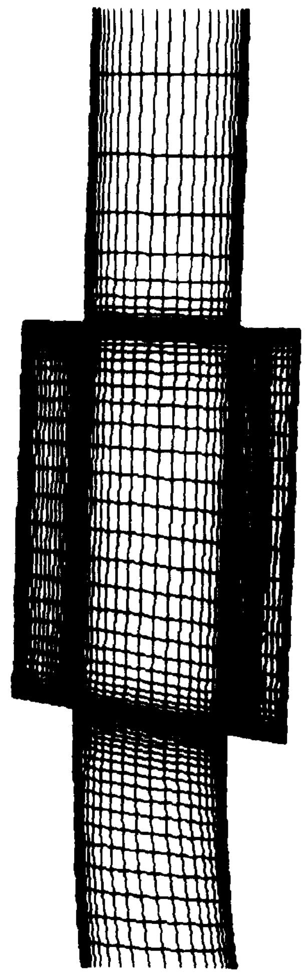

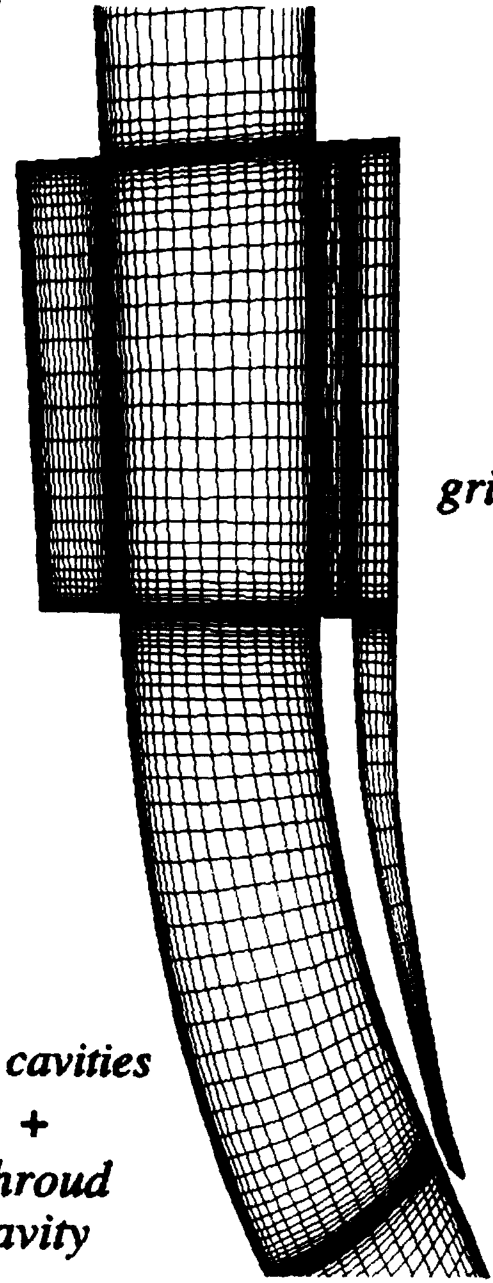

Advanced Impeller Concept

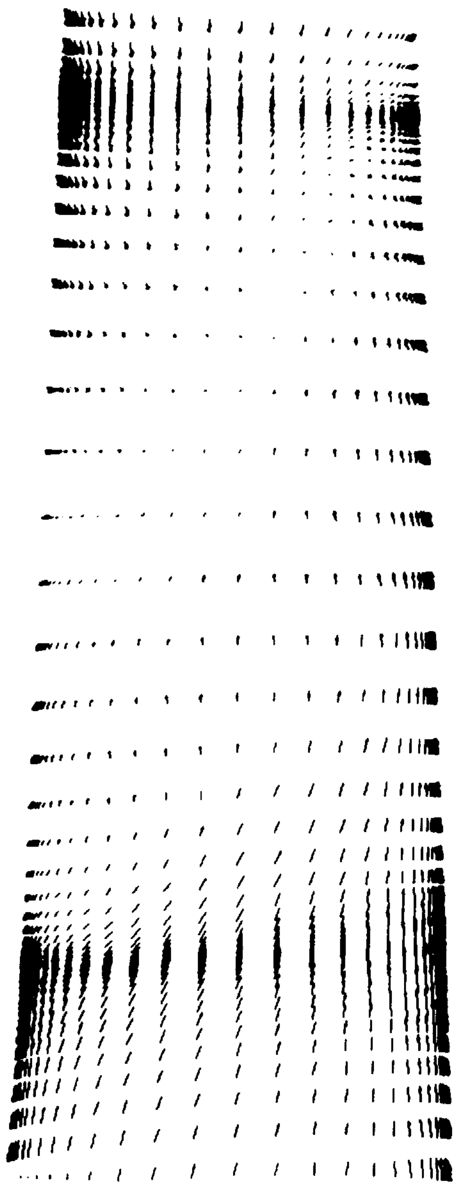

no cavity (slip b.c.)

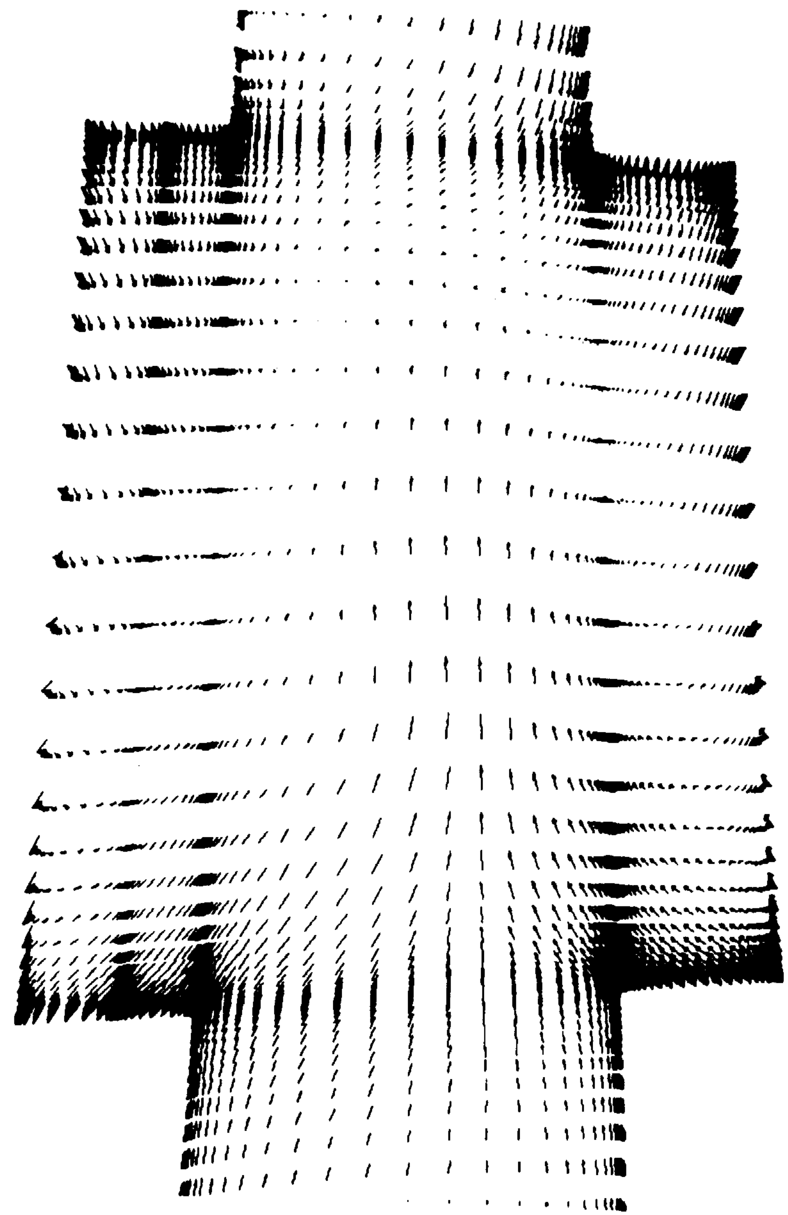

with exit cavities

Advanced Impeller Concept

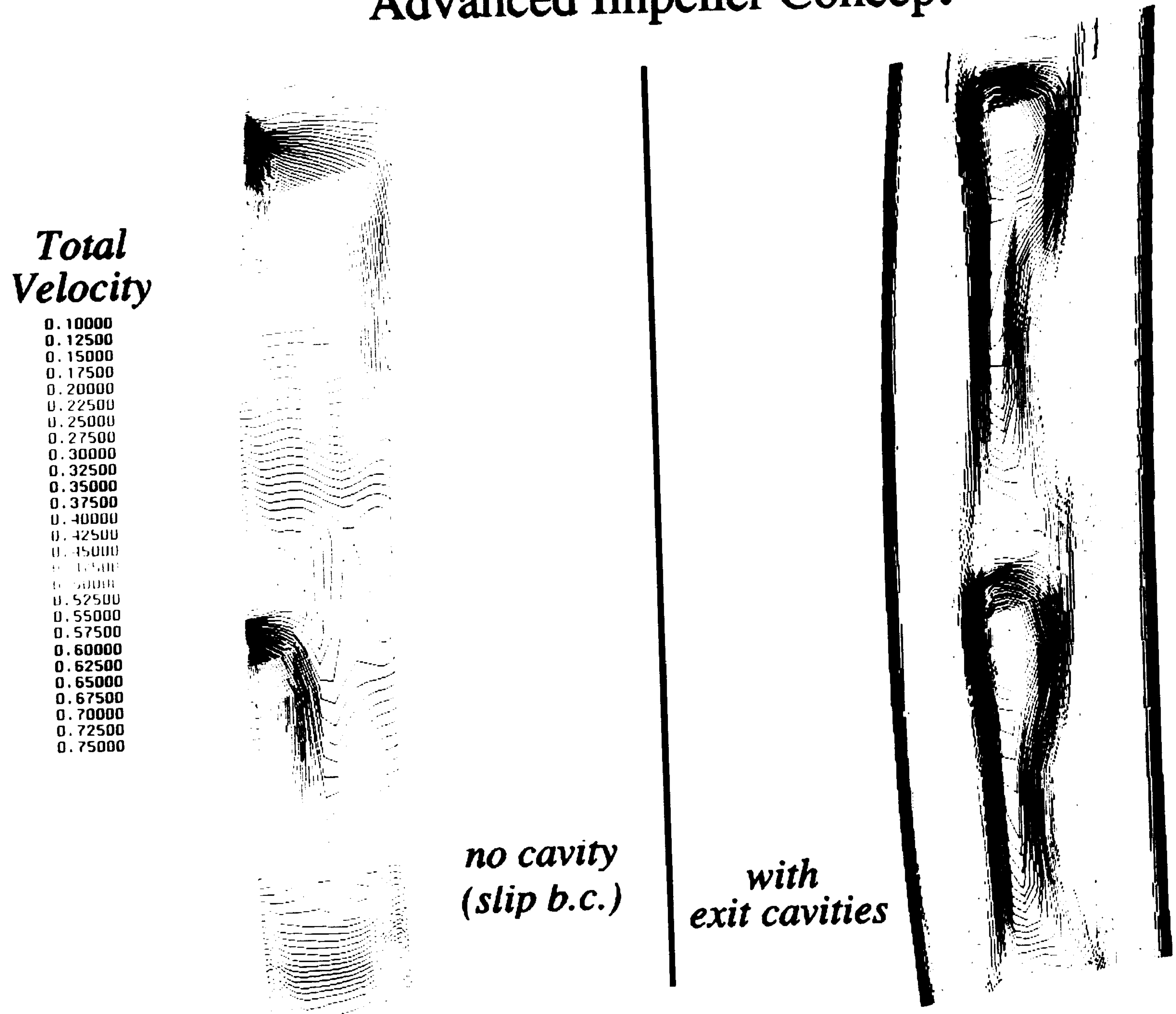

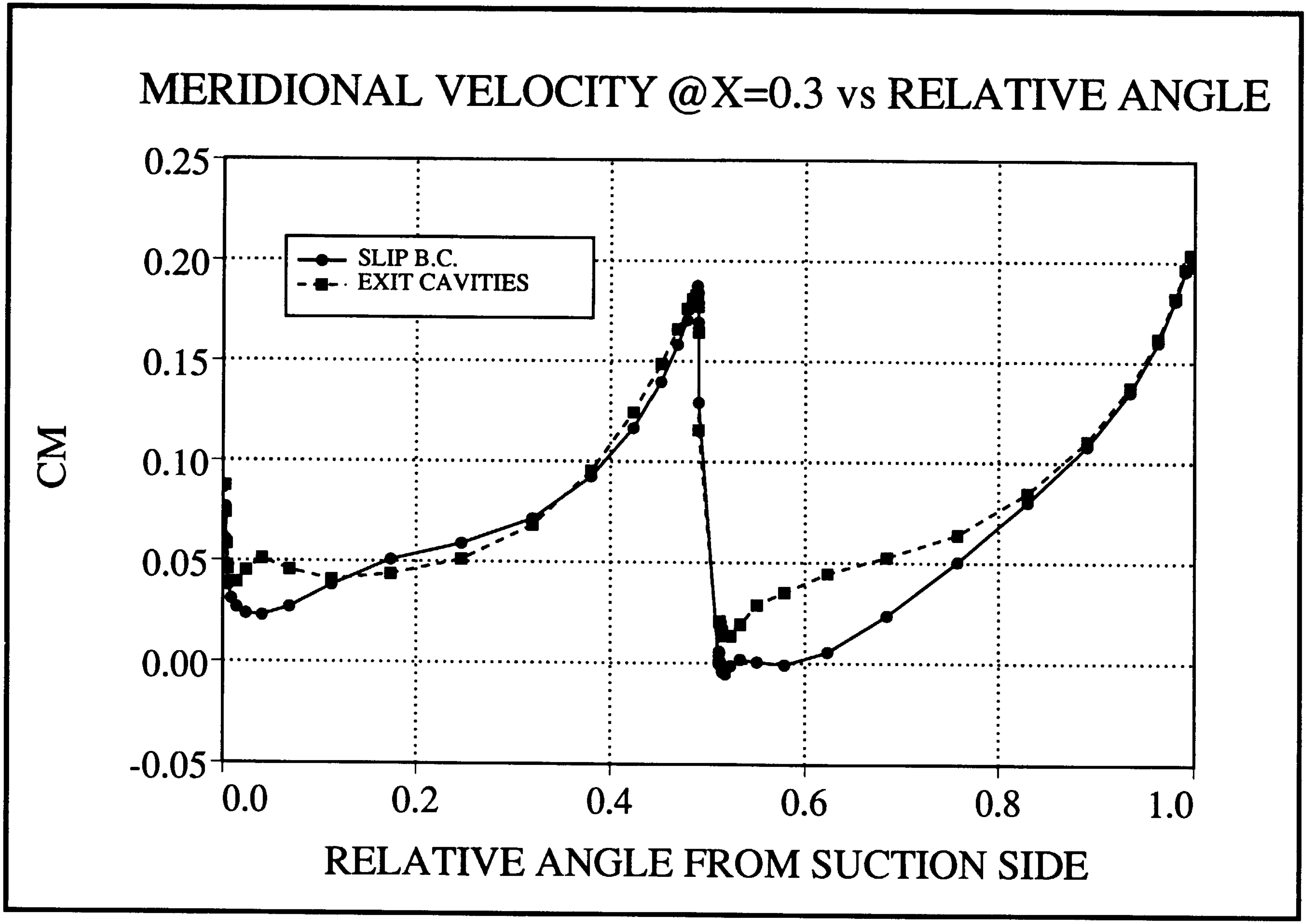
MERIDIONAL VELOCITY @X=0.3 vs RELATIVE ANGLE
SLIP B.C.
EXIT CAVITIES
CM
0.25
0.20
0.15
0.10
0.05
0.00
-0.05
0.0
0.2
0.4
0.6
0.8
1.0
RELATIVE ANGLE FROM SUCTION SIDE

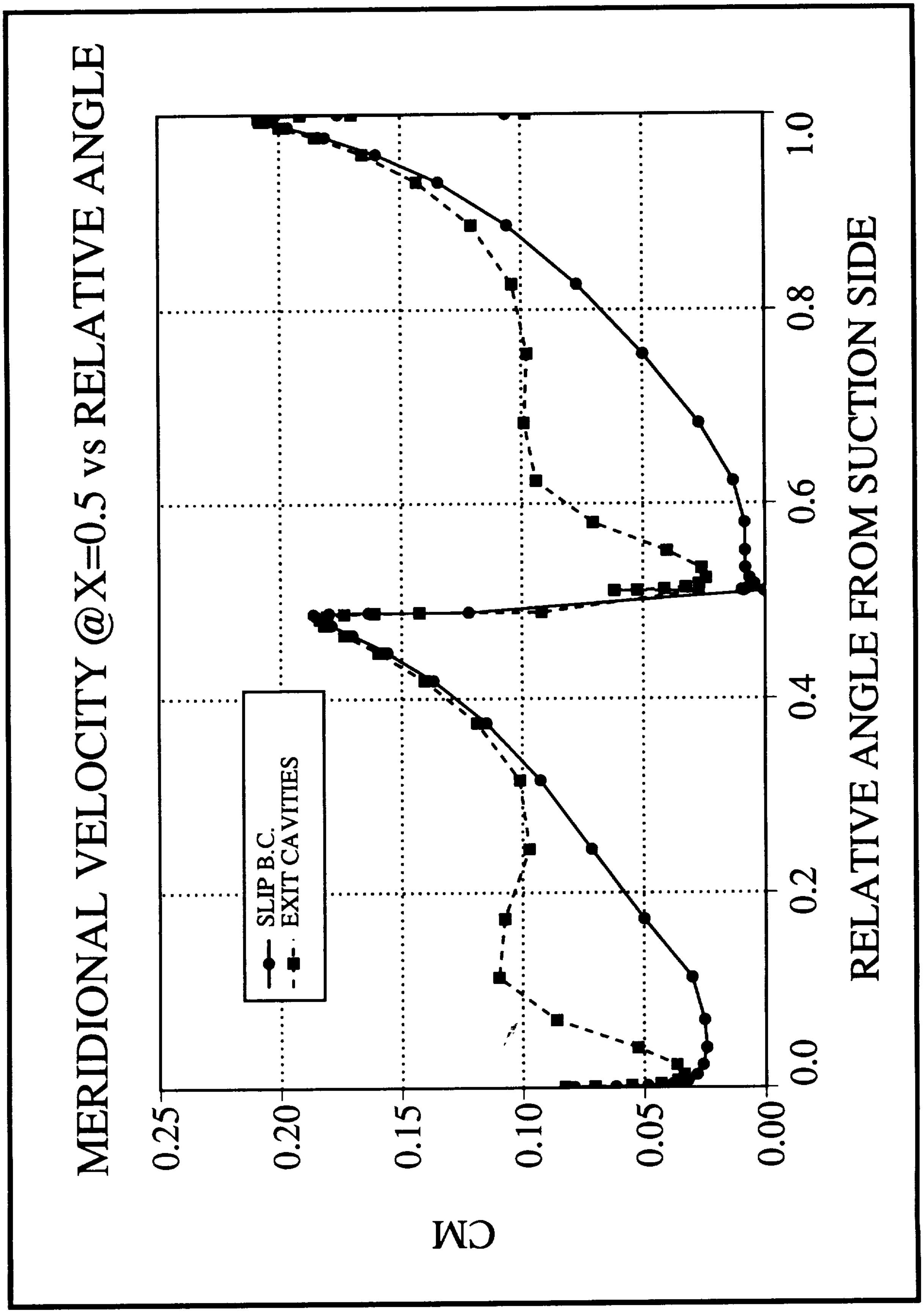
MERIDIONAL VELOCITY @X=0.5 vs RELATIVE ANGLE
CM
0.25
0.20
0.15
0.10
0.05
0.00
0.0
0.2
0.4
0.6
0.8
1.0
RELATIVE ANGLE FROM SUCTION SIDE
SLIP B.C.
EXIT CAVITIES

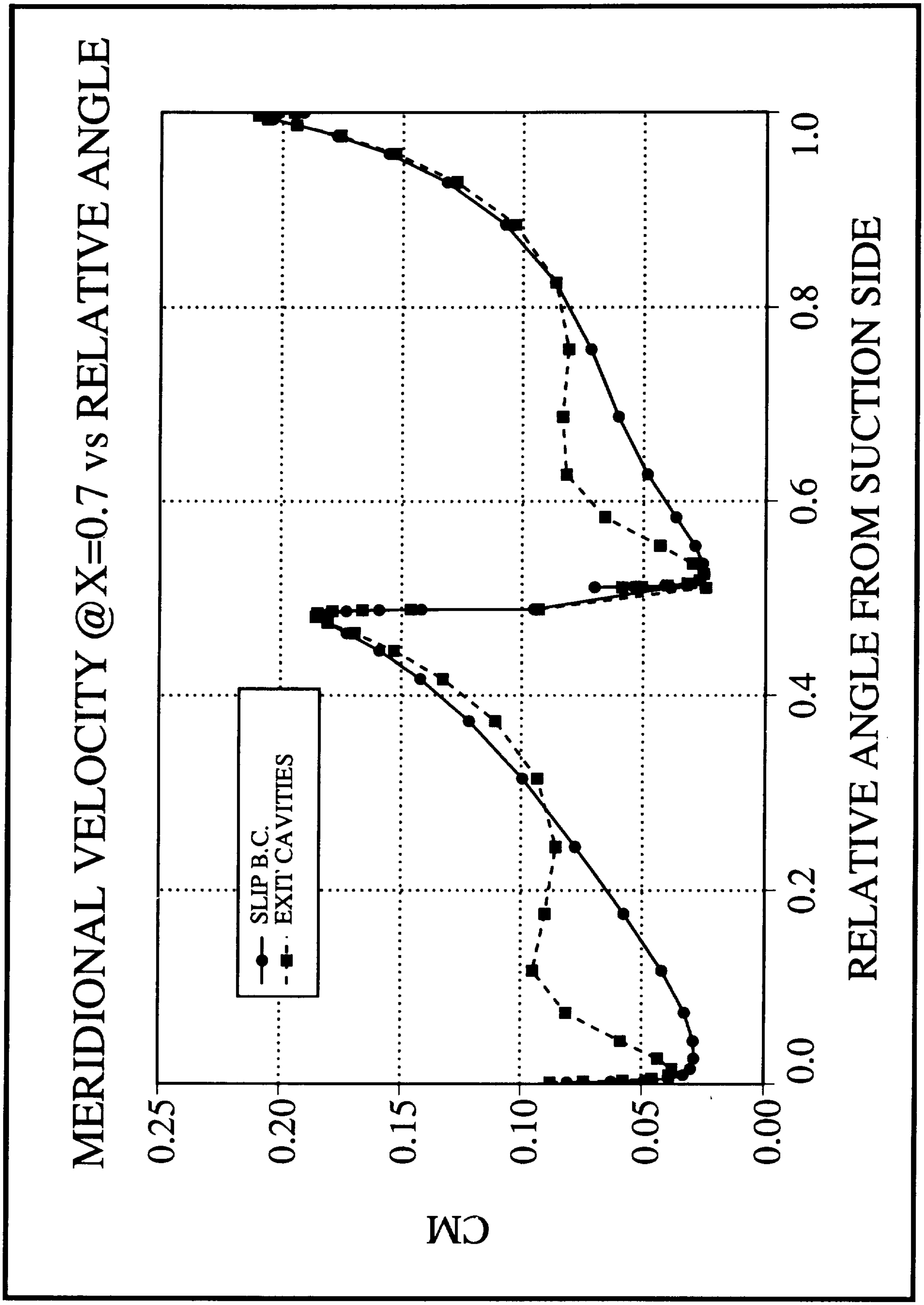
MERIDIONAL VELOCITY @X=0.7 vs RELATIVE ANGLE
CM
0.25
0.20
0.15
0.10
0.05
0.00
0.0
0.2
0.4
0.6
0.8
1.0
RELATIVE ANGLE FROM SUCTION SIDE
SLIP B.C.
EXIT CAVITIES

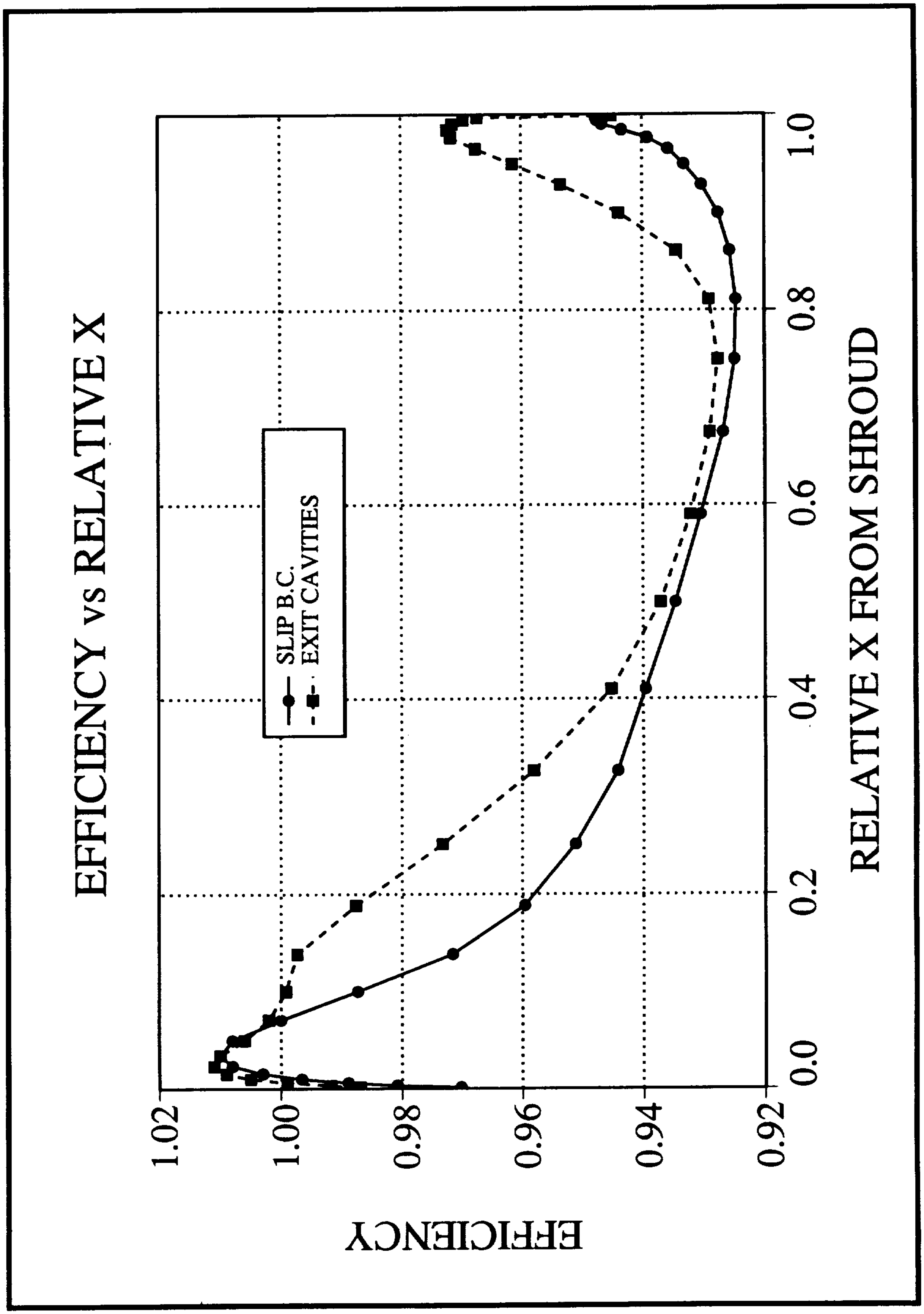
EFFICIENCY vs RELATIVE X
SLIP B.C.
EXIT CAVITIES
EFFICIENCY
RELATIVE X FROM SHROUD
1.02
1.00
0.98
0.96
0.94
0.92
0.0
0.2
0.4
0.6
0.8
1.0

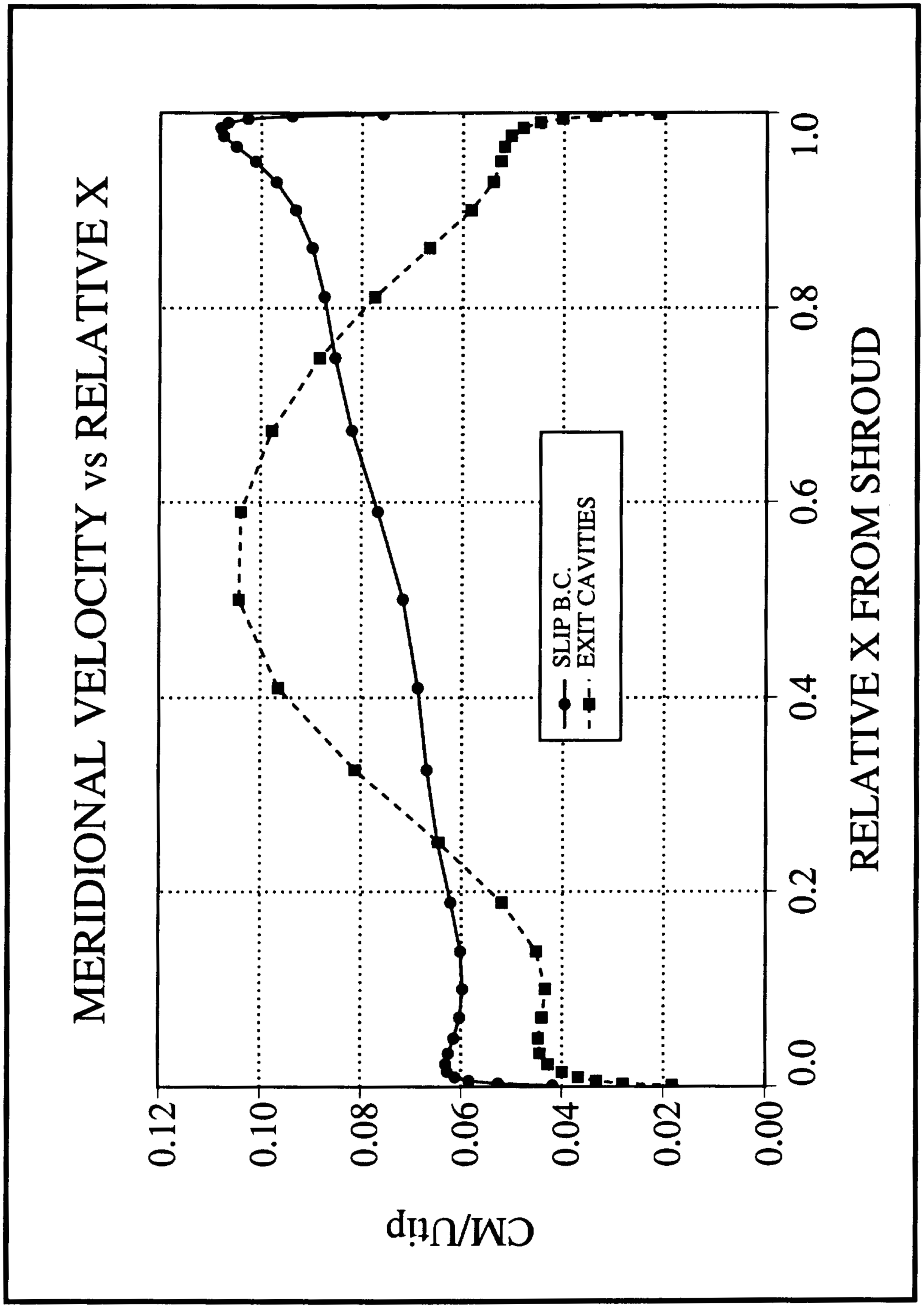
MERIDIONAL VELOCITY vs RELATIVE X
CM/Utip
RELATIVE X FROM SHROUD
SLIP B.C.
EXIT CAVITIES
0.00
0.02
0.04
0.06
0.08
0.10
0.12
0.0
0.2
0.4
0.6
0.8
1.0

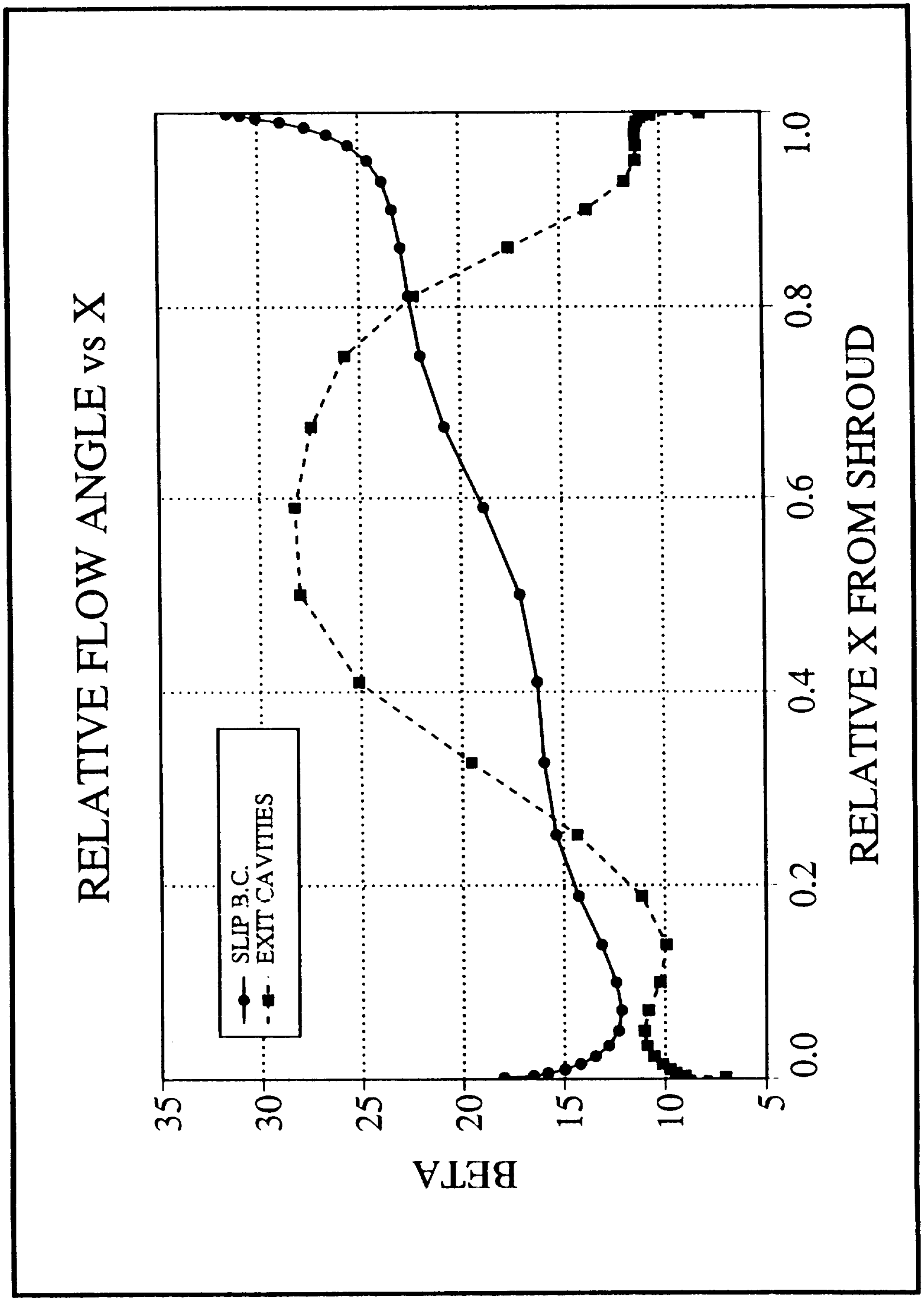
RELATIVE FLOW ANGLE vs X
BETA
35
30
25
20
15
10
5
0.0
0.2
0.4
0.6
0.8
1.0
SLIP B.C.
EXIT CAVITIES
RELATIVE X FROM SHROUD

Advanced Impeller Concept

particle traces
colored by
relative
total
velocity
magnitude

total
velocity

0.00000
0.05000
0.10000
0.15000
0.20000
0.25000
0.30000
0.35000
0.40000
0.45000
0.50000
0.55000
0.60000
0.65000
0.70000
0.75000
0.80000
0.85000
0.90000
0.95000
1.00000
1.05000
1.10000
1.15000
1.20000
1.25000
1.30000
1.35000
1.40000
1.45000
1.50000
1.55000
1.60000

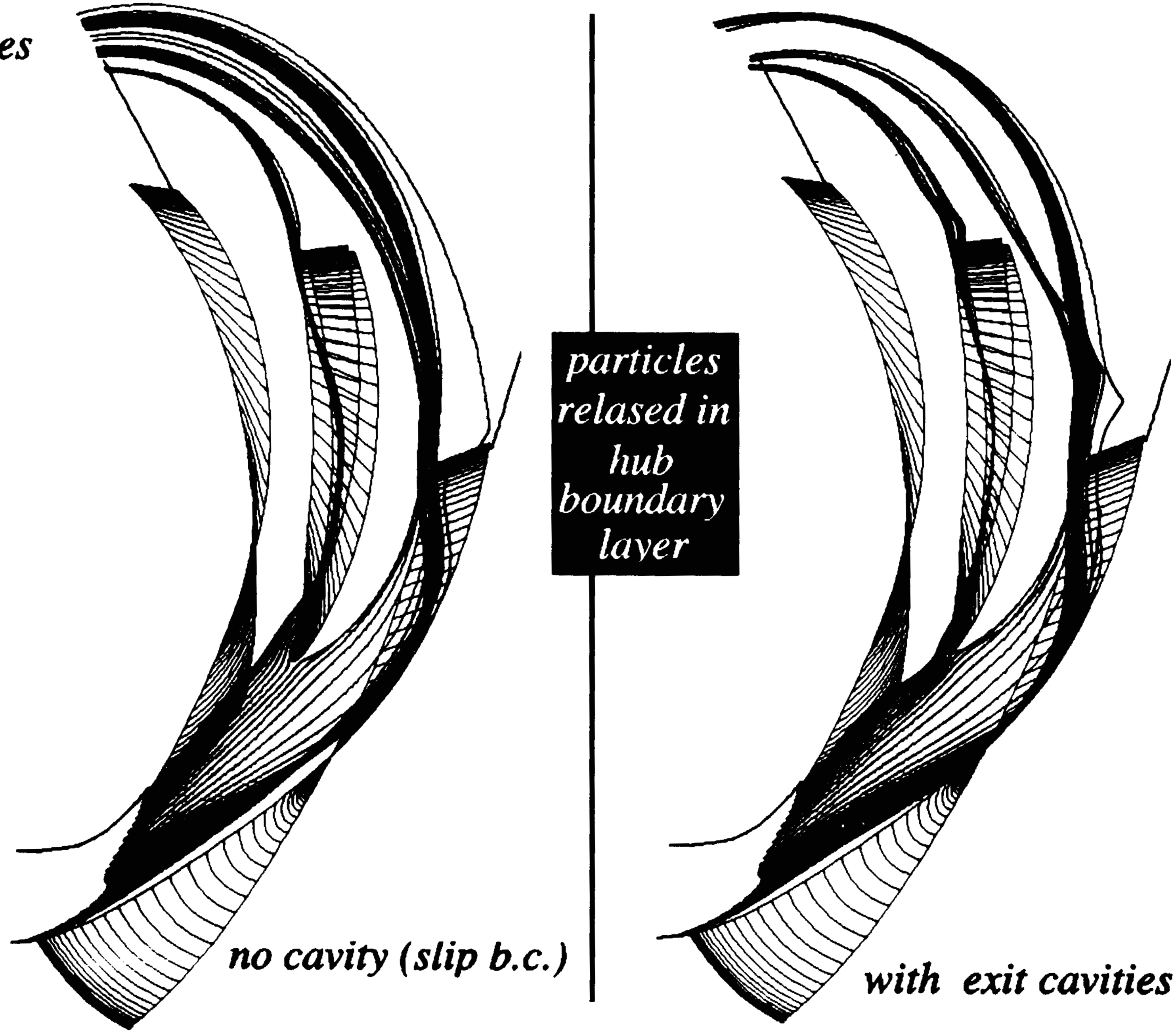

Advanced Impeller Concept

particle traces colored by relative total velocity magnitude

total velocity

0.00000
0.05000
0.10000
0.15000
0.20000
0.25000
0.30000
0.35000
0.40000
0.45000
0.50000
0.55000
0.60000
0.65000
0.70000
0.75000
0.80000
0.85000
0.90000
0.95000
1.00000
1.05000
1.10000
1.15000
1.20000
1.25000
1.30000
1.35000
1.40000
1.45000
1.50000
1.55000
1.60000

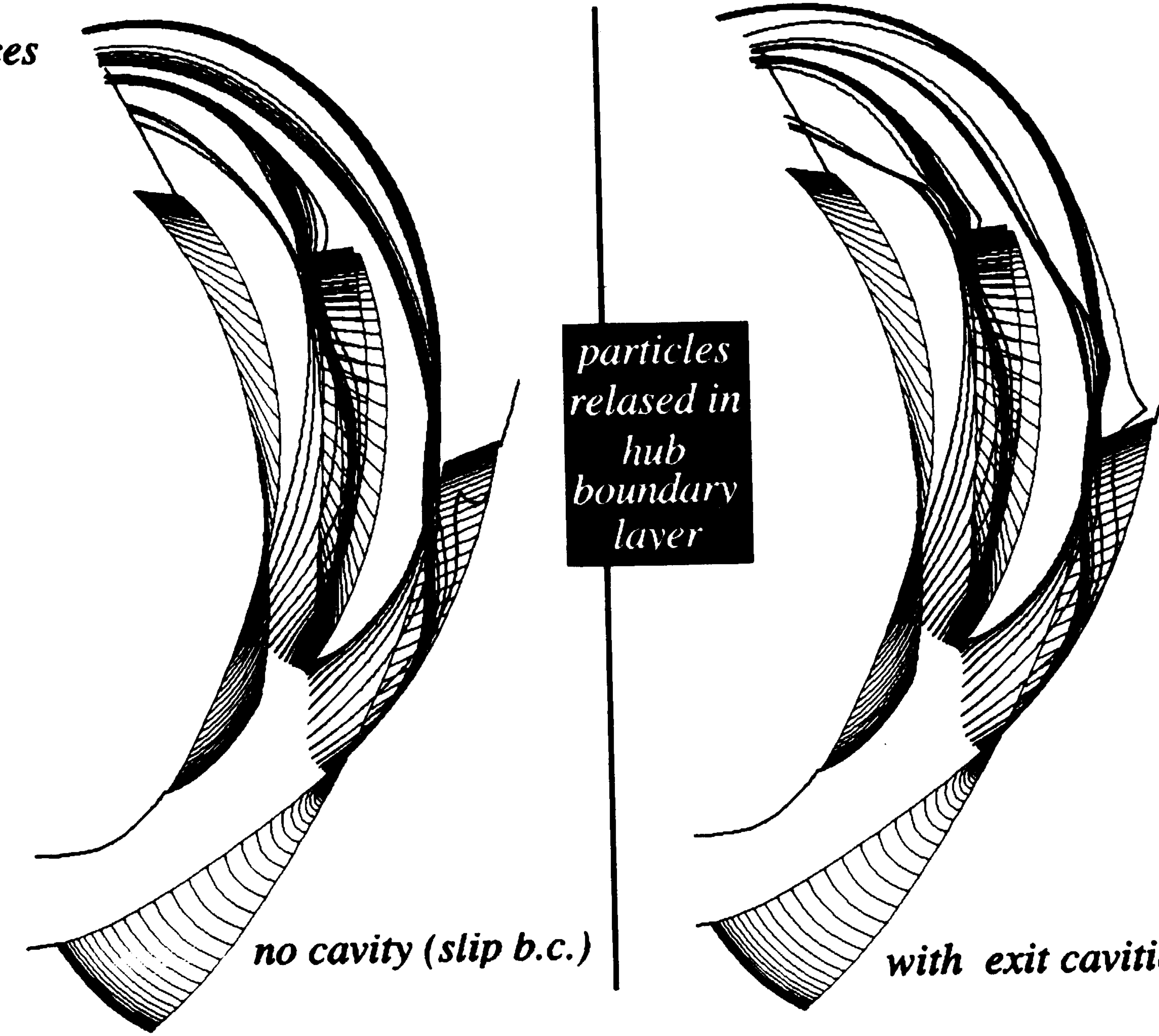

Advanced Impeller Concept

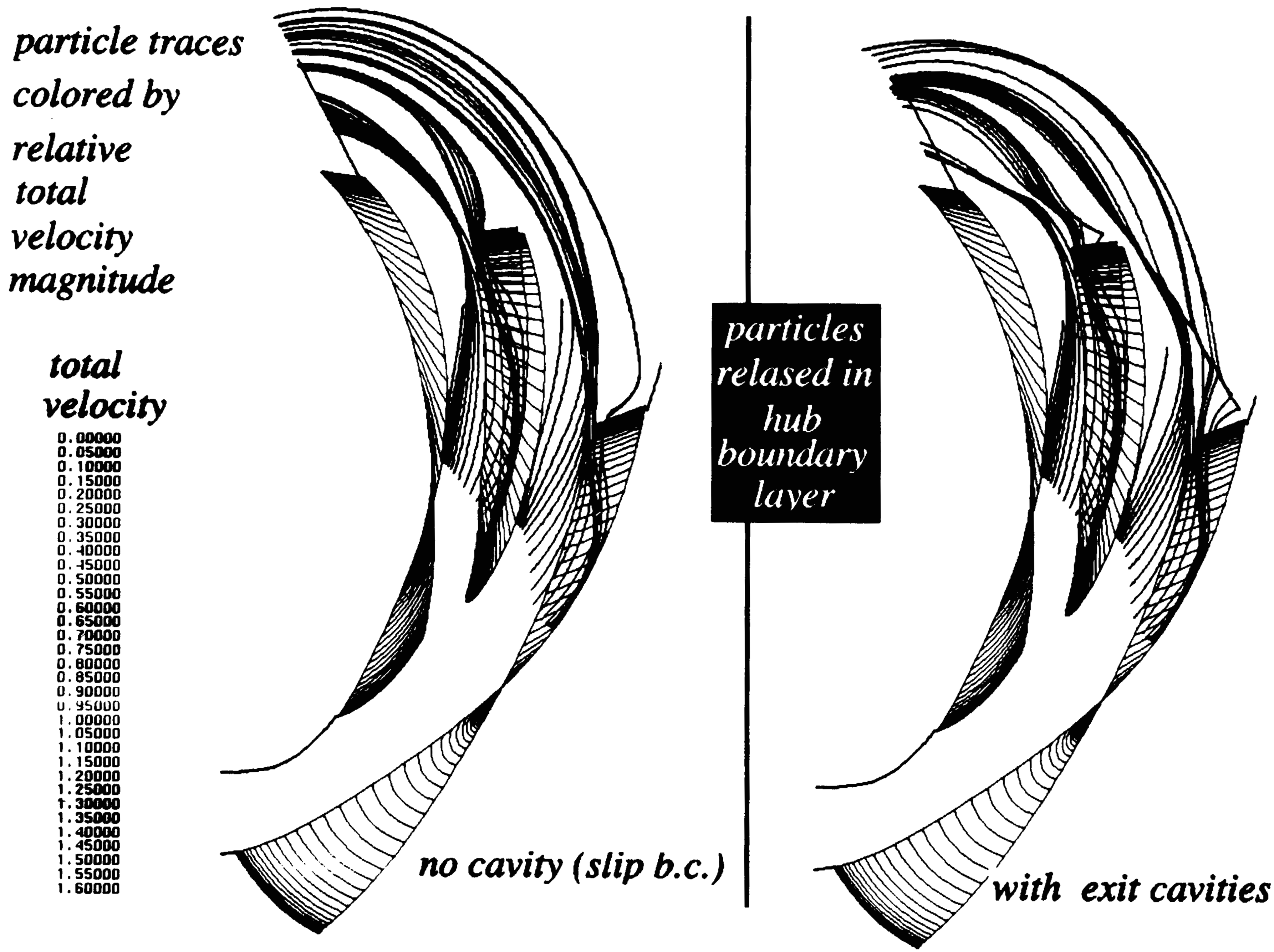

Advanced Impeller Concept

particle traces colored by relative total velocity magnitude

total velocity

0.00000
0.05000
0.10000
0.15000
0.20000
0.25000
0.30000
0.35000
0.40000
0.45000
0.50000
0.55000
0.60000
0.65000
0.70000
0.75000
0.80000
0.85000
0.90000
[illegible]
1.00000
1.05000
1.10000
1.15000
1.20000
1.25000
1.30000
1.35000
1.40000
1.45000
1.50000
1.55000
1.60000

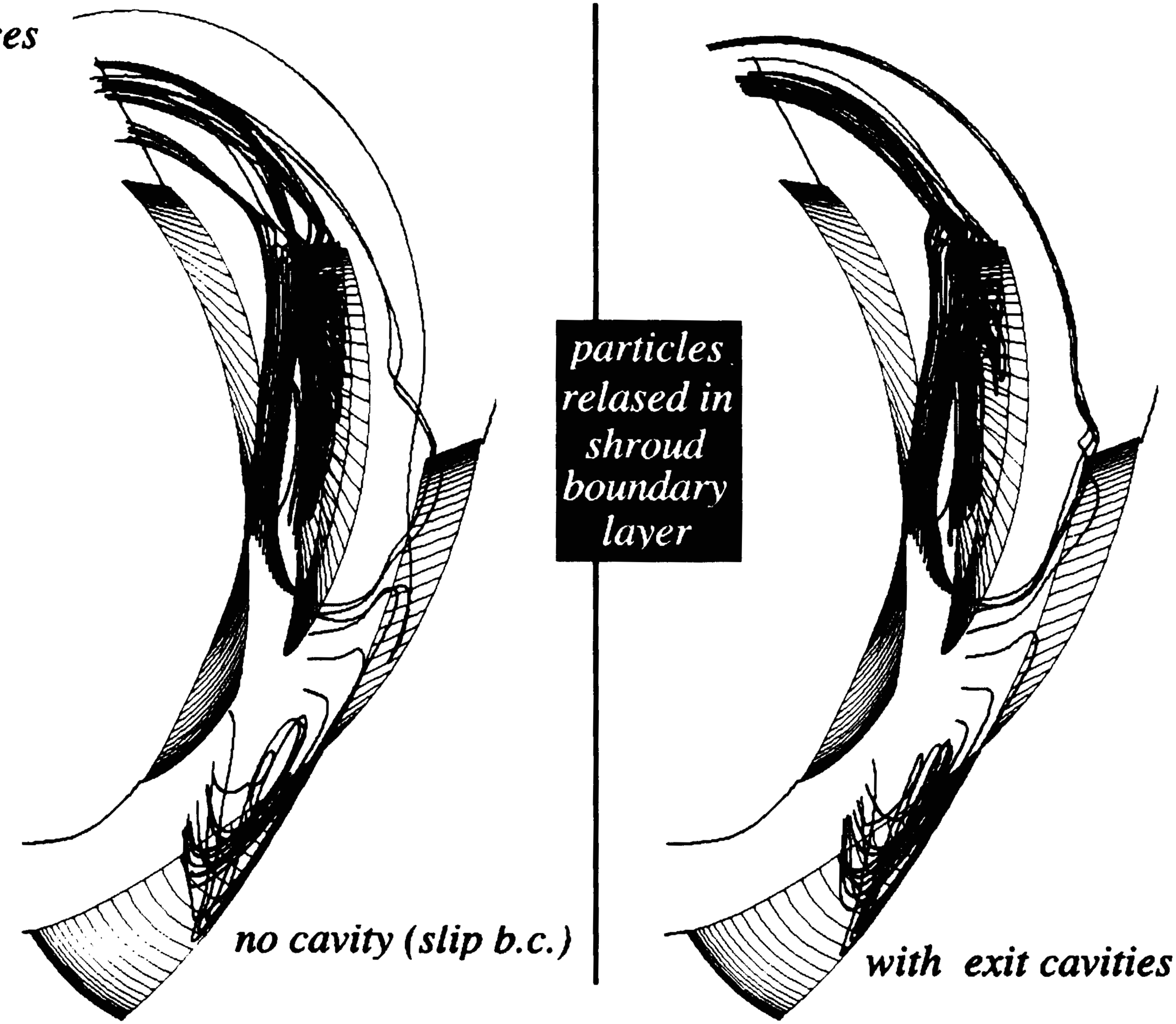

Advanced Impeller Concept

particle traces colored by relative total velocity magnitude

total velocity

0.00000
0.05000
0.10000
0.15000
0.20000
0.25000
0.30000
0.35000
0.40000
0.45000
0.50000
0.55000
0.60000
0.65000
0.70000
0.75000
0.80000
0.85000
0.90000
0.95000
1.00000
1.05000
1.10000
1.15000
1.20000
1.25000
1.30000
1.35000
1.40000
1.45000
1.50000
1.55000
1.60000

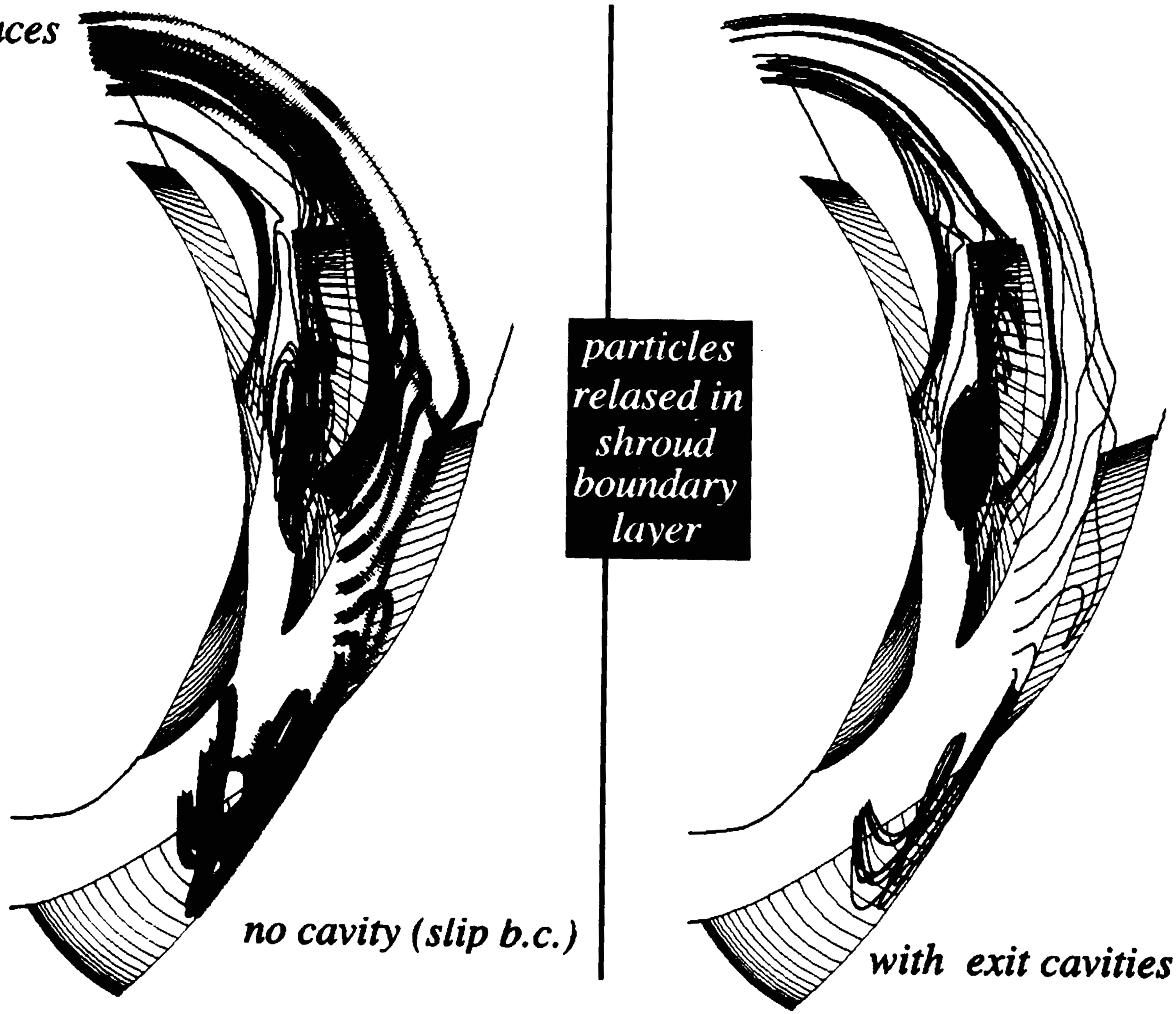

Summary

- Solution procedure for rocket engine pump analysis was validated using benchmark problems.
- Preliminary comparison of 11 inch SSME-HPFTP impeller results show good agreement with the available experimental data.
- Advanced impeller design was analyzed with the conditions obtained from experiments The effect of exit cavities was shown at the impeller exit plane.
- Future work will focus on impeller-diffuser interaction and unsteady rotor-stator interaction.

N95- 23628

3 4/ p- 23

THE INFLUENCE OF SWIRL BRAKES AND A TIP DISCHARGE ORIFICE ON THE ROTORDYNAMIC FORCES GENERATED BY DISCHARGE-TO-SUCTION LEAKAGE FLOWS IN SHROUDED CENTRIFUGAL PUMPS

J. M. Sivo, A. J. Acosta, C. E. Brennen, T. K. Caughey

California Institute of Technology
Division of Engineering and Applied Science
Pasadena, California 91125

ABSTRACT

Recent experiments conducted in the Rotor Force Test Facility at the California Institute of Technology have examined the effects of a tip leakage restriction and swirl brakes on the rotordynamic forces due to leakage flows on an impeller undergoing a prescribed circular whirl. The experiments simulate the leakage flow conditions and geometry of the Alternate Turbopump Design (ATD) of the Space Shuttle High Pressure Oxygen Turbopump and are critical to evaluating the pump's rotordynamic instability problems.

Previous experimental and analytical results have shown that discharge-to-suction leakage flows in the annulus of a shrouded centrifugal pump contribute substantially to the fluid induced rotordynamic forces. Also, previous experiments have shown that leakage inlet (pump discharge) swirl can increase the cross-coupled stiffness coefficient and hence increase the range of positive whirl for which the tangential force is destabilizing. In recent experimental work, the present authors demonstrated that when the swirl velocity within the leakage path is reduced by the introduction of ribs or swirl brakes, then a substantial decrease in both the destabilizing normal and tangential forces could be achieved.

Motivation for the present research is that previous experiments have shown that restrictions such as wear rings or orifices at pump inlets affect the leakage forces. Recent pump designs such as the Space Shuttle Alternate Turbopump Design (ATD) utilize tip orifices at discharge for the purpose of establishing axial thrust balance. The ATD has experienced rotordynamic instability problems and one may surmise that these tip discharge orifices may also have an important effect on the normal and tangential forces in the plane of impeller rotation. The present study determines if such tip leakage restrictions contribute to undesirable rotordynamic forces.

Additional motivation for the present study is that the widening of the leakage path annular clearance and the installation of swirl brakes in the ATD has been proposed to solve its instability problems. The present study assesses the effect of such a design modification on the rotordynamic forces.

The experimental apparatus consists of a solid or dummy impeller, a housing instrumented for pressure measurements, a rotating dynamometer and an eccentric whirl mechanism. The solid impeller is used so that leakage flow contributions to the forces are measured, but the main throughflow contributions are not experienced. The inner surface of the housing has been modified to accommodate meridional ribs or swirl brakes within the leakage annulus. In addition, the housing has been modified to accommodate a discharge orifice that qualitatively simulates one side of the balance piston orifice of the Space Shuttle ATD.

Results indicate the detrimental effects of a discharge orifice and the beneficial effects of brakes. Plots of the tangential and normal forces versus whirl ratio show a substantial increase in these forces along with destabilizing resonances at some positive whirl ratios when a discharge orifice is added. When brakes are added, some of the detrimental effects of the orifice are reduced. For the tangential force, a plot versus whirl ratio shows a significant reduction and a destabilizing resonance appears to be eliminated. For the normal force, although the overall force is not reduced, again a destabilizing resonance appears to be eliminated.

THE INFLUENCE OF SWIRL BRAKES AND A TIP DISCHARGE ORIFICE ON THE ROTORDYNAMIC FORCES GENERATED BY DISCHARGE-TO-SUCTION LEAKAGE FLOWS IN SHROUDED CENTRIFUGAL PUMPS

Joseph M. Sivo

California Institute of Technology
Division of Engineering and Applied Science
Pasadena, California 91125

4/20/93

A. J. Acosta

C. E. Brennen

T. K. Caughey

OUTLINE

- Background
- Rotordynamic Forces and Coefficients
- Test Apparatus
- Phase 1 Tests

  Effect of Swirl Brakes
- Phase 2 Tests

  Effect of Tip Discharge Orifice

  Effect of Brakes with Tip Discharge Orifice
- Conclusions
- Future Work

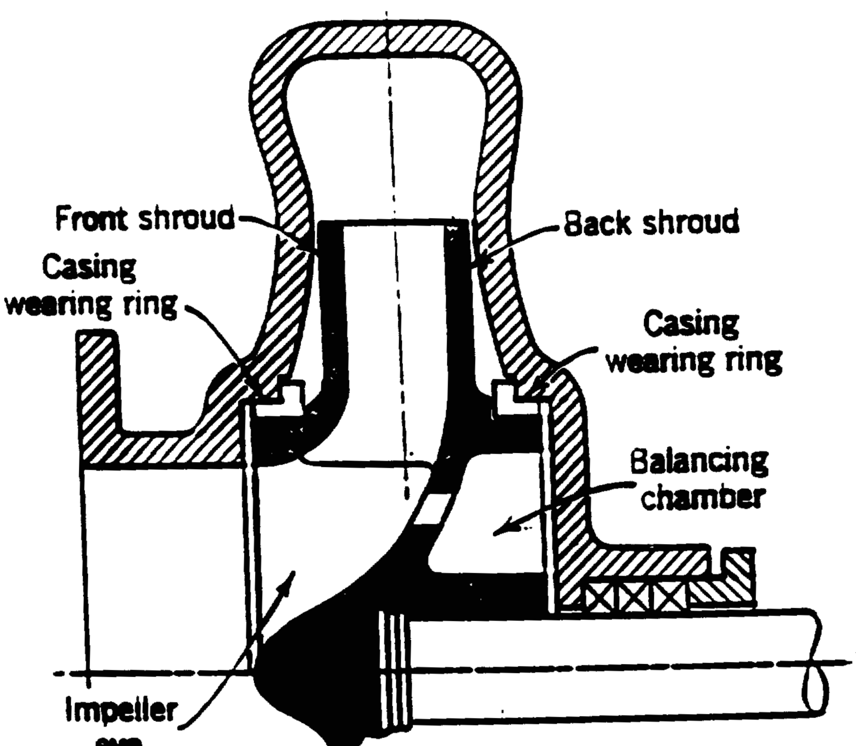

Single-suction impeller with a balancing chamber on the back.

ATD - HIGH PRESSURE OXIDIZER TURBOPUMP

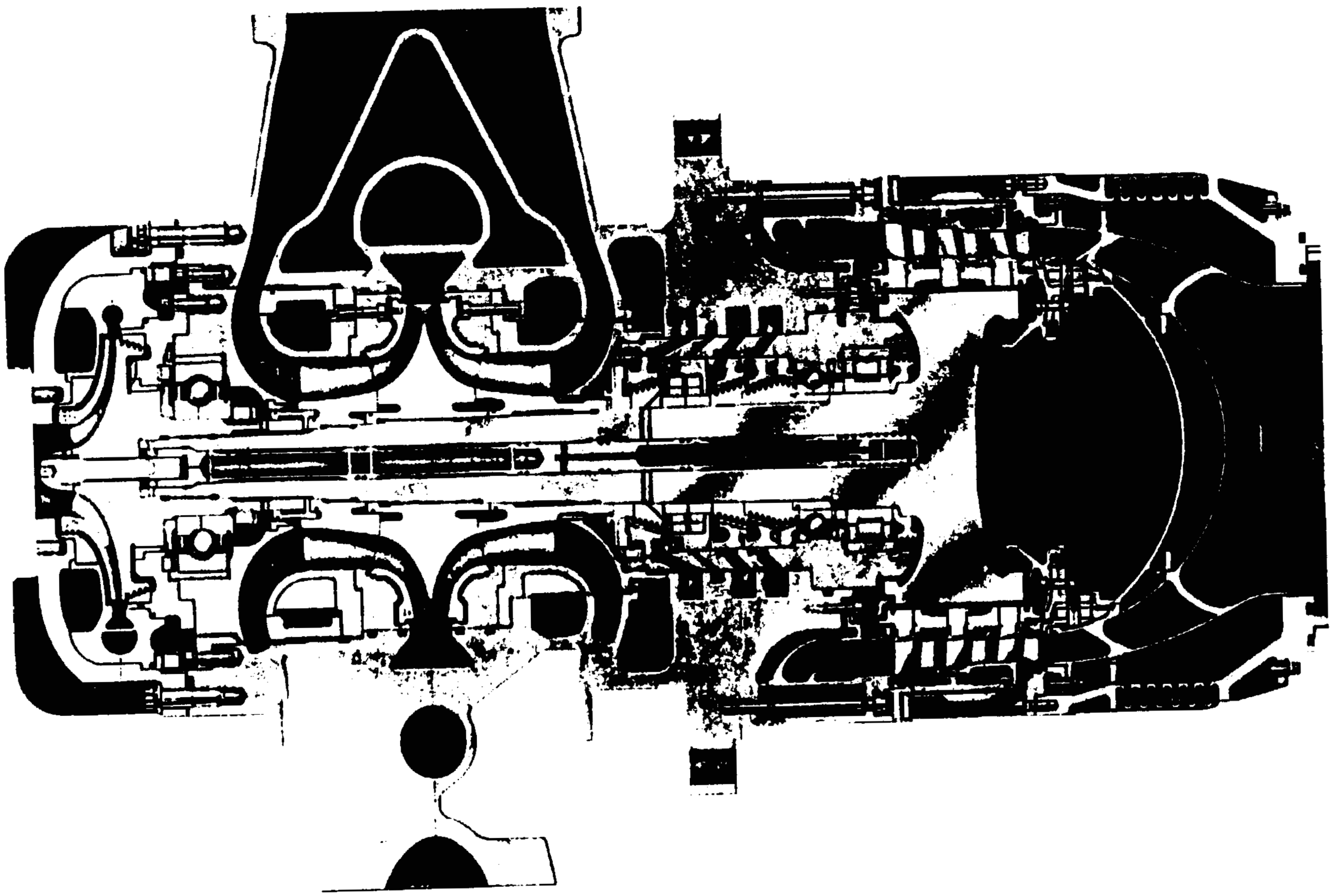

AVL380541 901810

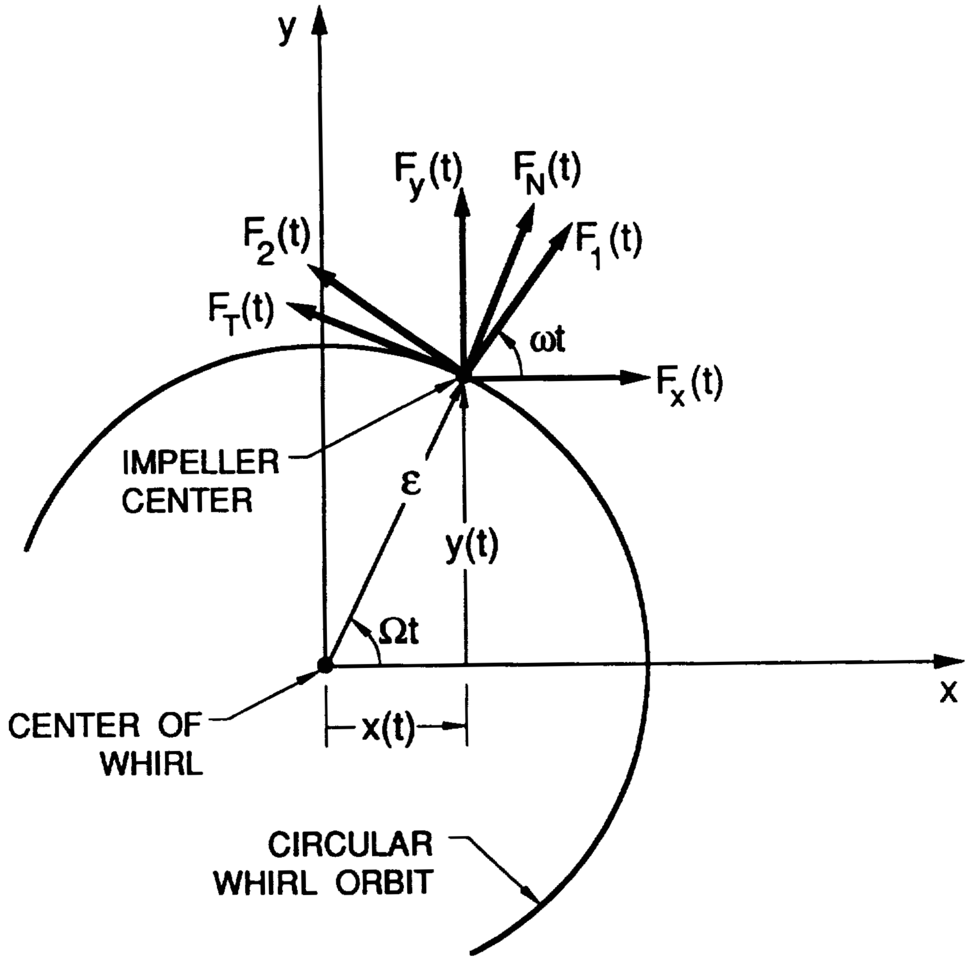

$$\begin{pmatrix} F_x(t) \\ F_y(t) \end{pmatrix} = \begin{pmatrix} F_{ox} \\ F_{oy} \end{pmatrix} + [A] \begin{pmatrix} x(t) \\ y(t) \end{pmatrix}$$

For a circular whirl orbit:

$$x^*(t) = \varepsilon cos(\Omega t)$$
$$y^*(t) = \varepsilon sin(\Omega t)$$

$$F_n^*(t) = \frac{1}{2}(A_{xx}^* + A_{yy}^*)\varepsilon$$

$$F_t^*(t) = \frac{1}{2}(-A_{xy}^* + A_{yx}^*)\varepsilon$$

ROTORDYNAMIC COEFFICIENTS

$$F_n = M\left(\frac{\Omega}{\omega}\right)^2 - c\left(\frac{\Omega}{\omega}\right) - K$$

$$F_t = -C\left(\frac{\Omega}{\omega}\right) + k$$

M = Direct Added Mass

C = Direct Damping

c = Cross-coupled Damping

K = Direct Stiffness

k = Cross-coupled Stiffness

k/C = Whirl Ratio

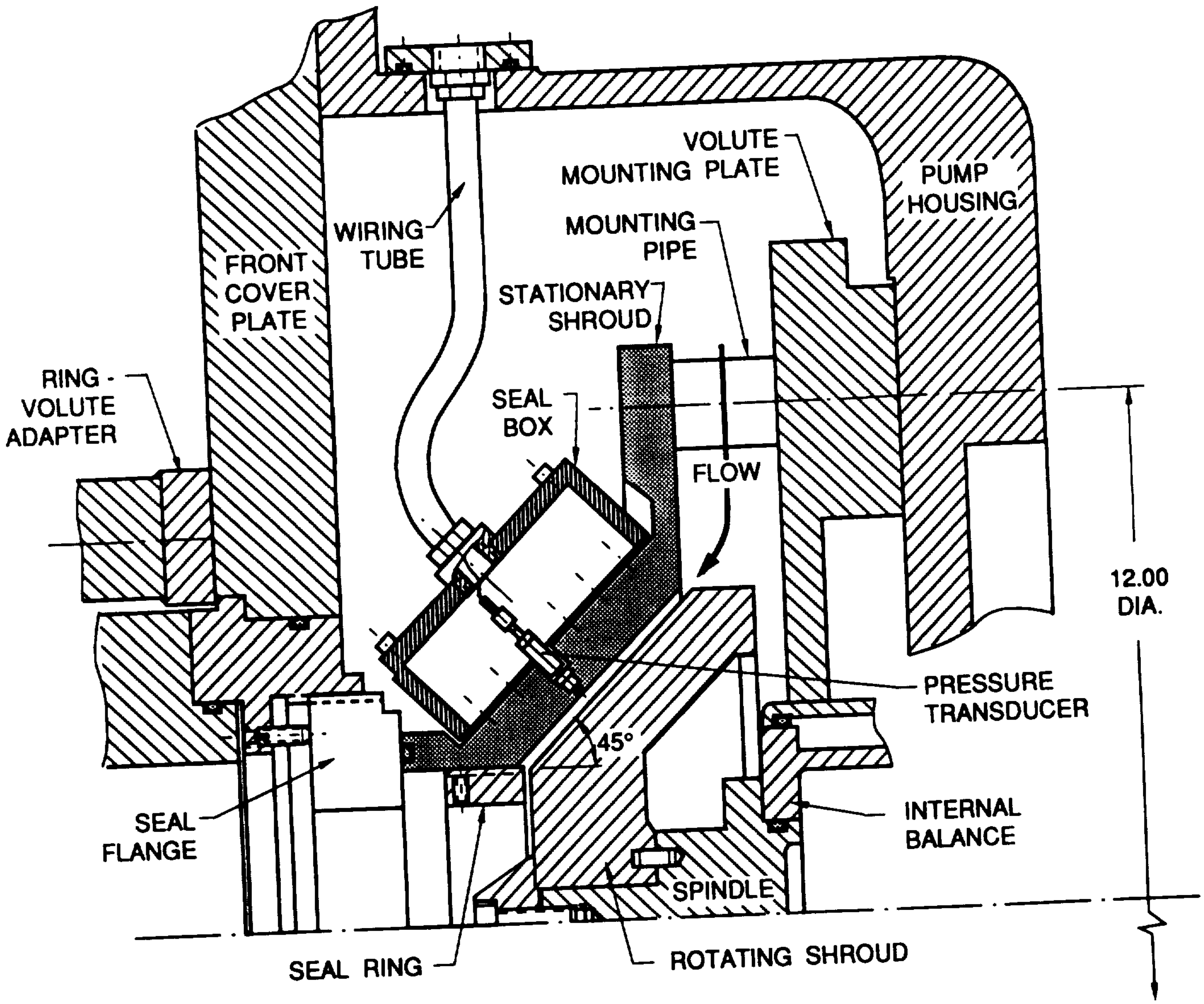

CALTECH LEAKAGE FORCE TEST APPARATUS

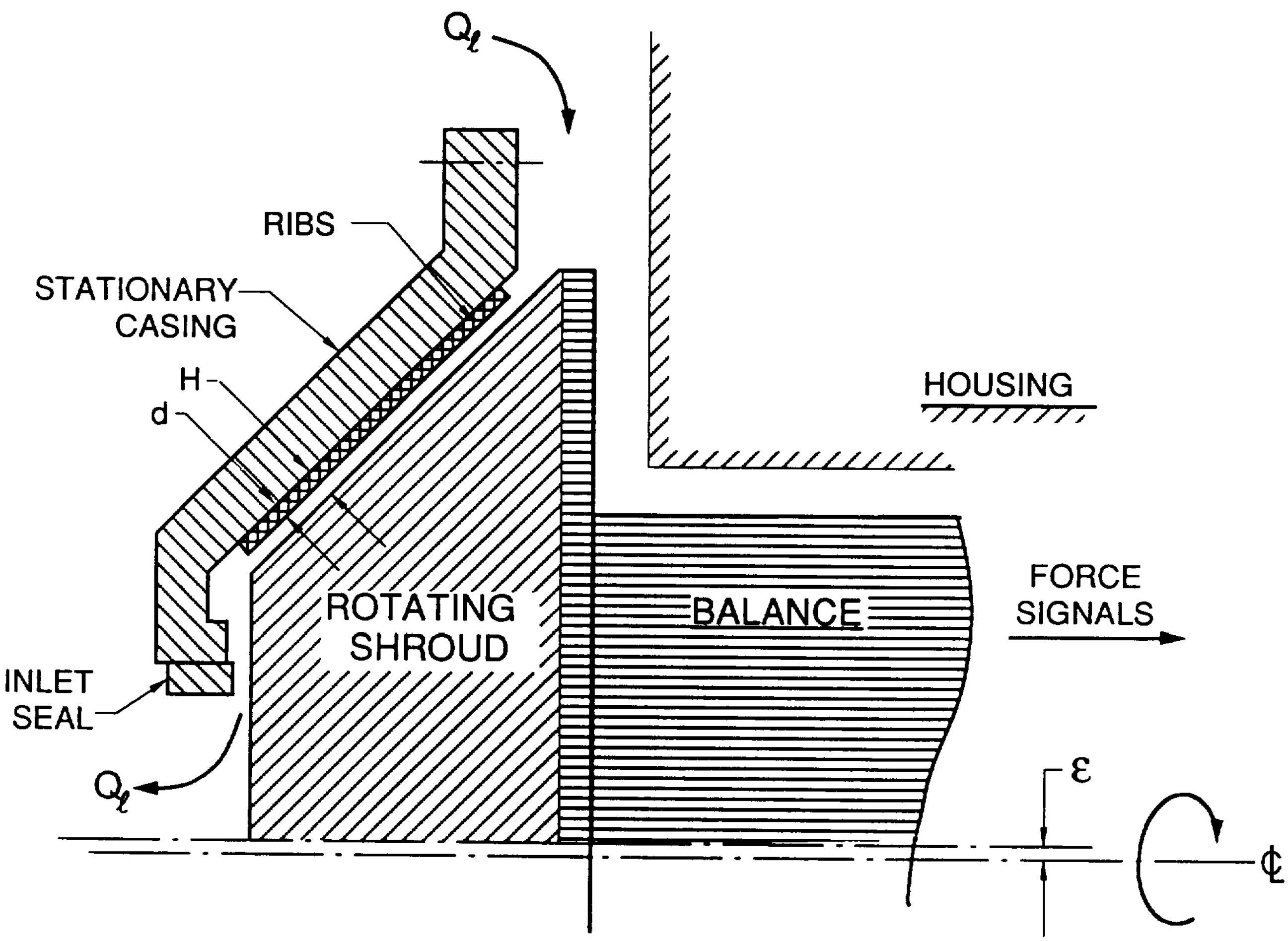

Q_ℓ
RIBS
STATIONARY CASING
H
d
HOUSING
ROTATING SHROUD
BALANCE
FORCE SIGNALS
INLET SEAL
Q_ℓ
ε
℄

TEST MATRIX

Table 1. Tests Without Inlet Swirl

RPM	Ω/ω	Brakes	Q (GPM)	ϕ
1000	−0.9 to +0.9	0	0	0.0
			10	0.026
			20	0.052
			30	0.077
		4	0	0.0
			10	0.026
			20	0.052
			30	0.077
		8	0	0.0
			10	0.026
			20	0.052
			30	0.077
2000	−0.6 to +0.7	0	0	0.0
			10	0.013
			20	0.026
			30	0.039
		4	0	0.0
			10	0.013
			20	0.026
			30	0.039
		8	0	0.0
			10	0.013
			20	0.026
			30	0.039

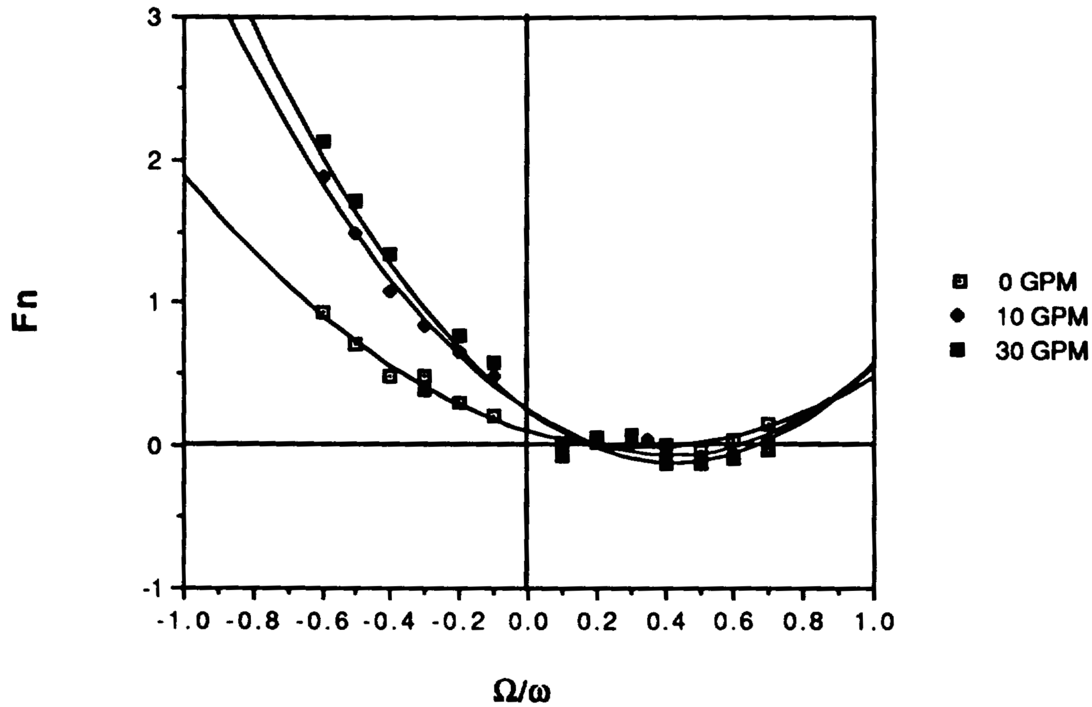

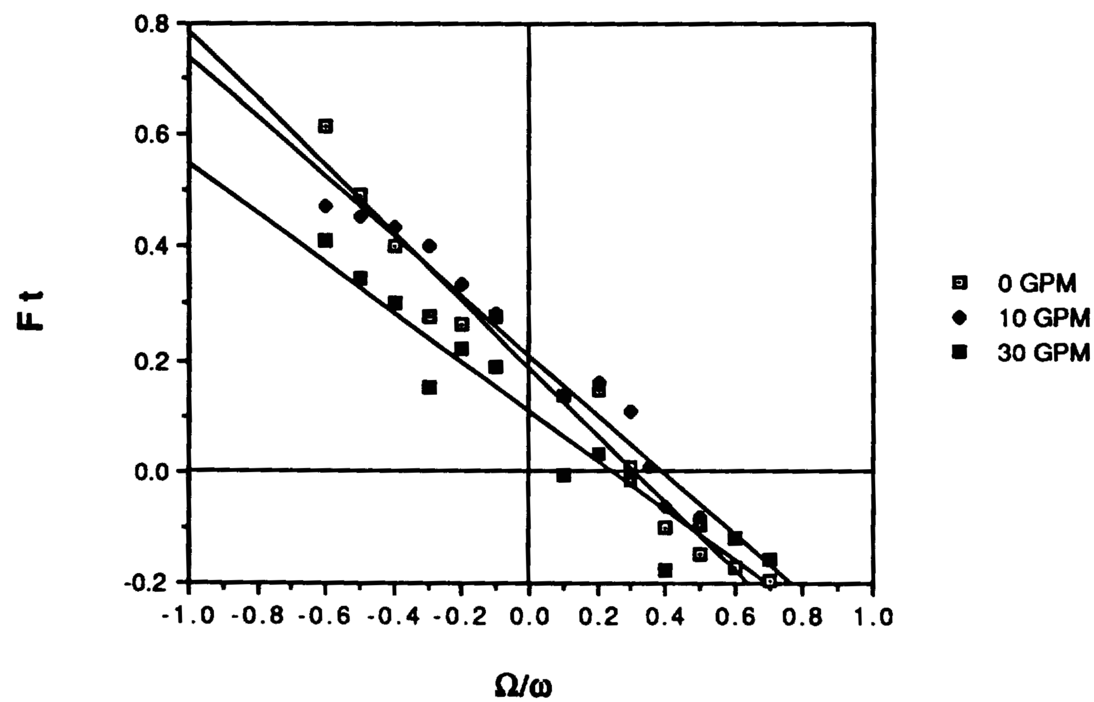

Figure (I) Dimensionless normal and tangential forces at 2000 RPM with 0 swirl brakes and flow rates of 0, 10 and 30 GPM.

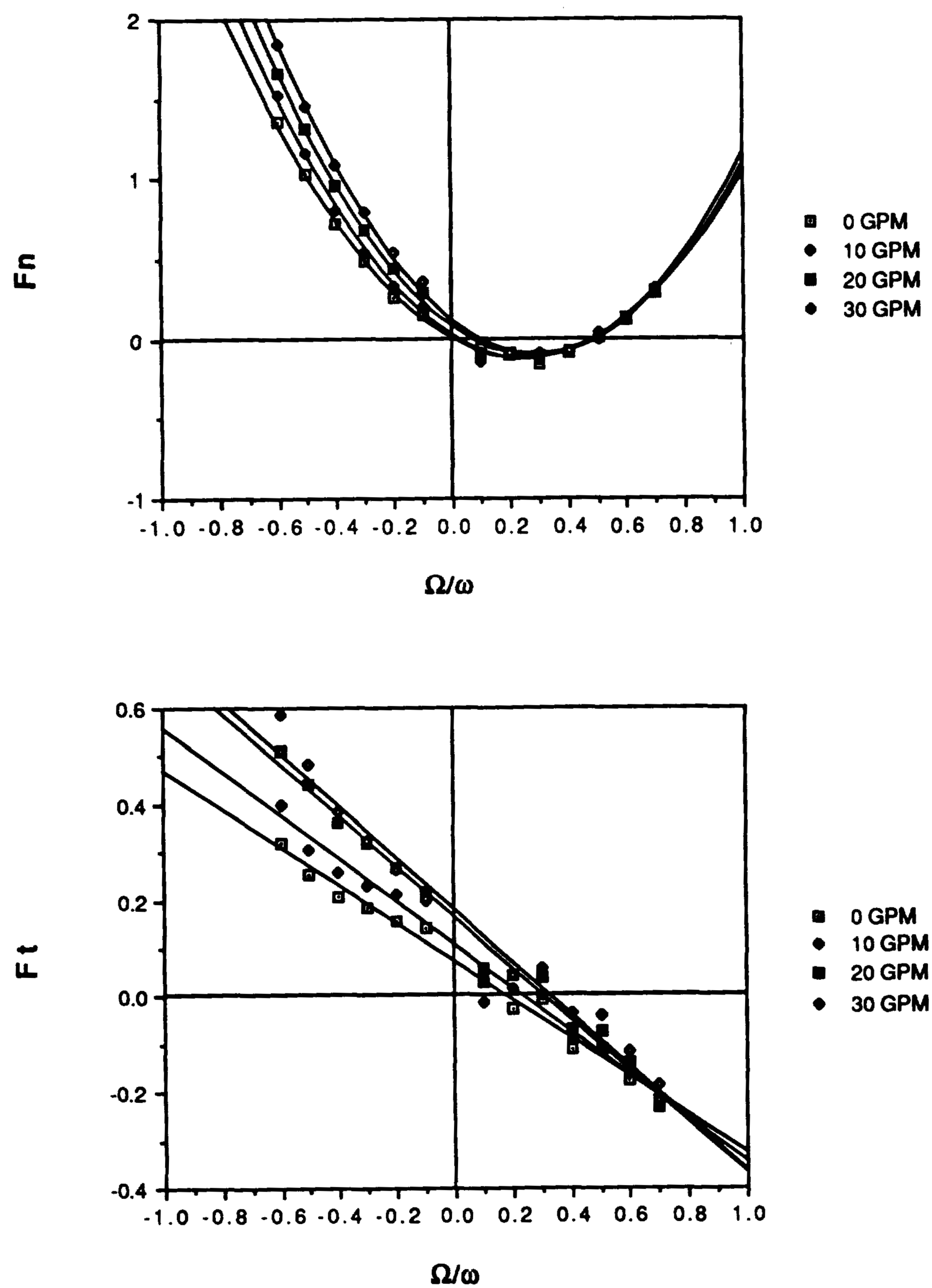

Figure (2) Dimensionless normal and tangential forces at 2000 RPM with 4 swirl brakes and flow rates of 0, 10 and 30 GPM.

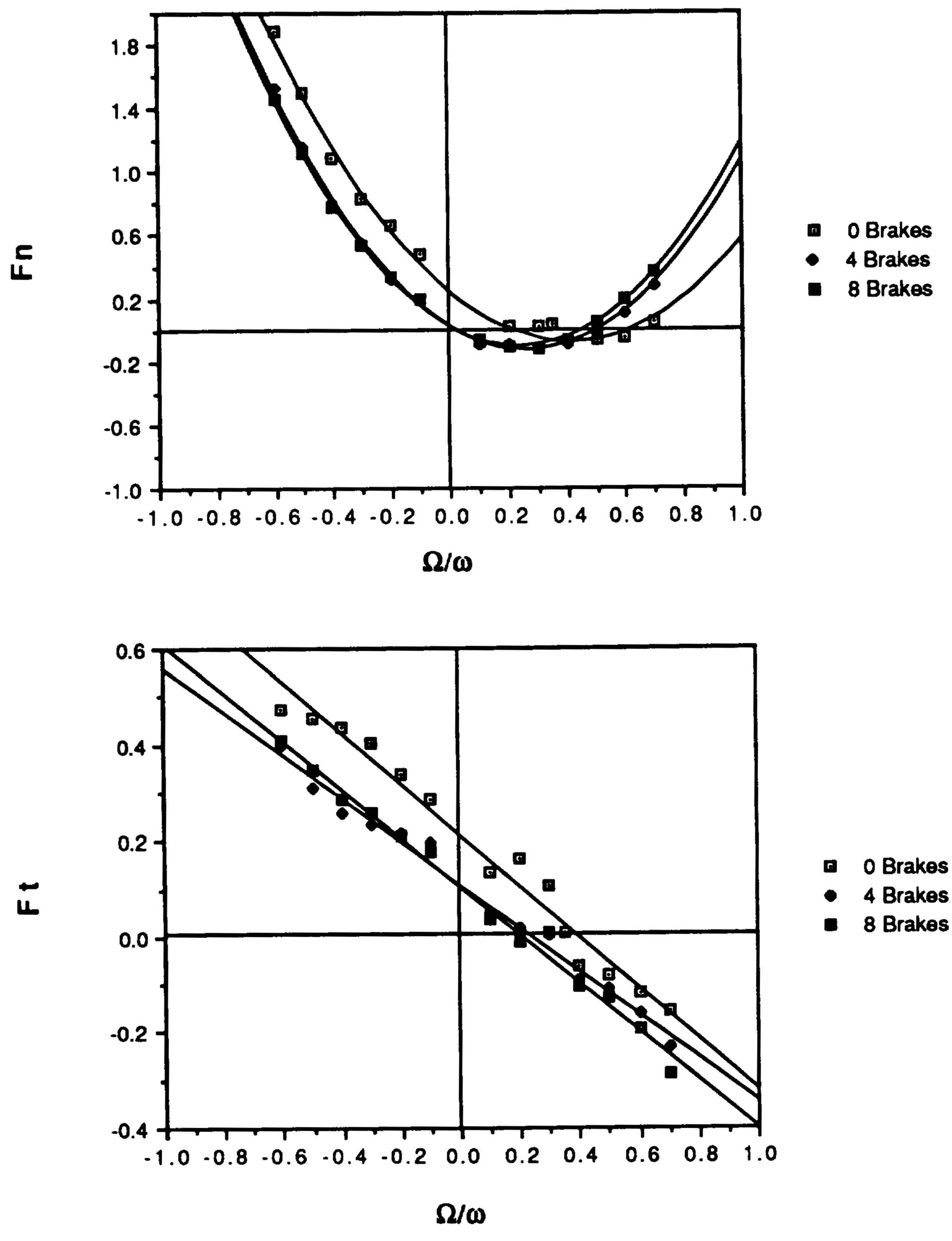

Figure (3) Dimensionless normal and tangential forces at 2000 RPM and a flow rate of 10 GPM for 0, 4 and 8 swirl brakes.

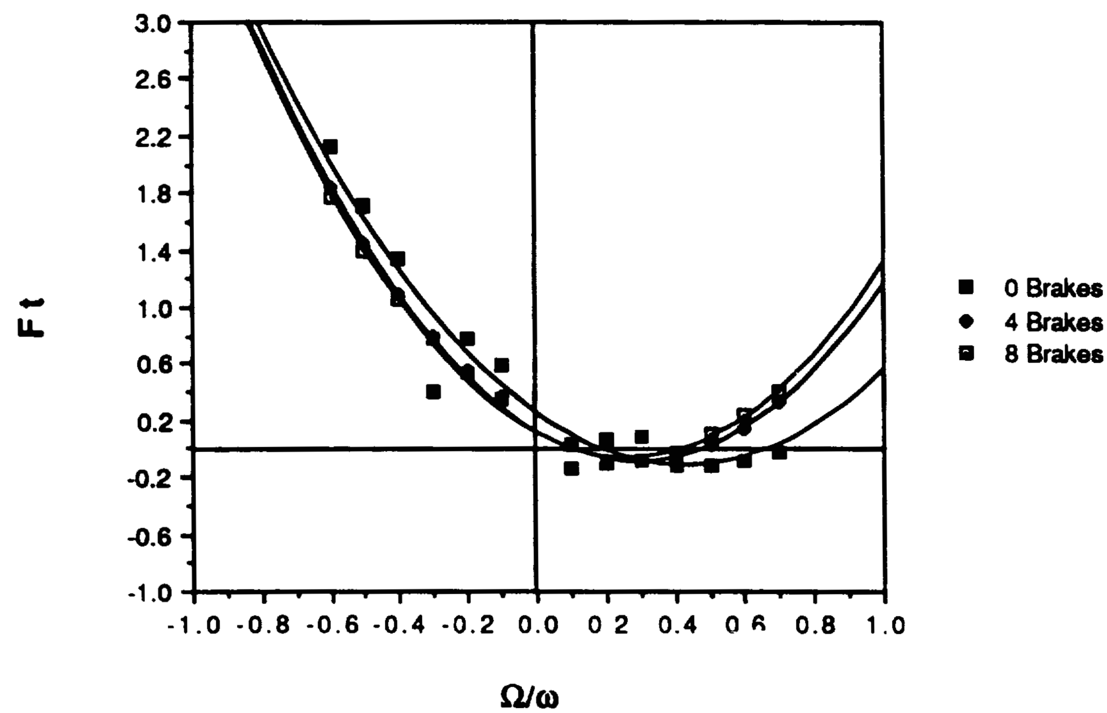

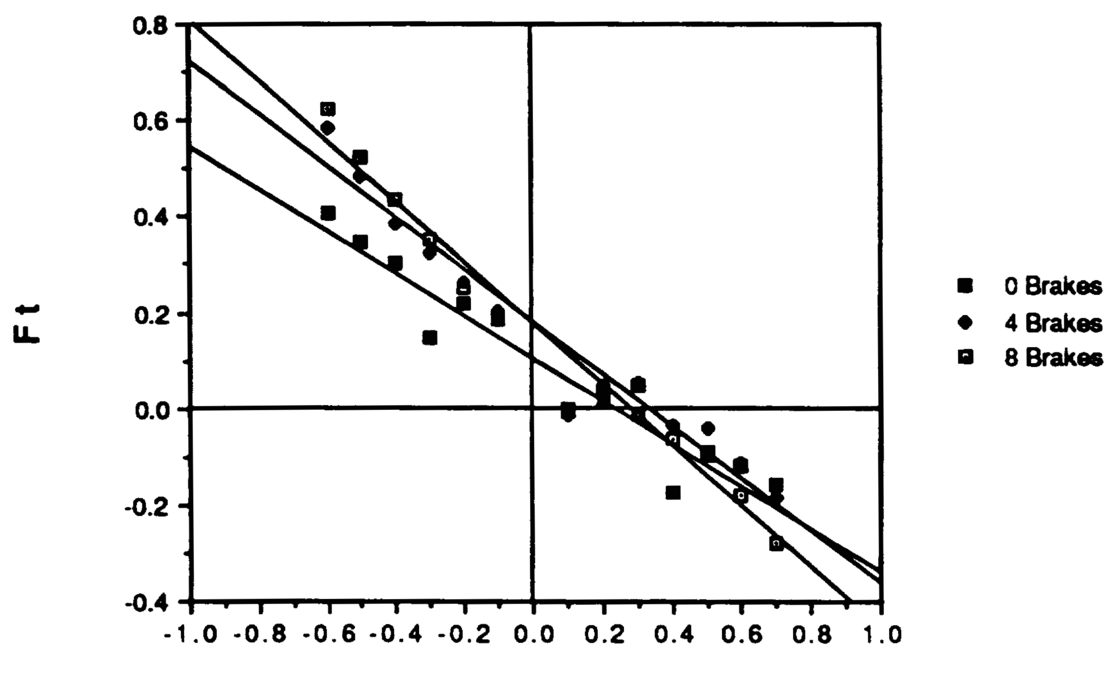

Figure (4) Dimensionless normal and tangential forces at 2000 RPM and a flow rate of 30 GPM for 0, 4 and 8 swirl brakes.

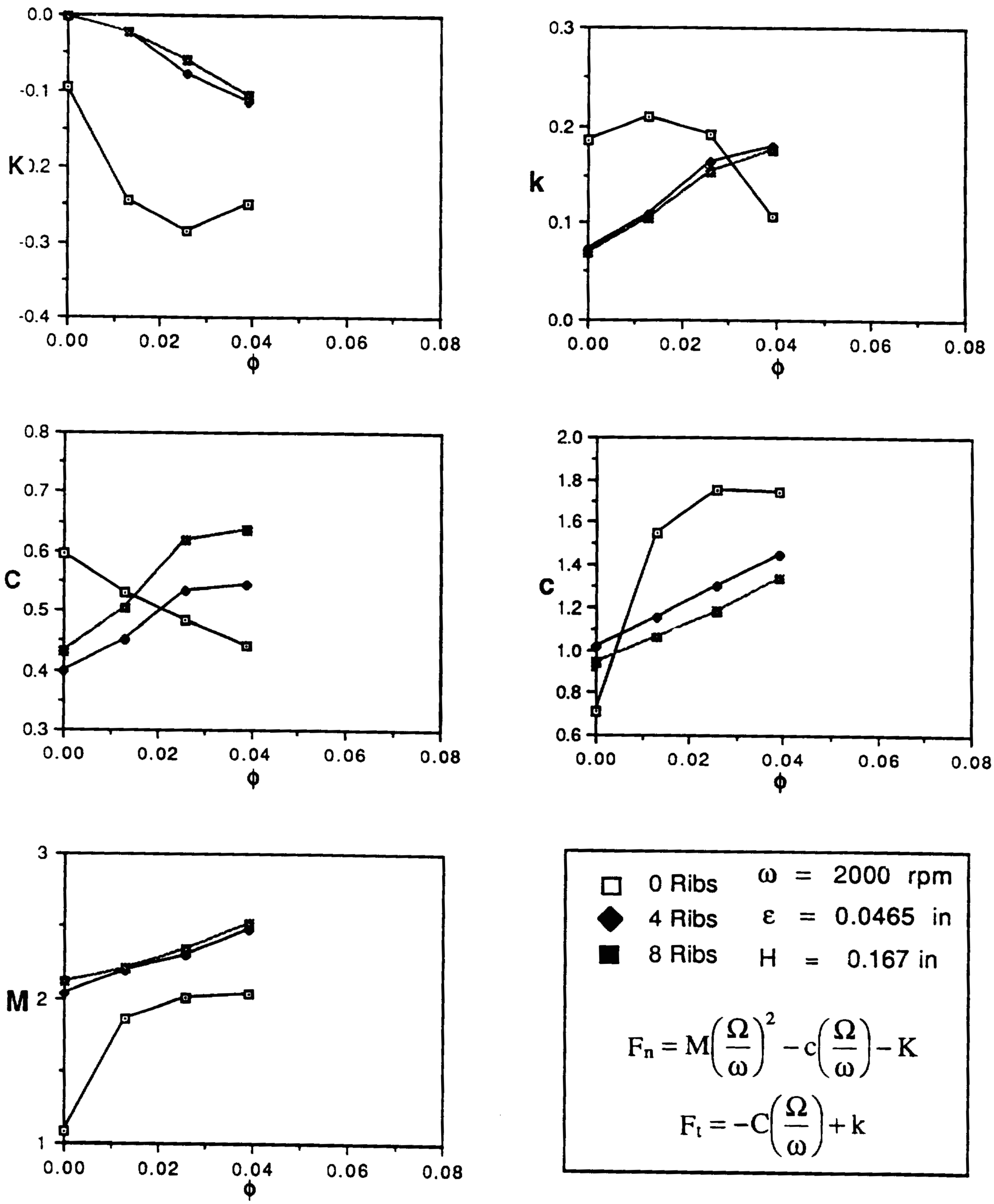

$$F_n = M\left(\frac{\Omega}{\omega}\right)^2 - c\left(\frac{\Omega}{\omega}\right) - K$$

$$F_t = -C\left(\frac{\Omega}{\omega}\right) + k$$

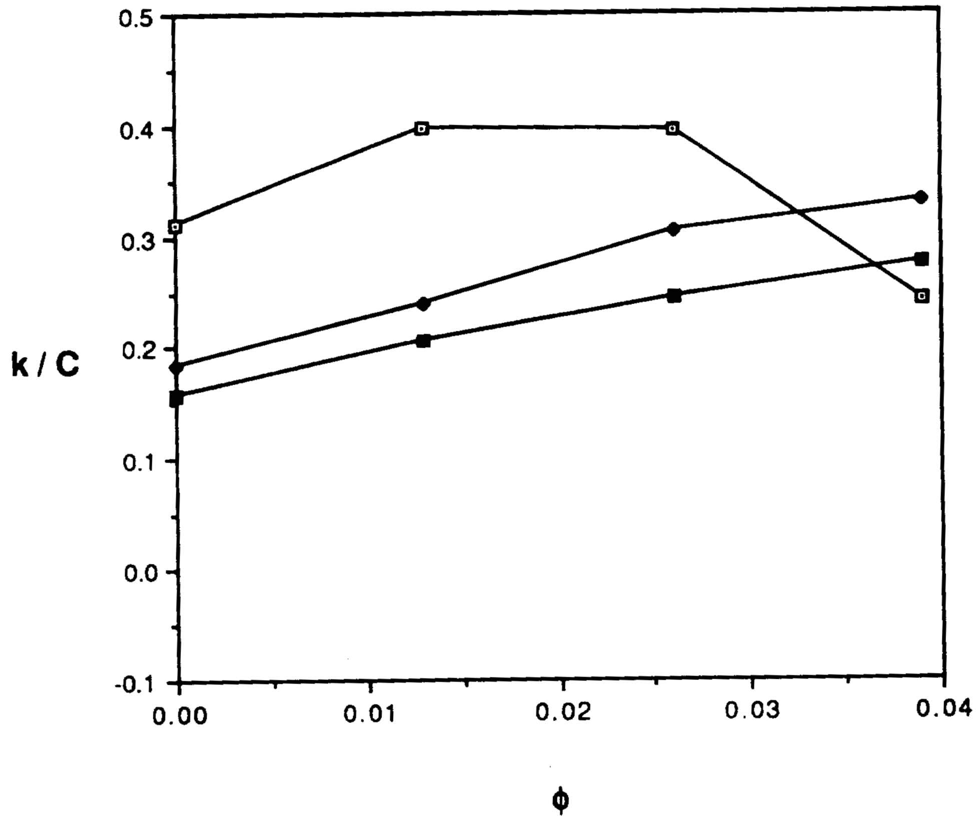

0 Ribs ω = 2000 rpm

4 Ribs ε = 0.0465 in

8 Ribs H = 0.167 in

$$F_n = M\left(\frac{\Omega}{\omega}\right)^2 - c\left(\frac{\Omega}{\omega}\right) - K$$

$$F_t = -C\left(\frac{\Omega}{\omega}\right) + k$$

CONCLUSIONS FOR PHASE 1

1. The addition of brakes reduces the destabilizing normal force for all flow rates tested.

2. For flow rates below $\phi = 0.025$, the addition of brakes reduces the tangential force and whirl ratio.

ATD - HIGH PRESSURE OXIDIZER TURBOPUMP

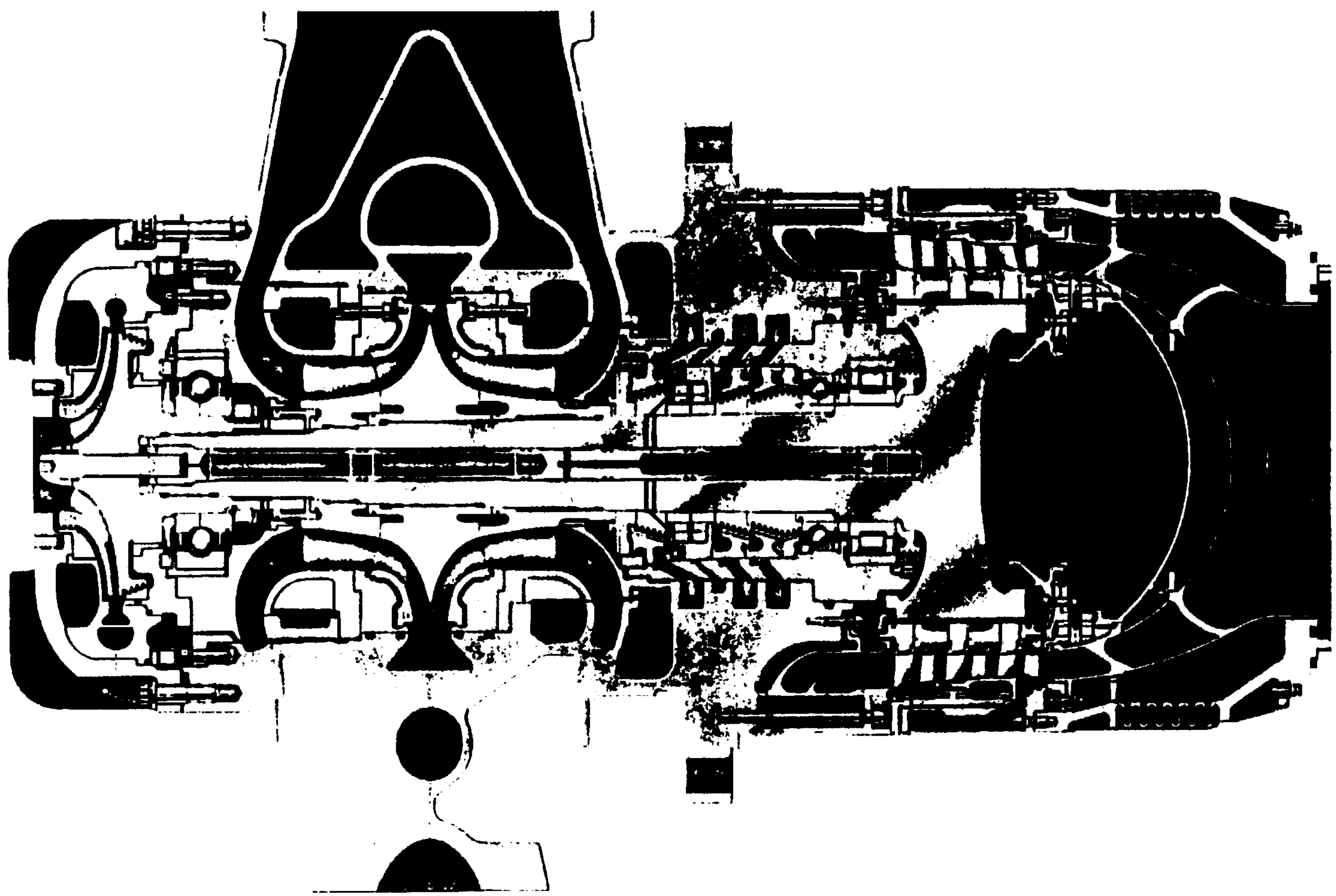

AVL380541 901810

Leakage Inlet Seal for ATD HPOTP

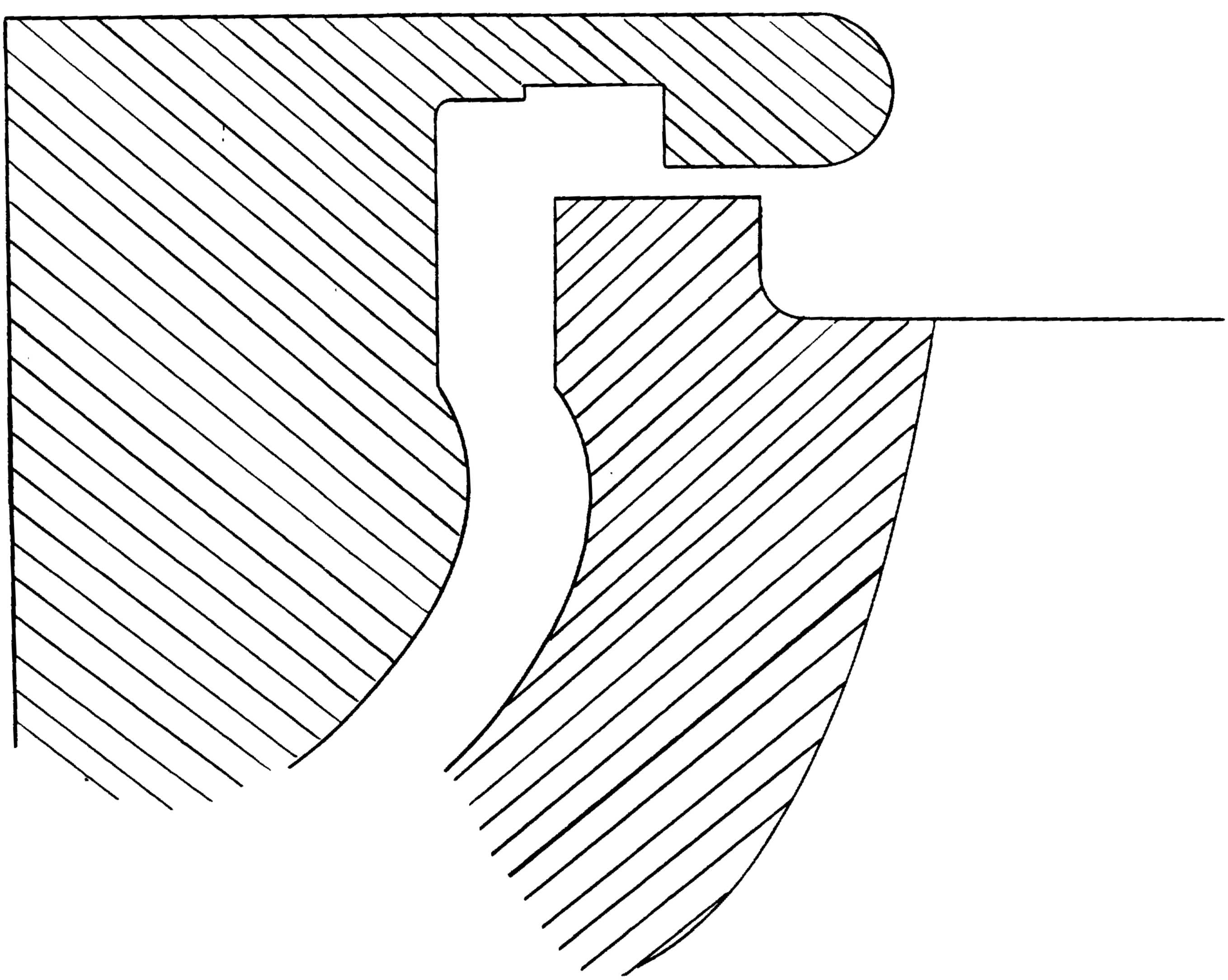

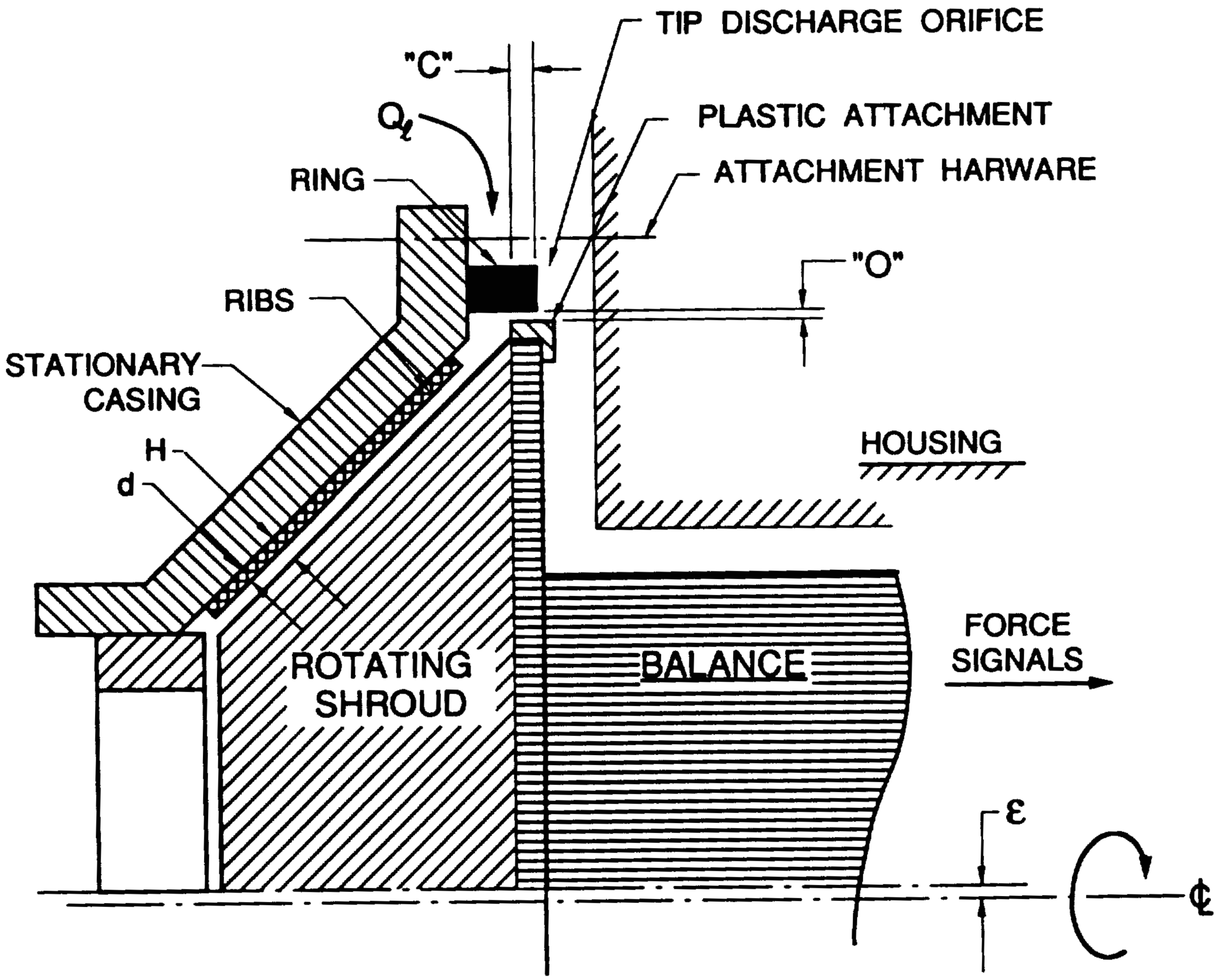

RADIAL TIP DISCHARGE ORIFICE

Comparison Plot (2000 RPM, Face Seal = 0.05 in, 10 GPM)
No Brakes

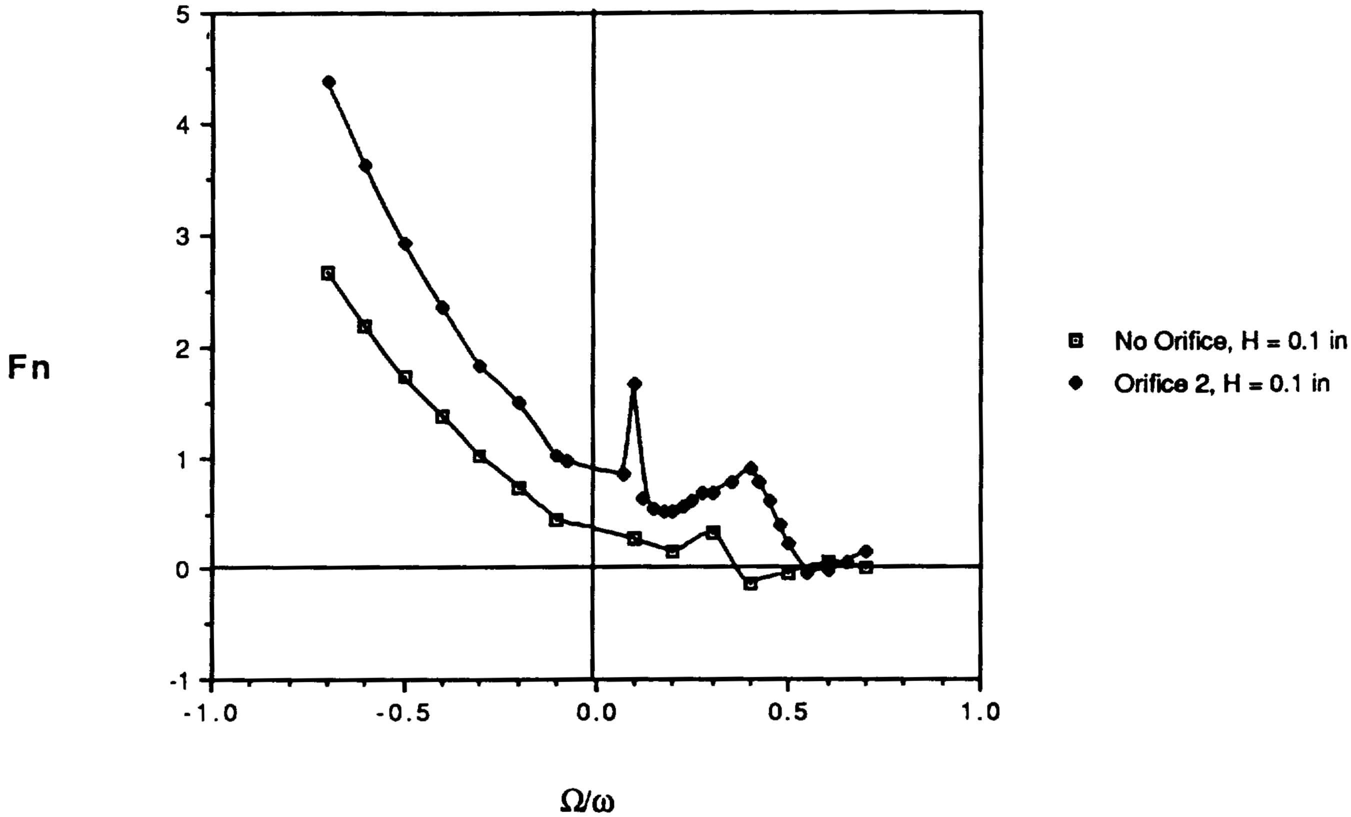

Comparison Plot (2000 RPM, Face Seal = 0.05 in, 10 GPM)
No Brakes

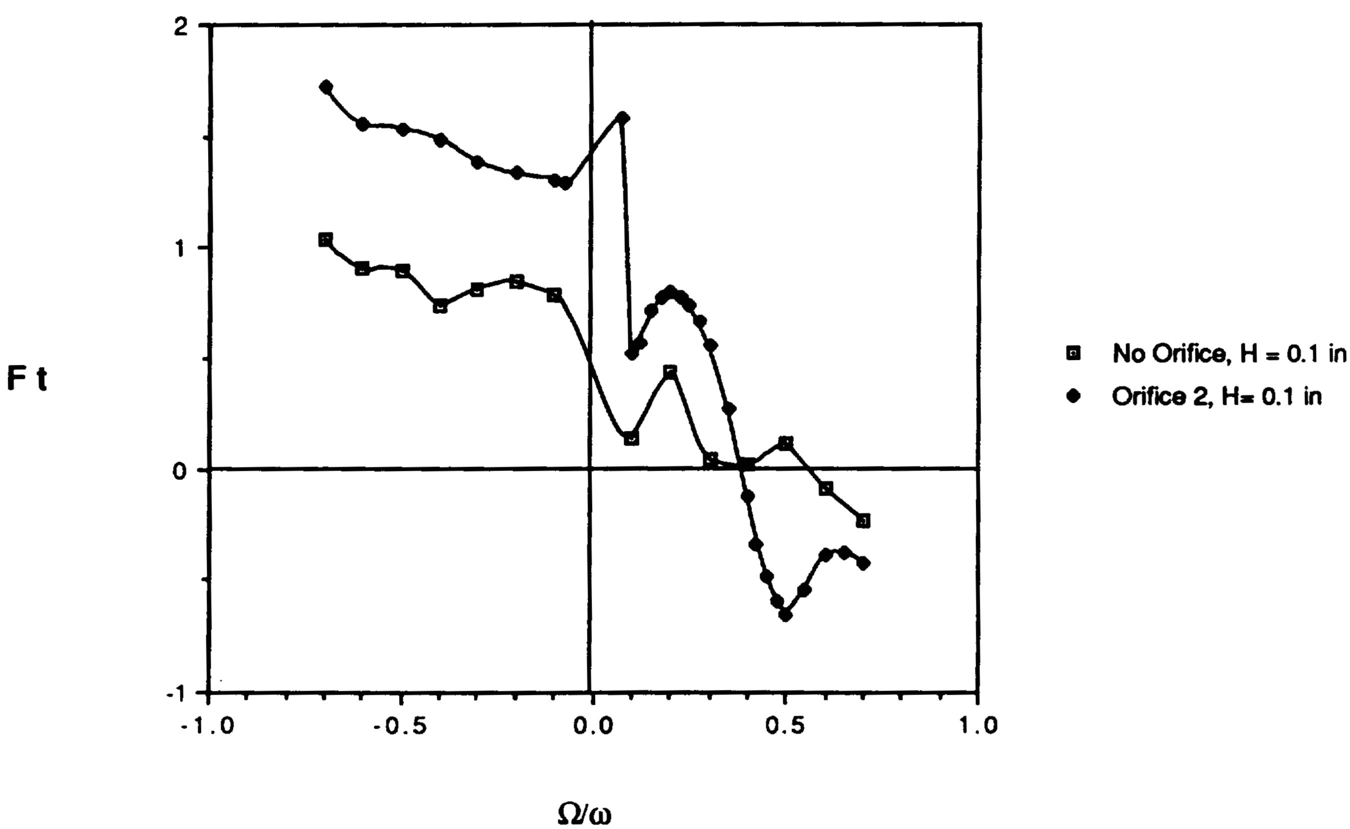

Comparison Plot (2000 RPM, Face Seal = 0.05 in, 10 GPM)
Orifice 2

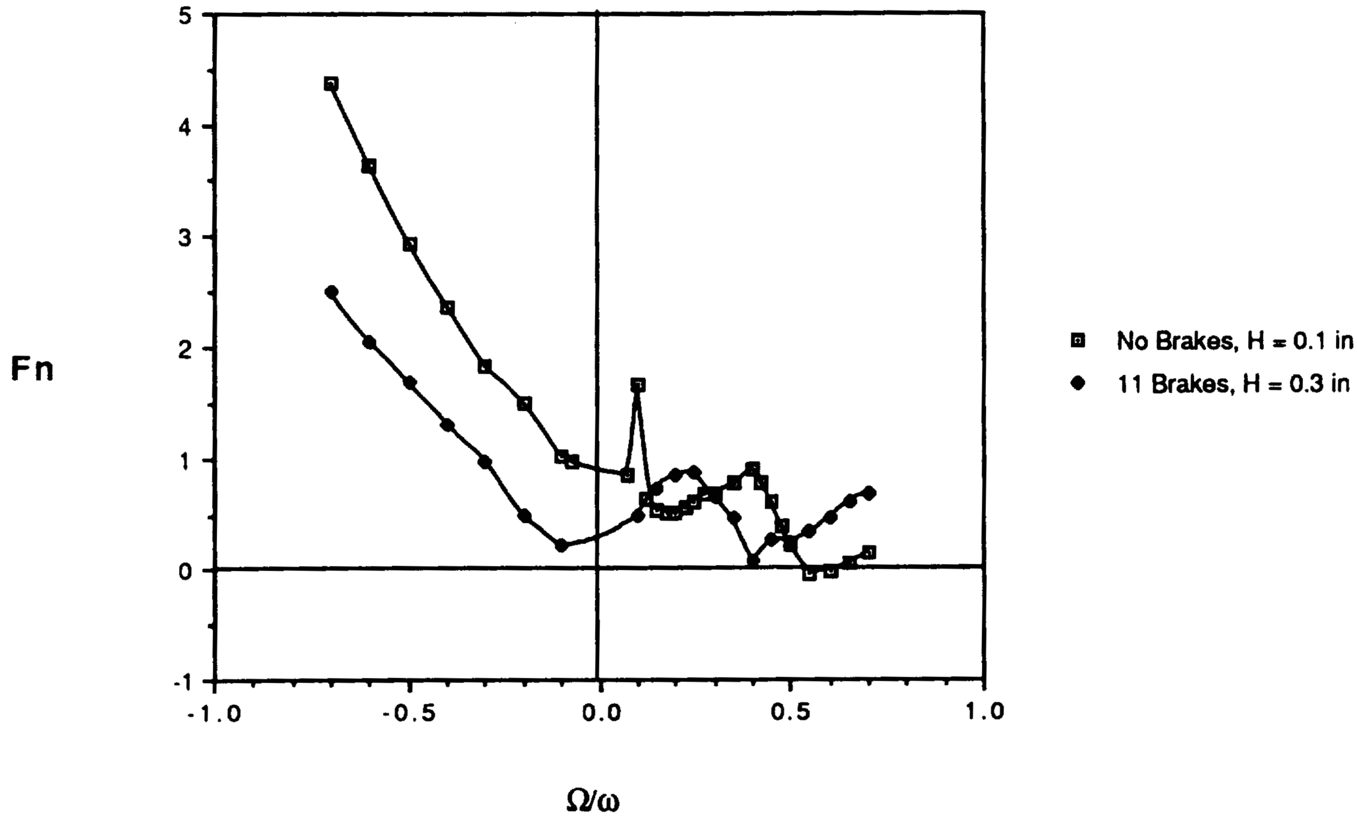

Comparison Plot (2000 RPM, Face Seal = 0.05 in, 10 GPM)
Orifice 2

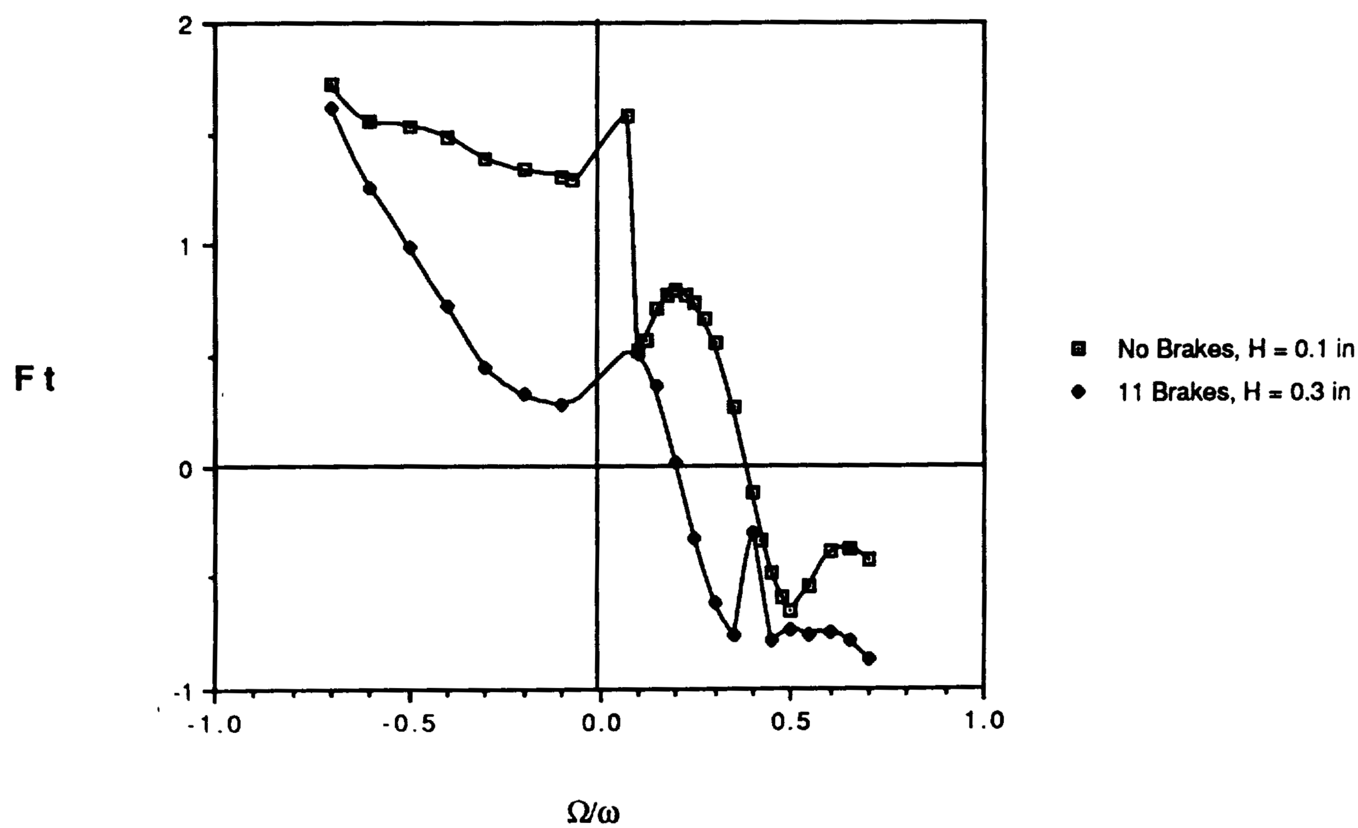

CONCLUSIONS FOR PHASE 2

1. A tip discharge orifice of the type used for the Alternate Turbopump Design (ATD) of the Space Shuttle High Pressure Oxygen Turbopump is destabilizing.

2. The design modification of widening the leakage path annular clearance and installation of 11 swirl brakes in the ATD would reduce some of the detrimental effects of the orifice.

N95- 23629

S/4-34

p. 14

ADAPTATION OF THE ADVANCED SPRAY COMBUSTION CODE TO CAVITATING FLOW PROBLEMS

Pak-Yan Liang
Rocketdyne Division, Rockwell International

ABSTRACT

A very important consideration in turbopump design is the prediction and prevention of cavitation. Thus far conventional CFD codes have not been generally applicable to the treatment of cavitating flows. Taking advantage of its two-phase capability, the Advanced Spray Combustion Code is being modified to handle flows with transient as well as steady-state cavitation bubbles. The volume-of-fluid approach incorporated into the code is extended and augmented with a liquid phase energy equation and a simple evaporation model. The strategy adopted also successfully deals with the cavity closure issue. Simple test cases will be presented and remaining technical challenges will be discussed.

ADAPTATION OF THE ADVANCED SPRAY COMBUSTION CODE TO CAVITATING FLOW PROBLEMS

Pak-Yan Liang

11th Workshop For CFD Applications in Rocket Propulsion

NASA Marshall Space Flight Center

April 20-22, 1993

Rockwell International
Rocketdyne Division

CFD 93 013(A)-001/D1/PYL

VOLUME-OF-FLUID TWO-PHASE TRACKING SCHEME IMPLEMENTED IN BOTH ARICC AND GALACSY-2D:

GENERAL ALGORITHM FOR ANALYSIS OF COMBUSTION SYSTEMS

Rockwell International
Rocketdyne Division

CFD 93-013(A)-002/D2/PYL

VOF–BASED CELL PARTITIONING IN ASCOMB

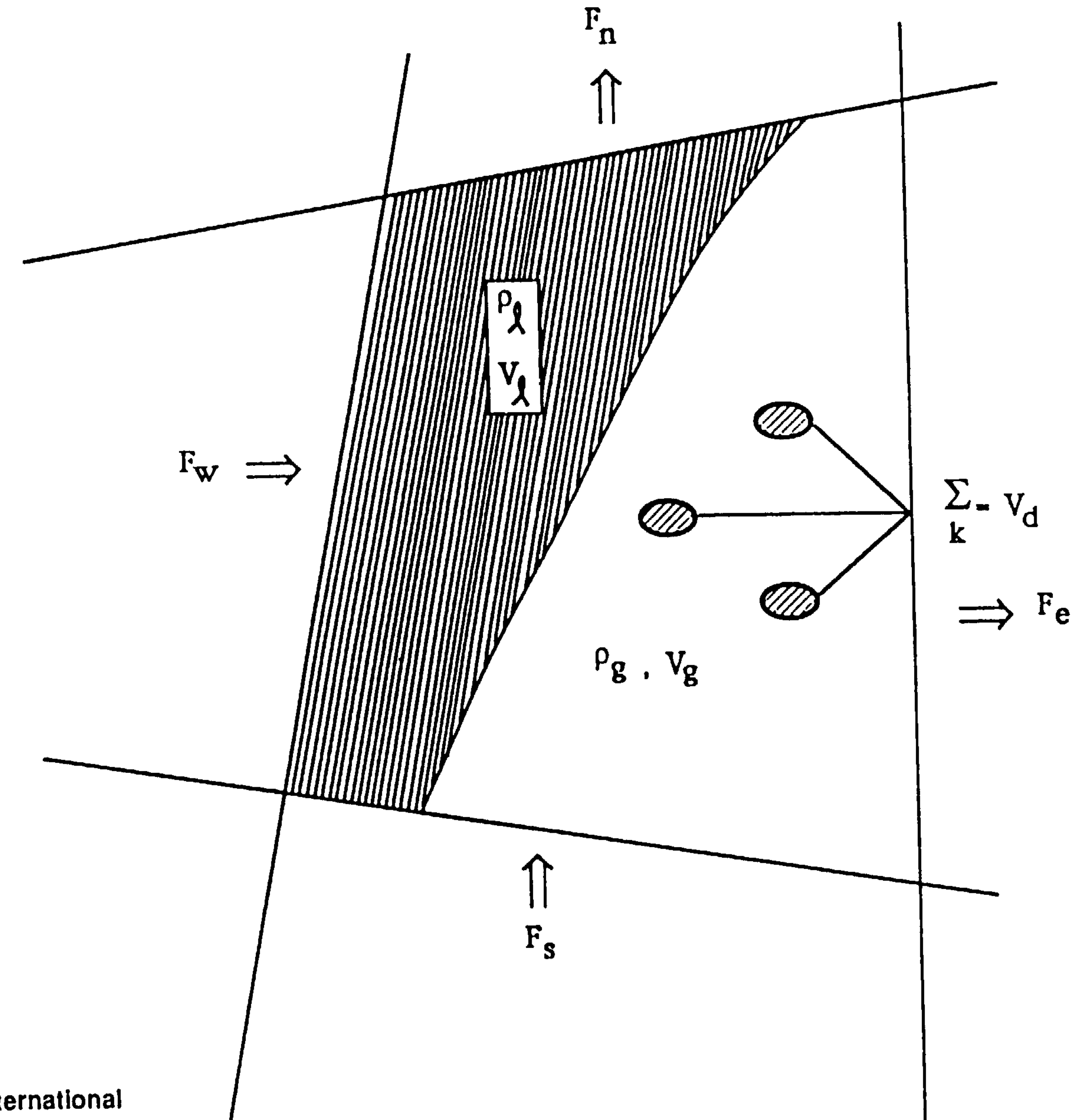

Rockwell International
Rocketdyne Division

CFD 92-058-012/D1/PYL

SUMMARY OF GOVERNING EQUATIONS

mass: $$\frac{\partial \bar{\rho}}{\partial t} + \nabla \bullet (\bar{\rho}\,\mathbf{u}) = \dot{\bar{\rho}}_d \quad \text{where} \quad \bar{\rho} = \mathcal{F}\rho_g + (1-\mathcal{F})\rho_\ell$$

momentum: $$\frac{\partial \bar{\rho}\mathbf{u}}{\partial t} + \nabla \bullet (\bar{\rho}\mathbf{u}\mathbf{u}) = -\nabla p - \nabla\left(\frac{2}{3}\bar{\rho}\bar{k}\right) + \nabla \bullet \underset{\approx}{\sigma} + \mathbf{S} + \bar{\rho}\mathbf{G}$$

internal energy: $$\frac{\partial \bar{\rho}\bar{I}}{\partial t} + \nabla \bullet (\bar{\rho}\bar{I}\mathbf{u}) = -p\nabla \bullet \mathbf{u} - \nabla \mathbf{J} + \bar{\rho}\bar{\varepsilon} + \underset{\text{chemistry}}{\dot{\mathbf{Q}}^c} + \underset{\text{spray}}{\dot{\mathbf{Q}}^s}$$

species m: $$\frac{\partial \bar{\rho}_m}{\partial t} + \nabla \bullet (\rho_m \mathbf{u}\mathcal{F}) = \mathcal{F}\nabla \bullet \left[\rho_g \mathcal{D} \nabla \left(\frac{\rho_m}{\rho_g}\right)\right] + \underset{\text{chemistry}}{\dot{\bar{\rho}}_m^c} + \underset{\text{evaporation}}{\dot{\bar{\rho}}_s \delta_{m,s}}$$

volume fraction: $$\frac{\partial \mathcal{F}}{\partial t} + \nabla \bullet \mathbf{u}\mathcal{F} = \dot{\mathcal{F}}_s = \frac{\text{net gas vol. outflux}}{\text{per unit total vol.}} = \frac{\dot{\bar{\rho}}_s}{\rho_g}$$

Rockwell International
Rockeldyne Division

CFD 93 013(A)-003/D1/PYL

OVERALL FLOW CHART FOR ASCOMB

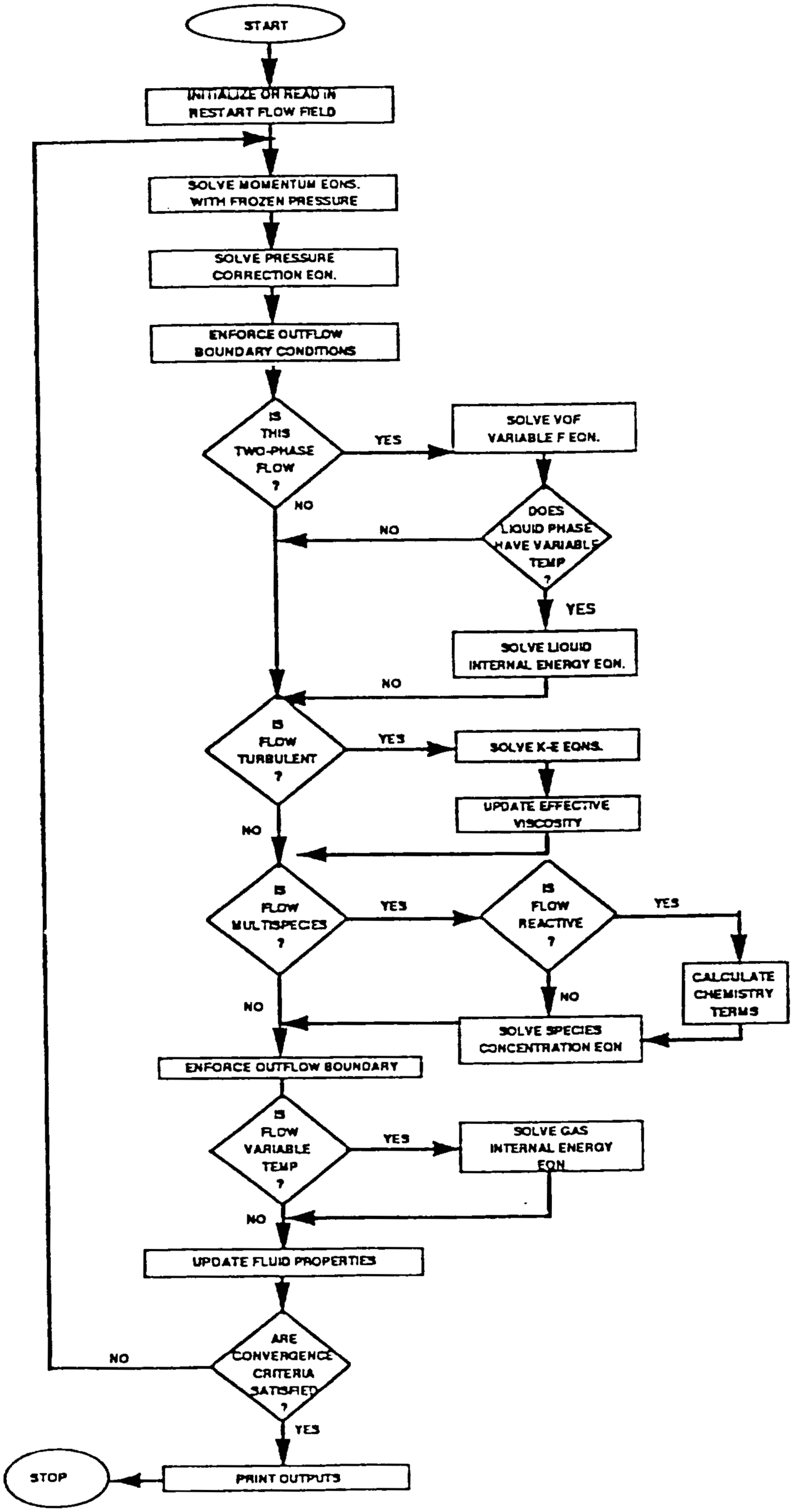

KEY SUBROUTINES

MODINP

CALCUV

CALCP

OUTBC

CALCF

CALCENL

CALCSC (ITE)
CALCSC (IED)

MODVIS

CHEM

CALCSP
OUTBC

CALCSC (IEN)
TEMPER

MODPRO

PRINT

SYNOPSIS OF SOLUTION APPROACH

- CAST ALL MATRIX EQUATIONS INTO GENERIC FORM

$$a_P \phi_P = \sum_m a_m \phi_m + C_P$$

WHERE

$$a_P = \sum_m a_m + \dot{\bar{\rho}}_s V_c$$

EXCEPT FOR $\mathcal{F}$-EQUATION, WHERE

$$a_P = \sum_m a_m + \sum_m \dot{V}_m$$

- KEEP COEFFICIENT MATRIX TO 5-DIAGONAL FOR 2D AND 7-DIAGONAL FOR 3D FLOWS BY DOING IMPLICIT DIFFERENCING ONLY FOR CONVECTION AND NORMAL DIFFUSION TERMS.

- SOLVE WITH STONE'S STRONGLY IMPLICIT PROCEDURE

Rockwell International
Rocketdyne Division

CFD 92 013(A)-005/O 1/PYL

OBSERVATIONS ON GENERAL FLOW CHARACTERISTICS THAT FORM THE BASIS OF SOLUTION STRATEGY

1. • VELOCITY COMPONENTS STRONGLY COUPLED TO EACH OTHER ONLY BY WAY OF PRESSURE; WEAKLY COUPLED TO TURBULENCE & TEMPERATURE FIELDS

   • HENCE, 2-STEP PRESSURE CORRECTION APPROACH OF "SIMPLE"

   • FLUX UPDATE INCLUDES DENSITY CORRECTION TERM FOR COMPRESSIBLE FLOWS, I.E.,

$$F_{gi} = F^*_{gi} + F'_{gi} + \hat{F}_{gi}$$

WHERE

$$F^*_{gi} = \mathcal{F}_i \, \rho^*_i (u^*_1 b^i_1 + u^*_2 b^i_2 + u^*_3 b^i_3)_i = \mathcal{F}_i \, \rho^*_i \, \dot{V}^*_i$$

$$F'_{gi} = \mathcal{F}_i \, \rho^*_i (u'_1 b^i_1 + u'_2 b^i_2 + u'_3 b^i_3)_i = \mathcal{F}_i \, \rho^*_i \, \dot{V}'_i$$

$$\hat{F}_{gi} = \mathcal{F}_i \, \rho'_i (u^*_1 b^i_1 + u^*_2 b^i_2 + u^*_3 b^i_3)_i = \mathcal{F}_i \, \rho'_i \, \dot{V}^*_i$$

OBSERVATIONS ON GENERAL FLOW CHARACTERISTICS THAT FORM THE BASIS OF SOLUTION STRATEGY

2\.

- WITH SECOND, DENSE LIQUID PHASE, ALL VARIABLES BECOME STRONGLY COUPLED TO THE $\mathcal{F}$-FIELD THROUGH THE CONVECTIVE MASS FLUXES

- TOTAL MASS FLUX GIVEN BY

$$F_i = F_{\ell i} + F_{gi}$$

WHERE

$$F_{\ell i} = \rho_\ell (1 - \mathcal{F}_i)(\dot{V}_i^* + \dot{V}_i')$$

- $\mathcal{F}$-FIELD MUST BE ALLOWED TO EVOLVE MORE SLOWLY THAN VELOCITY AND OTHER GAS SCALAR FILEDS, EXCEPT FOR TOTAL MASS CONSERVATION (PRESSURE-CORRECTION) ESP. WHEN BOILING IS INVOLVED

Rockwell International
Rocketdyne Division

CFD 93 013(A)-007/01/PYL

ADDITIONAL UPGRADES NEEDED TO TREAT CAVITATION PROBLEMS

1. VARIABLE TEMPERATURE/ADDITIONAL ENERGY EQUATION FOR THE LIQUID PHASE

   - EQUALIZATION OF TEMPERATURES IN PARTIALLY LIQUID CELLS ASSUMED

2. SIMPLE EVAPORATION (CAVITATION INCEPTION) MODEL REQUIRED

$$\dot{m} = E_p A_s (P_v - P)/\sqrt{2\pi RT}$$

Rockwell International
Rocketdyne Division

CFD 93 013(A)-008/D1/PYL

ADVANTAGES OF VOF-APPROACH OVER OTHER CAVITATION MODELS

- PHYSICALLY RIGOROUS DESCRIPTION FROM FIRST PRINCIPLES
- NO NEED FOR HEURISTIC CAVITY CLOSURE MODELS
- DESCRIBES FLOW FIELDS BOTH INSIDE AND OUTSIDE OF CAVITY
- NATURALLY HANDLES CLOUD CAVITATION, TRAVELING CAVITATION, VORTEX CAVITATION, AND VIBRATORY CAVITATION
- POTENTIALLY CAPABLE OF DESCRIBING CAVITATION BUBBLE COLLAPSE
- HIGHER ORDER EFFECTS (DIFFERENT ρ_ℓ/ρ_g RATIOS, FINITE EVAPORATION RATES, RECONDENSATION, ROUGHNESS EFFECTS ON CAVITATION INCEPTION ETC.) CAN BE ACCOMMODATED

Rockwell International
Rocketdyne Division

CFD 92 013(A)-009/D1/PYL

TYPICAL CONVERGENCE CHARACTERISTICS FOR NONREACTING CAVITATING FLOW

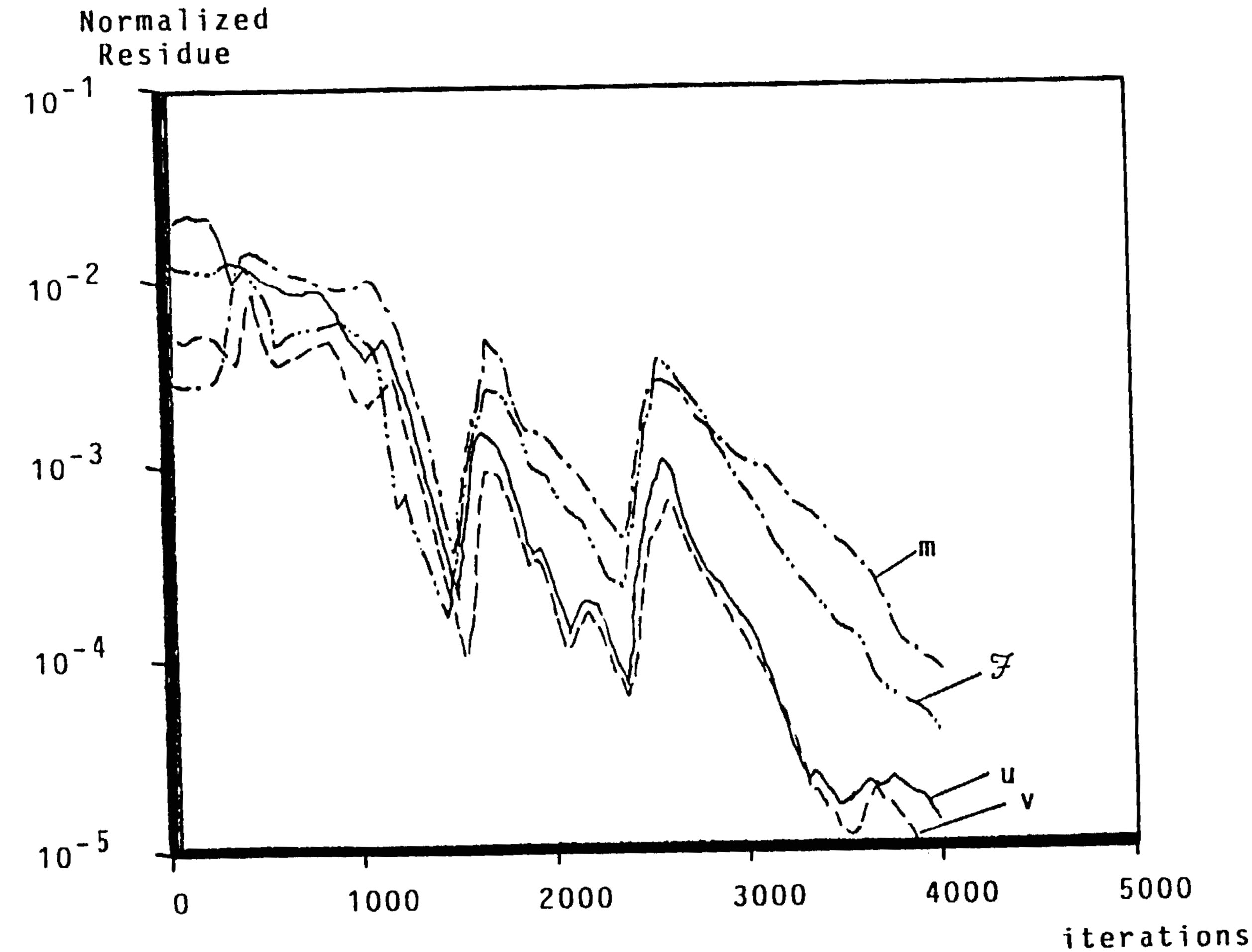

Rockwell International
Rocketdyne Division

CFD 93 013(A)-010/D1/PYL

STATUS OF THE CAVITATION UPGRADE SUBTASK

- **QUALITATIVELY AT LEAST, THE CAVITATION SCHEME NOW SEEMS TO FUNCTION PROPERLY**
  - STRAIGHT CHANNEL LIQUID FLOW WITH INCOMING GASEOUS "LAYER"
    - OVERALL CHANNEL PRESSURE RESPONDS CORRECTLY TO CHANGES IN VAPOR PRESSURE
    - NUMERICAL DIFFUSION OF VOF VARIABLE APPEARS TO BE ACCEPTABLE EVEN FOR FIRST ORDER UPWIND SCHEME
  - CURVED CHANNEL FLOW WITH CAVITATING BUBBLE ON CONVEX WALL
    - BUBBLE FORMATION AND TERMINATION PROPERLY CAPTURED
    - BUBBLE SIZE ADJUSTS TO CHANGES IN VELOCITY AND MAGNITUDE OF LIQUID EVAPORATION TERM

Rockwell International
Rocketdyne Division

CFD 92-065-001/D6/PYL

CONCLUDING REMARKS

- NUMERICAL STIFFNESS ISSUES STILL NEED CLOSER EXAMINATION
- SPATIAL DIFFERENCING OF $\mathscr{F}$-VARIABLE MAY NEED SOMETHING LESS DIFFUSIVE
- NEXT TEST CASES SHOULD EXPLORE TRUE POTENTIAL OF VOF-APPROACH E.G., TRAILING EDGE CAVITATION PROBLEMS

Rockwell International
Rocketdyne Division

CFD 93 013(A)-011/01/PYL

C-5

N95- 23630

S5-34
P. 20

Cavitation Modeling in Euler and Navier-Stokes Codes

Manish Deshpande, Jinzhang Feng, and Charles L. Merkle
Propulsion Engineering Research Center
The Pennsylvania State University
State College, PA

Many previous researchers have modeled sheet cavitation by means of a constant pressure solution in the cavity region coupled with a velocity potential formulation for the outer flow. The present paper discusses the issues involved in extending these cavitation models to Euler or Navier-Stokes codes. The approach taken is to start from a velocity potential model to ensure our results are compatible with those of previous researchers and available experimental data, and then to implement this model in both Euler and Navier-Stokes codes. The model is then augmented in the Navier-Stokes code by the inclusion of the energy equation which allows the effect of subcooling in the vicinity of the cavity interface to be modeled to take into account the experimentally observed reduction in cavity pressures that occurs in cryogenic fluids such as liquid hydrogen. Although our goal is to assess the practicality of implementing these cavitation models in existing three-dimensional, turbomachinery codes, the emphasis in the present paper will center on two-dimensional computations, most specifically isolated airfoils and cascades. Comparisons between velocity potential, Euler and Navier-Stokes implementations indicate they all produce consistent predictions. Comparisons with experimental results also indicate that the predictions are qualitatively correct and give a reasonable first estimate of sheet cavitation effects in both cryogenic and non-cryogenic fluids. The impact on CPU time and the code modifications required suggests that these models are appropriate for incorporation in current generation turbomachinery codes.

Computational Modeling of Cavitation

Charles L. Merkle, Jinzhang Feng and Manish Deshpande

Propulsion Engineering Research Center
Department of Mechanical Engineering
Penn State University

Objectives

- Extend Existing Cavitation Theories from Potential Flow to Euler/Navier-Stokes Solvers
- Identify Techiniques Needed to Incorporate Cavitation Models in Existing Turbomachinery Codes
- Add Additional Physics to Cavitation Model as Euler/Navier-Stokes Formulation Allows

Approach

Incorporate Cavitation Model in a Sequence of Platforms

- Potential Flow Model (Panel)
- Euler Analysis
- Navier-Stokes Analysis
- Navier-Stokes + Energy
    - Thermal Effects

Governing Equations

- **Navier-Stokes + Energy**

$$\Gamma^{-1}\frac{\partial Q}{\partial \tau}+\frac{\partial\left(E-E_v\right)}{\partial \xi}+\frac{\partial\left(F-F_v\right)}{\partial \eta}=H$$

- **Incompressible, Variable Properties**

$$Q=\begin{pmatrix} p \\ u \\ v \\ T \end{pmatrix},\ E=\begin{pmatrix} \rho u \\ \rho uu+p \\ \rho uv \\ \rho uT \end{pmatrix},\ F=\begin{pmatrix} \rho v \\ \rho uv \\ \rho vv+p \\ \rho vT \end{pmatrix},\ H=\begin{pmatrix} 0 \\ 0 \\ 0 \\ q \end{pmatrix}$$

Numerical Scheme

- 4-Stage Runge-Kutta Explicit Time-marching.
- Central Differencing in Space
- Local Time stepping
- Fourth order artificial viscosity used to prevent odd-even splitting.

Euler Analysis

- Extend Classical Potential Flow Model to Euler Eqns.
  - Cavity Treated as a Constant Pressure Region
- Solve Direct Problem
  - Specify Cavitation Pressure
  - Determine Inception Point and Cavity Length as Part of Solution
  - Use Closure Condition From Potential Methods

Navier-Stokes Analysis

- Implementation Analogous to Euler Analysis
- Advantages
  - Enables the solution of viscous, turbulent flows
  - Couples thermodynamics through energy equation
  - Important for Cryogenics

Cavitation Boundary Conditions

- Over-specified Boundary Conditions
  - Location of Solid Surface
  - Cavitation Pressure

- Cavity interface Location
  - "Linear" - B.C.'s transferred to Body Surface
  - "NonLinear" - B.C.'s applied on Interface
Computational Domain evolves with solution

Computational Steps

- Check pressure to identify cavitating points
- Trace cavity and ensure positive thickness
- Attach afterbody for finite thickness cavity
- Regrid domain (Nonlinear)

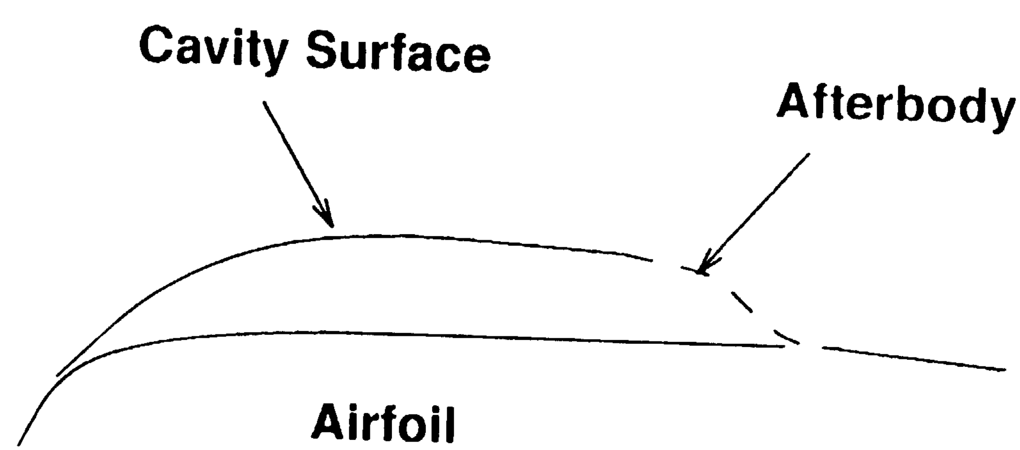

Code Validation

Non-cavitating NACA66(MOD) Shen and Dimotakis

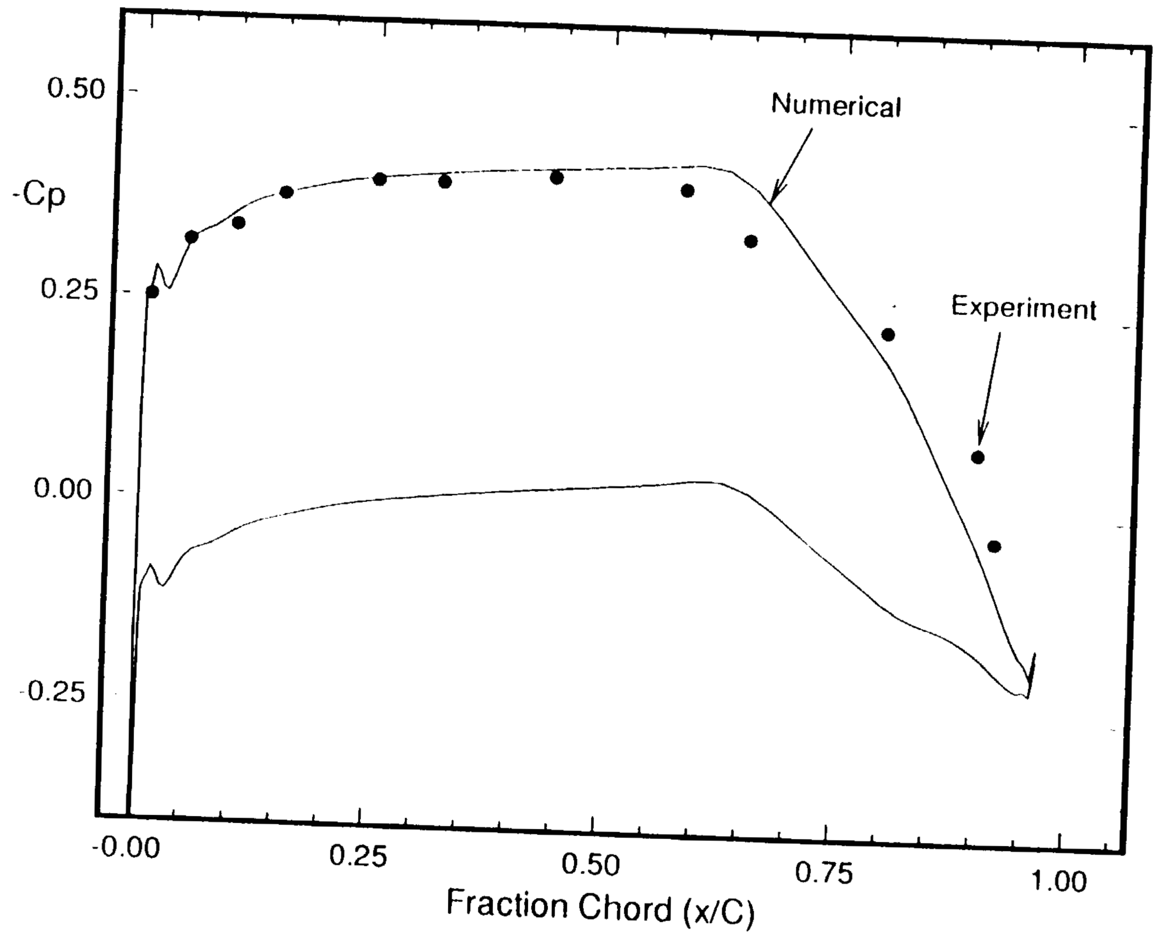

Navier-Stokes/Euler Comparison

NACA66 (MOD)
$\alpha = 4°$

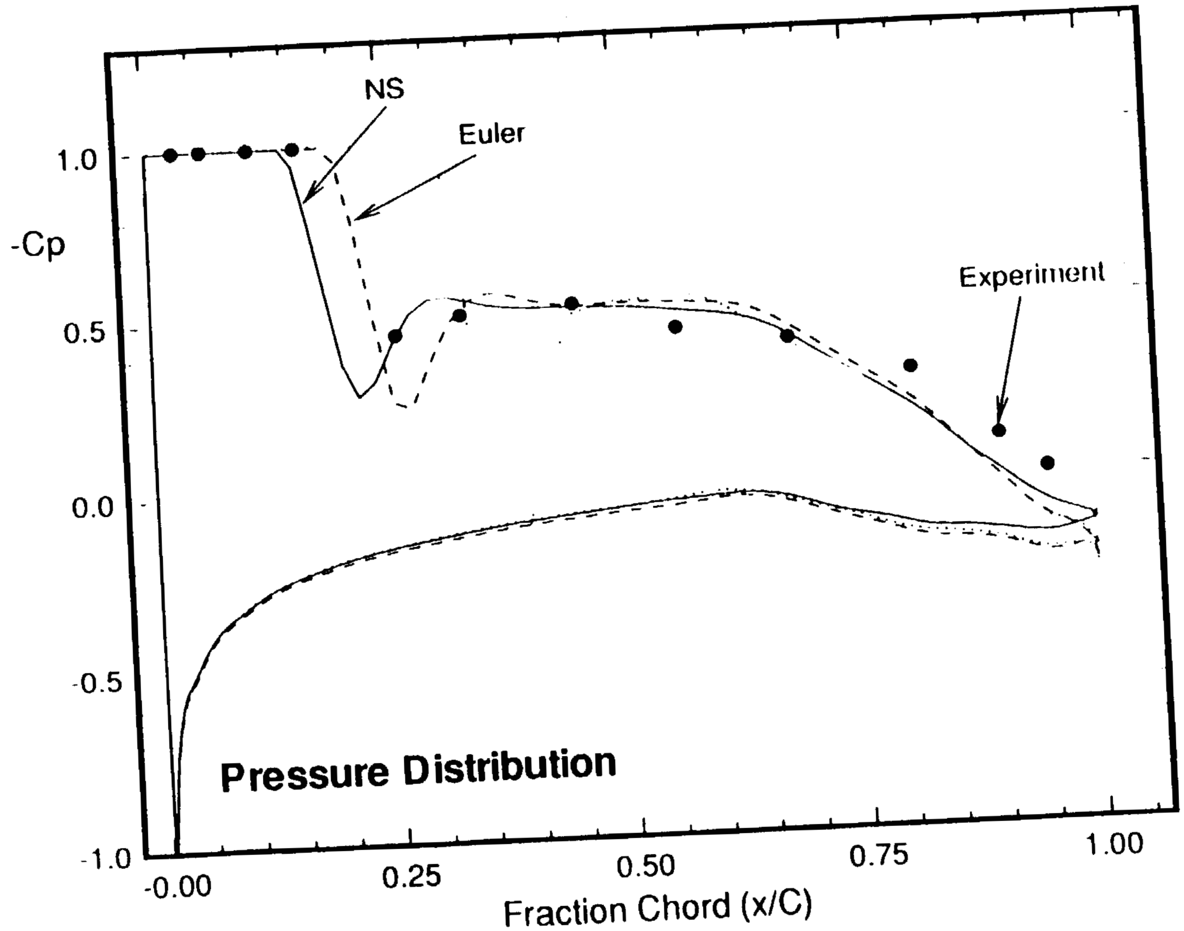

Cavitation Pressure Comparison

NACA66(MOD) - Shen and Dimotakis.

Pressure Distribution

$\alpha = 4°$

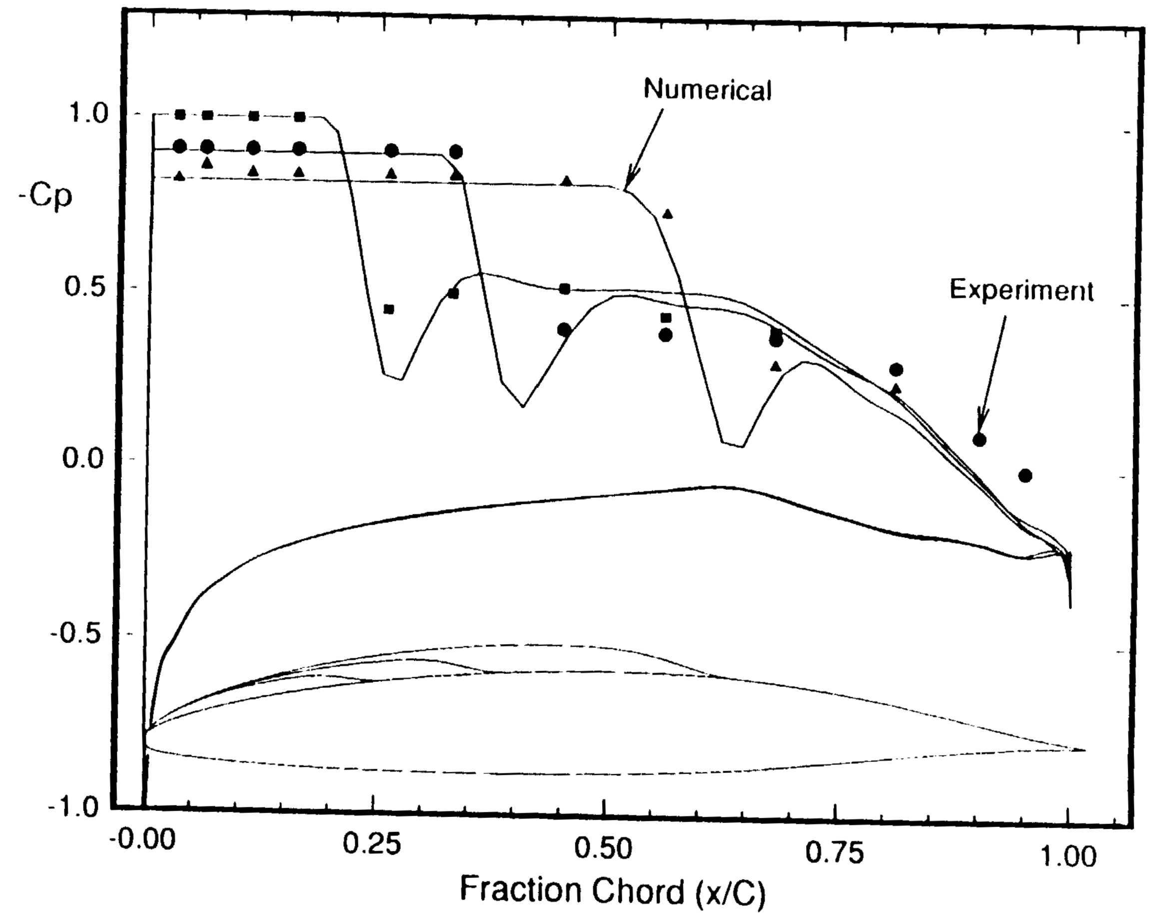

Cavitating Flowfield

NACA66 airfoil

Final Grid

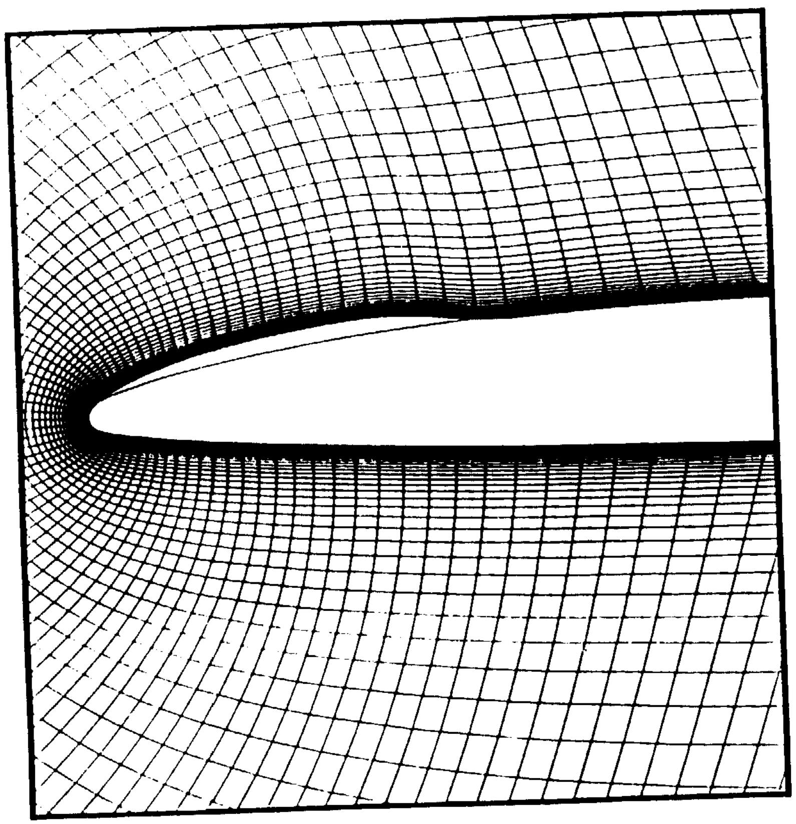

Pressure Contours

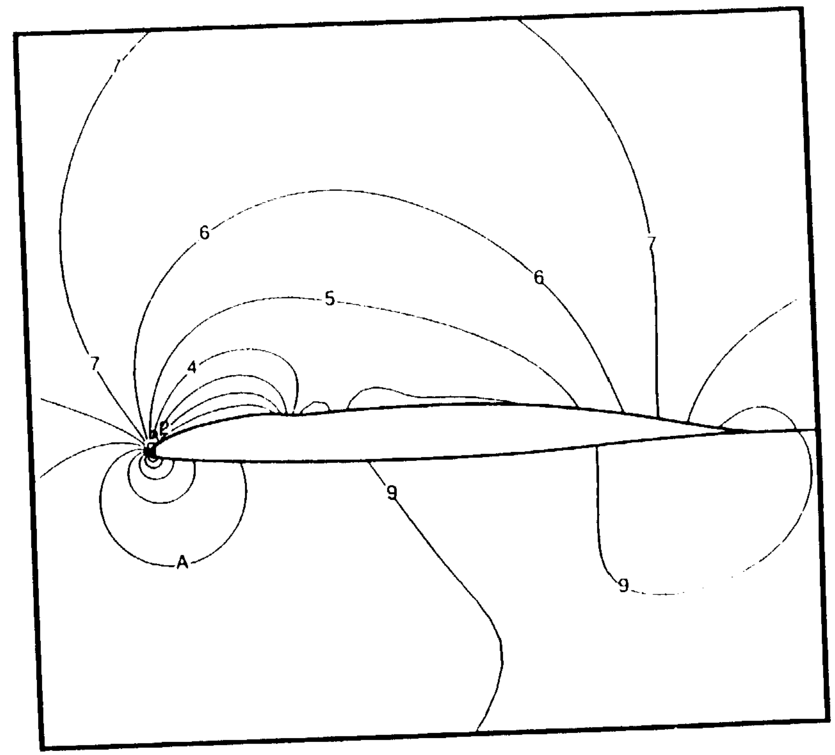

Cavity Length Comparison

NACA16009 hydrofoil - Dong (1983)
α/σ vs l/c

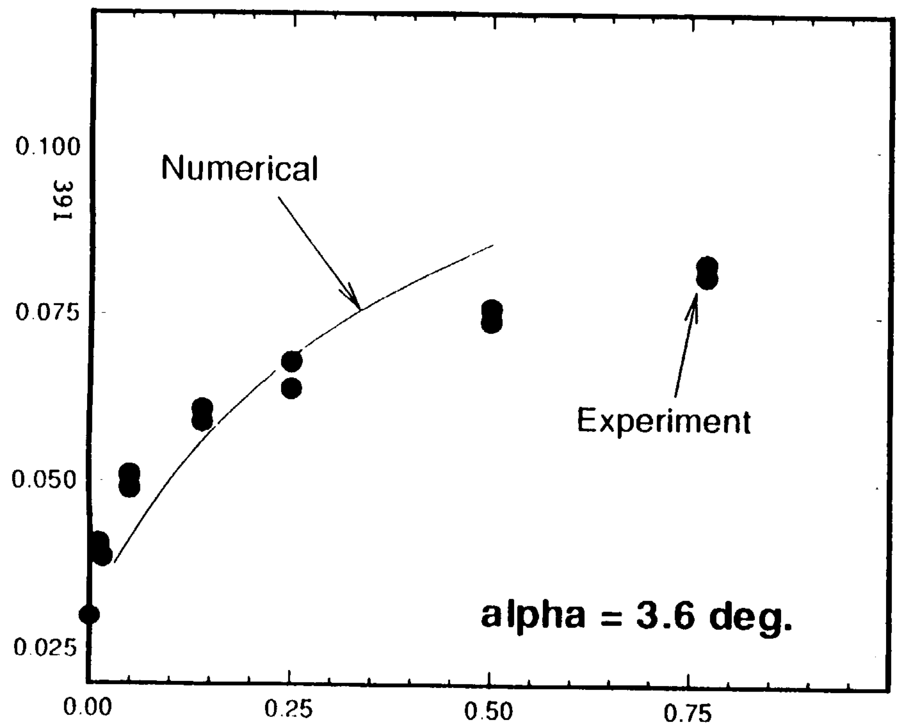

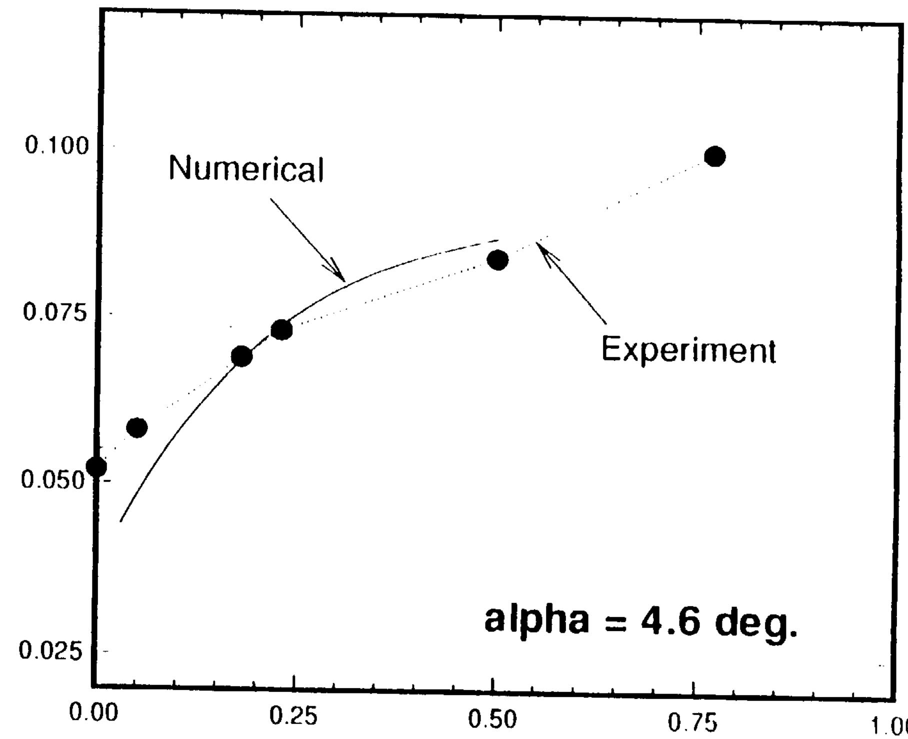

Midchord Cavitation

- Midchord Cavitation occurs on blades with Flat Pressure Distributions
- Difficult to predict with potential flow codes
  - No distinct Minimum Pressure Location.
- Good Prediction using Euler Analysis
  - Specification of Inception Point not required

Midchord Cavitation

NACA66(MOD) - Shen and Dimotakis

Pressure distribution
$\alpha \stackrel{o}{=} 1$

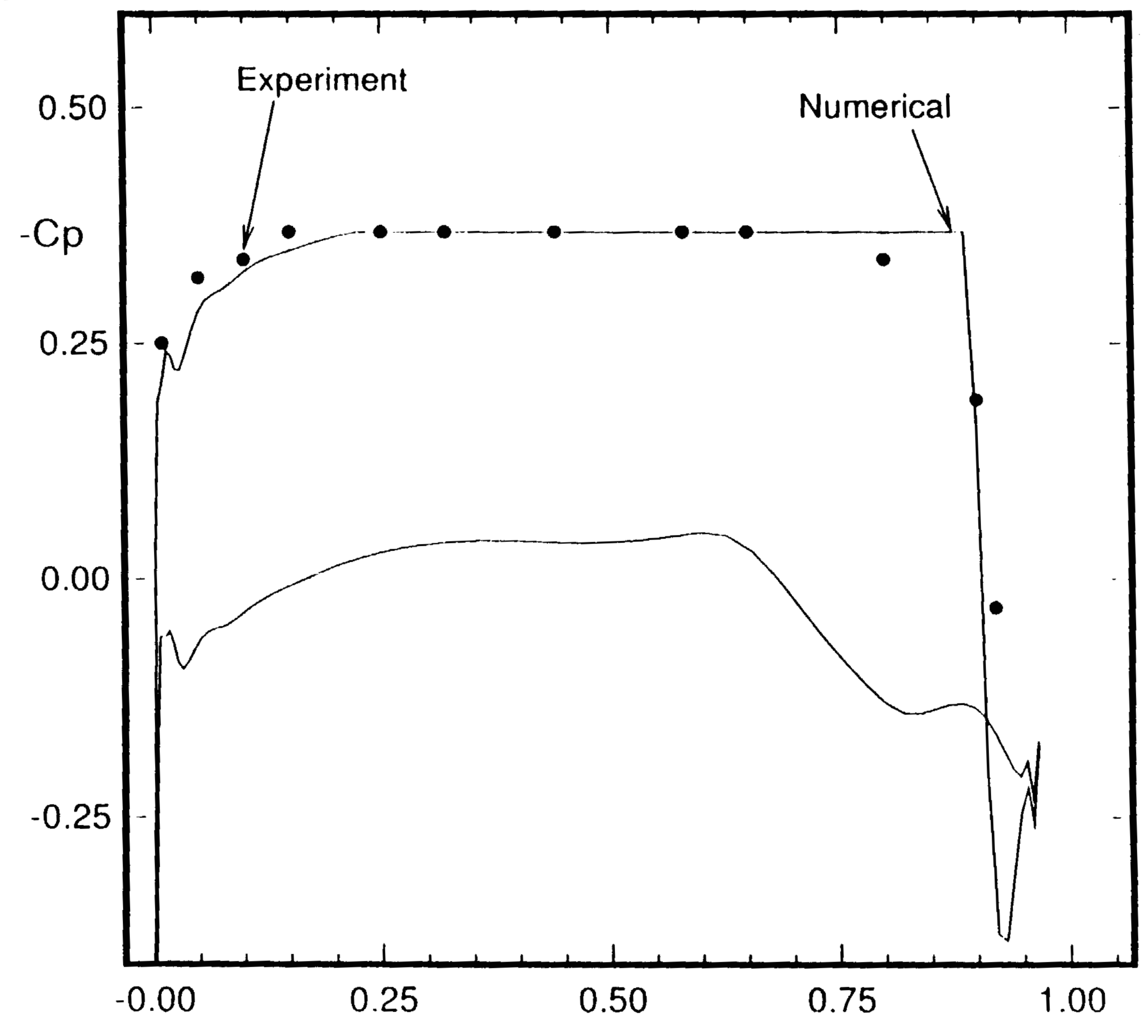

Effect of Cascade Spacing

NACA0012 Cascade

$\sigma = -0.5$

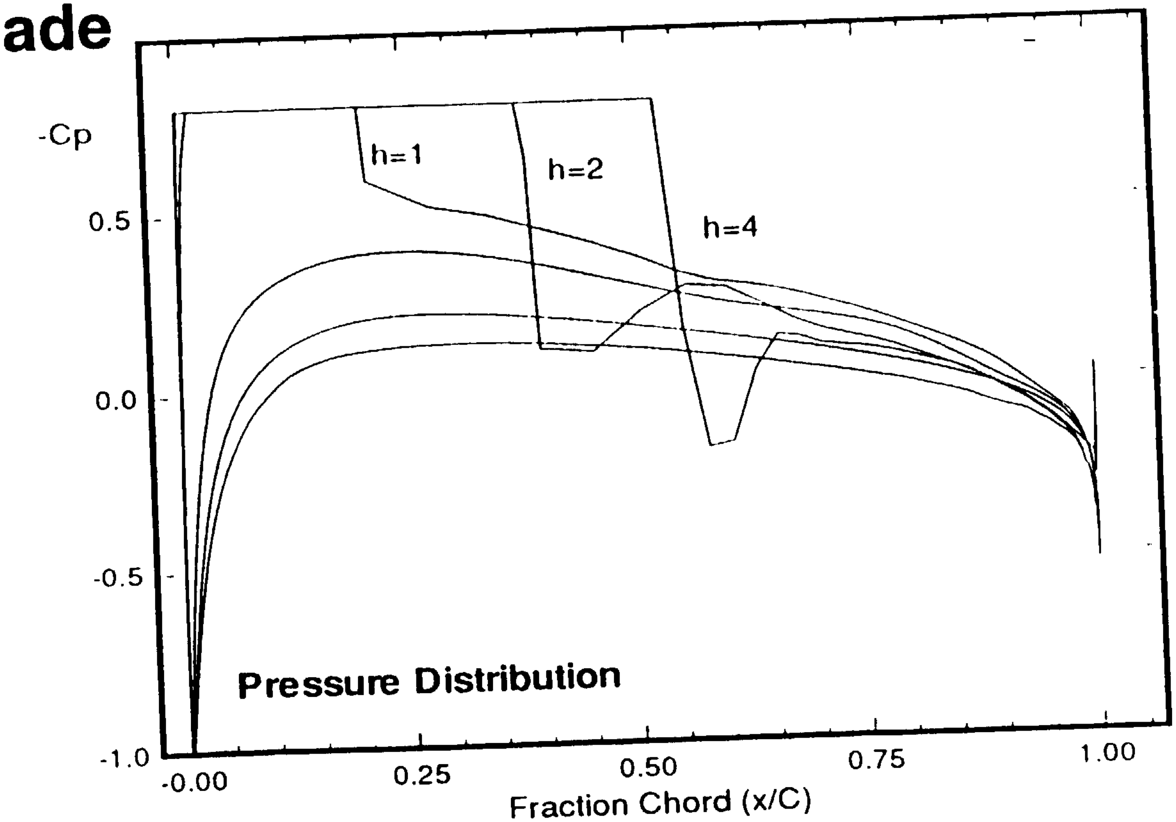

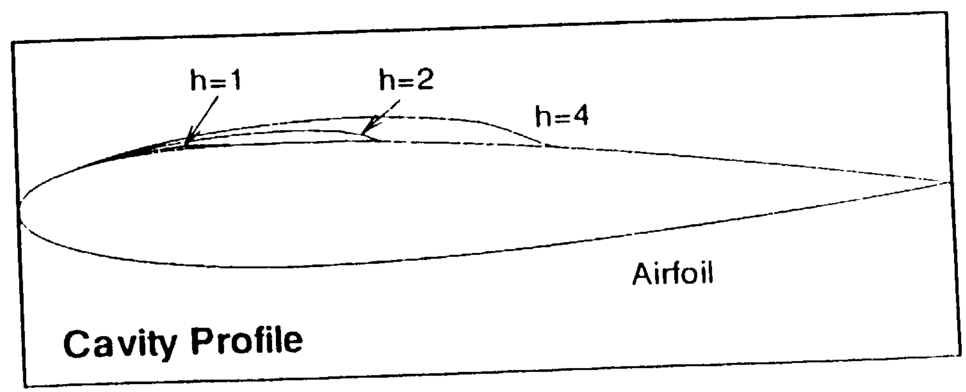

Thermodynamic Boundary Condition

- Energy Balance at Cavity interface

Heat Conducted into interface	=	Vaporization Rate x Latent Heat

- Determines the normal temperature gradient at surface
- Present Model Relates Vaporization Rate to Vapor Velocity

$$-u_c = u_\infty$$

Temperature Depression - Hydrogen

Hord (NASA CR-2156)

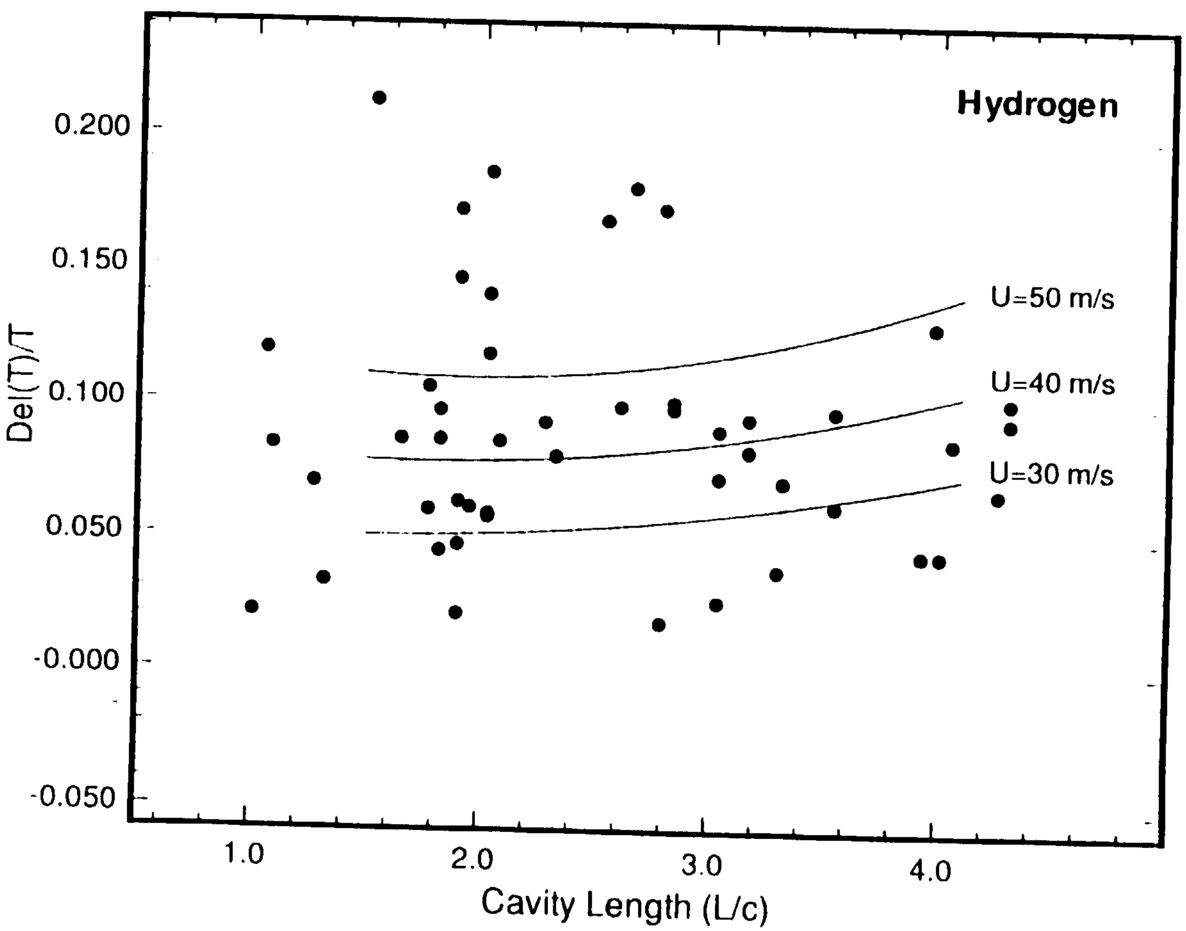

Temperature Depression - Nitrogen

Hord (NASA CR-2156)

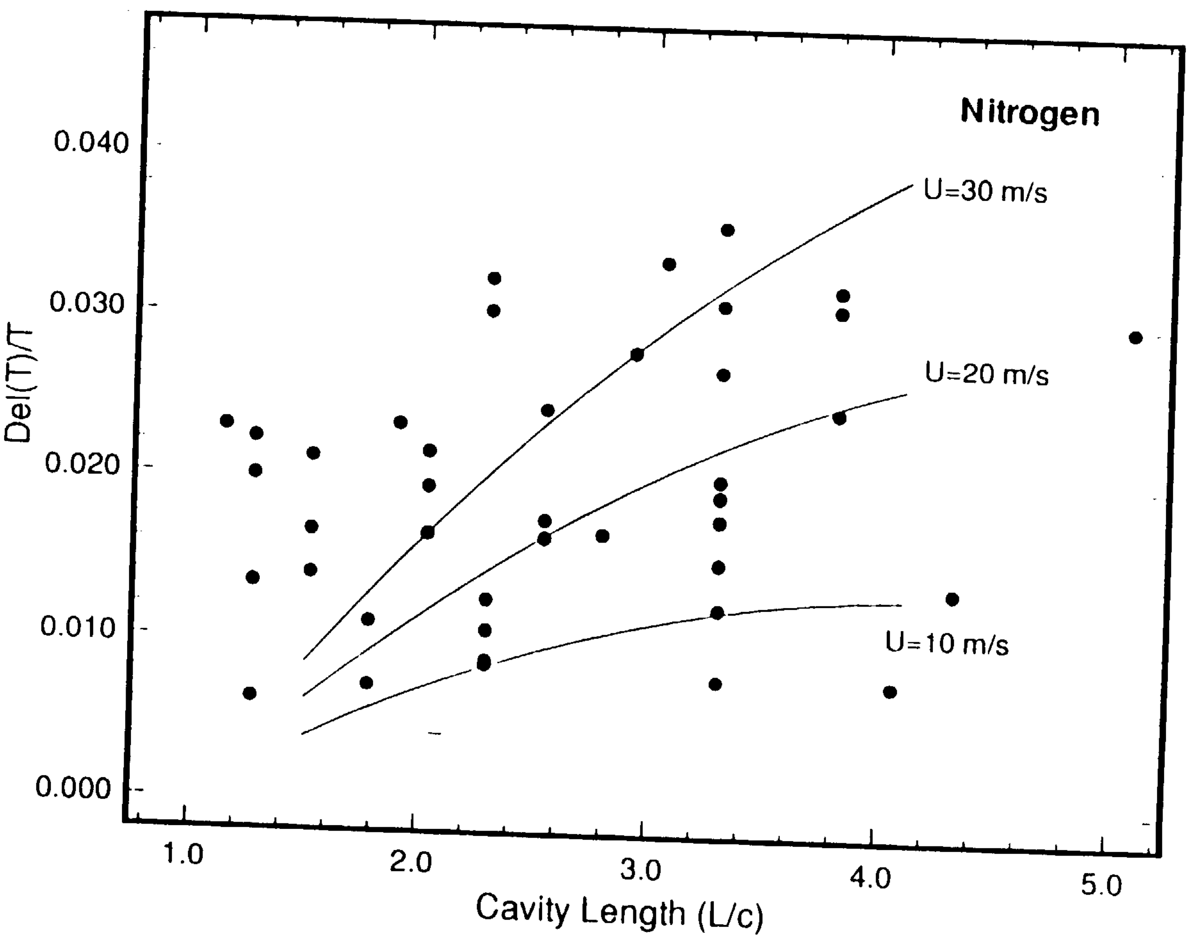

Temperature Depressions
Water, Hydrogen and Nitrogen

NACA0012 airfoil

$\alpha = 5^{\circ}$

$\sigma = -1.0$

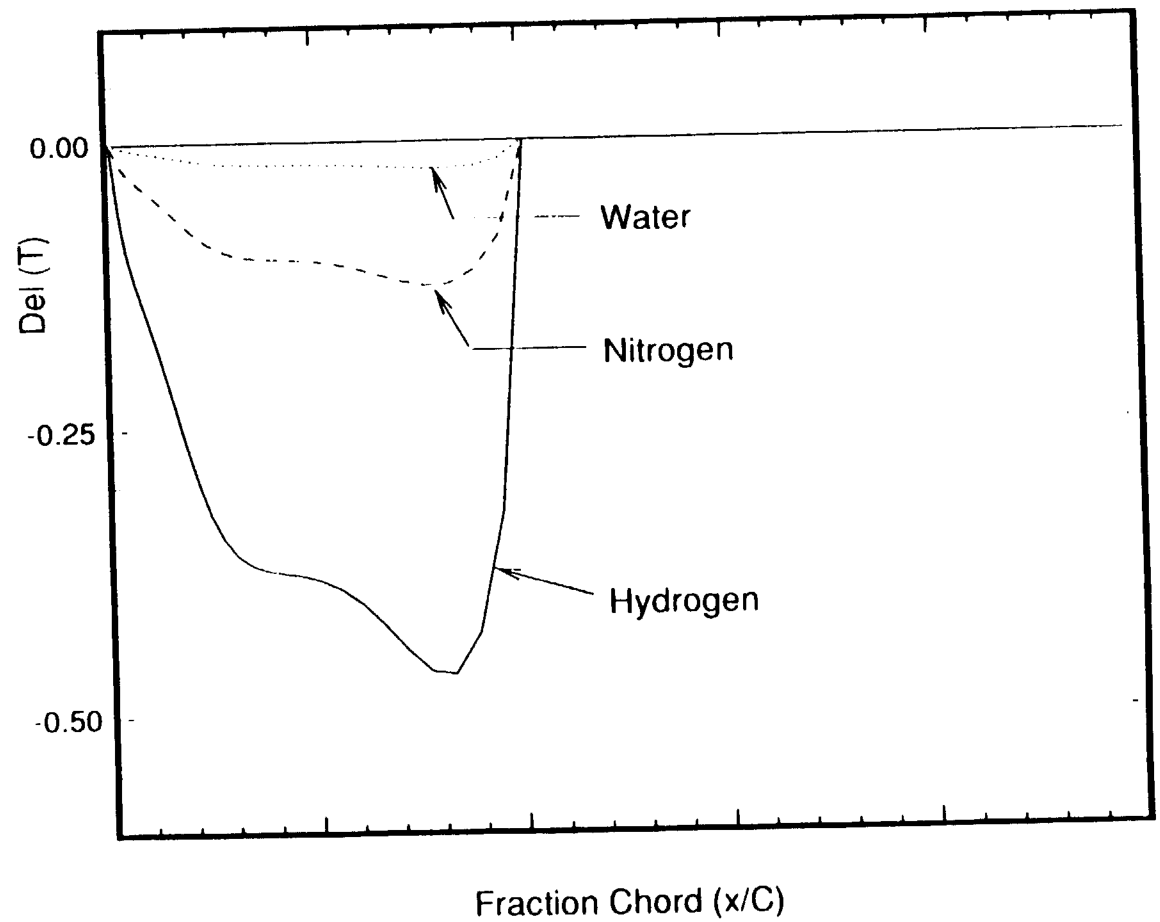

Impact of Thermal Effects on Cavitation

NACA0012 airfoil
$\alpha = 5^{\circ}$

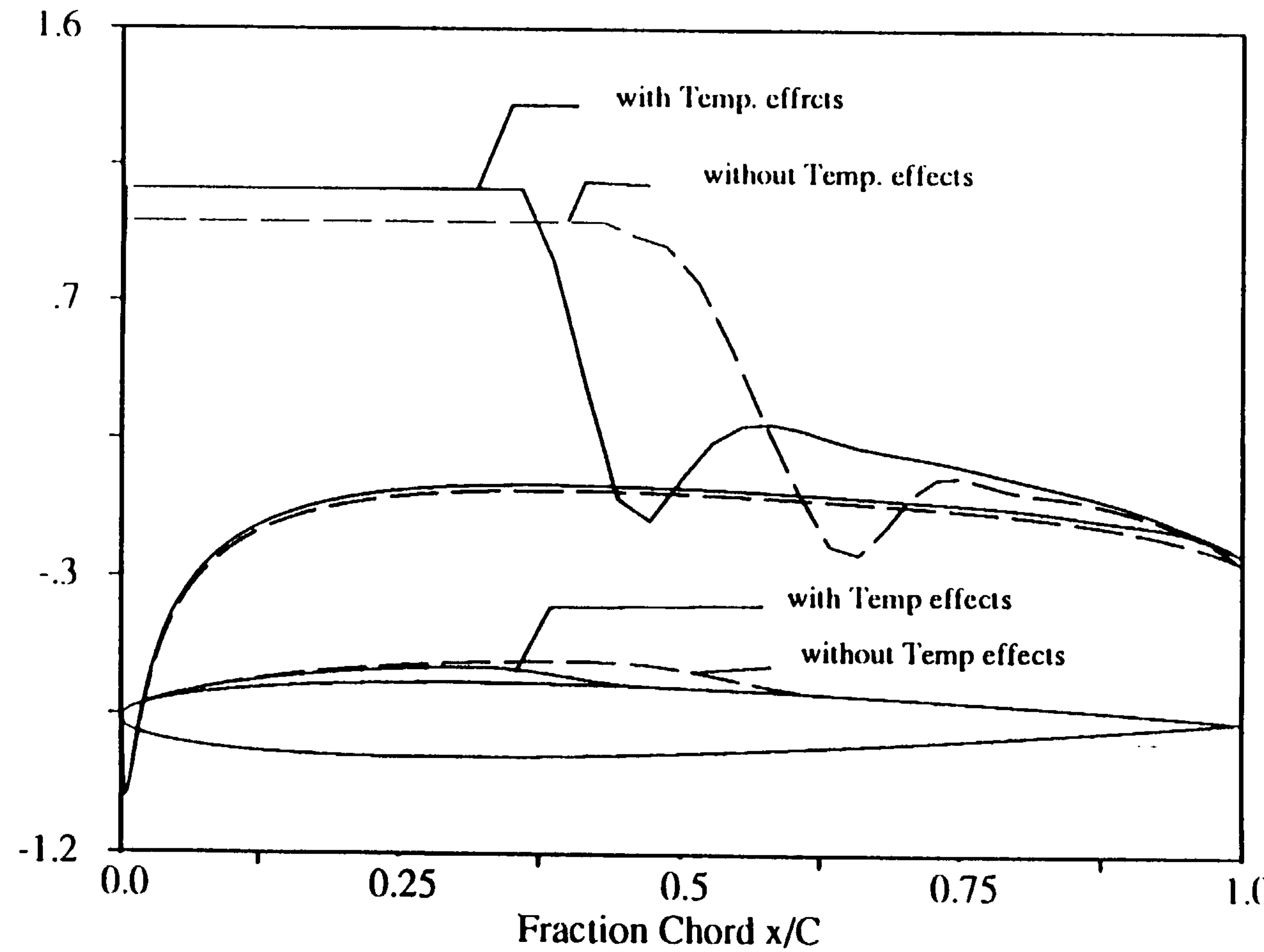

Summary

- Determines cavity length and inception point
- Good prediction of both pressure distribution and cavity geometry
- Capable of predicting midchord cavitation
- Cavity termination model used to predict pressure recovery.
- Easy to extend to more complex flows as well as to incorporate into design codes.
- Predictions of Panel, Euler and N-S are similar
  - BL's and Turbulence have little effect on Model Predictions

Summary

- Thermal Effects are significant in cryogenic fluids
  - Slope of Vapor Pressure/Temperature curve is steep
  - Near Super-critical Properties intensify Thermal Effect
  - Measurable Temperature Depression in liquid
- Effect requires coupled NS/Energy Solution
  - Thermal BL in Liquid
  - Predict Temperature Depression
  - Empirical model for vapor production rate
- Model predicts magnitude of temperature depression satisfactorily

N95- 23631

WORKSHOP FOR CFD APPLICATIONS IN ROCKET PROPULSION AT NASA-MSFC

Mehtab M. Pervaiz
April 20, 1993

S8-34
P. 20

Title: An Inducer CFD Solution and Effects Associated With Cavitation

This presentation describes a CFD analysis for an Alternate Turbopump Development (ATD) configuration. The analysis consists of a coupled configuration of the inducer and impeller. The work presented here is a joint collaboration of J. Garrett, J. Kuryla and myself.

Outline:

This view graph provides an outline of the current presentation. I will start with the ATD configuration for the inducer and impeller and the corresponding CFD solution. Subsequently, I will describe the current cavitation modeling approach that has been utilized on this configuration. A review of various cavitation modeling approaches will then be presented. Various suggestions and modeling ideas will then be presented for analyzing cavitation. The talk concludes with a brief summary and future plans.

14.6 Degree Inducer-Impeller with Splitters

This view graph shows the computational mesh for the inducer-impeller combination of the hub surface. The inducer and impeller rotate at the same RPM, with no clocking in between them. The configuration consists of a full inducer and impeller coupling with a continuous main blade that proceeds from the inducer leading edge to impeller trailing edge. A single set of splitters is apparent in the impeller. The figure shows the blades and splitters projecting out of the hub surface. Although there are four total main blade passages, only one was considered for analysis and periodic boundary conditions were applied before the leading edge of the inducer and after the trailing edge of the impeller main blade. There are 18 computational nodes in between the main blade passages. There are about 110 points along the flow direction.

Summary of Pressure Distribution Over the Full Configuration

This shows the pressure distribution on the full configuration (computational results produced with a multiplicity of four) with splitters. The top two figures show the pressure distribution on the suction and pressure sides of the blades and splitters and the hub surface is shown shaded. The bottom figures shows the pressure distributions on the hub, centerline and shroud surfaces whereas the blades and splitters shown in the grey shade. These figures indicate the existence of negative pressure near tip of the suction side of the inducer blade. The negative pressures are due to the fact that the CFD model assumes a single-phase flow and is incapable of modeling vapor where the local static pressure becomes lower than the vapor pressure.

Current Cavitation Model Applied to ATD Configuration

This viewgraph presents an approach that we have utilized at Pratt & Whitney for getting an estimate for the change in loading attributed to cavitation. The first step is to carry out a single phase 3-D CFD solution for the configuration at hand. For the ATD configuration, as shown in the previous figure, the CFD analysis shows that the static pressure on the suction side near the tip region becomes lower than local vapor pressure. Hence the effect of cavitation must only manifest itself near the suction side tip region and gradually diminish as one move towards the hub. The next step is to compute a 2-D potential flow cavitation sheet model corresponding to the conditions relevant at the blade tip. This potential flow cavitation sheet model has been developed by Penn State University for P&W. The model yields *cavitation correction factors*, Δp_{sheet}, for *pressure loads* as a function of tip chord length. These corrections must be multiplied with non-cavitated blade delta-pressures to obtain cavitated delta-pressures. Note that p is used here for pressure corrections, whereas P is used for static pressures. Next the tip sheet cavitation correction factors are scaled linearly such that no cavitation correction is needed at the hub. This yields a 2-D distribution of the correction factors, Δp_{cor}, on the blade surface. Thus in

$$\Delta p_{cor} = K(s,r)\Delta p_{sheet}$$

$K(s,r)$ represents the linear scaling transformation as a function of local arc length s measured from the inducer LE for a streamline at a local radius r and Δp_{cor} represents the multiplier for delta-pressure at all blade locations. Once the functional form of the delta-pressure corrections is known, it is multiplied at all the CFD blade locations to obtain a new distribution ΔP_{cor} for blade loads. This distribution is then used to compute the new suction side pressure corresponding to the CFD solution. The suction side pressure is given by:

$$P_s = P_p - \Delta P_{cor}$$

where P_p represents the pressure on the pressure side of the blade. As a sanity check, one should verify that the corrected pressure on the suction side remains above the vapor pressure. If this not achieved, then the 2-D sheet model should be repeated for other streamlines and the cavitation corrections determined by a bilinear interpolation.

Distribution of Cavitation Correction Factors

This viewgraph shows the functional form of the cavitation correction on the blade tip as a function of local arc length along the blade. The effect of factors greater than unity is to increase the pressure load downstream of the bubble, whereas for those locations where the bubble actually exists, the effect is to decrease the pressure loads. This can be thought of as a blockage effect which causes the variations in pressure. The figure also shows the effect of linearly scaling the correction factors and its diminishing effect as one goes from tip to hub. Note that this procedure should be regarded as rough estimate of the changes associated with cavitation. For this reason a more elaborate non-linear transfer function is not warranted. Ideally the cavitation correction procedure should a part of the CFD numerics.

Inducer Blade Delta Pressures

This figure shows a projected view of the inducer blade in the x-r plane. The top figure shows the blade pressure loads as predicted by the CFD code and before the cavitation correction is applied. The cavitation bubble is limited to the red region near the blade tip. The lower figure shows the pressure loads after the cavitation correction is applied. The effect of this correction is to locally decrease the load due to the blockage and to increase the loads downstream of it. The saw-tooth behavior relates to the axial coarseness of the mesh when the tip correction factors are linearly transferred to other locations.

Inducer Blade Suction-Side Pressures The top figure shows the blade suction side pressures as predicted by the CFD code and before the cavitation correction is applied on a projected x-r plane. Note that the pressures are substantially negative in the cavity region. The lower figure shows the suction side static pressure after the cavitation correction is applied. In this case all the pressures have become positive. The blockage effect is felt to about mid-span location at the tip. The blockage effect diminishes as one moves from tip to hub.

Linear Cavitation Model

I will now present some sheet cavitation models that one can consider. Some of these have been considered by Penn State. Additional ideas are presented that can provide a more accurate and simpler treatment of the cavitation problem. This viewgraph describes the linear cavitation sheet model. In such a model the cavity interface is treated as a streamline with a constant pressure equal to the vapor pressure. The approach is analogous to classical linear theory used in the potential flow codes. Interface conditions are transferred to the solid body and zero normal velocity condition is relaxed at the solid boundary. Thus the pressure of the solid boundary adjacent to the bubble will be equal to the vapor pressure. The relaxing of zero normal velocity condition at the solid boundary simply discards all flow quantities interior to the cavity and correct blockage effects are simulated outside of the cavity. The disadvantage of the approach is that it does not explicitly treat the vapor phase and that the approach is not robust. Since the approach handles only the liquid phase, the modeling can not be accurate for cryogenic fluids operating near the critical point. There can be certain cavity termination problems in 2-D which can only become worse in three spatial dimensions.

Non-Linear Cavitation Model

In the non-linear cavitation model, the cavity interface is again regarded as a streamline with a specified cavitation pressure. The basic difference between the linear and non-linear models is that the computational domain evolves with the solution procedure as a sequence of linear solutions followed by modifications of the domain to accommodate the cavity geometry. Thus the computational domain is regridded after locating the positions where the cross-over below the vapor pressure occurs. These cross-over points are recomputed subsequently for a better definition of the cavity. One can, in principle, iterate to a "correct" cavity geometry via these multiple passes. The disadvantage of the approach is that mesh movement may introduce significant grid distortions and the grid lines may actually cross for complicated configurations. Significant man power efforts are already spend in gridding complicated configurations, it will make sense to retain these meshes for a cavitating flow. Hence a non-linear cavitation approach that holds the base grid will be highly desirable. It should also be pointed out that regridding may only be suitable for box-like domains and may have significant problems for complex 3-D configurations. For example, there can be multiple cavities in a domain, or a cavity may be completely embedded in the domain and not hooked to a physical boundary. There are other disadvantages with respect to the physics of cavitation sheet models. If $p > p_v$, then the fluid remains a liquid; otherwise the fluid is in the vapor phase. No dynamics of the vapor phase are included in the computations, so for example, the change in volume in flashing to a vapor, or the collapse in volume due to condensation is not taken into account. These effects can be accounted by considering a multi-phase approach with more elaborate description of physics. However, the incorporation of two-phase flows can only be accommodated in a regridding methodology with some difficulty.

Proposed Cavitation Model

I will now present a non-linear two-phase sheet model in which a structured grid does not have to be regenerated. Firstly, for the sake of all subsequent discussion, consider the static pressure to be referenced from vapor pressure. Thus pressures below the vapor pressure are regarded as negative pressure for the liquid. First carry out a single phase (liquid) CFD solution to convergence. Regard cells with positive pressure on all nodes as liquid cells, regard cells with all negative node pressures as vapor cells for subsequent iterations, and regard all remaining cells as interface cells where both liquid and vapor fluxes will be carried out simultaneously. The third step is to determine the liquid vapor interface as zero crossing for pressure on the edges of interface cells. Consider a 2-D cell $acef$ shown in the viewgraph for reference. Treat the liquid-vapor interface bd locally as a streamline. This means that one should discard the velocity components normal to the streamline. Suppose u_b^p is the predicted value of velocity at the zero crossing point b based upon linear interpolation of the edge values ac. Let u_b^c be the corrected value of the velocity that discards the velocity component normal to the line bd. Then redo the flux balance for the liquid part of the cell on nodes $abdef$. Except for the pressure terms in the momentum and energy equations, the interface bd yields a zero flux. Thus the flux balance for x-momentum equation on the interface bd is simply:

$$\int_{bd} (\rho u^2 + p)dy - \rho uvdx = p_v \Delta y_{bd}.$$

Based upon the new flux balance, one can compute the "distribution formulas" for nodes aef. These distribution relations yield contribution of the cell flux balance to the corresponding nodes (See Ni's classical AIAA Journal Paper, 1985). A similar flux balance can be carried out for the vapor part of the cell. One can, in fact, regard the interface cell nodes to be multiply defined for vapor and liquid parts. Thus the liquid part will have real fluid values at nodes aef and fictitious values at node c. The flux balance can be carried out independently based upon the real and fictitious values and the nodes updated separately. This approach constitutes a simple two-phase approach to cavitation without the mesh regridding option. Note that I have not specifically stated anything about the physics of two-phase flows yet. A more elaborate two-phase approach without appropriate physics may only yield qualitatively correct answers. This follows on the next viewgraph.

Additional Modeling Enhancements

A more elaborate equation of state which is approximately valid in the gas/liquid two-phase region, as well as at moderately high temperatures is needed. A suitable model that describes the law of corresponding states can be easily implemented for the thermal equation of state (that relates pressure, density and temperature). This has to be coupled with a more representative caloric equation of state (that relates specific heat to temperature). One has to also employ a more accurate energy equation to describe two-phase flow physics. This basically includes latent heat of vaporization for the vapor phase. Certain cryogenic fluids, with critical temperatures below 50 K, exhibit quantum effects, and do not necessarily satisfy the principle of corresponding states. A more elaborate equation of state, possibly in the form of look up tables, may be needed for these fluids. Note that both liquid hydrogen and helium exhibit these quantum effects. Liquid hydrogen is a common fluid for rocket engine fuel pumps. Lastly, one can utilize mesh adaptation to locally subdivide the cells in the vicinity of liquid-vapor interface to impart additional spatial resolution. This will eliminate the need to carry out multi-valued flux balance, providing that the embedded cells are reasonably resolved. Note that embedded mesh adaptation does not regrid the "base" mesh, the skewness of the embedded meshes will only be limited by the skewness of the coarse mesh, and that cells can never cross if the base mesh is not crossed over. Pratt & Whitney already has suitable data base structure for handling this approach.

Closure

A CFD solution for ATD inducer/impeller pump configuration, with splitters, has been presented at the design point. This solution points to the existence of a cavitation bubble in the domain. Current cavitation approach employs a separate potential flow cavitation sheet model that yields cavitation correction factors for the CFD predicted pressure loads. Penn State University is currently studying linear and non-linear approaches for handling 3-D configurations. If a suitable linear cavitation approach can constitute a simple and effective model, we will implement such a model in the Pratt & Whitney design code. Additional enhancements for two-phase flows and more accurate physics will be considered as part of a long-term effort.

AN INDUCER CFD SOLUTION AND EFFECTS ASSOCIATED WITH CAVITATION

M. Pervaiz
J. Garrett
J. Kuryla

Pratt & Whitney, GESP
West Palm Beach, Florida

April 20, 1993

Presented At Workshop for CFD Applications in Rocket Propulsion, NASA–MSFC

OUTLINE

- Atd inducer/impeller CFD Analysis
- Current cavitation modeling approach
- Review of cavitation approaches
- Suggestions for future modeling
- Closure

ATD 14.6 Degree Inducer-Impeller with Splitters

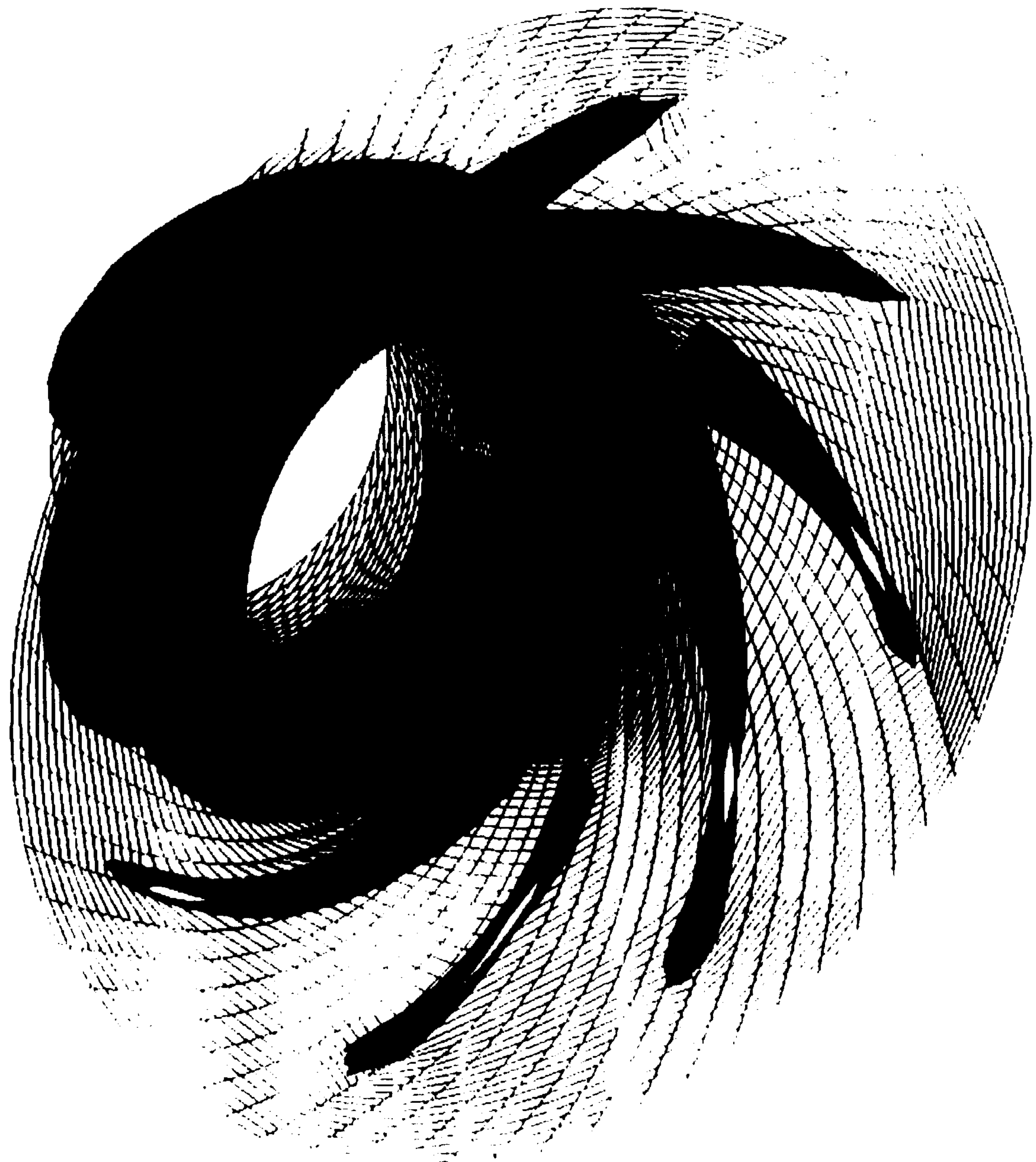

ATD 14.6 Degree Inducer Impeller w/ Splitter

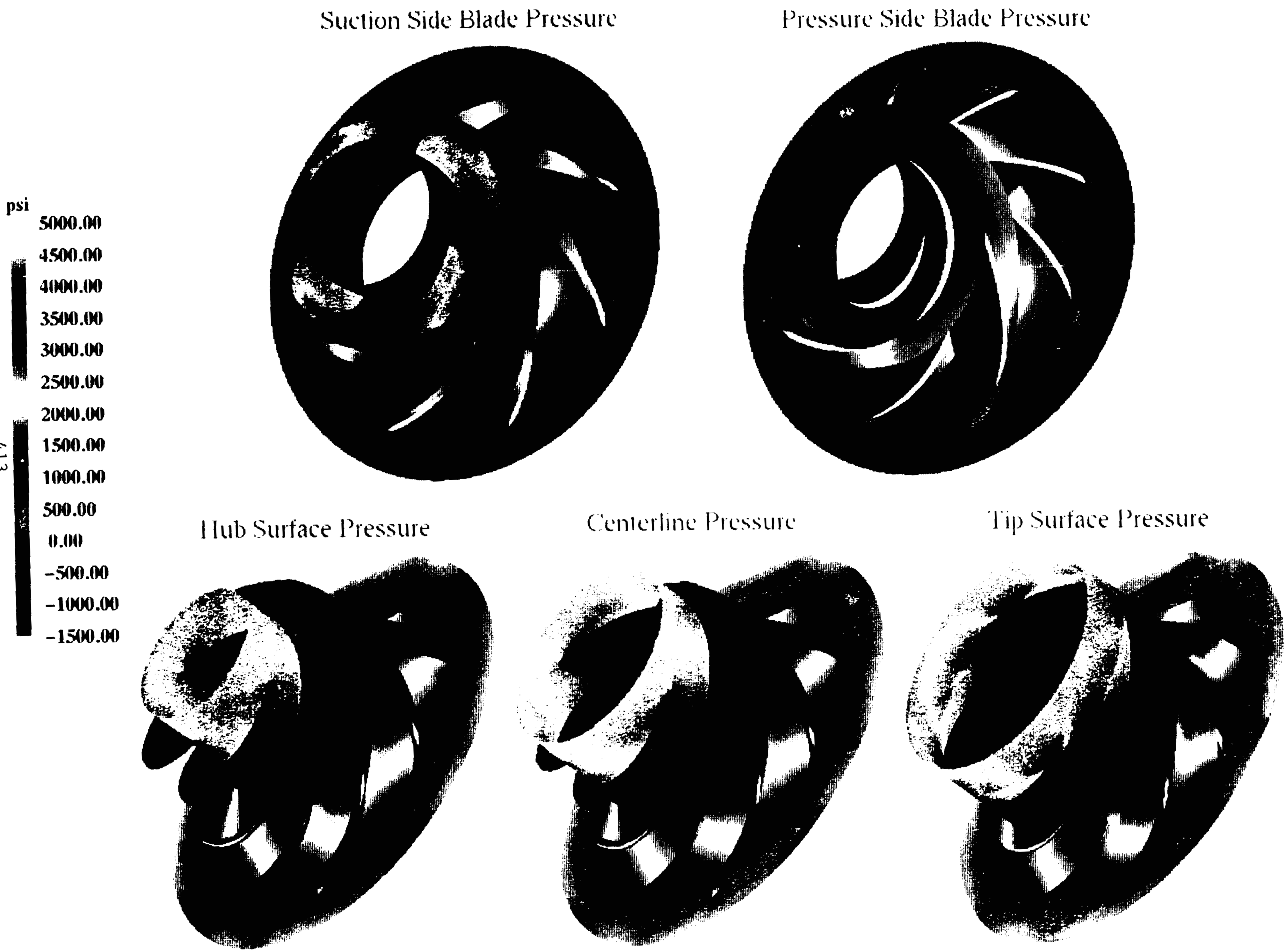

CURRENT CAVITATION PROCEDURE APPLIED TO ATD CONFIGURATION

- Compute single phase 3–D CFD solution for the ATD configuration. Calculation shows pressures less than vapor pressure on suction side near the blade tip.

- Compute 2–D potential flow cavitation sheet model to obtain cavitation correction factors for *pressure loads* as a function of tip chord length.

- Scale cavitation correction factors linearly such that no correction is needed at the hub. This yields a 2–D distribution on blade surface.

$$\Delta p_{cor} = K(s,r)\ \Delta p_{sheet}$$

- Transform cavitation correction factors for delta–pressure to suction side pressure in the CFD solution.

$$P_s = P_p - \Delta P_{cor}$$

- As a sanity check verify that the corrected suction pressure remains above the vapor pressure.

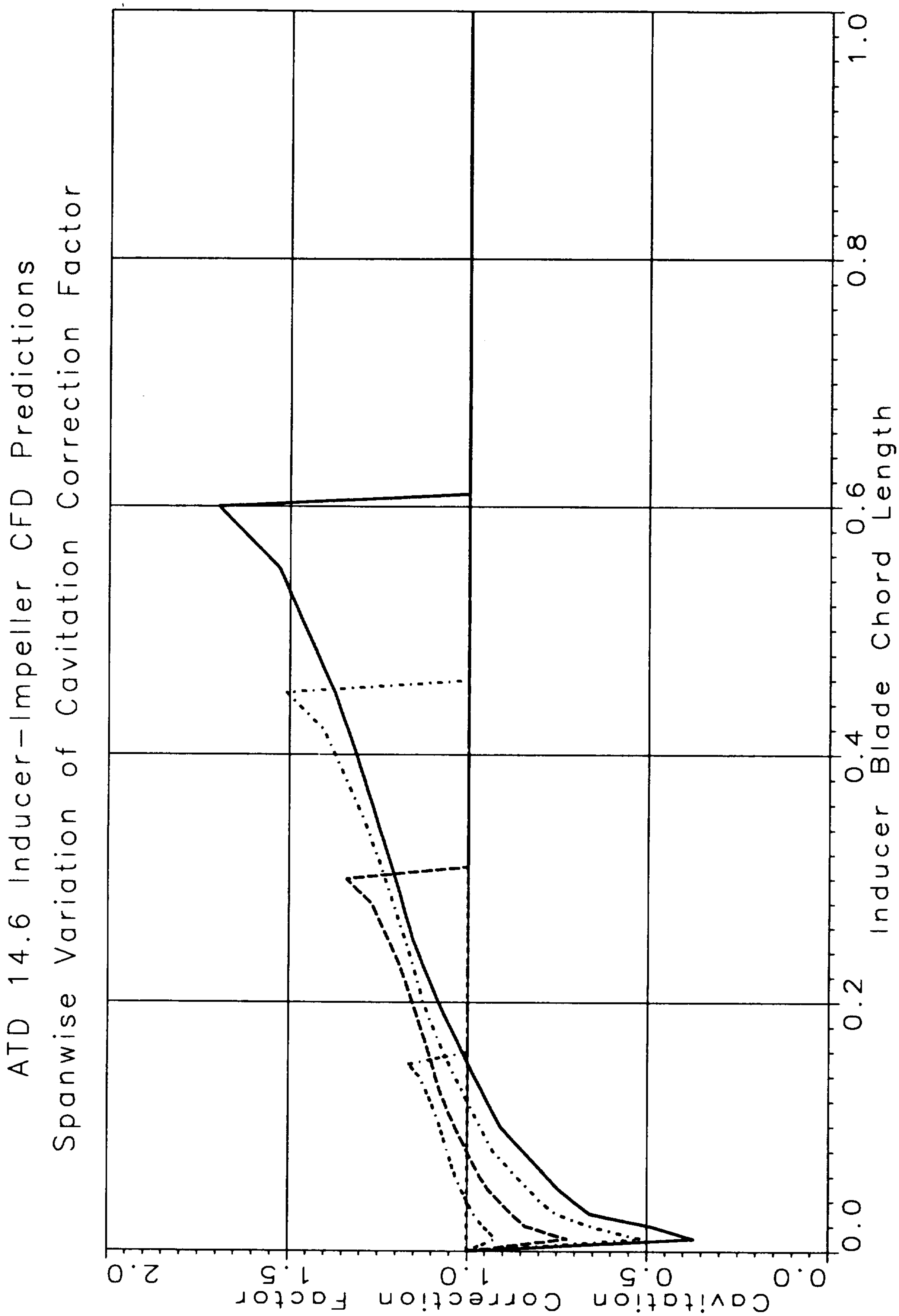
ATD 14.6 Inducer-Impeller CFD Predictions
Spanwise Variation of Cavitation Correction Factor
Inducer Blade Chord Length
Cavitation Correction Factor
0.0
0.2
0.4
0.6
0.8
1.0
0.0
0.5
1.0
1.5
2.0

ATD 14.6 Inducer–Impeller CFD Predictions
Inducer Blade Delta Pressures

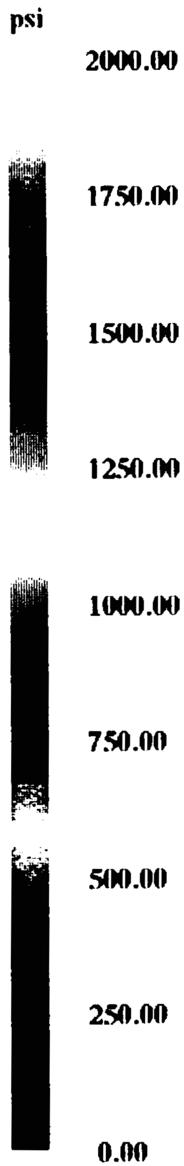

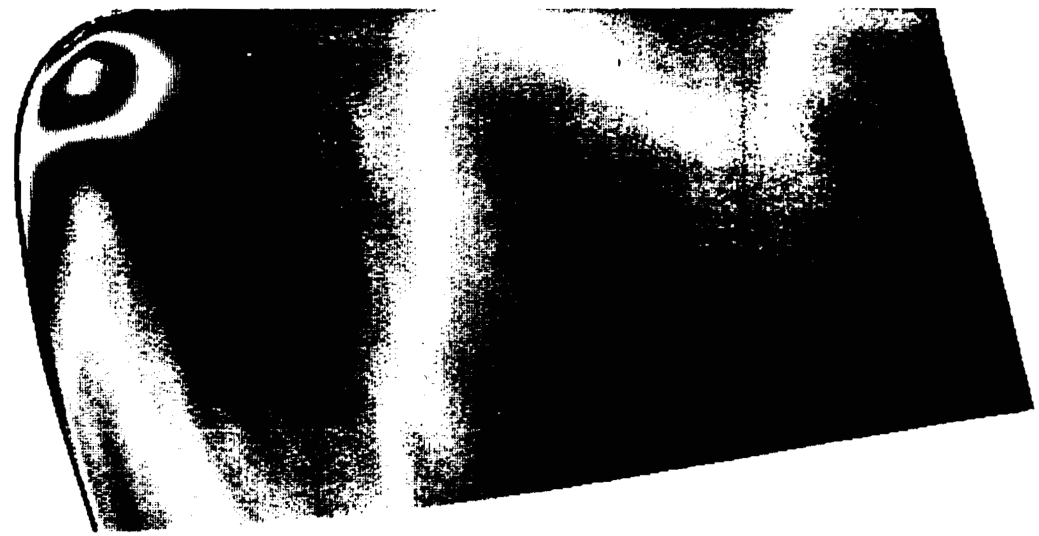

No Cavitation Correction

Corrected for Cavitation

ATD 14.6 Inducer–Impeller CFD Predictions
Inducer Blade Suction–Side Pressure

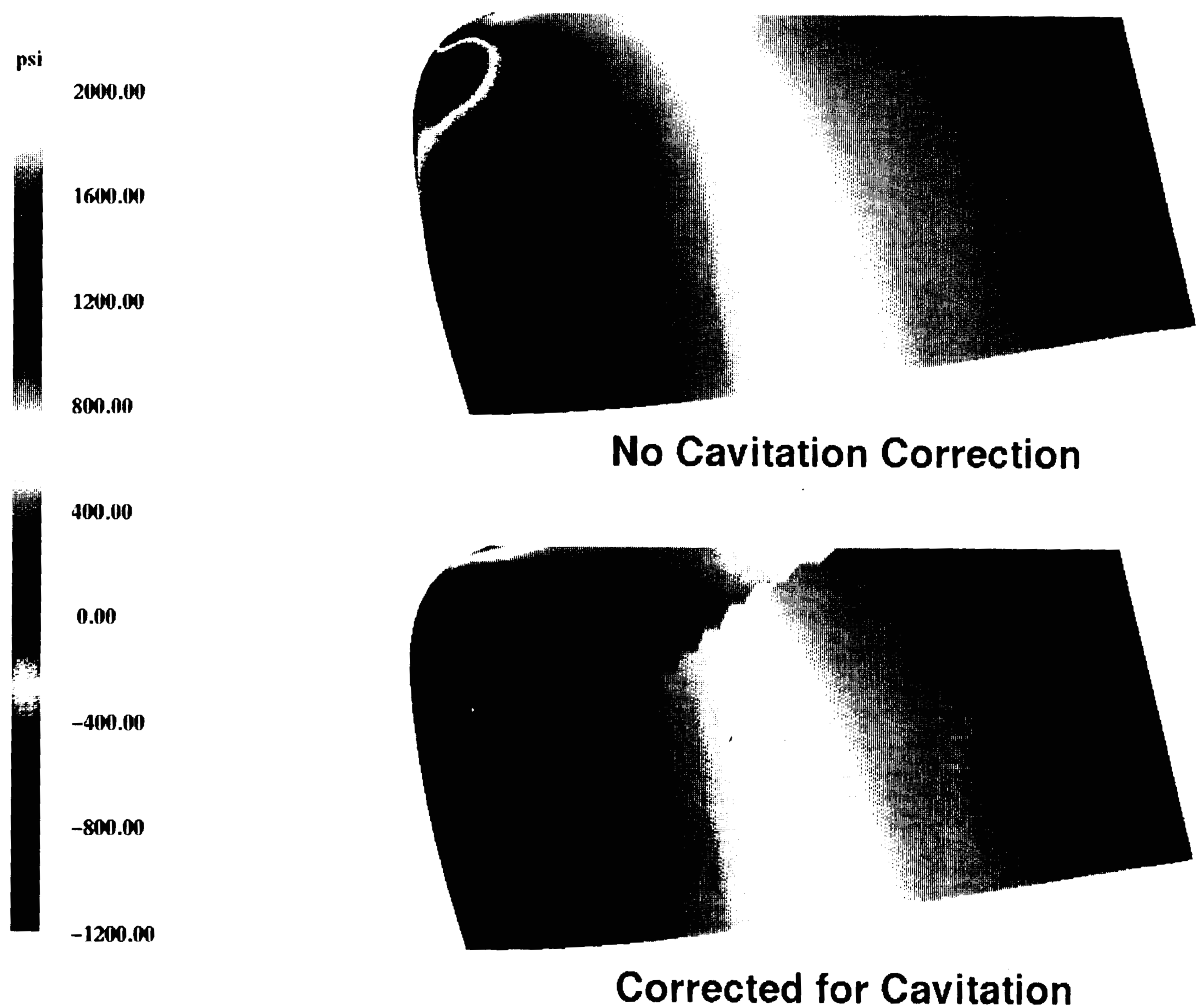

LINEAR CAVITATION MODEL

- Cavity interface is treated as a streamline
- Analogous to classical linear theory used in potential flow codes
- Interface conditions are transferred to the body surface
- Zero normal velocity condition is relaxed at solid boundaries
- Approach does not treat vapor phase.
- Approach is not robust – cavity termination problems

NON–LINEAR CAVITATION MODEL

- Cavity interface is treated as a streamline with a specified cavitation pressure

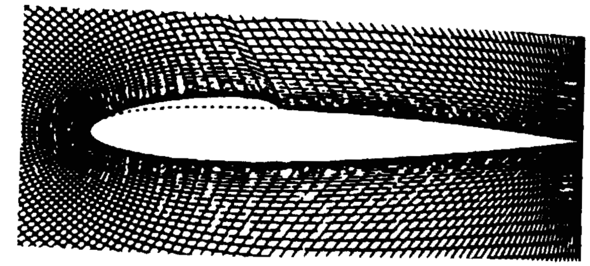

- Computational domain evolves with solution procedure as a sequence of linear solutions followed by modifications of the domain to accommodate cavity geometry.
- Mesh movement may introduce significant grid distortions and grid–lines may actually cross.
- Regridding may only be suitable for box–like domains and may have significant problems for complex 3–D configurations.
- 2–phase flows can be accommodated with difficulty.

PROPOSED CAVITATION MODEL

- Carry Out Flux Balance for Both Liquid and Vapor Cells Separately.

- Carry Out Flux Balance for Liquid and Vapor Parts of Interface Cells. These Cells Will Have Multiply Defined Values at Nodes.

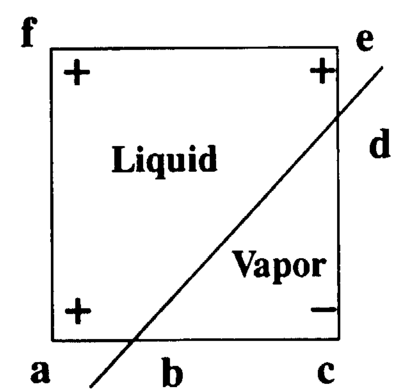

- Nodes a, e, f Have Real Values for Liquid and Fictitious Values For Vapor.
  Node c Has Real Values for Vapor and Fictitious Values for Liquid.

- Liquid and Vapor Nodes of Interface Cells Will Vary Independently.

- This Constitutes a Non−linear Multi−phase approximation to Cavitation Without the Mesh Regridding Option.

ADDITIONAL MODELING ENHANCEMENTS

- ☐ Employ a more elaborate equation of state which is approximately valid in gas/liquid two–phase region, as well as at moderately high temperature.
- ☐ Employ a more accurate energy equation to describe two–phase flow physics.
- ☐ Certain cryogenic fluids, with critical temperature below 50 K, exhibit quantum effects, and do not necessarily satisfy the principle of corresponding states.
- ☐ Embedded mesh adaptation can eliminate the need for carrying out multi–valued flux balance.

CLOSURE

- A CFD solution for ATD inducer/impeller with splitters is presented.
- Current cavitation approach employs a separate potential flow code that yields cavitation correction factors for the CFD solution.
- Penn State is studying linear and non–linear approaches for 3–D configurations.
- A suitable linear cavitation model will be implemented in the Pratt & Whitney design code.
- Additional enhancements will be considered in the future.

N95- 23632

CURRENT STATUS IN CAVITATION MODELING

by

Ashok K. Singhal and Ram K. Avva
CFD Research Corporation, Huntsville, AL

for presentation at
Open Forum on "Turbomachinery-Pumps-Cavitation"

11th Workshop for CFD Applications in Rocket Propulsion
NASA Marshall Space Flight Center, AL

April 20-22, 1993

Cavitation is a common problem for many engineering devices in which the main working fluid is in liquid state. In turbomachinery applications, cavitation generally occurs on the inlet side of pumps. The deleterious effects of cavitation include: lowered performance, load asymmetry, erosion and pitting of blade surfaces, vibration and noise, and reduction of the overall machine life.

Cavitation models in use today range from rather crude approximations to sophisticated bubble dynamics models. Details about bubble inception, growth and collapse are relevant to the prediction of blade erosion, but are not necessary to predict the performance of pumps. An engineering model of cavitation is proposed to predict the extent of cavitation and performance. The vapor volume fraction is used as an indicator variable to quantify cavitation. A two-phase flow approach is employed with the assumption of the thermal equilibrium between liquid and vapor. At present velocity slip between the two phases is selected. Preliminary analyses of 2D flows shows qualitatively correct results.

CFD Research Corporation
3325-D Triana Blvd. ■ Huntsville, AL 35805 ■ (205) 536-6576 ■ FAX: (205) 536-6590

CURRENT STATUS IN CAVITATION MODELING

by
A. K. Singhal and R. K. Avva

for Presentation at:
11*th* Workshop for CFD Applications in Rocket Propulsion
NASA Marshall Space Flight Center, AL

April 20-22, 1993

PA-93-8PR/01

BOILING VS CAVITATION

Boiling is phase change at constant pressure due to addition of external heat.

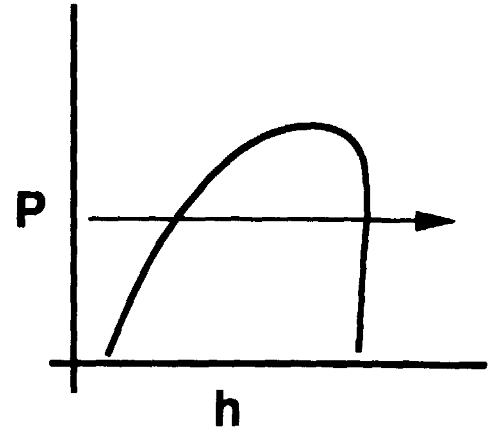

Cavitation is phase change due to lowering of hydrodynamic pressure under adiabatic conditions.

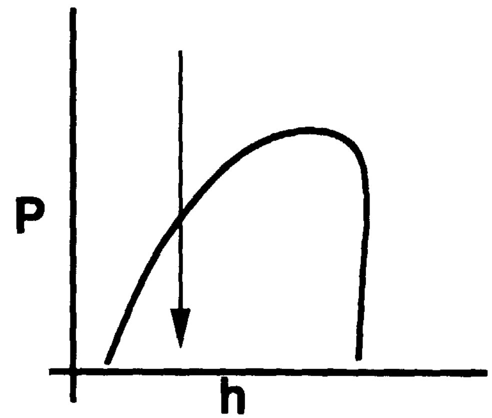

PA-93-8PR/02

HIERARCHY OF CAVITATION MODELS

CFDRC

LEVEL	METHODOLOGY
1	Single-phase flow analysis; identify cavitated zones where $P < P_V$
2	Single-phase flow analysis; Set $P = P_V$ in regions where $P < P_V$; iteratively identify cavitated zones
3	Two-phase flow analysis with a vapor source equation
4	Two-phase flow analysis with bubble-dynamics equations

PA-93-8PR/03

COMMENTS

CFDRC

- **Level 1 Approach:** O.K. but too conservative
- **Level 2 Approach:** too weak, and can be misleading
- **Level 3 Approach:** Acceptable and sufficient for performance prediction; Accuracy depends on Vapor Source Equation
- **Level 4 Approach:** Needed for accurate prediction of local damage sites of bubble bursting, *etc.*
- **Selected Approach:** Level 3

PA-93-8PR/04

TWO-PHASE FLOW METHODS

Method	Governing Equations	Velocity Slip	Interphase Friction
Homogenous	Mixture momentum Mixture continuity Mixutre enthalpy	0	–
Algebraic slip	Same as homogenous but with velocity-slip terms	Needs to be modeled	–
Two-fluid	Phasic momentum Mixture and/or Phasic continuity Mixture Enthalpy	$U_g - U_\ell$	Needs to be modeled
Eulerian-Lagrangian	Continuum equations for continuous phase Particle tracking	$U_g - U_\ell$	Needs to be modeled

PA-93-8PR/05

DENSITY CHANGES IN ENGINEERING FLOWS

FLOW TYPE	ρ_{max}/ρ_{min}
Buoyant Flows	1.1
Transonic Flows	2.0
Supersonic Flows	10.0
Reacting Flows	20.0
Cavitating Flows	1000.0

$$\frac{\partial \rho}{\partial p} \approx \frac{1}{C^2}$$

C= Sound Speed

Medium	Sound Speed (m/s)
Air	300
2ϕ Diesel	1.6

- Large density variations give rise to stiff equations
- Smaller sound speed slows down information propagation
- Cavitating flows offer a very stringent challenge to numerical schemes

PA-93-8PR/06

TEST PROBLEM

CFDRC

Geometry:	**Axisymmetric Orifice; D/d = 3**
Fluid:	**Diesel**
Flow Conditions:	**P_{exit} = 1 Bar; T = 187°C; ρ_{ℓ}/ρ_{v} = 283**
Study 1:	**Effect of varying inlet pressure**
Study 2:	**Effect of geometry change (rounded entrance; γ/R = 15%)**

PA-93-8PR/07

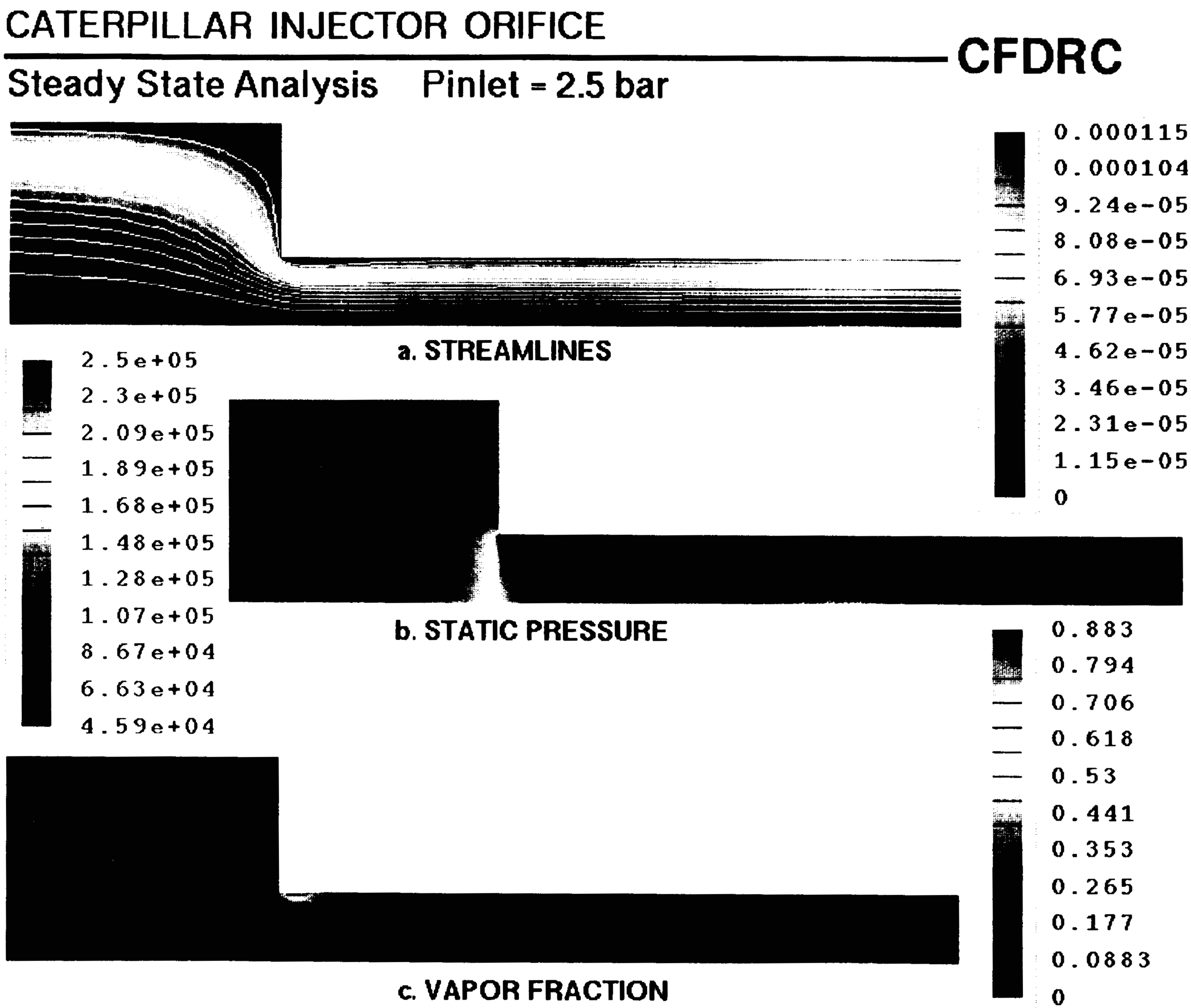

a. STREAMLINES

b. STATIC PRESSURE

c. VAPOR FRACTION

CATERPILLAR INJECTOR ORIFICE — CFDRC

Steady State Analysis   Pinlet = 3.0 bar

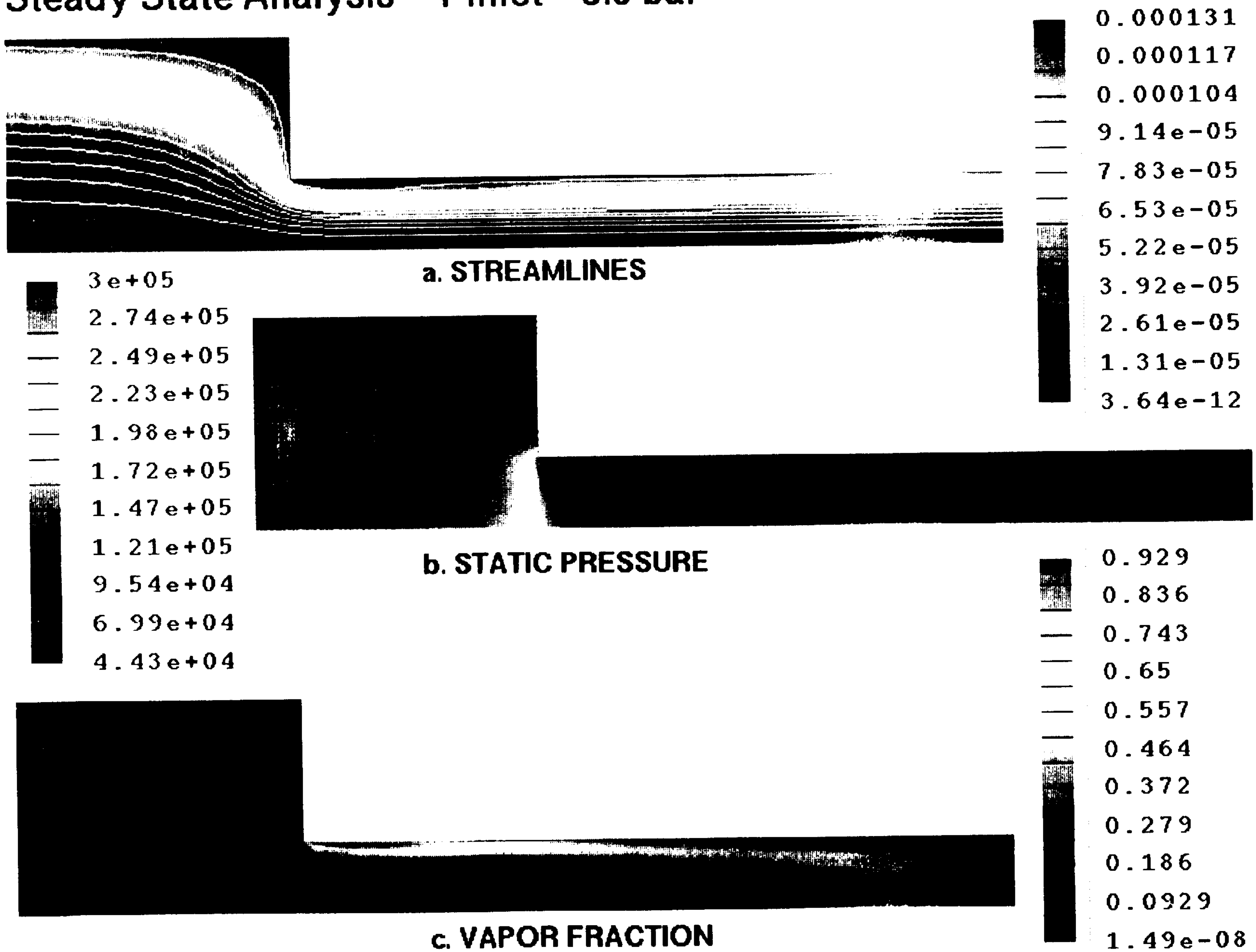

a. STREAMLINES

b. STATIC PRESSURE

c. VAPOR FRACTION

CATERPILLAR INJECTOR ORIFICE

CFDRC

Steady State Analysis   Pinlet = 10.0 bar

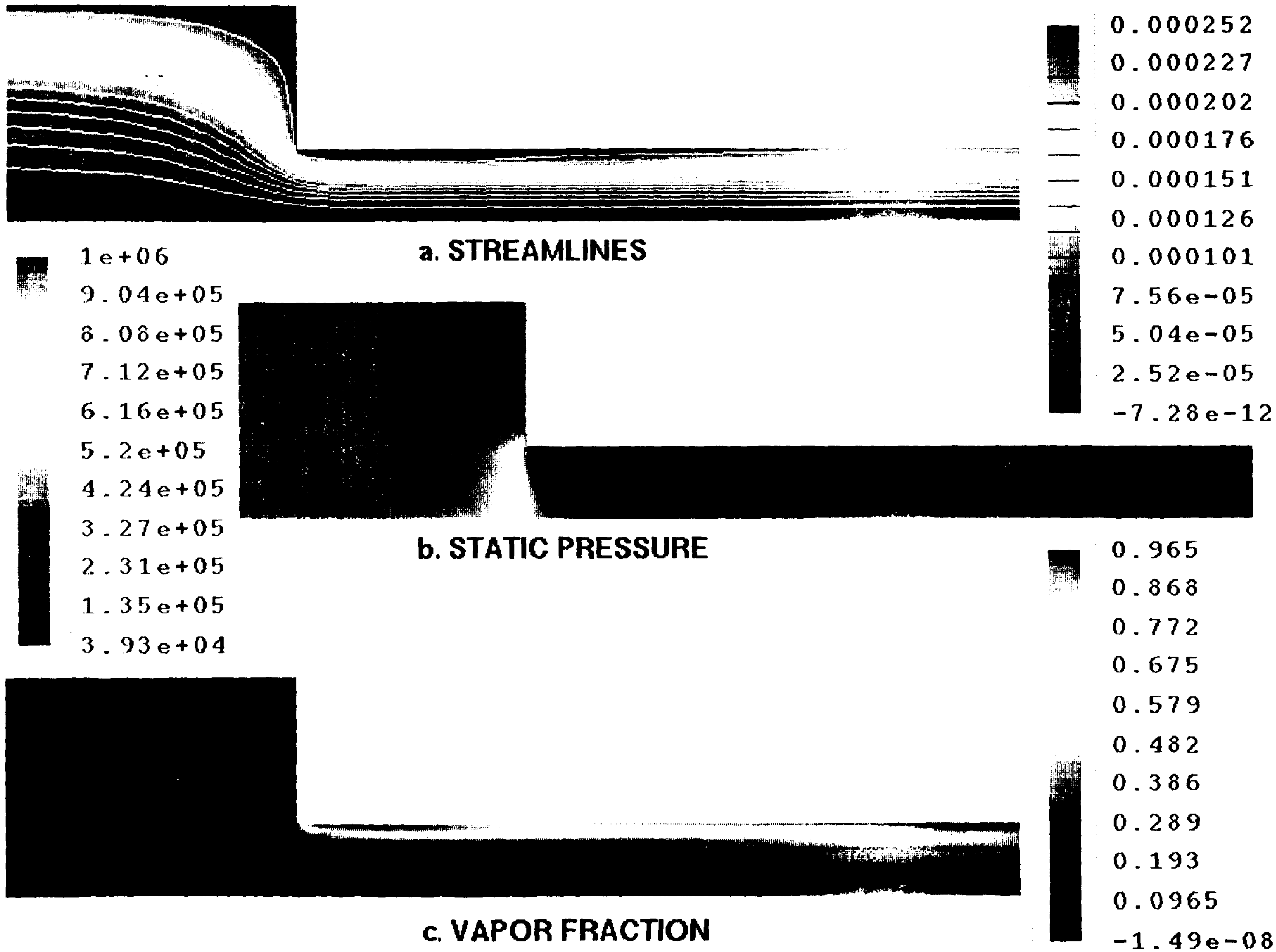

CATERPILLAR INJECTOR ORIFICE

CFDRC

Effect of Edge Shape on Void Fraction   Pinj=4 bar

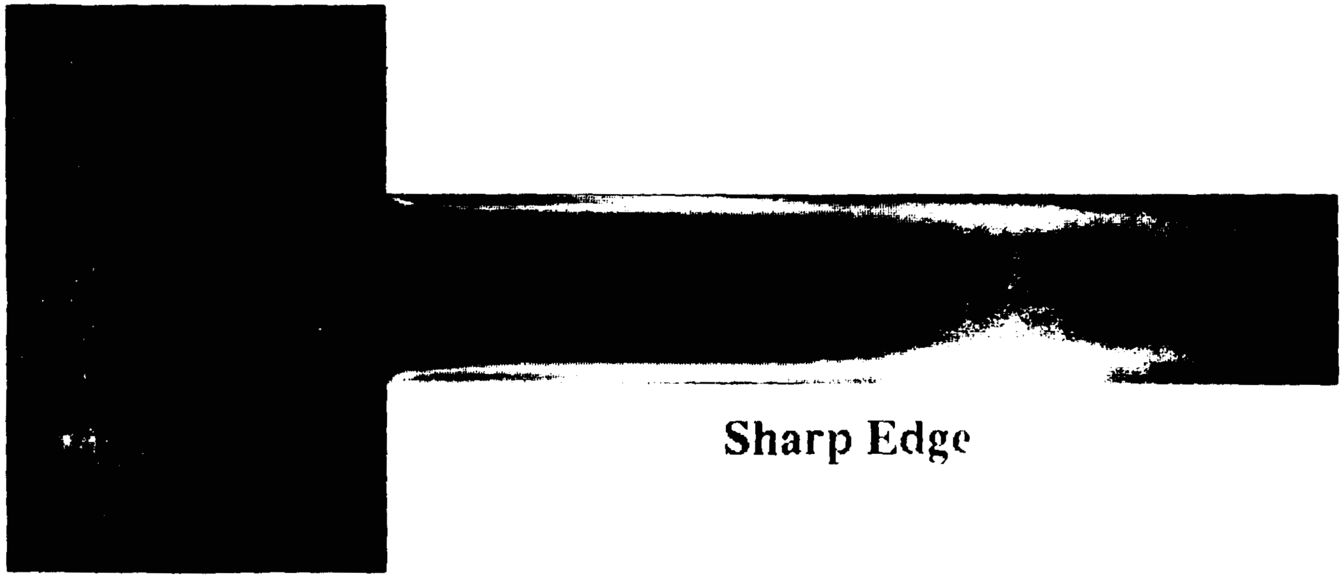

Sharp Edge

Rounded Edge

SUMMARY

CFDRC

- Test Problem Results:
  1) As inlet pressure increases, state of cavitation changes from subcritical to supercritical.
  2) The rounded entrance reduces cavitation.

- Preliminary results are encouraging

- Considerable future work needed for:
  1) Robustness and accuracy improvements of basic method.
  2) Adaptation for complex geometries with additional body forces (*e.g.* due to rotation)
  3) Validation under a variety of flow conditions.

PA-93-8PR/ 09

N95-23633

A GENERALIZED EULERIAN-LAGRANGIAN ANALYSIS, WITH APPLICATION TO LIQUID FLOWS WITH VAPOR BUBBLES†

Frederik J. de Jong and Meyya Meyyappan
Scientific Research Associates, Inc.
Glastonbury, CT

Presented at the
Workshop for Computational Fluid Dynamics Applications
in Rocket Propulsion

April 20-22, 1993

ABSTRACT

Under a NASA MSFC SBIR Phase II effort an analysis has been developed for liquid flows with vapor bubbles such as those in liquid rocket engine components. The analysis is based on a combined Eulerian-Lagrangian technique, in which Eulerian conservation equations are solved for the liquid phase, while Lagrangian equations of motion are integrated in computational coordinates for the vapor phase. The novel aspect of the Lagrangian analysis developed under this effort is that it combines features of the so-called particle distribution approach with those of the so-called particle trajectory approach and can, in fact, be considered as a generalization of both of those traditional methods. The result of this generalization is a reduction in CPU time and memory requirements. Particle time step (stability) limitations have been eliminated by semi-implicit integration of the particle equations of motion (and, for certain applications, the particle temperature equation), although practical limitations remain in effect for reasons of accuracy. The analysis has been applied to the simulation of cavitating flow through a single-bladed section of a labyrinth seal. Models for the simulation of bubble formation and growth have been included, as well as models for bubble drag and heat transfer. The results indicate that bubble formation is more or less "explosive": for a given flow field, the number density of bubble nucleation sites is very sensitive to the vapor properties and the surface tension. The bubble motion, on the other hand, is much less sensitive to these properties, but is affected strongly by the local pressure gradients in the flow field. In situations where either the material properties or the flow field are not known with sufficient accuracy, parametric studies can be carried out rapidly to assess the effect of the important variables. Future work will include application of the analysis to cavitation in inducer flow fields.

----

† This work was supported by NASA Marshall Space Flight Center under Contract NAS8-38959.

OBJECTIVE:

DEVELOPMENT OF AN ANALYSIS FOR LIQUID FLOWS WITH VAPOR BUBBLES (SUCH AS THOSE IN BEARINGS, SEALS, AND PUMPS) FOR USE IN DESIGN OF LIQUID ROCKET ENGINE COMPONENTS

APPROACH:

USE A COMBINED EULERIAN-LAGRANGIAN ANALYSIS

- CONTINUOUS (LIQUID) PHASE TREATED BY SOLVING EULERIAN CONSERVATION EQS. (N-S EQS.) WITH DISCRETE PHASE SOURCE TERMS
- DISCRETE (VAPOR BUBBLE) PHASE TREATED BY INTEGRATING LAGRANGIAN EQUATIONS OF MOTION IN COMPUTATIONAL COORDINATES

Scientific Research Associates

LAGRANGIAN ANALYSIS - METHODOLOGY

- GENERALIZATION OF PARTICLE TRAJECTORY AND PARTICLE DISTRIBUTION MODELS

  ⇒ REDUCED CPU TIME AND STORAGE REQUIREMENTS

- STABLE INTEGRATION OF LAGRANGIAN EQUATIONS OF MOTION IN COMPUTATIONAL COORDINATES

  ⇒ NO PARTICLE TIME STEP LIMITATION OTHER THAN FOR ACCURACY

Scientific Research Associates

LAGRANGIAN ANALYSIS - FEATURES

- LAGRANGIAN DISCRETE PHASE ANALYSIS INTERFACES WITH EULERIAN CONTINUOUS PHASE ANALYSIS VIA ONE SINGLE SUBROUTINE
- GENERALIZED ARRAY ADDRESSING AND INDEX / VARIABLE NUMBERING

  ⇒ LAGRANGIAN ANALYSIS CAN BE HOOKED UP TO A VARIETY OF EULERIAN CODES ("FLOW SOLVERS")

- CODE IS MODULAR W.R.T. PHYSICAL MODELS

Scientific Research Associates

APPLICATION TO VAPOR BUBBLES

- MODELS NEEDED FOR BUBBLE FORMATION, GROWTH / COLLAPSE AND MOTION
- CRITICAL PHYSICAL PARAMETERS:
  - SURFACE TENSION
  - VAPOR PRESSURE - TEMPERATURE RELATION (CLAUSIUS-CLAPEYRON EQUATION)

Scientific Research Associates

BUBBLE FORMATION

- NUCLEATION DUE TO LOCAL P DROP; USE HOMOGENEOUS NUCLEATION MODEL (KATZ AND BLANDER)

$$J\left(\frac{\text{NUCLEI}}{M^3 S}\right) = n\left(\frac{2\sigma}{\pi M}\right)^{1/2} \exp\left[\frac{-16\pi\sigma^3}{3\kappa T(P_e - P_L)^2}\right]$$

J : NUMBER OF NUCLEATION SITES PER UNIT VOLUME AND TIME

P_e : EQUILIBRIUM VAPOR PRESSURE

P_L : PRESSURE IN LIQUID

T : TEMPERATURE OF THE LIQUID

σ : SURFACE TENSION

k : BOLTZMANN CONSTANT

M : MOLECULAR WEIGHT

n : MOLECULAR NUMBER DENSITY IN LIQUID

Scientific Research Associates

BUBBLE GROWTH

- AFTER THE INITIAL GROWTH PERIOD (WHICH IS INERTIA CONTROLLED) THE PRESSURE INSIDE THE BUBBLE IS DETERMINED BY THE YOUNG-LAPLACE EQUATION

$$P_e - P_L = 2\sigma / R$$

- THE BUBBLE TEMPERATURE IS ASSUMED TO BE EQUAL TO THE SATURATION TEMPERATURE AT THE PRESSURE P_e
- BUBBLE GROWTH IS DETERMINED BY THE ENERGY EQUATION

Scientific Research Associates

ENERGY EQUATION FOR BUBBLE

$$q = m\, c_p \dot{T}_p + \dot{m}\, h_{fg}$$

c_p : VAPOR-PHASE SPECIFIC HEAT

h_{fg} : LATENT HEAT OF EVAPORATION

$\dot{m}$: BUBBLE MASS GROWTH RATE ("EVAPORATION RATE")

$\dot{T}_p$: RATE OF CHANGE OF BUBBLE TEMPERATURE

$$\dot{T}_p = \left(\frac{dT}{dp}\right)_{sat} \vec{U} \bullet \nabla p$$

Scientific Research Associated

HEAT TRANSFER RATE TO BUBBLE

$$q = Nu\, \pi\, D\, \kappa \left(T - T_p\right)$$

Nu : NUSSELT NUMBER

D : BUBBLE DIAMETER

κ : THERMAL CONDUCTIVITY OF THE LIQUID

T : LIQUID TEMPERATURE

T_P : BUBBLE TEMPERATURE

Scientific Research Associated

BUBBLE EQUATION OF MOTION

$$\vec{F} = m\left(1+\frac{\Delta_A}{2}\frac{\rho}{\rho_p}\right)\frac{d^2\vec{X}}{dt^2}$$

ρ : LIQUID DENSITY

ρ_p : VAPOR DENSITY

Δ_A : ADDED MASS COEFFICIENT (=1 FOR STOKES FLOW)

m : BUBBLE MASS

$\vec{X}$: BUBBLE POSITION VECTOR

$\vec{F}$: FORCE ON BUBBLE
- DRAG FORCE
- BUOYANCY
- PRESSURE GRADIENT

Scientific Research Associated

DRAG COEFFICIENT

- FOR BUBBLES

$$C_D\left(=\frac{2F_d}{\pi\rho a^2 u^2}\right) = 14.9 / Re^{0.78} \quad Re > 2$$

$$= 16 / Re \quad Re < 2$$

GOOD FIT TO NUMERICAL SOLUTION
COMPARES WELL WITH EXPERIMENTS, WIDELY USED

- FOR SOLID SPHERES

$$C_D = \frac{24}{Re}\,[1 + 0.15\, Re^{0.687}] \quad Re < 1000$$

$$= 0.438, \quad Re > 1000$$

- NOTE: FOR SAME a AND u, DRAG ON A BUBBLE IS SMALLER (FACTOR 6 FOR Re = 900)

Scientific Research Associates

COMPUTATIONAL TEST CASE

SINGLE BLADE LABYRINTH SEAL

APPROXIMATES ONE BLADE OF THE LOX PREBURNER

BOOST PUMP IMPELLER SEAL IN THE SSME

FLOW CONDITIONS:

INLET PRESSURE	: 3.67 MPa (532 psi)
INLET TEMPERATURE	: 130 K (234 °R)
DENSITY	: 1088 kg/m^3 (167.9 lb/ft^3)
PRESSURE DROP	: 1.47 MPa (213 psi)

Scientific Research Associated

GEOMETRY

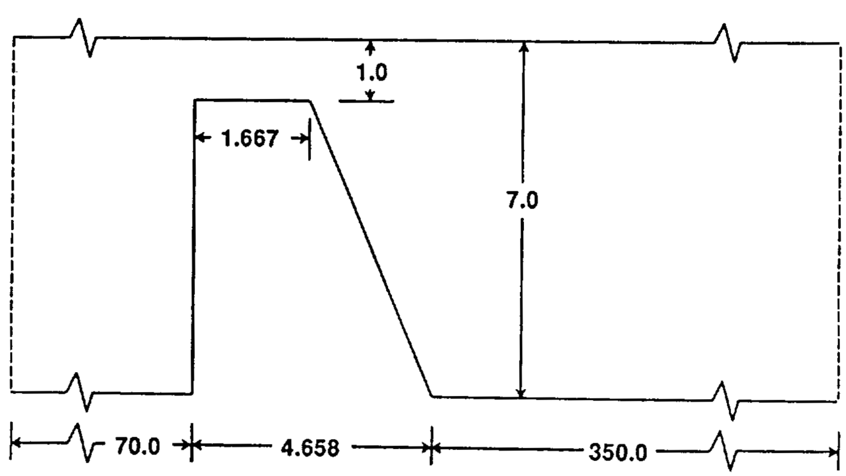

SEAL GAP: 1.524×10^{-4} m (0.006 inch)

Scientific Research Associated

COMPUTATIONAL GRID

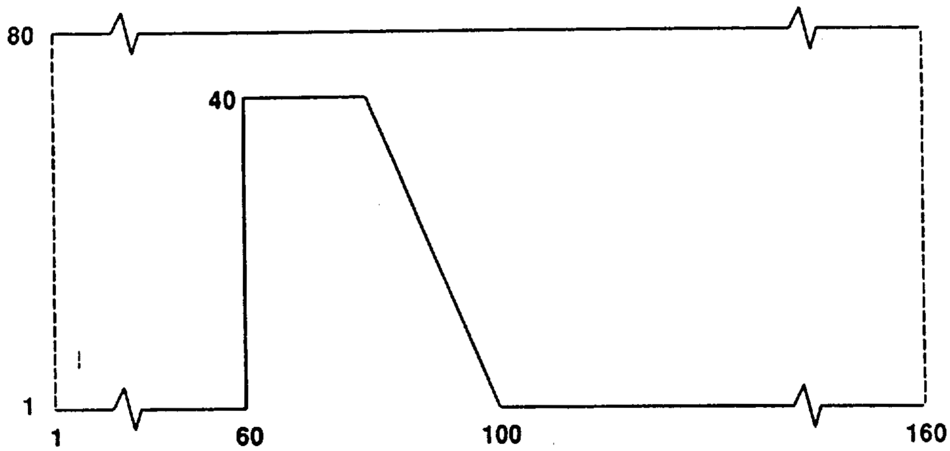

80 x 160 GRID

NEAR-WALL RESOLUTION IN THE GAP = 1.0×10^{-4} (= 0.015 μm)

Scientific Research Associated

COMPUTATIONAL GRID

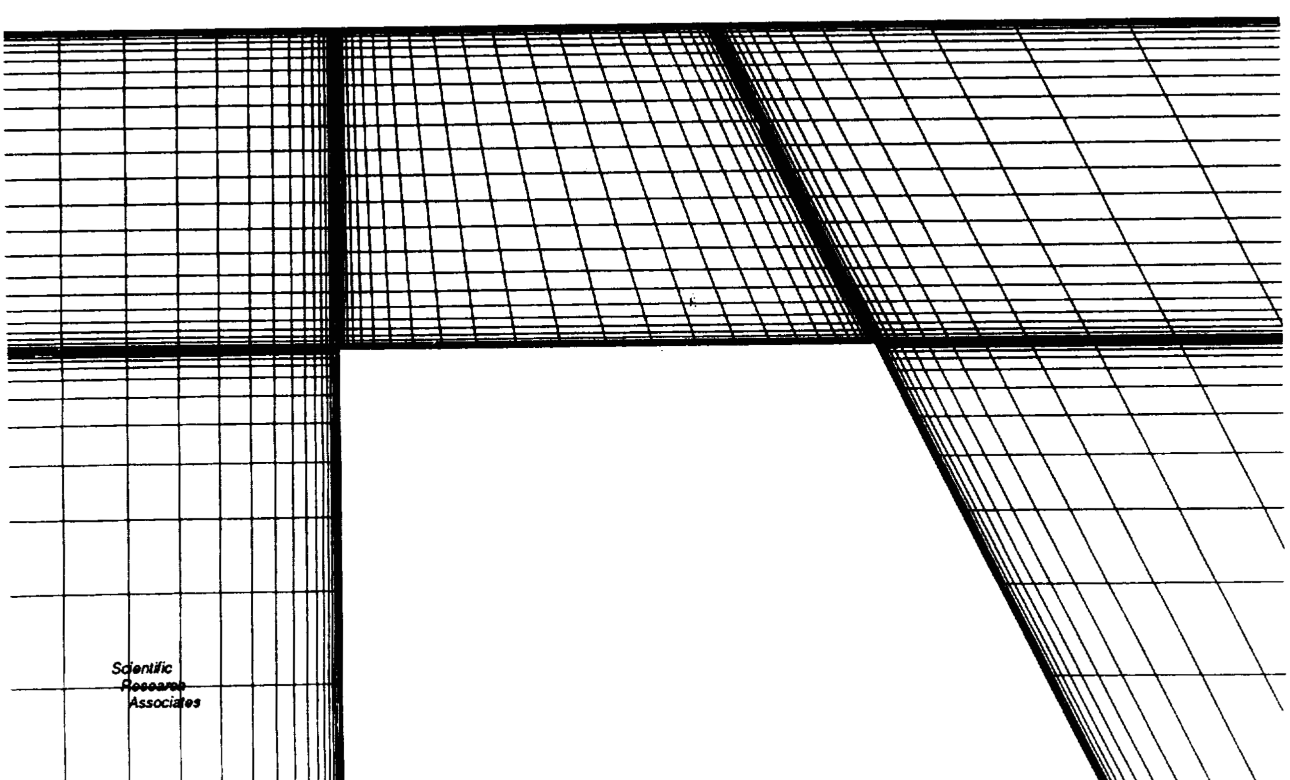

AXIAL VELOCITY

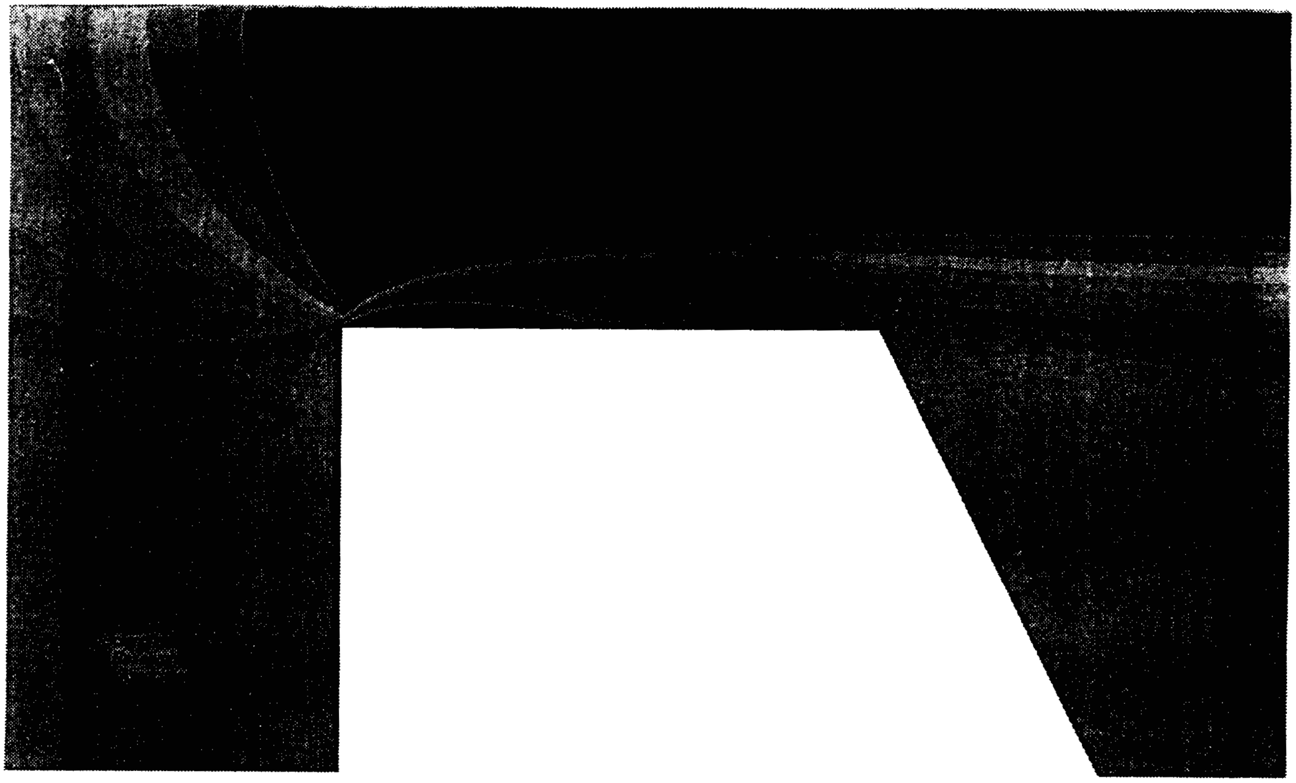

PRESSURE

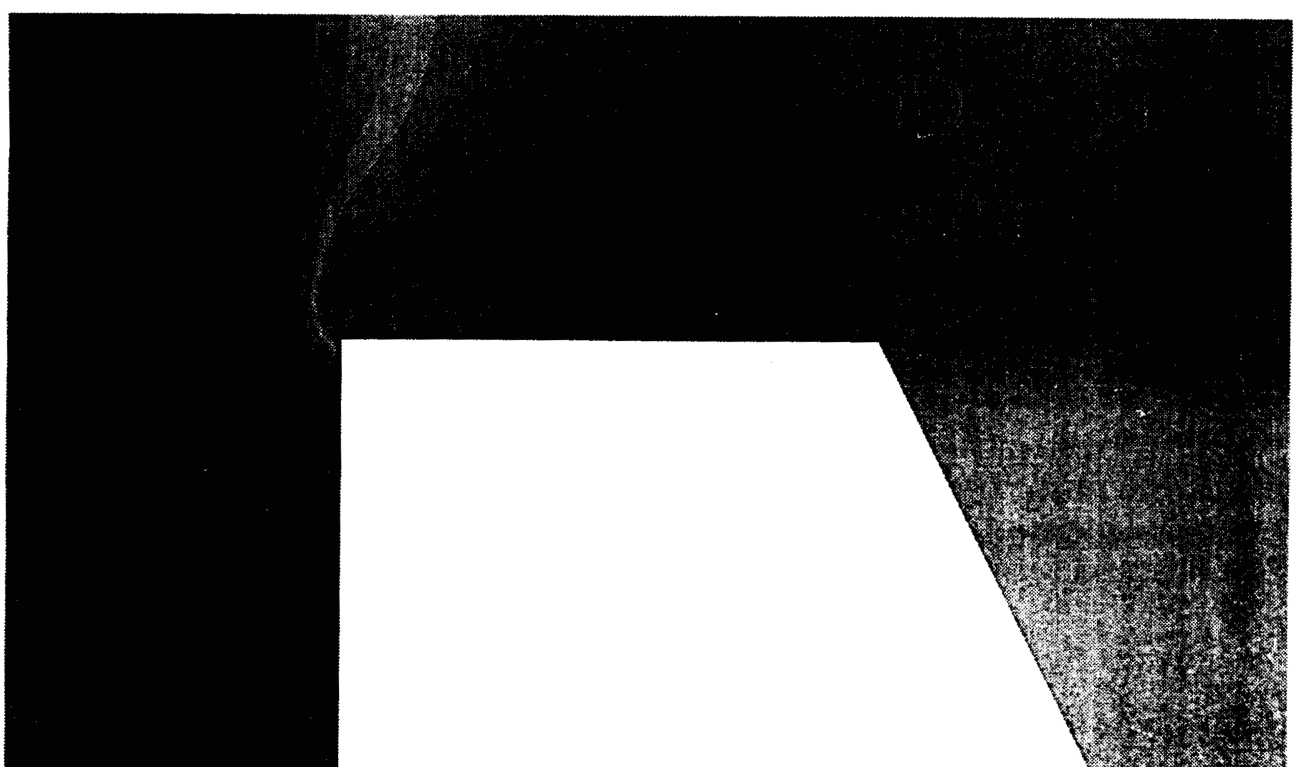

NUCLEATION SITE DENSITY

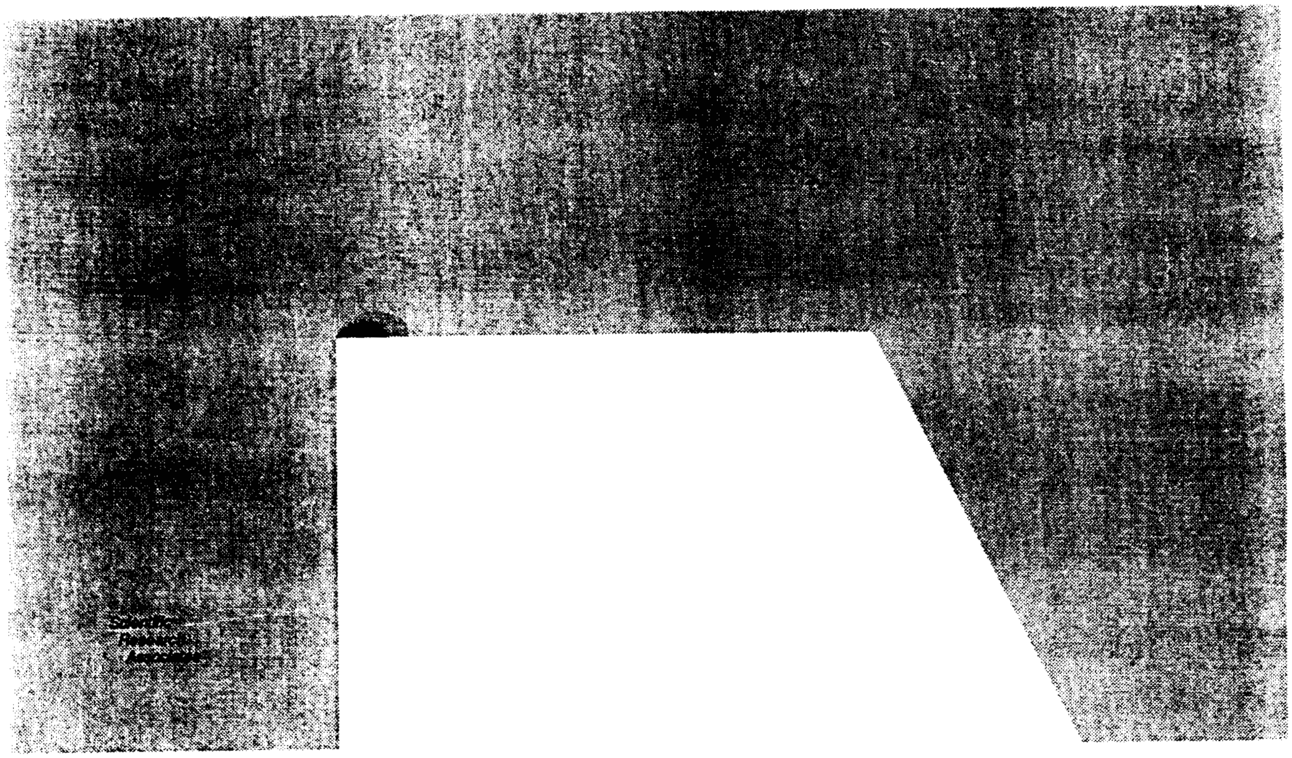

BUBBLE TRAJECTORIES

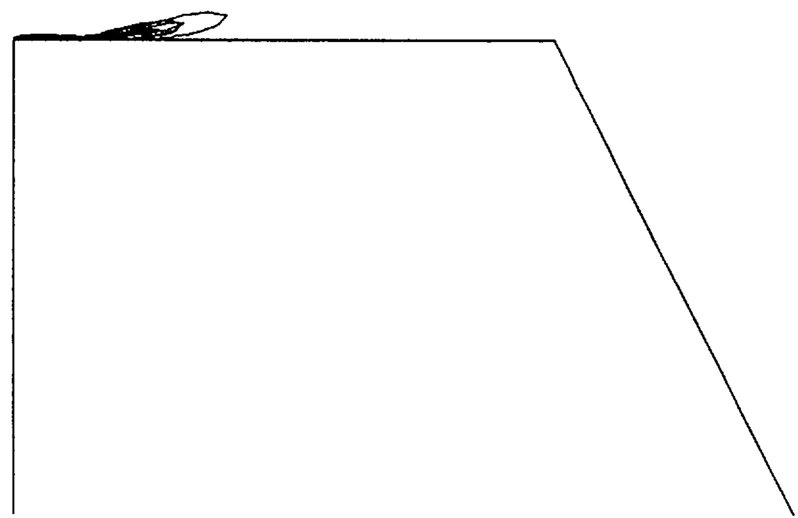

Scientific
Research
Associates

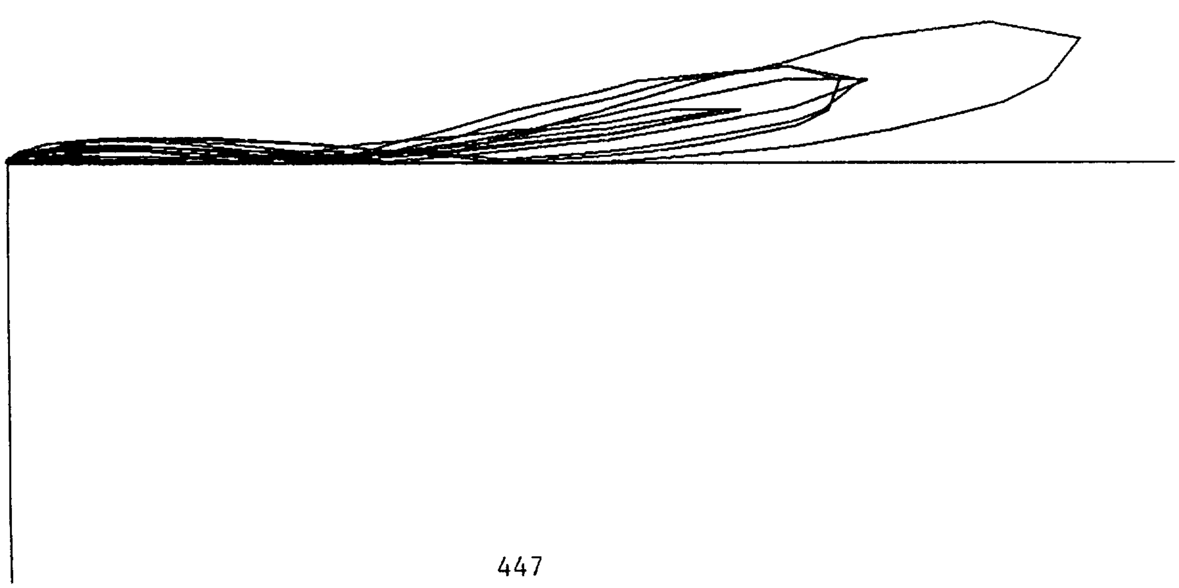

BUBBLE SIZE

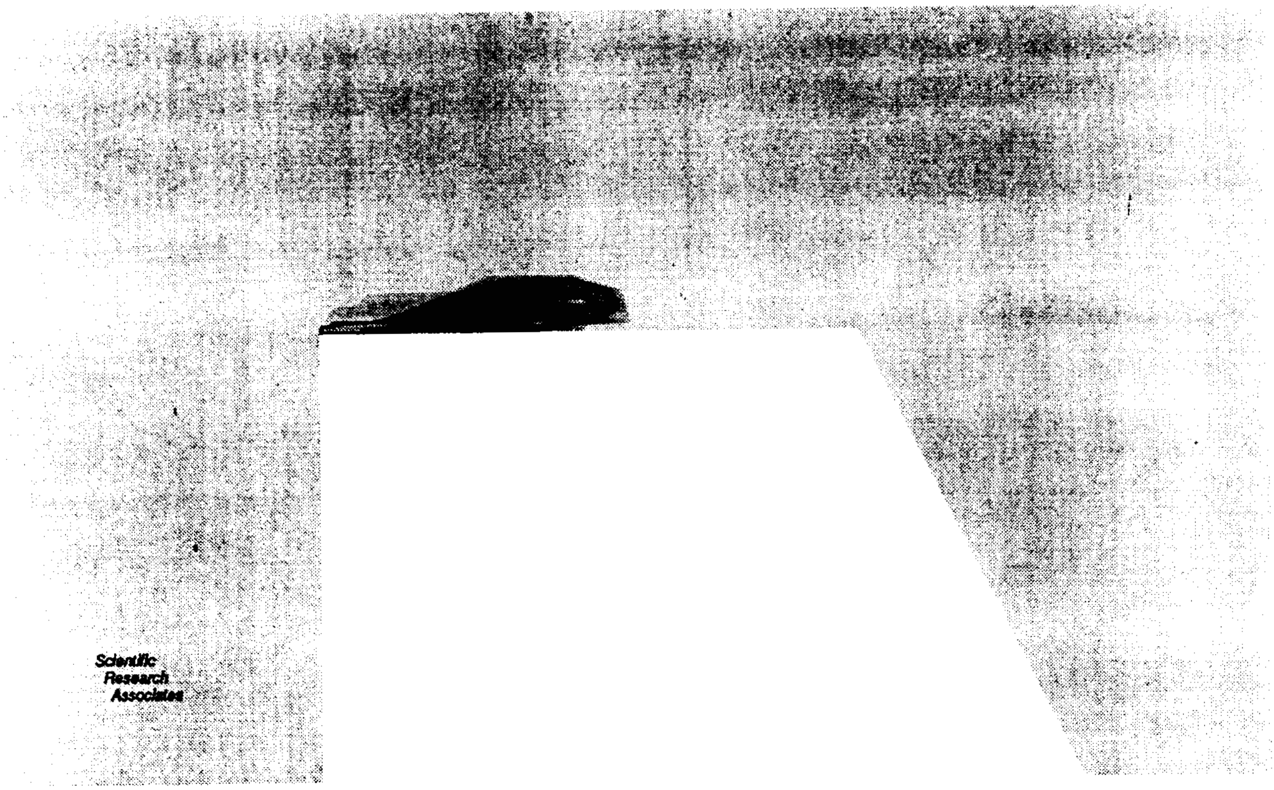

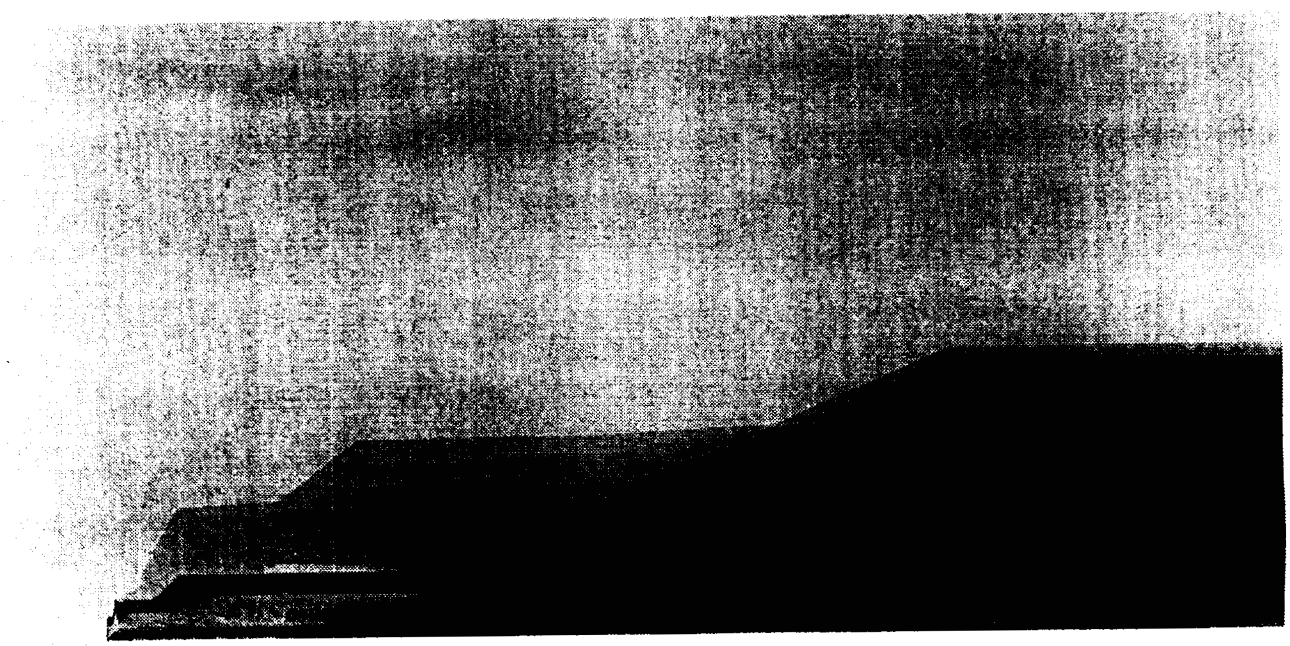

N95-23634

S19-34

On the Accuracy of CFD-Based Pressure Drop Predictions for Right-Angle Ducts

p. 13

A. Brankovic
Pratt & Whitney, Florida

The predictive capability of computational fluid dynamics (CFD) codes for turbulent flow through curved ducts is of significant importance to the design and performance analysis of modern rocket engine flowpaths. Code calibration and validation studies for this class of flow are desireable to estimate the performance margin and operating range of components designed using Navier-Stokes methods. Parametric experimental studies such as that of Weske (NACA ARR W-39) provided a wealth of performance data for the design of single- and compound elbow configurations with various cross-sections, curvature and aspect ratios at varying Reynolds numbers. In that work, the majority of data is presented in the form of loss coefficients, characterizing pressure losses due to duct curvature, and including losses due to wall friction. Using measured friction coefficients, losses of equivalent straight lengths of duct are subtracted, resulting in performance curves useful for design computations. These data are currently used in a CFD-based parametric study covering a broad range of operating conditions. Of particular interest for the accuracy of CFD predictions are the effects on pressure loss due to inlet boundary layer thickness (dependent on upstream development length), and the wall treatment for the turbulence equations (conventional wall functions vs. wall integration using a two-layer model). The experimental data are reassessed in the form of an error analysis, and are compared with CFD predictions for 18 computational cases. Grid-independence, grid spacing, and convergence requirements of the cases are discussed. Conclusions regarding the relative importance of the parametric variables will be presented.

ON THE ACCURACY OF CFD–BASED PRESSURE DROP PREDICTIONS FOR RIGHT–ANGLE DUCTS

by
Andreja Brankovic
Pratt & Whitney, Florida

Presented at
Workshop for CFD Applications
in Rocket Propulsion
NASA Marshall Space Flight Center
April 20–22, 1993

INTRODUCTION / OBJECTIVE

- Physics of flow in a right–angle ducts has much in common to that in a rocket engine flowpaths, i.e., large pressure loss, secondary flows, possible separation.

- Experimental pressure loss data have long been used for design of high performance single and compound elbow duct systems.

- Data from these early measurement programs, obtained over a wide range of operating conditions, provide an excellent source for CFD target data suitable for studies of B.C.'s, grid resolution, wall functions vs. integration to wall, etc.

- Present CFD test matrix designed to investigate experimentally–observed trends of pressure losses in right–angle ducts, due to varying Re #, duct aspect and curvature ratio.

EXPERIMENTAL DATASETS

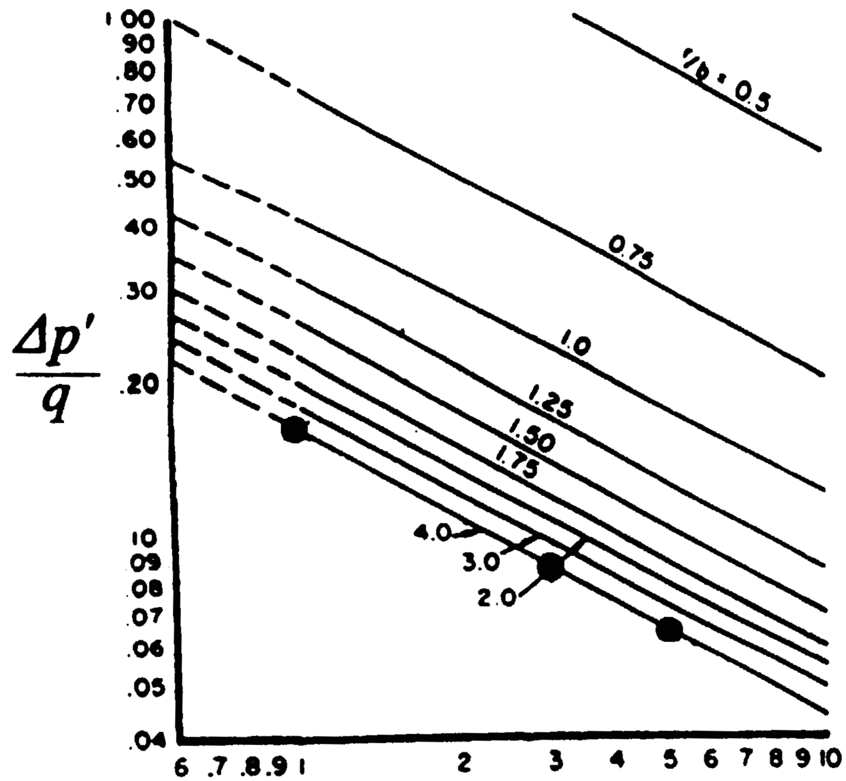

Aspect Ratio = a/b

$R_e = 10^5$

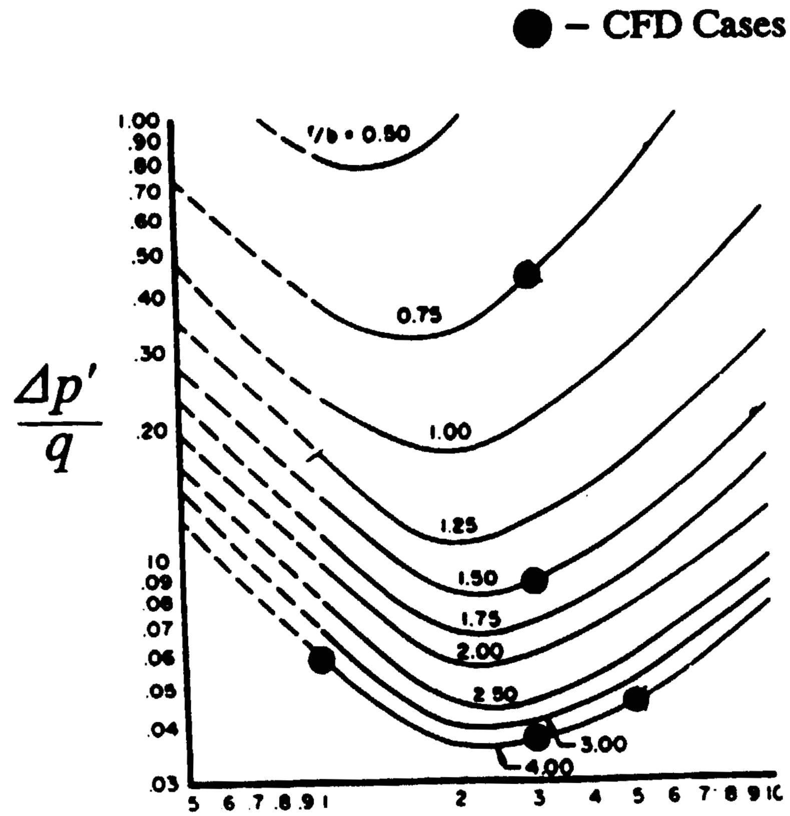

Aspect Ratio = a/b

$R_e = 6 \times 10^5$

Reference: Weske, J.R., "Pressure Loss in Ducts with Compound Elbows", NACA Wartime Report W–39 February 1943.

EXPERIMENTAL GEOMETRY

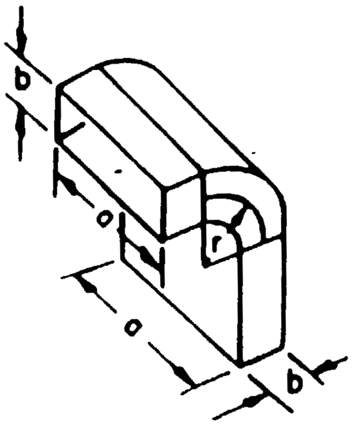

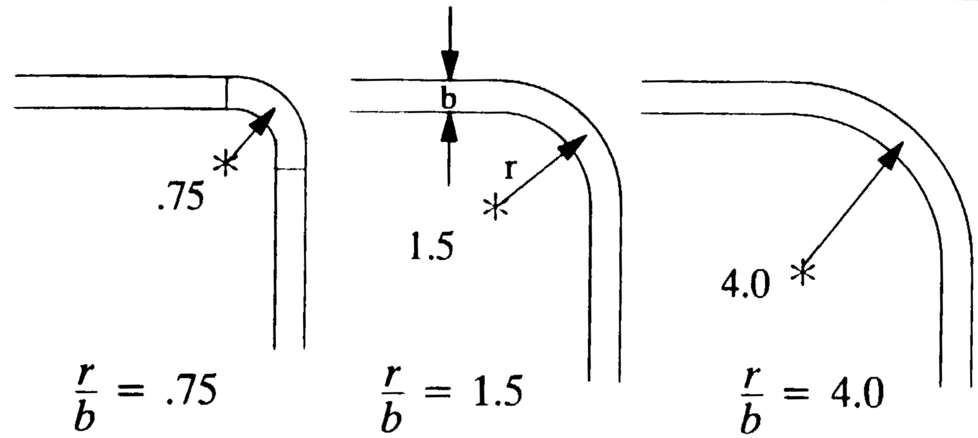

		Aspect Ratio (a/b)	Curvature Ratio (r/b)	Dimensions (a x b)	Hydraulic Diameter (D_H)	Mean Radius (R)
$R_e = 10^5$						
	1.	1:1	4.0	5.125″ x 5.125″	5.125″	20.75″
	2.	3:1	4.0	9.1875″ x 3.06″	4.5909″	12.25″
	3.	5:1	4.0	11.875″ x 2.375″	3.9583″	9.5″
$R_e = 6 X 10^5$						
	4.	1:1	4.0	5.125″ x 5.125″	5.125″	20.75″
	5.	3:1	4.0	9.1875″ x 3.06″	4.5909″	12.25″
	6.	3:1	1.5	9.1875″ x 3.06″	4.5909″	4.6″
	7.	3:1	0.75	9.1875″ x 3.06″	4.5909″	2.3″
	8.	5:1	4.0	11.875″ x 2.375″	3.9583″	9.5″

DATA REDUCTION METHOD

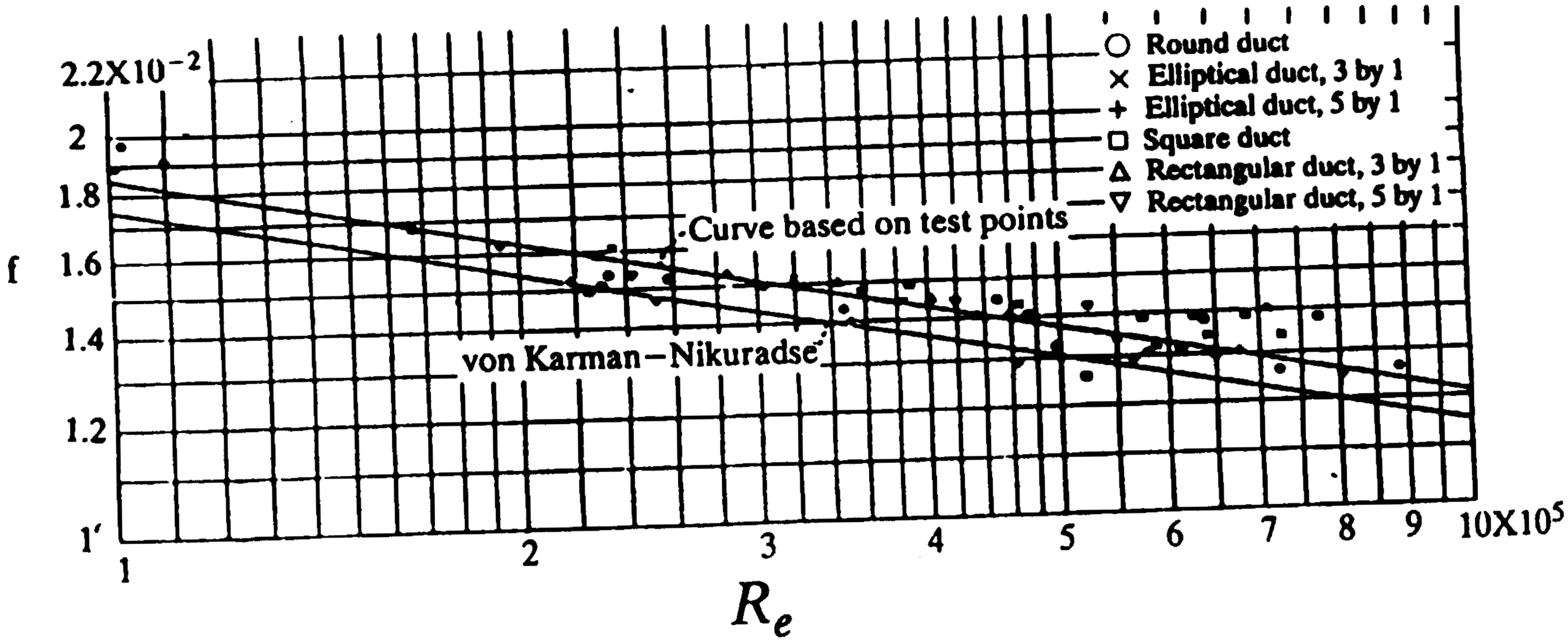

$$\frac{\Delta P'}{q} = \frac{\Delta P}{q} - f\left(\frac{L_1 + L_2 + L_c}{D_H}\right)$$

where: $\frac{\Delta P'}{q}$ = *pressure coefficient*

$q = .5\varrho Q^2$

L_1, L_2, L_c = *upstream, downstream, curve lengths*

f = *friction factor*

CFD NUMERICS

Grid Independence

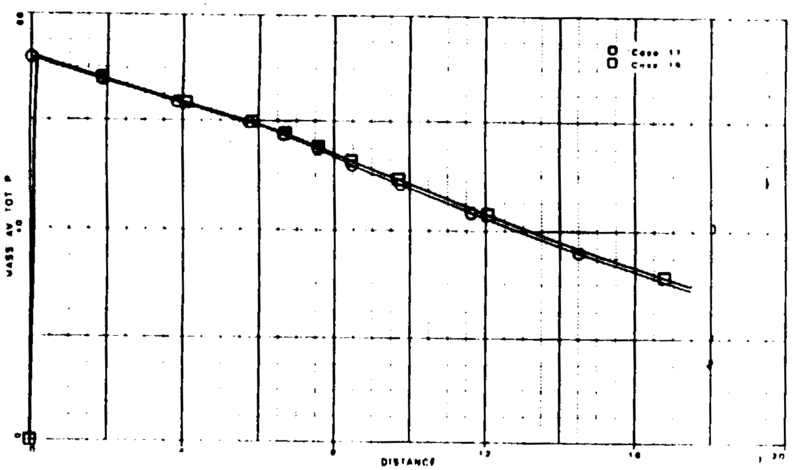

Total Pressure

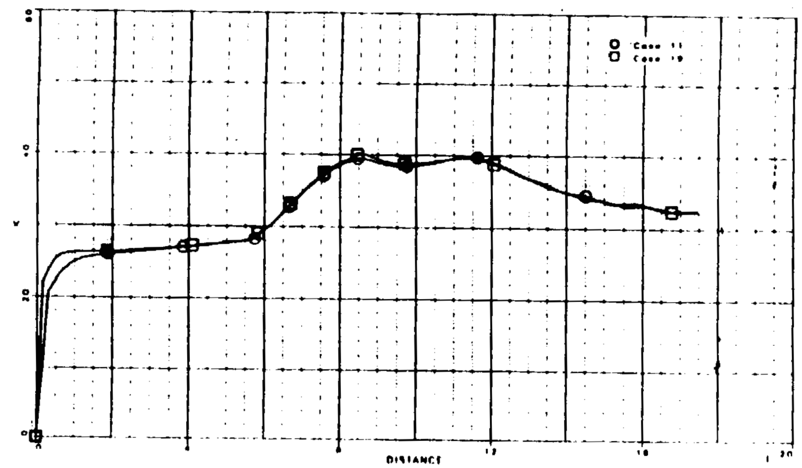

Turbulent Kinetic Energy

Coarse Mesh: 59 x 40 x 30 = 70,800 Points
Fine Mesh: 92 x 80 x 60 = 441,600 Points

Similar results obtained for wall function and wall integration models

PREDICTED vs. MEASURED RESULTS

Influence of Duct Aspect Ratio at $R_e = 10^5$

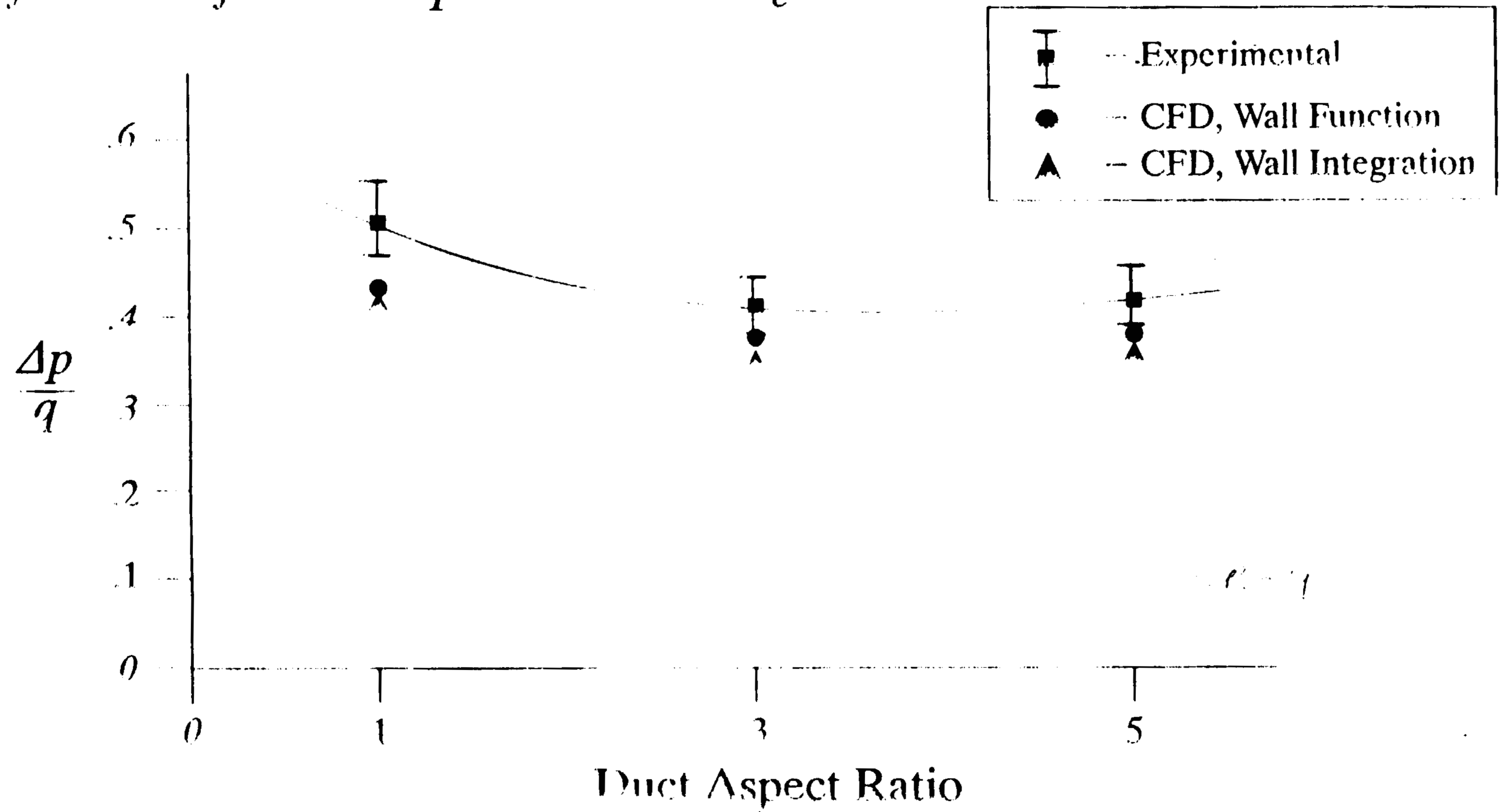

Data shows distinct minimum when plotted as

$$\frac{\Delta p}{q} \quad \text{instead of} \quad \frac{\Delta p'}{q}$$

COMPUTED FLOW STRUCTURE

Influence of Duct Aspect Ratio at $R_e = 10^5$

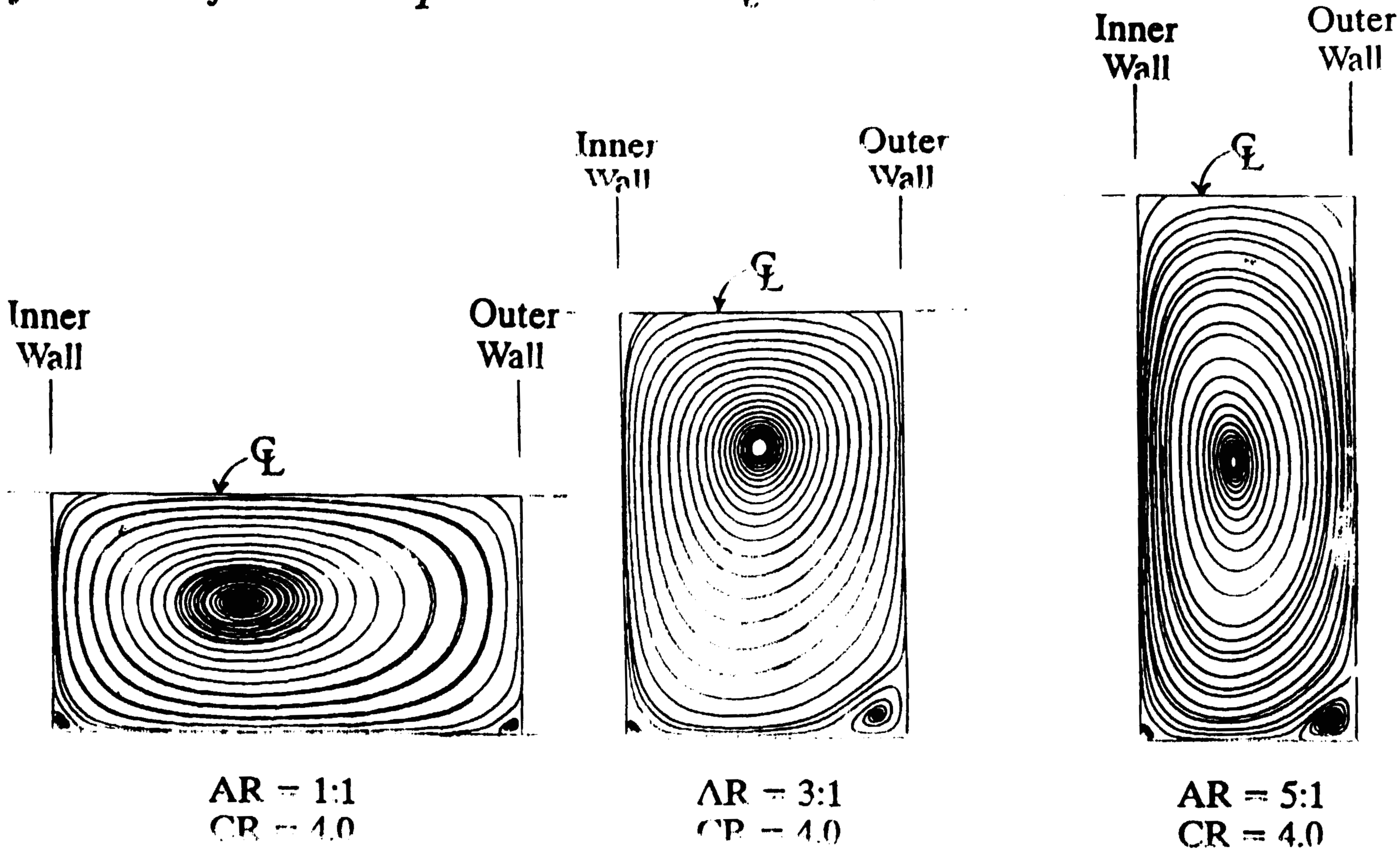

Shown at 48″ downstream of elbow exit plane

PREDICTED vs. MEASURED RESULTS

Influence of Duct Aspect Ratio at $R_e = 6 \times 10^5$

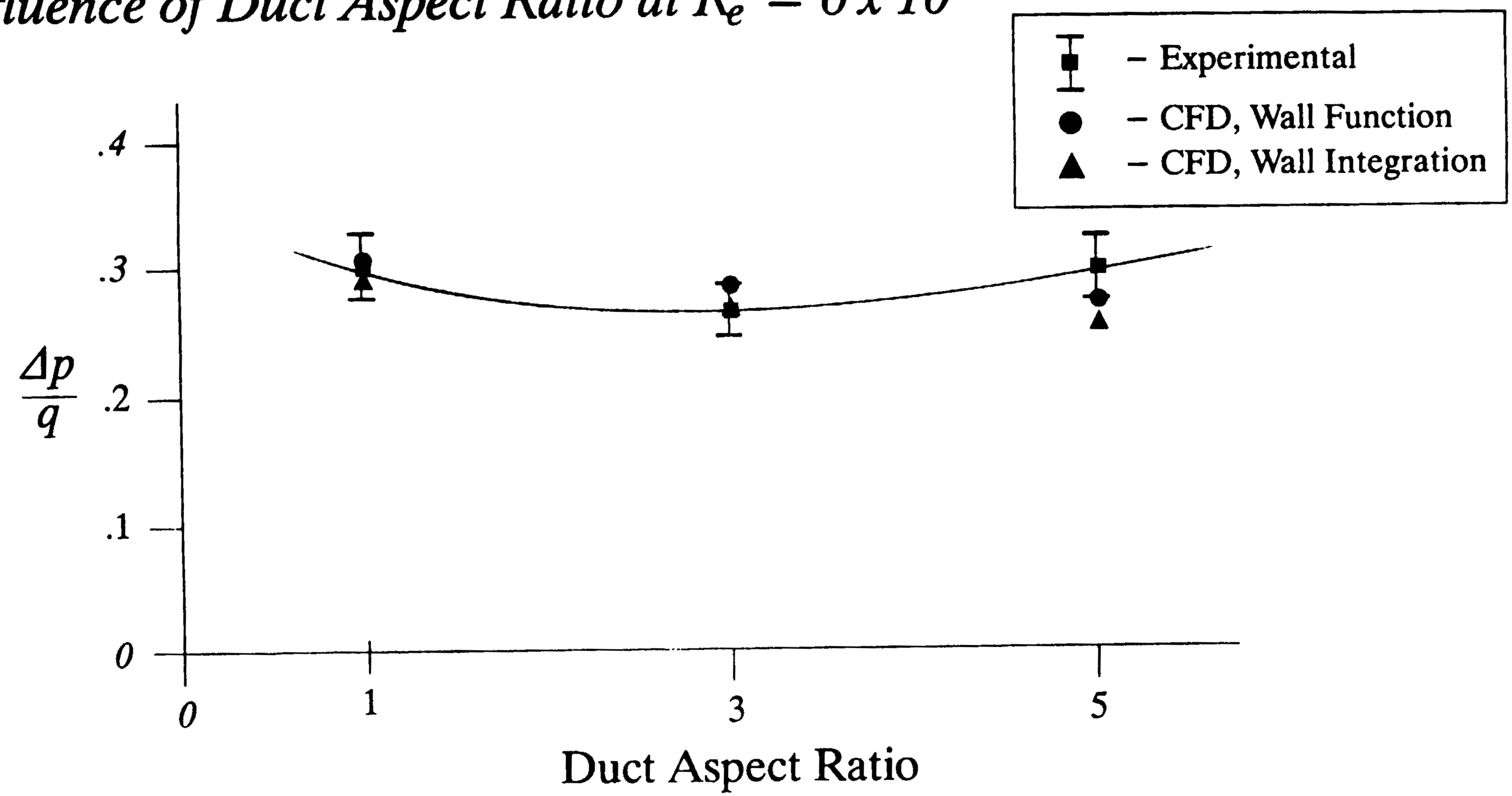

Minimum in data not as pronounced when plotted as

$$\frac{\Delta p}{q} \text{ instead of } \frac{\Delta p'}{q}$$

PREDICTED vs. MEASURED RESULTS

Influence of Duct Curvature Ratio at $R_e = 6 \times 10^5$

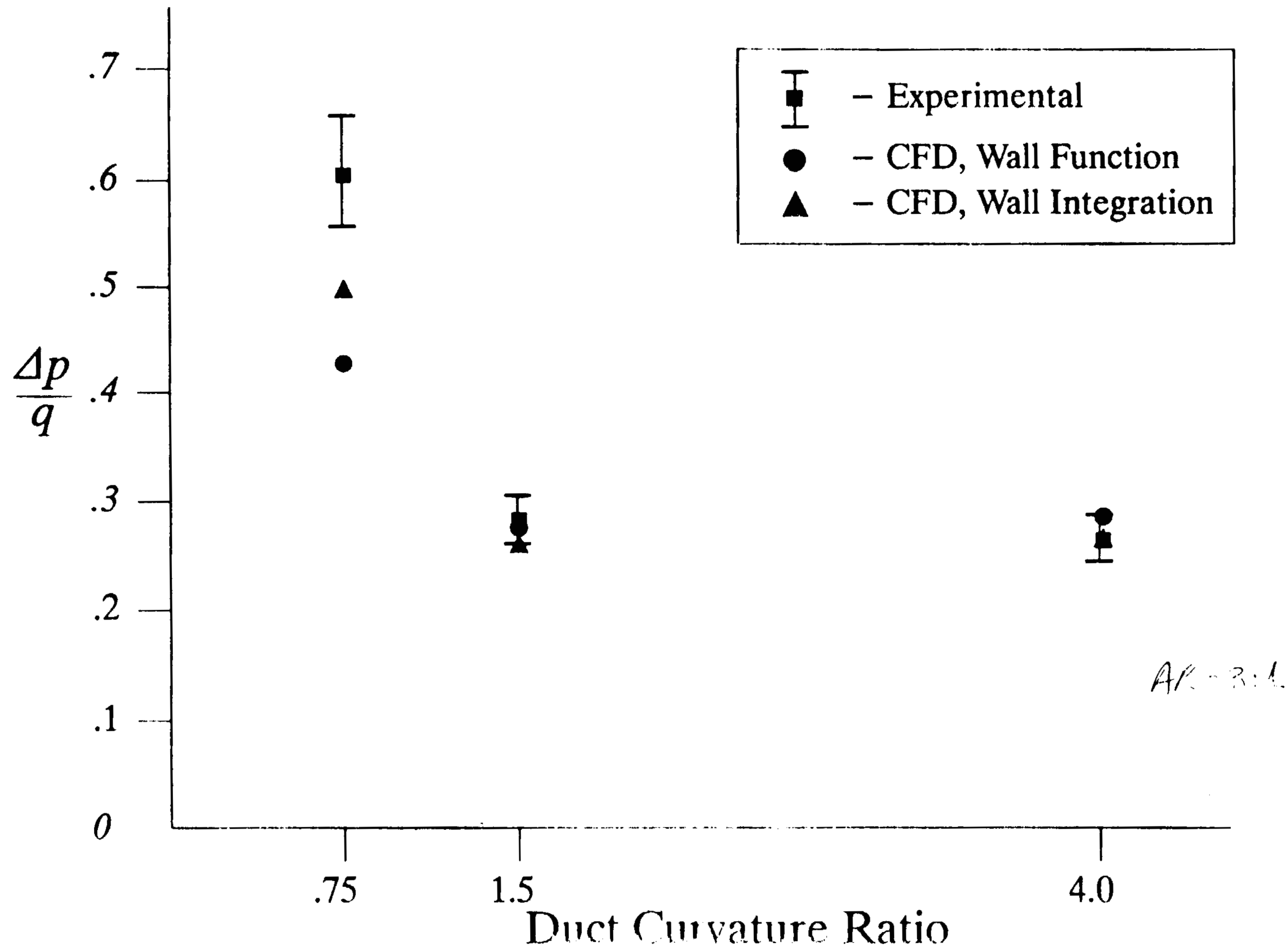

FLOW SEPARATION DETAILS

Turbulence Model Influences Shape, Location Of Separation Bubble

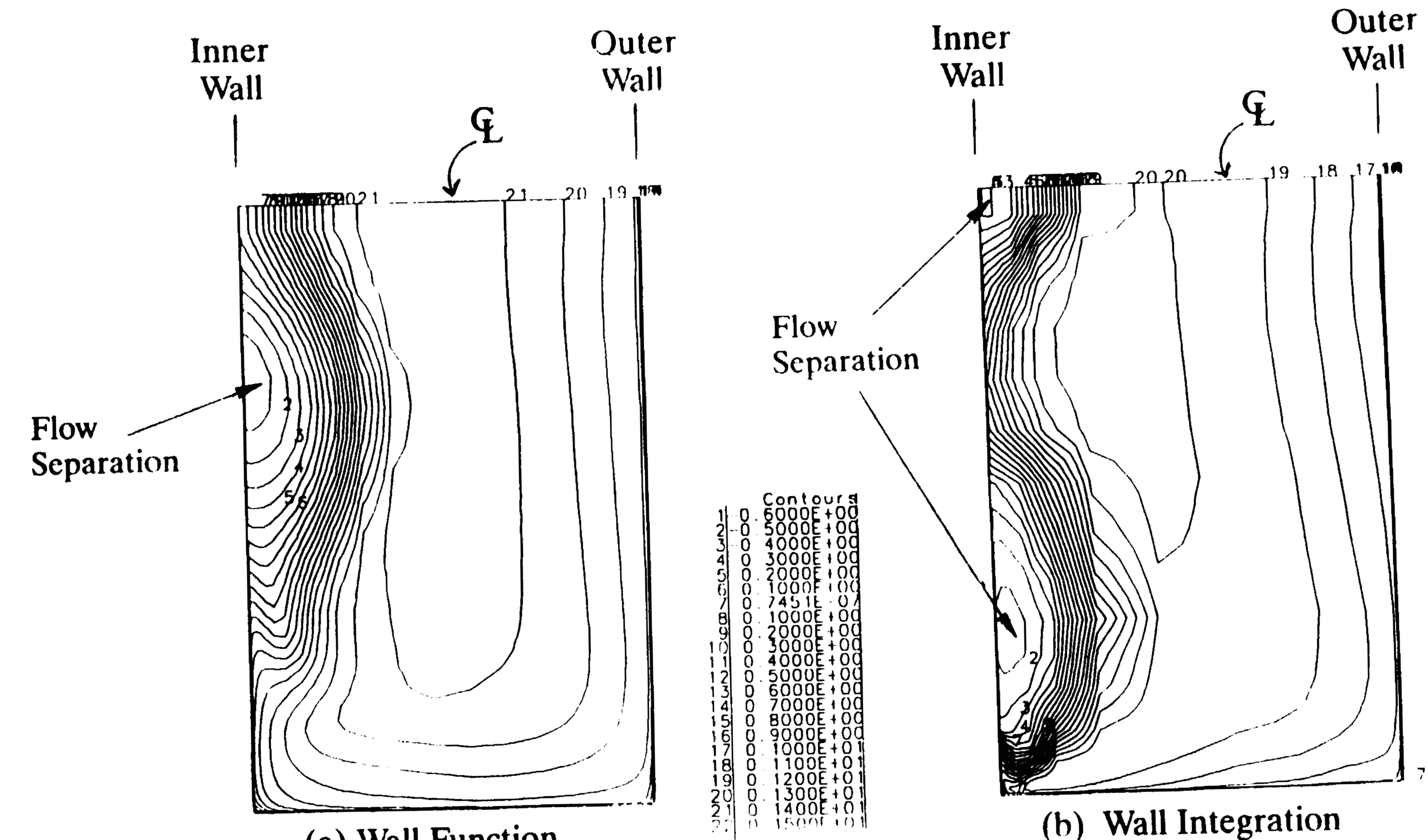

(a) Wall Function

(b) Wall Integration

Details of separated flow region for CR = 0.75, AR = 3:1, $R_e = 6 \times 10^5$.

CONCLUSIONS

- Details of experimental setup, uncertainty estimates, data reduction method critical to appropriate modeling of cases.
- CFD predictions usually within 15% of data for pressure drop across elbow; larger error associated with low curvature elbow due to flow separation.
- Wall function $k-\varepsilon$ model as good or better than wall integration model for loss calculations.
- Reynolds number effects shown in data are apparent, not real; variation of pressure loss due to duct aspect and curvature ratios has been captured by CFD model.

N95- 23635

CFD MODELING OF TURBULENT DUCT FLOWS FOR COOLANT CHANNEL ANALYSIS

Ronald J. Ungewitter and Daniel C. Chan
Rocketdyne Div. /Rockwell International
Canoga Park, Ca 91304

ABSTRACT

The design of modern liquid rocket engines requires the analysis of chamber coolant channels to maximize the heat transfer while minimizing the coolant flow. Coolant channels often do not remain at a constant cross section or at uniform curvature. New designs require higher aspect ratio coolant channels than previously used. To broaden the analysis capability and to complement standard analysis tools an investigation on the accuracy of CFD predictions for coolant channel flow has been initiated. Validation of CFD capabilities for coolant channel analysis will enhance the capabilities for optimizing design parameters without resorting to extensive experimental testing. The eventual goal is to use CFD to determine the flow fields of unique coolant channel designs and therefore determine critical heat transfer coefficients.

In this presentation the accuracy of a particular CFD code is evaluated for turbulent flows. The first part of the presentation is a comparison of numerical results to existing cold flow data for square curved ducts (NASA CR-3367, "Measurements of Laminar and Turbulent Flow in a Curved Duct with Thin Inlet Boundary Layers"). The results of this comparison show good agreement with the relatively coarse experimental data. The second part of the presentation compares two cases of higher aspect ratio channels (AR=2.5,10) to show changes in axial and secondary flow strength. These cases match experimental work presently in progress and will be used for future validation. The comparison shows increased secondary flow strength of the higher aspect ratio case due to the change in radius of curvature. The presentation includes a test case with a heated wall to demonstrate the program's capability. The presentation concludes with an outline of the procedure used to validate the CFD code for future design analysis.

CFD MODELING OF TURBULENT DUCT FLOWS FOR COOLANT CHANNEL ANALYSIS

BY

RONALD J. UNGEWITTER DANIEL C. CHAN

ROCKETDYNE DIV/ ROCKWELL INTERNATIONAL

MFSC CFD WORKSHOP APRIL 20-22 1993

Rockwell International
Rocketdyne Division

CFD MODELING OF TURBULENT DUCT FLOWS FOR COOLANT CHANNEL ANALYSIS

TOPICS

- INTRODUCTION
- TURBULENT VALIDATION: 90° CURVED SQUARE DUCT, Re=40000
- ASPECT RATIO EFFECTS: 60° CURVED RECTANGULAR DUCT, ASPECT RATIOS 2.5 & 10,
- CONSTANT TEMPERATURE WALL: Tw-Tin=200°C
- FUTURE EFFORTS

Rockwell International
Rocketdyne Division

CFD MODELING OF TURBULENT DUCT FLOWS FOR COOLANT CHANNEL ANALYSIS

BACKGROUND; LOCAL COOLANT CHANNEL HEAT FLUX IS DIFFICULT AND EXPENSIVE TO MEASURE BUT CAN BE CRITICAL TO COMBUSTION CHAMBER LIFE. IMPROVED ANALYTICAL CAPABILITIES ARE DESIRED FOR EVALUATING NEW COOLANT CHANNEL DESIGNS.

OBJECTIVE; DEMONSTRATE THE EXISTING CAPABILITIES OF CFD FOR MODELING TURBULENT SQUARE DUCT FLOWS FOR COOLANT CHANNEL ANALYSIS

APPROACH; COMPARE REACT3D CODE RESULTS OF CURVED CHANNEL CALCULATIONS TO EXPERIMENTAL DATA

Rockwell International
Rocketdyne Division

TURBULENT VALIDATION

- TURBULENT CURVED DUCT DATA FROM NASA CR-3367, Taylor, et. al.
- REACT3D PERFORMED WELL

  INCOMPRESSIBLE FNS
  TWO EQUATION TURBULENCE MODEL (WALL FUNCTIONS,)
  43 SPARC 10 CPU HOURS, 113,000 NODE GRID

- GOOD QUALITATIVE COMPARISONS OF AXIAL VELOCITY TO RELATIVELY COARSE EXPERIMENTAL DATA
- PRESSURE PREDICTIONS ALSO SHOW GOOD AGREEMENT

Rockwell International
Rocketdyne Division

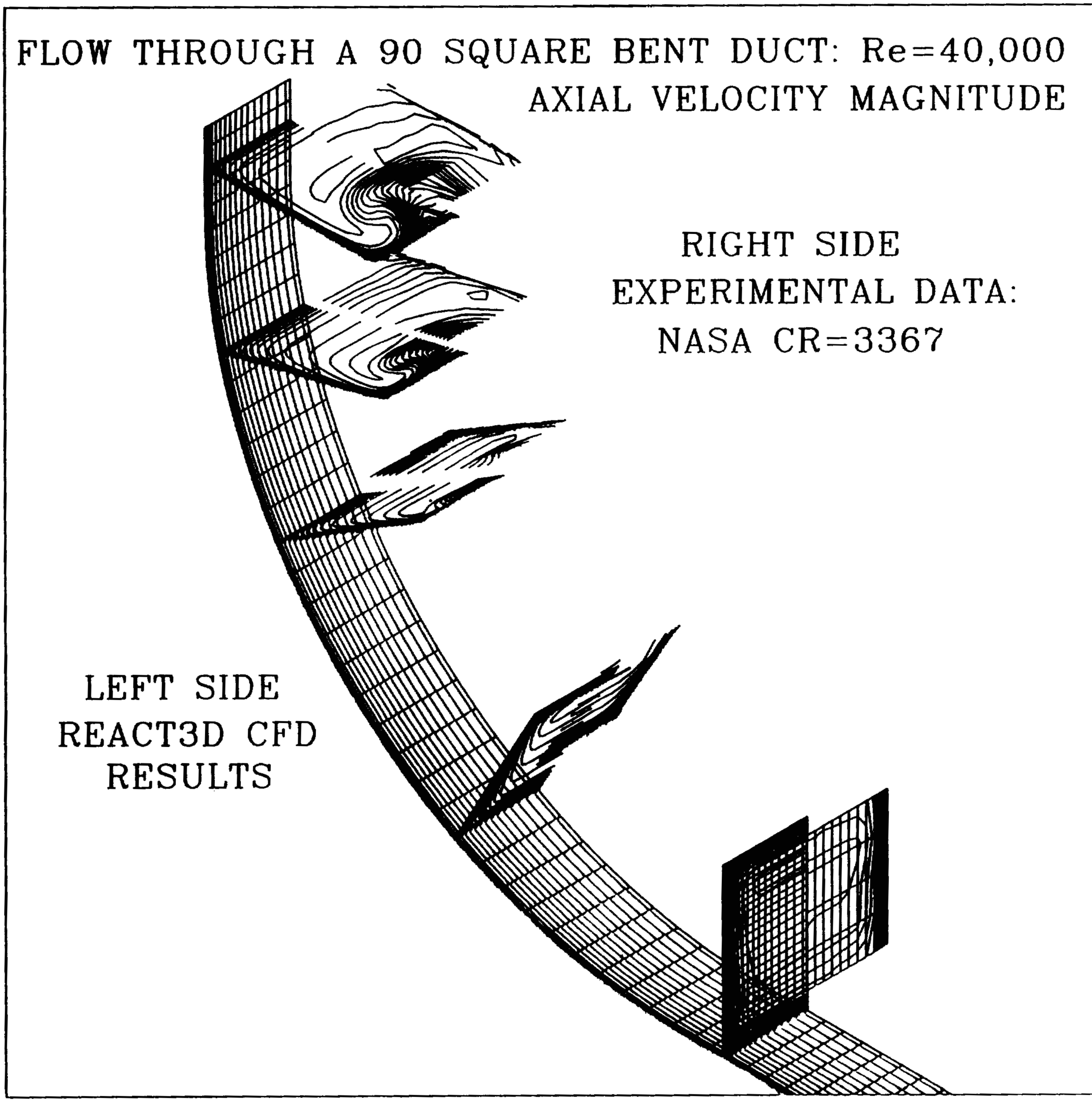

FLOW THROUGH A 90 SQUARE BENT DUCT: Re=40,000
AXIAL VELOCITY MAGNITUDE
RIGHT SIDE
EXPERIMENTAL DATA:
NASA CR=3367
LEFT SIDE
REACT3D CFD
RESULTS

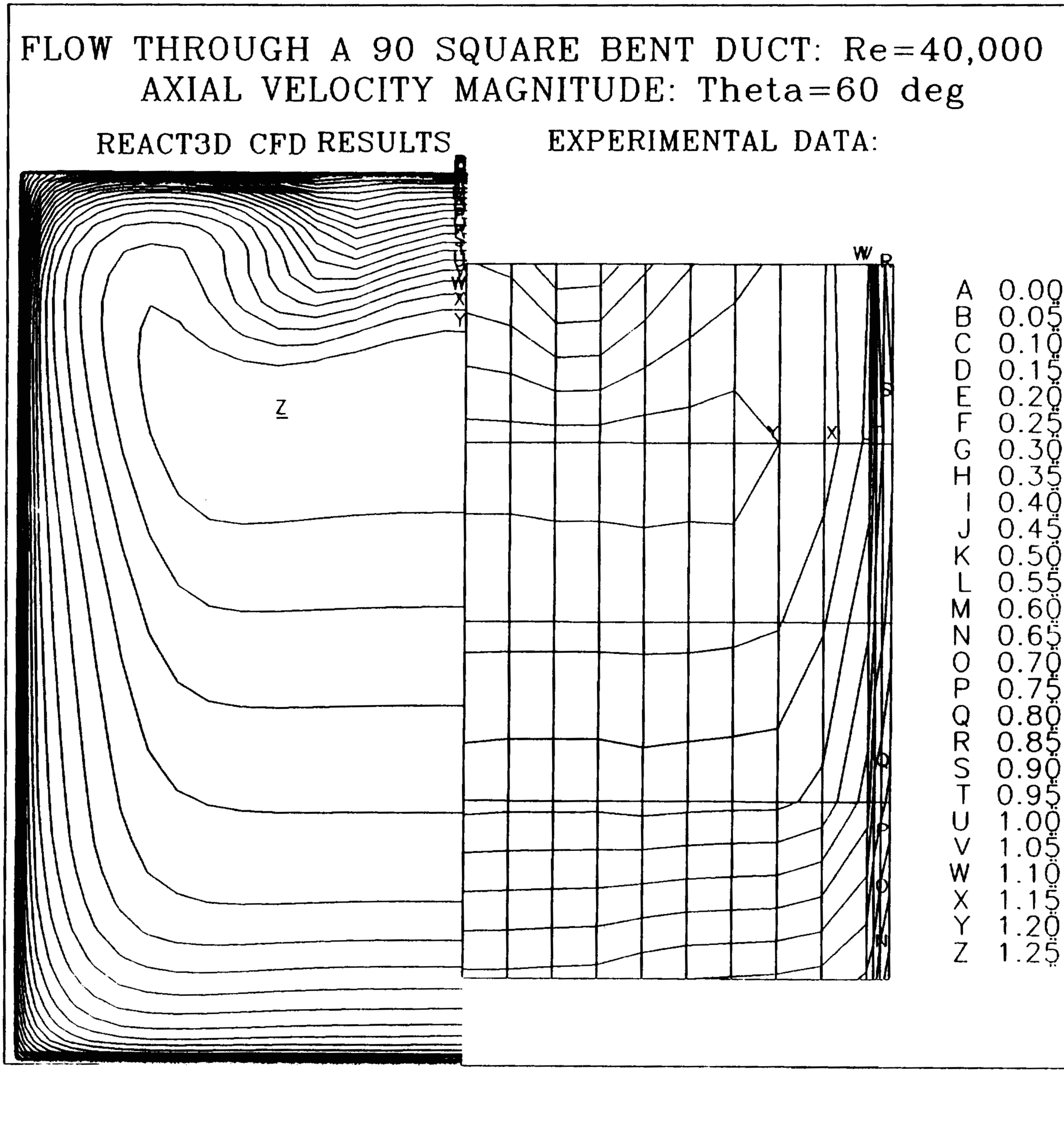

FLOW THROUGH A 90 SQUARE BENT DUCT: Re=40,000
AXIAL VELOCITY MAGNITUDE: Theta=60 deg
REACT3D CFD RESULTS
EXPERIMENTAL DATA:
A 0.00
B 0.05
C 0.10
D 0.15
E 0.20
F 0.25
G 0.30
H 0.35
I 0.40
J 0.45
K 0.50
L 0.55
M 0.60
N 0.65
O 0.70
P 0.75
Q 0.80
R 0.85
S 0.90
T 0.95
U 1.00
V 1.05
W 1.10
X 1.15
Y 1.20
Z 1.25

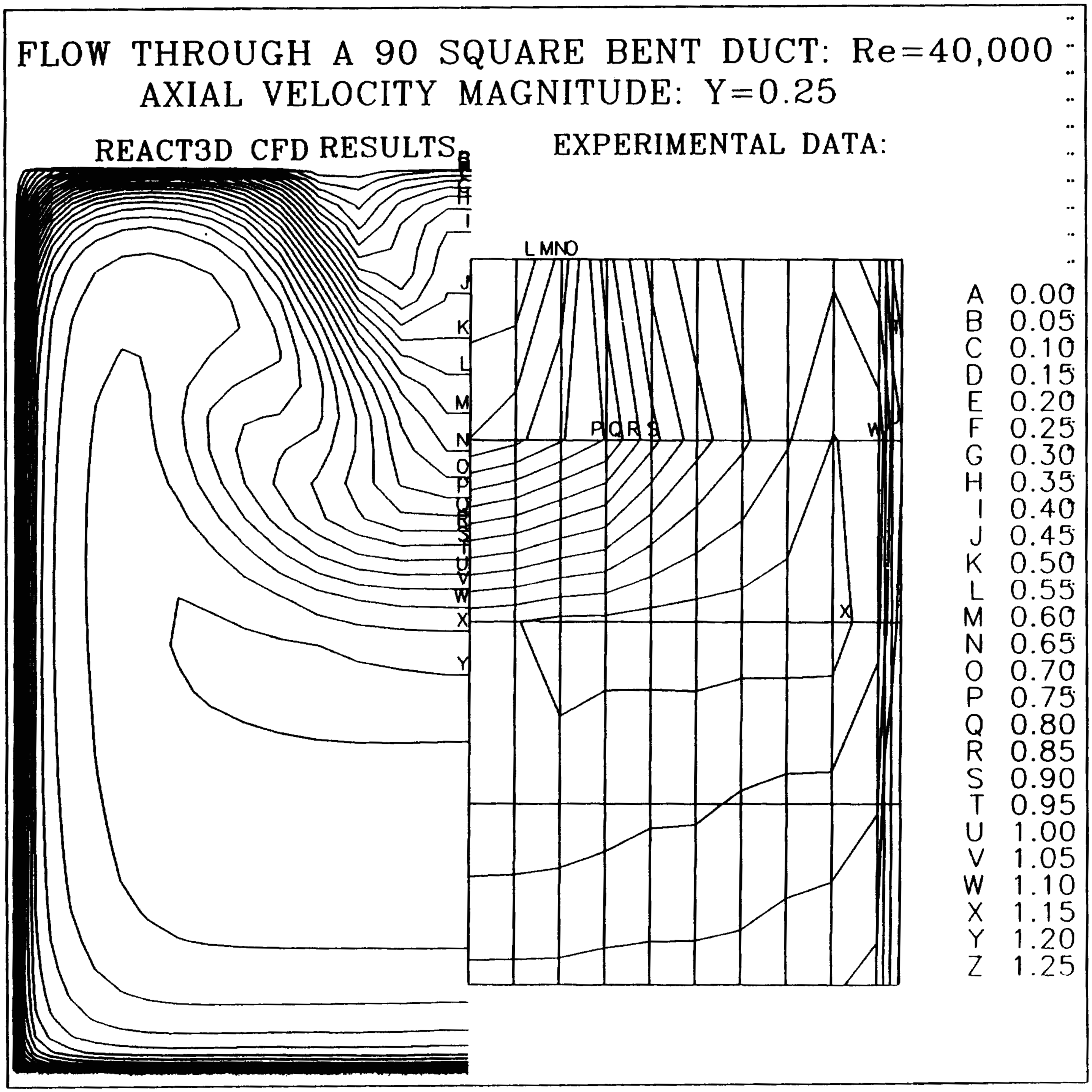
FLOW THROUGH A 90 SQUARE BENT DUCT: Re=40,000
AXIAL VELOCITY MAGNITUDE: Y=0.25
REACT3D CFD RESULTS
EXPERIMENTAL DATA:
A 0.00
B 0.05
C 0.10
D 0.15
E 0.20
F 0.25
G 0.30
H 0.35
I 0.40
J 0.45
K 0.50
L 0.55
M 0.60
N 0.65
O 0.70
P 0.75
Q 0.80
R 0.85
S 0.90
T 0.95
U 1.00
V 1.05
W 1.10
X 1.15
Y 1.20
Z 1.25

C-6.

TURBULENT VALIDATION

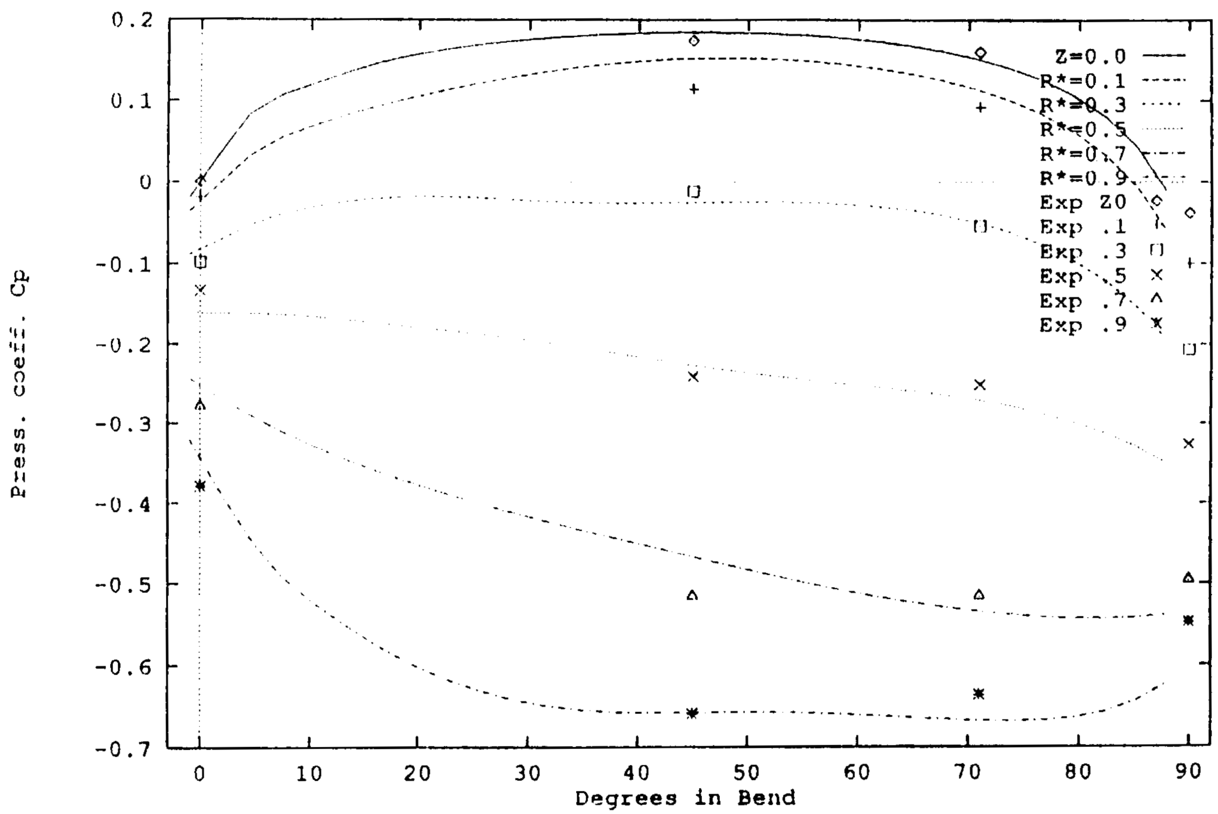

SOLID LINE; NUMERICAL

POINTS; EXPERIMENTAL

- **PRESSURE VALUES ARE ALONG THE OUTSIDE WALL, Z=0.0, AND SIDE WALLS, R*=0.1, 0.3,.05, 0.7, 0.9**

Rockwell International
Rocketdyne Division

ASPECT RATIO EFFECTS

- GEOMETRY MATCHES EXPERIMENTAL WORK IN PROGRESS
- 60° CURVED RECTANGULAR DUCTS, OUTSIDE RADIUS CONSTANT (RADIUS IS SCALED FROM SSME DESIGN)

ASPECT RATIO	Dh	RADIUS CURVATURE	REYNOLDS #	DEAN #
2.5	1.57"	37.3"	100,000	20500
10	2.0"	33.2"	127,000	31200

- TWO STEP SOLUTION PROCESS

  1) CALCULATE STRAIGHT DUCT SOLUTION (INLET CONDITION)
  2) CALCULATE CURVED DUCT SOLUTION

- NO SIGNIFICANT COMPUTATIONAL PROBLEMS WITH HIGH ASPECT RATIO COMPUTATIONAL CELLS
- SECONDARY FLOW MAGNITUDE GREATER FOR ASPECT RATIO OF 10

Rockwell International
Rocketdyne Division

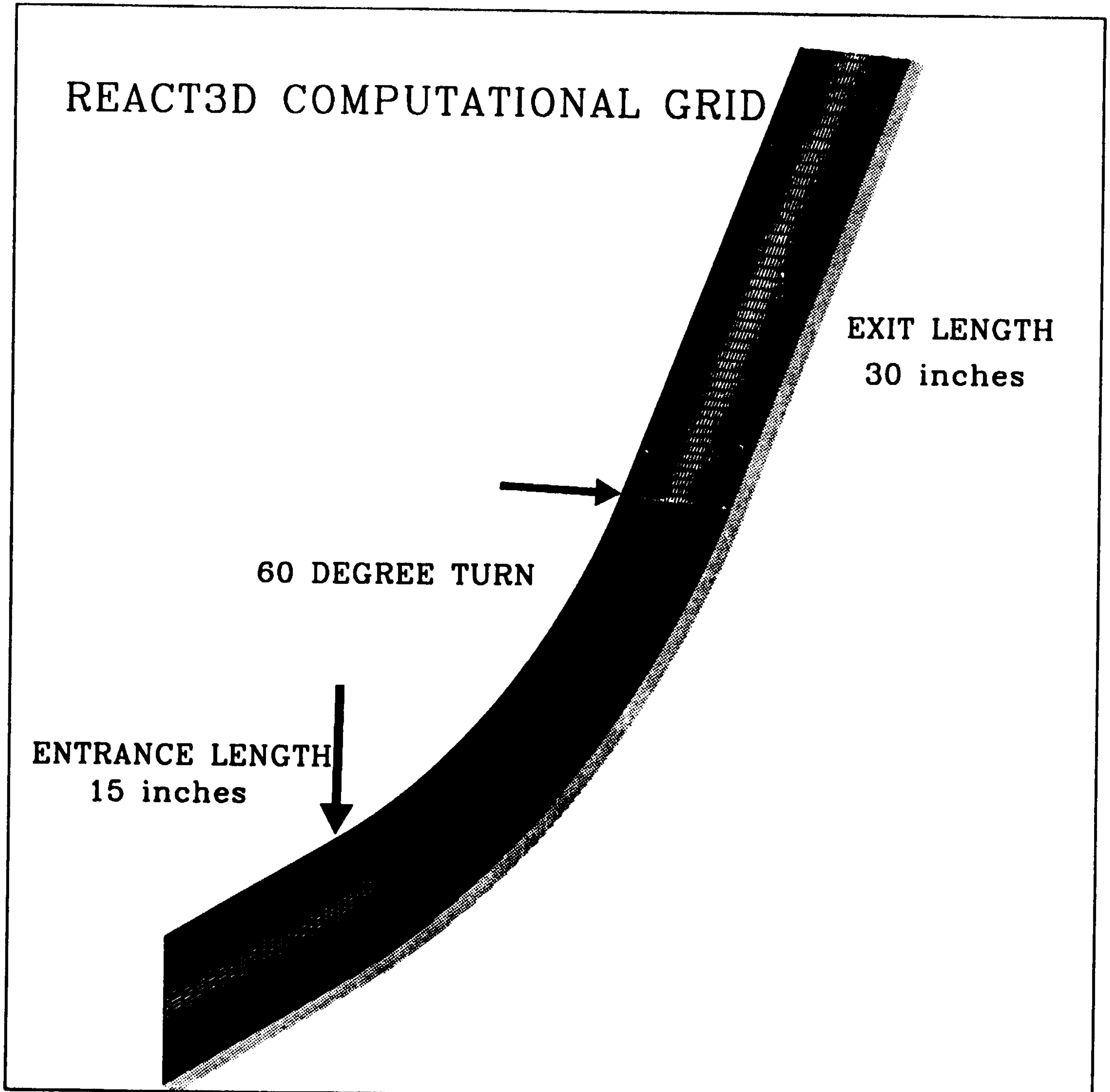
REACT3D COMPUTATIONAL GRID
EXIT LENGTH
30 inches
60 DEGREE TURN
ENTRANCE LENGTH
15 inches

REACT3D SOLUTION OF 60 DEG. RECT. DUCT
ASPECT RATIO=10, RE=127,000, THETA=0

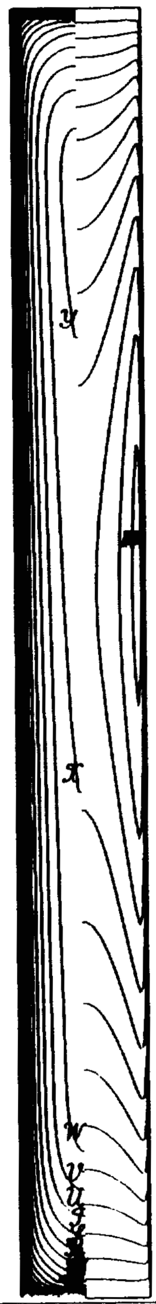

AXIAL VEL. MAG

A	0.00
B	0.05
C	0.10
D	0.15
E	0.20
F	0.25
G	0.30
H	0.35
I	0.40
J	0.45
K	0.50
L	0.55
M	0.60
N	0.65
O	0.70
P	0.75
Q	0.80
R	0.85
S	0.90
T	0.95
U	1.00
V	1.05
W	1.10
X	1.15
Y	1.20
Z	1.25
a	1.30
b	1.35

SECONDARY VEL. MAG.

A	0.000
B	0.005
C	0.010
D	0.015
E	0.020
F	0.025
G	0.030
H	0.035
I	0.040
J	0.045
K	0.050
L	0.055
M	0.060
N	0.065
O	0.070
P	0.075
Q	0.080
R	0.085
S	0.090
T	0.095
U	0.100

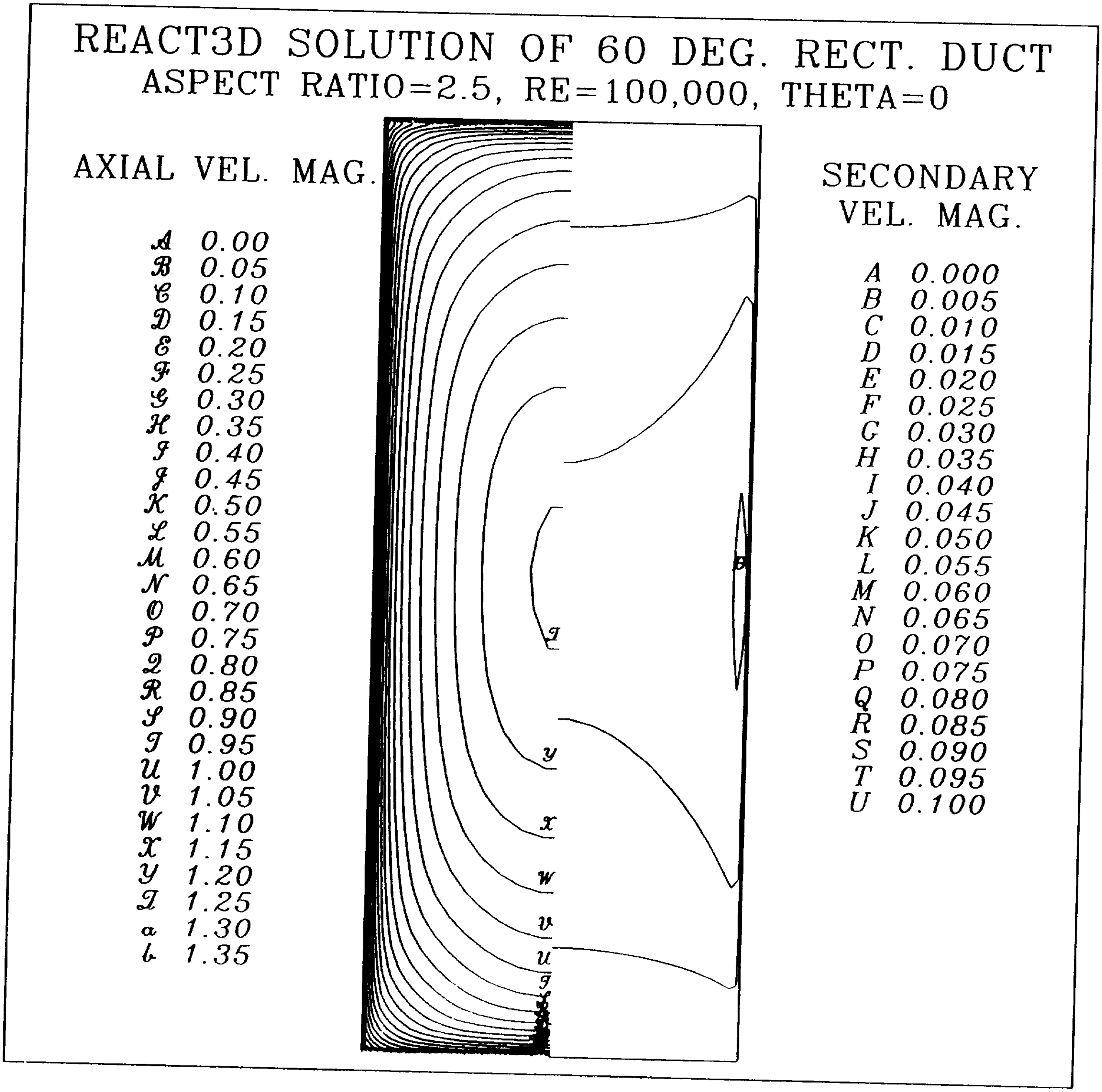
REACT3D SOLUTION OF 60 DEG. RECT. DUCT
ASPECT RATIO=2.5, RE=100,000, THETA=0
AXIAL VEL. MAG.
A 0.00
B 0.05
C 0.10
D 0.15
E 0.20
F 0.25
G 0.30
H 0.35
I 0.40
J 0.45
K 0.50
L 0.55
M 0.60
N 0.65
O 0.70
P 0.75
Q 0.80
R 0.85
S 0.90
T 0.95
U 1.00
V 1.05
W 1.10
X 1.15
Y 1.20
Z 1.25
a 1.30
b 1.35
SECONDARY VEL. MAG.
A 0.000
B 0.005
C 0.010
D 0.015
E 0.020
F 0.025
G 0.030
H 0.035
I 0.040
J 0.045
K 0.050
L 0.055
M 0.060
N 0.065
O 0.070
P 0.075
Q 0.080
R 0.085
S 0.090
T 0.095
U 0.100

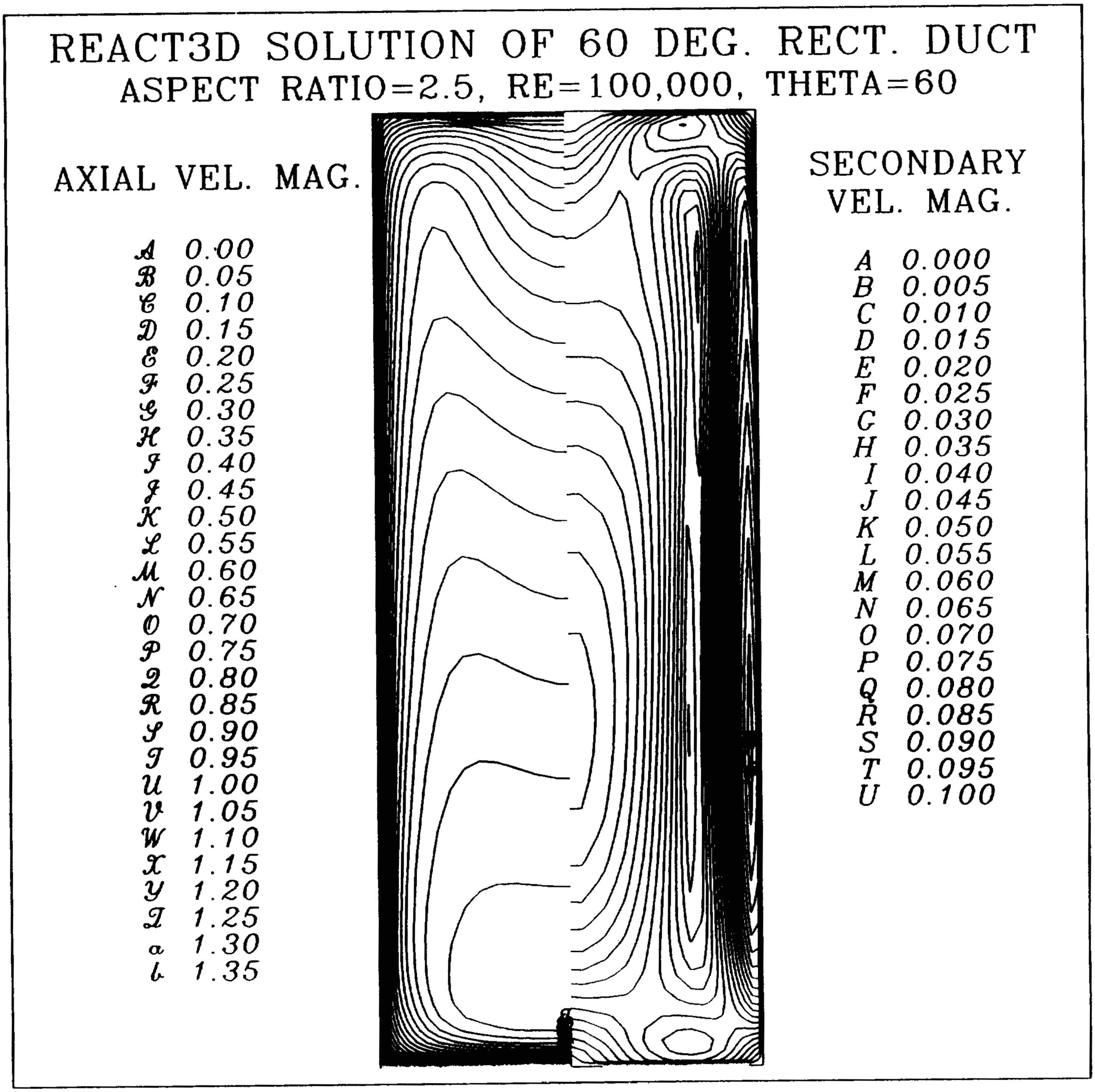
REACT3D SOLUTION OF 60 DEG. RECT. DUCT
ASPECT RATIO=2.5, RE=100,000, THETA=60
AXIAL VEL. MAG.
A 0.00
B 0.05
C 0.10
D 0.15
E 0.20
F 0.25
G 0.30
H 0.35
I 0.40
J 0.45
K 0.50
L 0.55
M 0.60
N 0.65
O 0.70
P 0.75
Q 0.80
R 0.85
S 0.90
T 0.95
U 1.00
V 1.05
W 1.10
X 1.15
Y 1.20
Z 1.25
a 1.30
b 1.35
SECONDARY VEL. MAG.
A 0.000
B 0.005
C 0.010
D 0.015
E 0.020
F 0.025
G 0.030
H 0.035
I 0.040
J 0.045
K 0.050
L 0.055
M 0.060
N 0.065
O 0.070
P 0.075
Q 0.080
R 0.085
S 0.090
T 0.095
U 0.100

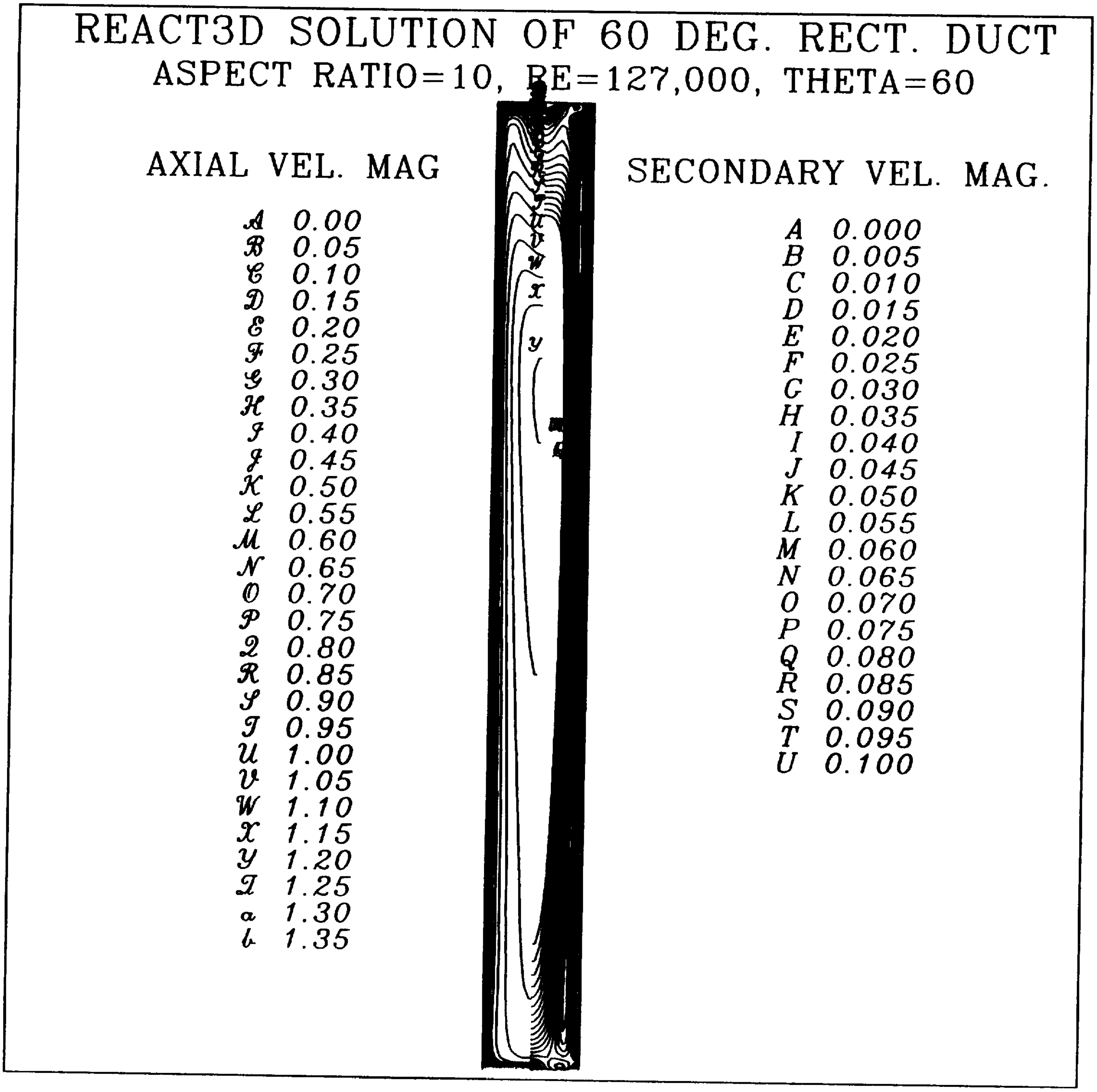
REACT3D SOLUTION OF 60 DEG. RECT. DUCT
ASPECT RATIO=10, RE=127,000, THETA=60
AXIAL VEL. MAG
A 0.00
B 0.05
C 0.10
D 0.15
E 0.20
F 0.25
G 0.30
H 0.35
I 0.40
J 0.45
K 0.50
L 0.55
M 0.60
N 0.65
O 0.70
P 0.75
Q 0.80
R 0.85
S 0.90
T 0.95
U 1.00
V 1.05
W 1.10
X 1.15
Y 1.20
Z 1.25
a 1.30
b 1.35
SECONDARY VEL. MAG.
A 0.000
B 0.005
C 0.010
D 0.015
E 0.020
F 0.025
G 0.030
H 0.035
I 0.040
J 0.045
K 0.050
L 0.055
M 0.060
N 0.065
O 0.070
P 0.075
Q 0.080
R 0.085
S 0.090
T 0.095
U 0.100

ASPECT RATIO EFFECTS

- HEATED WALL CALCULATIONS PERFORMED TO DEMONSTRATE CODE CAPABILITIES
- INITIAL ASSESSMENT OF HEAT TRANSFER EFFECTS OF HIGH ASPECT RATIO CHANNELS
- Tin-Tw=200 CASE SHOWS LIMITED IMPROVEMENT OF HEAT TRANSFER WITH INCREASED ASPECT RATIO

Rockwell International
Rocketdyne Division

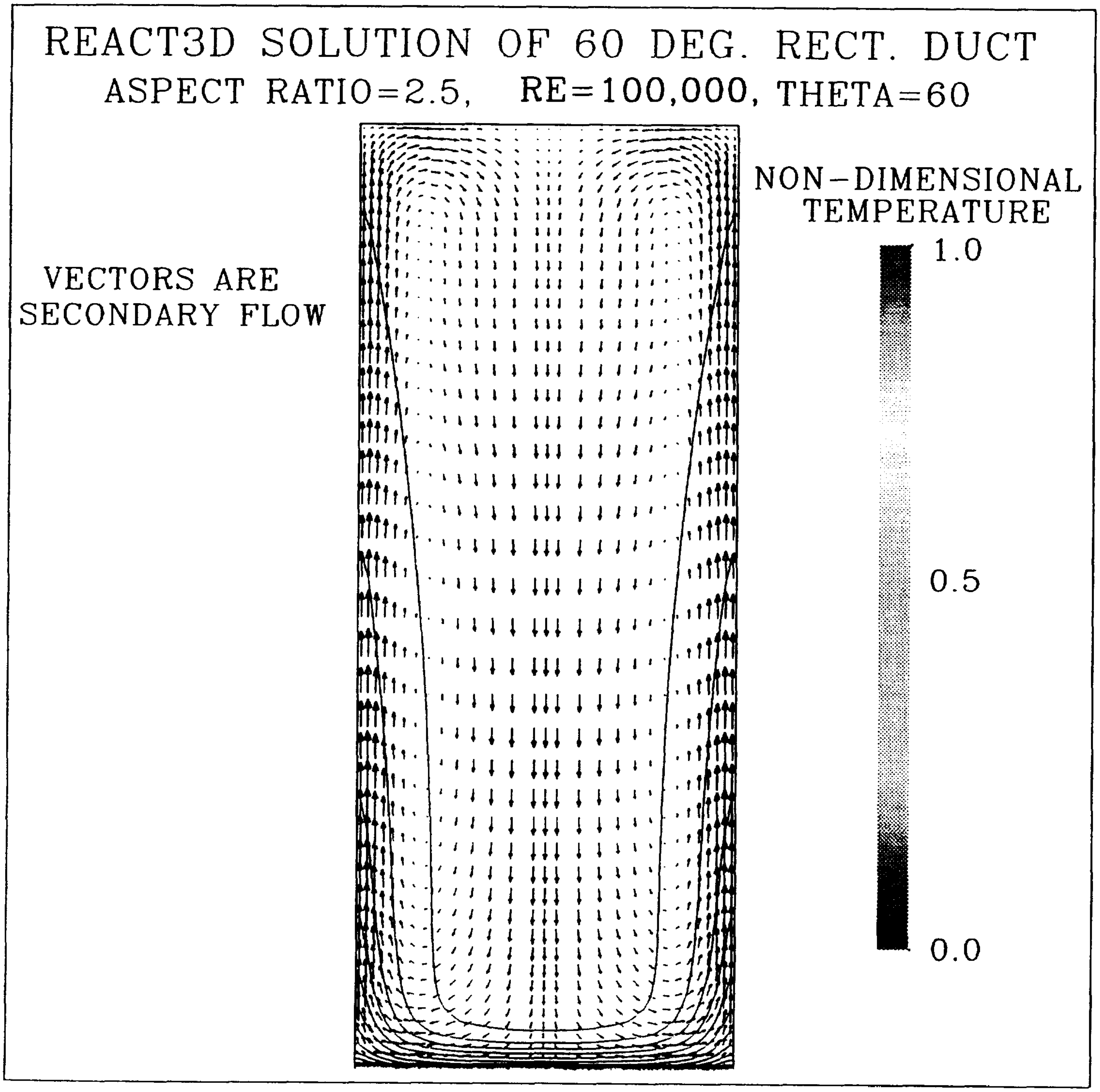
REACT3D SOLUTION OF 60 DEG. RECT. DUCT
ASPECT RATIO=2.5, RE=100,000, THETA=60
VECTORS ARE
SECONDARY FLOW
NON-DIMENSIONAL
TEMPERATURE
1.0
0.5
0.0

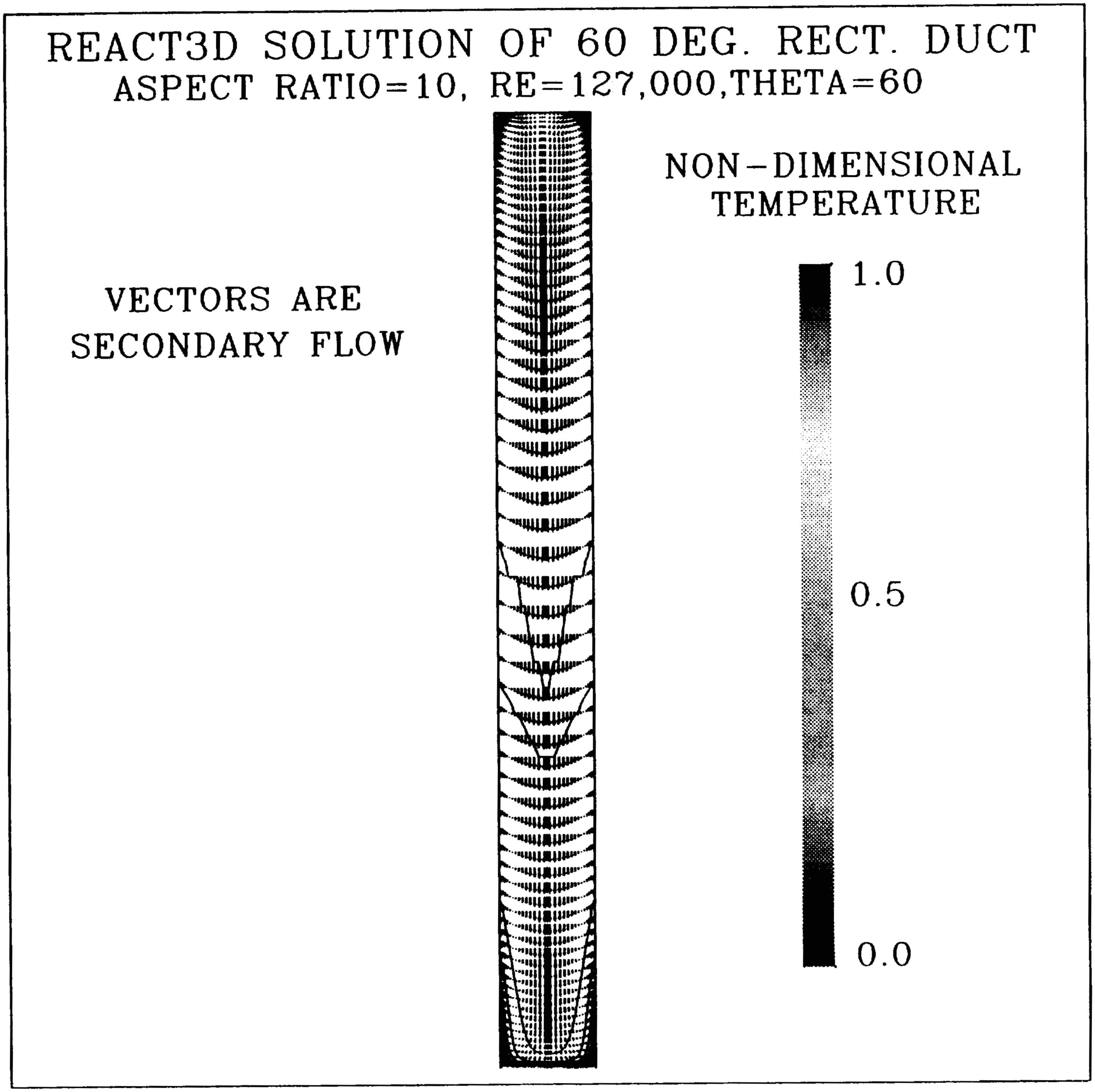
REACT3D SOLUTION OF 60 DEG. RECT. DUCT
ASPECT RATIO=10, RE=127,000,THETA=60
VECTORS ARE
SECONDARY FLOW
NON-DIMENSIONAL
TEMPERATURE
1.0
0.5
0.0

FUTURE PLANS

- COLLECT LDV DATA ON 60° CURVED DUCT FLOWS
- VALIDATE CFD SOLUTIONS TO DATA
- UPGRADE THERMOPHYSICAL PROPERTIES OF FLUIDS
- COLLECT HEAT TRANSFER DATA ON HIGH ASPECT RATIO CHANNELS
- VALIDATE CFD CODE ON HEAT TRANSFER DATA
- PERFORM PARAMETRIC STUDIES FOR COOLANT CHANNEL DESIGNS

Rockwell International
Rocketdyne Division

N95- 23636

FLOW AND HEAT TRANSFER IN 180-DEGREE TURN SQUARE DUCTS - EFFECTS OF TURNING CONFIGURATION AND SYSTEM ROTATION

Ten-See Wang
Computational Fluid Dynamics Branch
NASA - Marshall Space Flight Center
Marshall Space Flight Center, AL 35812

Ming-King Chyu
Department of Mechanical Engineering
Carnegie Mellon University
Pittsburgh, PA 15213

51-34

p. 19

ABSTRACT

Forced flow through channels connected by sharp bends is frequently encountered in various rocket and gas turbine engines. For example, the transfer ducts, the coolant channels surround the combustion chamber, the internal cooling passage in a blade or vane, the flow path in the fuel element of a nuclear rocket engine, the flow around a pressure relieve valve piston, and the recirculated base flow of multiple engine clustered nozzles. Transport phenomena involved in such a flow passage are complex and considered to be very different from those of conventional turning flow with relatively mild radii of curvature. While previous research pertaining to this subject has been focused primarily on the experimental heat transfer, very little analytical work is directed to understanding the flowfield and energy transport in the passage. Therefore, the primary goal of this paper is to benchmark the predicted wall heat fluxes using a state-of-the-art computational fluid dynamics (CFD) formulation against those of measurement for a rectangular turn duct. Other secondary goals include studying the effects of turning configurations, e.g., the semi-circular turn, and the rounded-corner turn, and the effect of system rotation. The computed heat fluxes for the rectangular turn duct compared favorably with those of the experimental data. The results show that the flow pattern, pressure drop, and heat transfer characteristics are different among the three turning configurations, and are substantially different with system rotation. Also demonstrated in this work is that the present computational approach is quite effective and efficient and will be suitable for flow and thermal modeling in rocket and turbine engine applications.

Flow and Heat Transfer in 180-Degree Turn Square Ducts - Effects of Turning Configuration and System Rotation

Ten-See Wang

Computational Fluid Dynamics Branch

NASA-Marshall Space Flight Center

Ming-King Chyu

Department of Mechanical Engineering

Carnegie Mellon University

11th Workshop for CFD in Rocket Propulsion

Main Sessions 5: Applications - Duct Flows

MSFC, Alabama

April 20, 1993

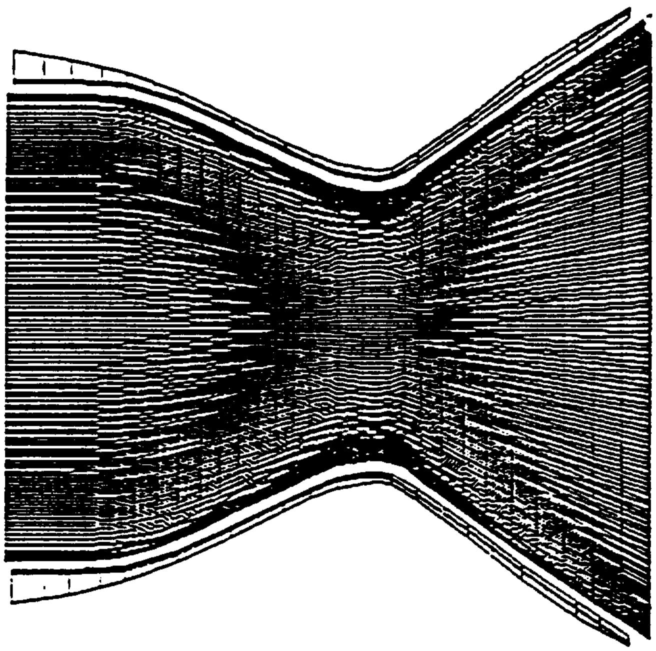

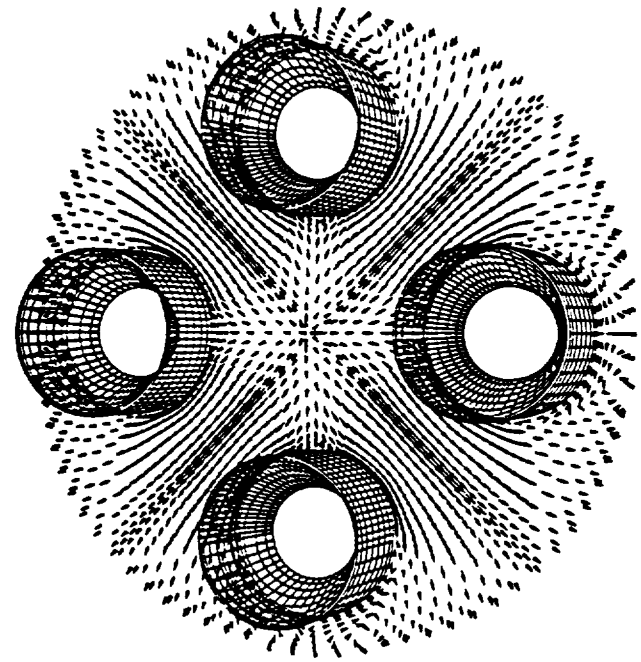

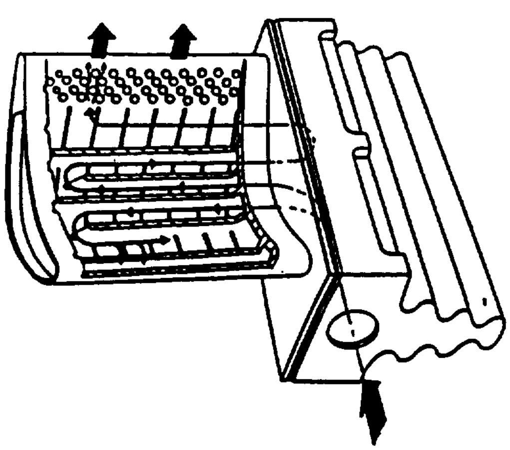

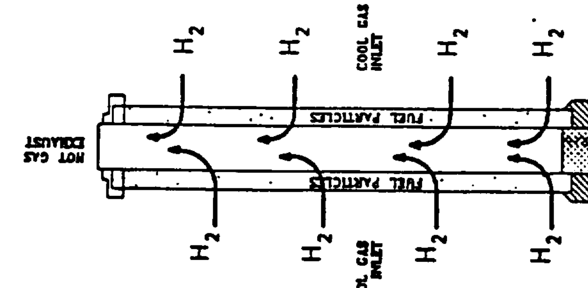
HOT GAS EXHAUST
FUEL PARTICLES
FUEL PARTICLES
COOL GAS INLET
COOL GAS INLET
END CLOSURE
H_2

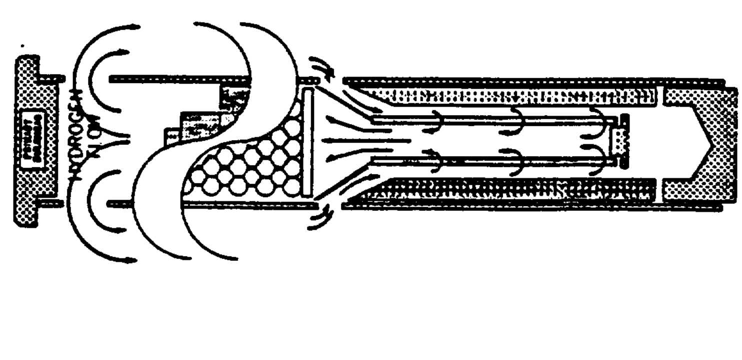
HYDROGEN FLOW

Objectives

- To obtain detailed information on the turbulent flowfield and its effects on the local heat transfer
- To benchmark the CFD solution with a two-pass sharp-turned square duct experiemnt
- To examine the influence of turn configuration and System rotation on the overall transport phenomena in the passage

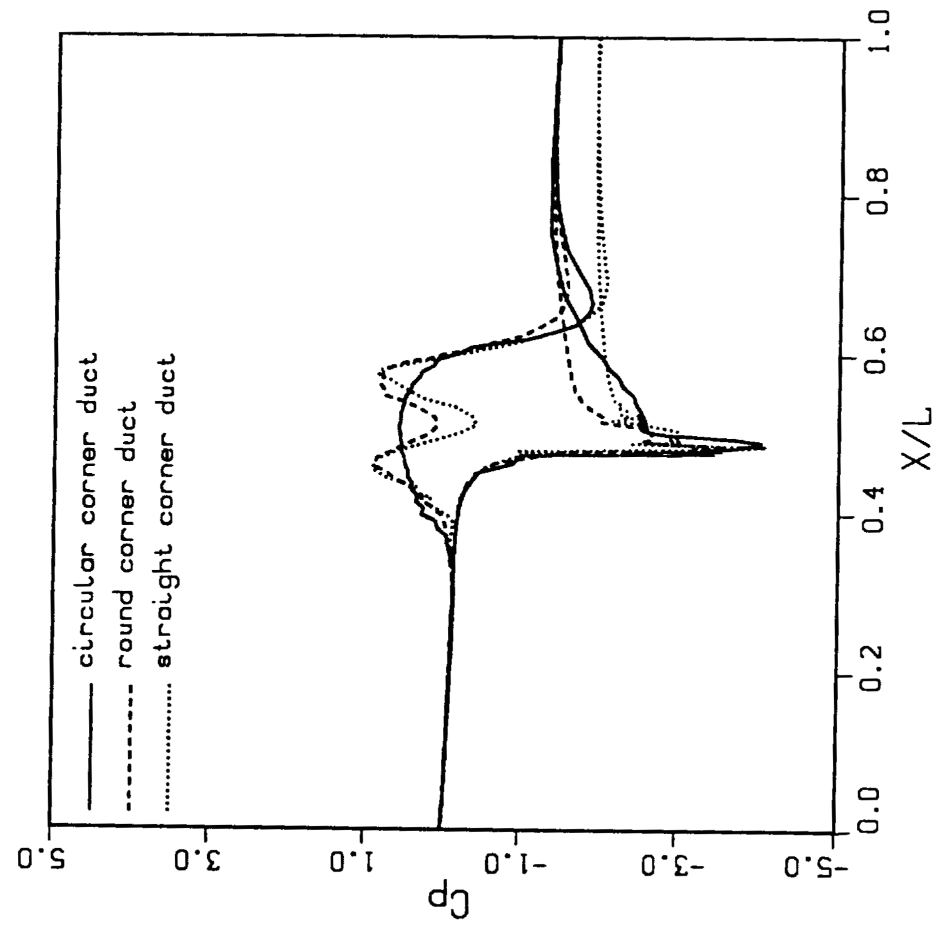

circular corner duct
round corner duct
straight corner duct
X/L
Cp
0.0
0.2
0.4
0.6
0.8
1.0
5.0
3.0
1.0
-1.0
-3.0
-5.0

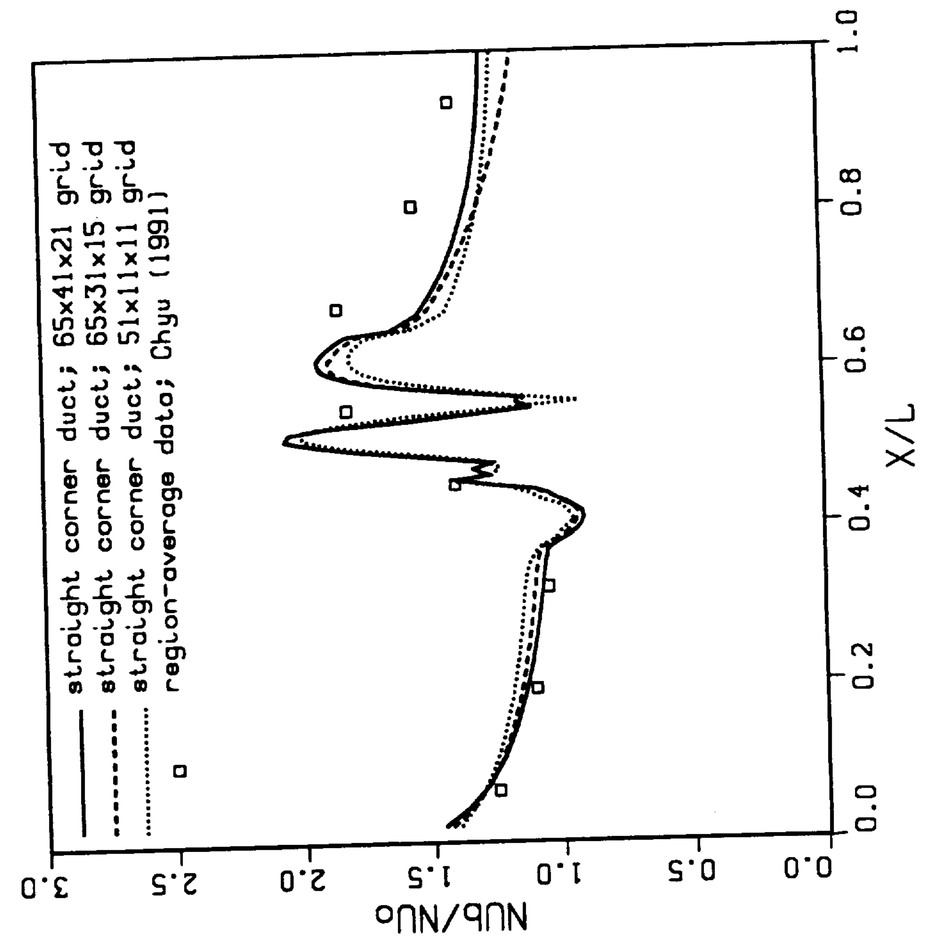
straight corner duct; 65x41x21 grid
straight corner duct; 65x31x15 grid
straight corner duct; 51x11x11 grid
region-average data; Chyu (1991)
NUb/NUo
X/L
0.0
0.5
1.0
1.5
2.0
2.5
3.0
0.0
0.2
0.4
0.6
0.8
1.0

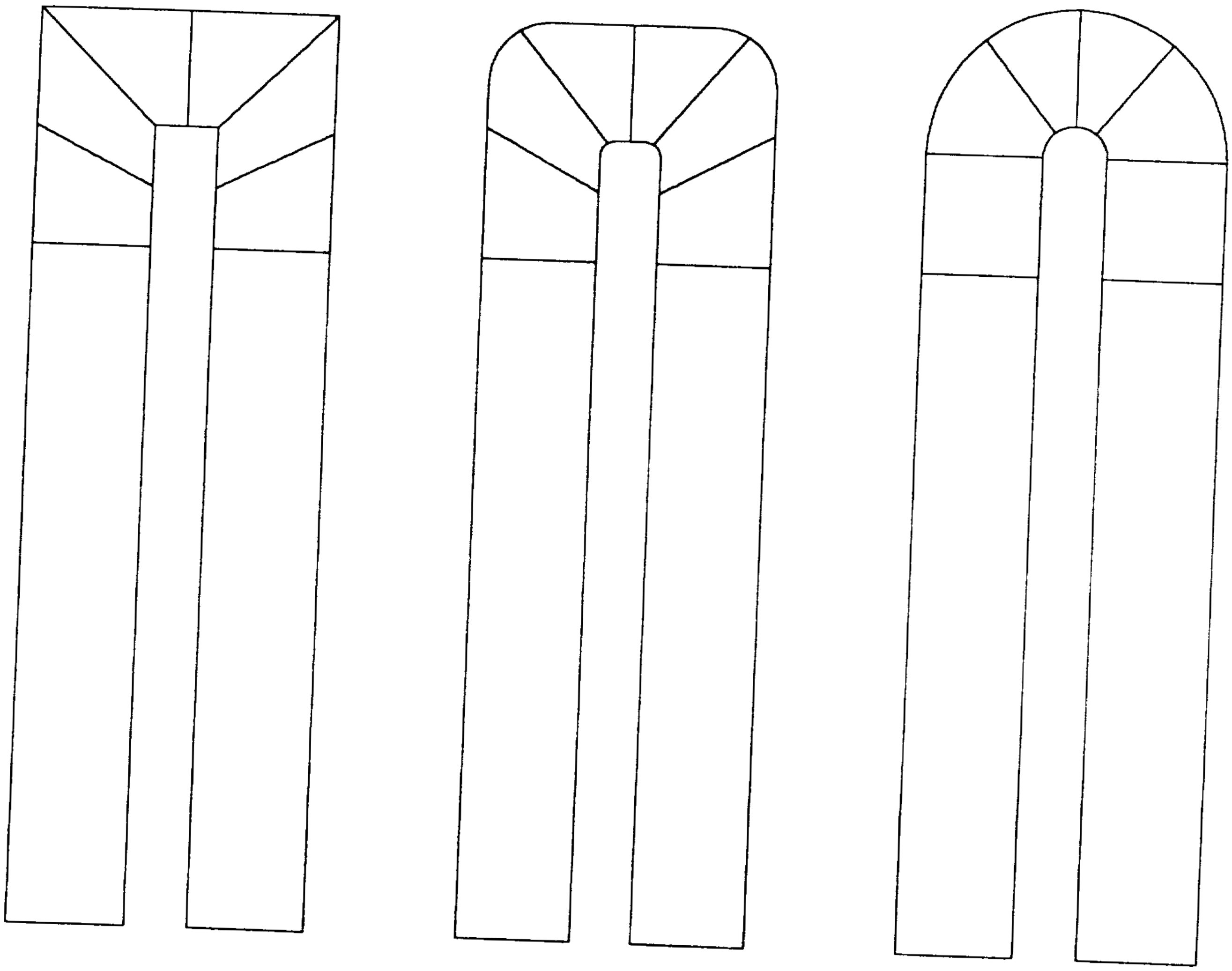

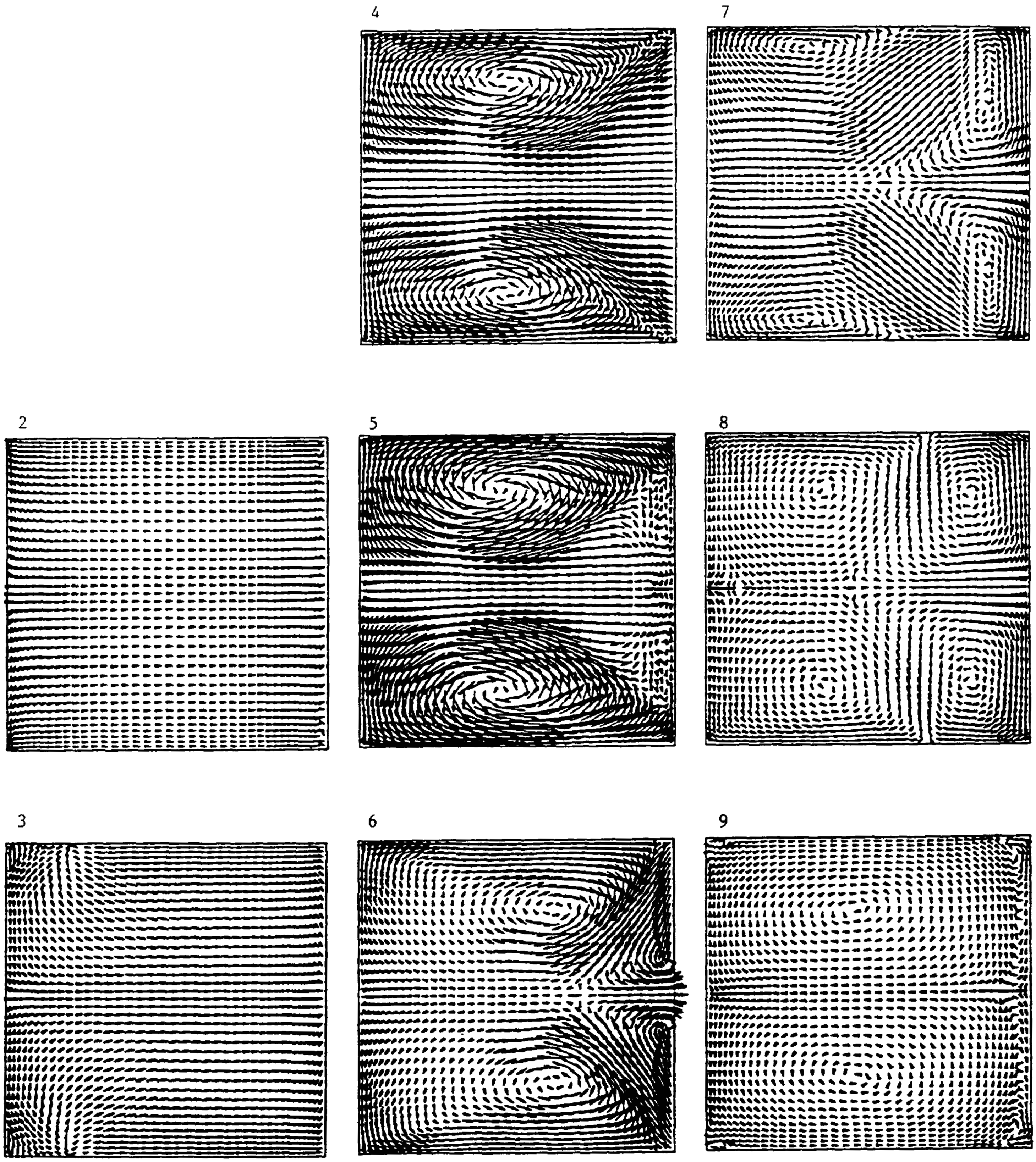

The evolution of the secondary flow pattern for a 180-degree turn straight-corner square duct

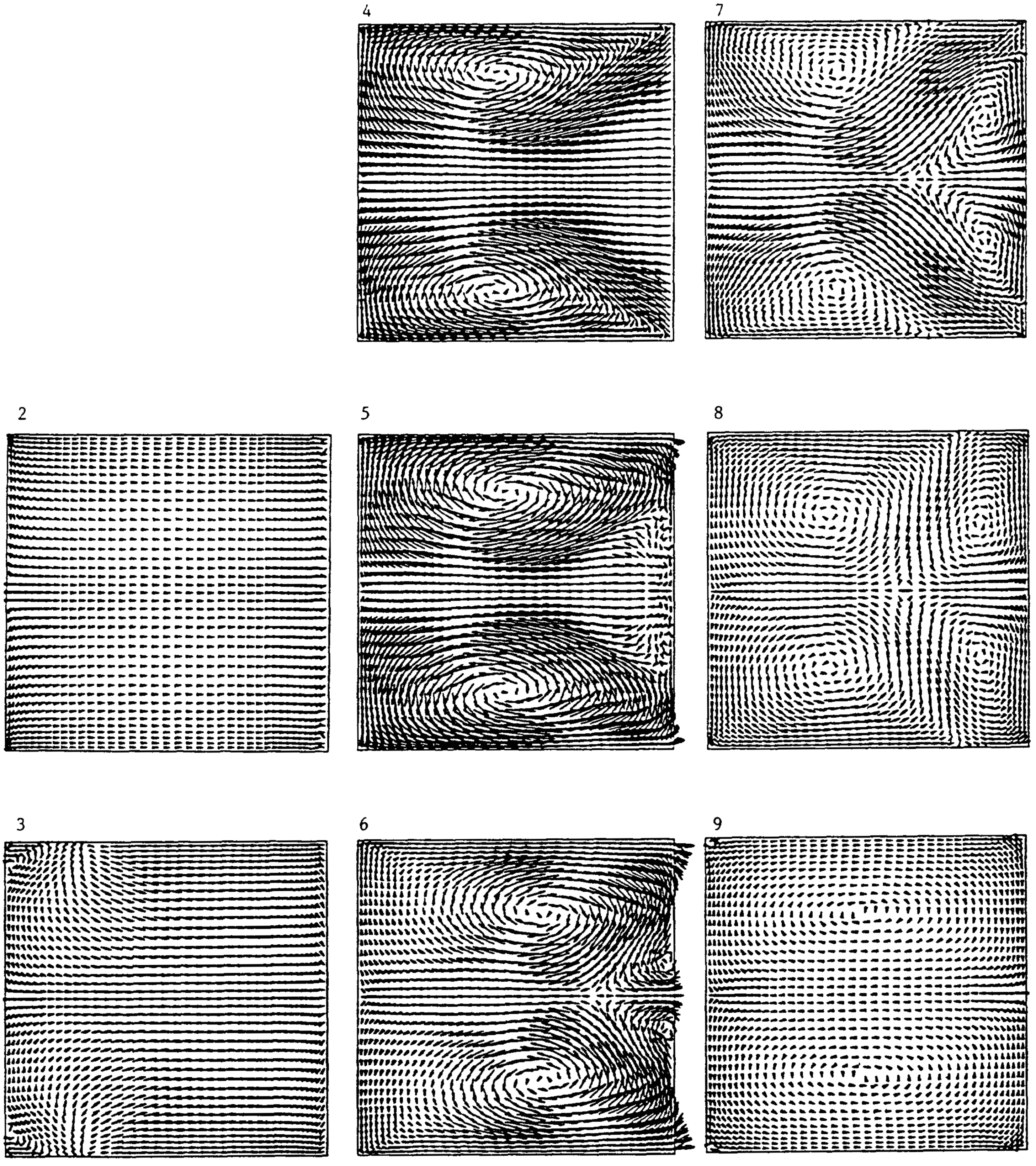

The evolution of the secondary flow pattern for a 180-degree turn round-corner square duct

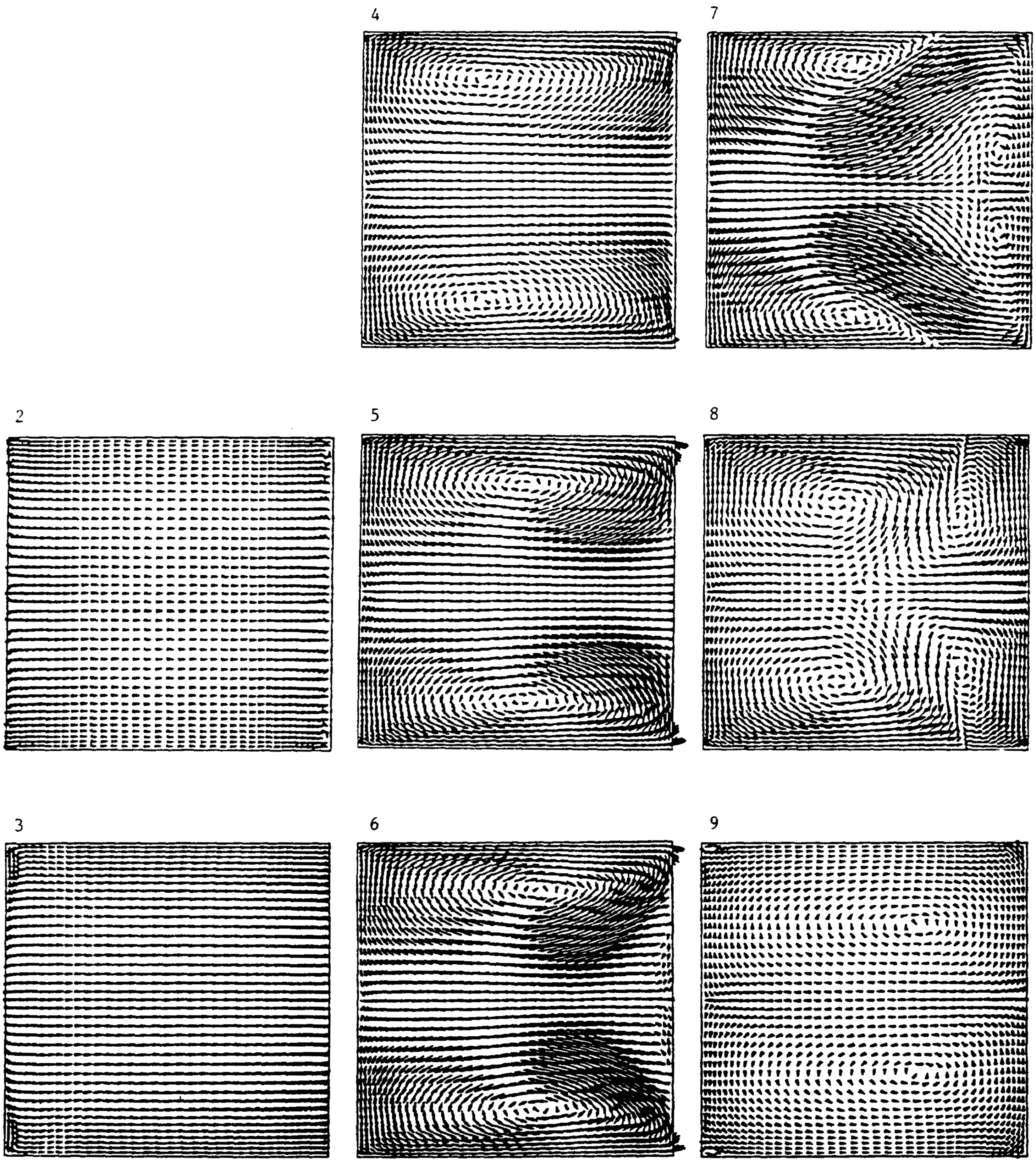

The evolution of the secondary flow pattern for a 180-degree turn circular-corner square duct

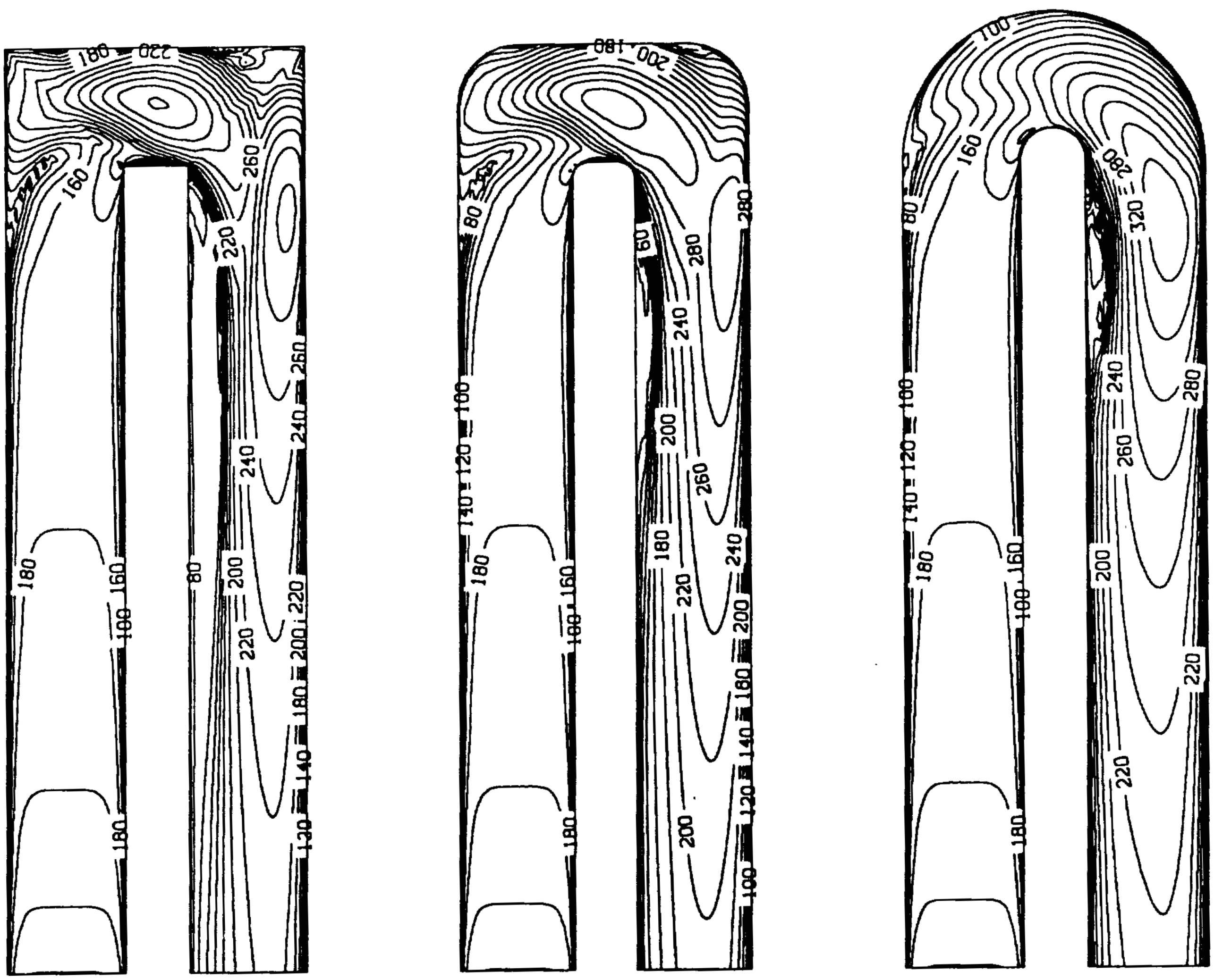

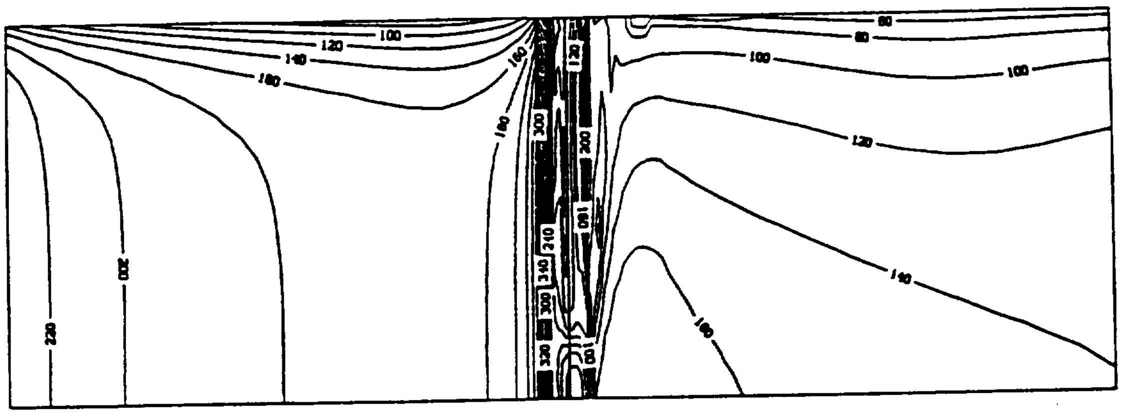
100
120
140
180
220
200
300
80
100
120
140
180

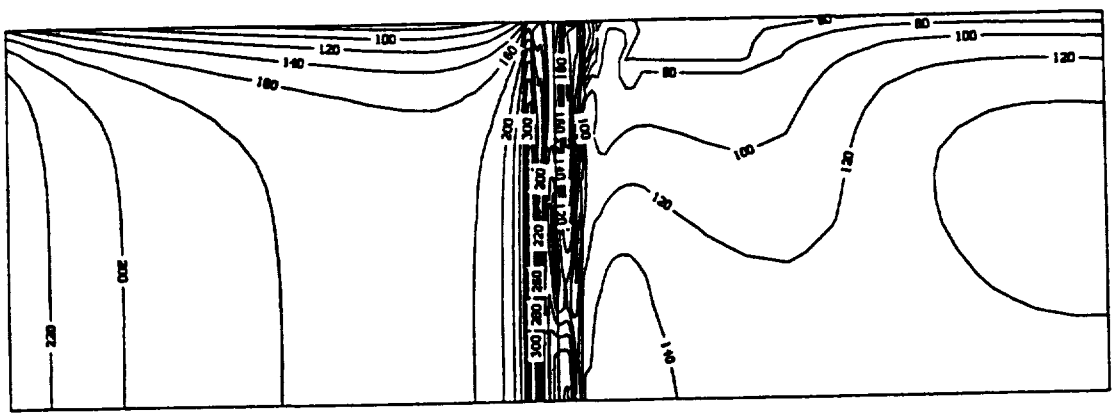
100
120
140
180
200
220
300
80
100
120
140

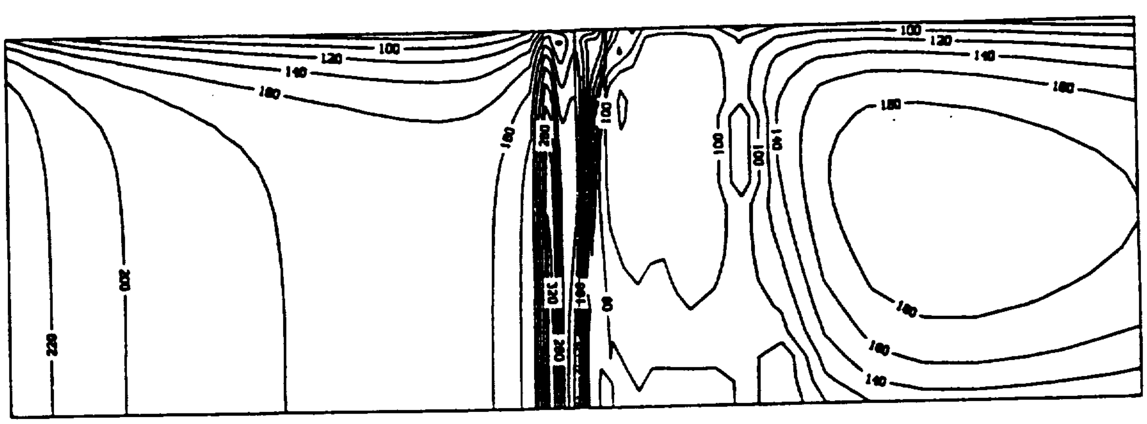
100
120
140
180
200
220
100
120
140
180
160

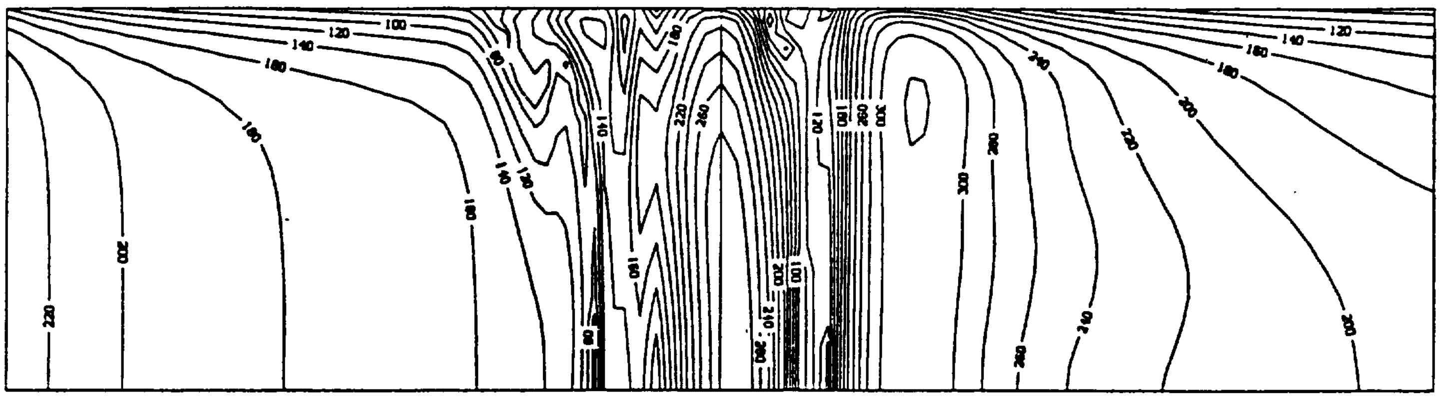

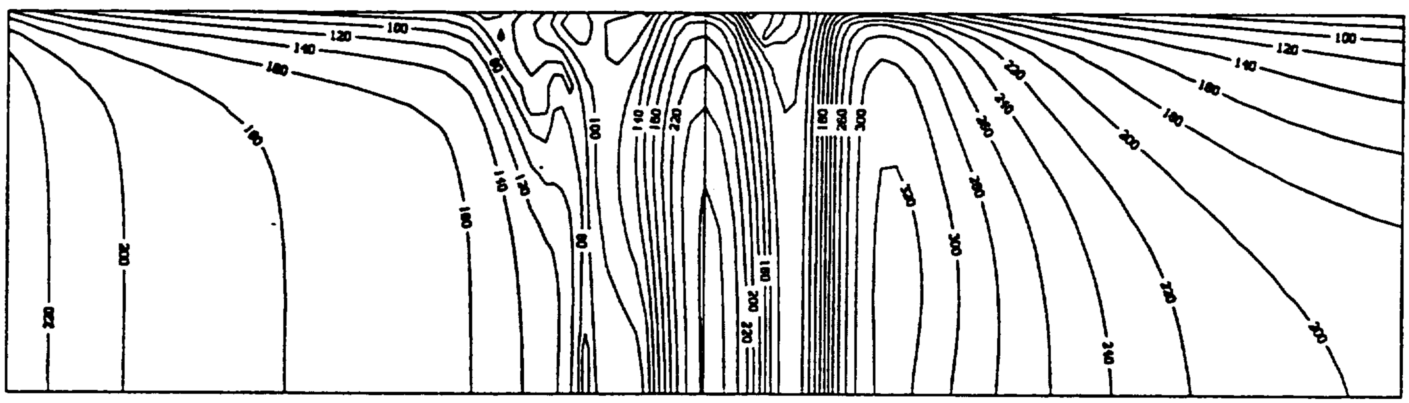

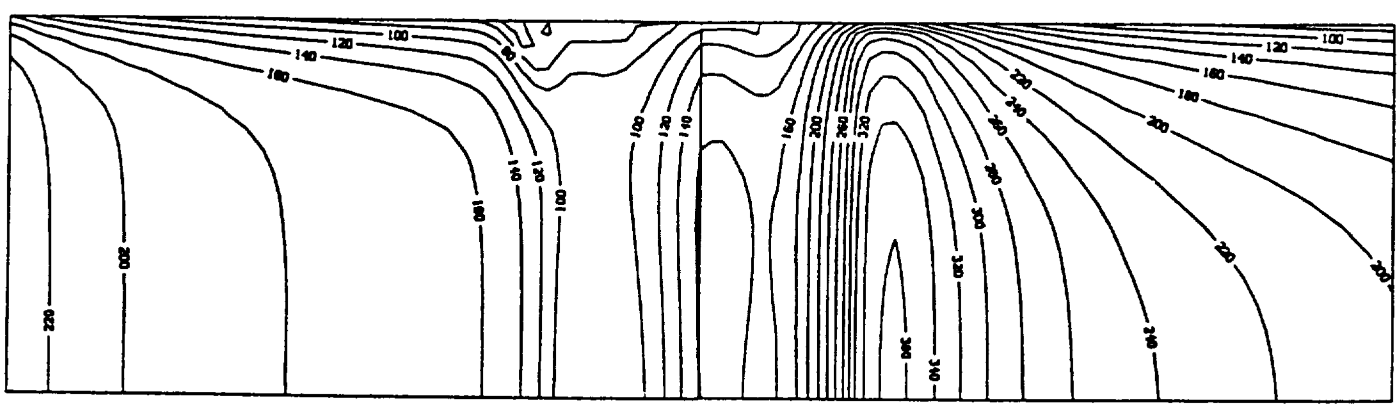

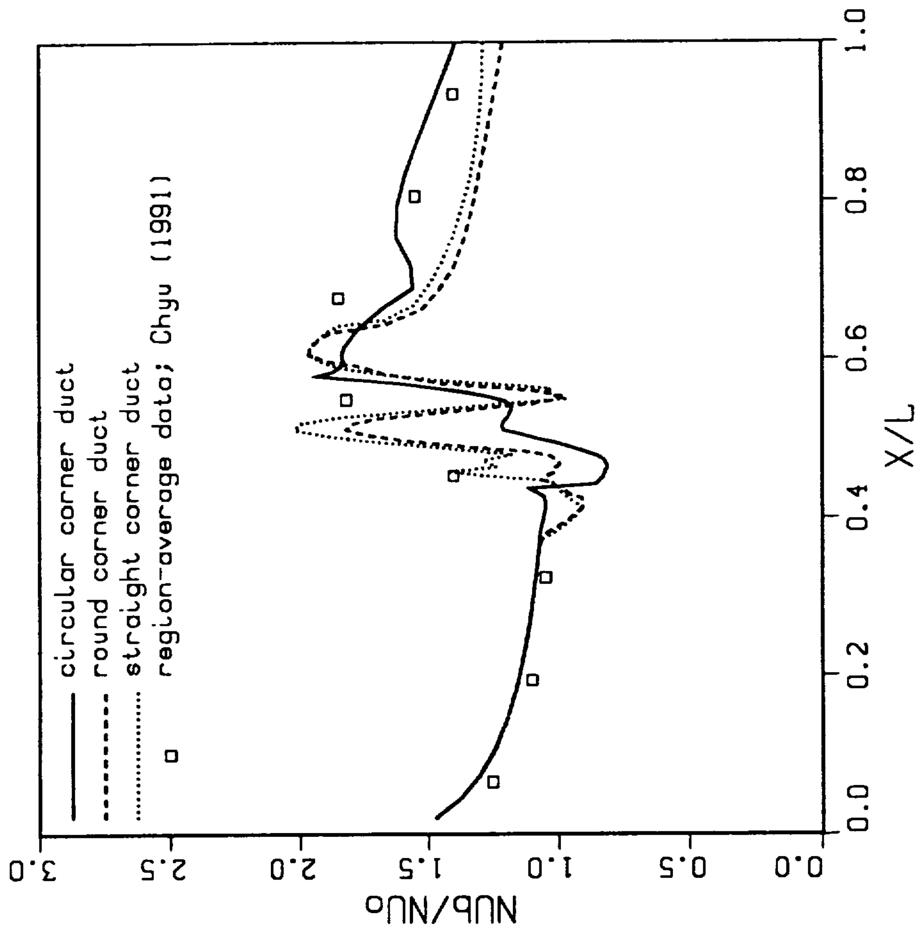

circular corner duct
round corner duct
straight corner duct
region-average data; Chyu (1991)
NUb/NUo
0.0
0.5
1.0
1.5
2.0
2.5
3.0
X/L
0.0
0.2
0.4
0.6
0.8
1.0

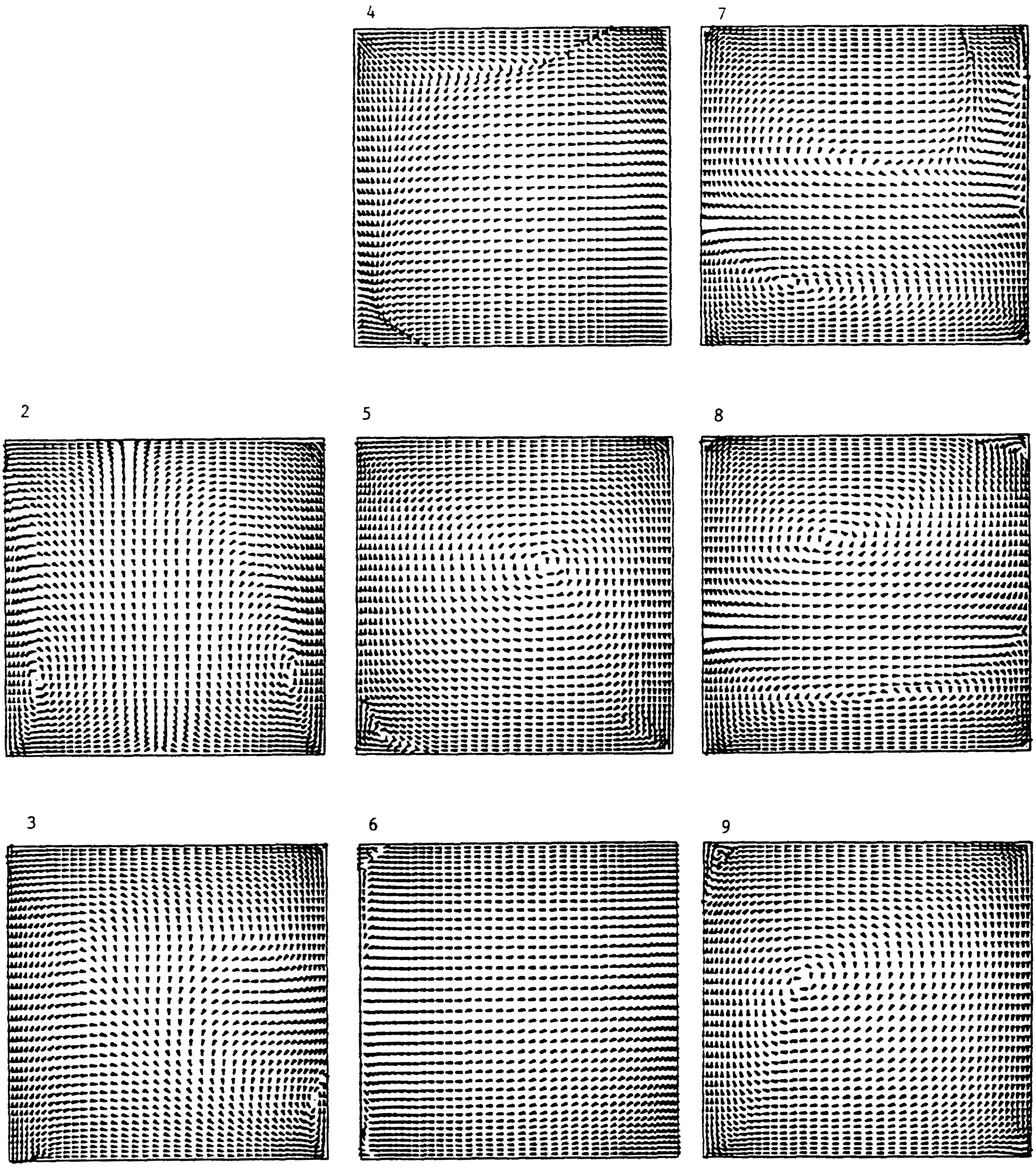

The evolution of the secondary flow pattern for a 180-degree turn straight-corner square duct with rotation

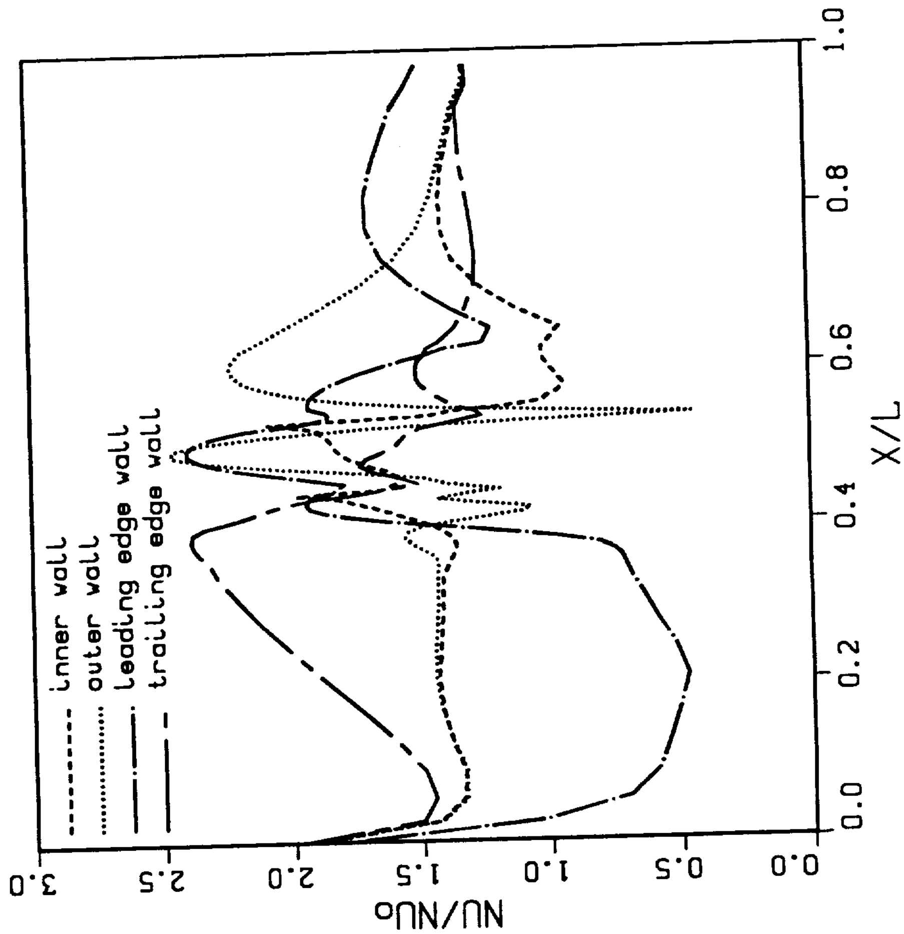
inner wall
outer wall
leading edge wall
trailing edge wall
X/L
NU/NUo
0.0
0.2
0.4
0.6
0.8
1.0
0.5
1.0
1.5
2.0
2.5
3.0

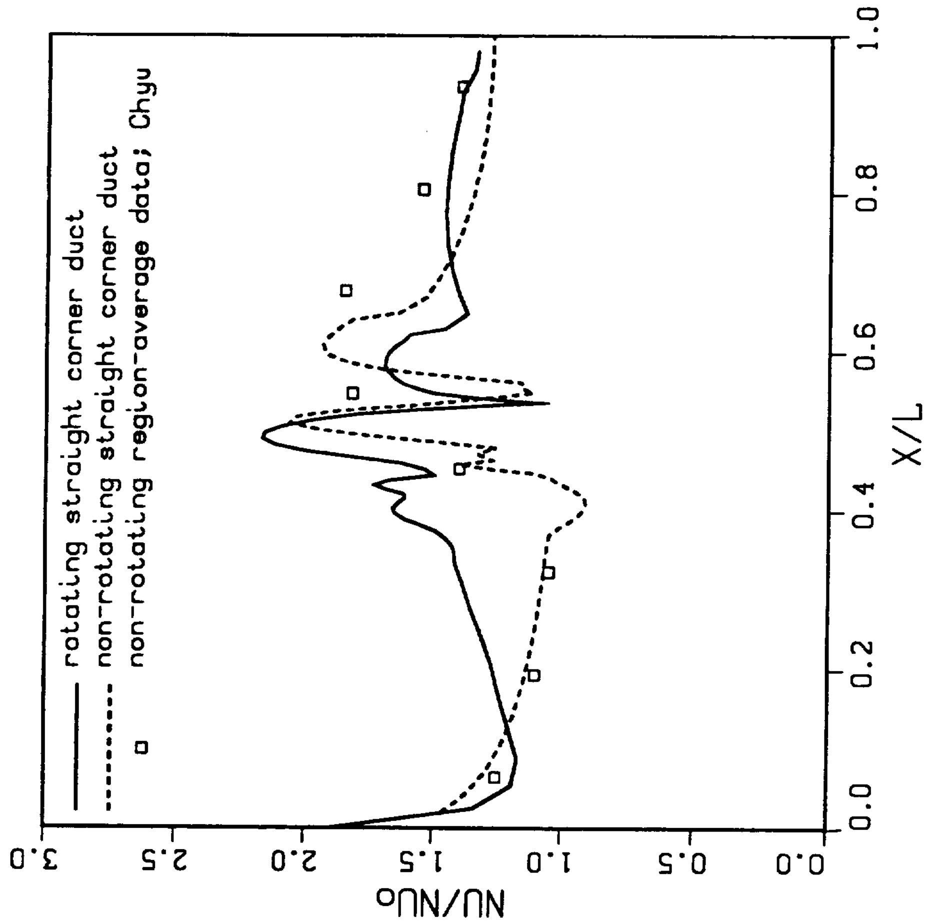
rotating straight corner duct
non-rotating straight corner duct
non-rotating region-average data; Chyu
NU/NU₀
X/L
0.0
0.5
1.0
1.5
2.0
2.5
3.0
0.0
0.2
0.4
0.6
0.8
1.0

The averaged total Nusselt numbers

	NUi	NUb	NUb/NUo
Circular-Corner Turn	184	210	1.3127
Round-Corner Turn	188	213	1.3321
Straight-Corner Turn	193	222	1.3837
Straight-Corner Turn with Rotation	217	250	1.5614

Conclusions

- Detailed information in flowfield, pressure drop and local heat transfer
- Favorable agreement with experimental data
- Complex features and strong turn-geometry dependence in post-turn secondary flows
- Straight-corner turn has highest turn-induced heat transfer enhancement
- Circular-corner turn has highest post-turn heat transfer
- System rotation enhances heat transfer

N95- 23637

Methodology for CFD Design Analysis of National Launch System Nozzle Manifold

p. 21

Scot L. Haire
Pratt & Whitney, West Palm Beach, FL

ABSTRACT

The current design environment dictates that high technology CFD (Computational Fluid Dynamics) analysis produce quality results in a timely manner if it is to be integrated into the design process. The design methodology outlined describes the CFD analysis of an NLS (National Launch System) nozzle film cooling manifold. The objective of the analysis was to obtain a qualitative estimate for the flow distribution within the manifold. A complex, 3D, multiple zone, structured grid was generated from a 3D CAD file of the geometry. An Euler solution was computed with a fully implicit compressible flow solver. Post processing consisted of full 3D color graphics and mass averaged performance. The result was a qualitative CFD solution that provided the design team with relevant information concerning the flow distribution in and performance characteristics of the film cooling manifold within an effective time frame. Also, this design methodology was the foundation for a quick turnaround CFD analysis of the next iteration in the manifold design.

METHODOLOGY FOR CFD ANALYSIS OF A NATIONAL LAUNCH SYSTEM FILM COOLING NOZZLE MANIFOLD

Scot Haire

Pratt & Whitney, GESP

West Palm Beach, Florida

April 20, 1993

Presented At Workshop for CFD Applications in Rocket Propulsion, NASA–MSFC

NLS MANIFOLD ANALYSIS

- Purpose of the analysis
- Manifold geometry
- Schedule limitations
- Pre–processing
  - Geometry modification
  - Grid generation
- Solution
- Post–processing
  - Color graphics
  - Performance
- Summary

ANALYSIS OBJECTIVE

To determine the flow distribution at the exit of the manifold without the effects of a choked orifice. This will identify the flow uniformity as a function of the volute manifold geometry alone.

STME FILM/CONVECTIVE COOLED NOZZLE

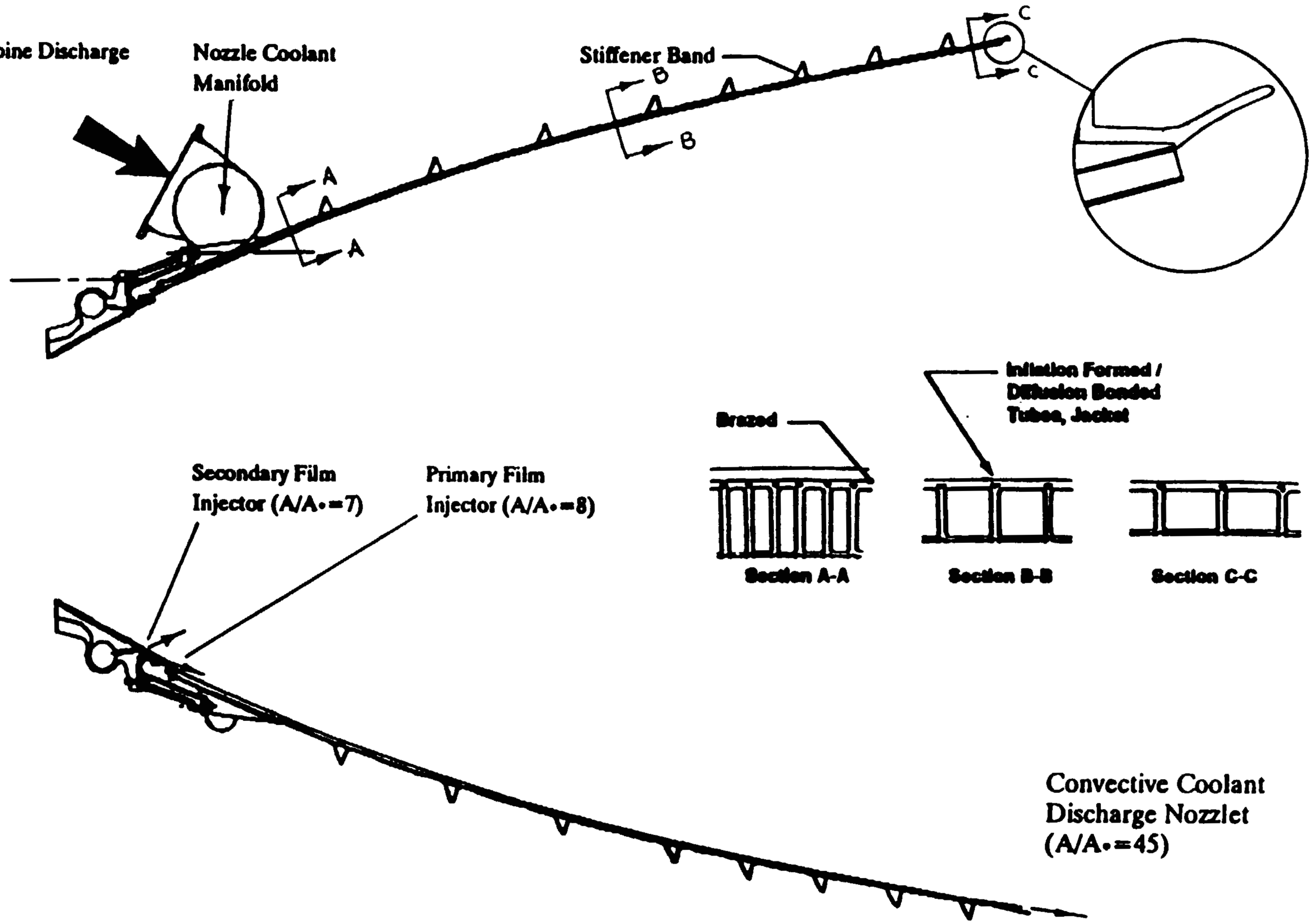

THIS PAGE LEFT BLANK INTENTIONALLY

SCHEDULE REQUIREMENT

STME Nozzle Manifold Development

PRELIMINARY

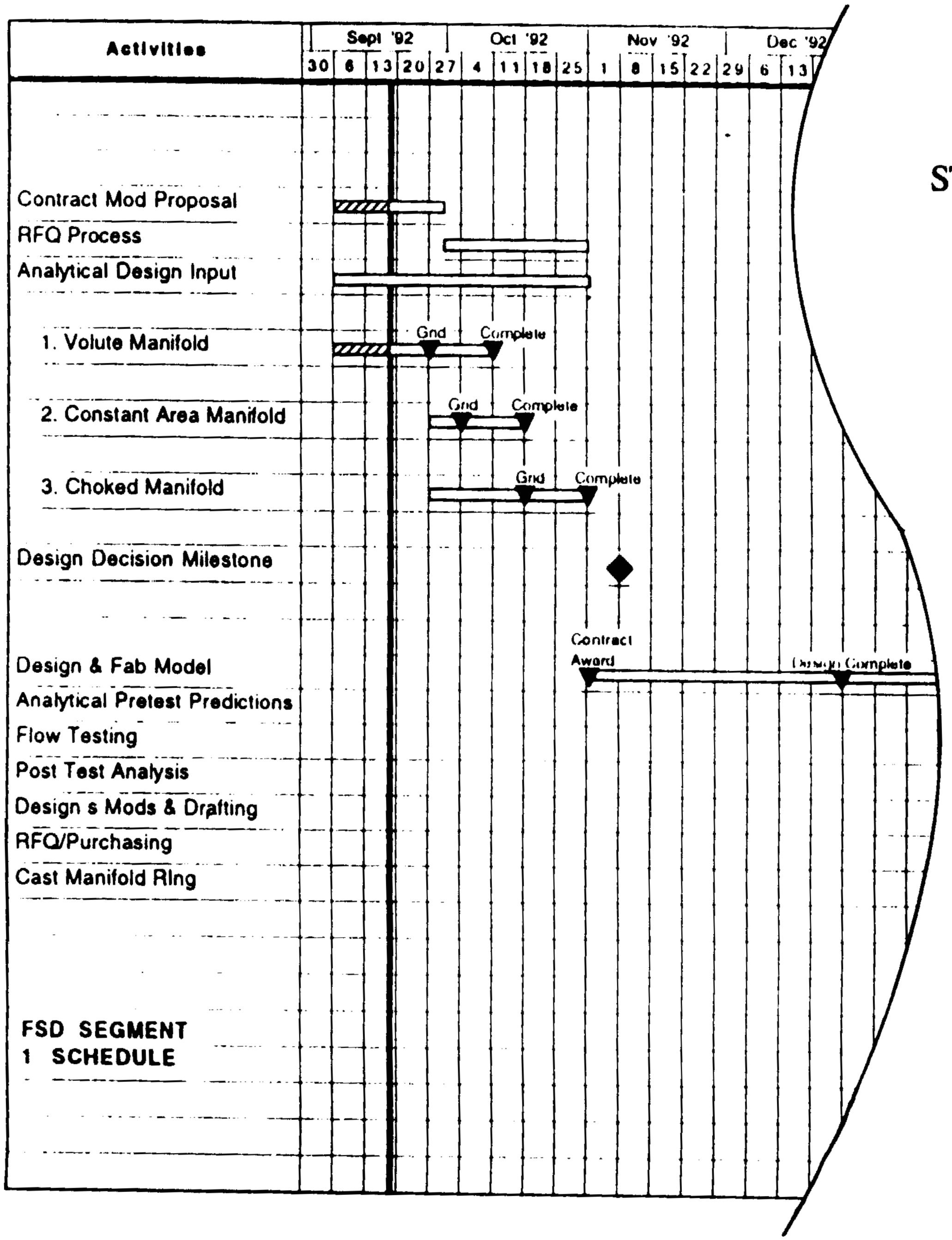

PRECEDING PAGE BLANK NOT FILMED

PRE–PROCESSING

- Geometry modification
  - Splitter vane
  - ICEM DDN (CDC)
- Grid generation
  - ICEM DDN, PADDAM, MULCAD (CDC)
  - $\sim$ 130,000 points
  - 19 zones
- Time to complete $\sim$ 7 days

Computational Grid Zones

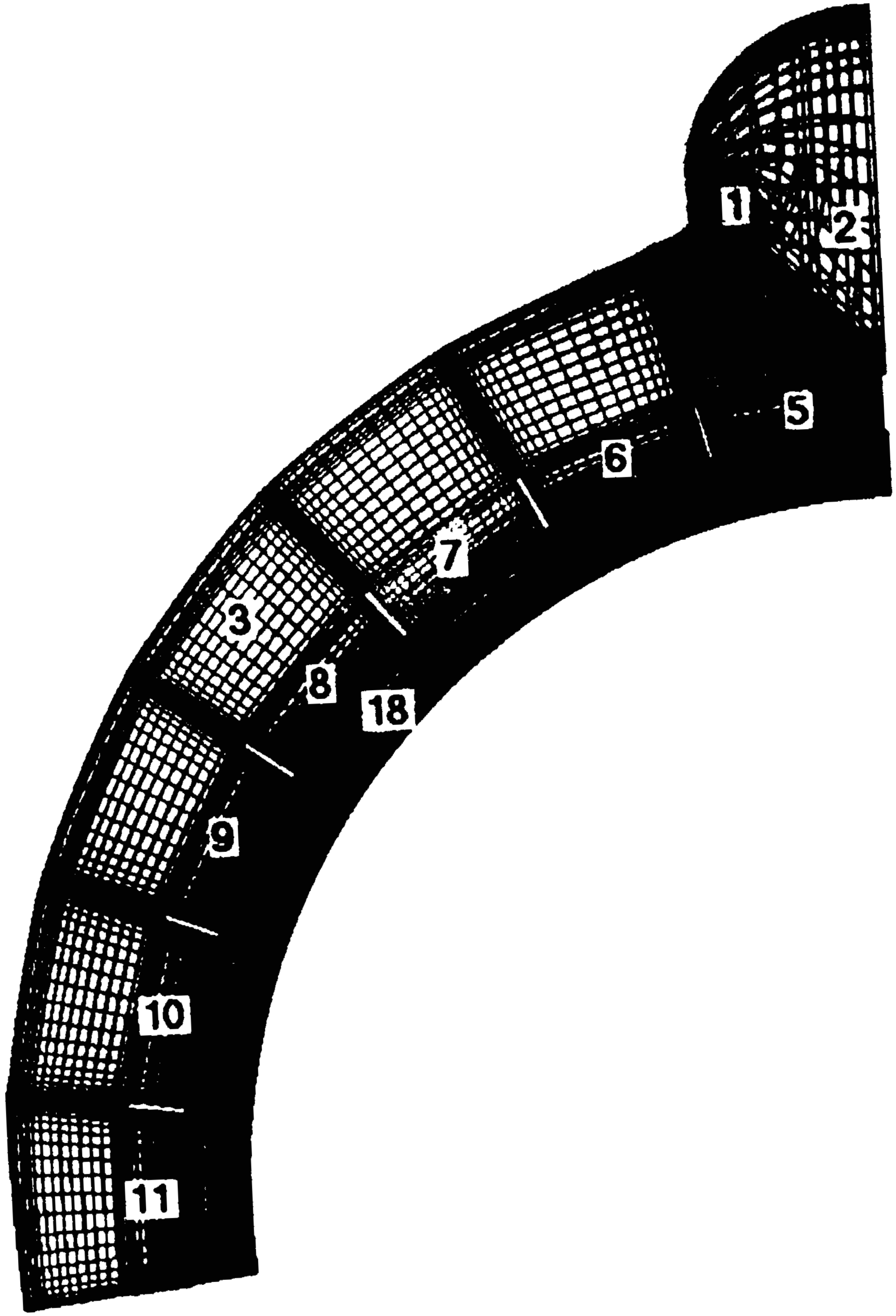

Computational Grid Zones

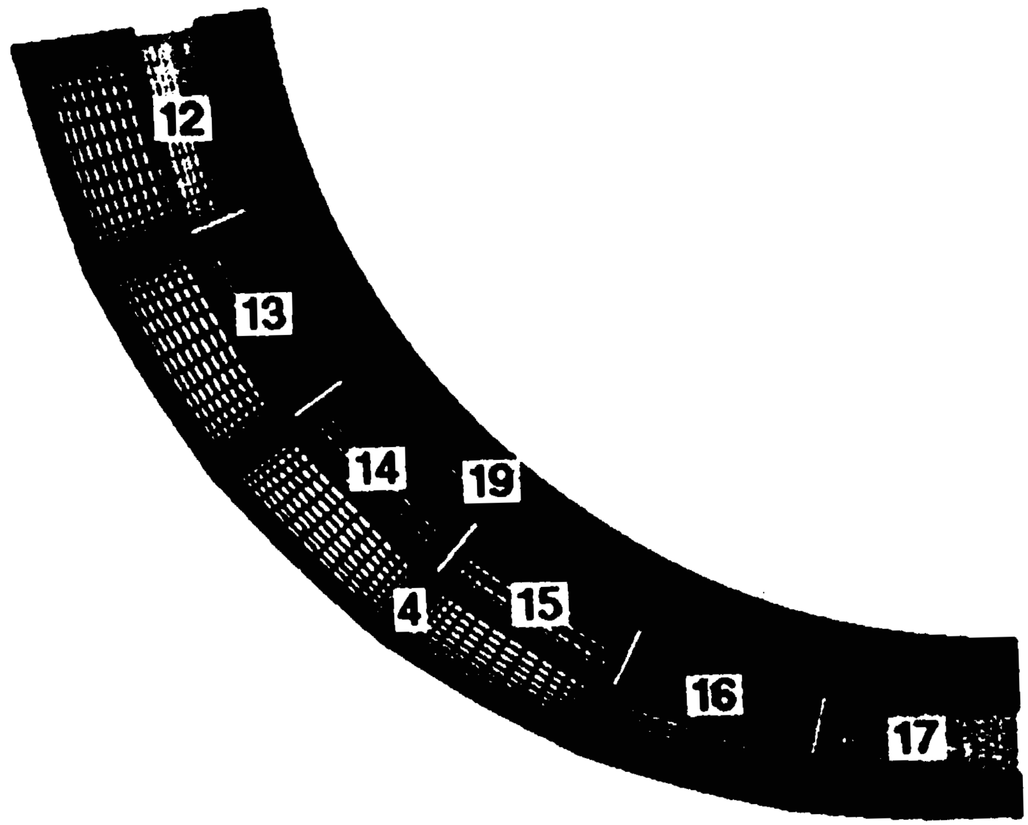

Computational Grid

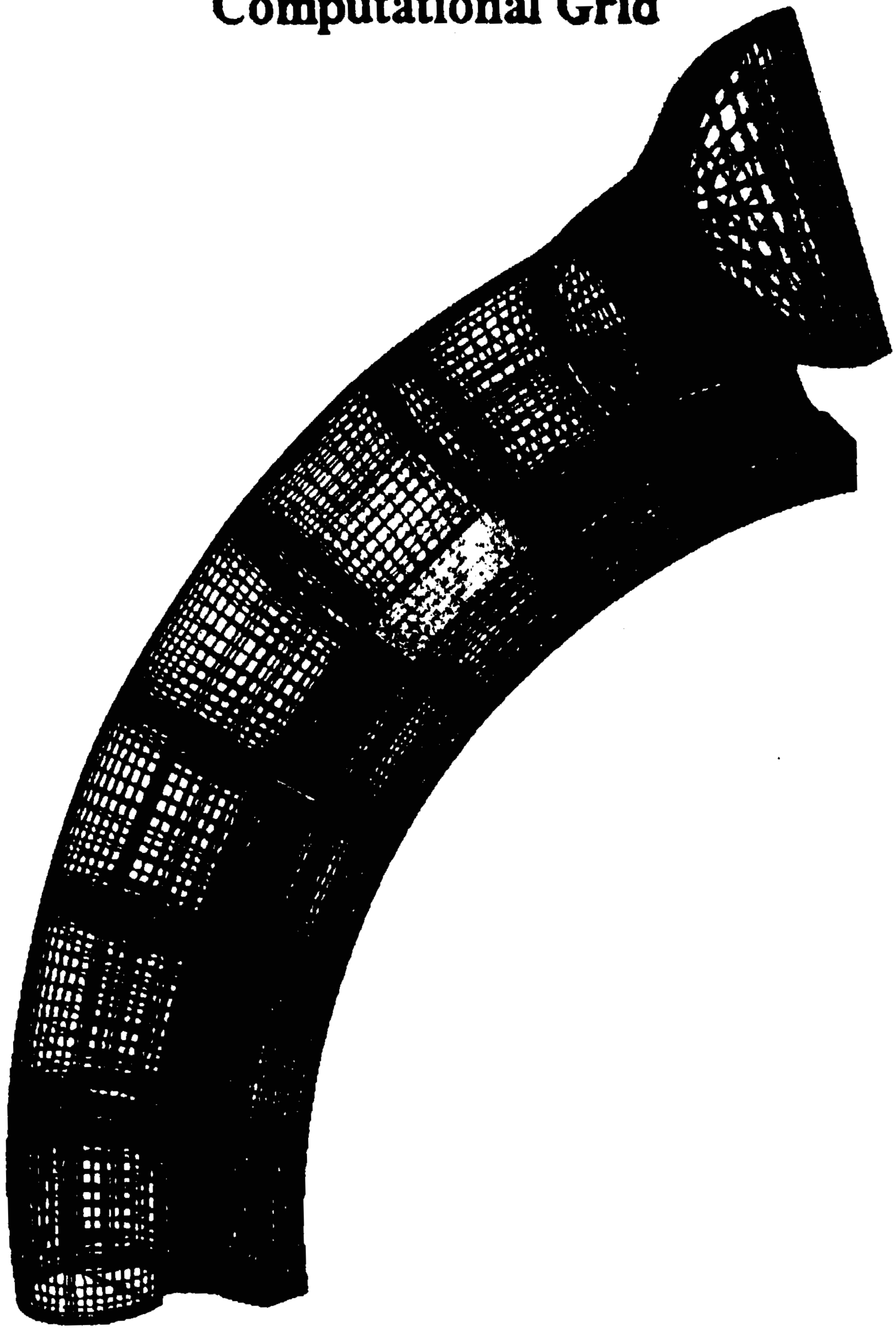

Computational Grid Cross Section

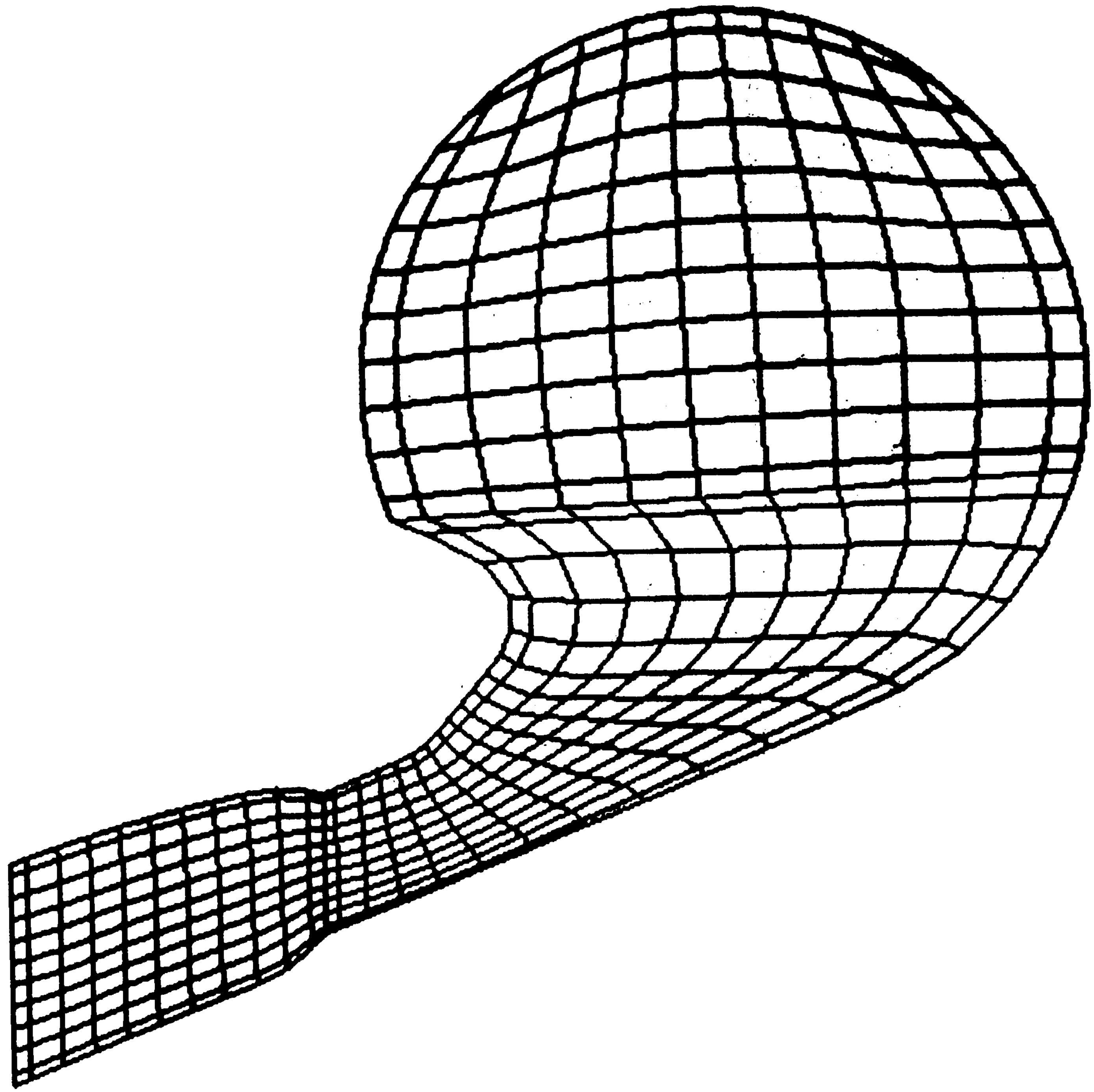

SOLUTION

- GASP 2.0 (AeroSoft)
  - Fully Implicit
  - Finite volume
- 64 MW SGI Machine
- Flow solution
  - 3–D inviscid (viscous)
  - 108 CPU hours ($\sim$ 5 days)
- Time to complete $\sim$ 7 days

POST PROCESSING

- Color graphics
  - FAST (NASA Ames)
  - Visualization of flow distribution
- Mass averaged performance
  - Pratt & Whitney utilities
  - Static pressure
  - Mach number
  - Mass flow rate

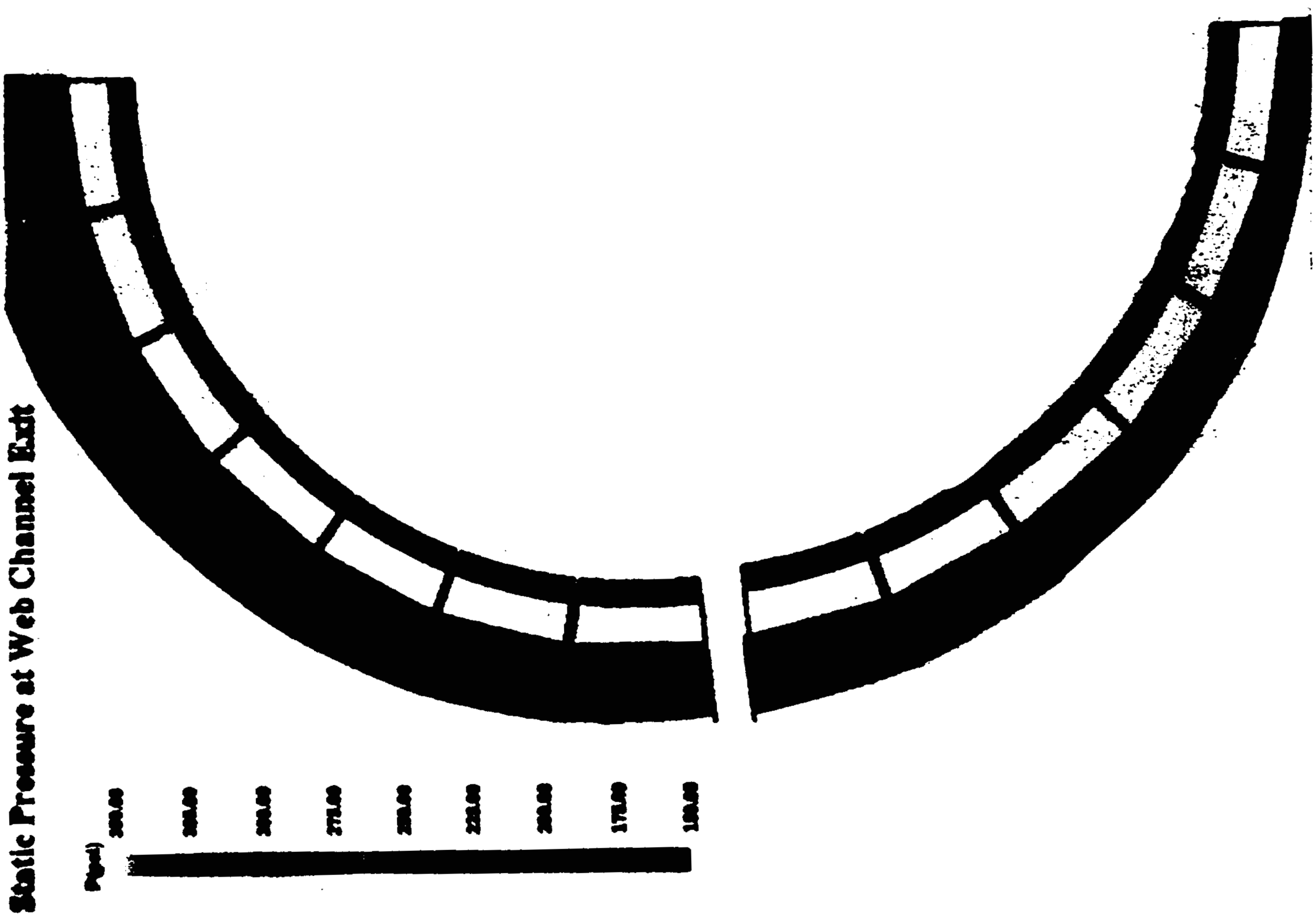
Static Pressure at Web Channel Exit

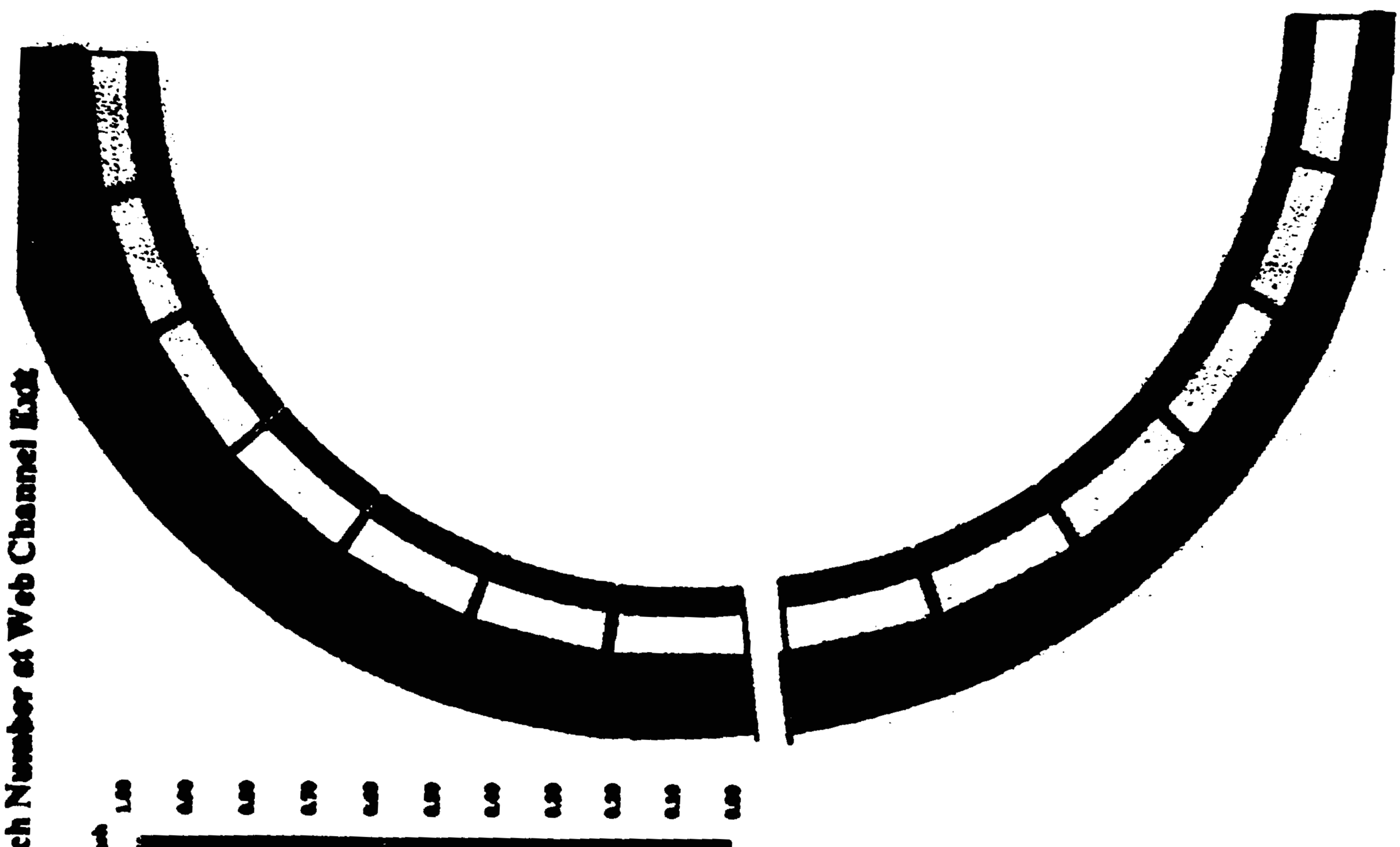
Mach Number at Web Channel Exit

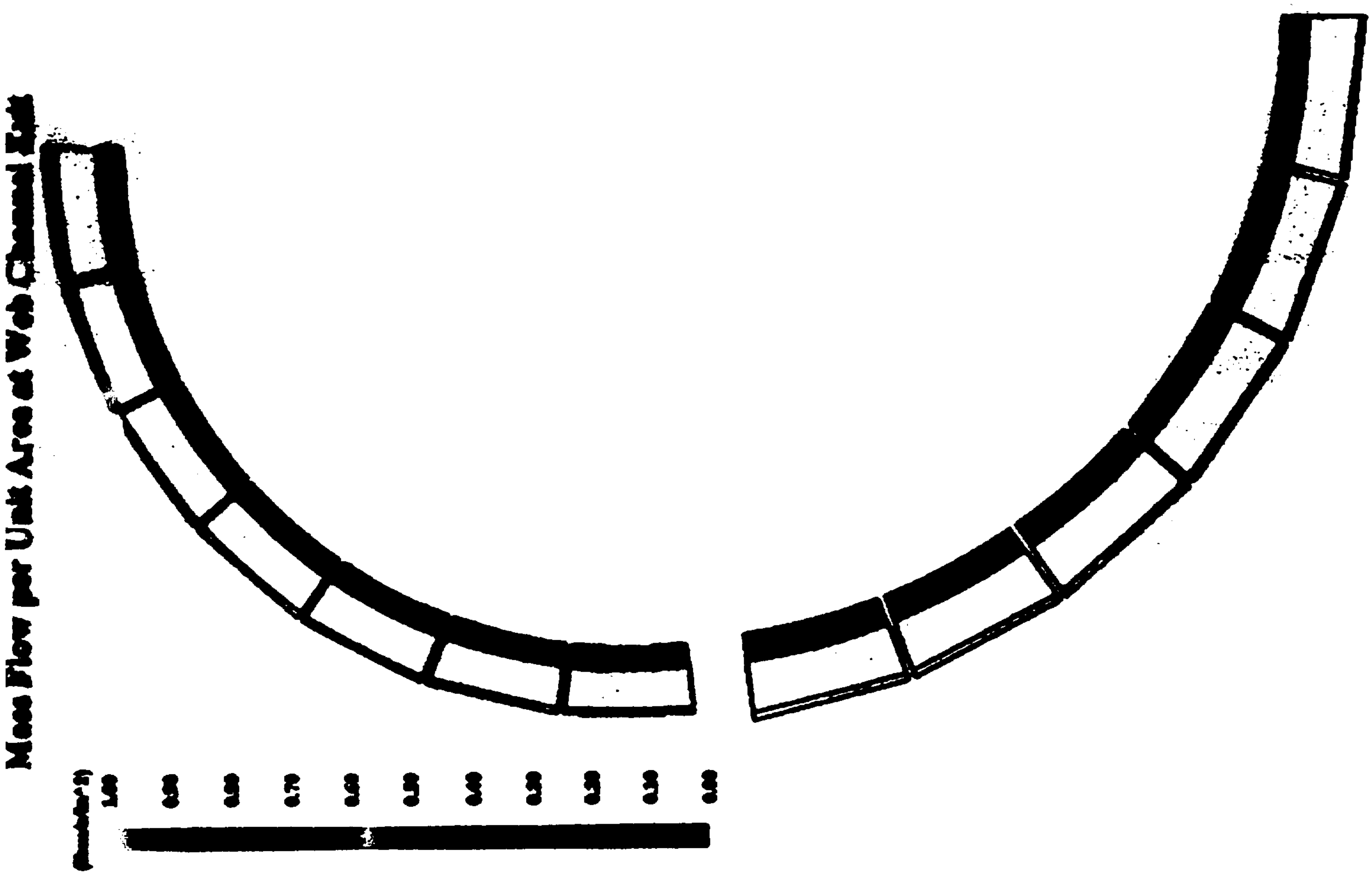
Mass Flow per Unit Area at Web Channel Exit

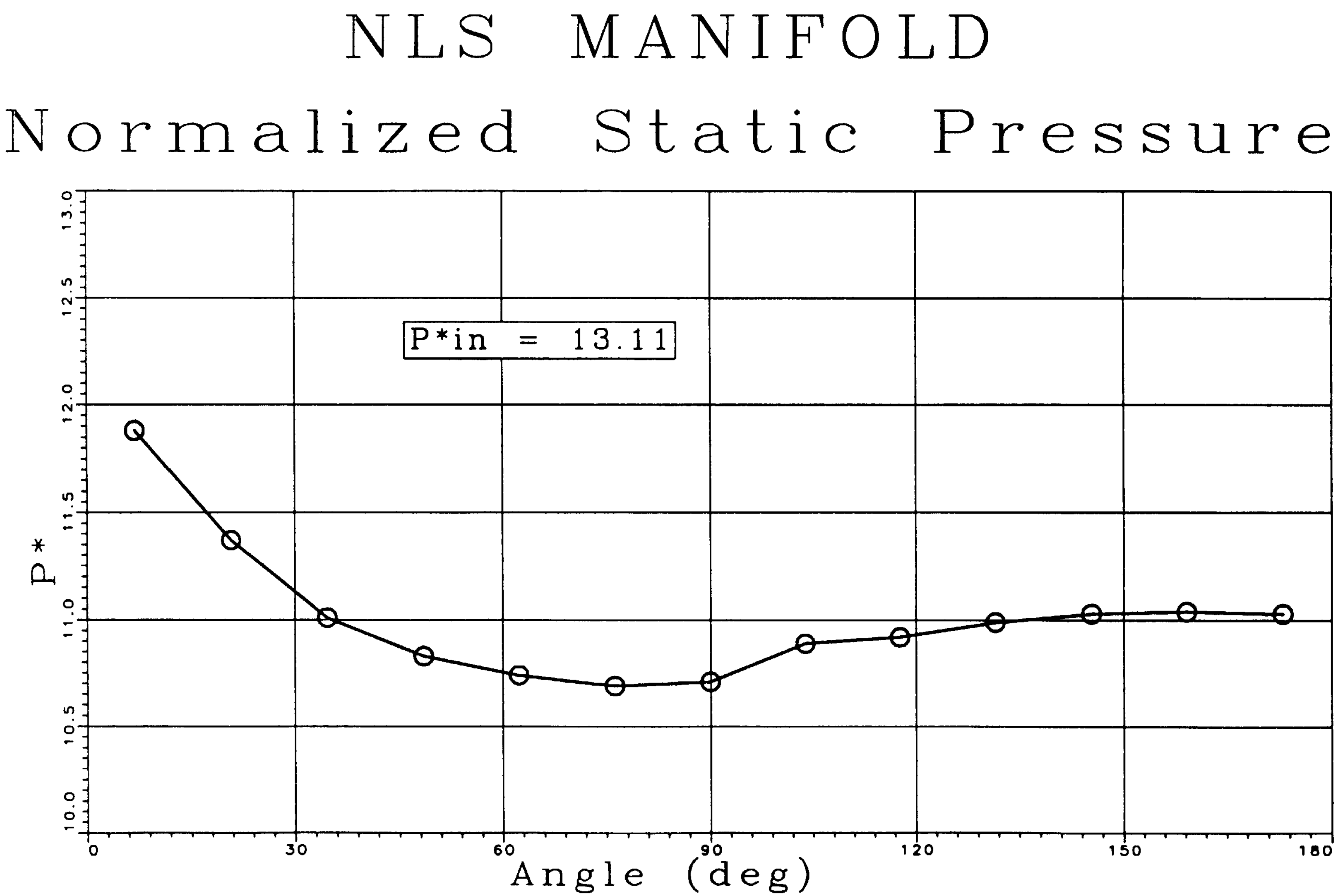

NLS MANIFOLD
Normalized Static Pressure
P*in = 13.11
P*
13.0
12.5
12.0
11.5
11.0
10.5
10.0
0
30
60
90
120
150
180
Angle (deg)

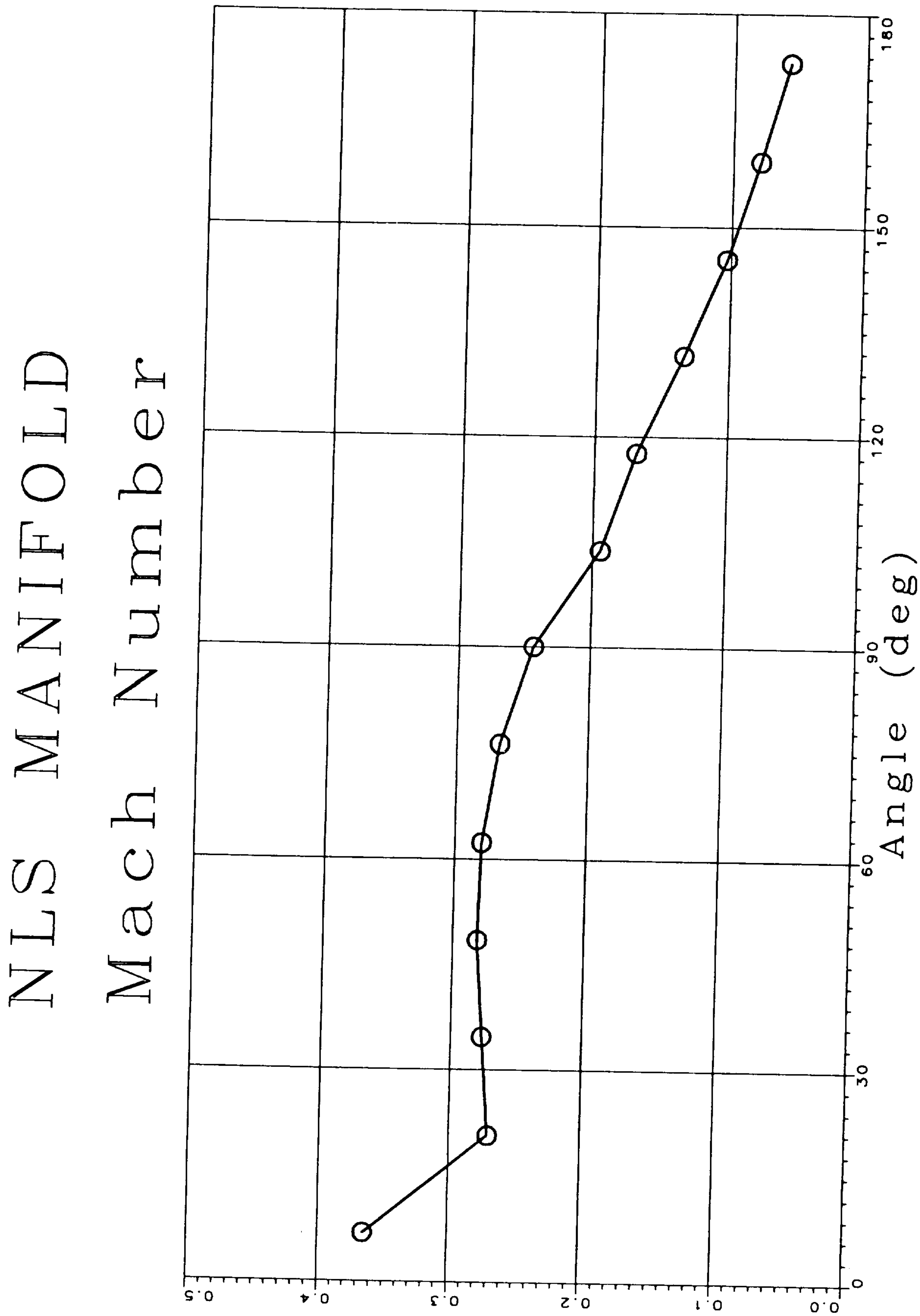
NLS MANIFOLD
Mach Number
Angle (deg)
0
30
60
90
120
150
180
0.0
0.1
0.2
0.3
0.4
0.5

NLS MANIFOLD
% Mass Flow

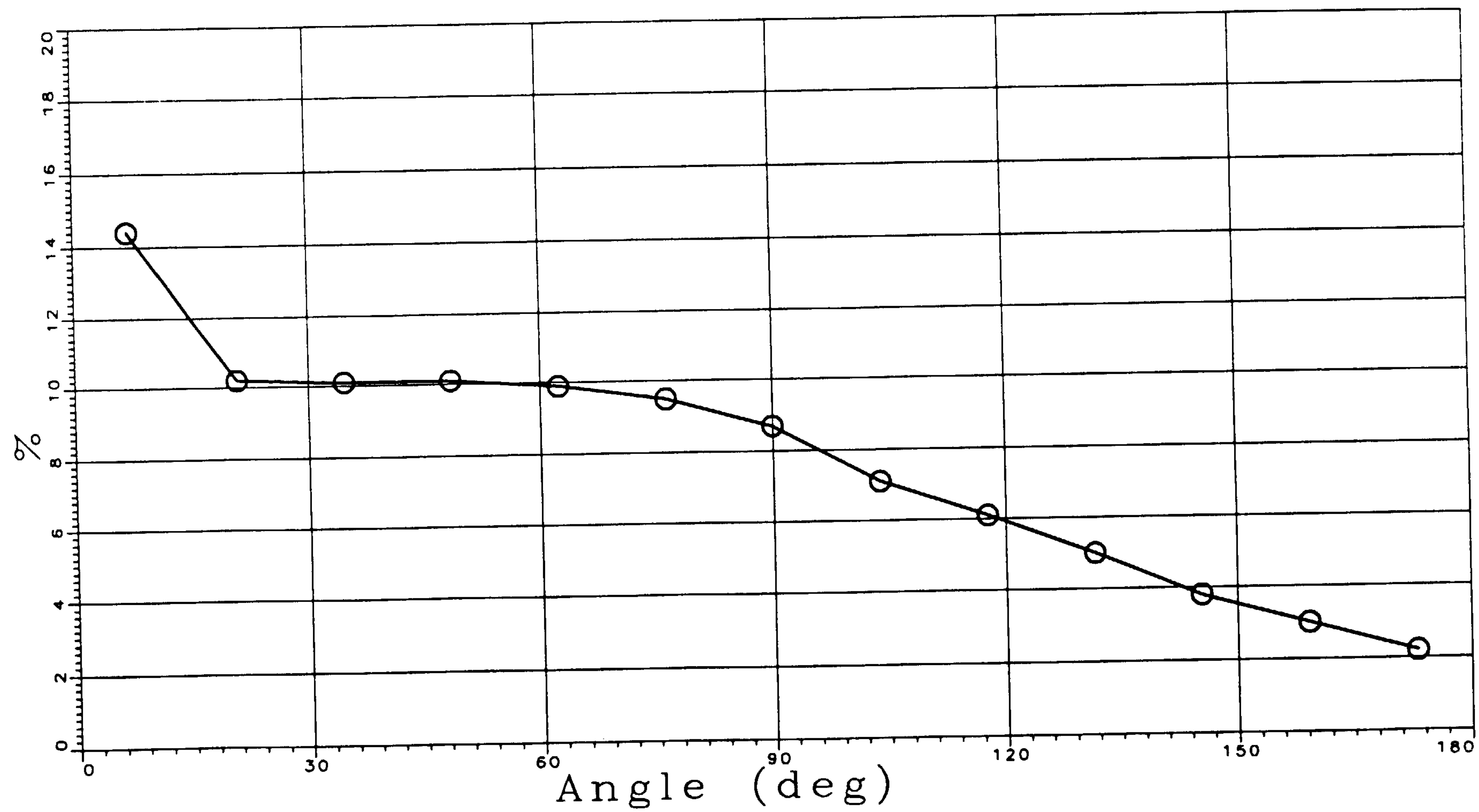

SUMMARY

- Working parameters
  - Limited time
  - Complex geometry
- Qualitative results
  - Mass averaged circumferential variations
- Timely response –
  - ~ 14 days for first analysis

ADVANCED MULTI-PHASE FLOW CFD MODEL DEVELOPMENT FOR SOLID ROCKET MOTOR FLOWFIELD ANALYSIS*

Paul Liaw, Y.S. Chen, and H. M. Shang
Engineering Sciences, Inc.
Huntsville, AL

D. Doran
ED 32, NASA Marshall Space Flight Center

p. 26

ABSTRACT

It is known that the simulations of solid rocket motor internal flow field with AL-based propellants require complex multi-phase turbulent flow model. The objective of this study is to develop an advanced particulate multi-phase flow model which includes the effects of particle dynamics, chemical reaction and hot gas flow turbulence. The inclusion of particle agglomeration, particle/gas reaction and mass transfer, particle collision, coalescence and breakup mechanisms in modeling the particle dynamics will allow the proposed model to realistically simulate the flowfield inside a solid rocket motor.

The Finite Difference Navier-Stokes numerical code FDNS is used to simulate the steady-state multi-phase particulate flow field for a 3-zone 2-D axisymmetric ASRM model and a 6-zone 3-D ASRM model at launch conditions. The 2-D model includes aft-end cavity and submerged nozzle. The 3-D model represents the whole ASRM geometry, including additional grain port area in the gas cavity and two inhibitors.

FDNS is a pressure based finite difference Navier-Stokes flow solver with time-accurate adaptive second-order upwind schemes, standard and extended k-ε models with compressibility corrections, multi-zone body-fitted formulations, and turbulence/particle interaction model. Eulerian/Lagrangian multi-phase solution method is applied for multi-zone mesh. To simulate the chemical reaction, penalty function corrected efficient finite-rate chemistry integration method is used in FDNS. For the AL particle combustion rate, the Hermsen correlation is employed. To simulate the turbulent dispersion of particles, the Gaussian probability distribution with standard deviation equal to $(2k/3)^{1/2}$ is used for the random turbulent velocity components.

The flow field in the aft-end cavity of the ASRM is analyzed to investigate its significant impact on the operation of the motor as well as its performance. It is known that heat flux and the pressure distributions in this region will cause recirculation and influence the design requirements. Chemical reaction of gas flow is a factor affecting the performance of the ASRM. An accurate analysis for chemically reacting flow is therefore important in the design of the ASRM. Twelve gas elements (H_2O, O_2, H_2, O, H, OH, CO, CO_2, CL, CL_2, HCL, and N_2) were considered for the chemical reaction in present study. For multi-phase calculations, the particulate phase was injected at the propellant grain surface. The particulate phase was assumed to be aluminum oxide (Al_2O_3) only. The mass fraction of the particulate phase was assumed to be 53% of the mixture.

The computational results reveal that the flow field near the juncture of aft-end cavity and the submerged nozzle is very complex. The effects of the turbulent particles affect the flow field significantly and provide better prediction of the ASRM performance. The multi-phase flow analysis using the FDNS code in the present research can be used as a design tool for solid rocket motor applications.

* This work is supported by NASA Marshall Space Flight Center under Contract NAS8-39398.

ADVANCED MULTI-PHASE FLOW CFD MODEL DEVELOPMENT FOR SOLID ROCKET MOTOR FLOWFIELD ANALYSIS

Paul Liaw, Y. S. Chen, and H. M. Shang
Engineering Sciences, Inc.

D. Doran
ED32, NASA Marshall Space Flight Center

11th Workshop for CFD Applications in Rocket Propulsion

April 20-22, 1993

ESI *Engineering Sciences, Inc.*

OBJECTIVE

1. BACKGROUND AND GENERAL APPROACH
2. NUMERICAL METHOD
3. ASRM APPLICATION --- CURRENT STATUS
4. CONCLUSIONS
5. FOLLOWING WORK

ESI Engineering Sciences, Inc.

BACKGROUND & GENERAL APPROACH

- SIMULATIONS OF SOLID ROCKET MOTOR INTERNAL FLOW FIELD WITH AL-BASED PROPELLANTS REQUIRE COMPLEX MULTI-PHASE TURBULENT FLOW MODEL

- CRUCIAL FACTORS SUCH AS THE PARTICLE SIZE DISTRIBUTIONS AND PARTICLE COMBUSTION INSIDE THE MOTOR ARE IMPORTANT FOR CORRECT DESCRIPTION OF THE FLOW FIELD AND GOOD PREDICTION OF THE MOTOR PERFORMANCE

ESI Engineering Sciences, Inc.

- SOME EXPERIMENTAL DATA EXIST FOR AL-AGGLOMERATES NEAR THE AP/HTPB/AL PROPELLANT WHICH CAN BE USED TO GENERATE INITIAL PARTICLE SIZES

- PARTICLE TRACKING METHODOLOGY WITH COMBUSTION MODEL IN TURBULENT HOT GAS SHALL BE EMPLOYED TO DESCRIBE THE PARTICLE BURNING AND SIZE REDISTRIBUTION HISTORY INSIDE THE MOTOR

- EXISTING MOTOR NOZZLE EXIT MEAN PARTICLE SIZE CORRELATION, D43, CAN BE USED TO ANCHOR THE MODEL PREDICTIONS

NUMERICAL METHOD

- PRESSURE BASED FINITE DIFFERENCE NAVIER-STOKES FLOW SOLVER (FDNS)
- TIME-ACCURATE ADAPTIVE SECOND-ORDER UPWIND SCHEMES
- STANDARD & EXTENDED k-ε TURBULENCE MODELS WITH COMPRESSIBILITY CORRECTIONS
- MULTI-ZONE BODY-FITTED FORMULATIONS

ESI Engineering Sciences, Inc.

- EULERIAN/LARGRANGIAN MULTI-PHASE SOLUTION METHOD FOR MULTI-ZONE MESH
- TURBULENCE/PARTICLE INTERACTION MODEL
- PENALTY FUNCTION CORRECTED EFFICIENT FINITE-RATE CHEMISTRY INTEGRATION METHOD
- HERMSEN CORRELATION EMPLOYED FOR THE AL PARTICLE COMBUSTION RATE

Turbulent Dispersion

The random turbulent velocity components were assumed to have Gaussian probability distribution with standard deviation equal to $(2k/3)^{1/2}$. Similar techniques have been used by, for example, Dukowicz and Gosman and Ioannides. The turbulent velocity components are thus computed using

$$u' = (4k/3)^{1/2} \, \mathrm{erf}^{-1}(2x-1)$$

where x is a random variable with uniform probability distribution between 0 and 1. The generated turbulent velocity components are added to the mean velocity field of the continuous phase in evaluating the interphase drag force.

ASRM APPLICATION -- CURRENT STATUS

- MODELS:

  1. 3-ZONE 2-D GEOMETRY (INCLUDING CHAMBER, AFT-END CAVITY, AND SUBMERGED NOZZLE)

  2. 6-ZONE 3-D GEOMETRY (INCLUDING CHAMBER, AFT-END CAVITY, SUBMERGED NOZZLE, INHIBITORS, AND GRAIN PORT)

- SIMULATION OF STEADY-STATE FLOW FIELD AT LAUNCH CONDITION

ESI Engineering Sciences, Inc.

THE ASRM

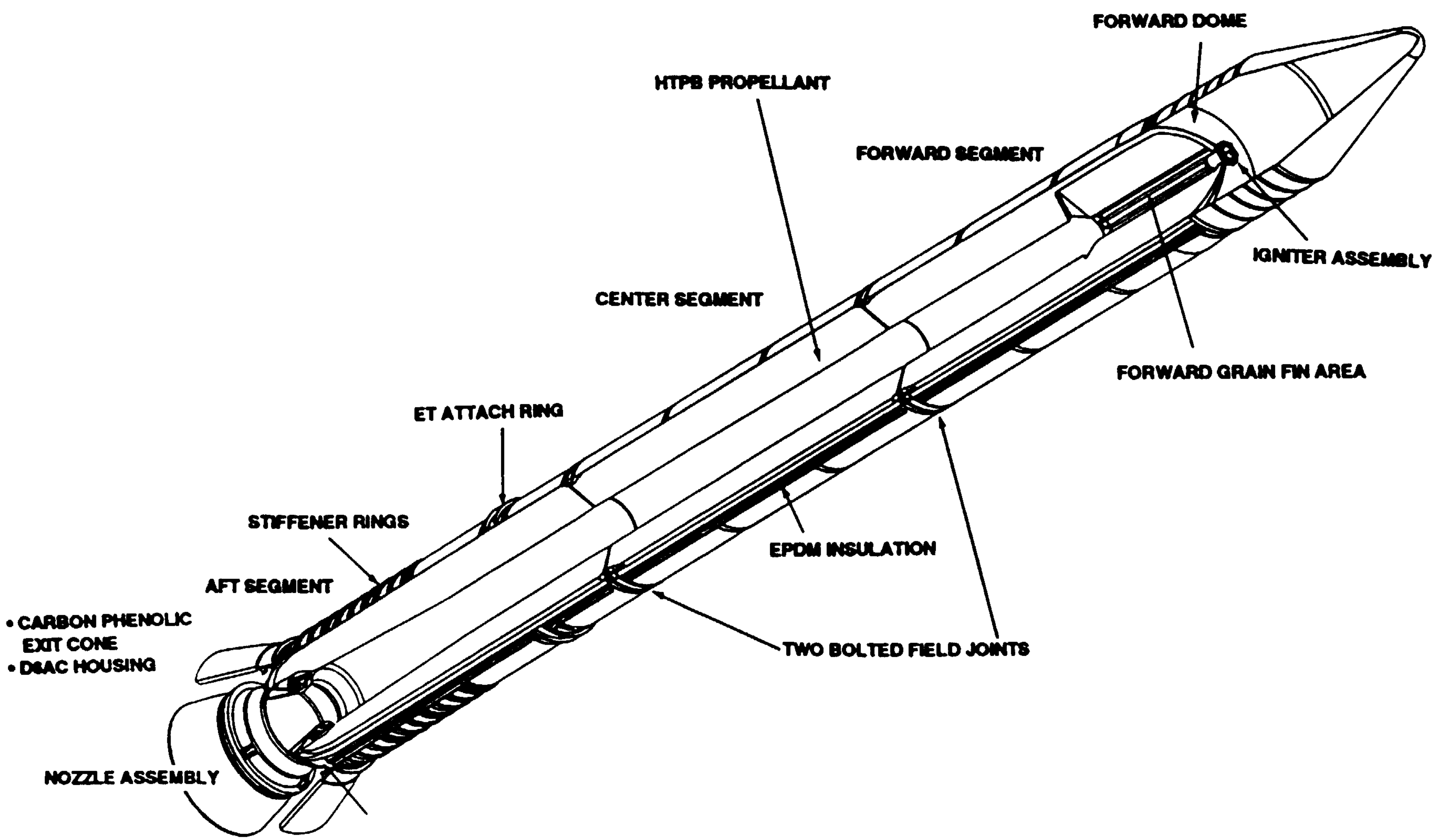

ESI Engineering Sciences, Inc.

ORIGINAL PAGE IS
OF POOR QUALITY

2-D GRID SYSTEM

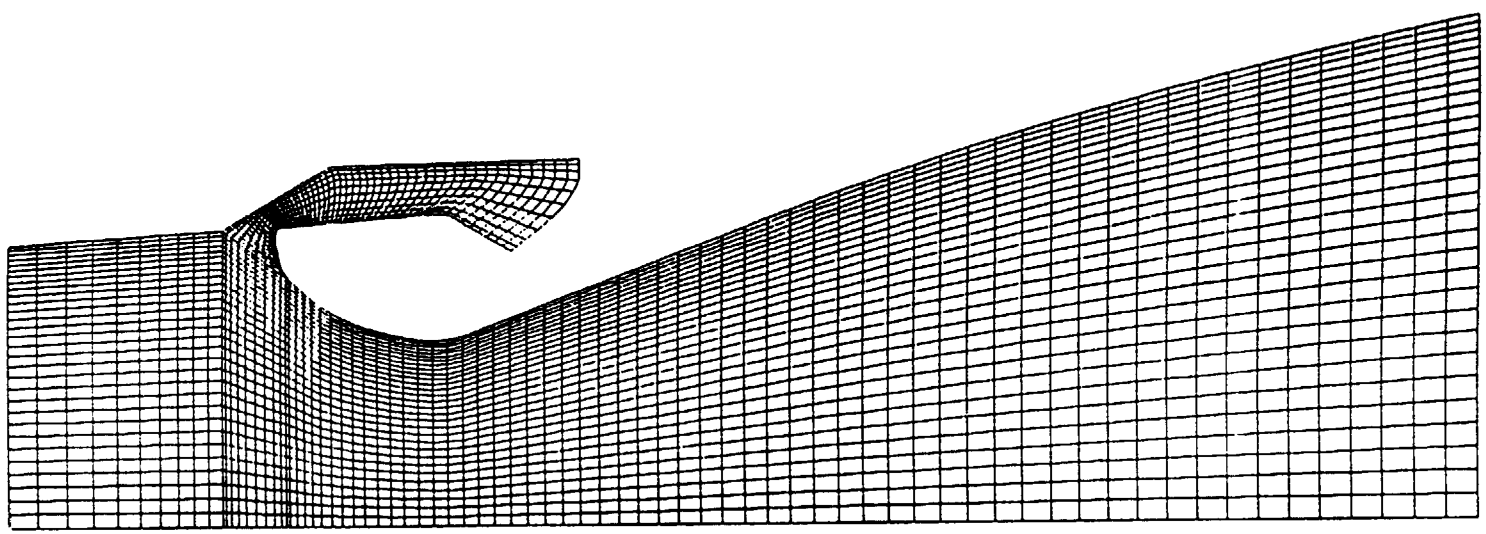

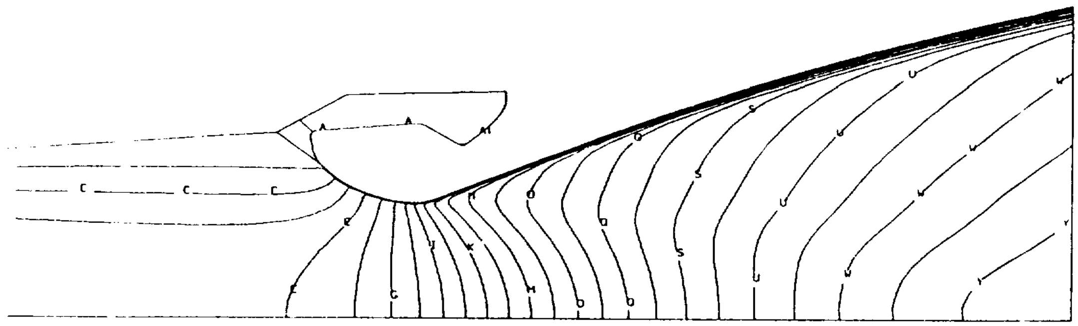

MACH NUMBER DISTRIBUTIONS NEAR THE NOZZLE (WITHOUT PARTICLE EFFECT)

CONTOUR LEVELS

ID	VALUES
A	0 0000E+00
B	1 4028E-01
C	2 8057E-01
D	4 2086E-01
E	5 6114E-01
F	7 0143E-01
G	8 4172E-01
H	9 8200E-01
I	1 1222E+00
J	1 2625E+00
K	1 4028E+00
L	1 5431E+00
M	1 6834E+00
N	1 8237E+00
O	1 9640E+00
P	2 1043E+00
Q	2 2445E+00
R	2 3848E+00
S	2 5251E+00
T	2 6654E+00
U	2 8057E+00
V	2 9460E+00
W	3 0863E+00
X	3 2265E+00
Y	3 3668E+00
Z	3 5071E+00

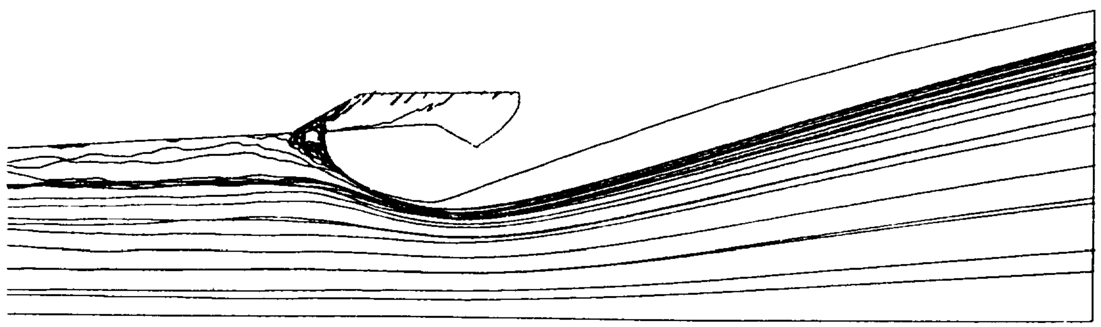

PARTICLE DISTRIBUTIONS NEAR THE NOZZLE

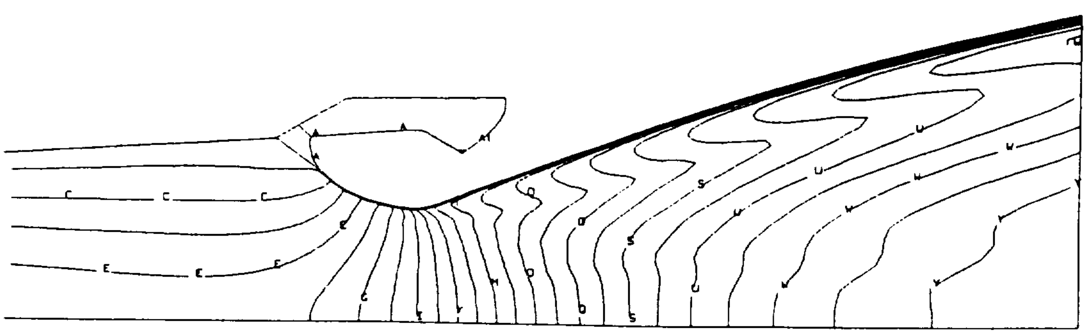

MACH NUMBER DISTRIBUTIONS (WITH PARTICLE EFFECT)

CONTOUR LEVELS

ID	VALUES
A	0 0000E+00
B	1 1885E-01
C	2 3770E-01
D	3 5655E-01
E	4 7540E-01
F	5 9425E-01
G	7 1310E-01
H	8 3195E-01
I	9 5080E-01
J	1 0696E+00
K	1 1885E+00
L	1 3073E+00
M	1 4262E+00
N	1 5450E+00
O	1 6639E+00
P	1 7827E+00
Q	1 9016E+00
R	2 0204E+00
S	2 1393E+00
T	2 2581E+00
U	2 3770E+00
V	2 4956E+00
W	2 6147E+00
X	2 7335E+00
Y	2 8524E+00
Z	2 9712E+00

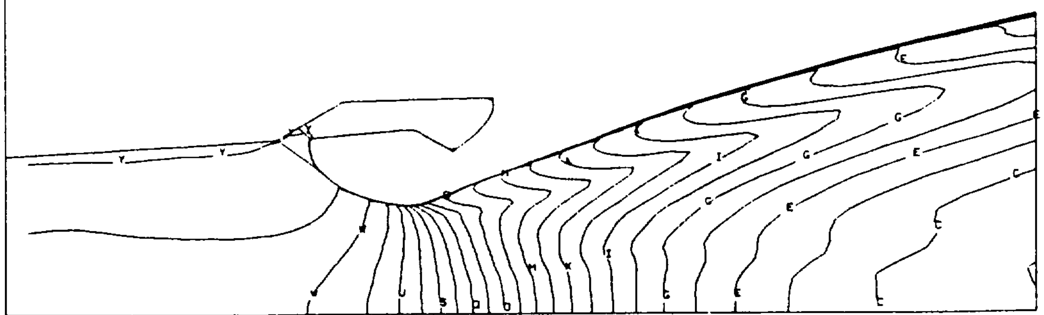

TEMPERATURE DISTRIBUTIONS (WITH PARTICLE EFFECT)

CONTOUR LEVELS

ID	VALUES
A	1 4698E+03
B	1 5513E+03
C	1 6329E+03
D	1 7144E+03
E	1 7959E+03
F	1 8774E+03
G	1 9590E+03
H	2 0405E+03
I	2 1220E+03
J	2 2035E+03
K	2 2851E+03
L	2 3666E+03
M	2 4481E+03
N	2 5296E+03
O	2 6112E+03
P	2 6927E+03
Q	2 7742E+03
R	2 8557E+03
S	2 9373E+03
T	3 0188E+03
U	3 1003E+03
V	3 1818E+03
W	3 2634E+03
X	3 3449E+03
Y	3 4264E+03
Z	3 5079E+03

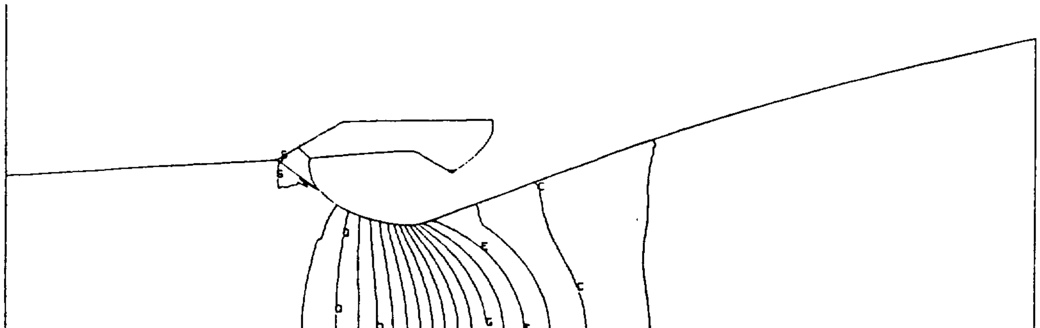

PRESSURE DISTRIBUTIONS (WITH PARTICLE EFFECT)

CONTOUR LEVELS

ID	VALUES
A	1 4183E+00
B	6 2819E+00
C	1 1145E+01
D	1 6009E+01
E	2 0872E+01
F	2 5736E+01
G	3 0599E+01
H	3 5463E+01
I	4 0326E+01
J	4 5190E+01
K	5 0053E+01
L	5 4917E+01
M	5 9781E+01
N	6 4644E+01
O	6 9508E+01
P	7 4371E+01
Q	7 9235E+01
R	8 4098E+01
S	8 9962E+01
T	9 3826E+01
U	9 8689E+01
V	1 0355E+02
W	1 0841E+02
X	1 1328E+02
Y	1 1814E+02
Z	1 2300E+02

ORIGINAL PAGE IS
OF POOR QUALITY

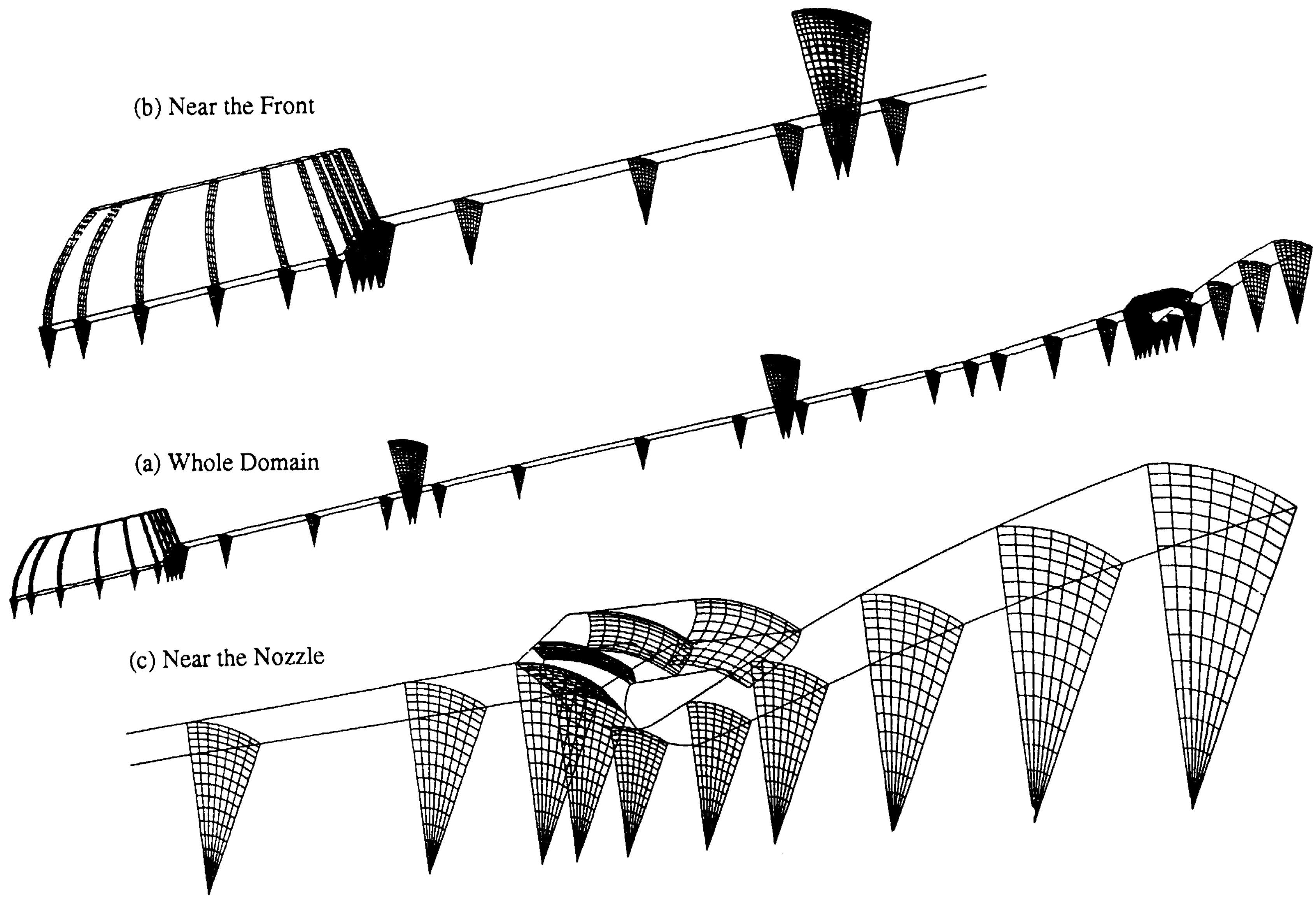

3-D GRID SYSTEM

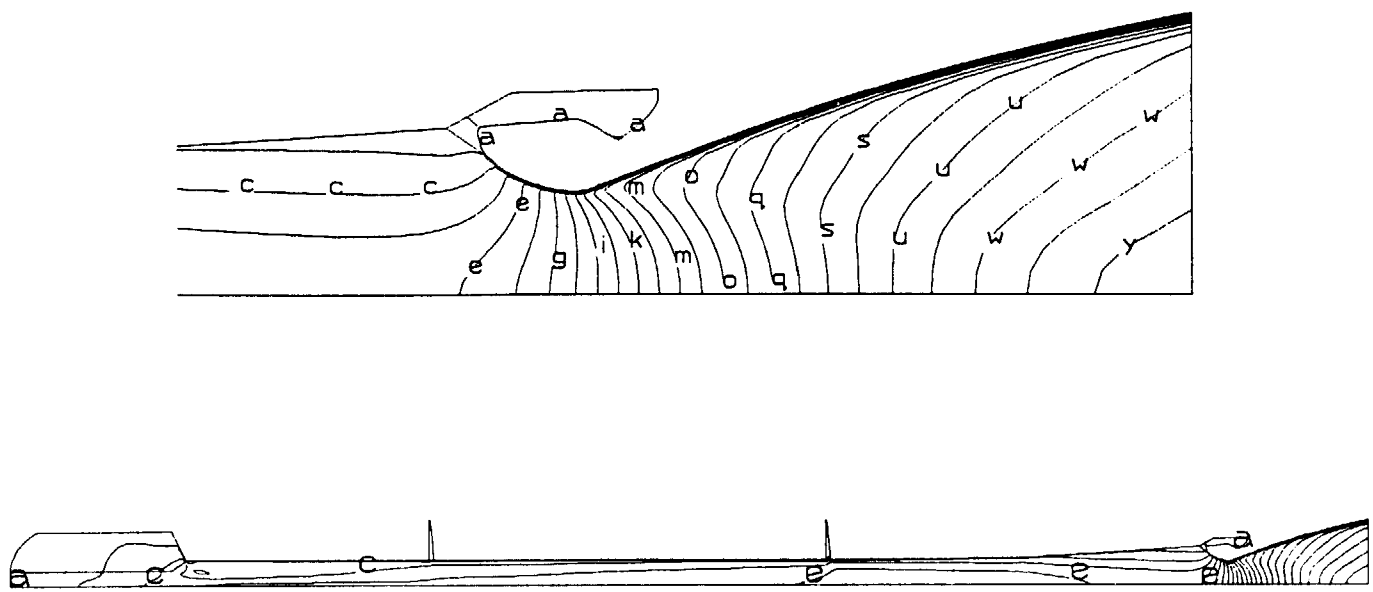

MACH NUMBER DISTRIBUTIONS (WITHOUT PARTICLES)

ESI Engineering Sciences, Inc.

PARTICLE DISTRIBUTIONS

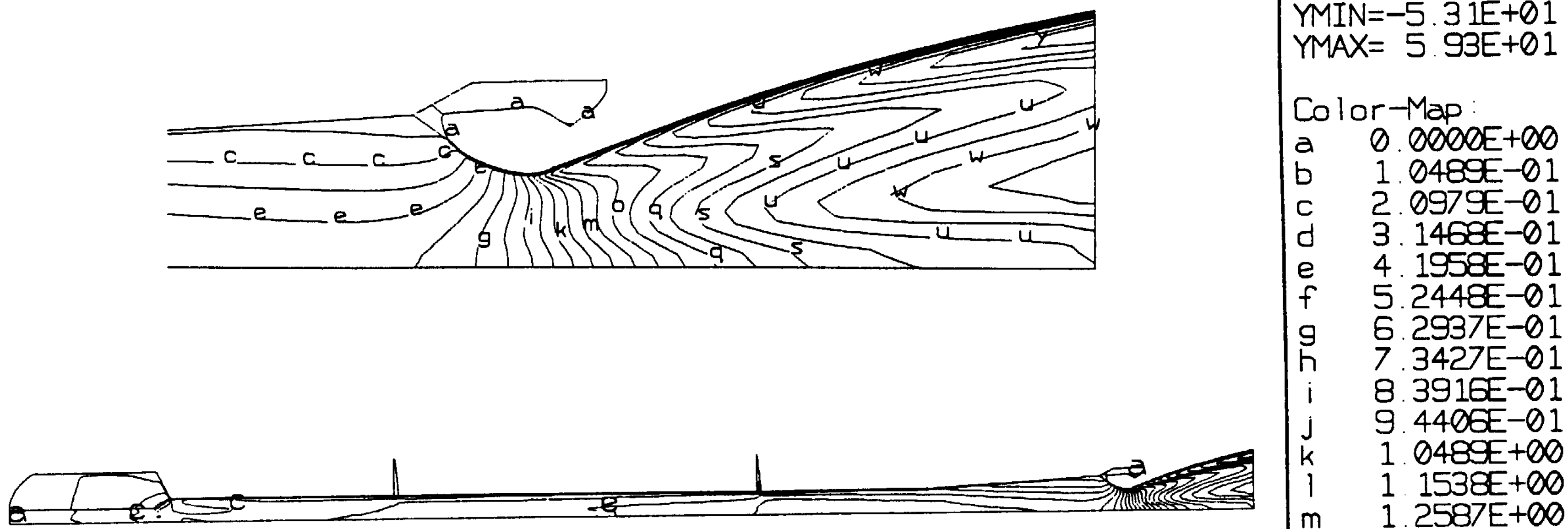

MACH NUMBER DISTRIBUTIONS (WITH PARTICLES)

ESI Engineering Sciences, Inc.

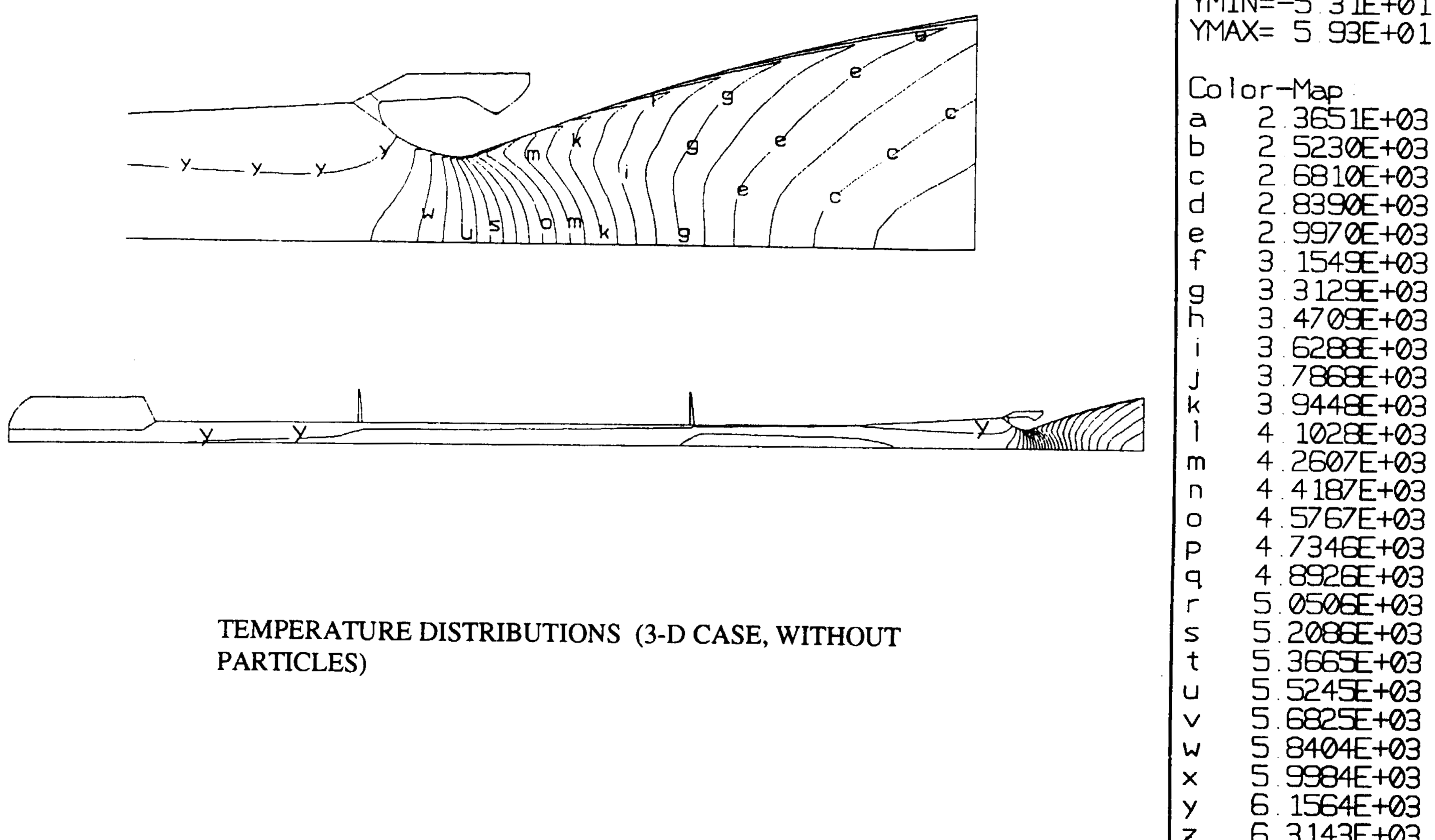

TEMPERATURE DISTRIBUTIONS (3-D CASE, WITHOUT PARTICLES)

ESI Engineering Sciences, Inc.

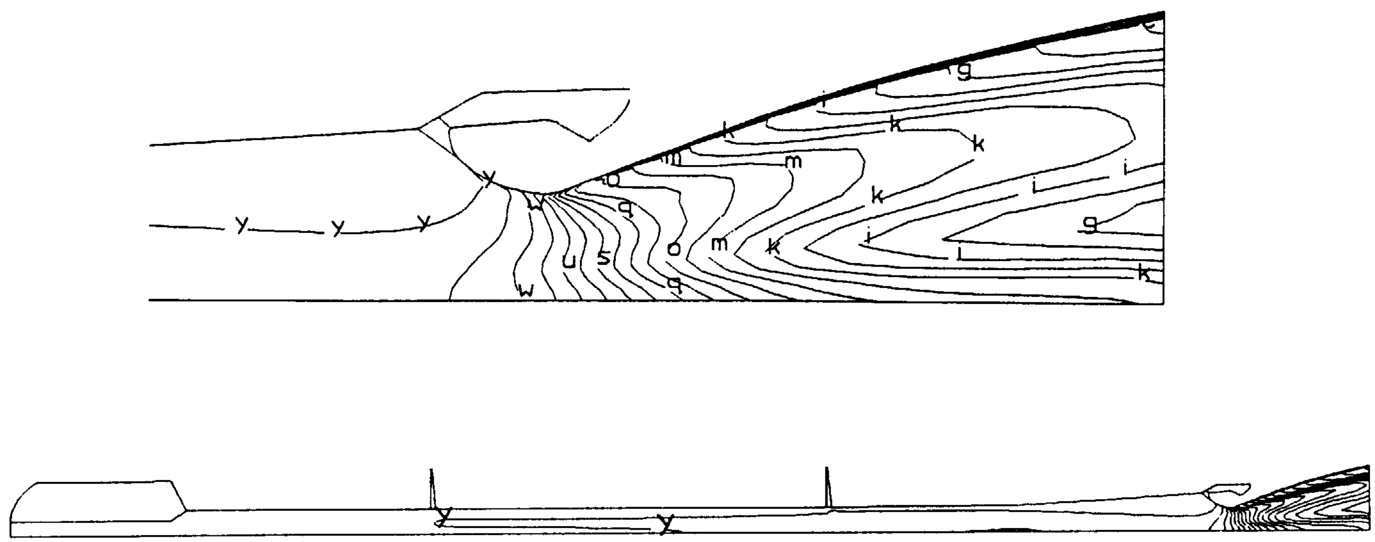

TEMPERATURE DISTRIBUTIONS (3-D CASE, WITH PARTICLES)

ESI Engineering Sciences, Inc.

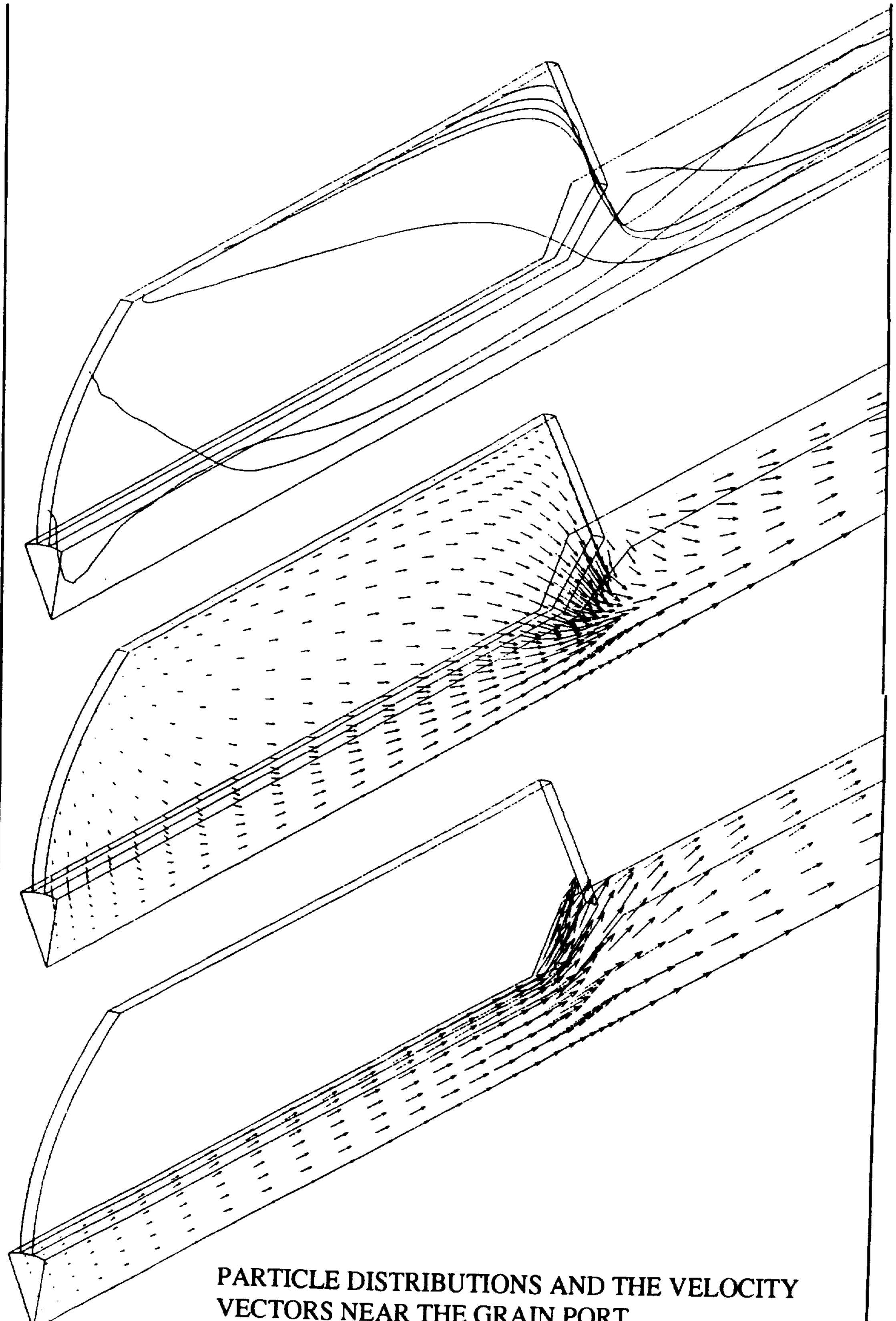

PARTICLE DISTRIBUTIONS AND THE VELOCITY VECTORS NEAR THE GRAIN PORT

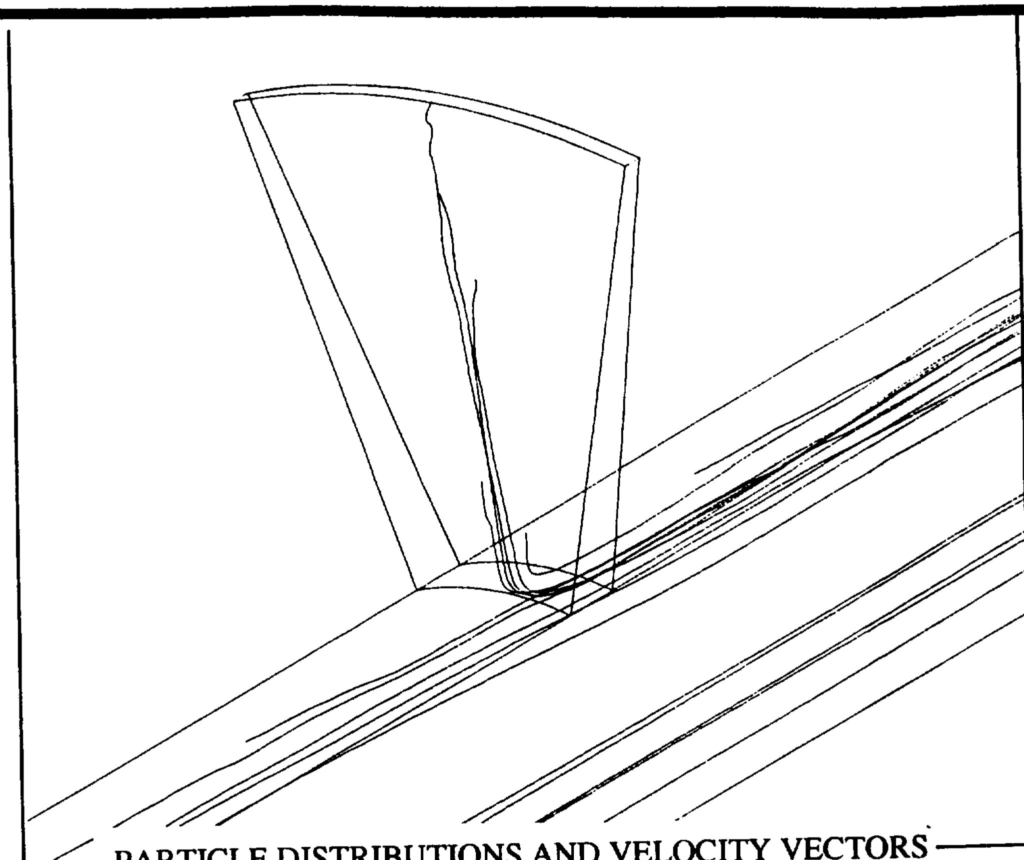

PARTICLE DISTRIBUTIONS AND VELOCITY VECTORS
NEAR THE FIRST INHIBITOR

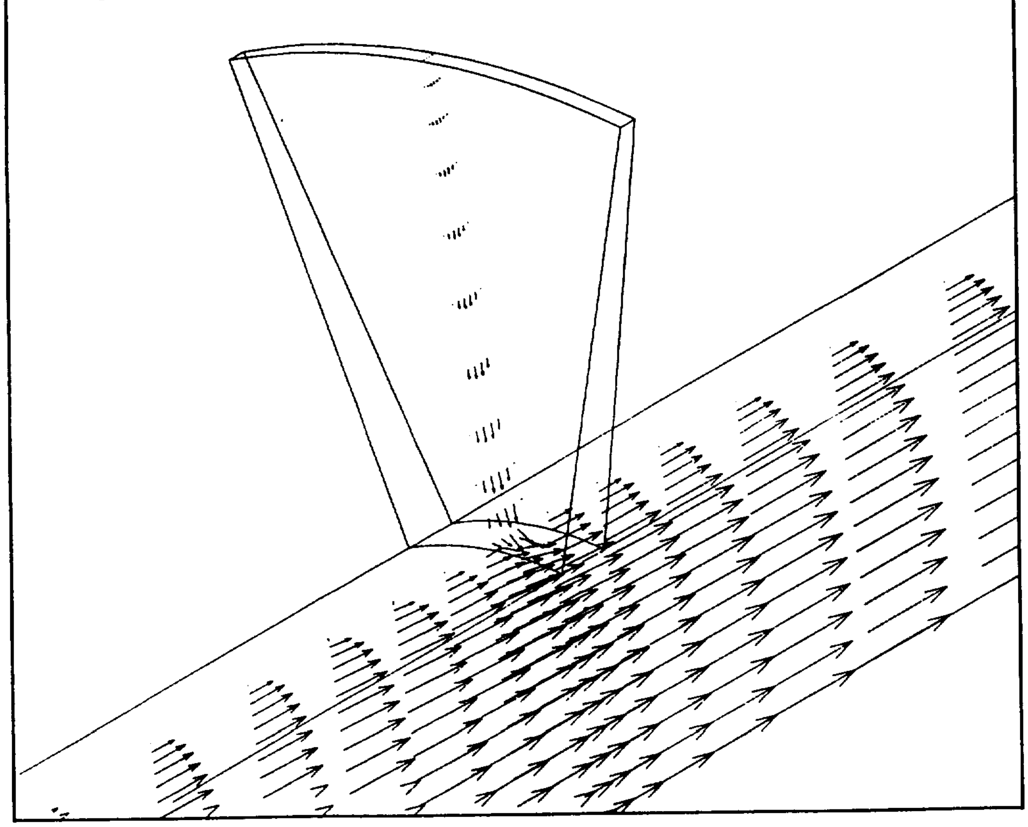

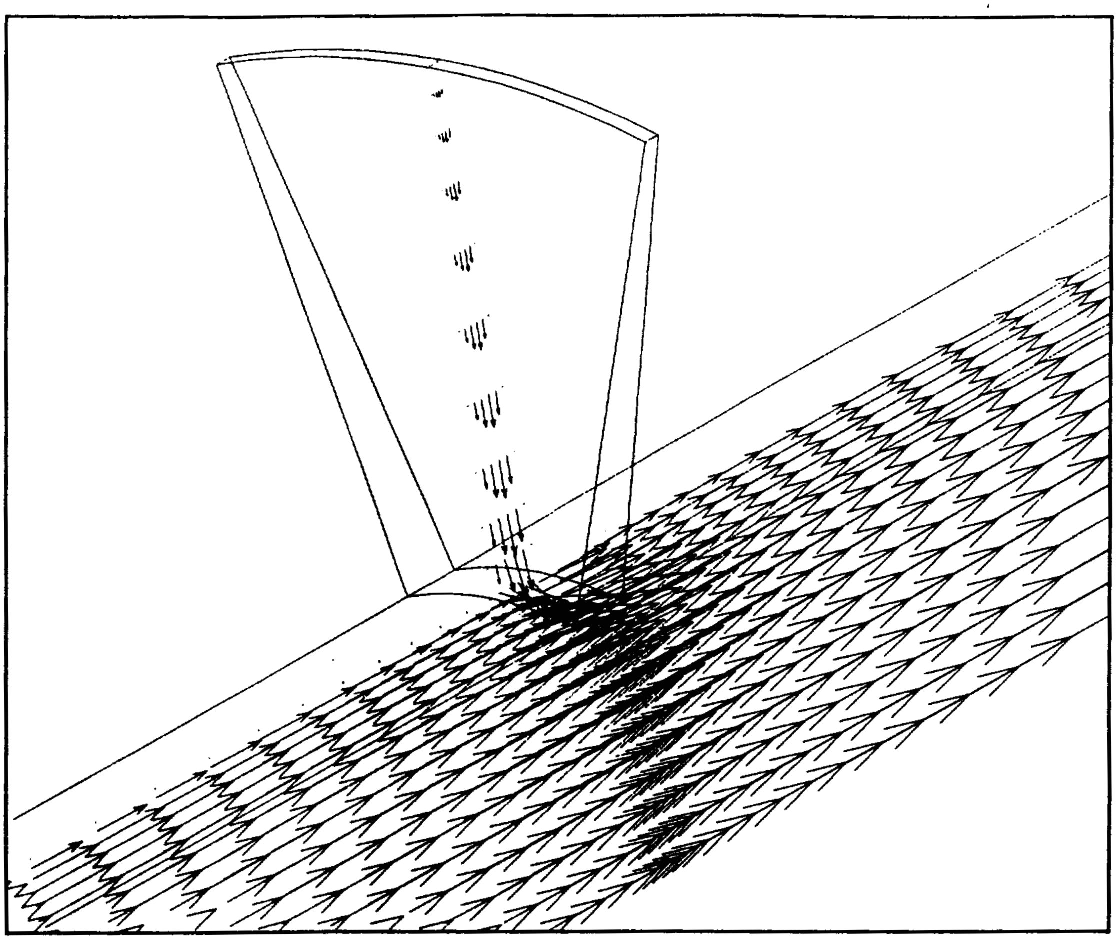

VELOCITY VECTORS NEAR THE SECOND INHIBITOR

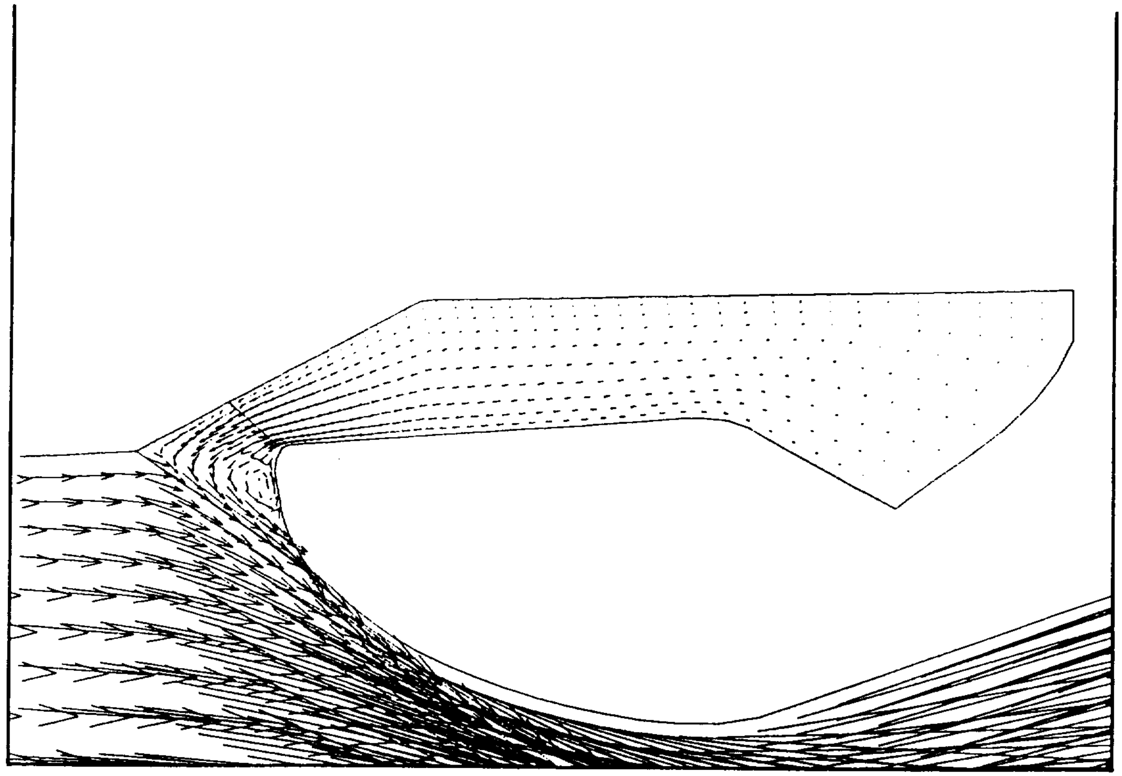

VELOCITY VECTORS FOR 2-D CASE (WITH PARTICLES)

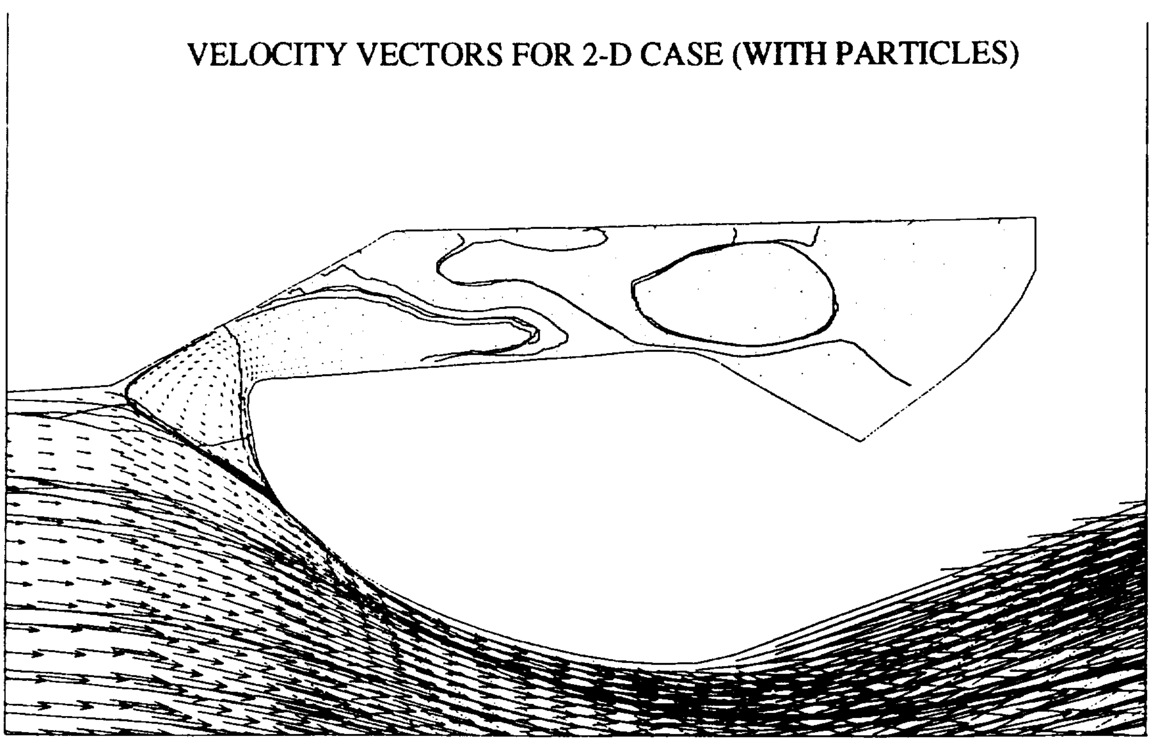

PARTICLE DISTRIBUTIONS AND VELOCITY VECTORS
FOR 3-D CASE (WITH PARTICLES)

PARTICLE TRAJECTORIES NEAR THE NOZZLE, 3-D CASE.

CONCLUSIONS

1. THE FDNS CODE SUCCESSFULLY PREDICTED THE MULTI-PHASE FLOW SIMULATION OF THE ASRM WITH CHEMICAL REACTION AND TURBULENT PARTICLES. THE COMPUTED FLOW FIELD IS REASONABLE BASED ON THE KNOWN DATA AND THE PHYSICAL POINT OF VIEW.

2. THE RECIRCULATION ZONE AT THE ENTRY OF THE AFT-END CAVITY IS PREDICTED CORRECTLY. MORE INVESTIGATIONS SHOULD BE DONE FOR FURTHER EVALUATION OF THE EFFECT ON THE PERFORMANCE OF ASRM DUE TO THE RECIRCULATION ZONE.

FOLLOWING WORK

- GENERATE AL AGGLOMERATE SIZE INITIAL CONDITIONS TREATMENT
- INVESTIGATE THE PARTICLE COMBUSTION AND COLLISION/BREAKUP MODELS FOR BENCHMARK TESTING CASES (NAVAL POST-GRADUATE DATA, FRENCH DATA, ETC.)
- INVESTIGATE THE EFFECT OF PARTICLE DEPOSITION ON THE CHAMBER WALL (MOVING BOUNDARY SCHEME WILL BE TESTED)

ESI Engineering Sciences, Inc.

N95- 23639

ASRM Multi-Port Igniter Flow Field Analysis

Lee Kania and Catherine Dumas
Sverdrup Technology, Inc.
620 Discovery Drive
Huntsville, AL 35806

Denise Doran
Computational Fluid Dynamics Branch
NASA - Marshall Space Flight Center
Marshall Space Flight Center, AL 35806

p. 19

Abstract

The Advanced Solid Rocket Motor (ASRM) program was initiated by NASA in response to the need for a new generation rocket motor capable of providing increased thrust levels over the existing Redesigned Solid Rocket Motor (RSRM) and thus augment the lifting capacity of the space shuttle orbiter. To achieve these higher thrust levels and improve motor reliability, advanced motor design concepts were employed. In the head end of the motor, for instance, the propellent cast has been changed from the conventional annular configuration to a "multi-slot" configuration in order to increase the burn surface area and guarantee rapid motor ignition. In addition, the igniter itself has been redesigned and currently features 12 exhaust ports in order to channel hot igniter combustion gases into the circumferential propellent slots. Due to the close proximity of the igniter ports to the propellent surfaces, new concerns over possible propellent deformation and erosive burning have arisen. The following documents the effort undertaken using computational fluid dynamics to perform a flow field analysis in the top end of the ASRM motor to determine flow field properties necessary to permit a subsequent propellent fin deformation analysis due to pressure loading and an assessment of the extent of erosive burning.

ASRM Multi-Port Igniter Flow Field Analysis

Lee Kania and Catherine Dumas
Sverdrup Technology

and

Denise Doran
NASA Marshall Space Flight Center

Sverdrup

ASRM Head End

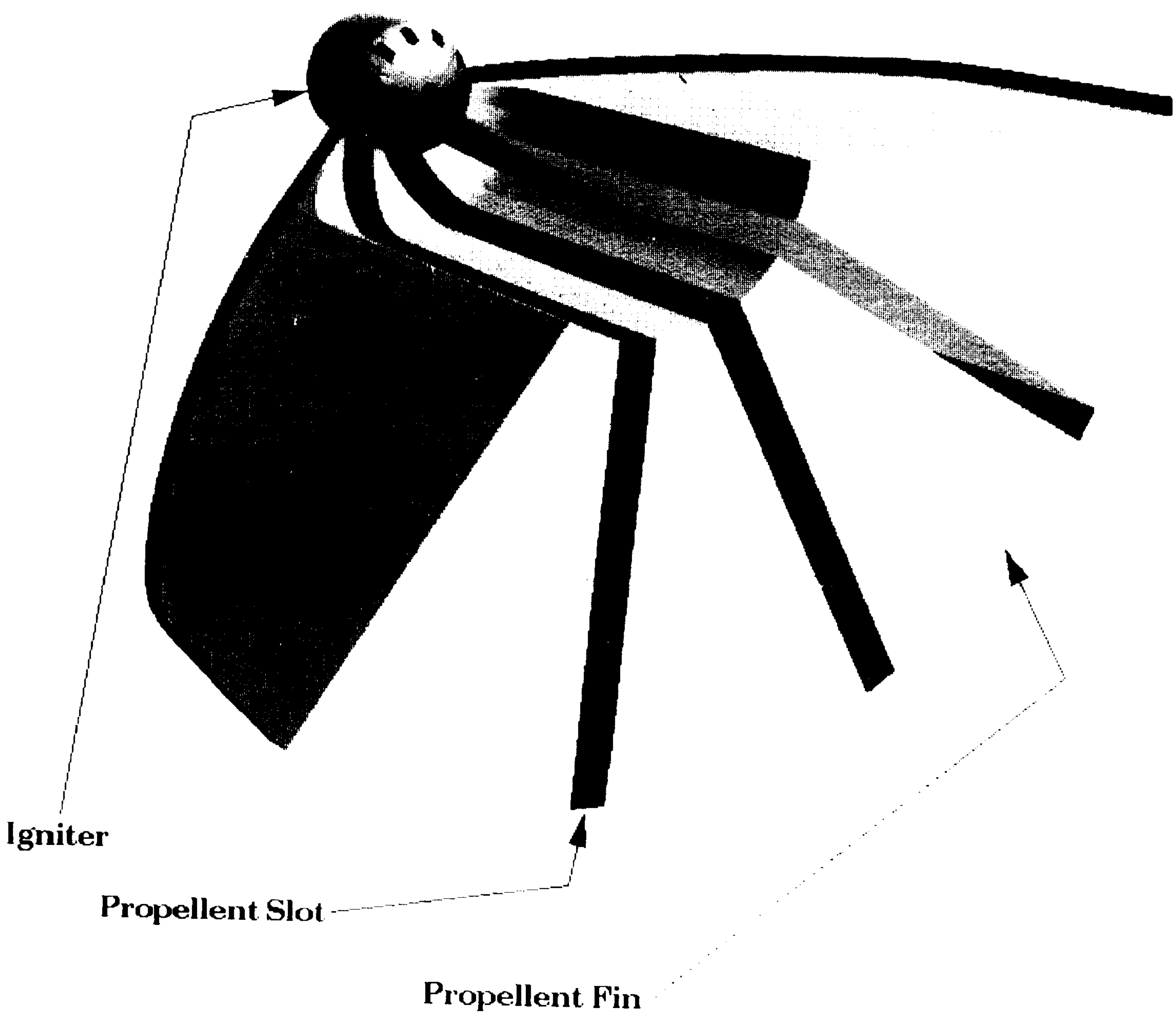

- Objective
  - Characterize ASRM Head End Flow Field
- Purpose
  - Estimate propellent surface pressures for deformation analysis
  - Quantify nature of impingement to assess erosive burning
- Approach
  - Three-dimensional CFD analysis
    * Utilize REFLEQS3D and FDNS
    * Physical discretization to include region from mid-slot to mid-fin
    * grid contains 169K points

Sverdrup

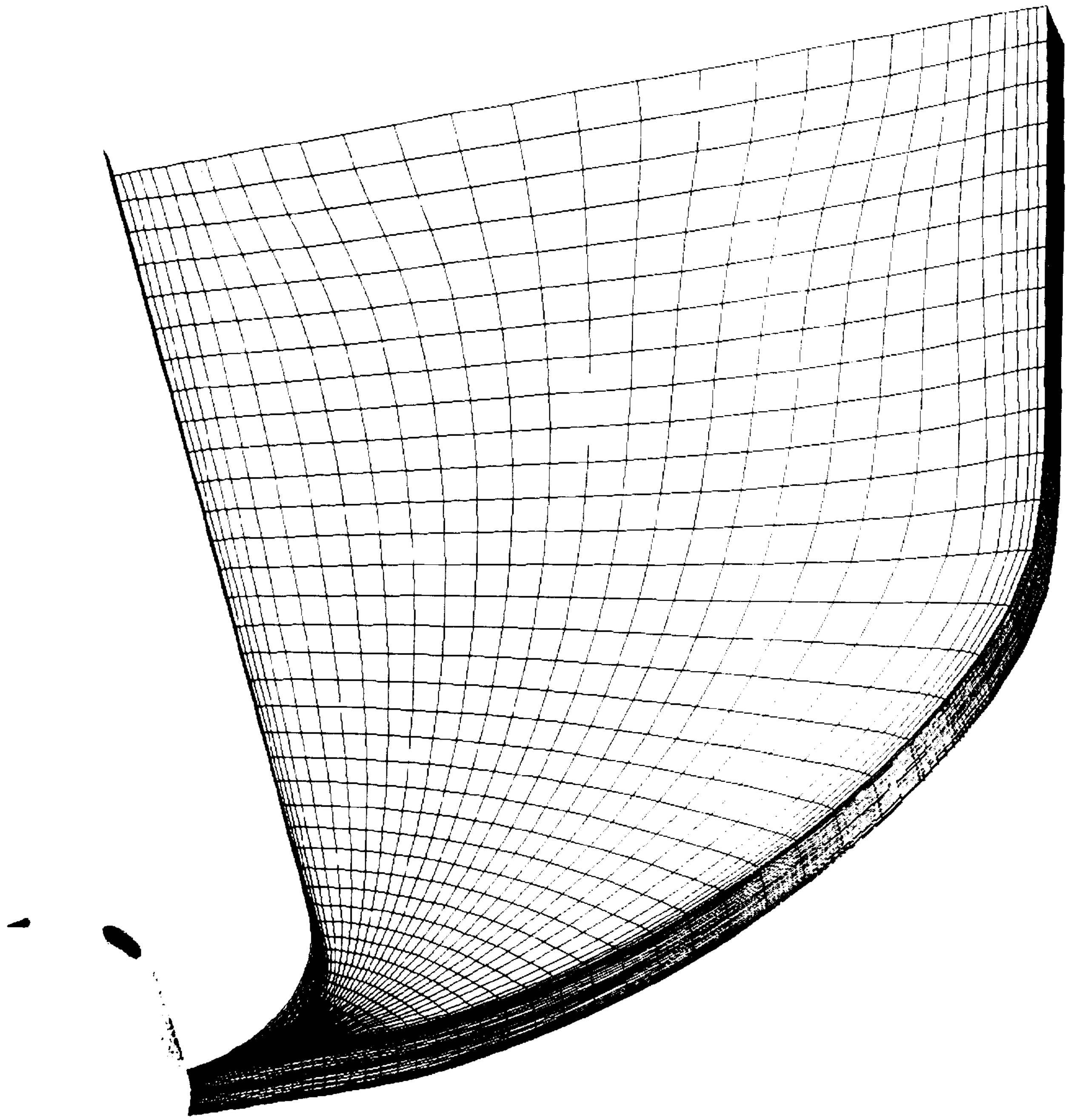

b.2.img

- Physical Models
  - Assume steady flow of a perfect gas
    - $\gamma = 1.166, \; R_{gas} = 1717.03$
  - $K - \epsilon$ turbulence model with wall functions

Sverdrup

- Igniter Port Flow Conditions
  - $P = 145{,}000$ psf
  - $T = 5861$ R
  - $M = 1.0$

Pressure Contours - Fin Surface (psf)

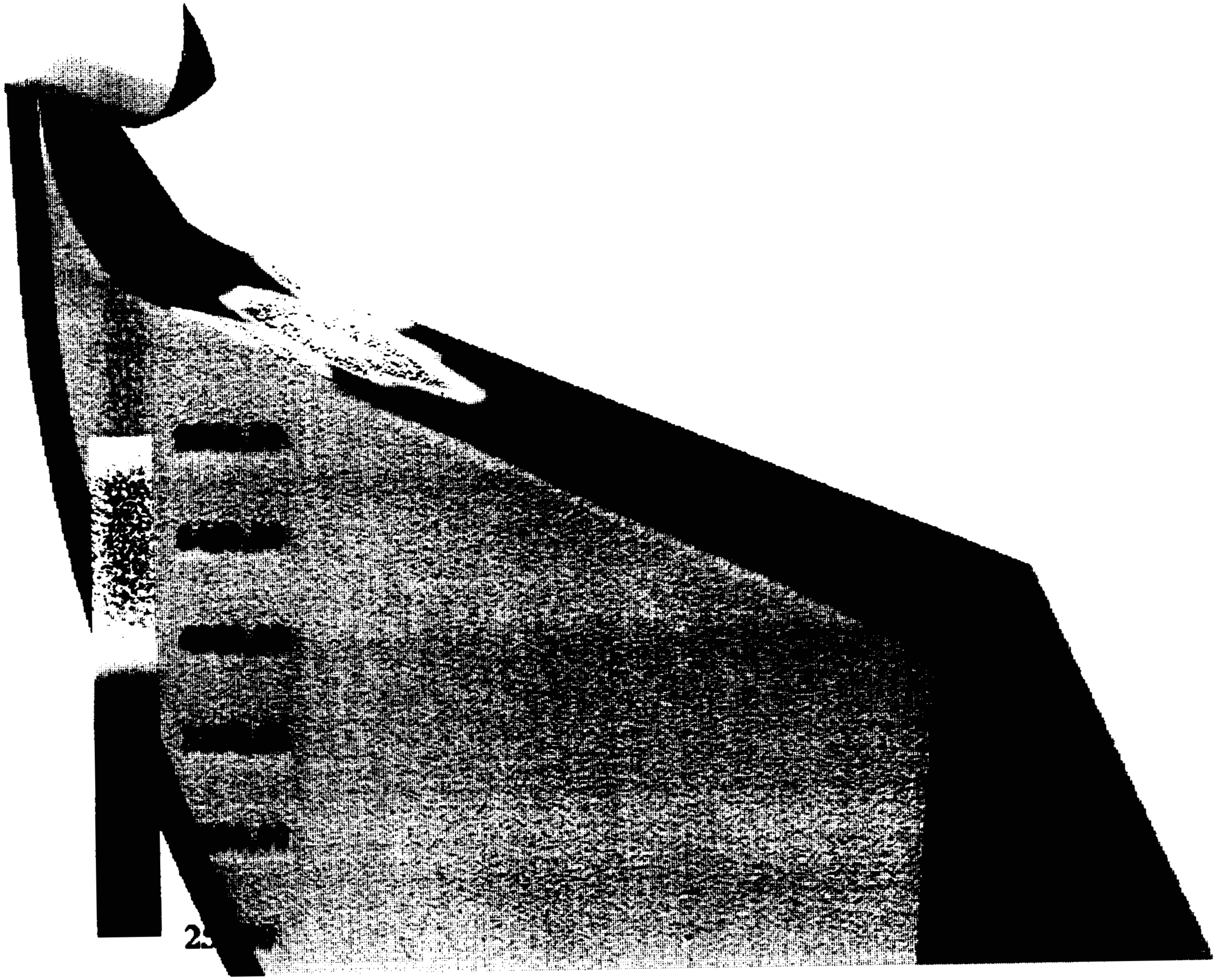

ORIGINAL PAGE IS
OF POOR QUALITY

Streamwise Mass Flux Contours

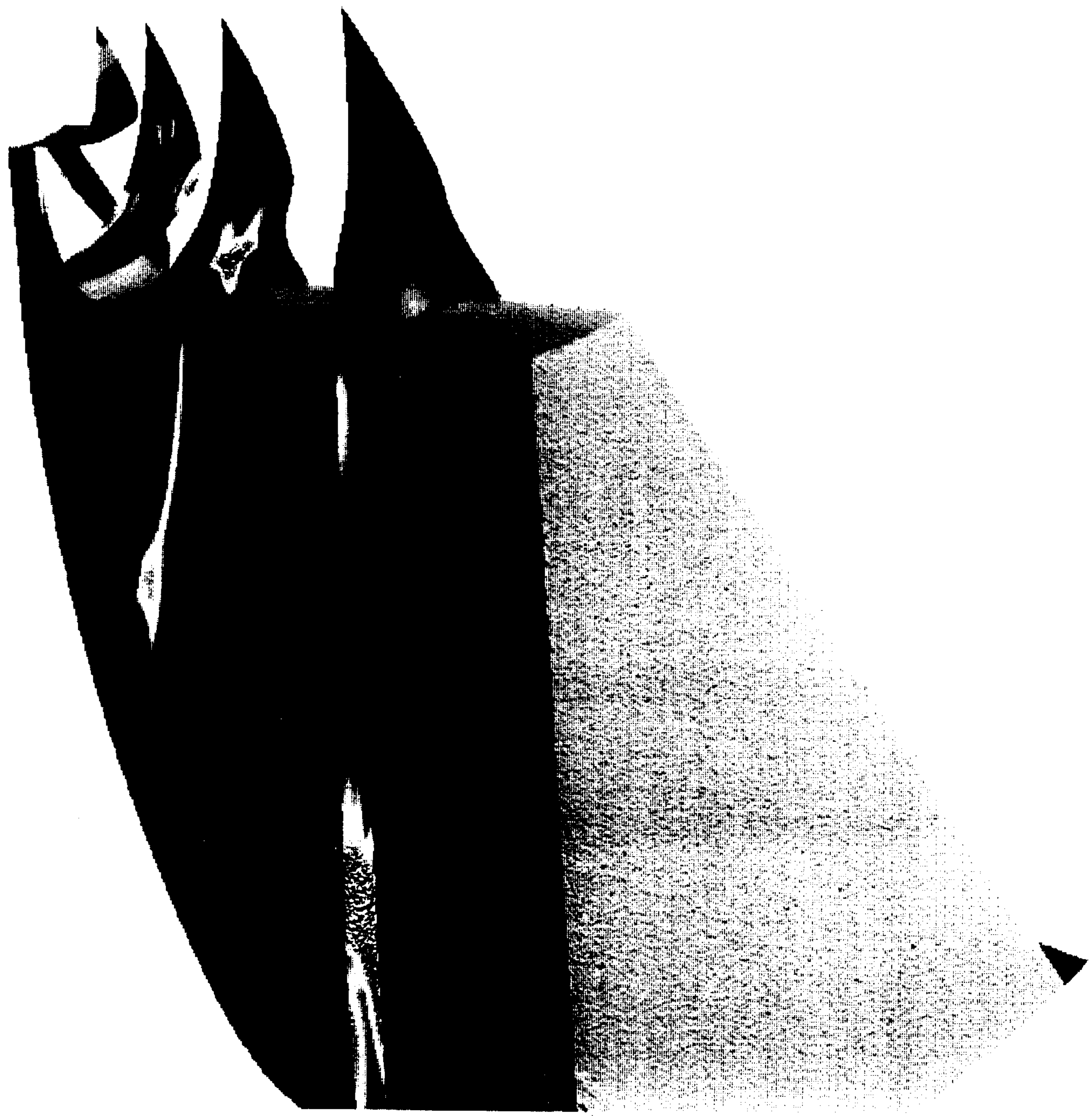

Transverse Mass Flux Contours

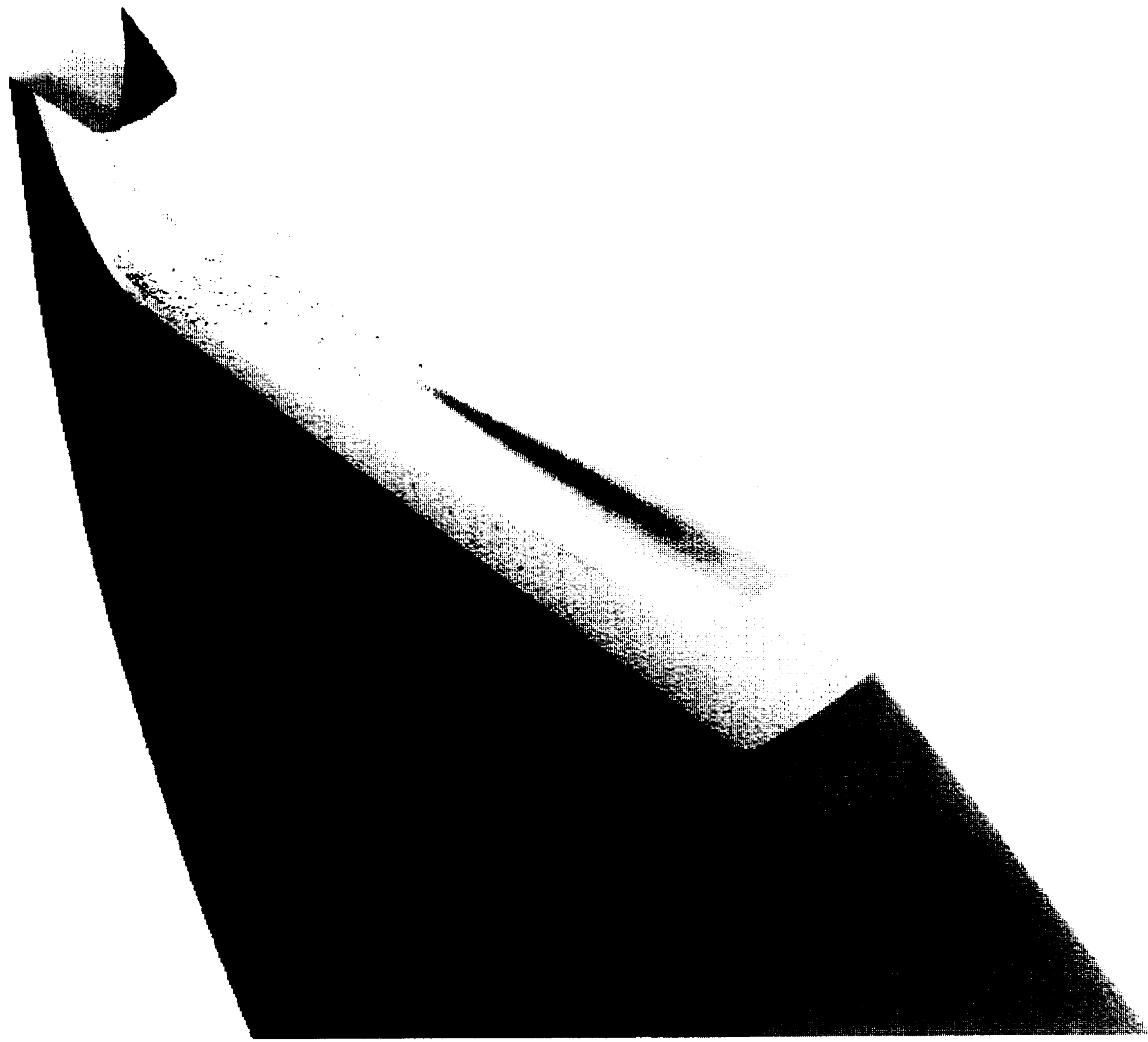

Transverse Mass Flux Contours

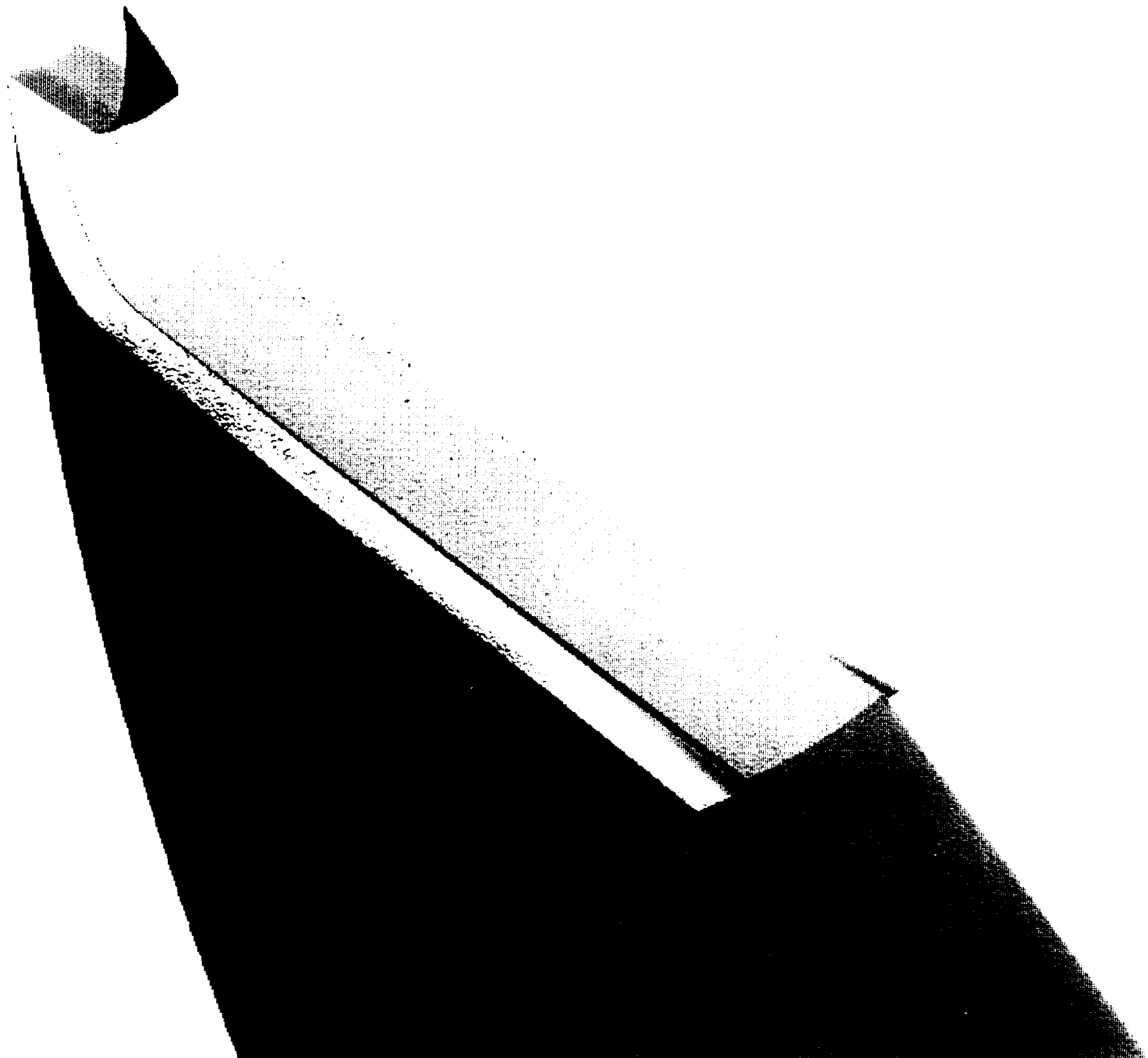

Mach Number Contours

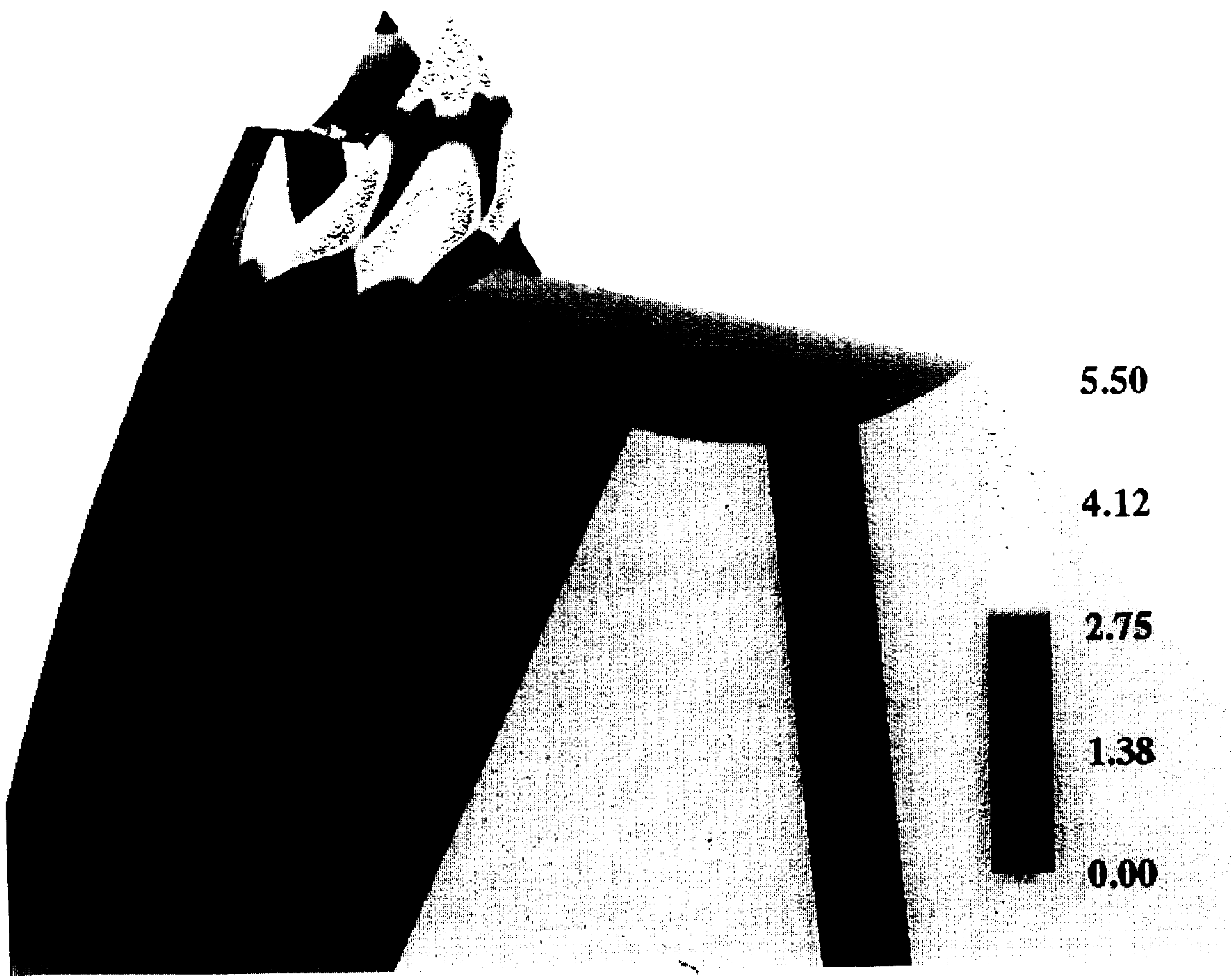

Mach Number Contours

Temperature Contours

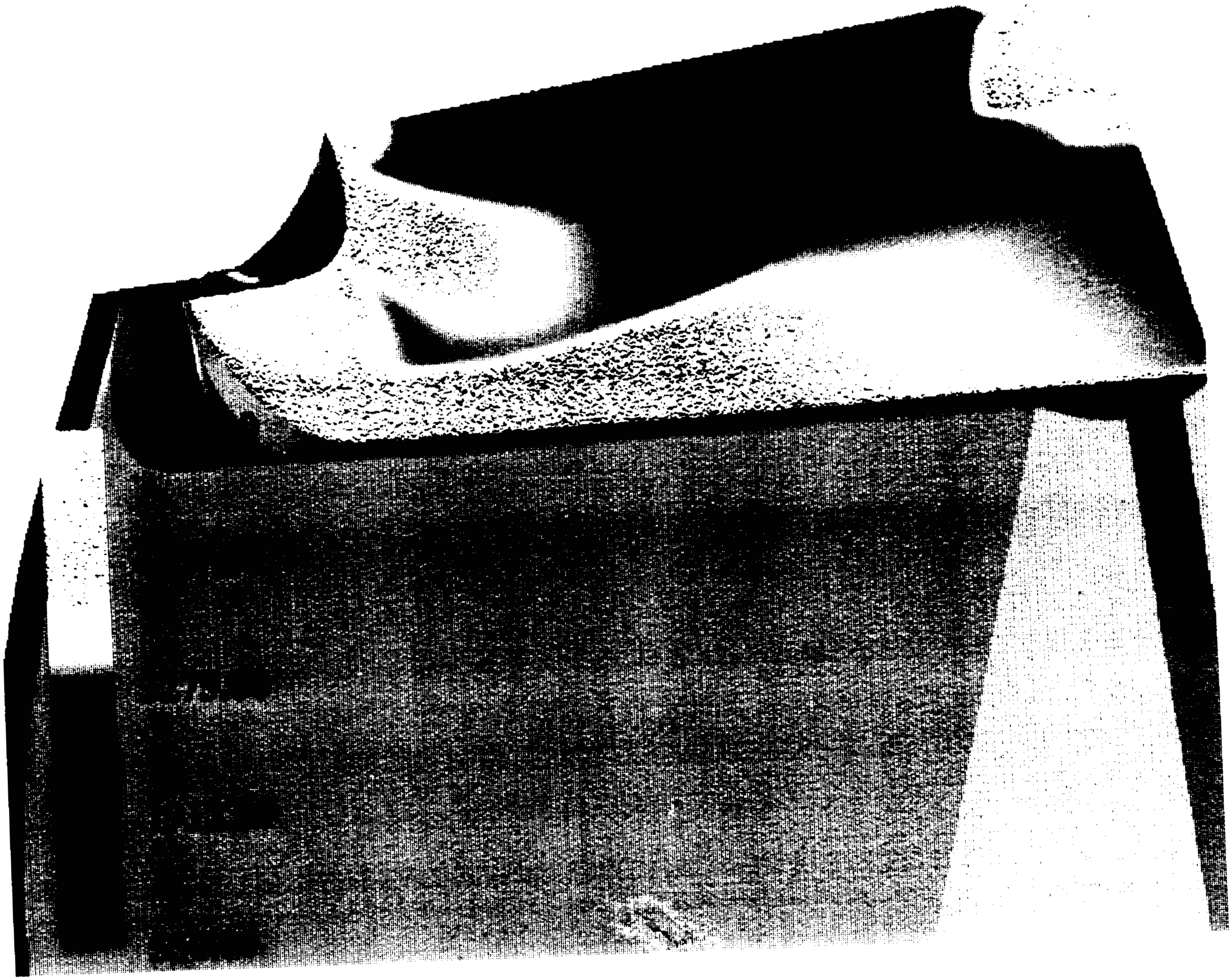

Temperature Contours

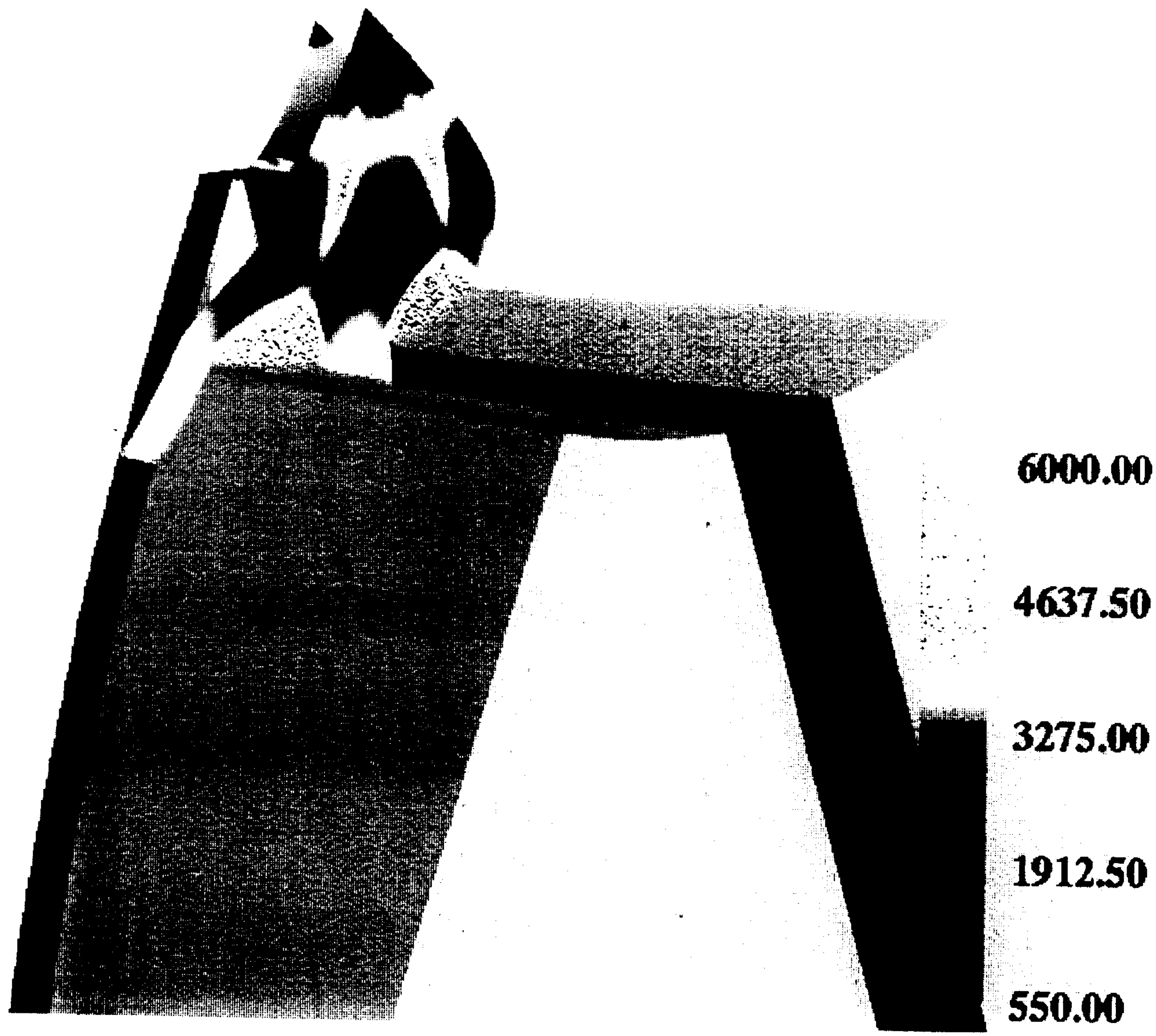

Near Field Velocity Vectors

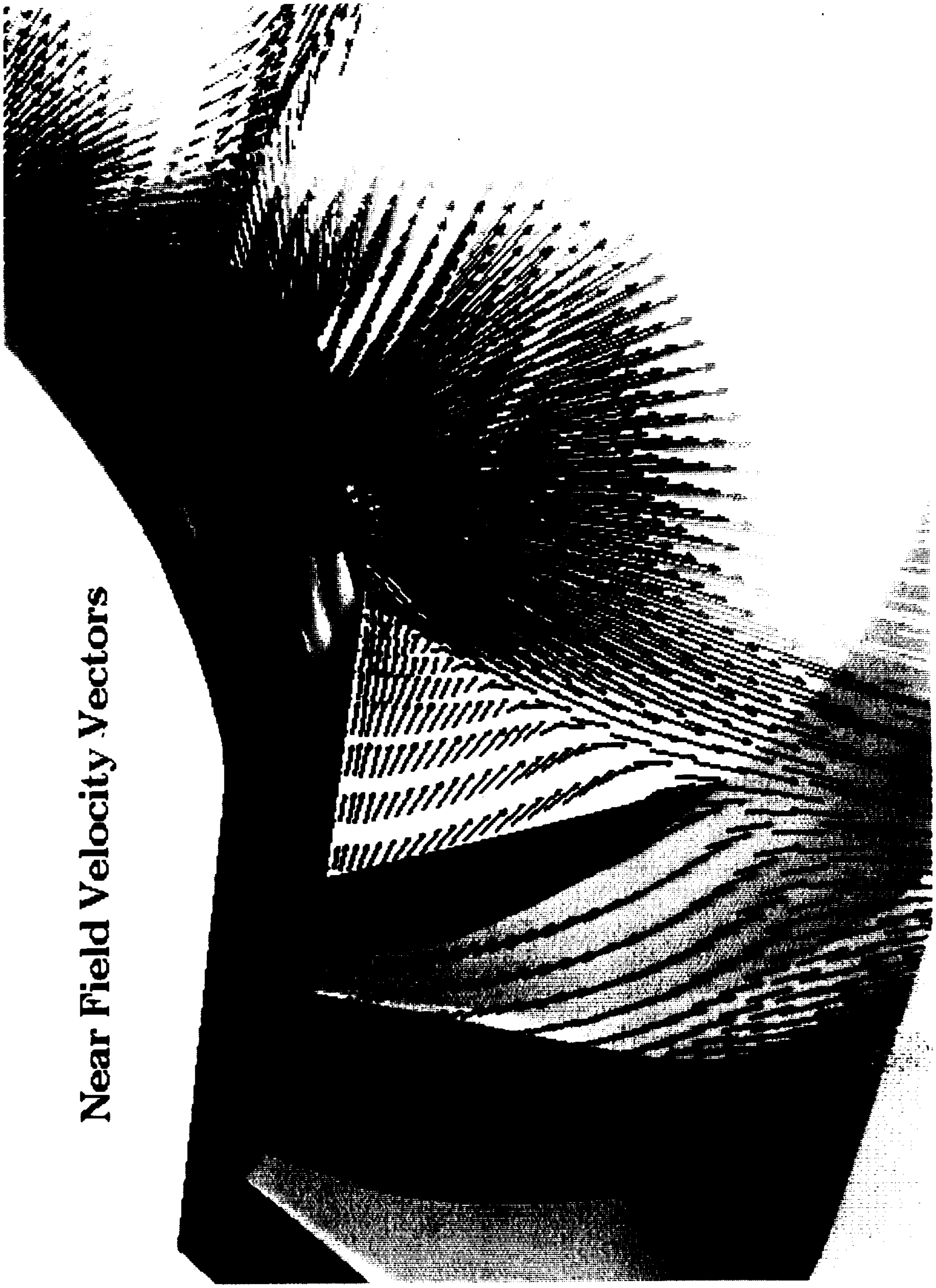

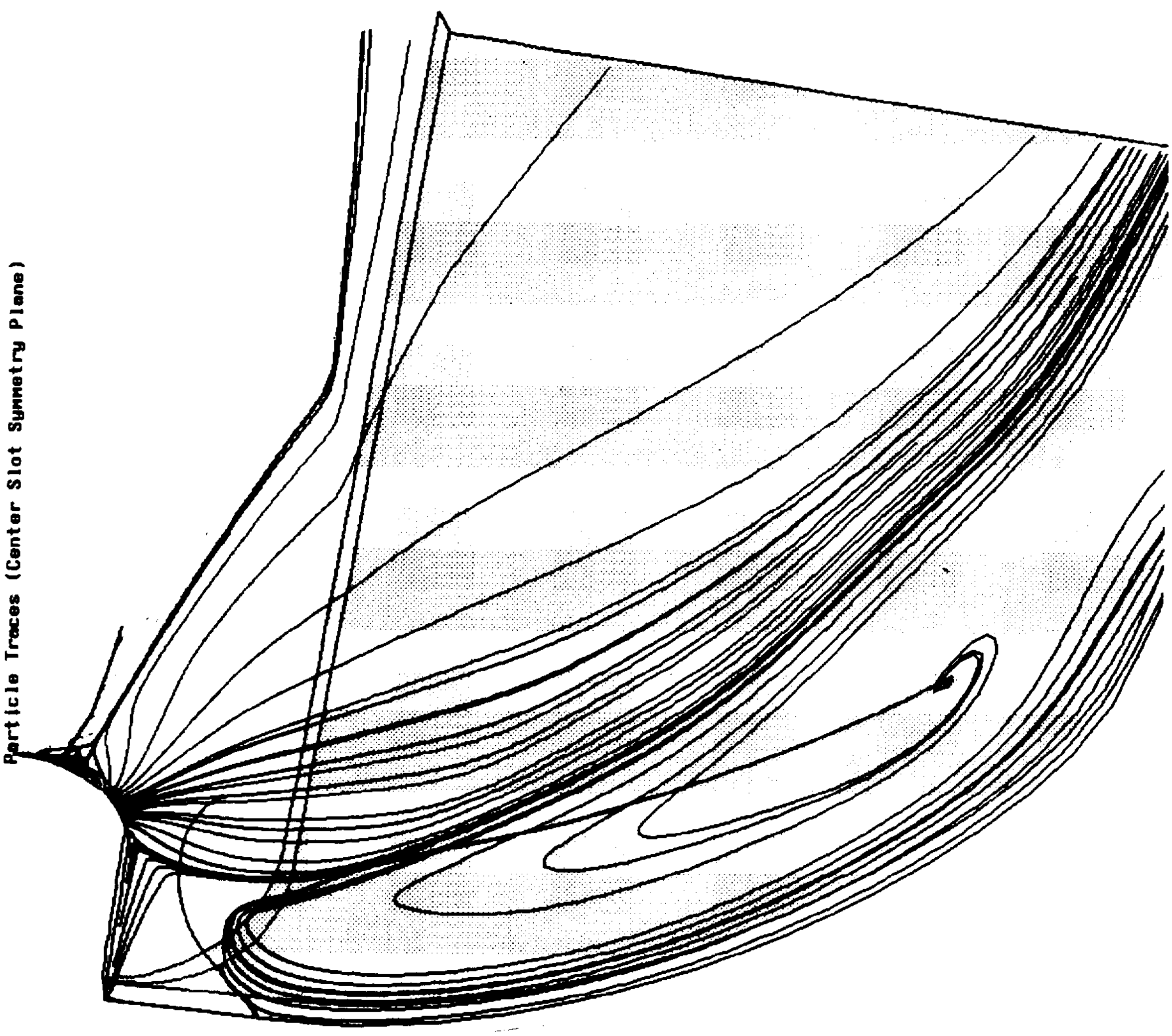

Particle Traces (Center Slot Symmetry Plane)

p.3.img

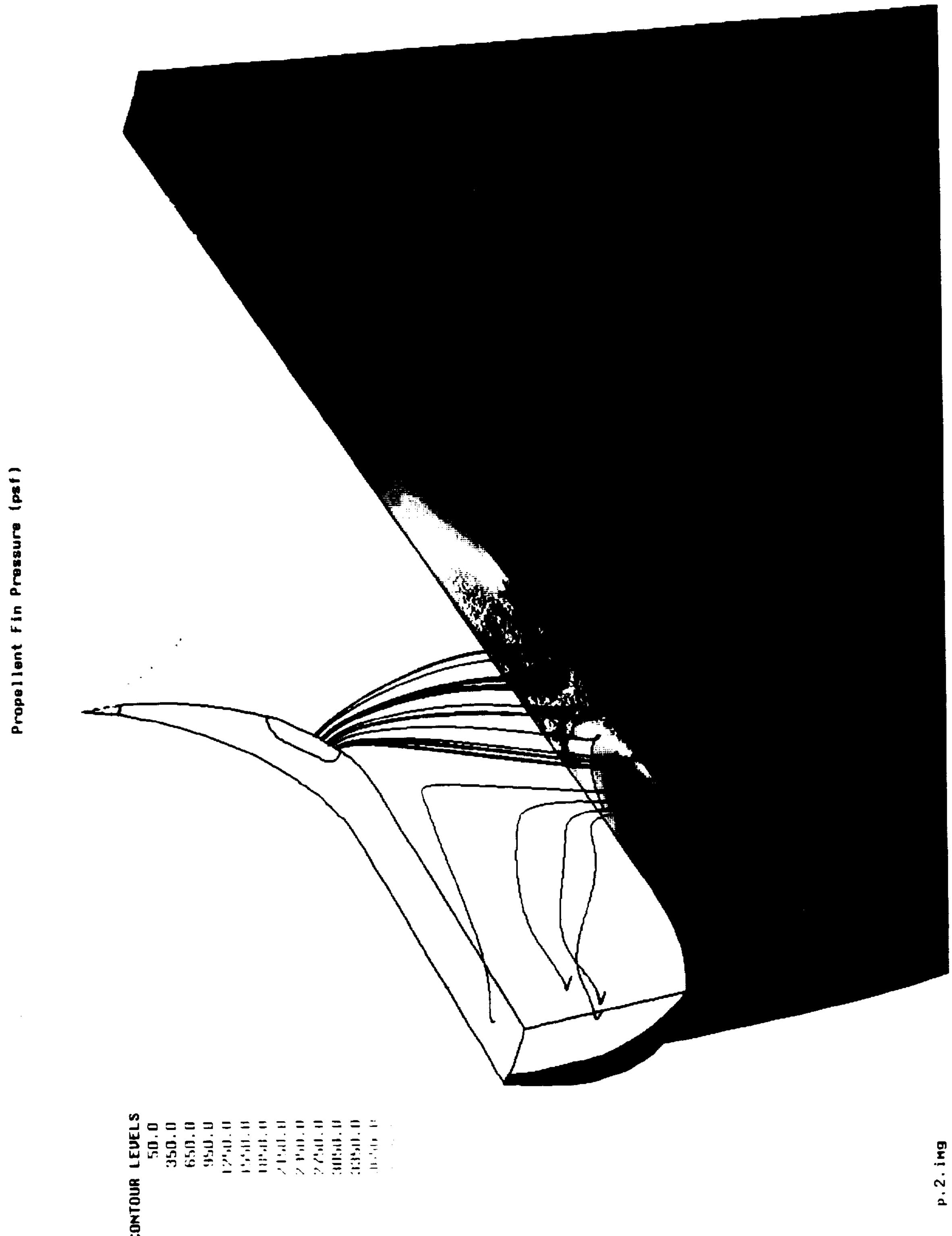

ORIGINAL PAGE IS
OF POOR QUALITY

- Conclusions
  - Rapid expansion of port flow plume causes pressure "hot" spots on fin surfaces
  - Subsequent propellent deformation and erosive burning analyses now required

NASA Sverdrup

IGNITION TRANSIENT CALCULATIONS IN THE SPACE SHUTTLE SOLID ROCKET MOTOR

Rhonald M. Jenkins and Winfred A. Foster, Jr.

Aerospace Engineering Department
Auburn University, Alabama

ABSTRACT

The work presented is part of an effort to develop a multi-dimensional ignition transient model for large solid propellant rocket motors. On the Space Shuttle, the ignition transient in the slot is induced when the igniter, itself a small rocket motor, is fired into the head-end portion of the main rocket motor. The computational results presented in this paper consider two different igniter configurations. The first configuration is a simulated Space Shuttle RSRM igniter which has one central nozzle that is parallel to the centerline of the motor. The second igniter configuration has a nozzle which is canted at an angle of 45° from the centerline of the motor. This paper presents a computational fluid dynamic (CFD) analyses of certain flow field characteristics inside the solid propellant star grain slot of the Space Shuttle during the ignition transient period of operation for each igniter configuration. The majority of studies made to date regarding ignition transient performance in solid rocket motors have concluded that the key parameter to be determined is the heat transfer rate to the propellant surface and hence the heat transfer coefficient between the gas and the propellant. In this paper the heat transfer coefficients, pressure and velocity distributions are calculated in the star slot. In order to validate the computational method and to attempt to establish a correlation between the flow field characteristics and the heat transfer rates a series of cold flow experimental investigations were conducted. The results of these experiments show excellent qualitative and quantitative agreement with the pressure and velocity distributions obtained from the CFD analysis. The CFD analysis utilized a classical pipe flow type correlation for the heat transfer rates. The experimental results provide an excellent qualitative comparison with regard to spatial distribution of the heat transfer rates as a function of nozzle configuration and igniter pressure. The results indicate that from a quantitative point of view that the pipe flow correlation gives reasonably good results. Furthermore, there appears to be a direct correlation between igniter pressure and an average Reynolds number in the star grain slot. This may lead to a simple method for modifying the convection heat transfer correlation. Calculated results of pressure-vs-time for the first 200 msec of motor firing of the Space Shuttle RSRM support the trends shown for the heat transfer rate comparisons between the cold flow CFD and experimental data.

ACKNOWLEDGEMENTS

Work performed under NASA Grants No. NAG8-683 and NAG8-923. Experimental work performed, in cooperation with MSFC (aerophysics division) personnel , in the special-purpose test section of the MSFC 14"x14" trisonic wind tunnel.

In particular, the assistance of John E. Hengel and Andrew W. Smith is acknowledged.

OUTLINE

Presentation of Cold-Flow Heat Transfer/ Aerodynamic Results for Flow in the Head-End Star Slot of the Space Shuttle SRM

- Single Port Igniter
- 45° Igniter (no center port)

Presentation of Flow Visualization Results for Three Igniter Configurations

- Single Port Igniter
- 45° Igniter (no center port)
- 45° Igniter (with center port)

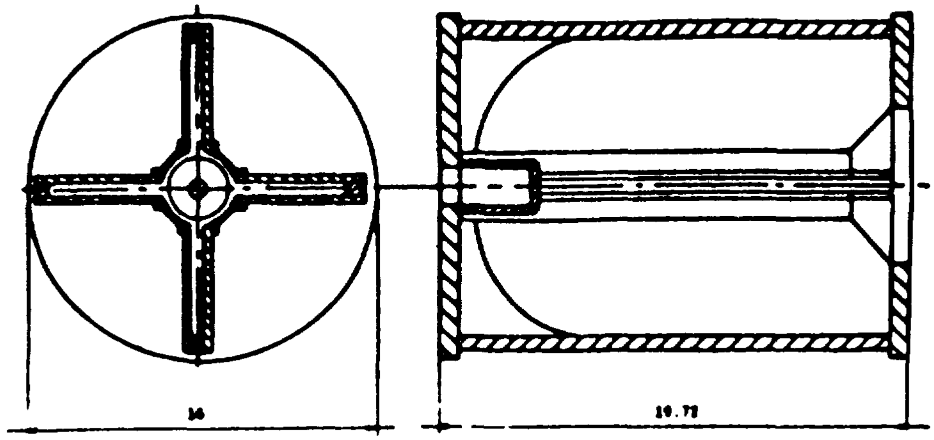
16
19.72

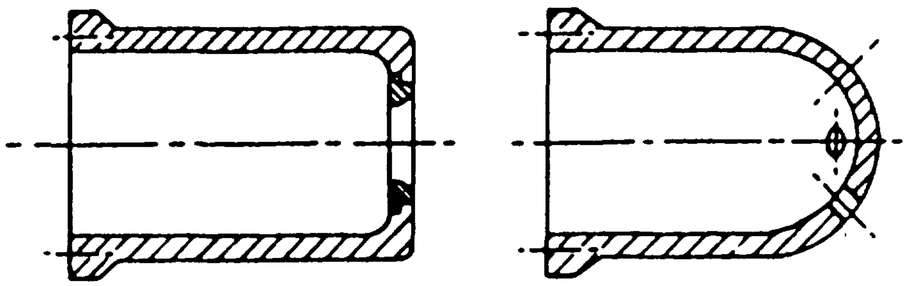

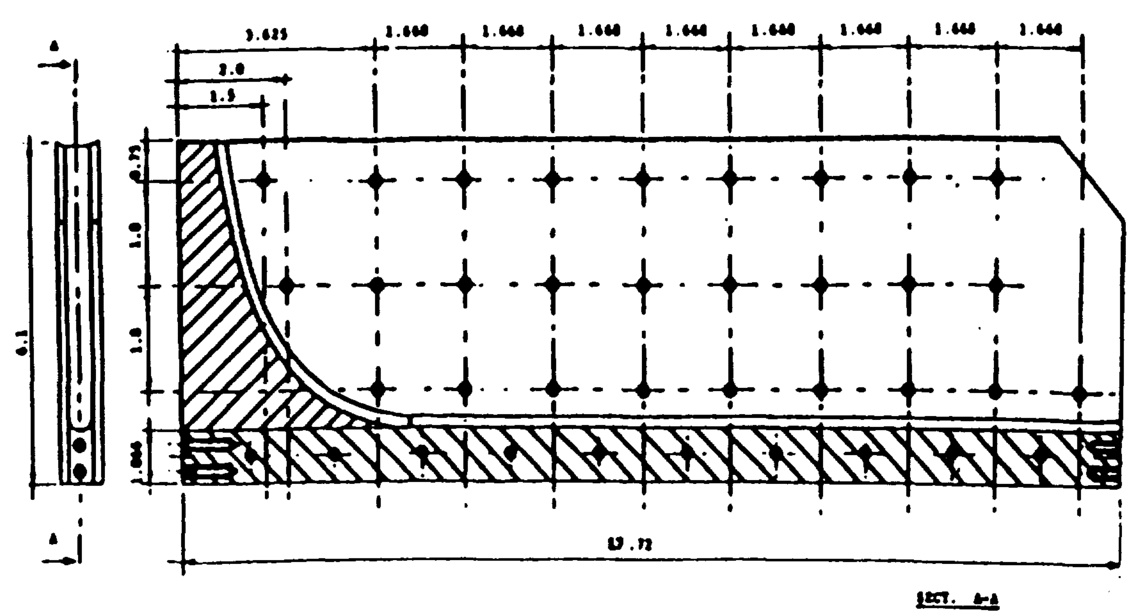
3.625
1.660
2.0
1.5
1.0
SECT. A-A

HEAT TRANSFER MODEL

Heat transfer from gas to wall is assumed to be by convection only.

The convection correlation utilized was originally derived for turbulent pipe flow, but can be adapted to arbitrary geometries. The correlation utilized is of the form

$$Nu = \frac{0.152 Re^{0.9} Pr}{0.833[2.25 \ln(0.114 Re^{0.9}) + 13.2 Pr - 5.8]}$$

where Re is based on the hydraulic diameter of the slot.

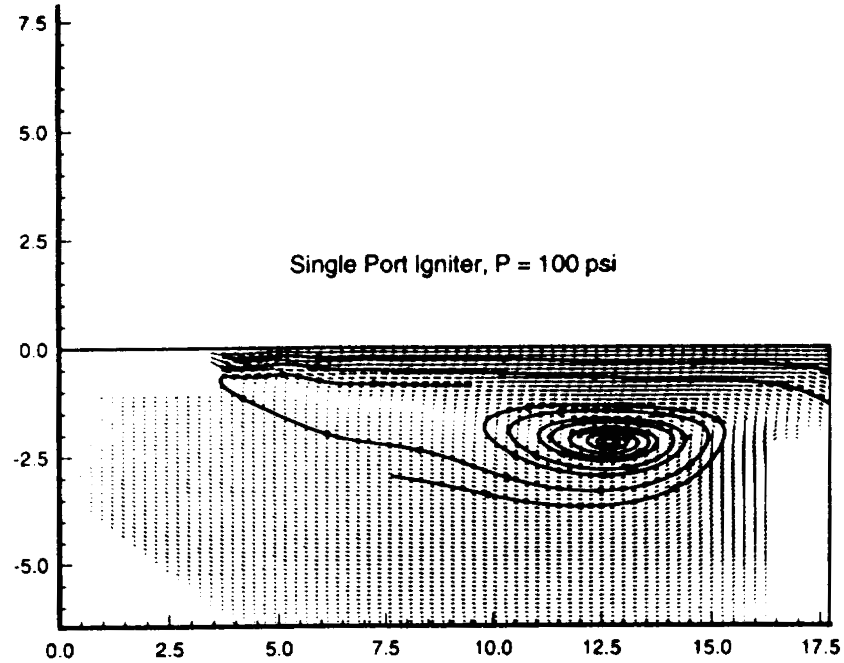
Single Port Igniter, P = 100 psi
7.5
5.0
2.5
0.0
-2.5
-5.0
0.0
2.5
5.0
7.5
10.0
12.5
15.0
17.5

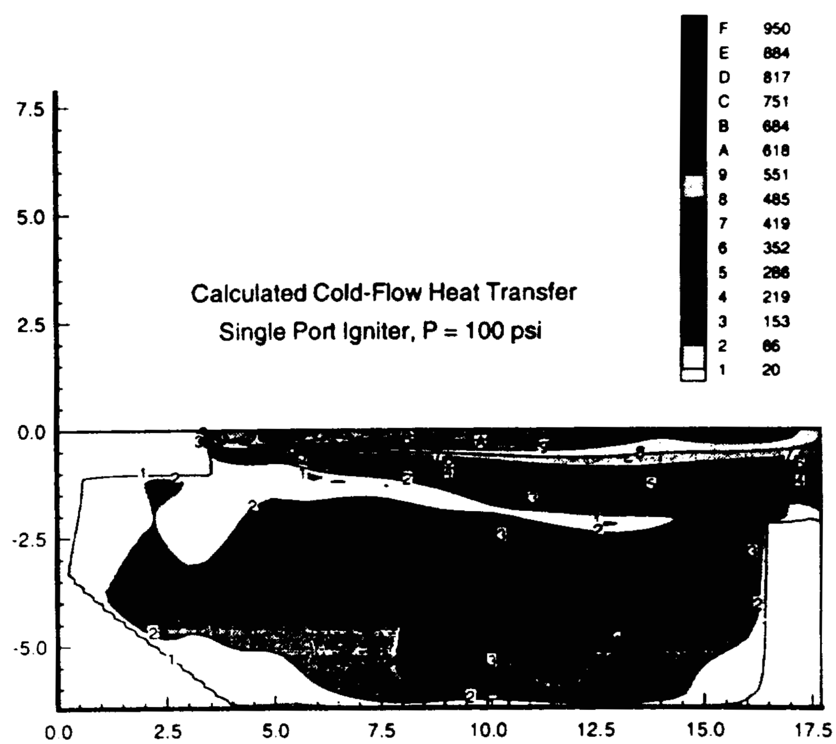
Calculated Cold-Flow Heat Transfer
Single Port Igniter, P = 100 psi
F 950
E 884
D 817
C 751
B 684
A 618
9 551
8 485
7 419
6 352
5 286
4 219
3 153
2 86
1 20
7.5
5.0
2.5
0.0
-2.5
-5.0
0.0
2.5
5.0
7.5
10.0
12.5
15.0
17.5

Calculated Heat Transfer, Single Port Igniter

$P_{igniter} = 100$ psi

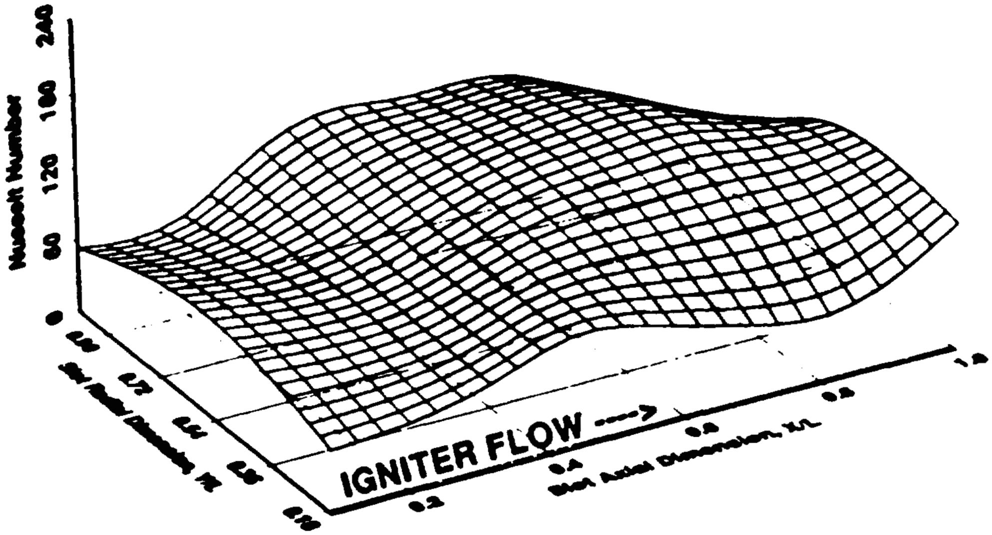

Measured Heat Transfer, Single Port Igniter

$P_{igniter} = 100$ psi

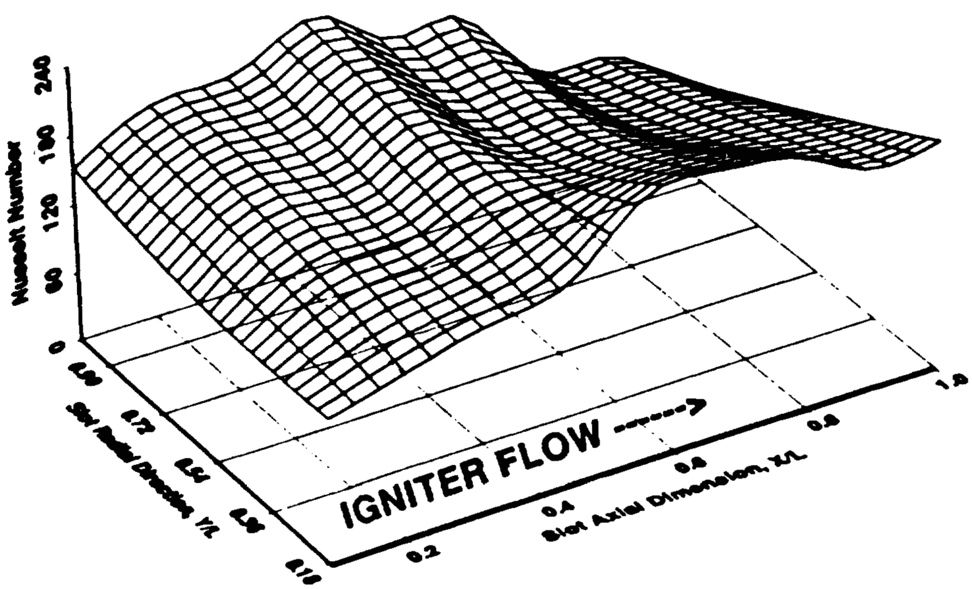

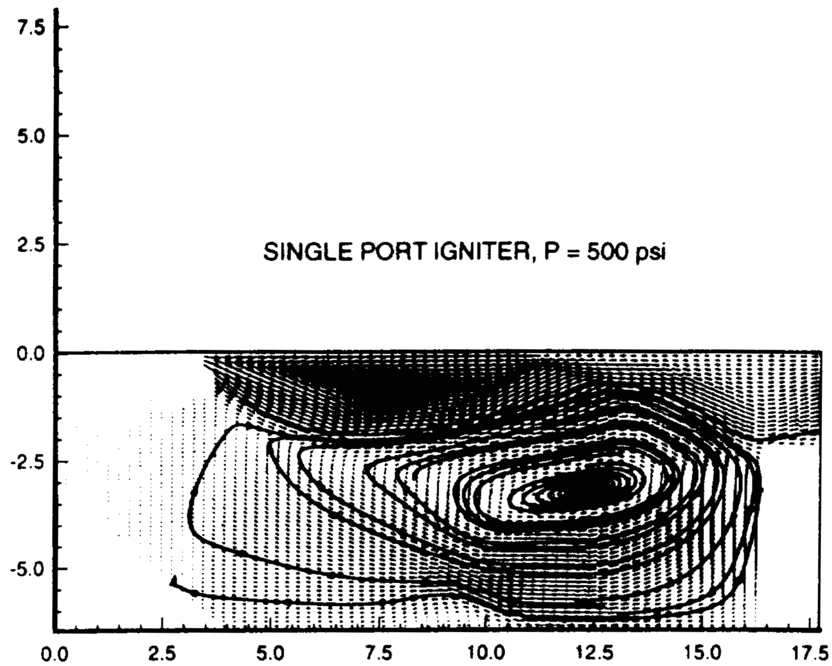
SINGLE PORT IGNITER, P = 500 psi
7.5
5.0
2.5
0.0
-2.5
-5.0
0.0
2.5
5.0
7.5
10.0
12.5
15.0
17.5

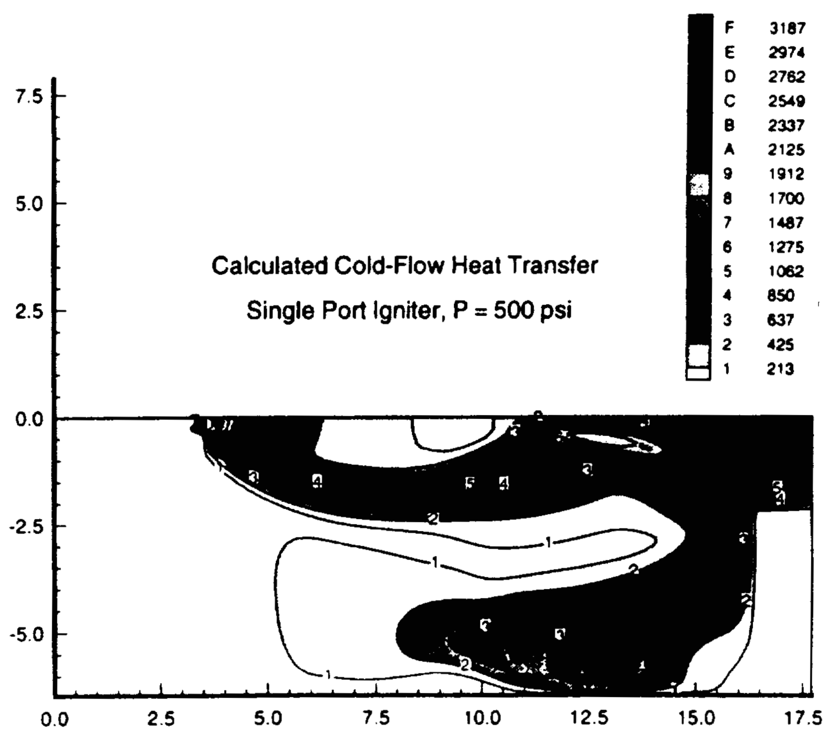
Calculated Cold-Flow Heat Transfer
Single Port Igniter, P = 500 psi
F 3187
E 2974
D 2762
C 2549
B 2337
A 2125
9 1912
8 1700
7 1487
6 1275
5 1062
4 850
3 637
2 425
1 213
7.5
5.0
2.5
0.0
-2.5
-5.0
0.0
2.5
5.0
7.5
10.0
12.5
15.0
17.5

Calculated Heat Transfer, Single Port Igniter

$P_{Igniter} = 500$ psi

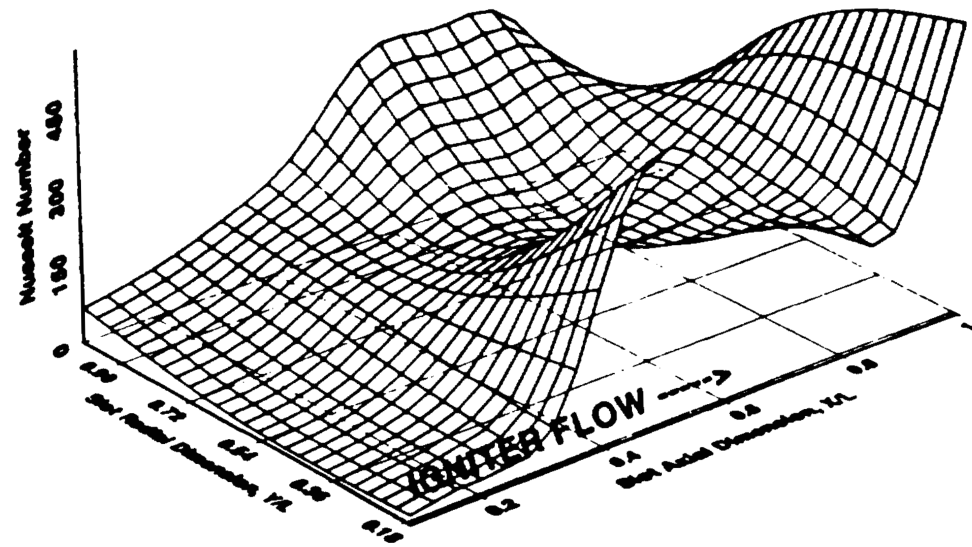

Measured Heat Transfer, Single Port Igniter

$P_{Igniter} = 500$ psi

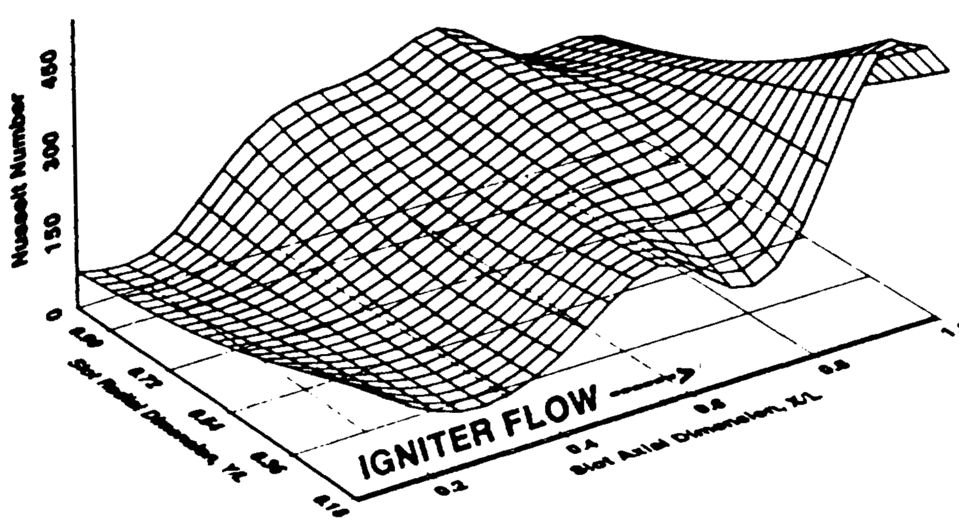

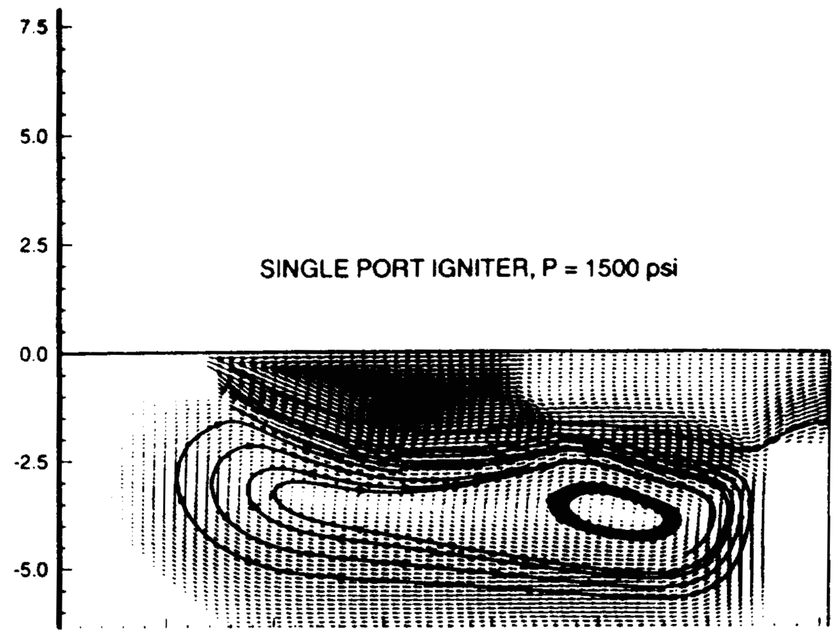
SINGLE PORT IGNITER, P = 1500 psi
7.5
5.0
2.5
0.0
-2.5
-5.0

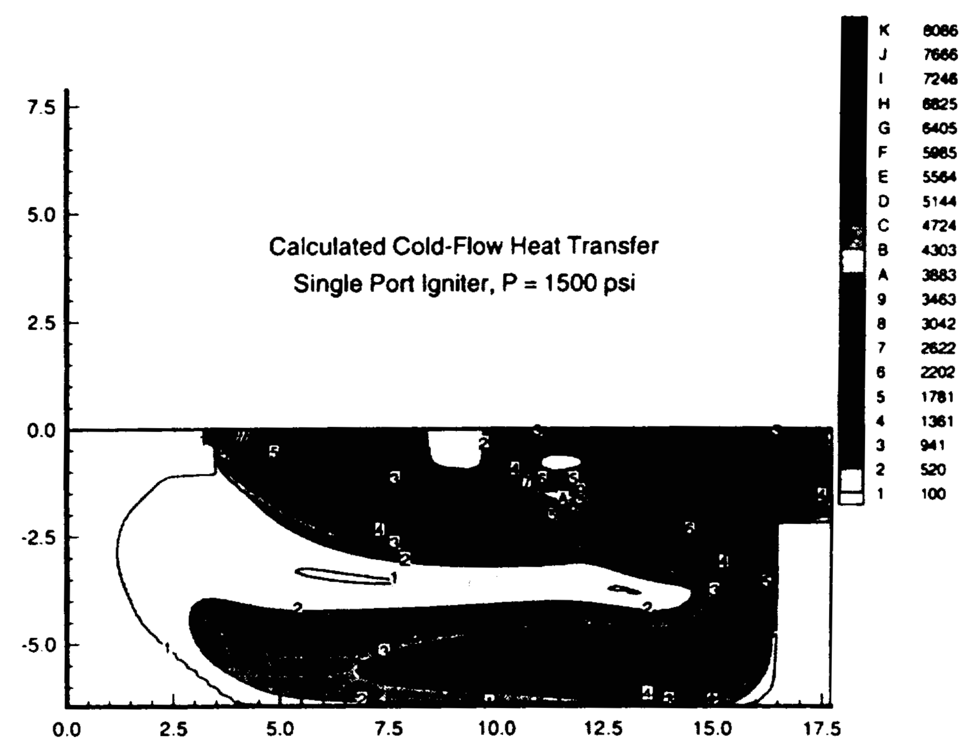
Calculated Cold-Flow Heat Transfer
Single Port Igniter, P = 1500 psi
7.5
5.0
2.5
0.0
-2.5
-5.0
0.0
2.5
5.0
7.5
10.0
12.5
15.0
17.5
K 8086
J 7666
I 7246
H 6825
G 6405
F 5985
E 5564
D 5144
C 4724
B 4303
A 3883
9 3463
8 3042
7 2622
6 2202
5 1781
4 1361
3 941
2 520
1 100

Calculated Heat Transfer, Single Port Igniter

$P_{Igniter}$ = 1500 psi

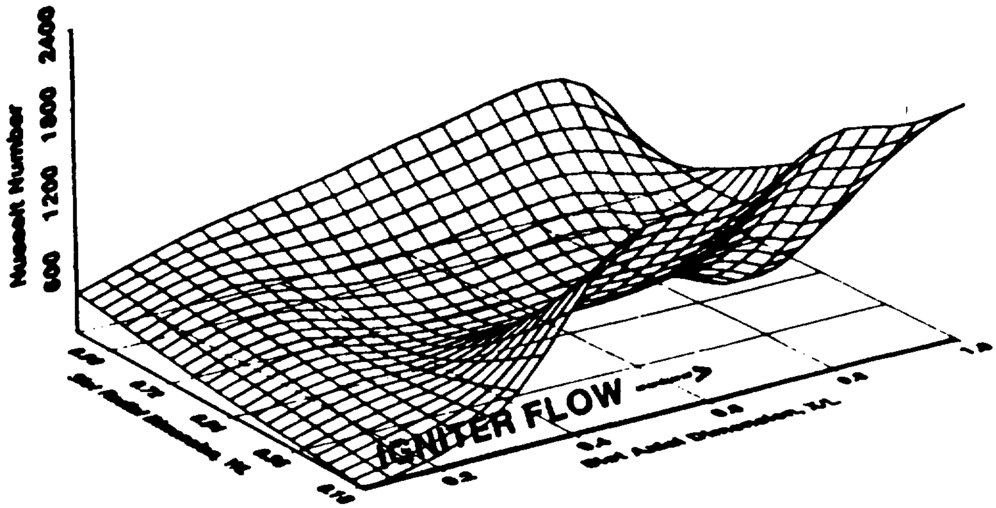

Measured Heat Transfer, Single Port Igniter

$P_{Igniter}$ = 1500 psi

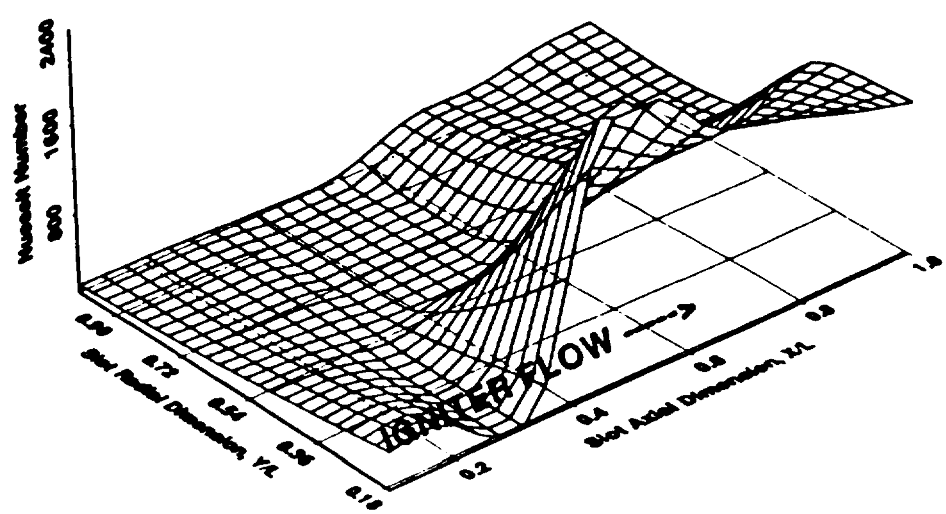

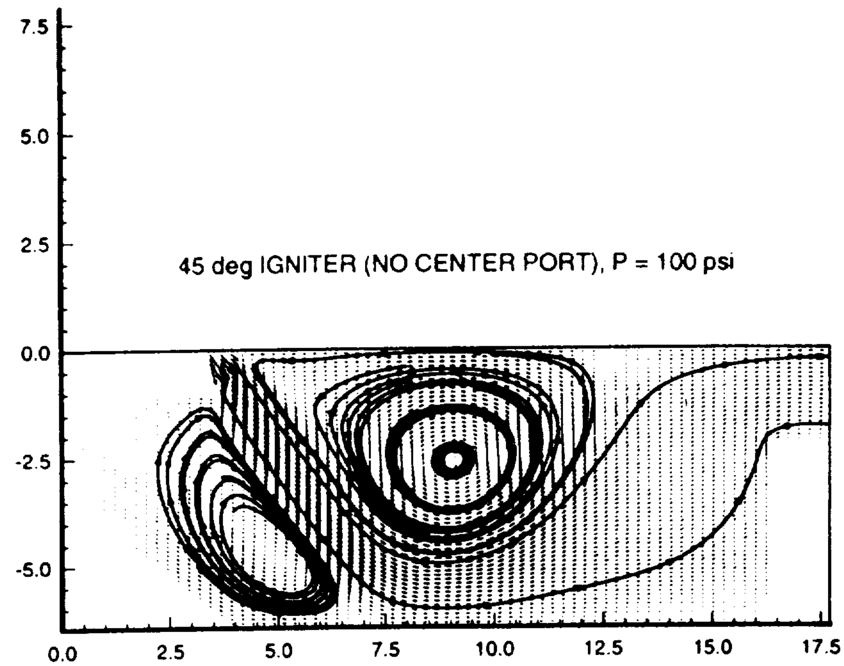

45 deg IGNITER (NO CENTER PORT), P = 100 psi
7.5
5.0
2.5
0.0
-2.5
-5.0
0.0
2.5
5.0
7.5
10.0
12.5
15.0
17.5

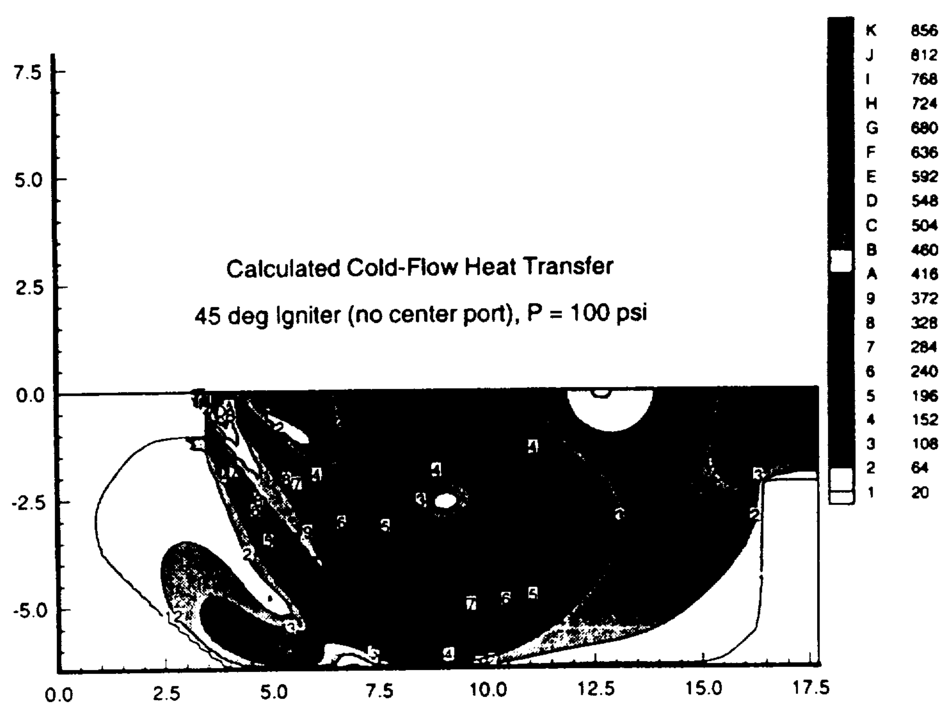

Calculated Cold-Flow Heat Transfer
45 deg Igniter (no center port), P = 100 psi
K 856
J 812
I 768
H 724
G 680
F 636
E 592
D 548
C 504
B 460
A 416
9 372
8 328
7 284
6 240
5 196
4 152
3 108
2 64
1 20
7.5
5.0
2.5
0.0
-2.5
-5.0
0.0
2.5
5.0
7.5
10.0
12.5
15.0
17.5

Calculated Heat Transfer, 45° Igniter

$P_{Igniter}$ = 100 psi

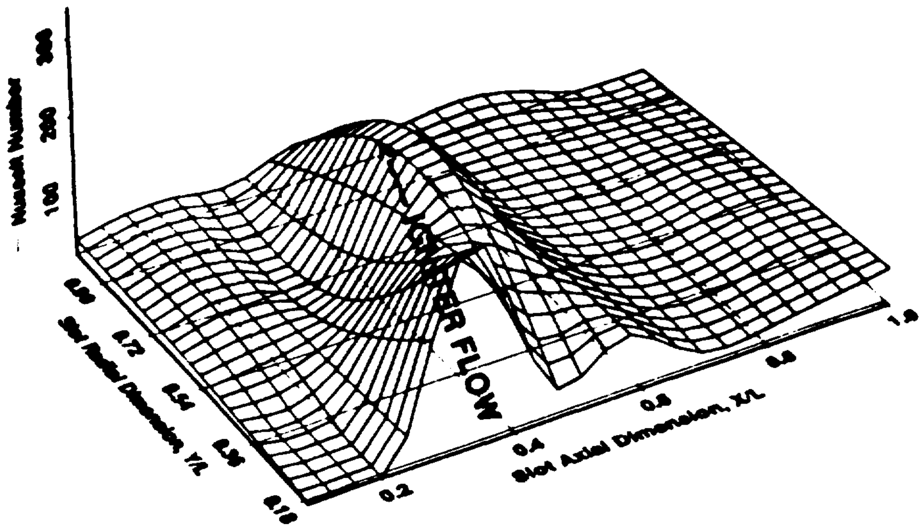

Measured Heat Transfer, 45° Igniter

$P_{Igniter}$ = 100 psi

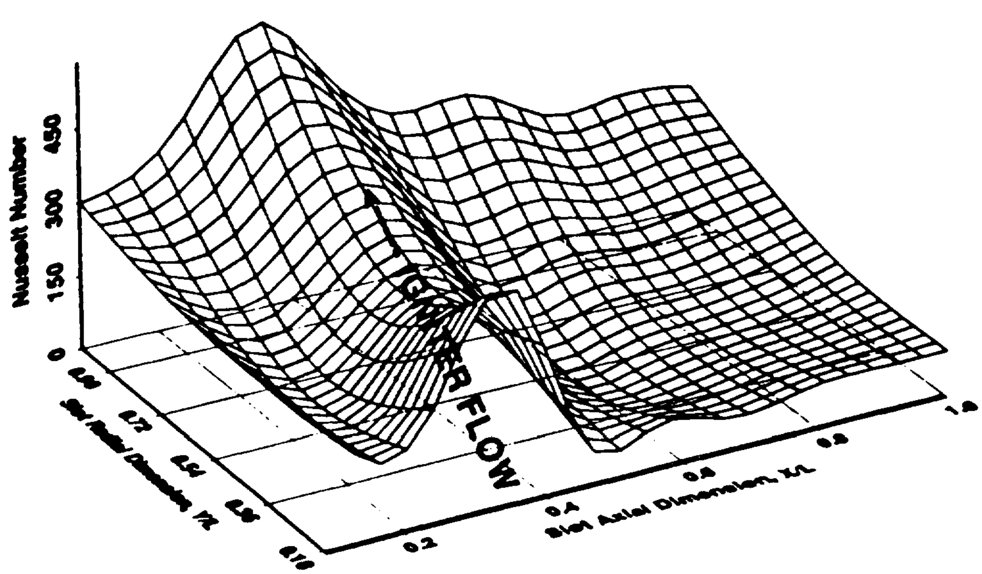

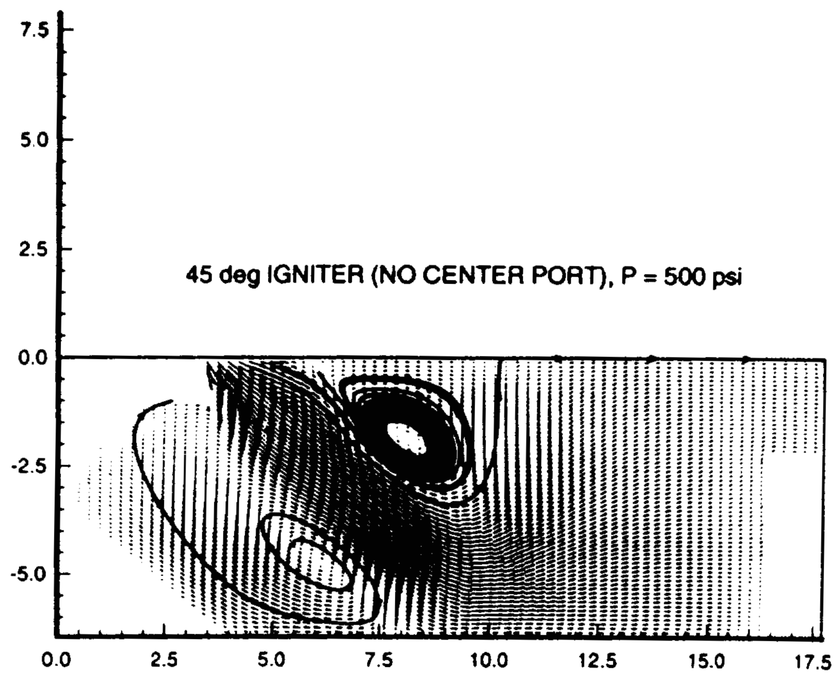
45 deg IGNITER (NO CENTER PORT), P = 500 psi
7.5
5.0
2.5
0.0
-2.5
-5.0
0.0
2.5
5.0
7.5
10.0
12.5
15.0
17.5

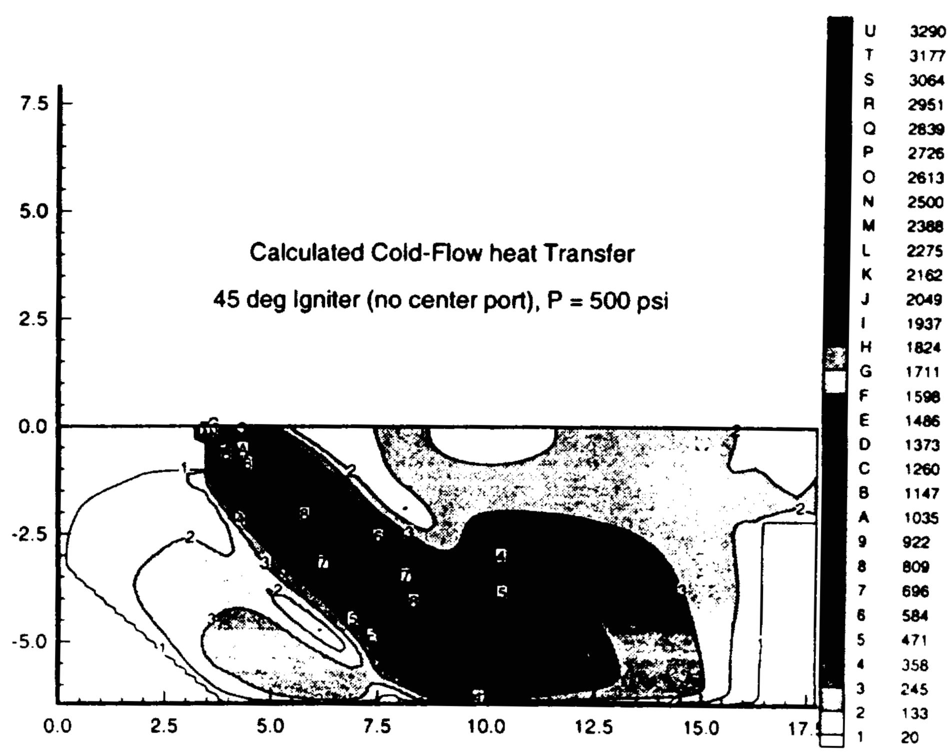
Calculated Cold-Flow heat Transfer
45 deg Igniter (no center port), P = 500 psi
U 3290
T 3177
S 3064
R 2951
Q 2839
P 2726
O 2613
N 2500
M 2388
L 2275
K 2162
J 2049
I 1937
H 1824
G 1711
F 1598
E 1486
D 1373
C 1260
B 1147
A 1035
9 922
8 809
7 696
6 584
5 471
4 358
3 245
2 133
1 20

Calculated Heat Transfer, 45° Igniter

$P_{Igniter}$ = 500 psi

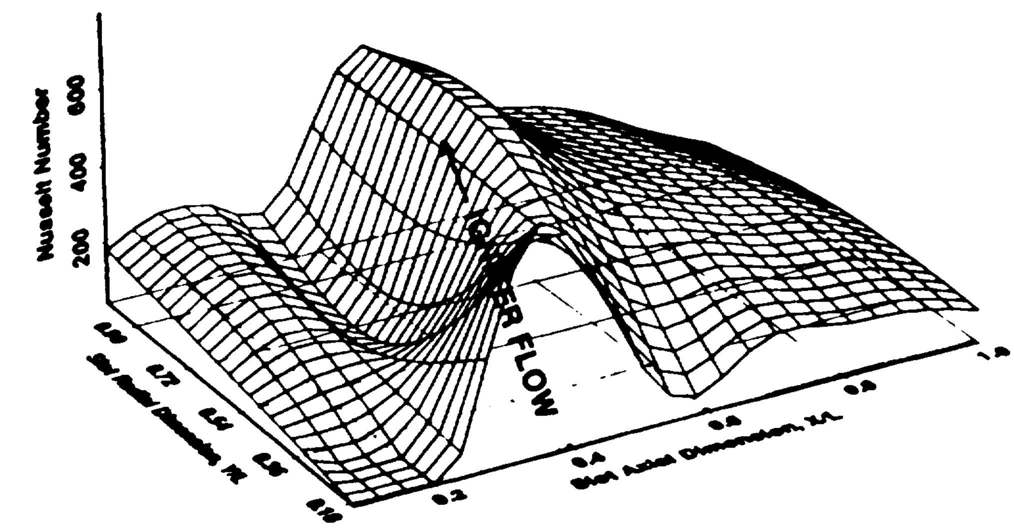

Measured Heat Transfer, 45° Igniter

$P_{Igniter}$ = 500 psi

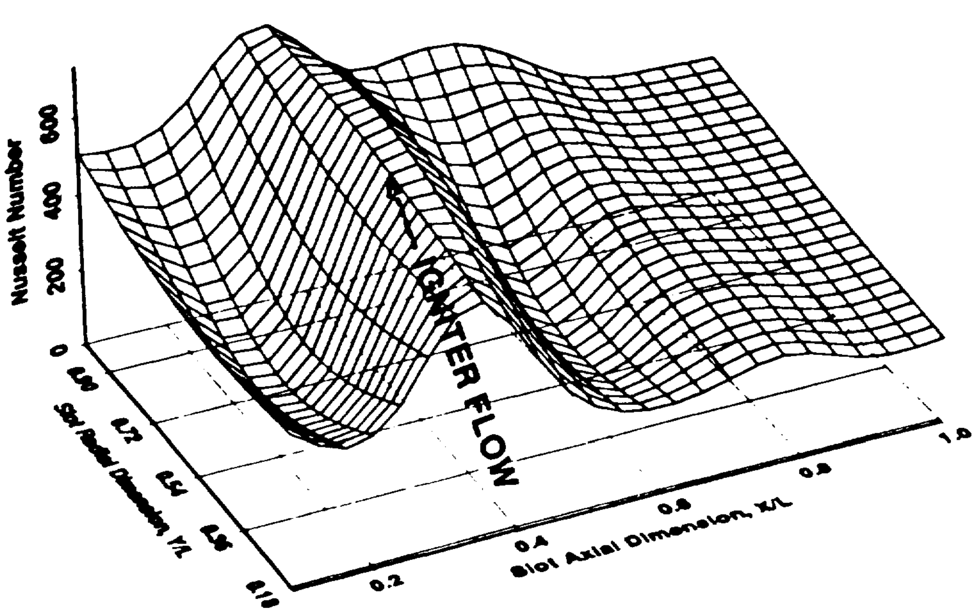

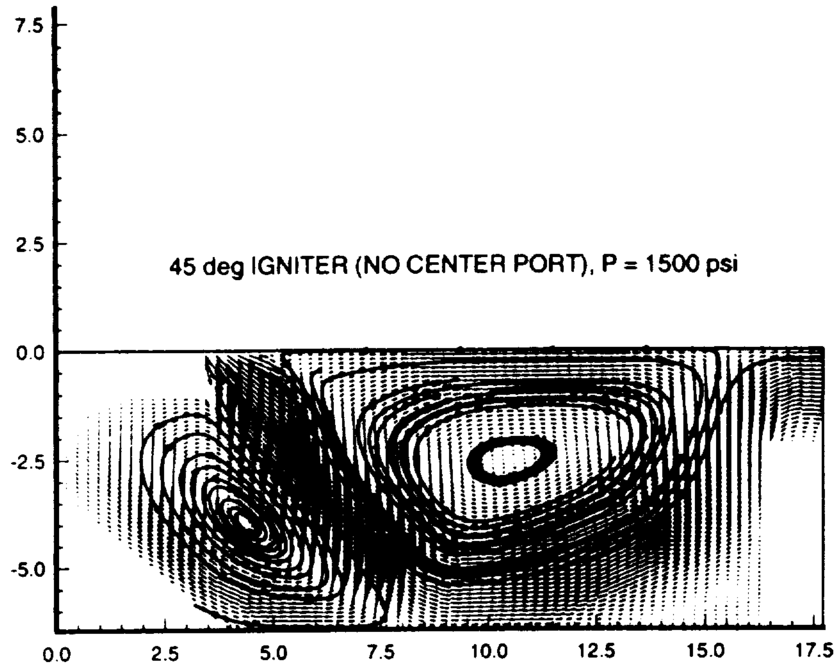
45 deg IGNITER (NO CENTER PORT), P = 1500 psi
7.5
5.0
2.5
0.0
-2.5
-5.0
0.0 2.5 5.0 7.5 10.0 12.5 15.0 17.5

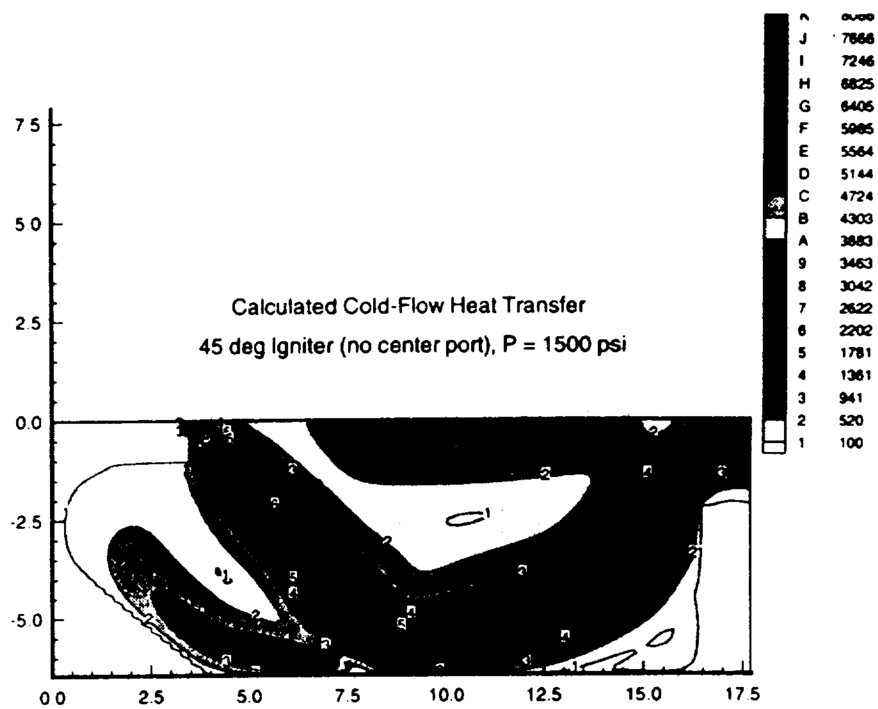
Calculated Cold-Flow Heat Transfer
45 deg Igniter (no center port), P = 1500 psi
J 7666
I 7246
H 6825
G 6405
F 5985
E 5564
D 5144
C 4724
B 4303
A 3883
9 3463
8 3042
7 2622
6 2202
5 1781
4 1361
3 941
2 520
1 100
7.5
5.0
2.5
0.0
-2.5
-5.0
0.0 2.5 5.0 7.5 10.0 12.5 15.0 17.5

Calculated Heat Transfer, 45° Igniter

$P_{Igniter}$ = 1500 psi

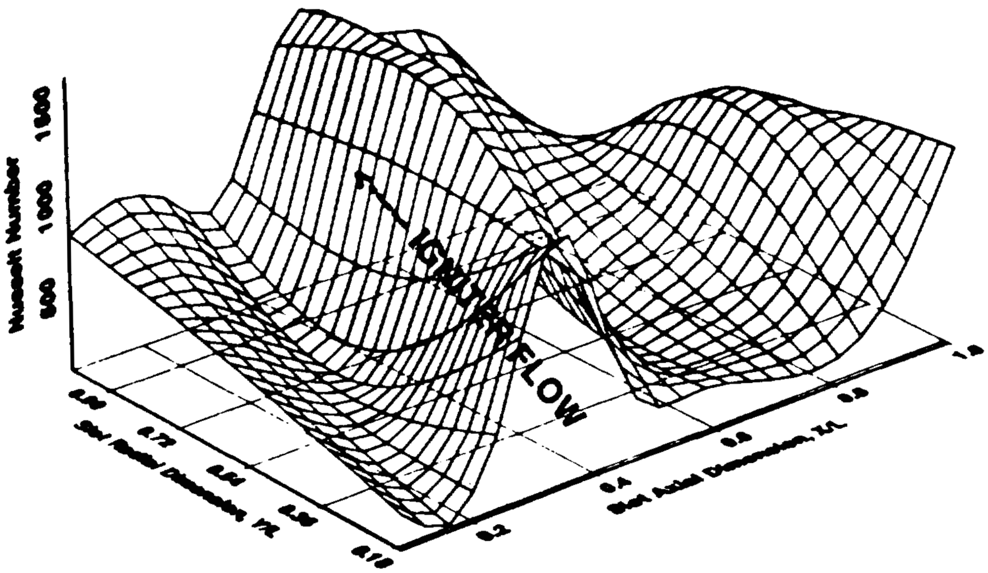

Measured Heat Transfer, 45° Igniter

$P_{Igniter}$ = 1500 psi

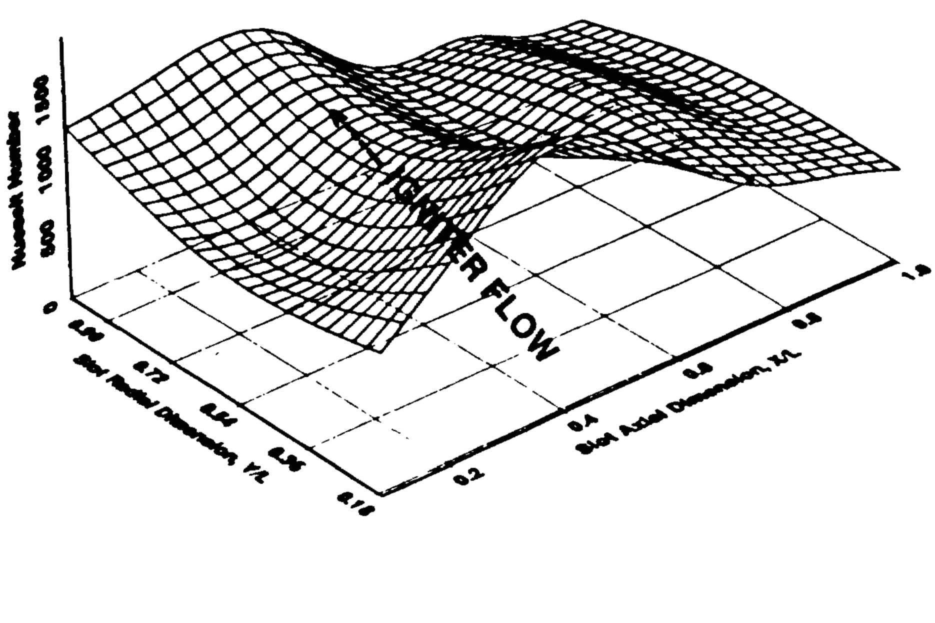

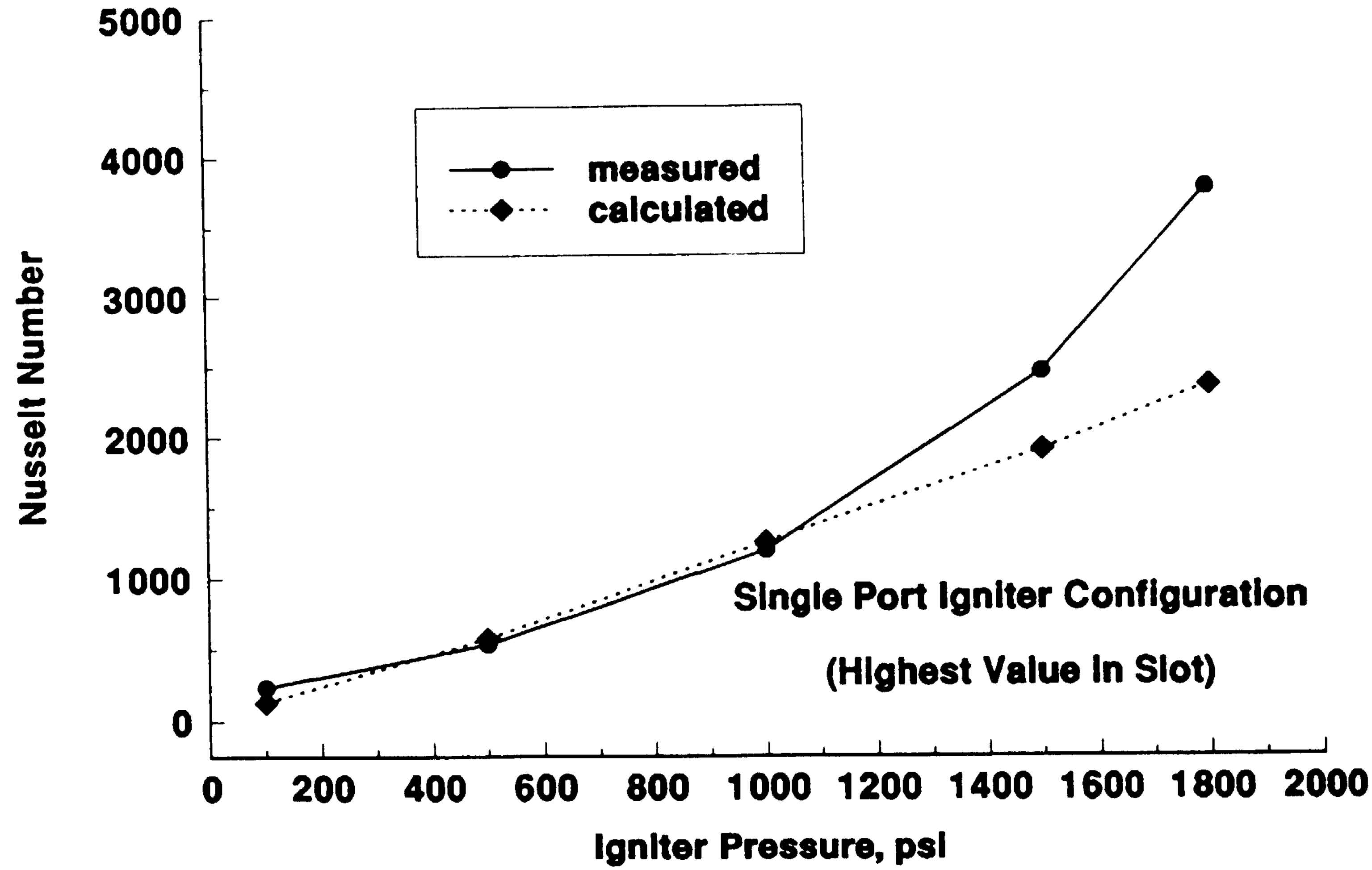

measured
calculated
Single Port Igniter Configuration
(Highest Value In Slot)
Nusselt Number
Igniter Pressure, psi
5000
4000
3000
2000
1000
0
200
400
600
800
1000
1200
1400
1600
1800
2000

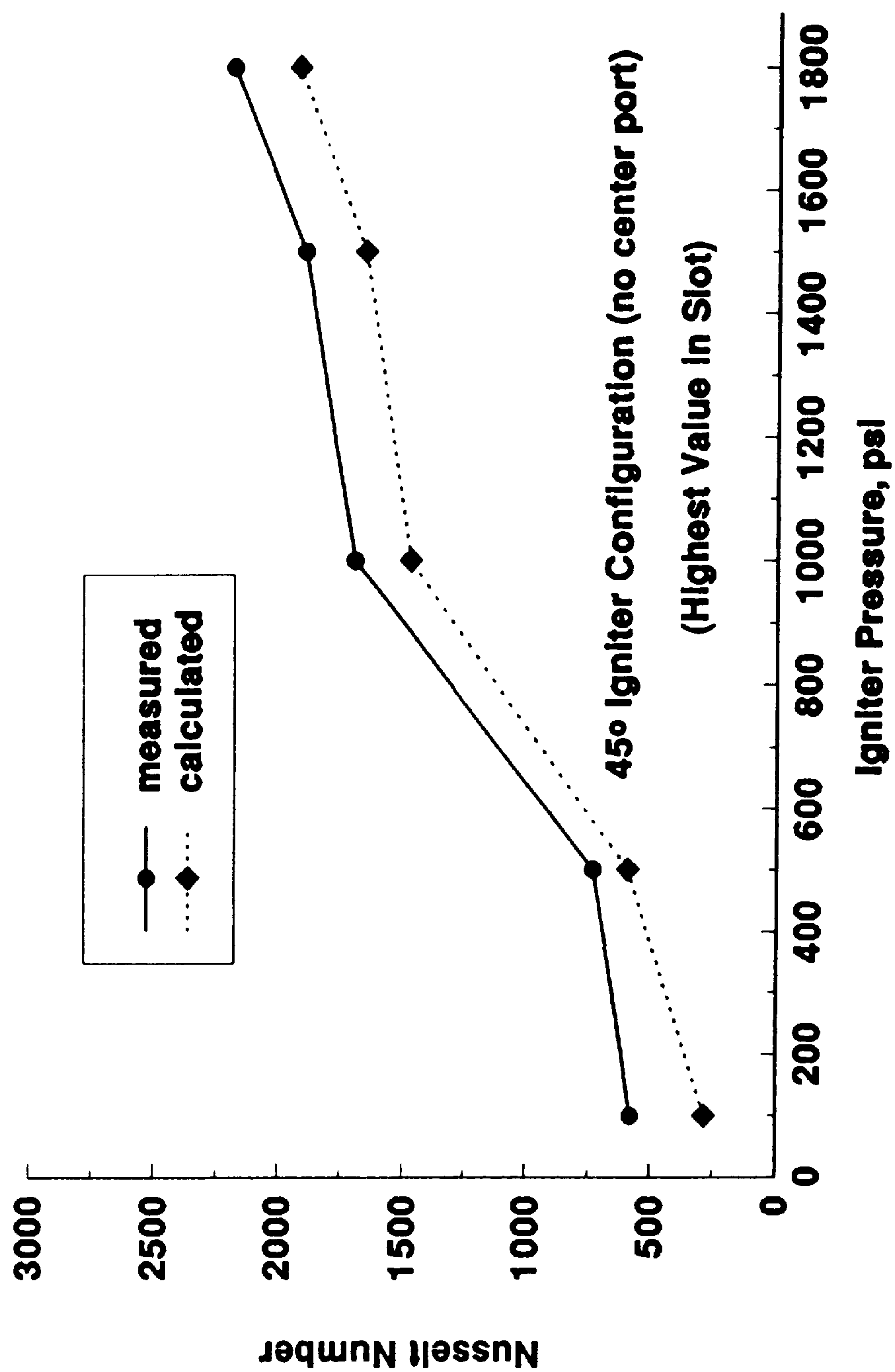

Nusselt Number
3000
2500
2000
1500
1000
500
0
0
200
400
600
800
1000
1200
1400
1600
1800
Igniter Pressure, psi
measured
calculated
45° Igniter Configuration (no center port)
(Highest Value in Slot)

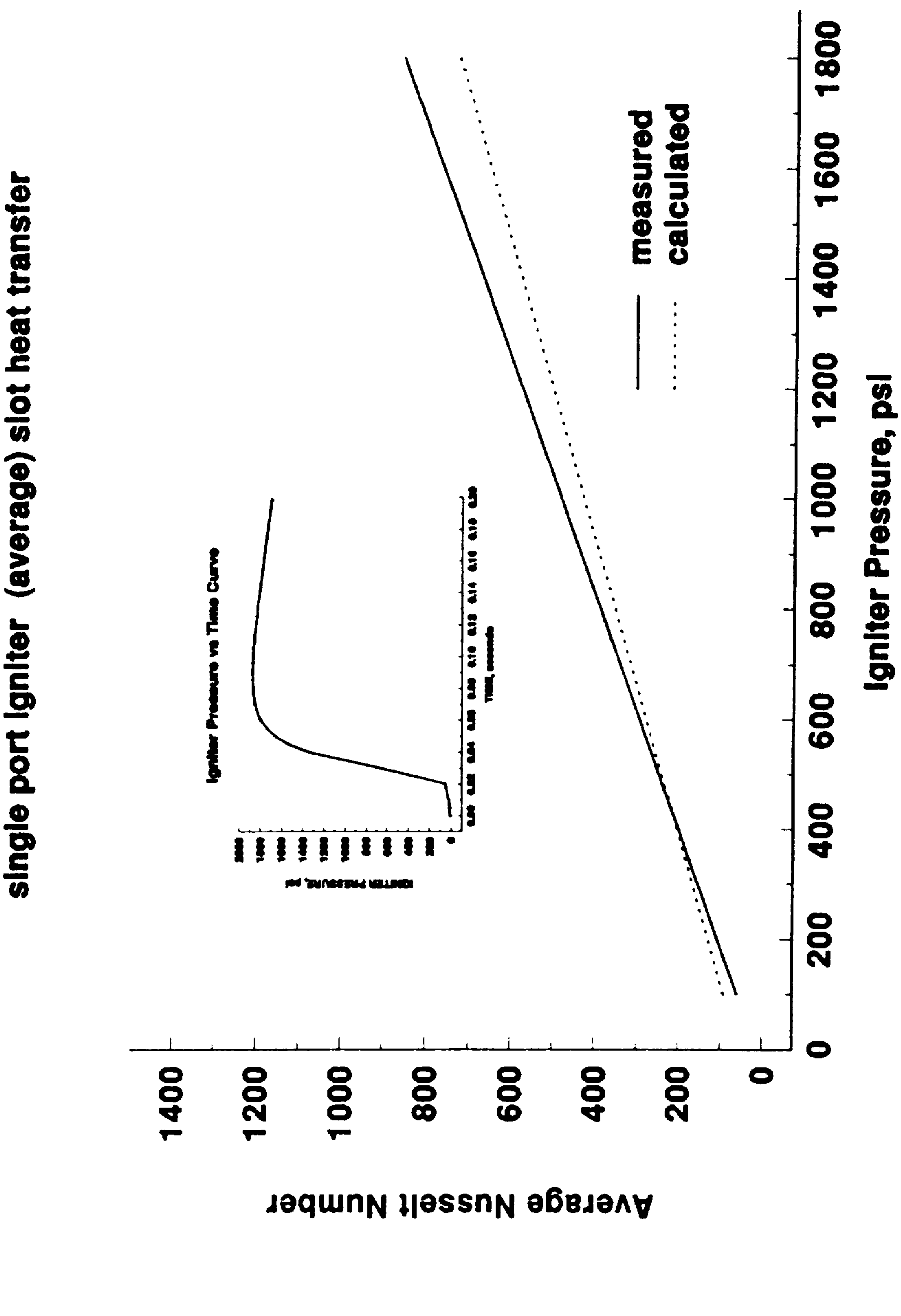
single port igniter (average) slot heat transfer
Average Nusselt Number
0
200
400
600
800
1000
1200
1400
Igniter Pressure, psi
0
200
400
600
800
1000
1200
1400
1600
1800
measured
calculated
Igniter Pressure vs Time Curve
IGNITER PRESSURE, psi
TIME, seconds

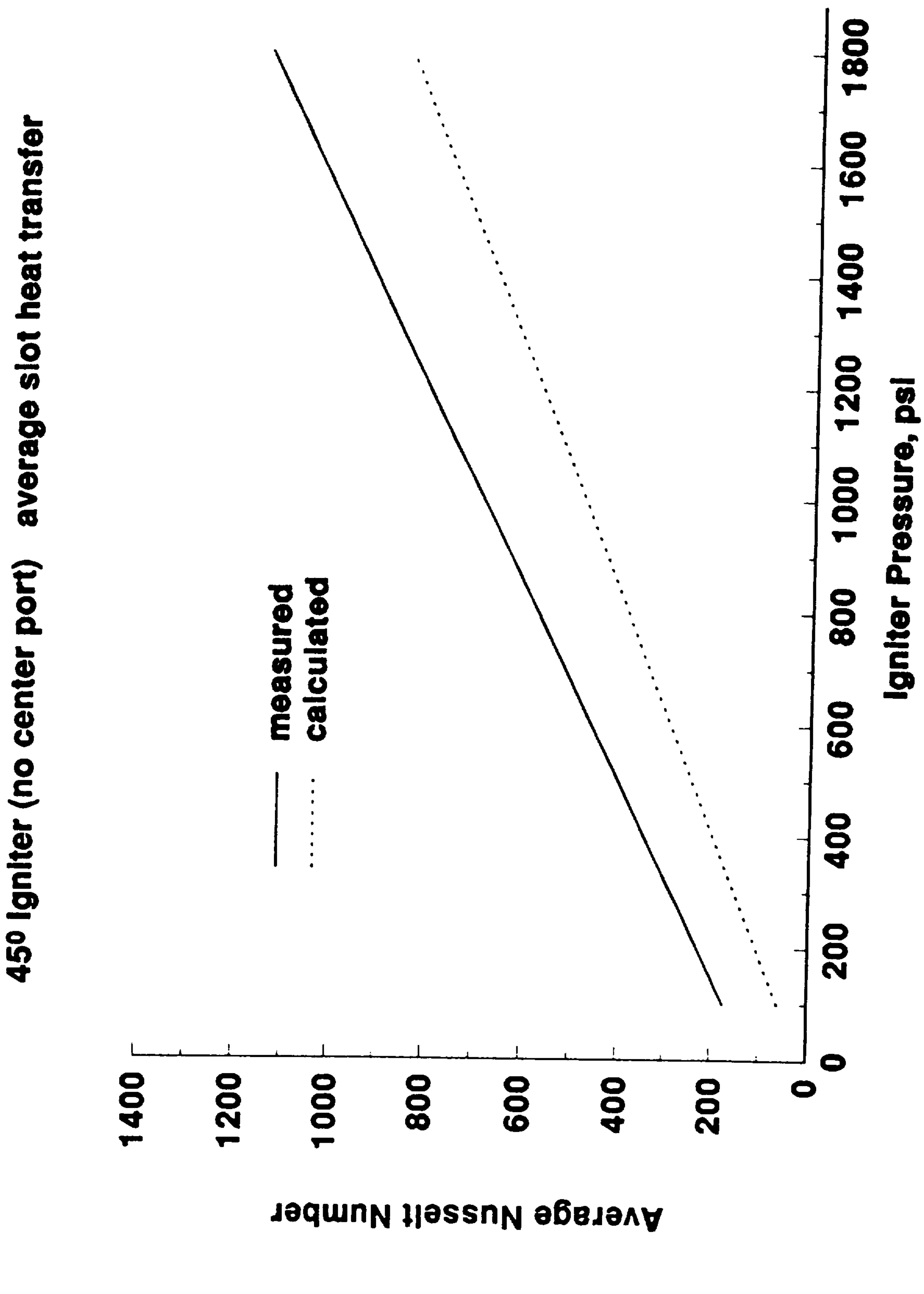

45⁰ Igniter (no center port)   average slot heat transfer
measured
calculated
Average Nusselt Number
0
200
400
600
800
1000
1200
1400
Igniter Pressure, psi
0
200
400
600
800
1000
1200
1400
1600
1800

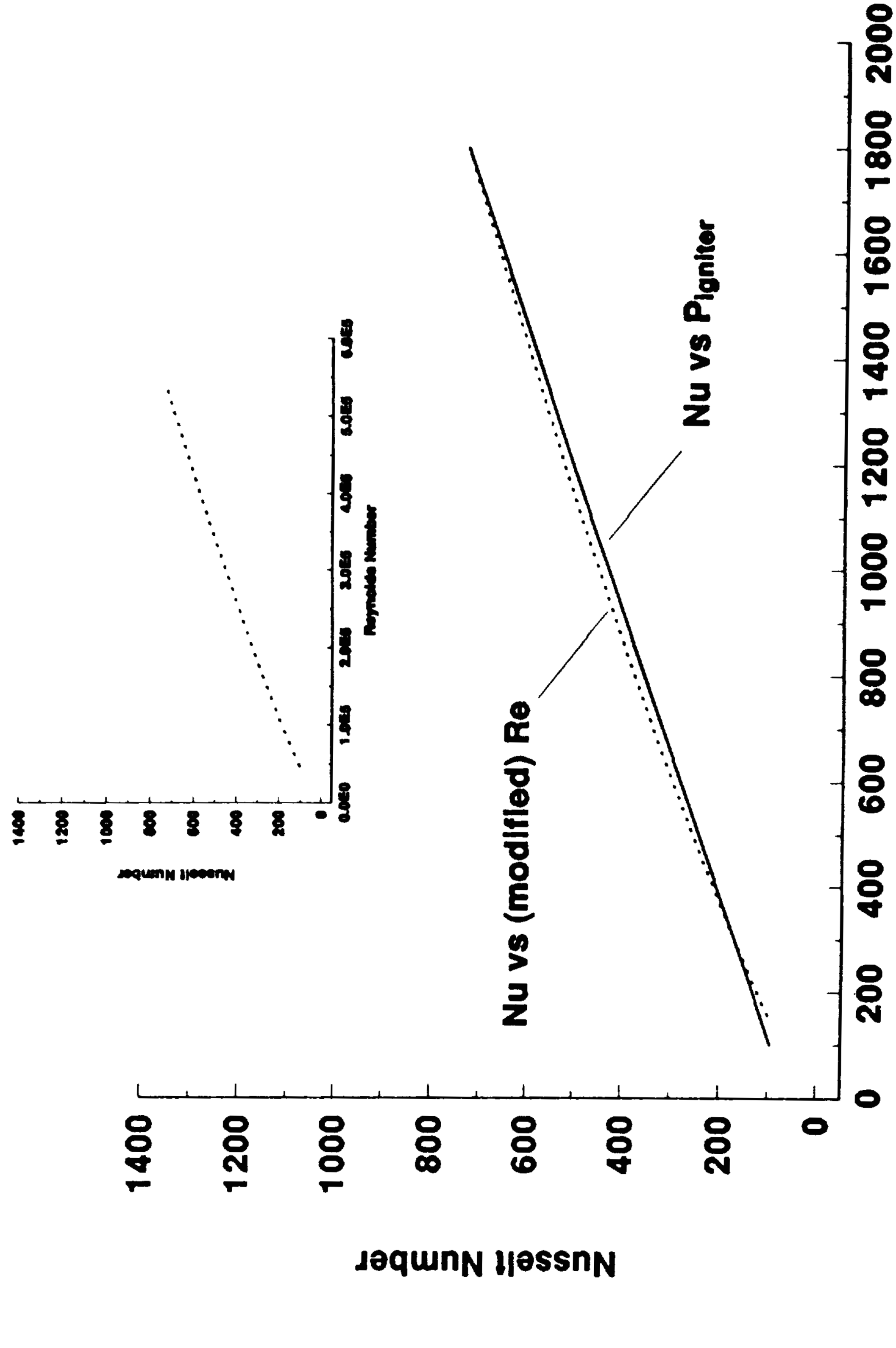

Nusselt Number
0
200
400
600
800
1000
1200
1400
0
200
400
600
800
1000
1200
1400
1600
1800
2000
Nu vs (modified) Re
Nu vs $P_{igniter}$
Nusselt Number
Reynolds Number

Sensitivity of Initial Shuttle Head-End Pressure to Assumed Heat Transfer Correlation

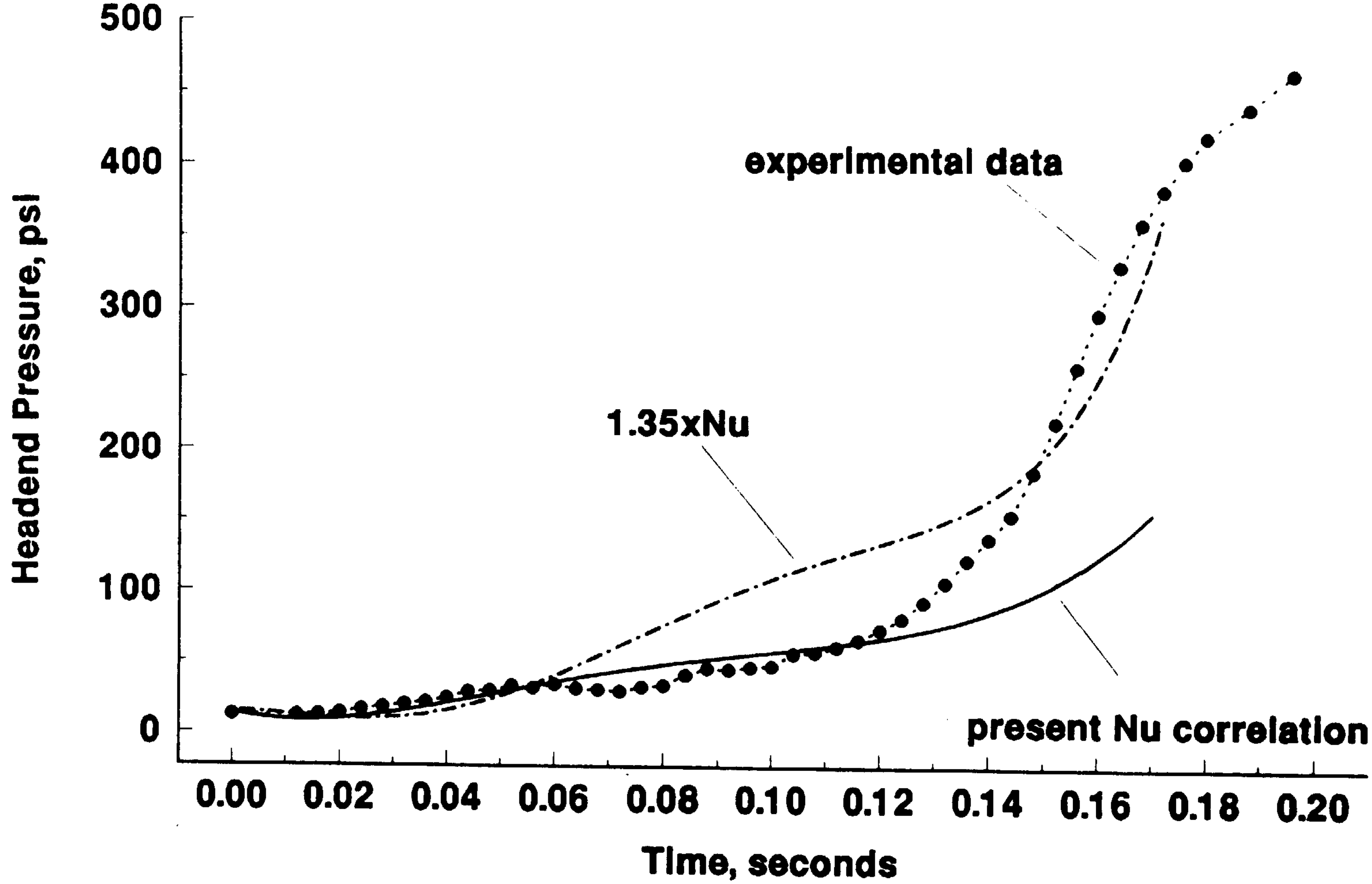

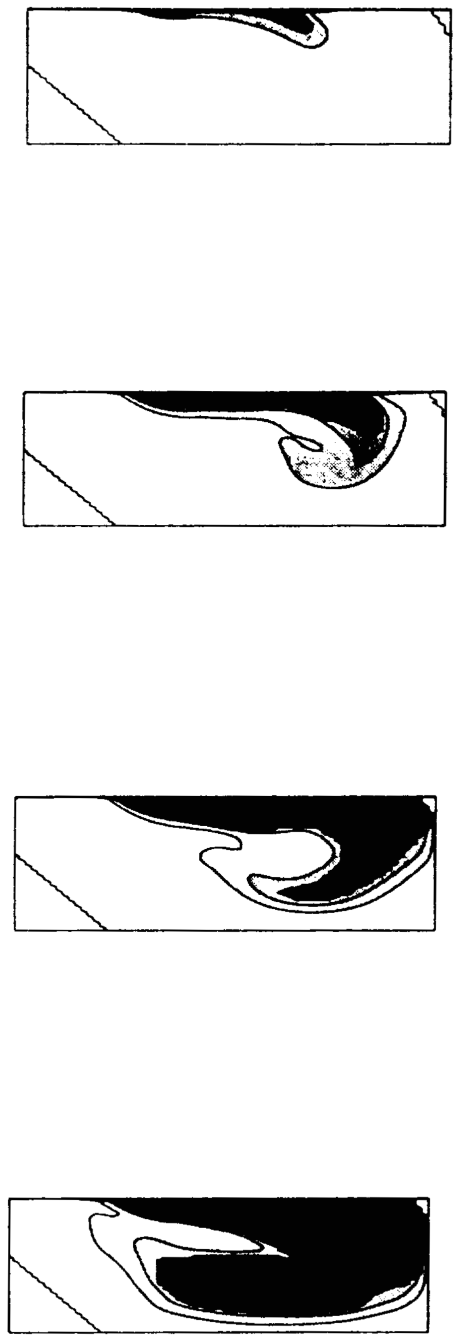

TYPICAL FLAME SPREAD CHARACTERISTICS: SINGLE PORT IGNITER

Conclusions: Work-to-Date

- Correlation between the convection heat transfer model utilized and the measured (cold flow) values of heat transfer is generally good.

- For the single port igniter, the heat transfer model utilized increasingly under-predicts the heat transfer as igniter pressure increases.

- For the 45° igniter with no center port, the heat transfer model under-predicts the heat transfer for all igniter pressures, with increasing under-prediction as igniter pressure increases.

- There appears to be a direct correlation between igniter pressure and an average Reynolds number in the star grain slot. This may lead to a simple method for modifying the convection heat transfer correlation.

- Calculated results of pressure-vs-time for the first 200 msec of motor firing of the Space Shuttle SRM tend to support the idea that heat transfer is under-predicted for higher igniter pressures.

AN INTERACTIVE TOOL FOR DISCRETE PHASE ANALYSIS IN TWO-PHASE FLOWS

Frederik J. de Jong and Stephen J. Thoren
Scientific Research Associates, Inc.
Glastonbury, CT

Presented at the
Workshop for Computational Fluid Dynamics Applications
in Rocket Propulsion

April 20-22, 1993

Abstract

Under a NASA MSFC SBIR Phase I effort an interactive software package has been developed for the analysis of discrete (particulate) phase dynamics in two-phase flows in which the discrete phase does not significantly affect the continuous phase. This package contains a Graphical User Interface (based on the X Window system and the Motif™ tool kit) coupled to a particle tracing program, which allows the user to interactively set up and run a case for which a continuous phase grid and flow field are available. The software has been applied to a solid rocket motor problem, to demonstrate its ease of use and its suitability for problems of engineering interest, and has been delivered to NASA Marshall Space Flight Center.

I. Introduction

Multiphase flow effects in liquid and solid propulsion systems have profound implications on performance and durability. For example, the dynamics of aluminum oxide particulates in an SRM affects the slag accumulation, thereby affecting the performance. A second example is particulate impingement on the motor casing and nozzle affecting durability via its influence on the thermal load on the insulator. The effect of the discrete phase on performance and durability can be very significant even when the concentration of the discrete phase is low enough to not alter the continuous phase flow field in a significant manner. Under the present effort a workstation-based analysis tool has been developed which can be used by analysts and designers to interactively assess the discrete phase effects during the development and testing of rocket propulsion systems. The workstation based software uses a Lagrangian analysis for the discrete phase motion and includes a Graphical User Interface allowing the user to interactively change the relevant parameters to conduct parametric studies. To demonstrate the suitability of the interactive software and its ease of use, it has been successfully applied to a two-dimensional solid rocket motor test problem.

The software consists basically of two parts: (i) the Graphical User Interface for input/output, and (ii) the computational analysis for the discrete phase dynamics. As description of these is given below.

II. Discrete Phase Analysis and Governing Equations

The present analysis is based on the Lagrangian analysis described by de Jong et al. [1]. Although originally part of a fully coupled two-phase flow analysis (see, for example, Madabhushi et al. [2] or de Jong and Sabnis [3]), this analysis has been adapted for stand-alone use, and does not, in its current form, depend on any flow solver. For a given computational grid and

continuous phase flow field, the stand-alone particle code integrates a Lagrangian equation of motion for each particle. A brief description of its relevant features is presented below.

II.1 Equation of Motion

The equation of motion for a particle can be written in the form

$$\frac{d^2\mathbf{X}}{dt^2} = \frac{\mathbf{F}}{m} \tag{1}$$

where **X** is the position vector of the particle, m is the particle mass, and **F** is the total force acting on the particle. In general, **F** contains "body" forces, such as those due to gravity or electro-magnetic fields, and the force acted upon the particle by the fluid (F_p). Integration of Eq. (1) yields

$$\frac{d\mathbf{X}}{dt} = \int_{t_0}^{t} \frac{\mathbf{F}}{m}\, d\tau + \left.\frac{d\mathbf{X}}{dt}\right|_{t_0} \tag{2}$$

At this stage a coordinate transformation **Y** = **Y**(**X**) is introduced to transform the equation of motion into the computational coordinate space corresponding to the grid used for the continuous phase analysis, i.e.

$$y^j = y^j(x_1, x_2, x_3) \qquad (j = 1,2,3)$$

where y^j are the computational coordinates (the components of **Y**) used in the continuous phase analysis and x_i are the physical coordinates (the components of **X**). Let **J** be the inverse of the transformation matrix, i.e. let **J** be the matrix with elements J_{ij}, where

$$J_{ij} = \frac{\partial y^i}{\partial x_j}$$

Then

$$\frac{d\mathbf{Y}}{dt} = \mathbf{J}\,\frac{d\mathbf{X}}{dt} \tag{3}$$

Substituting Eq. (2) into Eq. (3) yields

$$\frac{d\mathbf{Y}}{dt} = \mathbf{J}\int_{t_0}^{t} \frac{\mathbf{F}}{m}\, d\tau + \mathbf{J}\left.\frac{d\mathbf{X}}{dt}\right|_{t_0} \tag{4}$$

This equation can be integrated (assuming that **J**, **F**, and m are constant over the integration interval Δt) to yield

$$\Delta \mathbf{Y} = \tfrac{1}{2}\Delta t^2 \mathbf{J} \frac{\mathbf{F}}{m} + \Delta t \mathbf{J} \mathbf{U}_p |_{t_0} \tag{5}$$

where $\Delta\mathbf{Y}$ is the change in the coordinate space position vector (i.e. **Y**) during the period Δt. Equation (5) then provides the change in particle location (in computational space) for a given time interval Δt and starting location corresponding to $t = t_0$.

The transformation of the Lagrangian equations of motion from the physical coordinates to the computational, body-fitted coordinates used for the continuous phase analysis offers some very significant advantages. Since the motion of a particle is tracked in the computational coordinate space (via Eq. (5)), no searching is needed for the mesh cell in which a computational particle resides. This facilitates the computation of the force on the particle in the Lagrangian equation of motion. Also, tracking the motion in the computational space allows the estimation of the time taken by the particle to cross the boundaries of the grid cell where it currently resides. This estimate is used in the selection of sub-time steps (described below) used in integrating the equation of motion. Finally, the search for boundaries is simplified, which makes it easier to determine whether a particle has reached a solid boundary and should be reflected, or a particle has left the computational domain and should be omitted. This latter advantage is of major importance when the number of boundaries is large (see de Jong et al. [1] and McConnaughey et al. [4] for an interesting application).

Each particle is moved through the domain by integrating its Lagrangian equation of motion using a sequence of "sub-time steps" Δt_s. These sub-time steps are chosen as the minimum time for the particle to cross the nearest cell boundary and a kinematic time scale defined as a fraction (e.g. 0.1) of the ratio of particle velocity to acceleration. It should be noted that, for accuracy reasons, the maximum allowable sub-time step could be significantly different for different particles depending upon their location, mass, etc. The sub-time step approach has been adopted to provide an accurate representation of the particle motion, since at the end of each sub-time step the force on the particle is updated using the particle attributes and the continuous phase values corresponding to the new particle locations.

II.2 Force on a Particle

In Equation (1), the force **F** on the particle has been assumed to consist of a drag force, a gravitational acceleration force, and a force due to the pressure gradient in the liquid,

$$\mathbf{F} = \mathbf{F}_D + m\mathbf{g} - \frac{m}{\rho_p} \nabla p \tag{6}$$

where **g** is the (gravitational) acceleration vector, ρ_p is the particle density, p is the local pressure in the continuous phase and where the drag force $\mathbf{F}_D$ is given by

$$\mathbf{F}_D = \frac{1}{8} C_D \rho \pi D_p^2 |\mathbf{U}_R| \mathbf{U}_R \tag{7}$$

Here ρ is the density of the continuous phase, D_p is the particle diameter and $\mathbf{U}_R$ is the velocity of the particle relative to the continuous phase velocity. C_D is the drag coefficient, which is related to the particle Reynolds number

$$Re_p = \frac{\rho U_R D_p}{\mu} \tag{8}$$

(where μ is the viscosity of the continuous phase) via the expression

$$C_D = \frac{24}{Re_p}\left[1 + \frac{1}{6} Re_p^{2/3}\right] \qquad \text{for } Re_p < 1000$$

$$= 0.424 \qquad \text{for } Re_p > 1000 \tag{9}$$

The second term on the right hand side of Eq. (6) represents the gravitational (or other acceleration) effects, which could be significant for solid particles or liquid droplets in a gaseous continuous phase. The effect of buoyancy, on the other hand, which is included in the last term of Eq. (6), may not always be of importance.

II.3 Discrete Phase Turbulent Dispersion

In two-phase flows, the continuous phase turbulence results in dispersion of the discrete phase. This process is modeled by some researchers (see Abbas et al. [5]) by adding a "diffusion" velocity obtained from some phenomenological model to the particle velocity. In the present analysis, this effect is modeled by evaluating the fluid force on a particle using an instantaneous continuous phase velocity field rather than a mean velocity field. The instantaneous velocity components are obtained by adding stochastically generated turbulent velocity components to the mean velocity field for the continuous phase. If the continuous phase turbulence is assumed to be isotropic, and the random turbulent velocity components are assumed to have a Gaussian probability distribution with standard deviation σ, then

$$\sigma = \left[\frac{2k}{3}\right]^{2/3} \tag{9}$$

where k is the turbulent kinetic energy, and the random turbulent velocity components can be obtained as

$$\left[\frac{4k}{3}\right]^{1/2} \operatorname{erf}^{-1}(2x - 1) \tag{10}$$

where x is random variable with uniform probability distribution between 0 and 1 (i.e. x is a random number between 0 and 1). This latter result follows from the observation that if x is random variable with uniform probability distribution between 0 and 1, then $F^{-1}(x)$ is a random variable whose cumulative probability function is F. This technique offers a way to treat the effect of gas phase turbulence on the particulate phase dispersion in a manner which is less empirical than the techniques traditionally used with Eulerian-Eulerian analyses. Similar techniques for modeling the discrete phase turbulent dispersion have been used by, for example, Dukowicz [6], Gosman and Ioannides [7], and Hotchkiss [8].

If the turbulent energy k is not directly available, but an eddy viscosity μ_T and a mixing length ℓ are (for example, when a mixing length turbulence model is used in the continuous phase analysis), then k can be obtained from the relation

$$\mu_T = C_\mu^{\frac{1}{4}} \rho k^{\frac{1}{2}} \ell \tag{12}$$

where C_μ is a function of μ_T that can be determined from the expression

$$C_\mu = 0.09 \exp\left\{-\frac{2.5}{1 + 0.02 \frac{\mu_T}{\mu} C_\mu}\right\} \tag{13}$$

(cf. Launder and Spalding [10]).

III. Graphical User Interface

The Graphical User Interface (GUI) developed under the present effort is based on the X Window system and the Motif™ tool kit. Some advantages to using X and Motif™ include improved code portability, maintaining a consistent look and feel between applications and the ability to run the interface on one machine and to display it on another. Its portability was verified by compiling and running the GUI both on SGI 4D/25TG and IBM RS/6000 Workstations. The main window of the GUI contains a menubar with several pull-down menus (Fig. 1) that allow the user to perform functions associated with file I/O, problem specification, or output display. In most cases, selection of a menu item from a pull-down menu opens up a property window that provides the user with the requested input items. Depending on the item, user input is possible via type-ins, toggle buttons, selection from lists, or graphically by using the mouse. Some of the features of the GUI are:

(i) Grid and flow field files can be used in standard PLOT3D-type format.

(ii) Boundaries can be defined in the computational domain by adding or deleting "zones" or "blocks". Here a "zone" is defined as a region inside which there is a flow field, while a "block" is defined as a solid region (without a flow field). These "zones" or "blocks" can be specified graphically by using the mouse (Figs. 2-3). This approach allows the user to define complex (2-D) geometries without the need for code modifications.

(iii) To define the boundary type (such as inlet/exit, wall, or symmetry line) and the properties (restitution and friction coefficients) of a solid wall, this boundary can be selected by "clicking" on it. The boundary type can then be set by choosing the appropriate one from a menu (Fig. 4), while the relevant properties can be typed in.

(iv) The injection locations can be specified graphically by clicking on the desired grid points in the computational domain (Fig. 5). The particle properties at these locations (such as the particle velocity, its radius and its density) can be specified via type-ins. By defining default properties, only those properties that change from one particle to the next have to be typed in.

(v) Wherever possible, error and consistency checks are performed by the interface on user input prior to running the particle code. This helps to produce a more accurate input file and prevents needless execution of the particle code.

The Graphical User Interface is coupled to the particle code, so that it can be used both to set up and to run a particular problem. Execution of the particle tracking program under the GUI displays the particle traces while they are being computed; once the program is finished, the image can be manipulated interactively. A complete description of all the functions included in the GUI and guidelines for setting up and running a new case can be found in the User's Manual; on-line help is available for most functions.

IV. Application and Results

To demonstrate the suitability of the software package developed under the present effort and its ease of use for solid rocket motor applications, the Particle Trace Interface was used to set up and run particle trajectories in the so-called super BATES motor. The geometry of this motor is shown in Fig. 6. The flow field in this motor was computed with SRA's MINT code, on the grid shown in Fig. 6. This grid contains two "cut-out" regions, adjacent to the grain surface and the nozzle wall. The "full" grid is shown in Fig. 7. This grid, and the flow field, were then used as input to the Particle Trace Interface (PTI). Using the PTI, the boundaries of the computational domain were constructed by putting two "blocks" into the "zone" that comprised the full grid (cf. Fig. 5). Alternatively, it would have been possible to build up the domain as the union of three "zones", corresponding to the combustion chamber, the slot region, and the nozzle region. At this point it should be noted that Fig. 7 was actually obtained by displaying the grid in the PTI after it had been read in, while Fig. 6 was obtained by displaying the grid after the boundaries had been specified. Next, the PTI was used to define the "boundary conditions" (insofar as these are needed to determine the behavior of a particle when it reaches a boundary) and a set of particle injection locations (the solid circles in Fig. 5). Particle and flow field information was specified to complete the problem setup, after which the PTI was used to (interactively) execute the particle tracing code. Figs. 8 and 9 show the resulting particle traces (again obtained from the PTI). The whole operation was completed without exiting from the PTI.

Acknowledgements

This research was supported by the NASA George C. Marshall Space Flight Center under Contracts NAS8-39337 and NAS8-38959.

References

1. De Jong, F. J., Sabnis, J. S., and McConnaughey, P. K.: "A Combined Eulerian-Lagrangian Two-Phase Flow Analysis of SSME HPOTP Nozzle Plug Trajectories: Part I - Methodology", AIAA Paper 89-2347, AIAA/ASME/SAE/ASEE 25th Joint Propulsion Conference, July 1989.

2. Madabhushi, R.K., Sabnis, J.S., de Jong, F.J. and Gibeling, H.J.: "Calculation of Two-Phase Aft-Dome Flowfield in Solid Rocket Motors," *J. Propulsion and Power*, Vol. 7, 1991, pp. 178-184.

3. de Jong, F.J. and Sabnis, J.S.: "Simulation of Cryogenic Liquid Flows with Vapor Bubbles," AIAA Paper 91-2257, AIAA/SAE/ASME/ASEE 27th Joint Propulsion Conference, June 1991.

4. McConnaughey, P. K., Garcia, R., de Jong, F. J., Sabnis, J. S., and Pribik, D.A.: "A Combined Eulerian-Lagrangian Two-Phase Flow Analysis of SSME HPOTP Nozzle Plug Trajectories: Part II - Results", AIAA Paper 89-2348, AIAA/ASME/SAE/ASEE 25th Joint Propulsion Conference, July 1989.

5. Abbas, A. S., Kousa, S. S. and Lockwood, F. C.: "The Prediction of the Particle Laden Gas Flows," *Proc. 18th Symposium on Combustion,* Combustion Institute, 1981, pp. 1427-1438.

6. Dukowicz, J. K.: "A Particle-Fluid Model for Liquid Sprays", *J. Computational Physics*, Vol. 35, 1980, pp. 229-253.

7. Gosman, A. D. and Ioannides, E.: "Aspects of Computer Simulation of Liquid-Fueled Combustors," *J. Energy*, Vol. 7, 1983, pp. 482-490.

8. Hotchkiss, R. S.: "The Numerical Modeling of Air Transport in Street Canyons", Report LA-UR-74-1427, Los Alamos Scientific Laboratory, 1974.

9. Launder, B.E. and Spalding, D.B.: "The Numerical Computation of Turbulent Flows," *Computer Methods in Applied Mechanics and Engineering*, Vol. 3, 1974, pp. 269-289.

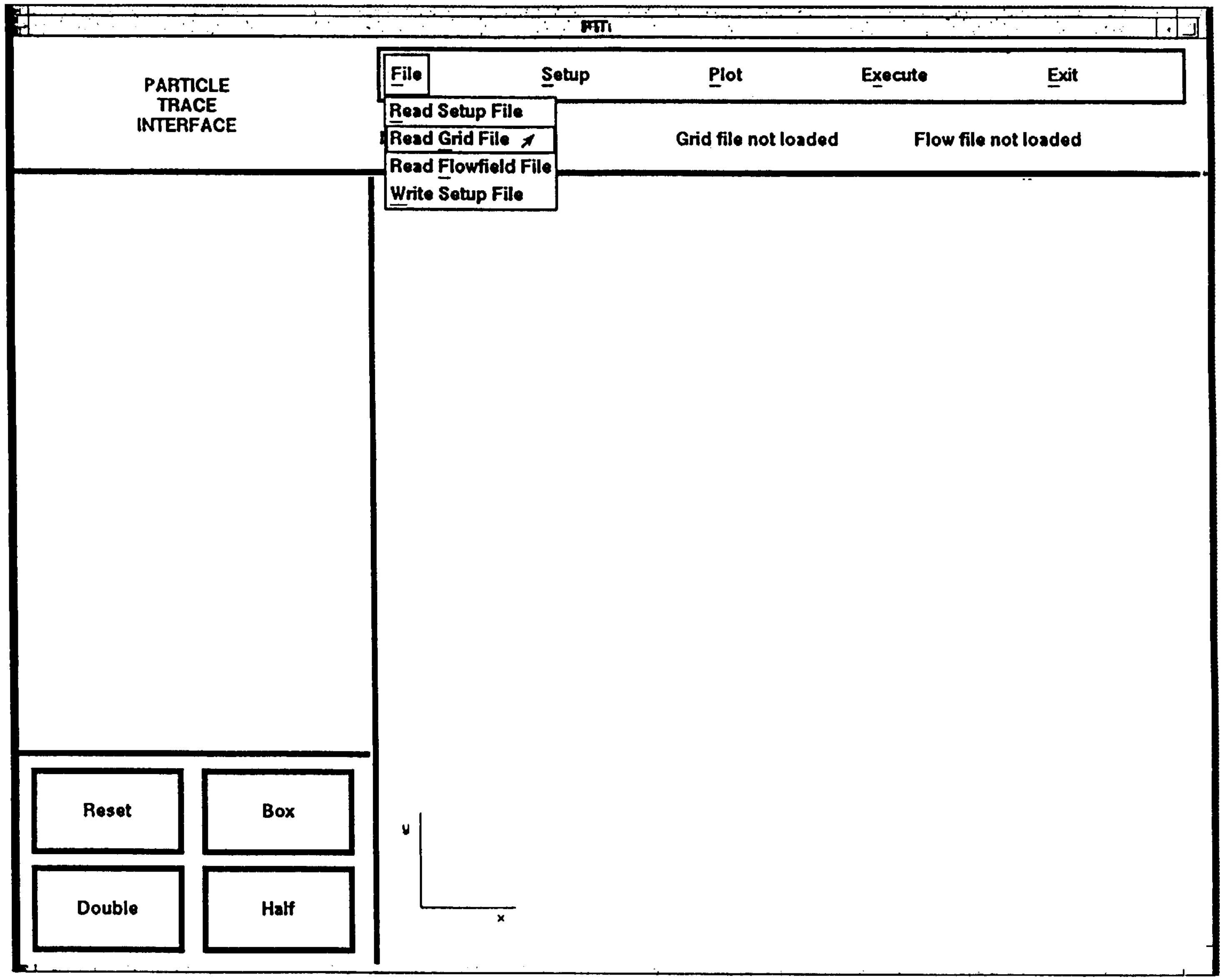

Figure 1. Main Panel of the Particle Trace Interface with the File Pulldown Menu.

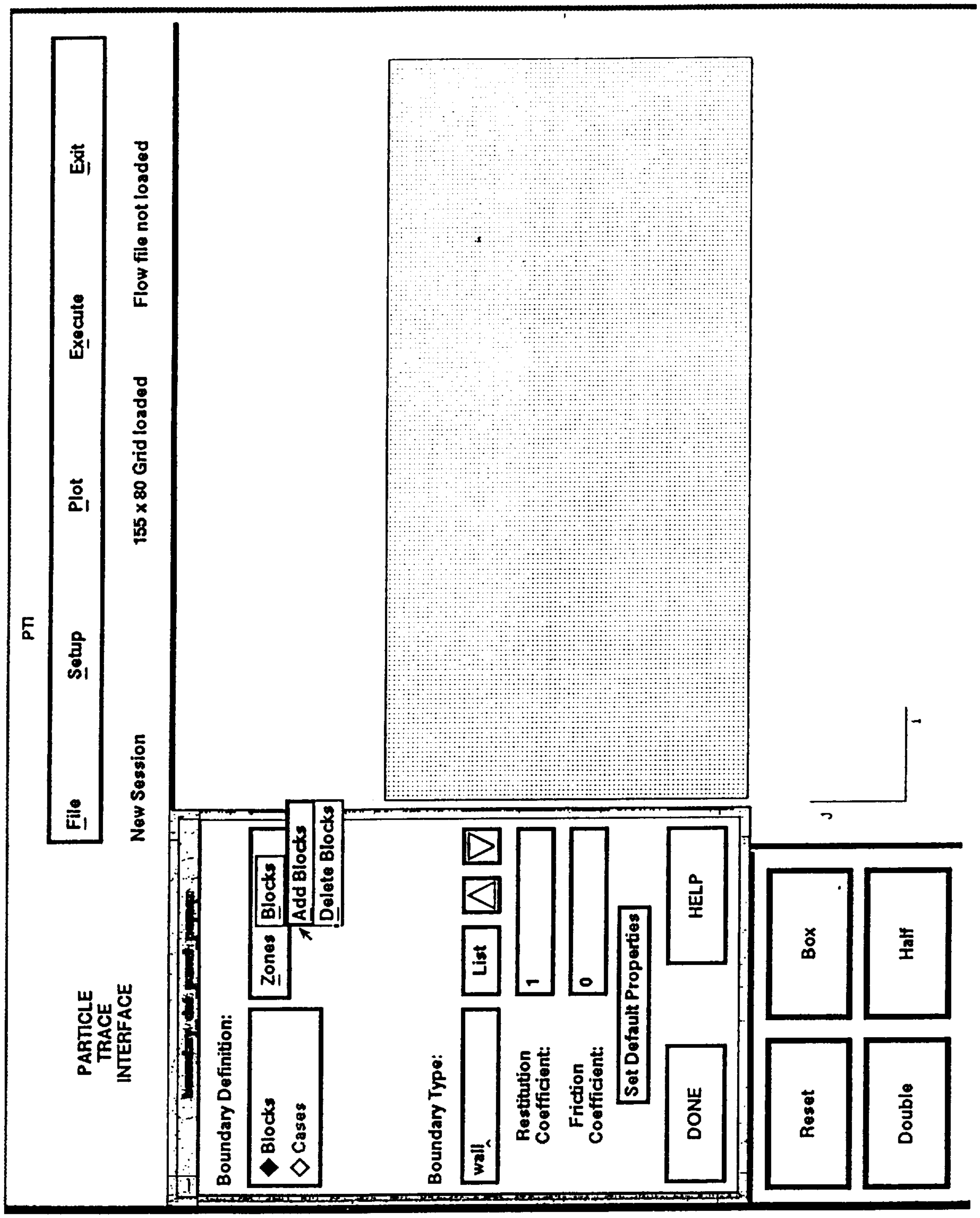

Figure 2. The Boundary Definition Window with the Blocks Pulldown Menu.

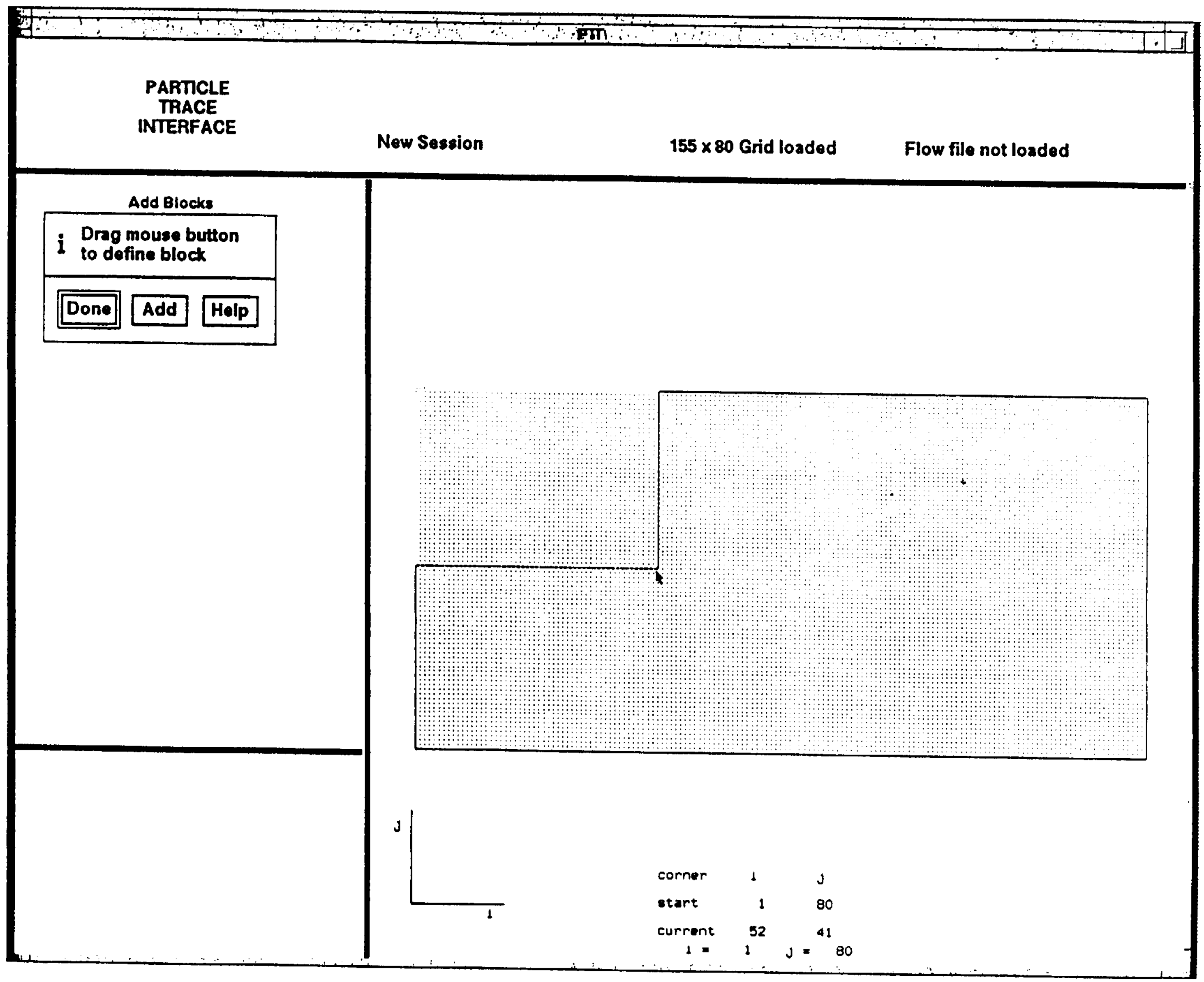

Figure 3. Adding a Block.

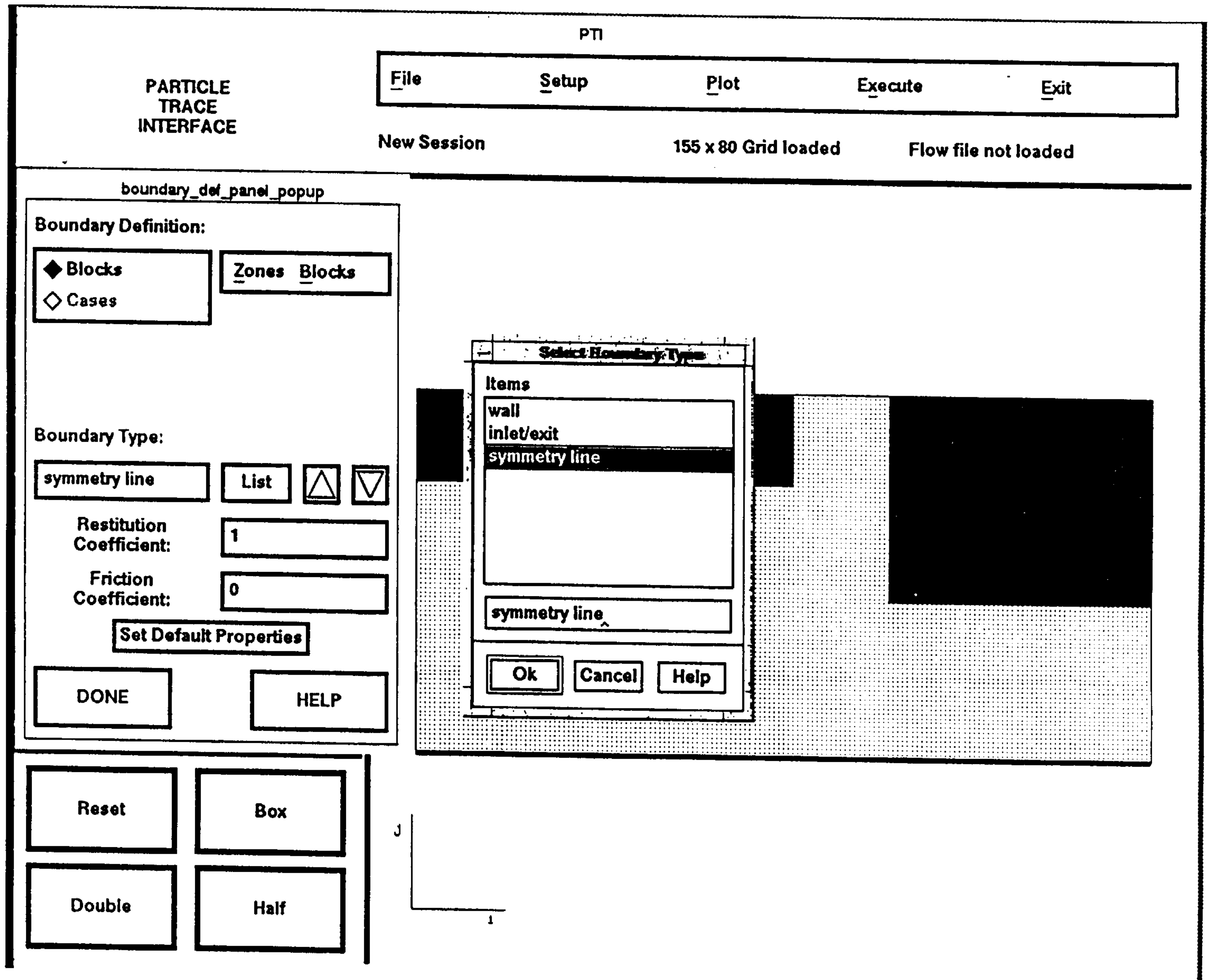

Figure 4. The Boundary Type Selection Window.

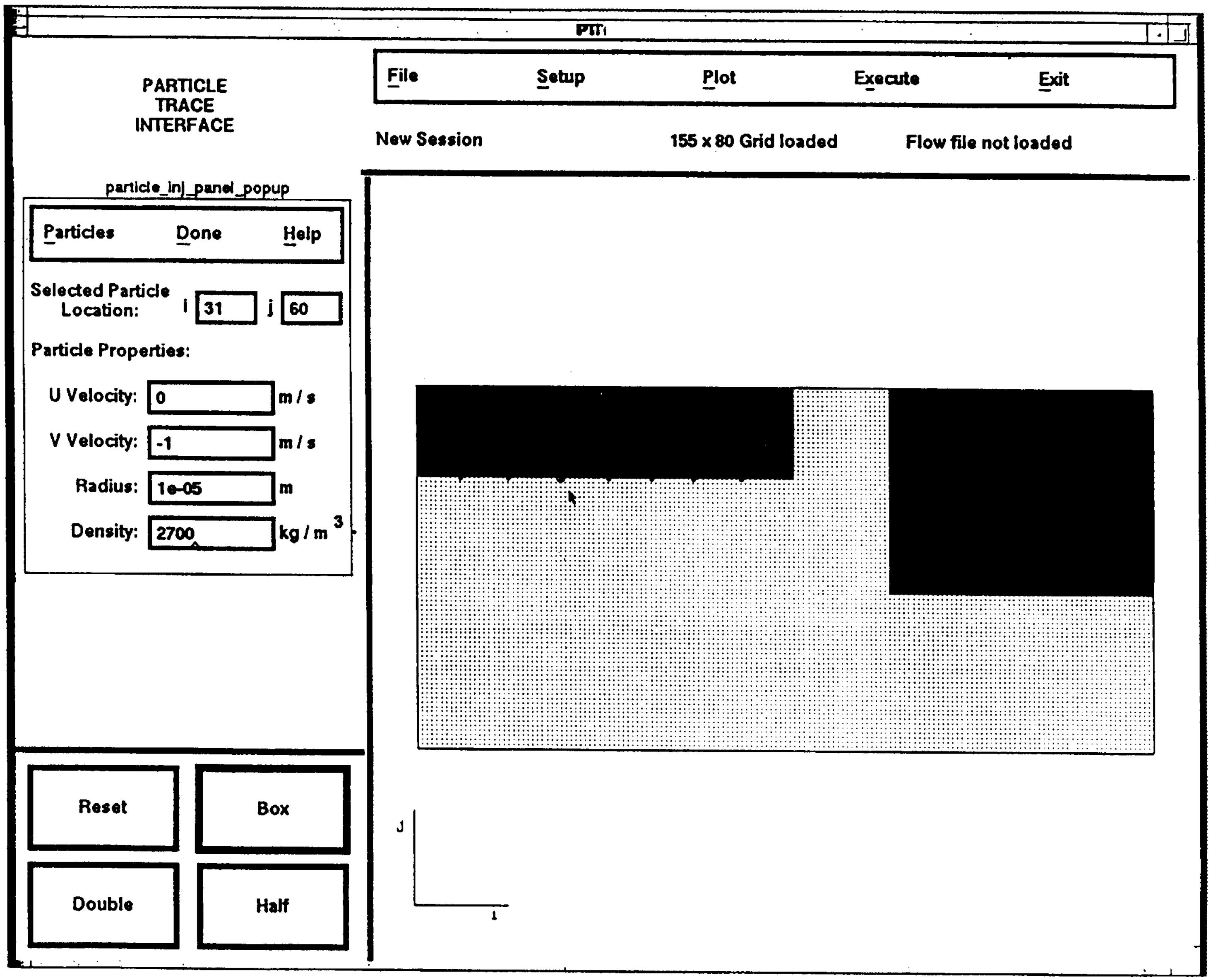

Figure 5. Display of Particle Injection Locations (Solid Circles).

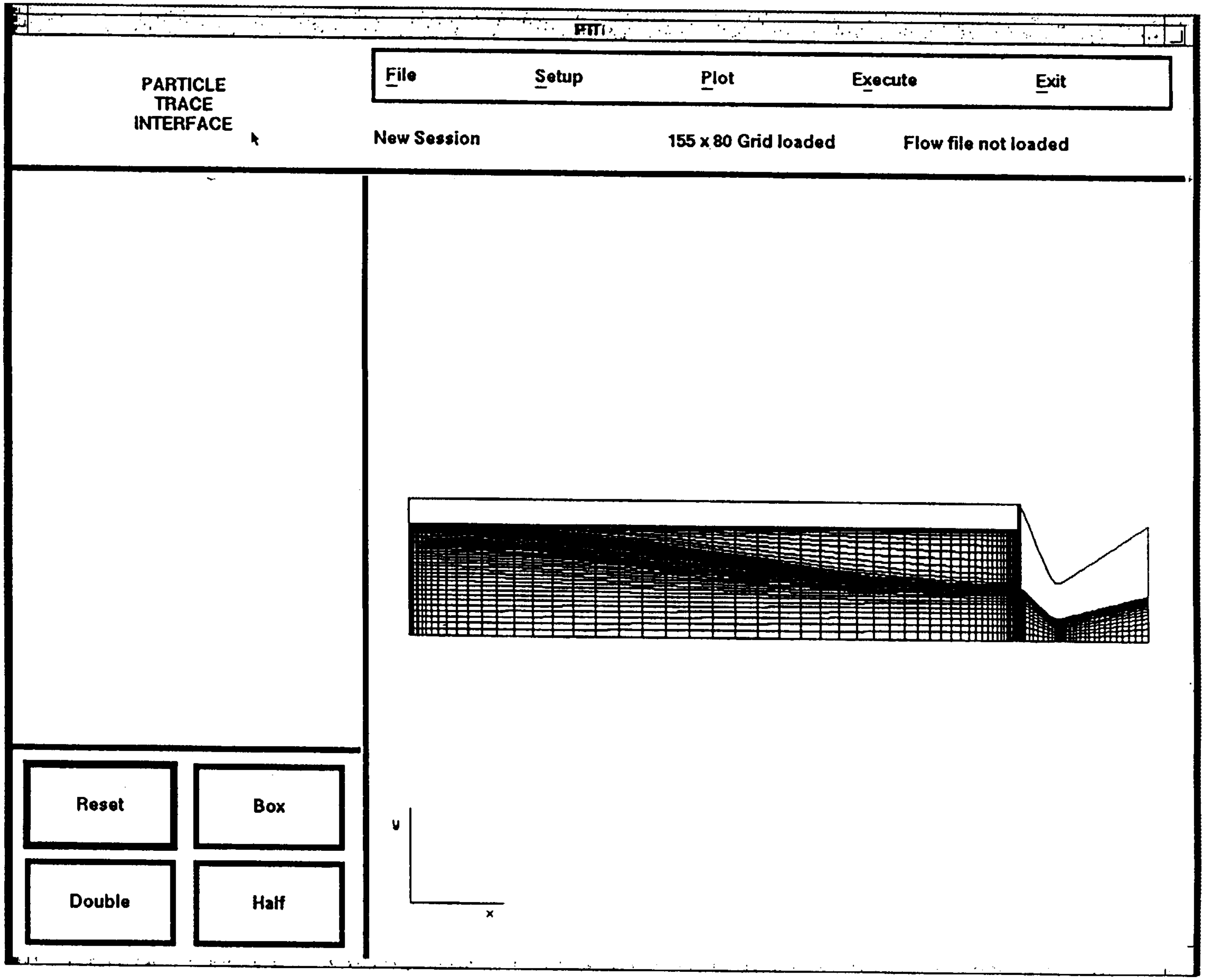

Figure 6. Super BATES Motor Geometry an Grid in the Physical Domain with Blocked-out Regions.

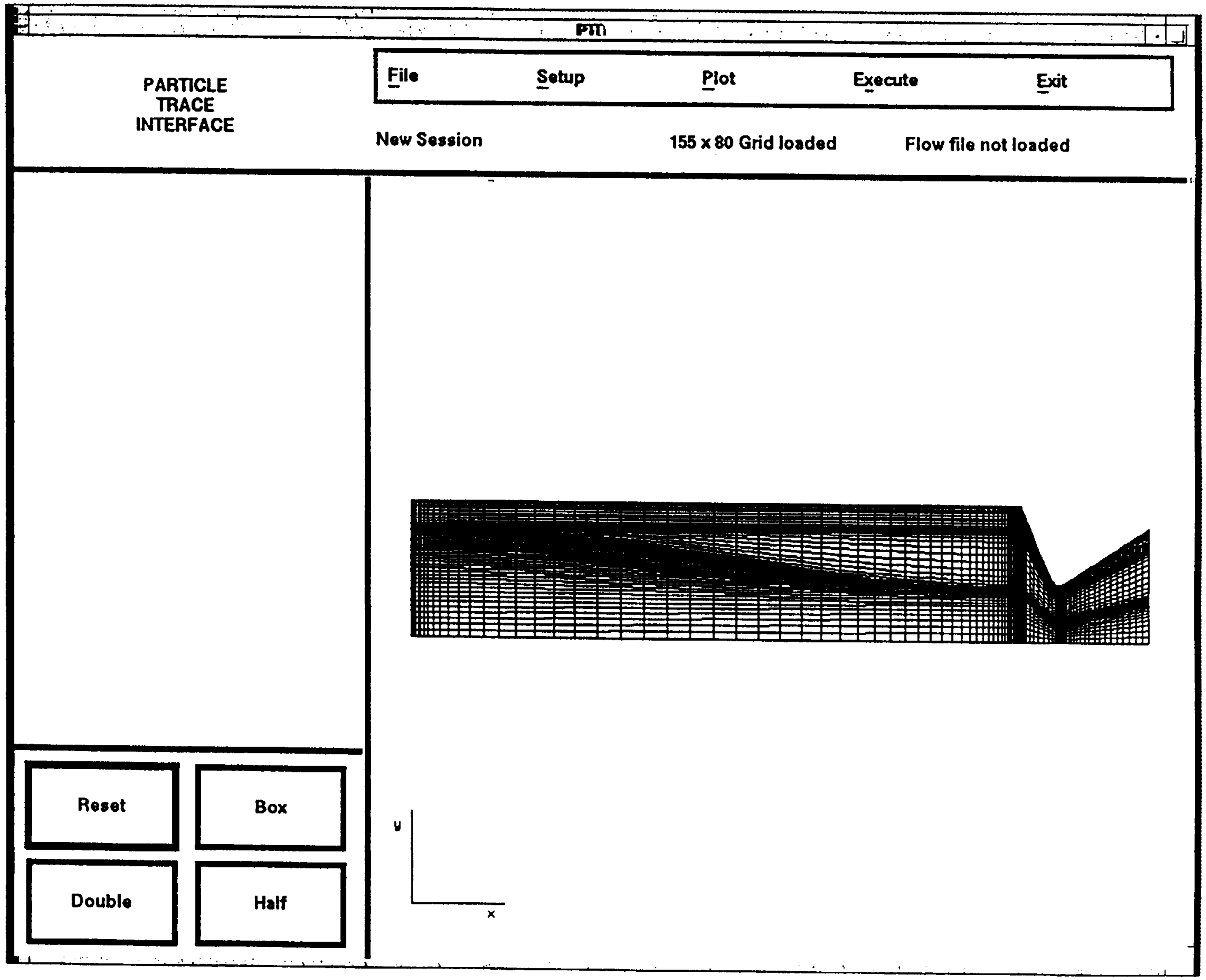

Figure 7. Full Grid in the Physical Domain.

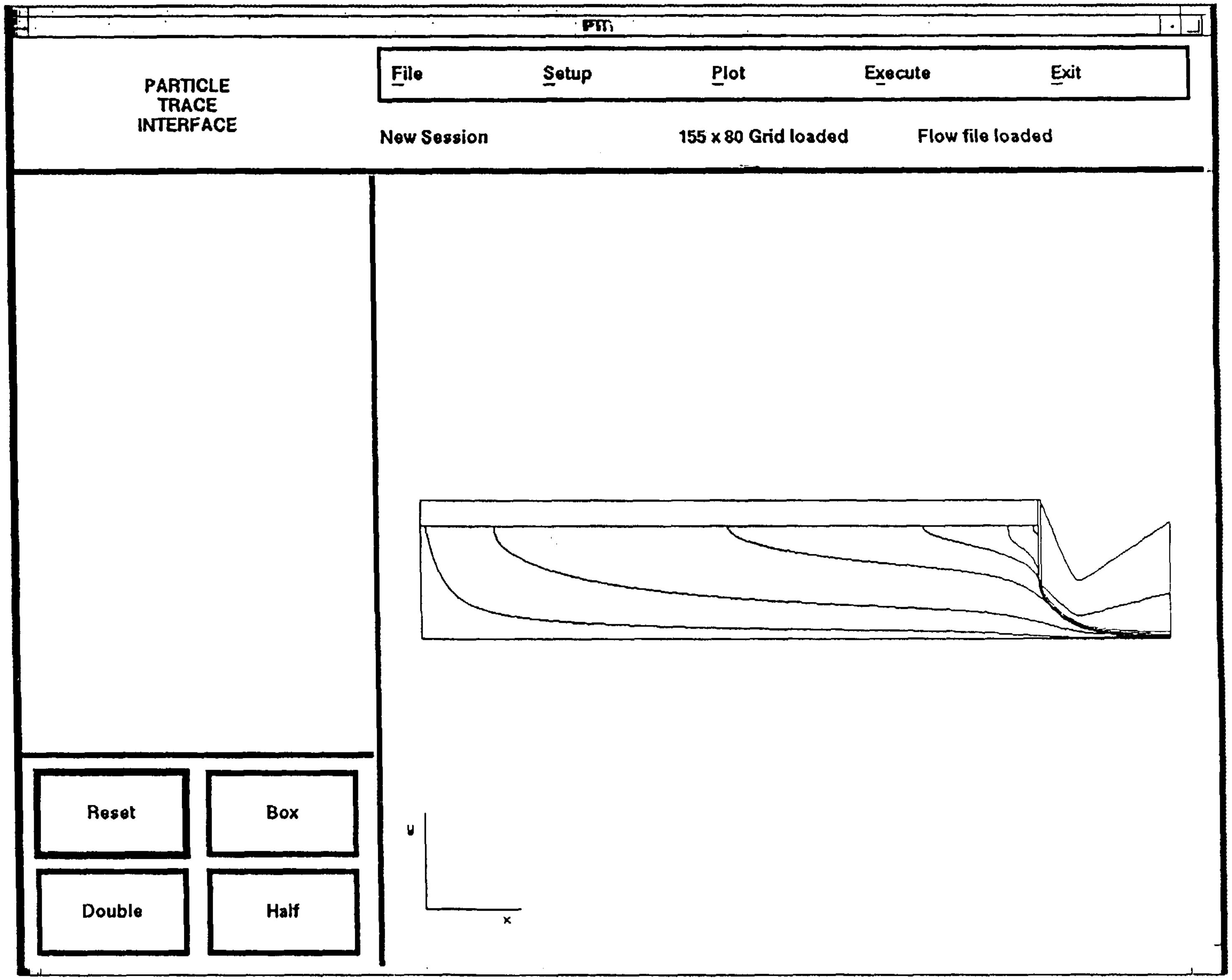

Figure 8. Particle Trajectories.

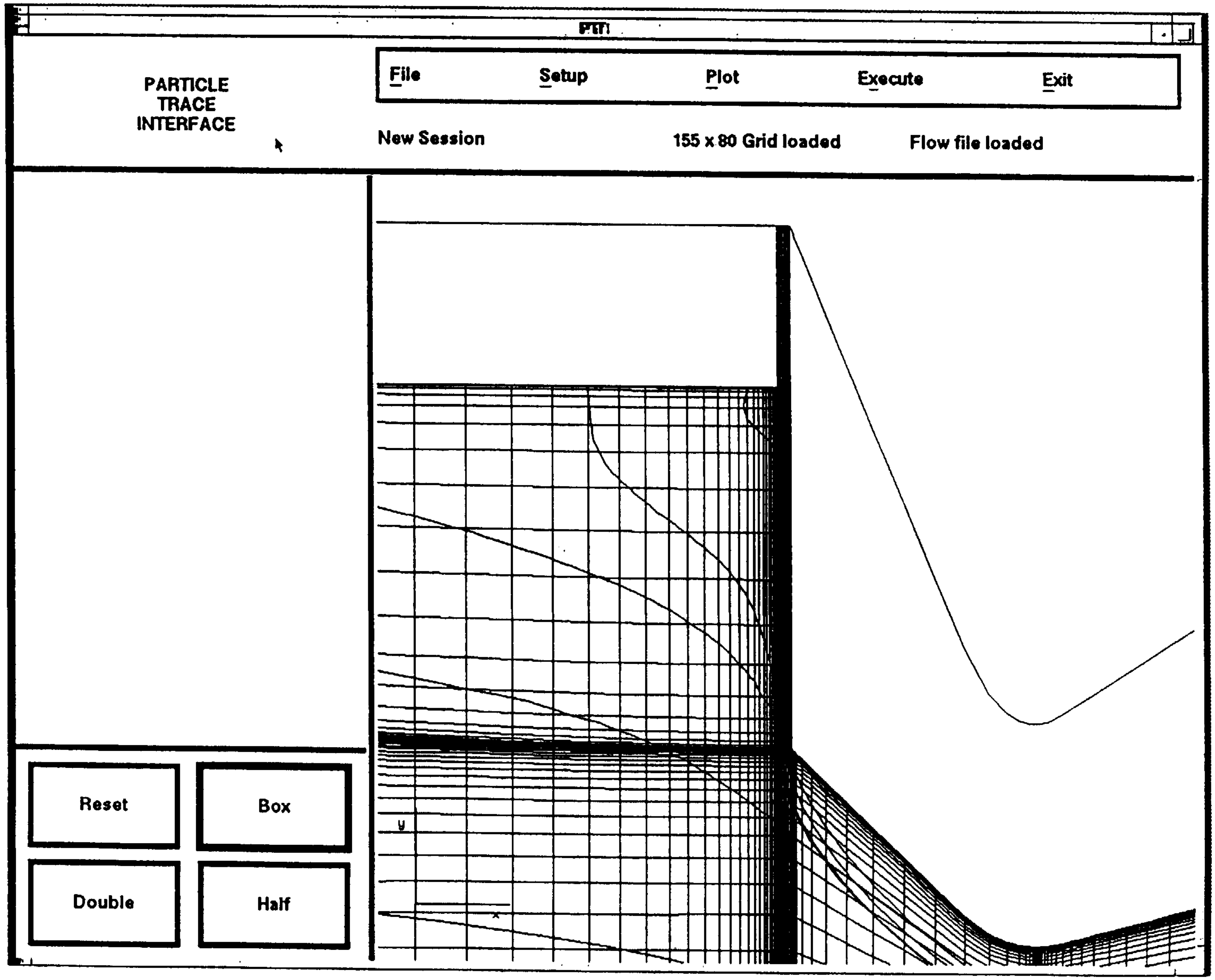

Figure 9. Particle Traces Overlaid on the Grid;
Enlarged View near the Aft End of the Motor.

N95- 23642

Flowfield Characterization in a LOX/GH_2 Propellant Rocket

S. Pal, M. D. Moser, H. M. Ryan, M. J. Foust and R. J. Santoro

Propulsion Engineering Research Center
and
Department of Mechanical Engineering
The Pennsylvania State University
University Park, PA 16802

Statement of Problem

There is a critical shortage of data pertaining to the flowfield characteristics in a liquid propellant rocket chamber for hot-fire conditions. For a liquid oxygen (LOX)/gaseous hydrogen (GH_2) propellant combination, either shear or swirl coaxial injectors are typically used to atomize the liquid propellant into drops. Understanding the atomization process under hot-fire conditions represents the first step in understanding the subsequent processes of vaporization, mixing and combustion. The flowfield here is two-phase and therefore experiments that detail the intact liquid jet, drop size and velocity, and combustion length are necessary for understanding the physics of the problem.

Objective of Work

The objective of the current work is to experimentally characterize the flowfield associated with an uni-element shear coaxial injector burning LOX/GH_2 propellants. These experiments were carried out in an optically-accessible rocket chamber operating at a high pressure ($\approx$400 psia). Quantitative measurements of drop size and velocity were obtained along with qualitative measurements of the disintegrating jet.

Approach

The experiments were conducted at the Cryogenic Combustion Laboratory at Penn State University. This laboratory provides the capability for firing both gaseous and liquid propellant sub-scale rocket engines. A modular rocket chamber which provides extensive optical access was designed for the experiments. The cross-section of the rocket is 50.8 mm (2 in.) square and the chamber length which can be easily varied was 248 mm (9.75 in.). The flowfield downstream of a shear coaxial injector was characterized using laser-based diagnostic techniques. The inner diameter of the LOX post was 3.43 mm (0.135 in.) and the post was recessed 3.78 mm (0.15 in.). The inner diameter of the fuel annulus was 4.19 mm (0.165 in.) and the outer diameter was 7.11 mm (0.28 in.). The nominal LOX and GH_2 flowrates were 0.11 kg/s (0.25 lbm/s) and 0.021 kg/s (0.047 lbm/s) respectively, thus resulting in a nominal O/F ratio of 5.3:1. These flow rates, coupled with the nozzle dimensions yielded a chamber pressure of 2.74 MPa ($\approx$400 psia). The duration of a test run was four seconds.

A Phase Doppler Particle Analyzer (PDPA) was used to measure LOX drop size and velocity at various radial locations for an axial position 63.5 mm (2.5 in.) downstream of the injector face. The measured Sauter Mean diameter (SMD) ranged from 110 μm at the centerline to about 60 μm at a 9.5 mm (0.375 in.) radial location. At greater radial locations, no drops were observed. The results indicate that under hot-fire conditions, the drops formed from the shear coaxial injector are confined to a narrow circumferential region.

Conclusions

These experiments represent the first time that drop sizes have been measured under combusting conditions for cryogenic propellants. These results are, in general, encouraging with respect to applications of laser-based diagnostics to LOX/GH_2 uni-element rocket studies. A comprehensive mapping of the flowfield will need to be completed to gain a thorough understanding of the physics of this complex problem.

Flowfield Characterization in a Liquid Oxygen/Gaseous Hydrogen Propellant Rocket

S. Pal, M. D. Moser, H. M. Ryan, M. J. Foust and R. J. Santoro

The Propulsion Engineering Research Center
The Pennsylvania State University
University Park, PA 16802

11th Workshop for CFD Applications in Rocket Propulsion

April 20-22, 1993

NASA Marshall Space Flight Center
Huntsville, Alabama

PRESENTATION OUTLINE

Motivation

Background

Objective

Experimental

- **Facility**
- **Rocket chamber**
- **Diagnostics**

Results

Summary

MOTIVATION

To obtain fundamental data under well characterized conditions

- **For gaseous propellant rockets**
- **For liquid propellant rockets**
- **For various injector types**

Fundamental data would form the basis for

- **Empirical correlation validation**
- **CFD code validation**

BACKGROUND

Atomization models typically are:

- Anchored to cold flow experimental results

  We and *Re* of cold flow experiments differ by an order of magnitude from actual rocket conditions

  Results have to be extrapolated

- Predicted from analytical models based on linear stability theory

Drop size data for hot-fire conditions would:

- Validate atomization models

- Validate methodology for extending cold flow data to hot flow conditions

- Develop hot-flow correlations for direct use in combustion models

OBJECTIVE

To characterize the flowfield downstream of a shear coaxial injector using LOX/GH_2 propellants under combusting conditions

- **Drop size and velocity measurements using Phase Doppler Interferometry**

- **Laser sheet visualizations of near breakup region**

FACILITY CAPABILITIES

Propulsion Engineering Research Center
Cryogenic Combustion Laboratory

Propellants:

- Gaseous Hydrogen
- Gaseous Methane
- Gaseous Oxygen
- Liquid Oxygen

Flow rates (maximum):

Gaseous oxygen:	0.1 lbm/s
Liquid oxygen:	1.0 lbm/s
Gaseous hydrogen:	0.25 lbm/s

Typical mixture ratios: 4 - 8

Maximum chamber operating pressure: 1000 psi

Typical test time: 1 - 5 s

Longer tests subject to hardware cooling and gas supply specifications

PENN STATE ROCKET

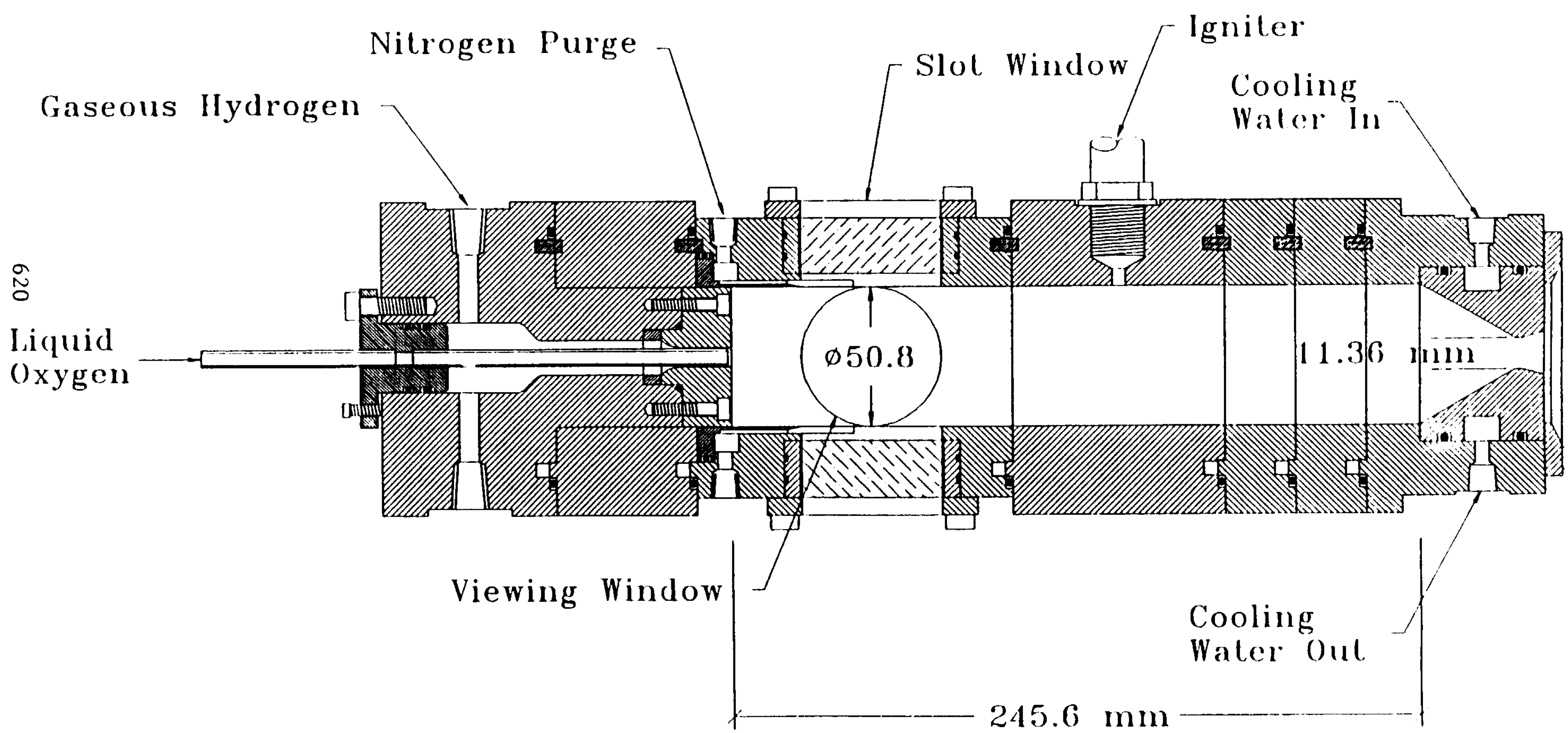

Cross-Sectional View of the Windowed Rocket Chamber

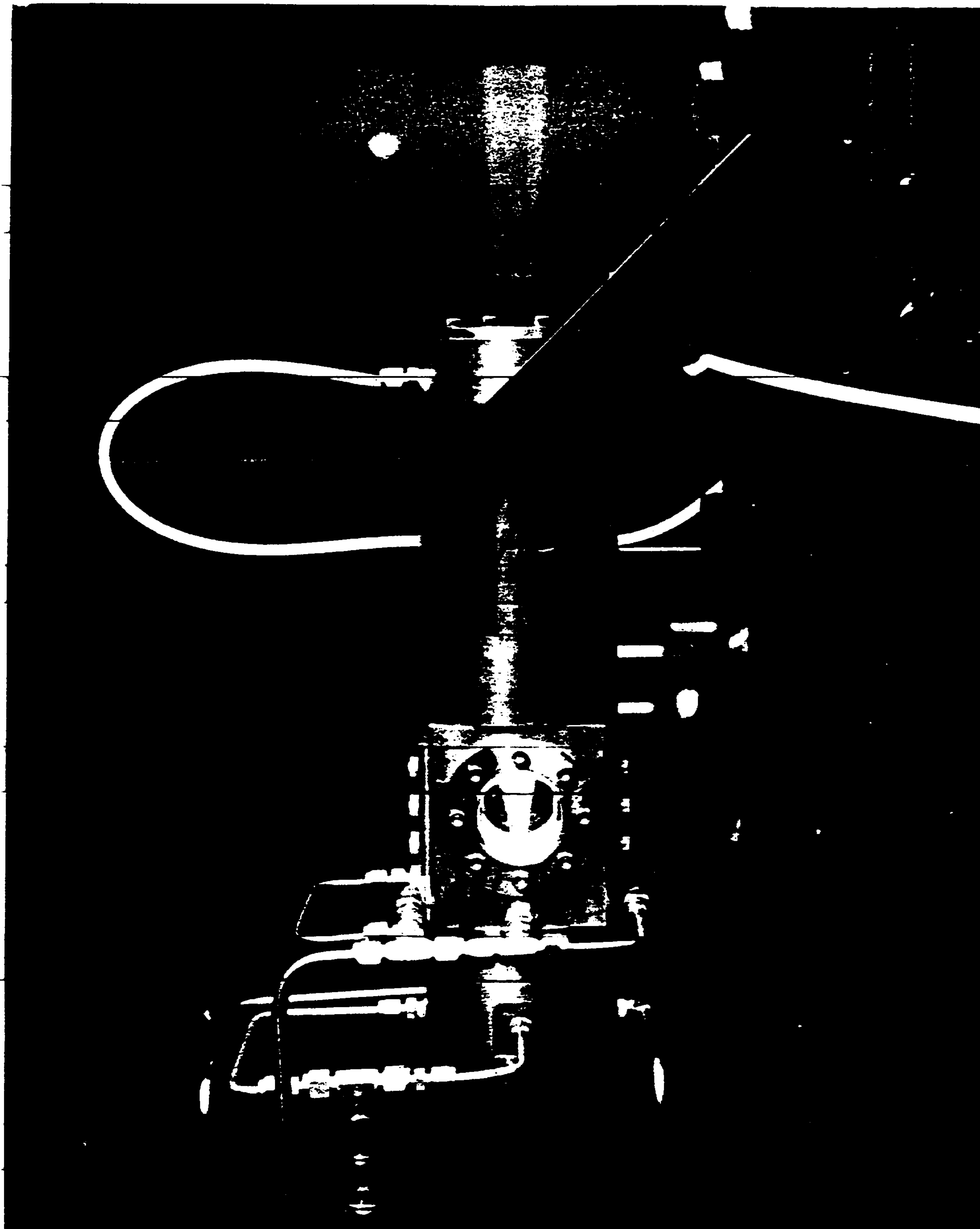

EXPERIMENTAL SCHEMATIC

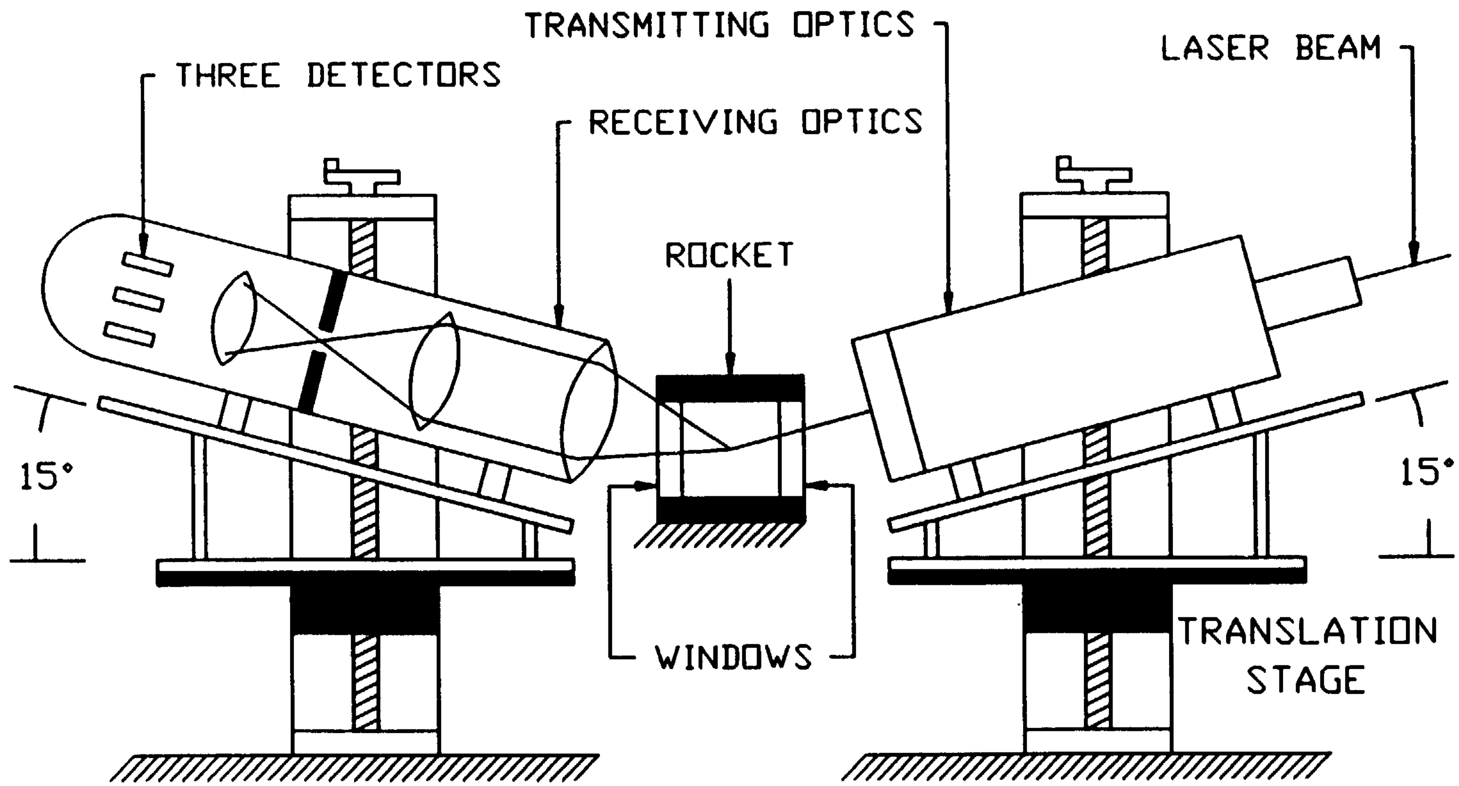

THIS PAGE LEFT BLANK INTENTIONALLY

TEST CONDITIONS

Chamber pressure	**2.67 Mpa (387 psia)**
LOX flowrate	**0.112 kg/s (0.245 lbm/s)**
GH_2 flowrate	**0.021 kg/s (0.045 lbm/s)**
Mixture ratio (O/F)	**5.4**
LOX velocity	**13.5 m/s (44.1 ft/s)**
GH_2 velocity	**381 m/s (1250 ft/s)**
Momentum ratio (F/O)	**5.22**
Velocity ratio (F/O)	**28.3**
Re[1]	**5.03×10^5**
We[2]	**2.06×10^5**

[1] $Re = \rho_l U_l \, d / \mu_l$
[2] $We = \rho_g (U_g - U_l)^2 d / \sigma$

MEAN DROP DIAMETER VS. RADIAL LOCATION
Z=63.5 mm (Z/d=18.5)

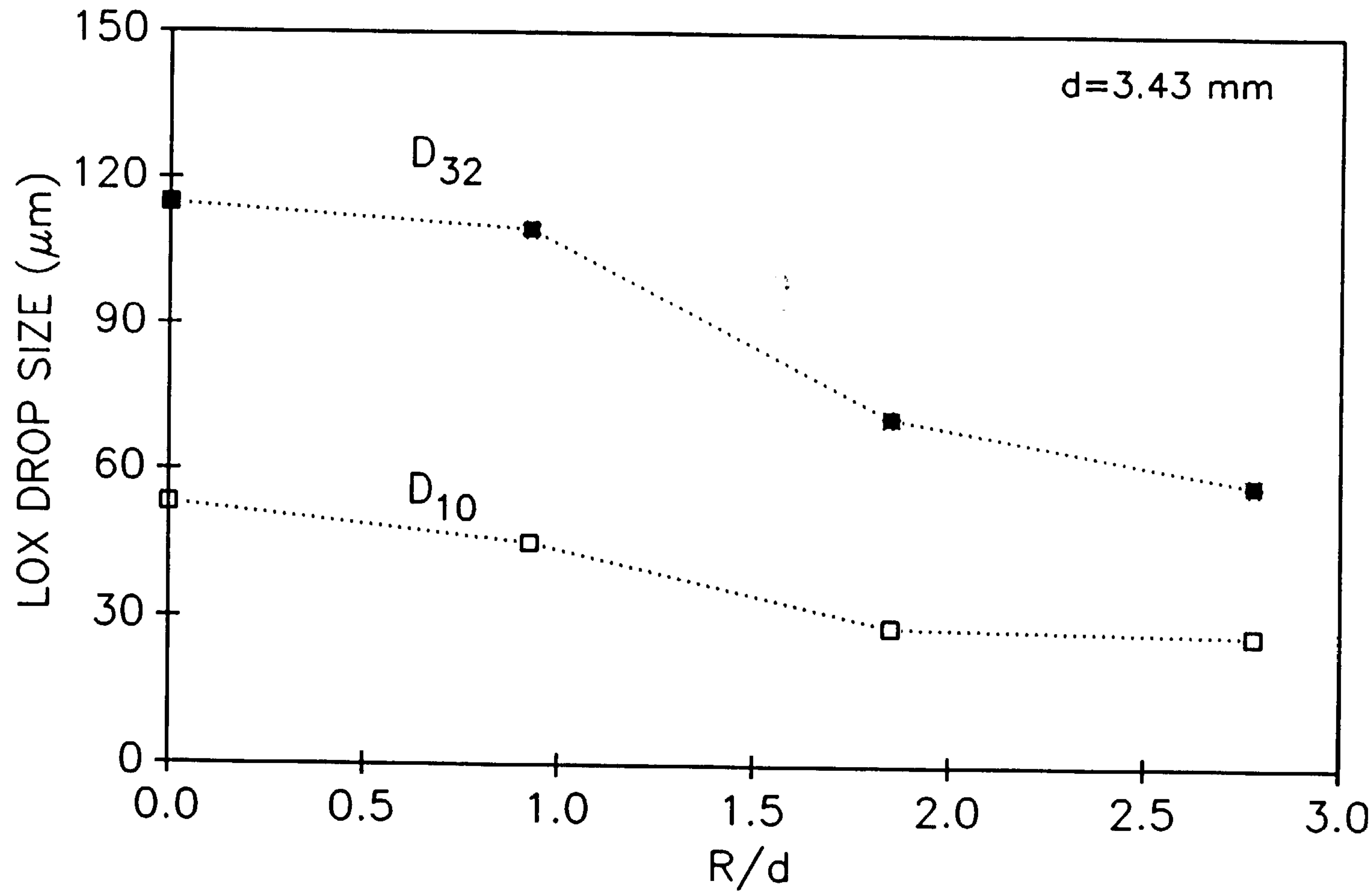

LOX DROP SIZE DISTRIBUTION

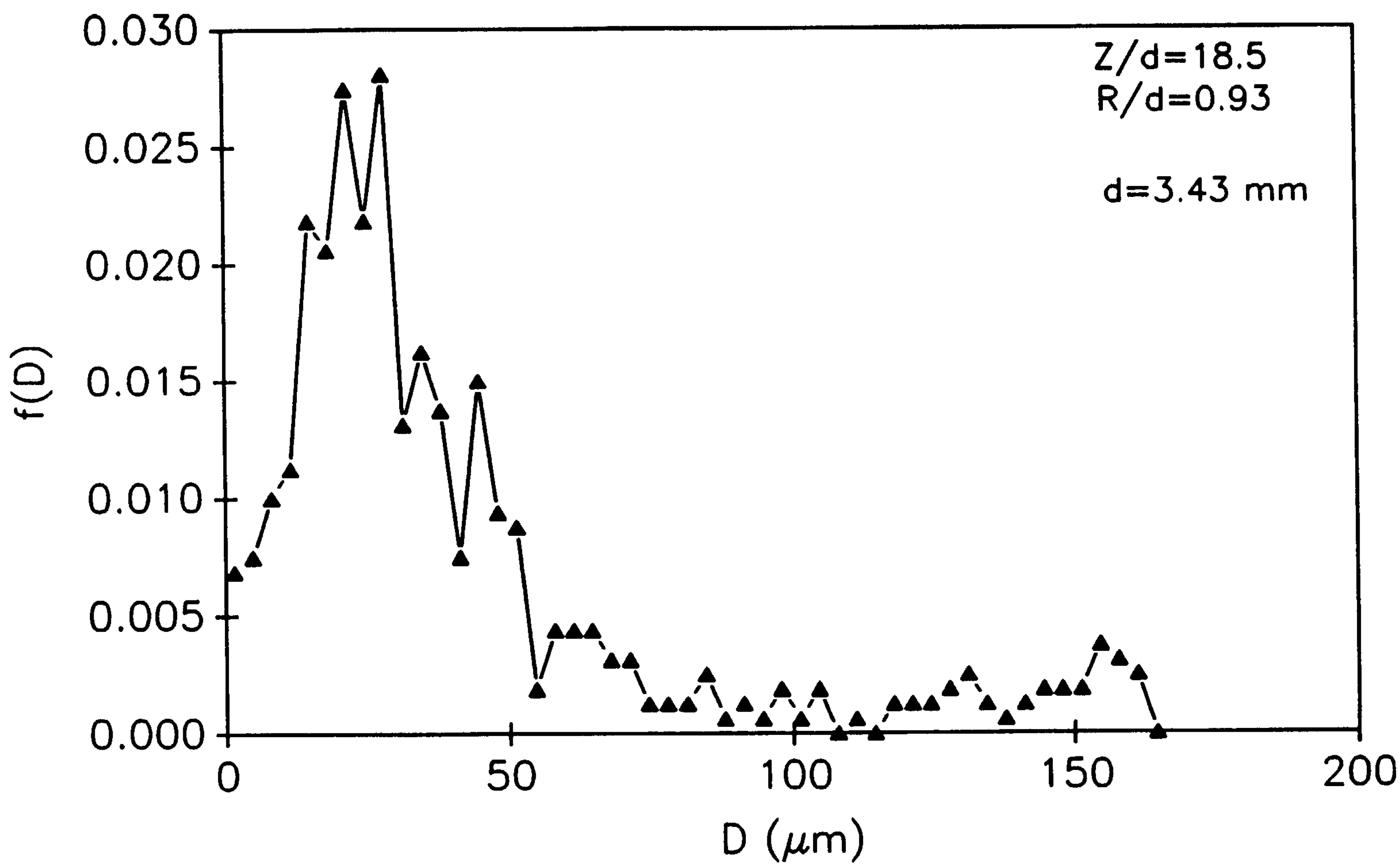

MEAN DROP VELOCITY VS. RADIAL LOCATION

Z=63.5 mm (Z/d=18.5)

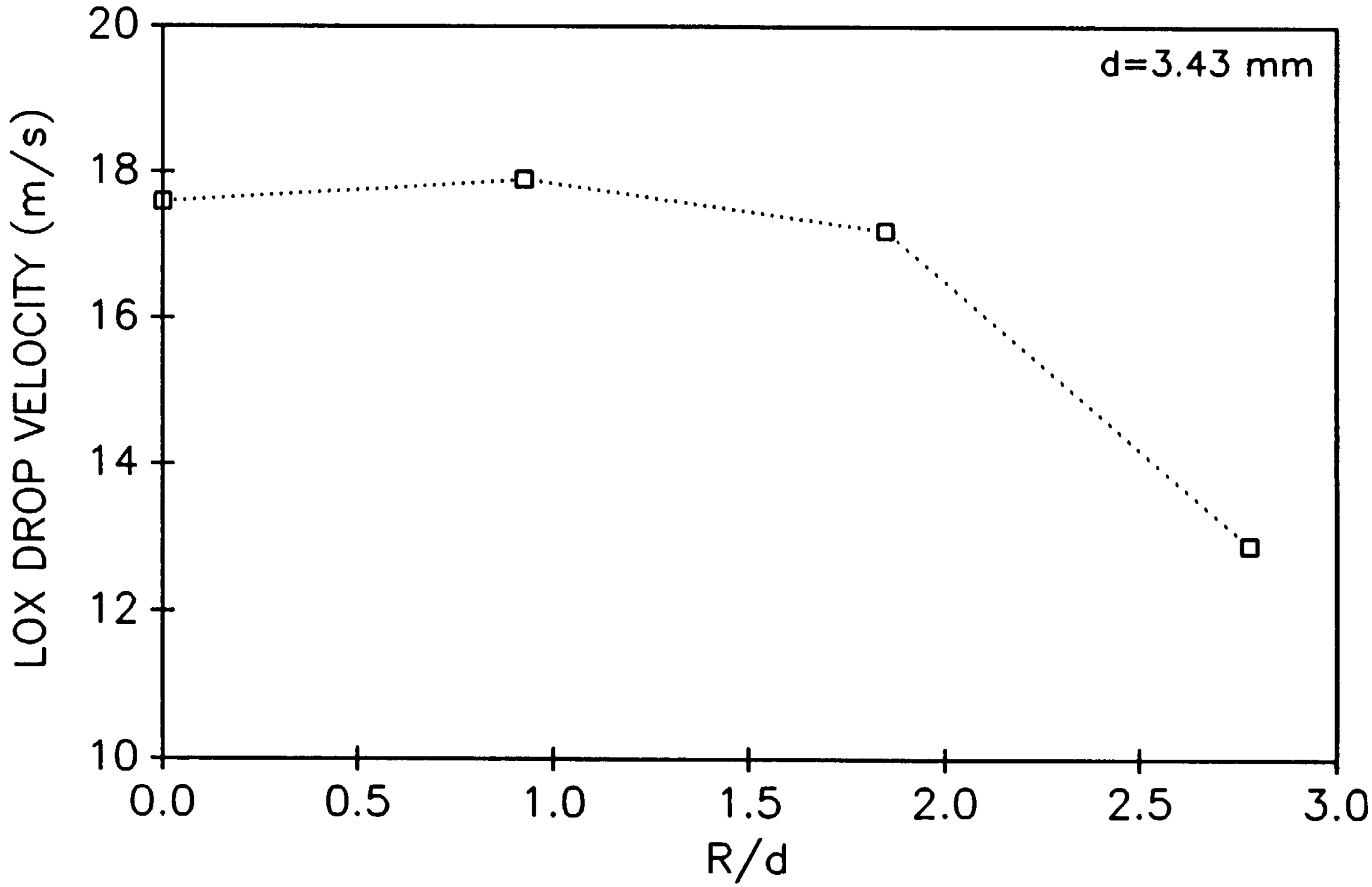

ROCKET PARAMETERS

Run	Chamber Pressure (MPa)/ (psia)	LOX Flowrate (kg/s)/ (lbm/s)	GH_2 Flowrate (kg/s)/ (lbm/s)	Mixture Ratio (O/F)	Momentum Ratio (F/O)	Velocity Ratio (F/O)	Re_l[1] ($\times 10^5$)	We_g[2] ($\times 10^5$)
1	2.79/404	0.120/ 0.264	0.021/ 0.047	5.6	4.70	26.8	4.97	1.61
2	2.72/395	0.110/ 0.243	0.021/ 0.047	5.2	5.58	29.2	5.11	1.95
3	2.73/396	0.113/ 0.250	0.021/ 0.047	5.3	5.19	27.9	5.25	2.07
4	2.43/352	0.103/ 0.227	0.019/ 0.041	5.5	5.41	29.3	4.80	2.59

[1] $Re_l = \rho_l U_l d / \mu_l$

[2] $We_g = \rho_g (U_g - U_l)^2 d / \sigma$

PDPA RESULTS

Axial Location, Z=63.5 mm (Z/d=18.5)
LOX Post I.D., d=3.43 mm

Run	R/d	D_{10} (μm)	D_{32} (μm)	V (m/s)	# Drops	% Val.	Run Time (sec.)
1	0.00	53.2	114.9	17.6	149	16%	1.41
2	0.93	45.1	109.7	17.9	484	21%	1.03
3	1.85	28.2	71.0	17.2	448	46%	1.52
4	2.78	26.8	57.5	12.9	45	62%	0.82

SHEAR-COAXIAL INJECTOR SPRAYS
Re_l vs. We_g

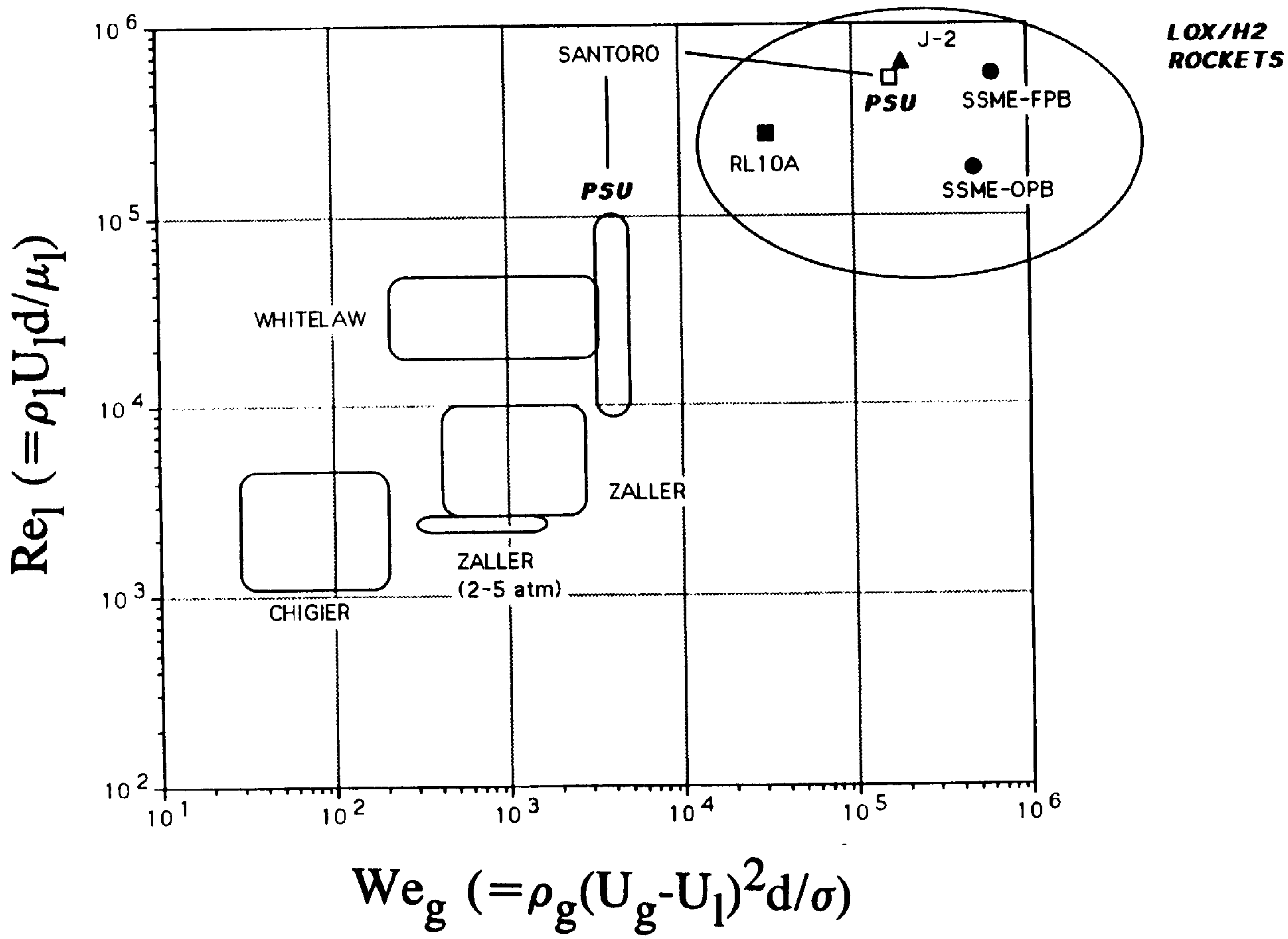

DROP SIZE EQUATIONS

NUKIYAMA/TANASAWA (1930) - *E*

$$\overline{D}_{32} = \frac{585}{V_r}\sqrt{\frac{\sigma}{\rho_l}} + 597\left(\frac{\mu_l}{\sqrt{\sigma\rho_l}}\right)^{0.45}\left(1000\frac{\dot{m}_l}{\rho_l}\frac{\rho_g}{\dot{m}_g}\right)^{1.5}$$

WEISS/WORSHAM (1959) - *SI

$$\overline{D}_{V0.5} = 0.61\left(1 + 1000\frac{\rho_g}{\rho_l}\right)\left(\frac{V_r\mu_l}{\sigma}\right)^{\frac{1}{3}}\left(\frac{\sigma}{\rho_g V_r^2}\right)\left(\frac{\rho_l\sigma\mu_g}{\mu_l^4}\left(\dot{m}_l + \dot{m}_g\right)\right)^{\frac{1}{12}}$$

MAYER (1961) - *SI

$$\overline{D}_{V0.5} = 9\pi\sqrt[3]{16}B\left(\frac{\mu_l\sqrt{\sigma}}{\rho_g V_g^2\sqrt{\rho_l}}\right)^{\frac{2}{3}}$$

LORENZETTO/LEFEBVRE (1977) - *SI

$$\overline{D}_{32} = 0.95\left(\frac{\sigma^{0.33}\dot{m}_l^{0.33}}{V_r\rho_l^{0.37}\rho_g^{0.3}}\right)\left(1 + \frac{\dot{m}_l}{\dot{m}_g}\right)^{1.7} + 0.13\mu_l\left(\frac{d}{\sigma\rho_l}\right)^{0.5}\left(1 + \frac{\dot{m}_l}{\dot{m}_g}\right)^{1.7}$$

ZALLER (1993) - *SI

$$\overline{D}_{30} = 3.62\left(\frac{\mu_g^{1.5}}{\rho_g\sigma^{1.5}}\right)\left(\frac{\dot{m}_l}{\dot{m}_g}\right)^{0.4}\frac{1}{V_r^{0.5}}$$

E	*English Units*	* *Dimensionally Correct*
SI	*Metric Units*	

DROP SIZE PREDICTIONS

CORRELATION	DROP DIAMETER	DROP SIZE (μm) HOT FIRE[1]	DROP SIZE (μm) COLD FLOW[2]
NUKIYAMA (1939)	D_{32}	1227	2325
LORENZETTO (1977)	D_{32}	440	5856
WEISS (1959)	$D_{V0.5}$	1.88	12.9
MAYER (1961)	$D_{V0.5}$	0.39	4.25
ZALLER (1993)	D_{30}	4.8	64.9

MEASURED DROP SIZE

[1] HOT FIRE : $58 < D_{32} < 115$

[2] COLD FLOW: $29 < D_{32} < 88$

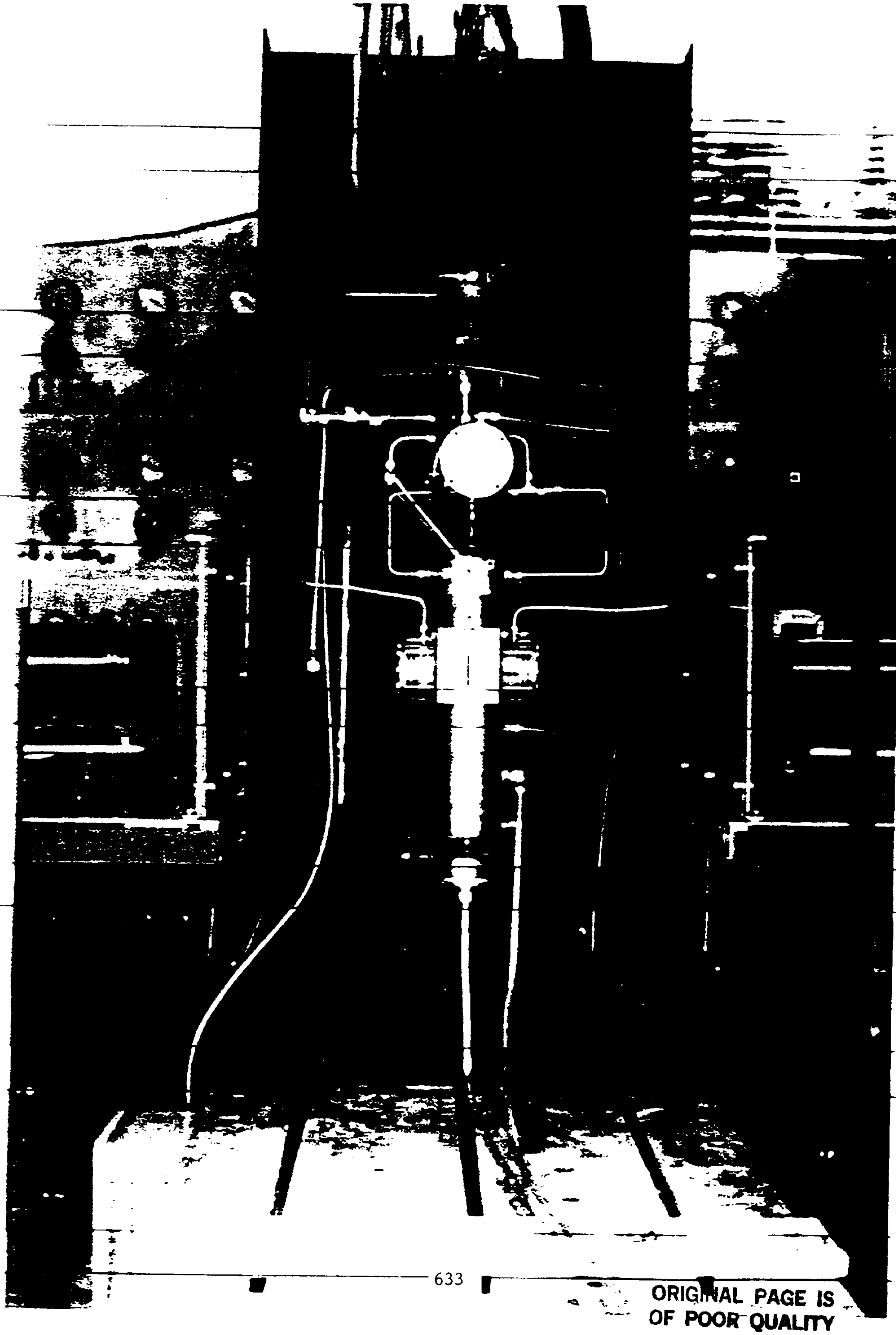

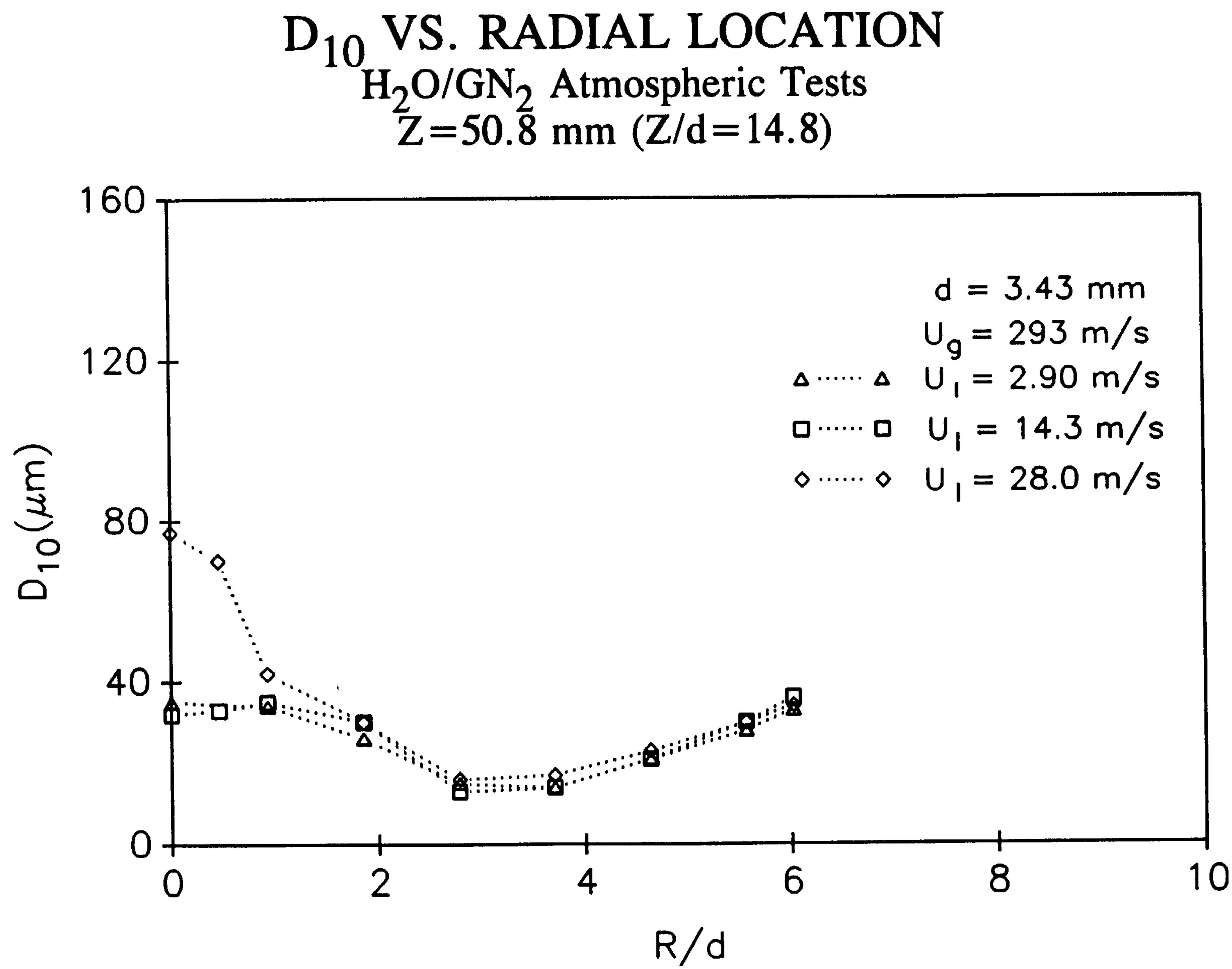
D_{10} VS. RADIAL LOCATION
H_2O/GN_2 Atmospheric Tests
Z=50.8 mm (Z/d=14.8)
d = 3.43 mm
U_g = 293 m/s
U_l = 2.90 m/s
U_l = 14.3 m/s
U_l = 28.0 m/s
$D_{10}(\mu m)$
R/d
0
40
80
120
160
0
2
4
6
8
10

D_{32} VS. RADIAL LOCATION

H_2O/GN_2 Atmospheric Tests

$Z=50.8$ mm ($Z/d=14.8$)

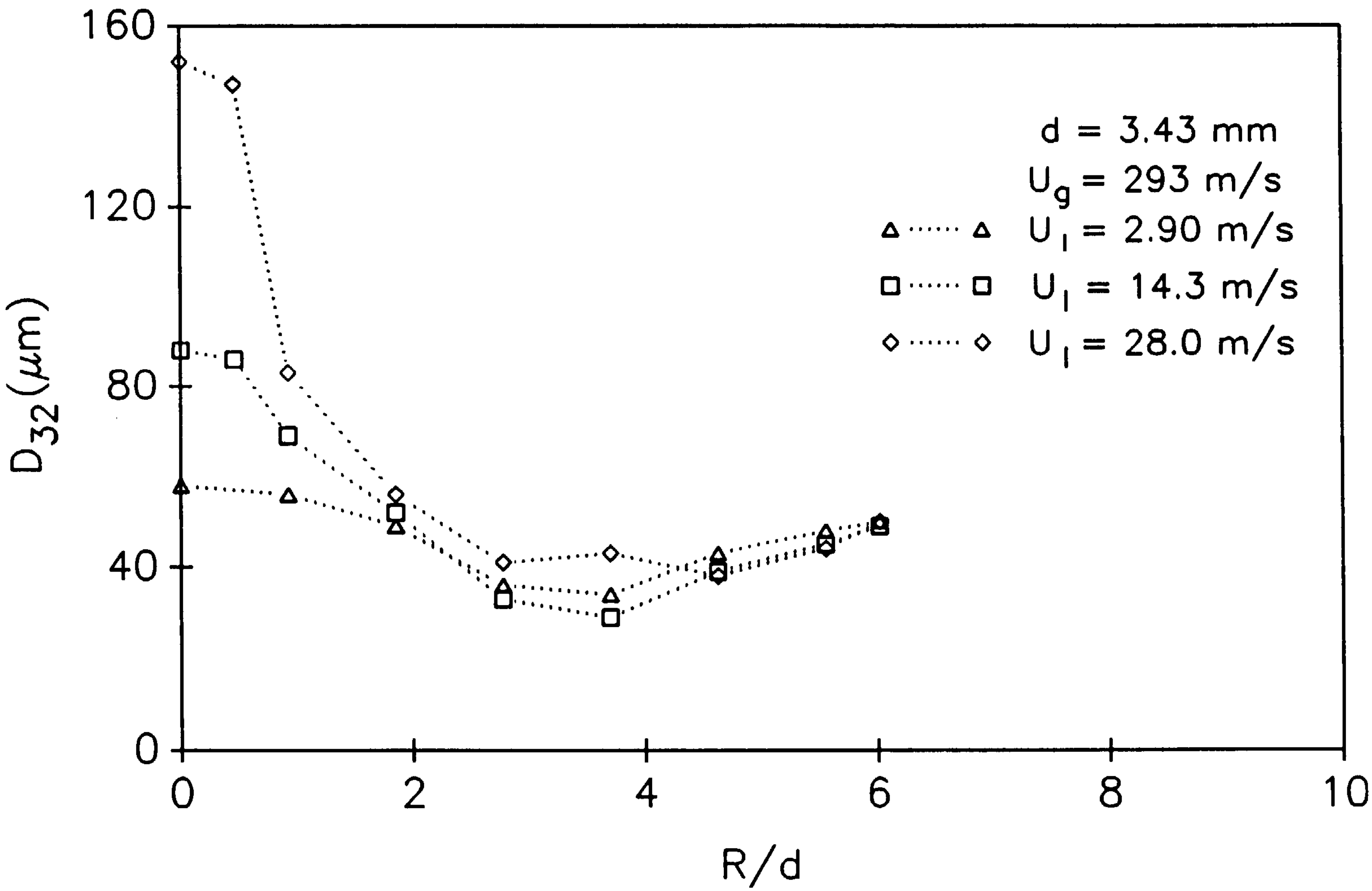

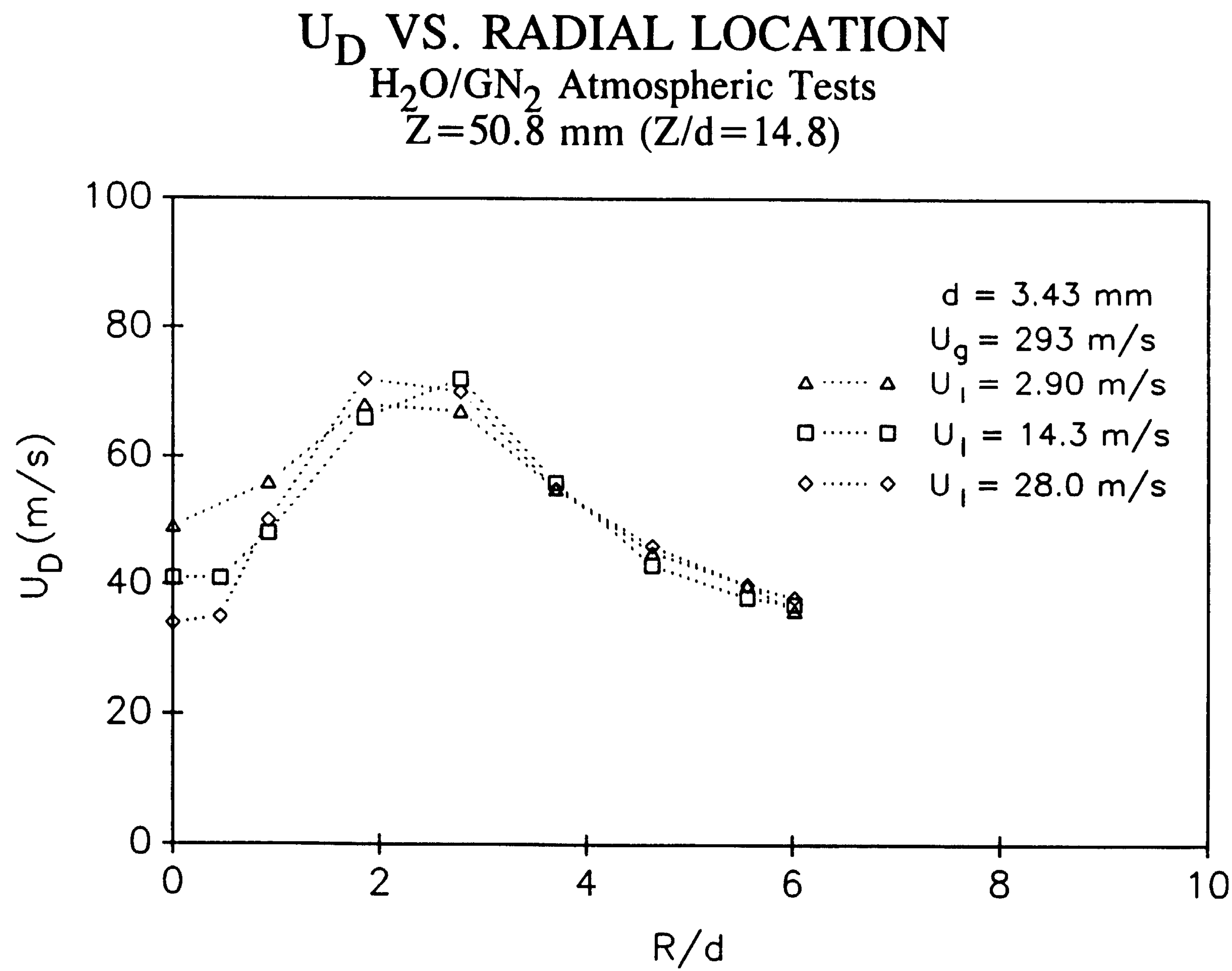
U_D VS. RADIAL LOCATION
H_2O/GN_2 Atmospheric Tests
Z=50.8 mm (Z/d=14.8)
100
80
60
40
20
0
U_D (m/s)
0
2
4
6
8
10
R/d
d = 3.43 mm
U_g = 293 m/s
U_l = 2.90 m/s
U_l = 14.3 m/s
U_l = 28.0 m/s

U_D' VS. RADIAL LOCATION
H_2O/GN_2 Atmospheric Tests
Z=50.8 mm (Z/d=14.8)

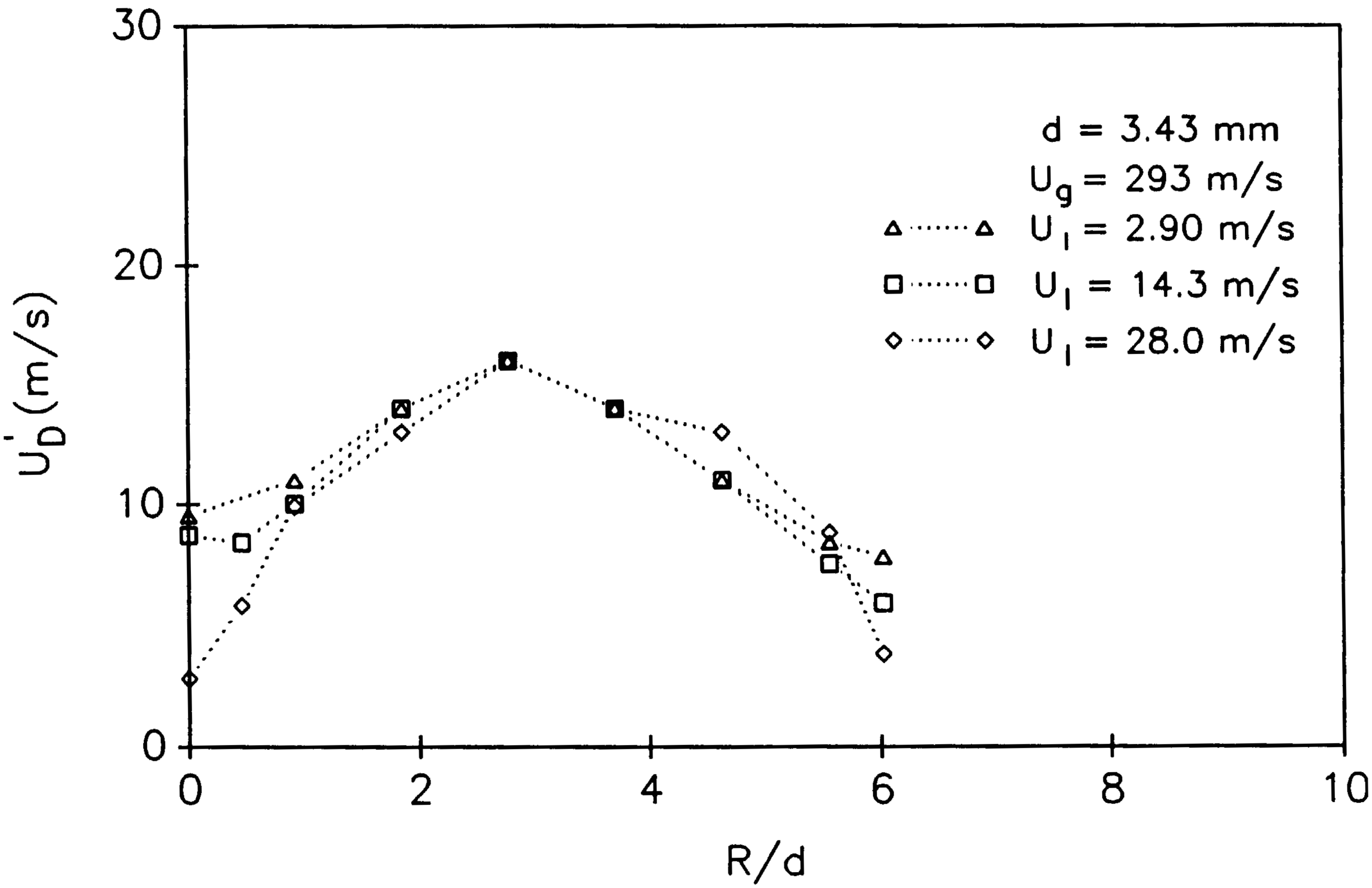

% VALIDATION VS. RADIAL LOCATION

H_2O/GN_2 Atmospheric Tests

Z=50.8 mm (Z/d=14.8)

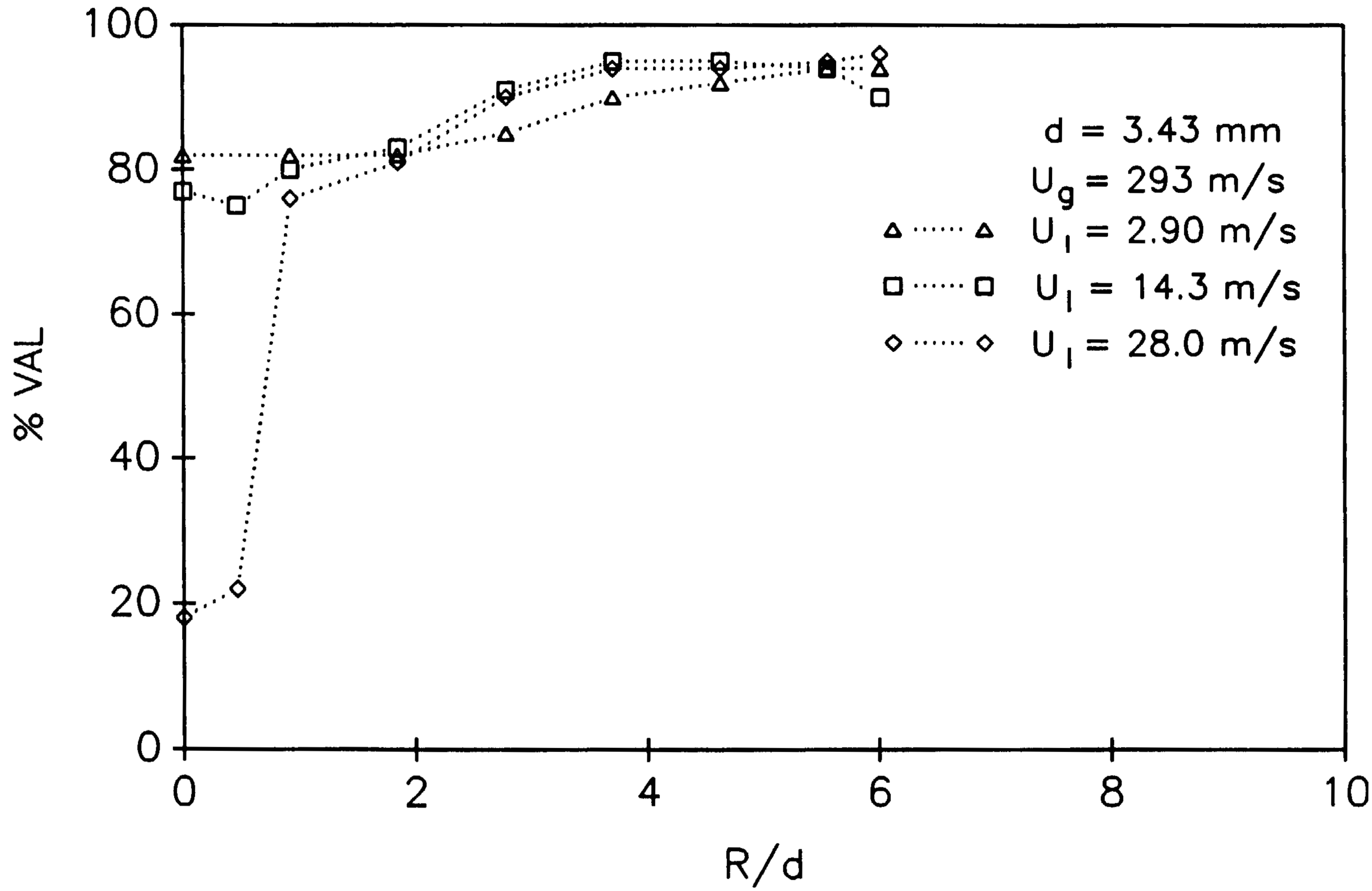

SAMPLES/SEC. VS. RADIAL LOCATION

H_2O/GN_2 Atmospheric Tests

Z=50.8 mm (Z/d=14.8)

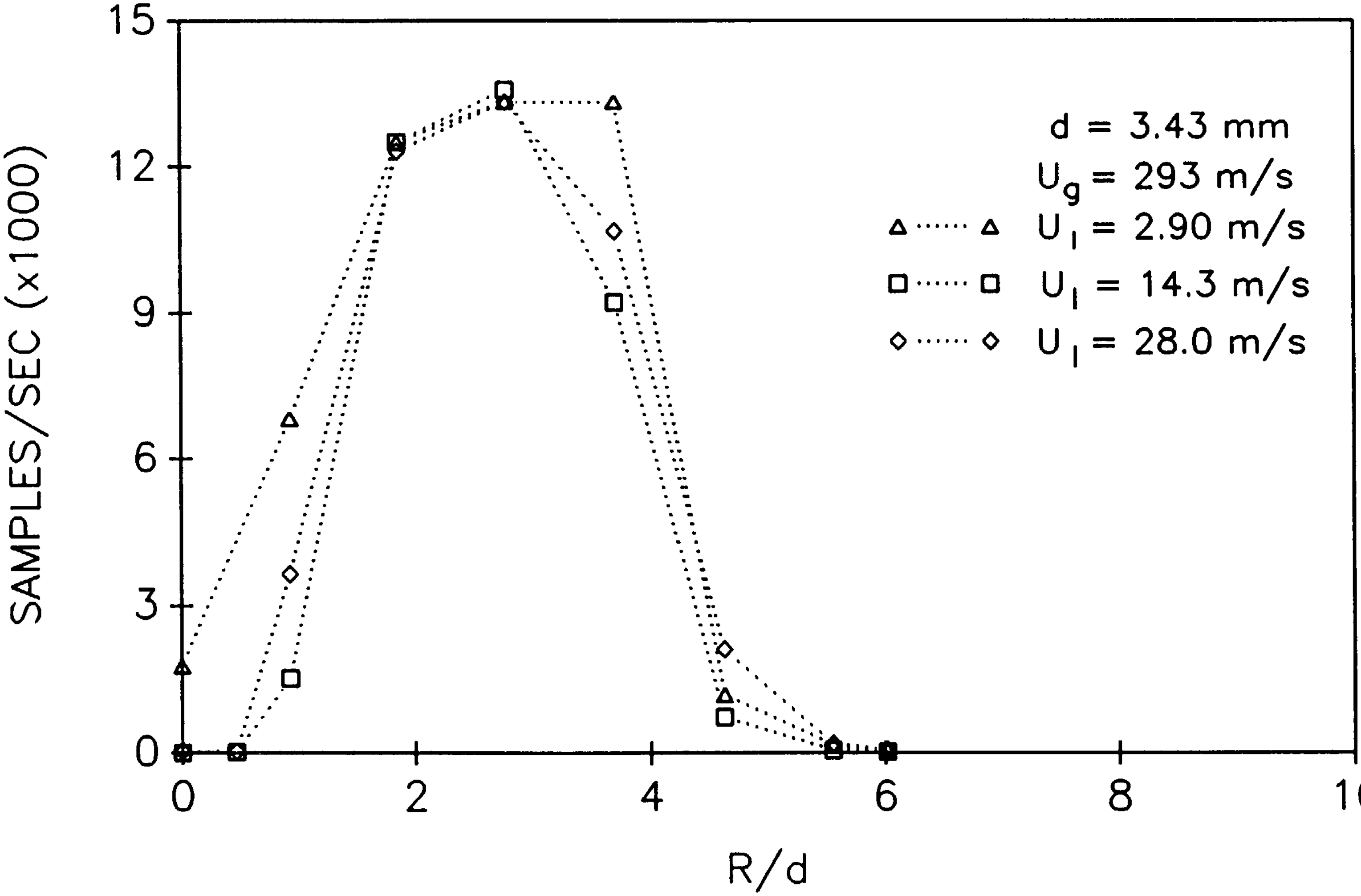

HOT FIRE/COLD FLOW COMPARISON

	HOT FIRE	COLD FLOW	RATIO (H.F./C.F.)
CHAMBER PRESSURE (psia)	387	14.7	26.3
LIQUID FLOWRATE (kg/s)	0.112	0.13	0.85
GAS FLOWRATE (kg/s)	0.021	0.009	2.3
MIXTURE RATIO (O/F)	5.4	14.5	0.37
LIQUID VELOCITY (m/s)	13.5	14.3	0.94
GAS VELOCITY (m/s)	381	290	1.3
VELOCITY RATIO (F/O)	28.3	20.3	1.4
Re_l $(=\rho_l U_l d/\mu_l)$	5.03×10^5	4.86×10^4	10.3
We_g $(=\rho_g (U_g-U_l)^2 d/\sigma)$	2.06×10^5	4.3×10^3	48

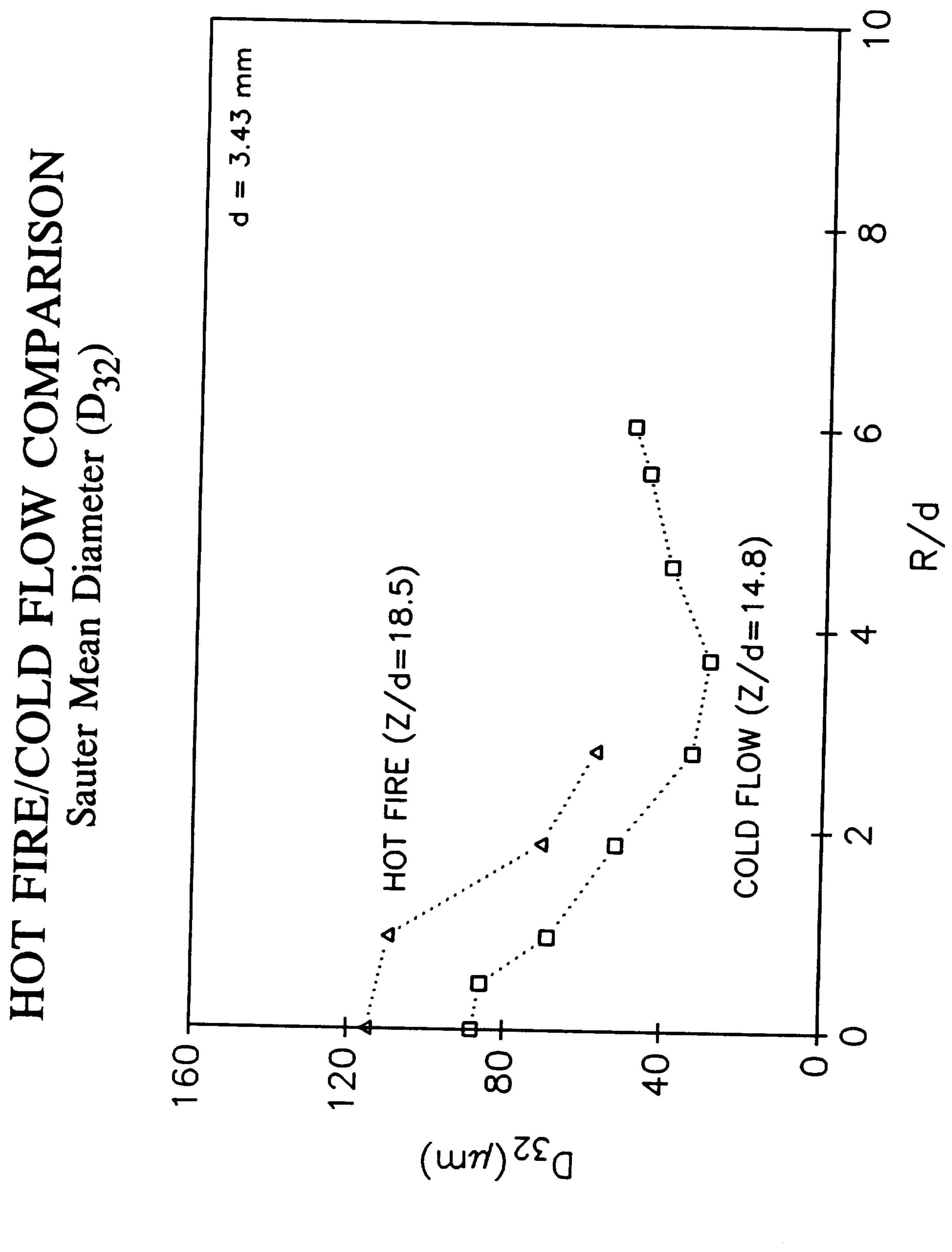
HOT FIRE/COLD FLOW COMPARISON
Sauter Mean Diameter (D_{32})
d = 3.43 mm
HOT FIRE (Z/d=18.5)
COLD FLOW (Z/d=14.8)
D_{32} (μm)
R/d
0
40
80
120
160
0
2
4
6
8
10

HOT FIRE/COLD FLOW COMPARISON

Mean Drop Velocity (U_D)

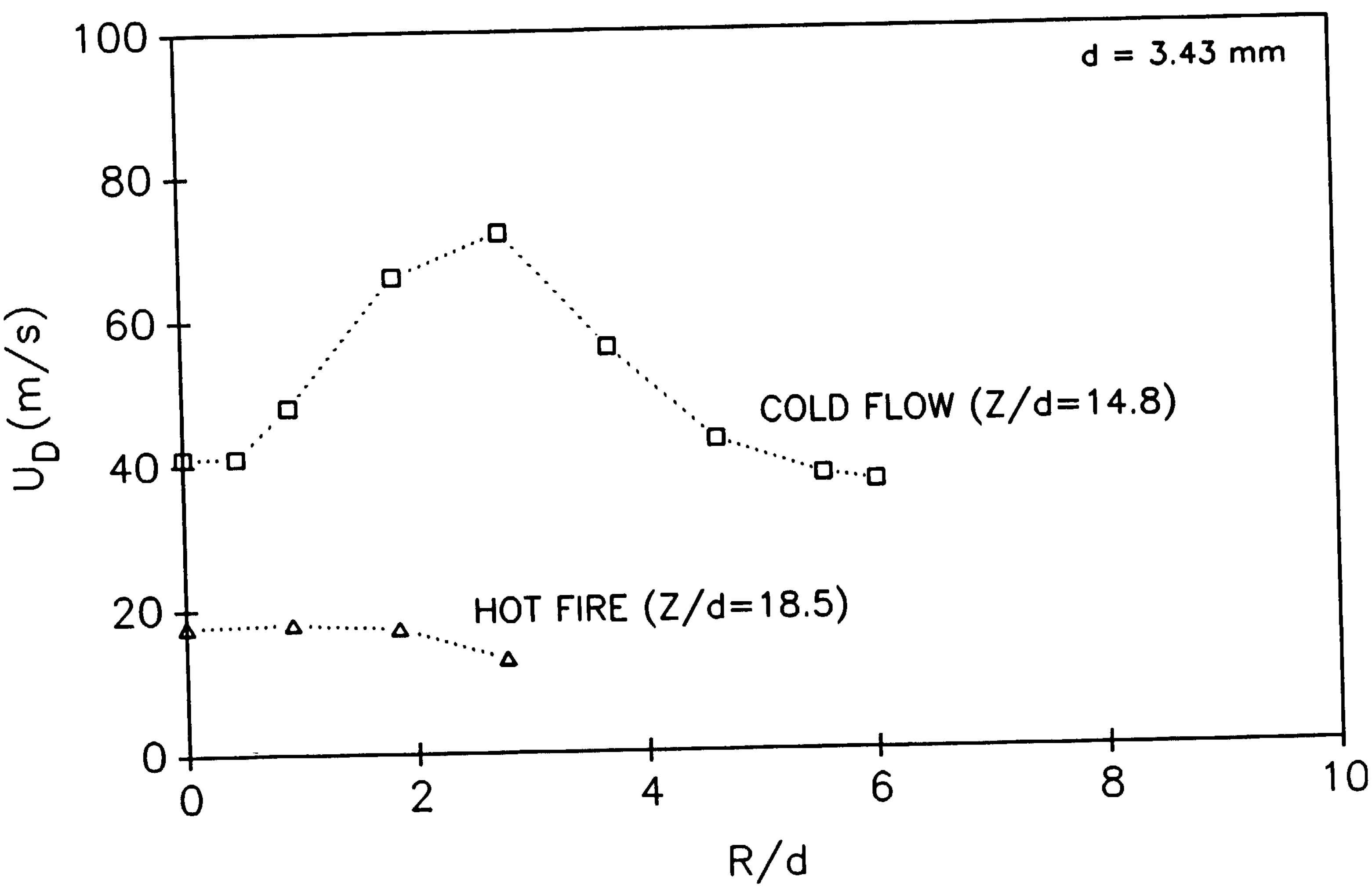

SUMMARY

- **Measured liquid oxygen drop size and velocity in combusting environment**

  - Intact core extends well beyond the injector

  - Drops confined to narrow region

- **Correlations based on cold flow data inadequate for predicting drop size in LOX/GH_2 combusting flow**

- **Compared drop measurements between cold flow and combusting conditions for similar liquid and gas flowrates**

  - Re_l and We_g differ by an order of magnitude

  - Mean drop size larger for hot fire conditions

ACKNOWLEDGEMENT

Funding by NASA Marshall Space Flight Center, contract NAS8-38862 and the Penn State NASA Propulsion Engineering Research Center, Contract NAGW 1356 supplement 2

N95- 23643

SPRAY COMBUSTION EXPERIMENTS AND NUMERICAL PREDICTIONS

by

Edward J. Mularz
U. S. Army Vehicle Propulsion Directorate, ARL
NASA Lewis Research Center

Daniel L. Bulzan
NASA Lewis Research Center

Kuo-Huey Chen
The University of Toledo

ABSTRACT

The next generation of commercial aircraft will include turbofan engines with performances significantly better than those in the current fleet. Control of particulate and gaseous emissions will also be an integral part of the engine design criteria. These performance and emission requirements present a technical challenge for the combustor: control of the fuel and air mixing and control of the local stoichiometry will have to be maintained much more rigorously than combustors in current production. A better understanding of the flow physics of liquid fuel spray combustion is necessary. This presentation describes recent experiments on spray combustion where detailed measurements of the spray characteristics were made, including local drop-size distributions and velocities. In addition, an advanced combustor CFD code has been under development and predictions from this code are presented and compared with measurements. Studies such as these will provide information to the advanced combustor designer on fuel spray quality and mixing effectiveness. Validation of new fast, robust, and efficient CFD codes will also enable the combustor designer to use them as valuable design tools for optimization of combustor concepts for the next generation of aircraft engines.

U.S. ARMY RESEARCH LABORATORY

NASA Lewis Research Center

SPRAY COMBUSTION EXPERIMENTS AND NUMERICAL PREDICTIONS

Edward J. Mularz
U.S. Army Research Laboratory
Lewis Research Center
Cleveland, Ohio

Daniel L. Bulzan
National Aeronautics and Space Administration
Lewis Research Center
Cleveland, Ohio

Kuo-Huey Chen
University of Toledo
Toledo, Ohio

OBJECTIVES

- Provide Measurements in Two-Phase, Reacting Flowfields for Better Understanding of Multiphase Flows and Serve as Database for Computer Model Validation
- Develop Robust, Efficient Computer Code for Internal, Chemical Reacting Flows
- Develop Numerical Solution Procedure to Efficiently Couple Spray Model with Strongly Implicit Flow Solution Algorithm
- Validation of CFD Code

COMBUSTOR

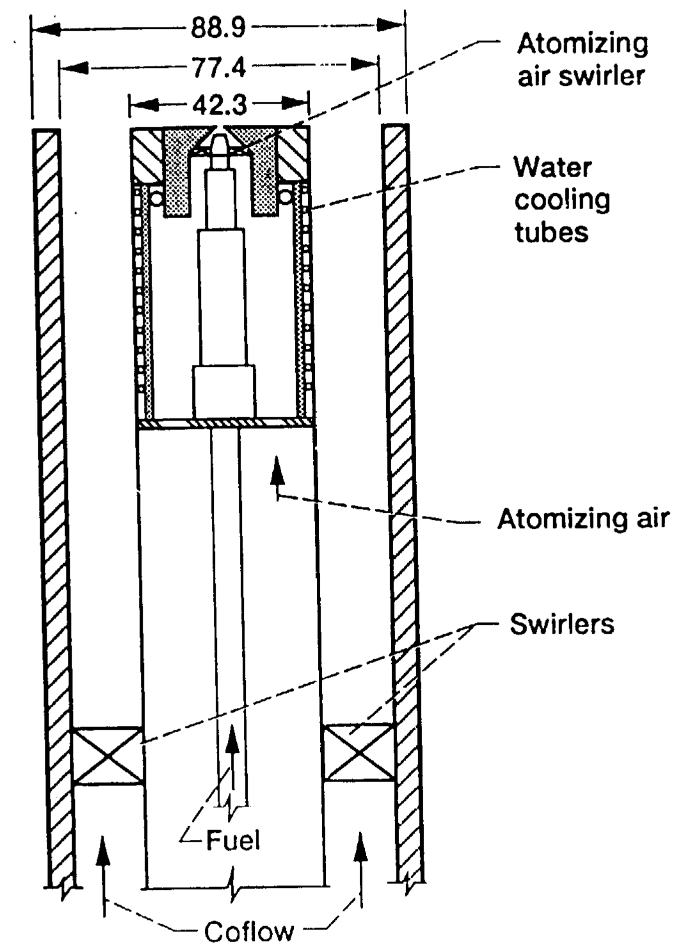
88.9
77.4
42.3
Atomizing air swirler
Water cooling tubes
Atomizing air
Swirlers
Fuel
Coflow

Gas Phase Velocity at 5 mm Downstream

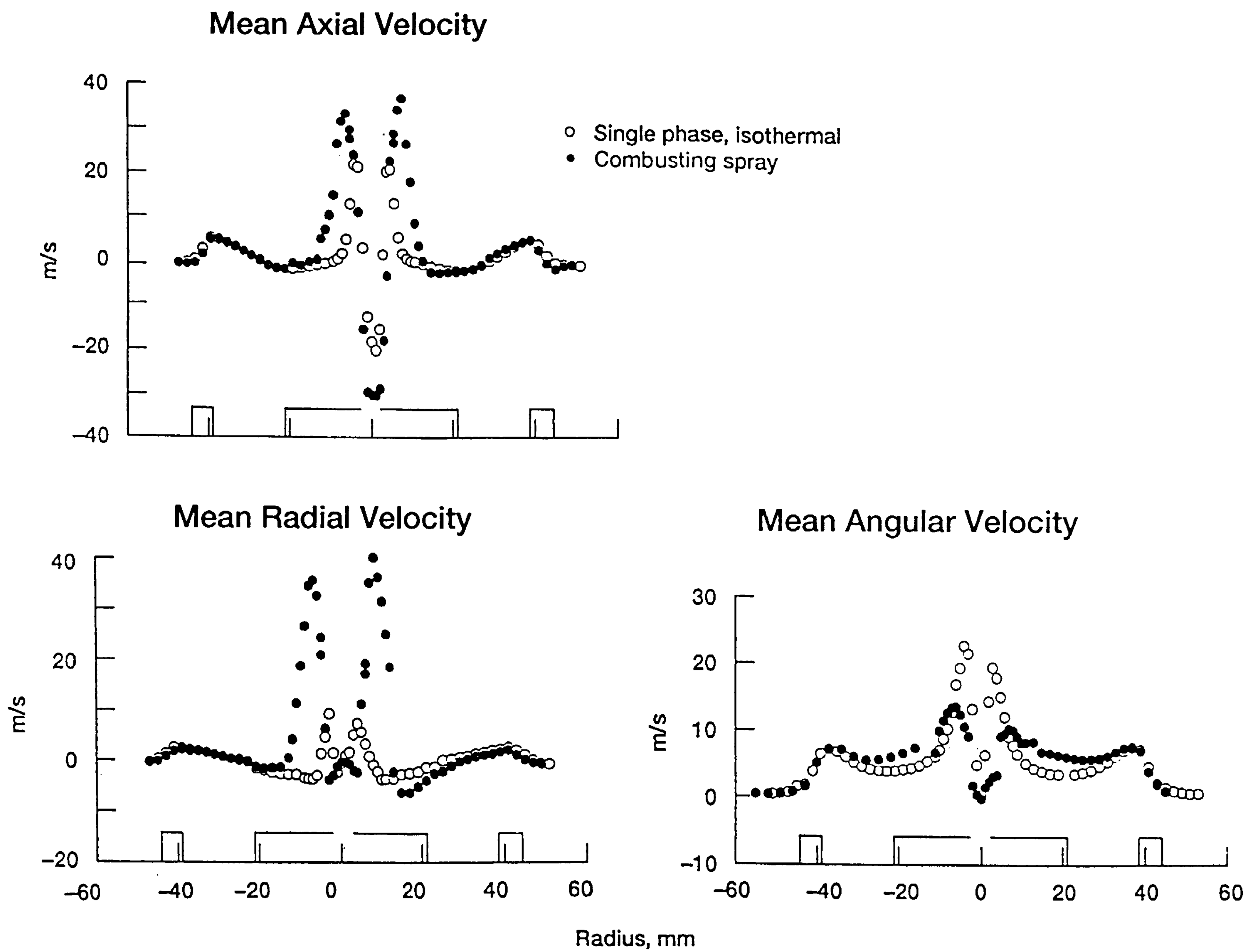

CD-93-65257

Gas Phase Velocity at 5 mm Downstream

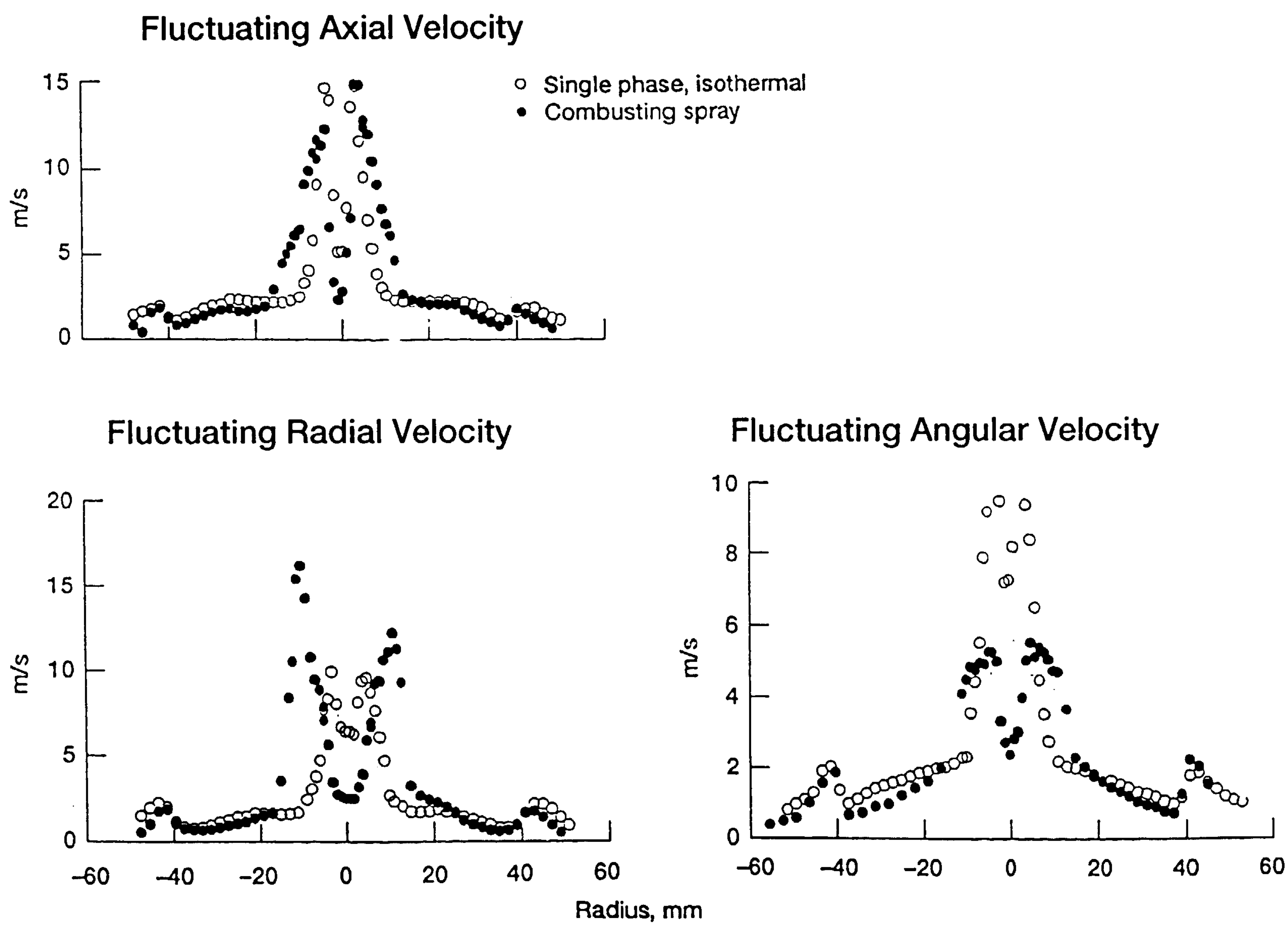

CD-93-65258

Drop Velocity at 5 mm Downstream

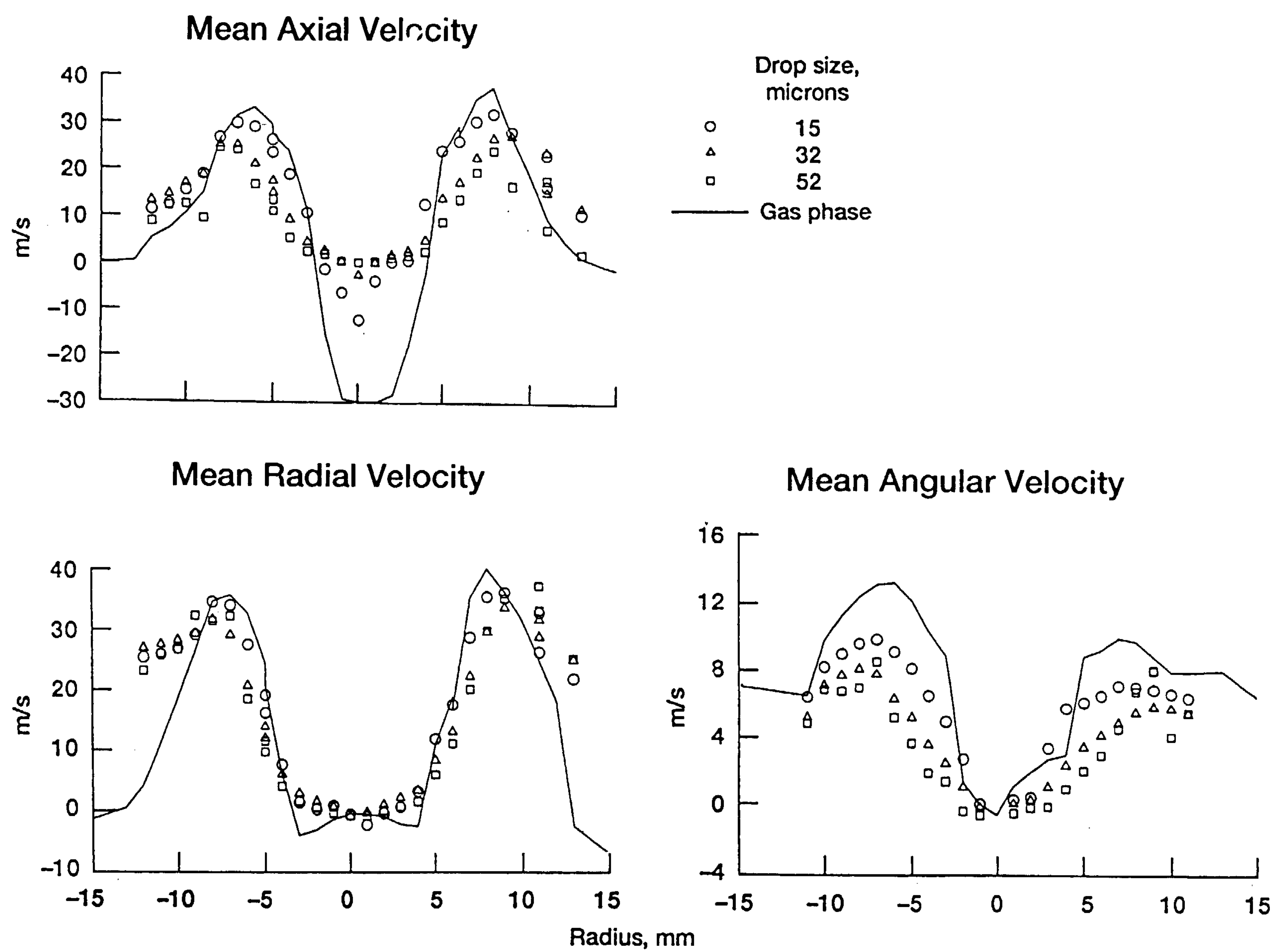

CD-93-65259

Drop Velocity at 5 mm Downstream

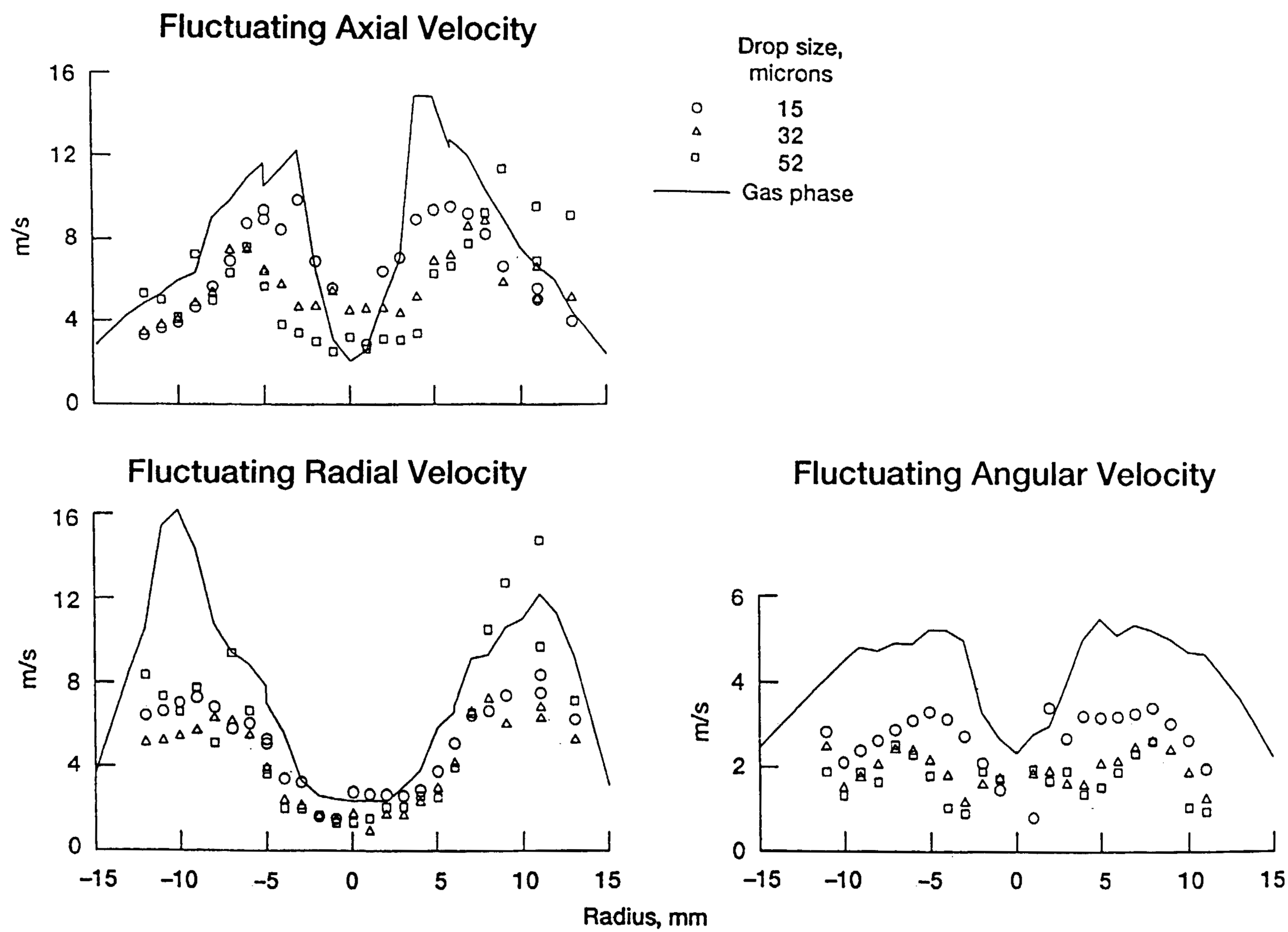

CD-93-65260

Drop Number Flux at 5 mm Downstream

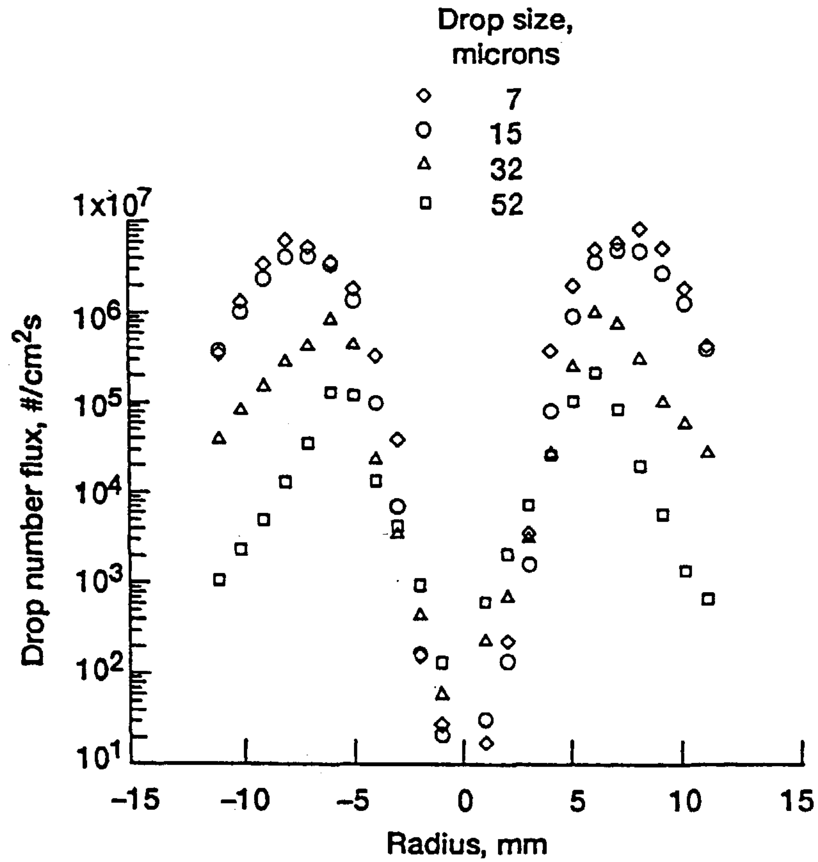

CD-93-65261

NUMERICAL ALGORITHM

- Gas-Phase - ALLSPD code
- Liquid-Phase
  - Droplet motion equations (ODE) - Runge-Kutta method.
  - Droplet internal equations (PDE) - implicit method (Thomas algorithm).
  - Determination of spray time step for integration.
  - Stochastic separate flow model.
- Interaction Between Two Phases

Difficulties with Compressible Flow Algorithms at Low Mach Numbers

- Disparities among system's eigenvalues (stiffness), u, $u + c$, $u - c$, resulting in significant slowdown in convergence rate.

- Singular behavior of pressure gradient term in momentum equations as Mach number approaches zero,

$$\rho^* u^{*2} + \frac{p^*}{\gamma M_r^2}$$

As Mach number is decreased, pressure variation ($\Delta p^* \propto M^2$) becomes of similar magnitude as roundoff error of the large pressure gradient term ($p^*/\gamma M_r^2$).

METHOD OF APPROACH

Pressure Singularity Problem

- Pressure decomposed into two parts:

$$p = p_o + p_g$$

  p_g replaces p in momentum equations and retains p_g as one of the unknowns.

- Employs conservative form of governing equations, but uses primitive variables

$$(p_g, u, v, h, Y_i)$$

  as unknowns. Conservation property preserved and pressure field accurately resolved for all Mach numbers.

Eigenvalue Stiffness Problem

- Pressure rescaled so that all eigenvalues have the same order of magnitude. Physical acoustic waves removed and replaced with pseudo-acoustic waves which travel at speed comparable to fluid convective velocity.

Particle Traces

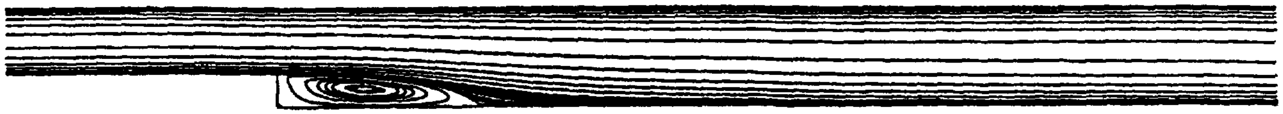

CD-93-65274

Mean Velocity Profiles

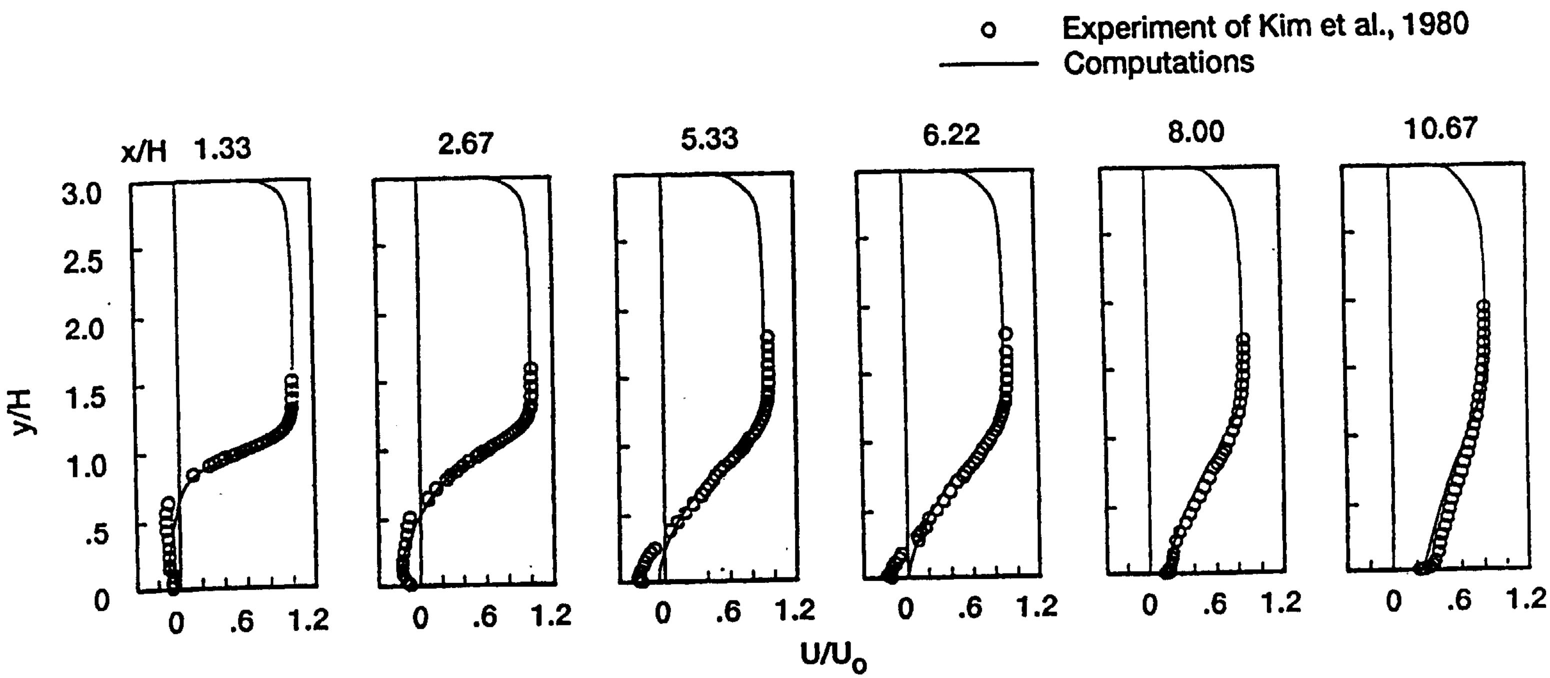

CD-93-65262

Turbulence Quanities

Turbulent Kinetic Energy

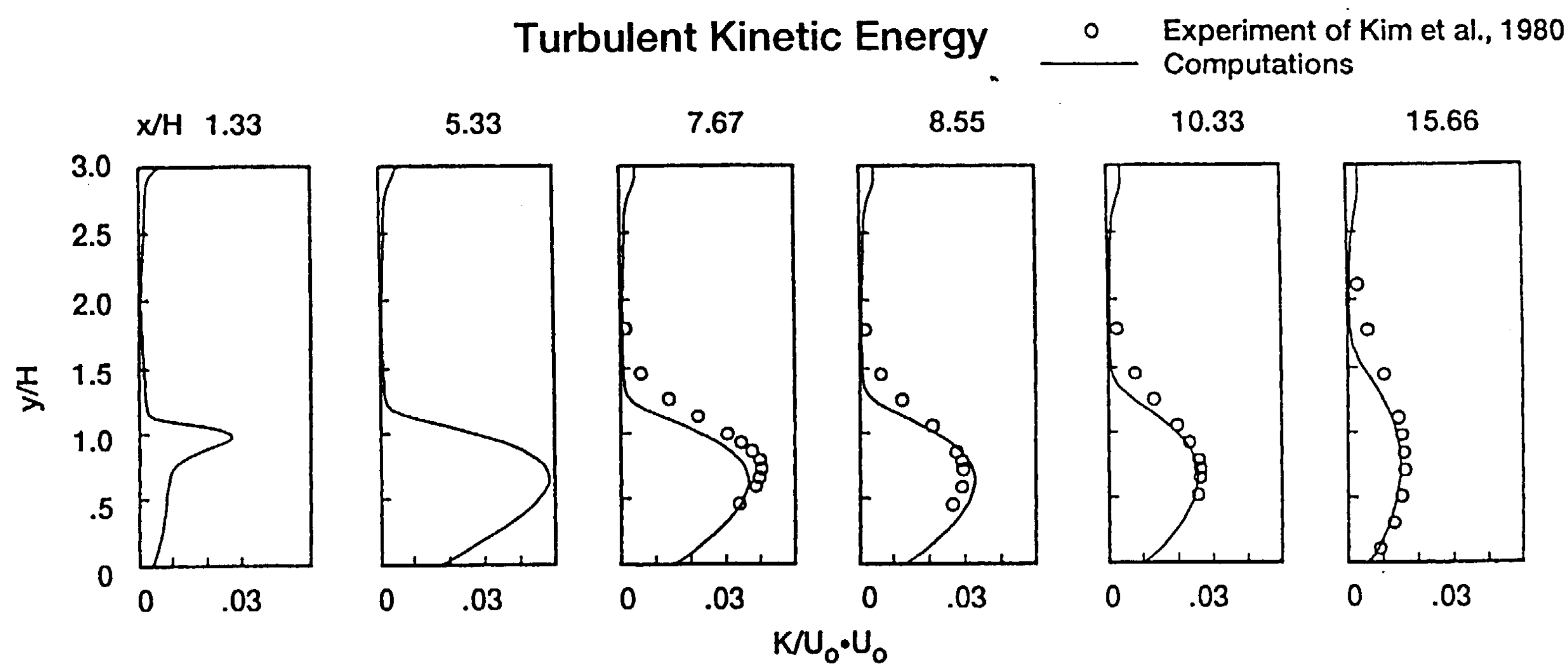

Turbulent Shear Stress

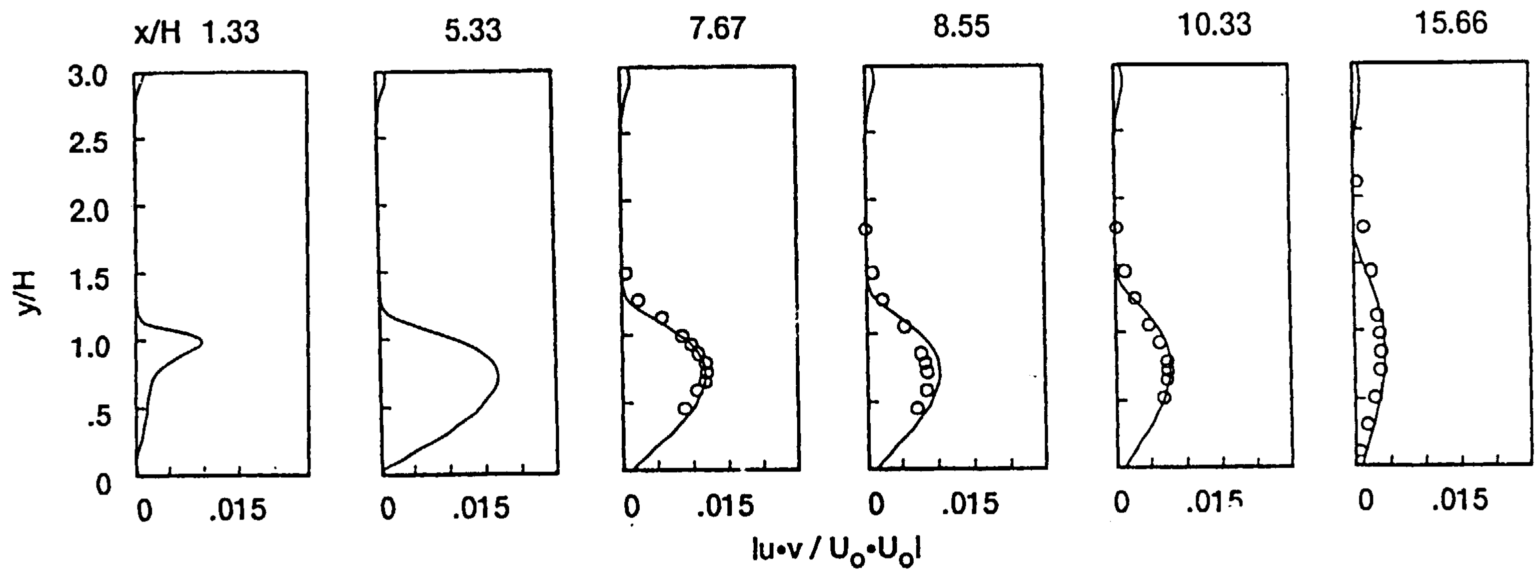

CD-93-65263

Particle Traces

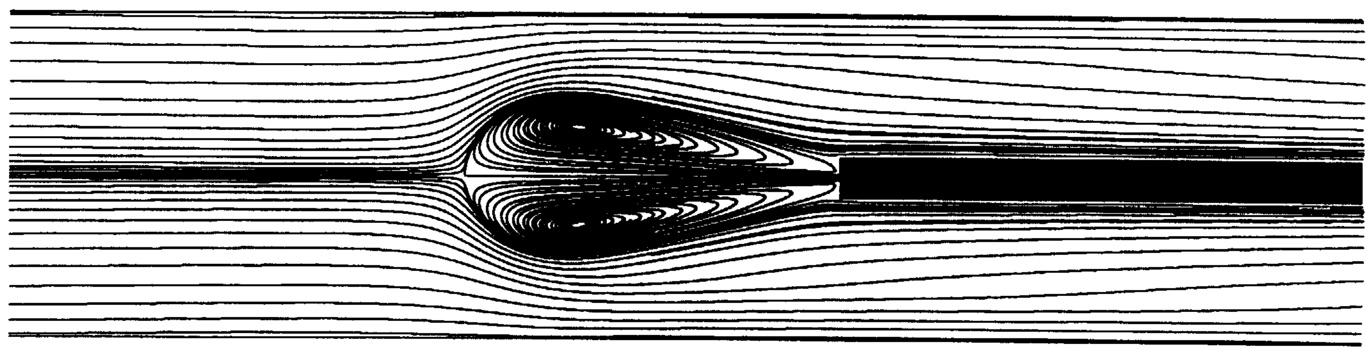

CD-93-65266

Velocity Vectors

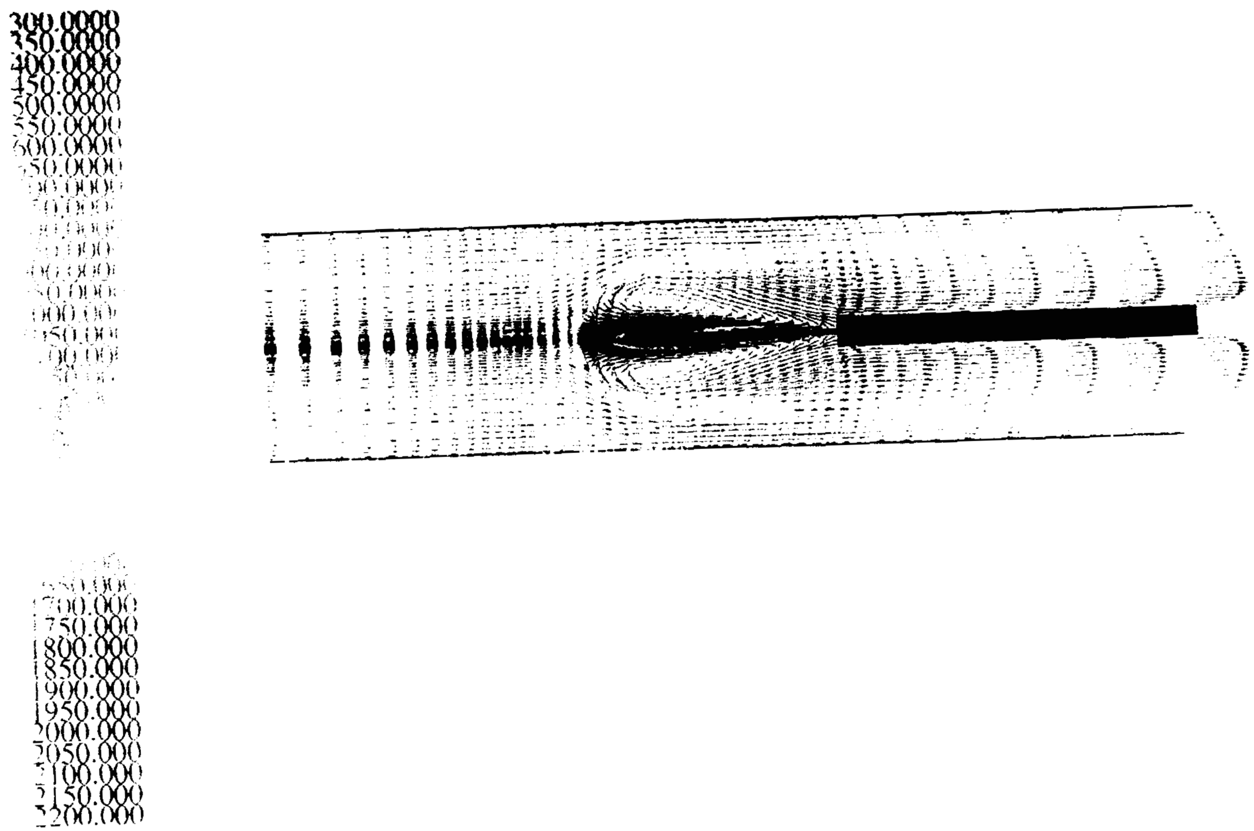

CD-93-65267

Gas Turbine Combustor

Grid

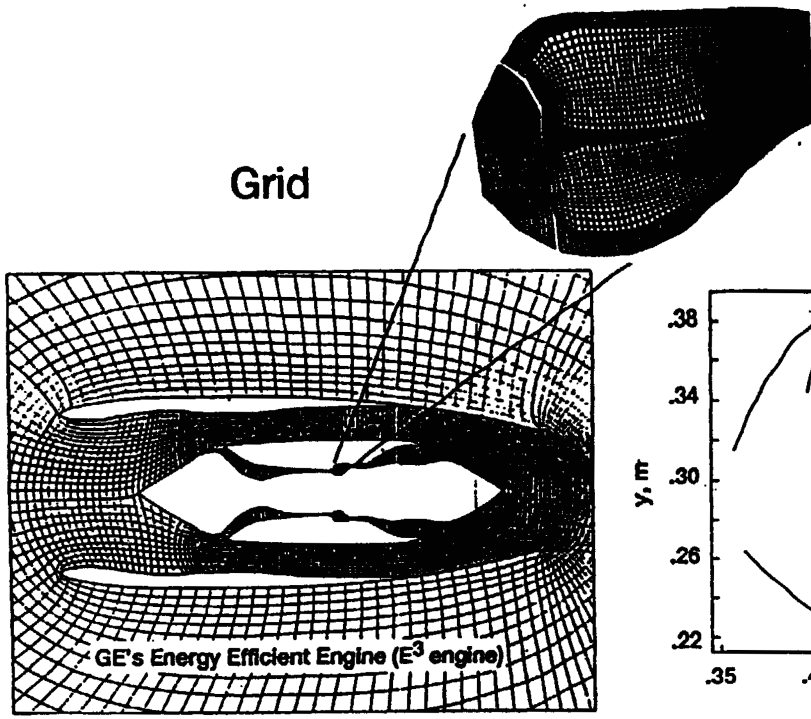

Drop Trajectories

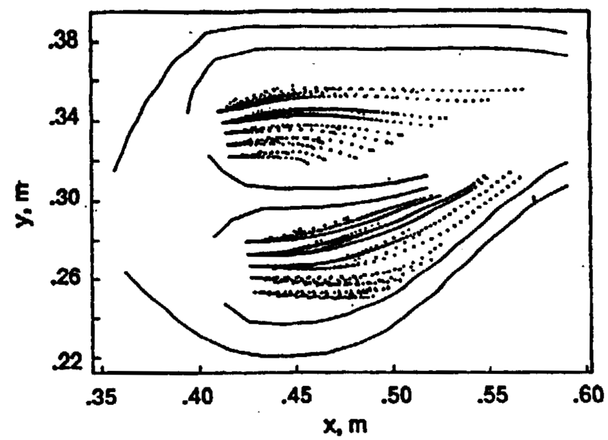

Noncombustion Flow
(Cold Flow, No Spray)

Spray Combustion Flow

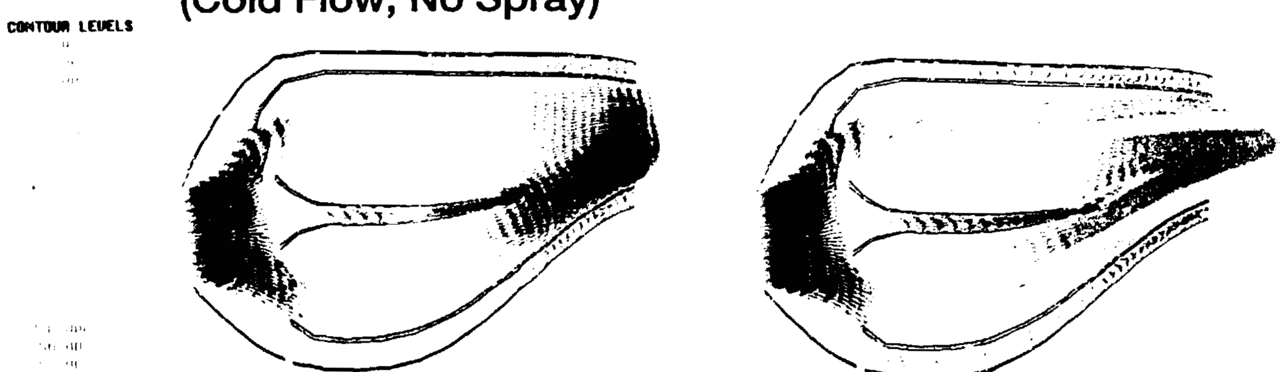

Velocity Vectors

CD-93-65268

SMD Distribution

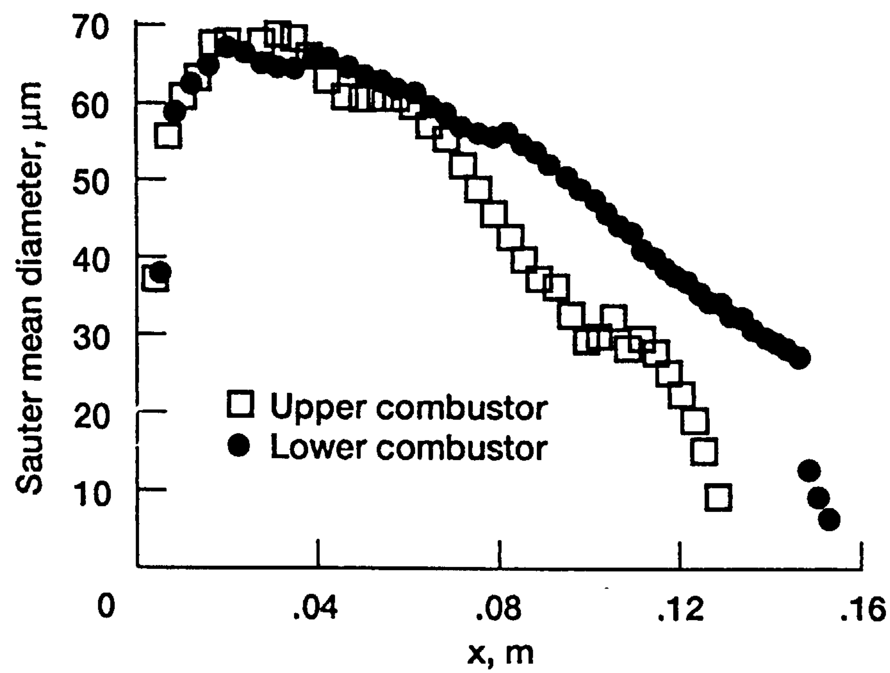

CD-93-65269

C-8

Convergence History

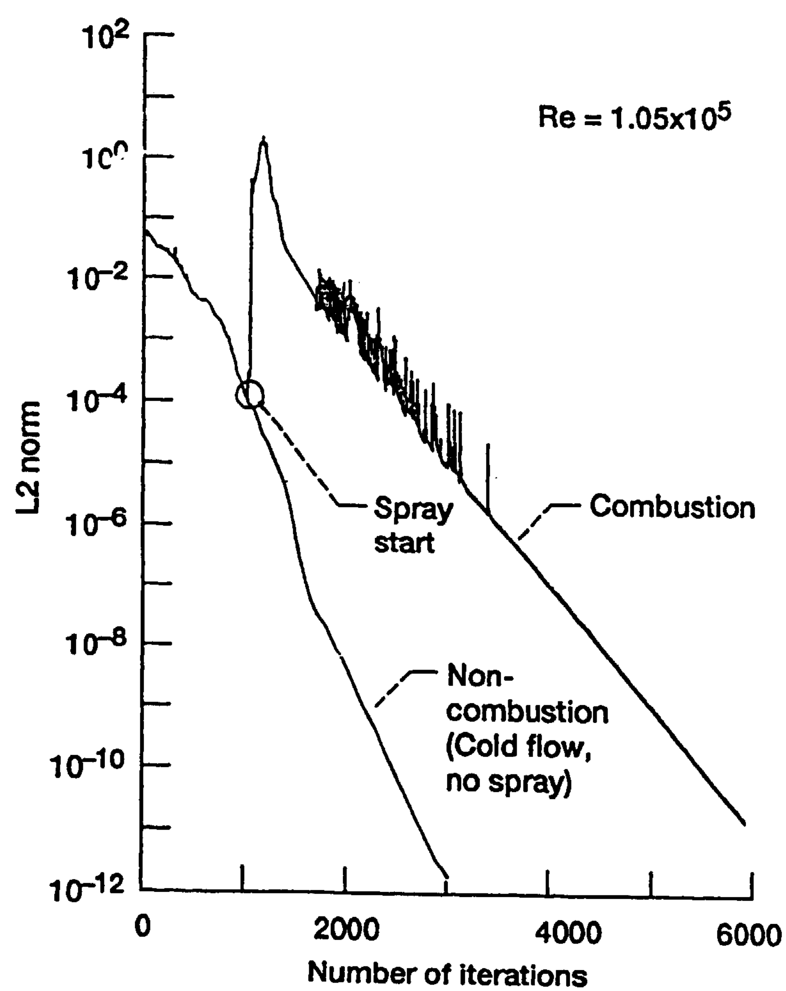

CD-93-65270

CONCLUSIONS

- Flowfield Symmetric Making Data Useful for Comparison With Axisymmetric Model Predictions
- Both Drop Size and Velocity are Important in Two-Phase, Reacting, Swirling Flowfields
- ALLSPD 2-D Algorithm Demonstrated for Non-Reacting, Turbulent Flow and Turbulent, Reacting, Single-Phase Flow
- Spray Model Incorporated into CFD Code and Preliminary Results Obtained for Two-Phase, Turbulent, Reacting Combustor Flowfield

N95- 23644

29-25
43763
p-21

PROGRESS IN ADVANCED SPRAY COMBUSTION CODE INTEGRATION

Pak-Yan Liang
Rocketdyne Division, Rockwell International

ABSTRACT

A multiyear project to assemble a robust, multiphase spray combustion code is now underway and gradually building up to full speed. The overall effort involves several university and government research teams as well as Rocketdyne. The first part of this paper will give an overview of the respective roles of the different participants involved, the master strategy, the evolutionary milestones, and an assessment of the state-of-the-art of various key components. The second half of this paper will highlight the progress made to-date in extending the baseline Navier-Stokes solver to handle multiphase, multispecies, chemically reactive sub- to supersonic flows. The major hurdles to overcome in order to achieve significant speed ups are delineated and the approaches to overcoming them will be discussed.

PROGRESS IN ADVANCED SPRAY COMBUSTION CODE INTEGRATION

Pak-Yan Liang

11th Workshop For CFD Applications in Rocket Propulsion

NASA Marshall Space Flight Center

April 20-22, 1993

Rockwell International
Rocketdyne Division

CFD 93 013-001/D1/PYL

I. GENESIS OF THE IDEA

-- VALUE OF THE FIRST GENERATION EXPERIENCE: ARICC --

- ARICC STILL REPRESENTS ONE OF THE MOST COMPREHENSIVE PACKAGES OF PHYSICAL MODELS IN ANY CFD CODE
- ARICC DEMONSTRATED THE FEASIBILITY OF FULLY COUPLED THREE-PHASE (DROPLETS, GAS, LIQUID) CFD IN A FINITE VOLUME FORMULATION
- ARICC HIGHLIGHTED THE CRITICALITY OF THE INTER-DISCIPLINARY APPROACH AD THE KEY ROLE OF SEVERAL PHYSICAL PROCESSES IN LIQUID PROPULSION: I.E., ATOMIZATION, EVAPORATION, DENSE SPRAY EFFECTS

Rockwell International
Rocketdyne Division

CFD 92-007-003/D1/PYL

I. GENESIS OF THE IDEA

- - MOTIVATION BEHIND THIS EFFORT - -

TO

ADVANCED STATUS OF MULTI-PHASE SPRAY COMBUSTION MODELING

FROM
A LEVEL OF

TECHNICAL FEASIBILITY → TO A LEVEL OF → ECONOMIC ATTRACTIVENESS

CF. EXTERNAL FLOW AERODYNAMIC CODES CIRCA 1980.

Rockwell International
Rocketdyne Division

CFD 92-007-009/D1/PYL

II. DETAILS OF THE PLAN

- **ORGANIZATIONAL OBJECTIVE: BROADENED SENSE OF OWNERSHIP THROUGH MULTI-PARTY INVOLVEMENT**

- **TECHNICAL OBJECTIVE: 3–5X REDUCTION IN TURNAROUND TIME THROUGH**
  - MODEST IMPROVEMENT IN COMPUTATIONAL EFFICIENCY
  - LARGE IMPROVEMENTS IN ROBUSTNESS
  - PROVISIONS FOR EVOLVING COMPUTER ARCHITECTURES

- **SCHEDULING OBJECTIVE: NEAR-TERM (3 YR), CLEAR-CUT PROJECT COMPLETION THROUGH USE OF**
  - PROVEN LOW RISK METHODOLOGY AS BASE
  - INCORPORATION OF NOVEL ENHANCEMENT FEATURES CURRENTLY BEING DEVELOPED IN OTHER TECHNOLOGY EFFORTS

Rockwell International
Rocketdyne Division

CFD 92-007-010/D1/PYL

APPLICATIONAL OBJECTIVE

OPTIMAL ENGINEER – MODEL INTERFACE (DESIGNER)

HOW TO MAKE CFD MODELS USABLE BY NON-CFD SPECIALISTS?

- EASY PARAMETRIC VARIATION OF HARDWARE GEOMETRY
- EASY VISUALIZATION OF FLOW FIELD AND HEAT LOADING
- EASY DIAGNOSIS OF NUMERICAL PROBLEMS

Rockwell International
Rocketdyne Division

CFD 93 010-003/D1/PYL

MOTIVATION

- **IMPROVED ROBUSTNESS OF NEXT-GENERATION CODE TO BE MEASURED IN TERMS OF**
  - OPERABILITY OVER WIDE RANGE OF DIFFERENT REGIMES
  - COMPUTATIONAL EFFICIENCY FOR BASELINE FLOW PROCESSES
  - INCREASED TOLERANCE OF LOCALLY OR TEMPORARILY STIFF PROCESSES

Rockwell International
Rocketdyne Division

CFD 93-013-002/D2/PYL

CODE INTEGRATION STRATEGY

- START WITH
  - PROVEN, PRESSURE-BASED METHODOLOGY OF REACT CODES (BASED ON WORK BY PERIC, 1985)
    - COLLOCATED, PRIMITIVE VARIABLES
    - SEQUENTIAL SOLVER
  - TRANSLPLANT ARICC MULTI-PHASE SUBMODELS
- CLOSELY COORDINATED 2D/3D AND SS/TIME-ACCURATE VERSIONS
- DEVELOP ADVANCED TECHNIQUES FOR OVERCOMING STIFFNESS
  - SOURCE TERM PRE-CONDITIONING
  - GRID ADAPTATION
  - CODING TECHNIQUE FOR PARALLEL COMPUTER ARCHITECTURES

Rockwell International
Rocketdyne Division

CFD 93 013-003/D1/PYL

TECHNICAL ROAD MAP FOR ADVANCED SPRAY COMBUSTION CODE

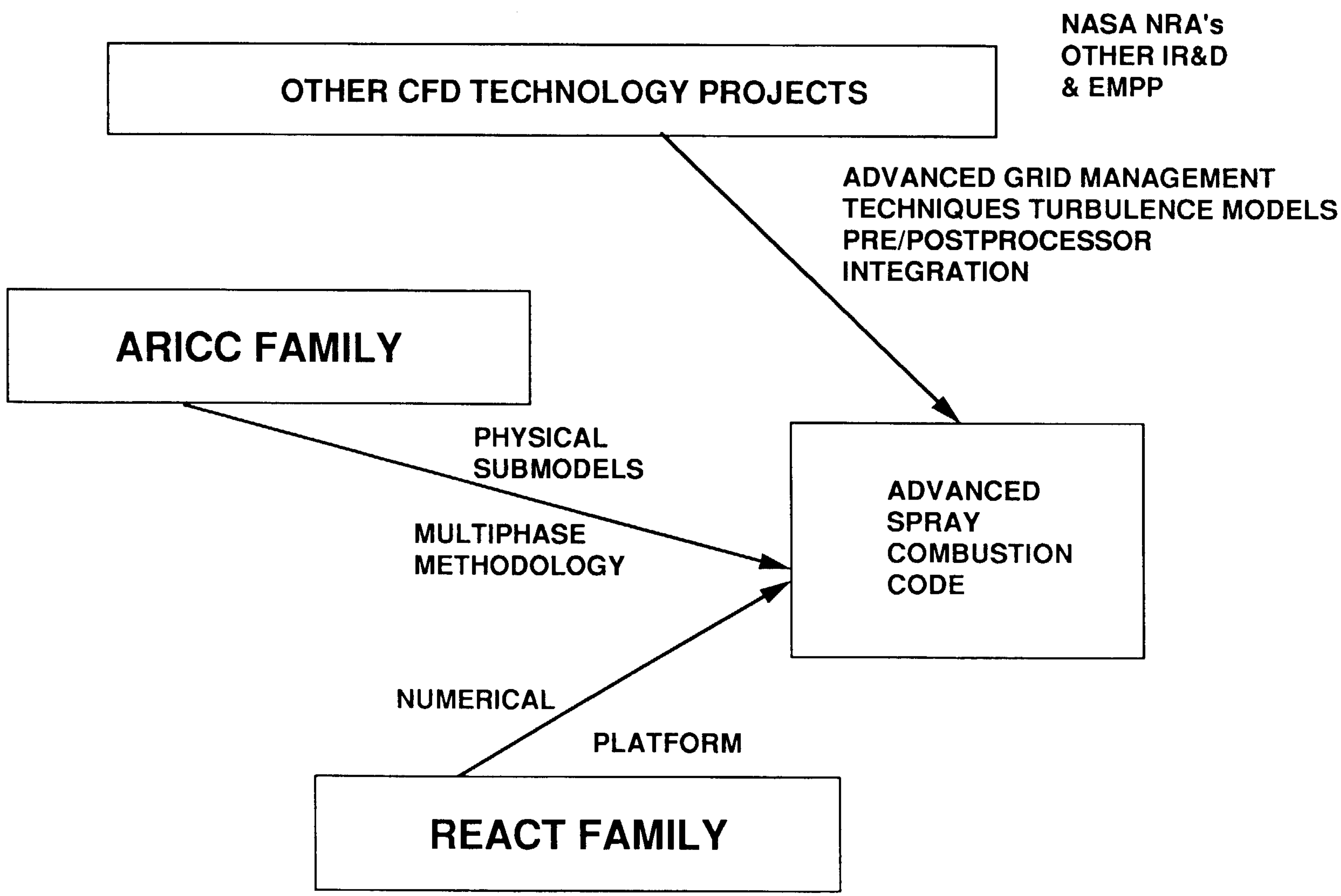

Rockwell International
Rocketdyne Division

CFD 92-013-004/D1/PYL

VOF–BASED CELL PARTITIONING IN ASCOMB

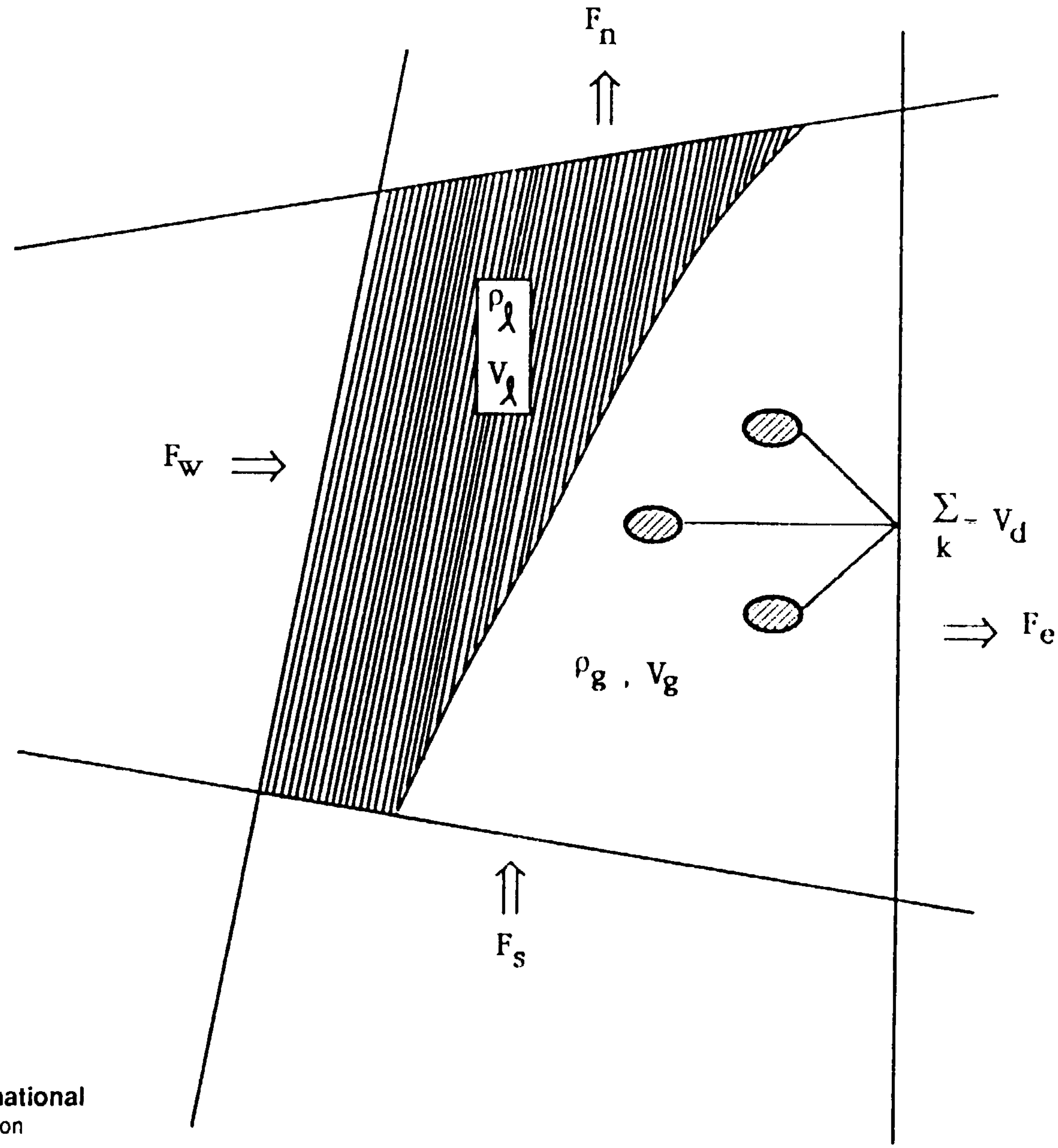

Rockwell International
Rocketdyne Division

CFD 92-058-012/D1/PYL

VOLUME-OF-FLUID TWO-PHASE TRACKING SCHEME IMPLEMENTED IN BOTH ARICC AND GALACSY-2D:

GENERAL ALGORITHM FOR ANALYSIS OF COMBUSTION SYSTEMS

SUMMARY OF GOVERNING EQUATIONS

mass:

$$\frac{\partial \bar{\rho}}{\partial t} + \nabla \bullet (\bar{\rho}\,\mathbf{u}) = \dot{\bar{\rho}}_d \quad \text{where} \quad \bar{\rho} = \mathcal{F}\rho_g + (1-\mathcal{F})\rho_\ell$$

momentum:

$$\frac{\partial \bar{\rho}\mathbf{u}}{\partial t} + \nabla \bullet (\bar{\rho}\mathbf{u}\mathbf{u}) = -\nabla p - \nabla(\tfrac{2}{3}\bar{\rho}\bar{k}) + \nabla \bullet \underset{\approx}{\sigma} + \mathbf{S} + \bar{\rho}\mathbf{G}$$

internal energy:

$$\frac{\partial \bar{\rho}\bar{I}}{\partial t} + \nabla \bullet (\bar{\rho}\bar{I}\mathbf{u}) = -p\nabla \bullet \mathbf{u} - \nabla \mathbf{J} + \bar{\rho}\bar{\varepsilon} + \underset{\text{chemistry}}{\dot{\mathbf{Q}}^c} + \underset{\text{spray}}{\dot{\mathbf{Q}}^s}$$

species m:

$$\frac{\partial \bar{\rho}_m}{\partial t} + \nabla \bullet (\rho_m \mathbf{u}\mathcal{F}) = \mathcal{F}\nabla \bullet \left[\rho_g \mathcal{D} \nabla \left(\frac{\rho_m}{\rho_g}\right)\right] + \underset{\text{chemistry}}{\dot{\bar{\rho}}_m^c} + \underset{\text{evaporation}}{\dot{\bar{\rho}}_s \delta_{m,s}}$$

volume fraction:

$$\frac{\partial \mathcal{F}}{\partial t} + \nabla \bullet \mathbf{u}\mathcal{F} = \dot{\mathcal{F}}_s = \frac{\text{net gas vol. outflux}}{\text{per unit total vol.}} = \frac{\dot{\bar{\rho}}_s}{\rho_g}$$

Rockwell International
Rocketdyne Division

CFD 93 013-004/D1/PYL

OVERALL FLOW CHART FOR ASCOMB

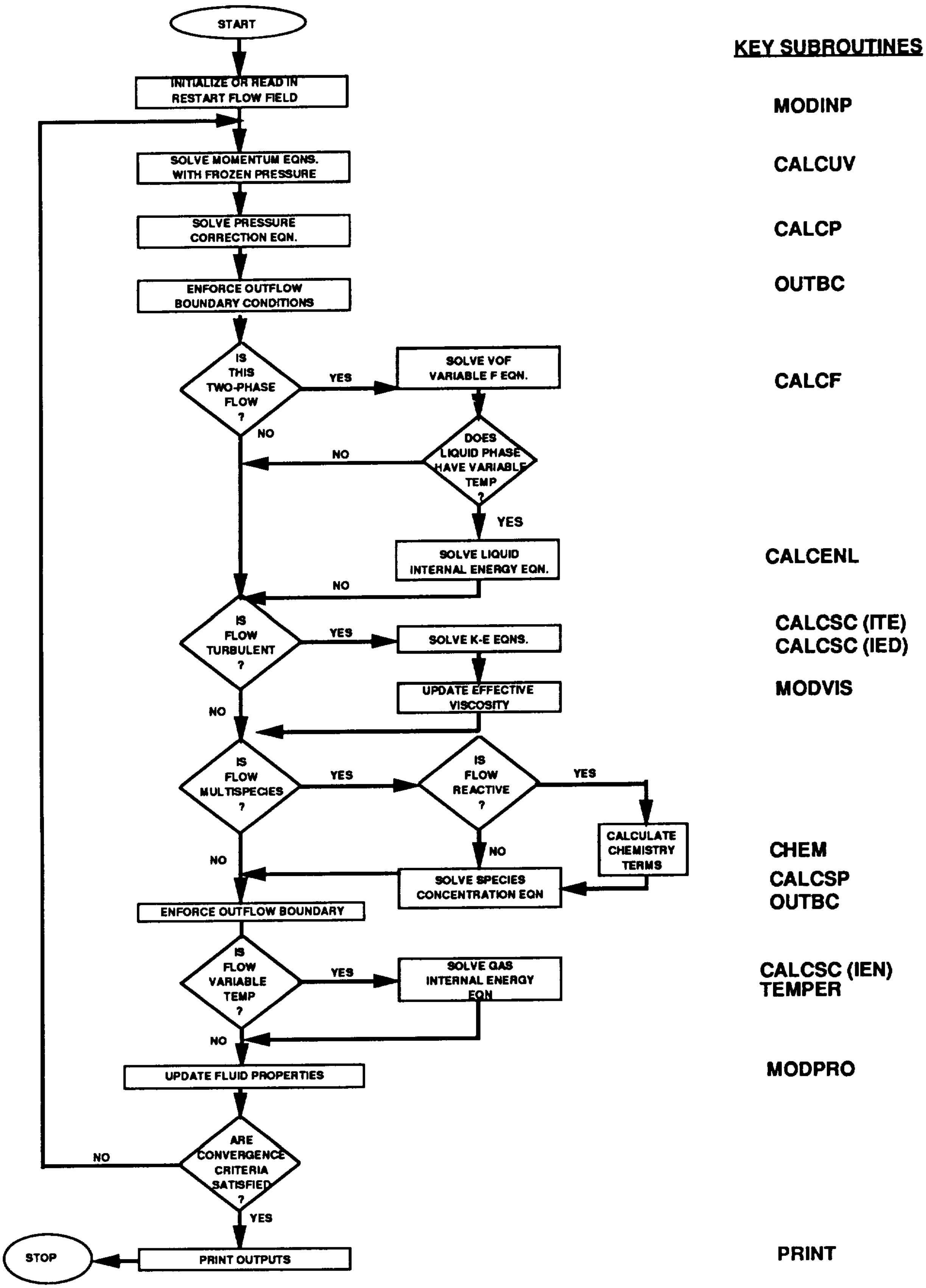

CFD 92-058-006/D4/PYL

SYNOPSIS OF SOLUTION APPROACH

- CAST ALL MATRIX EQUATIONS INTO GENERIC FORM

$$a_P \phi_P = \sum_m a_m \phi_m + C_P$$

WHERE

$$a_P = \sum_m a_m + \dot{\bar{\rho}}_s V_c$$

EXCEPT FOR $\mathcal{F}$-EQUATION, WHERE

$$a_P = \sum_m a_m + \sum_m \dot{V}_m$$

- KEEP COEFFICIENT MATRIX TO 5-DIAGONAL FOR 2D AND 7-DIAGONAL FOR 3D FLOWS BY DOING IMPLICIT DIFFERENCING ONLY FOR CONVECTION AND NORMAL DIFFUSION TERMS.

- SOLVE WITH STONE'S STRONGLY IMPLICIT PROCEDURE

Rockwell International
Rocketdyne Division

CFD 92 013-006/D1/PYL

OBSERVATIONS ON GENERAL FLOW CHARACTERISTICS THAT FORM THE BASIS OF SOLUTION STRATEGY

1\.

- VELOCITY COMPONENTS STRONGLY COUPLED TO EACH OTHER ONLY BY WAY OF PRESSURE; WEAKLY COUPLED TO TURBULENCE & TEMPERATURE FIELDS
- HENCE, 2-STEP PRESSURE CORRECTION APPROACH OF "SIMPLE"
- FLUX UPDATE INCLUDES DENSITY CORRECTION TERM FOR COMPRESSIBLE FLOWS, I.E.,

$$F_{gi} = F^{*}_{gi} + F'_{gi} + \hat{F}_{gi}$$

WHERE

$$F^{*}_{gi} = \mathscr{F}_i\, \rho^{*}_i (u^{*}_1 b^i_1 + u^{*}_2 b^i_2 + u^{*}_3 b^i_3)_i = \mathscr{F}_i\, \rho^{*}_i\, \dot{V}^{*}_i$$

$$F'_{gi} = \mathscr{F}_i\, \rho^{*}_i (u'_1 b^i_1 + u'_2 b^i_2 + u'_3 b^i_3)_i = \mathscr{F}_i\, \rho^{*}_i\, \dot{V}'_i$$

$$\hat{F}_{gi} = \mathscr{F}_i\, \rho'_i (u^{*}_1 b^i_1 + u^{*}_2 b^i_2 + u^{*}_3 b^i_3)_i = \mathscr{F}_i\, \rho'_i\, \dot{V}^{*}_i$$

CFD 93 013-006/01/PYL

COMPUTATIONAL MESH OF CONICAL NOZZLE TEST CASE

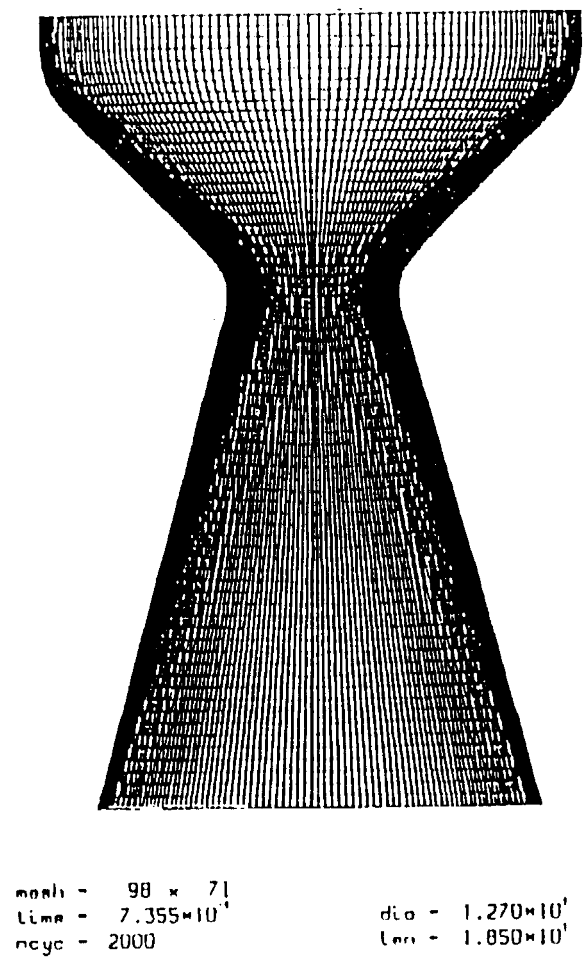

Rockwell International
Rocketdyne Division

CFD 92-058-010/D4/PYL

COMPARISON OF CENTERLINE AND WALL MACH NUMBER PROFILES FOR JPL CONICAL NOZZLE

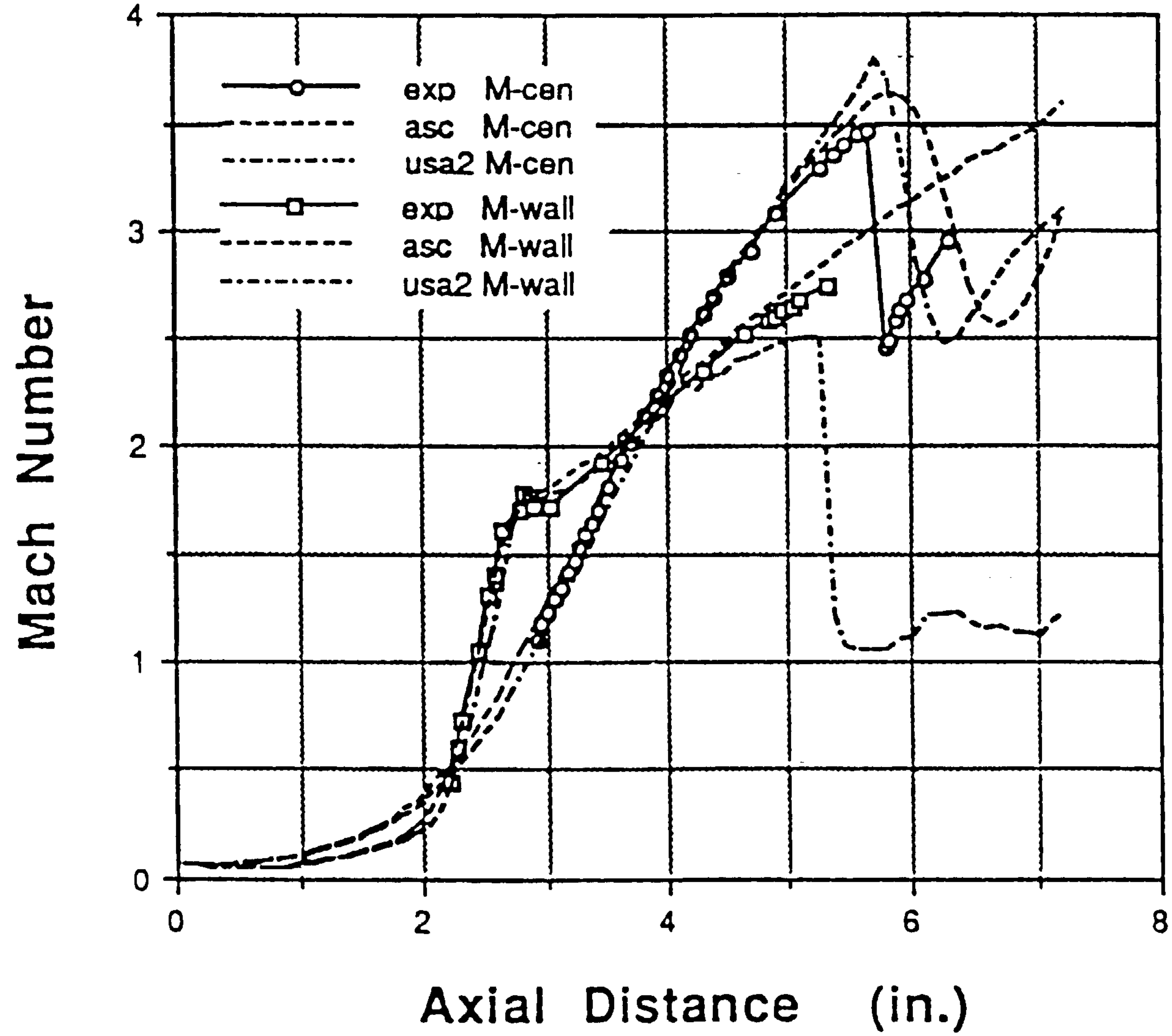

Rockwell International
Rocketdyne Division

CFD 92-058-007/D4/PYL

COMPARISON OF CENTERLINE AND WALL PRESSURE PROFILES FOR JPL CONICAL NOZZLE

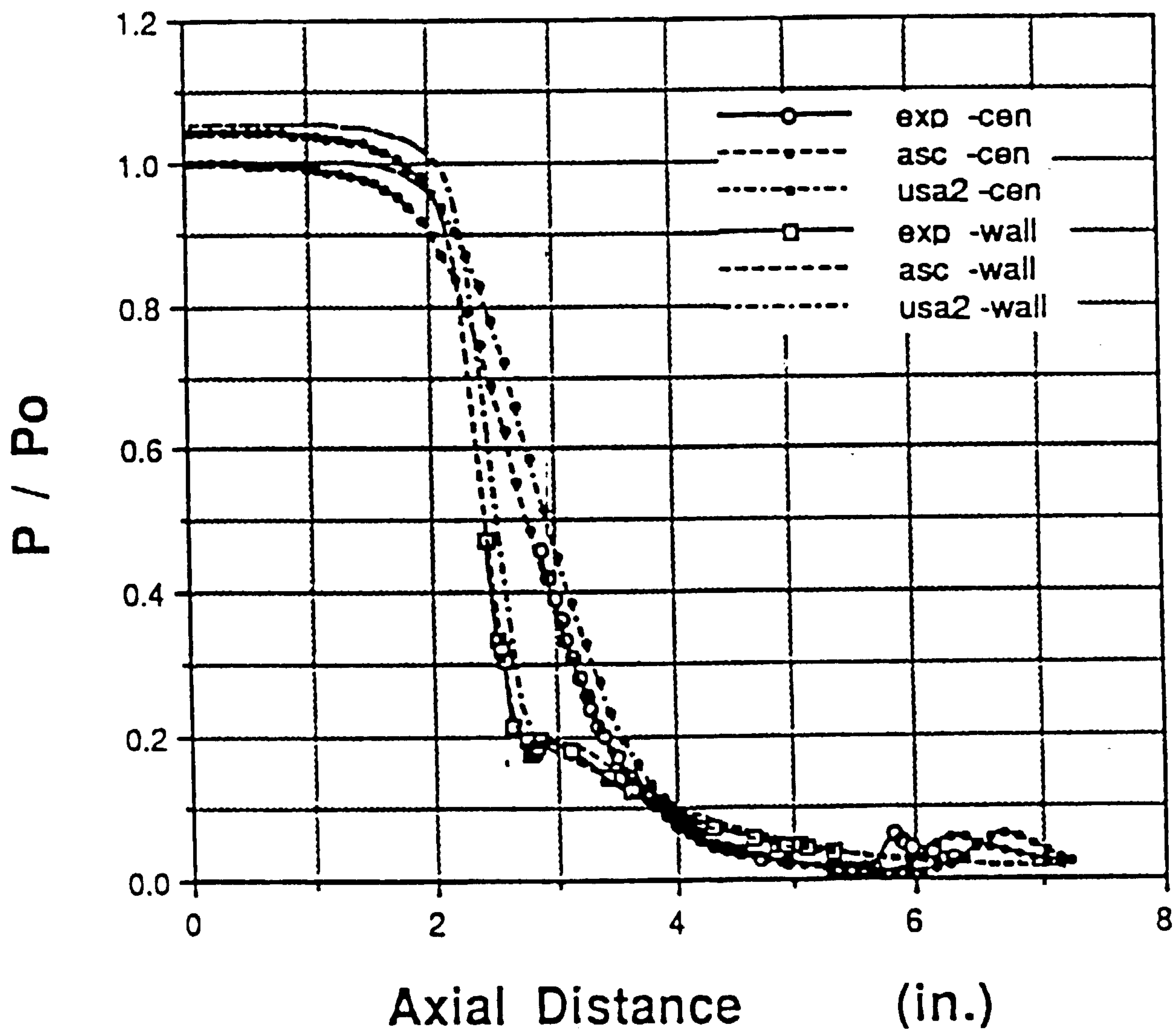

Rockwell International
Rocketdyne Division

CFD 92-058-008/D4/PYL

CHEMISTRY MODEL UPGRADE

- SUPER FAST EQUILIBRIUM PACKAGE FOR H/O CHEMISTRY IMPLEMENTED
- DIRECT CUBIC SOLVER, 8 SPECIES
- FOR EQUILIBRIUM SPECIES, TRANSPORT EQUATIONS FOR ATOMIC TOTAL RATHER THAN FOR INDIVIDUAL COMPOUNDS

1. $2(H_2) + 2(H_2O) + (OH) + (H) + (HO_2) + 2(H_2O_2) = (\hat{H})^\circ$
2. $2(O_2) + (H_2O) + (OH) + 2(HO_2) + 2(H_2O_2) + (O) = (\hat{O})^\circ$
3. $1/2\, O_2 + H_2 = H_2O \qquad (H_2O) = (K_{H_2O})(H_2)(\sqrt{O_2})$
4. $1/2\, H_2 + 1/2 O_2 = OH \qquad (OH) = (K_{OH})(\sqrt{H_2})(\sqrt{O_2})$
5. $1/2\, H_2 = H \qquad (H) = (K_H)(\sqrt{H_2})$
6. $1/2\, H_2 + O_2 = HO_2 \qquad (HO_2) = (K_{HO_2})(\sqrt{H_2})(O_2)$
7. $H_2 + O_2 = H_2O_2 \qquad (H_2O_2) = (K_{H_2O_2})(H_2)(O_2)$
8. $1/2\, O_2 = O \qquad (O) = (K_O)(\sqrt{O_2})$

- FOR KINETICS SPECIES, PREVIOUS GENERAL KINETICS MODEL IS RETAINED

CFD 93-013-003/D1/PYL

ADVANCED SPRAY COMBUSTION CODE PROGRAM MATURATION MILESTONES

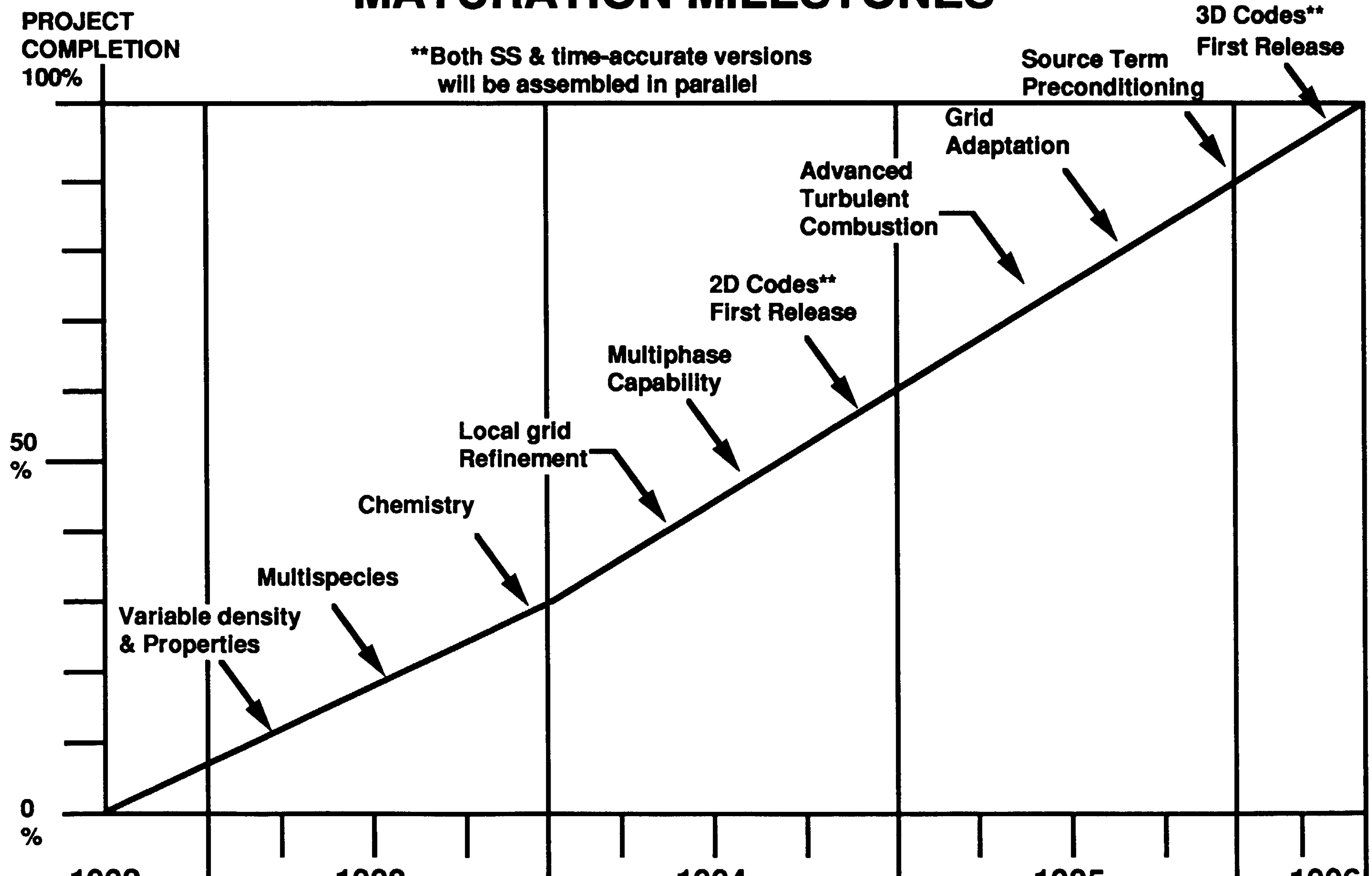

Rockwell International
Rocketdyne Division

CFD 93-013-009/D1/PYL

CONCLUDING REMARKS

- REACT PRESSURE-BASED METHODOLOGY HAS BEEN EXTENDED TO MULTI-PHASE, MULTI-SPECIES, SUPERSONIC FLOWS
- QUANTITATIVE VALIDATION IN PROGRESS
- GOAL OF 10X REDUCTION IN TURNAROUND TIME SEEMS ACHIEVABLE AT LEAST FOR SOME TYPES OF STEADY STATE FLOWS.
- UPCOMING ACTIVITY WILL FOCUS ON
    - LAGRANGIAN SPRAY REPRESENTATION COUPLING SCHEME
    - SOURCE TERM STIFFNESS MITIGATION

Rockwell International
Rocketdyne Division

CFD 93 013-008/D1/PYL

CFD Analysis of Spray Combustion and Radiation in OMV Thrust Chamber

by
M.G. Giridharan, A. Krishnan and A.J. Przekwas
CFD Research Corporation
Huntsville AL 35805
and
K. Gross
NASA Marshall Space Flight Center
Alabama 35812

ABSTRACT

The Variable Thrust Engine (VTE), developed by TRW, for the Orbit Maneuvering Vehicle (OMV) uses a hypergolic propellant combination of Monomethyl Hydrazine (MMH) and Nitrogen Tetroxide (NTO) as fuel and oxidizer, respectively. The propellants are pressure fed into the combustion chamber through a single pintle injection element. The performance of this engine is dependent on the pintle geometry and a number of complex physical phenomena and their mutual interactions. The most important among these are: (1) atomization of the liquid jets into fine droplets; (2) the motion of these droplets in the gas field; (3) vaporization of the droplets; (4) turbulent mixing of the fuel and oxidizer; and (5) hypergolic reaction between MMH and NTO.

Each of the above phenomena by itself poses a considerable challenge to the technical community. In a reactive flow field of the kind occurring inside the VTE, the mutual interactions between these physical processes tend to further complicate the analysis.

The objective of this work is to develop a comprehensive mathematical modeling methodology to analyze the flow field within the VTE. Using this model, the effect of flow parameters on various physical processes such as atomization, spray dynamics, combustion, and radiation is studied. This information can then be used to optimize design parameters and thus improve the performance of the engine.

The REFLEQS CFD Code is used for solving the fluid dynamic equations. The spray dynamics is modeled using the Eulerian-Lagrangian approach. The discrete ordinate method with 12 ordinate directions is used to predict the radiative heat transfer in the OMV combustion chamber, nozzle, and the heat shield. The hypergolic reaction between MMH and NTO is predicted using an equilibrium chemistry model with 13 species.

The results indicate that mixing and combustion is very sensitive to the droplet size. Smaller droplets evaporate faster than bigger droplets, leading to a well mixed zone in the combustion chamber. The radiative heat flux at combustion chamber and nozzle walls are an order of magnitude less than the conductive heat flux. Simulations performed with the heat shield show that a negligible amount of fluid is entrained into the heat shield region. However, the heat shield is shown to be effective in protecting the OMV structure surrounding the engine from the radiated heat.

CFD Research Corporation
3325-D Triana Blvd. ■ Huntsville, AL 35805 ■ (205) 536-6576 ■ FAX: (205) 536-6590

CFD ANALYSIS OF SPRAY COMBUSTION AND RADIATION IN OMV THRUST CHAMBER

by
M.G. Giridharan, A. Krishnan, and A.J. Przekwas
CFD Research Corporation
and
K. Gross
Marshall Space Flight Center

11th CFD Workshop
Marshall Space Flight Center

April 20-22, 1993

PA-93-4PR/01

OUTLINE

CFDRC

- Introduction
- Physical Models
    - Atomization Model
    - Spray Model
    - Combustion Model
    - Radiation Model
- REFLEQS Flow Solver
- Computational Results
- Conclusions

PA-93-4PR/02

INTRODUCTION

CFDRC

Variable Thrust Engine (VTE) for Orbital Maneuvering Vehicle (OMV)

- Planned for Operations in Outer Space
- Relatively Low Power Engine
- Continuous Thrust Variation from 0 to 100%
- Hypergolic Liquid Reactants:
  - Fuel - Monomethyl Hydrazine (MMH)
  - Oxidizer - Nitrogen Tetroxide (NTO)
- Pintle Injector

PA-93-4PR/03

INTRODUCTION

CFDRC

Important Issues

- Modeling Atomization is Crucial for Predicting Initial Drop Sizes
- Vaporization, Mixing and Combustion
- Effects of Radiation and Quantify Radiative Heat Loss

PA-93-4PR/04

PHYSICAL MODELS

Impinging Jets Atomization

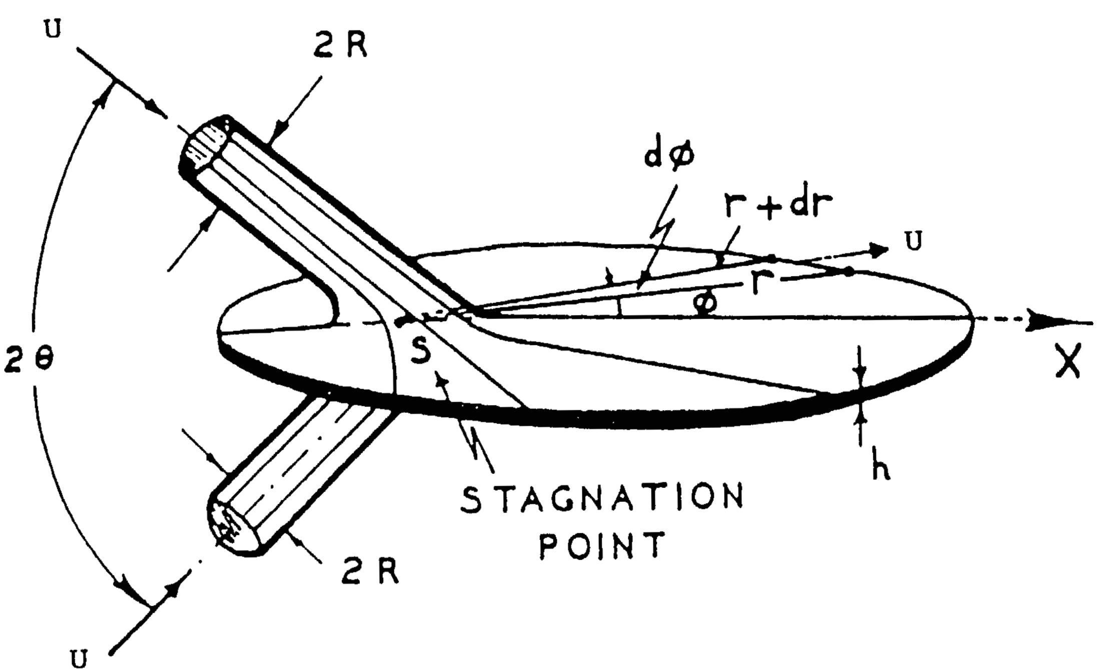

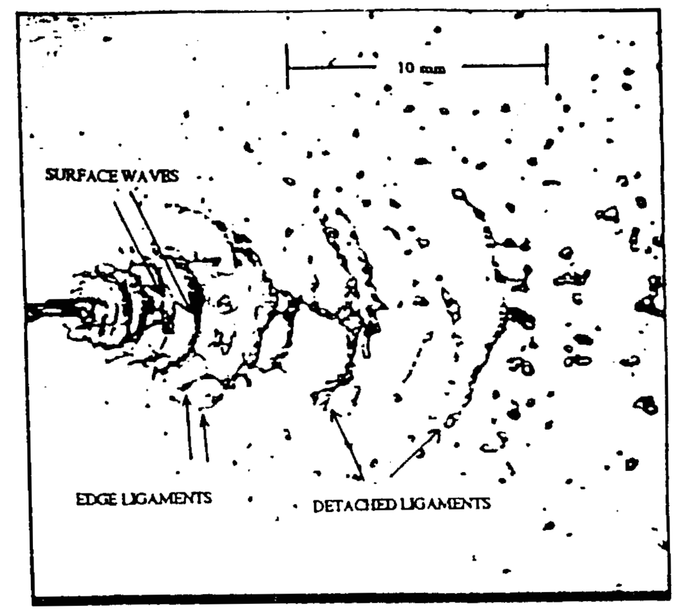

Anderson et al. (1992)

PA-93-4PR/05

PHYSICAL MODELS

CFDRC

Spray Model

- Eulerian-Lagrangian Approach
- Improved Version of PSI-CELL Method
- Deterministic Droplet Tracking
- Droplet Turbulent Dispersion Model based on Gosmann and Ioannides (1981)
- Droplet Size Distributions
- Coupled Droplet Source/Sink Terms for the Gas Phase

PA-93-4PR/08

PHYSICAL MODELS

CFDRC

Combustion Models

- Reaction between MMH & NTO is Hypergolic
- Instantaneous Chemistry
- Finite-Rate Chemistry
- Equilibrium Chemistry
  - based on the element potential method
  - minimization of Gibbs function of the system
  - 13 species (CH_6N_2, N_2O_4, H, H_2, H_2O, NO, CO, CH_4, N_2, O, OH, O_2, CO_2)

PA-93-4PR/09

PHYSICAL MODELS

CFDRC

Radiation Model

- Several Methods are Available
  - Flux Methods
  - Discrete Transfer Method
  - P-N Approximation
  - Monte-Carlo Method
  - Holtel's Zone Method
  - Discrete-Ordinate Method
- For Complex BFC Geometries such as OMV
- Study Effects of Radiation on the Flow
- Estimate Radiative Heat Flux

PA-93-4PR/10

PHYSICAL MODELS

CFDRC

Discrete-Ordinate Radiation Model

Radiative Transfer Equation

$$(\Omega \cdot \nabla) I = -(k + \sigma) I + k I_b + \frac{\sigma}{4\pi} \int_{\Omega = 4\pi} I \phi(\Omega' \to \Omega) \, d\Omega'$$

$I(r, \Omega)$ = Radiation Intensity
k = adsorption coefficient
σ = scattering coefficient
I_b = Black Body Intensity

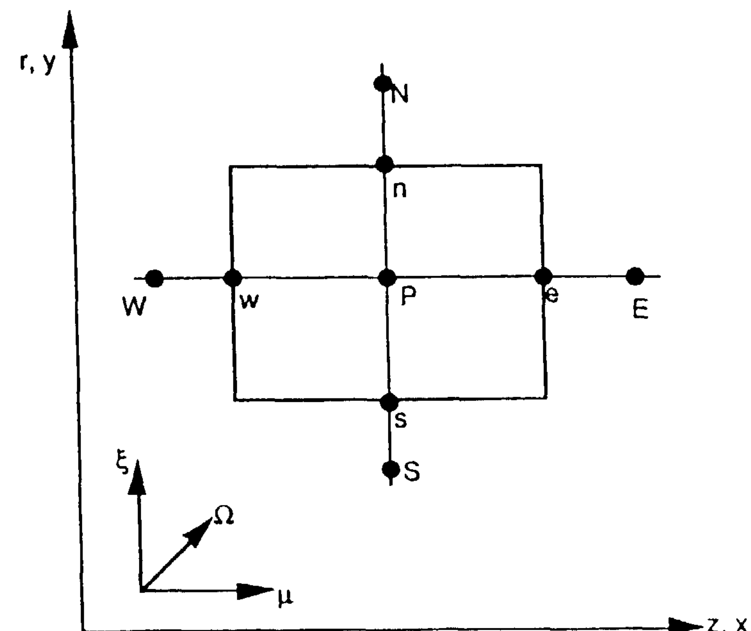

PA-93-4PR/11

REFLEQS FLOW SOLVER

CFDRC

- Solves Favre-Average Navier-Stokes Equations Using the Finite-Volume Approach
- Fully Implicit and Conservative Pressure-Based Solution Algorithm
- Cartesian and BFC Formulation
- k-ε Turbulence Model
- Source/Sink Terms Due to Spray, Combustion, and Radiation

PA-93-4PR/25

RESULTS

Radiation Model Validation

Temperature Distribution in a Square Enclosure (Bottom Wall - 1000°K, Other Walls - 0°K)

```
TEMP    CONTOURS
FMIN    5.063E+02
FMAX    8.796E+02
CONTOUR LEVELS
  1     5.063E+02
  2     5.260E+02
  3     5.456E+02
  4     5.653E+02
  5     5.849E+02
  6     6.046E+02
  7     6.242E+02
  8     6.439E+02
  9     6.635E+02
 10     6.831E+02
 11     7.028E+02
 12     7.224E+02
 13     7.421E+02
 14     7.617E+02
 15     7.814E+02
 16     8.010E+02
 17     8.207E+02
 18     8.403E+02
 19     8.599E+02
 20     8.796E+02
OK>
```

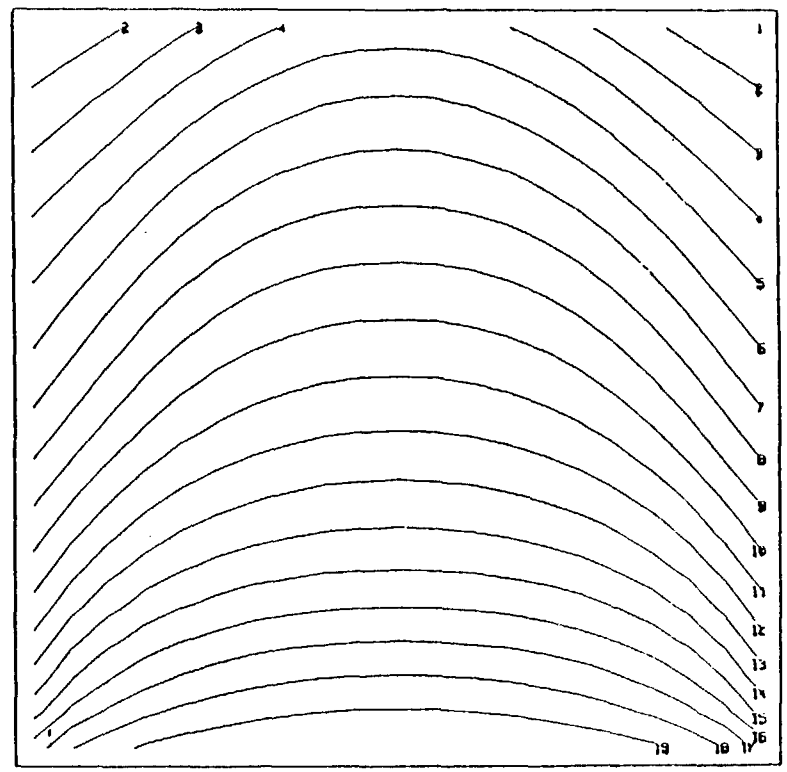

Grid Size 20 x 20

PA-93-4PR/13

RESULTS

Radiation Model Validation

CFDRC

Temperature Distribution in a Square Enclosure with Non-Orthogonal Grid

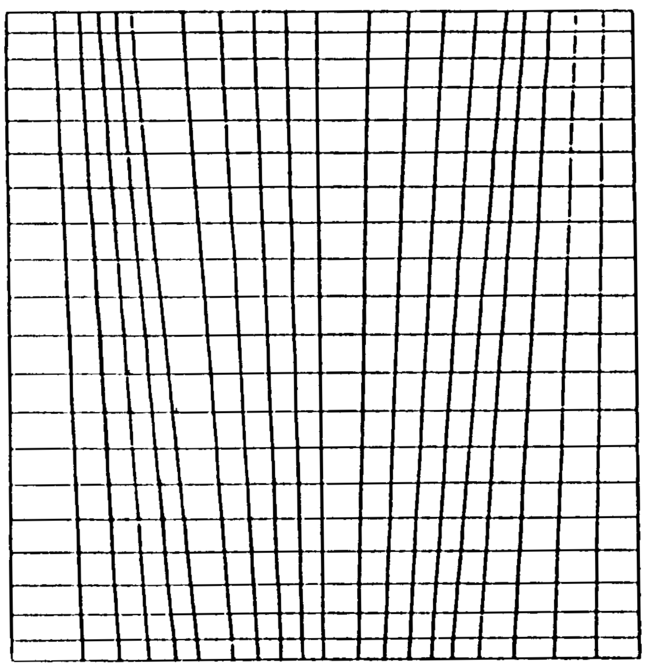

```
XY PLANE  1
TEMP  CONTOURS
FMIN  5.063E+02
FMAX  8.832E+02
CONTOUR LEVELS
  1   5.063E+02
  2   5.262E+02
  3   5.460E+02
  4   5.658E+02
  5   5.857E+02
  6   6.055E+02
  7   6.253E+02
  8   6.452E+02
  9   6.650E+02
 10   6.848E+02
 11   7.047E+02
 12   7.245E+02
 13   7.443E+02
 14   7.642E+02
 15   7.840E+02
 16   8.038E+02
 17   8.237E+02
 18   8.435E+02
 19   8.633E+02
 20   8.832E+02
OK>
```

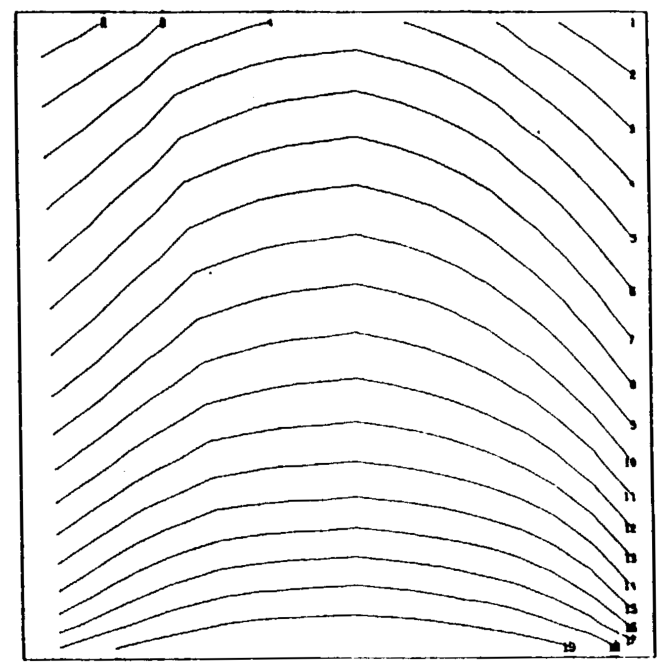

Grid Size 20 x 20

PA-93-4PR/14

RESULTS

Radiation Model Validation

Radiative Heat Transfer at the Hot Wall of a Square Enclosure for Various Absorption Cross-Sections

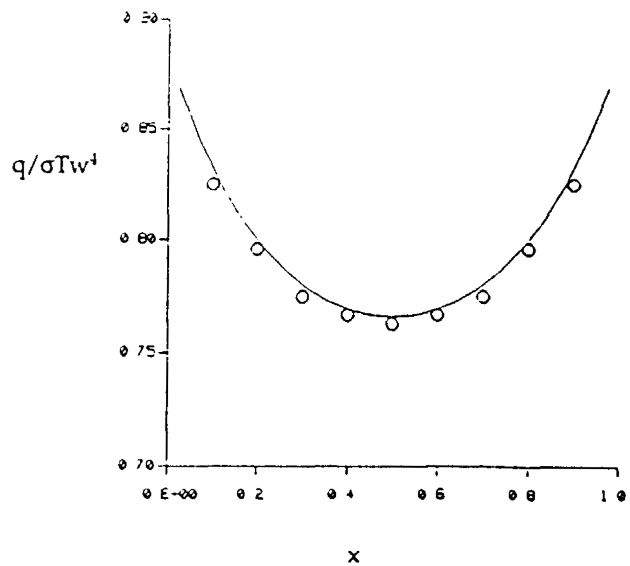

1.0

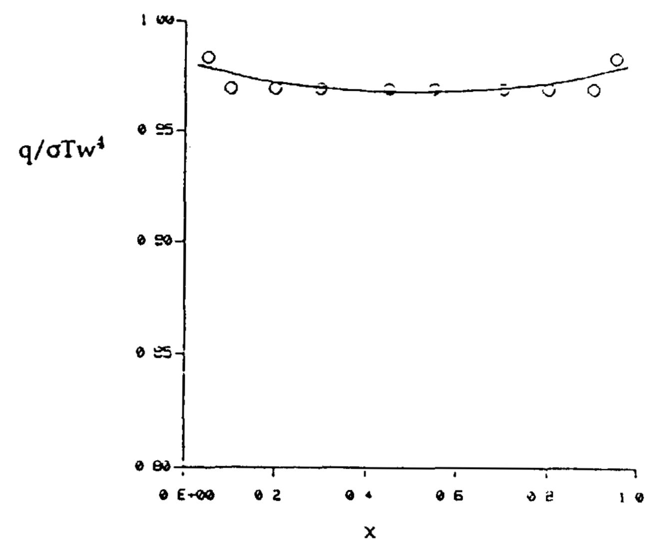

0.1

PA-93-4PR/15

Equilibrium Chemistry Model Validation

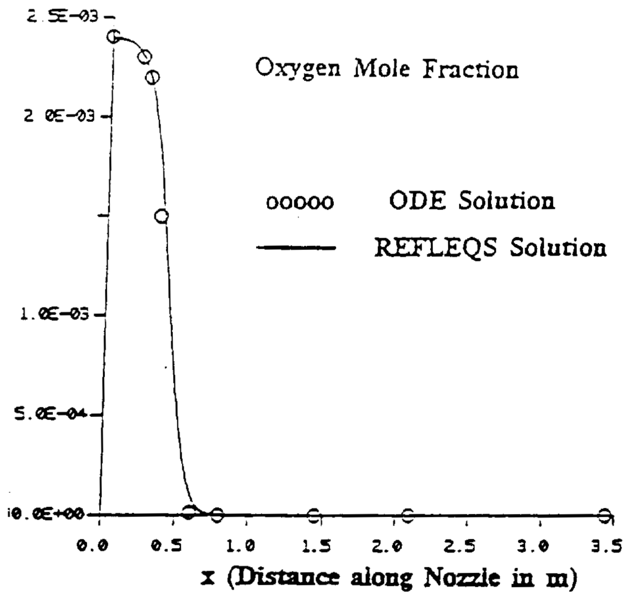

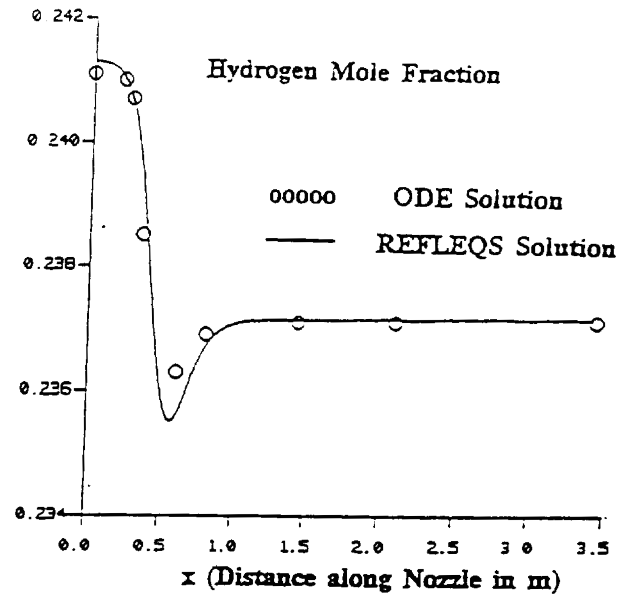

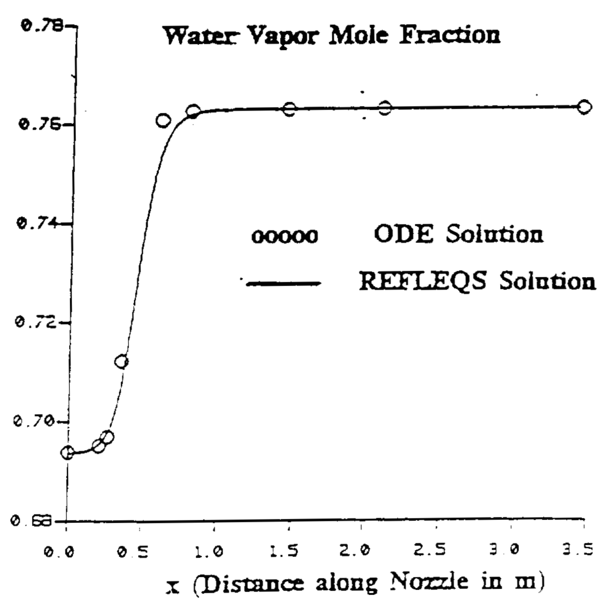

PA-93-4PR/22

TEMPERATURE DISTRIBUTION IN VTE CHAMBER/NOZZLE (GAS-GAS MODEL)

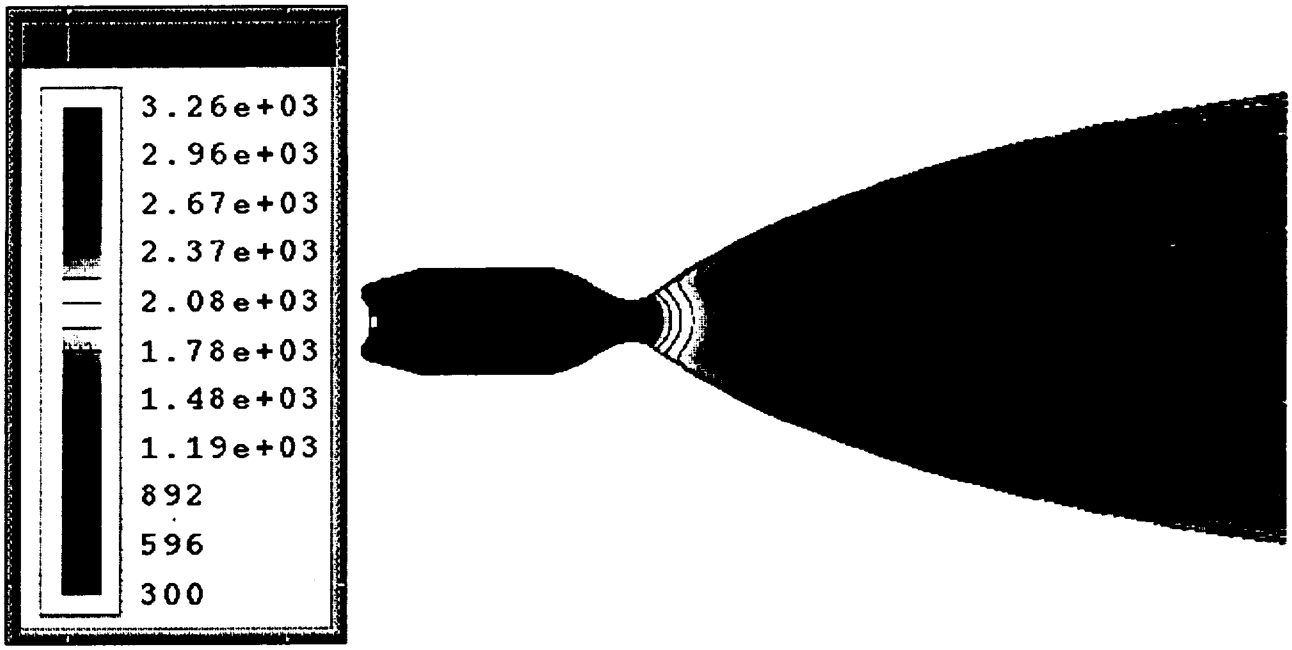

100% POWER LEVEL

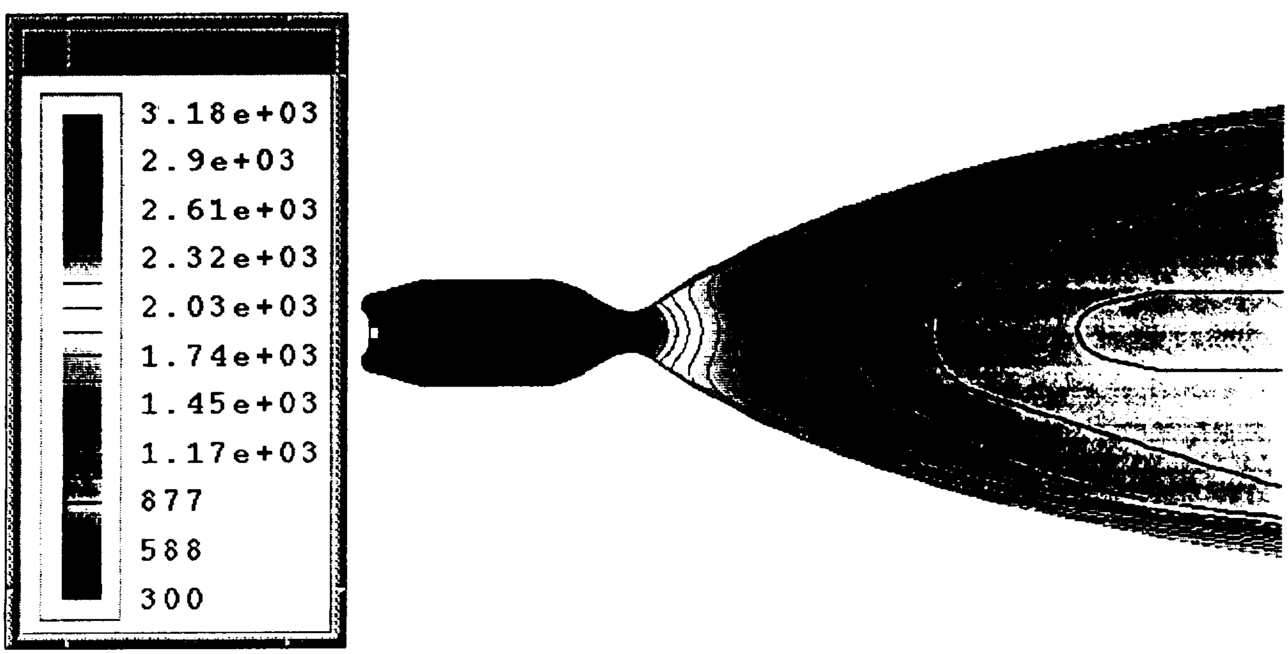

50% POWER LEVEL

Mach Number Distribution in VTE Chamber/Nozzle (Gas-Gas Model)

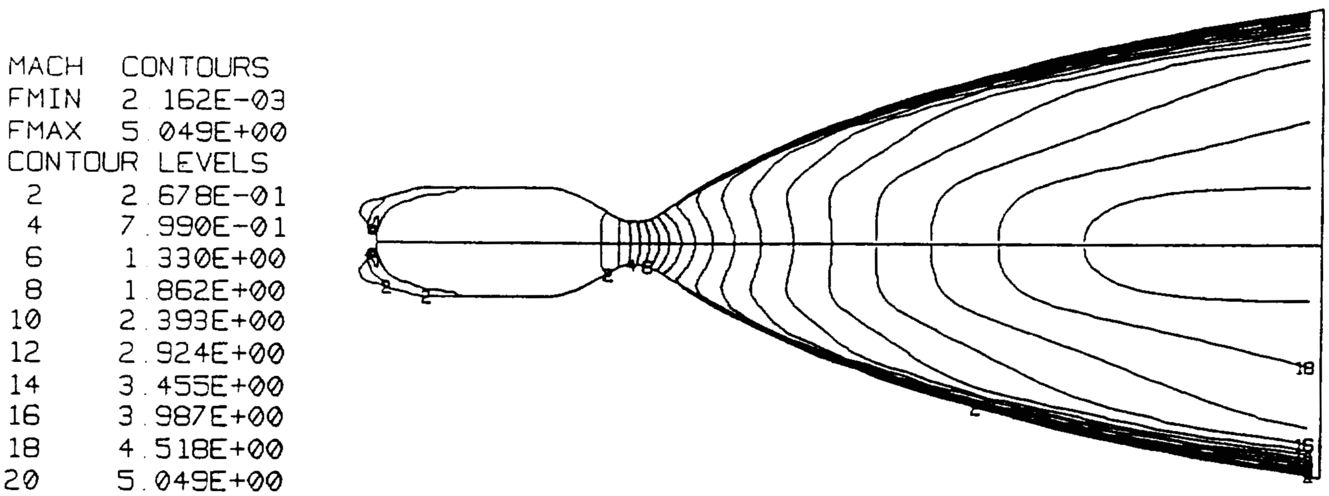

100% Power Level

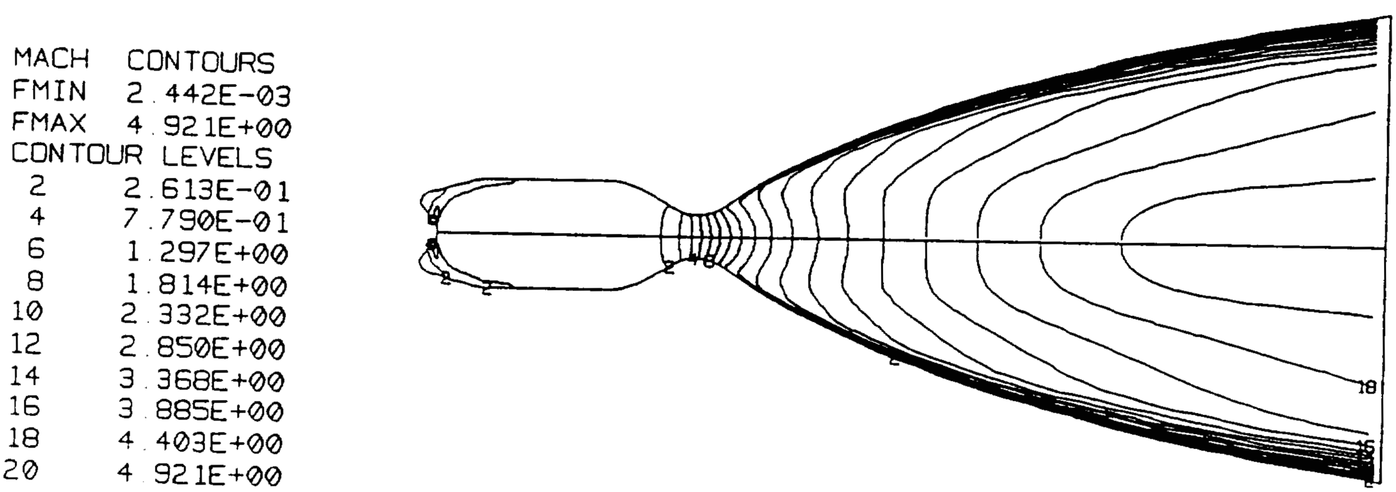

50% Power Level

RESULTS
Spray Model

Drop Size Distribution

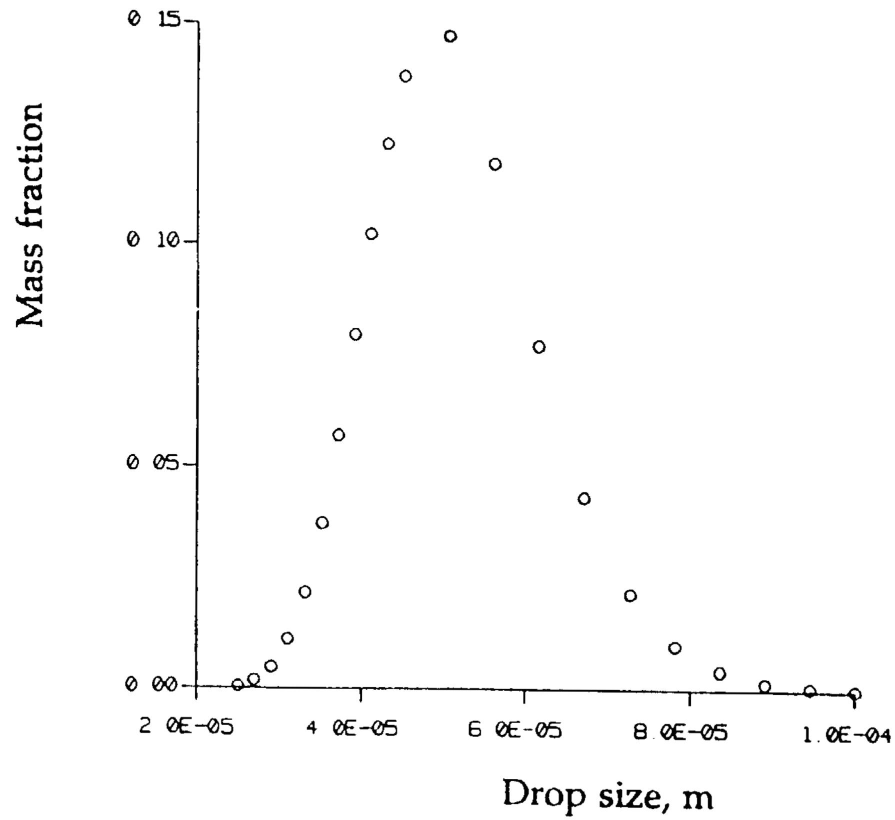

Droplet Trajectories

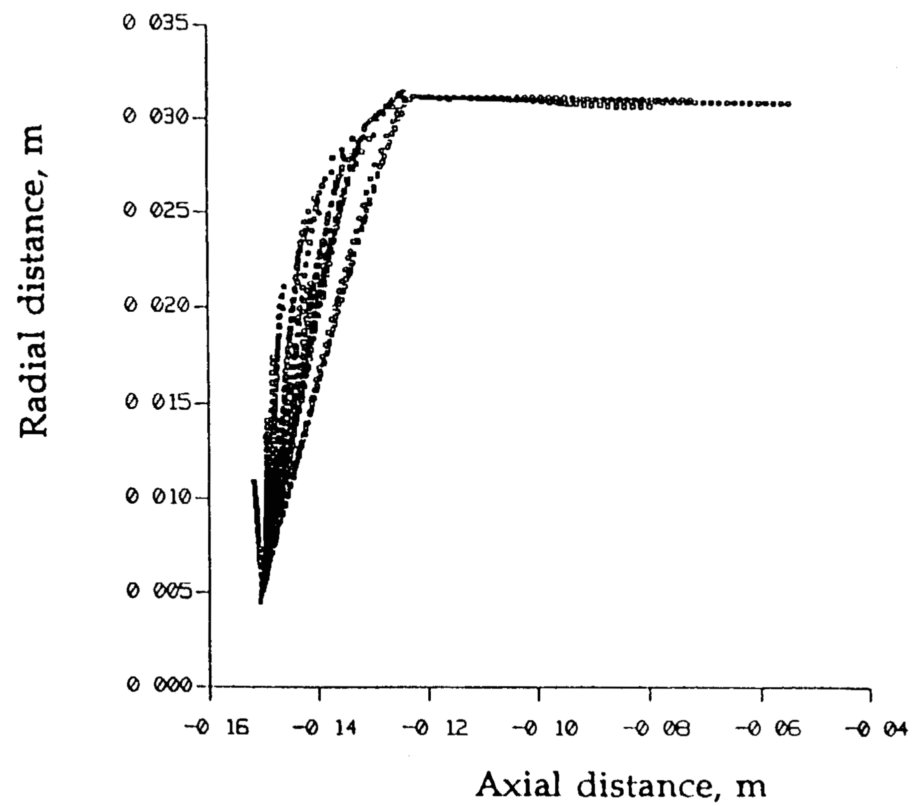

PA-93-4PR/17

TEMPERATURE DISTRIBUTION IN VTE CHAMBER/NOZZLE

(SPRAY MODEL)

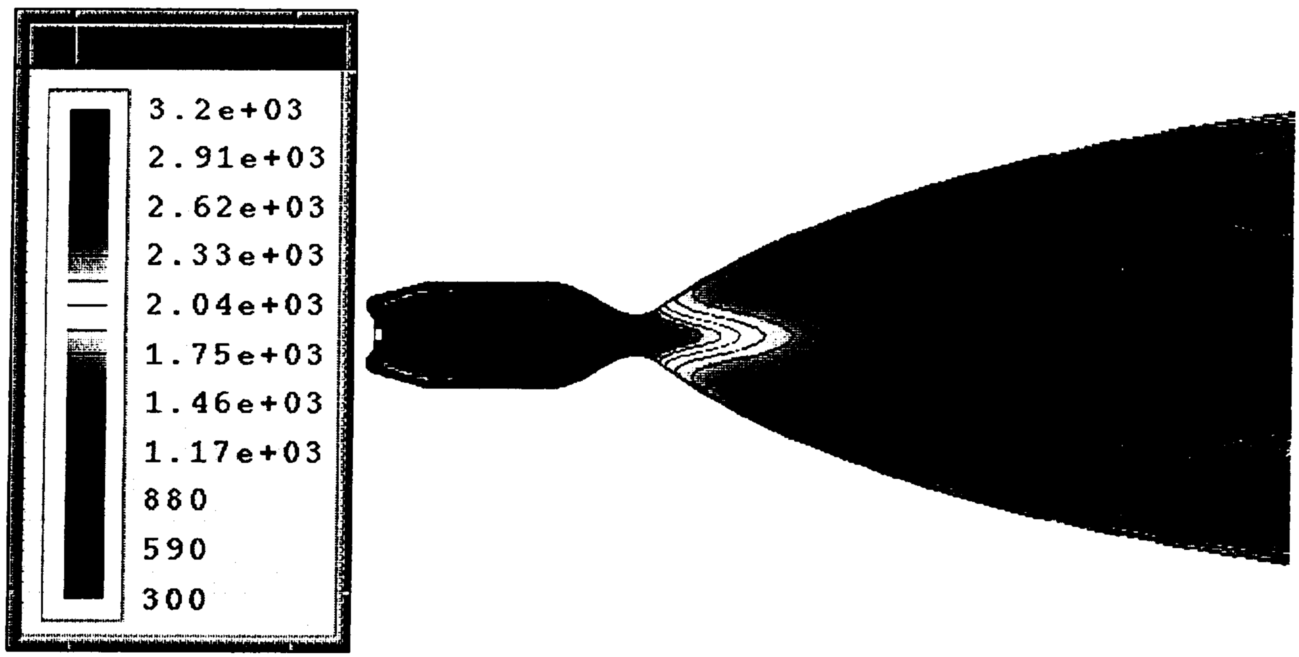

100% POWER LEVEL

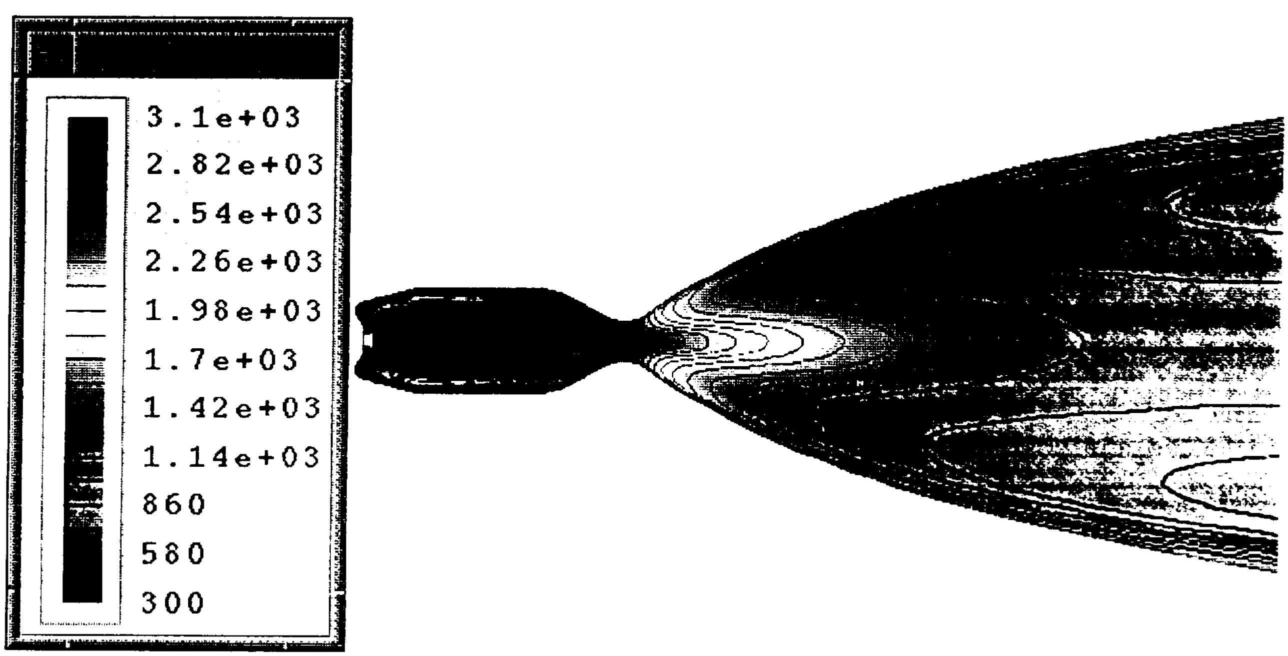

50% POWER LEVEL

Mach Number Distribution in VTE Chamber/Nozzle (Spray Model)

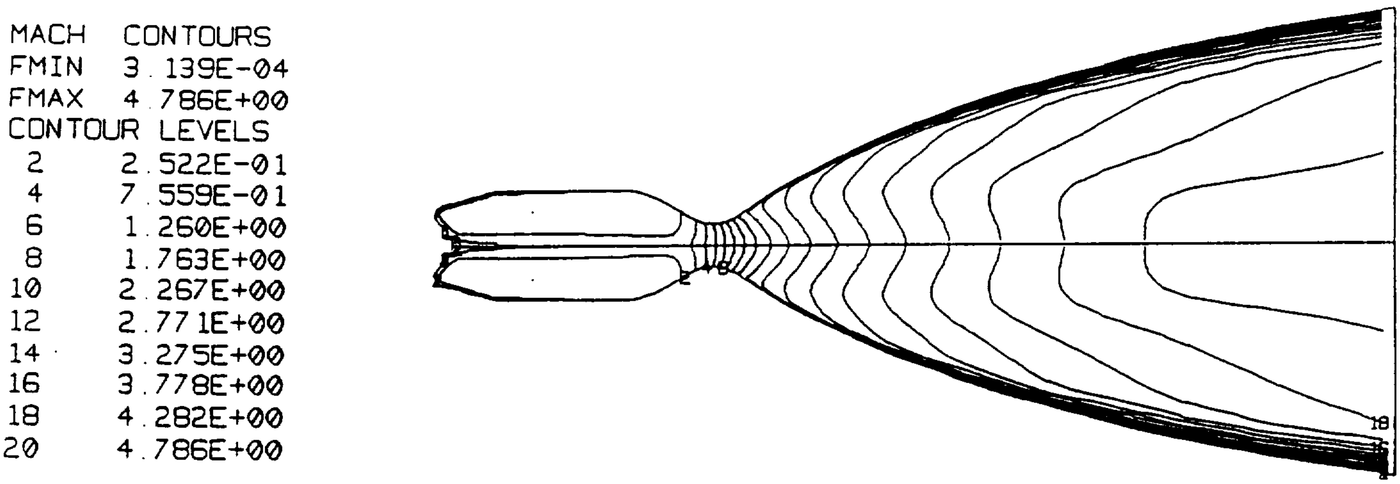

100% Power Level

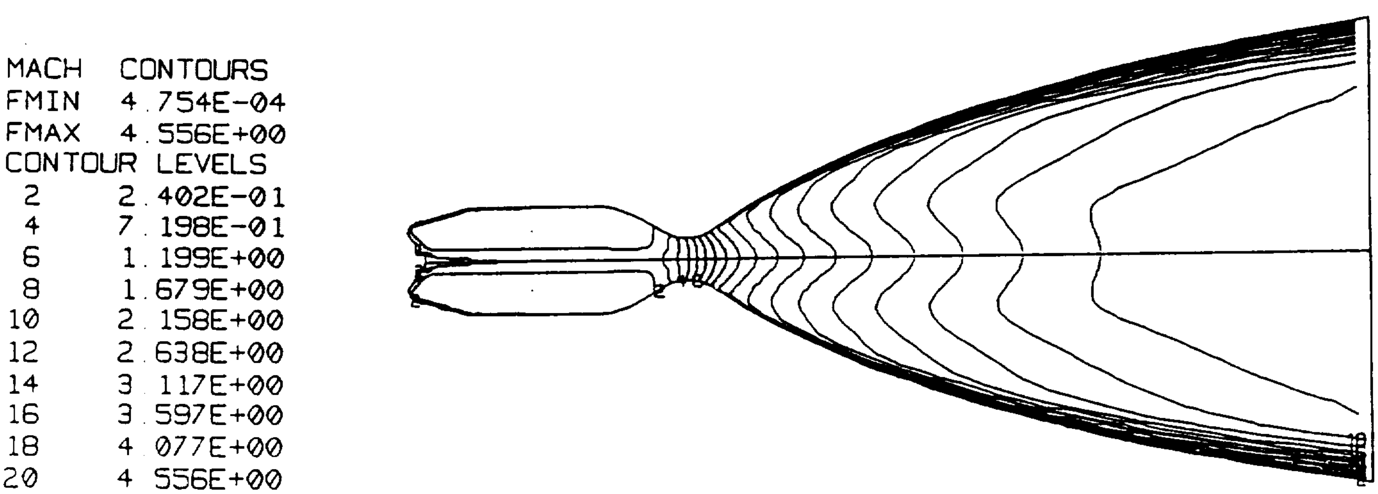

50% Power Level

PA-93-4PR/24

EVAPORATED NTO MASS DISTRIBUTION IN VTE CHAMBER (100% POWER LEVEL)

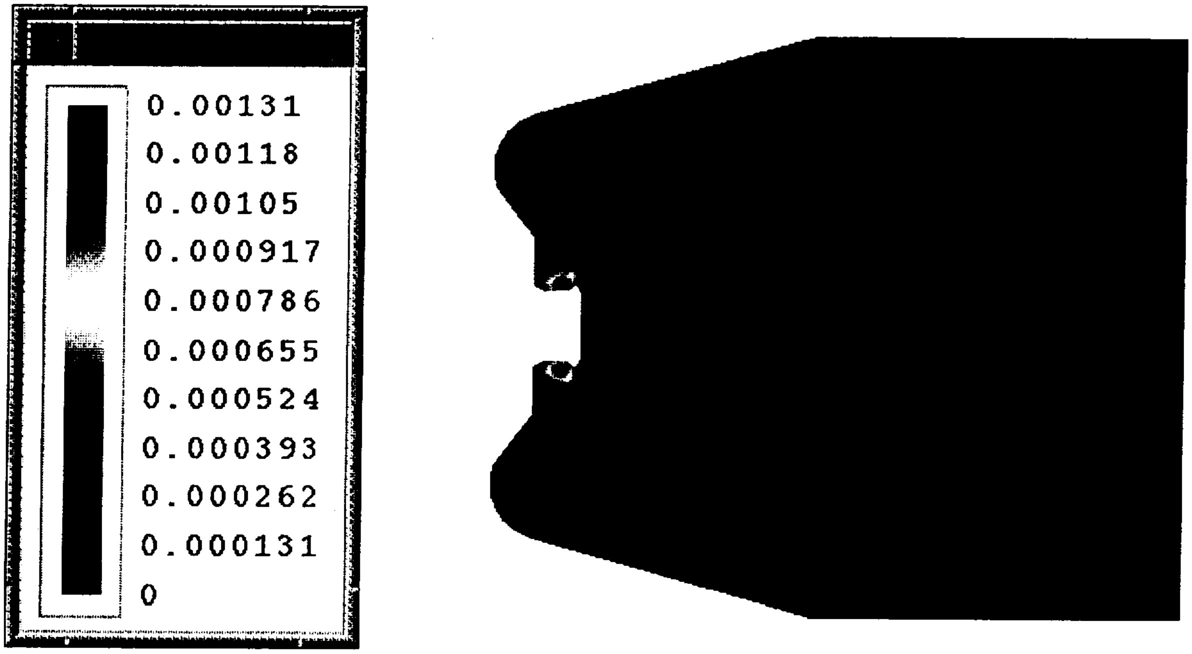

25 MICRON MEAN DROP SIZE

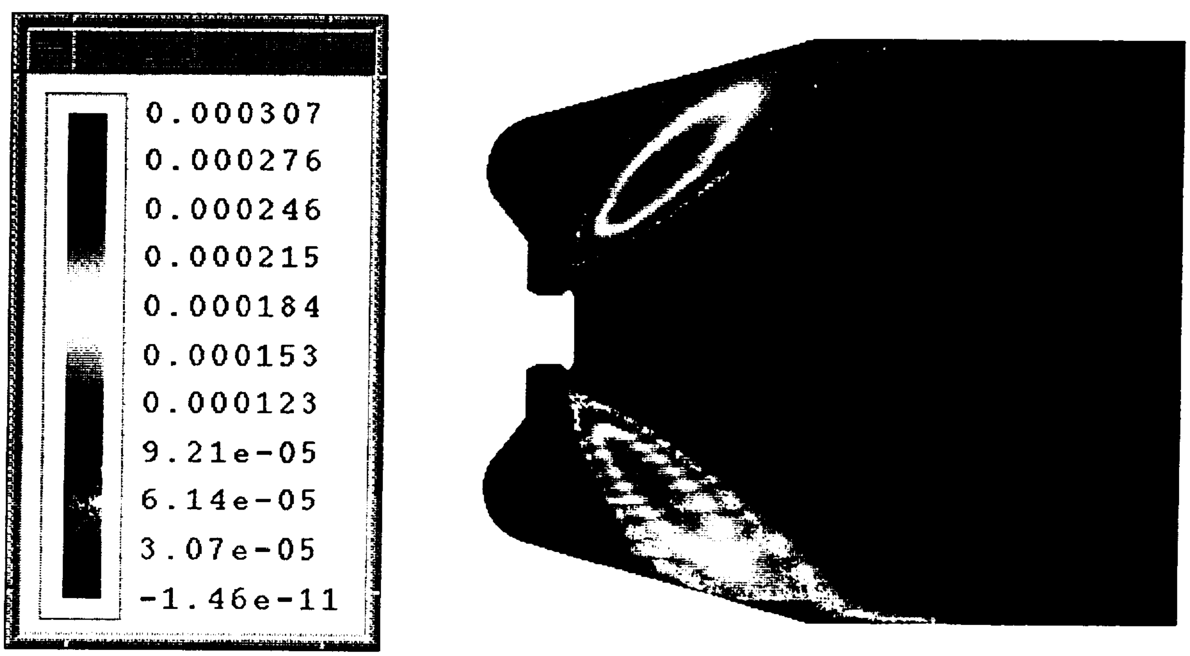

100 MICRON MEAN DROP SIZE

EFFECT OF RADIATION IN VTE CHAMBER/NOZZLE (TEMPERATURE DISTRIBUTION, 100% POWER LEVEL)

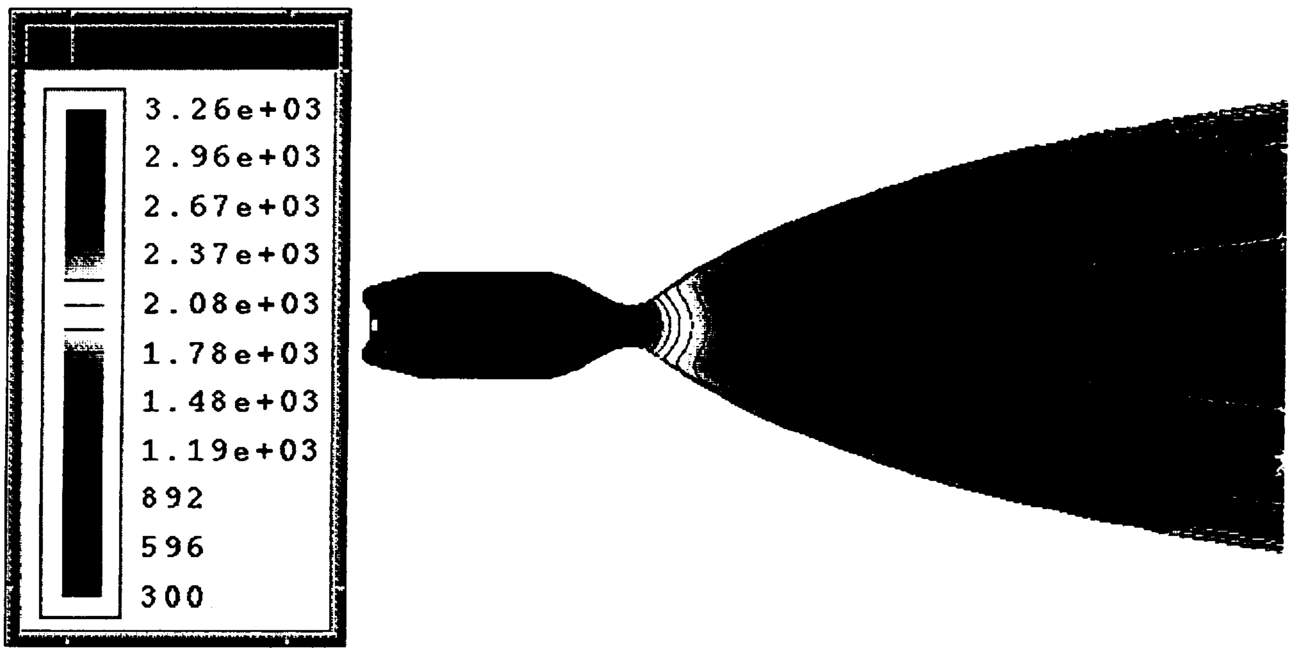

NO RADIATION

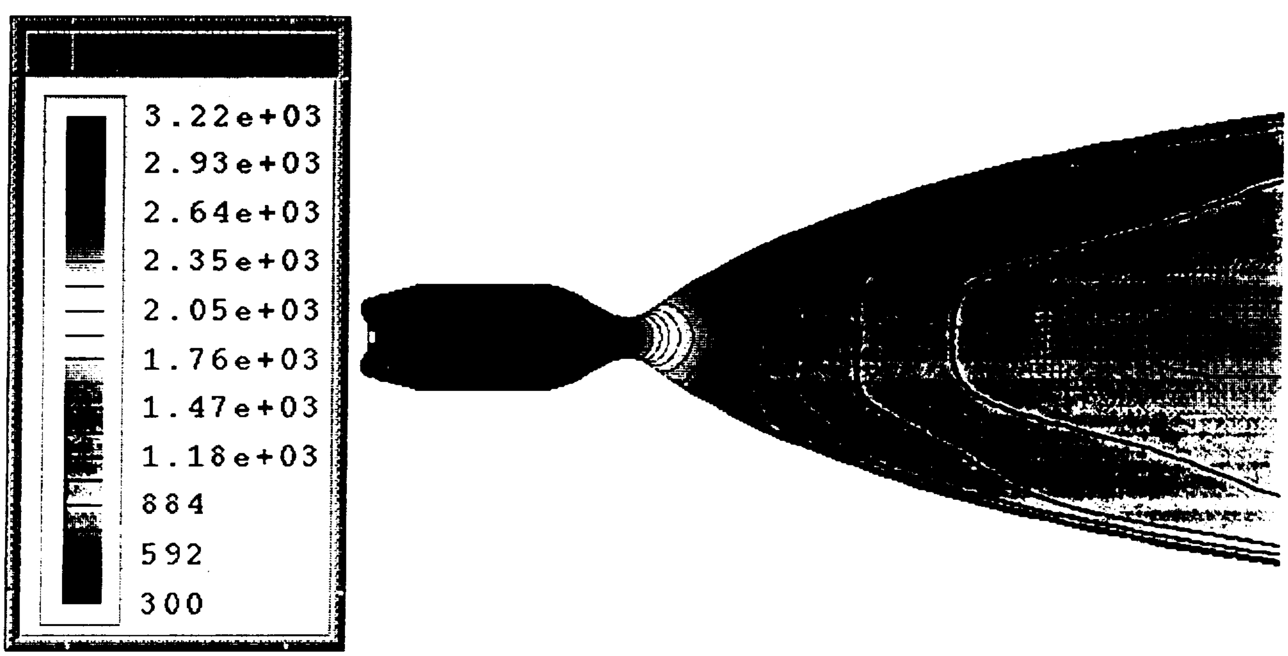

WITH RADIATION

RESULTS

Radiation Model

Comparison of Conductive and Radiative Heat Fluxes

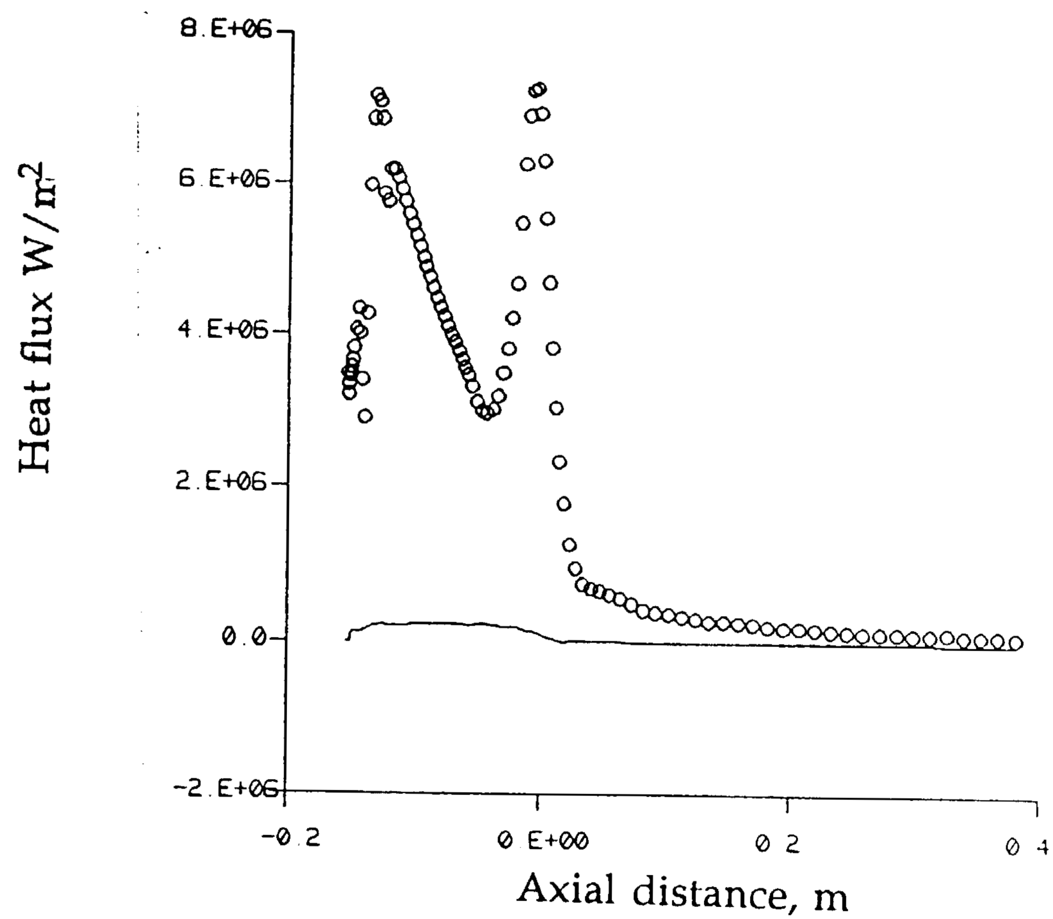

PA-93-4PR/19

RESULTS

CFDRC

Mach Number Distribution in VTE Chamber/Nozzle/Heat Shield

MACH CONTOURS

FMIN 2.140E-08

FMAX 4.817E+00

CONTOUR LEVELS

2	1.661E-01
4	4.983E-01
6	8.305E-01
8	1.163E+00
10	1.495E+00
12	1.827E+00
14	2.159E+00
16	2.492E+00
18	2.824E+00
20	3.156E+00
22	3.488E+00
24	3.821E+00
26	4.153E+00
28	4.485E+00
30	4.817E+00

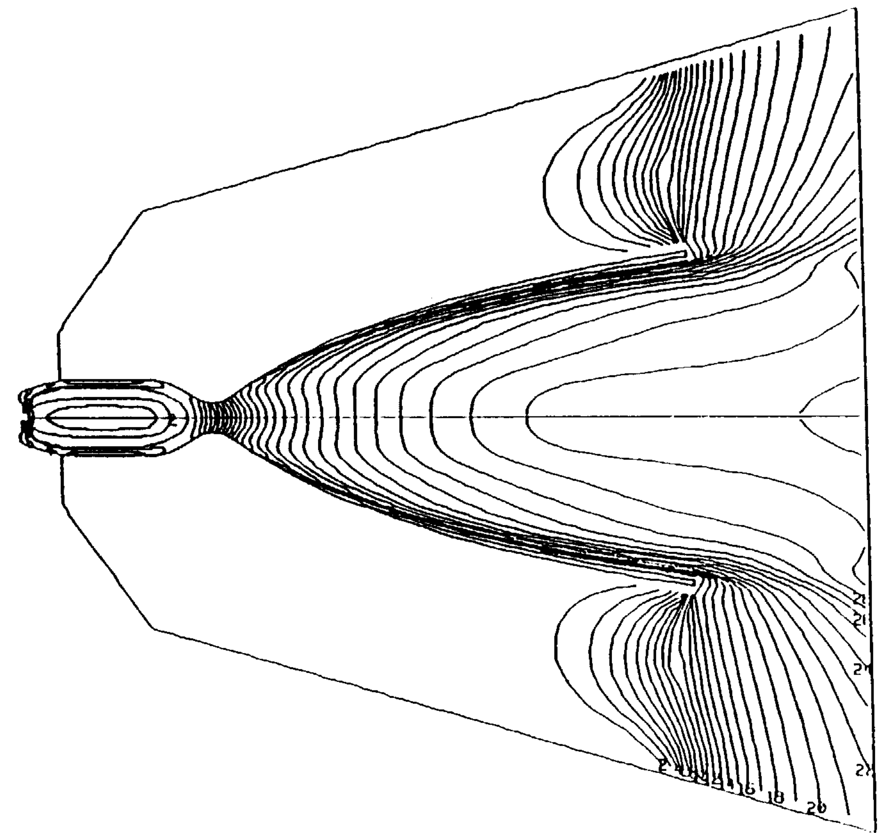

(Gas-Gas Model, 100% Power Level)

PA-93-4PR/21

EFFECT OF RADIATION IN VTE CHAMBER/NOZZLE/HEAT SHIELD (TEMPERATURE DISTRIBUTION, 100% POWER LEVEL)

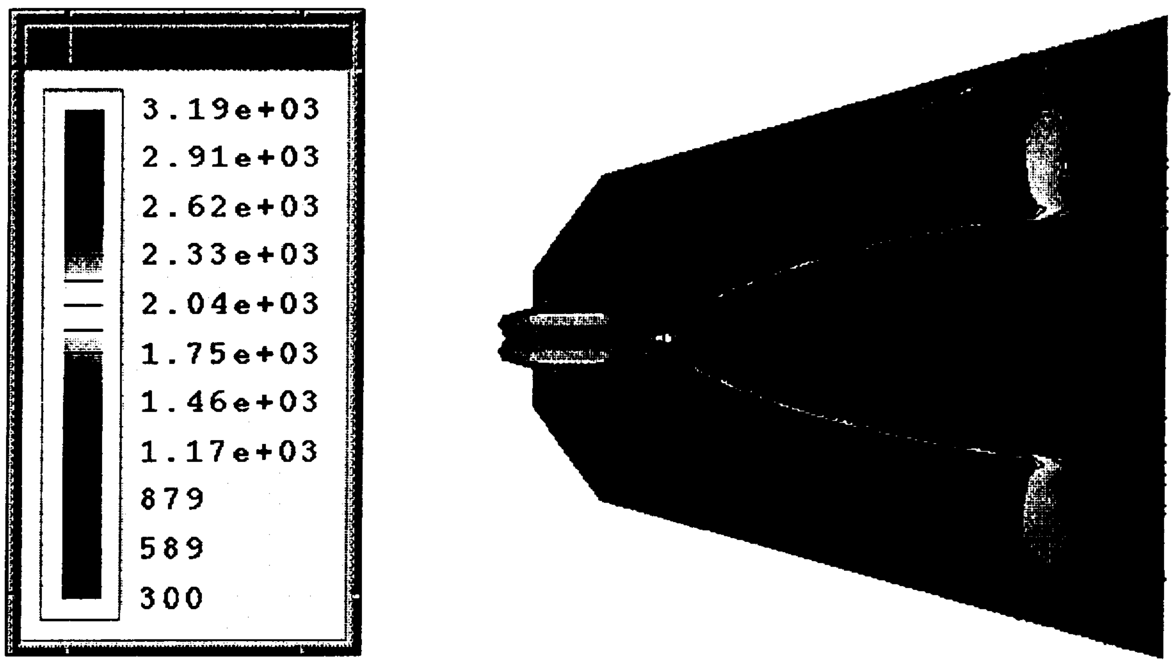

NO RADIATION

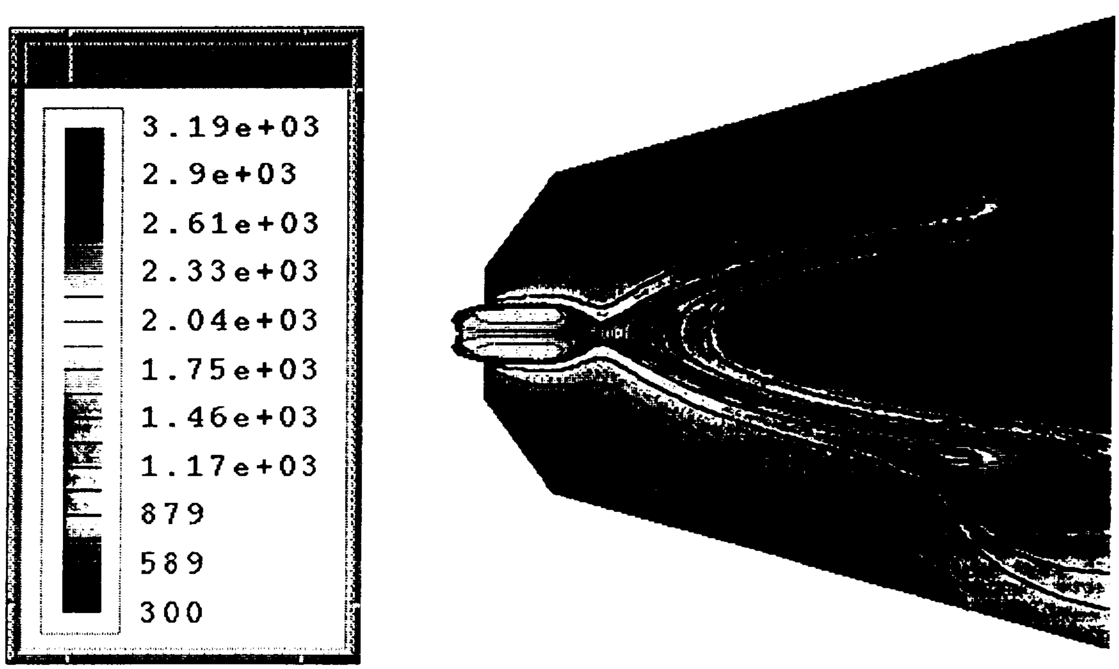

WITH RADIATION

RADIATIVE FLUX DISTRIBUTION IN VTE CHAMBER/NOZZLE
(100% POWER LEVEL)

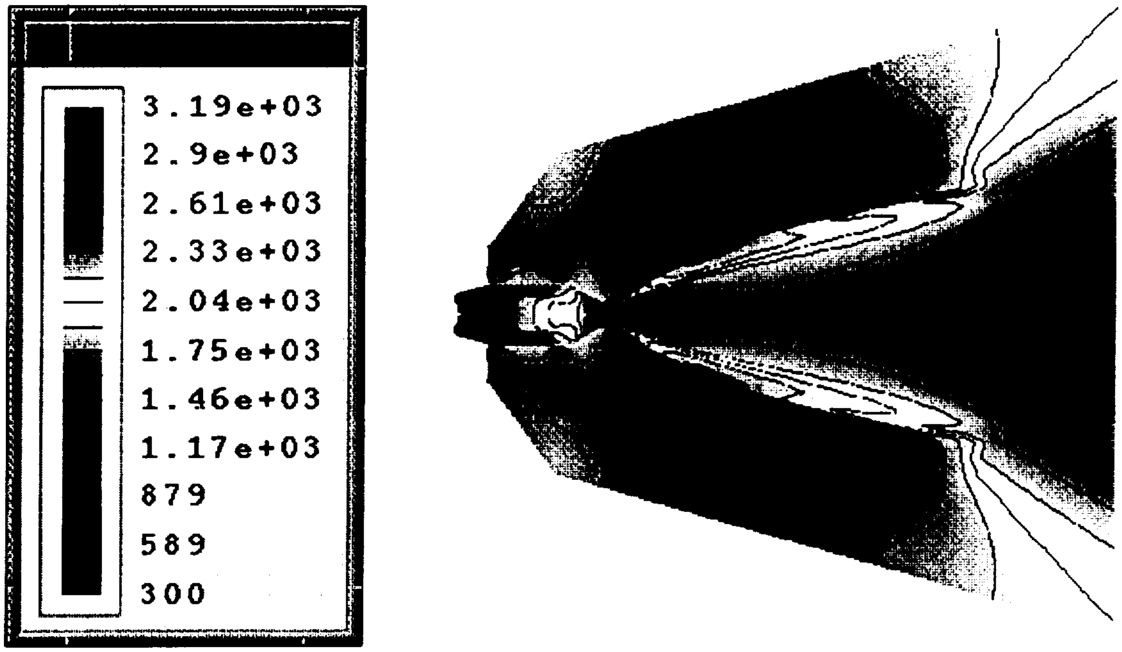

AXIAL RADIATIVE FLUX

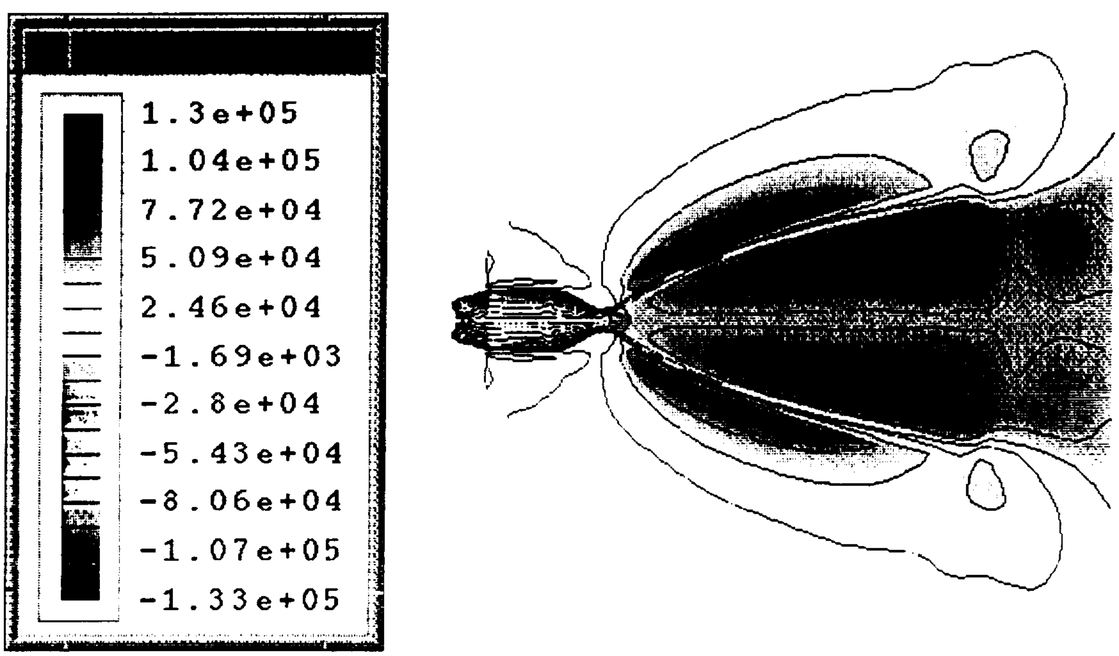

RADIAL RADIATIVE FLUX

CONCLUSIONS

CFDRC

- Evalutated the Performance of OMV/VTE at Various Power Levels
- BFC Radiation Model Based on the Discrete-Ordinate Method has been Implemented in the REFLEQS Code
- Simulations of Gas-Gas and Liquid Spray Models were Compared
- Smaller Droplets Evaporate Faster Leading to Better Mixing
- Radiative Effects on Flow and Heat Transfer are Insignificant
- Need an Advanced Model for Atomization Due to Impingement of Unlike Liquids

PA-93-4PR/26

N95- 23646

5

p. 31

Development of an Atomization Methodology for Spray Combustion

S. P. Seung, C. P. Chen
Department of Chemical Engineering
University of Alabama in Huntsville
Huntsville, AL 35899

and

Y. S. Chen
Engineering Sciences Inc.

ABSTRACT

In liquid rocket propulsion, the knowledge and the understanding of liquid-gas interfacial phenomena are very important. This is of keen importance for predicting the onset of cavitation occurring in swirl injection elements used in STME, as well as atomization processes in shear-induced injector's (co-axial) and impinging injector elements. From the fact that all the physical processes including droplets size distribution, droplet dispersion, mixing and combustion are controlled by atomization processes, it is expected that the successful incorporation of the volume of fraction (VOF) will greatly enhance the analytical capability for predicting spray combustion processes in liquid-fueled engines.

In this paper, a methodology is developed to define and track interfaces between two fluids in a non-orthogonal,body-fitted grids using a single fractional volume of fluid(VOF) variable to describe the distribution of the liquid phase in a gas-liquid flow field. This method was implemented in a matured CFD code MAST (Multiphase All-Speed Transient) utilizing the general PISO-C algorithm. For the preliminary study for analyzing the spray combustion and tracking the interface between two phase, we will report the progress on simulation of the instability on the liquid column, the surface wave instability and the droplet breakup from the liquid surface.

Development of an Atomization Methodology for Spray Combustion.

S.P. Seung, C.P. Chen
Department of Chemical Engineering
University of Alabama in Huntsville

and

Y.S.Chen
Engineering Sciences Inc.

Workshop for CFD Application in Rocket Propulsion
April 20 - 22, 1993

NASA/Marshall Space Flight Center.

INTRODUCTION.

- The dense and dilute spray combustion in liquid rocket engine.
- The onset of cavitation occurring in swirl injection elements used in STME.
- The atomization processes in shear-induced injector(co-axial) and impinging injector elements.

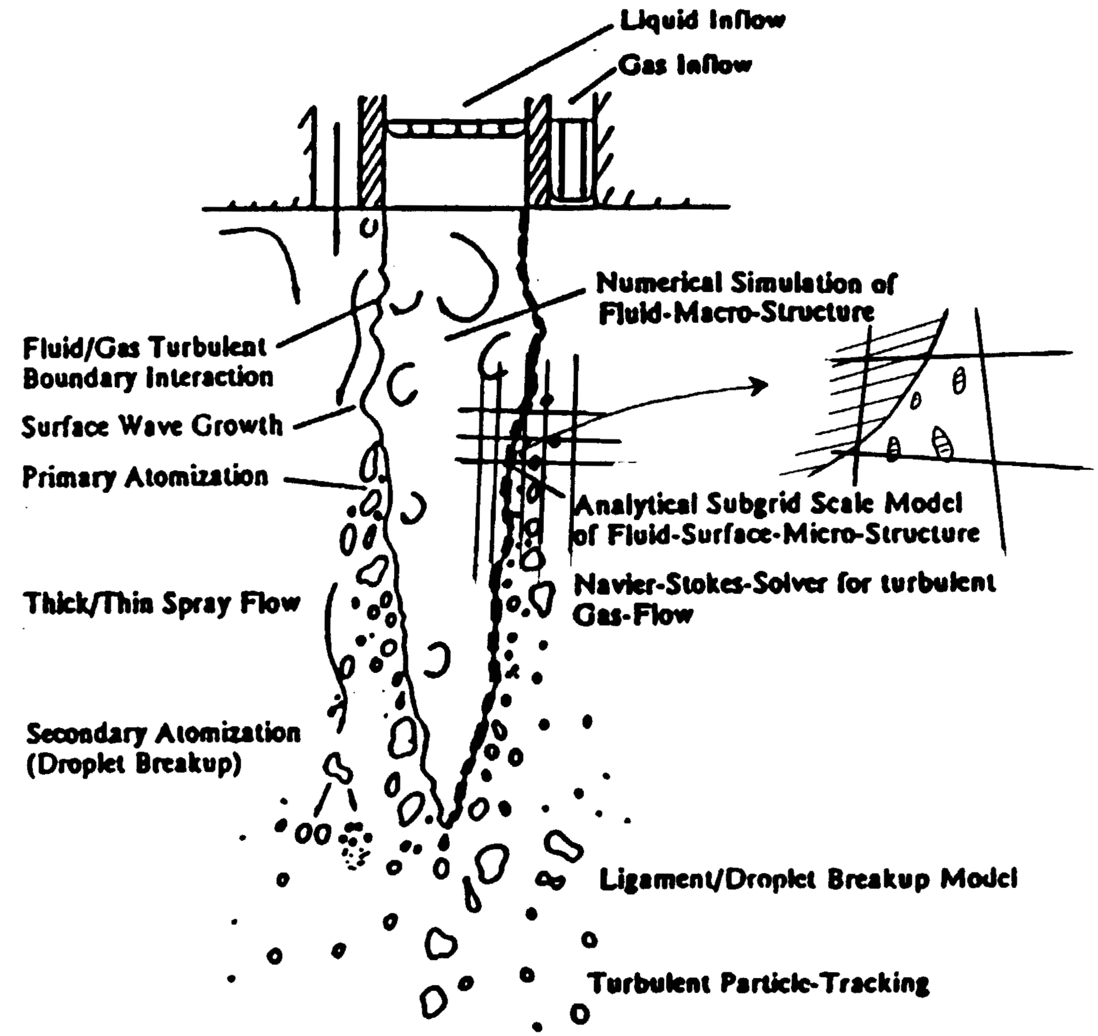

Coaxial Atomization Model and Phenomena

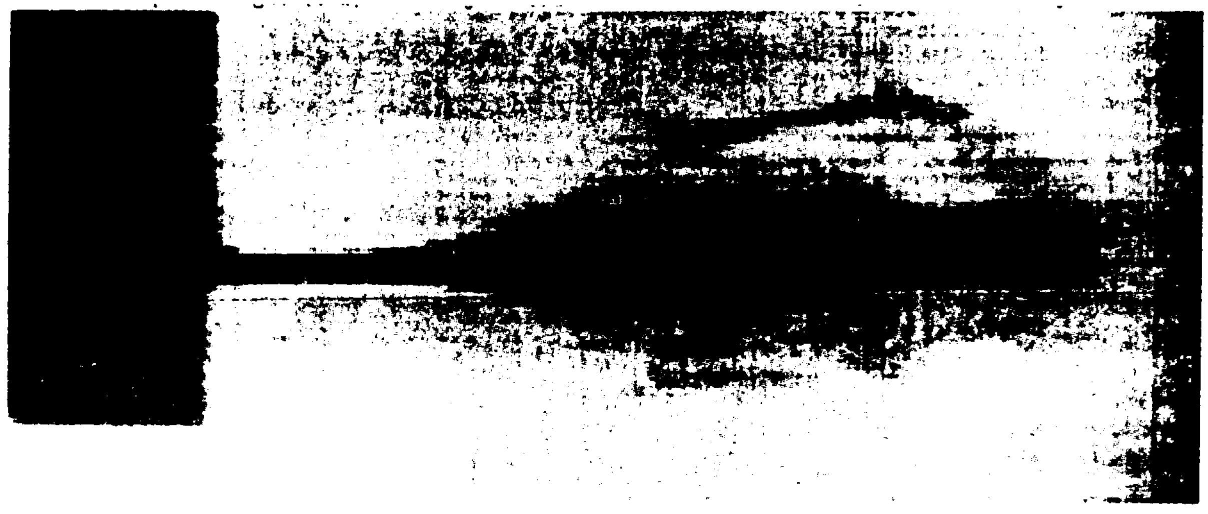

Enlarged Picture of a Liquid jet from X-ray Image

OBJECTIVES.

o To improve the analytical capability for predicting spray combustion processes in liquid-rocket engine.

o To develop <u>efficient</u> methodologies for spray combustion simulation.

- Droplet Dispersion.
- Dilute and Dense Spray.
- Atomization.

o To understand and study liquid-gas interfacial phenomena in liquid rocket propulsion.

METHODOLOGY.

o A strongly-coupled method has been developed to include the Lagrangian -Tracking scheme into a pressure-velocity coupling algorithm.

o Non-iterative PISOC Algorithm.

o Easy to include physical models.

- Evaporation
- Turbulence
- Collision and Breakup
- Finite Rate Chemistry

o Avoid global iteration between two phase.

o Time accurate after prescribed corrector steps

o Using VOF method (volume of fraction) to define and track the liquid-gas interfaces

APPROACHES.

o Stochastic Particle Tracking Technique
- Stochastic separated flow(SSF) model.
- Parcel PDF transport model.

o Incorporation of Dense Spray effects.
- Taylor analogy breakup(TAB) model.
- Reitz's wave instability model.
- Droplet collision and coalescence model.

o Eulerian-Lagrangian Frame.

o Atomization Model.
- Blob Injection.
- Volume of Fluid Method.

SHARP SURFACE BETWEEN TWO FLUIDS.

o Eulerian Volume of Fraction Method.

o VOF Equation.

$$\frac{\partial F}{\partial t} + \overline{V}\,\Delta_i F = 0$$

$$F(\bar{x},t) = \begin{cases} \text{if} \quad F=0.0 & \text{Gas} \\ \text{if} \quad 0 < F < 1.0 & \text{Free Surface} \\ \text{if} \quad F=1.0 & \text{Liquid} \end{cases}$$

o Chakravarthy & Osher High Order Upwind Scheme.

SURFACE TENSION EFFECT.

o Continuous Surface Force Procedure Used.

o Surface Tension treated as a limiting Body Force F_{SV} included in the momentum equation.

o Avoid Jump Conditions in Pressure corrections.

o Efficient.

o F_{SV} has to be calculated accurately.

$$F_{SV}(x) = \sigma \, \kappa(x) \, \Delta_i \, F(x) \, / \, [F]$$

σ : Surface tension coefficient

κ : Free surface curvature

Two-Way Coupling Scheme

- **Predictor Step**
  - **Solve Momentum Implicitly Including Two-Way Coupling Term,**

$$\left(\frac{\rho^{n-1}}{\Delta t} + A_p\right)U_i^* = H'(U_i^*) - \Delta_i p^n + S_{ui} + \frac{\rho^{n-1}U_i^n}{\Delta t} - S_p^n U_i^* + R_p^n$$

  - **Activate Droplet Injection, Evaporation, Breakup and Collision**
  - **Update Particle Velocity v_i^* and Relaxation Time τ^***

$$v_i^* = \frac{v_i^n + (U_i^* + u_i' + F_{bi}\tau^n)\frac{\Delta t}{\tau^n}}{1 + \frac{\Delta t}{\tau^n}}$$

  - **Evaluate Two-Way Coupling Terms, S_p^*, R_p^*, S_{ml}, and S_{hl}**

- **First Corrector Step**
  - **Momentum Equation is Approximated by**

$$(\frac{\rho^{n-1}}{\Delta t} + A_p)U_i^{**} = H'(U_i^*) - \Delta_i p^* + S_i + \frac{\rho^{n-1}U_i^n}{\Delta t} - S_p^* U_i^{**} + R_p^*$$

  - **Subtracted to Predictor Equation and Get New Velocity**

$$U_i^{**} = U_i^* - D_u^* \Delta_i (p^* - p^n) - D_u^* [(S_p^* - S_p^n)U_i^* - (R_p^* - R_p^n)]$$

$$D_u^* = (\frac{\rho^n}{\Delta t} + A_p + S_p^*)^{-1}$$

  - **Substitute into Continuity Equation and Obtain Pressure Correction Equation**

$$[\frac{1}{\Delta t R T^*} + \Delta_i(\frac{U_i^*}{RT^*}) - \Delta_i(\rho^{nT} D_u^* \Delta_i)](P^* - P^n) = -[\frac{\rho^{nT} - \rho^n}{\Delta t}$$
$$+ \Delta_i(\rho^{nT} U_i^*)] + S_{m,l} + \Delta_i\{\rho^{nT} D_u^* [(S_p^* - S_p^n)U_i^* - (R_{pi}^* - R_{pi}^n)]\}$$

<u>First Corrector Step (continued)</u>

- **Update Particle Velocity v_i^{**} and Relaxation Time τ^{**}**

$$v_i^{**} = \frac{v_i^n + (U_i^{**} + u_i' + F_{bi}\tau^*)\frac{\Delta t}{\tau^*}}{1 + \frac{\Delta t}{\tau^*}}$$

- **Evaluate S_p^{**} and R_p^{**}.**
- **Mean Velocity Field Satisfies the Continuity Constraint.**

VALIDATIONS & APPLICATIONS.

o Particle Dispersion.

o Non -evaporating Hollow-Cone Spray.

o Gas-Droplet round Jets.

o Non -evaporating and Evaporating Single Jet.

o Evaporating and Burning solid-Cone Spray.

o Liquid Column Instability Problem.

o Droplet Breakup Problem.

o Non- Evaporating Transient Solid-cone Spray.

o Measurements of Hiroyasu and Kadota.

o Liquid jet injected into high pressure chamber.

o Transient Flow.

o To compare jet penetration length and droplet size.

- Nozzle diameter : 300μm
- Injection pressure : 9.9 MPa
- Liquid fuel : diesel

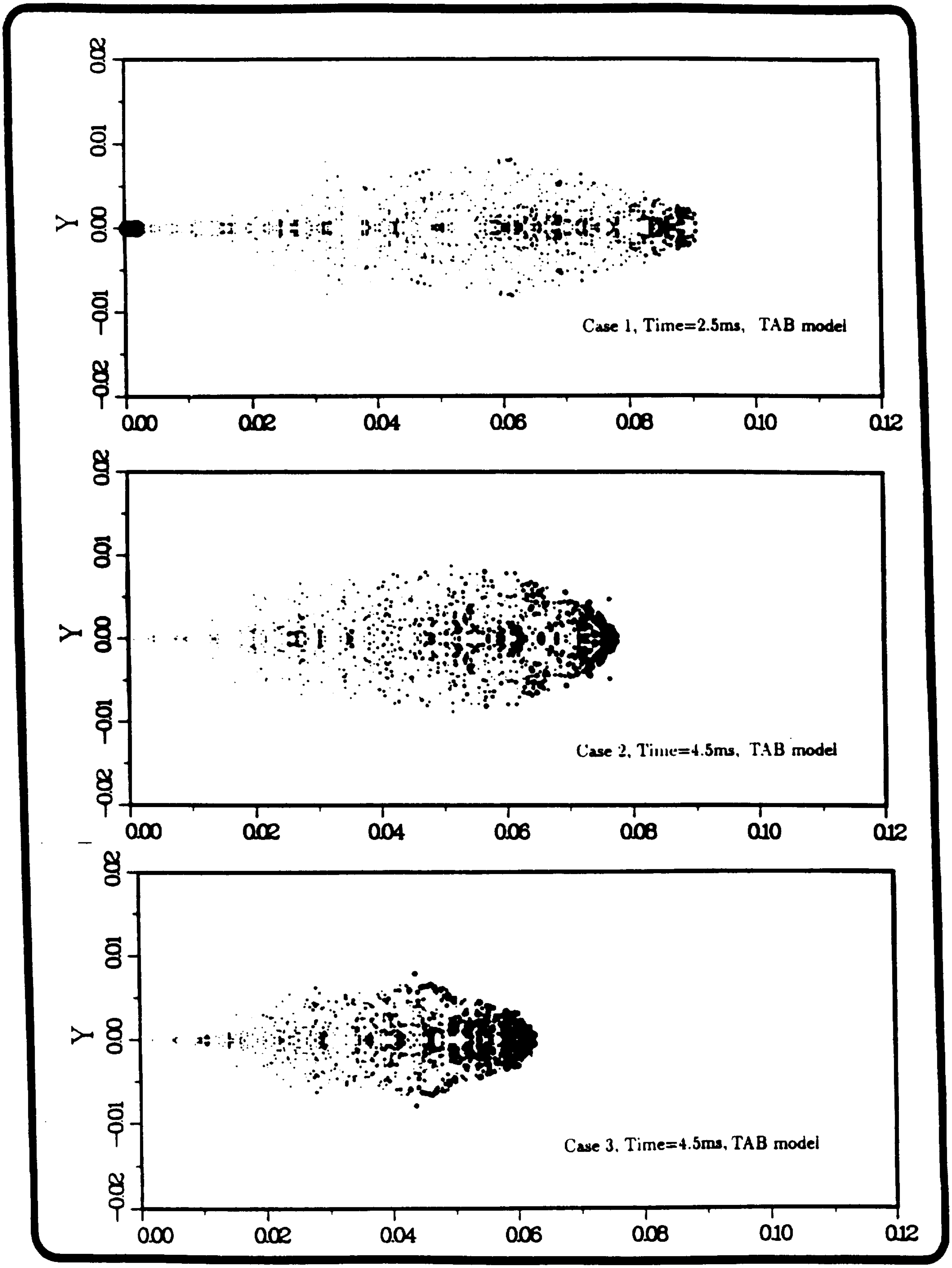
Case 1, Time=2.5ms, TAB model
Case 2, Time=4.5ms, TAB model
Case 3, Time=4.5ms, TAB model
Y
0.02
0.01
0.00
-0.01
-0.02
0.00
0.02
0.04
0.06
0.08
0.10
0.12

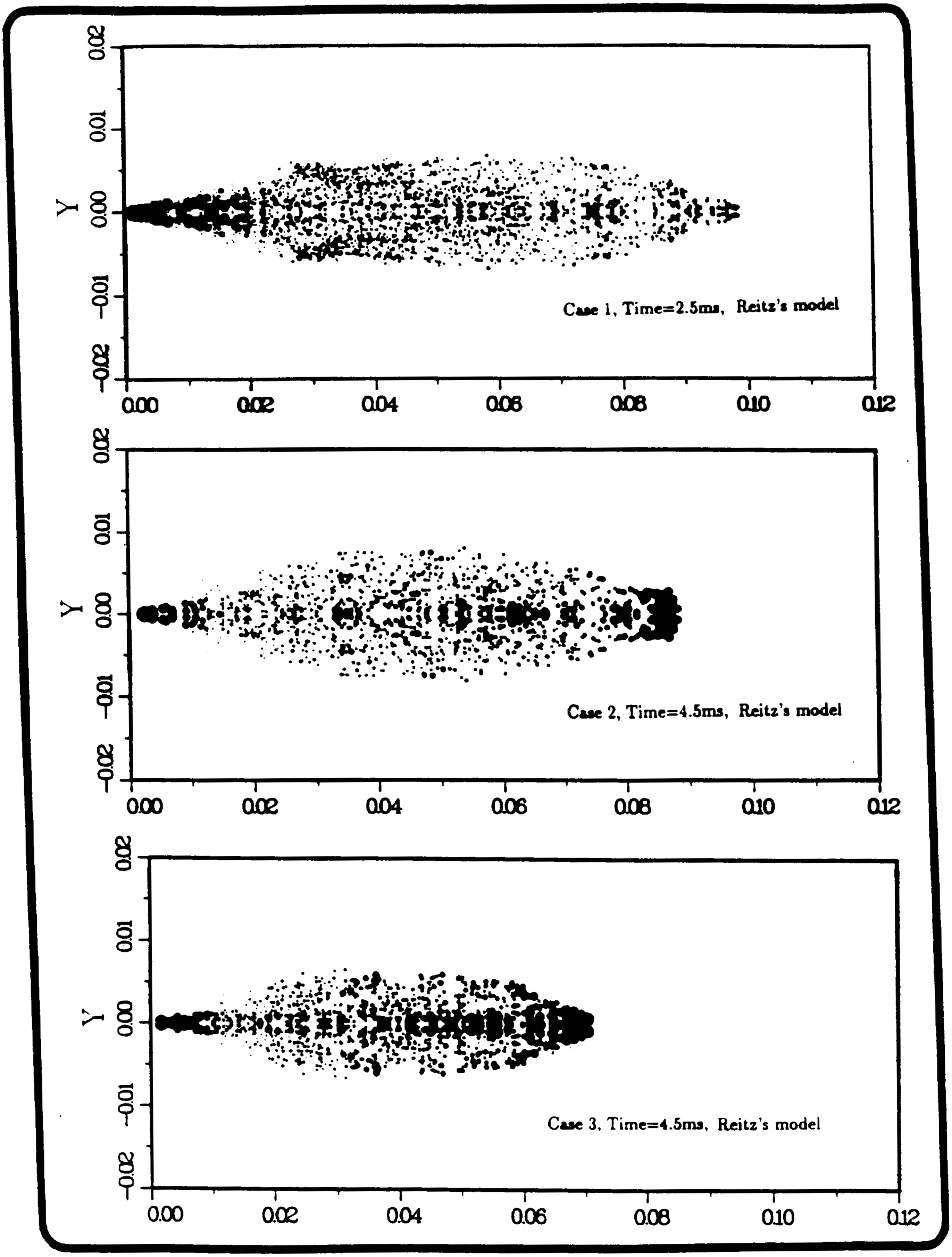
Y
0.02
0.01
0.00
-0.01
-0.02
0.00
0.02
0.04
0.06
0.08
0.10
0.12
Case 1, Time=2.5ms, Reitz's model
Case 2, Time=4.5ms, Reitz's model
Case 3, Time=4.5ms, Reitz's model

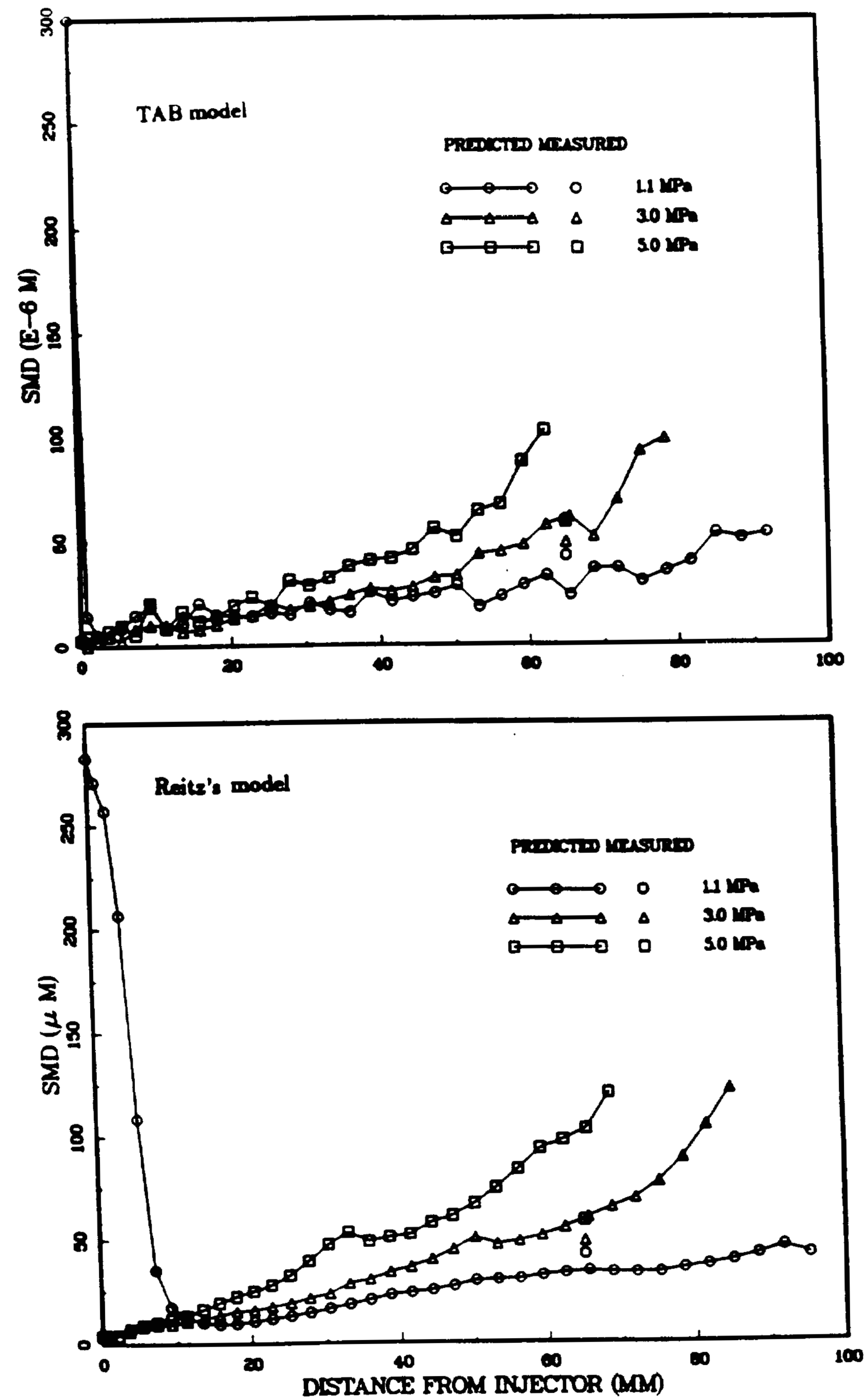

Sauter mean diameter ver. distance from the injector

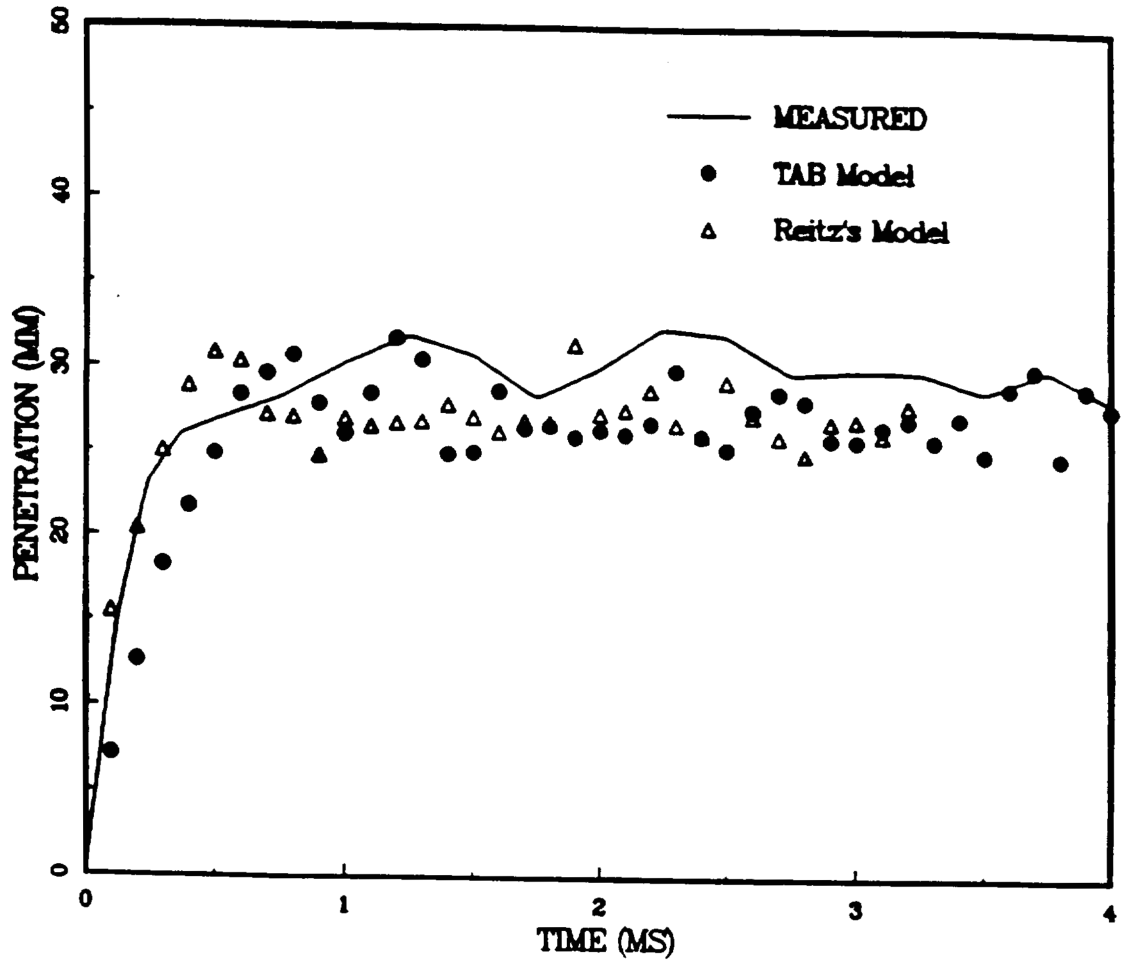

Spray tip penetration ver. time in an evaporating spray

o Evaporating and Burning Solid-Cone Spray.

o Measurement of Yokota et al.

o Liquid fuel (tridecane) injected into high pressure, high temperature nitrogen or air.

o Dense spray and turbulent.

o Liquid jet atomization and droplet secondary breakup.

o Single step chemical reaction .

$$C_{13}H_{28} + 20\ O_2 = 13\ CO_2 + 14\ H_2O$$

Test Conditions for the Measurement of Yokota et al.

Case	Pinj (MPa)	Pgas (MPa)	Tamb (K)	Minj (kg/s)	Atmosphere
Evaporating Spray	30	3.0	900	0.00326	N_2
Burning Spray	30	3.0	900	0.00326	*Air*

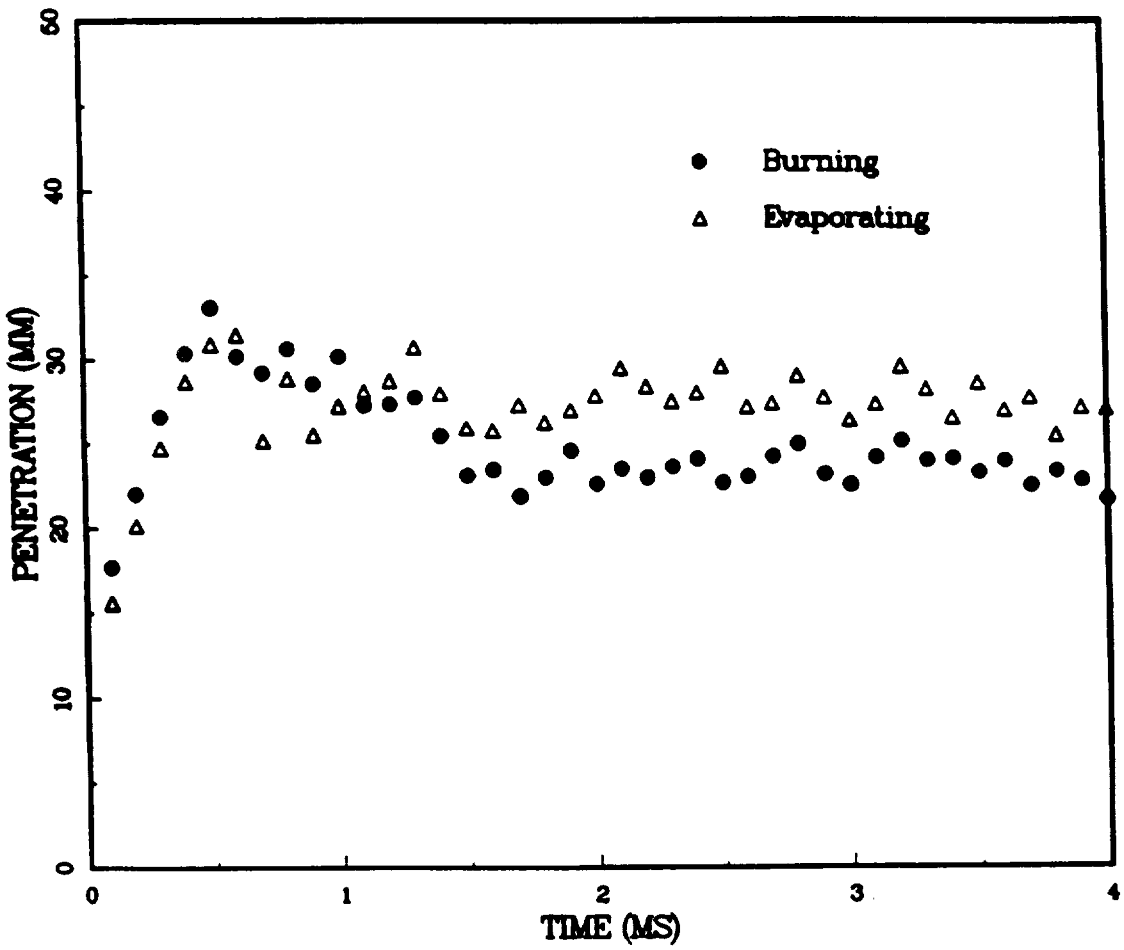

Comparison of penetration length ver. time for burning and evaporating sprays

o Liquid Column Instability Problem.

o Cylindrical Liquid Column.

- density : $1 g/cm^3$
- surface tension coefficient : 72.8 dyne/cm
- diameter : 0.1 cm
- length : 1 cm

o Initial perturbation.

$$0.001 \cdot R_0 \cdot COS(n\pi x/L)$$

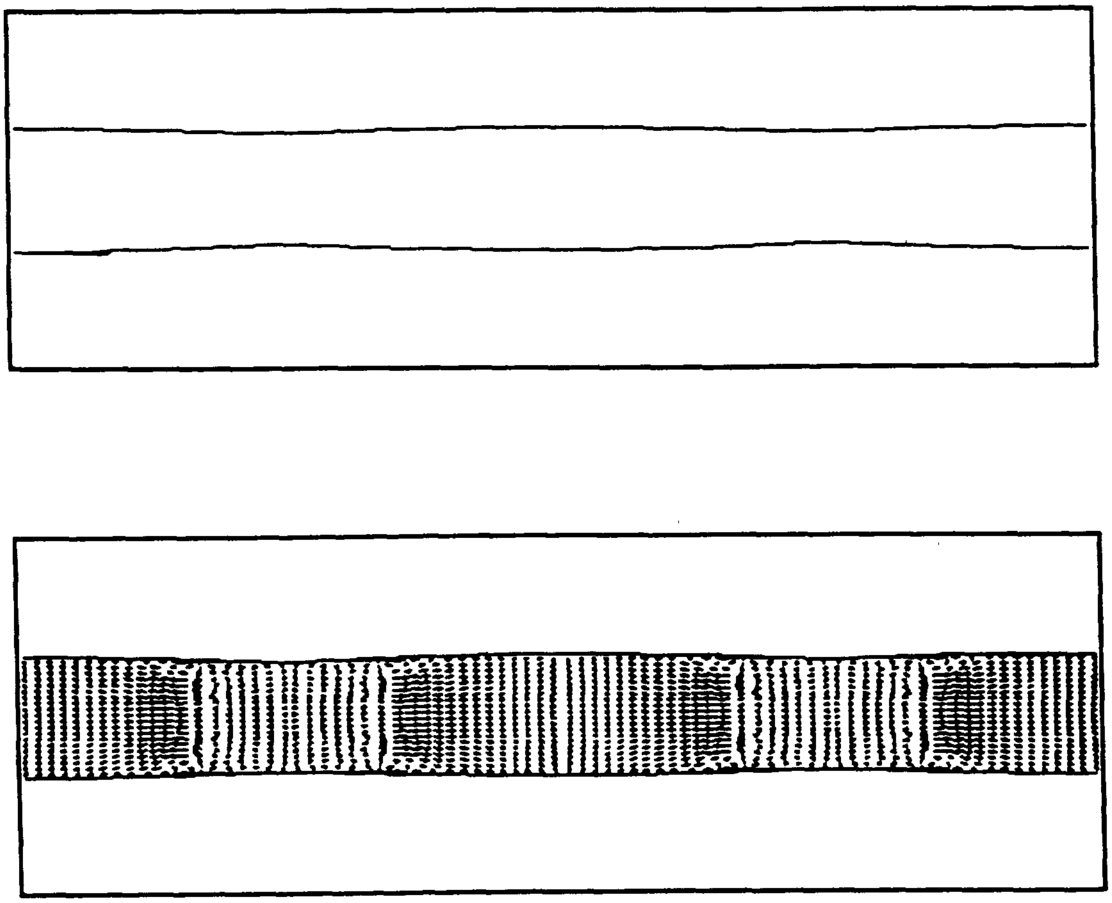

Liquid Column Jet Breakup Problem
Time = 2.501 x 10^{-2} sec   Cycle= 1114
(a) Surface
(b) Velocity vector

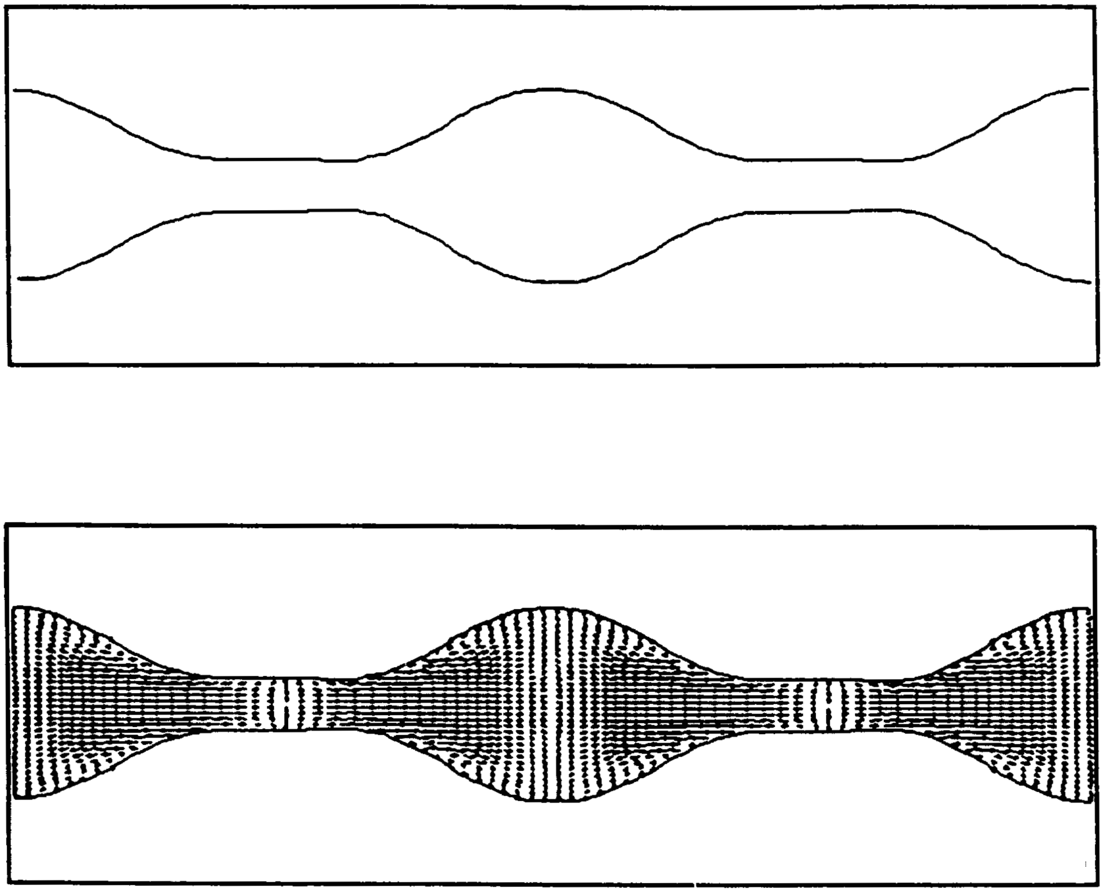

Liquid Column Jet Breakup Problem
Time = 3.700×10^{-2} sec   Cycle= 1647
(a) Surface
(b) Velocity vector

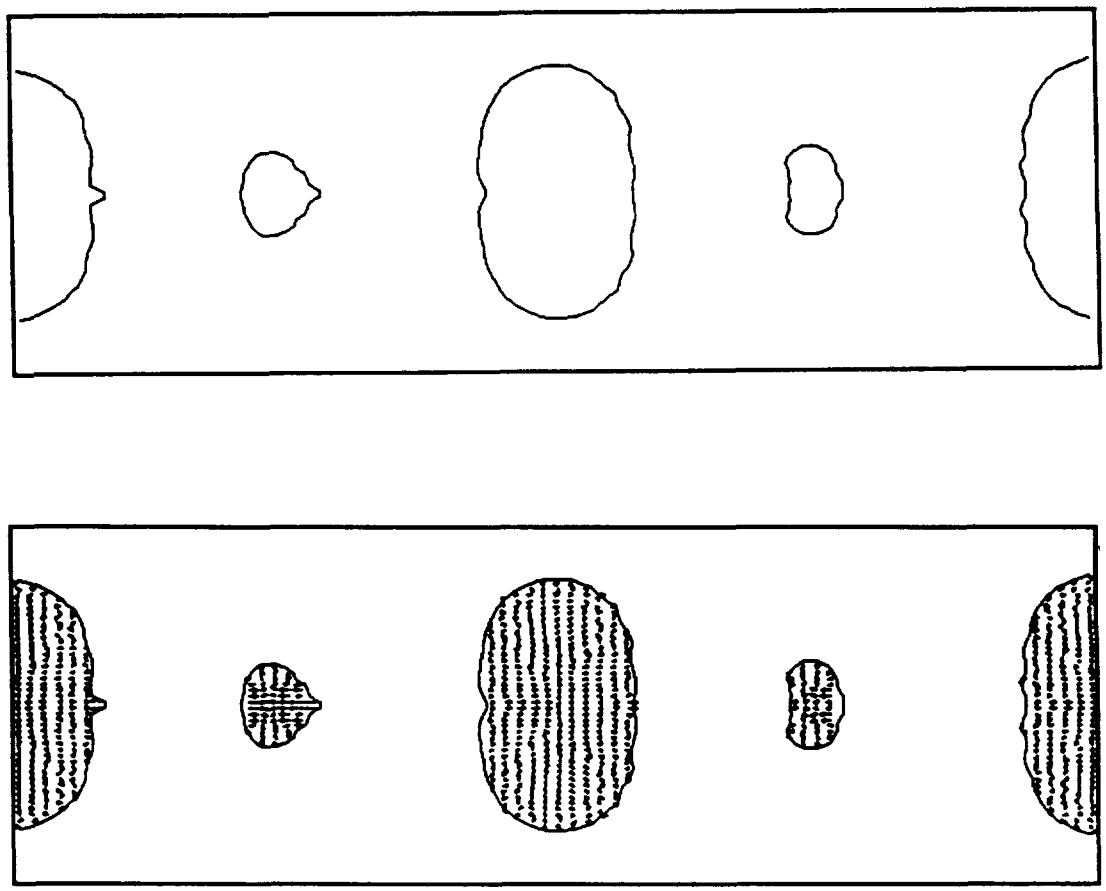

Liquid Column Jet Breakup Problem
Time $=4.002 \times 10^{-2}$ sec   Cycle= 1813
(a) Surface
(b) Velocity vector

o Liquid Droplet Breakup

o Liquid (Kerosene)

- density : 1g/cm^3
- surface tension coefficient :30.0 dyne/cm
- viscosity : 0.018 poise
- initial radius : 125 μm

o Gas (air)

- density : 1g/cm^3
- viscosity : 0.0018 poise
- initial velocity : 10000 cm/sec

o Physical domain : 1.25cm x 0.15cm

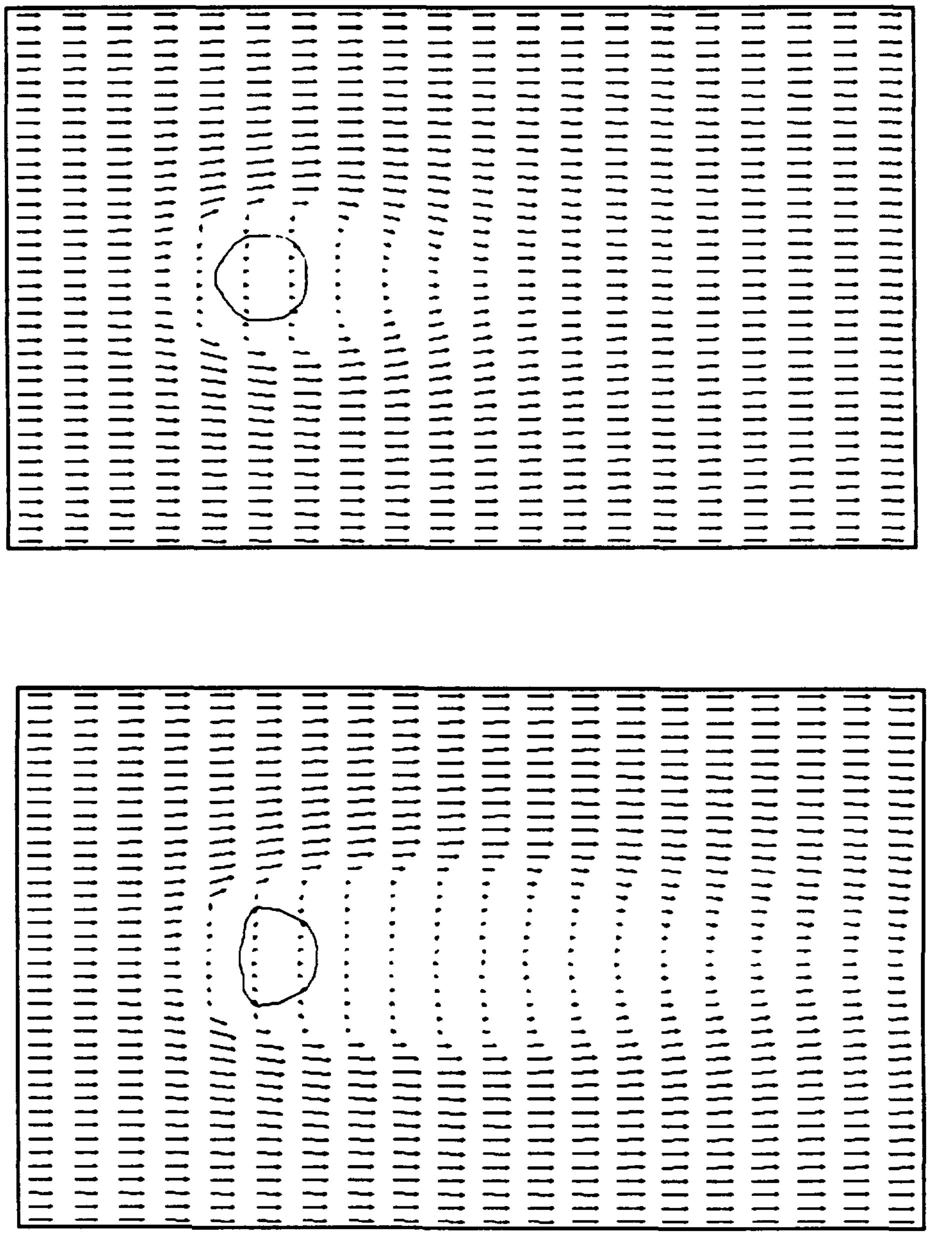

Liquid Droplet Breakup Problem
(a) Time = 4.078×10^{-6} sec   Cycle= 26
(b) Time = 1.909×10^{-5} sec   Cycle= 123

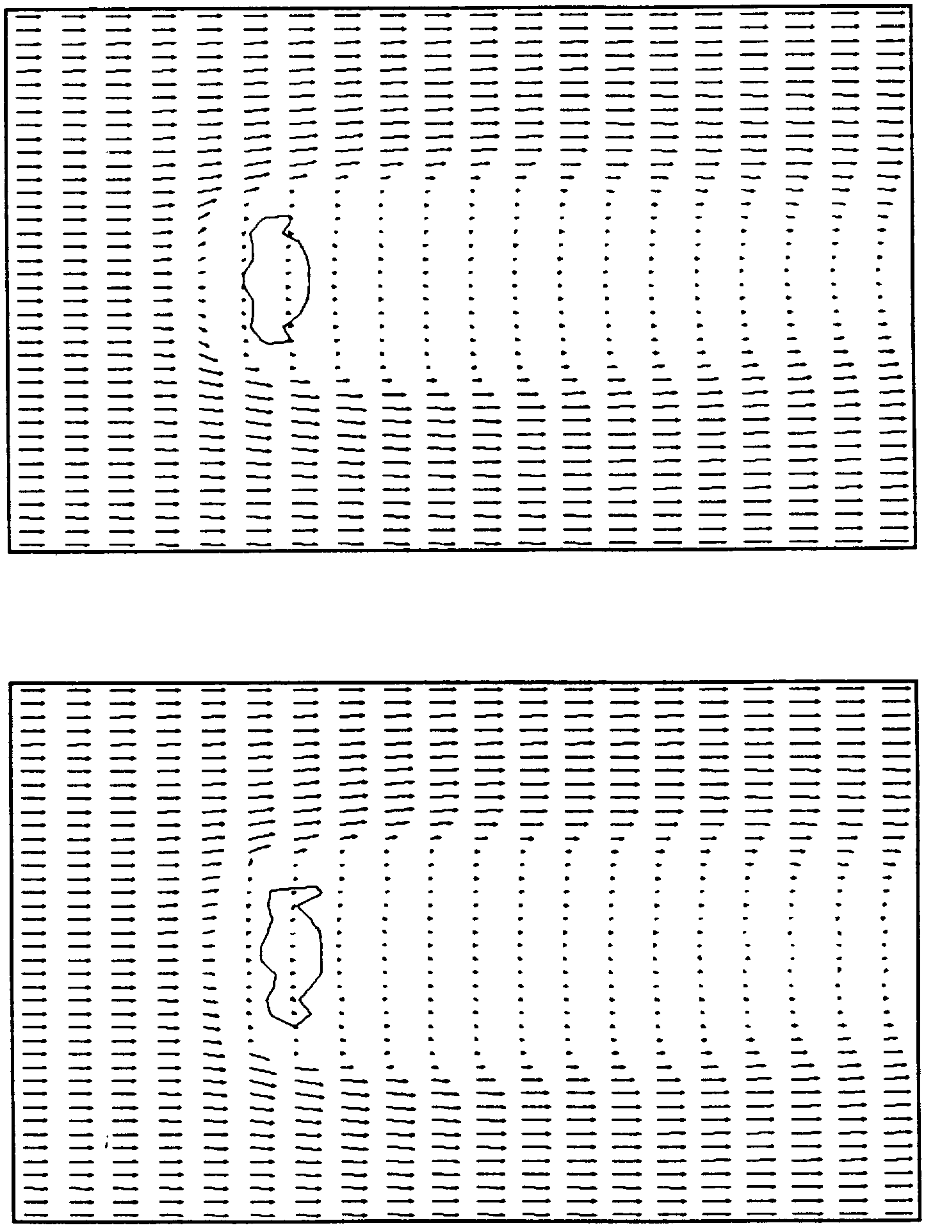

Liquid Droplet Breakup Problem
(a) Time = 3.410×10^{-5} sec Cycle= 219
(b) Time = 4.401×10^{-5} sec Cycle= 284

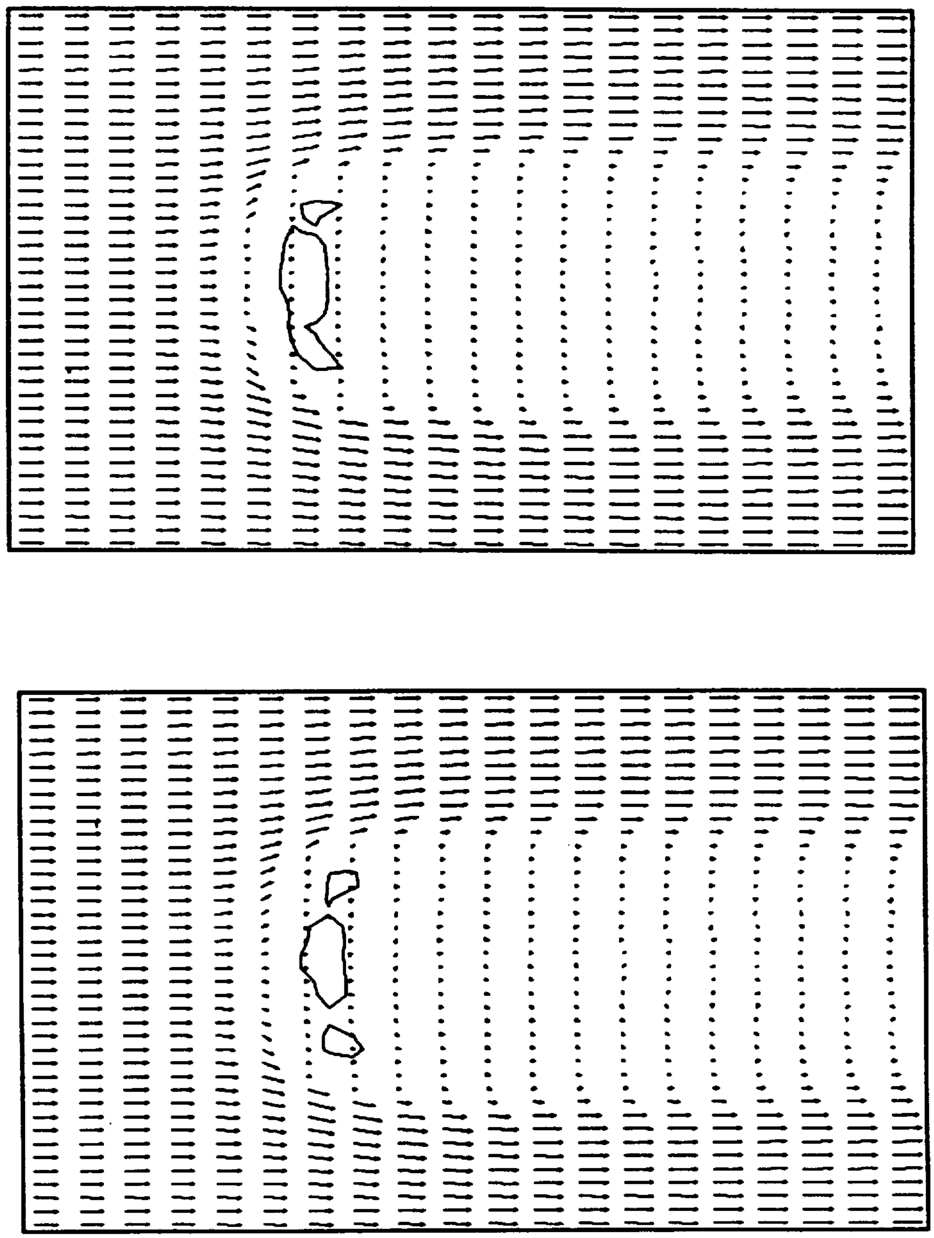

Liquid Droplet Breakup Problem
(a) Time = 5.409×10^{-5} sec   Cycle= 351
(b) Time = 5.911×10^{-5} sec   Cycle= 385

CONCLUSION AND WORK IN PROGRESS

o Preliminary Implementation of VOF in successful.

o Turbulence Effects will be included soon.

o Compressibility Effects is currently incorporated in the Gas Phase.

o Incorporation of other physical Submodels.

S32-34/
P. 20

MODELING OF NON-SPHERICAL DROPLET DYNAMICS

Z. T. Deng, G. S. Liaw
Alabama A&M University
Huntsville, AL 35762
(205) 851-5565

L. Chou
Induced Environment Branch
Fluid Dynamics Division, NASA/MSFC
Huntsville, AL 35812

ABSTRACT

A two-dimensional time-dependent computer code based on the modified Arbitrary Lagrangian Eulerian(ALE) technique has been developed to simulate non-spherical droplet dynamics and evaporation under convective flows at real rocket combustion chamber conditions. The equations of mass, momentum, energy and species are simultaneously solved for both liquid and gas phases with an accurate dynamic interface tracking. The jump boundary conditions across the deforming droplet surface are obtained by applying the integral forms of conservation of mass, momentum, and energy. At each time step, the interface geometry and flow properties at the droplet surface are implicitly solved by satisfying the interface boundary conditions. A Lagrangian technique was developed to track the arbitrarily moving interface between the liquid droplet and the external gas. An elliptic grid generator is adopted to dynamically reconstruct grids both inside and outside the droplet surface.

This code has been used to study droplet oscillation, droplet deformation/breakup, non-spherical droplet evaporation in both low and high pressure convective flows.

This presentation briefly describes the numerical algorithm for modeling of the non-spherical droplet dynamics and demonstrates the representative simulation results of non-spherical droplet evaporation at low and high pressure convective flows. Potential applications of this code to rocket combustor design and performance predictions are discussed.

Modeling of Non-Spherical Droplet Dynamics

Zheng-Tao Deng, Goang-Shin Liaw
Alabama A&M University
Huntsville, AL 35762

Lynn C. Chou
Induced Environment Branch
Fluid Dynamics Division
MSFC/NASA, Huntsville, AL 35812

1993 Workshop for CFD Application in Rocket Propulsion

Motivation:

- Droplet dynamics and vaporization process has been assumed to control combustor performance and combustion instability.
- Both experimental and theoretical studies on non-spherical droplet dynamics/combustion at realistic conditions are limited.
- High performance liquid rocket engines operate at chamber pressures exceeding the critical pressure of the propellants.

Objective:

To develop a comprehensive CFD model to predict non-spherical droplet dynamics and evaporation at both low- and high-pressure environments in realistic combustion chamber.

Model Description:

- Time-dependent, two-dimensional, viscous, compressible and/or incompressible flows in laboratory coordinates.
- Dynamic interface tracking and grid reconstruction.
- Two(one) species liquid droplet.
- Two(one) species compressible gas mixture(liquid).
- Surface tension force, heat, mass and momentum transfer across interface.
- Low/High pressure phase equilibrium.
- Modified Arbitrary-Lagrangian-Eulerian numerical method.

Gas-Liquid Interface Conditions:

- **Species concentration:**

$$\dot{m}Y_{gf} - \dot{m}Y_{lf} = \rho_g D \nabla \left(\frac{\rho_{gm}}{\rho_g} \right) \cdot \hat{n}$$

- **Continuity of mass flux:**

$$\rho_g \left(\vec{u}_g - \vec{U} \right) \cdot \hat{n} = \rho_l \left(\vec{u}_l - \vec{U} \right) \cdot \hat{n} = \dot{m}$$

- **Continuity of normal momentum flux:**

$$\dot{m} \left(\vec{u}_g - \vec{u}_l \right) \cdot \hat{n} = \left(P_g - P_l \right) \hat{n} - \tau_{gn} \cdot \hat{n} + \tau_{ln} \cdot \hat{n}$$

- **Continuity of energy flux:**

$$\dot{m} \left(E_g - E_l \right) = -\vec{u}_g \cdot \left(P_g - \tau_g \right) \cdot \hat{n} + \vec{u}_l \cdot \left(P_l - \tau_l \right) \cdot \hat{n} - \vec{J}_g \cdot \hat{n} + \vec{J}_l \cdot \hat{n}$$

Gas-Liquid Interface Conditions (Cont.):

- Low-Pressure Phase Equilibrium:
  - Clausius-Chapeyon vapor pressure formula.
  - Mass fraction based on vapor pressure and molecular weight.
- High-pressure Phase equilibrium: Redklich-Kwong equation of state with mixing rules of Chuen and Prausnitz.

$$T^{(v)} = T^{(l)}, \quad P^{(v)} = P^{(l)}, \quad \phi_i^{(v)} x_i^{(l)} = \phi_i^{(l)} x_i^{(l)}$$

- Iterative solution of surface temperature T_s, surface mass fraction Y_{gf} and surface pressure P_g, P_l.

Gas-Liquid Interface Conditions (Cont.):

- **Non-slip conditions:**

$$T_{gm} = T_{lm} = T_s$$

$$u_{gt} = u_{lt}$$

- **Surface pressure jump conditions:**

$$P_l - P_g = \sigma\left(T_s, Y_i\right)\left(\frac{1}{R_1} + \frac{1}{R_2}\right)$$

- **Surface tension coefficient** $\sigma(T_s, Y_i)$**: Model proposed by Brock and Bird.**

- **Radii of curvature at interface – Cubic Spline**

Dynamic Interface Tracking:

- Dynamic Lagrangian droplet surface tracking.
- Dynamic grid reconstruction based on Poisson Elliptic solver both inside and outside the droplet surface.

Low-Pressure Droplet Evaporation:

- **N-Heptane fuel, Oxygen gas**
- $P_{amb}/P_{cr} < 1.0$
- $P_{amb} = 1.0\ atm.$
- $W_e R_e^{-0.5} = 1.0$, **Parachute-type breakup.**

- **Parachute-type,** $8 \leq W_e \leq 40$, $0.2 \leq W_e R_e^{-0.5} \leq 1.6$
- **Striping-type,** $20 \leq W_e \leq 2 \times 10^4$, $1.0 \leq W_e R_e^{-0.5} \leq 20$

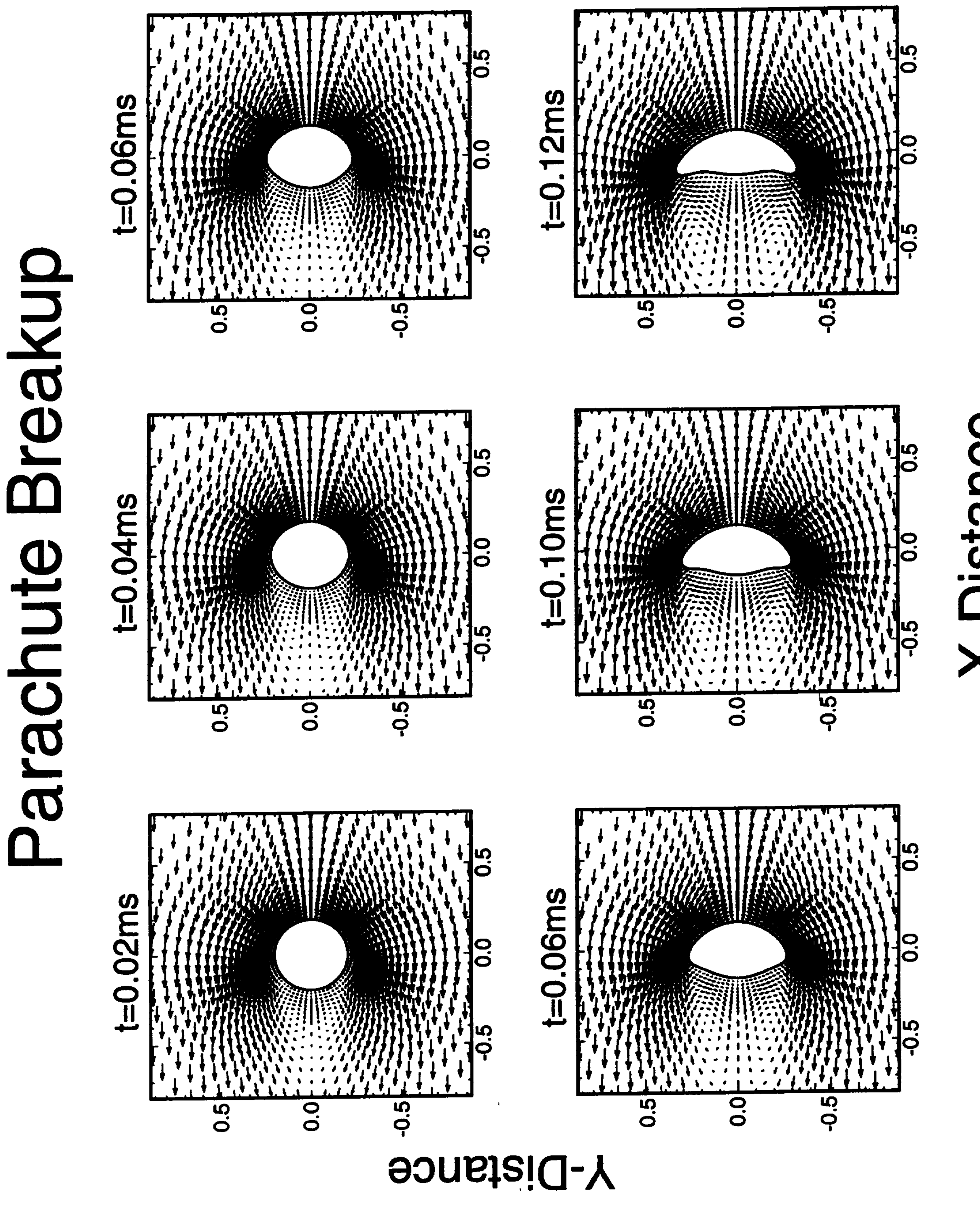
Parachute Breakup
t=0.02ms
t=0.04ms
t=0.06ms
t=0.06ms
t=0.10ms
t=0.12ms
0.5
0.0
-0.5
Y-Distance
X-Distance

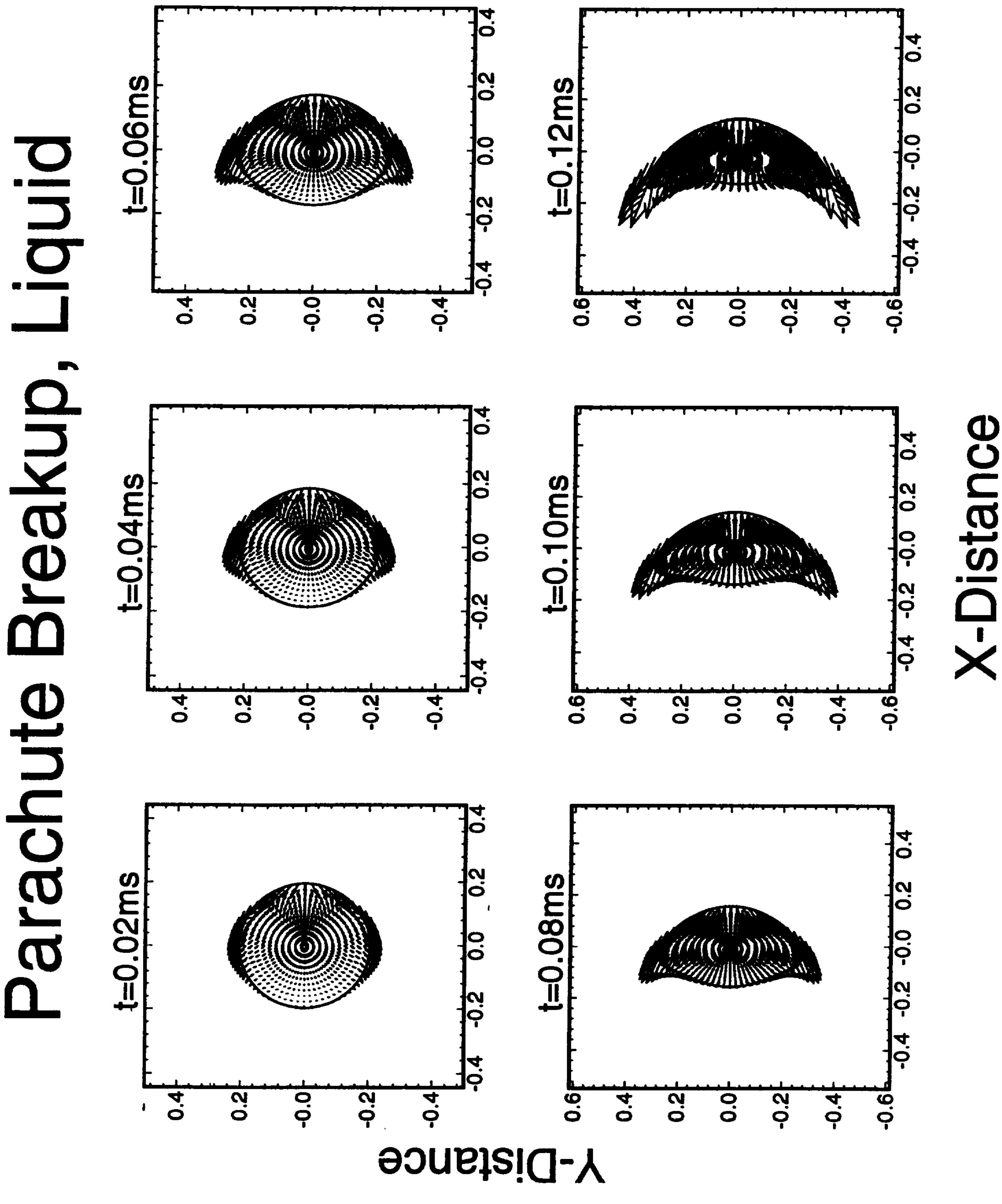
Parachute Breakup, Liquid
t=0.02ms
t=0.04ms
t=0.06ms
t=0.08ms
t=0.10ms
t=0.12ms
X-Distance
Y-Distance

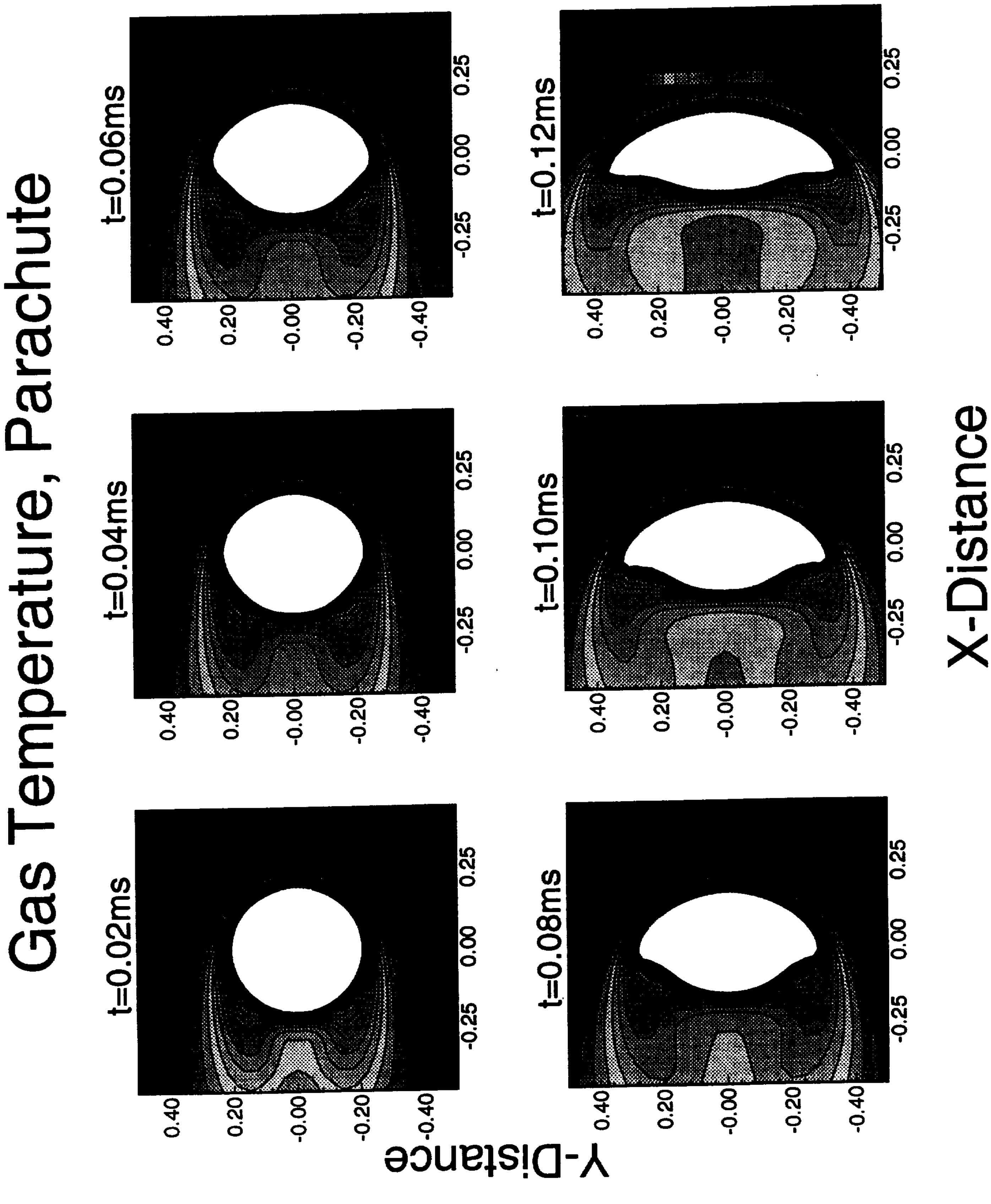

Gas Temperature, Parachute
t=0.02ms
t=0.04ms
t=0.06ms
t=0.08ms
t=0.10ms
t=0.12ms
0.40
0.20
-0.00
-0.20
-0.40
-0.25
0.00
0.25
Y-Distance
X-Distance

C-9.

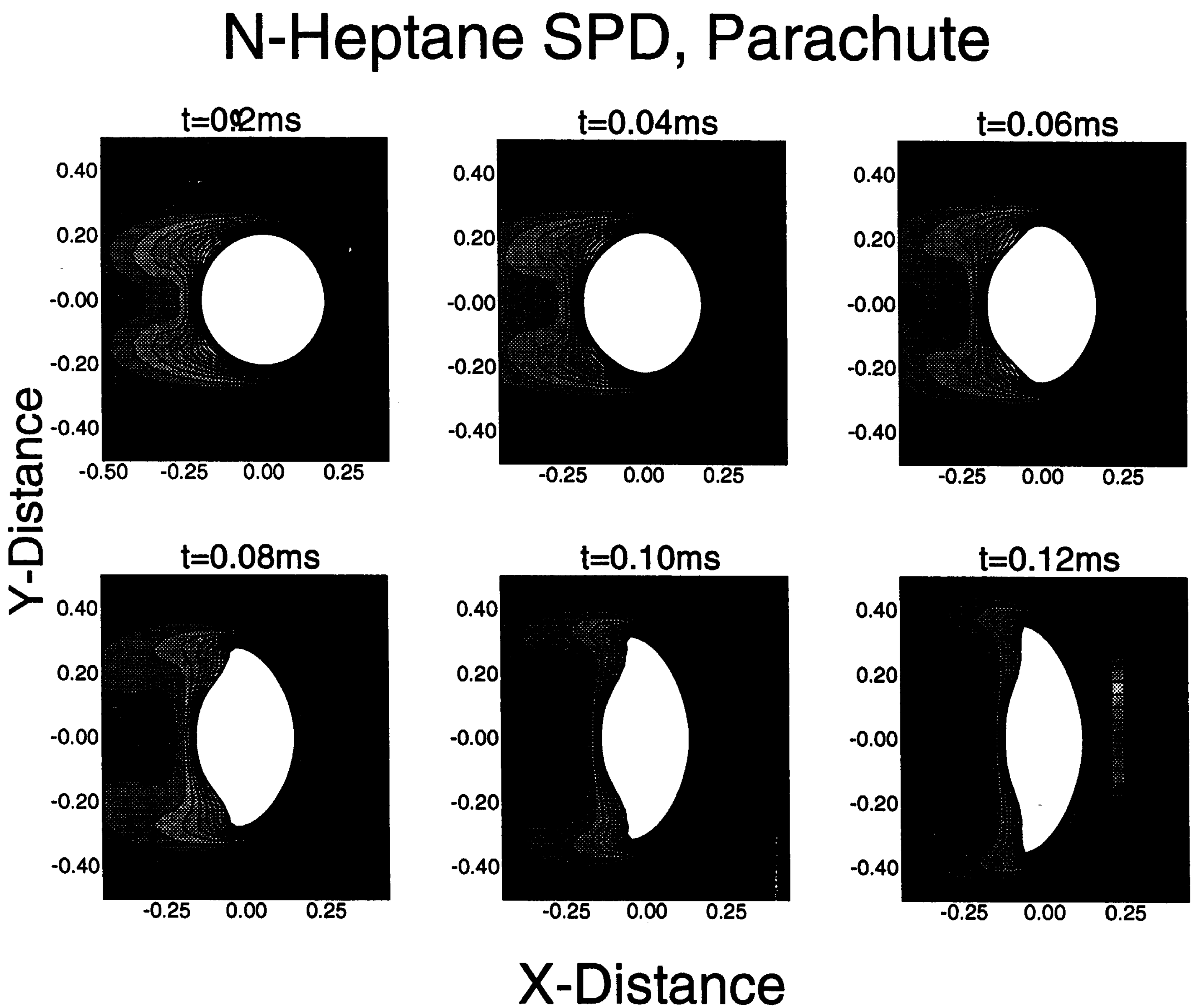
N-Heptane SPD, Parachute
t=0.02ms
t=0.04ms
t=0.06ms
t=0.08ms
t=0.10ms
t=0.12ms
0.40
0.20
-0.00
-0.20
-0.40
-0.50
-0.25
0.00
0.25
Y-Distance
X-Distance

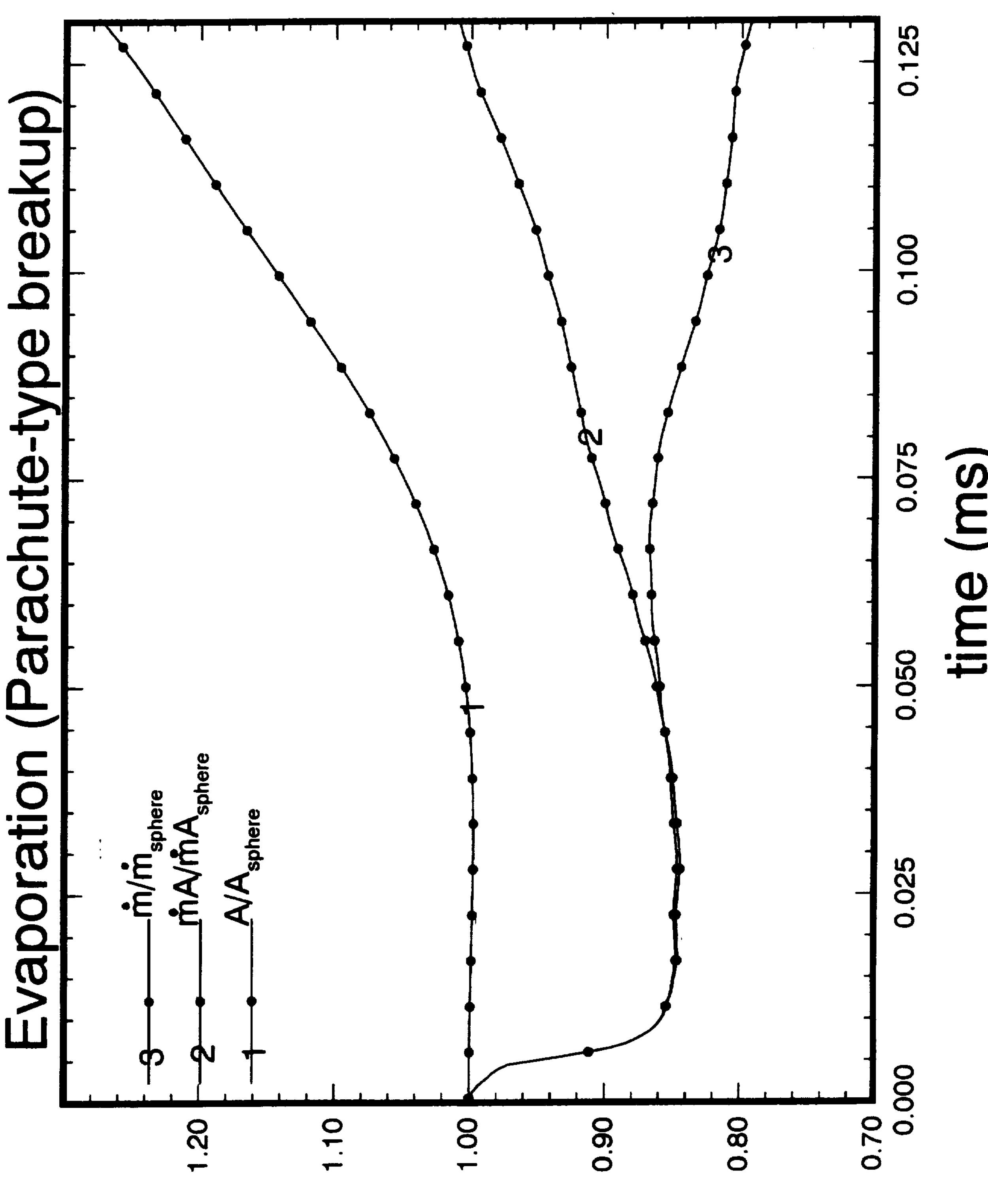
Evaporation (Parachute-type breakup)
time (ms)
0.000
0.025
0.050
0.075
0.100
0.125
0.70
0.80
0.90
1.00
1.10
1.20
3
2
1
ṁ/ṁsphere
ṁA/ṁAsphere
A/Asphere

High-Pressure Droplet Evaporation:

- **N-Heptane fuel droplet, hot Nitrogen gas.**
- $T_\infty = 1000K$, $D_0 = 200\mu m$
- $u_\infty = 2, 4, 8\ m/s$. **Oscillation, Bag, Striping.**
- $P_{amb}/P_{cr} = 1.4 > 1.0$, $T_{amb}/T_{cr} = 1.87$
- $P_{amb} = 4.0\ Mpascal.$

HP, Gas Velocity, 2M/S

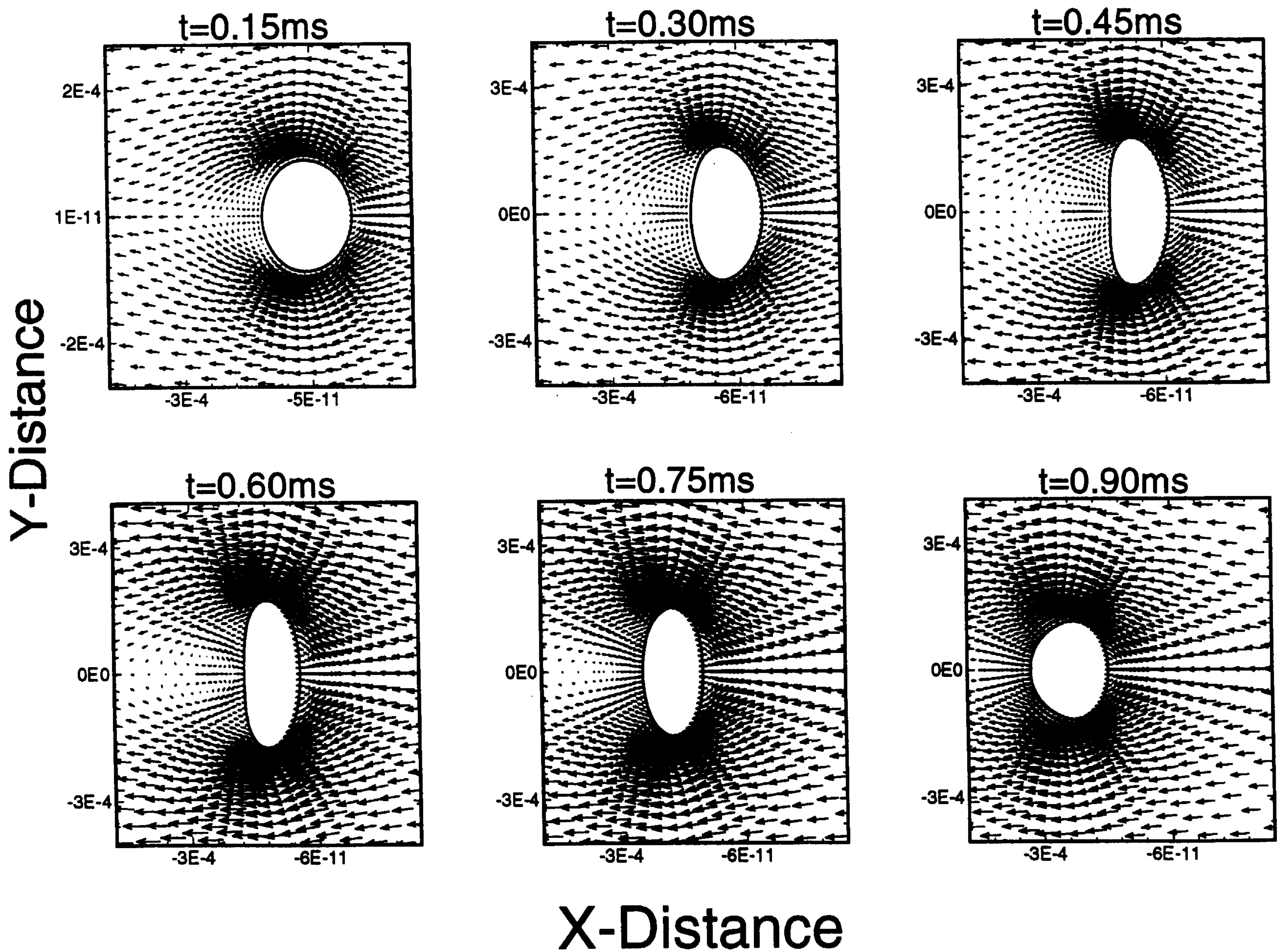

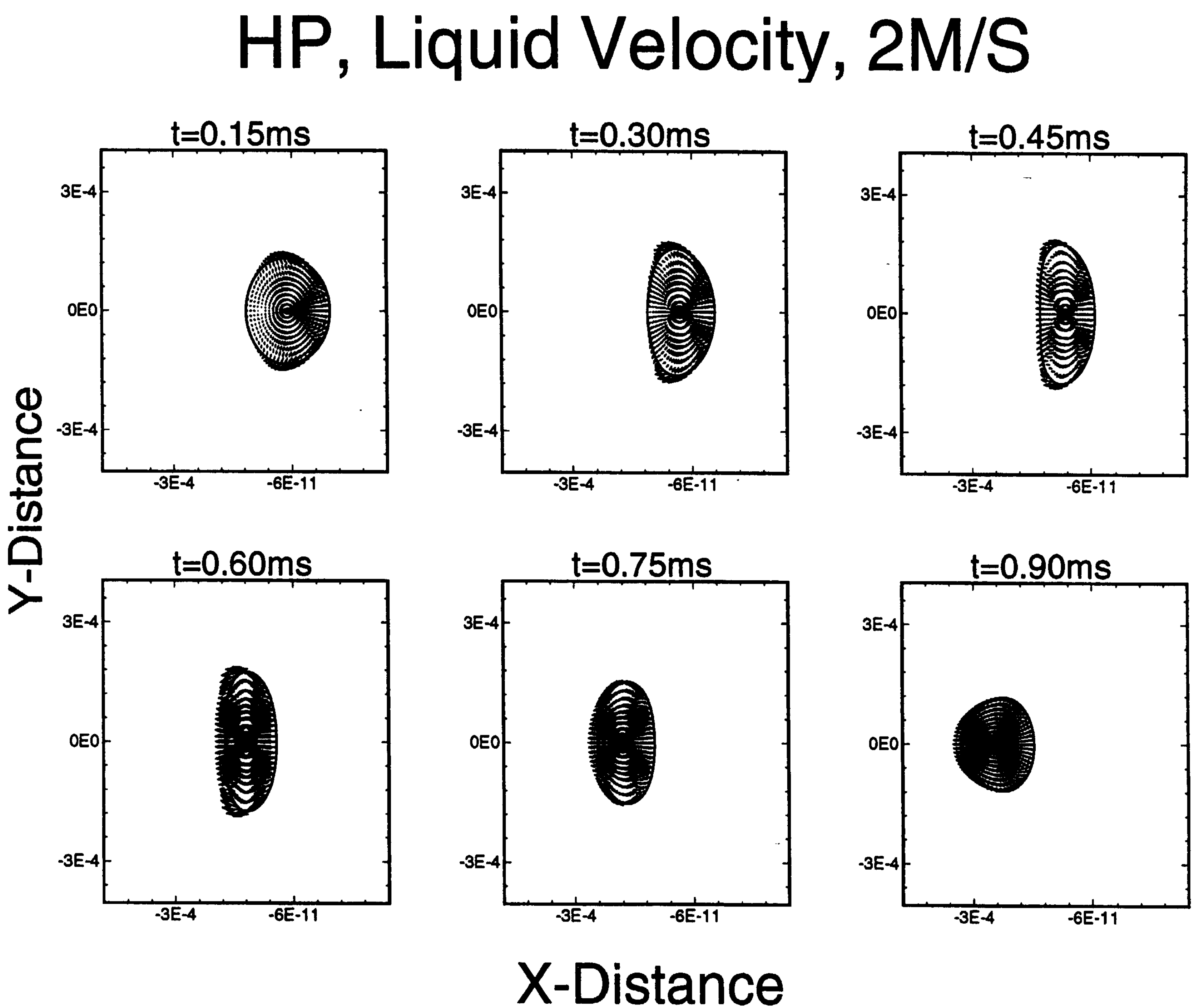
HP, Liquid Velocity, 2M/S
t=0.15ms
t=0.30ms
t=0.45ms
t=0.60ms
t=0.75ms
t=0.90ms
3E-4
0E0
-3E-4
-3E-4
-6E-11
Y-Distance
X-Distance

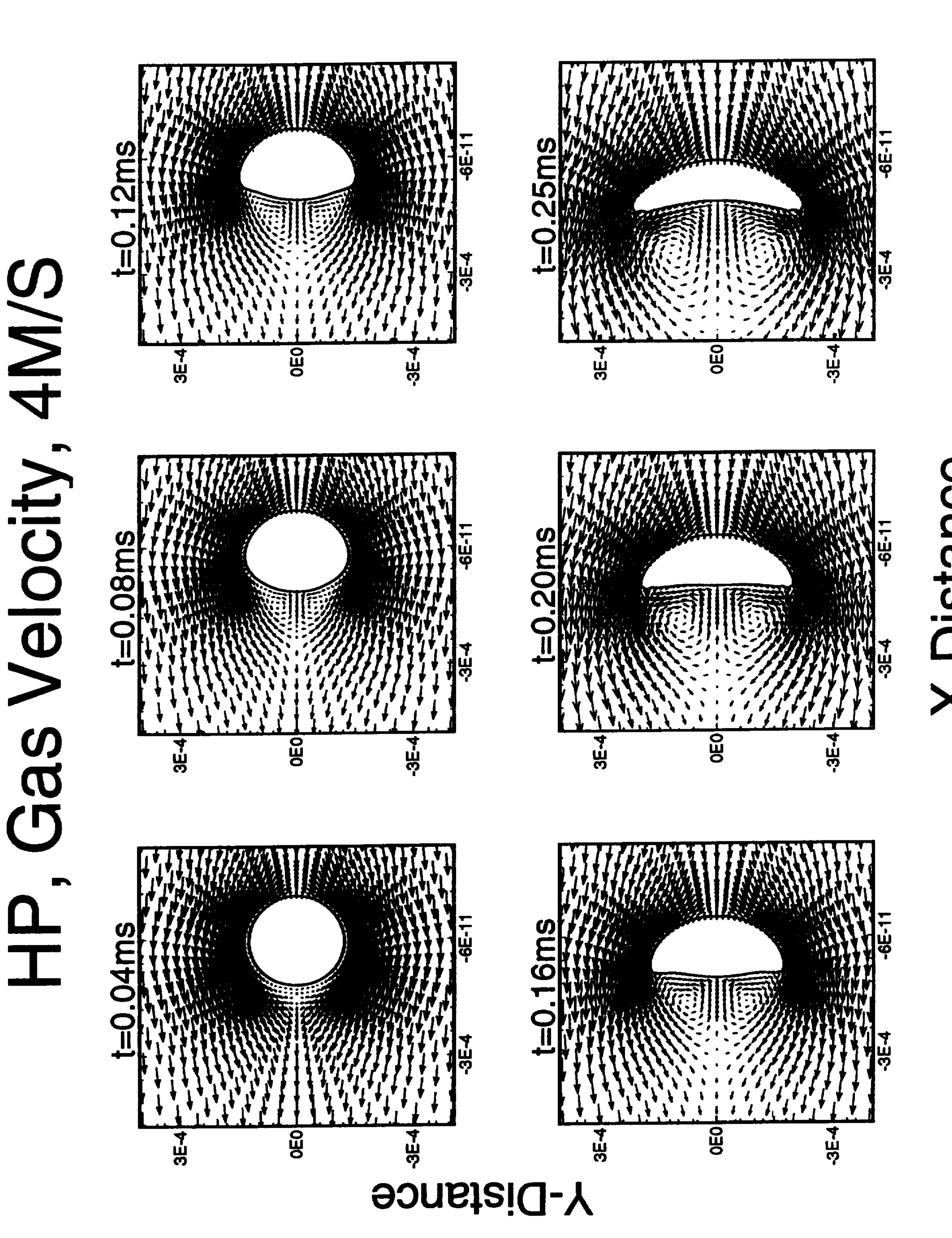

HP, Gas Velocity, 4M/S
t=0.04ms
t=0.08ms
t=0.12ms
t=0.16ms
t=0.20ms
t=0.25ms
3E-4
0E0
-3E-4
-3E-4
-6E-11
X-Distance
Y-Distance

HP, Gas Velocity, 8M/s

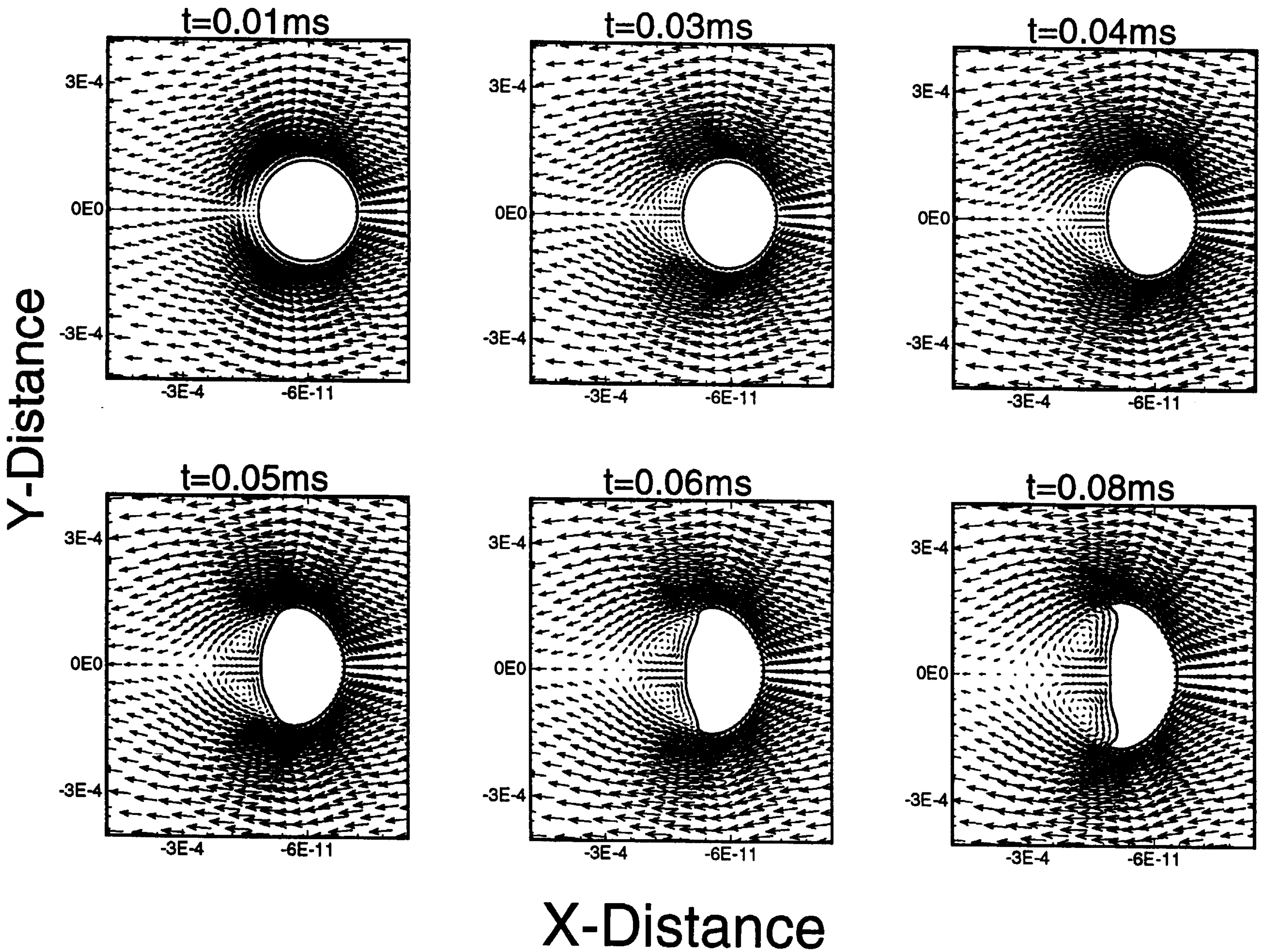

Conclusions and Recommendations:

- Established a two-dimensional model for non-spherical droplet dynamics and eveporation at both low and high pressure convective environments.
- Breakup is sensitive to gas relative velocity; insensitive to gas temperature.
- Fast engineering correlation to predict droplet behavior can be developed based on this model. Combined with available experimental data, a useful package can be provided for rocket engine combustor design.

N95-23648

S33-34
767
p. 24

Abstract for the Elventh CFD Working Group Meeting:

A Fine-Grid Model for the ASRM Aft Segment with Gimballed Nozzle

Presented By: Dr. Edward J. Reske

Results from computational fluid dynamic analyses for complex three-dimensional internal flows in the Advanced Solid Rocket Motor (ASRM) are presented. In particular, flow visualization and tabulated results from a fine-grid model consisting of 1.5 M grid points for the ASRM Aft Segment at the 19-second burn time with an 8-degree nozzle gimbal angle are shown. The results from this model will enable characterization of various aspects of the ASRM internal environment, and in particular will allow an assessment of the heat transfer and stresses exerted on the submerged nozzle, casing insulation, and nozzle-case joint.

A Fine-Grid Model for the ASRM Aft Segment With Gimballed Nozzle

Eleventh Workshop for CFD Applications in Rocket Propulsion

April 20-22, 1993

Ed Reske

MSFC, CFD Branch

Animation by Catherine Dumas, Sverdrup Technology

GEOMETRY

Fine Grid Model for ASRM at 19 seconds with 8-degree Gimbal Angle

Surface Geometry: Dimensions 127 X 311 X 37 = 1.46 M Grid Points

127x311x37 GRID

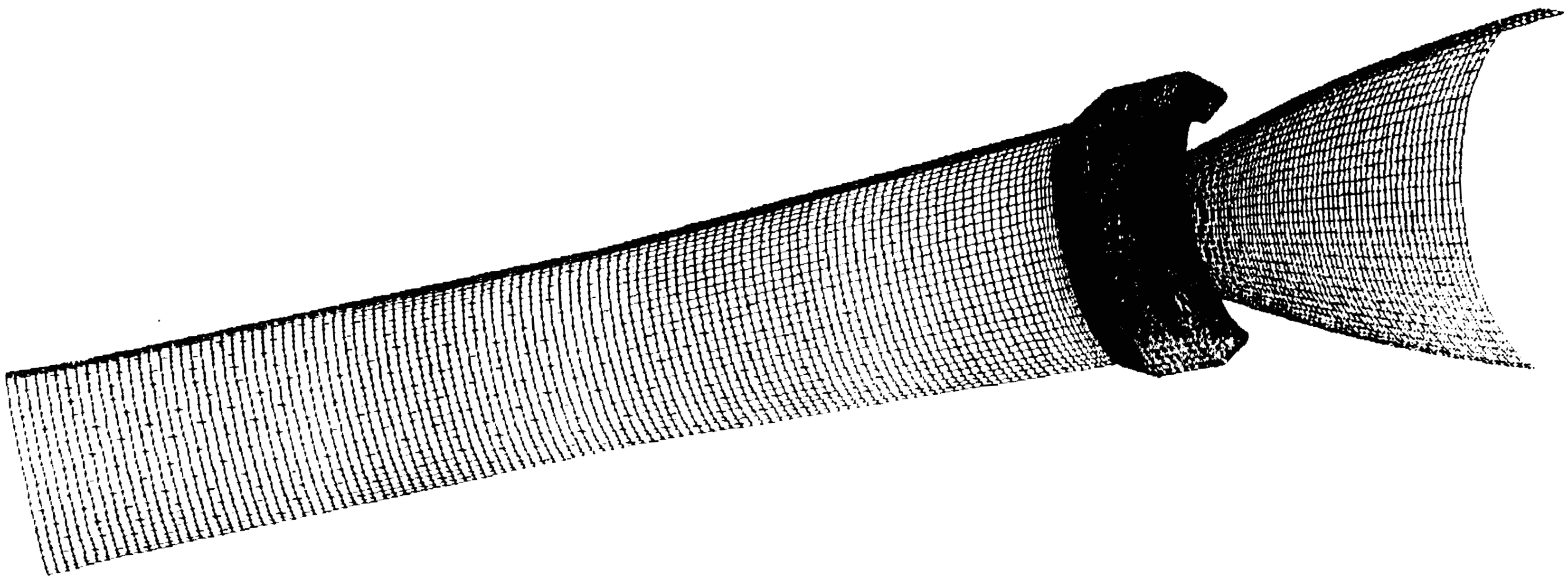

e19fg.2.img

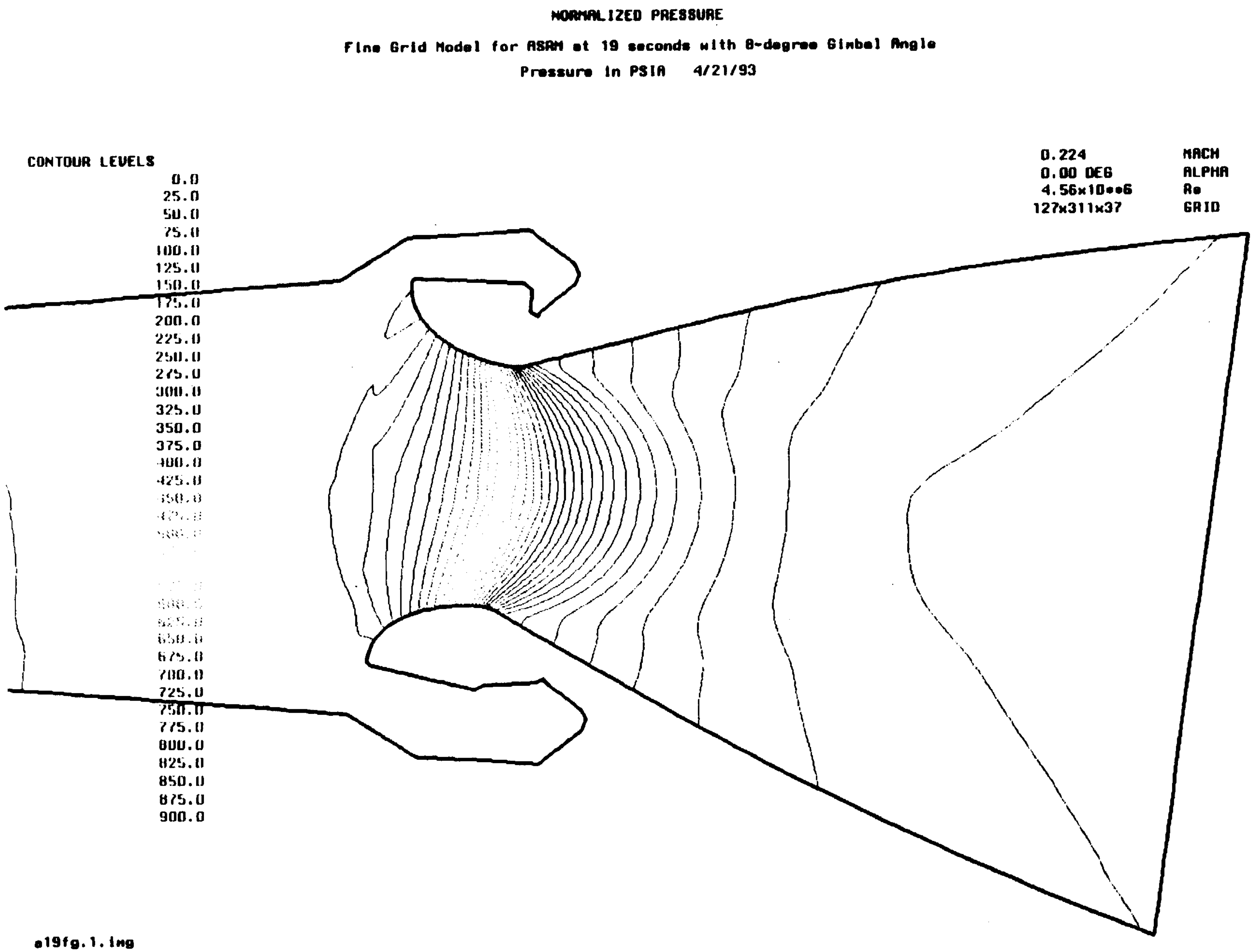

ORIGINAL PAGE IS
OF POOR QUALITY

MACH NUMBER

Fine Grid Model for ASRM at 19 seconds with 8-degree Gimbal Angle

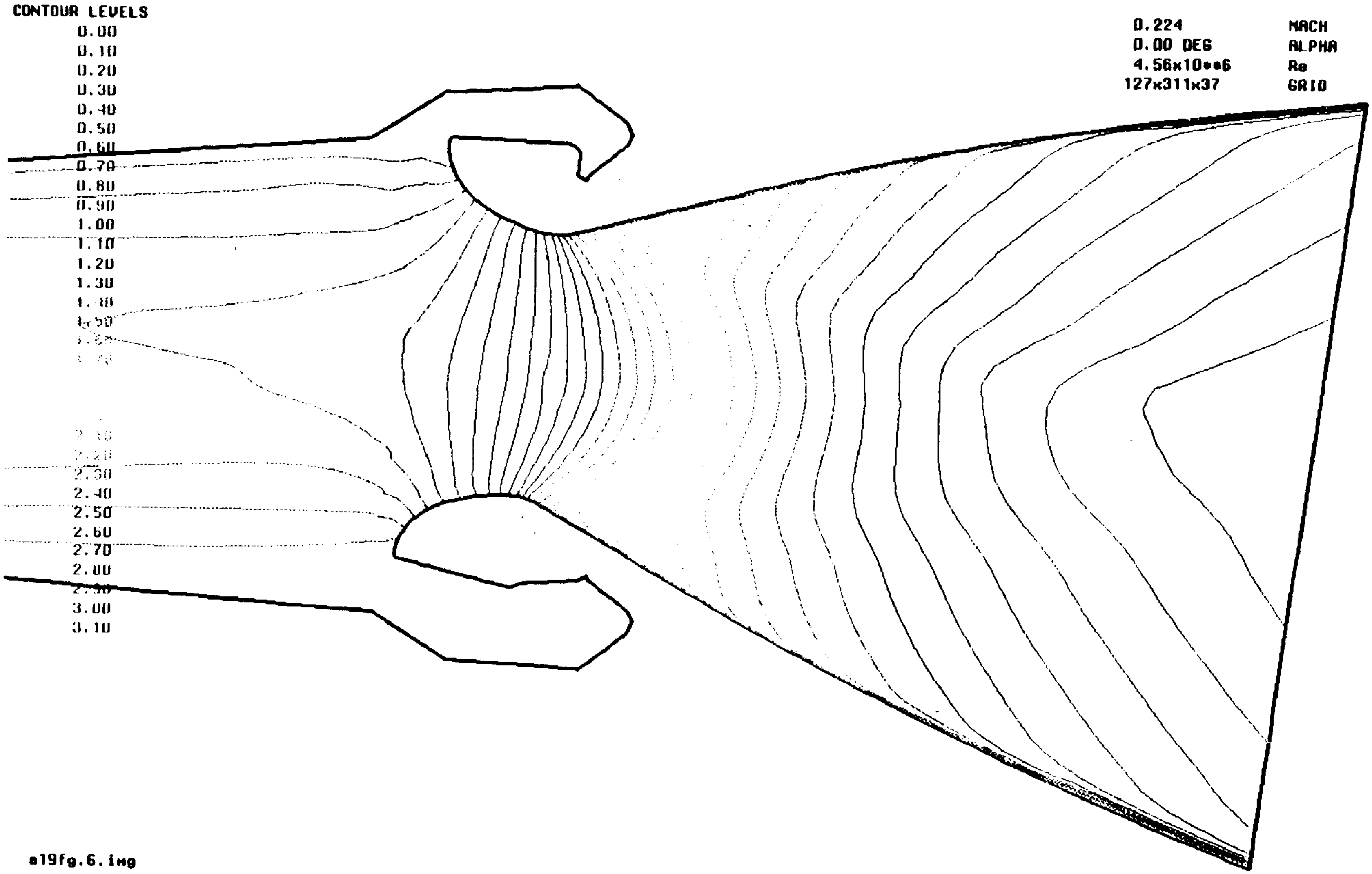

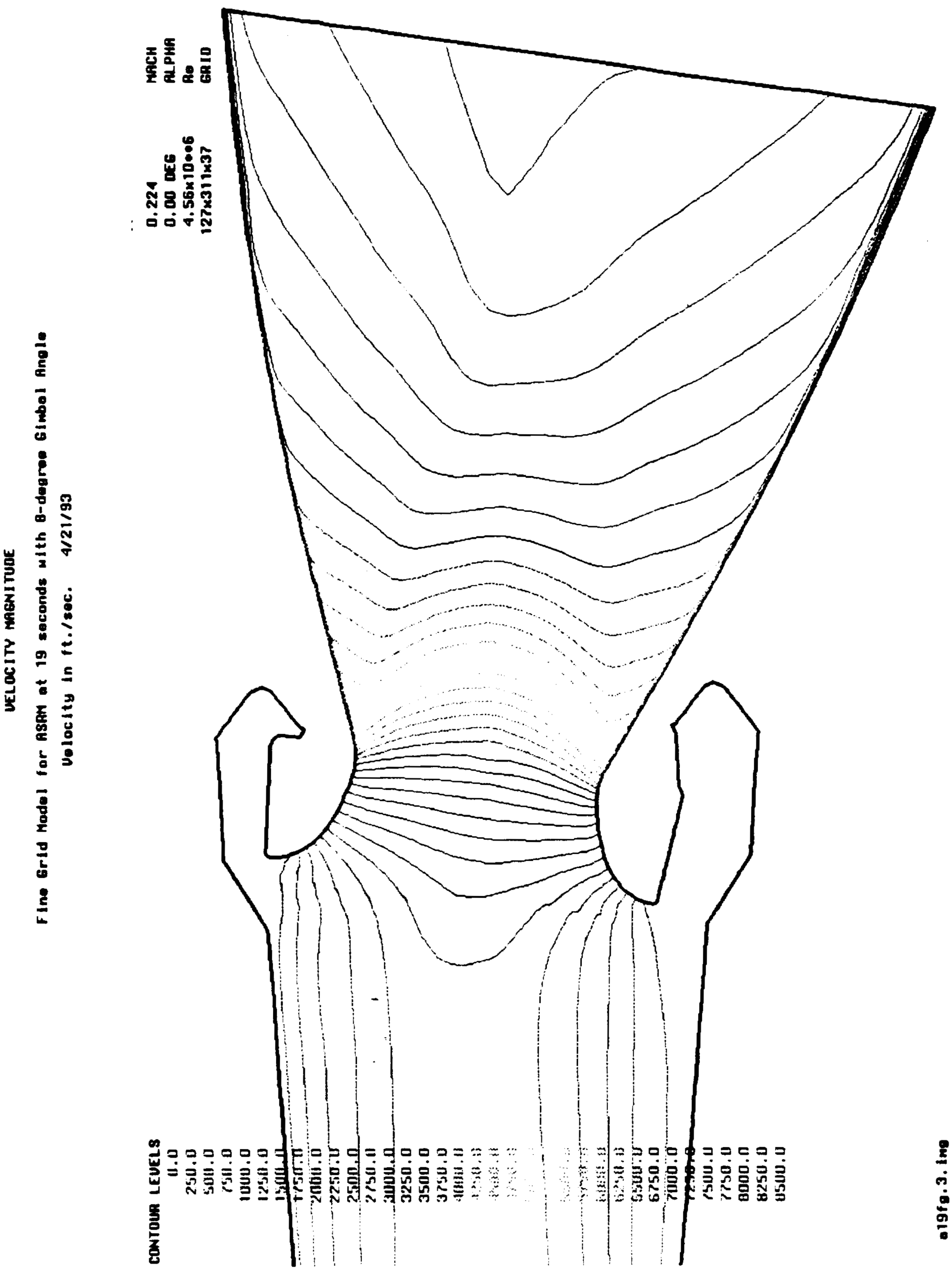

ORIGINAL PAGE IS
OF POOR QUALITY

V VELOCITY

Fine Grid Model for ASRM at 19 seconds with 8-degree Gimbal Angle

Velocity in ft./sec.   4/21/93

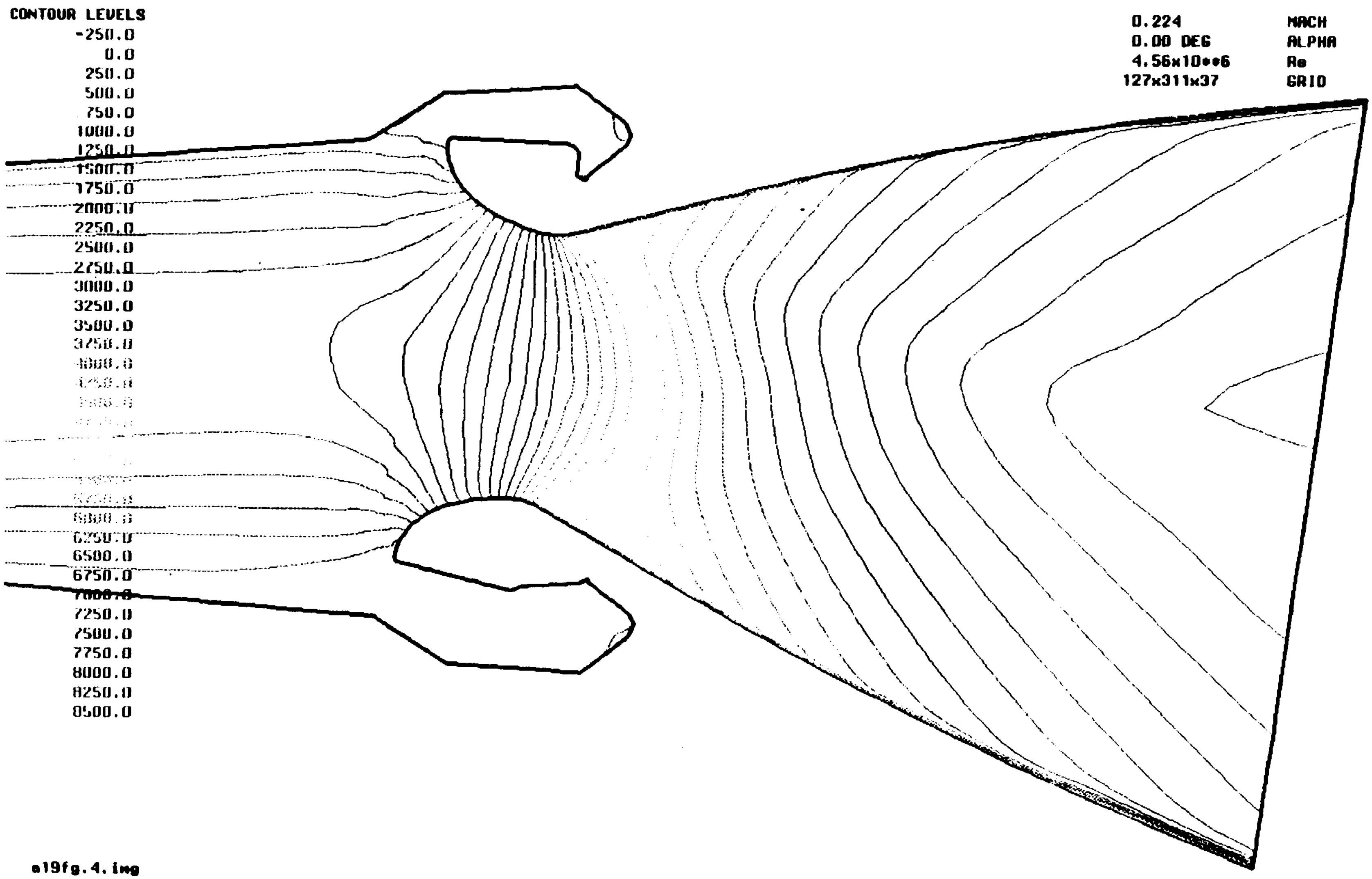

a19fg.4.img

U VELOCITY

Fine Grid Model for ASRM at 19 seconds with 8-degree Gimbal Angle

Velocity in ft./sec. 4/21/93

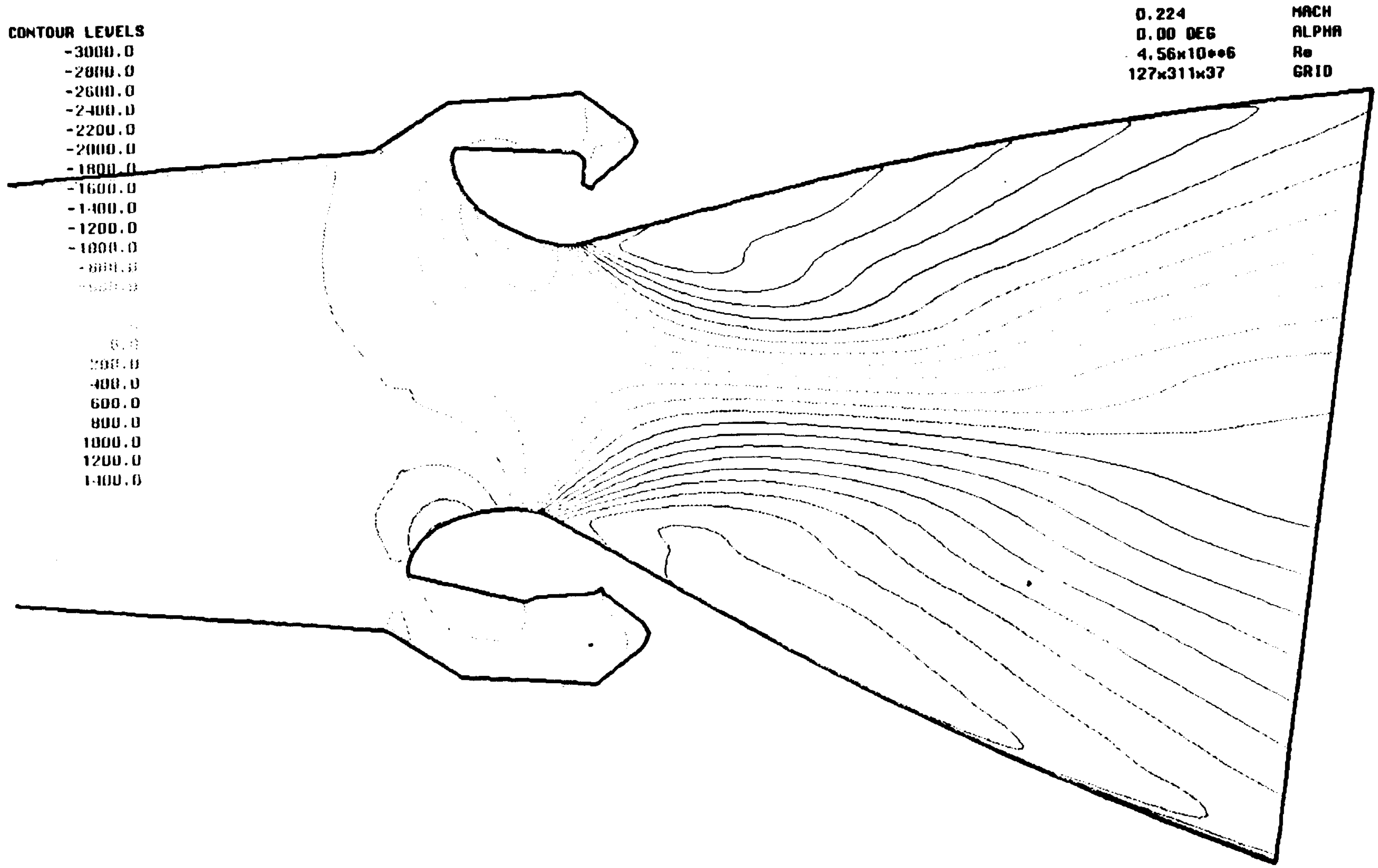

e19fg.5.img

PARTICLE TRACES

ASRM at 115 second burn time with nozzle gimballed at 8 degrees: 3/24/92

Solution "d" (after 3400 iterations)

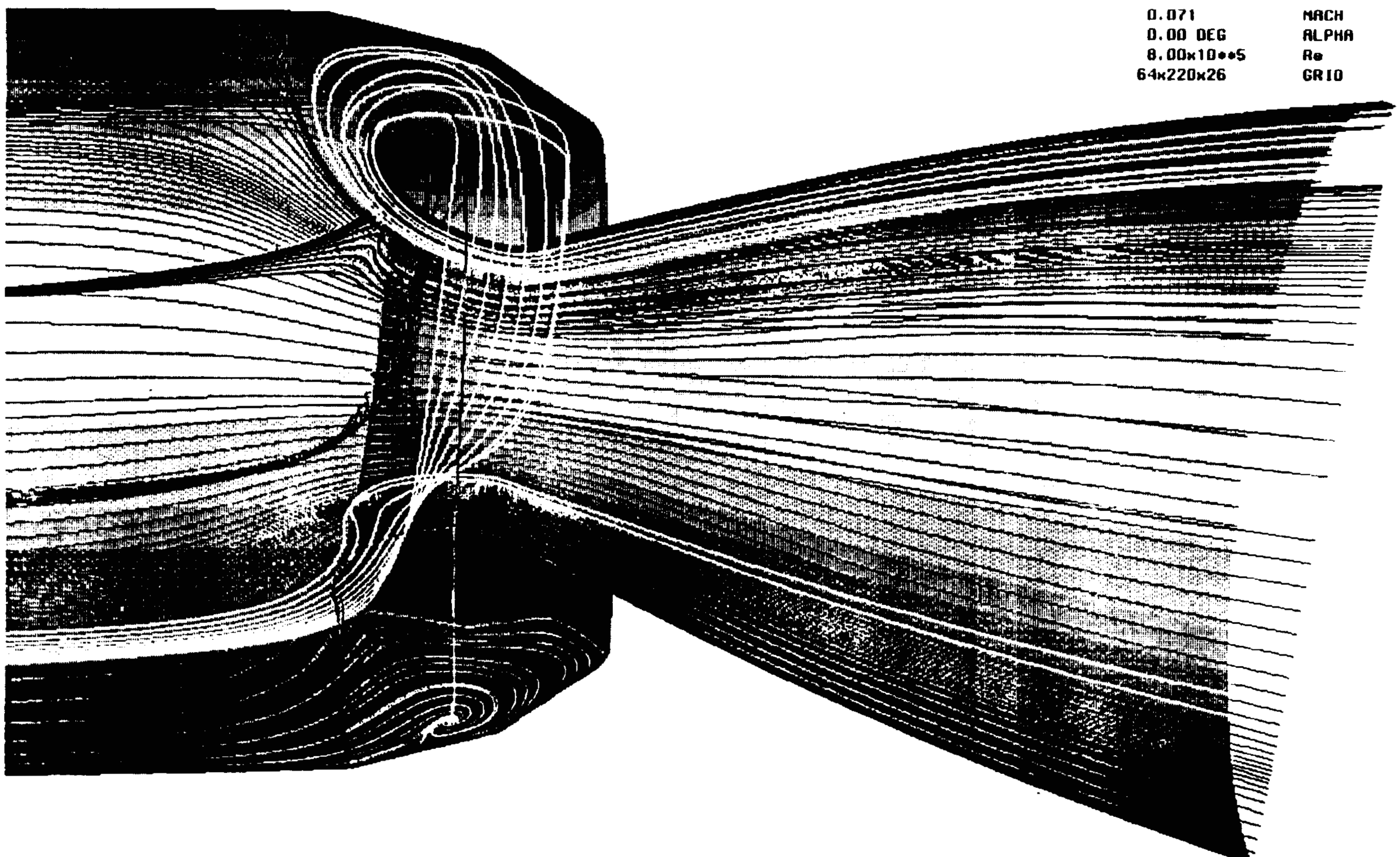

flowd.9.img

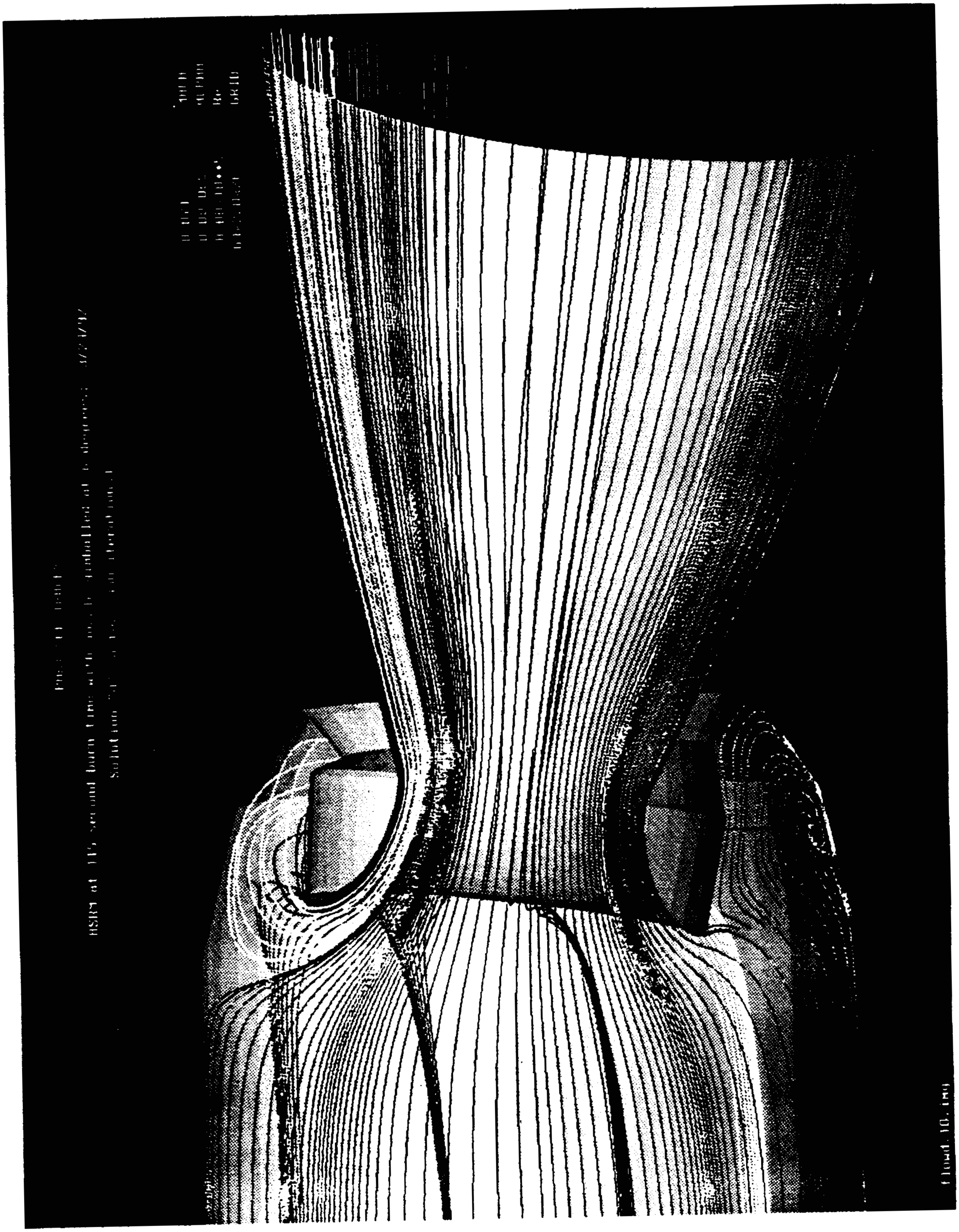

GEOMETRY

ASRM at 19 seconds with 8-degree Gimbal Angle

Station Locations on Nozzle Nose in K = 1 Plane

127x311x37 GRID

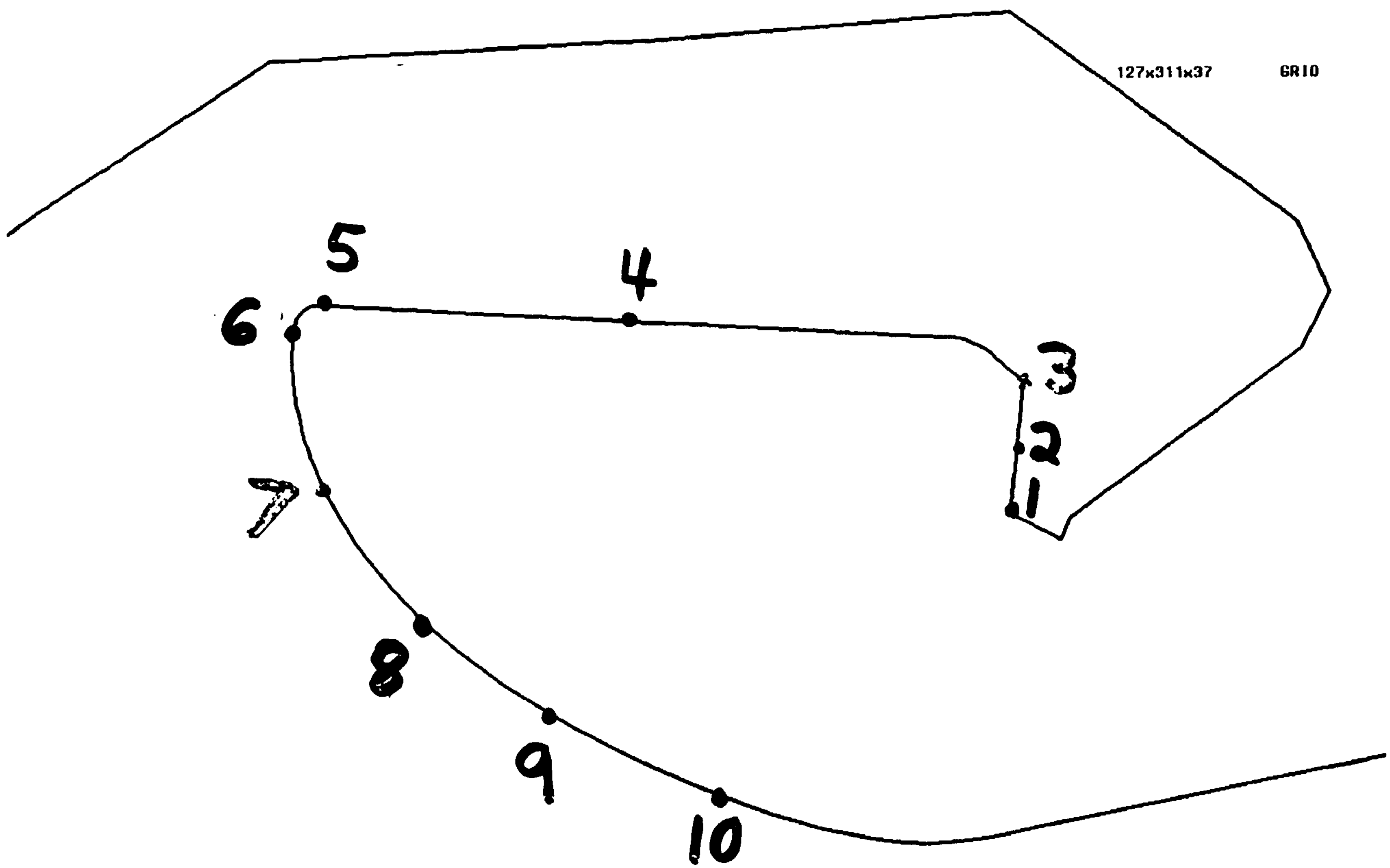

a19fg.1.img

GEOMETRY

ASRM at 19 seconds with 8-degree Gimbal Angle

Station Locations on Nozzle Nose in K = 1 Plane

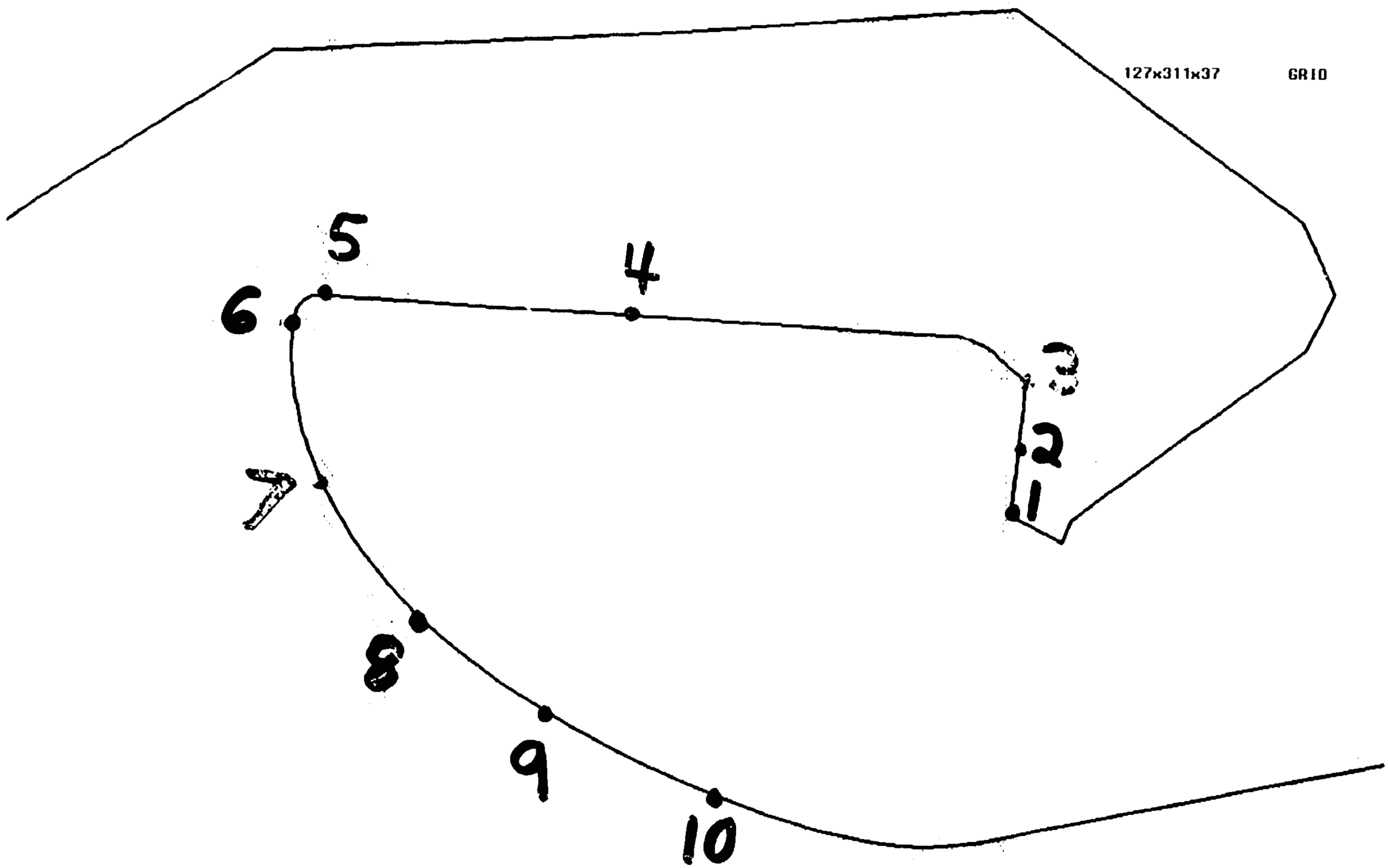

a19fg.1.img

Circumferential Pressure Variation

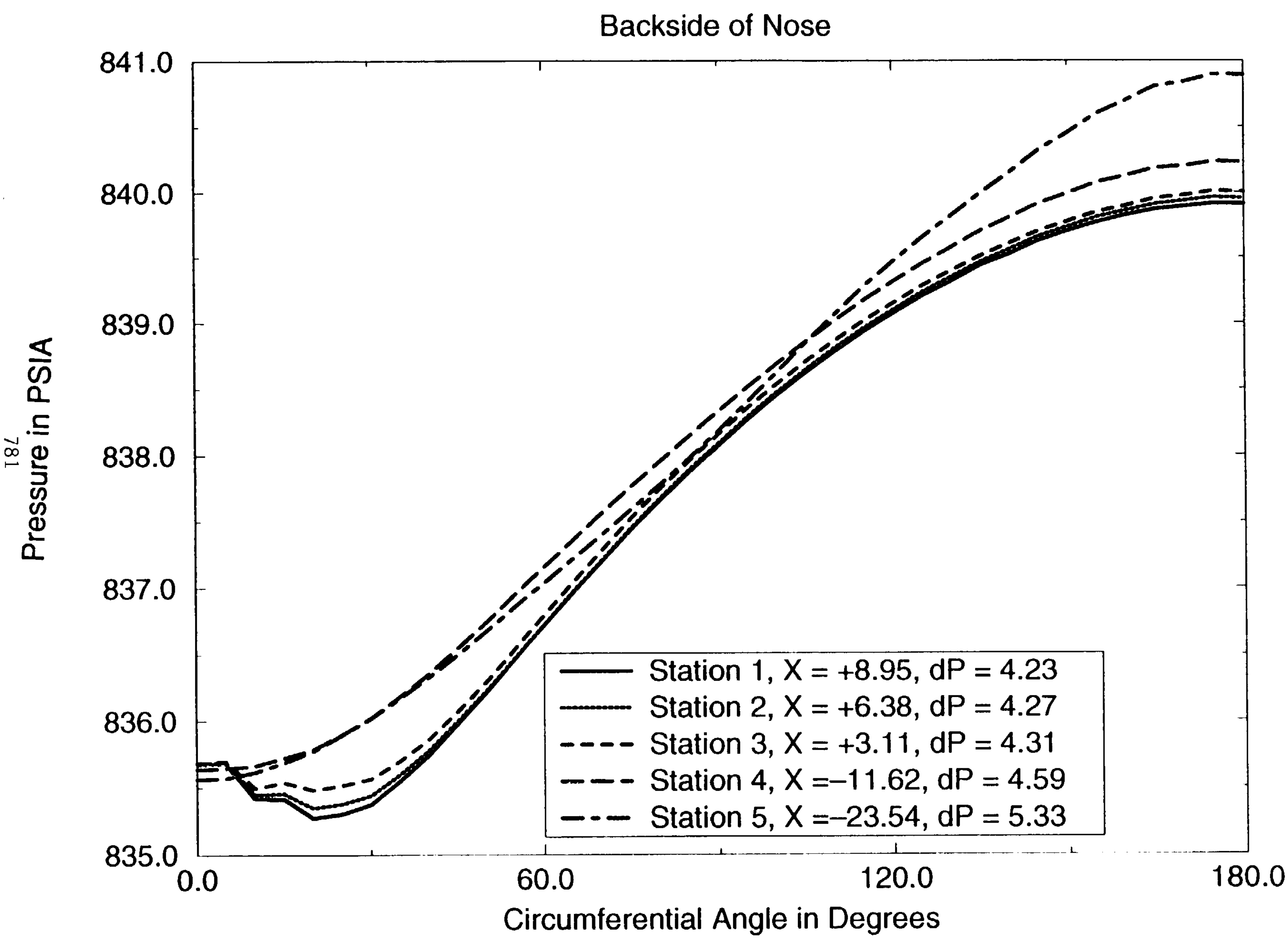

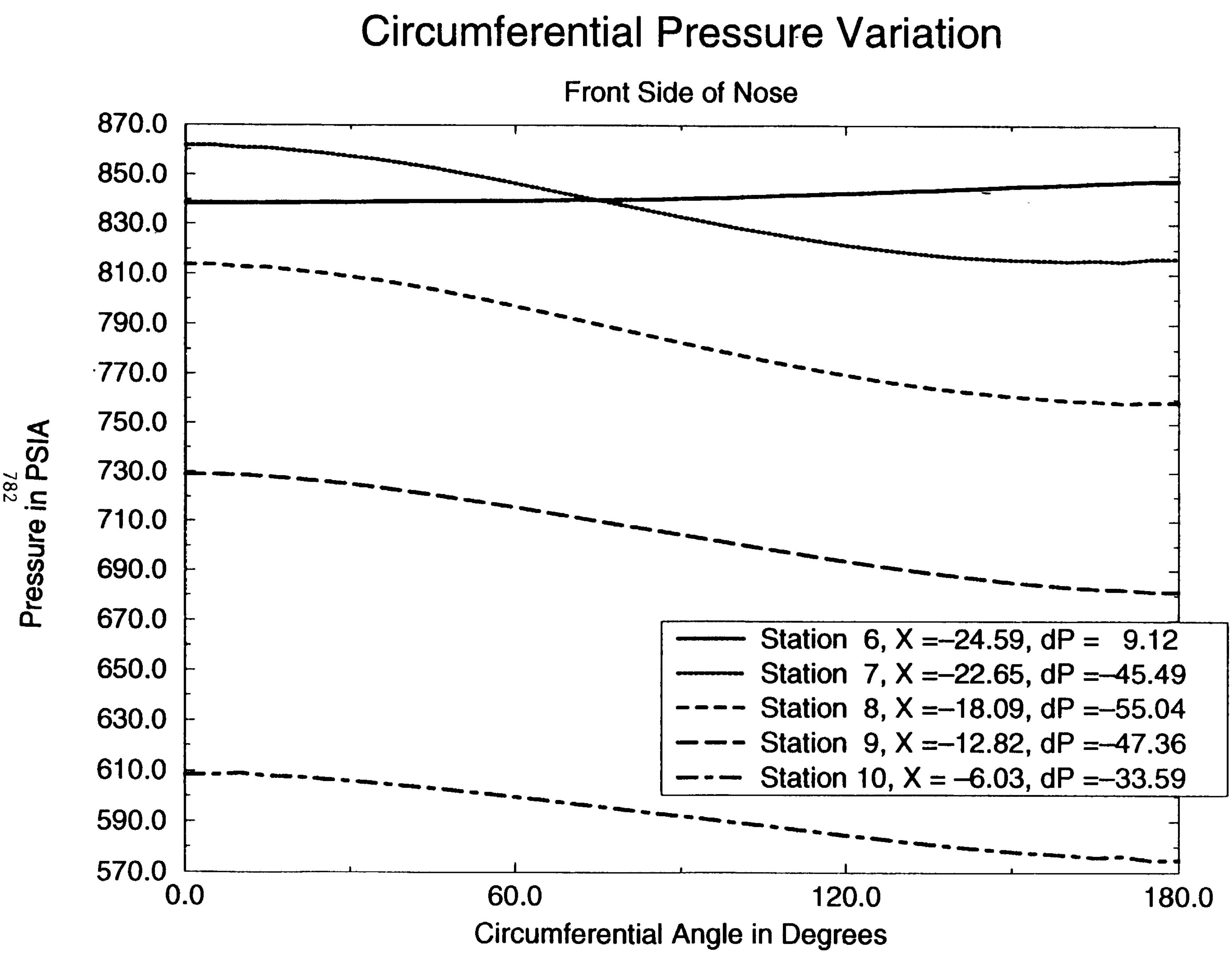

Circumferential Pressure Variation
Front Side of Nose
Pressure in PSIA
870.0
850.0
830.0
810.0
790.0
770.0
750.0
730.0
710.0
690.0
670.0
650.0
630.0
610.0
590.0
570.0
0.0
60.0
120.0
180.0
Circumferential Angle in Degrees
Station 6, X =−24.59, dP = 9.12
Station 7, X =−22.65, dP =−45.49
Station 8, X =−18.09, dP =−55.04
Station 9, X =−12.82, dP =−47.36
Station 10, X = −6.03, dP =−33.59

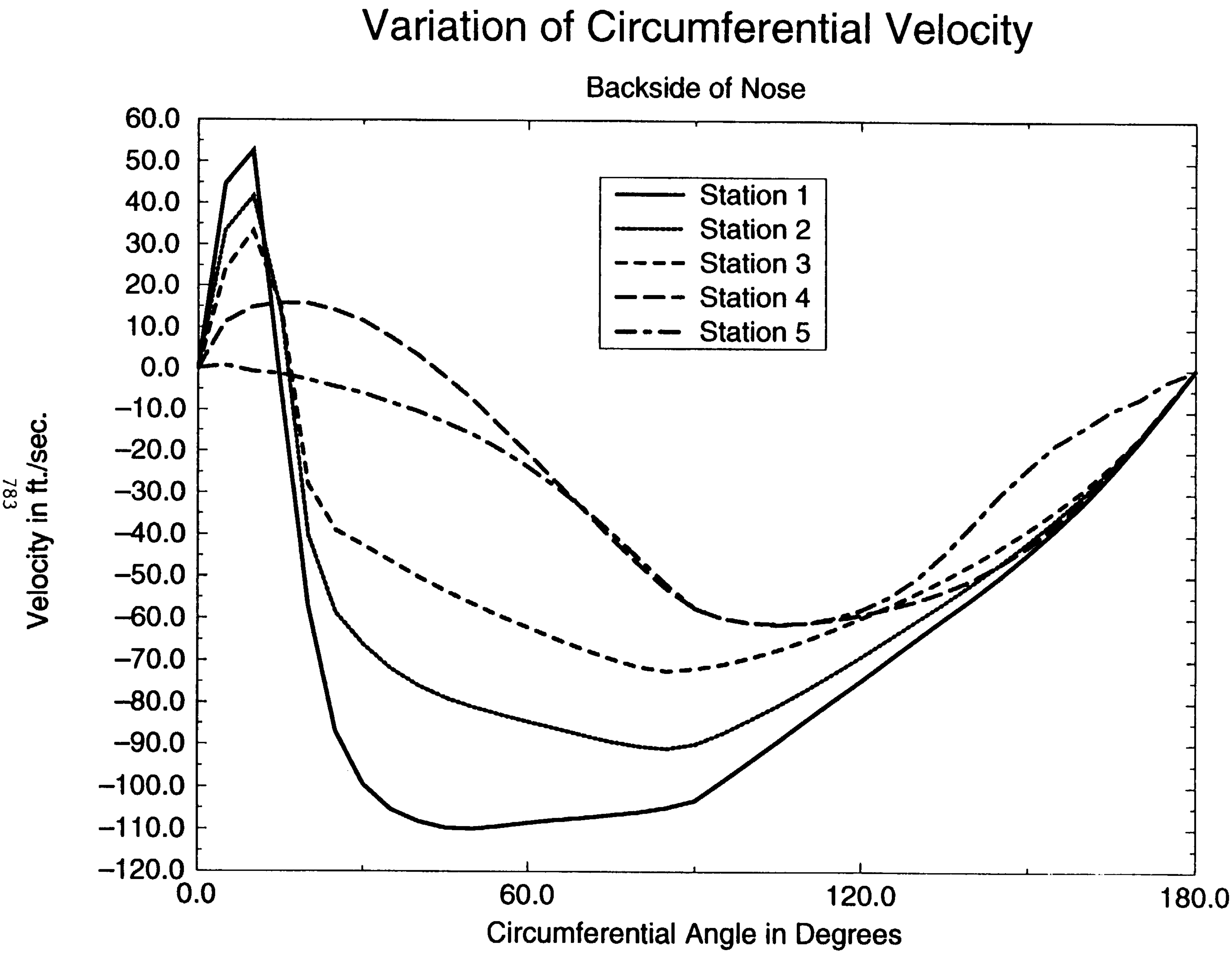
Variation of Circumferential Velocity
Backside of Nose
Station 1
Station 2
Station 3
Station 4
Station 5
Velocity in ft./sec.
Circumferential Angle in Degrees
60.0
50.0
40.0
30.0
20.0
10.0
0.0
−10.0
−20.0
−30.0
−40.0
−50.0
−60.0
−70.0
−80.0
−90.0
−100.0
−110.0
−120.0
0.0
60.0
120.0
180.0

Variation of Circumferential Velocity

Forward Side of Nose

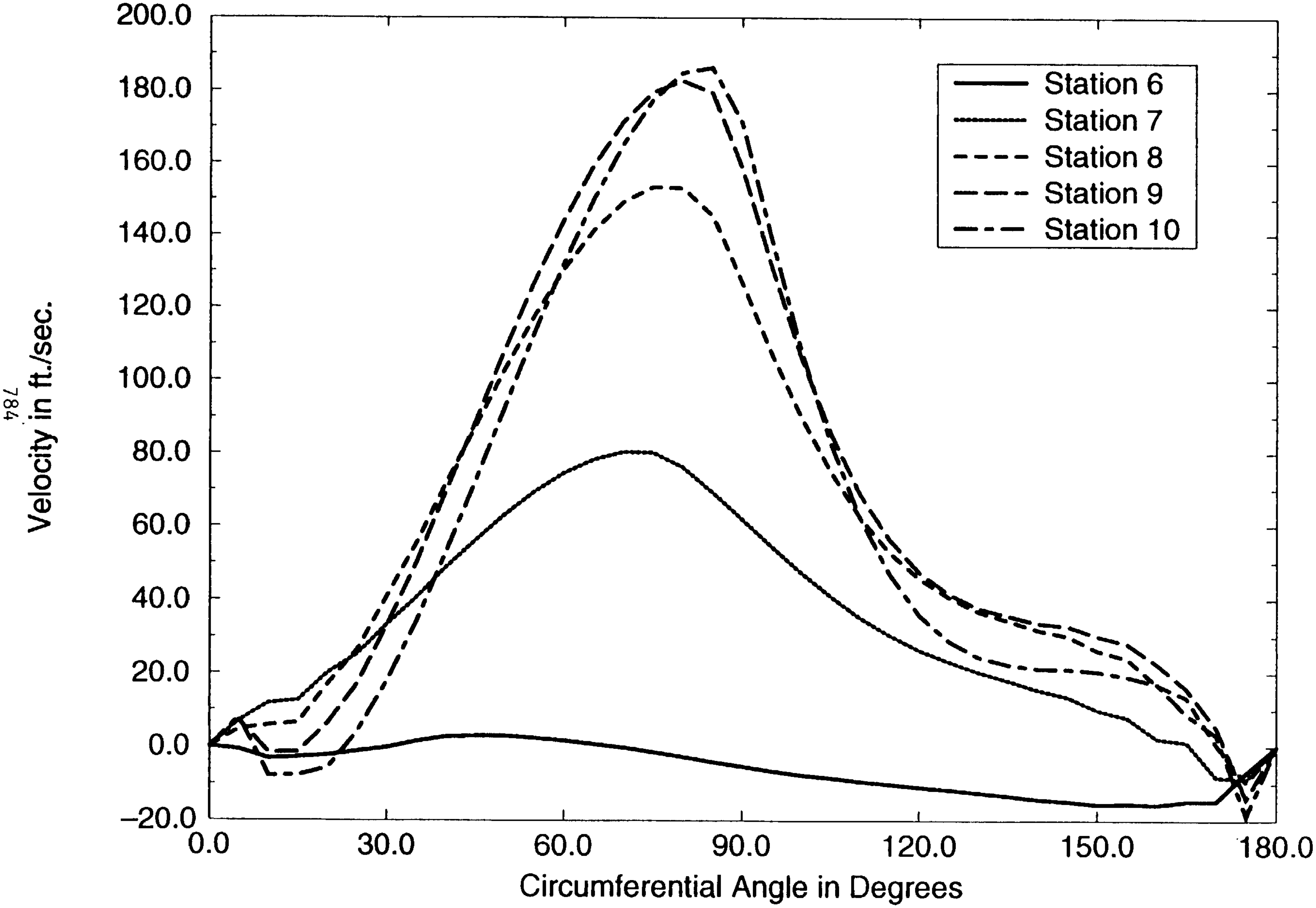

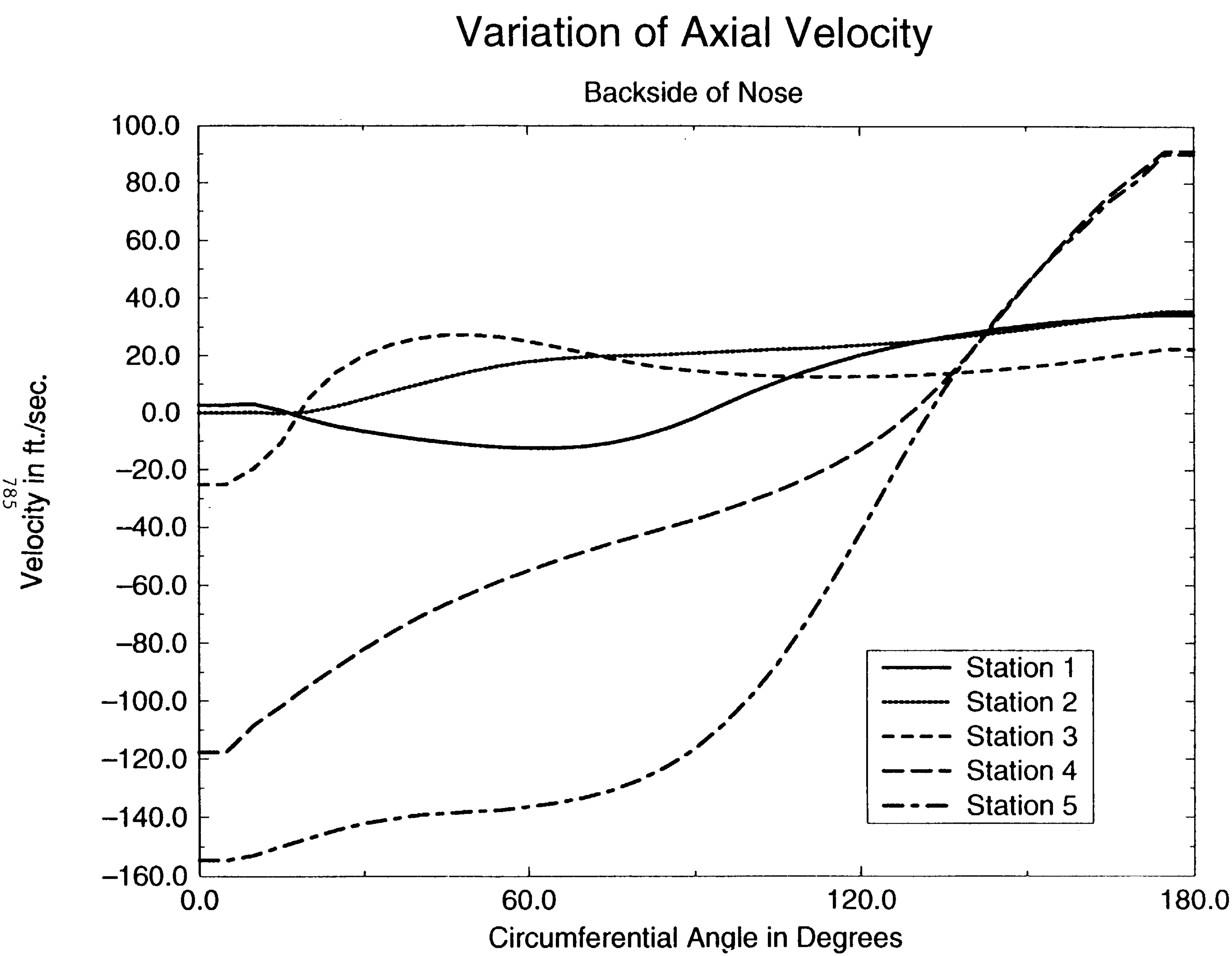

Variation of Axial Velocity
Backside of Nose
100.0
80.0
60.0
40.0
20.0
0.0
−20.0
−40.0
−60.0
−80.0
−100.0
−120.0
−140.0
−160.0
Velocity in ft./sec.
0.0
60.0
120.0
180.0
Circumferential Angle in Degrees
Station 1
Station 2
Station 3
Station 4
Station 5

Variation of Axial Velocity

Forward Side of Nose

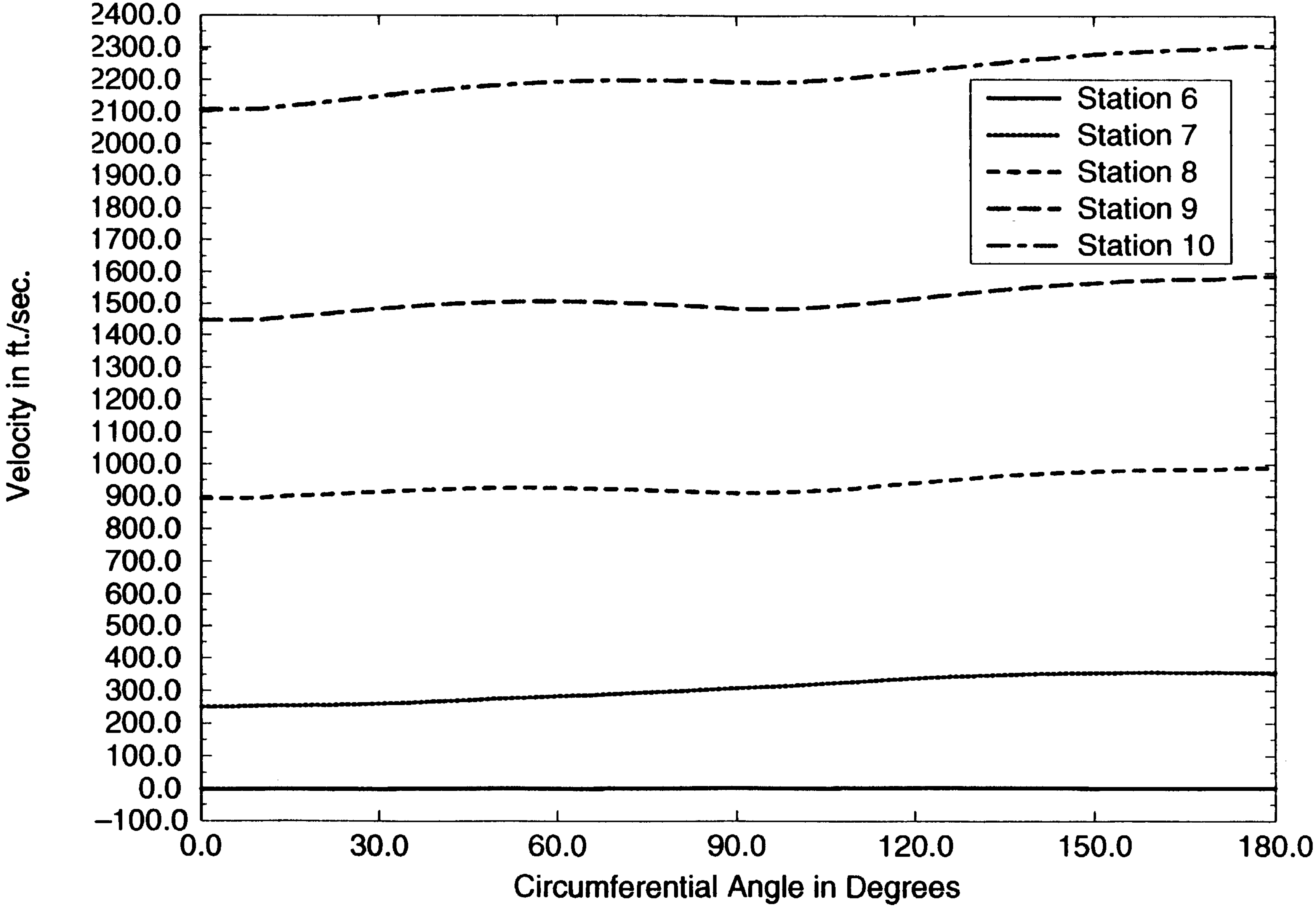

Variation of Radial Velocity

Backside of Nose

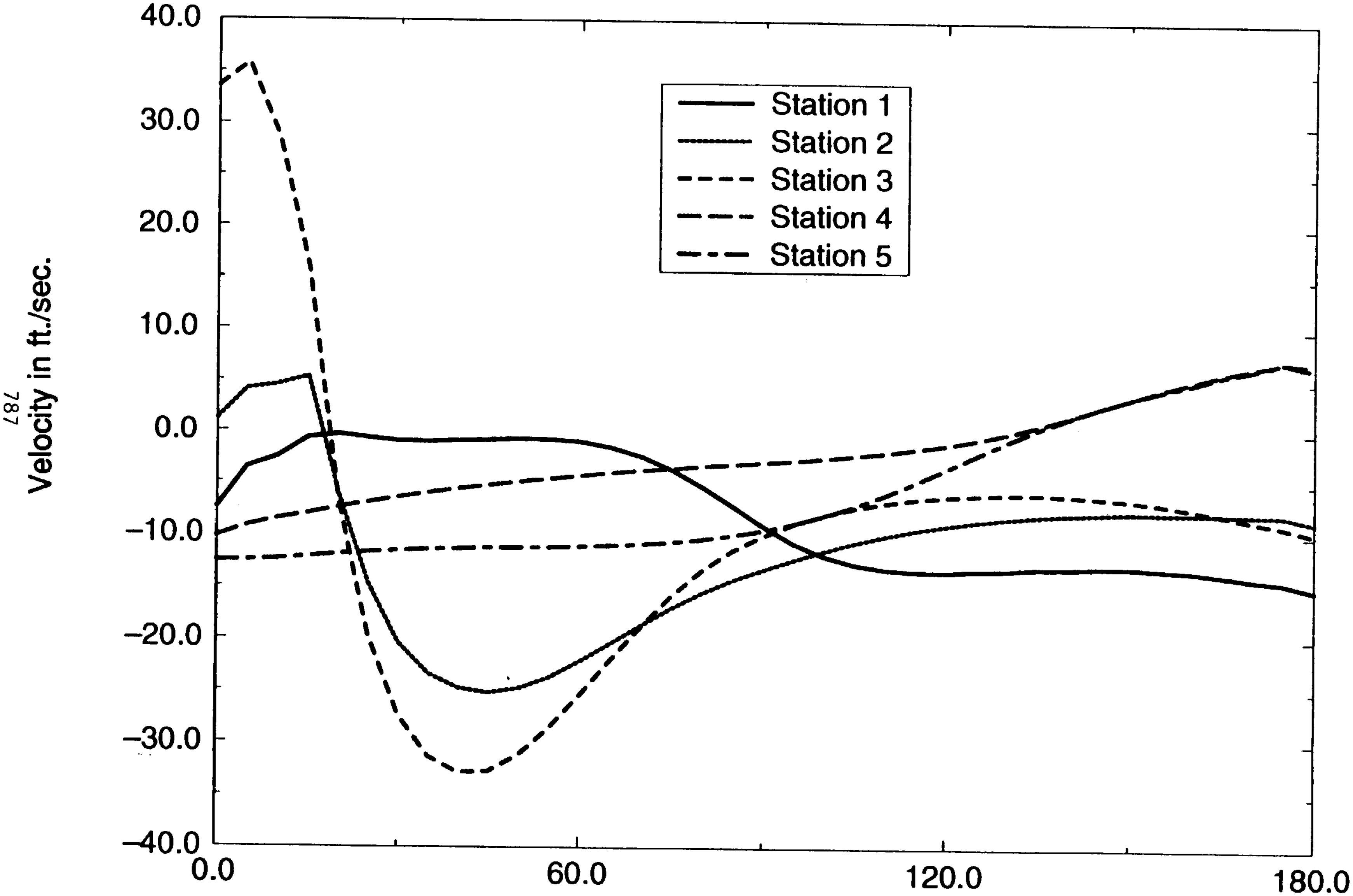

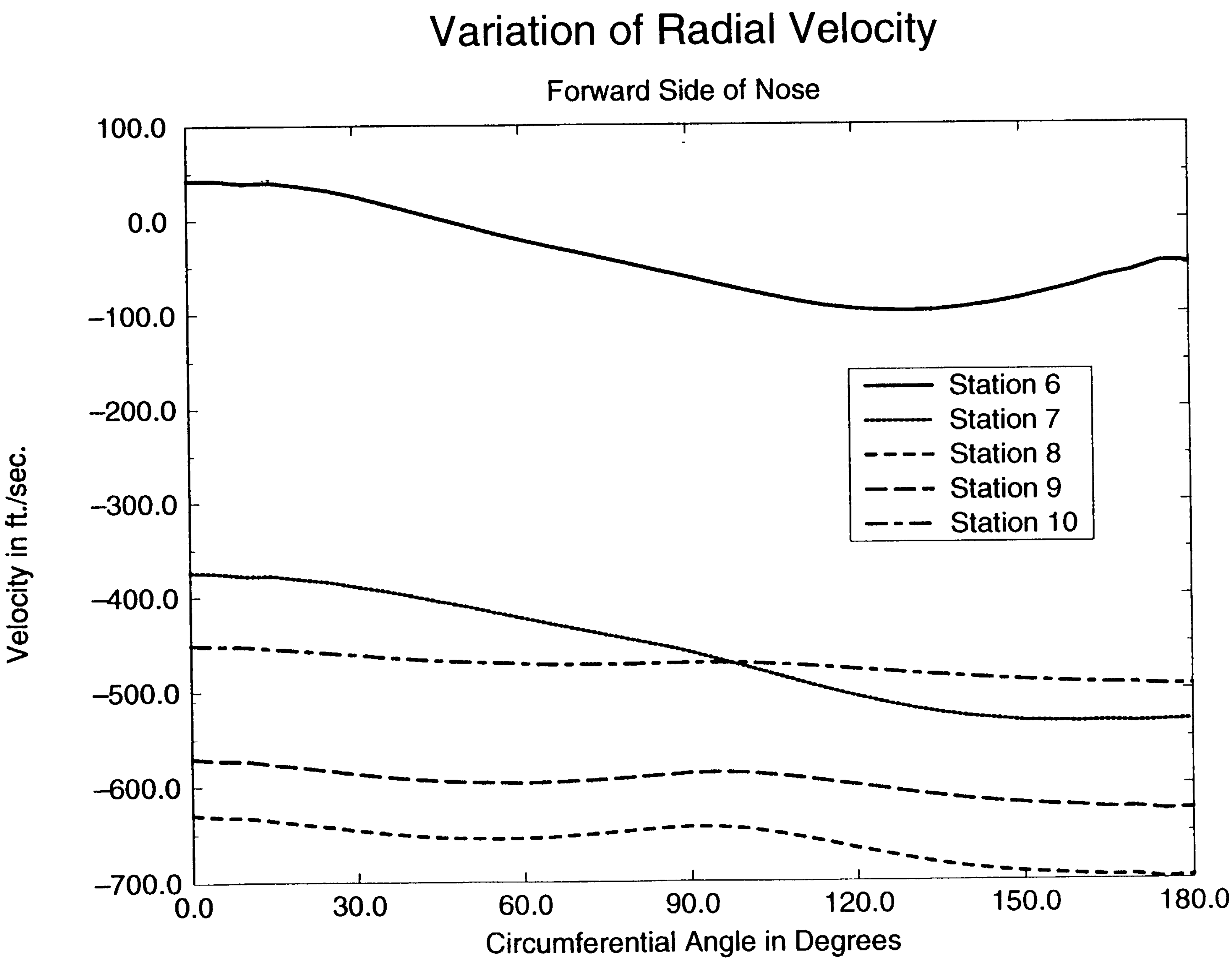
Variation of Radial Velocity
Forward Side of Nose
100.0
0.0
–100.0
–200.0
–300.0
–400.0
–500.0
–600.0
–700.0
Velocity in ft./sec.
0.0
30.0
60.0
90.0
120.0
150.0
180.0
Circumferential Angle in Degrees
Station 6
Station 7
Station 8
Station 9
Station 10

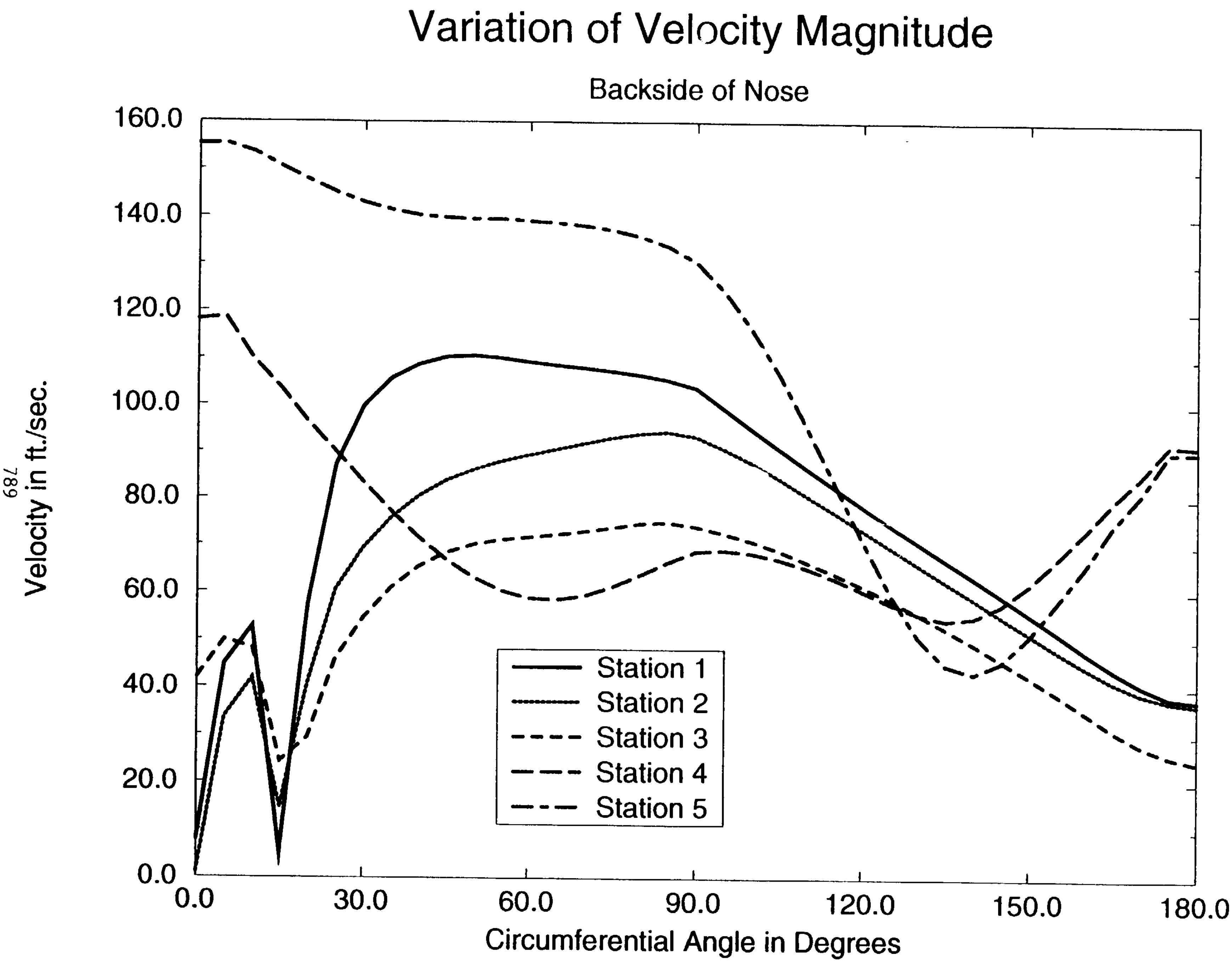
Variation of Velocity Magnitude
Backside of Nose
160.0
140.0
120.0
100.0
80.0
60.0
40.0
20.0
0.0
Velocity in ft./sec.
0.0
30.0
60.0
90.0
120.0
150.0
180.0
Circumferential Angle in Degrees
Station 1
Station 2
Station 3
Station 4
Station 5

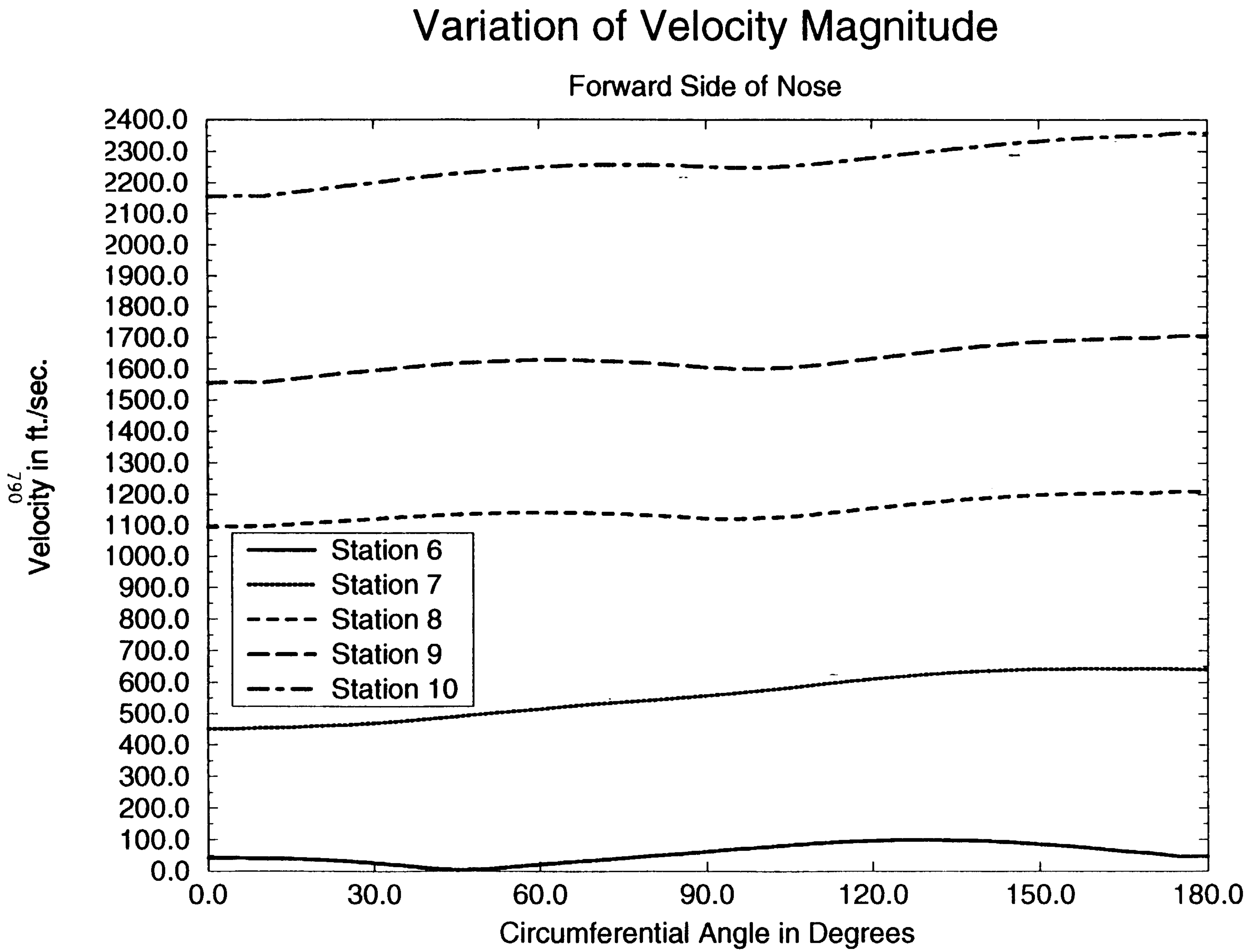

Variation of Velocity Magnitude
Forward Side of Nose
Velocity in ft./sec.
2400.0
2300.0
2200.0
2100.0
2000.0
1900.0
1800.0
1700.0
1600.0
1500.0
1400.0
1300.0
1200.0
1100.0
1000.0
900.0
800.0
700.0
600.0
500.0
400.0
300.0
200.0
100.0
0.0
0.0
30.0
60.0
90.0
120.0
150.0
180.0
Circumferential Angle in Degrees
Station 6
Station 7
Station 8
Station 9
Station 10

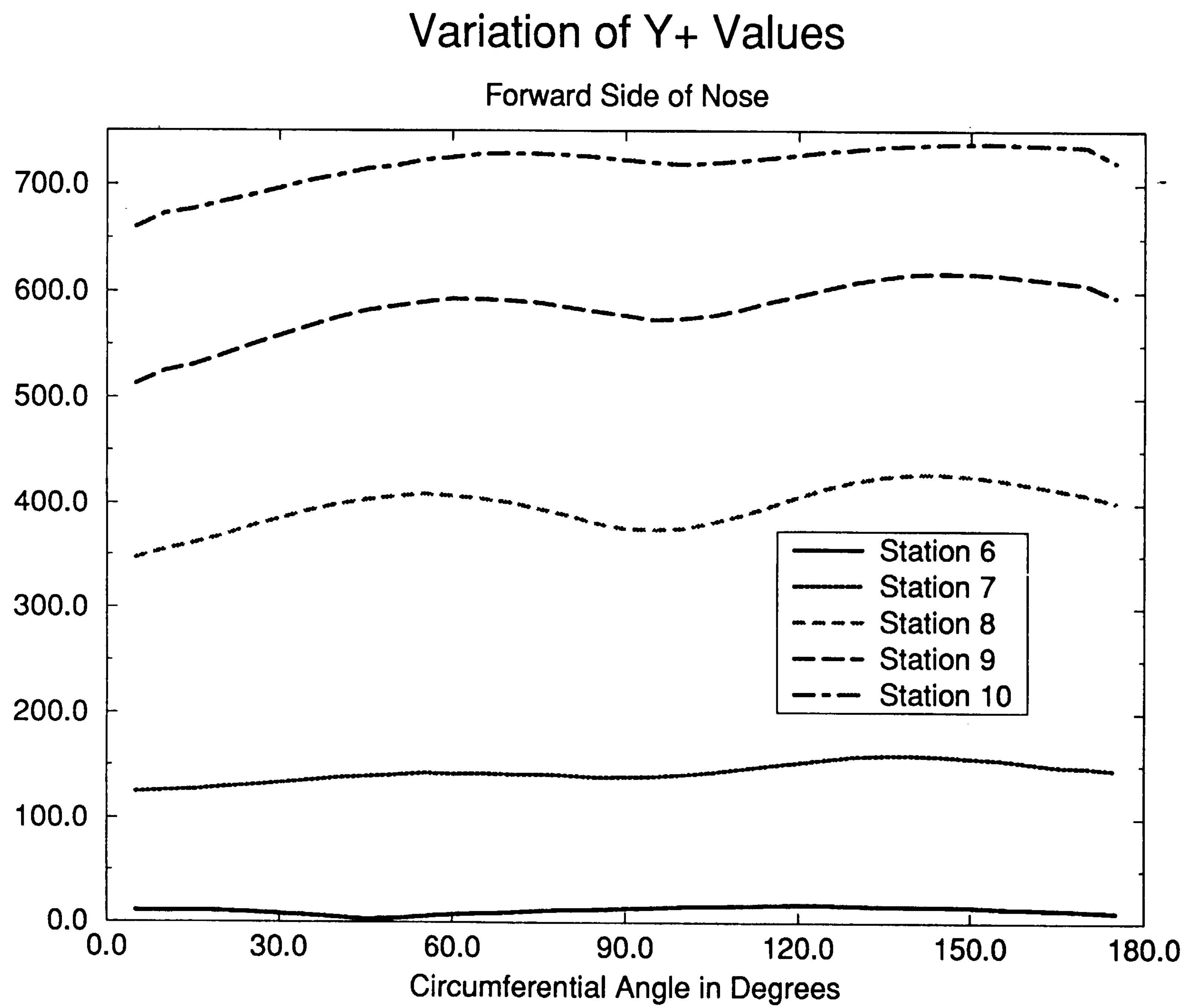
Variation of Y+ Values
Forward Side of Nose
700.0
600.0
500.0
400.0
300.0
200.0
100.0
0.0
0.0
30.0
60.0
90.0
120.0
150.0
180.0
Circumferential Angle in Degrees
Station 6
Station 7
Station 8
Station 9
Station 10

Variation of Y+ Values

Backside of Nose

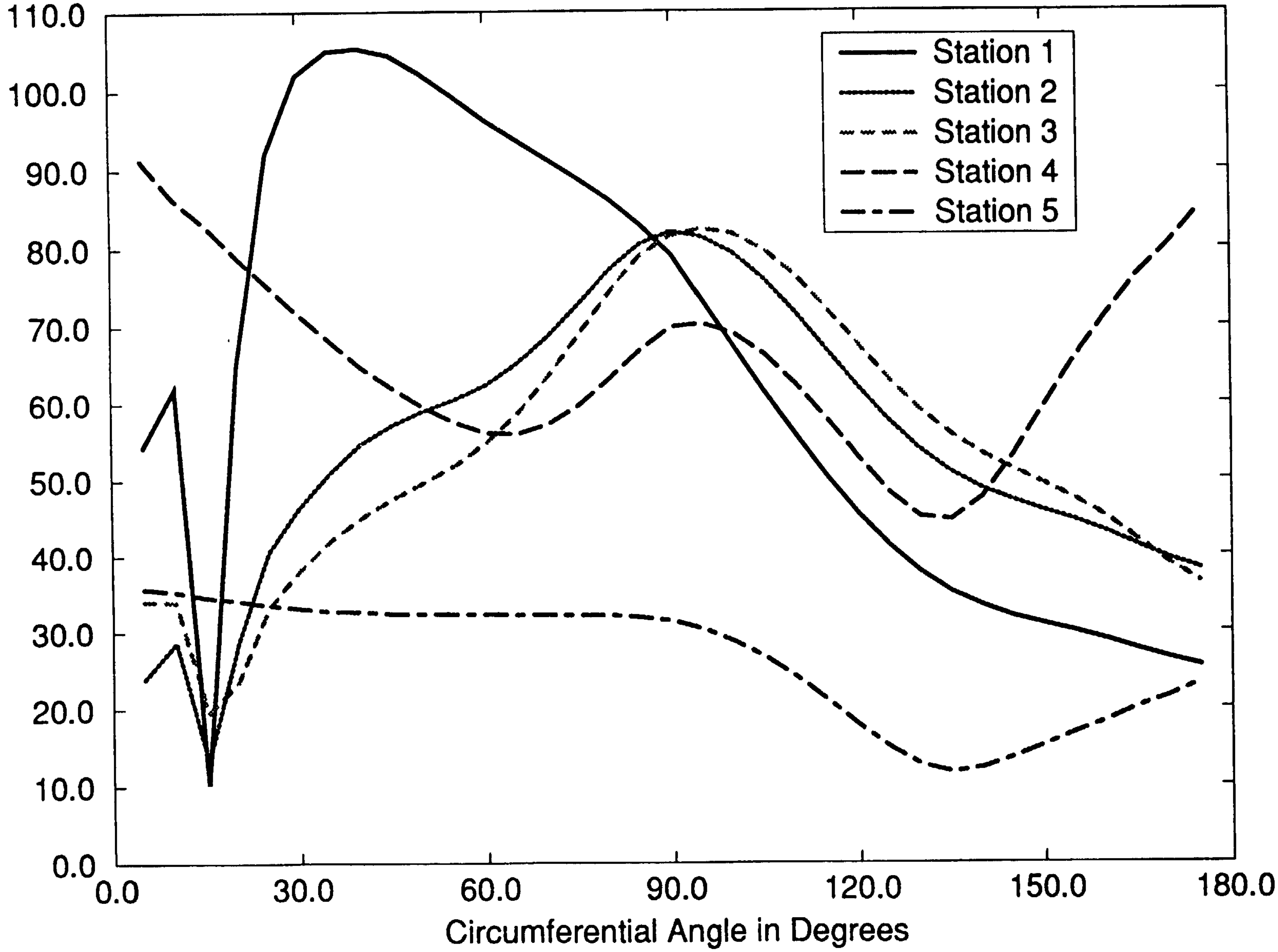

N95-23649 $-34-34$

Application of CFD Analyses to Design Support and Problem Resolution for ASRM and RSRM

p. 43

Richard A. Dill, ERC Incorporated
R. Harold Whitesides, ERC Incorporated

Abstract

The use of Navier-Stokes CFD codes to predict the internal flow field environment in a solid rocket motor is a very important analysis element during the design phase of a motor development program. These computational flow field solutions uncover a variety of potential problems associated with motor performance as well as suggesting solutions to these problems. CFD codes have also proven to be of great benefit in explaining problems associated with operational motors such as in the case of the pressure spike problem with the STS-54B flight motor. This paper presents results from analyses involving both motor design support and problem resolution. The issues discussed include the fluid dynamic/mechanical stress coupling at field joints relative to significant propellant deformations, the prediction of axial and radial pressure gradients in the motor associated with motor performance and propellant mechanical loading, the prediction of transition of the internal flow in the motor associated with erosive burning, the accumulation of slag at the field joints and in the submerged nozzle region, impingement of flow on the nozzle nose, and pressure gradients in the nozzle region of the motor.

The analyses presented in this paper have been performed using a two-dimensional axi-symmetric model. Fluent/BFC, a three dimensional Navier-Stokes flow field code, has been used to make the numerical calculations. This code utilizes a staggered grid formulation along with the SIMPLER numerical pressure-velocity coupling algorithm. Wall functions are used to represent the character of the viscous sub-layer flow, and an adjusted $\kappa-\varepsilon$ turbulence model especially configured for mass injection internal flows, is used to model the growth of turbulence in the motor port.

The topic of motor problem resolution is discussed by presenting solutions associated with the sixty-seven second burn time RSRM motor. The full motor internal flow environment for RSRM is discussed and the axial and radial pressure gradients are shown. The flow field environment and pressure gradients in the slots are also discussed. Particle traces from the burning propellant in the field joints are presented which show the tendency of the center and aft slots to collect slag. The flow field environment in the submerged nozzle region with and without slag in the submerged nozzle cavity is shown and specific flow field features which contribute to observed post-flight motor erosion patterns is discussed.

The design support analyses on the ASRM presented are for the zero second burn time geometry. The full motor flow field environment is presented along with axial and radial pressure gradients. Transition of the velocity profiles in the motor port is presented and the effect of the geometry flare in the bore at the aft end of the motor is shown. The aft slot deformation analysis is also presented. This analysis is an iterative coupled fluid dynamic/mechanical load analysis examining how two-dimensional flow field effects in the motor cause deformation of the propellant grain. The submerged nozzle region flow field is presented and discussed as it relates to the total pressure gradient observed in the aft end of the motor. The radial total pressure gradient is shown to be too great to allow the boot cavity motor pressure measurements to be compared with the nozzle end total pressure computed in ballistic runs.

Conclusions discussed in this paper consider flow field effects on the forward, center, and aft propellant grains except for the head end star grain region of the forward propellant segment. The field joints and the submerged nozzle are discussed as well. Conclusions relative to both the design evaluation of the ASRM and the RSRM scenarios explaining the pressure spikes were based on the flow field solutions presented in this paper.

APPLICATION OF CFD ANALYSES TO DESIGN SUPPORT AND PROBLEM RESOLUTION FOR ASRM AND RSRM

Richard A. Dill and R. Harold Whitesides

ERC, Inc.

Eleventh Annual CFD Working Group Meeting

Session 8

NASA/MSFC

April 21, 1993

CFD METHODOLOGY

- GOVERNING EQUATIONS ARE THE 3-D ENSEMBLE-AVERAGED NAVIER STOKES EQUATIONS IN CONSERVATION FORM
- CLOSURE OF THE EQUATIONS BY THE STANDARD TWO-EQUATION $\kappa-\varepsilon$ MODEL OF TURBULENCE
- WALL FUNCTIONS USED TO DETERMINE NEAR WALL GRADIENTS
- DISCRETIZATION METHOD
  - GOVERNING EQUATIONS ARE WRITTEN IN COMPONENT FORM USING CONTRAVARIANT VELOCITY COMPONENTS
  - THIS ALLOWS THE USE OF A BOUNDARY FITTED CURVILINEAR COORDINATE SYSTEM
  - NUMERICAL METHOD IS FINITE VOLUME BASED
  - STAGGERED GRID STORAGE SYSTEM IS USED
  - CONVECTION AND DIFFUSION FLUXES ARE APPROXIMATED USING A POWER-LAW SCHEME
  - TIME DERIVATIVES ARE CALCULATED USING A FULLY IMPLICIT FIRST ORDER SCHEME
- PRESSURE-VELOCITY COUPLING IS ACCOMPLISHED BY USING THE SIMPLER ALGORITHM
- SOLVER USES LINEARIZED BLOCK IMPLICIT SCHEME

ERC, Inc. 4/29/92

RSRM ANALYSIS OBJECTIVES

- DEFINE INTERNAL MOTOR FLOW ENVIRONMENT TO SUPPORT INVESTIGATION OF RSRM PRESSURE SPIKES (STS-54B)
- PROVIDE PRESSURE LOADS ON CASTABLE AND NBR INHIBITORS TO DETERMINE DEFORMED SHAPE AND FAILURE MODES
- PROVIDE DETAILED FLOW FIELD DEFINITION IN SUBMERGED NOSE NOZZLE REGION TO SUPPORT EVALUATION OF SLAG PHENOMENA
- DETERMINE RELATIVE PROPENSITY OF THE FORWARD, CENTER, AND AFT SLOTS FOR COLLECTING SLAG USING PARTICLE TRAJECTORY ANALYSIS

ERC, Inc.
4/21/93

RSRM Motor Geometry

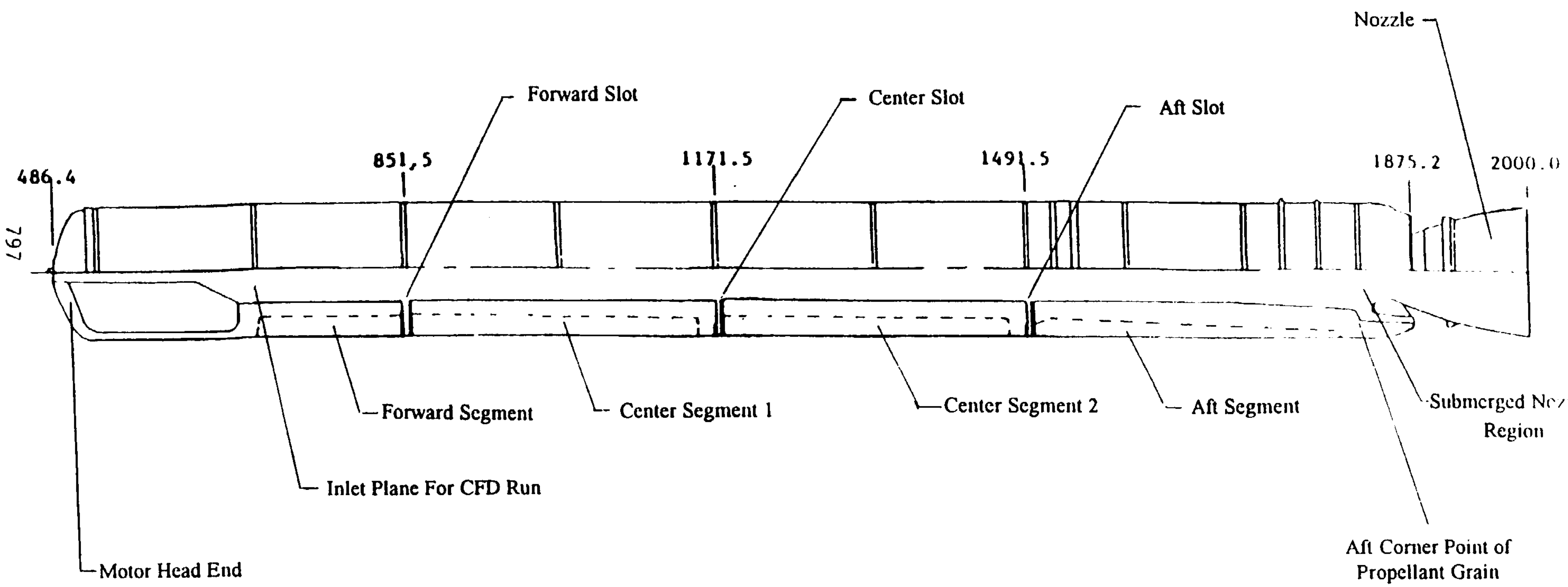

(Dashed Line Shows The 67 Second Burn Back)

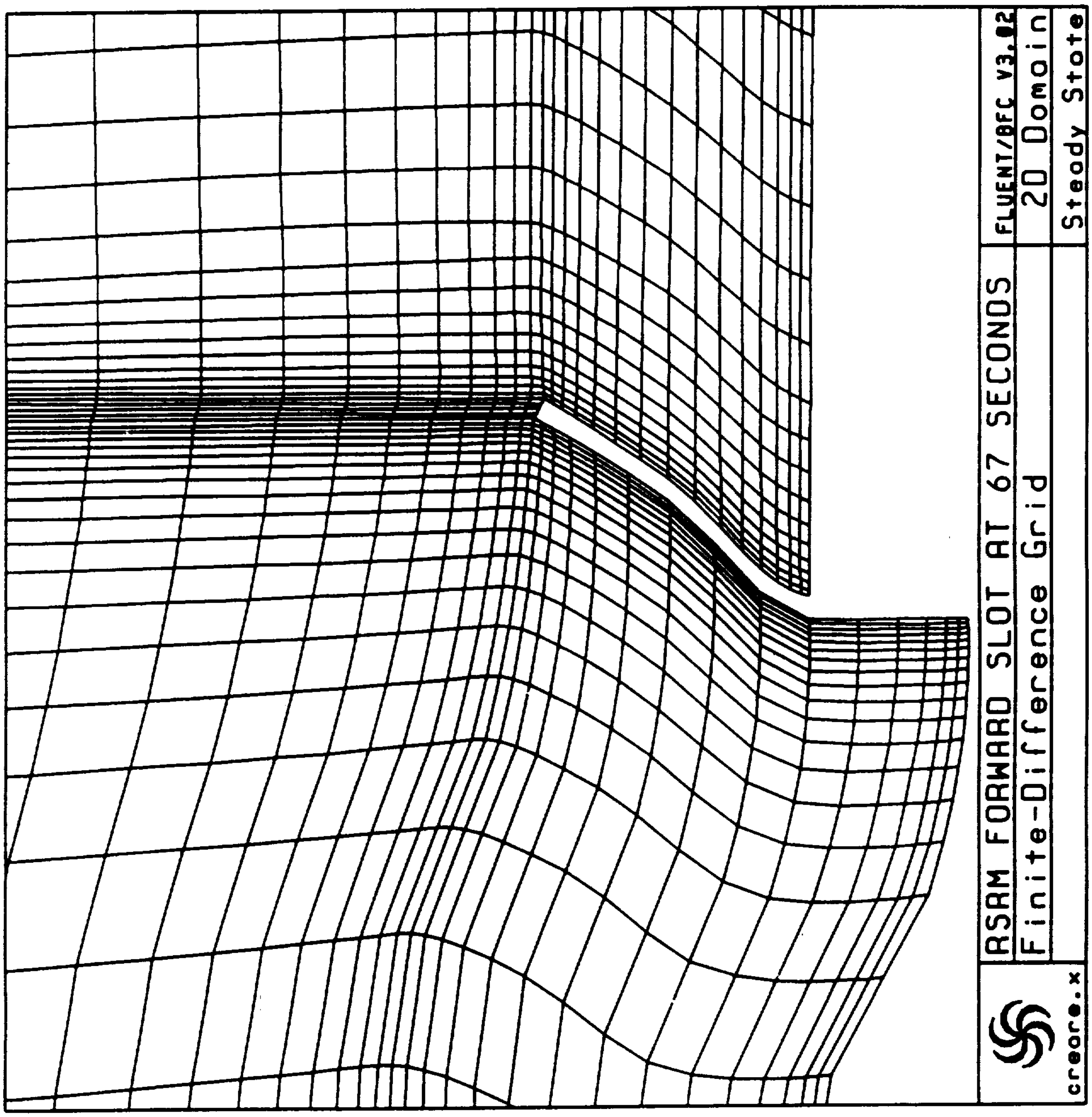

RSRM FORWARD SLOT AT 67 SECONDS
FLUENT/BFC V3.02
Finite-Difference Grid
2D Domain
Steady State
creare.x

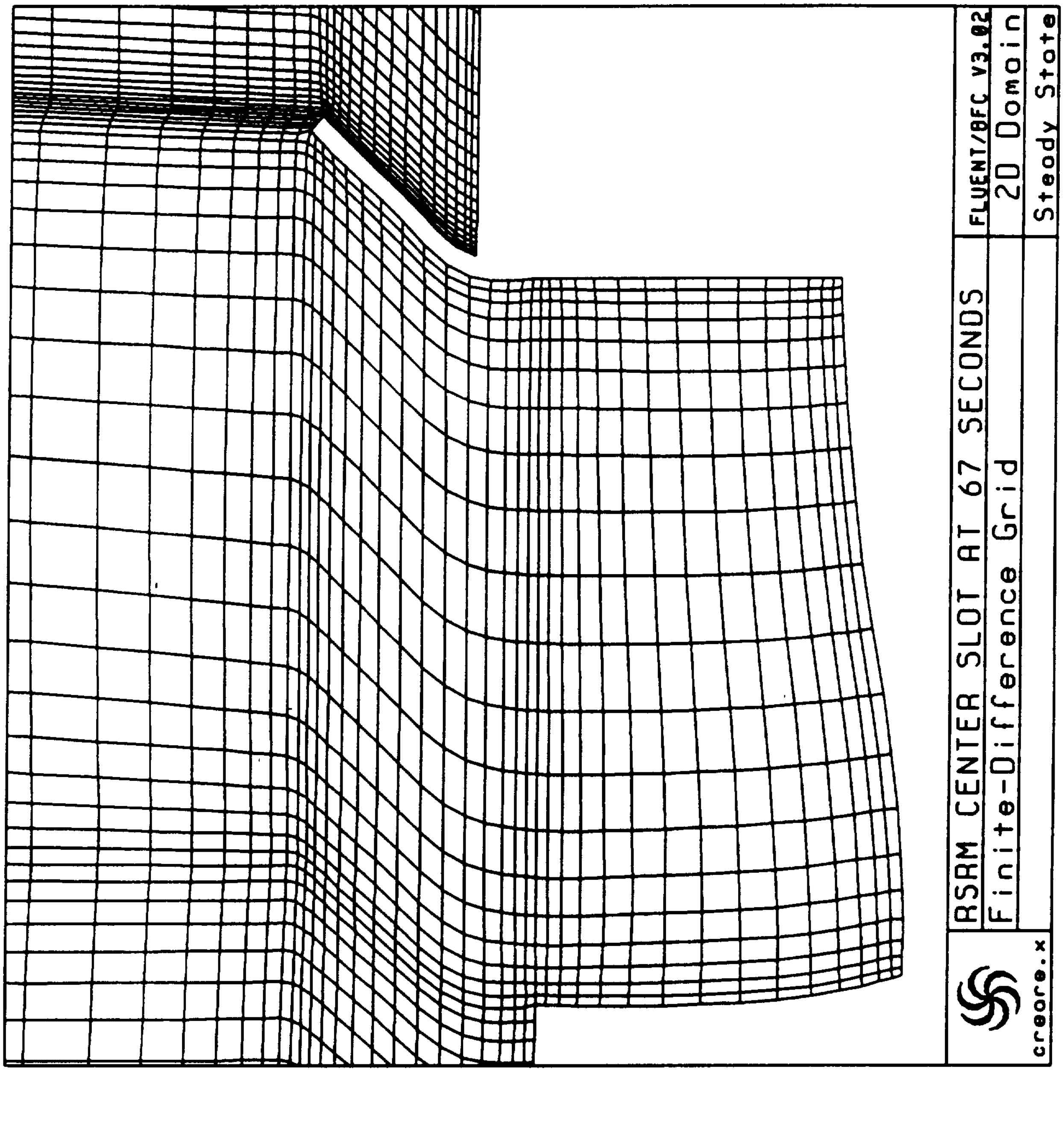
RSRM CENTER SLOT AT 67 SECONDS
Finite-Difference Grid
FLUENT/BFC V3.02
2D Domain
Steady State
creare.x

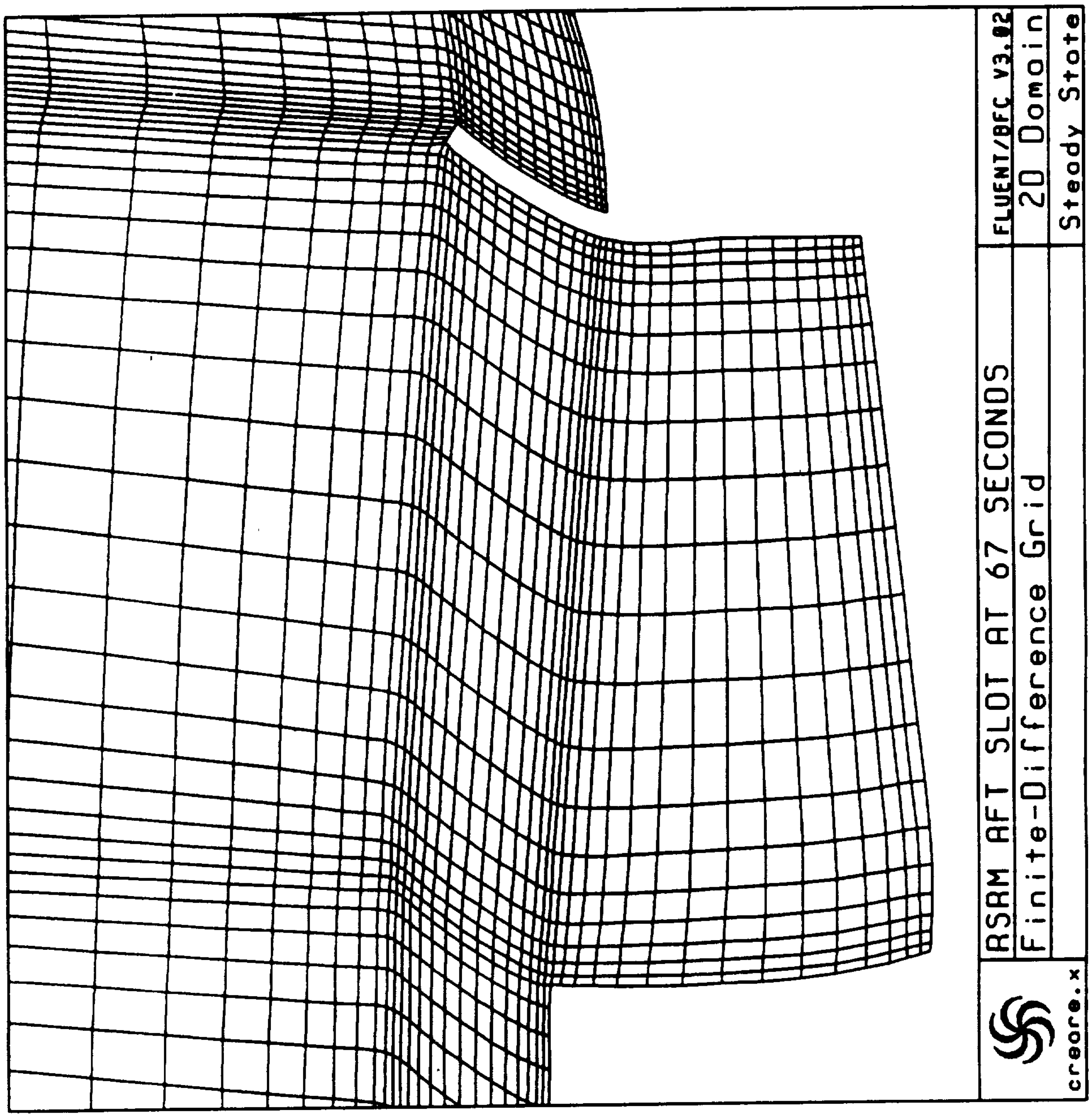
RSRM AFT SLOT AT 67 SECONDS
Finite-Difference Grid
FLUENT/BFC V3.02
2D Domain
Steady State
creare.x

RSRM MOTOR BOUNDARY CONDITIONS

67 SECOND MOTOR BURN TIME CONFIGURATION

MOTOR AFT SEGMENT END OF GRAIN PRESSURE	625.2 psia
HEAD END PORT VELOCITY	12.47 ft/sec
TOTAL TEMPERATURE	6093°K
$\dot{M}$ (FORWARD SEGMENT)	1555.9 lbm/sec
$\dot{M}$ (CENTER SEGMENT 1)	2587.5 lbm/sec
$\dot{M}$ (CENTER SEGMENT 2)	2578.6 lbm/sec
$\dot{M}$ (AFT SEGMENT)	2849 lbm/sec
MOLECULAR WEIGHT OF EQUIVALENT GAS	28.04
DYNAMIC VISCOSITY	6.189×10^{-5} lbm/ft-sec
SPECIFIC HEAT RATIO	1.138

ERC, Inc.
4/21/93

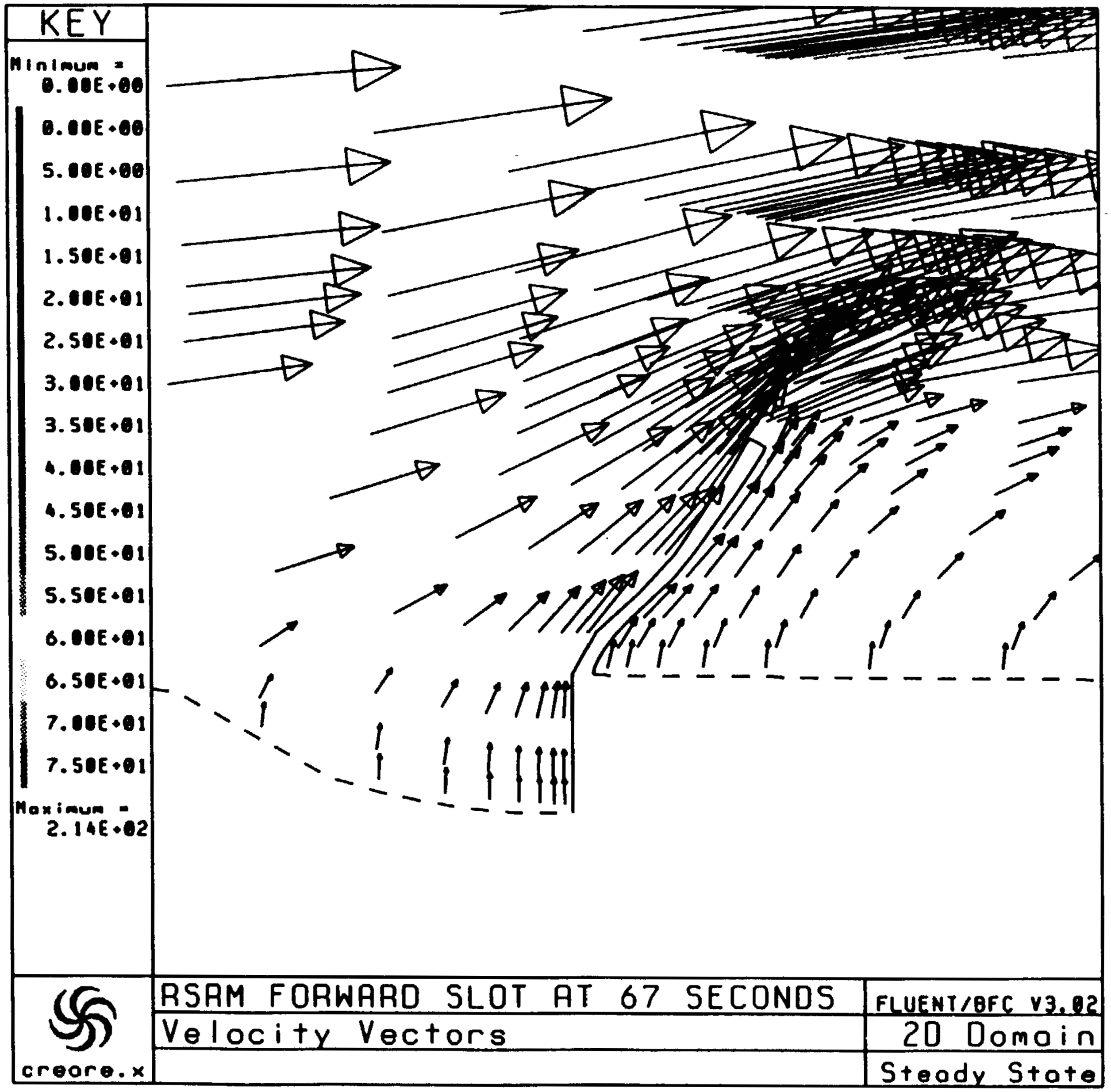
KEY
Minimum =
0.00E+00
0.00E+00
5.00E+00
1.00E+01
1.50E+01
2.00E+01
2.50E+01
3.00E+01
3.50E+01
4.00E+01
4.50E+01
5.00E+01
5.50E+01
6.00E+01
6.50E+01
7.00E+01
7.50E+01
Maximum =
2.14E+02
creare.x
RSAM FORWARD SLOT AT 67 SECONDS
Velocity Vectors
FLUENT/BFC V3.02
2D Domain
Steady State

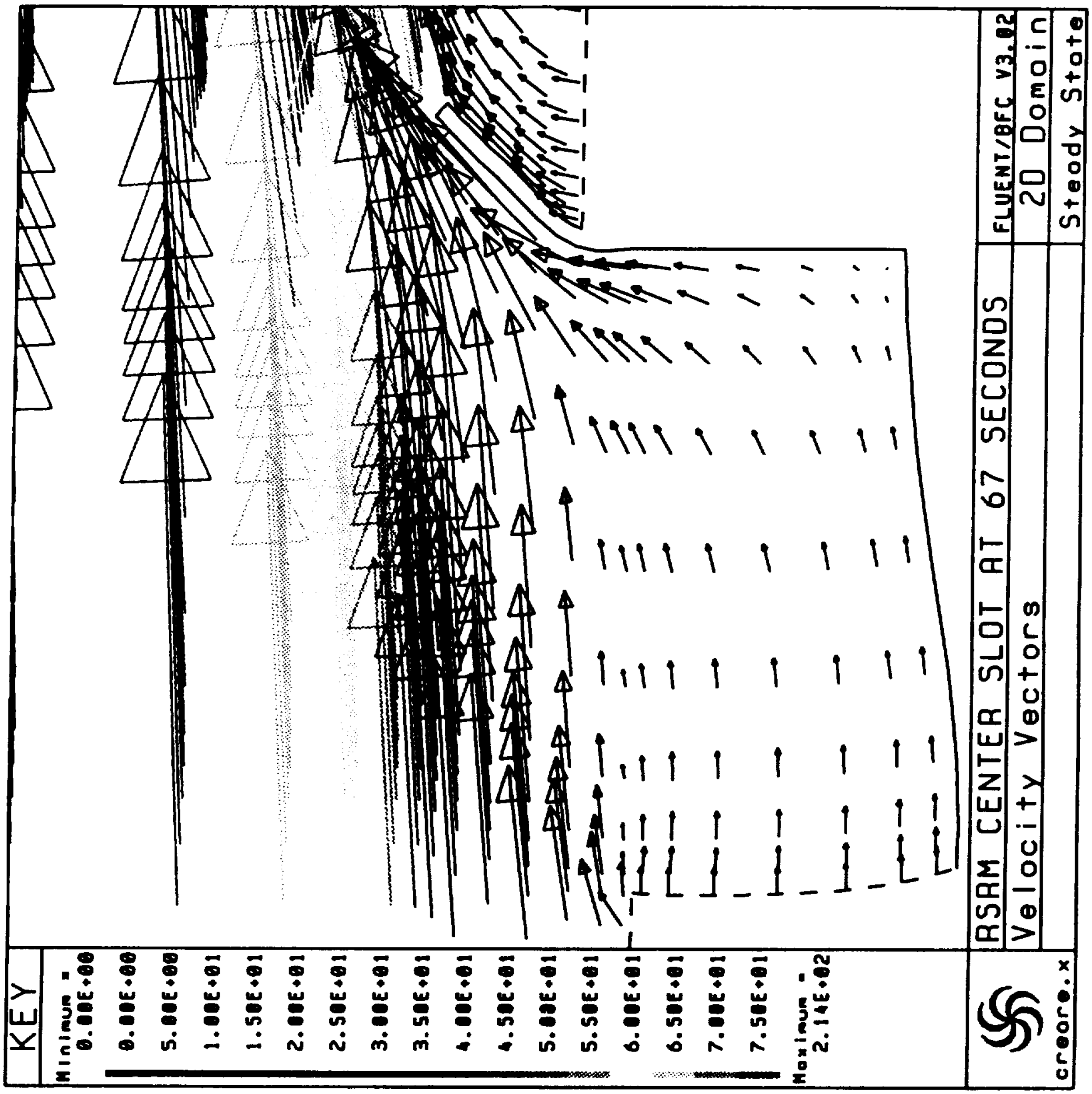
KEY
Minimum =
0.00E+00
0.00E+00
5.00E+00
1.00E+01
1.50E+01
2.00E+01
2.50E+01
3.00E+01
3.50E+01
4.00E+01
4.50E+01
5.00E+01
5.50E+01
6.00E+01
6.50E+01
7.00E+01
7.50E+01
Maximum =
2.14E+02
RSRM CENTER SLOT AT 67 SECONDS
Velocity Vectors
FLUENT/BFC V3.02
2D Domain
Steady State
creare.x

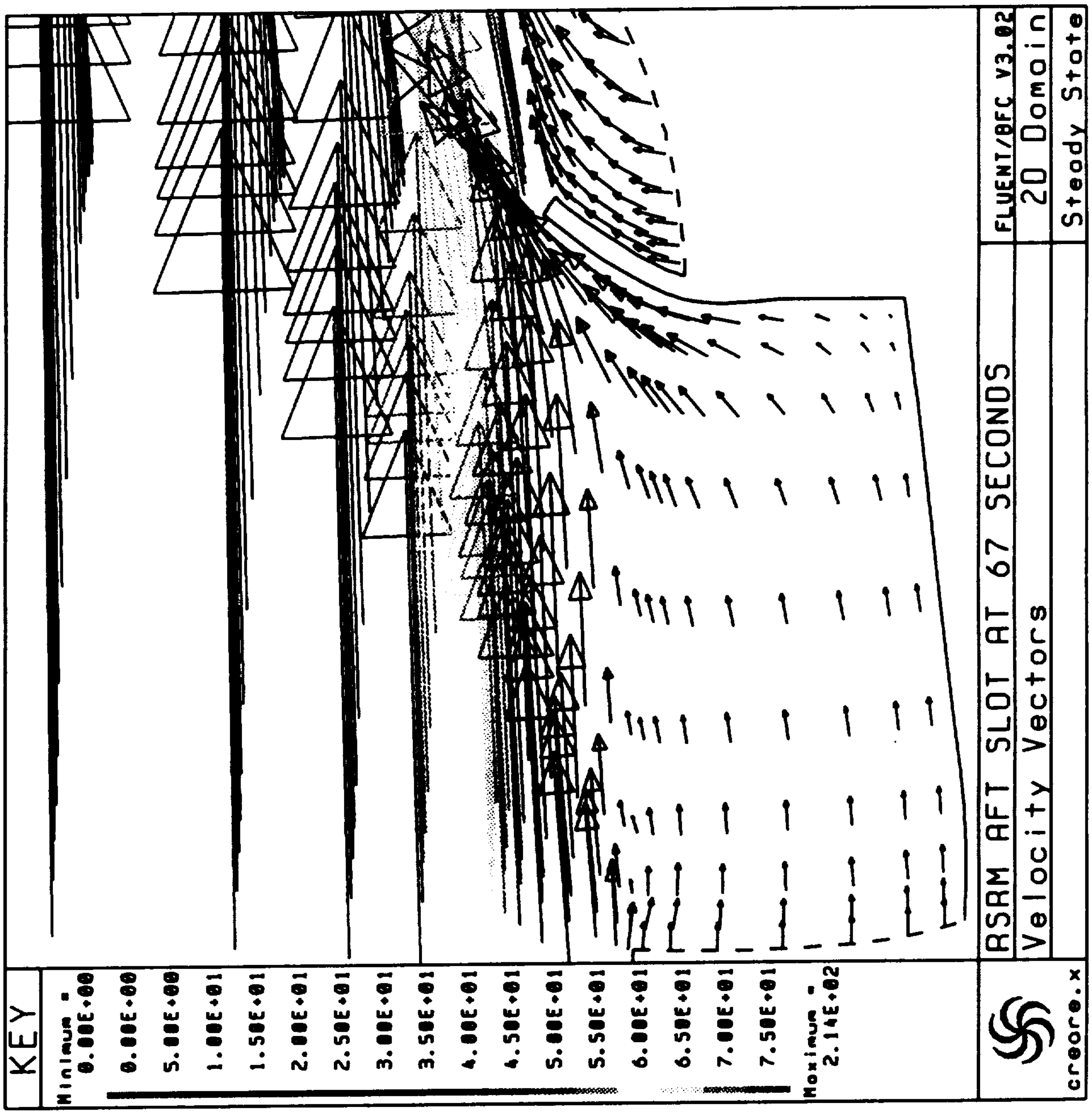
KEY
Minimum =
0.00E+00
0.00E+00
5.00E+00
1.00E+01
1.50E+01
2.00E+01
2.50E+01
3.00E+01
3.50E+01
4.00E+01
4.50E+01
5.00E+01
5.50E+01
6.00E+01
6.50E+01
7.00E+01
7.50E+01
Maximum =
2.14E+02
RSRM AFT SLOT AT 67 SECONDS
Velocity Vectors
FLUENT/BFC V3.02
2D Domain
Steady State
creare.x

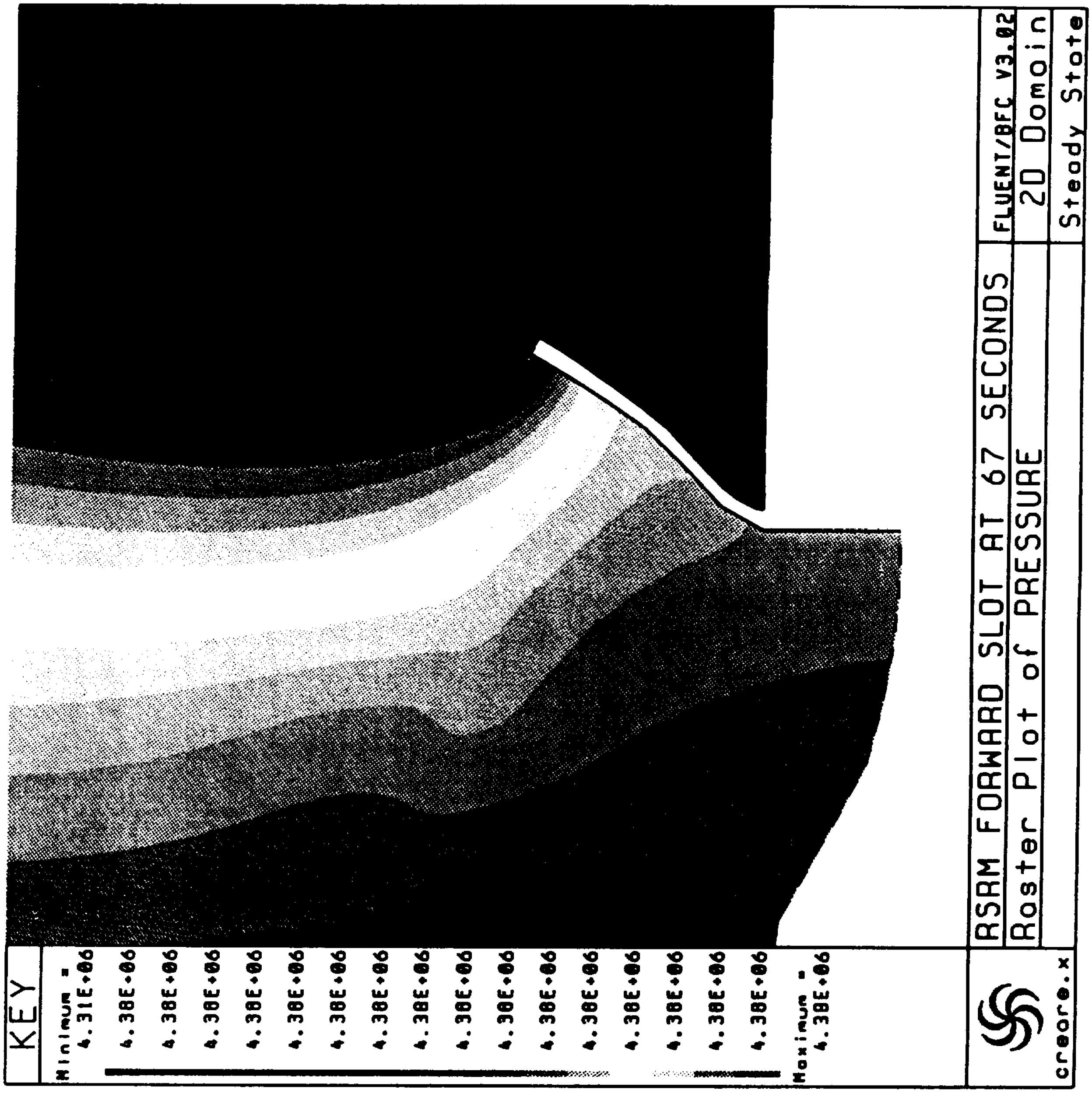

KEY
Minimum = 4.31E+06
4.38E+06
4.38E+06
4.38E+06
4.38E+06
4.38E+06
4.38E+06
4.38E+06
4.38E+06
4.38E+06
4.38E+06
4.38E+06
4.38E+06
4.38E+06
4.38E+06
4.38E+06
4.38E+06
Maximum = 4.38E+06
creare.x
RSRM FORWARD SLOT AT 67 SECONDS
Raster Plot of PRESSURE
FLUENT/BFC V3.02
2D Domain
Steady State

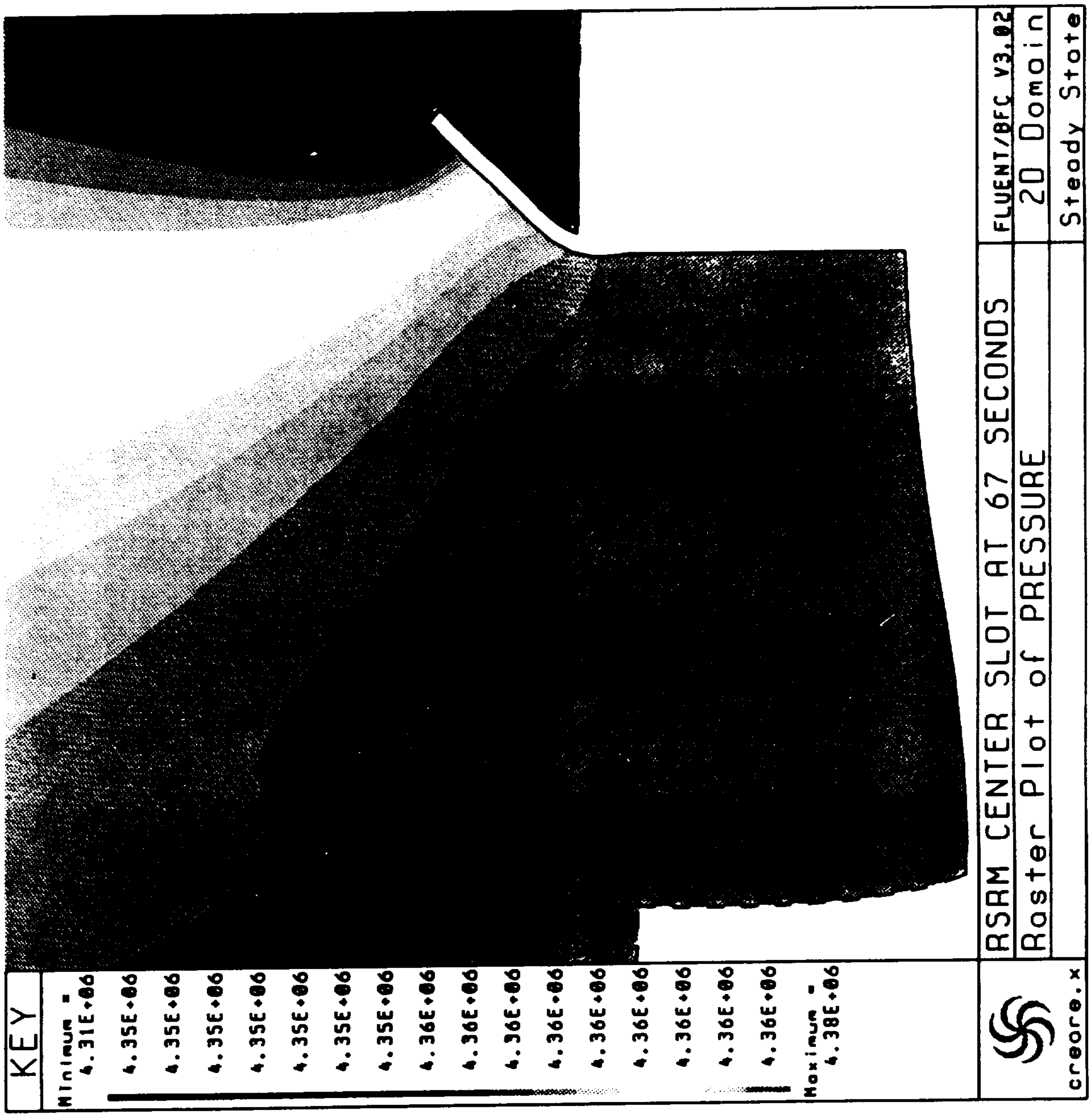
KEY
Minimum = 4.31E+06
4.35E+06
4.35E+06
4.35E+06
4.35E+06
4.35E+06
4.35E+06
4.36E+06
4.36E+06
4.36E+06
4.36E+06
4.36E+06
4.36E+06
4.36E+06
4.36E+06
4.36E+06
Maximum = 4.38E+06
creare.x
RSRM CENTER SLOT AT 67 SECONDS
Raster Plot of PRESSURE
FLUENT/BFC V3.02
2D Domain
Steady State

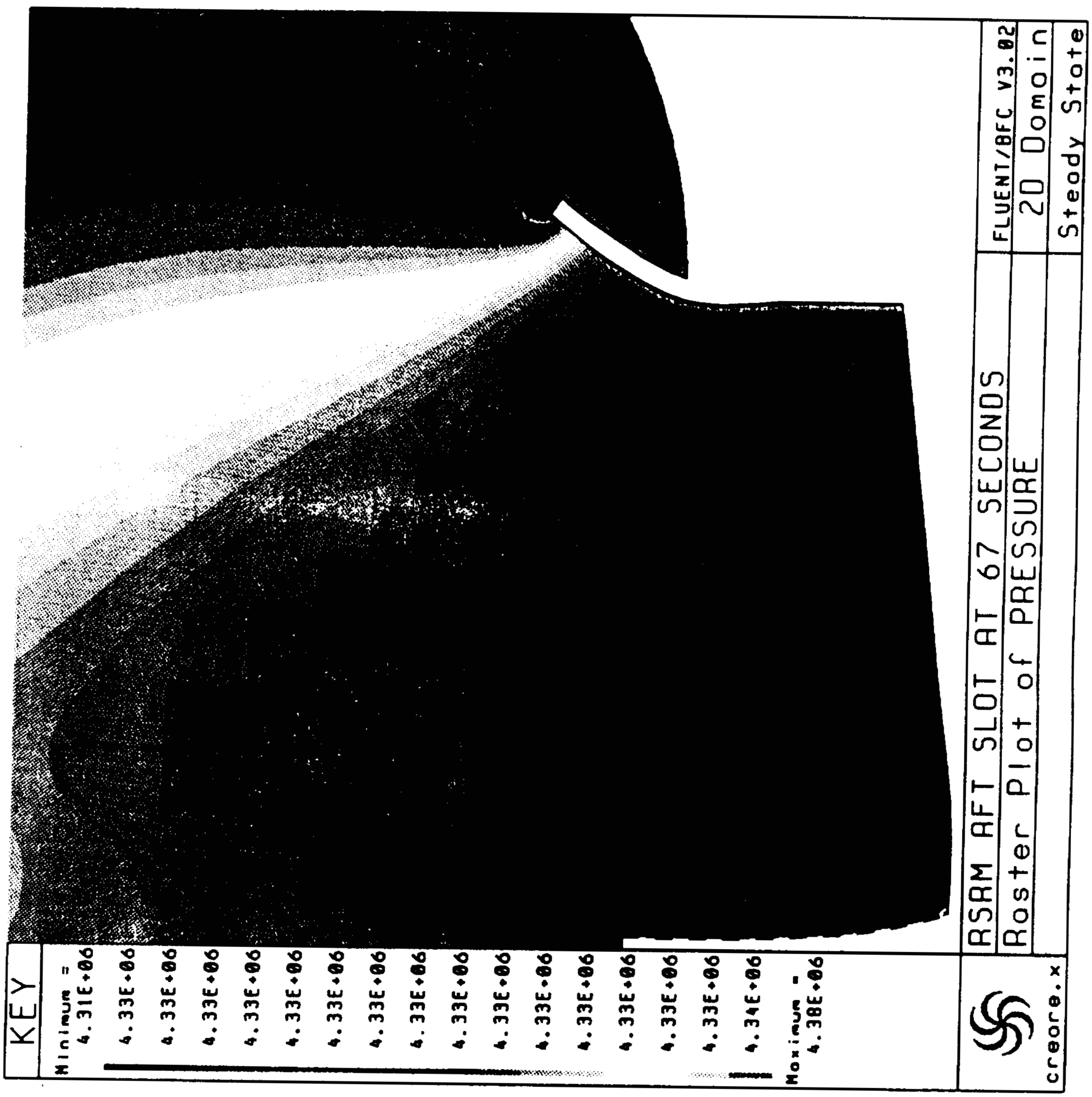
RSRM AFT SLOT AT 67 SECONDS
Raster Plot of PRESSURE
FLUENT/BFC V3.02
2D Domain
Steady State
KEY
Minimum =
4.31E+06
4.33E+06
4.33E+06
4.33E+06
4.33E+06
4.33E+06
4.33E+06
4.33E+06
4.33E+06
4.33E+06
4.33E+06
4.33E+06
4.33E+06
4.33E+06
4.33E+06
4.33E+06
4.34E+06
Maximum =
4.38E+06
creare.x

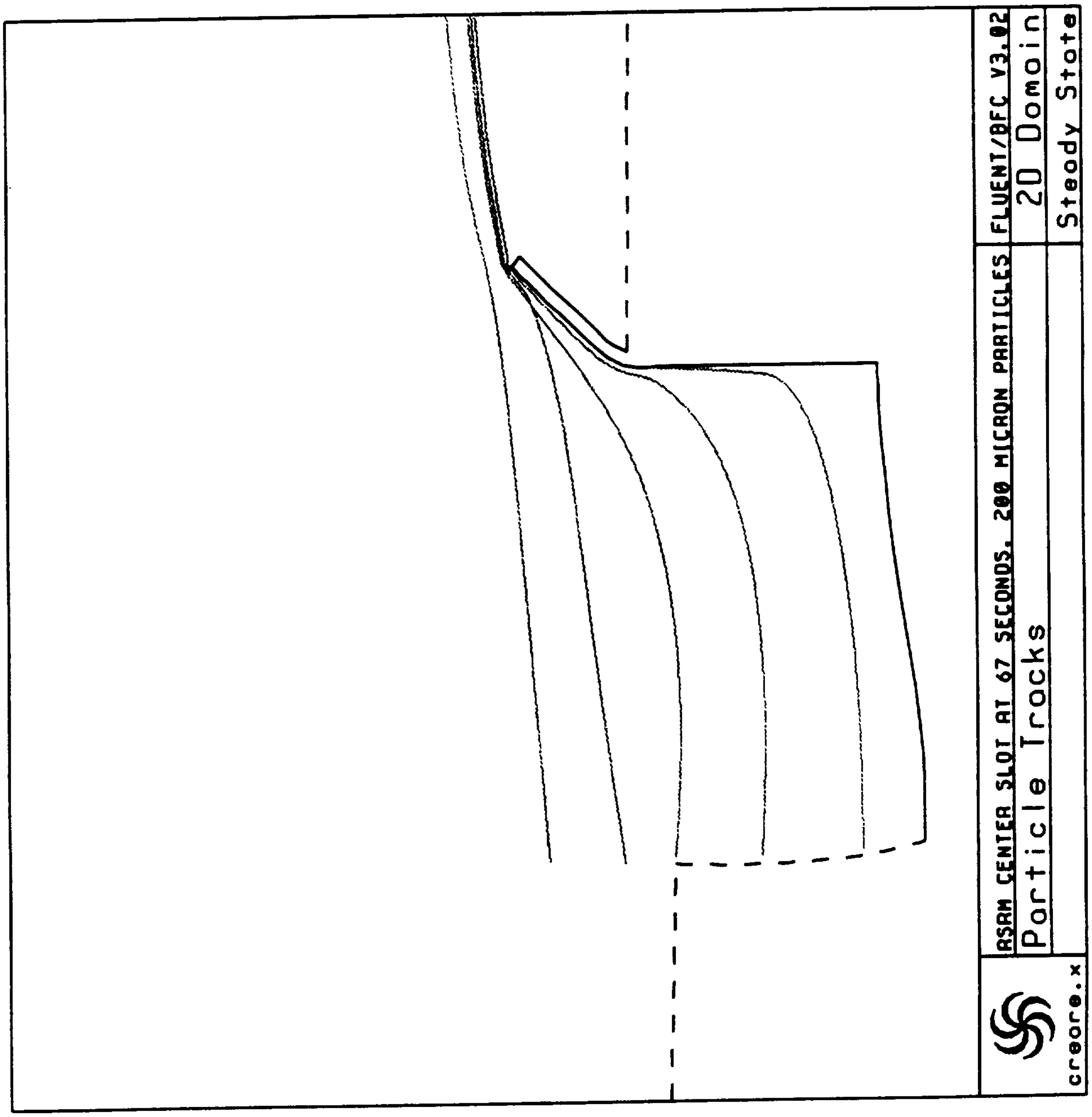
RSRM CENTER SLOT AT 67 SECONDS, 200 MICRON PARTICLES
FLUENT/BFC V3.02
Particle Tracks
2D Domain
Steady State
crsore.x

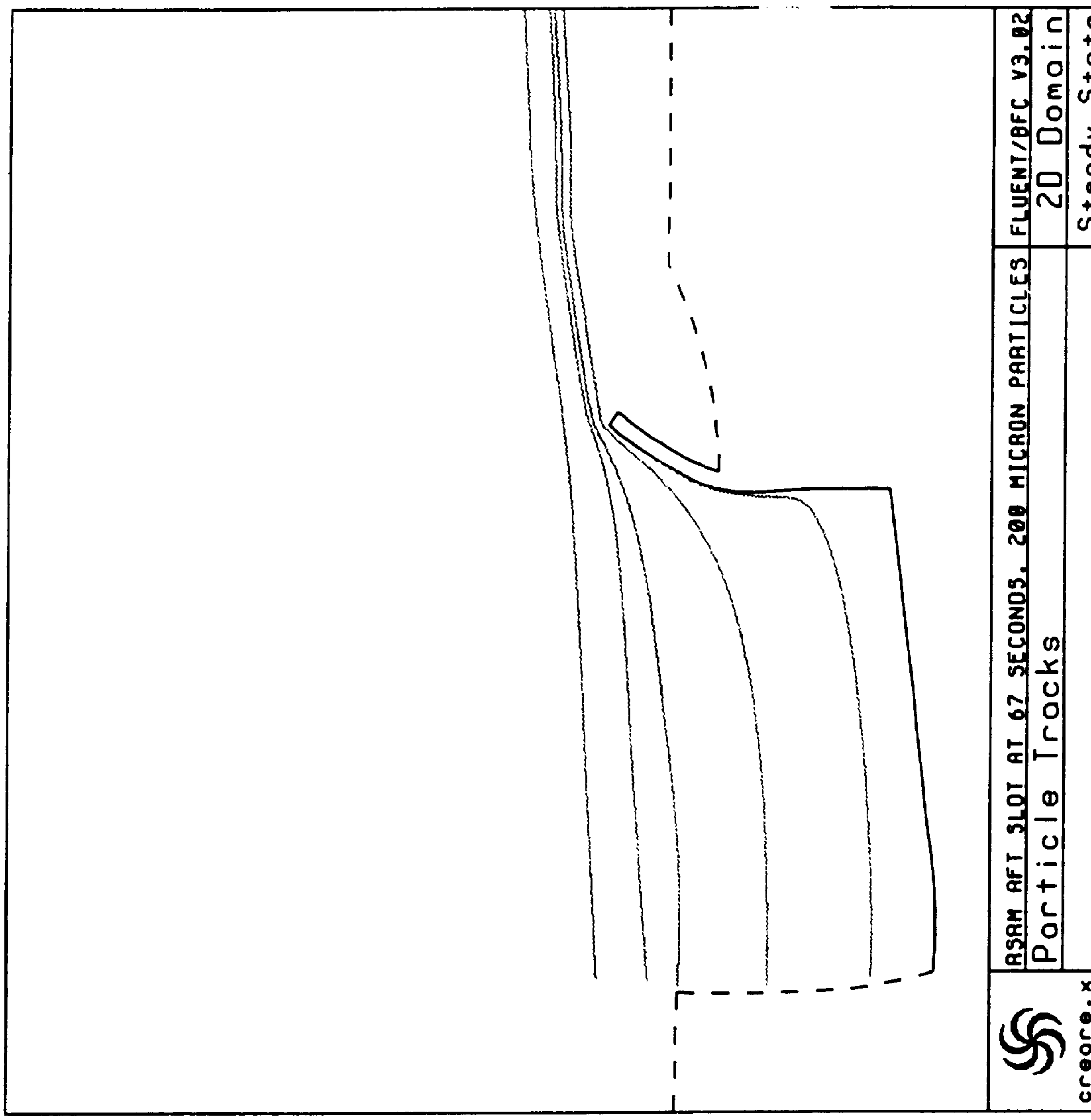
ASRM AFT SLOT AT 67 SECONDS, 200 MICRON PARTICLES
Particle Tracks
FLUENT/BFC V3.02
2D Domain
Steady State
creare.x

RSRM Motor Pressure at 67 Seconds

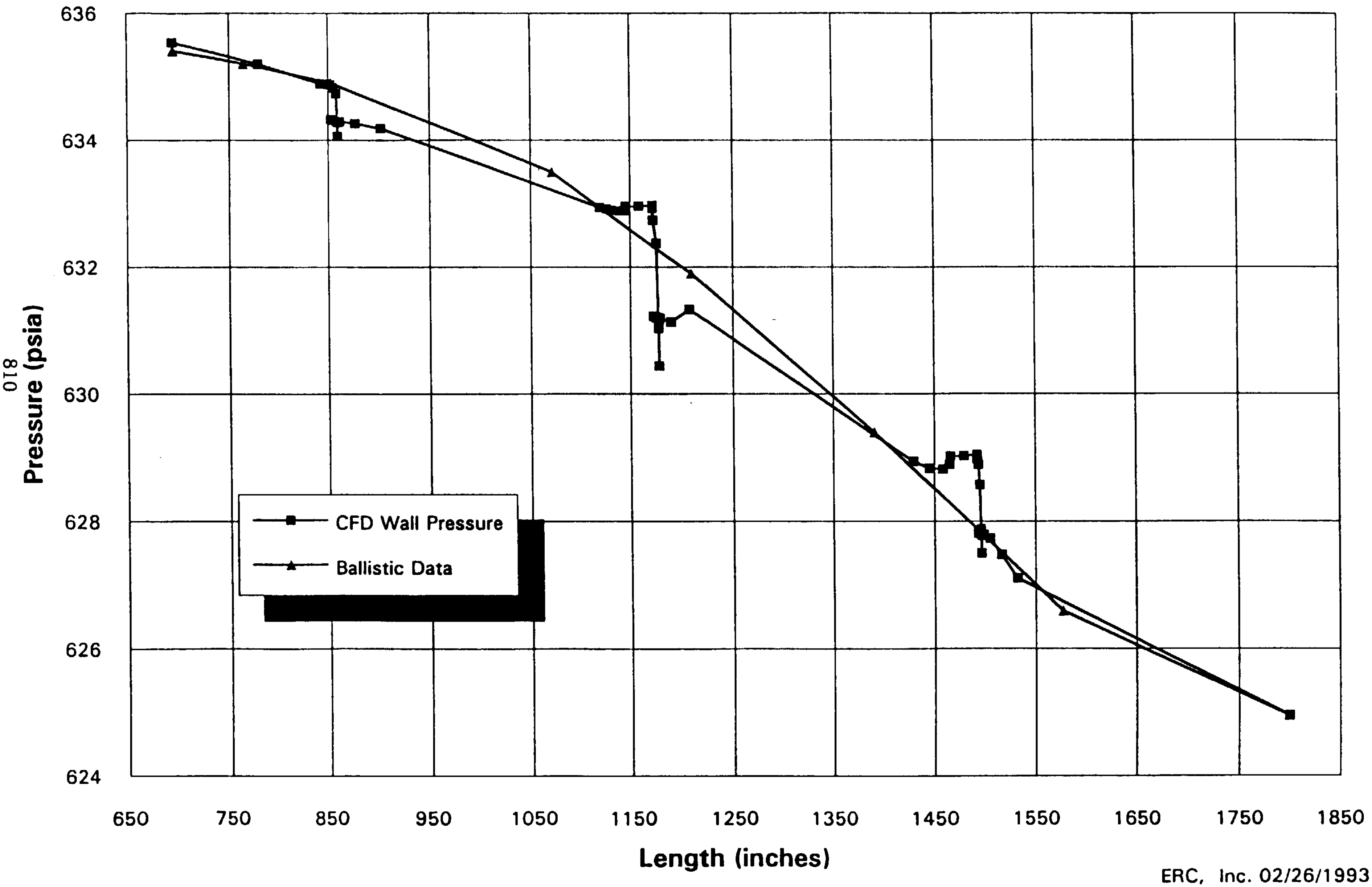

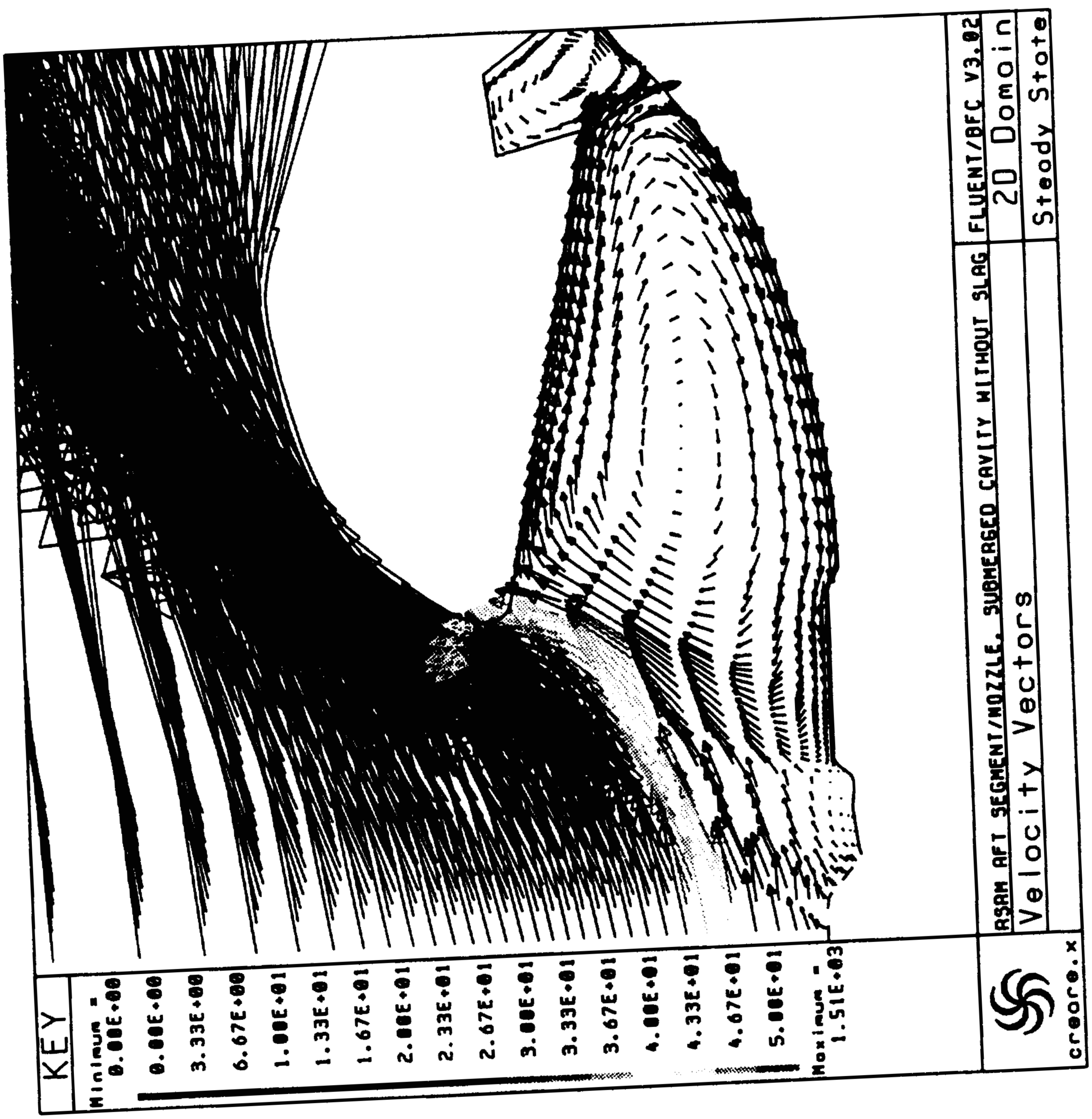
KEY
Minimum = 0.00E+00
0.00E+00
3.33E+00
6.67E+00
1.00E+01
1.33E+01
1.67E+01
2.00E+01
2.33E+01
2.67E+01
3.00E+01
3.33E+01
3.67E+01
4.00E+01
4.33E+01
4.67E+01
5.00E+01
Maximum = 1.51E+03
RSRM AFT SEGMENT/NOZZLE, SUBMERGED CAVITY WITHOUT SLAG
FLUENT/BFC V3.02
Velocity Vectors
2D Domain
Steady State
creare.x

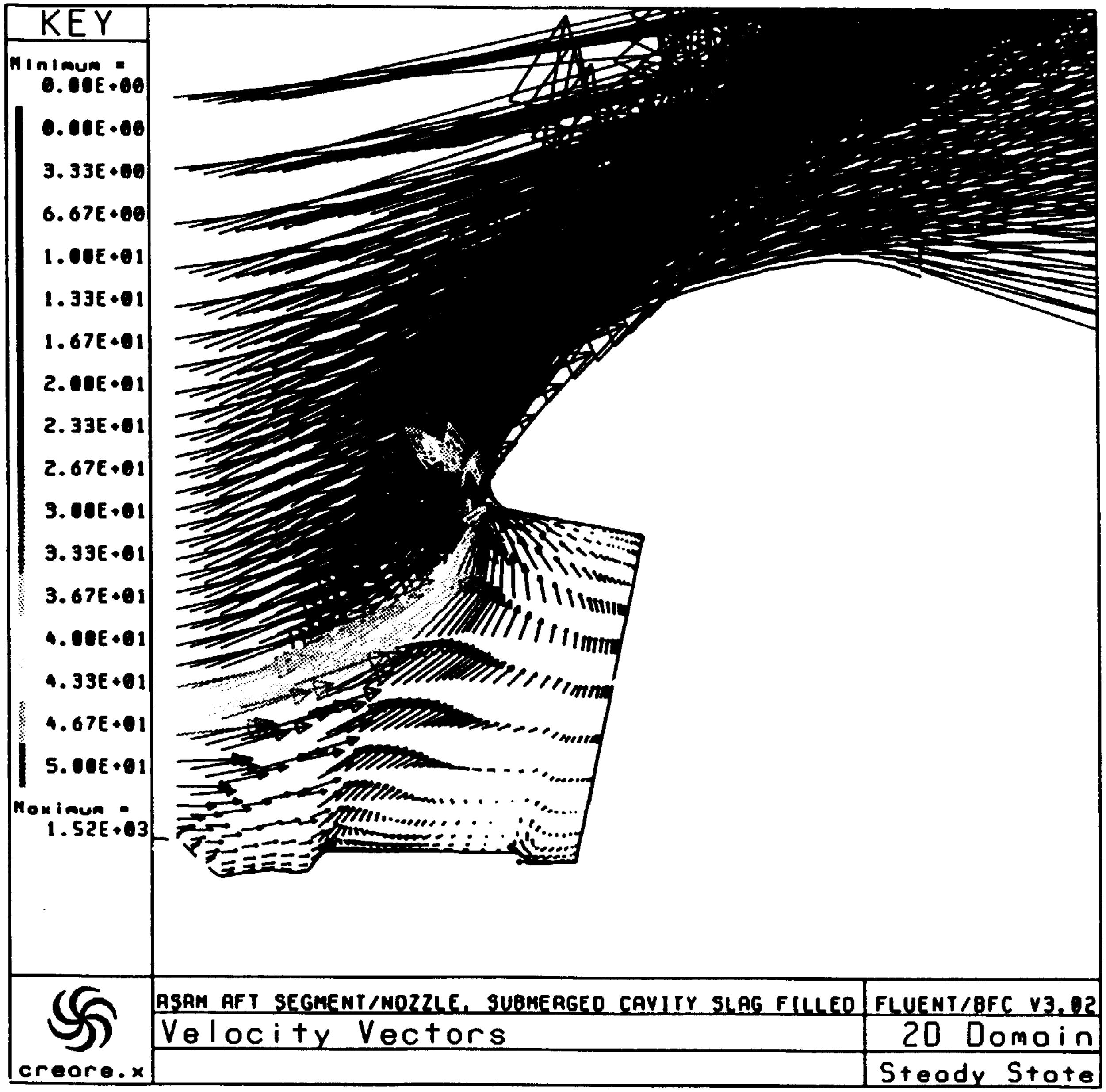
KEY
Minimum =
0.00E+00
0.00E+00
3.33E+00
6.67E+00
1.00E+01
1.33E+01
1.67E+01
2.00E+01
2.33E+01
2.67E+01
3.00E+01
3.33E+01
3.67E+01
4.00E+01
4.33E+01
4.67E+01
5.00E+01
Maximum =
1.52E+03
creare.x
RSRM AFT SEGMENT/NOZZLE, SUBMERGED CAVITY SLAG FILLED
Velocity Vectors
FLUENT/BFC V3.02
2D Domain
Steady State

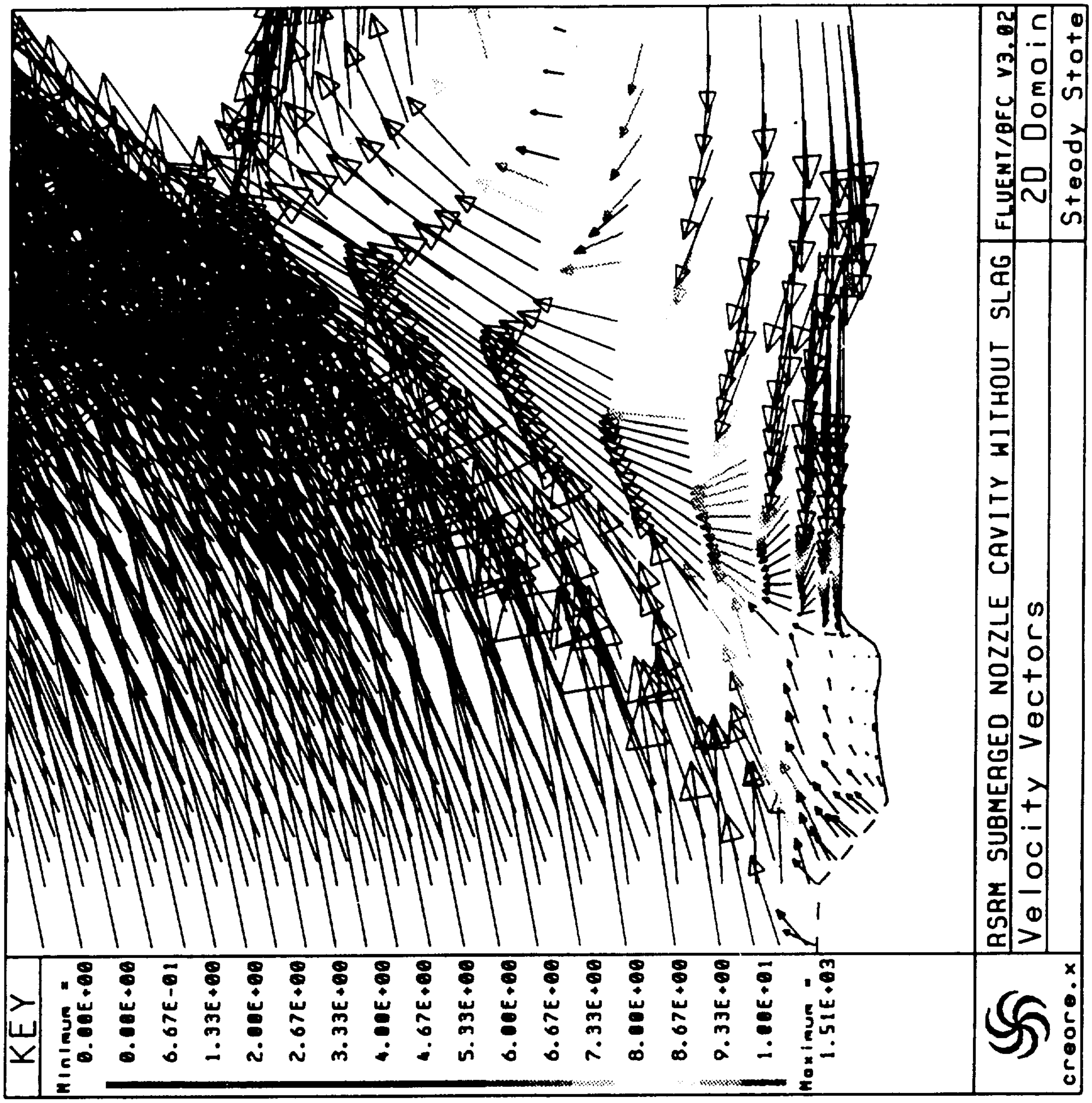
RSRM SUBMERGED NOZZLE CAVITY WITHOUT SLAG
Velocity Vectors
FLUENT/BFC V3.02
2D Domain
Steady State
creare.x
KEY
Minimum = 0.00E+00
0.00E+00
6.67E-01
1.33E+00
2.00E+00
2.67E+00
3.33E+00
4.00E+00
4.67E+00
5.33E+00
6.00E+00
6.67E+00
7.33E+00
8.00E+00
8.67E+00
9.33E+00
1.00E+01
Maximum = 1.51E+03

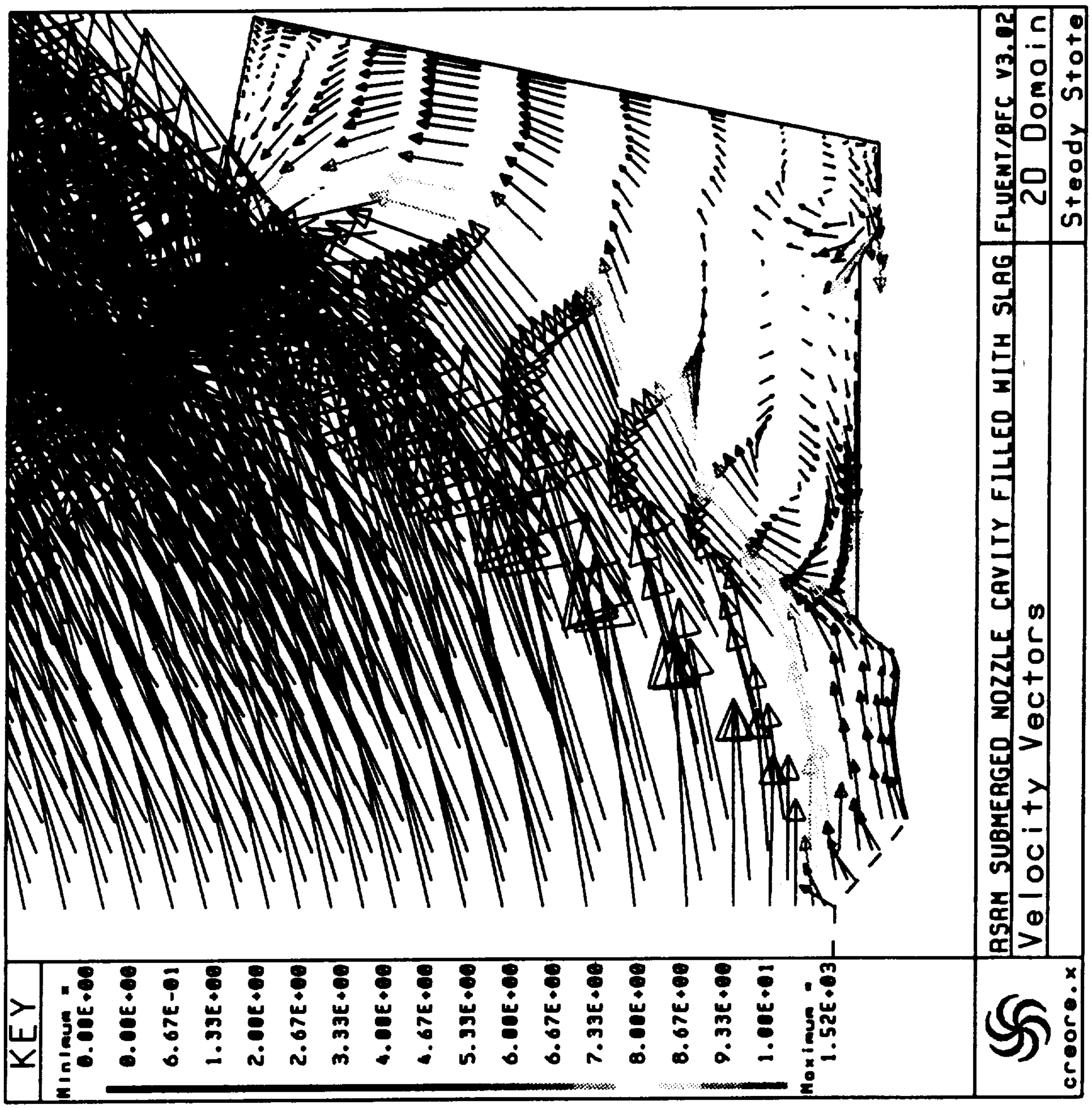
KEY
Minimum = 0.00E+00
0.00E+00
6.67E-01
1.33E+00
2.00E+00
2.67E+00
3.33E+00
4.00E+00
4.67E+00
5.33E+00
6.00E+00
6.67E+00
7.33E+00
8.00E+00
8.67E+00
9.33E+00
1.00E+01
Maximum = 1.52E+03
creare.x
RSRM SUBMERGED NOZZLE CAVITY FILLED WITH SLAG
FLUENT/BFC V3.02
Velocity Vectors
2D Domain
Steady State

RSRM ANALYSIS CONCLUSIONS

- INHIBITOR PRESSURE LOADS WERE PROVIDED AND USED TO DETERMINE CASTABLE INHIBITOR LOADS, DEFORMATION, AND FAILURE MECHANISMS

- AFT CASE FLOW FIELD SOLUTION OFFERED EXPLANATION OF ABNORMAL EROSION PATTERN AND SLAG EXPULSION MECHANISM

- PARTICLE TRAJECTORY ANALYSIS SHOWED PROPENSITY FOR COLLECTING SLAG GREATEST AT CENTER SLOT

ERC, Inc.
4/21/93

ASRM ANALYSIS OBJECTIVES

- DEFINE INTERNAL MOTOR FLOW ENVIRONMENT TO SUPPORT OVERALL MOTOR DESIGN EFFORT
- PROVIDE AXIAL MOTOR PORT PRESSURE GRADIENTS TO SUPPORT PERFORMANCE ANALYSIS AND TO PROVIDE PROPELLANT PRESSURE LOADS
- PROVIDE DETAILED TWO-DIMENSIONAL PRESSURE GRADIENTS AROUND JOINT SLOTS TO DETERMINE PROPELLANT DEFORMATIONS THROUGH AN INTERACTIVE CFD/STRUCTURAL ANALYSIS
- CALCULATE DEVELOPMENT OF VELOCITY PROFILES DOWN MOTOR PORT TO IDENTIFY TRANSITION AS IT MAY RELATE TO EROSIVE BURNING

ERC, Inc.
4/21/93

THE ASRM

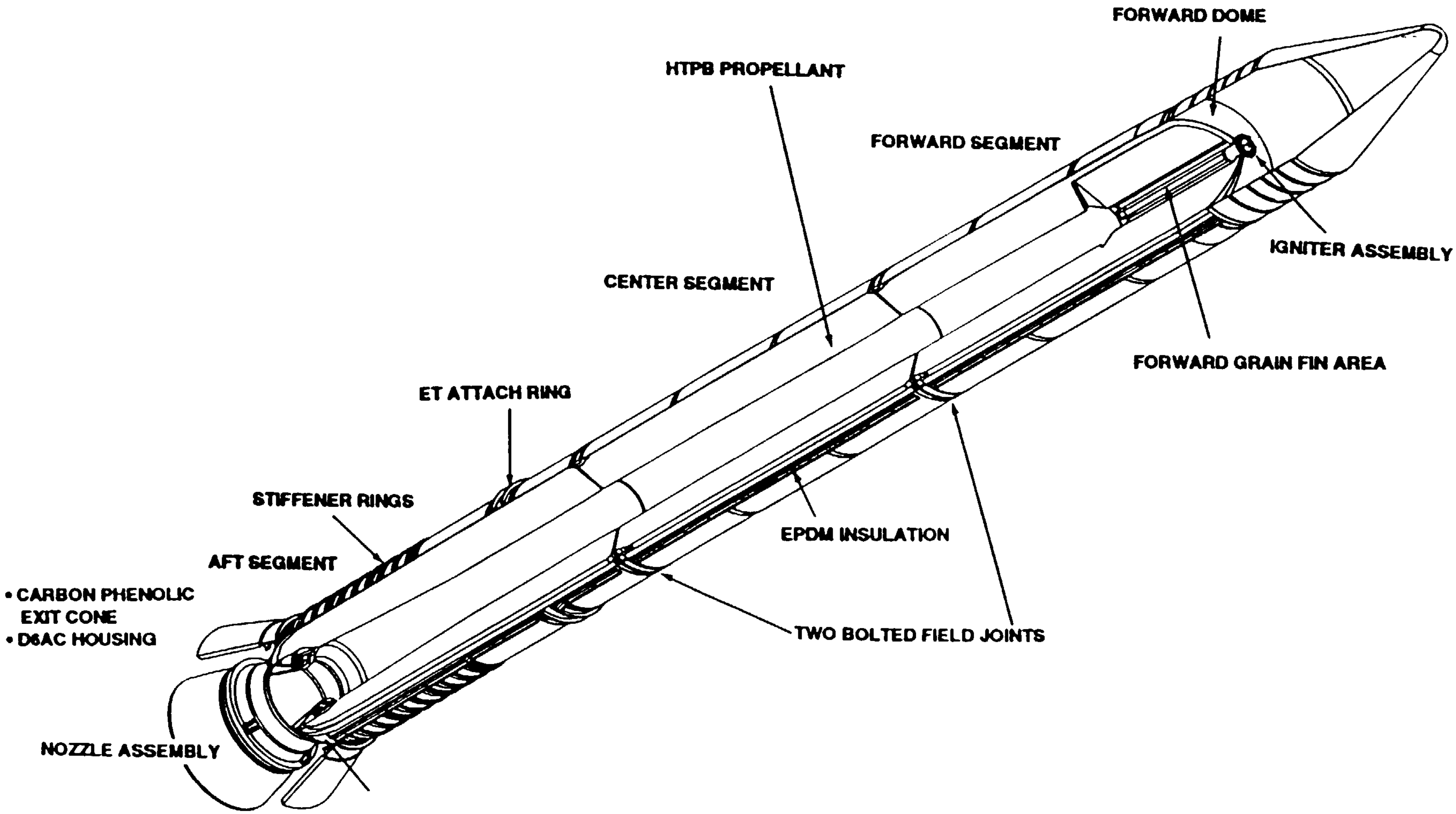

21/01/27

ASRM 2900F.00

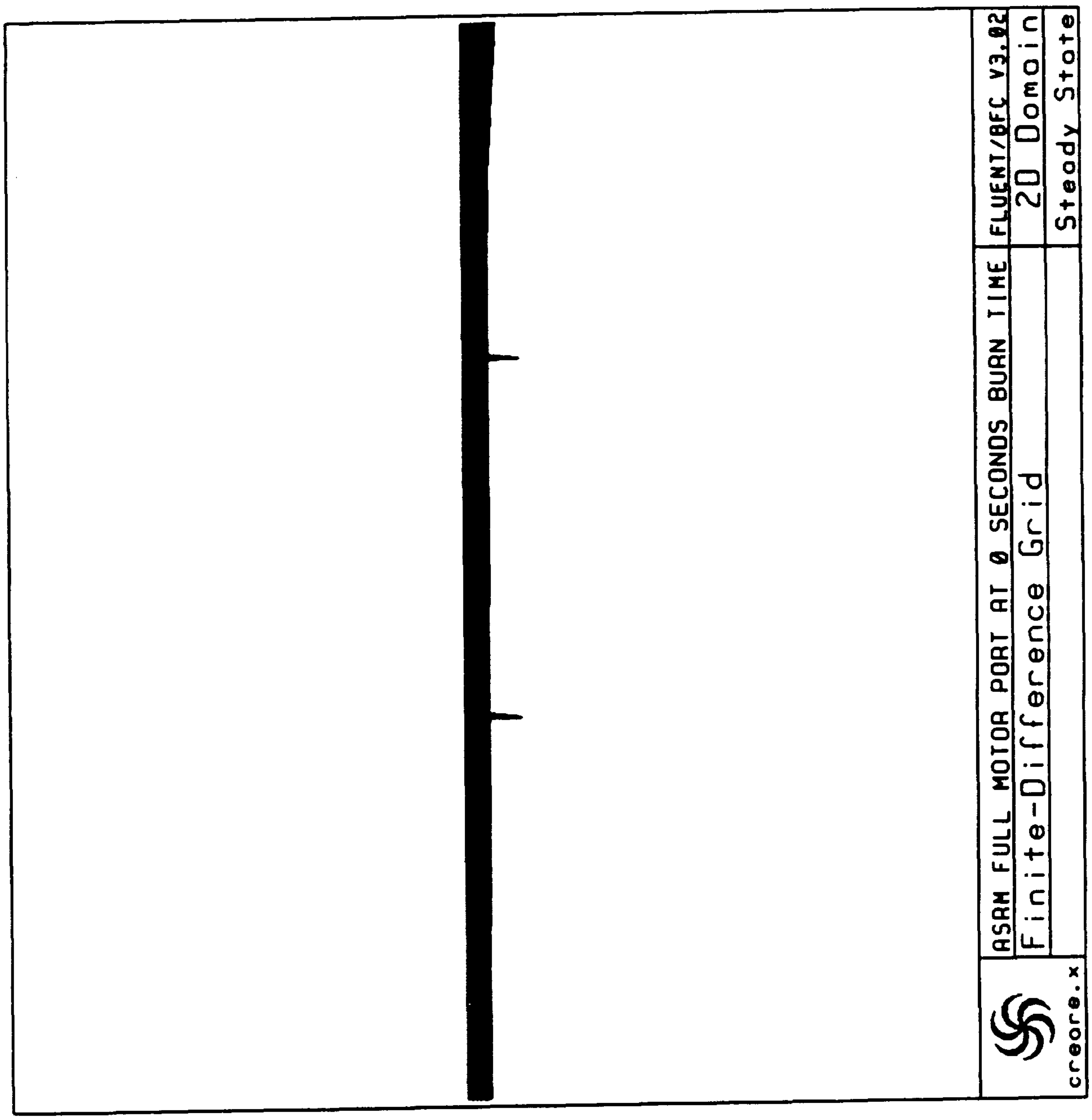
ASRM FULL MOTOR PORT AT 0 SECONDS BURN TIME
FLUENT/BFC V3.02
Finite-Difference Grid
2D Domain
Steady State
creare.x

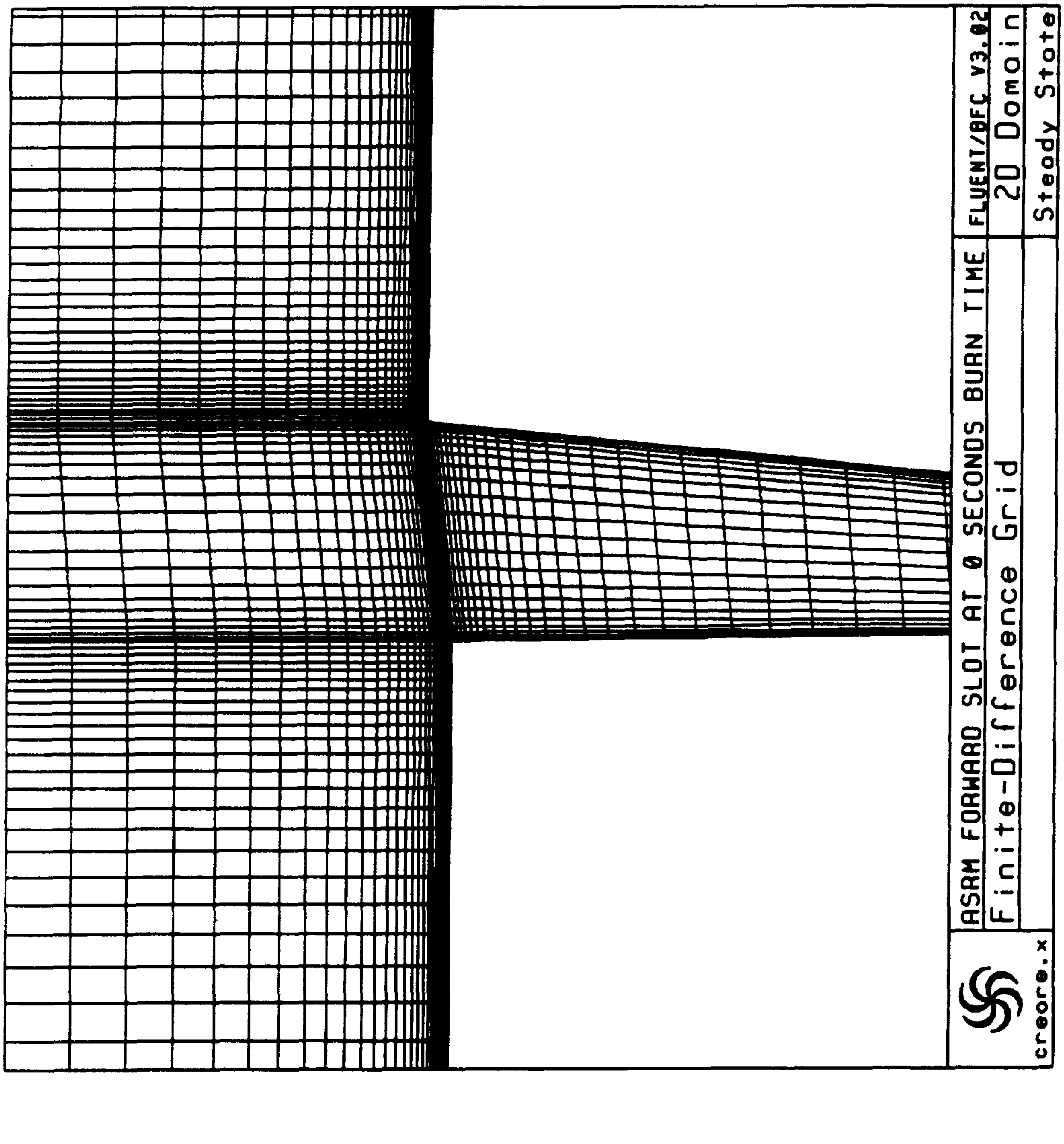
ASRM FORWARD SLOT AT 0 SECONDS BURN TIME
FLUENT/BFC V3.02
Finite-Difference Grid
2D Domain
Steady State
creare.x

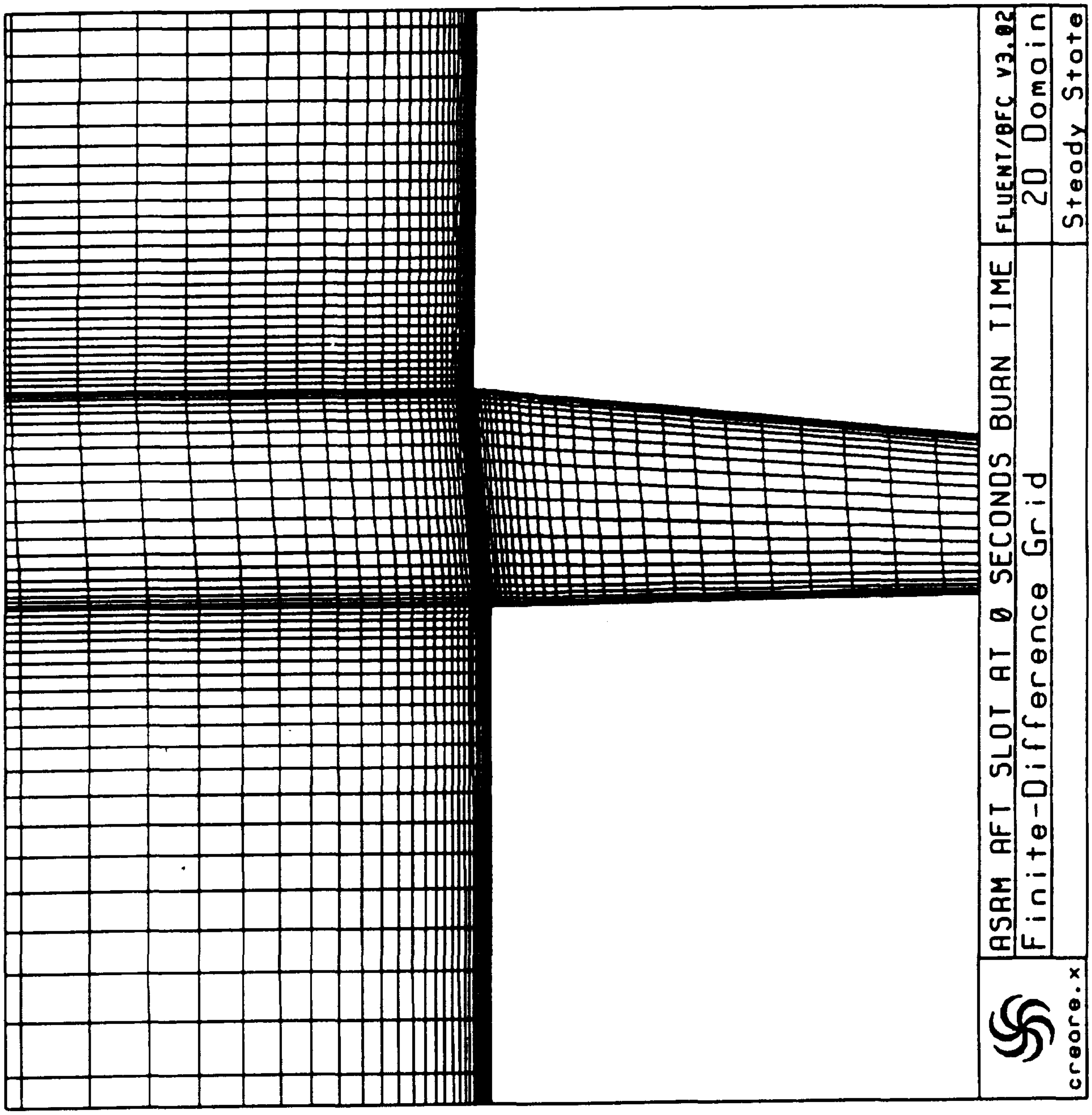
ASRM AFT SLOT AT Ø SECONDS BURN TIME
Finite-Difference Grid
FLUENT/BFC V3.02
2D Domain
Steady State
creare.x

ASRM MOTOR BOUNDARY CONDITIONS

0 SECOND MOTOR BURN TIME CONFIGURATION

MOTOR AFT SEGMENT END OF GRAIN PRESSURE	788 psia
TOTAL TEMPERATURE	6345°R
SPECIFIC HEAT RATIO	1.128
DYNAMIC VISCOSITY	6.34×10^{-5} lbm/ft-sec
MOLECULAR WEIGHT OF EQUIVALENT GAS	29.489
$\dot{M}$ FORWARD SEGMENT STAR GRAIN	5501 lbm/sec
$\dot{M}$ FORWARD SEGMENTS C. P.	1428 lbm/sec
$\dot{M}$ CENTER SEGMENT	2326 lbm/sec
$\dot{M}$ AFT SEGMENT	2415 lbm/sec

ERC, Inc.
4/21/93

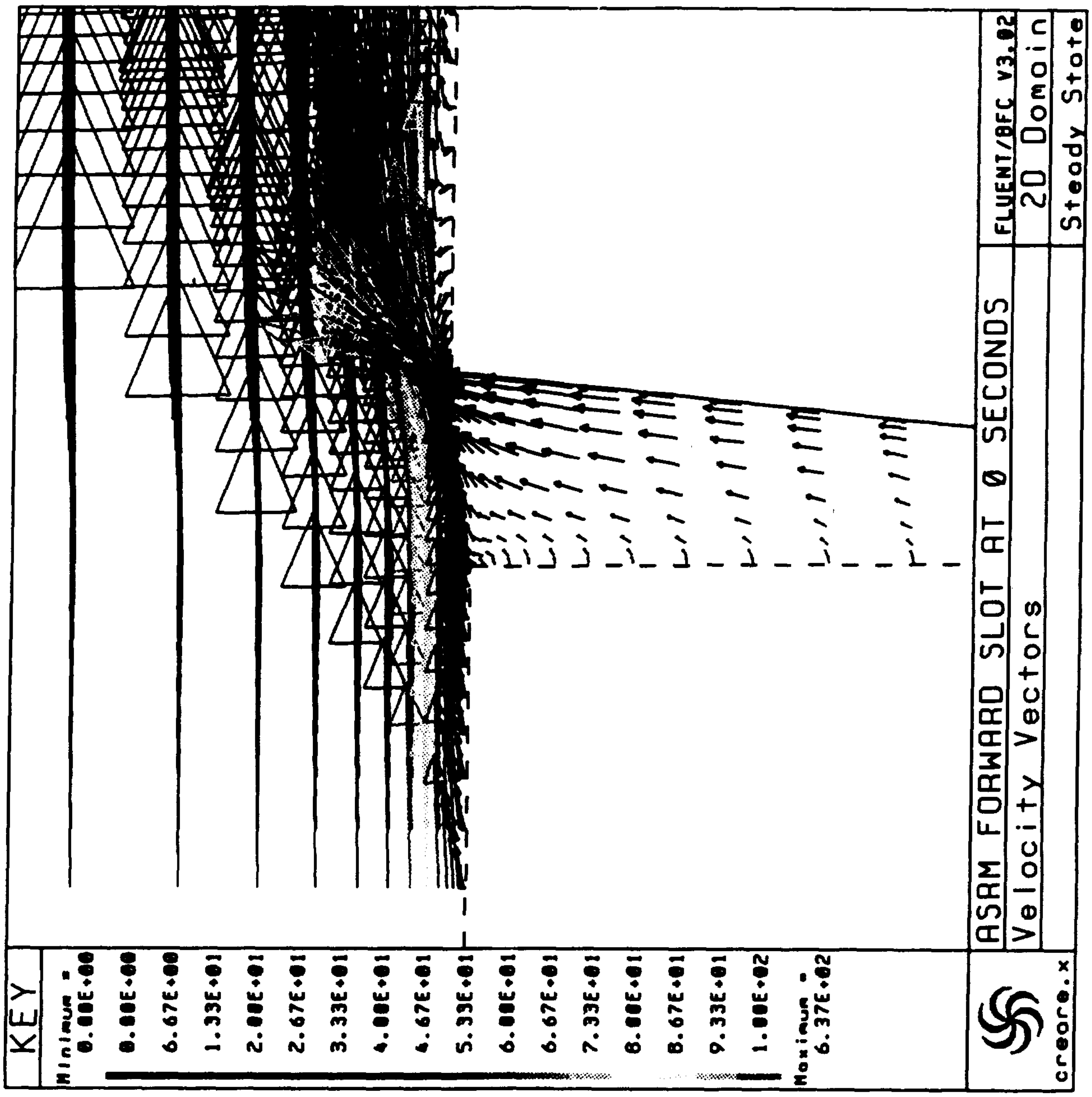
KEY
Minimum = 0.00E+00
0.00E+00
6.67E+00
1.33E+01
2.00E+01
2.67E+01
3.33E+01
4.00E+01
4.67E+01
5.33E+01
6.00E+01
6.67E+01
7.33E+01
8.00E+01
8.67E+01
9.33E+01
1.00E+02
Maximum = 6.37E+02
ASRM FORWARD SLOT AT 0 SECONDS
Velocity Vectors
FLUENT/BFC V3.02
2D Domain
Steady State
creare.x

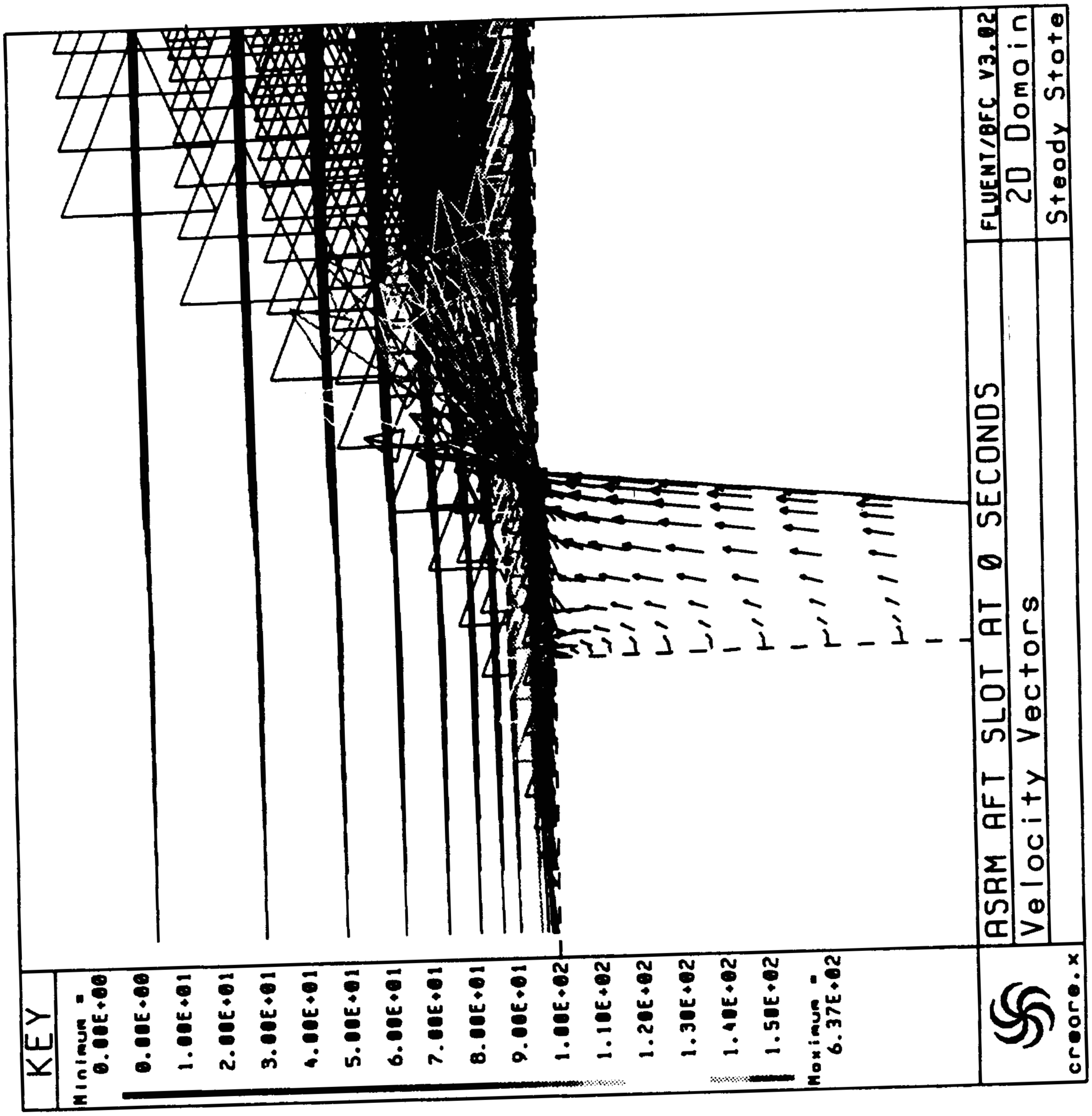
KEY
Minimum = 0.00E+00
0.00E+00
1.00E+01
2.00E+01
3.00E+01
4.00E+01
5.00E+01
6.00E+01
7.00E+01
8.00E+01
9.00E+01
1.00E+02
1.10E+02
1.20E+02
1.30E+02
1.40E+02
1.50E+02
Maximum = 6.37E+02
ASRM AFT SLOT AT 0 SECONDS
Velocity Vectors
FLUENT/BFC V3.02
2D Domain
Steady State
creare.x

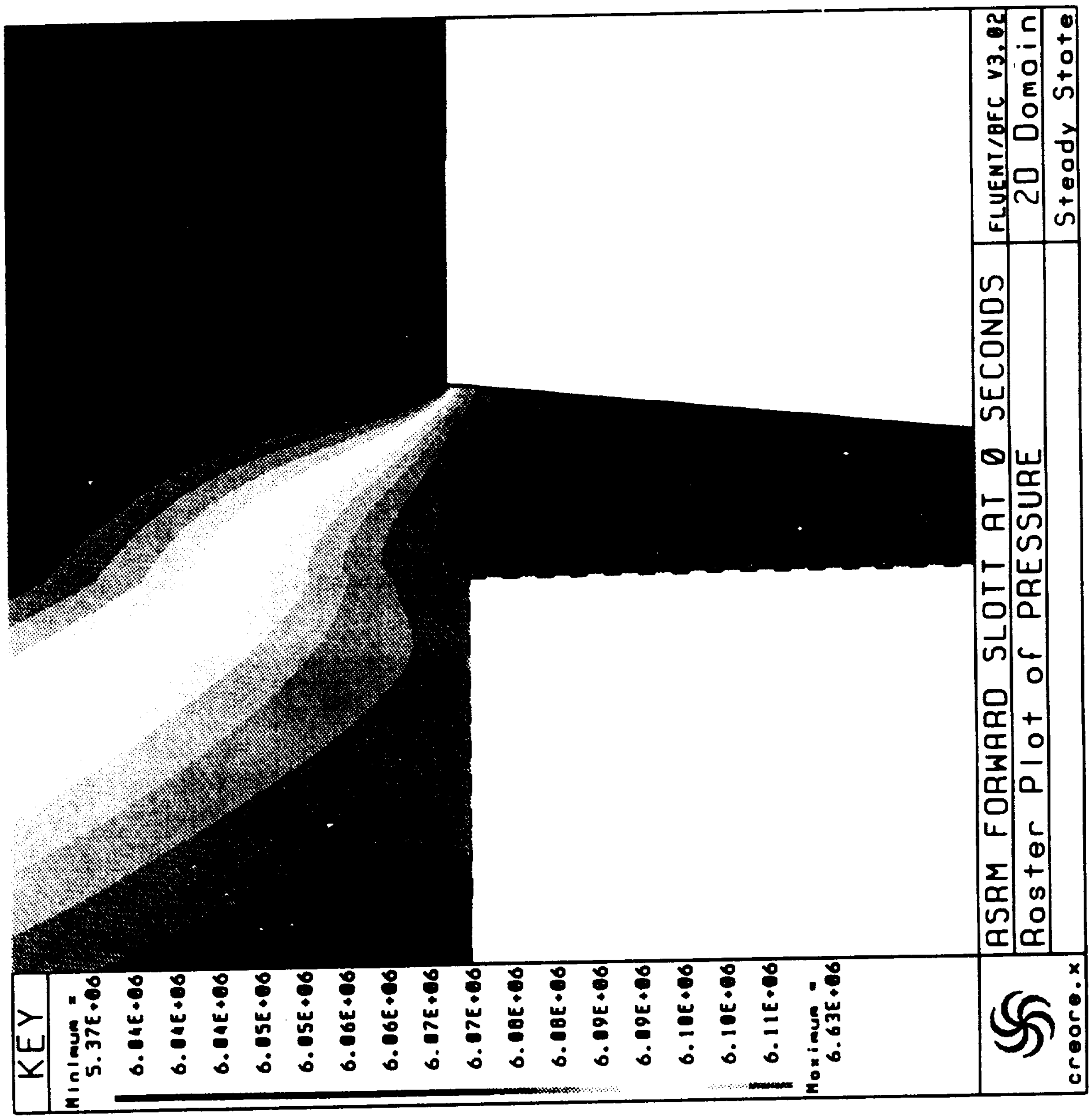
KEY
Minimum = 5.37E+06
6.04E+06
6.04E+06
6.04E+06
6.05E+06
6.05E+06
6.06E+06
6.06E+06
6.07E+06
6.07E+06
6.08E+06
6.08E+06
6.09E+06
6.09E+06
6.10E+06
6.10E+06
6.11E+06
Maximum = 6.63E+06
ASRM FORWARD SLOTT AT 0 SECONDS
Raster Plot of PRESSURE
FLUENT/BFC V3.02
2D Domain
Steady State
creare.x

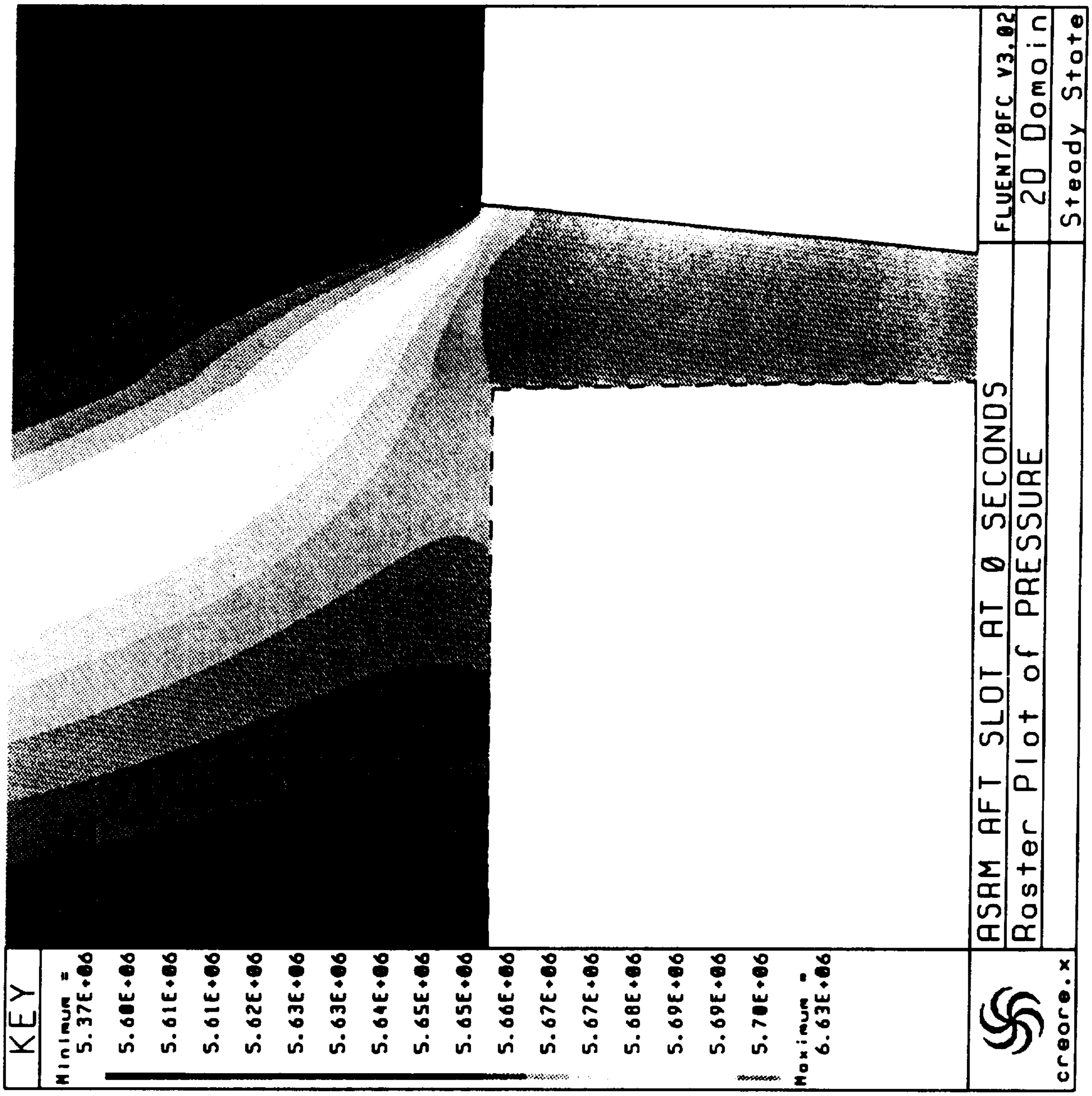
KEY
Minimum =
5.37E+06
5.60E+06
5.61E+06
5.61E+06
5.62E+06
5.63E+06
5.63E+06
5.64E+06
5.65E+06
5.65E+06
5.66E+06
5.67E+06
5.67E+06
5.68E+06
5.69E+06
5.69E+06
5.70E+06
Maximum =
6.63E+06
ASRM AFT SLOT AT Ø SECONDS
Raster Plot of PRESSURE
FLUENT/BFC V3.02
2D Domain
Steady State
creare.x

ASRM Full-Scale Motor Static Pressure

Adjusted k-e Model

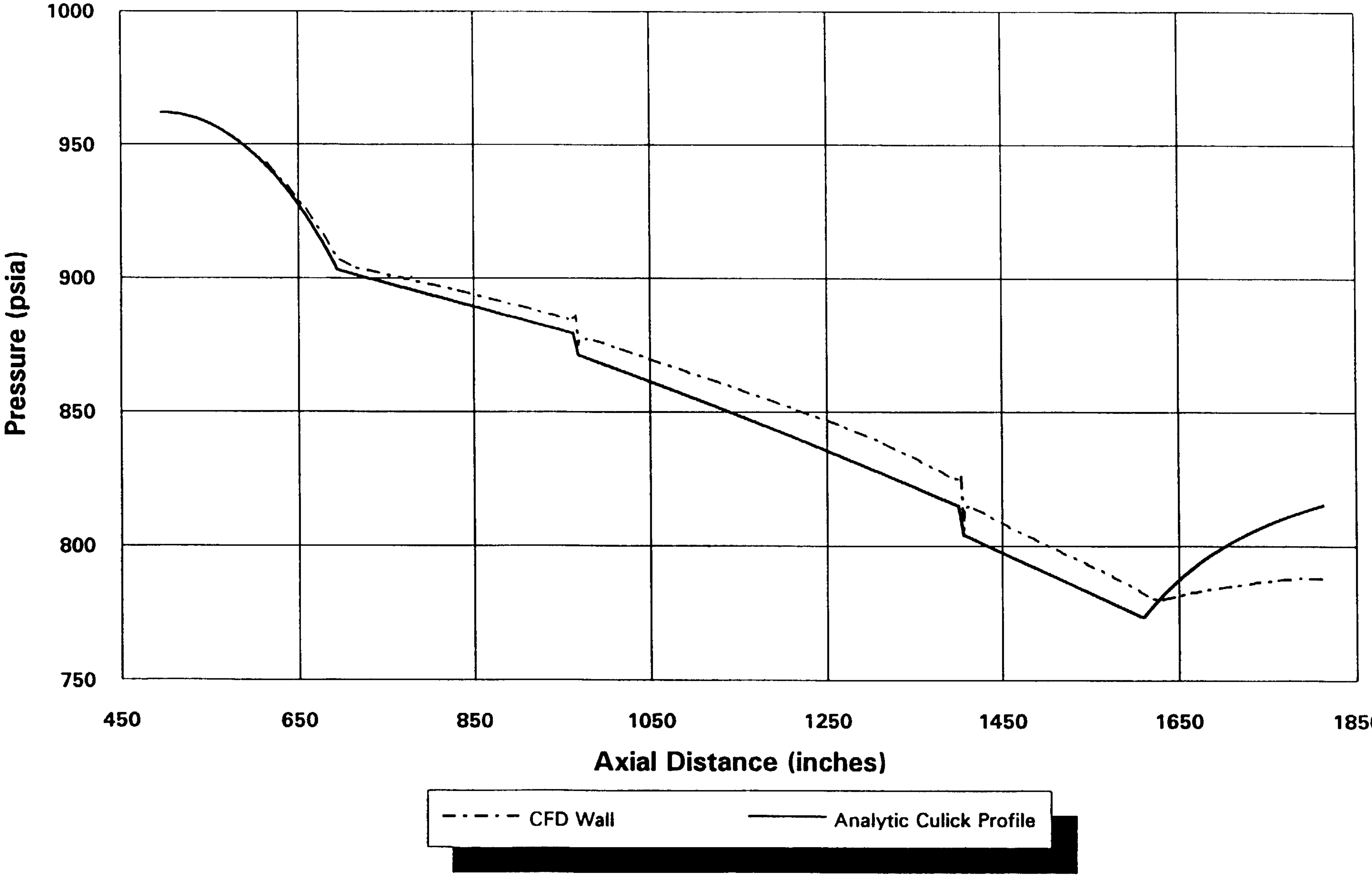

ERC, Inc. 11/03/92

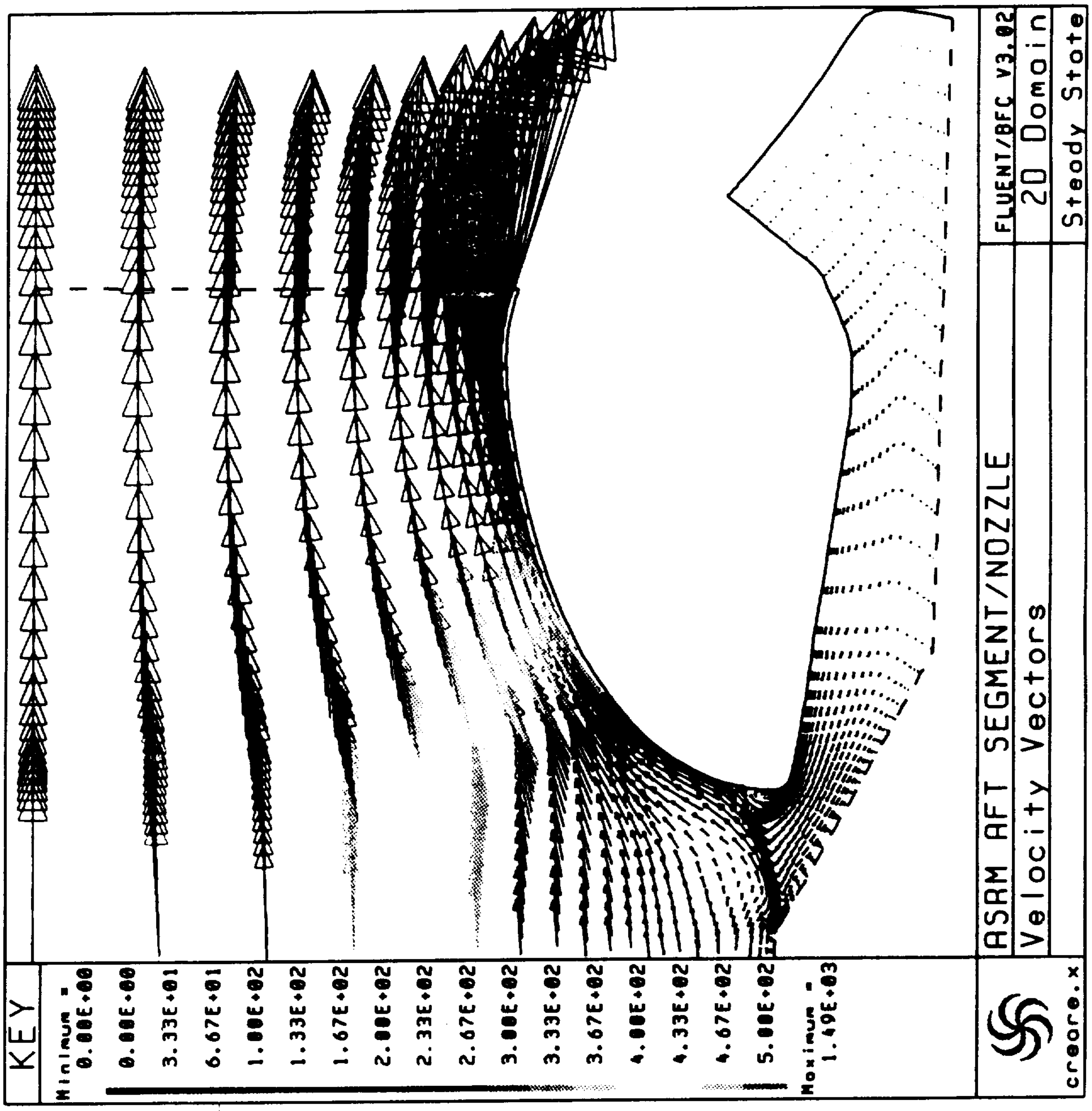

KEY
Minimum = 0.00E+00
0.00E+00
3.33E+01
6.67E+01
1.00E+02
1.33E+02
1.67E+02
2.00E+02
2.33E+02
2.67E+02
3.00E+02
3.33E+02
3.67E+02
4.00E+02
4.33E+02
4.67E+02
5.00E+02
Maximum = 1.49E+03
ASRM AFT SEGMENT/NOZZLE
Velocity Vectors
FLUENT/BFC V3.02
2D Domain
Steady State
creare.x

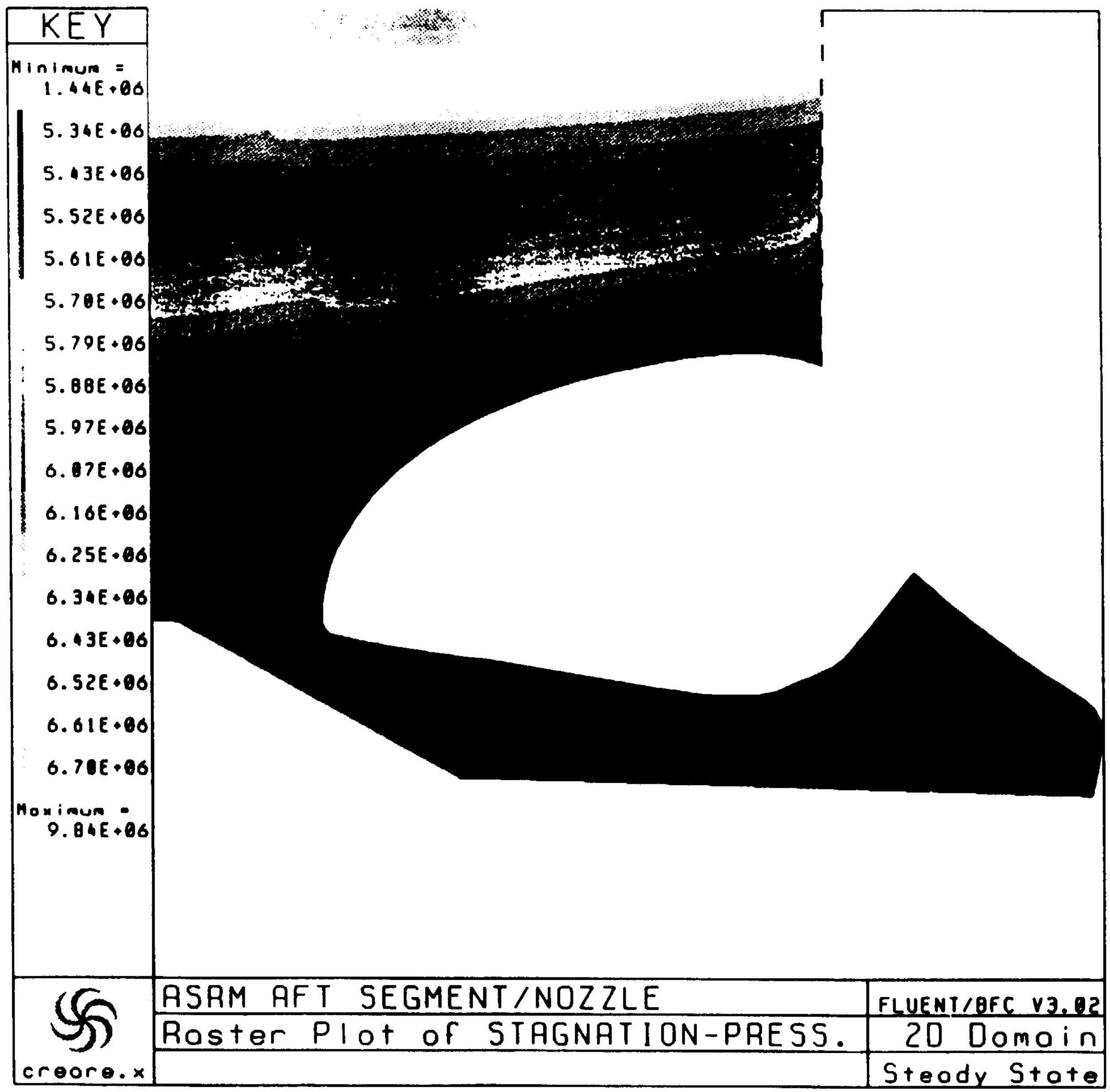
KEY
Minimum =
1.44E+06
5.34E+06
5.43E+06
5.52E+06
5.61E+06
5.70E+06
5.79E+06
5.88E+06
5.97E+06
6.07E+06
6.16E+06
6.25E+06
6.34E+06
6.43E+06
6.52E+06
6.61E+06
6.70E+06
Maximum =
9.84E+06
creare.x
ASRM AFT SEGMENT/NOZZLE
Raster Plot of STAGNATION-PRESS.
FLUENT/BFC V3.02
2D Domain
Steady State

ASRM Full-Scale Motor Velocity Profiles

Forward Slot Region

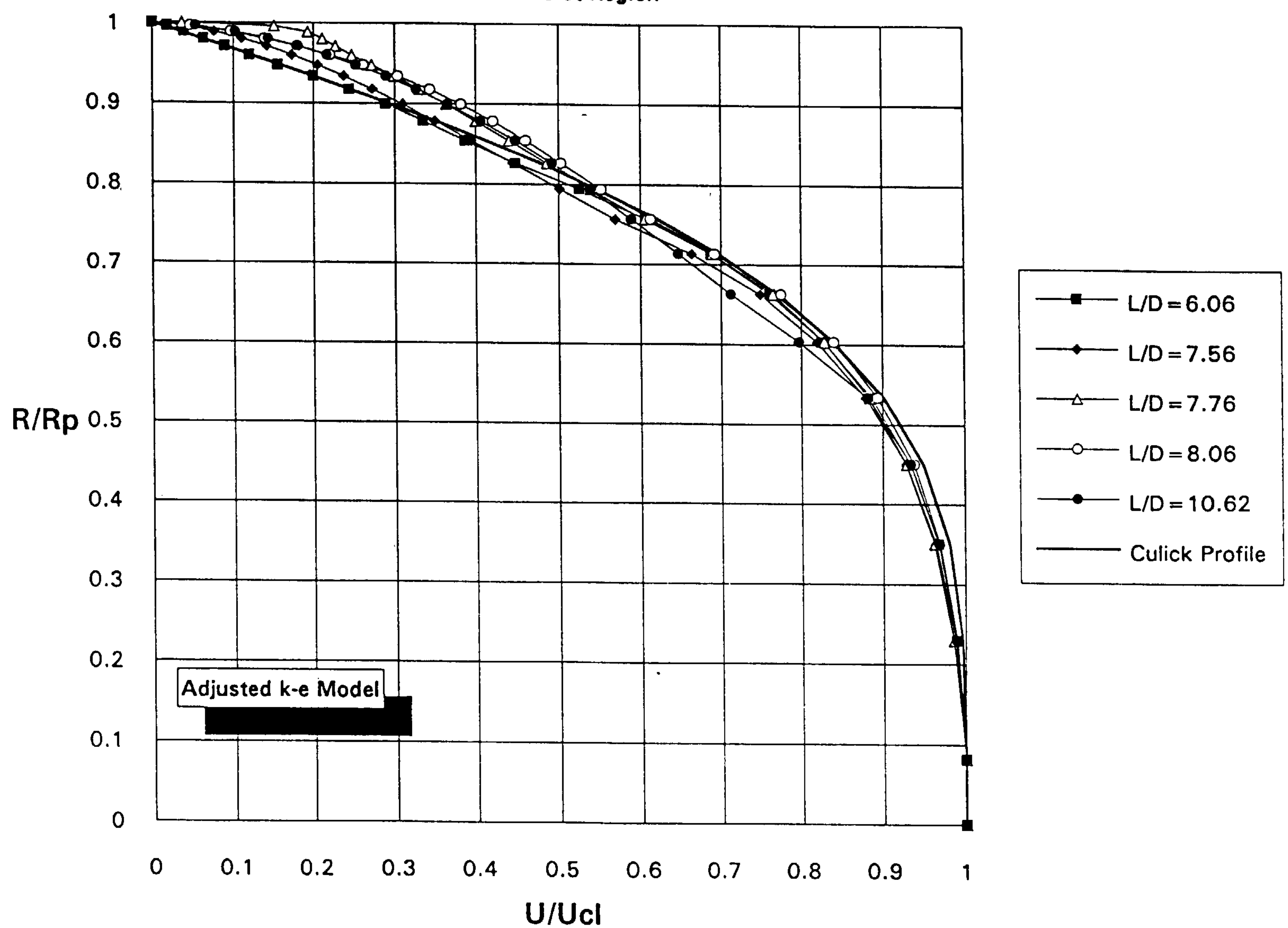

ERCI 07/06/92

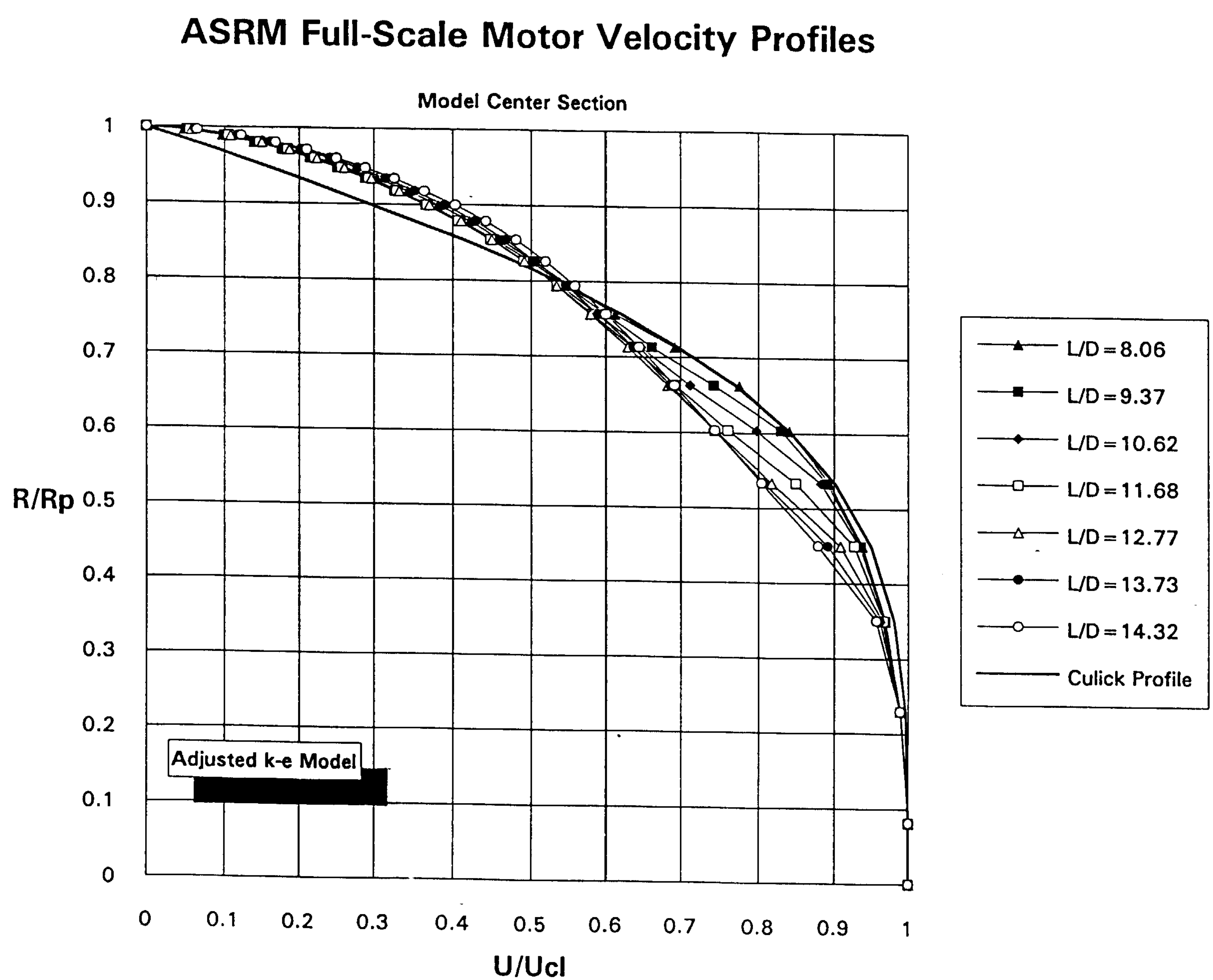
ASRM Full-Scale Motor Velocity Profiles
Model Center Section
R/Rp
U/Ucl
0
0.1
0.2
0.3
0.4
0.5
0.6
0.7
0.8
0.9
1
L/D = 8.06
L/D = 9.37
L/D = 10.62
L/D = 11.68
L/D = 12.77
L/D = 13.73
L/D = 14.32
Culick Profile
Adjusted k-e Model

ERCI 07/06/92

ASRM Full-Scale Motor Velocity Profiles

Aft Section

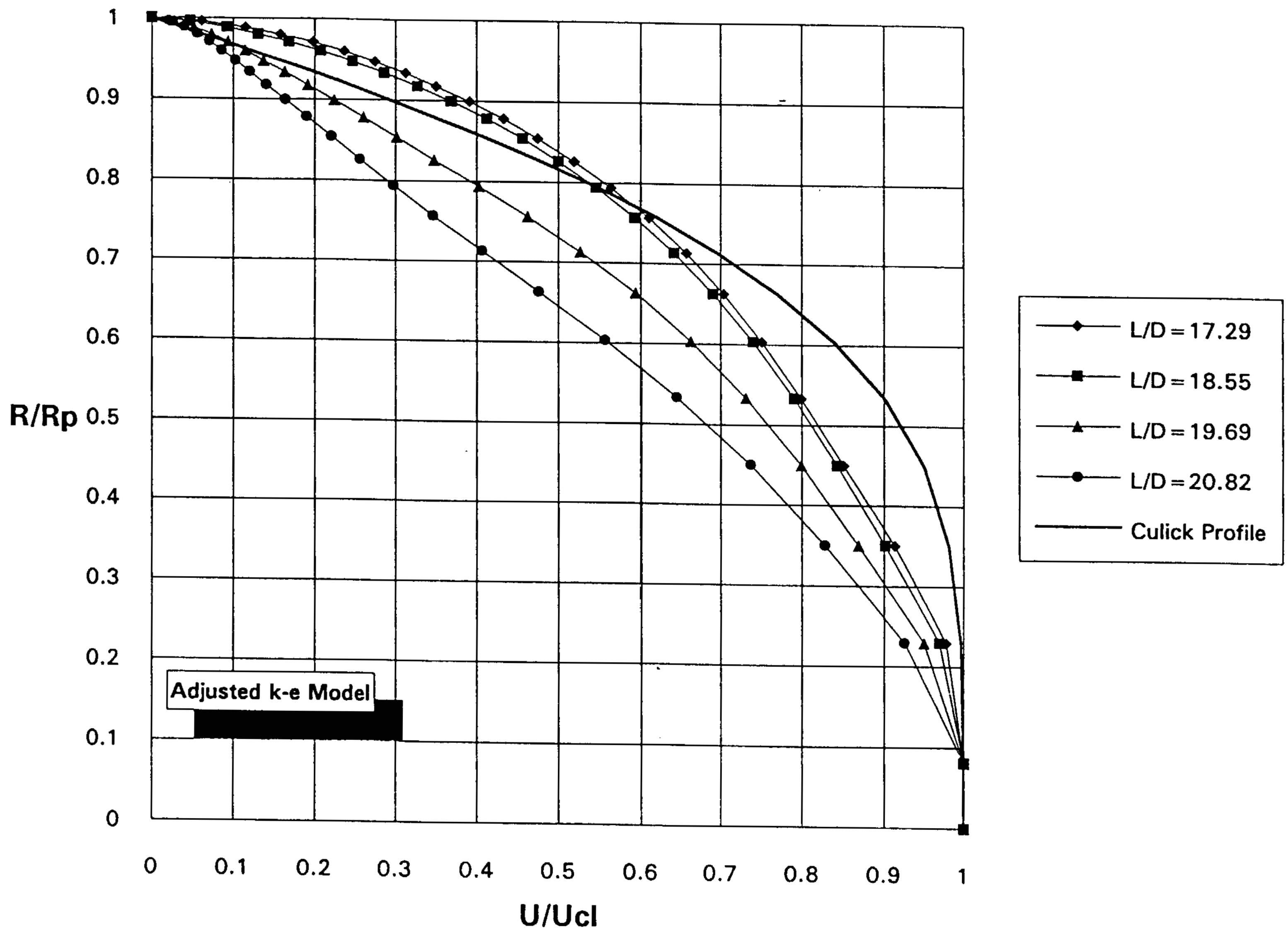

ERCI 07/14/92

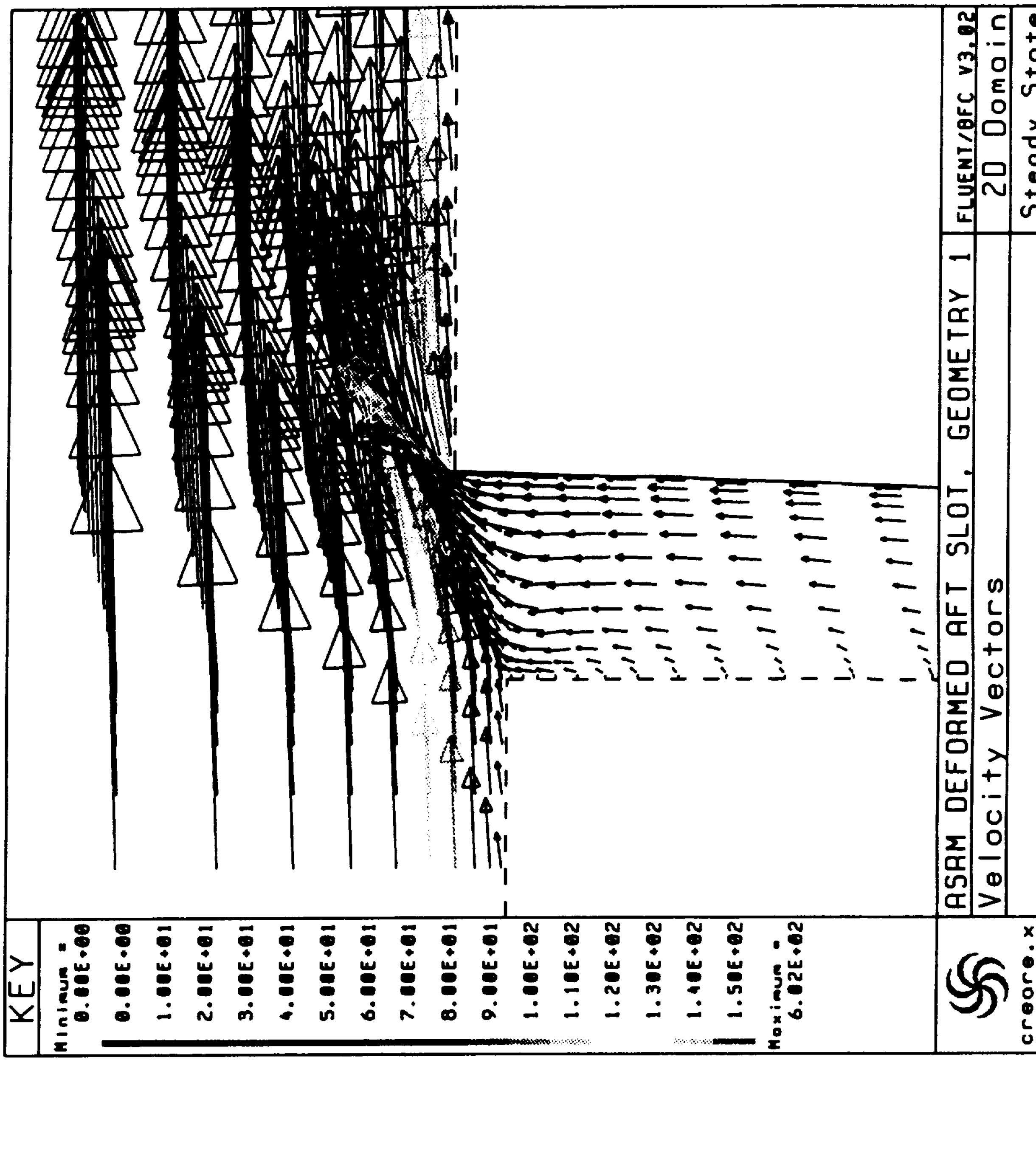
KEY
Minimum = 0.00E+00
0.00E+00
1.00E+01
2.00E+01
3.00E+01
4.00E+01
5.00E+01
6.00E+01
7.00E+01
8.00E+01
9.00E+01
1.00E+02
1.10E+02
1.20E+02
1.30E+02
1.40E+02
1.50E+02
Maximum = 6.02E+02
creare.x
ASRM DEFORMED AFT SLOT, GEOMETRY 1
Velocity Vectors
FLUENT/BFC V3.02
2D Domain
Steady State

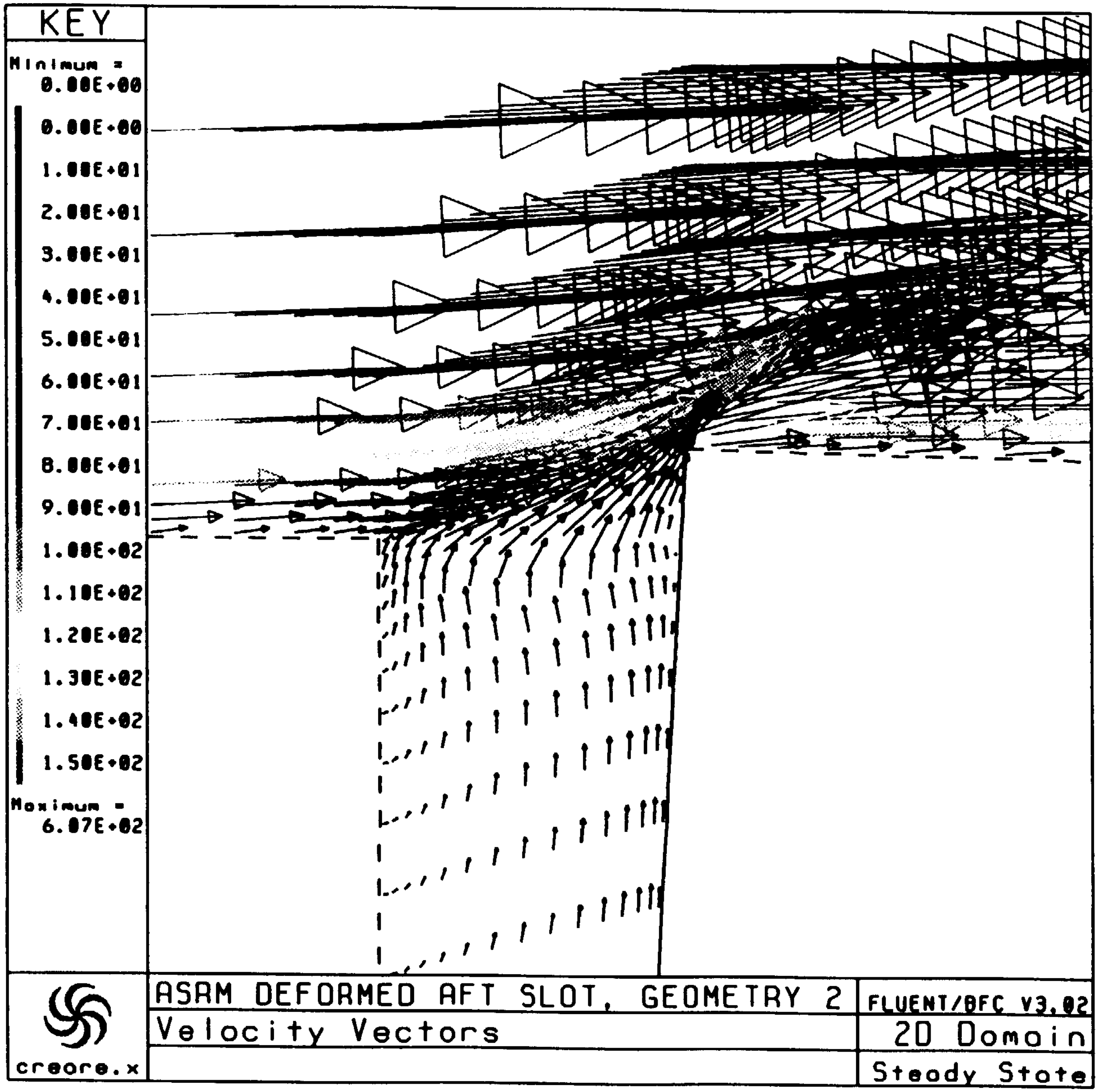
KEY
Minimum =
0.00E+00
0.00E+00
1.00E+01
2.00E+01
3.00E+01
4.00E+01
5.00E+01
6.00E+01
7.00E+01
8.00E+01
9.00E+01
1.00E+02
1.10E+02
1.20E+02
1.30E+02
1.40E+02
1.50E+02
Maximum =
6.07E+02
creare.x
ASRM DEFORMED AFT SLOT, GEOMETRY 2
Velocity Vectors
FLUENT/BFC V3.02
2D Domain
Steady State

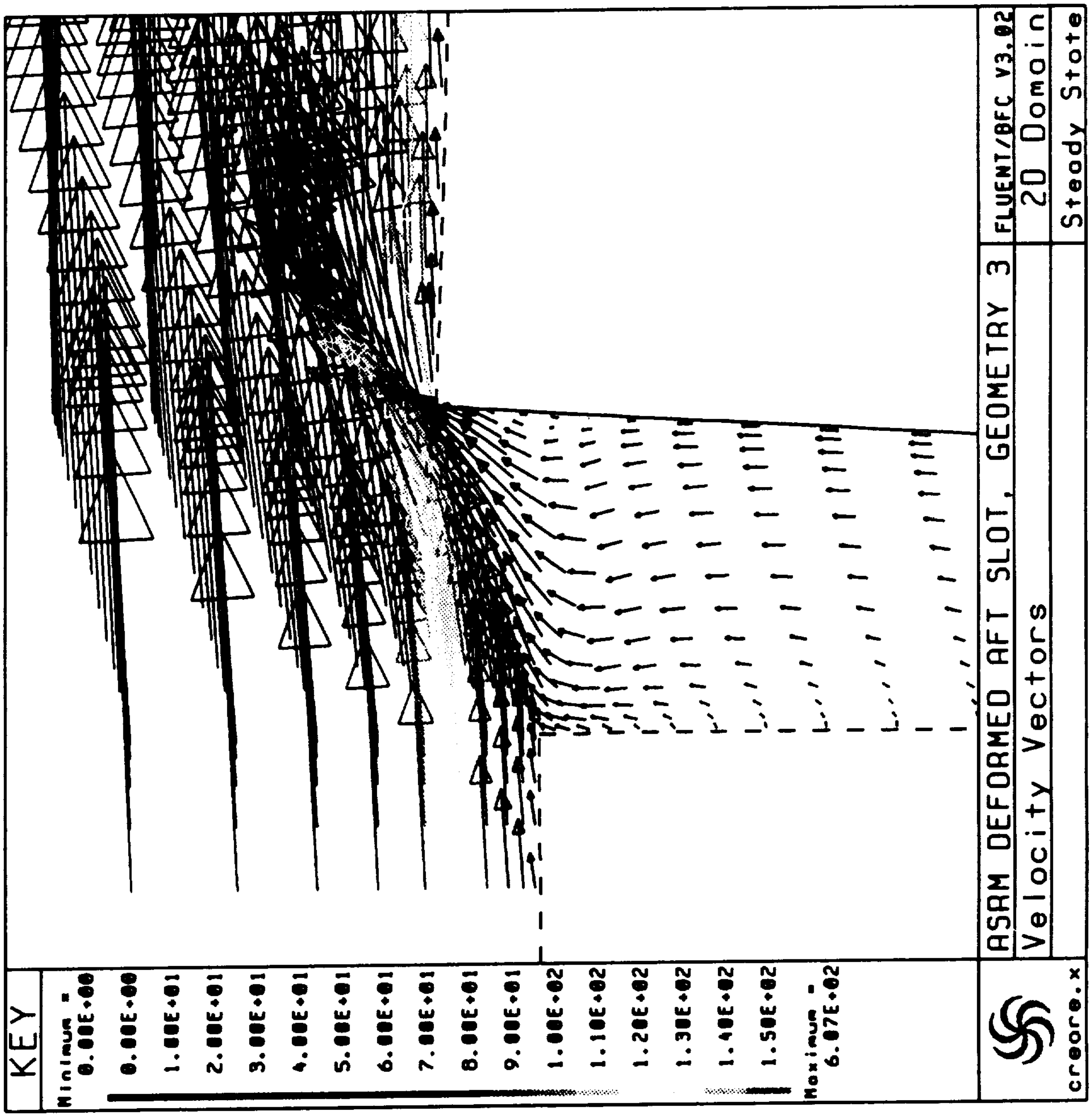
KEY
Minimum =
0.00E+00
0.00E+00
1.00E+01
2.00E+01
3.00E+01
4.00E+01
5.00E+01
6.00E+01
7.00E+01
8.00E+01
9.00E+01
1.00E+02
1.10E+02
1.20E+02
1.30E+02
1.40E+02
1.50E+02
Maximum =
6.07E+02
ASRM DEFORMED AFT SLOT, GEOMETRY 3
Velocity Vectors
FLUENT/BFC V3.02
2D Domain
Steady State
creare.x

ASRM ANALYSIS CONCLUSIONS

- MOTOR PORT PRESSURE GRADIENTS FROM CFD ANALYSES HAVE PROVIDED ADDITIONAL PERFORMANCE INFORMATION AND TEST DATA INTERPRETATION

- A SIGNIFICANT PORTION OF THE PROPELLANT DEFORMATION AT THE AFT SLOT IS DUE TO 2-D FLOW EFFECTS

- VELOCITY PROFILE TRANSITION ZONE AND EFFECT OF BORE GEOMETRY FLARE WAS PREDICTED BY CFD ANALYSIS

ERC, Inc.
4/21/93

N95- 23650

335-47
113767
p. 27

TIME-ACCURATE UNSTEADY FLOW SIMULATIONS SUPPORTING THE SRM T+68-SEC PRESSURE "SPIKE" ANOMALY INVESTIGATION (STS-54B)

by

N. S. Dougherty, D. W. Burnette, and J. B. Holt
Rockwell International
Space Systems Division
Huntsville, AL 35806

and

Jose Matienzo
MSFC/ED33
Marshall Space Flight Center, AL 35812

ABSTRACT

Time-accurate unsteady flow simulations are being performed supporting the SRM T+68-sec pressure "spike" anomaly investigation. The anomaly occurred in the RH SRM during the STS-54 flight (STS-54B) but not in the LH SRM (STS-54A) causing a momentary thrust mismatch approaching the allowable limit at that time into the flight. Full-motor internal flow simulations using the USA-2D axisymmetric code are in progress for the nominal propellant burn-back geometry and flow conditions at T+68-sec--P_C = 630 psi, γ = 1.1381, T_C = 6200 R, perfect gas without aluminum particulate. In a cooperative effort with other investigation team members, CFD-derived pressure loading on the NBR and castable inhibitors was used iteratively to obtain nominal deformed geometry of each inhibitor, and the deformed (bent back) inhibitor geometry was entered into this model. Deformed geometry was computed using structural finite-element models. A solution for the unsteady flow has been obtained for the nominal flow conditions (existing prior to the occurrence of the anomaly) showing sustained standing pressure oscillations at nominally 14.5 Hz in the motor IL acoustic mode that flight and static test data confirm to be normally present at this time. Average mass flow discharged from the nozzle was confirmed to be the nominal expected (9550 lbm/sec). The local inlet boundary condition is being perturbed at the location of the presumed reconstructed anomaly as identified by interior ballistics performance specialist team members. A time variation in local mass flow is used to simulate sudden increase in burning area due to localized propellant grain cracks. The solution will proceed to develop a pressure rise (proportional to total mass flow rate change squared). The volume-filling time constant (equivalent to 0.5 Hz) comes into play in shaping the rise rate of the developing pressure "spike" as it propagates at the speed of sound in both directions to the motor head end and nozzle. The objectives of the present analysis are to: (1) capture the dynamic responses of the motor combustion gas flow to correlate with available low-frequency (< 12.5 sample/sec) data and (2) observe the high-frequency (up to 50 Hz) characteristics of the response to determine any potentials for dynamic coupling.

PAGE 836 INTENTIONALLY BLANK

TIME-ACCURATE UNSTEADY FLOW SIMULATIONS SUPPORTING THE SRM T + 68 SEC PRESSURE "SPIKE" ANOMALY INVESTIGATION (STS-54B)

APRIL 21, 1993

N.S. Dougherty, D.W. Burnette, and J.B. Holt
Rockwell International
Huntsville, AL
and
J. Matienzo
MSFC/ED33

RENG002556.03

STS-54B SRM PRESSURE "SPIKE" ANOMALY INVESTIGATION

OBJECTIVE

- PERFORM TIME-ACCURATE CFD SIMULATIONS OF INTERNAL FLOW RESPONSE TO PRESSURE "SPIKE" ANOMALY ASSUMED TO BE CAUSED BY ALUMINUM OXIDE SLAG EJECTION THROUGH THE NOZZLE TO:

  1) CAPTURE DYNAMIC RESPONSES FOR CORRELATION WITH AVAILABLE 12.5 SAMPLE/SEC FLIGHT DATA, AND

  2) OBSERVE HIGH-FREQUENCY (UP TO 50 HZ) CHARACTERISTICS OF THE RESPONSE TO DETERMINE ANY POTENTIALS FOR DYNAMIC COUPLING

STS-54B SRM PRESSURE "SPIKE" ANOMALY INVESTIGATION

APPROACH

- DEVELOP THE UNSTEADY SOLUTION FOR THE MOTOR/NOZZLE FLOW AT T + 67 SEC
  - BENT-OVER INHIBITORS
- SIMULATE NOZZLE BLOCKAGE OF 39 IN^2 AT THROAT FOR"SPIKE" ANOMALY SCENARIO INITIATION
  - SUDDENLY APPLIED
  - REDUCED SMOOTH NOZZLE CONTOUR (LESS FLOW AREA WITHOUT EXTRANEOUS SHOCKS)
- COMPUTE MOTOR INTERNAL FLOW TRANSIENT UNTIL PEAK PRESSURE REACHED
  - OBSERVE CHARACTERISTICS
- RETURN NOZZLE GEOMETRY TO UNBLOCKED CONFIGURATION
  - BLOCKAGE SUDDENLY REMOVED
- COMPUTE MOTOR INTERNAL FLOW TRANSIENT TO RECOVERY

TIME-ACCURATE CFD ANALYSIS OF RSRM Pc ANOMALY T + 68 SEC

BASIC ASSUMPTIONS:

- PERFECT GAS
- ADIABATIC WALL
- NEGLECTS DAMPING FROM ALUMINUM PARTICULATE
- AXISYMMETRIC FLOW

SIMULATION/ANALYSIS TOOL:

- TIME-ACCURATE USA CODE (DEVELOPED BY ROCKWELL)
- CURRENTLY IN USE BY ED33 FOR RSRM AND ASRM VORTEX SHEDDING/ACOUSTIC INTERACTION STUDIES
- OUTPUTS PLOT 3D FILES IN MSFC STANDARDIZED FORMATS

STS-54B SRM PRESSURE "SPIKE" ANOMALY INVESTIGATION

MODELING APPROACH

BENEFITS

- CAN SHOW POTENTIALS FOR UNSTEADY BEHAVIOR
  - MOTOR ACOUSTIC MODE RESPONSE, INHIBITOR VORTEX SHEDDING, INHIBITOR DYNAMIC PRESSURE DIFFERENTIAL LOADING, MOTOR VOLUME-FILLING TIME CONSTANT, NOZZLE STAGNATION POINT MOVEMENT
- MATCHES 2D STEADY-FLOW CFD (MEAN VALUES)
  - PRESSURE, VELOCITY PROFILES, CALCULATED THRUST BEFORE THE "SPIKE"
- PROVIDES PRESSURE-VS-TIME TRANSIENT OVER FULL MOTOR LENGTH FOR SIMULATED "SPIKE" ANOMALY

AREAS FOR IMPROVEMENT

- REDUCE AFT DOME VOLUME GAS FILLING VOLUME BY THE VOLUME OF SLAG ACCUMULATION, ADD SLOSH MOTION DYNAMICS FOR THE POOLING SLAG
- DEVELOP 2-PHASE, TIME-DEPENDENT MODEL FOR AGGLOMERATED SLAG FLOW THROUGH THE NOZZLE TO INCLUDE SLAG MOMENTUM THRUST INCREMENT

Rockwell International

Space Systems Division

TIME-ACCURATE CFD ANALYSIS OF RSRM Pc ANOMALY T +68 SEC

Huntsville Operations

POSTULATED INTERNAL GEOMETRY AND SIMULATION CONDITIONS FOR RSRM @ T + 68 SEC

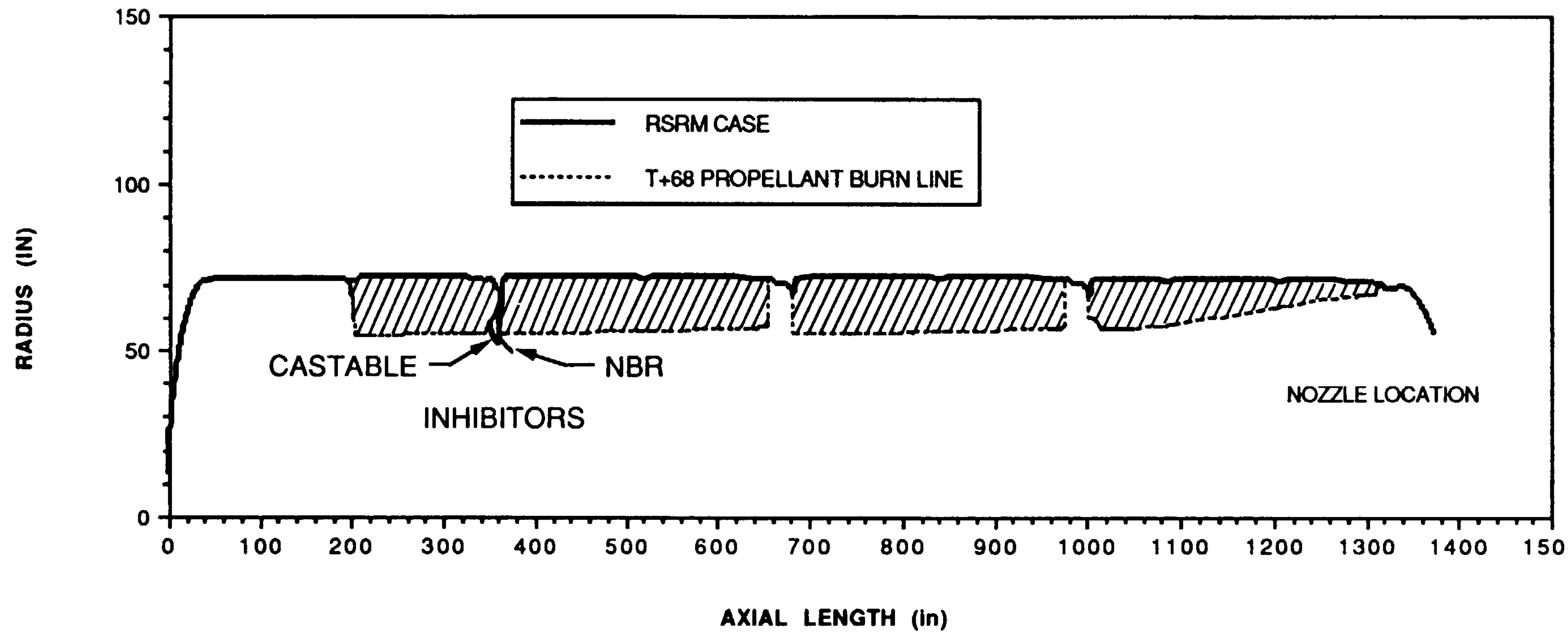

GAMMA 1.1381 (W/OUT ALUMINUM PARTICULATE)	PERFECT GAS
PRESSURE 629.7 PSI	SPEED OF SOUND 3493 FT/SEC
TEMP 3444.5 K (6200 R)	DENSITY (GAS) 1.575E-04 LB/IN^3

RENG002393.02

STS-54 RH PRESSURE PERTURBATION INVESTIGATION

STEADY STATE PRESSURE VS TIME (70°)

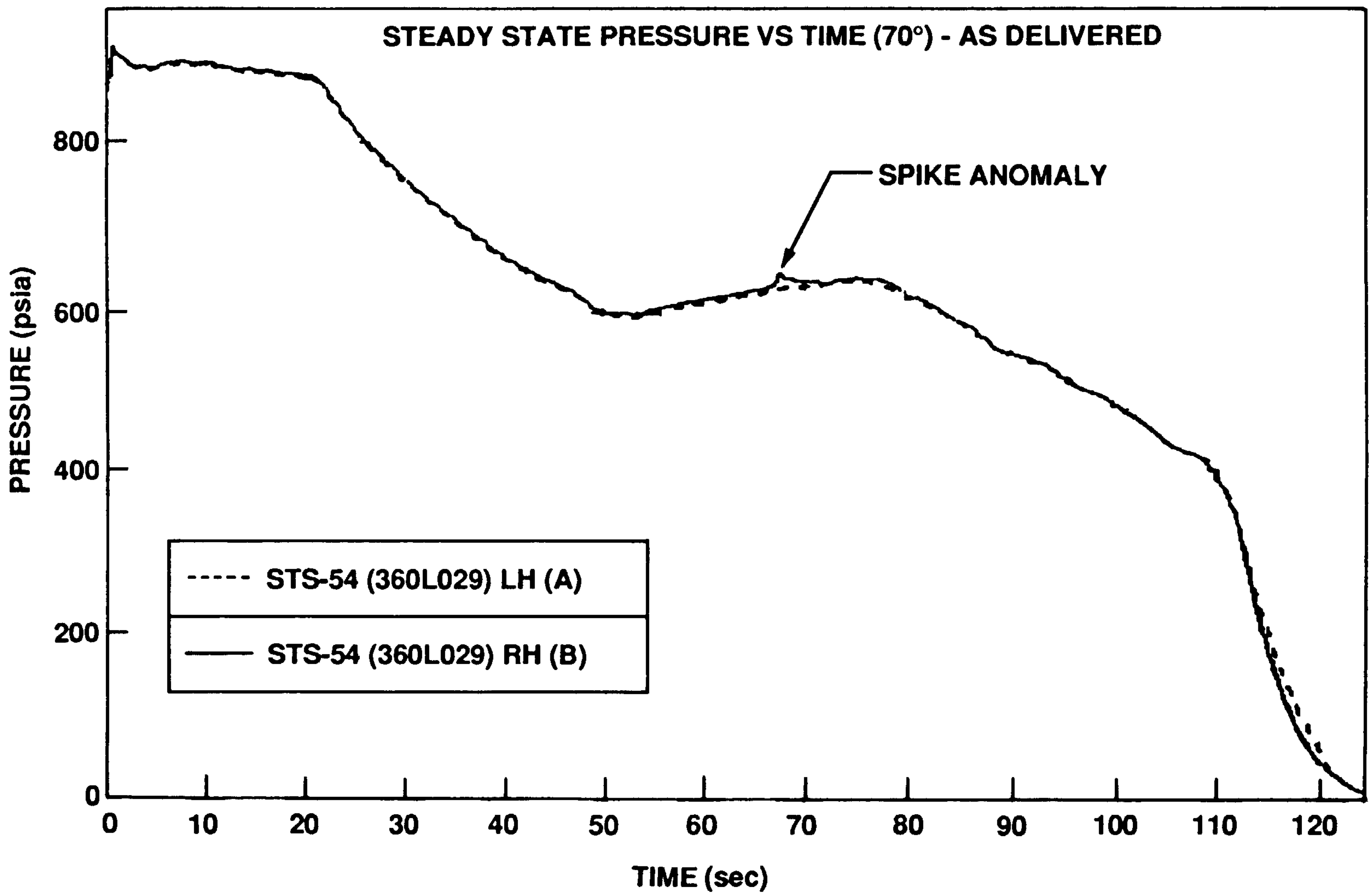

RENG002563.01

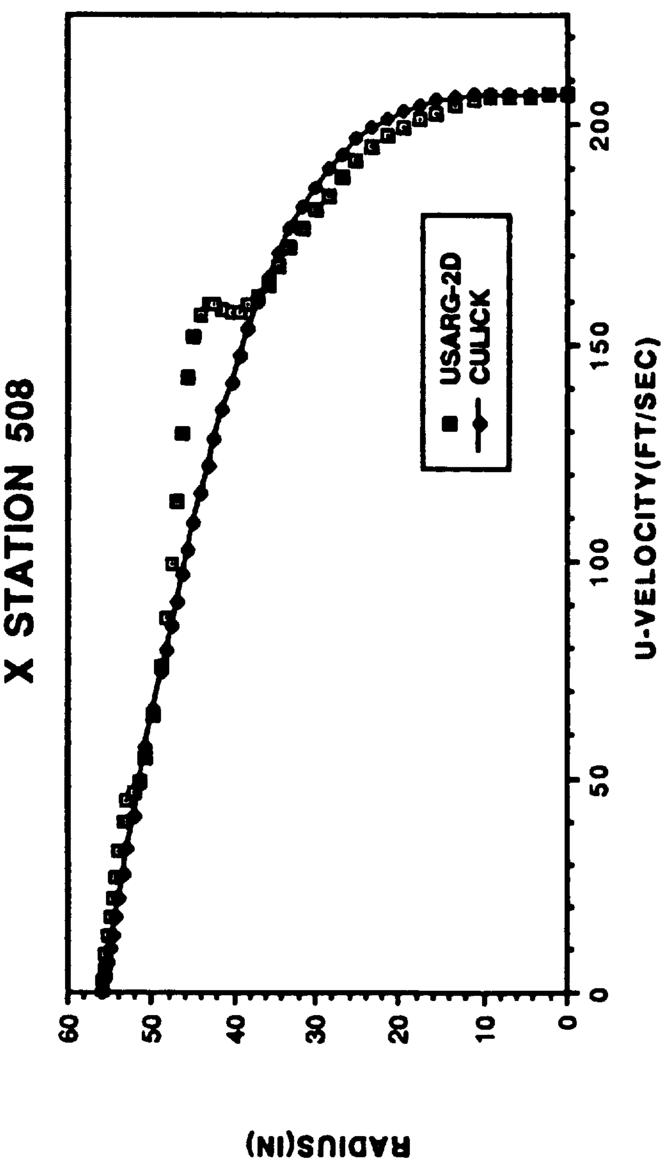
X STATION 508
USARG-2D
CULICK
U-VELOCITY(FT/SEC)
RADIUS(IN)

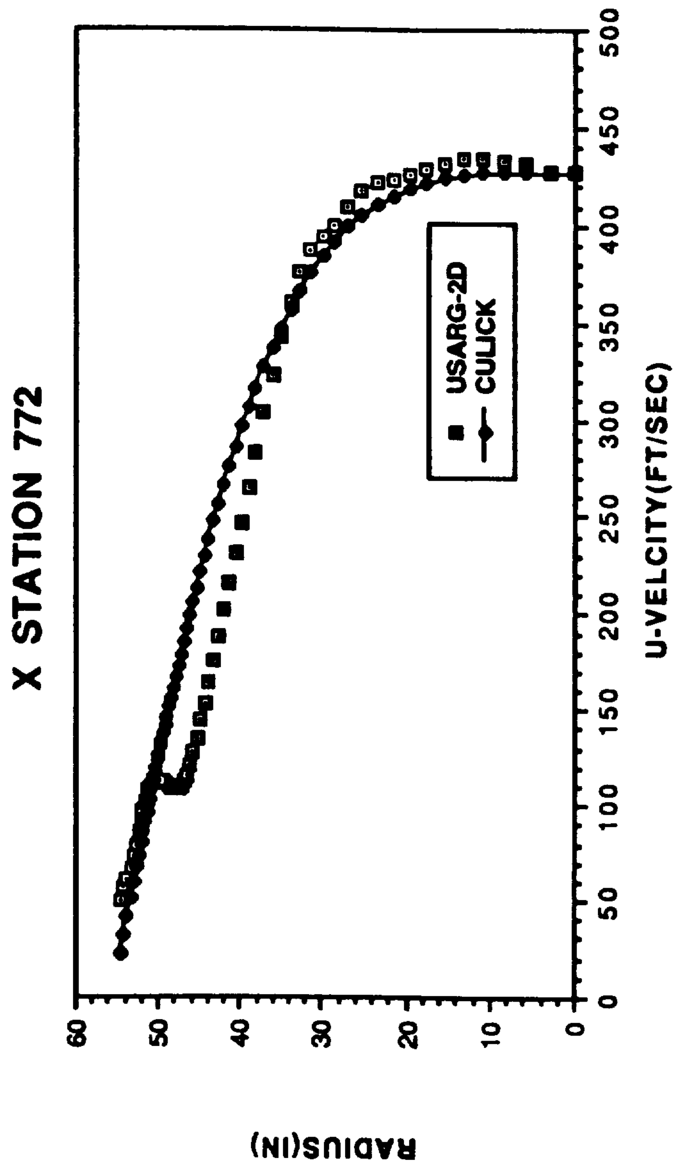
X STATION 772
USARG-2D
CULICK
U-VELCITY(FT/SEC)
RADIUS(IN)

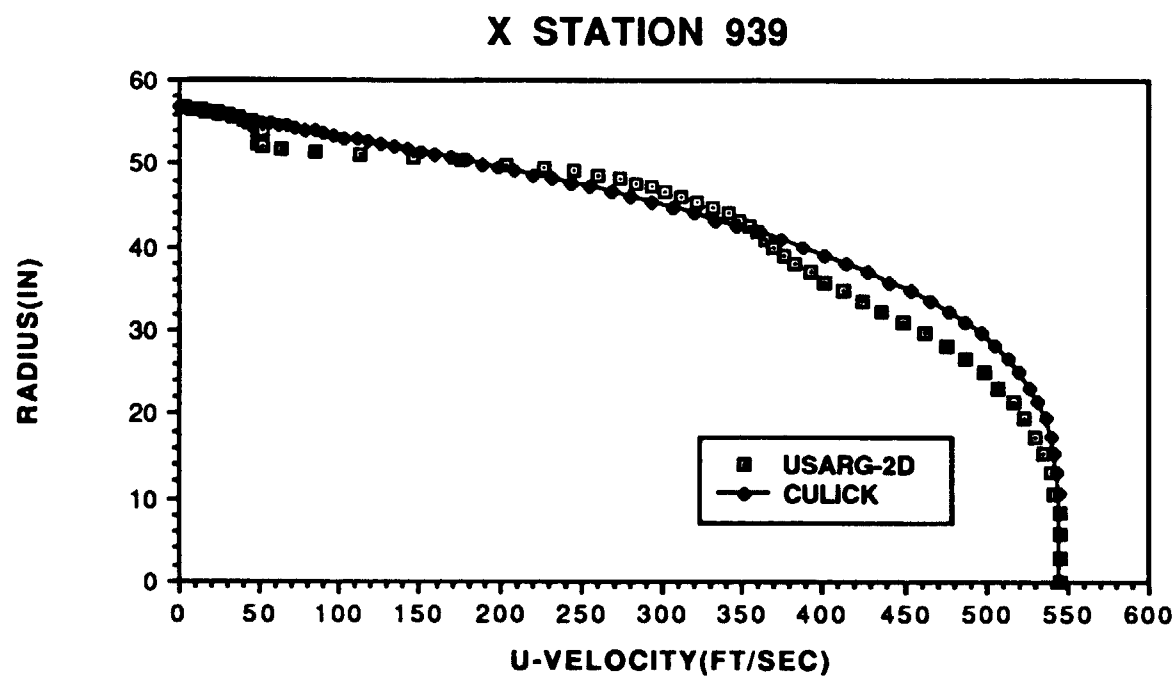
X STATION 939
RADIUS(IN)
U-VELOCITY(FT/SEC)
USARG-2D
CULICK

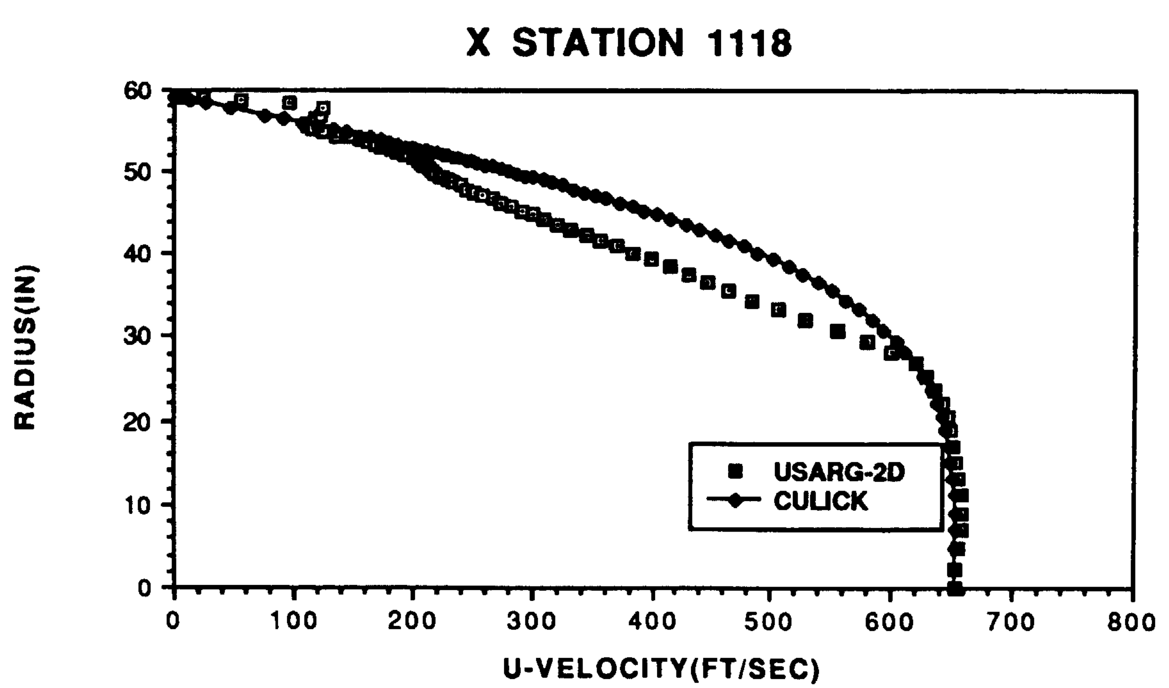
X STATION 1118
RADIUS(IN)
U-VELOCITY(FT/SEC)
USARG-2D
CULICK

X STATION 1256A

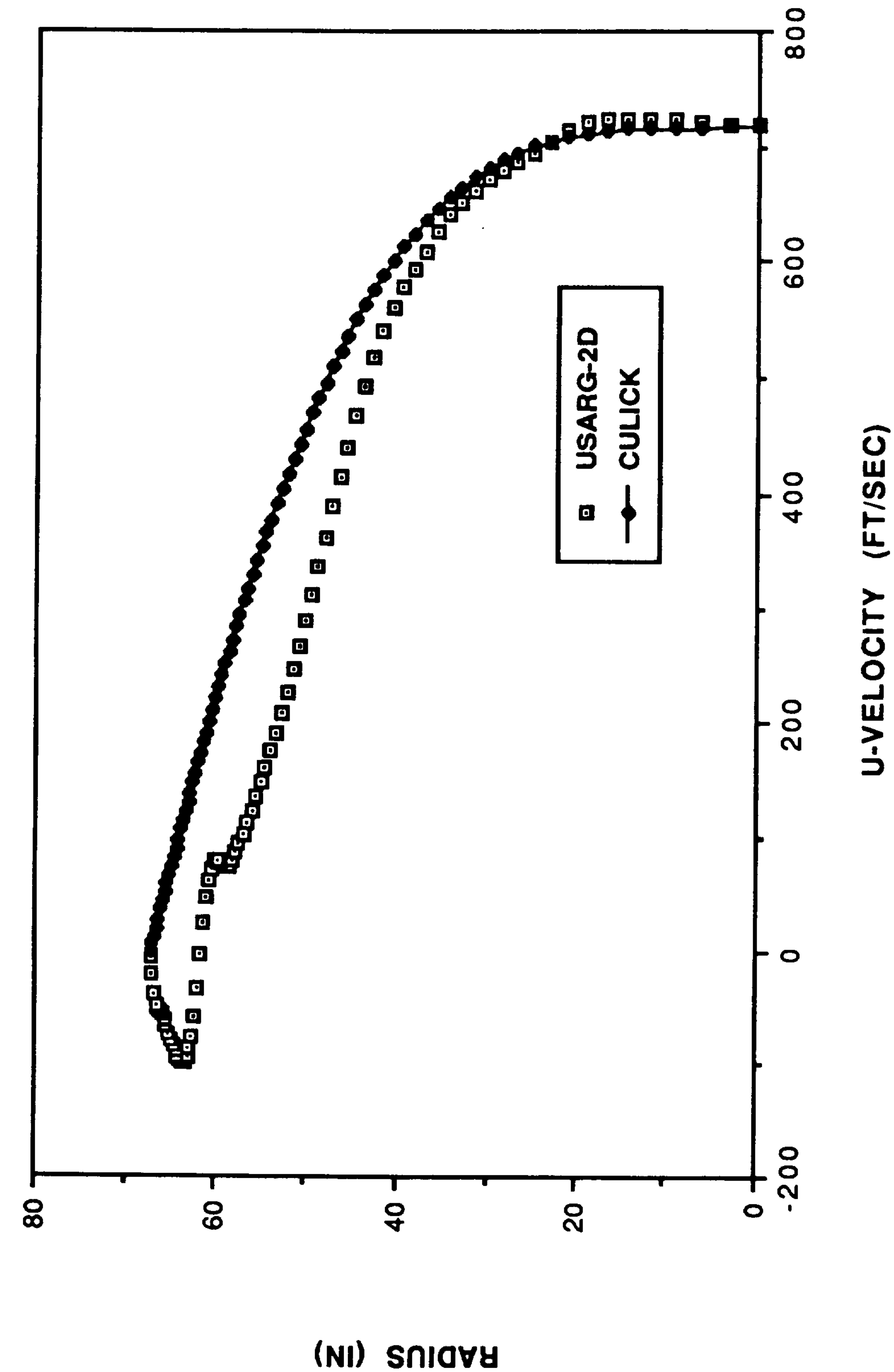

RSRM T+68 CFD SIMULATION
1ST LONGITUDINAL MODE (13.3 Hz)

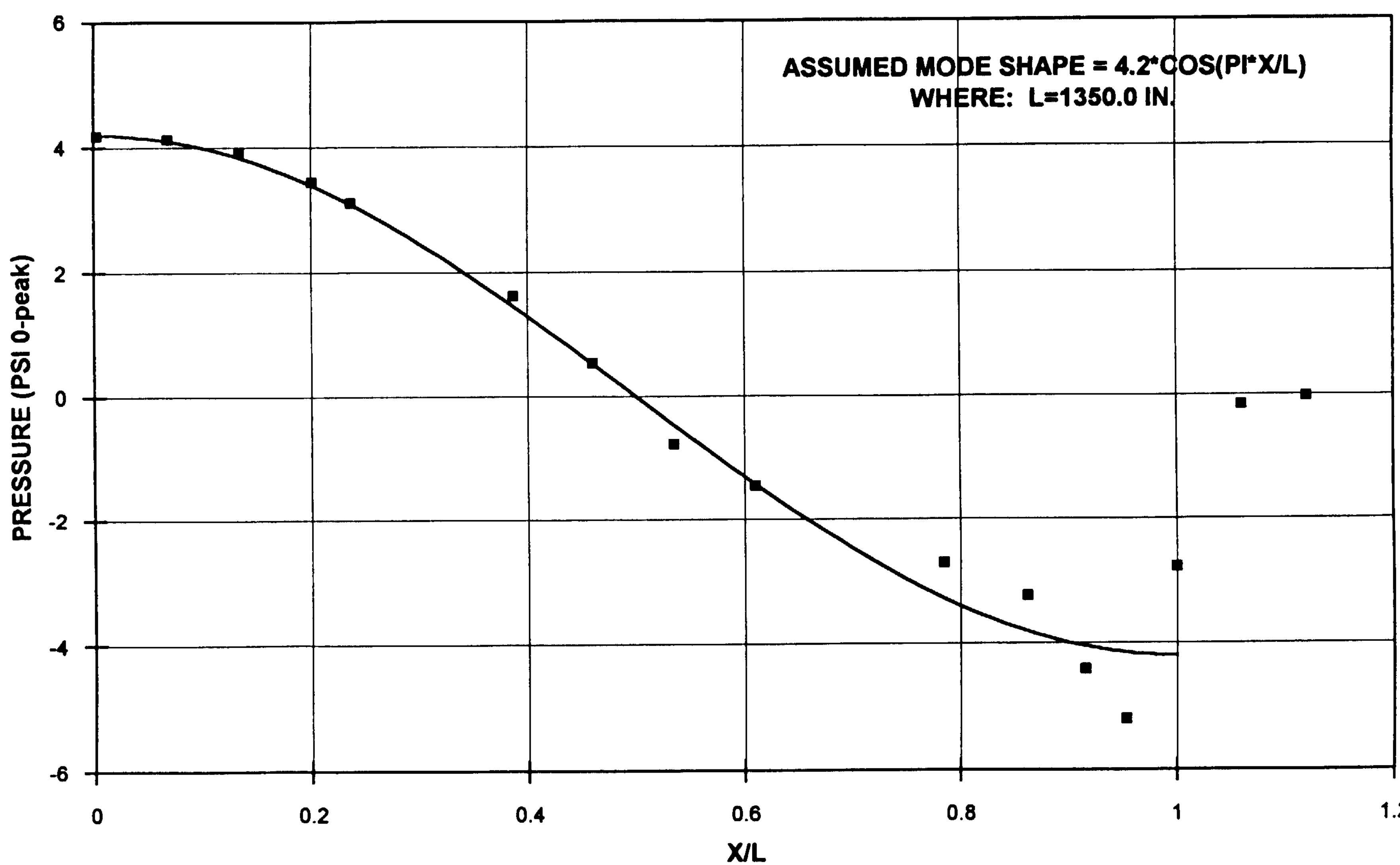

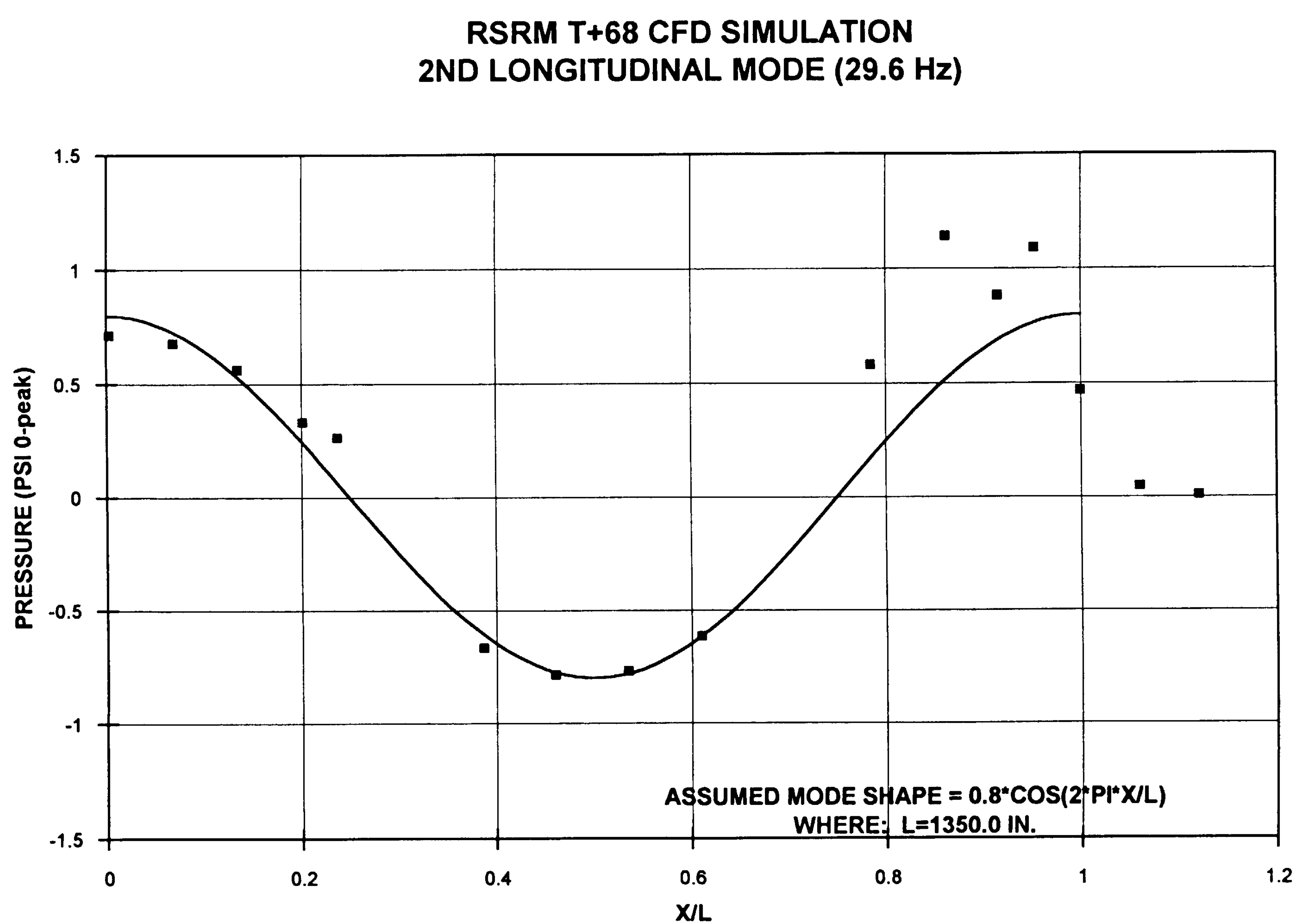

RSRM T+68 CFD SIMULATION
2ND LONGITUDINAL MODE (29.6 Hz)
PRESSURE (PSI 0-peak)
1.5
1
0.5
0
-0.5
-1
-1.5
0
0.2
0.4
0.6
0.8
1
1.2
X/L
ASSUMED MODE SHAPE = 0.8*COS(2*PI*X/L)
WHERE: L=1350.0 IN.

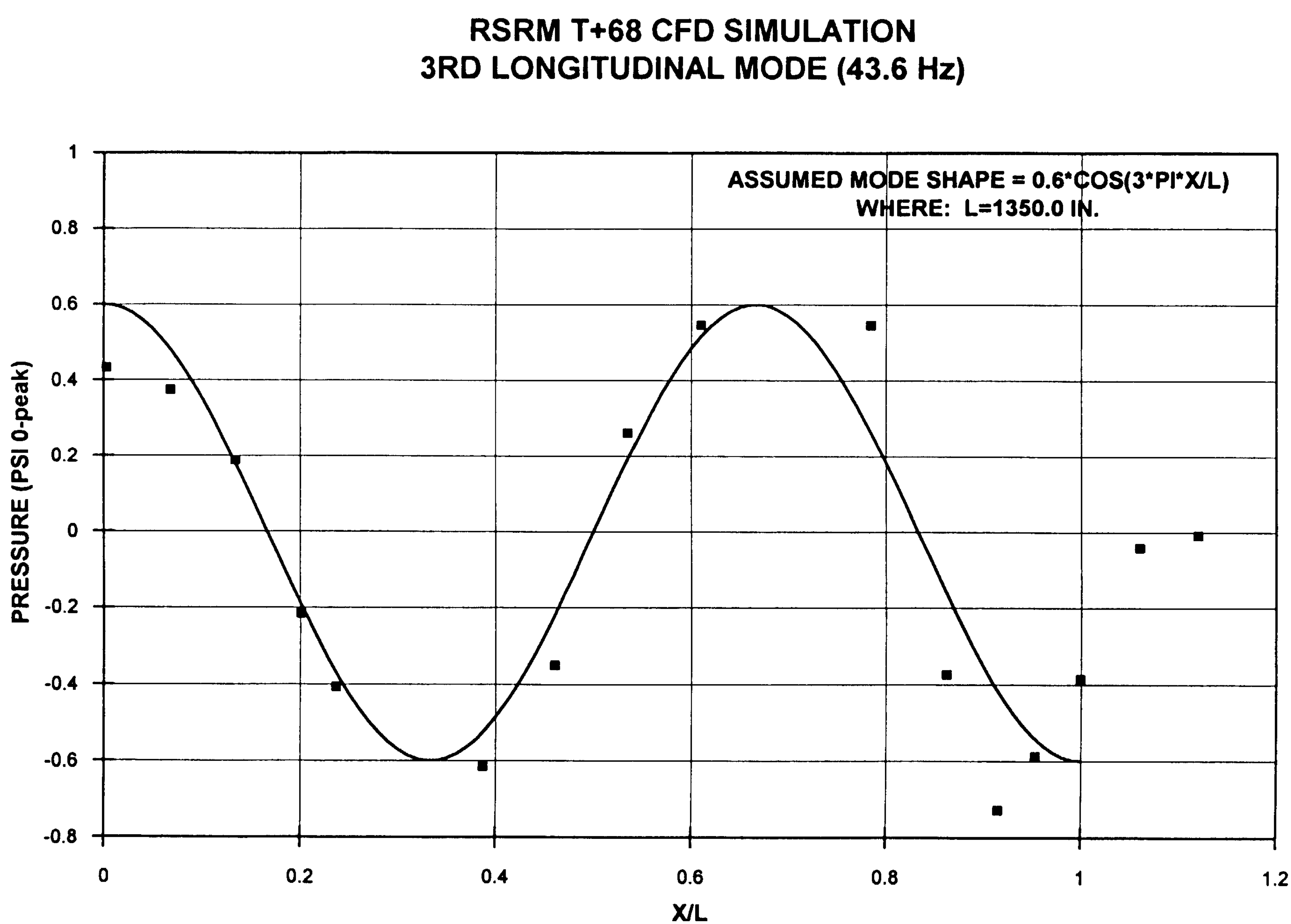
RSRM T+68 CFD SIMULATION
3RD LONGITUDINAL MODE (43.6 Hz)
ASSUMED MODE SHAPE = 0.6*COS(3*PI*X/L)
WHERE: L=1350.0 IN.
PRESSURE (PSI 0-peak)
X/L
1
0.8
0.6
0.4
0.2
0
-0.2
-0.4
-0.6
-0.8
0
0.2
0.4
0.6
0.8
1
1.2

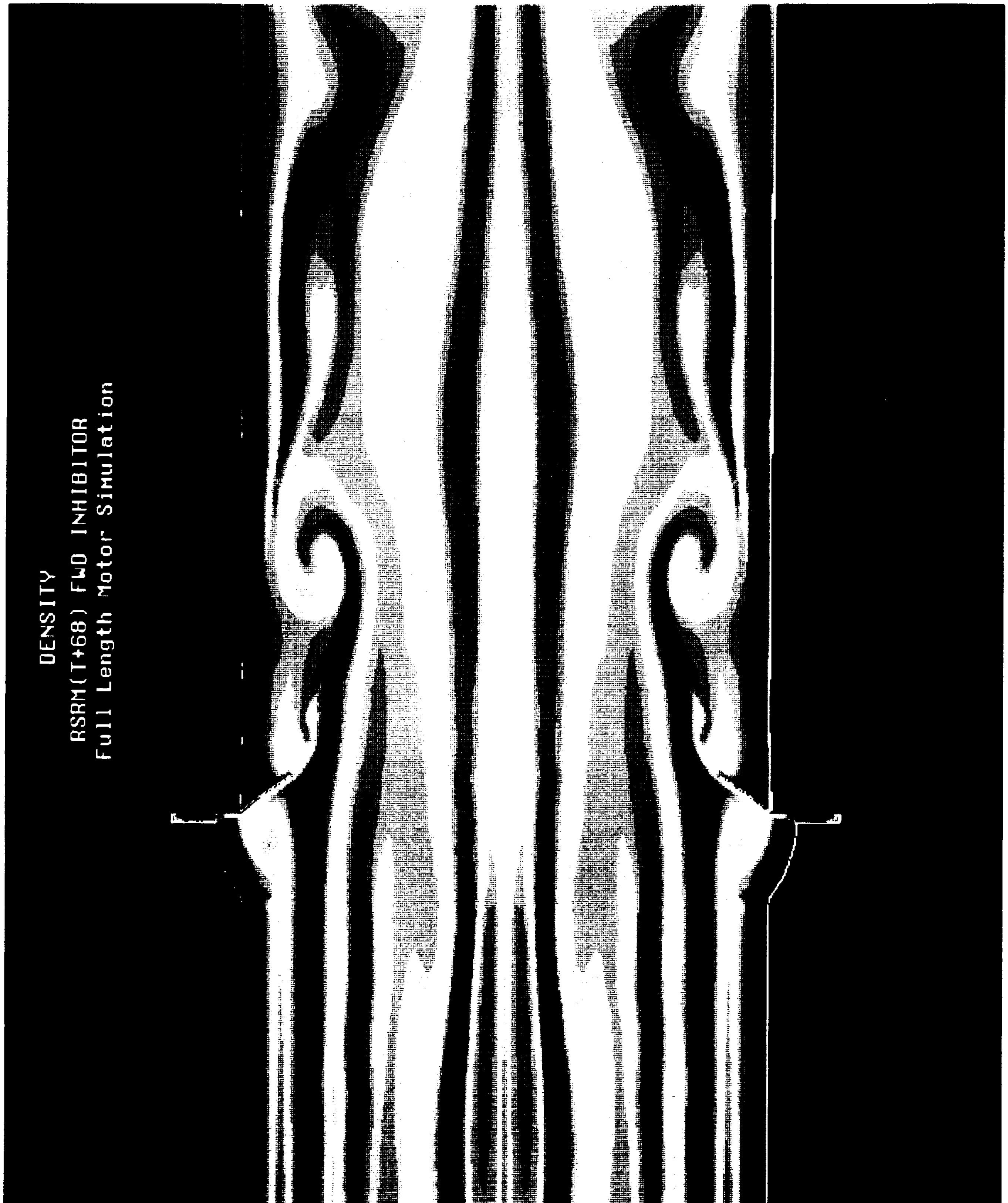
DENSITY
RSRM(T+68) FWD INHIBITOR
Full Length Motor Simulation

STS-54 RH PRESSURE PERTURBATION INVESTIGATION

CASTABLE INHIBITOR AND NBR INHIBITOR CONTACT

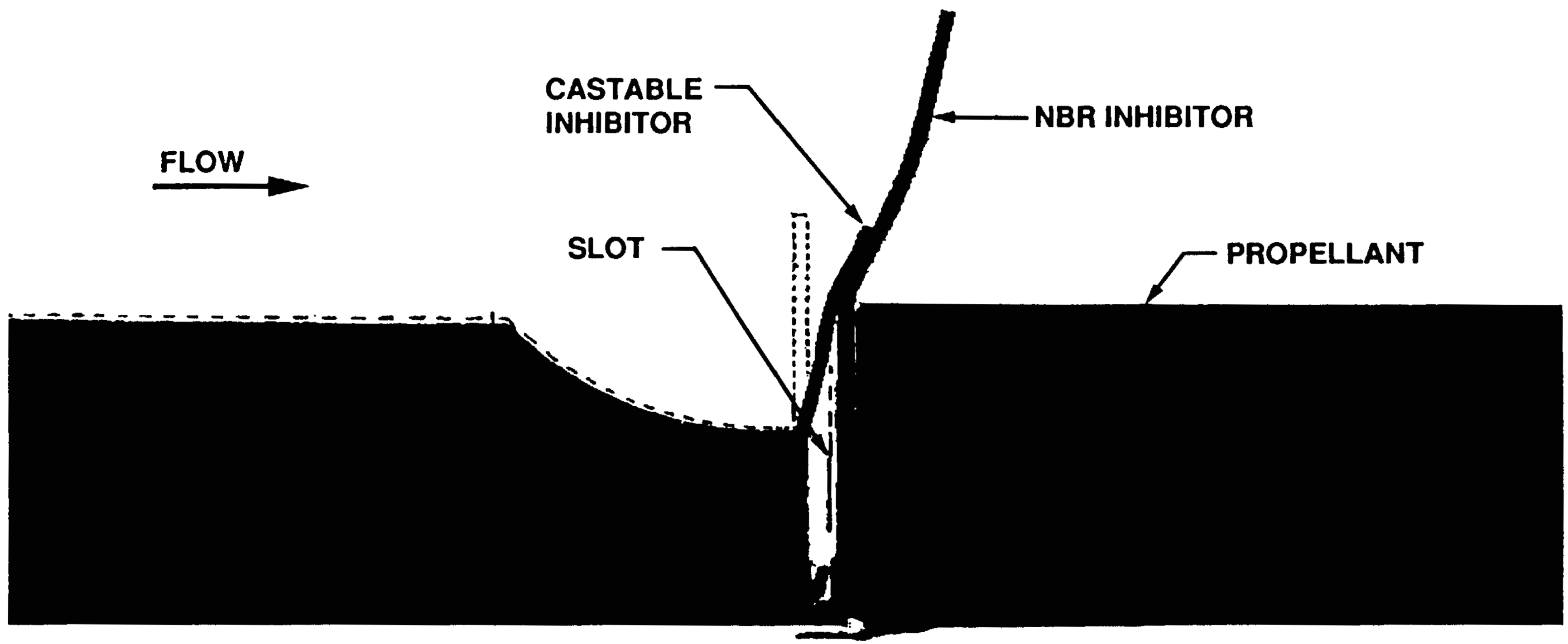

RENG002563.01

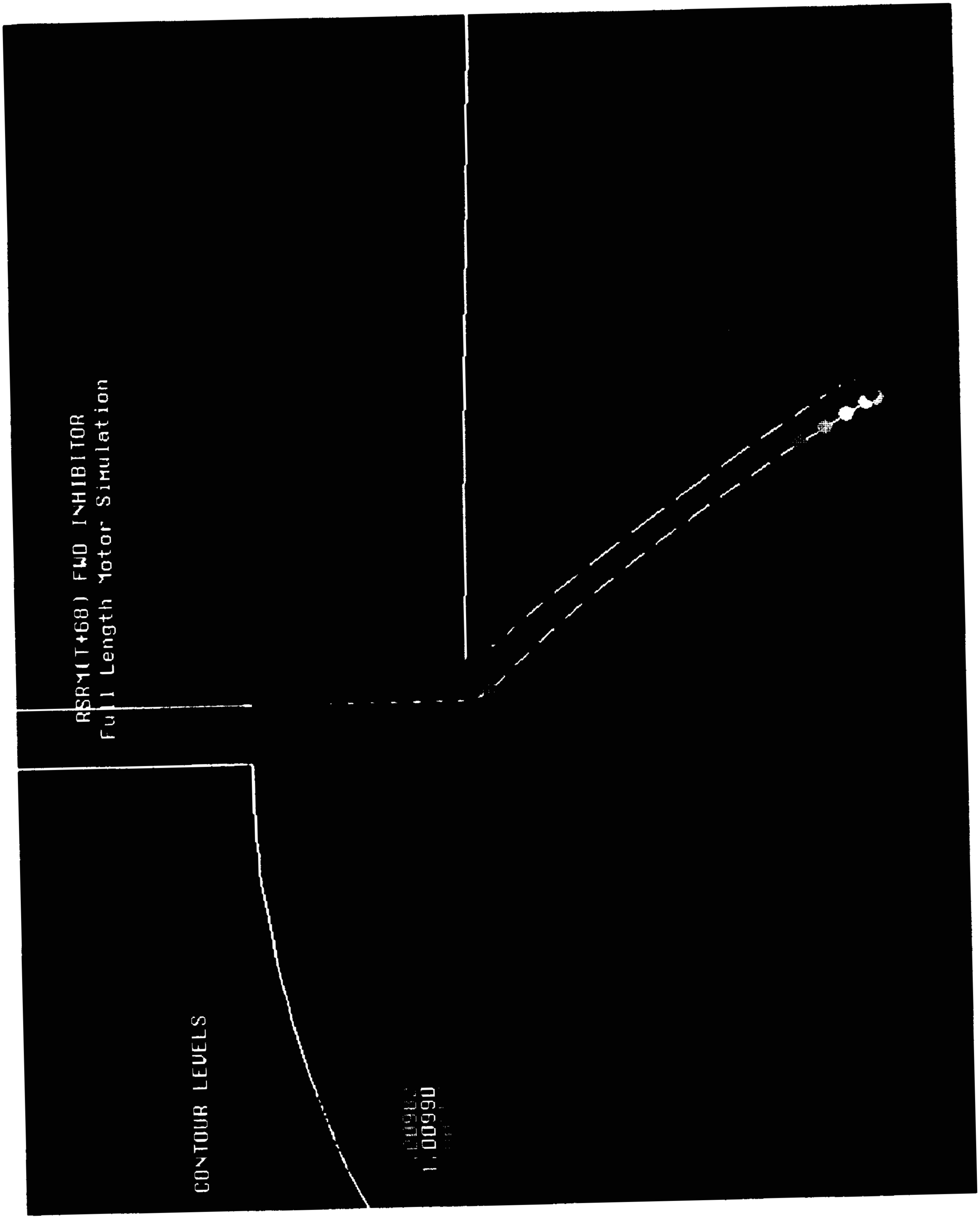

RSRM(T+68) FWD INHIBITOR
Full Length Motor Simulation
CONTOUR LEVELS
1.0099D

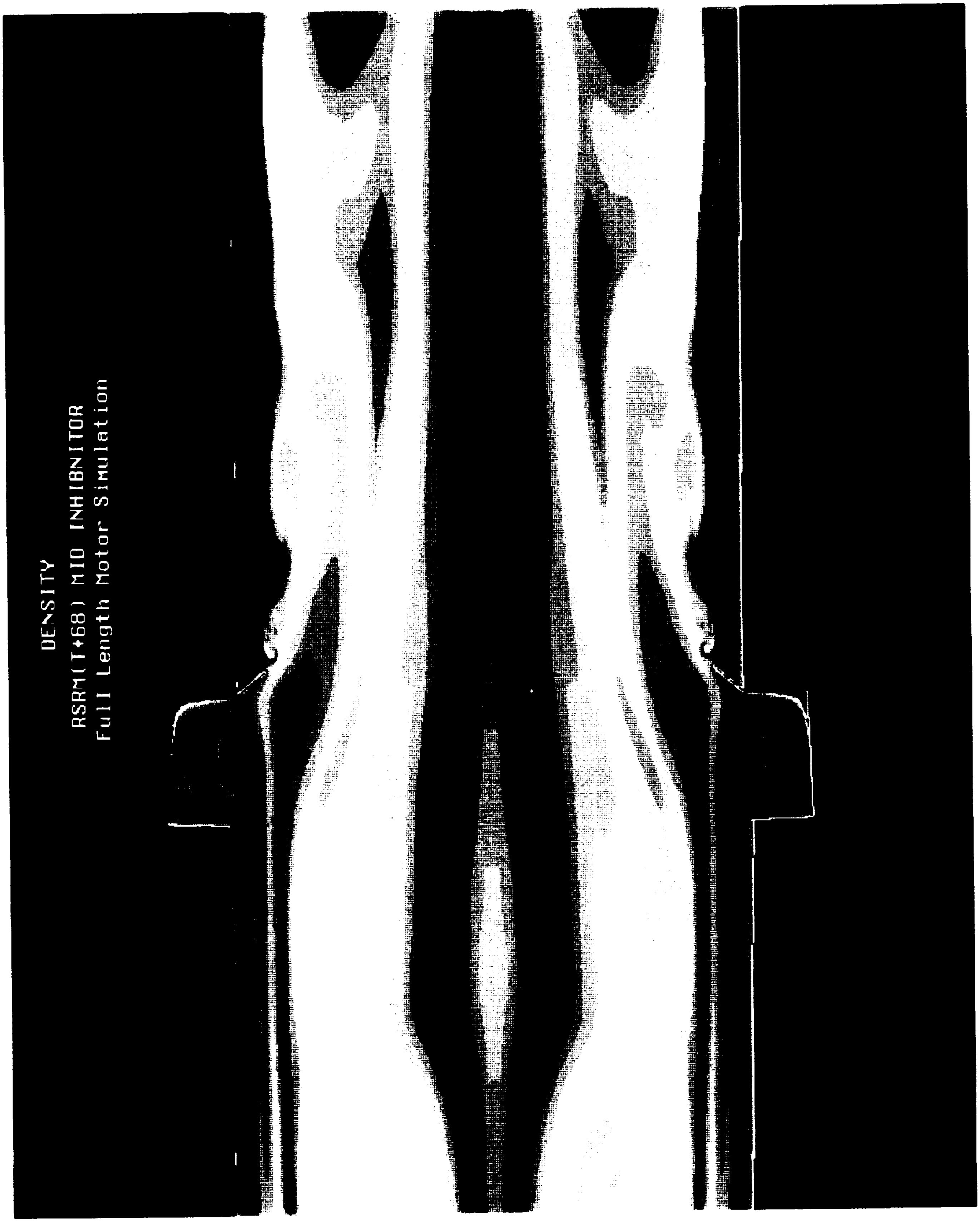
DENSITY
RSRM(T+68) MID INHIBNITOR
Full Length Motor Simulation

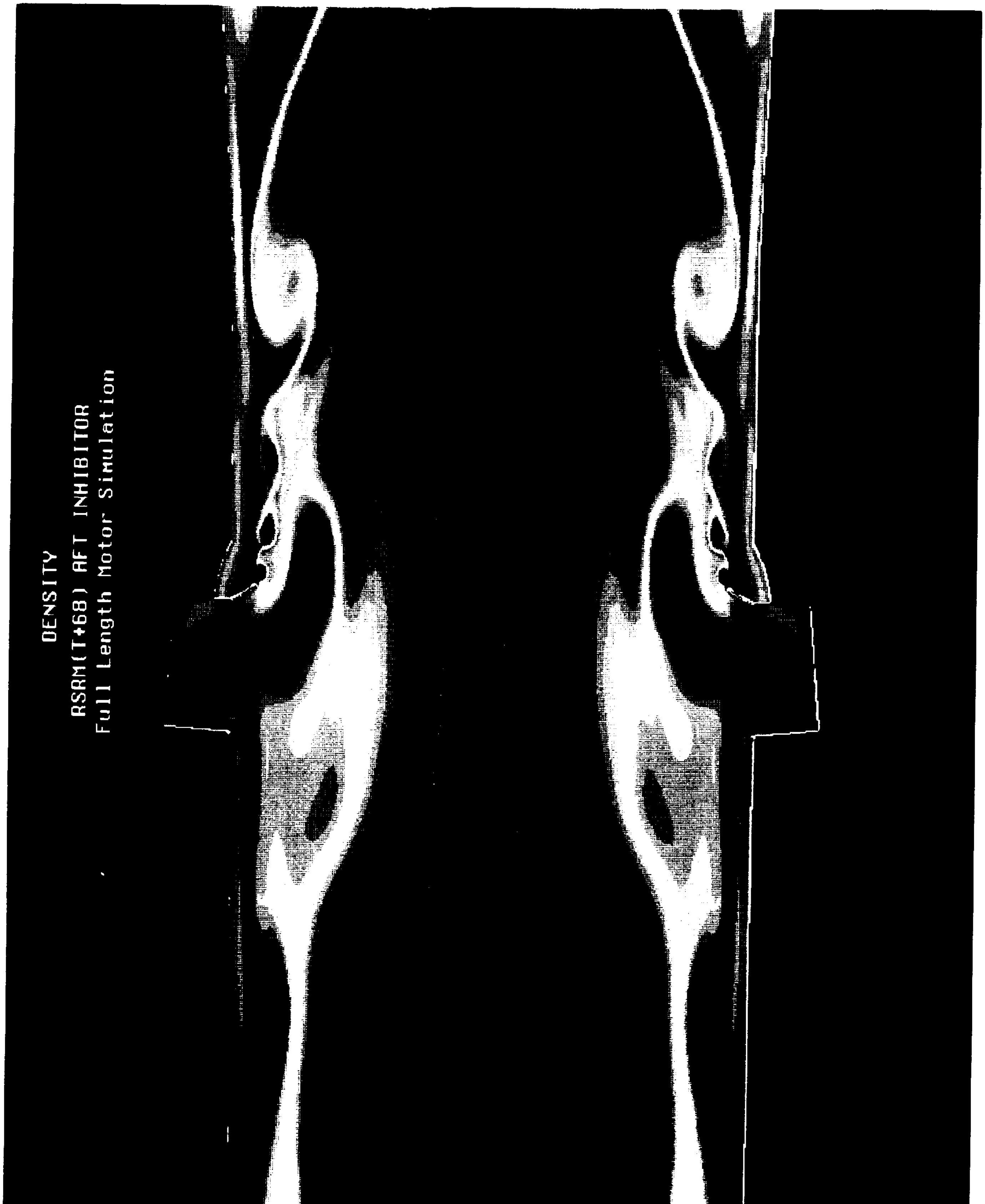
DENSITY
RSRM(T+68) AFT INHIBITOR
Full Length Motor Simulation

C-10.

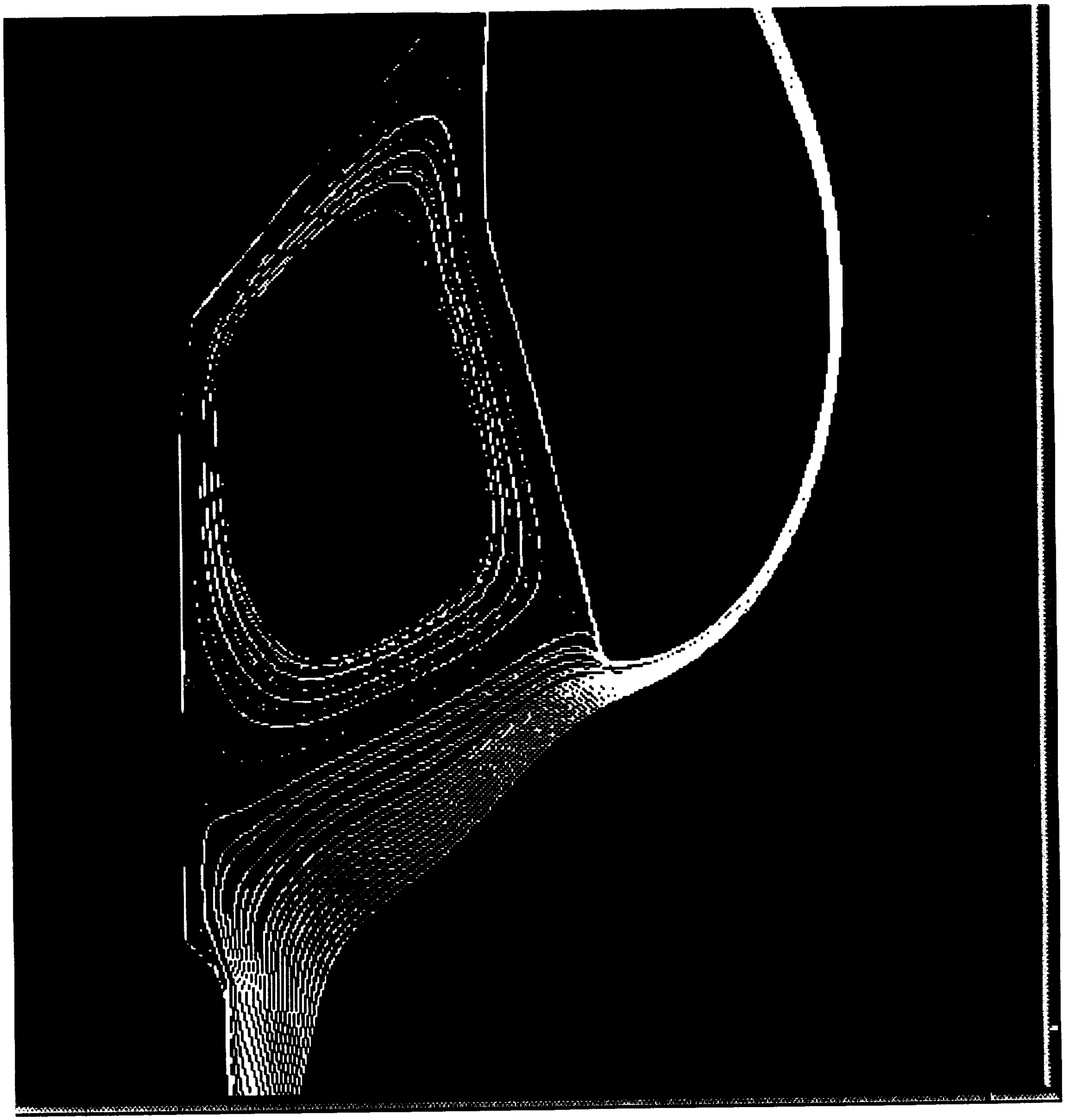

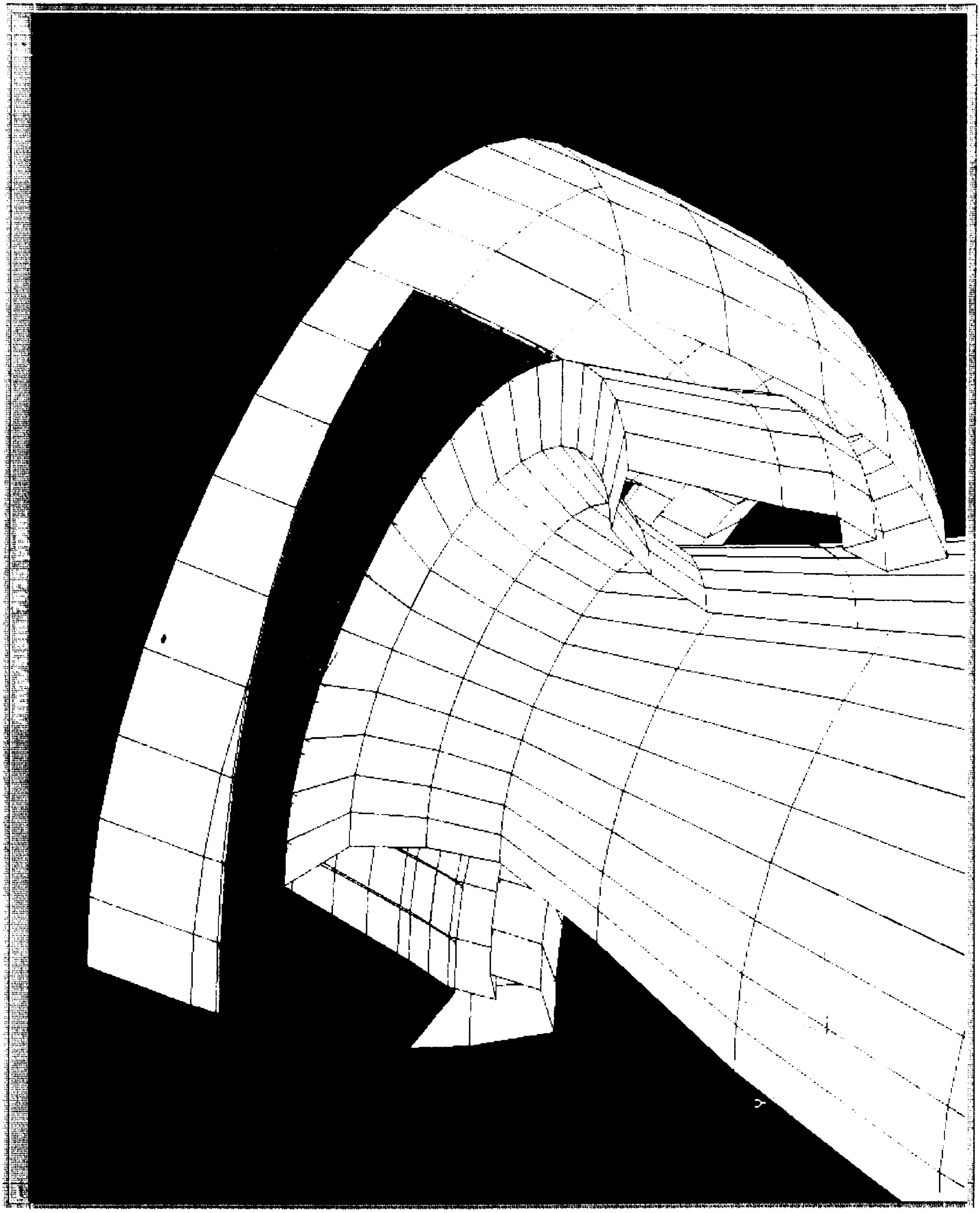

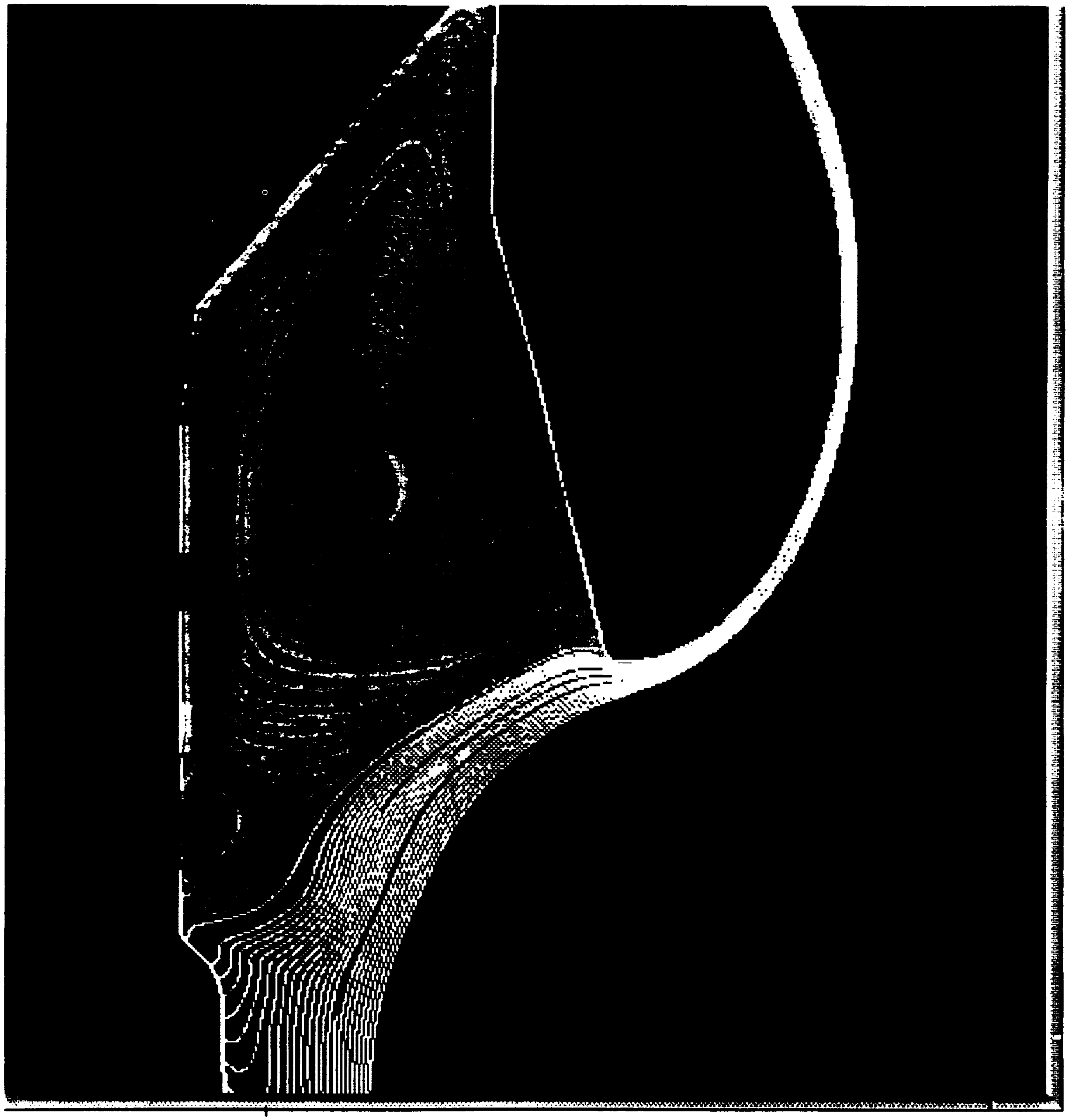

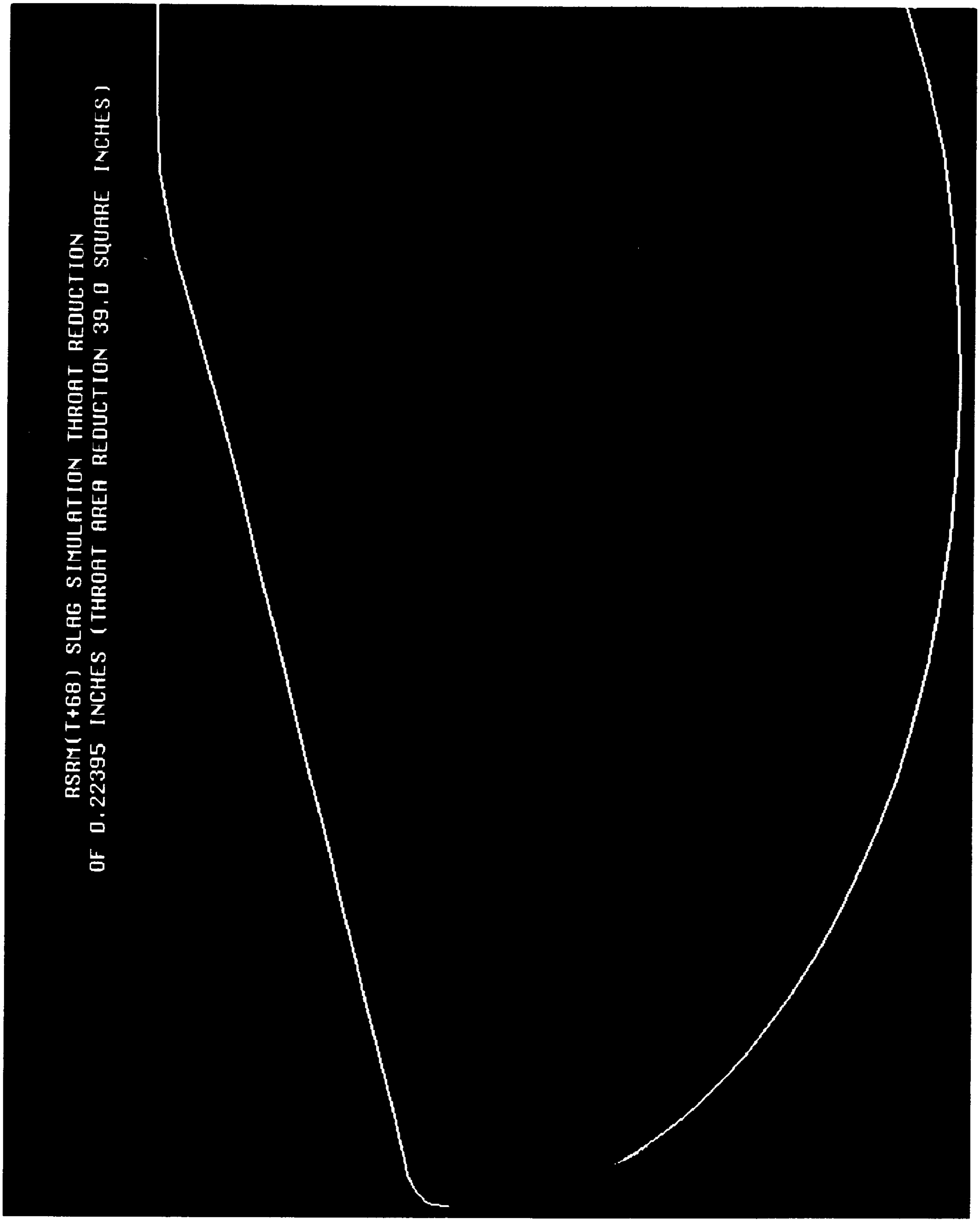
RSRM(T+68) SLAG SIMULATION THROAT REDUCTION
OF 0.22395 INCHES (THROAT AREA REDUCTION 39.0 SQUARE INCHES)

Rockwell International

Space Systems Division

TIME-ACCURATE CFD ANALYSIS OF RSRM Pc ANOMALY T + 68 SEC

Huntsville Operations

MOTOR RESPONSE TO SUDDEN 39 IN^2 THROAT AREA REDUCTION

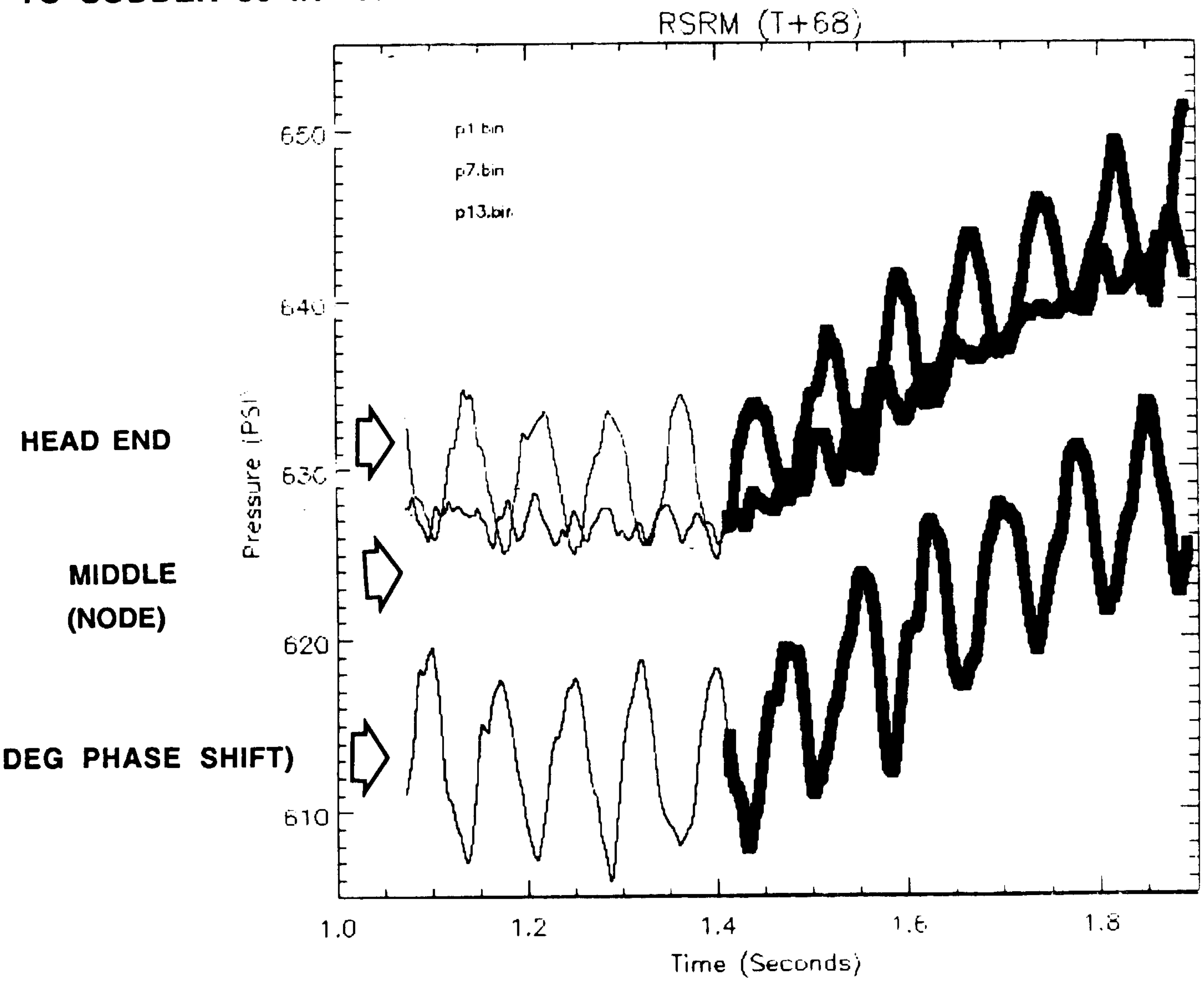

TIME-ACCURATE CFD ANALYSIS OF RSRM Pc ANOMALY T + 68 SEC

HIGH-PASS FILTERED HEAD END PRESSURE SHOWS ESSENTIALLY NO CHANGE IN LONGITUDINAL ACOUSTIC OSCILLATIONS AFTER BLOCKAGE IS INITIATED

RSRM T+68 Highpass

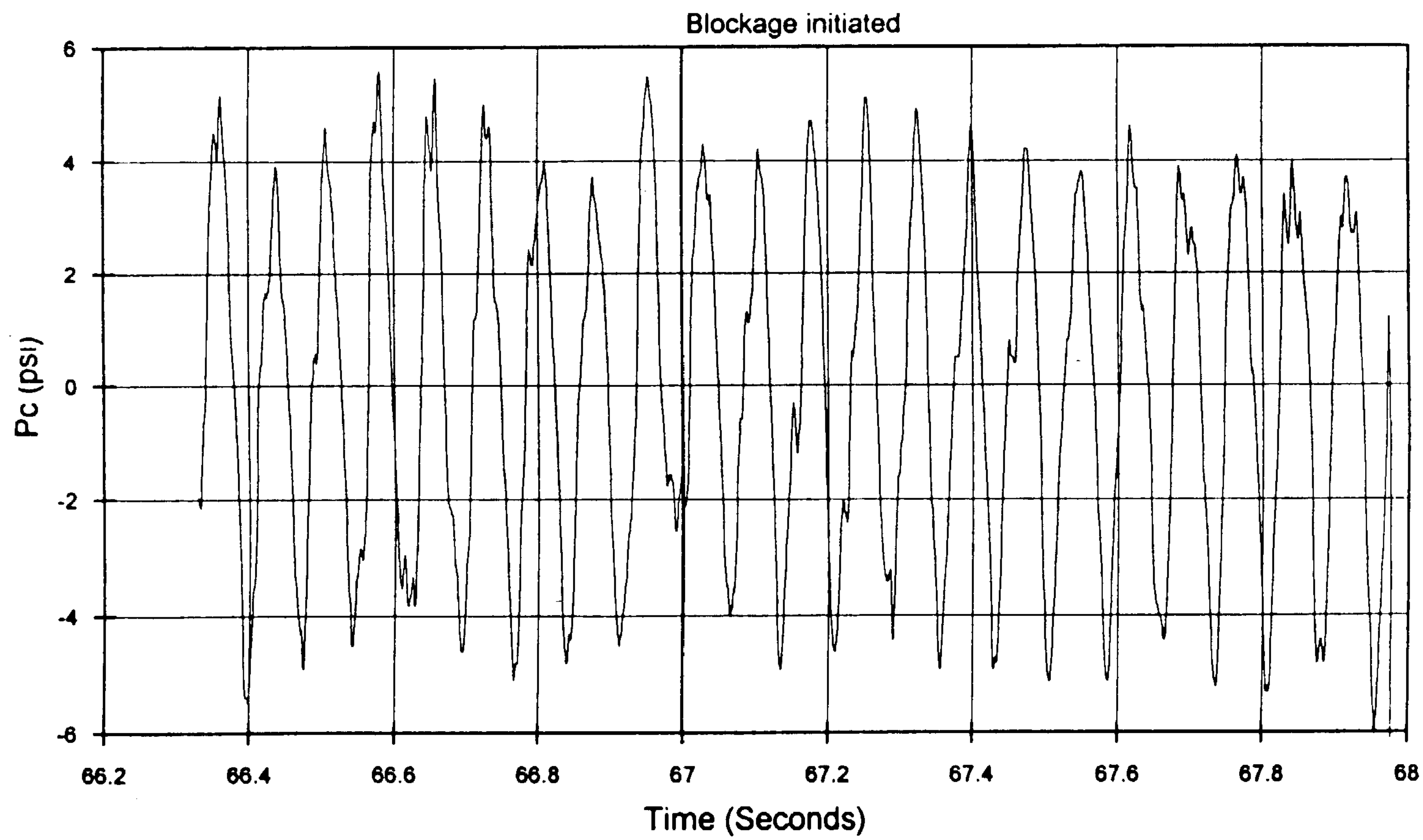

Rockwell International

Space Systems Division

TIME-ACCURATE CFD ANALYSIS OF RSRM Pc ANOMALY T + 68 SEC

Huntsville Operations

LOW-PASS FILTERED HEAD END PRESSURE RISE SHOWS CRITICALLY DAMPED RESPONSE (NO OVERSHOOT) AND T=0.293

Pc Rise Time Estimation

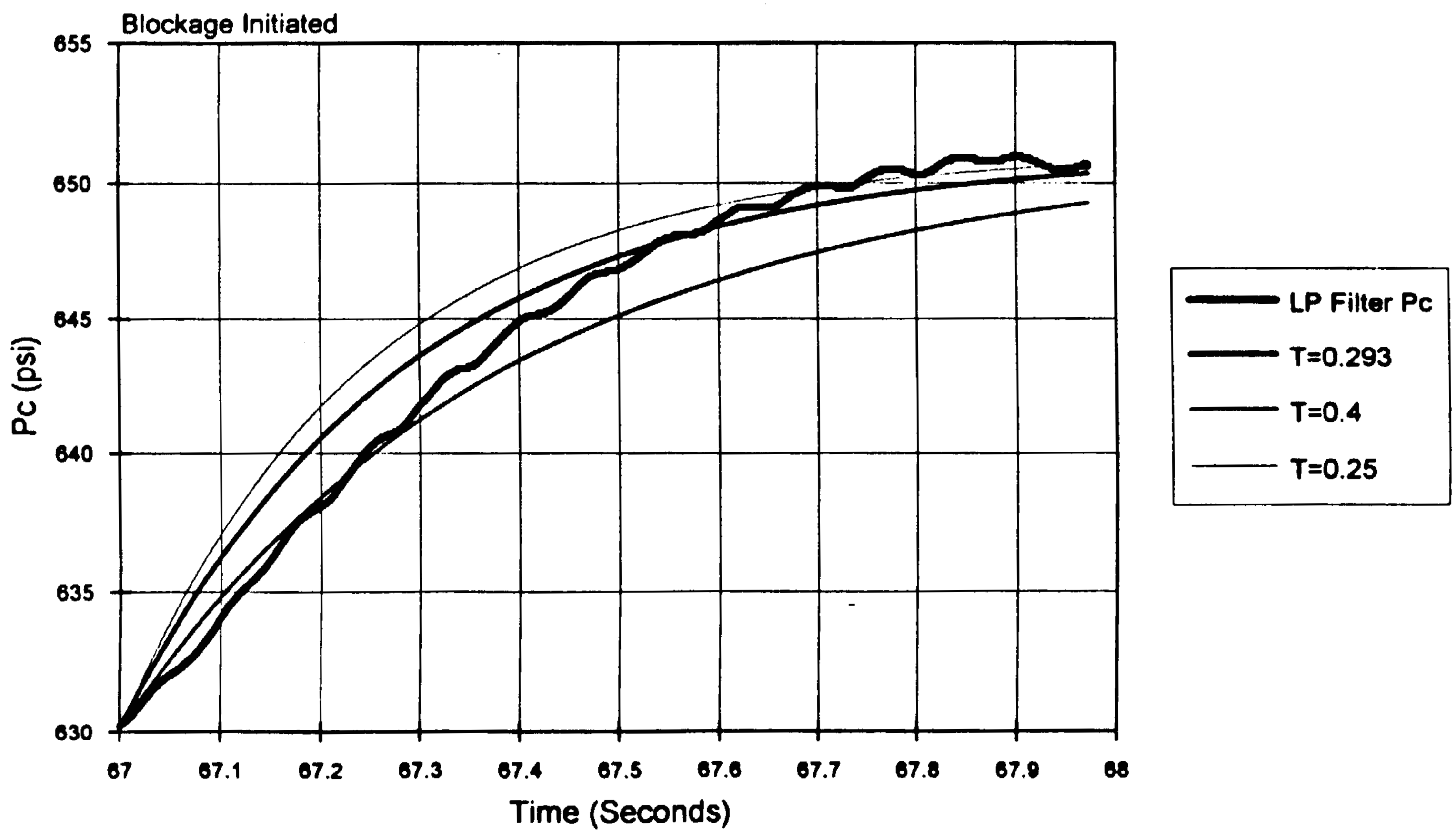

STS-54B SRM PRESSURE "SPIKE" ANOMALY INVESTIGATION

CONCLUSIONS

- FOR SUDDEN NOZZLE AREA REDUCTION, THEN RETURN TO NORMAL, WITH INHIBITOR AND SLAG POOLING GEOMETRY FIXED THERE IS NO APPARENT COUPLING WITH THE MOTOR 1L, 2L, OR 3L ACOUSTIC MODES IN THE "SPIKE" TRANSIENT

- THE "SPIKE" REACHES AN ASYMPTOTIC MAXIMUM PRESSURE AT THE HEAD END MEASUREMENT LOCATION IN 800 MSEC WITH A 300 MSEC TIME CONSTANT AND NO OVERSHOOT
  - GAS VOLUME-FILLING TIME

- FLIGHT ACCELERATION LOADS AND LARGE NOZZLE GIMBAL (>4.5 DEG) EFFECTS CAN BE ADDED FOR SIMULATING
  - SLAG SLOSHING MOTION DYNAMIC EFFECT
  - 3-D SLAG MIGRATION AS THE NOZZLE INLET MOVES DURING LARGE GIMBAL

RENG002559.02

N95- 23651

S20-34
43710
p. 14

Status of Axisymmetic CFD of an Eleven Inch Diameter Hybrid Rocket Motor

Joseph Ruf, ED32
Matthew R. Sullivan, EP54
Ten See Wang, ED32
NASA/Marshall Space Flight Center
Huntsville, AL.

Current status of a steady state, axisymmetric analysis of an experimental 11" diameter hybrid rocket motor internal flow field is given. The objective of this effort is to develop a steady state axisymmetric model of the 11" hybrid rocket motor which can be used as a design and/or analytical tool. A test hardware description, modeling approach, and future plans are given. The analysis was performed with FDNS implementing several finite rate chemistry sets. A converged solution for a two equation and five species set on a 'fine' grid is shown.

Status of Axisymmetric CFD Analysis of an Eleven Inch Diameter Hybrid Rocket Motor

Joseph H. Ruf
Matthew R. Sullivan
Ten See Wang
Marshall Space Flight Center

Status of Axisymmetric CFD Analysis of an Eleven Inch Diameter Hybrid Rocket Motor

- OBJECTIVE
- BACKGROUND
- APPROACH
- STATUS
- FUTURE PLANS

OBJECTIVE

- Develop a steady state axisymmetric model of 11" hybrid rocket motor which can be used as a design and analytical tool.

BACKGROUND

- 11" Hybrid Rocket Motor - solid fuel, gaseous oxidizer
  - fuel
    - solid grain 60% HTPB, 40 % escorez
    - initially at ambient temperature
  - oxidizer
    - GOX injected at ambient temperature
    - pressures of 300 to 1000 psig
  - geometry
    - 11 inch diameter casing, various port designs
    - total fuel grain length varies, 34, 68 or 102 inches

- 20 tests have been conducted with various configurations
  - Modeling test # 2 conditions
    - GOX injection pressure = 300 psi, flow rate = 6.8 lbm/s
    - GOX injected through 12 radial ports
    - overall o/f = 3.04
    - run duration 9.5 seconds
    - nozzle area ratio of 1.56

Cross Section of 11" Hybrid Rocket Motor

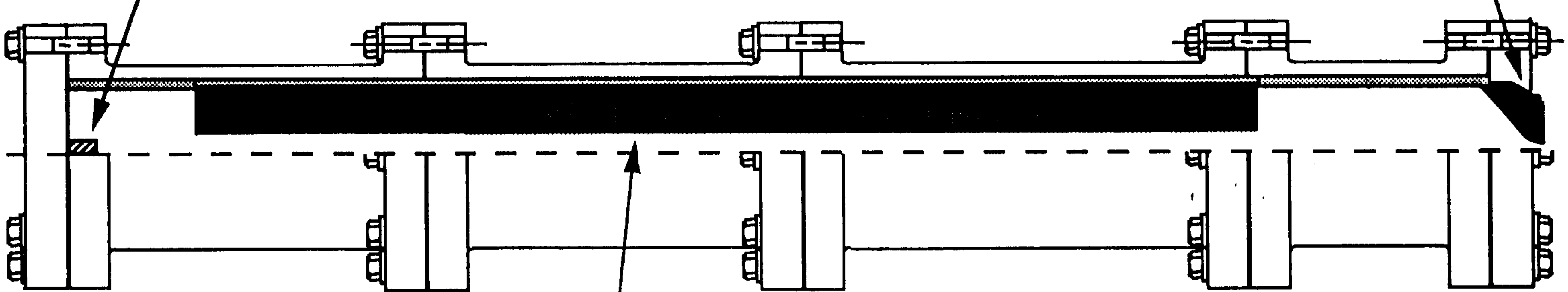

APPROACH

- Axisymmetric, three zone model
  - steady state, early in test
  - GOX injection ports modeled as equivalent area circumferential slot
    300 psia, flow rate=6.8 lbm/s, temperature=517 deg R
  - fuel grain modeled as blowing wall, uniform sublimation rate
    flow rate=2.27 lbm/s, temperature=1458 deg R

- Two grids implemented
  - 9800 and 21600 points

- Solution Procedure
  - begin with cold GOX, hot fuel, w/o reaction, subsonic flow
  - turn on chemistry, supersonic exit

- Six chemistry models tried
  - 5 species, 2 equations up to 11 species, 17 equations

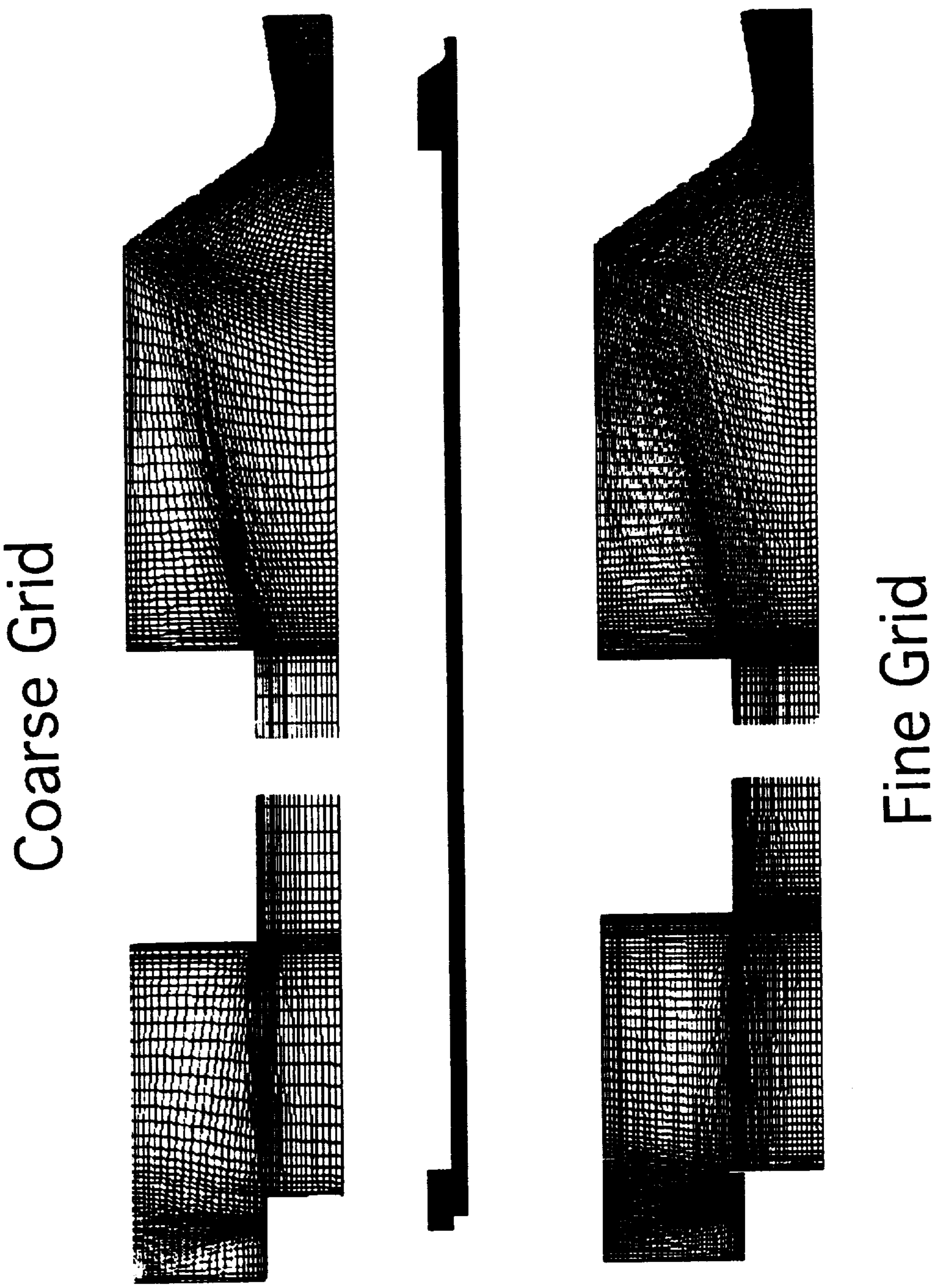
Coarse Grid
Fine Grid

STATUS

- Converged solutions obtained on both grids, grid dependent
- Flow field appears reasonable
  - mass balanced solutions
  - some zone interface effects at zone 1 and 2 boundary
- Temperature is too high, but trends appear correct

VELOCITY COLORED BY VELOCITY MAGNITUDE
Forward Mixing Chamber
(ft/s)

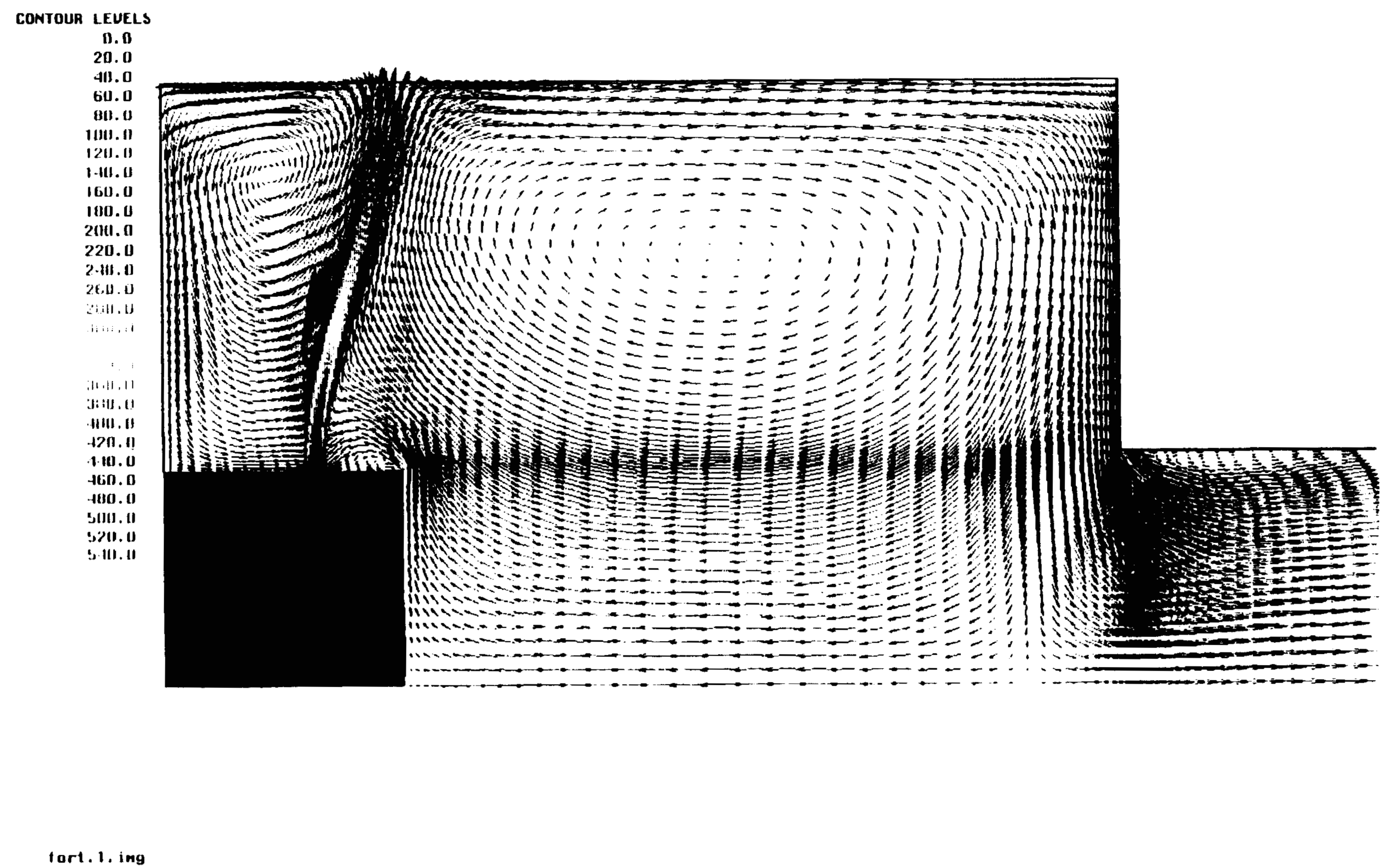

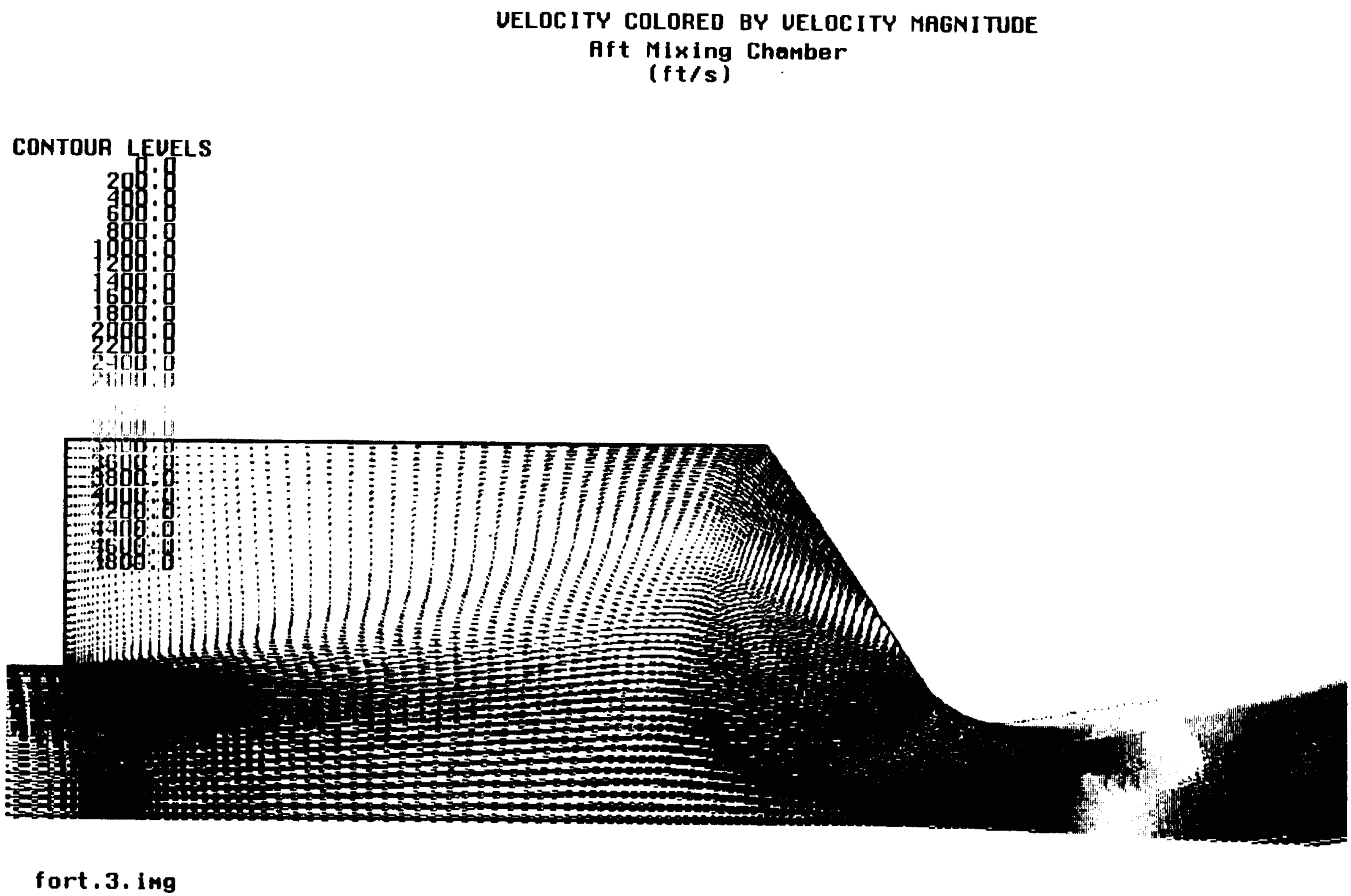

ORIGINAL PAGE IS
OF POOR QUALITY

Fine Grid Results

VELOCITY MAGNITUDE

PRESSURE

TEMPERATURE

Fine Grid Results

Mass Factions for a Two Equation Finite Rate Model

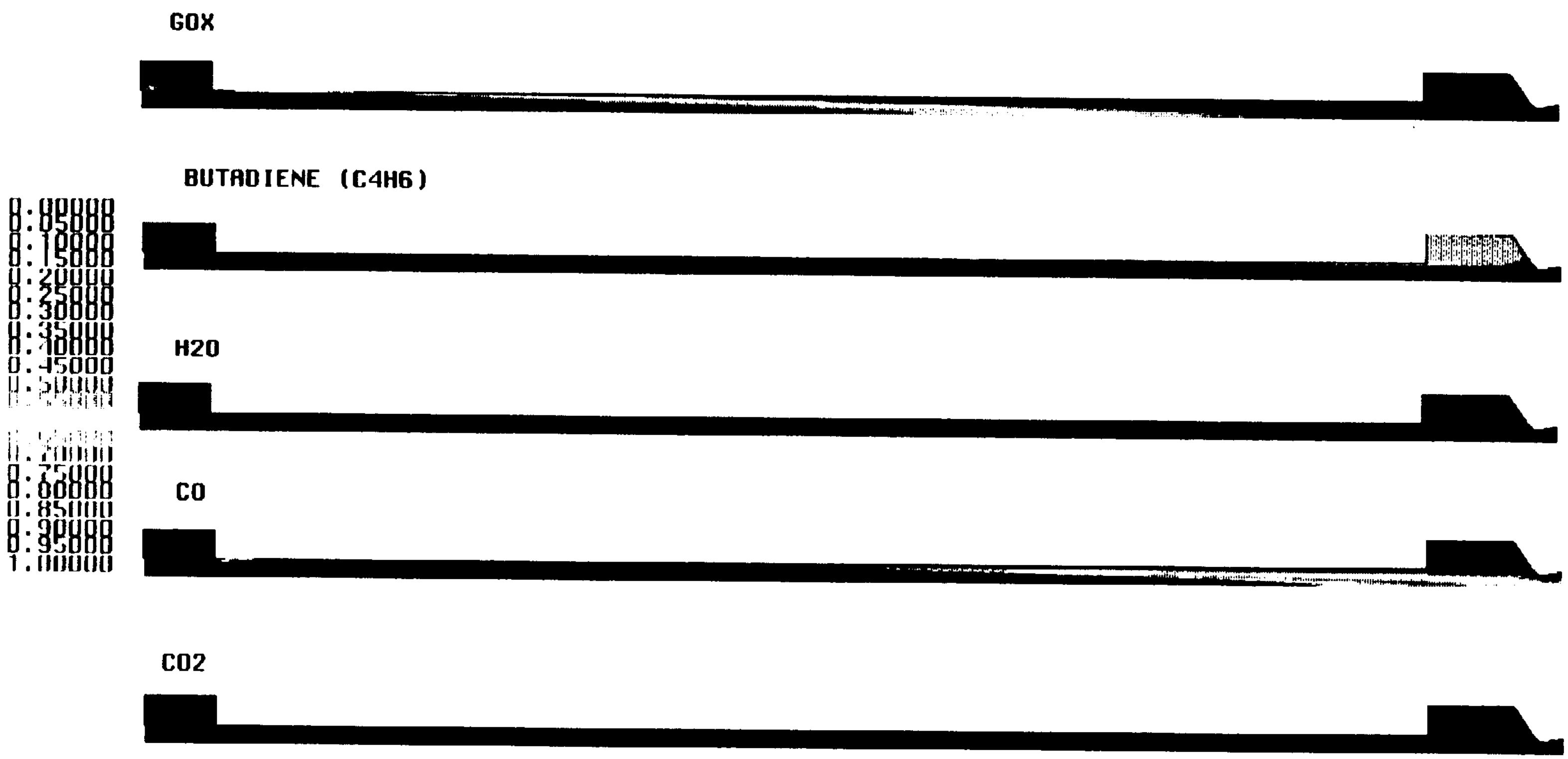

FUTURE PLANS

- determine 'best' chemistry model
- obtain a grid independent solution
- implement variable fuel sublimation rate in axial direction
- match limited test data

N95- 23652

Validation of a Computational Fluid Dynamics (CFD) Code for Supersonic Axisymmetric Base Flow

P. K. Tucker

NASA/Marshall Space Flight Center
Marshall Space Flight Center, AL

Abstract

The ability to accurately and efficiently calculate the flow structure in the base region of bodies of revolution in supersonic flight is a significant step in CFD code validation for applications ranging from base heating for rockets to drag for protectives.

The FDNS code is used to compute such a flow and the results are compared to benchmark quality experimental data. Flowfield calculations are presented for a cylindrical afterbody at $M = 2.46$ and angle of attack $\alpha = 0$. Grid independent solutions are compared to mean velocity profiles in the separated wake area and downstream of the reattachment point. Additionally, quantities such as turbulent kinetic energy and shear layer growth rates are compared to the data. Finally, the computed base pressures are compared to the measured values. An effort is made to elucidate the role of turbulence models in the flowfield predictions. The level of turbulent eddy viscosity, and its origin, are used to contrast the various turbulence models and compare the results to the experimental data.

Validation of a CFD Code for Supersonic Axisymmetric Afterbody Flow

Kevin Tucker

1993 CFD Conference

OVERVIEW

- Motivation
- Objectives
- Experimental Dataset
- Summary of Cases
- Results
  - Flow Structure
  - Data Comparisons
- Conclusion
  - Summary
  - Future Work

MOTIVATION

- Stemmed from NLS base heating study
- Need to predict base pressures in recirculating flows
- One step in a building-block validation approach for base flows

OBJECTIVES

- Determine factors which influence base pressure predictions
- Elucidate role of turbulence models for compressible, recirculating flows
- Provide guidance for 3-D base flow calculations

EXPERIMENTAL DATASET

UIUC Supersonic Afterbody (Dutton & Herrin)

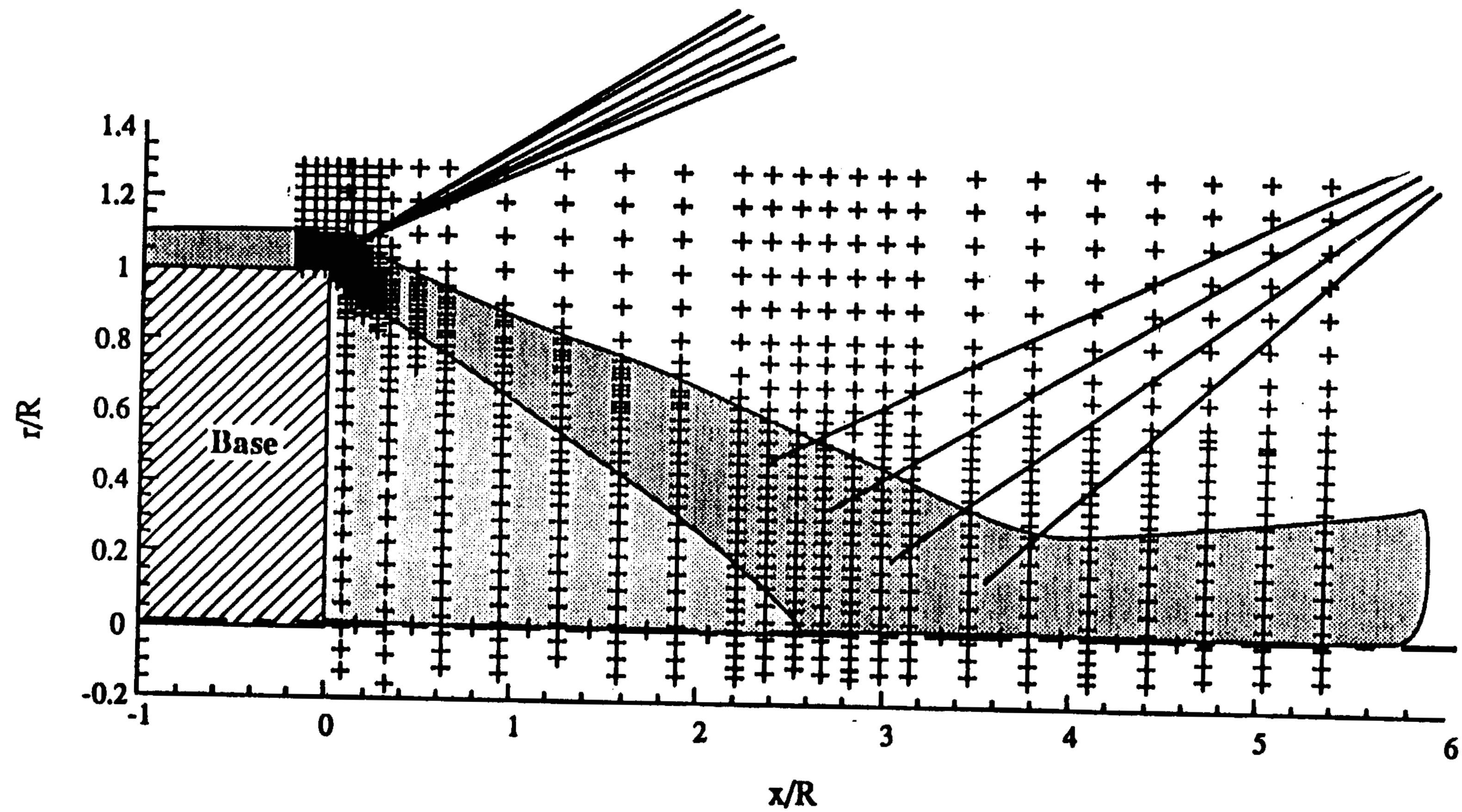

EXPERIMENTAL DATASET

Freestream Properties

- M=2.46
- U=1860.2 ft/sec
- P_o=74.7 psia
- T_o=532.8 R
- Re=1.6 e+7/ft

Boundary Layer Profile

- Boundary layer velocity profile-Sun & Childs curve fit for turbulent, compressible boundary layers
- Temperature-recovery factor of 0.89 (Kays & Crawford)
- Pressure-assumed constant static pressure thru boundary layer
- Density-calculated via equation of state
- Turbulent kinetic energy-interpolated from data onto grid

INLET VELOCITY PROFILE

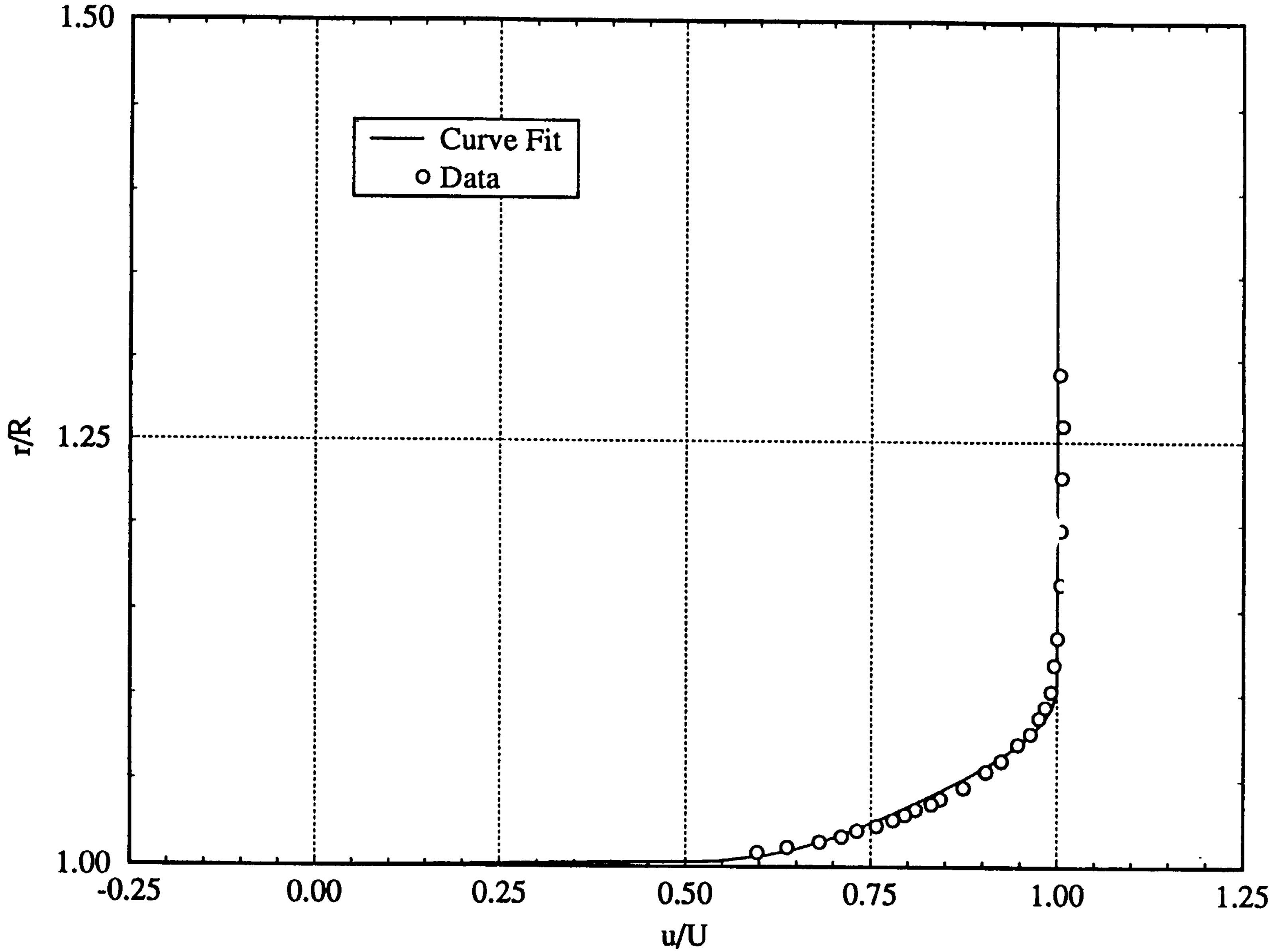

INLET TURBULENT KINETIC ENERGY PROFILE

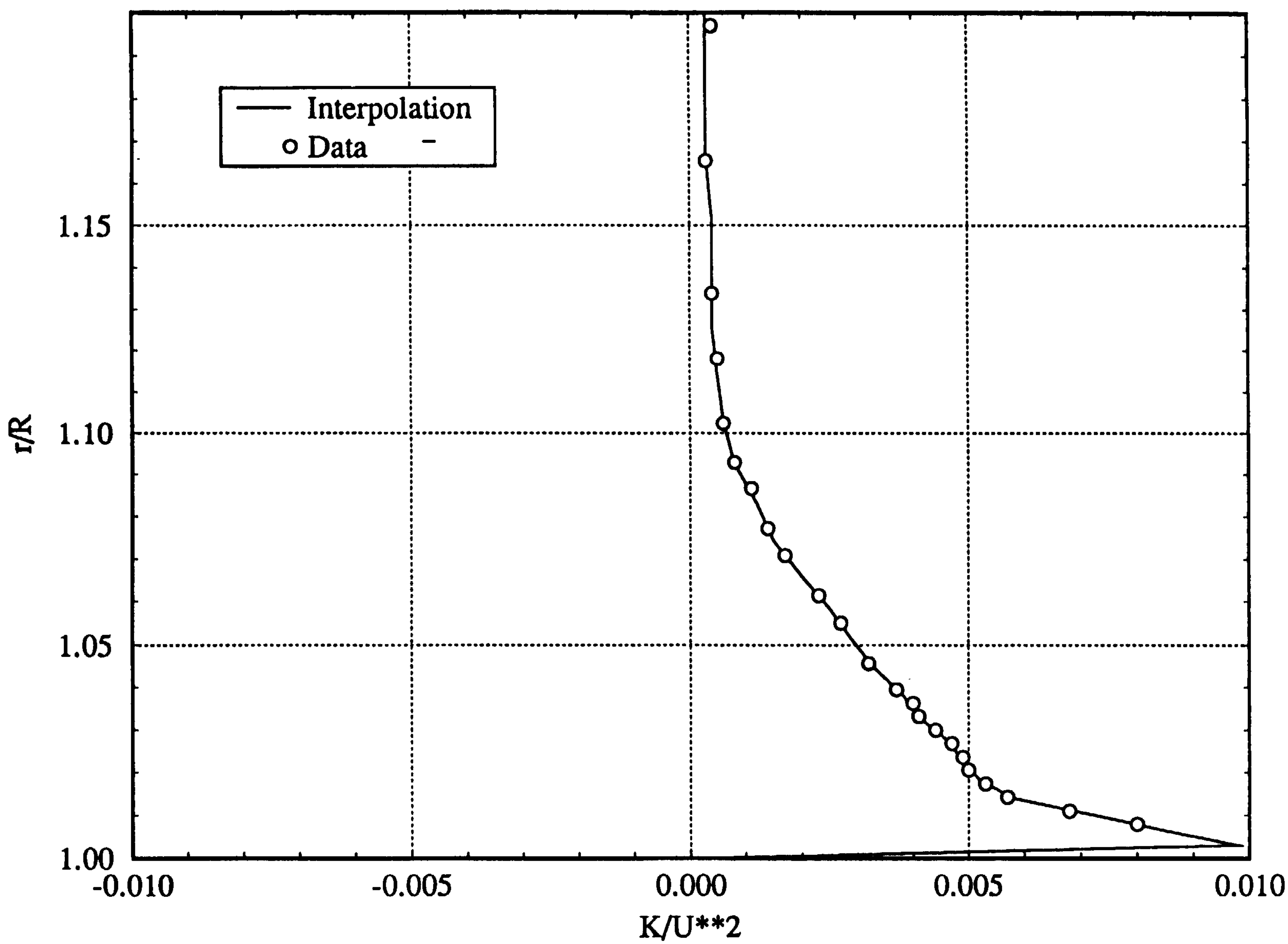

SUMMARY of CASES/RESULTS

Differencing Scheme	Turbulence Model	Reattachment	Avg. Base Press.
First order upwind	Standard k-e	-0.180	-0.310
First order upwind	Standard k-e, k-corr	0.000	-0.202
First order upwind	Standard k-e, e-corr	0.022	-0.186
First order upwind	Extended k-e	-0.045	-0.218
First order upwind	Extended k-e, k-corr	0.112	-0.140
First order upwind	Extended k-e, e-corr	0.131	-0.128
Second order upwind	Standard k-e, e-corr	0.052	-0.145
Second order upwind	Extended k-e, e-corr	0.191	-0.061
Second order central	Standard k-e, e-corr	0.052	-0.147
Second order central	Extended k-e, e-corr	0.180	-0.065
Third order upwind	**Standard k-e**	**-0.165**	**-0.300**
Third order upwind	Standard k-e, k-corr	0.034	-0.172
Third order upwind	Standard k-e, e-corr	0.052	-0.147
Third order upwind	Extended k-e	-0.008	-0.186
Third order upwind	**Extended k-e, k-corr**	**0.150**	**-0.087**
Third order upwind	Extended k-e, e-corr	-0.179	-0.065

TURBULENCE MODELS

- Standard k-ε model

$$\frac{\partial \rho k}{\partial t} + \frac{\partial}{x_i}\left(\rho u_i k + \mu_L \frac{\partial k}{\partial x_i}\right) = \rho \ (Pr - \varepsilon)$$

$$\frac{\partial \rho k}{\partial t} + \frac{\partial}{\partial x_i}\left(\rho u_i \varepsilon + \mu_L \frac{\partial \varepsilon}{\partial x_i}\right) = \rho \frac{\varepsilon}{k} \ (C_1 Pr - C_2 \varepsilon)$$

$$Pr = \frac{\mu_T}{\rho}\left\{\frac{1}{2}\left(\frac{\partial u_j}{\partial x_i} + \frac{\partial u_i}{\partial x_j}\right)^2 - \frac{2}{3}\left(\frac{\partial u_k}{\partial x_k}\right)^2\right\}$$

$$C_1 = 1.43 \quad C_2 = 1.92 \quad S_{C_k} = 1.0 \quad S_{C_\varepsilon} = 1.92$$

5-19714

TURBULENCE MODELS

- **Extended k-ε model**

$$C_1 = 1.15 + 0.25\left(\frac{Pr}{\varepsilon}\right)$$

$$C_2 = 1.90$$

$$S_{c_k} = 0.89$$

$$S_{c_\varepsilon} = 1.15$$

- k-correction

$\varepsilon = \left(1 + M_t^2\right)$ replaces ε in the k-eqn source term

where $M_t^2 = \frac{k}{a^2}$

GRID

AXISYMMETRIC AFTERBODY

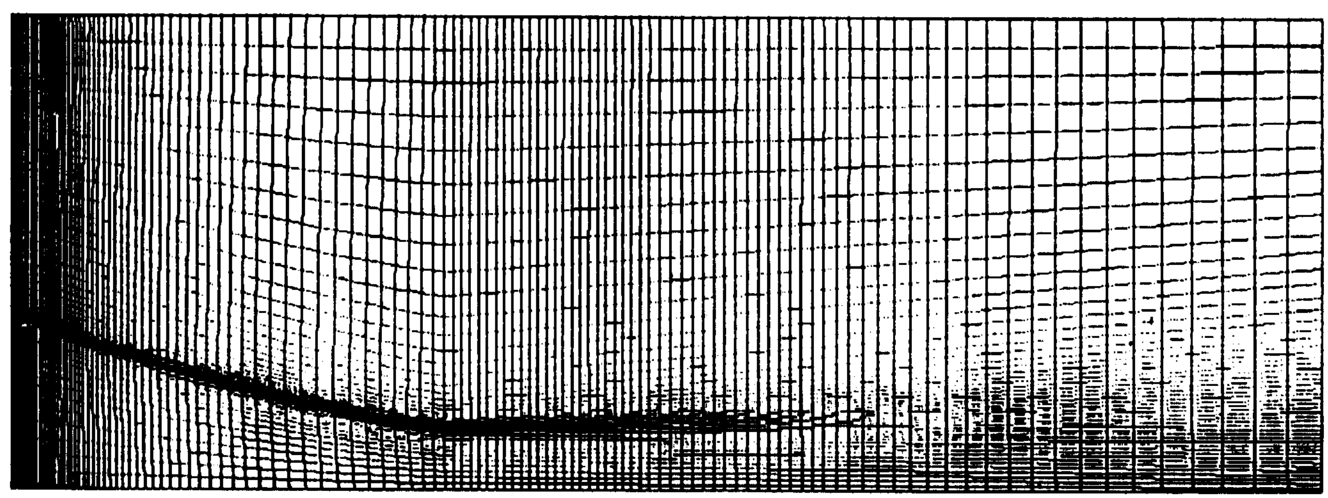

q17.8.img

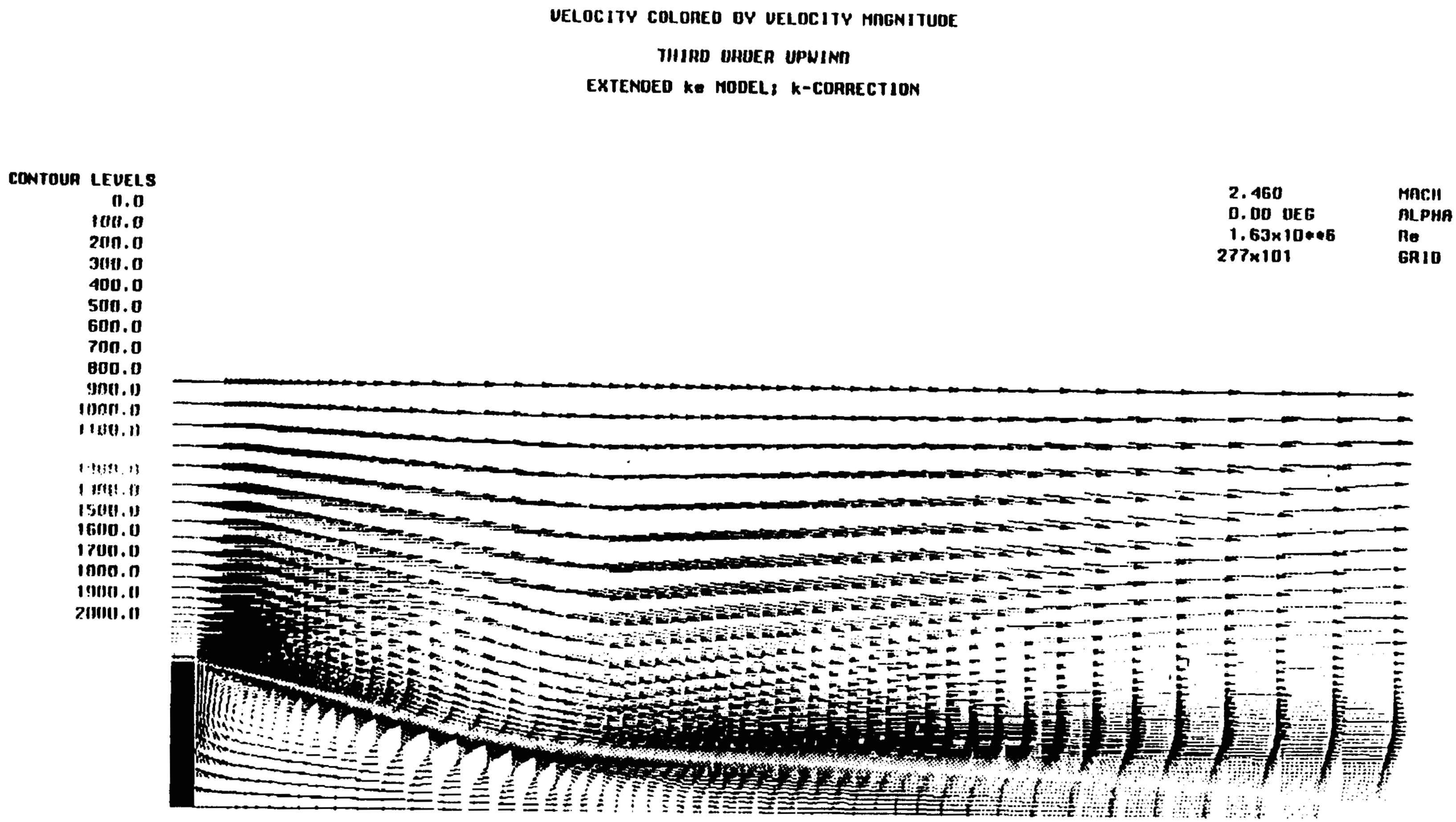
VELOCITY COLORED BY VELOCITY MAGNITUDE
THIRD ORDER UPWIND
EXTENDED ke MODEL; k-CORRECTION
CONTOUR LEVELS
0.0
100.0
200.0
300.0
400.0
500.0
600.0
700.0
800.0
900.0
1000.0
1100.0
1500.0
1600.0
1700.0
1800.0
1900.0
2000.0
2.460 MACH
0.00 DEG ALPHA
1.63x10**6 Re
277x101 GRID

q17.2.img

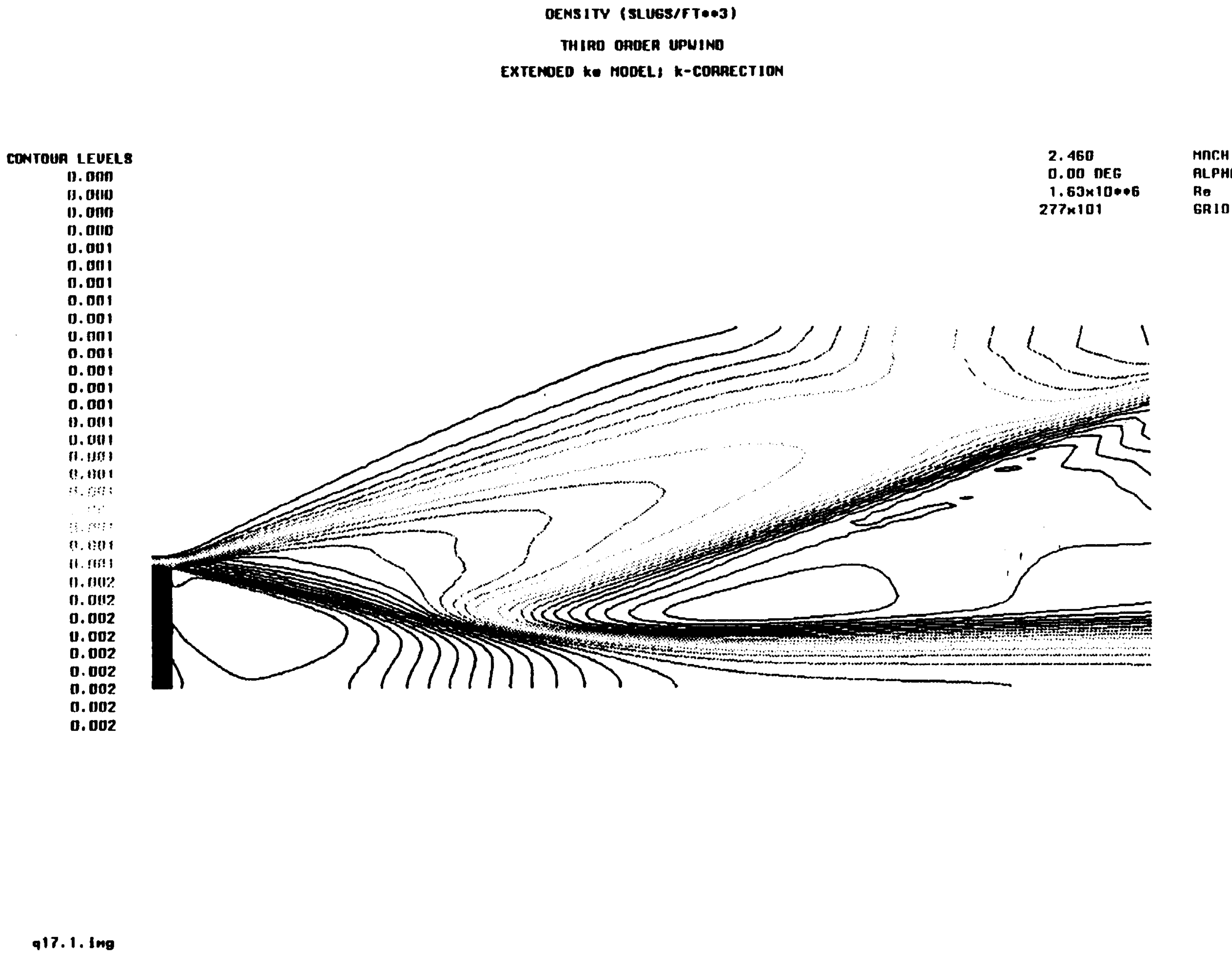

ORIGINAL PAGE IS
OF POOR QUALITY

PRESSURE (LB/FT**2)

THIRD ORDER UPWIND

EXTENDED ke MODEL; k-CORRECTION

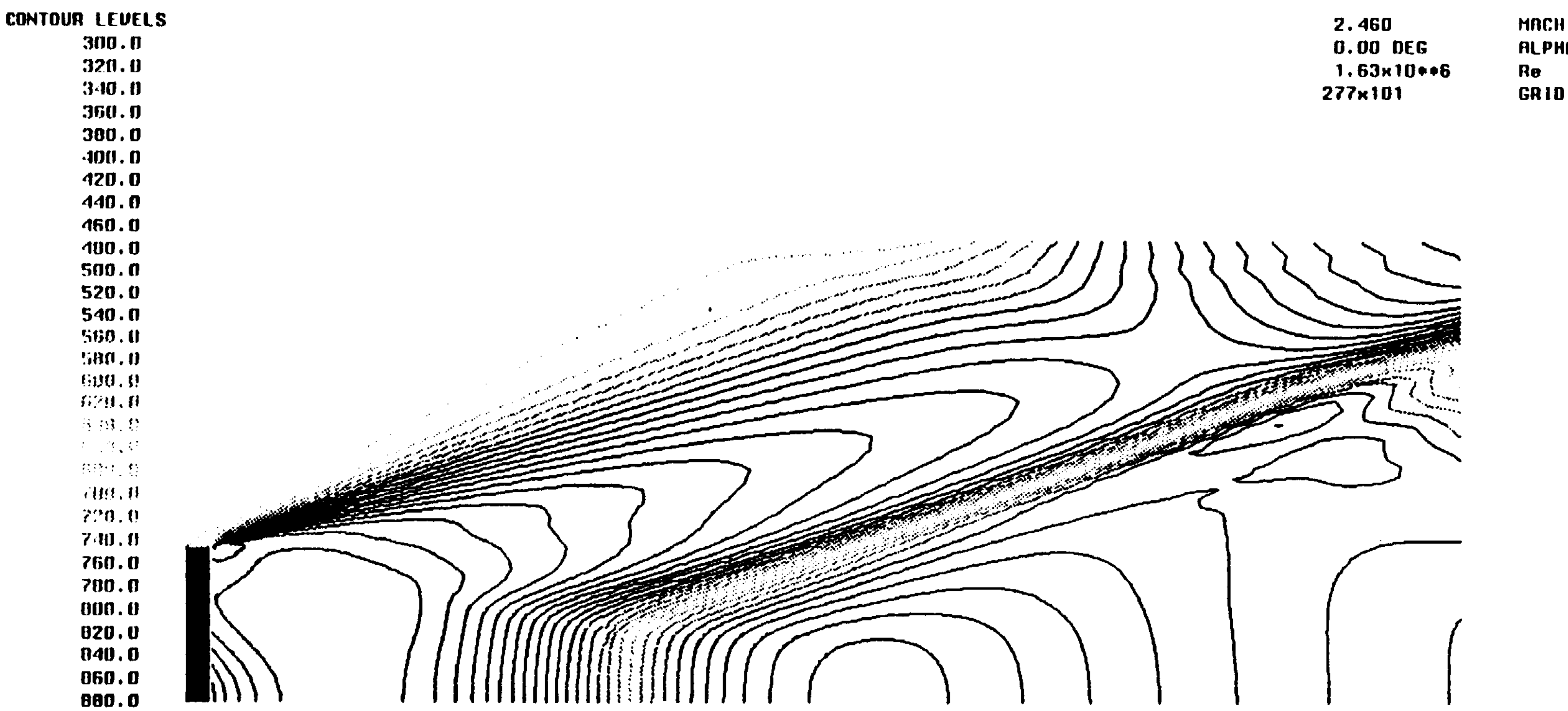

q17.3.img

MACH NUMBER

THIRD ORDER UPWIND

EXTENDED ke MODEL; k-CORRECTION

CONTOUR LEVELS
0.00
0.10
0.20
0.30
0.40
0.50
0.60
0.70
0.80
0.90
1.00
1.10
1.20
1.30
1.40
1.50
1.60
1.70
1.80
1.90
2.00
2.10
2.20
2.30
2.40
2.50
2.60
2.70
2.80
2.90

2.460	MACH
0.00 DEG	ALPHA
1.63x10**6	Re
277x101	GRID

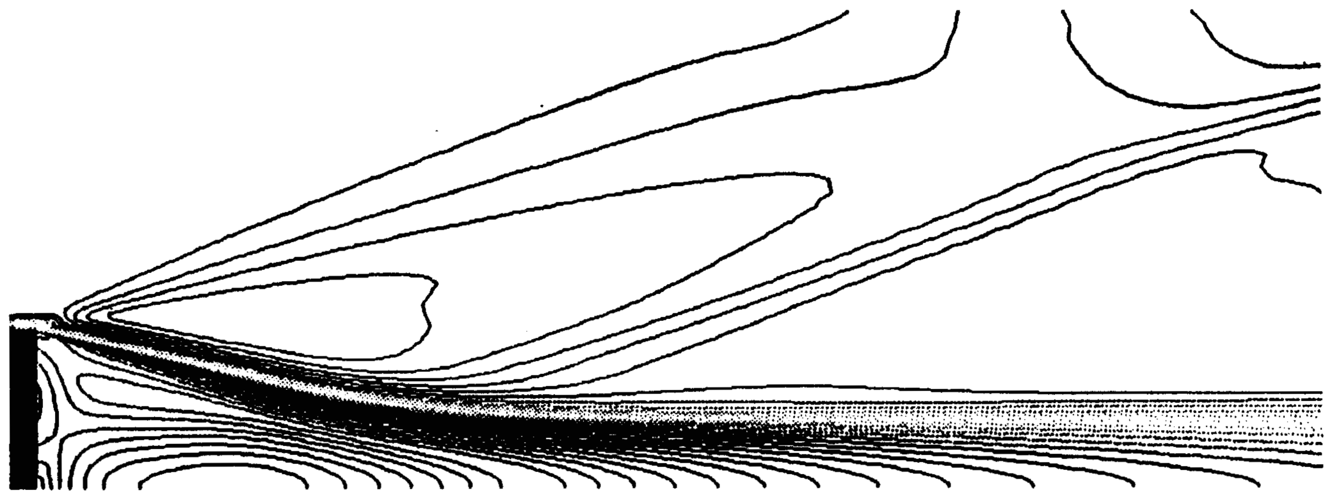

q17.5.img

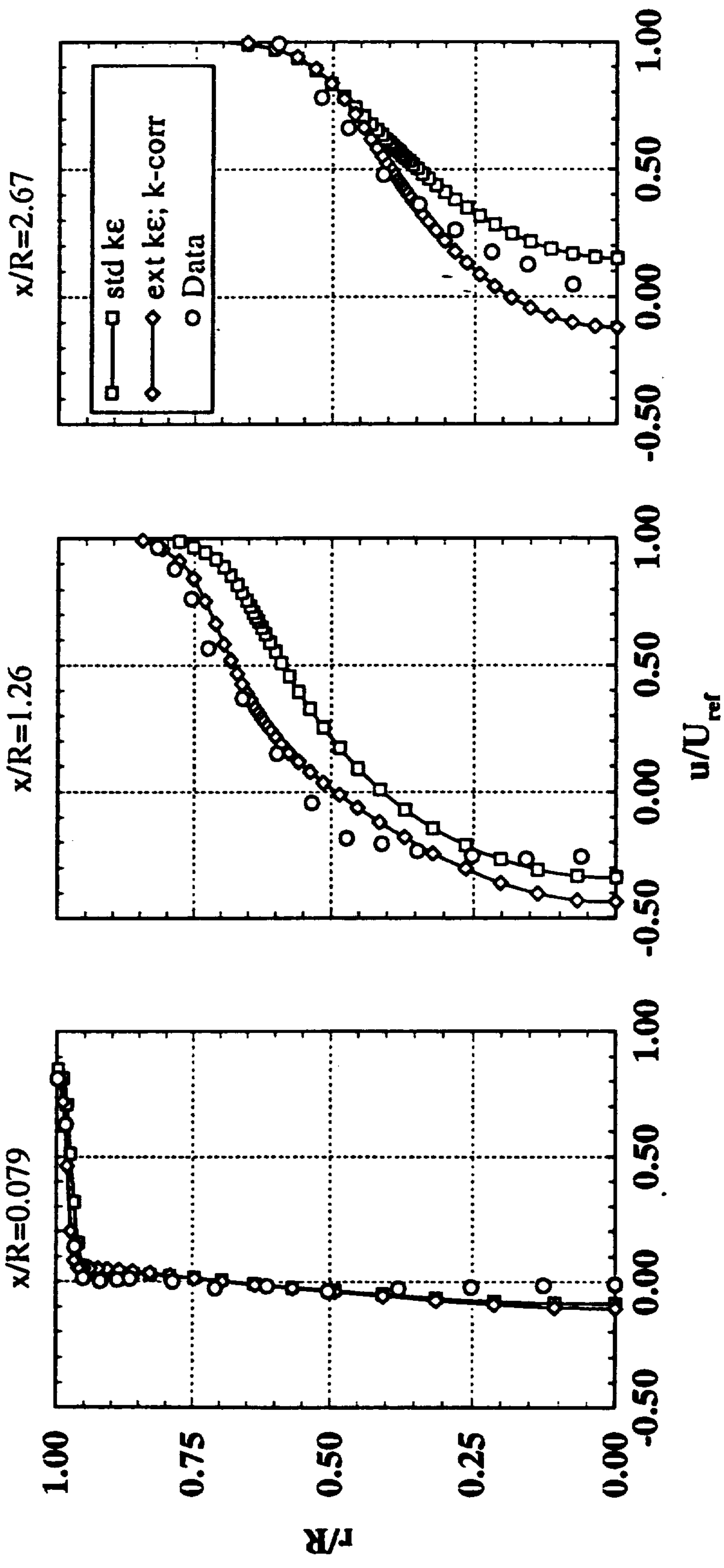

U-Velocity
x/R=0.079
x/R=1.26
x/R=2.67
std kε
ext kε; k-corr
Data
r/R
u/U_ref
1.00
0.75
0.50
0.25
0.00
-0.50
0.00
0.50
1.00

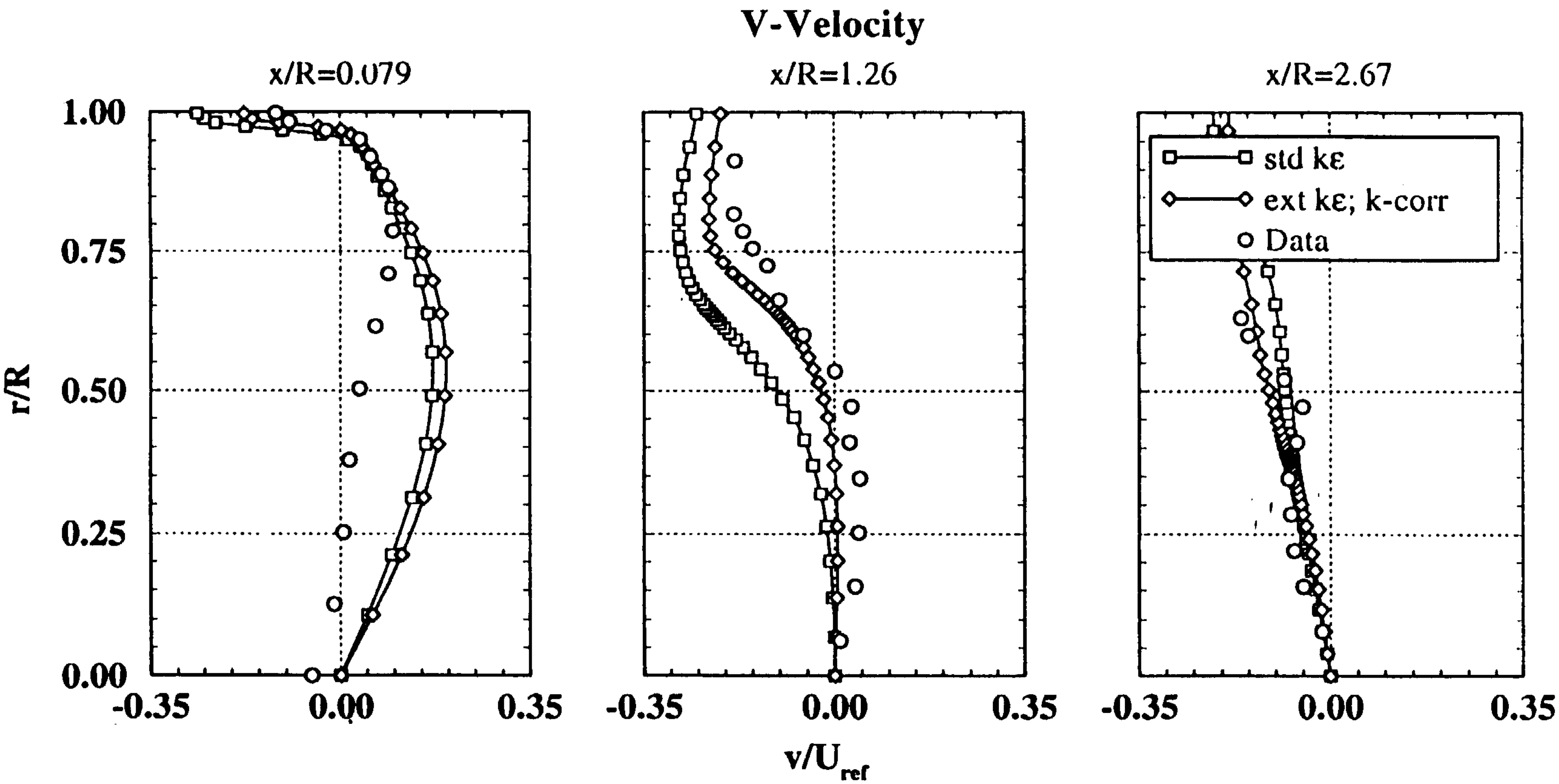
V-Velocity
x/R=0.079
x/R=1.26
x/R=2.67
std kε
ext kε; k-corr
Data
r/R
1.00
0.75
0.50
0.25
0.00
-0.35
0.00
0.35
v/U_ref

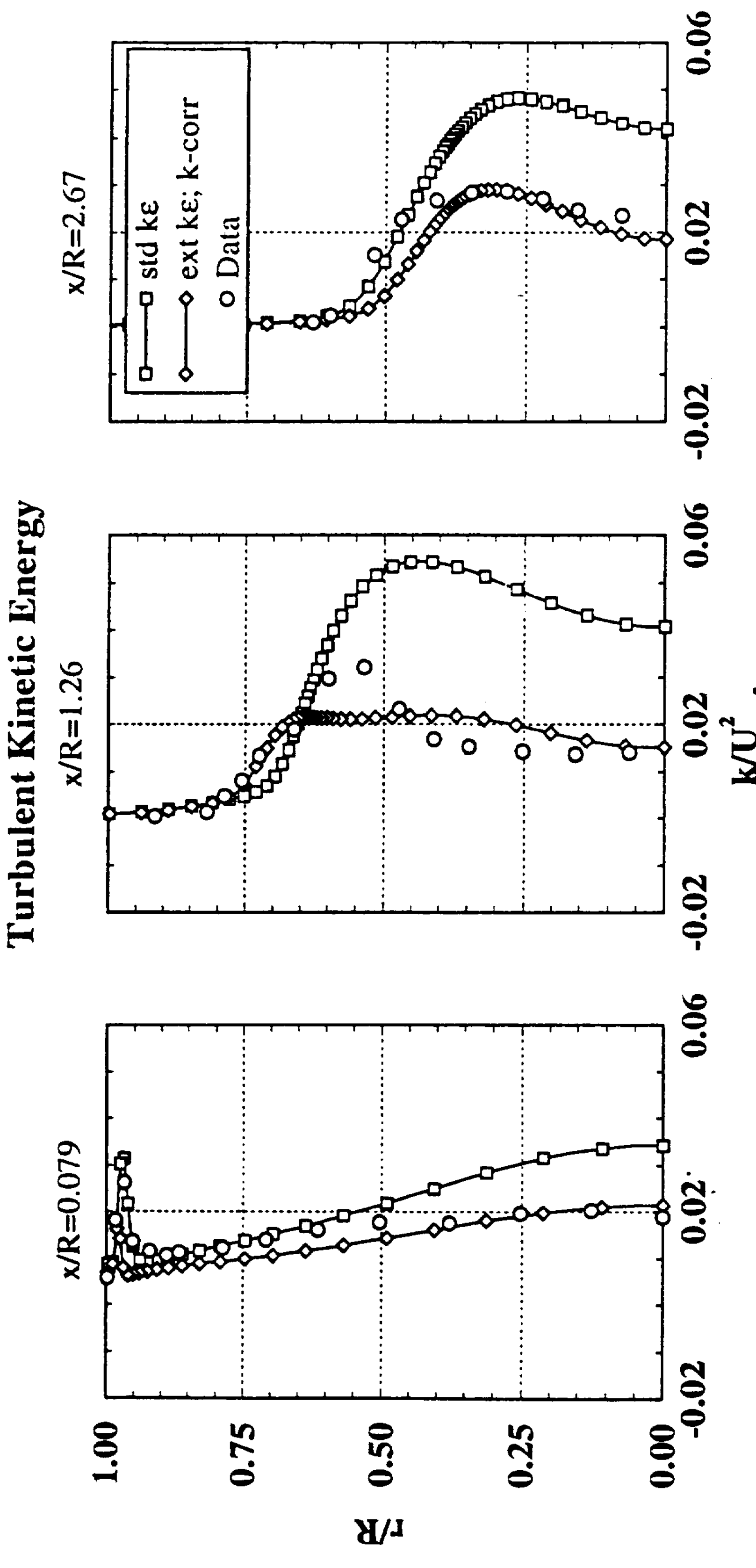
Turbulent Kinetic Energy
x/R=0.079
x/R=1.26
x/R=2.67
std kε
ext kε; k-corr
Data
r/R
1.00
0.75
0.50
0.25
0.00
-0.02
0.02
0.06
k/U²ref

SHEAR LAYER GROWTH

Standard kε Model

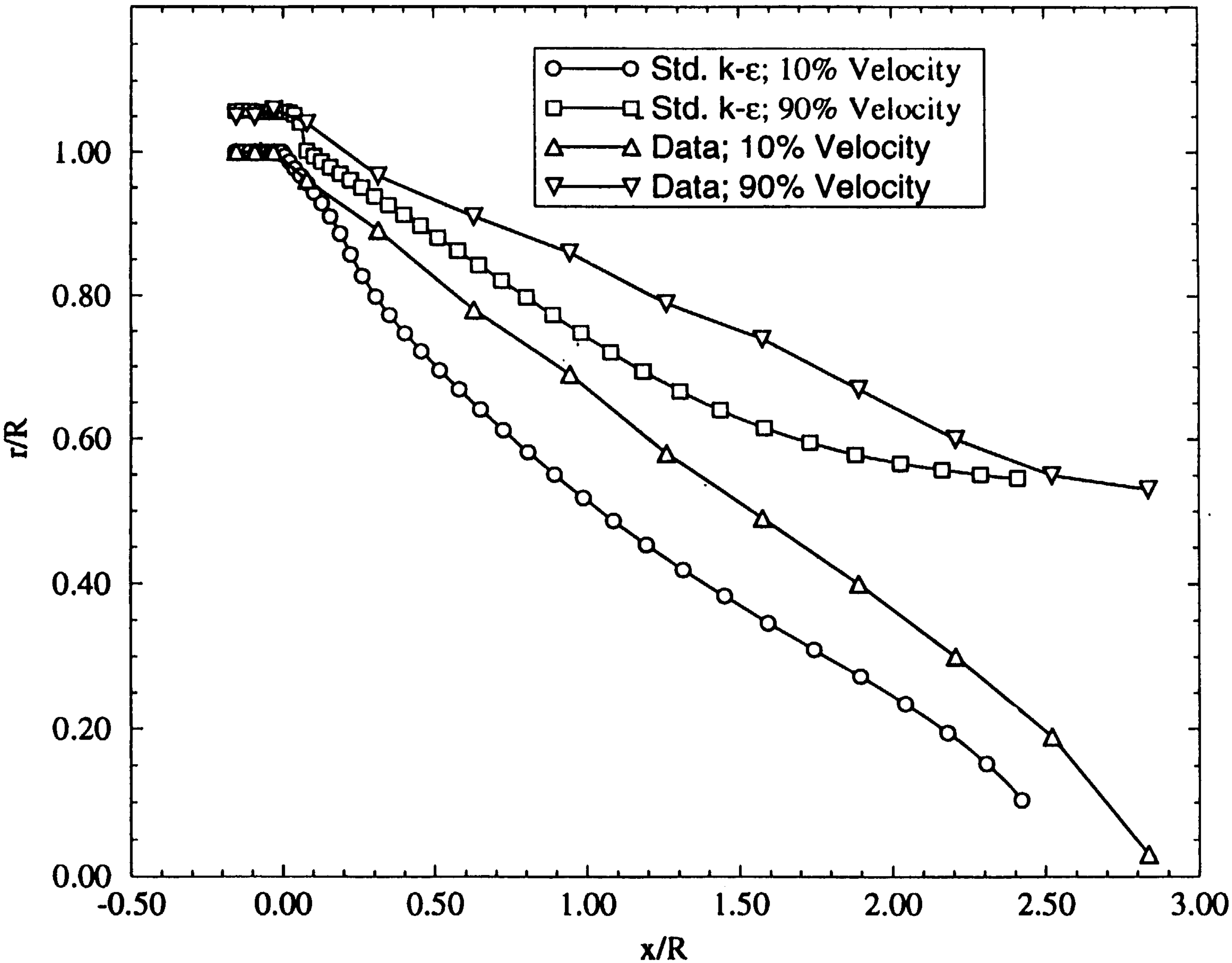

SHEAR LAYER GROWTH

Extended kε Model; k-Correction

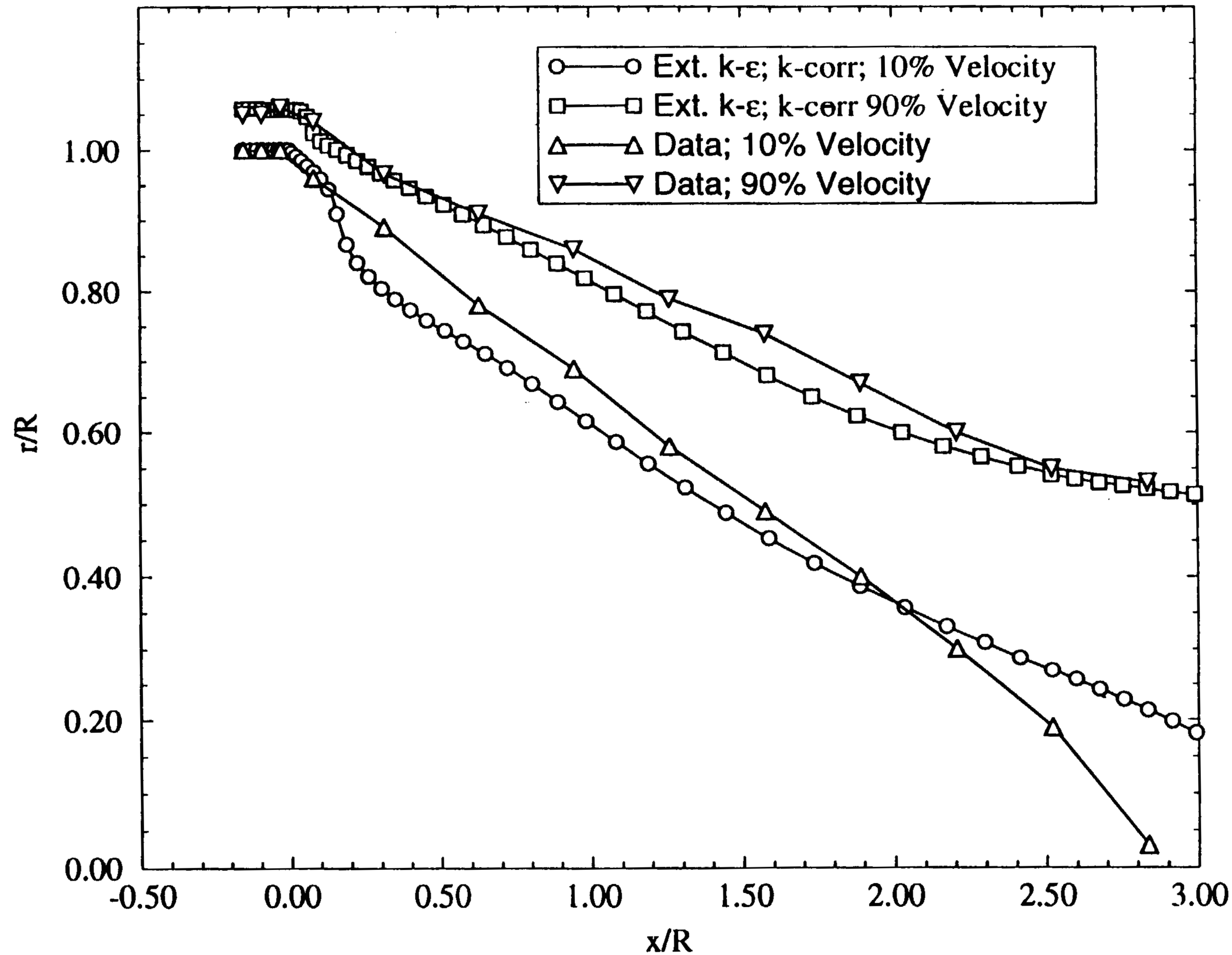

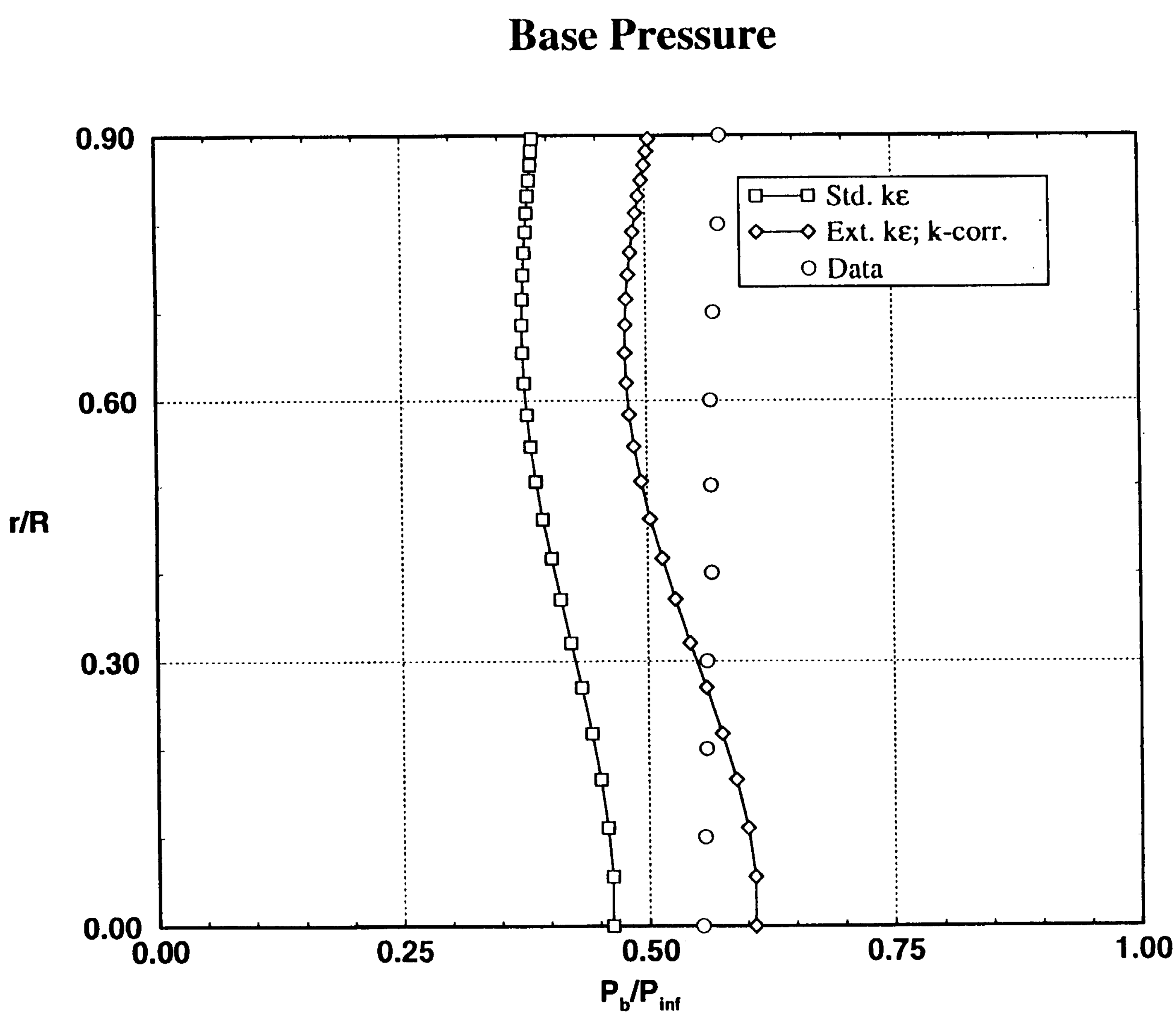
Base Pressure
Std. kε
Ext. kε; k-corr.
Data
r/R
0.90
0.60
0.30
0.00
0.00
0.25
0.50
0.75
1.00
P_b/P_{inf}

CONCLUSION

• Summary

-Predicted flowfield structure is qualitatively good for all cases

- Vorticity generation in shear layer makes problem more complex

- Standard k-e model over-predicts eddy viscosity resulting in:
  - Very low base pressure predictions
  - Under-predicted reattachment length
  - Over-predicted shear layer growth rate

- Extended k-e model with compressibility correction reduces eddy viscosity resulting in:
  - Much better (but still low) base pressures
  - Over-predicted reattachment length
  - Slightly underpredicted shear layer growth rate

- Overall, extended k-e model with compressibility correction gives better results

• Future Work

- Dilieate interaction between compressibility and turbulence generation/transport

- Address vorticity generation issue in highly compressible flowfield

- Complete coarse grid cases for guidance on 3-D problems

CODE VALIDATION STUDY FOR BASE FLOWS

Edward P. Ascoli, Adel H. Heiba, Ronald R. Lagnado,
Ronald J. Ungewitter, and Morgan Williams
Rocketdyne Div. /Rockwell International
Canoga Park, Ca 91304

P. 17

ABSTRACT

New and old rocket launch concepts recommend the clustering of motors for improved lift capability. The flowfield of the base region of the rocket is very complex and can contain high temperature plume gases. These hot gases can cause catastrophic problems if not adequately designed for. To assess the base region characteristics advanced computational fluid dynamics (CFD) is being used. As a precursor to these calculations the CFD code requires validation on base flows. The primary objective of this code validation study was to establish a high level of confidence in predicting base flows with the USA CFD code. USA has been extensively validated for fundamental flows and other applications. However, base heating flows have a number of unique characteristics so it was necessary to extend the existing validation for this class of problems.

In preparation for the planned NLS 1.5 Stage base heating analysis, six case sets were studied to extend the USA code validation data base. This presentation gives a cursive review of three of these cases. The cases presented include a 2D axi-symmetric study, a 3D real nozzle study, and a 3D multi-species study. The results of all the studies show good general agreement with data with no adjustments to the base numerical algorithms or physical models in the code. The study proved the capability of the USA code for modeling base flows within the accuracy of available data.

CODE VALIDATION STUDY FOR BASE FLOWS

BY

EDWARD P. ASCOLI, ADEL H. HEIBA,
RONALD R. LAGNADO, RONALD J UNGEWITTER, AND
MORGAN WILLIAMS
ROCKETDYNE DIV/ ROCKWELL INTERNATIONAL
MFSC CFD WORKSHOP APRIL 20-22 1993

Rockwell International
Rocketdyne Division

BASE HEATING STUDY VALIDATION OBJECTIVE AND APPROACH

OBJECTIVE

- ESTABLISH HIGH CONFIDENCE LEVEL IN PREDICTING BASE FLOWS
- ASSESS AND QUANTIFY PERFORMANCE OF EXISTING NUMERICAL ALGORITHMS AND PHYSICAL MODELS

APPROACH

- EXTEND EXISTING USA CODE VALIDATION TO BASE HEATING FLOWS
- BUILD UPON USA CODE VALIDATION ALREADY ESTABLISHED UNDER NASP PROGRAM

Rockwell International
Rockeldyne Division

CFD 92-042-020/03/SLB

SIX CASE SETS COMPLETED TO EXTEND USA CODE VALIDATION FOR BASE HEATING ANALYSIS

AEDC	Tangent ogive cylinder with centered propulsive jet	1 Case
AGARD	Nozzle afterbody parametric experimental study	9 Cases
YF-12	2-D aft-facing steps in high Reynolds number flow	9 Cases
AEROSPIKE	3-D single-stage-to-orbit demonstrator model	2 Cases
UVA	University of Virginia normal and axial injection	2 Cases
RHYME	Hypersonic flow over 10° ramp/injector	1 Case

Rockwell International
Rocketdyne Division

CFD 92-042-025/03/SLB

AGARD NOZZLE AFTERBODY CFD VALIDATION STUDY

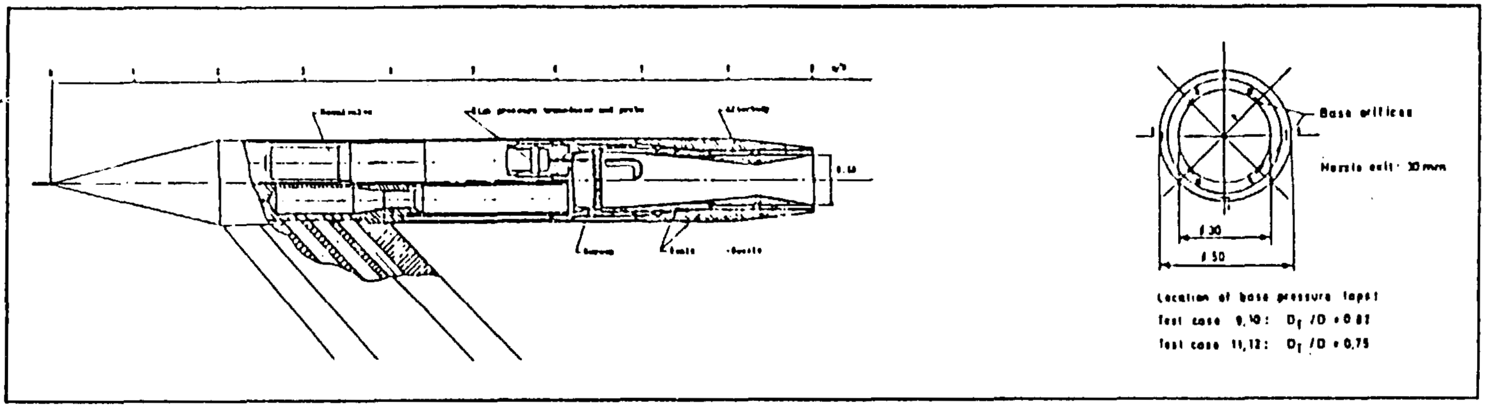

- **TEST DATA: PRESSURE TAPS ON BASE**

References:

AGARD Advisory Report No. 26, "Report of The Working Group on Aerodynamics of Aircraft Afterbody," June 1986.L.E. Putnam And N.C., Bissinger, "Results of AGARD

L.E. Putnam and N.C., Bissinger, "Results of AGARD Assessment of Prediction Capabilities for Nozzle Afterbody Flows," AIAA Paper No. 85-1464.

Rockwell International
Rocketdyne Division

CFD 92-042 031/D3/SL8

AGARD CFD MODELING APPROACH

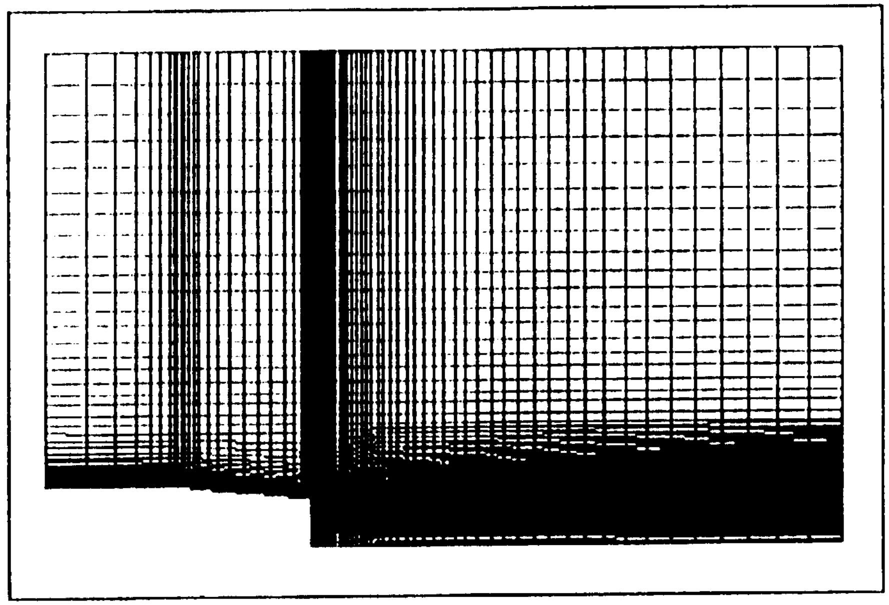

- 2 ZONE GRID WITH CLUSTERING ABOUT SHEAR LAYERS
- FULL NAVIER-STOKES ANALYSIS
- AXISYMMETRIC
- PERFECT GAS
- BALDWIN-LOMAX TURBULENCE MODEL

Rockwell International
Rocketdyne Division

CFD 92 042 032/D3/SLB

AGARD CFD VALIDATION STUDY CONCLUSIONS

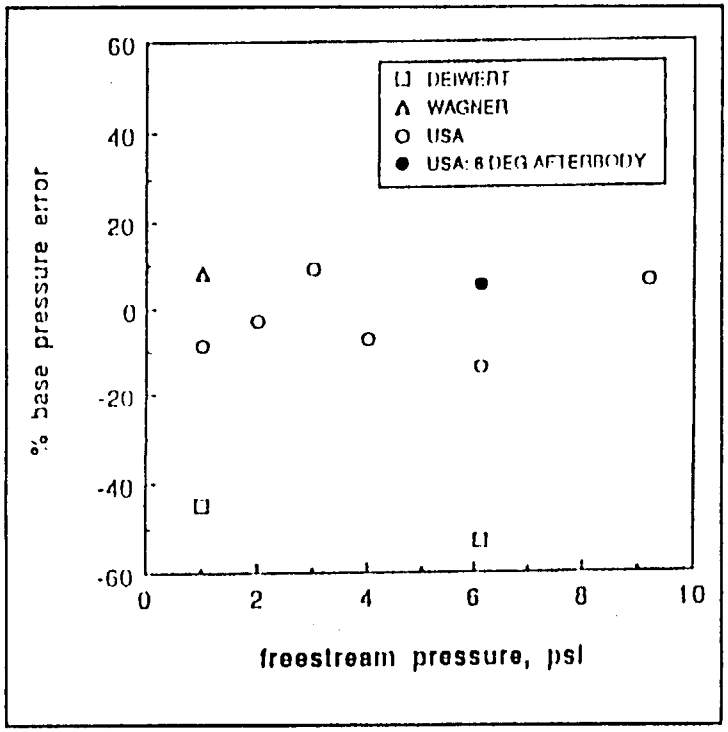

- % DEVIATION OF USA PREDICTIONS (o, •) FROM MEASURED BASE PRESSURE DATA (FNS + BALDWIN-LOMAX) IS GENERALLY WITHIN 10% FOR THE 7 CASES COMPLETED
- WAGNER'S CALCULATION (Δ) FOR THE THE CASE REPORTED (FNS + BALDWIN-LOMAX) SHOWS SIMILAR LEVEL OF AGREEMENT
- DEIWERT'S CALCULATIONS (□) FOR THE 2 CASES REPORTED (THIN-LAYER NS + BALDWIN LOMAX) ARE OFF BY AS MUCH AS 55% PROBABLY DUE TO THE TLNS LIMITATION
- OVERALL AGREEMENT APPEARS TO BE GOOD AND THE KEY FLOW FEATURES AT THE BASE ARE CAPTURED

Rockwell International
Rocketdyne Division

CFD 92 042 035/03/SI R

AEROSPIKE CFD VALIDATION STUDY

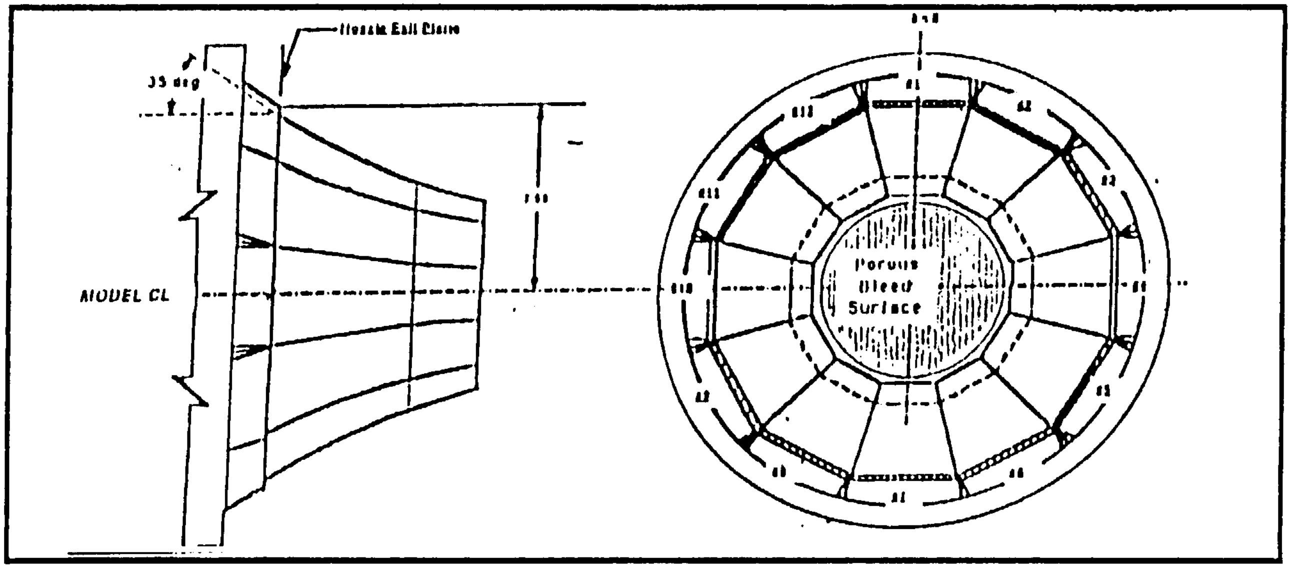

- **SSTO AEROSPIKE DEMONSTRATOR MODEL**
  - 12 MODULES, 11 THRUSTERS PER MODULE
- **TEST DATA**
- 37 PRESSURE TAPS ON NOZZLE SURFACE
- 21 PRESSURE TAPS ON BASE

Reference:

Kingsland, R.B., Petrilla, S., And Baker, W.M., "SSTO Aerospike Nozzle Demonstrator Test in the Fluidyne Channel No. 9 Test Facility," SSTO Pretest Conference, March 1991.

Rockwell International
Rocketdyne Division

CFD 92 042 04 1/D3/SI B

AEROSPIKE CFD MODELING APPROACH

- TWO COMPUTATIONAL ZONES
  - 1: UPSTREAM OF BASE
  - 2: DOWNSTREAM OF BASE
- 97,155 GRID POINTS

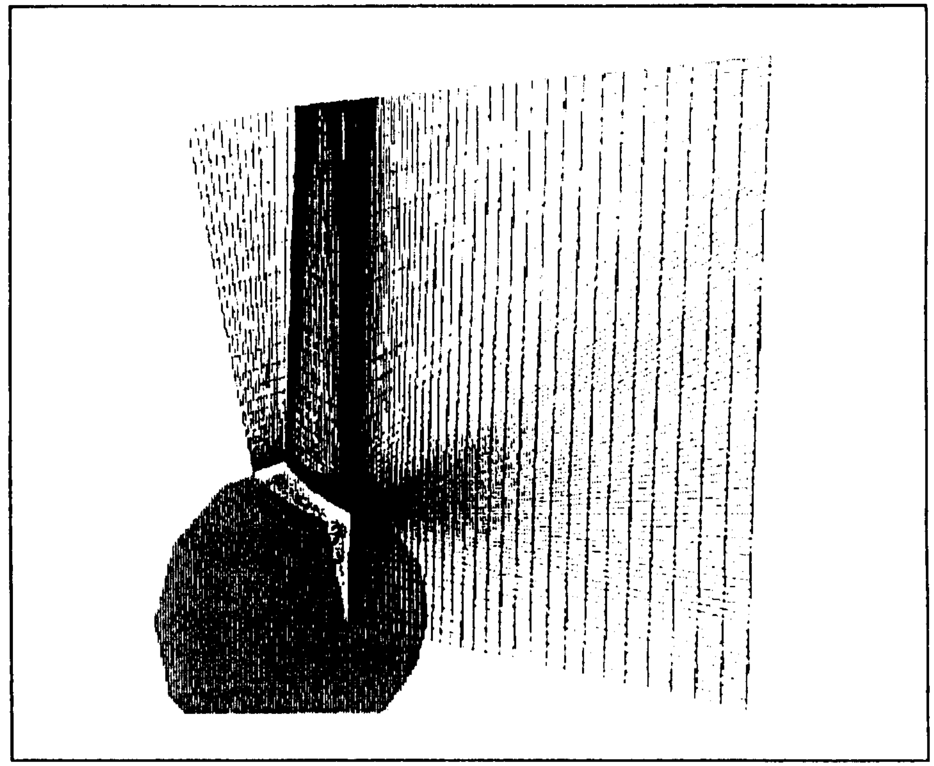

- 3-D NAVIER-STOKES ANALYSIS
- PERFECT GAS
- BALDWIN-LOMAX TURBULENCE MODEL

Rockwell International
Rocketdyne Division

CFD 92 042 042/D3/SI B

AEROSPIKE CFD ANALYSIS RESULTS

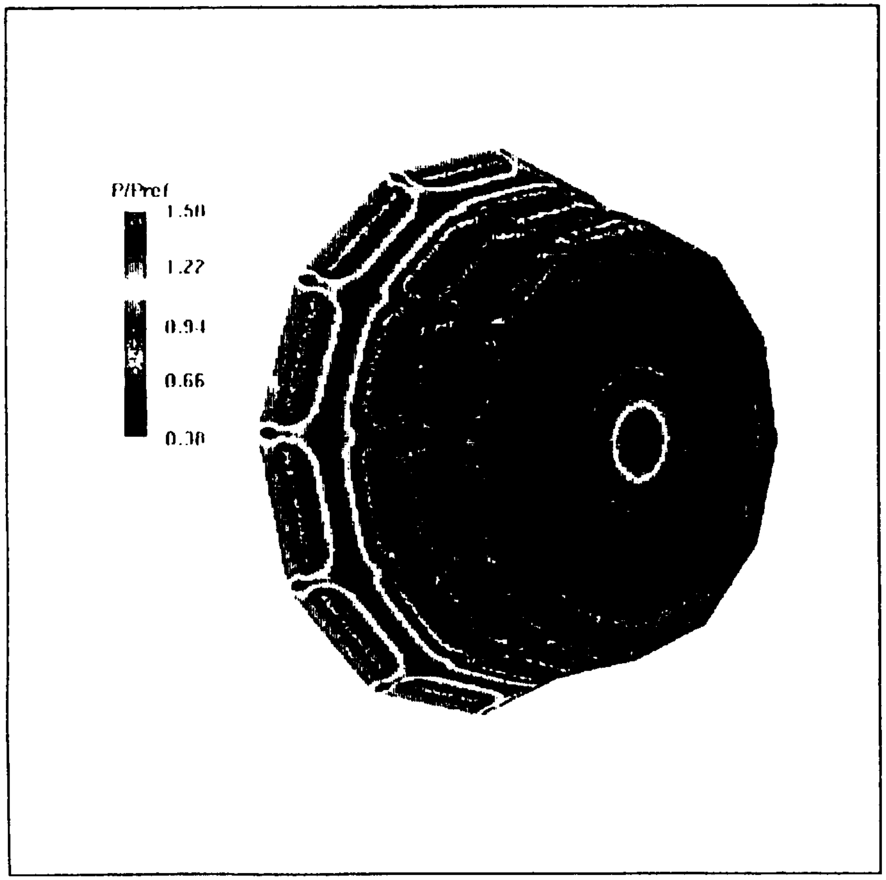

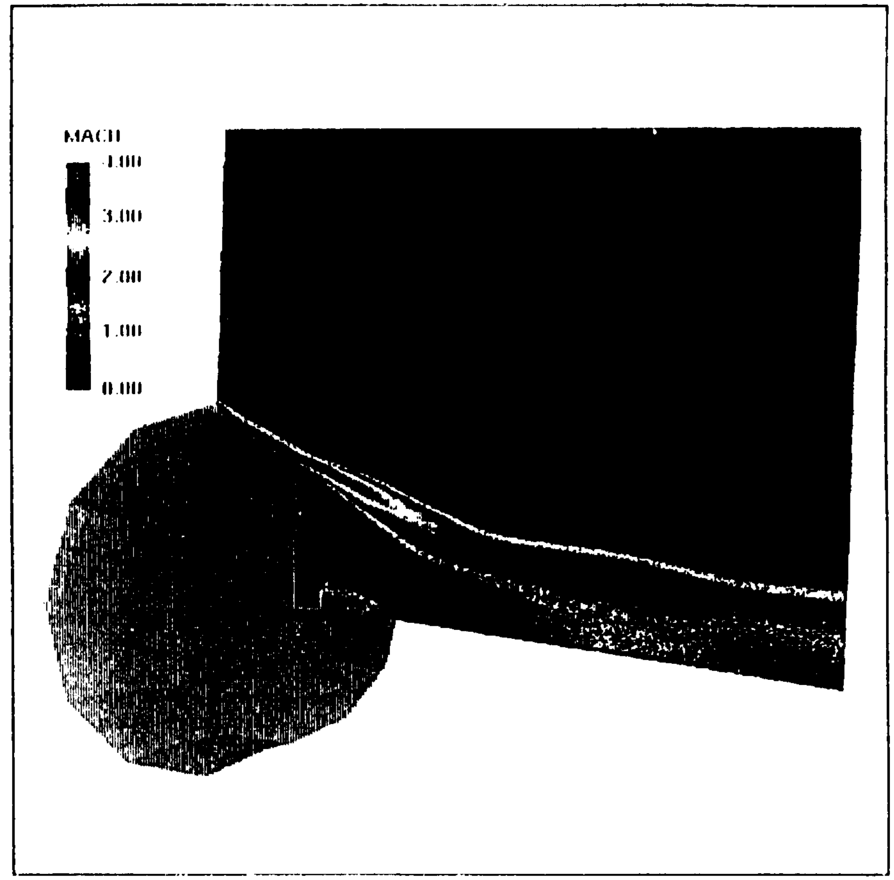

Rockwell International
Rocketdyne Division

CFD 92 042 043/D3/SLB

AEROSPIKE CFD ANALYSIS RESULTS (CONT'D)

LOW PRESSURE RATIO CASE

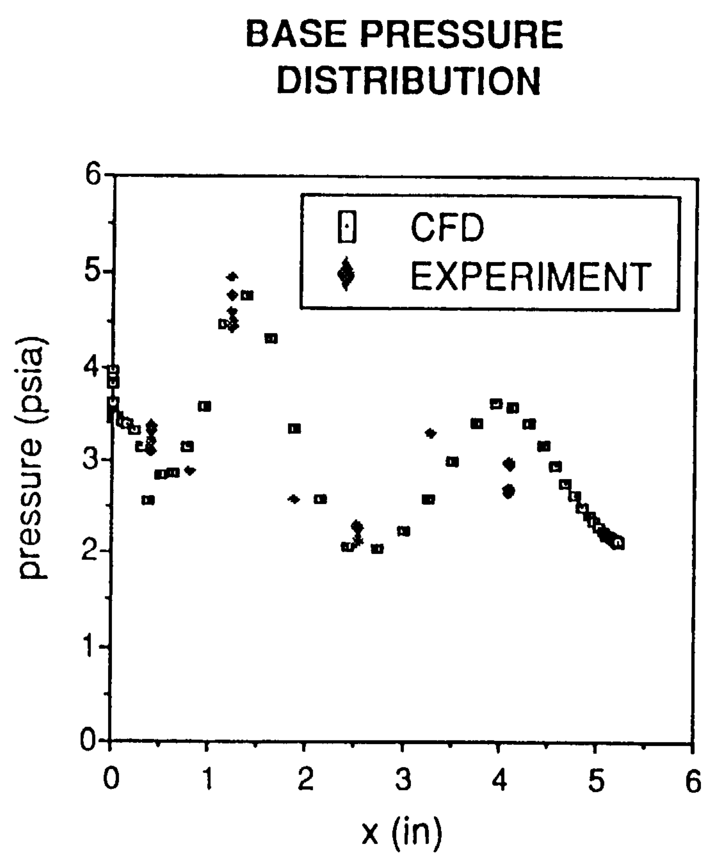

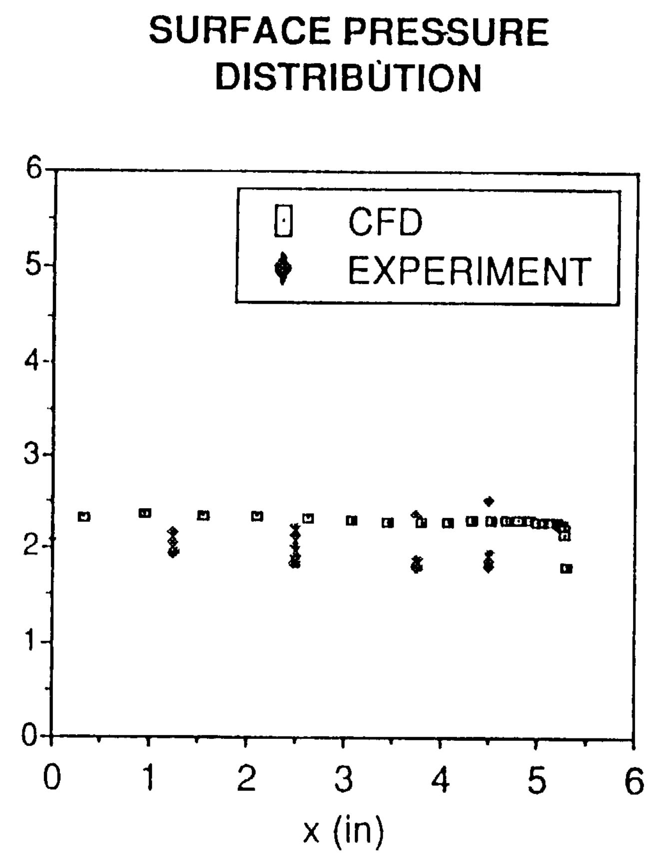

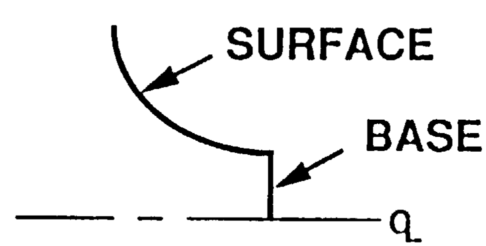

Rockwell International
Rocketdyne Division

CFD 92 042 044B/D3/SI B

UVA CFD VALIDATION STUDY

FLOW GEOMETRY

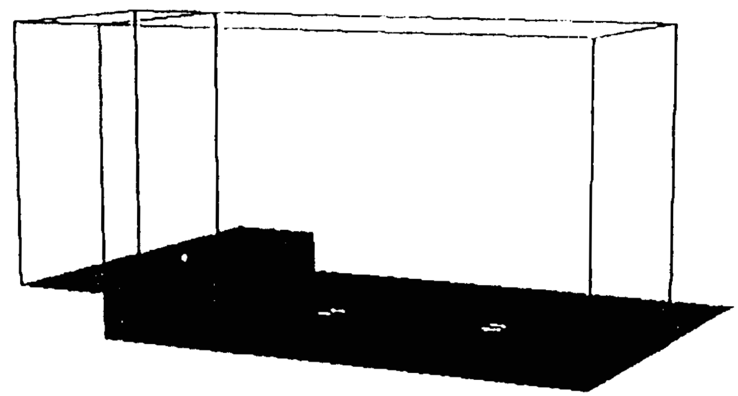

- **TEST DATA**
  - PLIF MEASUREMENTS FOR P, V, AND T
  - INJECTANT CONCENTRATION

Reference:

J. McDaniel, D. Fletcher, R. Hartfield and S. Hallo, "Staged Transverse Injection Into Mach 2 Flow Behind a Rearward-Facing Step: A 3-D Compressible Test Case for Hypersonic Combustor Code Validation," AIAA-91-5071.

Rockwell International
Rocketdyne Division

CFD 92-042-046/D3/SI B

UVA CFD MODELING APPROACH

COMPUTATIONAL GRID

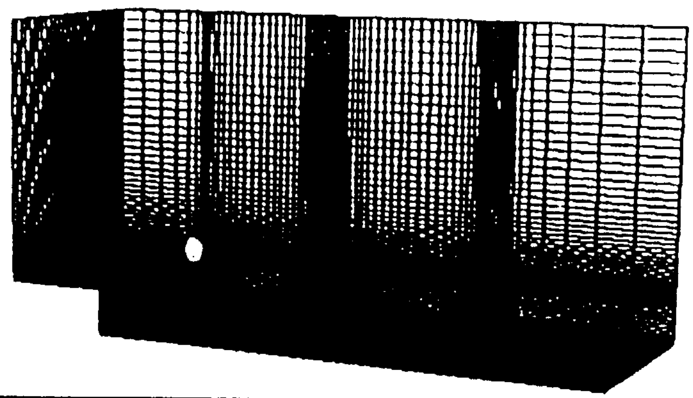

- TWO ZONE COMPUTATIONAL GRID WITH 171,532 POINTS
- 3-D NAVIER-STOKES ANALYSIS
- FROZEN CHEMISTRY WITH THREE SPECIES (O2, N2, AIR)
- 0-EQUATION GOLDBERG TURBULENCE MODEL

Rockwell International
Rockeldyne Division

CFD 92 042 047/D3/SI B

UVA CFD ANALYSIS RESULTS

CONCENTRATION CONTOURS OF INJECTANT

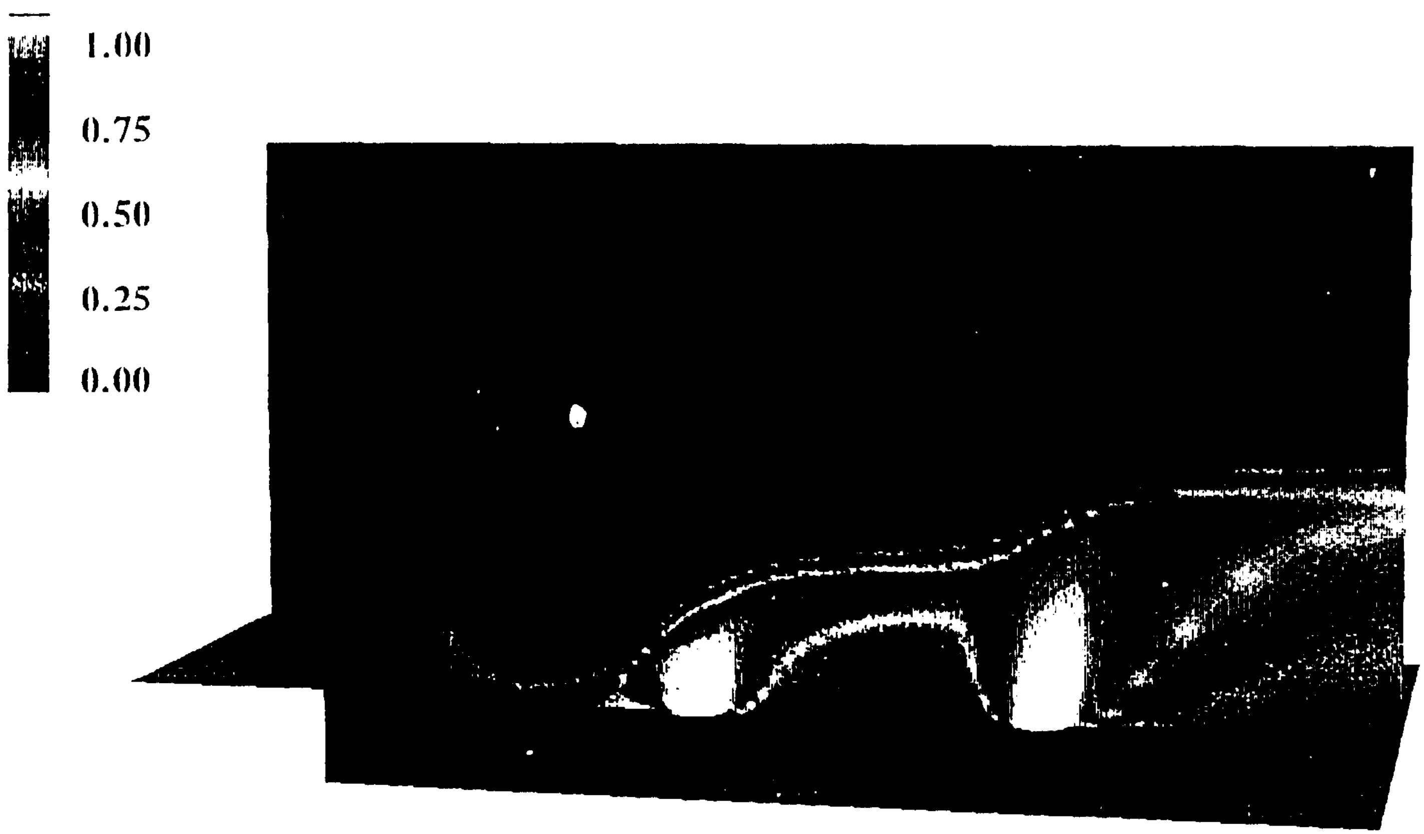

Rockwell International
Rocketdyne Division

CFD 92 042 048/03/SI 8

UVA CFD ANALYSIS RESULTS (CONT'D)

PRESSURE PROFILES AT CENTER OF 2ND JET (SYMMETRY PLANE)

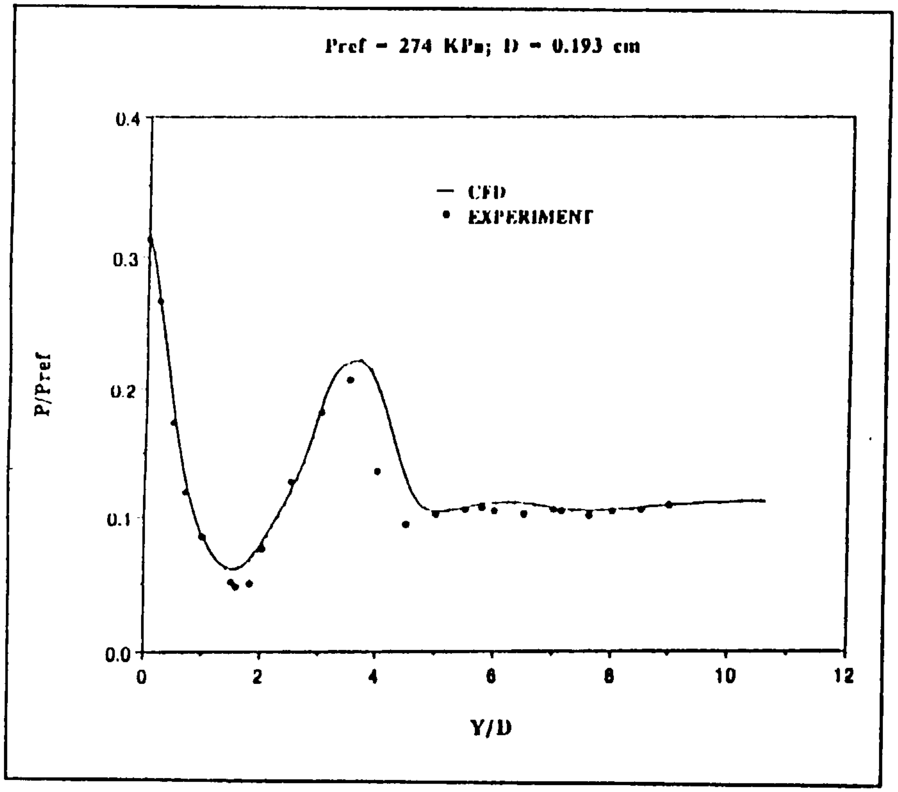

NORMAL VELOCITY PROFILES AT CENTER OF 2ND JET (SYMMETRY PLANE)

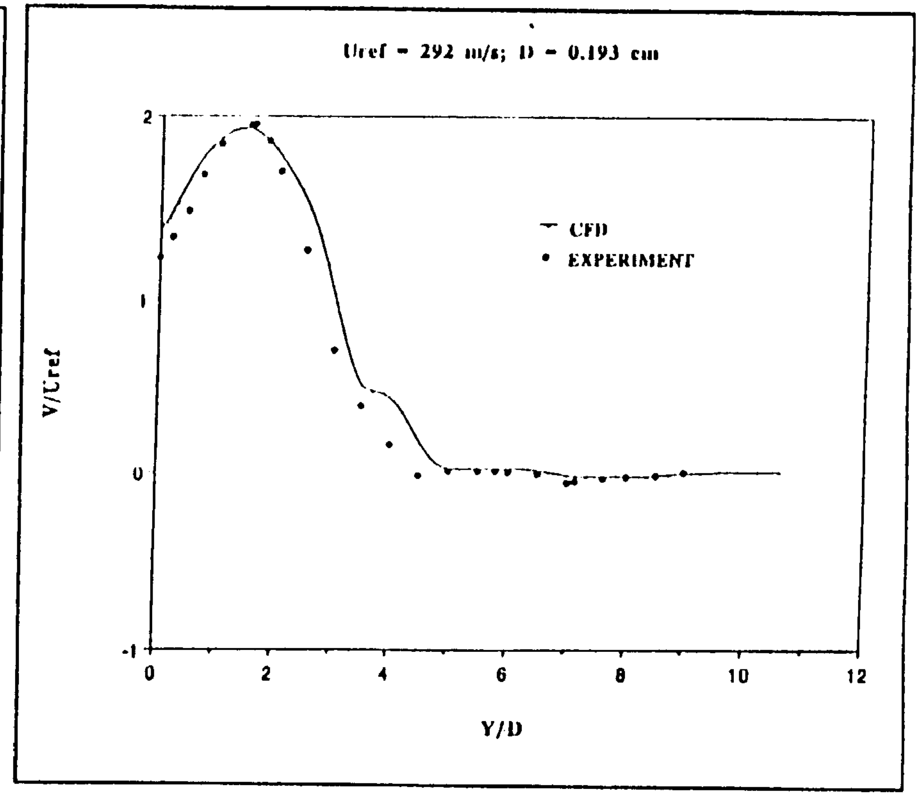

Rockwell International
Rocketdyne Division

CFD 92-042-049/D3/SLB

UVA CFD VALIDATION STUDY CONCLUSIONS

- **CALCULATIONS CAPTURE KEY FLOW FEATURES**
  - RECIRCULATION REGIONS BEHIND THE STEP AND AROUND THE INJECTORS
  - BOW AND BARREL SHOCKS
  - BASE PRESSURES
  - JET PENETRATION, SPREADING AND INTERACTION EFFECTS
- **PREDICTIONS SHOW GOOD AGREEMENT WITH TEST DATA**

Rockwell International
Rocketdyne Division

CFD 92-042-050/D3/SLB

CFD CODE VALIDATION ASSESSMENT

- **LEVEL OF AGREEMENT BETWEEN CALCULATIONS AND AVAILABLE DATA GENERALLY GOOD**
  - SOME CASES SHOW EXCELLENT AGREEMENT, OTHERS ARE GOOD TO ADEQUATE
  - OTHER THAN GRID REFINEMENT NO "ADJUSTMENTS" WERE MADE EITHER IN THE NUMERICAL ALGORITHMS OR PHYSICAL MODELS TO ACHIEVE BETTER AGREEMENT
  - MODELS USED IN THE VALIDATION WERE RESTRICTED TO THE SAME MODELS TO BE USED IN THE NLS CALCULATIONS

- **THERE IS A NEED FOR MORE CAREFULLY DESIGNED AND CONDUCTED EXPERIMENTS FOR CODE VALIDATION IN THE BASE HEATING AREA**

Rockwell International
Rocketdyne Division

CFD 92-042-055/D3/SLB

N95- 23654

FOUR-NOZZLE BENCHMARK WIND TUNNEL MODEL USA CODE SOLUTIONS FOR SIMULATION OF MULTIPLE ROCKET BASE FLOW RECIRCULATION AT 145,000 FT ALTITUDE

by

N. S. Dougherty and S. L. Johnson

Rockwell International
Space Systems Division
Huntsville, AL 35806

ABSTRACT

Multiple rocket exhaust plume interactions at high altitudes can produce base flow recirculation with attendant alteration of the base pressure coefficient and increased base heating. A search for a good wind tunnel benchmark problem to check grid clustering technique and turbulence modeling turned up the experiment done at AEDC in 1961 by Goethert and Matz on a 4.25-in. diameter domed missile base model with four rocket nozzles. This wind tunnel model with varied external bleed air flow for the base flow wake produced measured p/p_{ref} at the center of the base as high as 3.3 due to plume flow recirculation back onto the base. At that time in 1961, relatively inexpensive experimentation with air at $\gamma = 1.4$ and nozzle A_e/A^* of 10.6 and $\theta_n = 7.55$ deg with P_c = 155 psia simulated a LO_2/LH_2 rocket exhaust plume with $\gamma = 1.20$, A_e/A^* of 78 and P_c about 1,000 psia. An array of base pressure taps on the aft dome gave a clear measurement of the plume recirculation effects at p_∞ = 4.76 psfa corresponding to 145,000 ft altitude. Our CFD computations of the flow field with direct comparison of computed-versus-measured base pressure distribution (across the dome) provide detailed information on velocities and particle traces as well eddy viscosity in the base and nozzle region. The solution was obtained using a six-zone mesh with 284,000 grid points for one quadrant taking advantage of symmetry. Results are compared using a zero-equation algebraic and a one-equation pointwise R_t turbulence model (work in progress). Good agreement with the experimental pressure data was obtained with both; and this benchmark showed the importance of: (1) proper grid clustering and (2) proper choice of turbulence modeling for rocket plume problems/recirculation at high altitude.

FOUR-NOZZLE BENCHMARK WIND TUNNEL MODEL USA CODE SOLUTIONS FOR SIMULATION OF MULTIPLE ROCKET BASE FLOW RECIRCULATION AT 145,000 FT ALTITUDE

APRIL 21, 1993

N.S. Dougherty, and S.L. Johnson
Rockwell International
Huntsville, AL

RENG002558.01

FOUR-NOZZLE CLUSTER HIGH ALTITUDE BASE FLOW BENCHMARK

OBJECTIVE

- SHOW THE CAPABILITIES OF THE USA CODE TO SOLVE HIGH-ALTITUDE (> 100,000 FT) MISSILE CLUSTERED-NOZZLE BASE FLOW PROBLEMS AS TO SOLUTION ALGORITHM AND TURBULENCE MODEL (SEPARATE FROM CHEMISTRY OR ENERGY/HEAT TRANSFER SIMULATIONS).

FOUR-NOZZLE CLUSTER HIGH ALTITUDE BASE FLOW BENCHMARK

APPROACH

BENEFITS

- CLASSICAL EXPERIMENT FROM 1961 WITH AIR SIMULATES CLUSTERED LO_2/LH_2 ENGINES
- THIS BENCHMARK ISOLATES ALGORITHM, GRIDDING TECHNIQUE, AND TURBULENCE MODEL ACCURACIES
- EXCELLENT HIGH ALTITUDE EXPANSION TEST FOR THE CODE

NOTE - CHEMISTRY PACKAGE BENCHMARK CONDUCTED AND REPORTED SEPARATELY

AREAS FOR IMPROVEMENT

- ALTHOUGH GROSS FEATURES OF FLOW FIELD ADEQUATELY SIMULATED, AGREEMENT WITH BASE PRESSURE FLOW BETWEEN NOZZLES HAS REMAINING SMALL DISCREPANCY

RENG002570.01

FOUR-NOZZLE CLUSTER HIGH ALTITUDE BASE FLOW BENCHMARK

- ***EXPERIMENT DESCRIPTION***

THE CLUSTERED NOZZLE BASE FLOW EXPERIMENTS CONDUCTED IN 1961 BY R. J. MATZ AND D. W. LITTLE AT ARNOLD ENGINEERING DEVELOPMENT CENTER WERE SELECTED AS CFD BENCHMARK CASES FOR HIGH ALTITUDE PLUME INTERACTION EFFECTS. THE SPECIFIC CASE CHOSEN FOR SIMULATION IS DESCRIBED BELOW:

- Ae/At 10.63
- P_∞/Pc 0.000213
- Pc 155 psia
- h 145,000 FT (PRESSURE ALTITUDE)
- HIGH PRESSURE AIR UTILIZED TO SIMULATE PLUMES

THESE CONDITIONS ARE REPRESENTATIVE OF A FULL-SCALE CONFIGURATION WITH A NOZZLE AREA RATIO OF APPROXIMATELY 80 AND AN EXHAUST GAS SPECIFIC HEAT RATIO OF 1.2

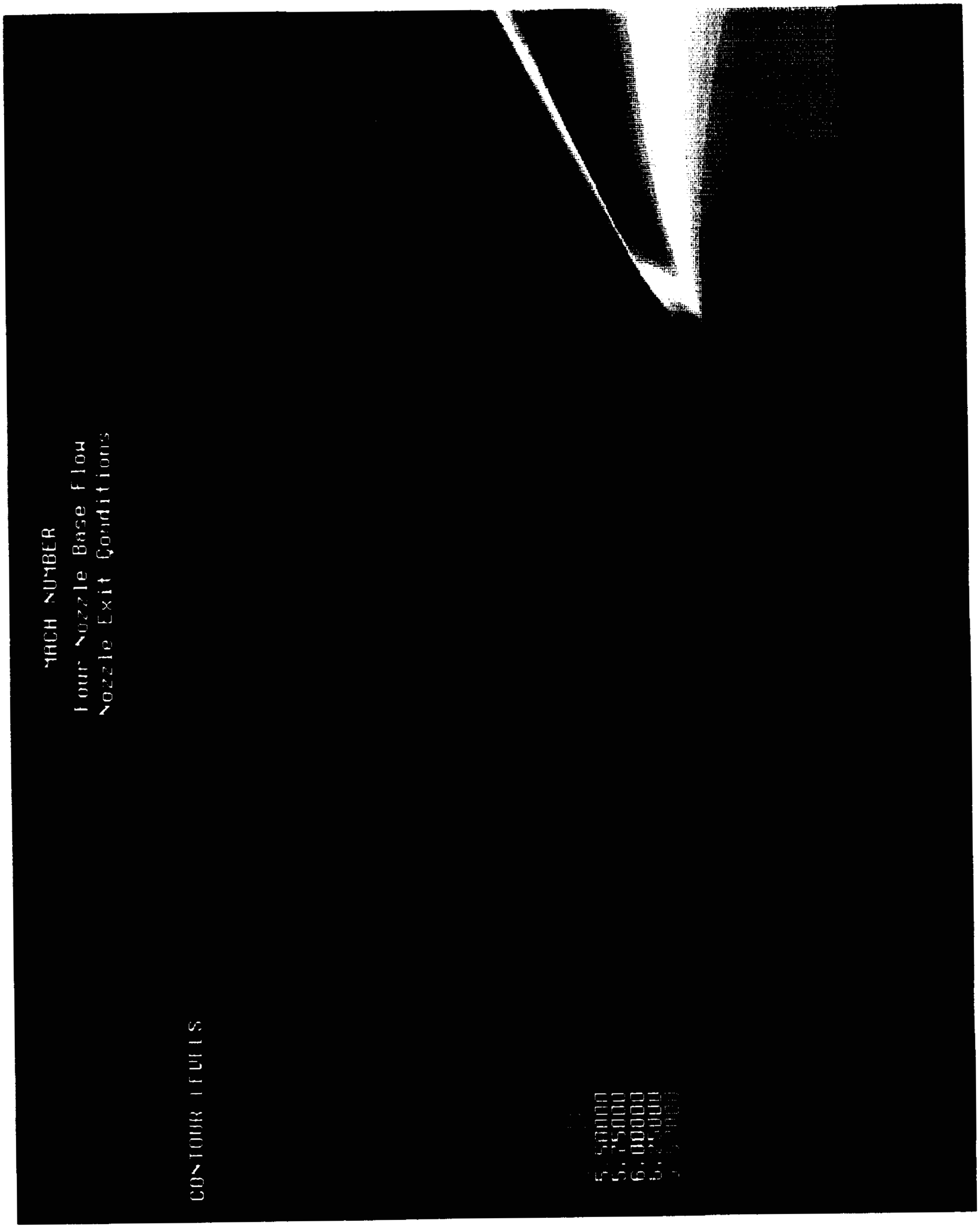
MACH NUMBER
Four Nozzle Base Flow
Nozzle Exit Conditions
CONTOUR LEVELS

Rockwell International

Space Systems Division

FOUR-NOZZLE CLUSTER HIGH ALTITUDE BASE FLOW BENCHMARK

Huntsville Operations

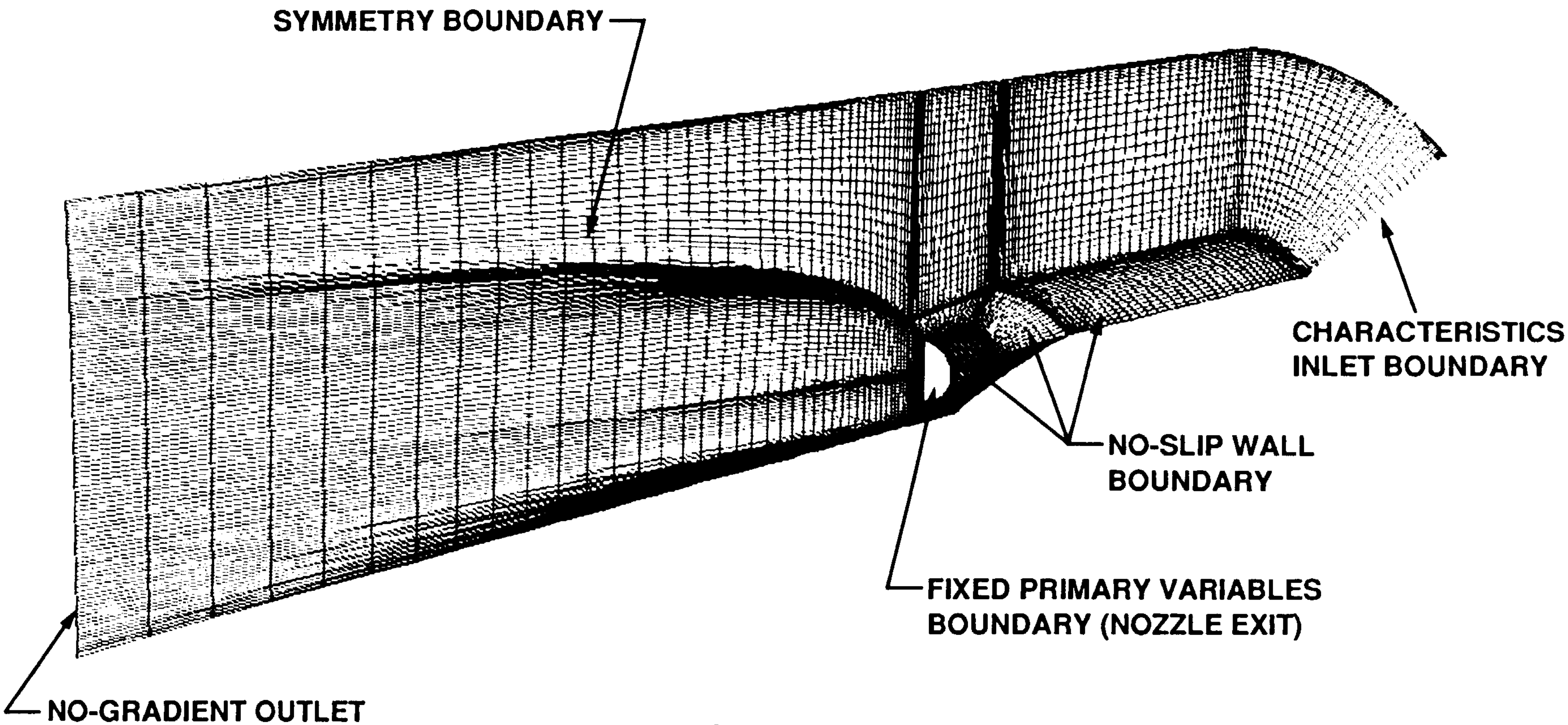

OUTER RADIUS IS A NO-SLIP WALL BOUNDARY (OMITTED FROM FIGURE FOR CLARITY)

RENG002571.01

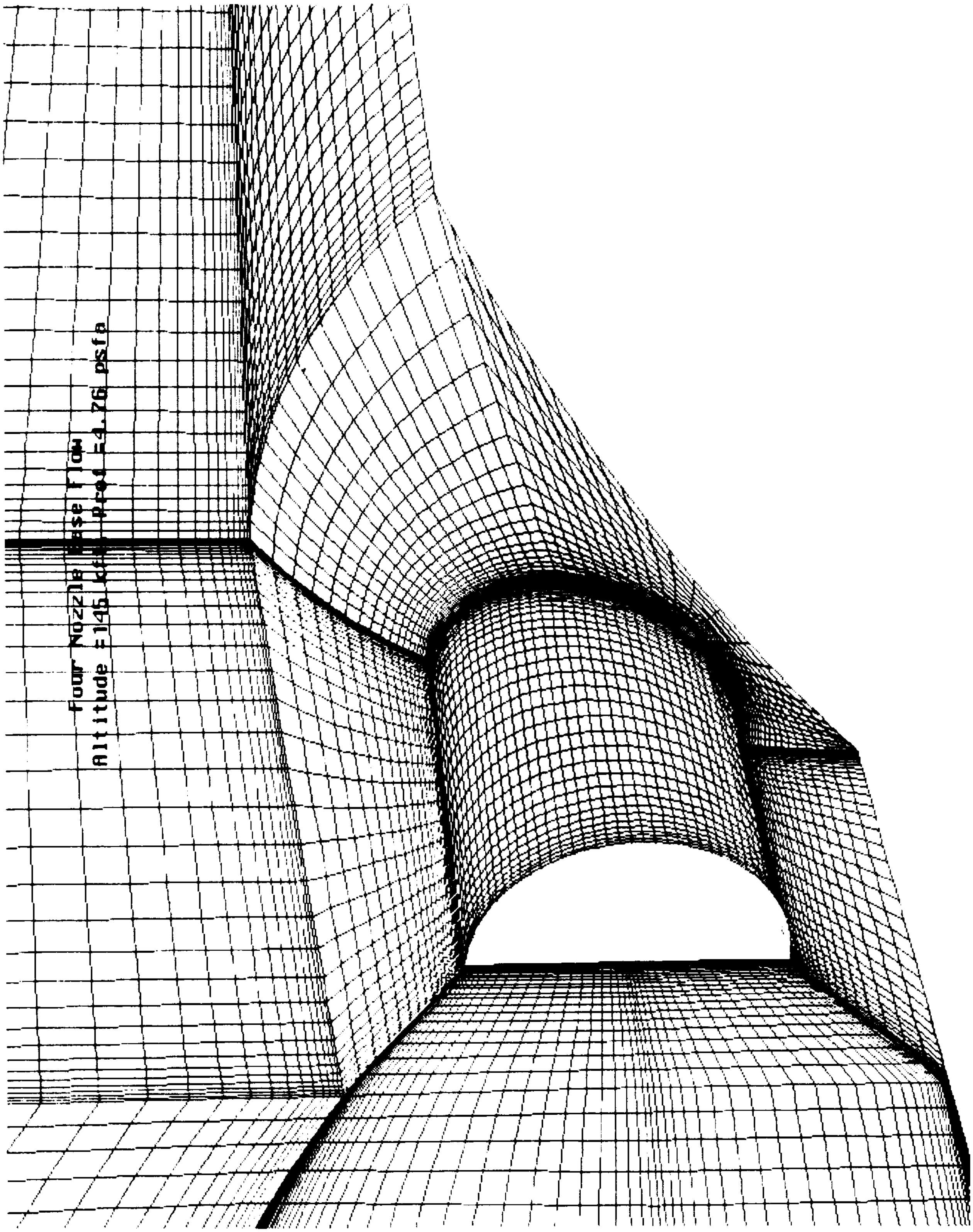

Four Nozzle Base Flow
Altitude =145 kft Pref =4.76 psfa

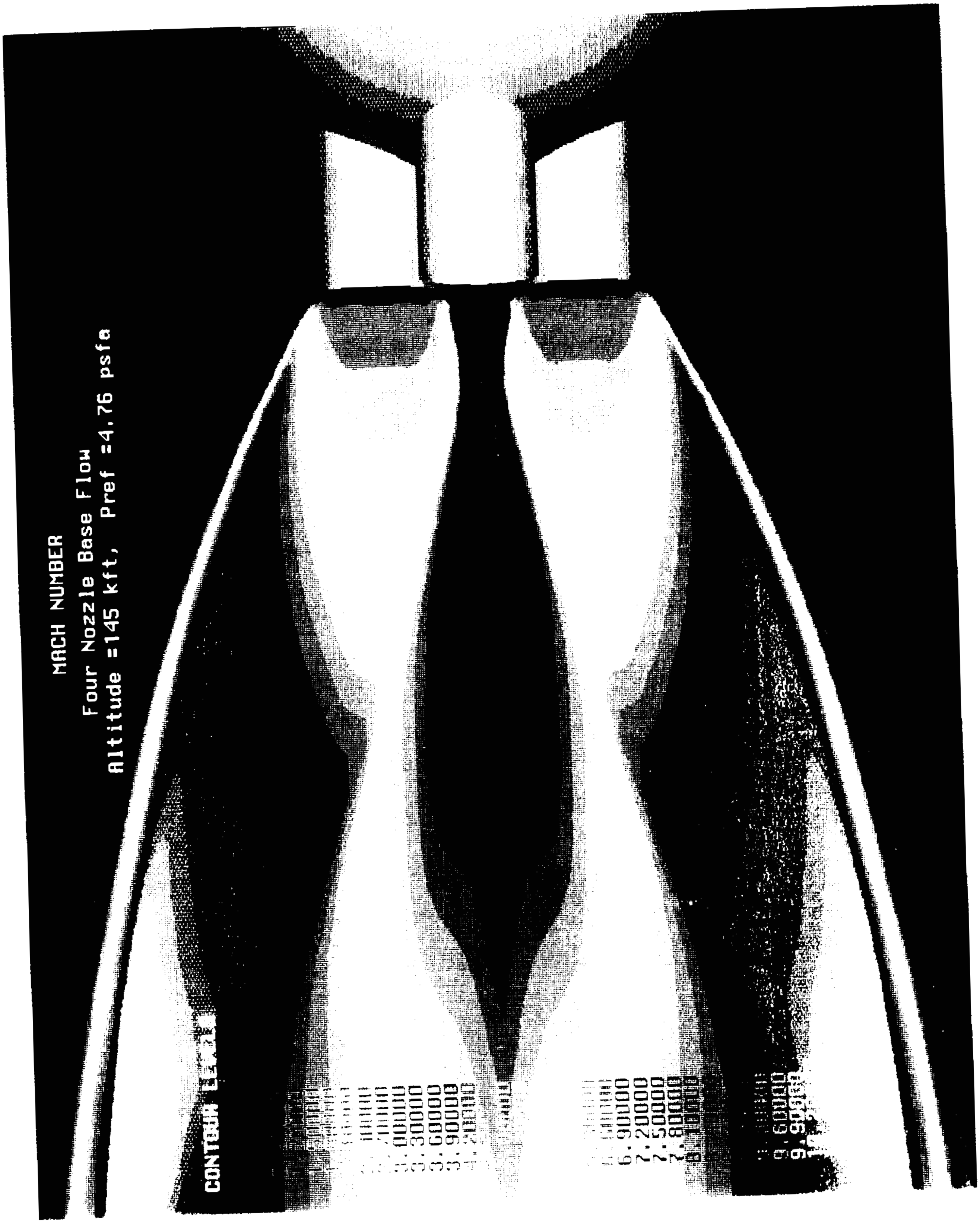
MACH NUMBER
Four Nozzle Base Flow
Altitude =145 kft, Pref =4.76 psfa
CONTOUR LEVELS
3.30000
3.60000
3.90000
6.90000
7.20000
7.50000
7.80000
8.10000
9.60000
9.90000

Rockwell International

Space Systems Division

FOUR-NOZZLE CLUSTER HIGH ALTITUDE BASE FLOW BENCHMARK

Huntsville Operations

DISCRIMINATING STREAMLINE FORMED AT THE INTERSECTION BETWEEN TWO PLUMES

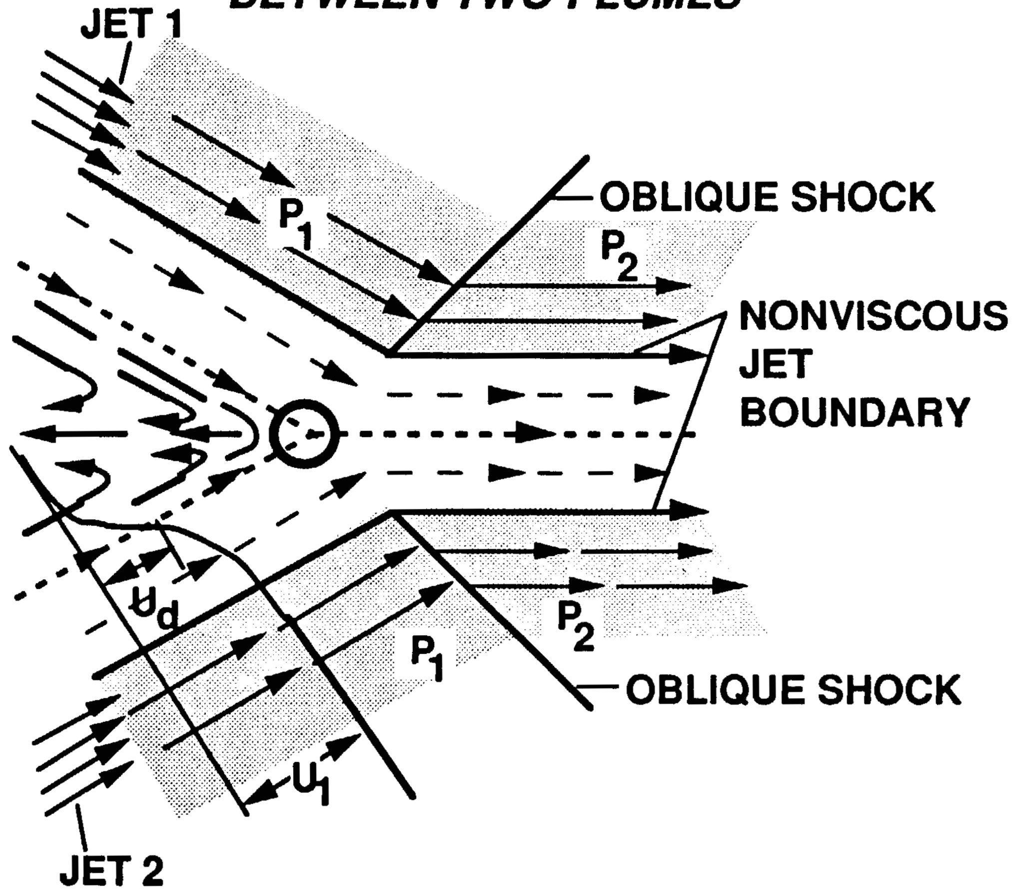

DISCRIMINATING STREAMLINE:

VELOCITY = U_d
MACH NUMBER = M_d

NORMAL SHOCK FOR M_d

$$P_s = P'_{ts} (M_d)$$

RENG002572.01

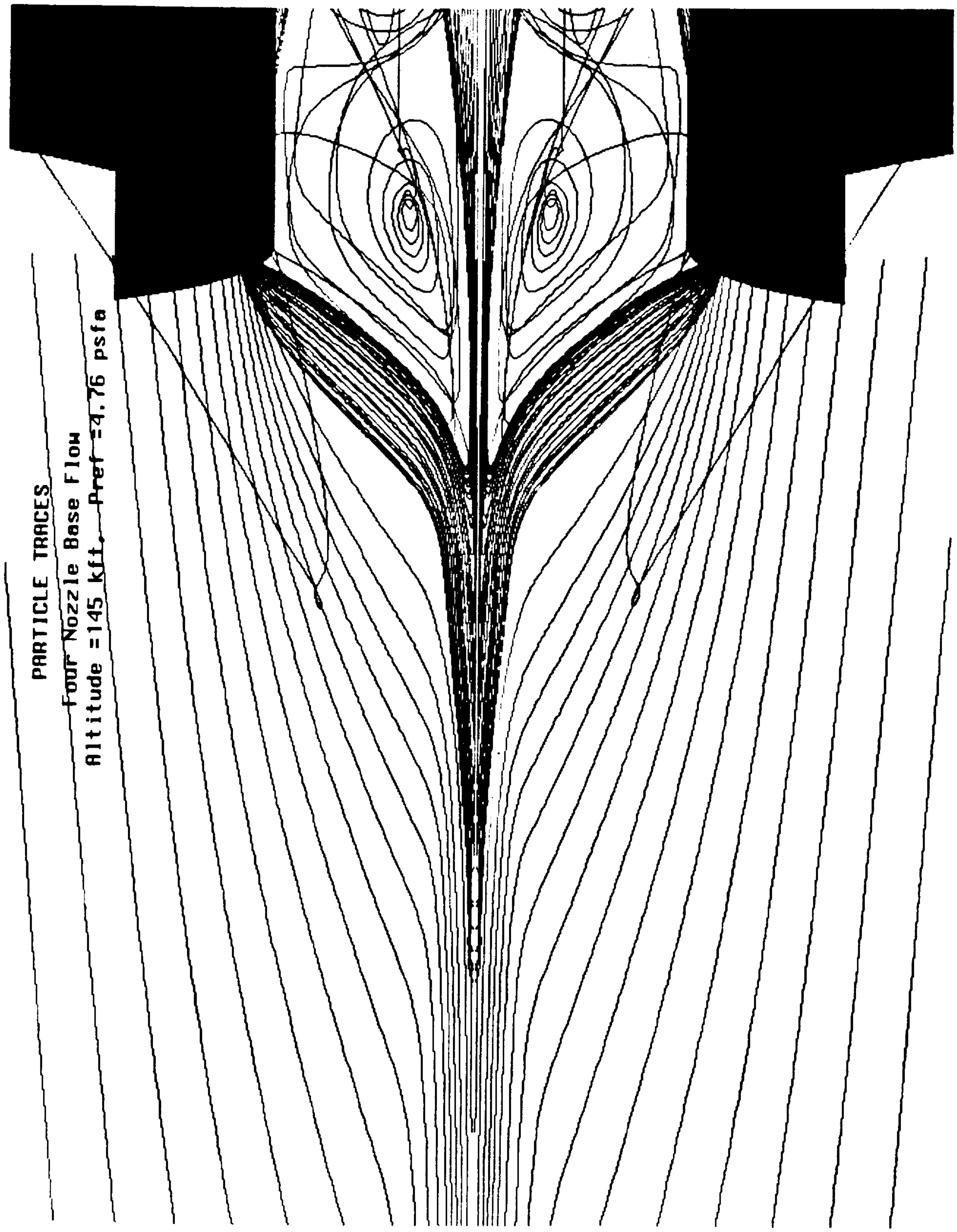
PARTICLE TRACES
Four Nozzle Base Flow
Altitude =145 kft, Pref =4.76 psfa

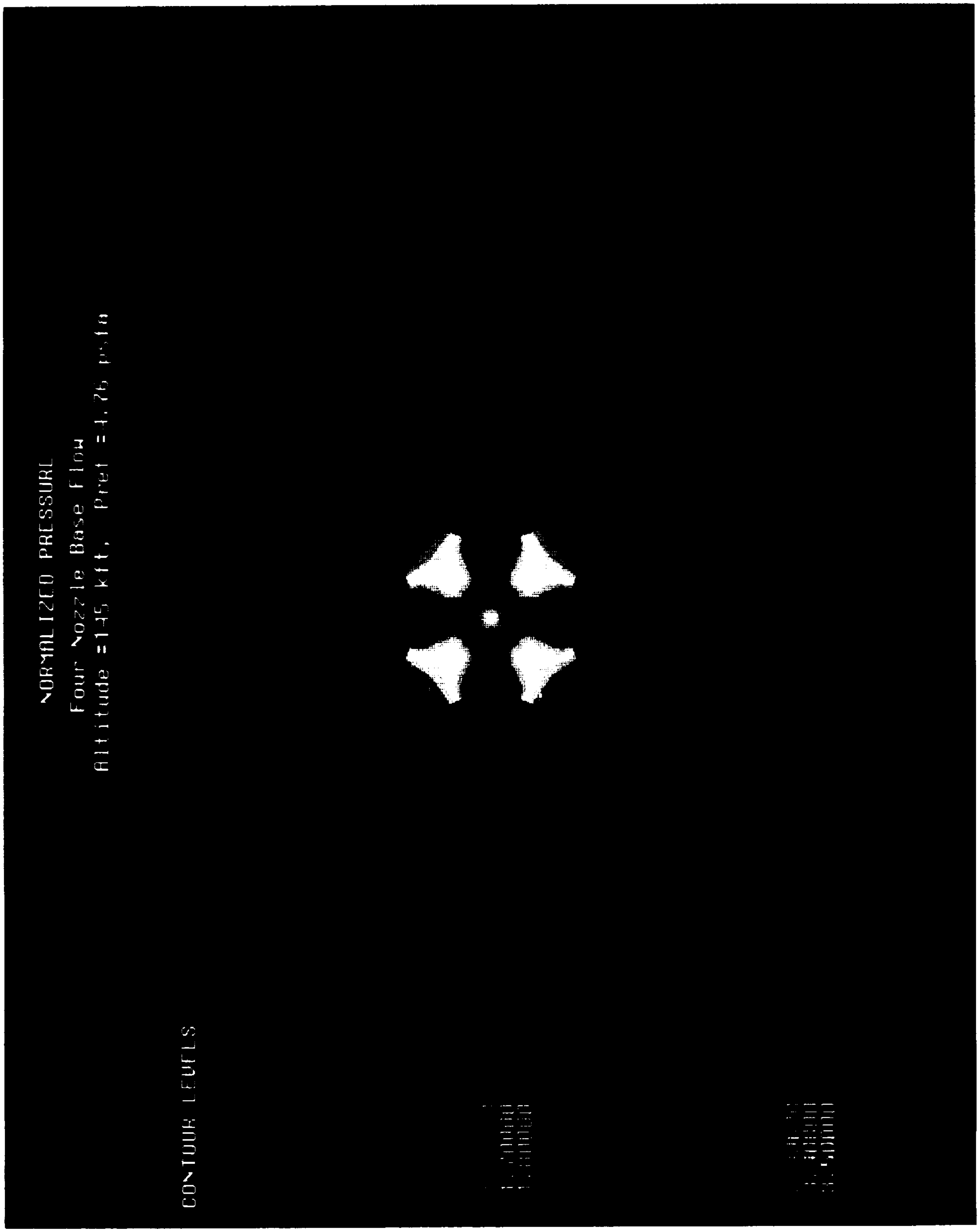
NORMALIZED PRESSURE
Four Nozzle Base Flow
Altitude =145 kft, Pref =4.76 psfa
CONTOUR LEVELS

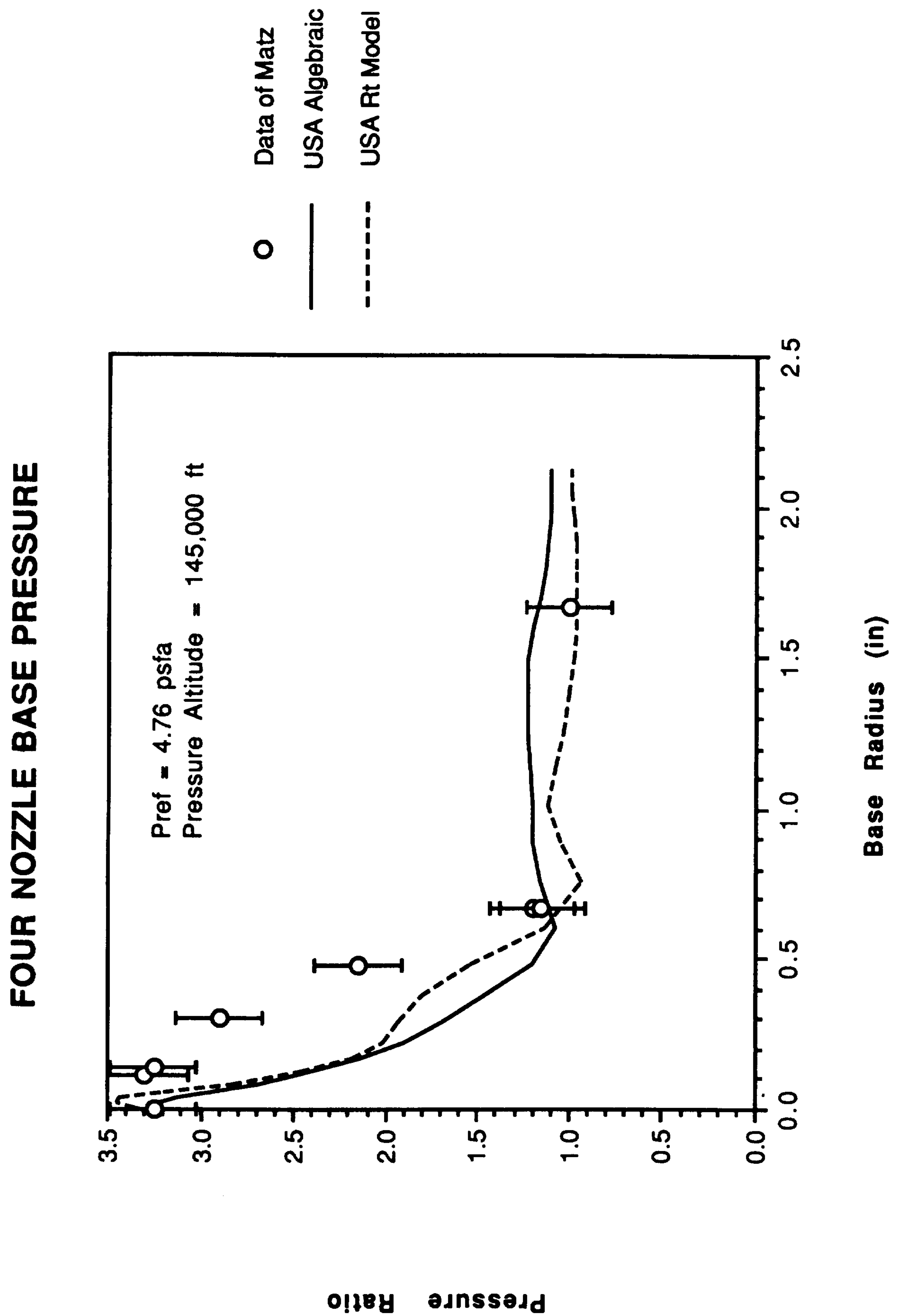
FOUR NOZZLE BASE PRESSURE
Pref = 4.76 psfa
Pressure Altitude = 145,000 ft
Data of Matz
USA Algebraic
USA Rt Model
Pressure Ratio
Base Radius (in)
0.0
0.5
1.0
1.5
2.0
2.5
3.0
3.5
0.0
0.5
1.0
1.5
2.0
2.5

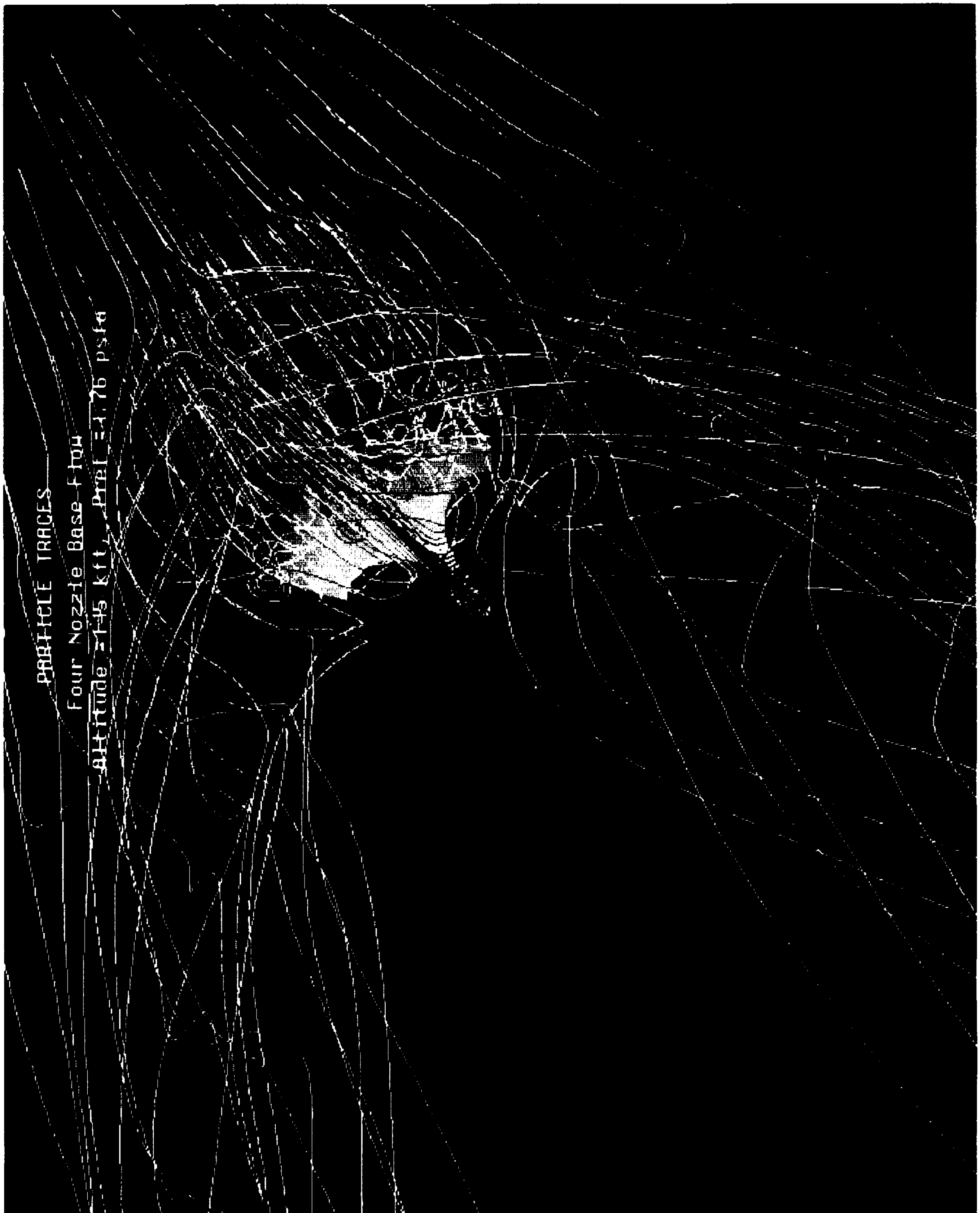
PARTICLE TRACES
Four Nozzle Base Flow
altitude = 145 kft, Pref = 4.76 psfa

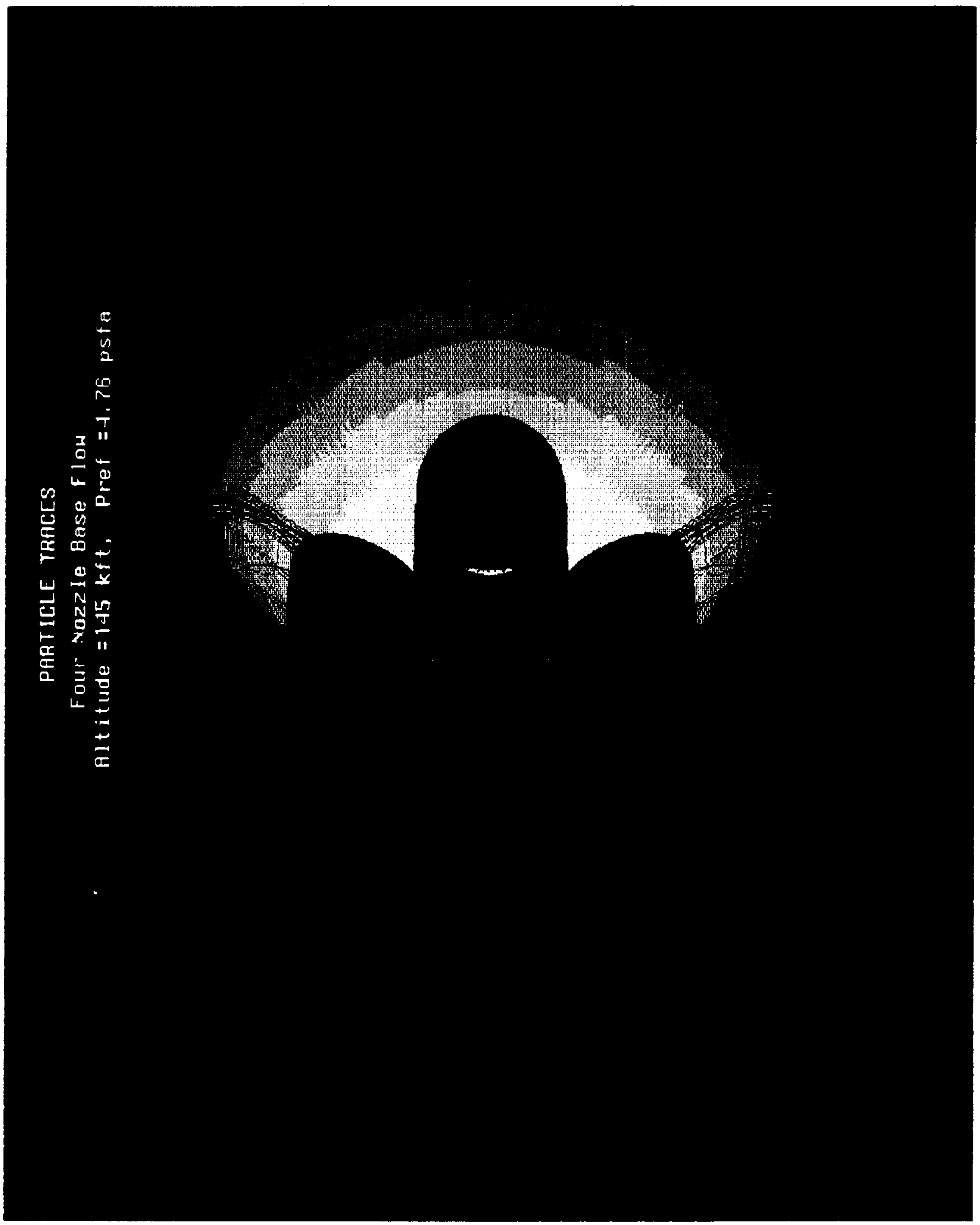
PARTICLE TRACES
Four Nozzle Base Flow
Altitude =145 kft, Pref =4.76 psfa

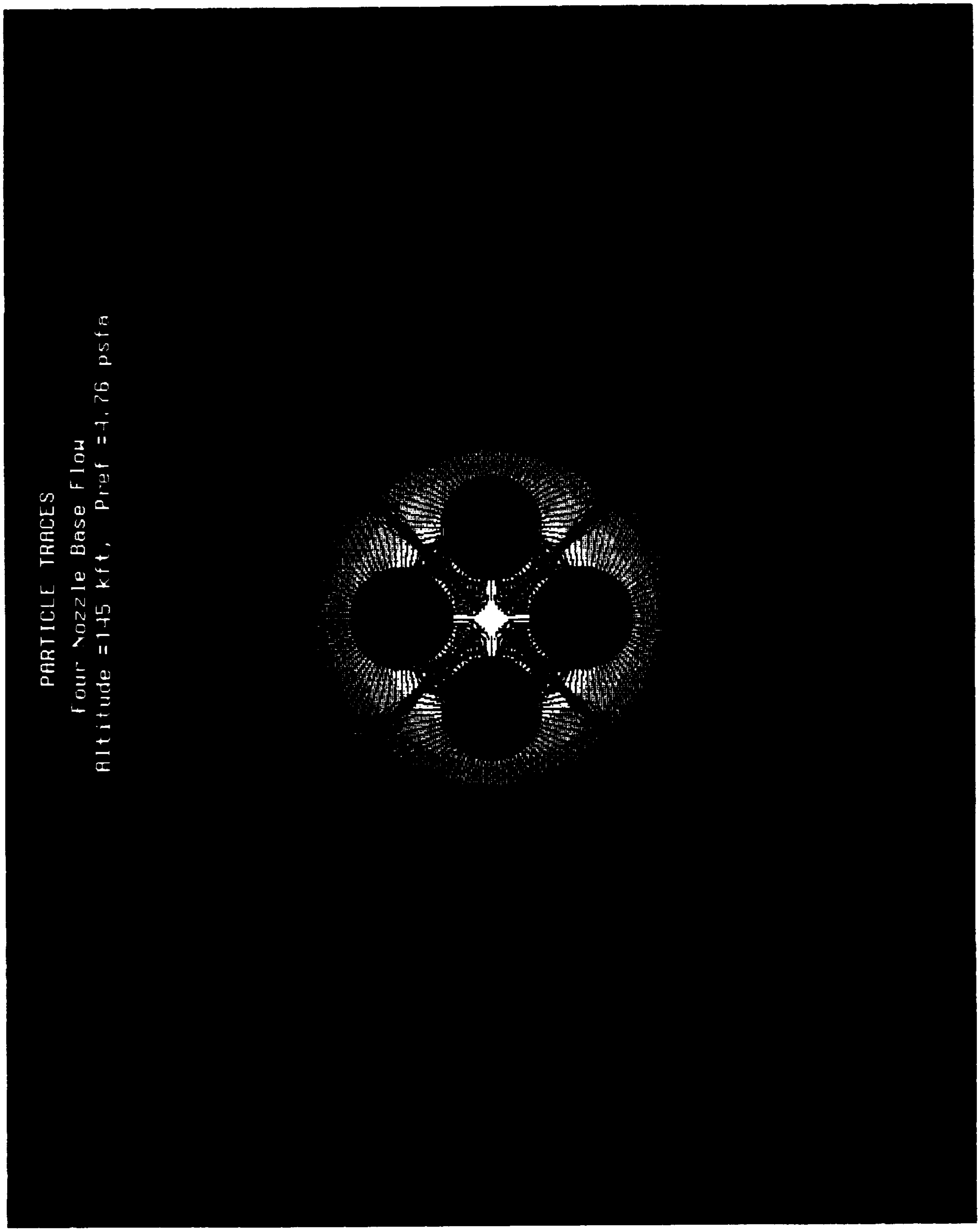

PARTICLE TRACES
Four Nozzle Base Flow
Altitude =145 kft,   Pref =4.76 psfa

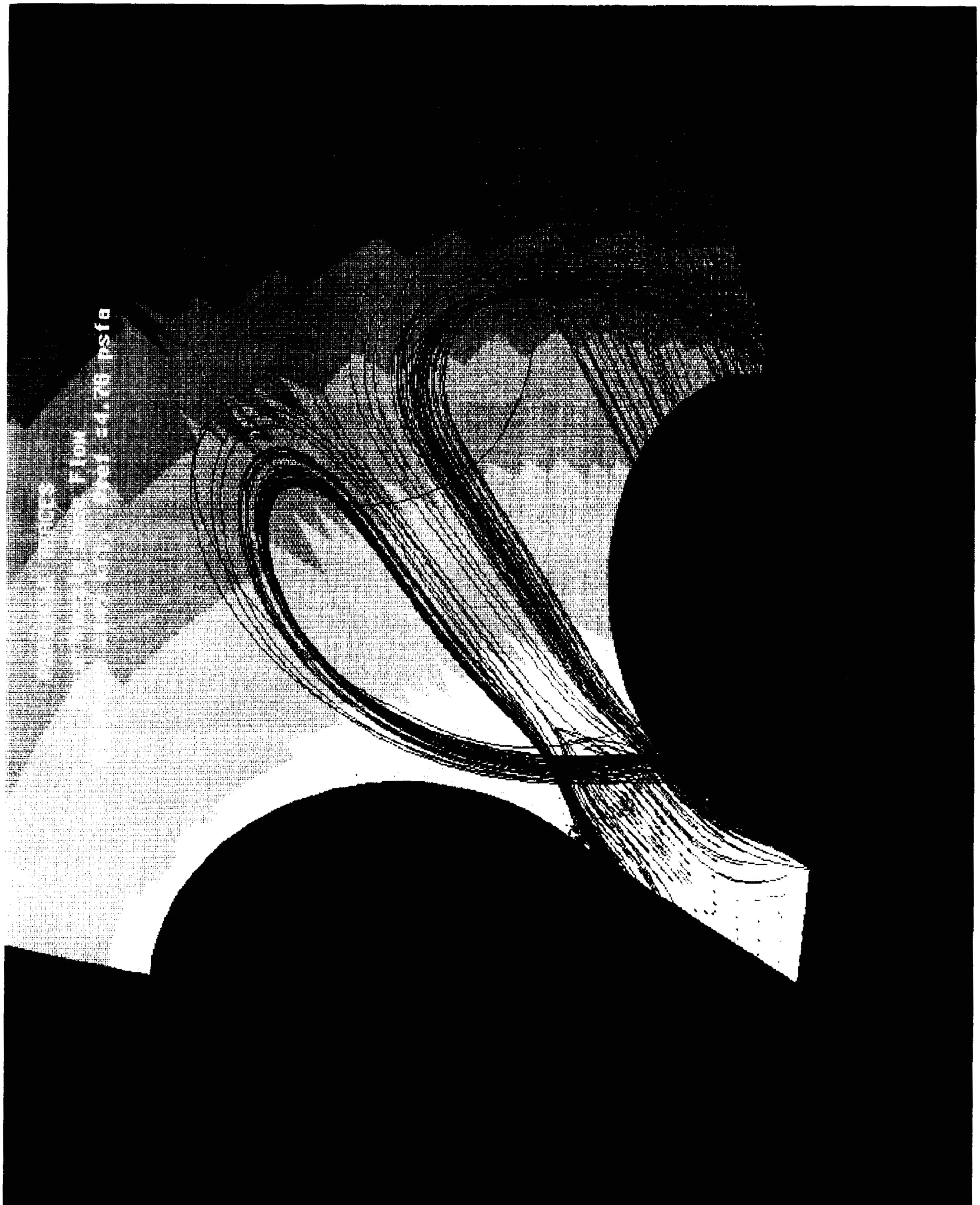

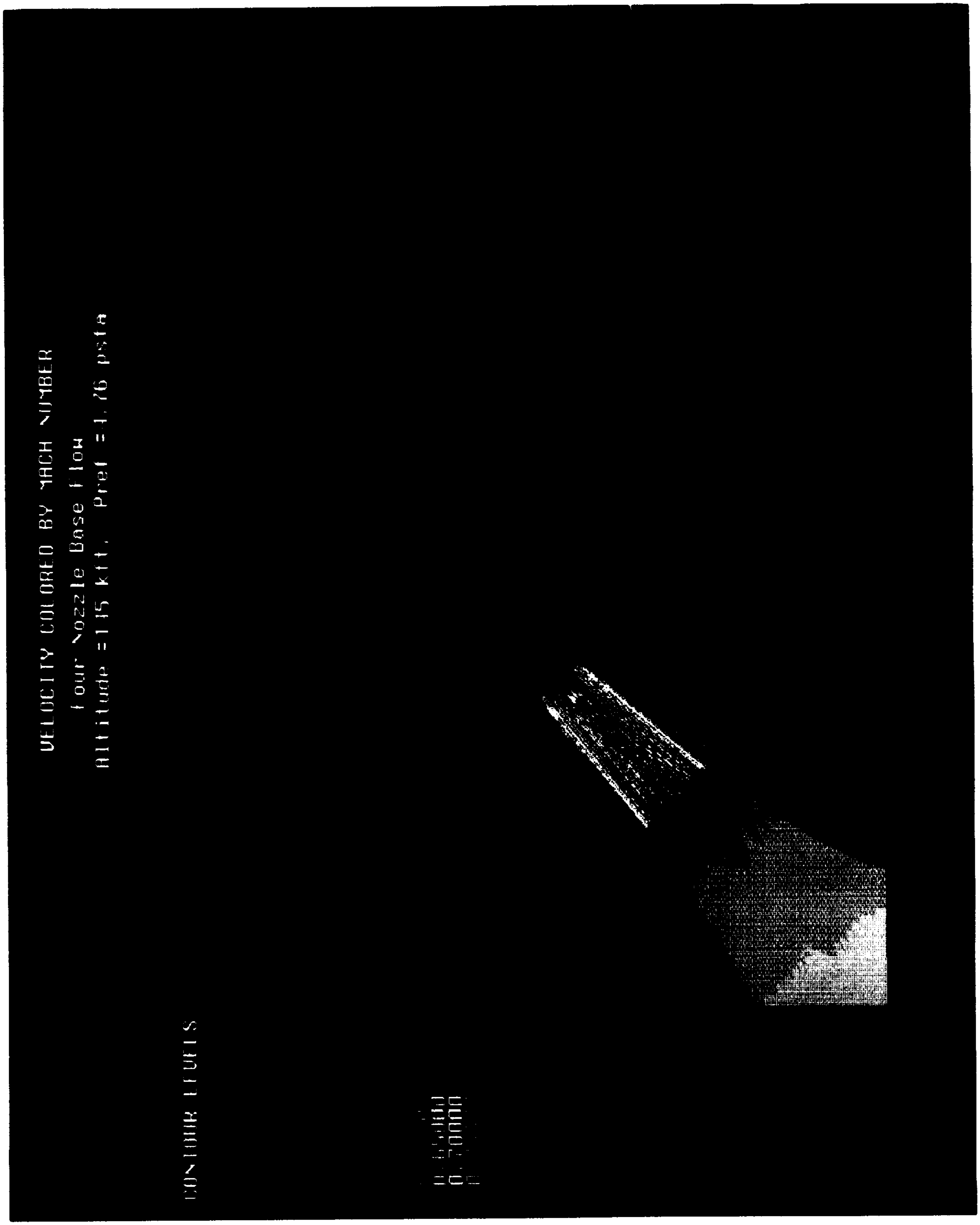
VELOCITY COLORED BY MACH NUMBER
Four Nozzle Base Flow
Altitude =115 kft, Pref =1.76 psfa
CONTOUR LEVELS

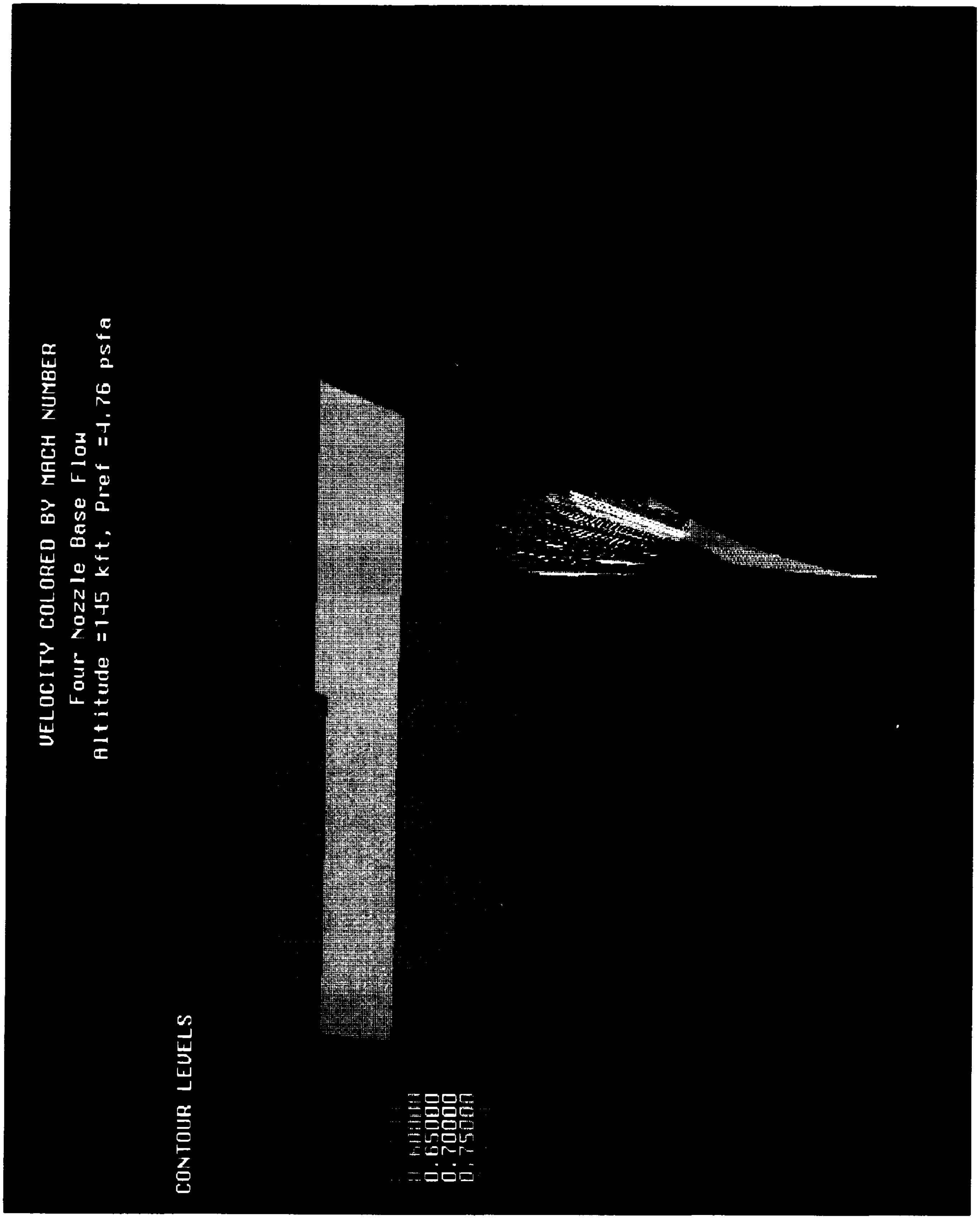

POOR QUALITY

FOUR-NOZZLE CLUSTER HIGH ALTITUDE BASE FLOW BENCHMARK

CONCLUSIONS

- BASE RECIRCULATION FLOW IN THE SIMULATION HAS THE SAME PATTERN AS THE EXPERIMENT
- THERE WAS AN EXCELLENT AGREEMENT WITH THE MAXIMUM PRESSURE AT THE CENTER OF THE BASE (3.3 X FREE-STREAM)
- SMALL DISAGREEMENT IN PRESSURE PROFILE ACROSS THE BASE BETWEEN NOZZLES REMAINS AFTER SEVERAL TRIAL VARIATIONS IN GRID AND TURBULENCE MODELING

RENG002565.02

NUMERICAL STUDY OF BASE PRESSURE CHARACTERISTIC CURVE FOR A FOUR-ENGINE CLUSTERED NOZZLE CONFIGURATION

Ten-See Wang
Computational Fluid Dynamics Branch
NASA - Marshall Space Flight Center
Marshall Space Flight Center, AL 35812

Abstract

Excessive base heating has been a problem for many launch vehicles. For certain design such as the direct dump of turbine exhaust in the nozzle section and at the nozzle lip of the Space Transportation Systems Engine (STME), the potential burning of the turbine exhaust in the base region have caused a tremendous concern. Two conventional approaches have been considered for predicting the base environment: (1) empirical approach, and (2) experimental approach. The empirical approach uses a combination of data correlations and semi-theoretical calculations. It works best for linear problems, simple physics and geometry. However, it is highly suspecious when complex geometry and flow physics are involved, especially when the subject is out of historical database. The experimental approach is often used to establish database for engineering analysis. However, it is qualitative at best for base flow problems. Other criticisms include the inability to simulate forebody boundary layer correctly, the interference effect from tunnel wall, and the inability to scale all pertinent parameters. Furthermore, there is a contention that the information extrapolated from subscale tests with combustion is unconservative.

One potential alternative to the conventional methods is the computational fluid dynamics (CFD), which has none of the above restrictions and is becoming more feasible due to maturing algorithms and advancing computer technology. It provides more details of the flowfield and is only limited by the computer resources. However, it has its share of criticism as a predictive tool for base environment. One major concern is that CFD has not been extensively tested for base flow problems. It is therefore imperative that CFD be assessed and benchmarked satisfactorily for base flows.

In this study, the turbulent base flowfield of a experimental investigation for a four-engine clustered nozzle is numerically benchmarked using a pressure based CFD method. Since the cold air was the medium, accurate prediction of the base pressure distributions at high altitudes is the primary goal. Other factors which may influence the numerical results such as the effects of grid density, turbulence model, differencing scheme, and boundary conditions are also being addressed. Preliminary result of the computed base pressure agreed reasonably well with that of the measurement. Basic base flow features such as the reverse jet, wall jet, recompression shock, and static pressure field in plane of impingement have been captured.

Numerical Study of Base Pressure Characteristic Curve for a Four-Engine Clustered Nozzle Configuration

Ten-See Wang
Computational Fluid Dynamics Branch
NASA-Marshall Space Flight Center

11th Workshop for CFD Applications in Rocket Propulsion
Main Session 9: Combustion - Nozzle/plume - Benchmark
MSFC, Alabama
April 21, 1993

OBJECTIVE

- ☆ To benchmark a cold flow experiment for a four-engine clustered nozzle base flowfield with a CFD model

Base environment predictive methods

★ The empirical approach

- works best for linear problems, simple physics, and simple geometry
- highly suspicious when complex geometry and complex physics such as base flows are involved
- especially when the subject is out of historical database

★ The experimental approach

- often used to establish a database for engineering analysis
- qualitative at best for base flow applications
- inability to simulate forebody boundary layers
- possible interference effect from tunnel wall
- inability to scale all pertinent parameters
- information extrapolated from subscale test with combustion is unconservative

Base environment predictive methods

★ The CFD approach

- has none of the above restrictions
- is becoming more feasible due to maturing algorithms and advancing computer technology
- provides subtle details of flow physics
- is only limited by computer resources

CFD Methodology

- ❄ Non-Staggered Grid Pressure Based Method
- ❄ Curvilinear Transformed Navier-Stokes Equations
- ❄ Predictor plus Multi-Corrector Solution Procedure for Efficient Time Marching
- ❄ Second and Fourth-Order Central Plus Upwind Dissipation for the Convective Terms
- ❄ Two-Equation Turbulence Model

Parametric Study

- Grid Resolution
  - four 2-zone 3D grid were generated
  - Grid A: 34,030 points
  - Grid B, C, and D: 113,202 points
- Turbulence Model
- Inlet boundary condition
- Convective dissipation parameter

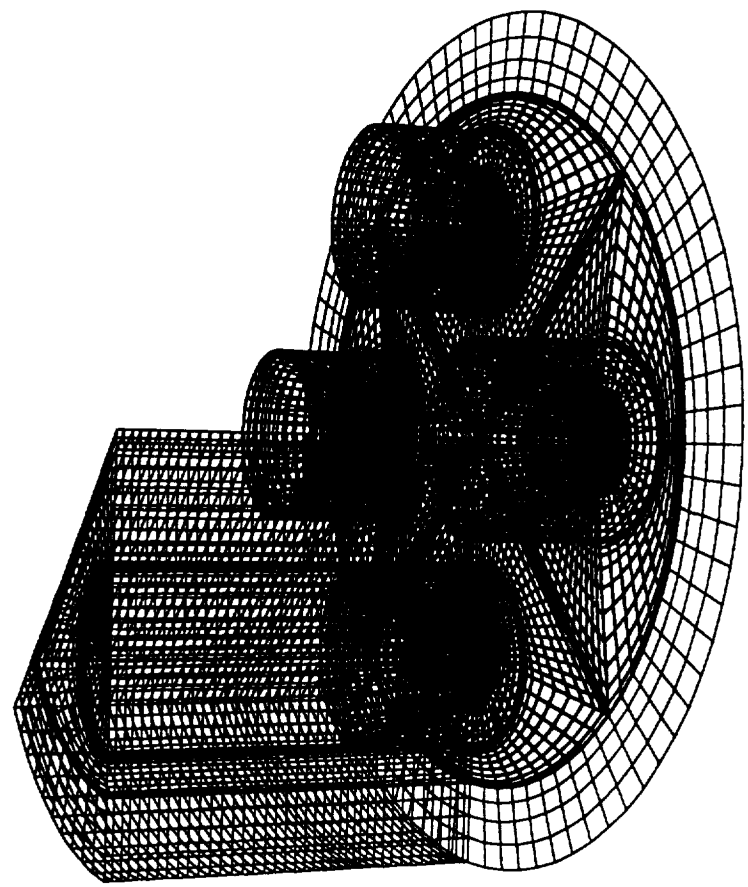

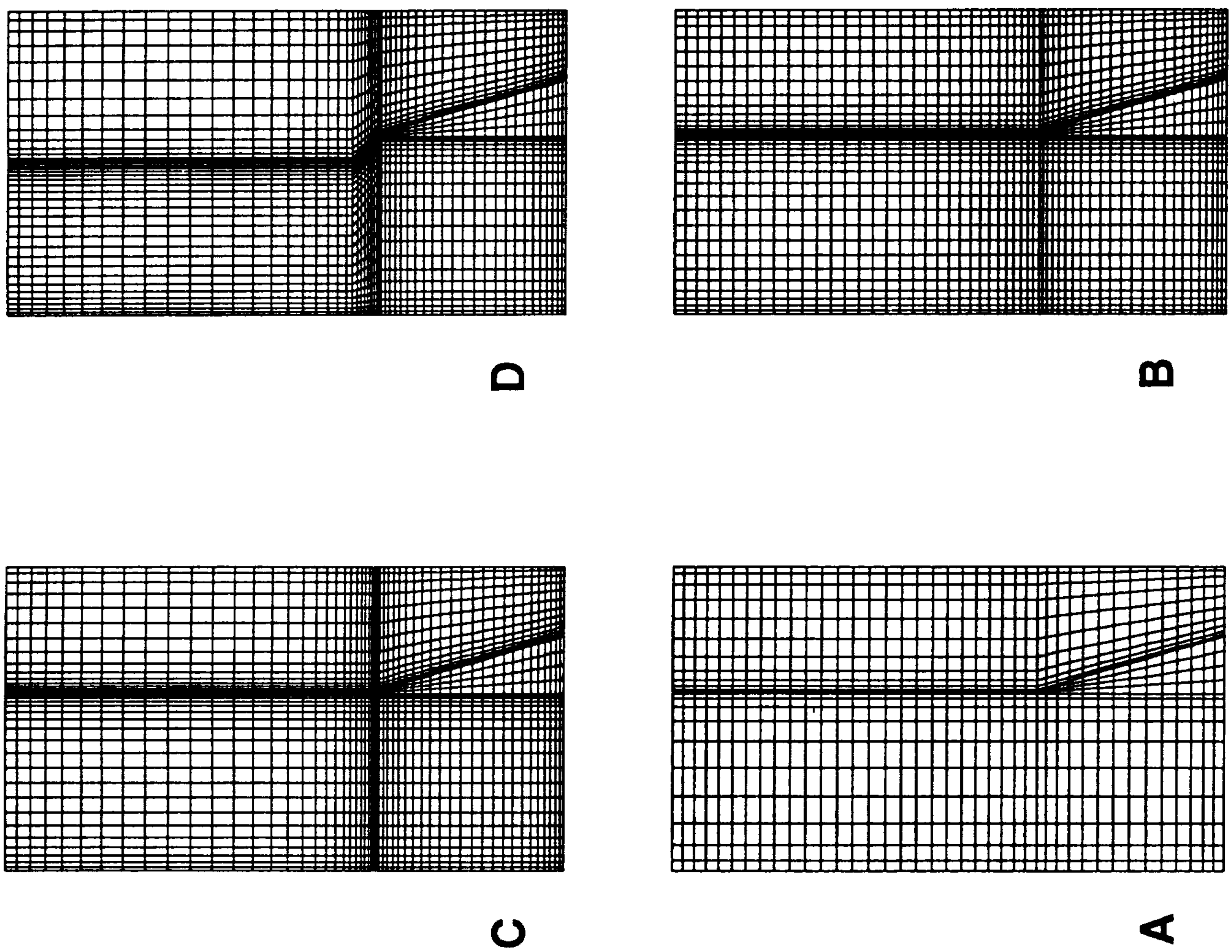
D
B
C
A

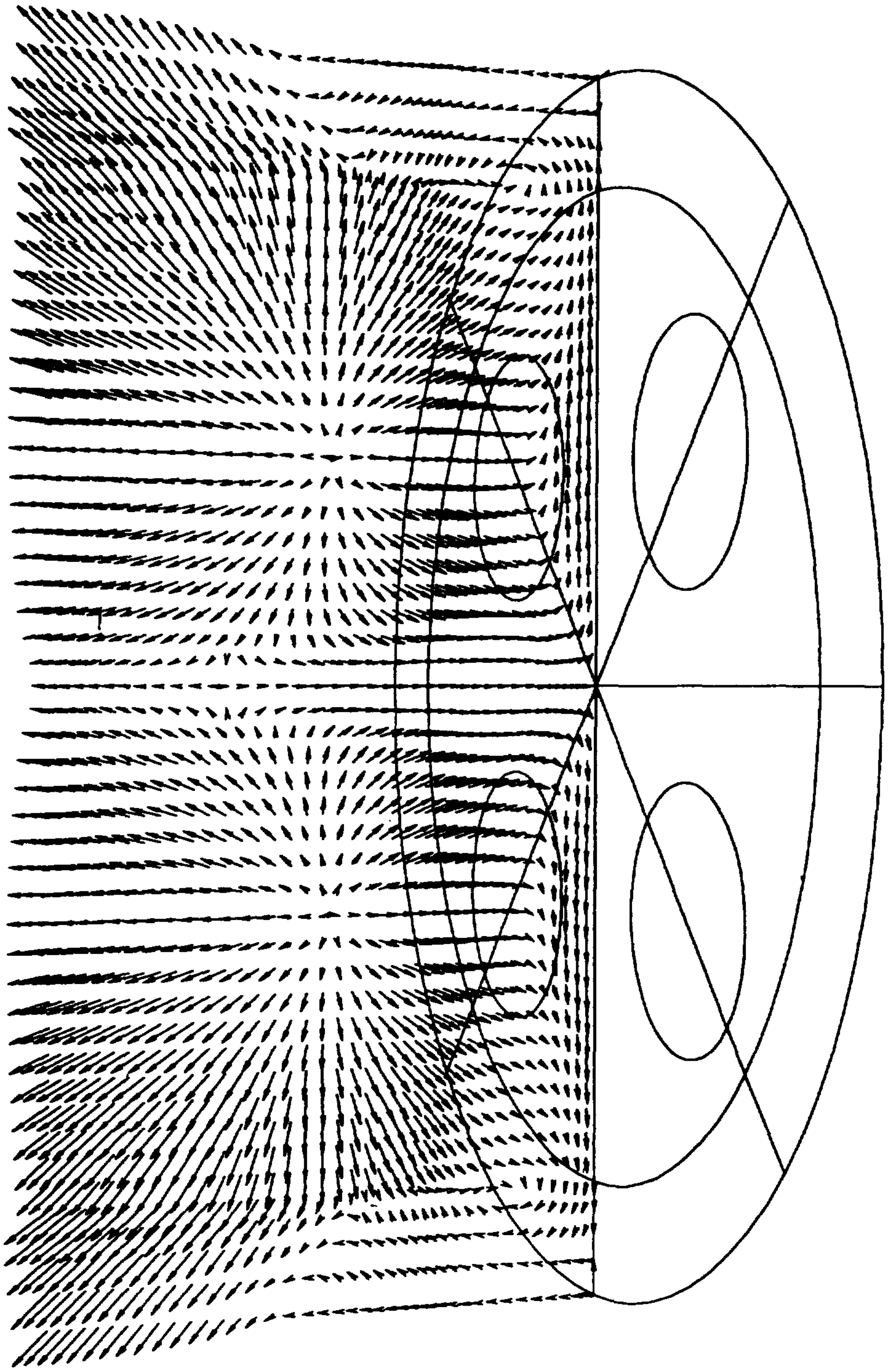

C-11.

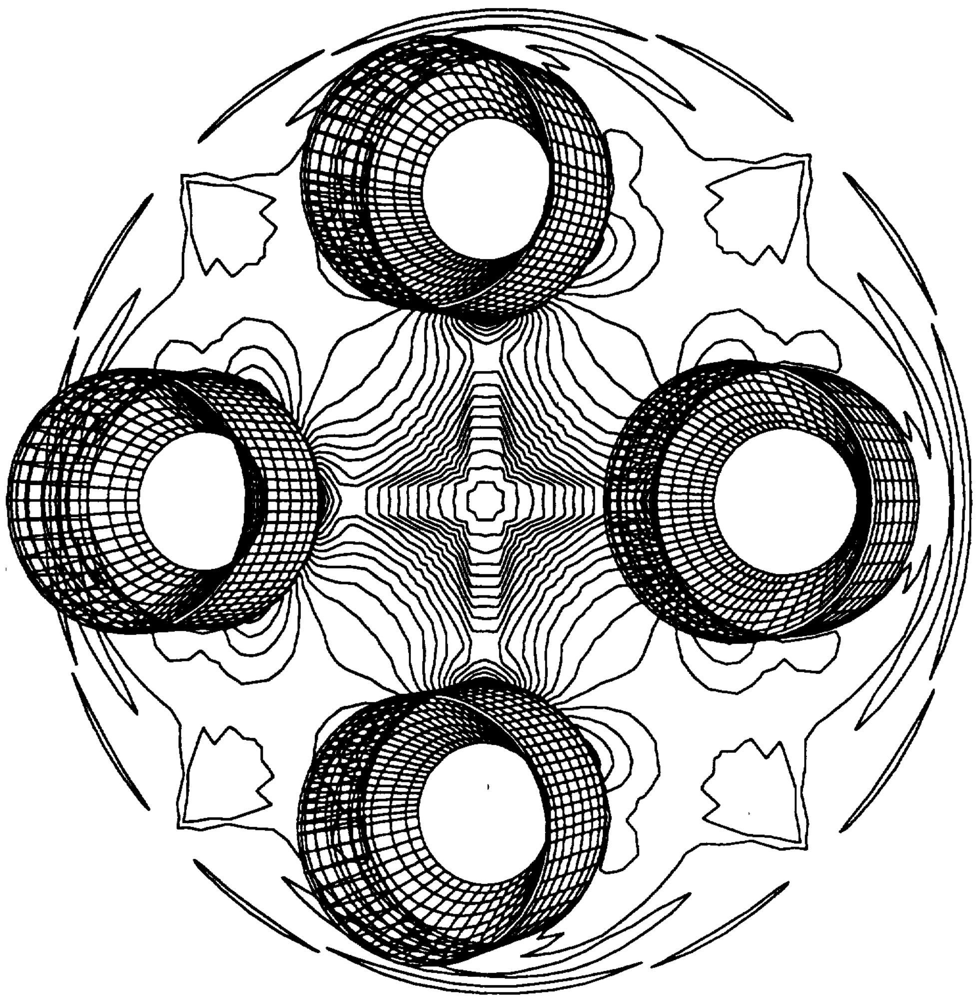

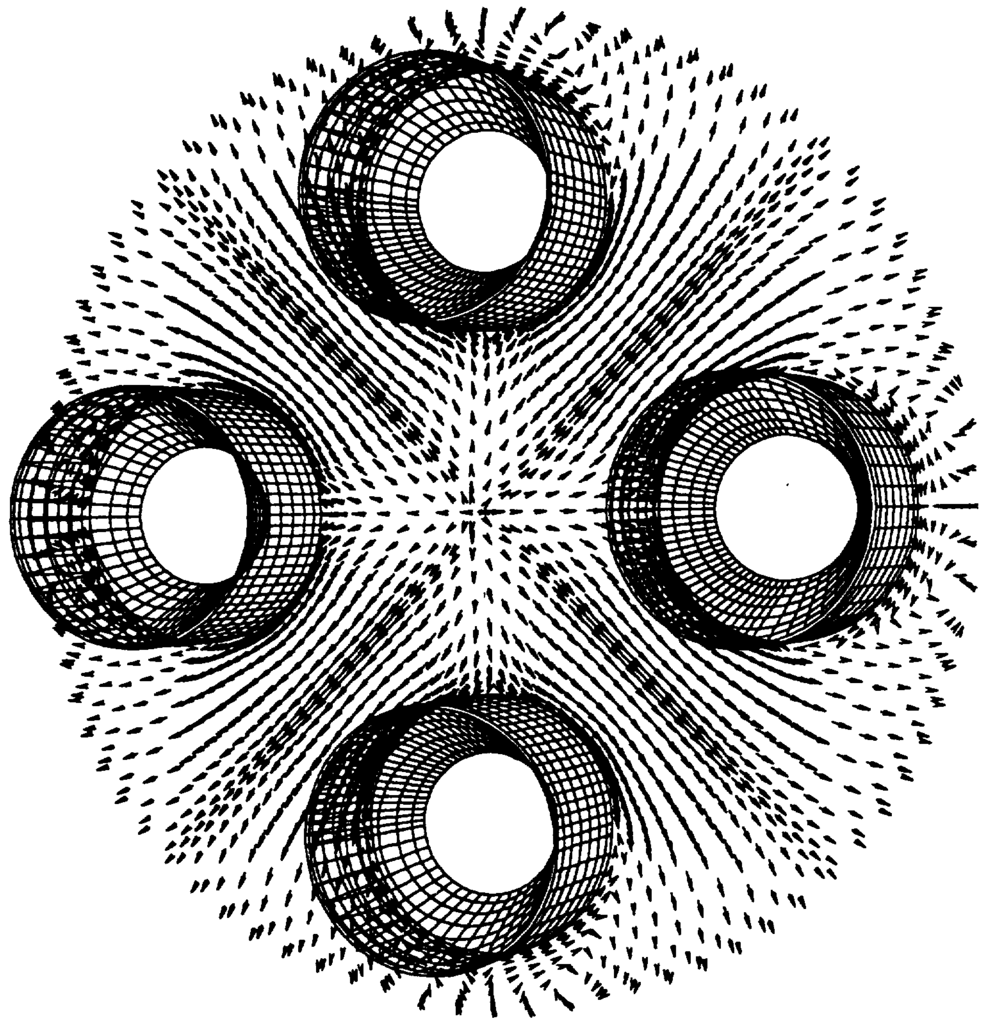

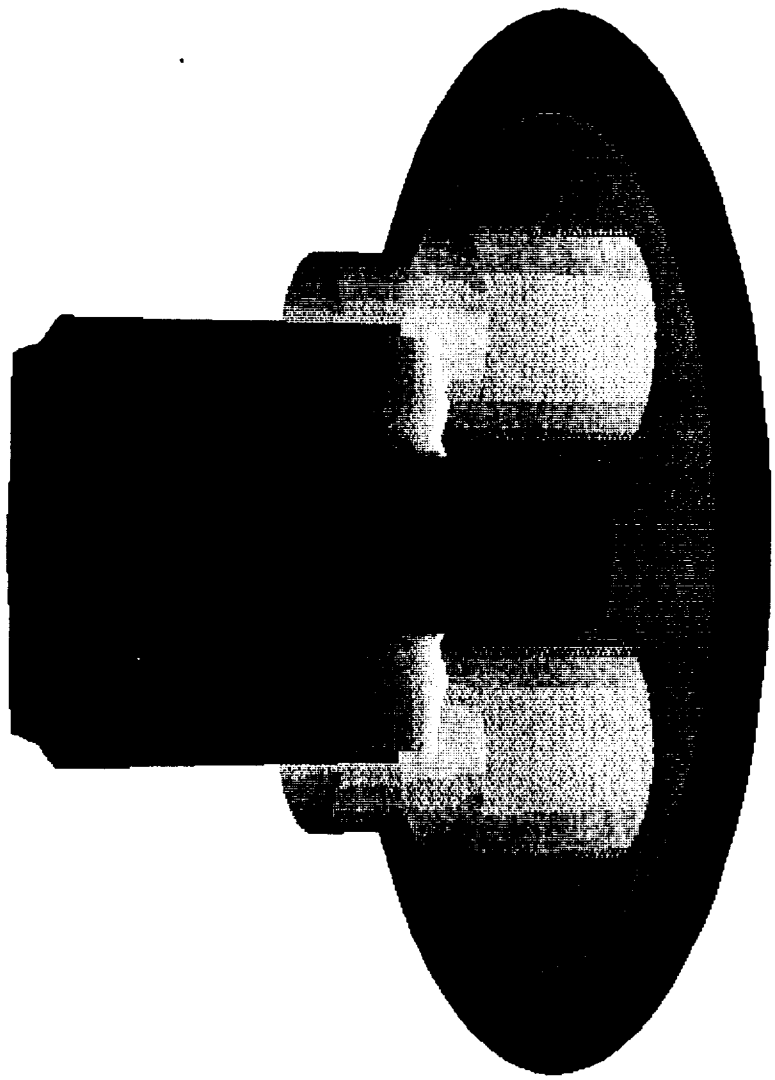

pmfmg4bw.1.img

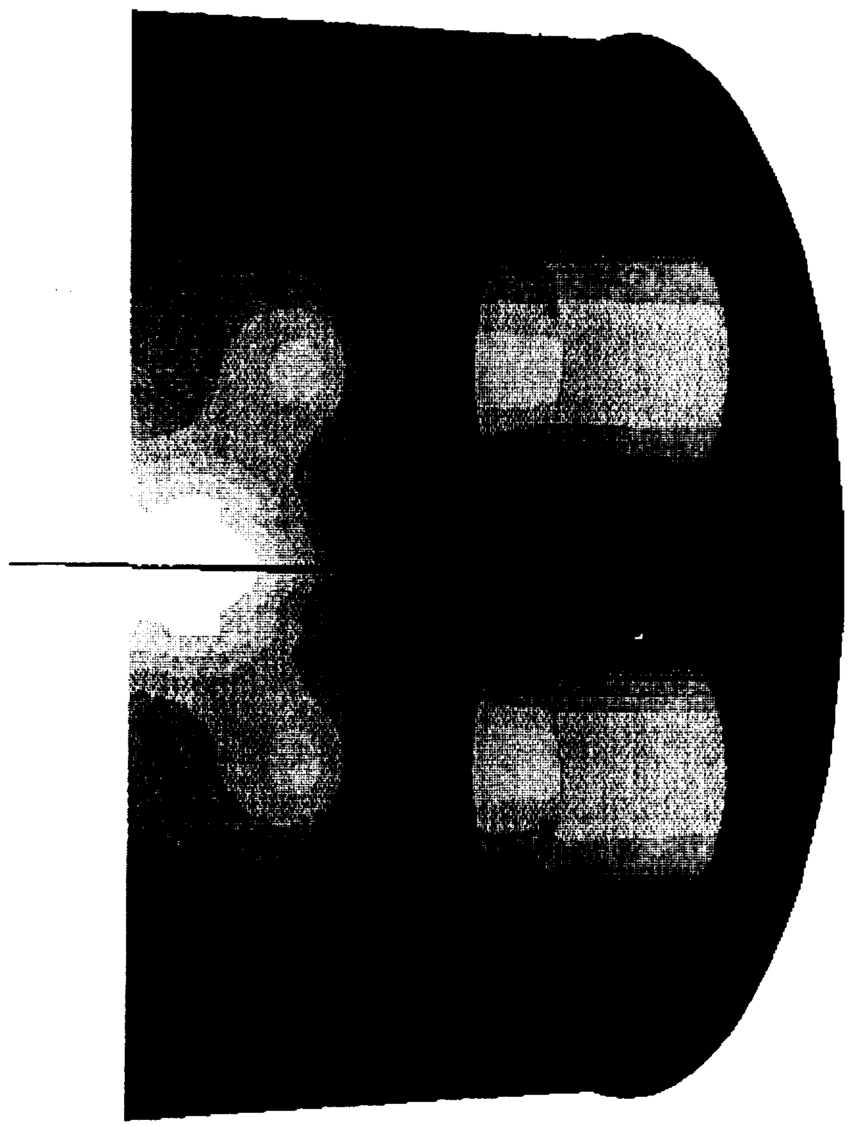

pmfmg4bw.2.img

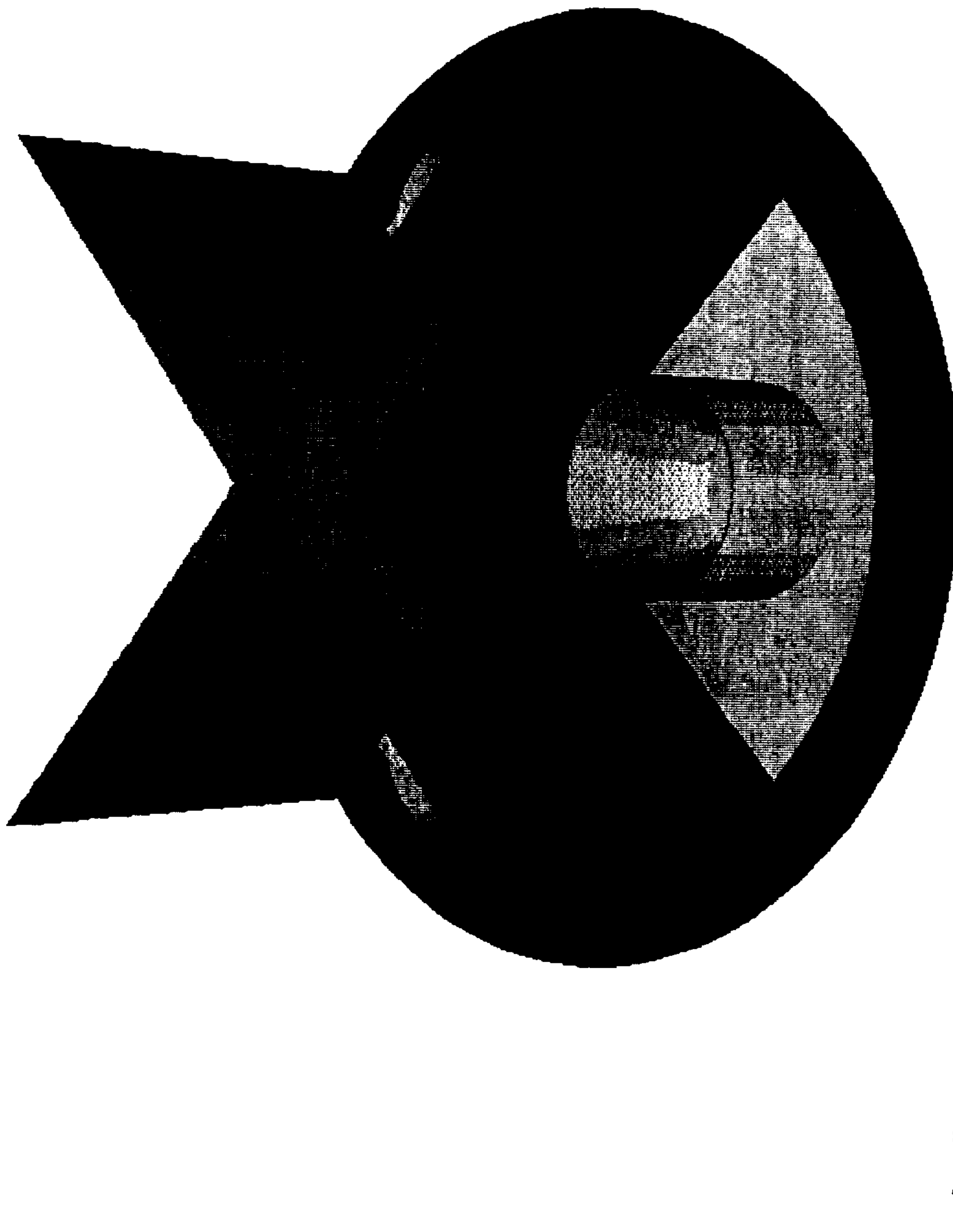

pwfmg4bw.3.img

RADIAL BASE PRESSURE DISTRIBUTION

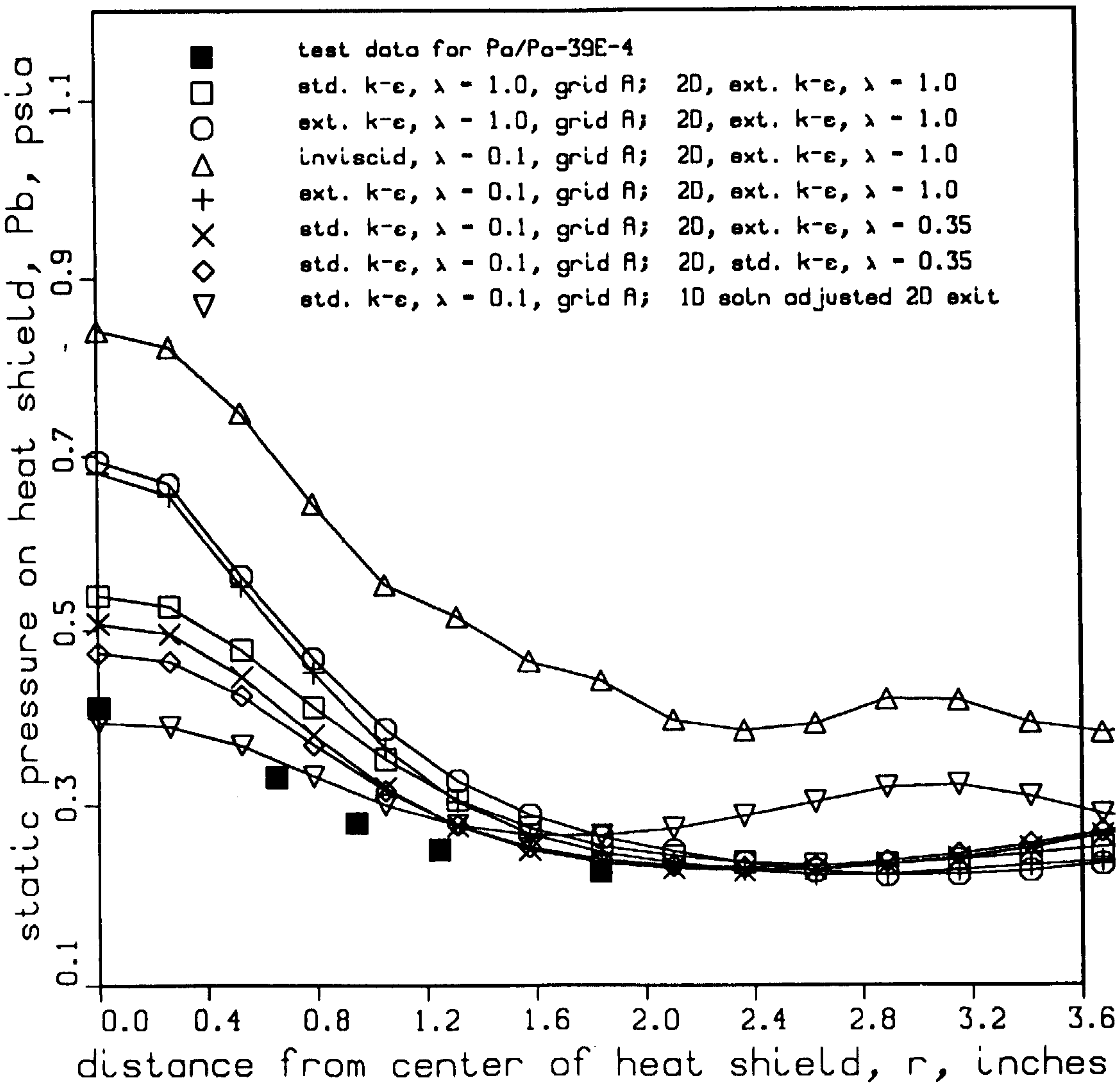

RADIAL BASE PRESSURE DISTRIBUTION

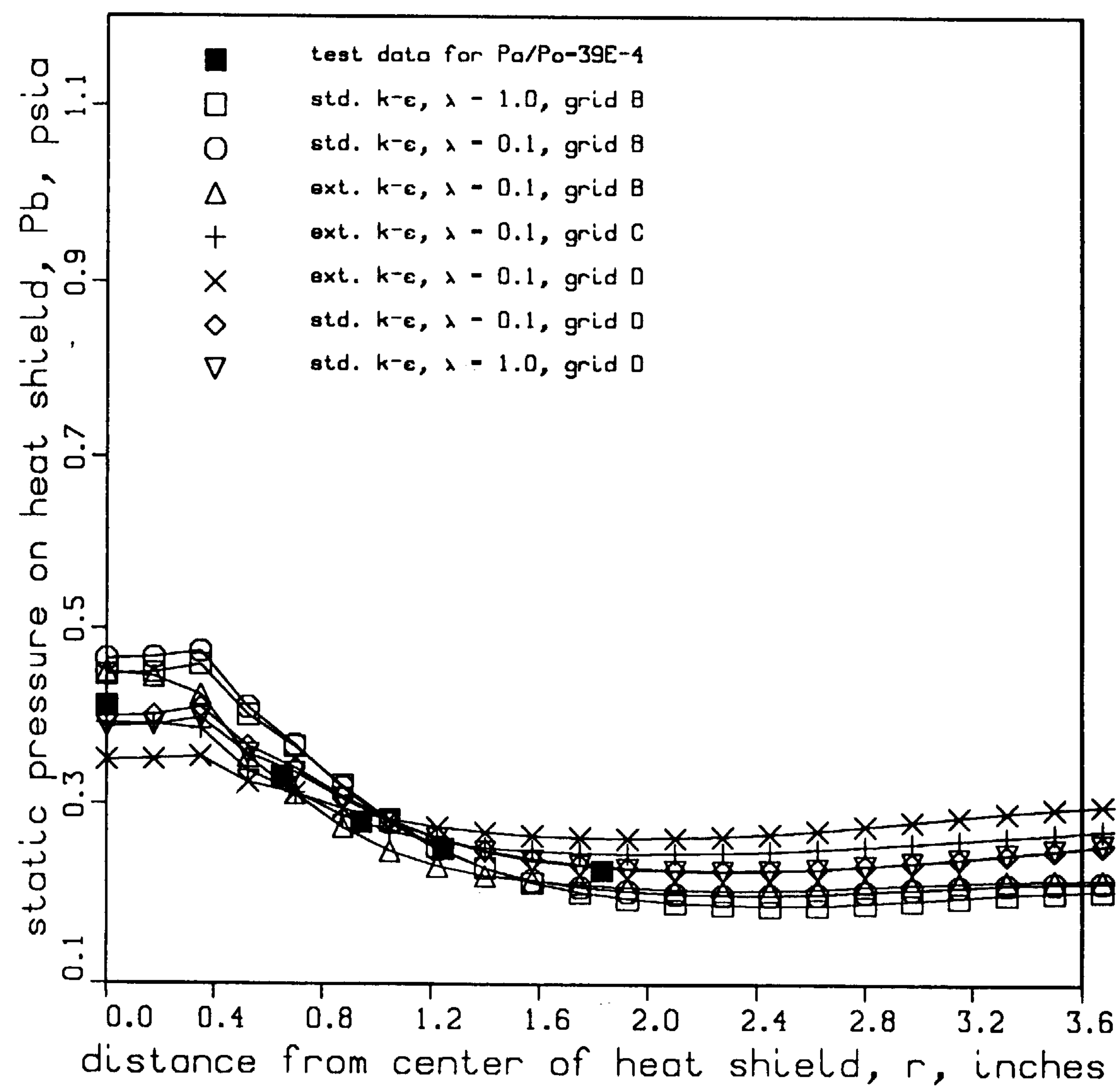

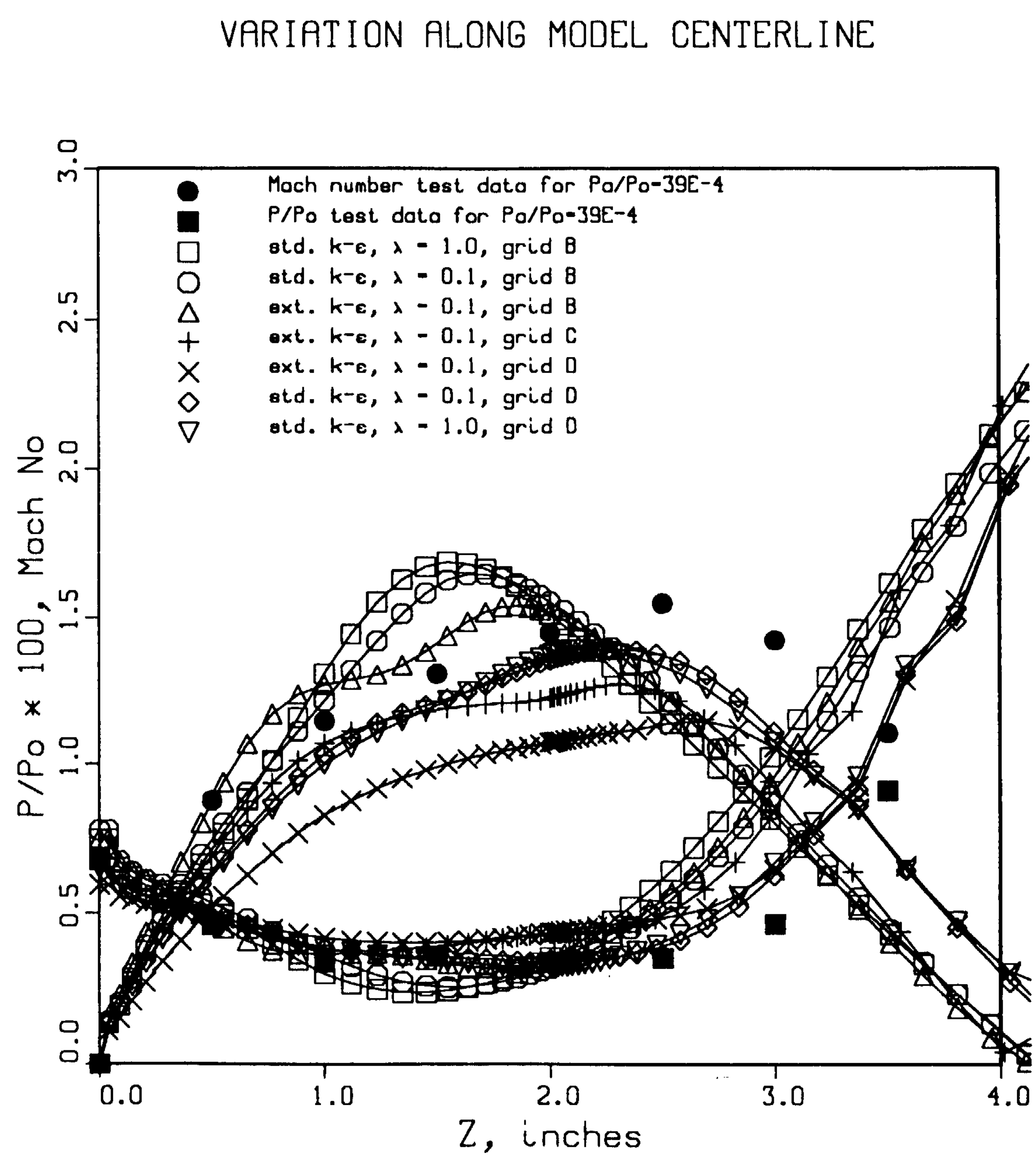
VARIATION ALONG MODEL CENTERLINE
Mach number test data for Pa/Po=39E-4
P/Po test data for Pa/Po=39E-4
std. k-ε, λ = 1.0, grid B
std. k-ε, λ = 0.1, grid B
ext. k-ε, λ = 0.1, grid B
ext. k-ε, λ = 0.1, grid C
ext. k-ε, λ = 0.1, grid D
std. k-ε, λ = 0.1, grid D
std. k-ε, λ = 1.0, grid D
P/Po * 100, Mach No
Z, inches
0.0
0.5
1.0
1.5
2.0
2.5
3.0
0.0
1.0
2.0
3.0
4.0

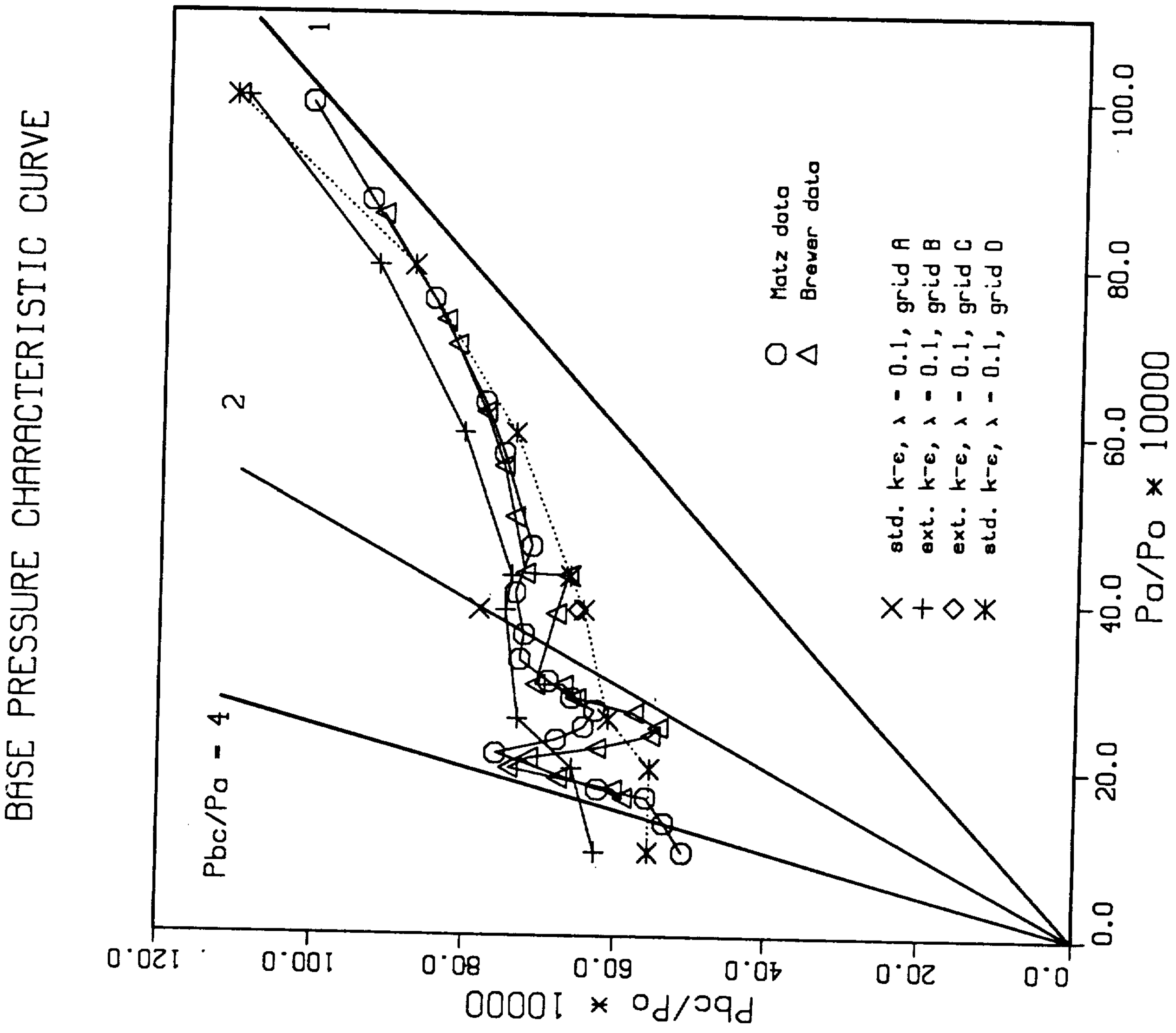
BASE PRESSURE CHARACTERISTIC CURVE
Pbc/Pa - 4
2
1
Matz data
Brewer data
std. k-ε, λ - 0.1, grid A
ext. k-ε, λ - 0.1, grid B
ext. k-ε, λ - 0.1, grid C
std. k-ε, λ - 0.1, grid D
0.0
20.0
40.0
60.0
80.0
100.0
120.0
Pa/Po * 10000
Pbc/Po * 10000

SUMMARY

- ☆ Qualitative base flow features such as the reverse jet, wall jet, recompression shock, and plume-plume impingement have been captured.
- ☆ Quantitative results such as the radial base flow distribution, Mach number and static pressure variations along model center line, and the base pressure characteristic curve agreed reasonable well with those of the experiment
- ☆ Parametric study indicated that the grid resolution and turbulence model are two important parameters which determine the accuracy of a base flow solution
- ☆ The potential of using CFD as a predictive tool for base environment prediction is demonstrated

Future work

- ☆ Grid adapted flowfield solution
- ☆ Hot flow multi-engine base flowfield benchmarking
- ☆ Combustion flow multi-engine base flowfield benchmarking
- ☆ Flight vehicle forbody and base environment simulation

REPORT DOCUMENTATION PAGE

Form Approved
OMB No. 0704-0188

1. AGENCY USE ONLY *(Leave blank)*	2. REPORT DATE	3. REPORT TYPE AND DATES COVERED
	July 1993	Conference Publication

4. TITLE AND SUBTITLE

Eleventh Workshop for Computational Fluid Dynamic Applications in Rocket Propulsion—Part I

5. FUNDING NUMBERS

6. AUTHOR(S)

R.W. Williams, Compiler

7. PERFORMING ORGANIZATION NAME(S) AND ADDRESS(ES)

George C. Marshall Space Flight Center
Marshall Space Flight Center, Alabama 35812

8. PERFORMING ORGANIZATION REPORT NUMBER

M-726

9. SPONSORING/MONITORING AGENCY NAME(S) AND ADDRESS(ES)

National Aeronautics and Space Administration
Washington, DC 20546

10. SPONSORING/MONITORING AGENCY REPORT NUMBER

NASA CP-3221

11. SUPPLEMENTARY NOTES

Prepared by Structures and Dynamics Laboratory, Science and Engineering Directorate.

12a. DISTRIBUTION/AVAILABILITY STATEMENT

Subject Category: 34
Unclassified—Unlimited

12b. DISTRIBUTION CODE

13. ABSTRACT *(Maximum 200 words)*

Conference publication includes ... resentations
given at the Eleventh Workshop for Co ... ocket Propulsion
held at George C. Marshall Space Flig ... he workshop is to
discuss experimental and computation ... n. The workshop is
an open meeting for government, ind ... are discussed
including computational fluid dynam ... lsion,
turbomachinery, combustion, heat tr

14. SUBJECT TERMS spray, injector, computational fluid dynamics, rocket propulsion, liquid rocket, solid rocket, turbopump, turbomachinery, combustion, methodology, impeller, inducer, heat transfer, grid generation, nozzle, plume

15. NUMBER OF PAGES 970

16. PRICE CODE A99

17. SECURITY CLASSIFICATION OF REPORT	18. SECURITY CLASSIFICATION OF THIS PAGE	19. SECURITY CLASSIFICATION OF ABSTRACT	20. LIMITATION OF ABSTRACT
Unclassified	Unclassified	Unclassified	Unlimited

NSN 7540-01-280-5500

Standard Form 298 (Rev 2-89)
Prescribed by ANSI Std Z39-18
298-102